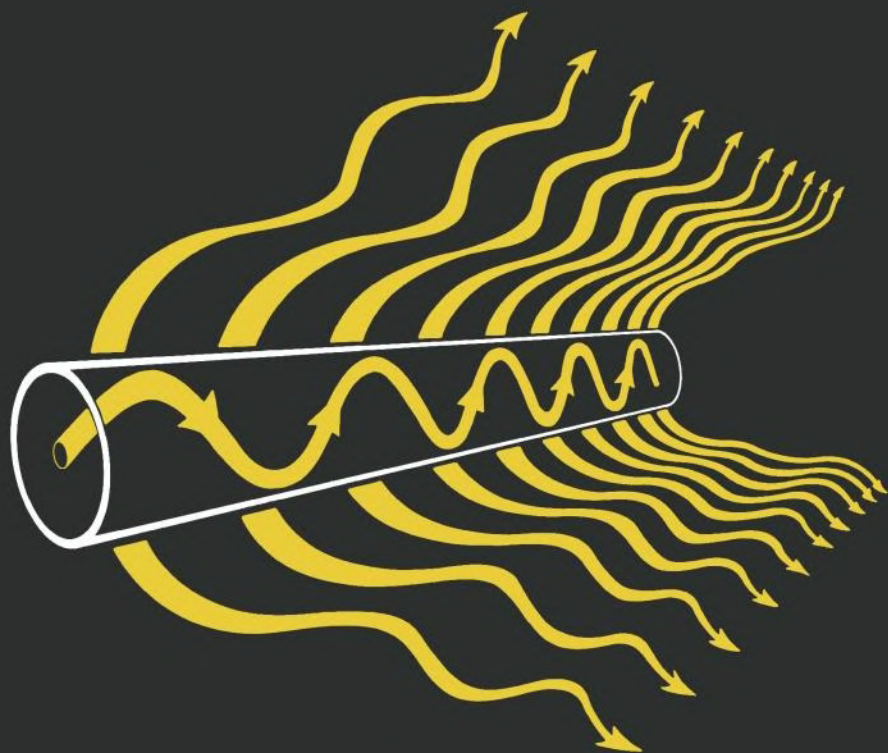


Optical Waveguide Theory

Allan W. Snyder *and* John D. Love



RAY PARAMETERS

$(n_{co}^2 - n_{cl}^2)^{1/2}$	Numerical aperture
$\{n^2(r) - n_{cl}^2\}^{1/2}$	Local numerical aperture
$\theta_c(r) = \sin^{-1} \left\{ 1 - \frac{n_{cl}^2}{n^2(r)} \right\}^{1/2}$ $= \cos^{-1} \left\{ \frac{n_{cl}}{n(r)} \right\}$	Complement of local critical angle
$\theta_z(r)$	Angle between path and axial direction
$\theta_\phi(r)$	Angle between projection of path onto fiber cross-section and azimuthal direction
$\alpha(r)$	Angle between path and radial direction
$\bar{\beta} = n(r) \cos \theta_z(r)$	Axial invariant
$T = \frac{r}{\rho} n(r) \sin \theta_z(r) \cos \theta_\phi(r)$	Azimuthal invariant
r_{ic}	Radius of inner caustic
r_{tp}	Radius of turning-point caustic
$r_{rad} = \frac{\rho l}{(n_{cl}^2 - \bar{\beta}^2)^{1/2}}$	Radius of radiation caustic
$z_p = \frac{1}{N}$	Ray half-period along fiber axis
$N = \frac{1}{z_p}$	Number of reflections or turning points per unit length of fiber
L_p	Geometric path length per half-period
L_o	Optical path length per half-period
$v_g = \frac{c}{n(r)}$	Local speed of light
t	Ray transit time

WAVEGUIDE OR FIBER PARAMETERS

$n(x, y)$ or $n(r)$	Refractive-index profile
$n^2(x, y) = n_{\text{co}}^2 \{1 - 2\Delta f(x, y)\}$ $n^2(r) = n_{\text{co}}^2 \{1 - 2\Delta f(r)\}$	Profile representation ($f \geq 0$)
$n_g = n - \lambda \frac{\partial n}{\partial \lambda}$	Group index
$\Delta = \frac{n_{\text{co}}^2 - n_{\text{cl}}^2}{2n_{\text{co}}^2} = \frac{\sin^2 \theta_c}{2}$	Profile height parameter
$\theta_c = \sin^{-1} \left\{ 1 - \frac{n_{\text{cl}}^2}{n_{\text{co}}^2} \right\}^{1/2} = \cos^{-1} \left(\frac{n_{\text{cl}}}{n_{\text{co}}} \right)$	Complement of the critical angle
$n_{\text{co}} \quad (f = 0)$	Maximum core index
$n_{\text{cl}} = n_{\text{co}}(1 - 2\Delta)^{1/2} \quad (f = 1)$	Uniform cladding index
$S = 1 - f$	Profile shape
$\Omega = \int_{A_{\infty}} (1 - f) dA = \int_{A_{\infty}} S dA$	Profile volume
A_{∞}	Infinite cross-section
A_{co}	Core cross-section
ρ	Core radius or half-width
λ	Free-space wavelength
$k = \frac{2\pi}{\lambda} = \frac{V}{\rho n_{\text{co}}(2\Delta)^{1/2}}$	Free-space wavenumber
$V = k\rho(n_{\text{co}}^2 - n_{\text{cl}}^2)^{1/2} = k\rho n_{\text{co}}(2\Delta)^{1/2}$ $= k\rho n_{\text{co}} \sin \theta_c$	Waveguide or fiber parameter
$n_{\text{co}} \cong n_{\text{cl}} \text{ or } \Delta \ll 1$ $\Delta \cong \frac{n_{\text{co}} - n_{\text{cl}}}{n_{\text{co}}}$ $\theta_c \cong (2\Delta)^{1/2} \cong \left(1 - \frac{n_{\text{cl}}^2}{n_{\text{co}}^2} \right)^{1/2} \cong \cos^{-1} \left(\frac{n_{\text{cl}}}{n_{\text{co}}} \right)$	Weak-guidance or paraxial approximation

Optical Waveguide Theory

Optical Waveguide Theory

ALLAN W. SNYDER

JOHN D. LOVE

*Institute of Advanced Studies
Australian National University
Canberra, Australia*

LONDON NEW YORK
Chapman and Hall

First published 1983 by
Chapman and Hall Ltd
11 New Fetter Lane, London EC4P 4EE
Published in the USA by
Chapman and Hall
733 Third Avenue, New York NY10017

© 1983 Allan W. Snyder and John D. Love

J. W. Arrowsmith Ltd., Bristol

ISBN 0 412 09950 0 (cased)
ISBN 0 412 24250 8 (Science Paperback)

This title is available in both hardbound and paperback editions. The paperback edition is sold subject to the condition that it shall not, by way of trade or otherwise, be lent, re-sold, hired out, or otherwise circulated without the publisher's prior consent in any form of binding or cover other than that in which it is published and without a similar condition including this condition being imposed on the subsequent purchaser.

All rights reserved. No part of this book may be reprinted, or reproduced or utilized in any form or by any electronic, mechanical or other means, now known or hereafter invented, including photocopying and recording, or in any information storage and retrieval system, without permission in writing from the Publisher.

British Library Cataloguing in Publication Data

Snyder, Allan W.

Optical waveguide theory.

1. Optical waveguides

I. Title	II. Love, John D.
535.8'9	QC448

ISBN-13: 978-0-412-24250-2

e-ISBN-13: 978-1-4613-2813-1

DOI: 10.1007/978-1-4613-2813-1

Library of Congress Cataloging in Publication Data

Snyder, Allan W., 1940–

Optical waveguide theory.

(Science paperbacks; 190)

Bibliography: p.

Includes index.

1. Optical wave guides. I. Love, John D.

II. Title. III. Series.

TA1800.S69 1983 621.36'9 83-7463

ISBN-13: 978-0-412-24250-2

e-ISBN-13: 978-1-4613-2813-1

DOI: 10.1007/978-1-4613-2813-1

Contents

Preface

vii

Part I Ray Analysis of Multimode Optical Waveguides

Introduction to Part I	3
1 Bound rays of planar waveguides	6
2 Bound rays of fibers	26
3 Pulse spreading	51
4 Fiber illumination and pulse shape	63
5 Nonuniform fibers	89
6 Material absorption	120
7 Leaky rays	134
8 Spatial transient	154
9 Bends	179
10 Diffraction phenomena	189

Part II Electromagnetic Analysis of Optical Waveguides

Introduction to Part II	205
11 Fundamental properties of modes	208
12 Waveguides with exact solutions	238
13 Weakly guiding waveguides	280
14 Circular fibers	301
15 Gaussian approximation for circular fibers	336
16 Noncircular waveguides	354
17 Gaussian approximation for noncircular fibers	366
18 Modes of perturbed fibers	374
19 Slowly varying waveguides	407
20 Illumination, tilts and offsets	420
21 Sources within fibers	442
22 Nonuniform fibers	460
23 Bends	474
24 Leaky modes	487
25 Radiation modes	514

vi Contents

26	Decomposition of the radiation field	534
27	Mode coupling	542
28	Local-mode coupling	553
29	Cross-talk	567

Part III Supplementary Material

	Introduction to Part III	589
30	Maxwell's equations	590
31	Modal methods for Maxwell's equations	601
32	Weak-guidance approximation	623
33	Modal methods for the scalar wave equation	640
34	Green's function methods	656
35	Rays and local plane waves	666
36	Rays and asymptotic modal methods	692
37	Mathematical formulae	709
	<i>Author index</i>	721
	<i>Subject index</i>	724

Preface

This text is intended to provide an in-depth, self-contained, treatment of optical waveguide theory. We have attempted to emphasize the underlying physical processes, stressing conceptual aspects, and have developed the mathematical analysis to parallel the physical intuition. We also provide comprehensive supplementary sections both to augment any deficiencies in mathematical background and to provide a self-consistent and rigorous mathematical approach. To assist in understanding, each chapter concentrates principally on a single idea and is therefore comparatively short. Furthermore, over 150 problems with complete solutions are given to demonstrate applications of the theory. Accordingly, through simplicity of approach and numerous examples, this book is accessible to undergraduates. Many fundamental topics are presented here for the first time, but, more importantly, the material is brought together to give a unified treatment of basic ideas using the simplest approach possible. To achieve such a goal required a maturation of the subject, and thus the text was intentionally developed over a protracted period of the last 10 years.

Layout of material

The book is divided into three parts. Part I presents those geometrical and elementary ray methods necessary for the analysis of propagation on multimode optical waveguides. Part II provides the electromagnetic theory approach, with emphasis on waveguides that propagate only one or a few modes. For these waveguides, the methods of Part I are inaccurate. Part III offers supplementary sections on mathematical methods, mainly to augment the more physical discussion of Parts I and II. It is possible to read Part II without Part I, although this is not recommended. Furthermore, while all chapters need not be read sequentially, we recommend familiarity at least with the topics of each chapter. Assistance on this and other matters is given in the introductions to Parts I and II.

References

The references we cite are those with which we are most familiar and which have helped us understand the subject as presented here. While there has been no attempt to give credit to each contributor, we have tried to cite the original

papers which brought new and important methods to the theory of optical waveguides covered in this text.

Suggestions for instruction

Because our primary goal is to produce a comprehensive treatment, we have, for completeness, intentionally developed all sections in their most logical order. Consequently, with restricted interests in mind, it is not necessary to read every chapter. In this regard, we offer advice to the reader throughout the text. In particular, for a first reading of the subject, only selected chapters need be read to grasp the essential concepts. Thus, for a short course consisting of, say, 30 1-hour lectures extending over a 10 week period, we recommend reading most of Chapters 1, 3, 5, 6 and 10 in Part I and Chapters 11, 12, 13, 14, 15, 19 and 20 in Part II. With this plan, the primary omission concerns radiation losses.

Acknowledgements

Finally, we owe much thanks to many individuals. Dr C. Pask, our colleague and close collaborator, offered many helpful suggestions in all aspects. Dr A. Ankiewicz performed an indispensable task in helping to check the analysis. Over the years, our many research students contributed greatly through their inquiring and critical minds, together with their own valuable research. Accordingly, we give particular thanks to Drs K. F. Barrell, M. C. Campbell, D. J. Carpenter, C. D. Hussey, P. D. McIntyre, R. A. Sammut, I. A. White, C. Winkler and W. R. Young, together with our present students R. J. Black, F. Rühl and I. Skinner. The typing of the final drafts was undertaken by Miss Diana Alex and Mrs Pauline Wallace, and the figures were drawn by Mrs Sandra Smith.

PART I

Ray Analysis of Multimode Optical Waveguides

Introduction to Part I

An optical waveguide is a dielectric structure that transports energy at wavelengths in the infrared or visible portions of the electromagnetic spectrum. In practice, waveguides used for optical communications are highly flexible fibers composed of nearly transparent dielectric materials. The cross-section of these fibers is small—comparable to a human hair—and generally is divisible into three layers as shown in Fig. I-1. The central region is the *core*, which is surrounded by the *cladding*, which in turn is surrounded by a protective jacket. Within the core, the *refractive-index profile* n can be *uniform* or *graded*, while the cladding index is typically uniform. The two situations correspond to the *step*-

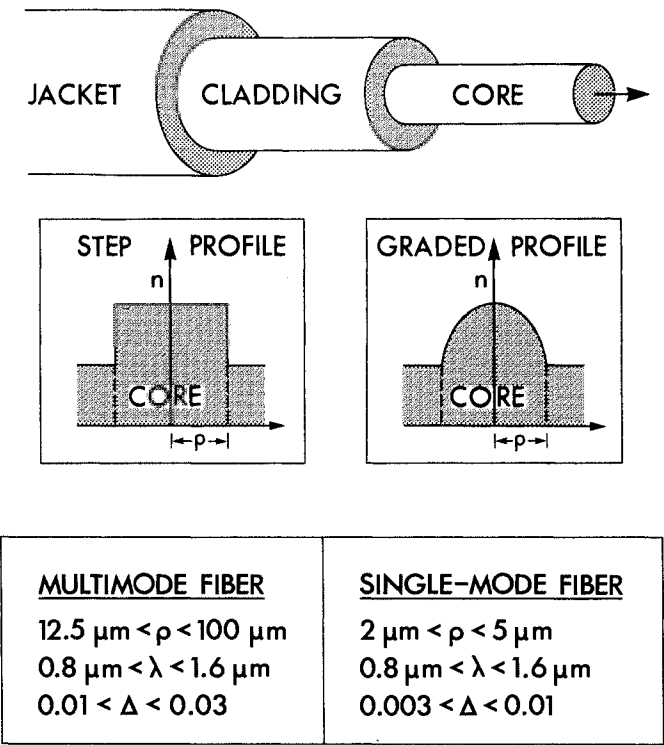


Fig. I-1 Nomenclature, profiles and ranges of dimensions for typical optical fibers, where ρ is the core radius, λ is the free-space wavelength of light and $\Delta = (1 - n_{cl}^2/n_{co}^2)/2$ [1].

4 Optical Waveguide Theory

index and *graded-index* profiles shown in the insets in Fig. I-1. It is necessary that the core index be greater than the cladding index, at least in some region of the cross-section, if guidance is to take place. For the majority of applications, most of the light energy propagates in the core and only a small fraction travels in the cladding. The jacket is almost optically isolated from the core, so for this reason we usually ignore its effect and assume an unbounded cladding for simplicity in the analysis.

Multimode and single-mode waveguides

Optical waveguides can be conveniently divided into two subclasses called *multimode* waveguides (with comparatively large cores) and *single-mode* waveguides (with comparatively small cores). The demarcation between the two is discussed in Section 10-3, and in Chapters 11 and 12. Multimode waveguides obey the condition $(2\pi\rho/\lambda)(n_{co}^2 - n_{cl}^2)^{1/2} \gg 1$, where ρ is a linear dimension in the core, e.g. the radius of the fiber core, λ is the wavelength of light in free space, n_{co} is the maximum refractive index in the core and n_{cl} is the uniform refractive index in the cladding. These waveguides are the subject of Part I, while, in Part II, we are more concerned with single-mode and few-mode waveguides. The range of dimensions for fibers presently used in long distance communications is given in Fig. I-1 [1]. For the constituency of these fibers we refer the reader elsewhere [2, 3].

Ray tracing

Electromagnetic propagation along optical waveguides is described exactly by Maxwell's equations. However, it is well known that classical geometric optics provides an approximate description of light propagation in regions where the refractive index varies only slightly over a distance comparable to the wavelength of light. This is typical of multimode optical waveguides used for communication. Thus, the most direct and conceptually simple way to describe light propagation in multimode waveguides is by tracing rays along the core. Accordingly, *the first five chapters are based on classical geometric optics only*. Those readers interested in the reduction of the solutions of Maxwell's equations to classical geometric optics are referred to the beginning of Chapter 35.

Wave effects

By using classical geometric optics, *we ignore all wave effects*. In multimode waveguides, wave effects are usually negligible, as we show in Chapter 10, but there are exceptional situations when such effects accumulate exponentially with the distance light travels. In these cases, wave effects must be retained,

since they can have a significant influence in long waveguides. Examples include power losses due to radiation, absorption by the cladding, and radiation from bends, and are discussed in Chapters 6 to 9. In each situation, we modify the classical geometric optics description by taking into account the local plane wave nature of light.

Modal description

There is an alternative approach to describing propagation in multimode waveguides, which relies on the small-wavelength limit of the electromagnetic modes of an optical waveguide. While this leads to results identical to those of classical geometric optics, it requires unnecessary algebraic manipulation, in addition to a knowledge of mode theory. This alternative approach is outlined later in Chapter 36, and can be regarded as an example which shows how Maxwell's equations lead to the results of Part I in the limit of small wavelength.

Pulse spreading

The phenomenon of greatest practical interest in fibers used for long-distance communications is *the spread of pulses as they propagate along the fiber*. For idealized multimode fibers, pulse spreading is easily described by classical geometric optics, as we show in Chapter 3. If attention is limited to pulse spreading, it is sufficient to cover Chapter 3, together with a few results from Chapter 1. However, our purpose in Part I is more ambitious, since we lay the foundation for a comprehensive geometric optics treatment of optical waveguides. In this way, we can more fully appreciate the consequences of departures from the ideal conditions desired in practice.

REFERENCES

1. Keck, D. B. (1981) 'Fiber design for cables.' Third International Conference on Integrated Optics and Optical Fiber Communications, San Francisco, April, 1981.
2. Miller, S. E. and Chynoweth, A. G. (eds.) (1979) *Optical Fiber Communications*, Academic Press, New York.
3. Midwinter, J. E. (1979) *Optical Fibers for Transmission*, Wiley, New York.

CHAPTER 1

Bound rays of planar waveguides

1-1 Planar waveguides	7
Step-profile planar waveguides	8
1-2 Construction of ray paths	8
1-3 Ray invariant	10
1-4 Ray-path parameters	10
1-5 Ray transit time	12
Graded-profile planar waveguides	13
1-6 Construction of ray paths	13
1-7 Ray invariant	16
1-8 Ray-path parameters	16
1-9 Ray transit time	18
Weakly guiding waveguides	20
1-10 Paraxial approximation	20
Graded profiles with analytical solutions	21
1-11 <i>Example: Parabolic profile</i>	21
1-12 <i>Example: Hyperbolic secant profile</i>	23
1-13 <i>Example: Clad power-law profiles</i>	24
Asymmetric waveguides	25
References	25

We begin our ray analysis of multimode optical waveguides with the planar, or slab waveguide, which is the simplest dielectric structure for illustrating the principles involved, and has application in integrated optics. Since we can analyse its light transmission characteristics in terms of a superposition of ray paths, it is important to fully appreciate the behavior of individual rays. In this chapter we study the trajectories of rays within planar waveguides, concentrating on those rays – the *bound rays* – which propagate without loss of energy on

a nonabsorbing waveguide, and can, therefore, propagate arbitrarily large distances.

1-1 Planar waveguides

The planar, or slab, waveguide is illustrated in Fig. 1-1. It consists typically of a *core* layer of thickness 2ρ sandwiched between two layers which form the *cladding*. As explained in the Introduction, we assume, for simplicity, that the cladding is unbounded. The planes $x = \pm \rho$ are the *core-cladding interfaces*. Since the waveguide extends indefinitely in all directions orthogonal to the x -axis, the problem is two dimensional. The z -axis is located along the axis of the waveguide midway between the interfaces. The refractive-index profile $n(x)$ in Fig. 1-1 can be uniform or graded across the core, and assumes a uniform value n_{cl} in the cladding. It is necessary that the core refractive index take some values greater than n_{cl} for the waveguide to have guidance properties. Furthermore, we assume in this chapter that the profile does not vary with z , so that the waveguide is *translationally invariant*, or *cylindrically symmetric*.

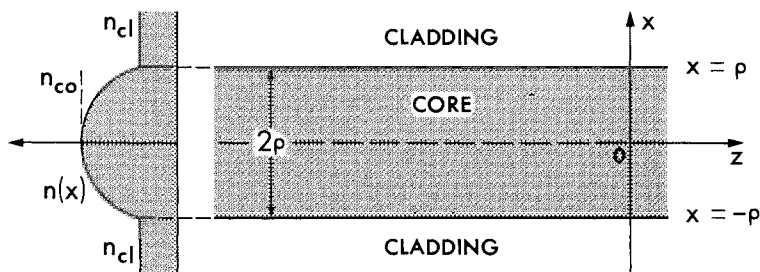


Fig. 1-1 Nomenclature and coordinates for describing planar waveguides. A representative graded profile varies over the core and is uniform over the cladding, assumed unbounded.

The parameters defined in Fig. 1-1 can be combined with the free-space wavelength λ of the light propagating along the waveguide to form a single dimensionless parameter V , known as the *waveguide parameter*, or *waveguide frequency*. If n_{co} is the maximum value of $n(x)$, which need not concur with the on-axis value $n(0)$, then we define

$$V = \frac{2\pi\rho}{\lambda} (n_{co}^2 - n_{cl}^2)^{1/2}. \quad (1-1)$$

Alternative forms for V are given inside the front cover. The ray theory presented here is restricted to *multimode waveguides*, i.e. waveguides satisfying $V \gg 1$, for reasons discussed in Chapters 10 and 36.

STEP-PROFILE PLANAR WAVEGUIDES

With reference to Fig. 1-2, the step-index planar waveguide has the refractive-index profile defined by

$$n(x) = n_{co}, \quad -\rho < x < \rho; \quad n(x) = n_{cl}, \quad |x| > \rho, \quad (1-2)$$

where n_{co} and n_{cl} are constants and $n_{co} > n_{cl}$. We now show how to construct ray paths within the core using ray tracing and Snell's laws. One of the most important problems is to determine the conditions necessary for a ray to be *bound*, i.e. the ray propagates along the nonabsorbing waveguide without loss of power.

1-2 Construction of ray paths

Propagation within the uniform core of the step-index waveguide of Fig. 1-2 is along straight lines. If a ray originates at P on one interface and makes angle θ_z with the waveguide axis, it will meet the opposite interface at Q as shown. The

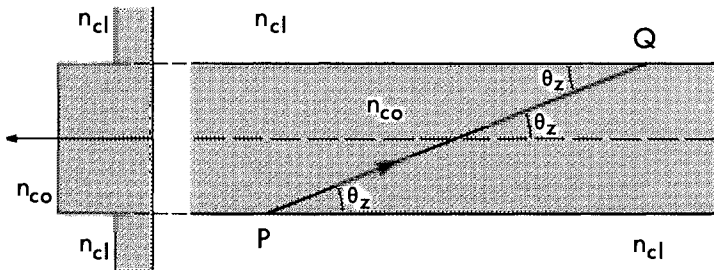


Fig. 1-2 Propagation along a straight line between interfaces in the core of a step-profile planar waveguide.

situation at Q is equivalent to incidence at an interface between two half-spaces of refractive indices n_{co} and n_{cl} as shown in Fig. 1-3. Reflection in this situation is governed by Snell's law [1, 2]. While these laws are usually expressed in terms of angles relative to the normal QN, as in Section 35-2, we prefer to retain the complementary angle θ_z . The reason will become apparent in Chapter 2 when classifying ray paths within optical fibers. Thus, in terms of complementary angles, the incident ray at Q is *totally internally reflected* if $0 \leq \theta_z < \theta_c$, and is partly reflected and partly *refracted* if $\theta_c < \theta_z \leq \pi/2$, where θ_c is the *complement of the critical angle*, defined by

$$\theta_c = \cos^{-1} \left\{ \frac{n_{cl}}{n_{co}} \right\} = \sin^{-1} \left\{ 1 - \frac{n_{cl}^2}{n_{co}^2} \right\}^{1/2}. \quad (1-3)$$

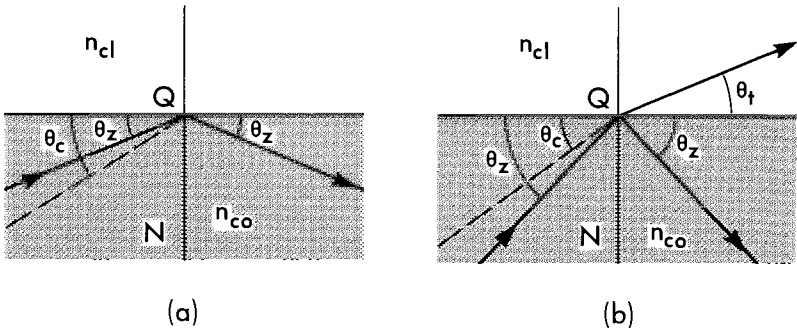


Fig. 1-3 Reflection at a planar interface between unbounded regions of refractive indices n_{co} and n_{cl} , showing (a) total internal reflection and (b) partial reflection and refraction.

In the first case, Fig. 1-3(a) shows the reflected ray leaving the interface at the same angle θ_z as the incident ray, while in the second case, Fig. 1-3(b) shows that the ray bifurcates, part of it being reflected at angle θ_z and part of it being transmitted into the cladding at angle θ_t to the interface, which satisfies Snell's law

$$n_{co} \cos \theta_z = n_{cl} \cos \theta_t. \quad (1-4)$$

Only total internal reflection returns all the ray power, i.e. the energy flowing along the ray, back into the core medium.

Ray trajectory

A ray is reflected from the interface back into the core at angle θ_z regardless of whether partial or total reflection occurs. If we repeat this procedure at successive reflections from the interfaces, we construct the zig-zag paths, or *trajectories*, of Fig. 1-4. Path (a) is for a ray that is totally reflected at every reflection. We refer to this as a *bound ray*, since its path is entirely confined within the core. Path (b) is for a ray that is partly reflected at each reflection. We refer to this as a *refracting ray*. The rays may be categorized by the value of θ_z according to

Bound rays:	$0 \leq \theta_z < \theta_c,$	(1-5a)
Refracting rays:	$\theta_c \leq \theta_z \leq \pi/2.$	(1-5b)

Since the power of a bound ray is totally reflected back into the core at every reflection, *the ray can propagate indefinitely without any loss of power.* A

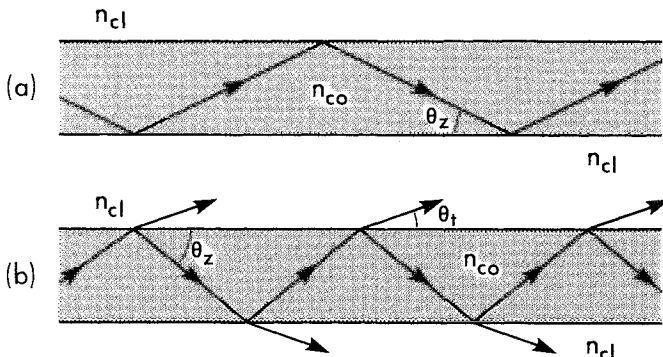


Fig. 1-4 Zig-zag paths within the core of a step-profile planar waveguide for (a) bound rays and (b) refracting rays.

refracting ray loses a fraction of its power at each reflection and therefore attenuates as it propagates. This is pursued further in Chapter 7.

1-3 Ray invariant

The periodic shape of the ray path in Fig. 1-4 is a consequence of the translational invariance of the waveguide, and gives rise to a *ray invariant* $\bar{\beta}$ which is constant along the path and specifies the ray direction at any position in the cross-section. For the step-profile waveguide, invariance is expressed by Eq. (1-4), so we set

$$\bar{\beta} = n_{co} \cos \theta_z = n_{cl} \cos \theta_t. \quad (1-6)$$

While this is a trivial observation for a step profile, and of no particular advantage, the introduction of the ray invariant simplifies the description of ray paths on *graded* profiles, as we show in Section 1-7. The relationship between the ray invariant and the direction of propagation enables us to classify rays according to their value of $\bar{\beta}$. We deduce from Eq. (1-5) that

$$\text{Bound rays:} \quad n_{cl} < \bar{\beta} \leq n_{co}, \quad (1-7a)$$

$$\text{Refracting rays:} \quad 0 \leq \bar{\beta} < n_{cl} \quad (1-7b)$$

which classifies all rays of the waveguide.

1-4 Ray-path parameters

It is useful to introduce parameters that characterize ray propagation, as it is these parameters, rather than the spatial dependence of the ray path, that are

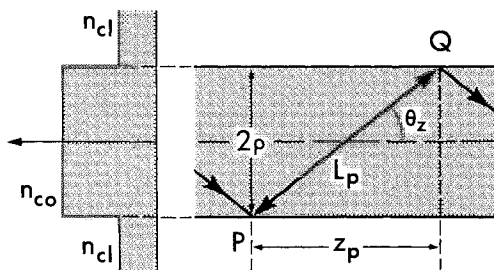


Fig. 1-5 Path length L_p and ray half-period z_p for a ray in the core of a step-profile planar waveguide.

important. Together with the ray invariant of the previous section, they are frequently used in subsequent chapters. The ray trajectory in Fig. 1-5 is fully characterized once the angle θ_z is prescribed. We define the *path length* L_p between successive reflections to be the distance PQ. This is useful in the absorption problems of Chapter 6. By geometry

$$L_p = \frac{2\rho}{\sin \theta_z} = \frac{2\rho n_{co}}{(n_{co}^2 - \bar{\beta}^2)^{1/2}}, \quad (1-8)$$

where $\bar{\beta}$ is defined by Eq. (1-6). For the ray transit time below, we require the *optical path length* L_o . In a homogeneous medium this is given by the product of path length and refractive index. Accordingly

$$L_o = n_{co} L_p = \frac{2\rho n_{co}}{\sin \theta_z} = \frac{2\rho n_{co}^2}{(n_{co}^2 - \bar{\beta}^2)^{1/2}}. \quad (1-9)$$

A quantity which will appear frequently in attenuation problems is the *ray half-period* z_p . This is the distance between successive reflections, measured along the waveguide axis. Thus

$$z_p = \frac{2\rho}{\tan \theta_z} = L_p \cos \theta_z = \frac{2\rho \bar{\beta}}{(n_{co}^2 - \bar{\beta}^2)^{1/2}}. \quad (1-10)$$

Closely related is the *number of reflections* N per unit length of the waveguide, which is the reciprocal of the ray half-period. Hence

$$N = \frac{1}{z_p} = \frac{\tan \theta_z}{2\rho}. \quad (1-11)$$

It is clear from these definitions that over arbitrary distance z along the waveguide, the accumulated path length, optical path length and number of

reflections are given proportionately by

$$\frac{z}{z_p} L_p; \quad \frac{z}{z_p} L_o; \quad Nz = \frac{z}{z_p}, \quad (1-12)$$

respectively. For reference, these parameters are repeated in Table 1-1, page 19.

1-5 Ray transit time

The most important quantity required to describe pulse spreading is the *ray transit time* t . This is the time a ray takes to propagate distance z along the waveguide, following the zig-zag ray path in Fig. 1-4. The velocity of light v_g along the path is given by

$$v_g = c/n_{co}, \quad (1-13)$$

where c is the free-space speed of light and n_{co} the core refractive index. The transit time then follows from Eqs. (1-6) to (1-12) as

$$t = \frac{z}{z_p} \frac{L_p}{v_g} = \frac{z}{z_p} \frac{L_o}{c} = \frac{z}{c} \frac{n_{co}^2}{\beta} = \frac{z}{c} \frac{n_{co}}{\cos \theta_z}, \quad (1-14)$$

so that the greater θ_z , the longer the transit time.

Material dispersion

We can account for *material dispersion*, which occurs when the refractive index varies with the wavelength of light λ , i.e. $n_{co} = n_{co}(\lambda)$. This requires more sophisticated reasoning relying on treating a ray as if it were a plane wave in local regions. We show that this is justifiable in Section 35-3. Ray energy propagates at the group velocity v_g , which is given by Eq. (1-13) in a *dispersionless* medium, but, allowing for material dispersion, it has the more general form [3]

$$v_g = c \left\{ n_{co}(\lambda) - \lambda \frac{dn_{co}(\lambda)}{d\lambda} \right\}^{-1}. \quad (1-15)$$

It is convenient to introduce the *group index* n_g , defined by

$$n_g = n_{co}(\lambda) - \lambda \frac{dn_{co}(\lambda)}{d\lambda}, \quad (1-16)$$

in which case, the transit time is expressible as

$$t = \frac{z}{c} \frac{n_g}{\cos \theta_z} = \frac{z}{c} \frac{n_g n_{co}}{\beta}, \quad (1-17)$$

and varies with both θ_z and λ .

GRADED-PROFILE PLANAR WAVEGUIDES

The description of ray propagation on the step profile is readily generalized to allow for a graded profile. For simplicity, we consider profiles of the type in Fig. 1-1 when only the core is graded. Our results are readily generalized to profiles that are graded in the cladding as well.

1-6 Construction of ray paths

When the refractive-index profile is graded, the trajectory of a ray is determined by the *ray path*, or *eikonal equation*, in terms of the profile $n(\mathbf{r})$ according to [1, 2]

$$\frac{d}{ds} \left\{ n(\mathbf{r}) \frac{d\mathbf{r}}{ds} \right\} = \nabla n(\mathbf{r}). \quad (1-18)$$

where s is the distance along the ray path and \mathbf{r} is the position vector of a point on the ray path, as shown in Fig. 1-6. This equation can be regarded as a generalization of Snell's law, and is derivable by various methods [4]. The graded profile can be viewed as the limit of many thin uniform layers. Application of Snell's law of Eq. (1-4) to each layer leads to Eq. (1-18) in this limit. Alternatively, Eq. (1-18) can be found using least-time principles; it is also the limit $\lambda \rightarrow 0$ of Maxwell's equations, where λ is the wavelength [1, 2]. When n is constant, $\nabla n = 0$, and the ray trajectories are straight lines; otherwise the ∇n term accounts for curvature of the ray path in the plane containing ∇n .

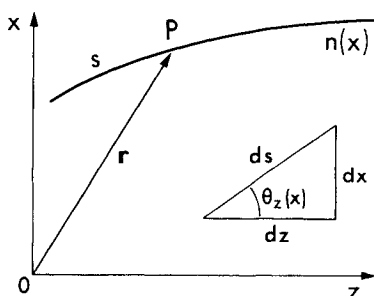


Fig. 1-6 Point P distance s along a ray path in a medium of variable refractive index $n(x)$ is described by position vector $\mathbf{r} = (x, z)$. Angle $\theta_z(x)$ is between the tangent to the path and the z -axis, and ds along the path has components dx and dz shown in the inset.

Component equations of the ray-path equation

On a planar waveguide, the refractive-index profile $n(x)$ depends only on x , so that each position (x, z) on the ray path is determined by the two component equations of Eq. (1-18) in the x - and z -directions

$$\frac{d}{ds} \left\{ n(x) \frac{dx}{ds} \right\} = \frac{dn(x)}{dx}; \quad \frac{d}{ds} \left\{ n(x) \frac{dz}{ds} \right\} = 0. \quad (1-19)$$

To facilitate physical interpretation of these equations, we introduce the angle $\theta_z(x)$, defined as the angle between the tangent to the path and the z , or waveguide, axis in Fig. 1-6. It then follows that

$$\frac{dx}{ds} = \sin \theta_z(x); \quad \frac{dz}{ds} = \cos \theta_z(x). \quad (1-20)$$

The second equation in Eq. (1-19) is integrable, and leads to

$$n(x) \cos \theta_z(x) = n(0) \cos \theta_z(0), \quad (1-21)$$

for all values of x . This is the generalization of Snell's law of Eq. (1-4) for a graded medium, namely that $n(x) \cos \theta_z(x)$ is a constant independent of position along the ray path. For a given profile the path is specified once the initial angle $\theta_z(0)$ is prescribed.

Turning-point caustic

We also deduce from Eq. (1-21) that when $n(x)$ decreases away from the waveguide axis, there may be a position in the core at which $\theta_z(x) = 0$, depending on the value of $\theta_z(0)$. Beyond this position the ray cannot propagate. We call this position the *turning point* x_{tp} , which is the solution of

$$n(x_{tp}) = n(0) \cos \theta_z(0); \quad 0 \leq x_{tp} \leq \rho. \quad (1-22)$$

If we combine curvature of the ray path with the notion of the turning point, then the ray path must qualitatively look like the path in Fig. 1-7(a) when Eq. (1-22) has a solution, and like Fig. 1-7(b) when Eq. (1-22) has no solution. In the first case the ray path bends continuously until it returns to the axis, and in the second case it reaches the interface, where it is totally transmitted. Since the profile is assumed continuous across the interface, the angles of incidence and transmission are all equal, and $\theta_t = \theta_z(\rho)$. The dashed line at $x = x_{tp}$ is the locus of turning points for all rays with the same value of $\theta_z(0)$, and is often called the *ray caustic* or *turning-point caustic*.

Characteristics of the ray path

We can build up the ray trajectory along the waveguide by repeated superposition of the path in Fig. 1-7. Assuming that the profile is symmetric, i.e.

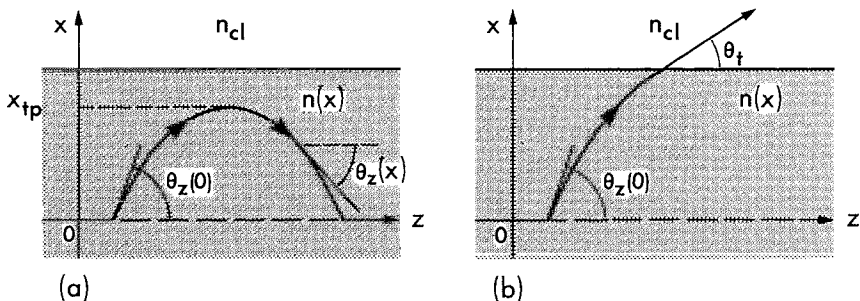


Fig. 1-7 Ray paths in the region $x \geq 0$ of a graded-profile planar waveguide showing (a) a ray touching the turning point at x_{tp} and (b) a ray reaching the interface where it is transmitted.

$n(-x) = n(x)$, this generates the sinusoidal-like path in Fig. 1-8. The path never reaches the interface, so that no power is lost, and thus it represents a *bound ray*. A ray path reaching the interface is lost from the core and is called a *refracting ray* in analogy with refracting rays on the step-profile waveguide.

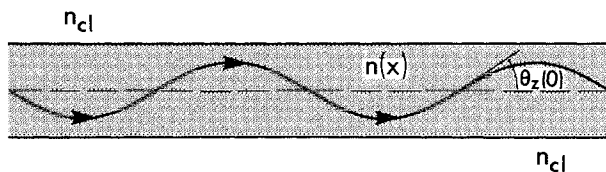


Fig. 1-8 Sinusoidal-like bound-ray path within the core of a graded-profile planar waveguide.

The delineation between the two classes is provided by the path that just reaches the interface, i.e. the one which has $x_{tp} = \rho$. If we denote the corresponding value of $\theta_z(0)$ by $\theta_c(0)$, we deduce from Eq. (1-22) that

$$\cos \theta_c(0) = n(\rho)/n(0) = n_{cl}/n_{co}, \quad (1-23)$$

assuming that $n(0) = n_{co}$ is the maximum value of $n(x)$. Thus, rays in graded-profile waveguides may be categorized according to the value of $\theta_z(0)$ by

$$\text{Bound rays:} \quad 0 \leq \theta_z(0) < \theta_c(0), \quad (1-24a)$$

$$\text{Refracting rays:} \quad \theta_c(0) < \theta_z(0) \leq \pi/2. \quad (1-24b)$$

The solution of Eq. (1-19) for the ray paths is discussed in Section 1-8.

1-7 Ray invariant

In Section 1-3 we introduced the concept of the ray invariant $\bar{\beta}$. For graded-profile waveguides, we use Eqs. (1-20) and (1-21) to define [5]

$$\bar{\beta} = n(x) \cos \theta_z(x) = n(x) \frac{dz}{ds}. \quad (1-25)$$

Hence $\bar{\beta}$ is constant along a trajectory. It also determines the direction of the ray at any position along its trajectory, and the position of the turning point x_{tp} . Since $\theta_z(x) = 0$ at the turning point, we deduce that

$$n(x_{tp}) = \bar{\beta}, \quad (1-26)$$

and there is a one-to-one correspondence between x_{tp} and $\bar{\beta}$. The ray classification of Eq. (1-24) is expressible in terms of $\bar{\beta}$. When $x = 0$ and $\theta_z(0) = \theta_c(0)$ in Eq. (1-25), we deduce from Eq. (1-23) that $\bar{\beta} = n_{cl}$. Thus

$$\text{Bound rays:} \quad n_{cl} < \bar{\beta} \leq n_{co}, \quad (1-27a)$$

$$\text{Refracting rays:} \quad 0 \leq \bar{\beta} < n_{cl}. \quad (1-27b)$$

where n_{co} is the maximum value of $n(x)$.

1-8 Ray-path parameters

It is useful to introduce parameters which characterize ray propagation in graded-profile waveguides, for use in subsequent chapters. These include the parameters introduced in Section 1-4 for the step-profile waveguide, whose definitions are readily generalized to apply to graded profiles. While this is facilitated by first deriving an explicit solution of Eq. (1-19) for the ray path, in practice we rarely require the dependence of the ray on position. We use Eq. (1-25) to replace ds and dz in the first equation of Eq. (1-19), and on rearrangement obtain

$$\bar{\beta}^2 \frac{d^2 x}{dz^2} = \frac{1}{2} \frac{dn^2(x)}{dx}. \quad (1-28)$$

Setting $d^2 x/dz^2 = x' dx'/dx$, where $x' = dx/dz$, integration leads to

$$\bar{\beta} \frac{dx}{dz} = \{n^2(x) - \bar{\beta}^2\}^{1/2}, \quad (1-29)$$

since $dx/dz = 0$ and $n(x) = \bar{\beta}$ at $x = x_{tp}$. A second integration gives

$$z(x) = \bar{\beta} \int_0^x \frac{dx}{\{n^2(x) - \bar{\beta}^2\}^{1/2}}, \quad (1-30)$$

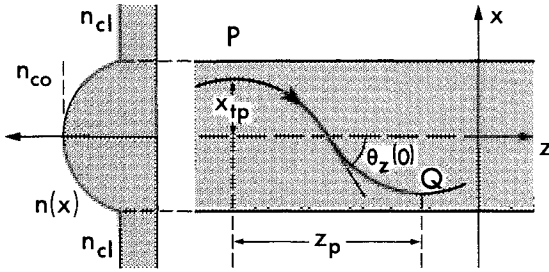


Fig. 1-9 Ray half-period z_p for a bound ray in the core of a graded-profile planar waveguide. The path length L_p is measured along the path from P and Q.

assuming $z = 0$ when $x = 0$. This integral gives the ray path explicitly for bound rays when $0 \leq x \leq x_{tp}$, and for refracting rays when $0 \leq x \leq \rho$.

The ray-path parameters are calculated with reference to Fig. 1-9 which shows a bound-ray path between successive turning points P and Q, separated by the ray half-period z_p measured along the axis. The path length L_p and the optical path length L_o are defined by path integrals

$$L_p = \int_P^Q ds; \quad L_o = \int_P^Q n(x) ds, \quad (1-31)$$

where s is the distance along the path. We use Eq. (1-25) to replace ds by dz and Eq. (1-29) to replace dz by dx , whence

$$L_p = \int_{-x_{tp}}^{x_{tp}} \frac{n(x) dx}{\{n^2(x) - \bar{\beta}^2\}^{1/2}}; \quad L_o = \int_{-x_{tp}}^{x_{tp}} \frac{n^2(x) dx}{\{n^2(x) - \bar{\beta}^2\}^{1/2}}. \quad (1-32)$$

The ray half-period z_p follows from Eq. (1-30) as

$$z_p = \bar{\beta} \int_{-x_{tp}}^{x_{tp}} \frac{dx}{\{n^2(x) - \bar{\beta}^2\}^{1/2}}. \quad (1-33)$$

which also determines $N = 1/z_p$, the number of turning points on the ray path per unit length of waveguide. When the profile is symmetric, the integrals can be evaluated for $0 \leq x \leq x_{tp}$ and the resulting expression doubled.

Complement of the local critical angle

It is conceptually helpful in understanding graded-profile waveguides to introduce a further parameter. We recall from Section 1-2 that, at *any* position in the core cross-section of a step-profile waveguide, all bound rays propagate at angles within the range $0 \leq \theta_z < \theta_c$, where θ_c is the complement of the critical angle. However, for graded-profile waveguides, the range of values of $\theta_z(x)$ for

bound rays varies with position. On the axis, this range is given by Eq. (1-24a), while at the interface there are no bound rays. Accordingly, we define *the complement of the local critical angle* $\theta_c(x)$ by

$$\cos \theta_c(x) = \frac{n_{cl}}{n(x)}; \quad \sin \theta_c(x) = \left\{ 1 - \frac{n_{cl}^2}{n^2(x)} \right\}^{1/2}, \quad (1-34)$$

so that at position x , the range of angles for bound rays is given by

$$0 \leq \theta_z(x) \leq \theta_c(x); \quad 0 \leq x \leq \rho \quad (1-35)$$

which reduces to Eq. (1-24a) when $x = 0$, and gives $\theta_z(x) = 0$ when $x = \rho$. All of the above parameters, together with the transit time of the following section are included in Table 1-1.

1-9 Ray transit time

The ray transit time for graded-profile waveguides is determined by integrating along the curved ray path in Fig. 1-8. The local speed of light varies continuously as $c/n(x)$, where c is the free-space speed of light and $n(x)$ is the profile, whence the transit time over distance z along the waveguide is given by

$$t = \frac{1}{c} \int n(x) ds = \frac{1}{c\beta} \int n^2(x) dz. \quad (1-36)$$

The second integral follows from Eq. (1-25) and integration is along the path $x = x(z)$. For arbitrary z this integral does not have a simple form, but it can be approximated as follows. We deduce from Eq. (1-31) that the transit time over a ray half-period z_p is L_o/c , where L_o is the optical path length. Thus, if z is divisible *exactly* into an integral number of half-periods, the transit time is expressible as

$$t = zL_o/(cz_p). \quad (1-37)$$

In general z is not divisible into an integral number of half-periods, but when $z \gg z_p$ it is clear that Eq. (1-37) is an accurate approximation to Eq. (1-36).

Equalization of transit time

Graded profiles tend to equalize the transit times of different rays. There is a simple explanation for this. As a ray propagates further from the axis, $n(x)$ decreases, thus increasing the local speed of light $c/n(x)$. This increase in speed compensates, in part, for the extra distance travelled by the ray off axis. For the hyperbolic secant profile this equalization is exact, as we show in Section 1-12.

Table 1-1 Ray-path parameters for planar waveguides. The half-period, path length and optical path length are measured between successive reflection or turning points, and the transit time is over length z of the waveguide. The number of reflection or turning points per unit length is $N = 1/z_p$, and ρ is the core half-width or profile scaling length. The caustic x_p is the solution of $n(x) = \bar{\beta}$.

	Profile $n^2(x)$	Ray half-period $z_p = 1/N$	Path length L_p	Optical path length L_o	Transit time t
Step	$\frac{n_{co}^2}{n_{cl}^2}; x < \rho$ ----- $\frac{n_{cl}^2}{n_{co}^2}; x > \rho$	$\frac{2\rho\bar{\beta}}{(n_{co}^2 - \bar{\beta}^2)^{1/2}}$	$\frac{2\rho n_{co}}{(n_{co}^2 - \bar{\beta}^2)^{1/2}}$	$\frac{2\rho n_{co}^2}{(n_{co}^2 - \bar{\beta}^2)^{1/2}}$	$\frac{z}{c} \frac{n_{co}^2}{\bar{\beta}}$
Graded	$\frac{n^2(x)}{n_{cl}^2}; x < \rho$ ----- $\frac{n^2(x)}{n_{cl}^2}; x > \rho$	$\frac{1}{\bar{\beta}} \int_{-x_p}^{x_p} \frac{dx}{\{n^2(x) - \bar{\beta}^2\}^{1/2}}$	$\int_{-x_p}^{x_p} \frac{n(x) dx}{\{n^2(x) - \bar{\beta}^2\}^{1/2}}$	$\int_{-x_p}^{x_p} \frac{n^2(x) dx}{\{n^2(x) - \bar{\beta}^2\}^{1/2}}$	$\frac{z}{c} \frac{L_o}{z_p}$
Parabolic	$n_{co}^2 \left\{ 1 - 2\Delta \left(\frac{x}{\rho} \right)^2 \right\}$	$\frac{\pi\rho\bar{\beta}}{n_{co}\sqrt{(2\Delta)}}$	$\frac{z_p}{4} \left\{ \frac{3n_{co}}{\bar{\beta}} + \frac{\bar{\beta}}{n_{co}} \right\}$ $\Delta \ll 1$	$\frac{z_p}{2} \left\{ \frac{n_{co}^2}{\bar{\beta}} + \bar{\beta} \right\}$	$\frac{z}{2c} \frac{n_{co}}{\bar{\beta}} \left\{ \frac{\bar{\beta}}{n_{co}} + \frac{n_{co}}{\bar{\beta}} \right\}$
Hyperbolic secant	$n_{co}^2 \operatorname{sech}^2 \left\{ \sqrt{(2\Delta) \frac{x}{\rho}} \right\}$	$\frac{\pi\rho}{\sqrt{(2\Delta)}}$	$\frac{z_p}{2} \left\{ 1 + \frac{n_{co}}{\bar{\beta}} \right\}$ $\Delta \ll 1$	$z_p n_{co}$	$\frac{z}{c} n_{co}$
Clad power law	$n_{co}^2 \left\{ 1 - 2\Delta \left \frac{x}{\rho} \right ^q \right\};$ $ x < \rho$ ----- $\frac{n_{cl}^2}{n_{co}^2}; x > \rho$	$\frac{\sqrt{(2\pi)\bar{\beta}x_p} \left(\frac{\rho}{x_p} \right)^{q/2}}{qn_{co}\sqrt{\Delta}} \times \frac{\Gamma(1/q)}{\Gamma(1/q + 1/2)}$	$\frac{z_p}{\{q+2\}} \left\{ \frac{\bar{\beta}}{n_{co}} + (q+1) \frac{n_{co}}{\bar{\beta}} \right\}$ $\Delta \ll 1$	$\frac{n_{co}}{z_p q + 2} \left\{ q \frac{n_{co}}{\bar{\beta}} + \frac{2\bar{\beta}}{n_{co}} \right\}$	$\frac{z}{c} \frac{n_{co}}{(q+2)} \left\{ q \frac{n_{co}}{\bar{\beta}} + \frac{2\bar{\beta}}{n_{co}} \right\}$
$\bar{\beta} = n_{co} \cos \theta_z$: step profile		$\bar{\beta} = n(x) \cos \theta_z(x) = n(x_p)$: graded profile			$2\Delta = 1 - \frac{n_{cl}^2}{n_{co}^2}$

Material dispersion

The discussion of material-dispersion effects on group velocity in Section 1-5 is readily extended to include graded media, in which case the profile $n(x)$ appearing in the first integral on the right of Eq. (1-36) is replaced by the group index n_g . Hence

$$t = \frac{1}{c} \int n_g(x, \lambda) ds; \quad n_g = n(x, \lambda) - \lambda \frac{\partial n}{\partial \lambda}(x, \lambda). \quad (1-38a)$$

Furthermore, by paralleling the derivation of Eq. (1-37) from Eq. (1-36)

$$\boxed{t = \frac{z}{c} \frac{L_m}{z_p};} \quad L_m = \int_{-x_{tp}}^{x_{tp}} \frac{n_g(x, \lambda) n(x, \lambda)}{\{n^2(x, \lambda) - \bar{\beta}^2\}^{1/2}} dx, \quad (1-38b)$$

so that L_m replaces the optical path length L_o in Eq. (1-37).

WEAKLY GUIDING WAVEGUIDES

Optical waveguides used for communications purposes are usually *weakly guiding*, i.e. the variation between the maximum and minimum values of the profile is small – typically less than 1% of the maximum value. In Part II, we frequently take advantage of this fact, as it leads to considerable algebraic simplification, and is useful in problems which would otherwise be intractable. Here we examine some of the consequences of weak guidance on ray analysis.

1-10 Paraxial approximation

When the maximum and minimum refractive index values are similar, it follows from Eqs. (1-3) and (1-23) that the complementary critical angles θ_c and $\theta_c(0)$ are both small, so that

$$\sin \theta_c \cong \theta_c \cong (1 - n_c^2/n_{co}^2)^{1/2}, \quad (1-39)$$

and similarly for $\theta_c(0)$. The range of bound-ray directions in Eqs. (1-5a) and (1-24a) is therefore small, and each bound ray propagates nearly parallel to the axis. This situation is known as the *paraxial approximation*.

The paraxial approximation does not lead to a simplification of the ray path equations of Eq. (1-19). This is evident from Eq. (1-30), since $\bar{\beta}$ is constant and $n(x)$ takes values down to and including $\bar{\beta}$. However, the paraxial approximation is helpful in simplifying the expression for the path length L_p in Eq. (1-32), by using the following approximation for the profile. The profile can be

expressed in the general form

$$n^2(x) = n_{co}^2 \{1 - 2\Delta f(x)\}, \quad (1-40)$$

where n_{co} is the maximum value of the profile, $f(x)$ is a nonnegative function and Δ is a constant which we define by

$$2\Delta = 1 - n_{cl}^2/n_{co}^2 = \sin^2 \theta_c, \quad (1-41)$$

using Eq. (1-3). In the uniform cladding $n(x) = n_{cl}$ and $f(x) = 1$. This definition of Δ ensures that $\Delta \ll 1$ in the weak-guidance approximation, i.e. when $n_{co} \cong n_{cl}$. Thus, to lowest order, Δ is the fractional difference between n_{co} and n_{cl} , or a measure of the profile height, i.e.

$$\Delta \cong \frac{\theta_c^2}{2} \cong \frac{n_{co} - n_{cl}}{n_{co}}, \quad n_{co} \cong n_{cl} \quad \text{or} \quad \theta_c \ll 1, \quad (1-42)$$

and will therefore be called the *profile height parameter*. When $\Delta f(x) \ll 1$, we deduce from Eq. (1-40) the approximation

$$n(x) \cong n_{co} \{1 - \Delta f(x)\}, \quad (1-43)$$

which is used to determine L_p in the examples below.

GRADED PROFILES WITH ANALYTICAL SOLUTIONS

To illustrate the use of the formal results for graded-profile waveguides, we consider examples of profiles which have analytical solutions for some or all of the ray-path quantities of interest, including solutions within the weak-guidance approximation. The more important parameters are also included in Table 1-1.

1-11 Example: Parabolic profile

Our first example is the infinite parabolic profile, which corresponds to the $q = 2$ solid curve and the dotted extension in Fig. 1-10 and is defined by

$$n^2(x) = n_{co}^2 \{1 - 2\Delta(x/\rho)^2\}; \quad -\infty < x < \infty, \quad (1-44)$$

where ρ is a measure of the profile width or a scaling parameter. This profile varies continuously over the infinite cross-section of the waveguide, but is unphysical since $n^2(x) \rightarrow -\infty$ as $x \rightarrow \pm \infty$. Nevertheless, it is one of the simplest profiles for understanding propagation and is the building block for the clad parabolic profile of Section 1-13 below. Because the profile is infinite, *every* ray path has a turning point at a

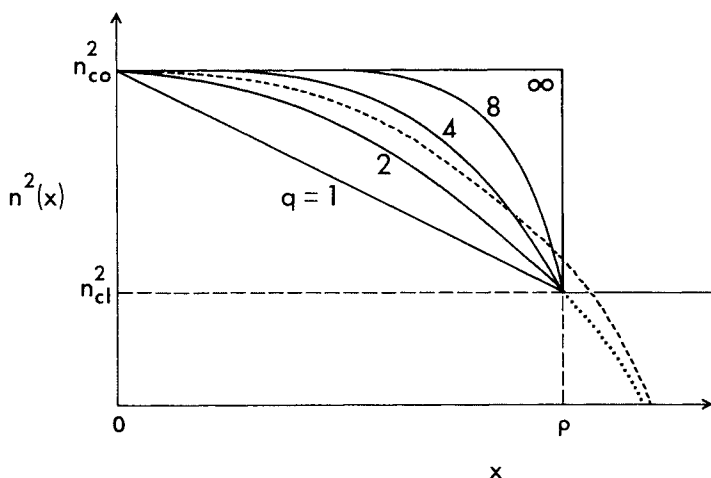


Fig. 1-10 Plots of the power-law profiles of Eq. (1-59) for various values of q . The clad parabolic profile corresponds to $q = 2$ and the step profile to $q = \infty$. The hyperbolic secant profile of Eq. (1-51) is shown dashed, and the dotted extension to the $q = 2$ core profile denotes the (infinite) parabolic profile of Eq. (1-44).

finite distance from the axis, found from Eq. (1-26) to be given by

$$x_{tp} = \pm \rho \frac{(n_{co}^2 - \bar{\beta}^2)^{1/2}}{n_{co}\sqrt{(2\Delta)}} = \pm \rho \frac{\sin \theta_z(0)}{\sin \theta_c(0)} \cong \pm \rho \frac{\theta_z(0)}{\theta_c(0)}, \quad (1-45)$$

where the last form applies in the paraxial approximation. Thus, the greater the angle $\theta_z(0)$, or the smaller $\bar{\beta}$, the further the turning point from the axis. As there is no solution for the path in Eq. (1-30) beyond the turning points, *all* rays are bound, and the range of invariant for bound rays satisfies

$$0 \leq \bar{\beta} \leq n_{co}. \quad (1-46)$$

We substitute Eq. (1-45) into Eq. (1-30), and use the transformation $x = x_{tp} \sin w$ to obtain an integral over w which is readily evaluated. This gives the ray path

$$x = x_{tp} \sin \left\{ \pi \frac{z}{z_p} \right\}; \quad z_p = \frac{1}{N} = \frac{\pi \rho \bar{\beta}}{n_{co}\sqrt{(2\Delta)}}, \quad (1-47)$$

where z_p is the ray half-period, found in a similar manner from Eq. (1-33). Using the same transformation, the optical path length of Eq. (1-32) is

$$L_o = z_p(n_{co}^2 + \bar{\beta}^2)/(2\bar{\beta}), \quad (1-48)$$

while the path length is expressible in terms of the complete elliptic integral of the second kind $E(v)$ through Eq. (37-103). Within the weak-guidance approximation of

Eq. (1-43), we obtain a simpler expression when $\Delta \ll 1$. Hence

$$L_p = \rho \left(\frac{2}{\Delta} \right)^{1/2} E \left(2\Delta \frac{x_{ip}^2}{\rho^2} \right) \cong \frac{z_p}{4} \left\{ \frac{3n_{co}}{\bar{\beta}} + \frac{\bar{\beta}}{n_{co}} \right\}. \quad (1-49)$$

Finally, the ray transit time of Eq. (1-37) follows directly from Eqs. (1-48) and (1-47) as

$$t = z(\bar{\beta}^2 + n_{co}^2)/(2c\bar{\beta}). \quad (1-50)$$

Compared with the step-profile expression of Eq. (1-14), transit times are partially equalized for reasons explained in Section 1-9.

1-12 Example: Hyperbolic secant profile

This profile is graded over the infinite cross-section, as denoted by the dashed curve in Fig. 1-10, and is defined by

$$n^2(x) = n_{co}^2 \operatorname{sech}^2(\sqrt{(2\Delta)x/\rho}); \quad -\infty < x < \infty. \quad (1-51)$$

As $n(x) \rightarrow 0$ when $x \rightarrow \pm \infty$, all rays are again bound, and the ray invariant satisfies Eq. (1-46). Substituting the profile into Eq. (1-26), we find that the turning points are given by

$$x_{ip} = \rho(2\Delta)^{-1/2} \cosh^{-1}(n_{co}/\bar{\beta}). \quad (1-52)$$

If in Eq. (1-30) we make the transformation $\sinh(\sqrt{(2\Delta)x/\rho}) = (n_{co}^2/\bar{\beta}^2 - 1)^{1/2} \sin w$, we obtain an integral over w which is known and leads to the equation for the ray path

$$x = \frac{\rho}{\sqrt{(2\Delta)}} \sinh^{-1} \left\{ \sinh \left(\frac{\sqrt{(2\Delta)x_{ip}}}{\rho} \right) \sin \left(\pi \frac{z}{z_p} \right) \right\}; \quad z_p = \frac{1}{N} = \frac{\pi\rho}{\sqrt{(2\Delta)}}. \quad (1-53)$$

The ray half-period follows from Eq. (1-33) in a similar manner. The same transformation of the optical path length integral in Eq. (1-32) leads to a second integral which is evaluated from Eq. (37-112). We obtain

$$L_o = n_{co} z_p. \quad (1-54)$$

Thus, both the ray half-period and optical path length are independent of $\bar{\beta}$, and, therefore, of the inclination of the ray path where it crosses the waveguide axis. For the path length, the above transformation is combined with a second transformation $w = \pi/2 - \theta$ to express the integral in a form which is proportional to the complete elliptic function $K(v)$ of the first kind, defined by Eq. (37-103)

$$L_p = \frac{2}{\pi} z_p K \left(\frac{n_{co}^2 - \bar{\beta}^2}{n_{co}^2} \right). \quad (1-55)$$

Within the weak-guidance approximation, we eliminate $\Delta f(x)$ between Eqs. (1-40) and (1-43), whence correct to order Δ

$$n(x) \cong \{n_{co}^2 + n^2(x)\}/(2n_{co}); \quad \Delta \ll 1. \quad (1-56)$$

We then deduce from Eqs. (1-32) and (1-33) that

$$L_p \cong (n_{co}^2 z_p + L_o \bar{\beta}) / (2\bar{\beta} n_{co}) = z_p (\bar{\beta} + n_{co}) / (2\bar{\beta}). \quad (1-57)$$

The ray transit time of Eq. (1-37) follows immediately from Eqs. (1-54) and (1-53) as

$$t = z n_{co} / c. \quad (1-58)$$

Thus the transit time is identical for all rays and is equal to the transit time for a ray propagating along the waveguide axis [6].

1-13 Example: Clad power-law profiles

Our final examples are the clad power-law profiles defined by [7]

$$n^2(x) = n_{co}^2 [1 - 2\Delta |x/\rho|^q]; \quad -\rho \leq x \leq \rho, \quad (1-59a)$$

$$= n_{cl}^2 = n_{co}^2 [1 - 2\Delta]; \quad |x| \geq \rho, \quad (1-59b)$$

where q is a positive constant. These profiles correspond to the solid curves in Fig. 1-10. The step profile corresponds to the limit $q \rightarrow \infty$ and the clad parabolic profile to $q = 2$. For the power-law profiles, the range of values of $\bar{\beta}$ for bound rays is given by Eq. (1-27a). Subject to this restriction, all the results for the parabolic profile of Section 1-11 apply to the clad parabolic profile, since the two profiles of Eqs. (1-44) and (1-59a) are identical within the core, and the path parameters for bound rays do not depend on the presence of the cladding. For arbitrary values of q , the position of the turning points is found by substituting Eq. (1-59a) into Eq. (1-26). Hence

$$x_{tp} = \pm \rho \left\{ \frac{n_{co}^2 - \bar{\beta}^2}{2n_{co}^2 \Delta} \right\}^{1/q} = \pm \rho \left\{ \frac{\sin \theta_z(0)}{\sin \theta_c(0)} \right\}^{2/q} \cong \pm \rho \left\{ \frac{\theta_z(0)}{\theta_c(0)} \right\}^{2/q} \quad (1-60)$$

where the last expression applies within the paraxial approximation. There is no general solution of Eq. (1-30) for the ray path, but solutions can be obtained for particular values of q , e.g. when $q = 2$ the path is given by Eq. (1-47). We do not pursue other solutions here. The ray half-period can be expressed analytically for all q . We transform the integral in Eq. (1-33) by setting $w = (x/x_{tp})^q$ and recognize the resultant form as the beta function of Eq. (37-104). In terms of the gamma function, Eq. (37-105) leads to

$$z_p = \frac{1}{N} = \frac{\bar{\beta}}{q} \left(\frac{2\pi}{\Delta} \right)^{1/2} \frac{x_{tp}}{n_{co}} \left\{ \frac{\rho}{x_{tp}} \right\}^{q/2} \frac{\Gamma(1/q)}{\Gamma(1/q + 1/2)}. \quad (1-61)$$

The same transformation is applied to the optical path-length integral of Eq. (1-32), and with the help of the recurrence formula for gamma functions in Eq. (37-106a), we find by a similar procedure that

$$L_o = \frac{z_p}{q+2} \left\{ q \frac{n_{co}^2}{\bar{\beta}} + 2\bar{\beta} \right\}. \quad (1-62)$$

The path-length integral in Eq. (1-32) can only be evaluated exactly for certain values of q ; e.g. $q = 2$. However, within the paraxial approximation of Eq. (1-43), L_p can be

derived by analogy with L_o as [5]

$$L_p \cong \frac{z_p}{q+2} \left\{ \frac{\bar{\beta}}{n_{co}} + (q+1) \frac{n_{co}}{\bar{\beta}} \right\}; \quad \Delta \ll 1, \quad (1-63)$$

correct to order Δ . Finally the ray transit time of Eq. (1-37) follows immediately from Eq. (1-62) as [5]

$$t = \frac{z}{c} \frac{n_{co}}{q+2} \left\{ q \frac{n_{co}}{\bar{\beta}} + \frac{2\bar{\beta}}{n_{co}} \right\}. \quad (1-64)$$

Thus the range of transit times decreases as $q \rightarrow 2$ for reasons discussed in Section 1-9.

ASYMMETRIC WAVEGUIDES

So far in this chapter we have investigated ray propagation on planar waveguides assuming a symmetric refractive-index profile, i.e. $n(-x) = n(x)$. However, the methods for constructing paths are just as easily applied to waveguides with *asymmetric profiles*. The only significant difference in construction is that while it is sufficient to know the path of a ray over *half a ray period* in order to determine its trajectory along a *symmetric waveguide*, we need to know the path of a ray over *a whole ray period* to correctly determine its trajectory along an *asymmetric waveguide*. The path parameters are given by the appropriately modified expressions for symmetric profiles.

REFERENCES

1. Born, M., and Wolf, E. (1970) *Principles of Optics*, Pergamon Press, Oxford.
2. Marcuse, D. (1972) *Light Transmission Optics*, Van Nostrand, New York.
3. Jackson, J. D. (1967) *Classical Electrodynamics*, Wiley, New York.
4. Krueger, D. A. (1980) Spatial varying index of refraction: an open ended undergraduate topic. *Am. J. Phys.*, **48**, 183-8.
5. Ankiewicz, A. and Pask, C. (1977) Geometric optics approach to light acceptance and propagation in graded index fibres. *Opt. Quant. Elect.*, **9**, 87-109.
6. Fletcher, A., Murphy, T. and Young, A. (1954) Solutions of two optical problems. *Proc. Roy. Soc.*, **A223**, 216-25.
7. Gloge, D. and Marcattili, E. A. J. (1973) Multimode theory of graded-core fibres. *Bell Syst. Tech. J.*, **52**, 1563-78.

CHAPTER 2

Bound rays of fibers

2-1 Circular fibers	27
Step-profile fibers	28
2-2 Construction of ray paths	28
2-3 Ray invariants	31
2-4 Ray-path parameters	31
2-5 Ray transit time	32
Graded-profile fibers	32
2-6 Construction of ray paths and ray invariants	32
2-7 Classification of rays	35
2-8 Ray-path parameters	38
2-9 Ray transit time	42
Graded profiles with analytical solutions	42
2-10 <i>Example: Parabolic profile</i>	43
2-11 <i>Example: Clad power-law profiles</i>	44
Noncircular fibers	45
2-12 Ray-path equations	45
2-13 <i>Example: Homogeneous-function profiles</i>	46
2-14 <i>Example: Separable profiles</i>	47
2-15 <i>Example: Parabolic elliptical profile</i>	49
References	49

In Chapter 1 we established the basic concepts for the ray analysis of planar waveguides. Here we extend the analysis to optical fibers, which are used for high-capacity communication over long distances. As far as ray tracing is concerned, the only difference between fibers and planar waveguides is the introduction of the third dimension. Thus, although the ray concepts are the same as in Chapter 1, the analysis and resulting expressions are generally more complicated because of the fiber geometry. Nevertheless, one of the important results of this chapter shows that the ray transit times for step and clad power-law profile fibers of both circular and noncircular cross-sections are identical to

those of the corresponding planar waveguides. If this remarkable simplification is acceptable without proof, then pulse spreading in such fibers can be studied directly by proceeding to Chapter 3 and omitting this chapter at a first reading.

Most of the chapter is devoted to the construction of ray paths and their classification on circular fibers with axisymmetric profiles. However, we also consider noncircular fibers since cross-sections can differ from circular symmetry in practice, e.g. elliptical fibers. Finally, since this chapter parallels Chapter 1 to a large extent, it may be helpful to compare the results of corresponding sections.

2-1 Circular fibers

An optical fiber is illustrated in Fig. 2-1. Unless otherwise stated, the *core* is assumed to have a circularly symmetric cross-section of radius ρ , surrounded by the *cladding*, which, for simplicity, is assumed unbounded. The *core-cladding interface* is the cylindrical surface $r = \rho$. Over the core, the axisymmetric refractive-index profile $n(r)$ is either uniform or graded, and it takes the uniform value n_{cl} in the cladding.

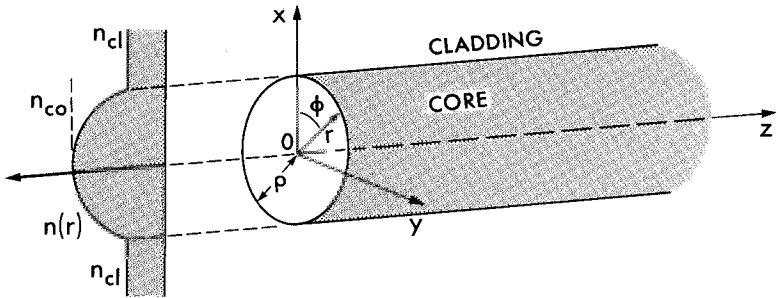


Fig. 2-1 Nomenclature for describing circular fibers. Cartesian coordinates x, y, z and cylindrical polar coordinates r, ϕ, z are oriented so that the z -axis lies along the fiber axis. A representative graded profile varies over the core and is uniform over the cladding, assumed unbounded.

The dimensionless parameter V of Eq. (1-1) also applies to fibers, and will be referred to as the *fiber parameter*. Thus

$$V = \frac{2\pi\rho}{\lambda} (n_{co}^2 - n_{cl}^2)^{1/2}, \quad (2-1)$$

where n_{co} is the maximum value of $n(r)$, ρ the core radius, and λ the free-space wavelength of light. The quantity $(n_{co}^2 - n_{cl}^2)^{1/2}$ is often referred to as the *numerical aperture* of the fiber, while a related expression $\{n^2(r) - n_{cl}^2\}^{1/2}$ is

sometimes called the *local numerical aperture*. The ray theory presented here is restricted to multimode fibers with $V \gg 1$ for reasons discussed in Chapters 10 and 36.

STEP-PROFILE FIBERS

With reference to Fig. 2-1, the step-profile fiber has the refractive-index profile defined by

$$n(r) = n_{co}, \quad 0 \leq r < \rho; \quad n(r) = n_{cl}, \quad \rho < r < \infty, \quad (2-2)$$

where $n_{co} > n_{cl}$. We now determine ray paths within the core.

2-2 Construction of ray paths

The path of each ray within the core is constructed by generalizing the methods of Section 1-2. Between reflections the ray follows a straight line and, on reflection from the interface, its direction is determined by Snell's laws. Thus, the incident ray, reflected ray and normal, or radial direction, lie in the same plane, and the angles of incidence and reflection relative to the normal are equal. This leads to paths such as those shown in Fig. 2-2.

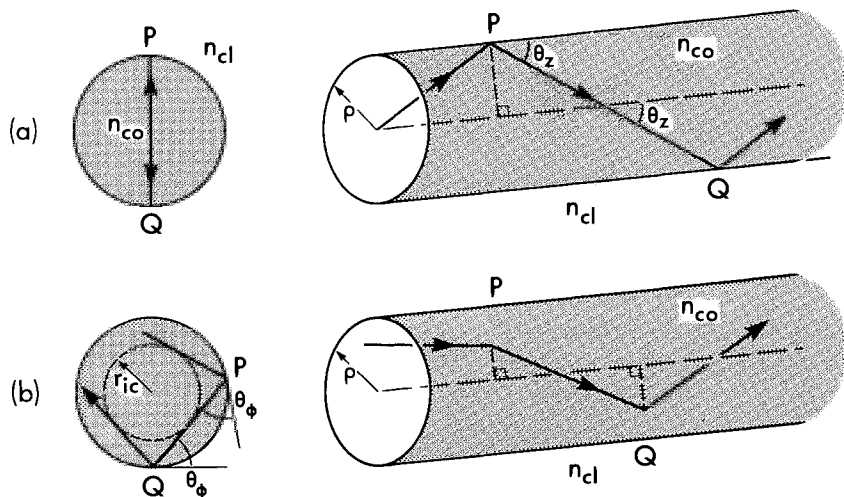


Fig. 2-2 Ray paths within the core of a step-index fiber showing (a) the zig-zag path of a meridional ray and (b) the helical path of a skew ray, together with their projections onto the core cross-section.

Meridional and skew rays

It is convenient to distinguish between rays which cross the fiber axis between reflections—known as *meridional rays*—and rays which never cross the fiber axis—known as *skew rays*. We see from Fig. 2-2(a) that meridional rays lie in a plane of width 2ρ through the axis. Consequently, they have properties identical with rays of the corresponding planar waveguide, and Table 1-1, page 19, applies to meridional rays of fibers, if the cartesian coordinate x is replaced by the cylindrical polar coordinate r of Fig. 2-1. Skew rays, on the other hand, follow a helical path, whose projection onto the cross-section is a regular polygon—not necessarily closed—as shown in Fig. 2-2(b). The midpoints between successive reflections all touch a cylindrical surface of radius r_{ic} , known as the *inner caustic*.

We label meridional rays with the angle θ_z between the path and the z -direction, as used in Section 1-2. Accordingly, the ranges of θ_z for bound and refracting meridional rays are given by Eq. (1-5), where for the step profile of Eq. (2-2), the complement of the critical angle θ_c retains the definition of Eq. (1-3).

To specify the trajectory of a skew ray, it is clear from Fig. 2-2(b) that, in addition to the inclination θ_z to the axial direction, we need a second angle to indicate the skewness. We define θ_ϕ to be the angle in the core cross-section between the tangent to the interface and the projection of the ray path, as shown in Fig. 2-2(b). By geometry θ_ϕ has the same value at every reflection.

Direction angles

The angles θ_ϕ and θ_z are spherical polar angles relative to the axial direction PQ in Fig. 2-3, which also shows the angle α between the incident and reflected rays and the normal. By taking projections, the three direction angles are related by

$$\cos \alpha = \sin \theta_z \sin \theta_\phi. \quad (2-3)$$

The radius r_{ic} of the inner caustic in Fig. 2-2(b) is given by

$$r_{ic} = \rho \cos \theta_\phi, \quad (2-4)$$

and thus depends only on the skewness angle. For meridional rays $\theta_\phi = \pi/2$ and $r_{ic} = 0$.

Classification of rays

Snell's laws of Section 35-2 predict that a ray will refract at P in Fig. 2-3 if $\alpha < \alpha_c$, where α_c is the critical angle defined by

$$\sin \alpha_c = n_{cl}/n_{co} = \cos \theta_c, \quad (2-5)$$

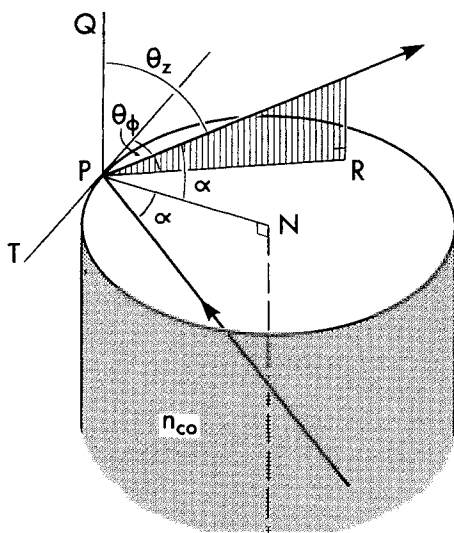


Fig. 2-3 Angles for describing reflection of a ray incident at P on the interface of a step-profile fiber. Relative to the normal PN, the angle of incidence or reflection is α . Both incident and reflected rays make angles θ_z , with the axial direction PQ, and θ_ϕ in the cross-section between the tangent PT and the path projection, i.e. PR for the reflected ray.

and will undergo total internal reflection if $\alpha > \alpha_c$. We are therefore inclined to believe that *all* rays with $\alpha > \alpha_c$ are bound, whereas, in fact, only certain rays satisfying this condition are bound. This is because Snell's laws are derived for reflection from a planar interface, whereas the fiber interface is curved. As we show in Section 2-7, the condition for a ray to be bound is $0 \leq \theta_z < \theta_c$, independent of θ_ϕ . This is derived from the ray-path equation and is identical to Eq. (1-5a) for the planar waveguide. However, for the fiber, it represents a cone of angles at each position in the core cross-section, and includes both meridional and skew rays. The remaining skew-ray directions which are not included in either bound or refracting rays belong to a third class of rays called *tunneling rays* [1], for reasons discussed in Section 2-7. Rays which are not bound, i.e. tunneling and refracting rays, are known as *leaky rays*.

To summarize, rays on step-profile fibers may be categorized according to the values of the angles θ_z , θ_ϕ and α by

Bound rays:	$0 \leq \theta_z < \theta_c$,	(2-6a)
Refracting rays:	$0 \leq \alpha < \alpha_c$,	(2-6b)
Tunneling rays:	$\theta_c \leq \theta_z \leq \pi/2$ and $\alpha_c \leq \alpha \leq \pi/2$,	(2-6c)

where α_c and θ_c are defined in Eq. (2-5) and the angles are illustrated in Fig. 2-3.

2-3 Ray invariants

We showed by geometry in the previous section that the angles θ_z and θ_ϕ are constant along a particular ray path. It is convenient to define two invariants in terms of these angles. The first invariant $\bar{\beta}$ is identical to Eq. (1-6) and accounts for the translational invariance of the fiber along its axis, and the second invariant \bar{l} , which is related to the skewness angle θ_ϕ , accounts for the azimuthal symmetry of the fiber. We define \bar{l} so that it will be consistent with the corresponding expression for graded profiles in Eq. (2-17). Hence

$$\bar{\beta} = n_{co} \cos \theta_z; \quad \bar{l} = n_{co} \sin \theta_z \cos \theta_\phi, \quad (2-7a)$$

$$\bar{\beta}^2 + \bar{l}^2 = n_{co}^2 \sin^2 \alpha, \quad (2-7b)$$

where the latter result follows from Eq. (2-3). For meridional rays $\bar{l} = 0$ and for skew rays $\bar{l} > 0$. Rays can be classified in terms of these invariants. We deduce from Eqs. (2-5) to (2-7) that, regardless of the value of \bar{l} , a ray is *bound* if $n_{cl} < \bar{\beta} \leq n_{co}$ and is *leaky* if $0 \leq \bar{\beta} < n_{cl}$. The subdivision of leaky rays into *tunneling* and *refracting* rays depends on the value of \bar{l} according to the following criteria, as may be verified

$$\text{Bound rays:} \quad n_{cl} < \bar{\beta} \leq n_{co}, \quad (2-8a)$$

$$\text{Refracting rays:} \quad 0 \leq \bar{\beta}^2 + \bar{l}^2 < n_{cl}^2, \quad (2-8b)$$

$$\text{Tunneling rays:} \quad n_{cl}^2 < \bar{\beta}^2 + \bar{l}^2 \leq n_{co}^2 \quad \text{and} \quad 0 \leq \bar{\beta} < n_{cl}. \quad (2-8c)$$

Given $\bar{\beta}$ for a bound ray, the values of \bar{l} lie in the range $0 \leq \bar{l} \leq n_{co}^2 - \bar{\beta}^2$.

2-4 Ray-path parameters

The definitions of ray-path parameters introduced in Section 1-4 are readily extended to include the skew ray paths of Fig. 2-2(b). Using the angles θ_z and θ_ϕ in Fig. 2-3 and the ray invariants of Eq. (2-7), the path length L_p from P to Q is found by geometry to be

$$L_p = 2\rho \frac{\sin \theta_\phi}{\sin \theta_z} = 2\rho n_{co} \frac{(n_{co}^2 - \bar{\beta}^2 - \bar{l}^2)^{1/2}}{n_{co}^2 - \bar{\beta}^2}. \quad (2-9)$$

The optical path length L_o follows immediately as

$$L_o = n_{co} L_p = 2\rho n_{co} \frac{\sin \theta_\phi}{\sin \theta_z} = 2\rho n_{co}^2 \frac{(n_{co}^2 - \bar{\beta}^2 - \bar{l}^2)^{1/2}}{n_{co}^2 - \bar{\beta}^2}. \quad (2-10)$$

The ray half-period z_p and the number of reflections per unit length of fiber N are given by

$$z_p = \frac{1}{N} = L_p \cos \theta_z = 2\rho \frac{\sin \theta_\phi}{\tan \theta_z} = 2\rho \bar{\beta} \frac{(n_{co}^2 - \bar{\beta}^2 - l^2)^{1/2}}{n_{co}^2 - \bar{\beta}^2}. \quad (2-11)$$

The accumulated path length, optical path length and number of reflections over length z of fiber are then given by Eq. (1-12). For convenience, these parameters are included in Table 2-1 below.

2-5 Ray transit time

In Section 1-5 we defined the ray transit time t as the time taken for a ray to propagate distance z along a waveguide. For the step-profile fiber, we deduce from Eqs. (1-14), (2-10) and (2-11) that

$$t = \frac{z}{z_p} \frac{L_o}{c} = \frac{z}{c} \frac{n_{co}}{\cos \theta_z} = \frac{z}{c} \frac{n_{co}^2}{\bar{\beta}}, \quad (2-12)$$

where $\bar{\beta}$ is the ray invariant of Eq. (2-7). Thus *the ray transit time is independent of ray skewness, and depends only on the axial angle θ_z* . As Eq. (2-12) is identical to Eq. (1-14), pulse transmission is no more difficult to study on fibers than on planar waveguides with step profiles, as we show in Chapter 3. If the effects of material dispersion are incorporated, then the transit time is given by Eq. (1-17).

For handy reference we have included definitions of all quantities relevant to the description of propagation on step-profile fibers and planar waveguides inside the front cover.

GRADED-PROFILE FIBERS

Here we extend the ray-tracing analysis of step-profile fibers to fibers with a graded core. This extension can be generalized to include profiles that are graded over the infinite cross-section.

2-6 Construction of ray paths and ray invariants

Our starting point is the ray-path equation of Eq. (1-18) for general graded media. When the refractive-index profile $n(r)$ of Fig. 2-1 is axisymmetric, we show in Section 35-4 that the component equations in the radial, azimuthal

and longitudinal directions are [2]

$$\frac{d}{ds} \left\{ n(r) \frac{dr}{ds} \right\} - r n(r) \left(\frac{d\phi}{ds} \right)^2 = \frac{dn(r)}{dr}, \quad (2-13a)$$

$$\frac{d}{ds} \left\{ n(r) \frac{d\phi}{ds} \right\} + \frac{2n(r)}{r} \frac{d\phi}{ds} \frac{dr}{ds} = 0, \quad (2-13b)$$

$$\frac{d}{ds} \left\{ n(r) \frac{dz}{ds} \right\} = 0, \quad (2-13c)$$

respectively, where s is the distance along the ray path, and (r, ϕ, z) are cylindrical polar coordinates defined in Fig. 2-1. To help interpret these equations, we generalize the definitions of the angles θ_z , θ_ϕ and α of Fig. 2-3. Thus, at radius r , $\theta_z(r)$ is the angle between the path tangent and the axial direction, and $\theta_\phi(r)$ is the angle in the core cross-section between the projection of the path tangent and the azimuthal direction, as shown in Fig. 2-4(c). If $\alpha(r)$ is the angle between the path tangent and the radial direction, then, by analogy with Eq. (2-3), all three angles are related by

$$\cos \alpha(r) = \sin \theta_z(r) \sin \theta_\phi(r), \quad (2-14)$$

at each position along the path. We then deduce by resolution that

$$\frac{dr}{ds} = \cos \alpha(r); \quad \frac{dz}{ds} = \cos \theta_z(r), \quad (2-15a)$$

$$\frac{d\phi}{ds} = \frac{1}{r} \sin \theta_z(r) \cos \theta_\phi(r), \quad (2-15b)$$

where the latter relationship follows from the identity $ds^2 = dr^2 + r^2 d\phi^2 + dz^2$.

Ray invariants

Integration of Eq. (2-13c) leads to the ray invariant $\bar{\beta}$ for graded-profile fibers

$$\bar{\beta} = n(r) \frac{dz}{ds} = n(r) \cos \theta_z(r). \quad (2-16)$$

This invariant is identical to Eq. (1-25) for graded-profile planar waveguides, and is associated with the translational invariance of the fiber.

We can integrate Eq. (2-13b) after multiplication by r^2 , and obtain a second invariant expressible in the dimensionless form [3]

$$\bar{l} = \frac{r^2}{\rho} n(r) \frac{d\phi}{ds} = \frac{r}{\rho} n(r) \sin \theta_z(r) \cos \theta_\phi(r), \quad (2-17)$$

where ρ is the core radius. This invariant arises because the profile is axisymmetric. If we eliminate $\theta_z(r)$ between the two equations, the skewness angle $\theta_\phi(r)$ can be directly related to the profile by

$$\cos \theta_\phi(r) = \frac{\rho}{r} \frac{\bar{T}}{\{n^2(r) - \bar{\beta}^2\}^{1/2}}. \quad (2-18)$$

We note that $\theta_\phi(r) = \pi/2$ for meridional rays ($\bar{T} = 0$). Our choice of \bar{T} in Eq. (2-7) for the step-profile is now clear, since it corresponds to Eq. (2-17) when $r = \rho$ and $n(r) = n_{co}$.

Characteristics of the ray path

The general shape of the ray paths can be deduced from the paths of Fig. 1-8 for a graded-profile planar waveguide and the paths of Fig. 2-2 for the step-profile fiber. Assuming that the paths are confined to the core, they have the characteristic forms shown in Fig. 2-4. Meridional rays cross the fiber axis

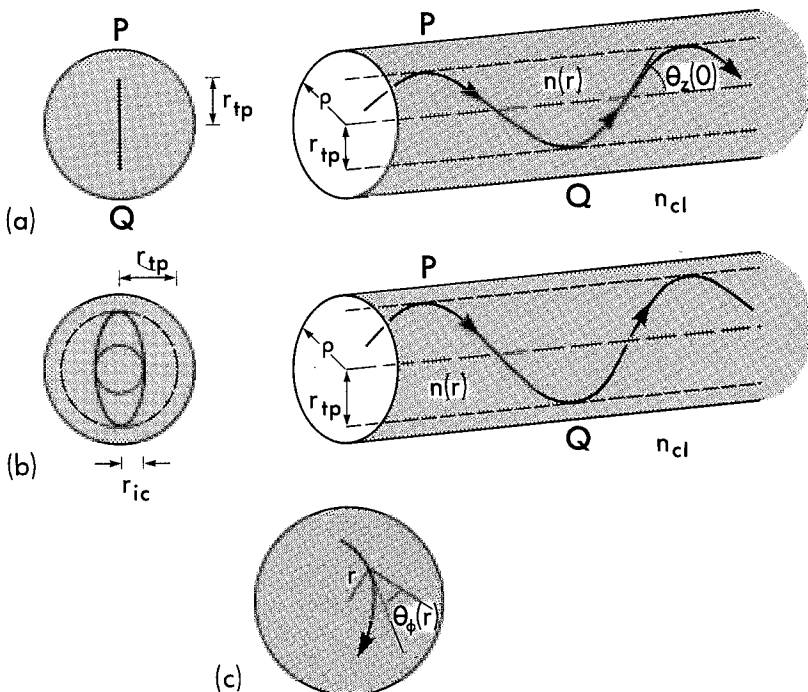


Fig. 2-4 Ray paths within the core of a graded-profile fiber showing (a) a meridional path and (b) a skew path, together with their projections onto the core cross-section. The angle $\theta_\phi(r)$ between the projection and the azimuthal direction is shown in (c).

between successive turning points. They lie in planes and are identical to the rays in graded-profile planar waveguides. Thus Table 1-1, page 19, applies to meridional rays on fibers if the cartesian coordinate x is replaced by the radial coordinate r . Skew rays follow a helical path, such as the one shown in Fig. 2-4(b), and alternately touch the cylindrical surfaces $r = r_{ic}$ and $r = r_{tp}$ corresponding to the inner and turning-point caustics, respectively. At both caustics it is clear by definition that $\theta_\phi(r) = 0$. Thus, for a given profile we deduce from Eq. (2-18) that r_{ic} and r_{tp} are the roots of $g(r)$, where

$$g(r) \equiv n^2(r) - \bar{\beta}^2 - \bar{L}^2 \frac{\rho^2}{r^2} = 0. \quad (2-19)$$

For meridional rays $\bar{L} = 0$ and $r_{ic} = 0$.

2-7 Classification of rays

A simple method for classifying rays on graded-profile fibers uses the ray equation to determine the range of values of the radial coordinate r for which rays can propagate. This is accomplished by expressing the radial component of the ray-path equation in Eq. (2-13a) as a relationship between r and z . We use Eq. (2-16) to replace ds by dz , and substitute for $d\phi/ds$ from Eq. (2-17). This leads to

$$\bar{\beta}^2 \frac{d^2 r}{dz^2} - \bar{L}^2 \frac{\rho^2}{r^3} = \frac{1}{2} \frac{dn^2(r)}{dr}, \quad (2-20)$$

which is integrable on setting $d^2 r/dz^2 = r' dr'/dr$, where $r' = dr/dz$, and leads to

$$\boxed{\bar{\beta}^2 \left(\frac{dr}{dz} \right)^2 = g(r) = n^2(r) - \bar{\beta}^2 - \bar{L}^2 \frac{\rho^2}{r^2}}, \quad (2-21)$$

since $dr/dz = 0$ and $g(r_{tp}) = 0$ at $r = r_{tp}$. We see immediately that ray paths can exist only if the right side is non negative. This criterion determines the range of values of r for a given profile. *It is not necessary to determine the actual path to categorize rays.*

Bound and refracting rays

For convenience, we assume that $n(r)$ decreases monotonically from its maximum value n_{co} on the axis in Fig. 2-1, to its minimum value at the interface where it coincides with the cladding index, i.e. $n(\rho) = n_{cl}$. A refracting ray must reach the interface, which requires $g(\rho) > 0$. In Eq. (2-21), this is equivalent to requiring that $0 \leq \bar{\beta}^2 + \bar{L}^2 < n_{cl}^2$, and there is then only the one root r_{ic} of $g(r)$ in the core, as shown schematically in Fig. 2-5(c). For a ray to be bound, $g(r) < 0$

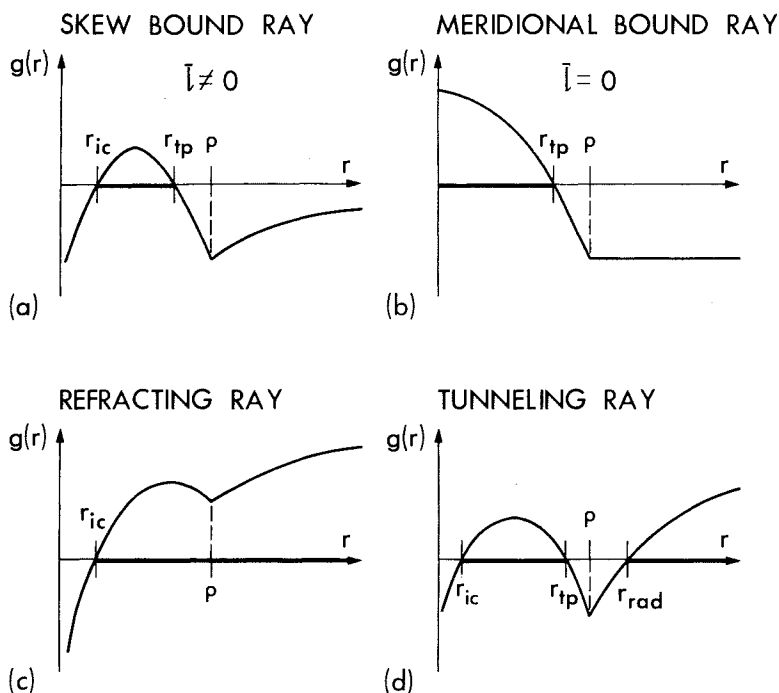


Fig. 2-5 Schematic indication of the basic shape of $g(r)$ of Eq. (2-21) for a typical graded fiber. Rays propagate only when $g(r) > 0$, indicated by the thick line along the axis [3].

everywhere in the cladding, and Eq. (2-21) shows that this requires $n_{cl} < \bar{\beta} \leq n_{co}$, which is identical with Eq. (1-27a) for the planar waveguide. A skew bound-ray path lies between the roots r_{ic} and r_{tp} of $g(r)$, as shown in Fig. 2-5(a), and a meridional ray lies between the fiber axis and r_{tp} , as shown in Fig. 2-5(b).

Tunneling rays

The above discussion leaves ranges of values of $\bar{\beta}$ and \bar{l} which represent neither bound nor refracting rays and satisfy the two conditions

$$\bar{\beta} < n_{cl} \quad \text{and} \quad n_{cl}^2 < \bar{\beta}^2 + \bar{l}^2. \quad (2-22)$$

These values of the invariants correspond to a class of rays called *tunneling rays*. The name tunneling is derived from the fact that these rays appear to tunnel a finite distance into the cladding [1], in analogy to the mechanism of frustrated total internal reflection [4]. To deduce this, we note in Eq. (2-21) that $g(\rho) < 0$ when Eq. (2-22) is satisfied. However, if we examine $g(r)$ in the

cladding, we find that $g(r)$ is positive for all values of r beyond a certain radius r_{rad} given by the condition $g(r_{\text{rad}}) = 0$. Hence

$$r_{\text{rad}} = \rho \bar{l} / (n_{\text{cl}}^2 - \bar{\beta}^2)^{1/2}, \quad (2-23)$$

which defines the *radiation caustic*. The second condition in Eq. (2-22) ensures that $r_{\text{rad}} > \rho$. In other words, there is a ray path in the cladding which extends indefinitely beyond r_{rad} and as the cladding index is uniform, this path is a straight line. The core and cladding paths are separated by the region $r_{\text{tp}} < r < r_{\text{rad}}$ in which propagation cannot take place. It is helpful to refer to the variation of $g(r)$ in Fig. 2-5(d), and to the part of a tunneling-ray path on a graded-profile fiber illustrated by the two views in Fig. 2-6, which show the origin of the cladding path on the radiation caustic relative to the turning point of the path in the core. While the ray equation tells us nothing about the physical mechanism connecting the two regions comprising the path of a tunneling ray, the situation in Fig. 2-6 suggests that some power is lost from the core to the cladding by a tunneling mechanism analogous to frustrated total internal reflection. We verify this suggestion in Chapter 7.

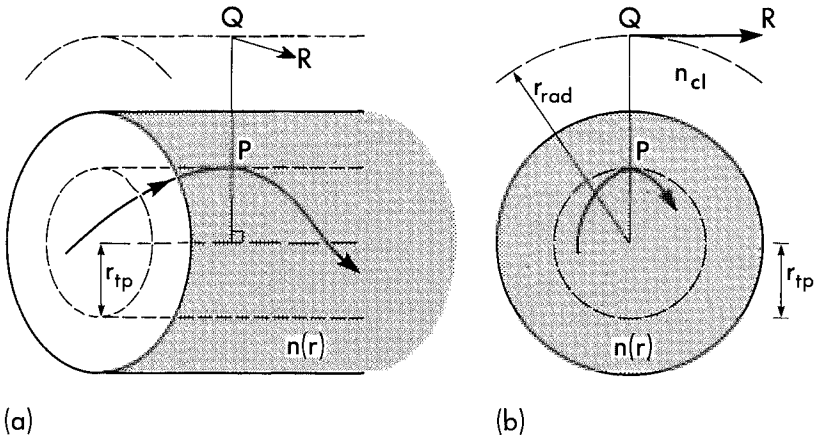


Fig. 2-6 Section of a tunneling ray path on a graded-profile fiber. In (a) the core path touches the turning-point caustic at P. Radiation originates at Q in the cladding and propagates along QR tangential to the radiation caustic. The projection onto the fiber cross-section is shown in (b).

Summary

The classification in Eq. (2-8) for rays on the step-profile fiber can also be deduced from the above discussion, and is a special case of the classification for

graded-profile fibers, since the step profile may be regarded as the extreme limit of a graded profile when all the grading occurs at the interface. Hence rays on clad fibers are *bound* if $n_{cl} < \bar{\beta} \leq n_{co}$ and are *leaky* if $0 \leq \bar{\beta} < n_{cl}$, regardless of the value of \bar{l} . However, the division of leaky rays into *refracting* and *tunneling* rays does depend on the value of \bar{l} . Thus [3]

$$\text{Bound rays: } n_{cl} < \bar{\beta} \leq n_{co}, \quad (2-24a)$$

$$\text{Refracting rays: } 0 \leq \bar{\beta}^2 + \bar{l}^2 < n_{cl}^2, \quad (2-24b)$$

$$\text{Tunneling rays: } \bar{\beta}_{min} \leq \bar{\beta} < n_{cl} \quad \text{and} \quad n_{cl}^2 - \bar{\beta}^2 \leq \bar{l}^2 \leq \bar{l}_{max}^2(\bar{\beta}) \quad (2-24c)$$

where $\bar{\beta}_{min}$ and $\bar{l}_{max}(\bar{\beta})$ for tunneling rays depend on the profile. Given $\bar{\beta}$ for a bound ray, the values of \bar{l} lie in the range $0 \leq \bar{l} \leq \bar{l}_{max}(\bar{\beta})$. These regions are depicted schematically in the $\bar{\beta}$ - \bar{l} plane of Fig. 2-7 for (a) the step profile of Eq. (2-8), and (b) the clad power-law profiles of Eq. (2-43), where $\bar{l}_{max}(\bar{\beta})$ is given by Eq. (4-53) and $\bar{\beta}_{min}$ by Eq. (8-10).

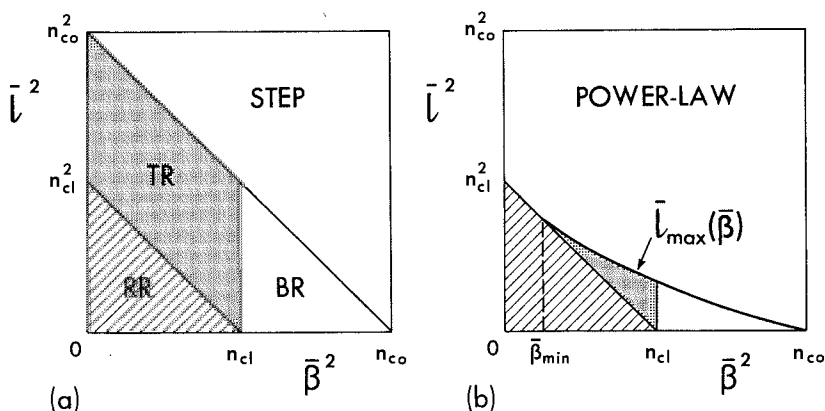


Fig. 2-7 Schematic distribution of rays on circular fibers according to the value of the invariants $\bar{\beta}$ and \bar{l} for (a) the step-profile of Eq. (2-8) and (b) the clad power-law fibers of Eq. (2-43) [3]. Shading denotes tunneling rays (TR) and hatching denotes refracting rays (RR). Bound rays (BR) occupy the unshaded regions.

2-8 Ray-path parameters

Each ray of the graded-profile fiber is characterized by the invariants $\bar{\beta}$ and \bar{l} . For most purposes in subsequent chapters the ray trajectory is unimportant, and it is sufficient to know only the values of the ray-path parameters. The

integral of the ray equation of Eq. (2-13a) is given by Eq. (2-21), and a second integration leads to

$$z = z_0 + \bar{\beta} \int_{r_0}^r \frac{dr}{g(r)^{1/2}}; \quad g(r) = n^2(r) - \bar{\beta}^2 - \bar{l}^2 \frac{\rho^2}{r^2}, \quad (2-25)$$

where (r_0, z_0) is a fixed point on the path, which for bound rays satisfies $r_{ic} \leq r_0 \leq r_{tp}$, where r_{ic} and r_{tp} are the roots of $g(r)$. The path length L_p and optical path length L_o are measured along the path in Fig. 2-4 between successive points P and Q at which the path touches the turning-point caustic. By symmetry, the midpoint touches the inner caustic if the path is skew, or crosses the axis if the path is meridional. Consequently

$$L_p = \int_P^Q ds; \quad L_o = \int_P^Q n(r) ds, \quad (2-26)$$

where integration is along the path. We use Eq. (2-16) to replace ds by dz , and Eq. (2-21) to replace dz by dr . Thus

$$L_p = 2 \int_{r_{ic}}^{r_{tp}} \frac{n(r) dr}{g(r)^{1/2}}; \quad L_o = 2 \int_{r_{ic}}^{r_{tp}} \frac{n^2(r) dr}{g(r)^{1/2}}, \quad (2-27)$$

where $g(r)$ is defined in Eq. (2-25). The ray half-period z_p is the axial distance between P and Q in Fig. 2-4, whence

$$z_p = \frac{1}{N} = \int_P^Q dz = 2\bar{\beta} \int_{r_{ic}}^{r_{tp}} \frac{dr}{g(r)^{1/2}}, \quad (2-28)$$

where N is the number of turning points per unit length of fiber. In the above expressions we set $\bar{l} = 0$ and $r_{ic} = 0$ for meridional rays. All these expressions, together with the transit time of the following section are included in Table 2-1.

Complement of the local critical angle

In Section 1-8 we introduced the notion of the complement of the local critical angle for graded-profile planar waveguides. By analogy, the complement of the local critical angle, $\theta_c(r)$, for fibers is defined in terms of the profile by

$$\cos \theta_c(r) = \frac{n_{cl}}{n(r)}; \quad \sin \theta_c(r) = \left\{ 1 - \frac{n_{cl}^2}{n^2(r)} \right\}^{1/2}. \quad (2-29)$$

The range of values of $\theta_z(r)$ for bound rays at radius r is then

$$0 \leq \theta_z(r) < \theta_c(r); \quad 0 \leq r \leq \rho. \quad (2-30)$$

At the interface there are no bound rays, i.e. $\theta_c(\rho) = 0$, and, provided $n(0) = n_{co}$, $0 < \theta_z(0) \leq \theta_c(0)$ on axis, which includes the step-profile fiber range of Eq. (2-6a).

Table 2-1 Ray-path parameters for optical fibers. The half-period, path length and optical path length are measured between successive reflection or turning points, and the transit time is over length z of fiber. The number of reflection or turning points per unit length of fiber is $N = 1/z_p$, and ρ is the core radius or profile scaling length. Both r_c and r_{tp} are roots of $g(r) = 0$.

	Profile $n^2(r)$	Ray half-period $z_p = 1/N$	Path length, L_p	Optical path length L_o	Transit time t
Step	$n_{co}^2; 0 \leq r < \rho$	$\frac{2\rho\beta g(\rho)^{1/2}}{n_{co}^2 - \beta^2}$	$\frac{2\rho n_{co} g(\rho)^{1/2}}{n_{co}^2 - \beta^2}$	$\frac{2\rho n_{co}^2 g(\rho)^{1/2}}{n_{co}^2 - \beta^2}$	$\frac{z n_{co}^2}{c \beta}$
	$n_{cl}^2; \rho < r < \infty$		$g(\rho) = n_{co}^2 - \beta^2 - \bar{r}^2$		
Graded	$n^2(r); 0 \leq r \leq \rho$	$\frac{2\beta \int_{r_c}^{r_{tp}} dr}{\int_{r_c}^{r_{tp}} g(r)^{1/2} dr}$	$\frac{2 \int_{r_c}^{r_{tp}} n(r) dr}{\int_{r_c}^{r_{tp}} g(r)^{1/2} dr}$	$2 \int_{r_c}^{r_{tp}} \frac{n^2(r) dr}{g(r)^{1/2}}$	$\frac{z L_o}{c z_p}$
	$n_{cl}^2; \rho \leq r < \infty$		$g(r) = n^2(r) - \beta^2 - \bar{r}^2 \rho^2 / r^2$		
Parabolic	$n_{co}^2 \left\{ 1 - 2\Delta \left(\frac{r}{\rho} \right)^2 \right\}$	$\frac{\pi \rho \beta}{n_{co} \sqrt{2\Delta}}$	$\frac{z_p}{4} \left\{ \frac{3n_{co}}{\beta} + \frac{\beta}{n_{co}} \right\} \Delta \ll 1$	$\frac{z_p}{2} \left\{ \frac{n_{co}^2}{\beta} + \beta \right\}$	$\frac{z n_{co}}{2 c} \left\{ \frac{\beta}{n_{co}} + \frac{n_{co}}{\beta} \right\}$

	Profile $n^2(r)$	Ray half-period $z_p = 1/N$	Path length L_p	Optical path length L_o	Transit time t
Clad power law	$n_{co}^2 \left\{ 1 - 2\Delta \left(\frac{r}{\rho} \right)^q \right\};$ $0 \leq r < \rho \quad \text{---} \quad \text{---}$ $n_{cl}^2; \rho \leq r < \infty$	Only for $q = 2$ above and for $T = 0$ in Table 1-1, page 19	$\frac{z_p}{(q+2)} \left\{ (q+1) \frac{n_{co}}{\bar{\beta}} + \frac{\bar{\beta}}{n_{co}} \right\}$ $\Delta \ll 1$	$\frac{z_p}{(q+2)} \left\{ q \frac{n_{co}^2}{\bar{\beta}} + 2\bar{\beta} \right\}$	$\frac{z}{c} \frac{n_{co}}{(q+2)} \left\{ q \frac{n_{co}}{\bar{\beta}} + 2 \frac{\bar{\beta}}{n_{co}} \right\}$
Noncircular power law	$n_{co}^2 \{ 1 - 2\Delta f(x, y) \}$ $f = \left[\left \frac{x}{\rho_x} \right ^p + \left \frac{y}{\rho_y} \right ^p \right]^{q/p}$ $-\infty < x, y < \infty$		Ray trajectory not periodic		$\frac{z}{c} \frac{n_{co}}{(q+2)} \left\{ q \frac{n_{co}}{\bar{\beta}} + 2 \frac{\bar{\beta}}{n_{co}} \right\}$
$\bar{\beta} = n_{co} \cos \theta_z; \quad T = n_{co} \sin \theta_z \cos \theta_\phi$; step profile			$\bar{\beta} = n(r) \cos \theta_z(r); \quad T = n(r) \sin \theta_z(r) \cos \theta_\phi(r)$; graded profile		

2-9 Ray transit time

The transit time t over length z of a fiber is given by analogy with Eq. (1-36) as

$$t = \frac{1}{c} \int n(r) ds = \frac{1}{c\bar{\beta}} \int_0^z n^2(r) dz, \quad (2-31)$$

in terms of Eq. (2-16), where the second integral is along the path $r = r(z)$. It follows from the discussion of Section 1-9, that *the transit time for fibers has the same form as for planar waveguides*. Thus, provided $z \gg z_p$, we deduce from Eq. (1-37) that

$$t = zL_o/(cz_p), \quad (2-32)$$

where L_o is the optical path length of Eq. (2-27) and z_p the ray half-period of Eq. (2-28). Material dispersion can be included by replacing $n(r)$ with the group index n_g in the first integral in Eq. (2-31). By analogy with Eq. (1-38a), we deduce that

$$t = \frac{1}{c} \int n_g(r, \lambda) ds; \quad n_g(r, \lambda) = n(r, \lambda) - \lambda \frac{\partial n}{\partial \lambda}(r, \lambda), \quad (2-33a)$$

and the corresponding expressions to Eq. (1-38b) become

$$t = \frac{z}{c} \frac{L_m}{z_p}; \quad L_m = 2 \int_{r_{ic}}^{r_{ip}} \frac{n_g(r, \lambda)n(r, \lambda)}{g(r, \lambda)^{1/2}} dr, \quad (2-33b)$$

where $g(r, \lambda)$ is defined by Eq. (2-25) with $n(r)$ replaced by $n(r, \lambda)$.

We emphasize that, in general, the transit times depend on both $\bar{\beta}$ and \bar{l} , and reduce to the corresponding expressions for planar waveguides only in the case of meridional rays. However, transit times are independent of \bar{l} , i.e. independent of skewness, for certain profiles, including the step and clad power-law profiles, as we show below. We also recall from Section 1-9 that *graded profiles tend to equalize transit times compared to the step profile*. Unlike planar waveguides, though, *there is no known profile for which complete equalization of all ray transit times on a fiber is possible*.

GRADED PROFILES WITH ANALYTICAL SOLUTIONS

Here we consider examples of graded-profile fibers which lead to analytical expressions for some or all of the ray-path parameters of interest. We can use the paraxial approximation of Section 1-10 to simplify determination of the path length. The results are included in Table 2-1.

2-10 Example: Parabolic profile

We first consider the infinite parabolic profile defined by

$$n^2(r) = n_{co}^2 \{1 - 2\Delta(r/\rho)^2\}; \quad 0 \leq r < \infty, \quad (2-34)$$

where Δ is defined by Eq. (1-41) and ρ is a scaling length that characterizes the profile width. As explained in Section 1-11, this profile is unphysical but is useful for understanding propagation, as it leads to simple expressions for virtually all ray-path parameters. Every ray path is bound, which is expressed by Eq. (1-46). Substituting Eq. (2-34) into Eq. (2-19) and solving the resultant quadratic equation in r^2 , we deduce that the radii of the inner caustic and turning-point caustic are

$$r_{ic} = \frac{\rho}{2n_{co}\Delta^{1/2}} [(n_{co}^2 - \bar{\beta}^2) - \{(n_{co}^2 - \bar{\beta}^2)^2 - 8\Delta\bar{l}^2 n_{co}^2\}^{1/2}]^{1/2}, \quad (2-35a)$$

$$r_{tp} = \frac{\rho}{2n_{co}\Delta^{1/2}} [(n_{co}^2 - \bar{\beta}^2) + \{(n_{co}^2 - \bar{\beta}^2)^2 - 8\Delta\bar{l}^2 n_{co}^2\}^{1/2}]^{1/2}, \quad (2-35b)$$

respectively. If we assume $z = 0$ at $r = r_{ic}$ and factorize the path integral of Eq. (2-25) with the help of Eq. (2-35), then

$$z = \frac{\rho\bar{\beta}}{n_{co}\sqrt{(2\Delta)}} \int_{r_{ic}}^r \frac{r dr}{(r_{tp}^2 - r^2)^{1/2} (r^2 - r_{ic}^2)^{1/2}}. \quad (2-36)$$

This is a standard integral, whose solution is given by Eq. (37-121), and on rearrangement we obtain

$$r = \left\{ \frac{r_{ic}^2 + r_{tp}^2}{2} - \frac{r_{tp}^2 - r_{ic}^2}{2} \cos\left(\frac{2z}{\rho} \frac{n_{co}\sqrt{(2\Delta)}}{\bar{\beta}}\right) \right\}^{1/2}. \quad (2-37)$$

The projection of this path onto the cross-section is a closed ellipse. The ray half-period z_p of Eq. (2-28) is the axial distance between successive positions at which $r = r_{tp}$, which corresponds to an increase of 2π in the argument of the cosine function in Eq. (2-37). Hence

$$z_p = 1/N = \pi\rho\bar{\beta}/(n_{co}\sqrt{(2\Delta)}), \quad (2-38)$$

where N is the number of turning points per unit length of fiber. The optical path length L_o is obtained by substituting Eq. (2-34) into the second integral in Eq. (2-27). By analogy with Eq. (2-36), we find with the help of Eq. (2-28) that

$$L_o = \frac{n_{co}^2}{\bar{\beta}} z_p - \frac{2n_{co}\sqrt{(2\Delta)}}{\rho} \int_{r_{ic}}^{r_{tp}} \frac{r^3 dr}{(r_{tp}^2 - r^2)^{1/2} (r^2 - r_{ic}^2)^{1/2}}. \quad (2-39)$$

The standard integral is deduced from Eq. (37-122), and with the aid of Eqs. (2-35) and (2-38) is expressible as

$$L_o = z_p (\bar{\beta}^2 + n_{co}^2)/(2\bar{\beta}). \quad (2-40)$$

The first integral in Eq. (2-27) for the path length is not expressible in closed form, but may be evaluated within the paraxial approximation. When $\Delta \ll 1$, we approximate $n(r)$

in the manner of Eq. (1-43), and by analogy with Eq. (2-39) find that

$$L_p \cong \frac{n_{co}}{\bar{\beta}} z_p - \frac{\sqrt{(2\Delta)}}{\rho} \int_{r_{ic}}^{r_{tp}} \frac{r^3 dr}{(r_{tp}^2 - r^2)^{1/2} (r^2 - r_{ic}^2)^{1/2}}, \quad (2-41a)$$

$$= \frac{z_p}{4} \left\{ \frac{3n_{co}}{\bar{\beta}} + \frac{\bar{\beta}}{n_{co}} \right\}; \quad \Delta \ll 1, \quad (2-41b)$$

with the help of Eqs. (2-35), (2-38) and (37-122). Finally, the ray transit time t of Eq. (2-32) follows directly from Eq. (2-40) as

$$t = z(\bar{\beta}^2 + n_{co}^2)/(2c\bar{\beta}), \quad (2-42)$$

which is identical to the planar waveguide result of Eq. (1-50).

2-11 Example: Clad power-law profiles

The clad power-law profiles are defined by

$$n^2(r) = n_{co}^2 [1 - 2\Delta(r/\rho)^q]; \quad 0 \leq r \leq \rho, \quad (2-43a)$$

$$= n_{cl}^2 = n_{co}^2 [1 - 2\Delta]; \quad \rho \leq r < \infty, \quad (2-43b)$$

where q is a positive constant. These profiles are illustrated in Fig. 1-10 with x replaced by r . The range of values of $\bar{\beta}$ for bound rays is given by Eq. (2-24a). For arbitrary skew-ray trajectories with $\bar{l} > 0$, only the ray transit time can be expressed in simple closed form. Path parameters for meridional rays are given in Table 1-1, page 19, with x replaced by r . As pointed out in Section 1-13, the results for the parabolic profile apply to the clad parabolic profile, since the ray-path parameters for bound rays are independent of the presence of the cladding. To determine the transit time for bound rays, we substitute Eq. (2-43a) into Eq. (2-27) for the optical path length, and rearrange as

$$L_o = \frac{n_{co}^2}{\bar{\beta}} z_p - \frac{4n_{co}^2 \Delta}{\rho^q} \int_{r_{ic}}^{r_{tp}} \frac{r^q}{g(r)^{1/2}} dr, \quad (2-44a)$$

$$g(r) = n_{co}^2 - \bar{\beta}^2 - \bar{l}^2 \frac{\rho^2}{r^2} - 2n_{co}^2 \Delta \left(\frac{r}{\rho} \right)^q, \quad (2-44b)$$

where z_p is the ray half-period of Eq. (2-28). To evaluate the integral we use a property of power-law profiles. Integrating the integral I in Eq. (2-44a) by parts gives

$$I \equiv \int_{r_{ic}}^{r_{tp}} g(r)^{1/2} dr = \int_{r_{ic}}^{r_{tp}} \frac{r}{2g(r)^{1/2}} \left\{ 2qn_{co}^2 \Delta \frac{r^{q-1}}{\rho^q} - \frac{2\bar{l}^2 \rho^2}{r^3} \right\} dr, \quad (2-45)$$

since $g(r) = 0$ at r_{ic} and r_{tp} . Rearranging and substituting from Eq. (2-44b) leads to

$$I = I + \int_{r_{ic}}^{r_{tp}} \frac{1}{g(r)^{1/2}} \left\{ \bar{\beta}^2 - n_{co}^2 + (q+2)n_{co}^2 \Delta \left(\frac{r}{\rho} \right)^q \right\} dr, \quad (2-46)$$

and we deduce from Eq. (2-28) that

$$\int_{r_{ic}}^{r_{ip}} \frac{r^q dr}{g(r)^{1/2}} = \frac{\rho^q (n_{co}^2 - \bar{\beta}^2)}{2(q+2)n_{co}^2 \Delta \bar{\beta}} z_p, \quad (2-47)$$

which gives L_o explicitly in Eq. (2-44a). Substituting into Eq. (2-32), we finally obtain [3]

$$t = \frac{z}{c} \frac{n_{co}}{(q+2)} \left\{ q \frac{n_{co}}{\bar{\beta}} + \frac{2\bar{\beta}}{n_{co}} \right\}, \quad (2-48)$$

which is identical to the planar waveguide result of Eq. (1-64).

NONCIRCULAR FIBERS

So far in this chapter we have considered only fibers with circular cross-sections. In practice, cross-sections can vary quite significantly from circular symmetry, e.g. elliptical fibers. We therefore extend our analysis to fibers with noncircular cross-sections and refractive-index profiles. Ray methods can be applied to fibers of arbitrary noncircularity, provided only that the fiber is multimoded. Ray paths on circular fibers can be described in terms of the ray invariants $\bar{\beta}$ and \bar{l} associated with translational and azimuthal symmetries, but noncircular fibers have only translational symmetry, and thus a ray analysis is in general more complicated than for circular fibers. Furthermore, noncircular fibers can support a new class of ray paths. In addition to the ray paths on circular fibers which are either bound, refracting or tunneling, there is a fourth category called *tunneling-refracting* rays [5]. These rays are leaky, and suffer power loss by tunneling at successive reflection or turning points along their paths, and are then partly or totally lost to the cladding by refraction.

2-12 Ray-path equations

The ray-path equation of Eq. (1-18) has component equations parallel to the cartesian axes in Fig. 2-1 given by

$$\frac{d}{ds} \left\{ n(x, y) \frac{dx}{ds} \right\} = \frac{\partial n(x, y)}{\partial x}; \quad \frac{d}{ds} \left\{ n(x, y) \frac{dy}{ds} \right\} = \frac{\partial n(x, y)}{\partial y}, \quad (2-49a)$$

$$\frac{d}{ds} \left\{ n(x, y) \frac{dz}{ds} \right\} = 0, \quad (2-49b)$$

where s is the distance along the ray path, and $n(x, y)$ is the profile. The last equation leads to the ray invariant $\bar{\beta}$, which is now defined by

$$\bar{\beta} = n(x, y) \frac{dz}{ds} = n(x, y) \cos \theta_z(x, y), \quad (2-50)$$

where $\theta_z(x, y)$ is the angle between the tangent to the path and the axial direction, and $x = x(z)$, $y = y(z)$ along the path. If we use $\bar{\beta}$ to eliminate ds from Eq. (2-49a), we obtain the ray path equations

$$2\bar{\beta}^2 \frac{d^2 x}{dz^2} = \frac{\partial n^2(x, y)}{\partial x}; \quad 2\bar{\beta}^2 \frac{d^2 y}{dz^2} = \frac{\partial n^2(x, y)}{\partial y}. \quad (2-51)$$

Noting that $ds^2 = dx^2 + dy^2 + dz^2$ and substituting from Eq. (2-50), we deduce that

$$\left(\frac{dx}{dz}\right)^2 + \left(\frac{dy}{dz}\right)^2 = \frac{n^2(x, y)}{\bar{\beta}^2} - 1, \quad (2-52)$$

along each path. This is the first integral of the ray-path equations. If $n(x, y)$ takes uniform value n_{cl} in the cladding, then we deduce from Eq. (2-52) that there are no paths in the cladding if $\bar{\beta} > n_{cl}$, i.e. the ray is bound. Furthermore, if n_{co} is the maximum value of $n(x, y)$ in the core, then Eq. (2-50) tells us that $\bar{\beta}$ cannot exceed n_{co} . Accordingly *the invariant $\bar{\beta}$ for bound rays lies in the range $n_{cl} < \bar{\beta} \leq n_{co}$ and is independent of both the profile shape and the cross-sectional geometry of the fiber.*

Ray transit time

The local speed of light is $c/n(x, y)$, and thus the transit time over distance z along the fiber is given by the path integral

$$t = \frac{1}{c} \int n(x, y) ds = \frac{1}{c\bar{\beta}} \int_0^z n^2(x, y) dz, \quad (2-53)$$

where in the second expression $x = x(z)$, $y = y(z)$, and we have used Eq. (2-50).

2-13 Example: Homogeneous-function profiles

We consider noncircular fibers with profiles expressible in terms of an arbitrary *homogeneous function* $f(x, y)$ in the form

$$n^2(x, y) = n_{co}^2 \{1 - 2\Delta f(x, y)\}; \quad -\infty < x, y < \infty. \quad (2-54a)$$

A homogeneous function of degree q has the properties that if a is a constant, then

$$f(ax, ay) = a^q f(x, y); \quad x(\partial f / \partial x) + y(\partial f / \partial y) = qf. \quad (2-54b)$$

An example is the class of noncircular power-law profiles defined by [5]

$$n^2(x, y) = n_{co}^2 \left\{ 1 - 2\Delta \left[\left| \frac{x}{\rho_x} \right|^p + \left| \frac{y}{\rho_y} \right|^p \right]^{q/p} \right\}, \quad (2-55)$$

where p is the *shape parameter*, and ρ_x, ρ_y are scaling lengths. This class includes the power-law profiles of Eq (2-43a) for circular fibers, when $\rho_x = \rho_y = \rho$, $p = 2$ and $r^2 = x^2 + y^2$. For an arbitrary homogeneous function, the transit time integral in Eq. (2-53) can be evaluated explicitly. This is accomplished by examining the variation in the cylindrical polar radius $r = (x^2 + y^2)^{1/2}$. We take the second derivative of this relation with respect to z and substitute Eqs. (2-51), (2-52) and (2-54) to obtain

$$\bar{\beta}^2 \frac{d^2 r^2}{dz^2} = 2\{n^2(x, y) - \bar{\beta}^2\} - 2n_{co}^2 \Delta \left\{ x \frac{\partial f}{\partial x}(x, y) + y \frac{\partial f}{\partial y}(x, y) \right\}, \quad (2-56a)$$

$$= (q + 2)n^2(x, y) - qn_{co}^2 - 2\bar{\beta}^2. \quad (2-56b)$$

On integrating with respect to z , the left side reduces to $\bar{\beta}^2 [dr^2/dz]^2_0$ which, when compared with terms on the right linear in z , can be ignored if z is sufficiently large. The right side contains the transit time integral of Eq. (2-53), and on rearrangement we have [5]

$$t = \frac{z}{c} \frac{n_{co}}{q + 2} \left\{ q \frac{n_{co}}{\bar{\beta}} + 2 \frac{\bar{\beta}}{n_{co}} \right\}, \quad (2-57)$$

which is identical with the transit time of Eq. (2-48) for clad power-law profiles on circular fibers, and Eq. (2-12) for the step profile in the limit $q \rightarrow \infty$. Thus we have the remarkable result that *the transit time is independent of both fiber noncircularity and ray skewness for homogeneous function profiles.*

2-14 Example: Separable profiles

A separable profile has refractive index which is expressible as [6]

$$n^2(x, y) = n_{co}^2 \{1 - 2\Delta[f(x) + g(y)]\}, \quad -\infty < x, y < \infty, \quad (2-58)$$

where $f(x)$ and $g(y)$ are functions of x and y , respectively. The ray-path equations of Eq. (2-51) for these profiles decouple into two ordinary differential equations which can be expressed in the forms

$$\frac{d}{dx} \left(\frac{dx}{dz} \right)^2 = -\Omega^2 \frac{df(x)}{dx}; \quad \frac{d}{dy} \left(\frac{dy}{dz} \right)^2 = -\Omega^2 \frac{dg(y)}{dy}, \quad (2-59)$$

where $\Omega = n_{co} \sqrt{(2\Delta)/\bar{\beta}}$. On integrating and rearranging, the ray path is given by

$$z = \frac{1}{\Omega} \int_{x_0}^x \frac{dx}{\{f(x_{tp}) - f(x)\}^{1/2}} = \frac{1}{\Omega} \int_{y_0}^y \frac{dy}{\{g(y_{tp}) - g(y)\}^{1/2}}, \quad (2-60)$$

assuming that the ray originates at x_0, y_0 in the fiber cross-section at $z = 0$. The turning points x_{tp} and y_{tp} are determined by the initial direction of the ray.

Characteristics of the ray path

For a given path, the turning-point caustic is the surface defined by points x_{tp}, y_{tp} at which $dx/dz = 0$ and $dy/dz = 0$. If we assume that both $f(x)$ and $g(y)$ are increasing

functions, then $n(x, y)$ decreases away from the fiber axis, and the turning-point caustic is a rectangle, as shown in Fig. 2-8(a), with sides equal in length to $2x_{tp}$ and $2y_{tp}$, respectively. In general, the projection of the path onto the cross-section eventually

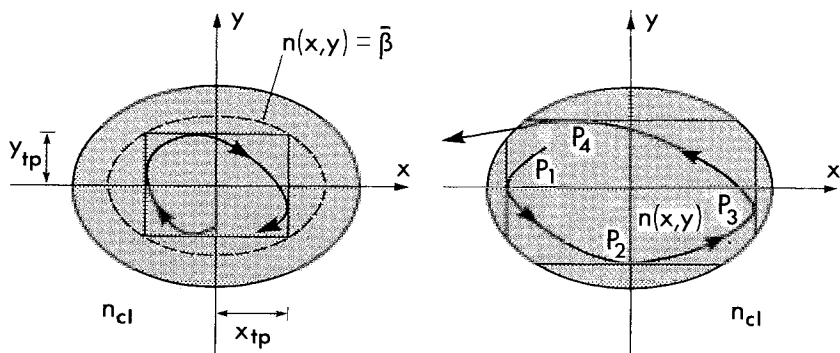


Fig. 2-8 Rectangular turning-point caustics for fibers with the separable profiles of Eq. (2-58), showing (a) a bound-ray caustic and (b) a tunneling-refracting ray caustic [5].

touches the rectangle at every point and completely fills the rectangle, provided the fiber is infinitely long. If we substitute the first integral of Eq. (2-59) into Eq. (2-52) and rearrange, we find that

$$\bar{\beta}^2 = n_{co}^2 \{1 - 2\Delta[f(x_{tp}) + g(y_{tp})]\}, \quad (2-61)$$

which, on comparison with Eq. (2-58), requires that the corners of the rectangle lie on a contour of constant refractive index defined by $n(x, y) = \bar{\beta}$. This contour in Fig. 2-8(a) is the envelope defined by all possible rectangles satisfying Eq. (2-61), which correspond to paths with different initial conditions but with the same value of $\bar{\beta}$.

Classification of rays

We now consider clad profiles, so that $n(x, y)$ takes uniform value n_{cl} beyond the interface. Furthermore, we assume $n(x, y)$ takes its maximum value n_{co} , at $x = y = 0$. As we showed in Section 2-12, bound rays have invariants in the range $n_{cl} < \bar{\beta} \leq n_{co}$, corresponding to rectangles with envelopes lying between the interface, $\bar{\beta} = n_{cl}$, and the axis, $\bar{\beta} = n_{co}$. For bound rays, every rectangular caustic lies completely within the core cross-section. For the remaining leaky rays, with $0 \leq \bar{\beta} \leq n_{cl}$, only part of each rectangle can be contained within the core, as shown by the example in Fig. 2-8(b). A typical path touches the envelope at P_1 , P_2 , P_3 and P_4 in succession. In the hatched region between the envelope and the interface no ray propagates, but $\bar{\beta} < n_{cl}$ and Eq. (2-52) shows that there are paths in the cladding. Consequently we associate the reflections at P_1 , P_2 , P_3 and P_4 with energy lost by tunneling, as discussed in Section 2-7. After P_4 the ray meets the interface and is lost to the cladding, i.e. refracts. Hence, we have a new type of ray which undergoes tunneling and refraction at different points

along its path. These rays which propagate only on noncircular fibers are called *tunneling-refracting rays* [5].

2-15 Example: Parabolic elliptical profile

The fiber has the profile defined by

$$n^2(x, y) = n_{co}^2 \left\{ 1 - 2\Delta \left(\frac{x^2}{\rho_x^2} + \frac{y^2}{\rho_y^2} \right) \right\}, \quad (2-62)$$

where ρ_x and ρ_y are the lengths of the semi-major and semi-minor axes, and contours of constant refractive index are ellipses with a common *eccentricity* e defined by $e = (1 - \rho_y^2/\rho_x^2)^{1/2}$. This profile is an example which is both a homogeneous function profile, corresponding to Eq. (2-55) with $p = q = 2$, and a separable profile, corresponding to Eq. (2-58) with $f(x) = x^2/\rho_x^2$ and $g(y) = y^2/\rho_y^2$. Consequently the transit time is given by Eq. (2-57) with $q = 2$, and the ray-path equations of Eq. (2-59) can be written as

$$\frac{d^2x}{dz^2} = -\frac{\Omega^2}{\rho_x^2} x; \quad \frac{d^2y}{dz^2} = -\frac{\Omega^2}{\rho_y^2} y, \quad (2-63)$$

where $\Omega = n_{co}\sqrt{(2\Delta)/\beta}$. These are the harmonic equations with solution [5,6]

$$x = (x_{tp}^2 - x_0^2)^{1/2} \sin(\Omega z/\rho_x) + x_0 \cos(\Omega z/\rho_x), \quad (2-64a)$$

$$y = (y_{tp}^2 - y_0^2)^{1/2} \sin(\Omega z/\rho_y) + y_0 \cos(\Omega z/\rho_y), \quad (2-64b)$$

where x_0, y_0 is the position of the ray in the cross-section at $z = 0$, and $\pm x_{tp}, \pm y_{tp}$ are the positions of the turning-point caustics. In this form, Eq. (2-64) satisfies both Eqs. (2-52) and (2-61), as may be verified. For arbitrary eccentricity these paths completely fill the rectangular caustic of Fig. 2-8(b), but when ρ_y/ρ_x is a rational fraction, i.e. $m\rho_x = n\rho_y$, where m and n are integers, the path projection is a closed Lissajous figure. In the limit $\rho_x = \rho_y = \rho$ these paths reduce to the closed ellipses in the cross-section of the circular fiber discussed in Section 2-10.

REFERENCES

1. Snyder, A. W. (1974) Leaky-ray theory of optical waveguides of circular cross-section. *Appl. Phys.*, **4**, 273-98.
2. Rawson, E. G., Herriott, D. R. and McKenna, J. (1970) Analysis of refractive index distributions in cylindrical, graded-index glass rods (GRIN) used as image relays. *Appl. Opt.*, **9**, 753-9.
3. Ankiewicz, A. and Pask, C. (1977) Geometric optics approach to light acceptance and propagation in graded-index fibres. *Opt. Quant. Elect.*, **9**, 87-109.
4. Lipson, S. G. and Lipson, H. (1969) *Optical Physics*, Cambridge University Press, p. 80.

5. Barrell, K. F. and Pask, C. (1979) Geometric optics analysis of non-circular graded-index fibres. *Opt. Quant. Elect.*, **11**, 237–51.
6. Ankiewicz, A. (1979) Ray theory of graded non-circular optical fibres. *Opt. Quant. Elect.*, **11**, 197–203.

Pulse spreading

Ray dispersion in planar waveguides	52
3-1 Step profile	52
3-2 Clad power-law profiles	53
Ray dispersion in fibers	55
3-3 Noncircular fibers	57
Material and profile dispersion	57
3-4 Material dispersion	57
3-5 Profile dispersion	58
3-6 Linear dispersion	58
3-7 <i>Example: Step-profile fiber</i>	58
3-8 <i>Example: Clad power-law profile fibers</i>	59
3-9 Nonlinear dispersion	60
References	61

The transmission of information along optical fibers is normally achieved by sending out a sequence of pulses of light energy. However, as an individual pulse propagates, it spreads out, due to the dispersive properties of the fiber. Clearly if this spread becomes sufficiently large the pulse will overlap with adjacent pulses, leading to a decrease in information-carrying capacity because of the loss of resolution at the end of the fiber.

In Chapters 1 and 2 we introduced the notion of ray transit time. The main contribution to pulse spreading is due to the obvious fact that the ray transit time is different for different ray paths. This effect is known as *ray dispersion*, and is sometimes referred to as *intermodal dispersion*, since early investigation used electromagnetic analysis in terms of modes [1], rather than ray theory. In addition to ray dispersion, *material dispersion* also affects pulse spreading. This effect arises because the materials constituting the fiber have a refractive index which varies with the wavelength of light.

The main purpose of this chapter is to show that pulse spreading depends on the refractive-index profile, and to demonstrate how it can be minimized by a suitable choice of profile. We first examine planar waveguides, for which it is possible to achieve zero pulse spread, and then circular and noncircular fibers.

Initially we assume that the waveguide is composed of materials which are nondispersive. We subsequently determine the modification due to material dispersion. Only bound rays are included in the present chapter, as they characterize the transmission properties of long fibers. *The major conclusion of this chapter is that pulse spreading on fibers is minimized if the profile has an approximately parabolic profile.*

Initial conditions

Throughout the chapter, we assume that the pulse originates at time $t = 0$ at the *endface* $z = 0$ of a waveguide of arbitrary profile and length z as shown in Fig. 3-1. The pulse is assumed to be composed of bound rays only, all of which are excited simultaneously at $z = 0$. For convenience, the initial pulse spread is assumed to be zero. In practice, sources excite pulses of finite duration; the spread along the fiber is then found by superposition.

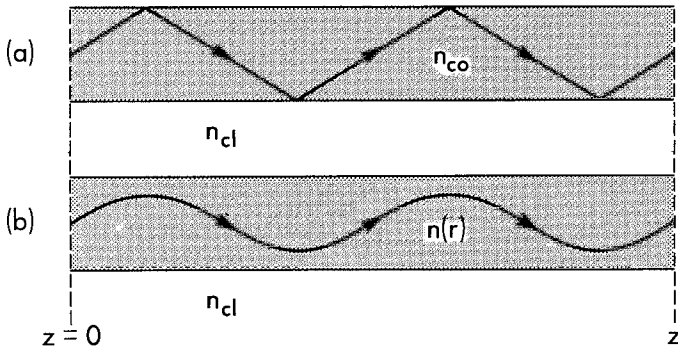


Fig. 3-1 Pulse propagation is described in terms of a superposition of bound rays, each ray propagating distance z along (a) a step-profile waveguide or (b) a graded-profile waveguide.

RAY DISPERSION IN PLANAR WAVEGUIDES

The simplest structures for calculating dispersion are the planar waveguides of Chapter 1. We start with the step profile and progress to graded profiles.

3-1 Step profile

We recall from Fig. 1-4(a) that bound rays propagate along a zig-zag path at angle θ_z to the axis in the core of the waveguide. The range of values of θ_z for bound rays is given by Eq. (1-5a) as $0 \leq \theta_z < \theta_c$, where θ_c is the complement of the critical angle defined inside the front cover. The transit time t of Eq. (1-14)

varies inversely with $\cos \theta_z$. Consequently, the minimum transit time t_{\min} corresponds to $\theta_z = 0$, i.e. to rays propagating parallel to the axis, and the maximum transit time t_{\max} corresponds to $\theta_z = \theta_c$. Thus

$$t_{\min} = \frac{z}{c} n_{\text{co}}; \quad t_{\max} = \frac{z}{c} \frac{n_{\text{co}}}{\cos \theta_c} = \frac{z}{c} \frac{n_{\text{co}}^2}{n_{\text{cl}}}, \quad (3-1)$$

where n_{co} and n_{cl} are the core and cladding indices, z is the length of the waveguide and c is the free-space speed of light. Thus the pulse spread, or ray dispersion, t_d in time, is the difference between the maximum and minimum transit times given by

$$t_d = t_{\max} - t_{\min} = \frac{z}{c} n_{\text{co}} \left\{ \frac{n_{\text{co}}}{n_{\text{cl}}} - 1 \right\} = \frac{z}{c} n_{\text{co}} \{ (1 - 2\Delta)^{-1/2} - 1 \}, \quad (3-2)$$

in terms of the profile height parameter defined inside the front cover. The greater the length of the waveguide, the greater pulse spreading becomes. For weakly guiding waveguides, when $n_{\text{co}} \cong n_{\text{cl}}$, we deduce from Eq. (1-42) that

$$t_d \cong z n_{\text{co}} \Delta / c \cong z n_{\text{co}} \theta_c^2 / 2c, \quad (3-3)$$

since $\Delta, \theta_c \ll 1$. Hence dispersion can be reduced by making the index difference smaller, which is one of the reasons why practical waveguides have small values of Δ or, equivalently, θ_c .

Spatial spread

An alternative way to regard dispersion is to think of the *spatial* spread z_d of the pulse, as it propagates. This spread is the distance between the front of the pulse, propagating with speed c/n_{co} , and the rear of the pulse, propagating with speed $cn_{\text{cl}}/n_{\text{co}}^2$. Thus after time t , the spread is given by

$$z_d = \frac{ct}{n_{\text{co}}} \left\{ 1 - \frac{n_{\text{cl}}}{n_{\text{co}}} \right\} \cong \frac{ct}{n_{\text{co}}} \Delta \cong \frac{ct}{n_{\text{co}}} \frac{\theta_c^2}{2}, \quad (3-4)$$

where the approximations apply to weakly guiding waveguides and paraxial rays. Clearly the spatial spread increases with increasing waveguide length.

Finally we note that the description of pulse spreading given by Eq. (3-2) is the simplest of a number of possibilities, which includes the r.m.s. width of the impulse response described in Section 4-20.

3-2 Clad power-law profiles

It is possible to reduce pulse spreading from its value for the step profile by grading the core. We recall from Eq. (1-13) that the velocity along a ray is

$c/n(x)$, where $n(x)$ is the core refractive-index profile. Hence, the smaller the index, the higher the velocity becomes. Clearly, if we can arrange for those rays with trajectories that extend farther from the axis to pass through regions with smaller index values, we can equalize transit times for different rays. This compensation scheme exactly equalizes the transit times of all rays on the planar waveguide with a hyperbolic secant profile [2], as we showed in Section 1-12. However, on a fiber with the same profile, only the meridional-ray transit times are equalized. *There is no known profile which equalizes transit times for all rays both skew and meridional.* Accordingly, the clad power-law profiles, which have transit times independent of skewness [1,3,4], as we showed in Section 1-13, are of great practical importance for fibers.

Optimum profile

The clad power-law profiles for planar waveguides are defined by Eq. (1-59) and illustrated in Fig. 1-10. Here we determine which of these profiles, i.e. the value of q , gives minimal pulse spreading. Unlike the step-profile waveguide, it is not immediately obvious from the geometry of the sinusoidal-like ray paths

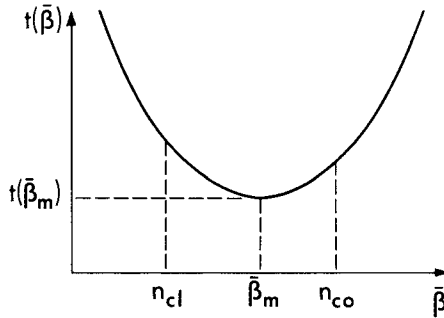


Fig. 3-2 Variation of the transit time t with $\bar{\beta}$ on a power-law profile waveguide.

of Fig. 1-8 and the profile grading, which paths correspond to the maximum and minimum transit times for each profile. The transit time for a bound ray is given by Table 1-1, page 19, in terms of the ray invariant $\bar{\beta}$ and the profile exponent q by

$$t(\bar{\beta}) = \frac{z}{c} \frac{n_{co}}{q+2} \left\{ q \frac{n_{co}}{\bar{\beta}} + 2 \frac{\bar{\beta}}{n_{co}} \right\}; \quad n_{cl} < \bar{\beta} \leq n_{co}. \quad (3-5)$$

If we plot $t(\bar{\beta})$ as a function of $\bar{\beta}$ for an arbitrary value of q , we obtain the characteristic parabola-like dependence in Fig. 3-2. The minimum transit time occurs at $\bar{\beta} = \bar{\beta}_m$ for a given value of q , where by differentiation

$$t(\bar{\beta}_m) = \frac{z}{c} \frac{(8q)^{1/2}}{q+2} n_{co}; \quad \bar{\beta}_m = \left(\frac{q}{2} \right)^{1/2} n_{co}. \quad (3-6)$$

There are three cases to consider because $\bar{\beta}_m$ will not always lie in the range of $\bar{\beta}$ for bound rays in Eq. (3-5). The maximum and minimum transit times, t_{\max} and t_{\min} , respectively, in each case are deduced from Fig. 3-2, and the corresponding pulse width t_d is given by

$$t_d = t_{\max} - t_{\min} = t(n_{cl}) - t(n_{co}); q \geq 2, \quad (3-7a)$$

$$= \sup \left\{ \begin{array}{l} t(n_{cl}) - t(\bar{\beta}_m) \\ t(n_{co}) - t(\bar{\beta}_m) \end{array} \right\}; \quad 2 - 4\Delta \leq q \leq 2, \quad (3-7b)$$

$$= t(n_{co}) - t(n_{cl}); \quad 0 < q \leq 2 - 4\Delta, \quad (3-7d)$$

for each value of q , where sup denotes the larger of the two expressions. The value $q = q_{\text{opt}}$ which minimizes the dispersion t_d , can be found either by formal differentiation or by the following simple argument. If we substitute for $t(\bar{\beta})$ from Eqs. (3-5) and (3-6) it is easy to verify that t_d increases with increasing values of q in Eqs. (3-7a) and (3-7b), and increases with decreasing values of q in Eqs. (3-7c) and (3-7d). The minimum value of t_d must therefore occur when Eqs. (3-7b) and (3-7c) are equal. Either way we find that this occurs when [3,4]

$$q_{\text{opt}} = 2(1 - 2\Delta)^{1/2} \cong 2 - 2\Delta \cong 2 - \theta_c^2, \quad (3-8)$$

with a corresponding minimum pulse spread

$$t_d = \frac{z}{c} \frac{(n_{co}^{1/2} - n_{cl}^{1/2})^2}{n_{co} + n_{cl}} n_{co} \cong \frac{z}{c} \frac{\Delta^2}{8} n_{co} \cong \frac{z}{c} \frac{\theta_c^4}{32} n_{co}. \quad (3-9)$$

The approximations in these equations are for weakly guiding fibers and paraxial rays. Hence *the optimum profile is close to parabolic*. The pulse width is a factor of $\Delta/8$, or $\theta_c^2/16$, times that for the step profile, in Eq. (3-3), and is therefore considerably reduced. Since $1/t_d$ is one measure of the information-carrying capacity of a waveguide, we deduce that capacity is increased by a factor of $8/\Delta$, or $16/\theta_c^2$. We plot t_d of Eq. (3-7) as the normalized time ct_d/zn_{co} against q , corresponding to the solid curve in Fig. 3-3, for $\Delta = 0.01$ or $\theta_c \cong 0.14$. There is a cusp at q_{opt} , which means that *ray dispersion is very sensitive to small variations about q_{opt}* . For example, when $q = q_{\text{opt}} \pm \Delta$, the pulse width increases by a factor of nearly 10. The normalized pulse width for a step profile with the same value of Δ is included for comparison.

RAY DISPERSION IN FIBERS

Pulse spreading in fibers is investigated in exactly the same manner as for planar waveguides. The added complication is that we must include skew rays

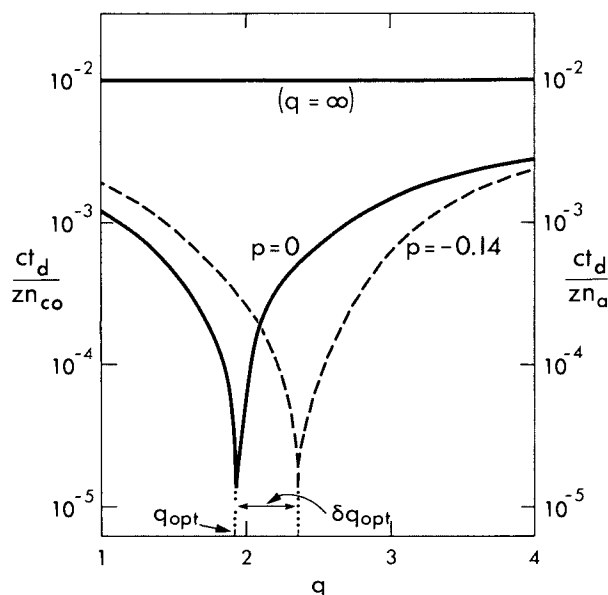


Fig. 3-3 The solid curve is the normalized pulse width ct_d/zn_{co} of Eq. (3-7) for clad power-law profiles as a function of q , and the horizontal line is the corresponding value of Eq. (3-2) for the step profile. When the fiber materials are dispersive, the dashed curve plots the normalized pulse width ct_d/zn_a , which shifts the optimum profile exponent from $q_{opt} \cong 1.98$ to $q_{opt} + \delta q_{opt} \cong 2.26$, assuming weak guidance [4]. For all three plots $\Delta = 0.01$, or $\theta_c \cong 0.14$.

as well as meridional rays. We showed in Chapter 2 that meridional rays have the same properties as rays on planar waveguides, and therefore have the same transit times, whereas transit times for skew rays generally depend on both ray invariants $\bar{\beta}$ and \bar{l} . However, we recall from Table 2-1, page 40, that the transit times for skew rays on step and clad power-law profile fibers are independent of \bar{l} and are therefore identical to the corresponding meridional-ray transit times. Consequently, ray dispersion on the step-profile fiber is given by the same expressions as for the step-profile planar waveguide, i.e. by Eqs. (3-2) and (3-3). Similarly, the optimum exponent and minimum pulse spread for clad power-law profile fibers are given by the corresponding solutions for the planar waveguide in Eqs. (3-8) and (3-9).

It is clear from the discussion at the beginning of Section 3-2 that there is no ray dispersion on the planar waveguide with a hyperbolic secant profile. However, on the fiber with the same profile, ray dispersion is no longer zero. There is no known profile which has zero ray dispersion for both skew and meridional rays.

3-3 Noncircular fibers

We showed in Section 2-13 that the transit time for a step-profile fiber is independent of the cross-sectional geometry. Consequently Eqs. (3-2) and (3-3) give the ray dispersion for step-profile fibers of arbitrary cross-section. We also found in Section 2-13 that the ray transit time for the noncircular, clad power-law profiles of Eq. (2-55) is identical to the transit time for the symmetric, clad power-law profiles in Table 2-1, page 40, i.e. dependent on $\bar{\beta}$ only. Thus Eqs. (3-8) and (3-9) also give the optimum profile and minimum pulse spread for those noncircular profiles [5], which includes the clad parabolic-profile fiber of elliptical cross-section. In other words, *ray dispersion on step-profile fibers of arbitrary cross-section and clad power-law profile fibers of noncircular cross-section is also given by the corresponding solutions for planar waveguides.*

MATERIAL AND PROFILE DISPERSION

The analysis of pulse spreading so far in this chapter has assumed that the waveguide materials are nondispersive. Here we allow for the effects of dispersive materials which constitute the waveguide or fiber. Although material dispersion by itself is usually small, we show in Section 3-8 that it can have a dramatic effect on pulse spreading when combined with ray dispersion.

3-4 Material dispersion

Sources of light which are nominally monochromatic, with wavelength λ , have a small inherent spread $\delta\lambda$ in wavelength associated with them, and practical waveguides are composed of materials that are dispersive. Dispersiveness is described by the variation – usually very slight – of the refractive-index profile with wavelength, e.g. $n = n(r, \lambda)$ for circular fibers. Consequently, *rays excited at different wavelengths and following the same path will propagate at different speeds.* This leads to a form of pulse spreading quite apart from ray dispersion, as we can demonstrate with a simple example. Consider rays propagating parallel to the axis over length z of a step-profile waveguide with core index $n_{co}(\lambda)$. The transit time at wavelength λ is given by Eq. (1-17) in terms of the group index n_g of Eq. (1-16). When $\theta_z = 0$, we have $\bar{\beta} = n_{co}$ and consequently

$$t = \frac{z}{c} \left\{ n_{co}(\lambda) - \lambda \frac{dn_{co}(\lambda)}{d\lambda} \right\}. \quad (3-10)$$

Since $\delta\lambda \ll \lambda$, the pulse width t_d is given approximately by

$$t_d \cong \left| \frac{\partial t}{\partial \lambda} \right| \delta\lambda = \frac{z\lambda}{c} \left| \frac{d^2 n_{co}(\lambda)}{d\lambda^2} \right| \delta\lambda, \quad (3-11)$$

and pulse spreading varies with the second derivative of the profile [6]. In practice, however, this spread is small compared to the profile dispersion discussed below.

3-5 Profile dispersion

We can now investigate how material dispersion and ray dispersion interact to influence pulse spreading. It is convenient to use *profile dispersion* to describe the combination of the two effects [3]. Surprisingly, we find that pulse spreading is significantly affected by material dispersion, even when the second derivative $\partial^2 n / \partial \lambda^2$ is zero. This is because the component $d\Delta/d\lambda$ of the first derivative $\partial n / \partial \lambda$ is of crucial importance in the interplay between the two forms of dispersion, as we show in the example of Section 3-8 below. We first consider the specific dependence of the profile on wavelength. Although we illustrate the principles of profile dispersion using fibers in the following sections, since fibers are of major practical importance, we could just as easily use planar waveguides.

3-6 Linear dispersion

When the fiber materials are dispersive, it has been found experimentally that, to a first approximation, we may assume a model for the profile of the form [7,8]

$$n^2(r, \lambda) = n_{co}^2(\lambda) \{1 - 2\Delta(\lambda)f(r)\}, \quad (3-12)$$

in which the *profile variation* $f(r)$ is independent of wavelength. This approximation is sometimes called *linear dispersion*, because, in the weak-guidance approximation ($\Delta \ll 1$), the group index is a linear function of n . If we set $n \cong n_{co}(\lambda) \{1 - \Delta(\lambda)f(r)\}$ in Eq. (2-33a), it is straightforward to show that

$$n_g = a(\lambda)n + b(\lambda), \quad (3-13)$$

where a and b are functions of λ only. We adopt this model in the examples.

3-7 Example: Step-profile fiber

The core and cladding indices of the step-profile fiber are $n_{co}(\lambda)$ and $n_{cl}(\lambda)$, respectively, when the materials are dispersive. We showed in Section 2-5 that the ray transit time in this situation is identical to the planar-waveguide expression of Eq. (1-17), which involves the group index n_g of Eq. (1-16). By analogy with the derivation in Section 3-1, we deduce that the pulse spread is given by

$$t_d(\lambda) = \frac{z}{c} n_{co}(\lambda) \left\{ \frac{n_{co}(\lambda)}{n_{cl}(\lambda)} - 1 \right\} \left[1 - \frac{\lambda}{n_{co}(\lambda)} \frac{dn_{co}(\lambda)}{d\lambda} \right], \quad (3-14a)$$

$$\cong \frac{z}{c} n_{co}(\lambda) \Delta(\lambda) \left[1 - \frac{\lambda}{n_{co}(\lambda)} \frac{dn_{co}(\lambda)}{d\lambda} \right], \quad (3-14b)$$

where the approximate result is valid in the weak-guidance approximation, when $\Delta(\lambda) \cong 1 - n_{\text{cl}}(\lambda)/n_{\text{co}}(\lambda) \ll 1$. We can then identify the first term within the square brackets of Eq. (3-14b) with ray dispersion and the second term with material dispersion.

3-8 Example: Clad power-law profile fibers

It follows from Eq. (3-12) that, in the presence of material dispersion, these profiles must have the following forms to satisfy the linear-dispersion criterion

$$n^2(r, \lambda) = n_{\text{co}}^2(\lambda) \left\{ 1 - 2\Delta(\lambda) \left(\frac{r}{\rho} \right)^q \right\}; \quad 0 \leq r \leq \rho, \quad (3-15a)$$

$$= n_{\text{cl}}^2(\lambda) = n_{\text{co}}^2(\lambda) \{1 - 2\Delta(\lambda)\}; \quad \rho \leq r < \infty, \quad (3-15b)$$

where the profile exponent q is independent of λ . The transit time in this situation is determined from Eq. (2-33b). If we substitute Eq. (3-15a) into the group index of Eq. (2-33a), then the expression for L_m in Eq. (2-33b) can be rearranged as

$$L_m = \frac{n_a n_{\text{co}}(\lambda)}{\bar{\beta}} z_p - 2n_a n_{\text{co}}(\lambda) \Delta(\lambda) (2-p) \int_{r_{\text{ic}}}^{r_{\text{tp}}} \frac{(r/\rho)^q}{g(r)^{1/2}} dr, \quad (3-16)$$

where $\bar{\beta}$, z_p , r_{tp} , r_{ic} and $g(r)$ depend implicitly on λ by replacing $n(r)$ with $n(r, \lambda)$ in their definitions. The on-axis group index n_a and the measure of off-axis material dispersion p are functions of wavelength only defined by

$$n_a = n_{\text{co}}(\lambda) - \lambda \frac{dn_{\text{co}}(\lambda)}{d\lambda}; \quad p = \frac{n_{\text{co}}(\lambda)}{n_a} \frac{\lambda}{\Delta(\lambda)} \frac{d\Delta(\lambda)}{d\lambda}. \quad (3-17)$$

The integral in Eq. (3-16) follows from Eq. (2-47), and on substituting into Eq. (2-33b), the ray transit time is given by

$$t = \frac{z}{c} \frac{n_a}{q+2} \left\{ (p+q) \frac{n_{\text{co}}}{\bar{\beta}} + (2-p) \frac{\bar{\beta}}{n_{\text{co}}} \right\}; \quad n_{\text{cl}}(\lambda) < \bar{\beta} \leq n_{\text{co}}(\lambda). \quad (3-18)$$

Thus, the ray transit time is independent of skewness and is identical to the corresponding planar waveguide expression within the linear-dispersion approximation to material dispersion. It is implicit that p is small in these expressions.

Optimum profile

The profile which minimizes pulse spreading is derived from Eq. (3-18) using the procedure described in Section 3-2. Hence the minimum transit time and the corresponding ray invariant are found to be

$$t(\bar{\beta}_m) = \frac{z}{c} \frac{2n_a}{q+2} (p+q)^{1/2} (2-p)^{1/2}; \quad \bar{\beta}_m = \left\{ \frac{p+q}{2-p} \right\}^{1/2} n_{\text{co}}. \quad (3-19)$$

The optimum profile $q = \bar{q}_{\text{opt}}$ is readily shown to be [4]

$$\bar{q}_{\text{opt}} = 2(1 - 2\Delta)^{1/2} - p\{1 + (1 - 2\Delta)^{1/2}\} \cong 2(1 - p) - \Delta(2 - p), \quad (3-20)$$

and the corresponding minimum pulse spread is given by

$$\bar{t}_d = \frac{z(n_{\text{co}}^{1/2} - n_{\text{cl}}^{1/2})^2}{c(n_{\text{co}} + n_{\text{cl}})} n_a \cong n_a \frac{z\Delta^2}{c8} \cong n_a \frac{z\theta_c^4}{c32}, \quad (3-21)$$

where $n_{\text{co}} = n_{\text{co}}(\lambda)$, $n_{\text{cl}} = n_{\text{cl}}(\lambda)$ and the approximate expressions apply within the weak-guidance approximation, or, equivalently, for paraxial rays. Thus, although the dispersion minimum is independent of p , it varies with wavelength through the implicit dependence of Δ and n_a on λ .

Sensitivity of the dispersion minimum

The slight change in value of the optimum profile exponent from q_{opt} to \bar{q}_{opt} due to profile dispersion is given approximately by $\delta q_{\text{opt}} = -2p$, assuming the weak-guidance expressions in Eqs. (3-8) and (3-20). Although δq_{opt} is small, it nevertheless has a dramatic effect on pulse dispersion. We calculate the ray dispersion $t_d = t_{\text{max}} - t_{\text{min}}$ from Eq. (3-18) by analogy with Eq. (3-7), and plot the normalized pulse width ct_d/n_a against q as the dashed curve in Fig. 3-3, assuming $p = -0.14$ and $\Delta = 0.01$ [4]. The solid curve, $p = 0$, ignores material dispersion. Thus, the effect of profile dispersion is to shift the cusp at the optimum profile distance δq_{opt} as shown. However, *the change in pulse width from the solid to the dashed curves in the neighborhood of $q = q_{\text{opt}}$ is almost two orders of magnitude*. In practice, it is often true that $|p| \gg \Delta$, in which case profile dispersion dominates ray dispersion in determining the optimum profile.

3-9 Nonlinear dispersion

If the profile $n(r, \lambda)$ does not satisfy the linear-dispersion condition of Eq. (3-13), then we have *nonlinear dispersion*. The separable term $2\Delta(\lambda)f(r)$ in Eq. (3-12) is replaced by $F(\lambda, r)$, which is not expressible in separable form, e.g. the clad power-law profiles of Eq. (3-15) when the exponent is wavelength dependent. The determination of the optimal profile is then a virtually intractable problem by analytical methods. However, if we make certain simplifying assumptions about the form of the transit time, we can pose the problem in a different and more tractable way.

We recall from Section 3-8, that in the case of linear dispersion the transit time of Eq. (3-18) for clad power-law profiles has a simple dependence on the invariant $\bar{\beta}$, which in turn leads directly to the optimum profile of Eq. (3-20).

When the dispersion is nonlinear, we assume a transit time with the same functional dependence on $\bar{\beta}$, which takes the form

$$t = \frac{z}{c} \left\{ A \frac{n_{co}}{\bar{\beta}} + B \frac{\bar{\beta}}{n_{co}} \right\}, \quad (3-22)$$

where A and B are independent of $\bar{\beta}$. Once A and B are prescribed, the optimum profile is therefore readily determined. The problem is to determine profiles whose transit times satisfy Eq. (3-22). Such profiles help provide flexibility in designing fibers. The detailed derivation is given elsewhere [9, 10], and shows that a sufficient condition for $F(\lambda, r)$ to lead to Eq. (3-22) is

$$r \frac{\partial F}{\partial r} + D \frac{n_{co}}{n_a} \lambda \frac{\partial F}{\partial \lambda} - 2(D-1)F = 0, \quad (3-23)$$

where n_a is defined in Eq. (3-17), and D is an arbitrary function of wavelength. The general solution of this equation is

$$F = \left(\frac{\lambda}{rn_{co}} \right)^2 G(\chi); \quad \chi = \frac{r}{\rho} \exp \left\{ - \int_0^\lambda \frac{n_a d\lambda}{\lambda D n_{co}} \right\}. \quad (3-24)$$

If the special case when G is a simple power, i.e. $G(\chi) = \chi^{q+2}$ with q constant, $F(\lambda, r)$ is separable and leads to a set of power-law profiles, similar to Eq. (3-15), with linear dispersion. An alternative solution of Eq. (3-23) expands F as a power series in r/ρ for each wavelength [11]. These solutions can be used to improve the minimum dispersion characteristics of fibers.

REFERENCES

1. Gloge, D. and Marcanti, E. A. J. (1973) Multimode theory of graded-core fibres, *Bell Syst. Tech. J.*, **52**, 1563-78.
2. Fletcher, A., Murphy, T. and Young, A. (1954) Solutions of two optical problems. *Proc. Roy. Soc.*, **A223**, 216-25.
3. Olshansky, R. and Keck, D. B. (1976) Pulse broadening in graded-index optical fibres. *Appl. Opt.*, **15**, 483-91.
4. Ankiewicz, A. and Pask, C. (1977) Geometric optics approach to light acceptance and propagation in graded index fibres. *Opt. Quant. Elect.*, **9**, 87-109.
5. Barrell, K. F. and Pask, C. (1979) Geometric optics analysis of non-circular graded-index fibres. *Opt. Quant. Elect.*, **11**, 237-51.
6. Jackson, J. D. (1967) *Classical Electrodynamics*, Wiley, New York, pp. 208-15.
7. Adams, M. J., Payne, D. N., Sladen, F. M. E. and Hartog, A. H. (1978) Wavelength-dispersive properties of glasses for optical fibres: the germania enigma. *Electron. Lett.*, **14**, 703-5.
8. Hammond, C. R. (1978) Silica-based binary glass system: wavelength dispersive properties and composition in optical fibres. *Opt. Quant. Elect.*, **10**, 163-70.

62 Optical Waveguide Theory

9. Marcatili, E. A. J. (1977) Modal dispersion in optical fibres with arbitrary numerical aperture and profile dispersion. *Bell Syst. Tech. J.*, **56**, 49–63.
10. Pask, C. (1978) On the derivations and interpretation of the Marcatili profile condition for optical fibres. *Electron. Lett.*, **14**, 13–15.
11. Olshansky, R. (1978) Optical waveguides with low pulse dispersion over an extended spectral range. *Electron. Lett.*, **14**, 330–1.

CHAPTER 4

Fiber illumination and pulse shape

Sources of illumination	65
4-1 Diffuse or Lambertian source	65
4-2 Collimated beam	66
Transmission across the endface	66
4-3 Reflection and refraction	67
4-4 Power transmission	68
Diffuse illumination	69
4-5 Total source power	69
4-6 Total bound-ray power	70
4-7 <i>Example: Step and clad power-law profiles</i>	71
4-8 Nonuniform illumination	72
Collimated-beam illumination	73
4-9 <i>Example: Step profile</i>	73
4-10 <i>Example: Graded profiles</i>	74
Lens illumination	74
4-11 Collimated beam	74
4-12 <i>Example: Intensity distribution</i>	75
4-13 <i>Example: Oblique incidence</i>	76
4-14 Diffuse source	76
4-15 <i>Example: Intensity distribution</i>	78
4-16 Partially diffuse source	79
Power distribution among bound rays	79
4-17 Derivation of the distribution function	79
4-18 Distribution function dependent on $\bar{\beta}$ only	82
4-19 <i>Example: Step and clad power-law profiles</i>	82
Impulse response	83
4-20 Ray transit times dependent on $\bar{\beta}$ only	84
4-21 <i>Example: Step profile</i>	85
4-22 <i>Example: Clad power-law profiles</i>	86
	63

4-23 Ray transit times dependent on both invariants	87
4-24 Material dispersion	88

References	88
-------------------	-----------

In the previous chapter we described pulse spreading by the maximum temporal width possible, $t_{\max} - t_{\min}$. Now we investigate pulse spreading more closely by examining the shape of the pulse as it propagates, i.e. the distribution of energy within the pulse, or *impulse response*. We derive the pulse shape at time t due to an impulse of initially zero width, from which we can describe the response of a pulse of arbitrary initial shape by convolution. The analysis includes only bound rays, since they characterize the transmission properties of long fibers.

Multimode fibers are typically illuminated by diffuse sources. For such sources, the impulse response of a step or clad parabolic profile is a virtually rectangular pulse of width $t_{\max} - t_{\min}$. Hence, the maximum temporal width is an accurate description of the response for these cases. Nevertheless, we emphasize that pulse shape is acutely sensitive to small deviations from the parabolic profile.

In order to determine pulse shape, it is necessary to study the illumination and light acceptance properties of a fiber. Accordingly, we consider how light power emitted from various sources enters the fiber core and is distributed among the various bound-ray directions. The material of this chapter is required in Chapter 8 to determine the impulse response of short fibers, when a significant fraction of power is carried by leaky rays, and also in Chapter 6, where we show how core and cladding absorption can greatly distort the impulse response from the rectangular shapes mentioned above.

Ray tubes

We discussed the characteristics of individual ray paths in Chapters 1 and 2. In

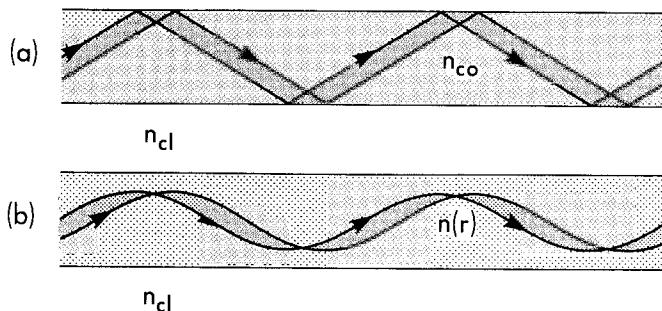


Fig. 4-1 Ray tubes on fibers with (a) a step profile and (b) a graded profile.

this chapter we determine the distribution of power among the various ray directions. Since the power of an individual ray is undefined, it is useful to introduce the concept of a *ray tube*, i.e. a tube of rays of infinitesimal cross-section, with each ray propagating in the same direction, or, equivalently, having the same values of the ray invariants β and \bar{l} . Tubes for step- and graded-profile fibers are illustrated in Fig. 4-1. This concept is the ray analogy of the flux tube of electromagnetic theory [1], and is discussed in more detail in Section 35-3. Light power flows parallel to the ray direction and the total power flow within the tube is constant along its length. *Throughout the rest of Part I, we take the word rays to mean ray tubes whenever discussing power.*

SOURCES OF ILLUMINATION

A source is specified by the distribution of power among all the ray directions emitted from each differential element dA of its surface area. For example, the source in Fig. 4-2 emits light within a cone of half-angle θ_s . Light emitted at

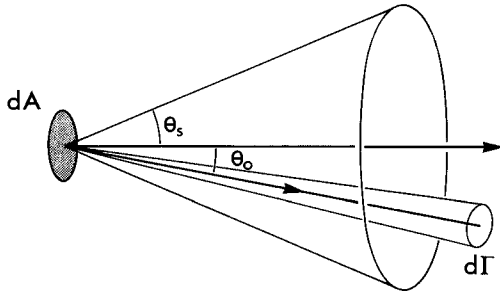


Fig. 4-2 Elemental source area dA emits light into solid angle $d\Gamma$ within a cone of half-angle θ_s .

angle θ_0 to the normal has *intensity* $I(\theta_0)$ per unit solid angle per unit area of source. Thus the element of power dP radiated is given by

$$dP = I(\theta_0)d\Gamma dA, \quad 0 \leq \theta_0 \leq \theta_s; \quad dP = 0, \quad \theta_s \leq \theta_0 \leq \pi/2, \quad (4-1)$$

where $d\Gamma$ is the element of solid angle as shown. We now define the two types of source used throughout Part I.

4-1 Diffuse or Lambertian source

A *diffuse* or *Lambertian source* [2] is one where each differential area dA of source area emits light in all directions, i.e. $\theta_s = \pi/2$ in Eq. (4-1). The cross-section of such a source is illustrated schematically in Fig. 4-3(a). This is the most typical source in practice and approximates the output of a light-emitting

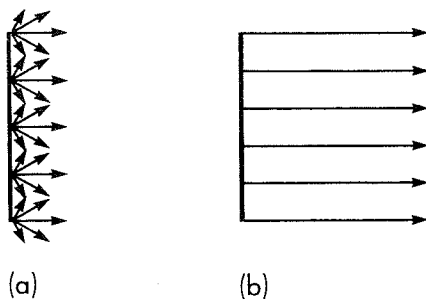


Fig. 4-3 Cross-sections of (a) a diffuse or Lambertian source, and (b) a collimated beam.

diode (LED). The intensity distribution is given by [2]

$$I(\theta_0) = I_0 \cos \theta_0; \quad 0 \leq \theta_0 \leq \pi/2, \quad (4-2)$$

where I_0 is a constant. However the LED can also be nonuniform, with the light output decreasing towards the boundaries of the source. In such cases I_0 depends on the cylindrical radius r from the center of the source, assumed axisymmetric, and can be approximated by a Gaussian distribution

$$I_0(r) = A \exp(-\alpha r^2 / \rho_s^2), \quad (4-3)$$

where ρ_s is the source radius and A , α are positive constants.

Partially diffuse source

When the directions of light emission do not occupy the full range of values of θ_0 in Eq. (4-2), i.e. $0 \leq \theta_0 \leq \theta_s < \pi/2$ as illustrated in Fig. 4-2, the source is called a *partially diffuse source*.

4-2 Collimated beam

A source of finite cross-section which radiates along its axial direction only produces a *collimated beam*, as shown in Fig. 4-3(b). Each differential element dA of the source area emits light in the direction $\theta_s = 0$ of Fig. 4-2. For a uniform beam, the intensity of Eq. (4-1) is constant I_0 over the beam cross-section and approximates the output from a laser.

TRANSMISSION ACROSS THE ENDFACE

We now determine the behavior of a ray as it passes from the source, across the fiber endface and into the core. If the refractive index n_0 of the medium

containing the source differs from the core index, we must first correct for both the change of ray direction due to refraction and the loss of power by reflection.

4-3 Reflection and refraction

The source is located in a uniform medium of refractive index n_0 , and is assumed to be sufficiently large that it fully illuminates at least the core cross-section of the fiber endface, as is normally the case in practice. A ray from the source is incident on the endface $z = 0$ at Q in Fig. 4-4, and makes angle θ_0 with the normal QN, or axial, direction. The polar coordinates of Q on the endface are (r, ϕ) relative to the x -axis. We consider only rays incident over the core; a ray incident over the cladding cannot become a bound ray in the core.

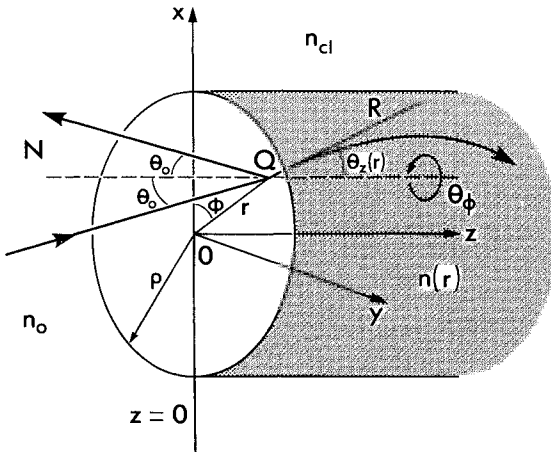


Fig. 4-4 Reflection and refraction of a source ray at Q on the fiber endface. Polar coordinates (r, ϕ) define the position of Q, and the projection of the ray path onto the endface makes angle θ_ϕ with the azimuthal direction at Q.

Snell's laws

For convenience we assume that $n_0 < n_{cl}$, where the uniform cladding index n_{cl} is the smallest value of the fiber profile $n(r)$. This condition is usually satisfied since the most common source medium is air, for which $n_0 = 1$. It also ensures that the incident ray in Fig. 4-4 is partly reflected at angle θ_0 and partly refracted, or transmitted, for all values of θ_0 . The transmission angle $\theta_z(r)$ is the angle between the normal QN and the tangent QR at $z = 0$ to the ray trajectory in the core of the fiber, and is related to θ_0 by Snell's law

$$n_0 \sin \theta_0 = n(r) \sin \theta_z(r); \quad 0 \leq \theta_0 \leq \pi/2. \quad (4-4)$$

The initial position and direction of the core path determine the ray invariant $\bar{\beta}$ by substituting Eq. (4-4) into Eq. (2-16). This leads to the expression in Eq. (4-5). We also deduce from Snell's laws that since the source ray, transmitted ray and normal are coplanar, the skewness of the ray relative to the fiber axis is unchanged on crossing the endface. If θ_ϕ is the angle between the projection of the incident ray onto the endface and the azimuthal, or ϕ , direction in Fig. 4-4, then the second ray invariant \bar{l} for the path in the core is obtained by substituting Eq. (4-4) into Eq. (2-17) with $\theta_\phi(r) = \theta_\phi$. Hence

$$\bar{\beta} = \{n^2(r) - n_0^2 \sin^2 \theta_0\}^{1/2}; \quad \bar{l} = \frac{r}{\rho} n_0 \sin \theta_0 \cos \theta_\phi, \quad (4-5)$$

so that each source ray defines the values of the invariants describing the continuation of its path within the fiber core.

Maximum angle of incidence

We define $\theta_m(r)$ to be the maximum value of θ_0 in Fig. 4-4 for which a source ray can propagate in the fiber core as a bound ray. The range of values of $\theta_z(r)$ for a ray to be bound is given by Eq. (2-30), assuming that $n(r)$ decreases monotonically from the fiber axis to the interface. By setting $\theta_0 = \theta_m(r)$ in Eq. (4-4), we deduce that $\theta_m(r)$ satisfies

$$n_0 \sin \theta_m(r) = n(r) \sin \theta_c(r) = \{n^2(r) - n_{cl}^2\}^{1/2}, \quad (4-6)$$

where $\theta_c(r)$ is the complement of the local critical angle defined by Eq. (2-29). For the step profile, $n(r)$ is replaced by n_{co} and $\theta_c(r)$ by θ_c . Within the paraxial approximation $\theta_c(r) \ll 1$, and thus $\theta_m(r) \cong n(r)\theta_c(r)/n_0$.

4-4 Power transmission

The index n_0 of the source medium usually differs from that of the core, and hence not all of the source power can be transmitted into the core. However, a maximum of about 4 per cent of source power is reflected from the endface in practice, as we now show, so that we can usually neglect this effect. If the fiber has a step profile, the fraction T of power transmitted into the core is given by the classical Fresnel coefficient for reflection at a planar dielectric interface. Since the fiber is multimoded, the electromagnetic fields behave like plane waves in any small region of the endface, and plane-wave arguments are applicable, as discussed in Section 35-3. For simplicity we restrict attention to the weak-guidance, or paraxial approximation, when bound rays propagate virtually parallel to the fiber axis, i.e. normal to the endface. The fraction of power transmitted into the core when $\theta_0 \cong 0$ is given by the first expression in

Eq. (35-21) with n_{cl} replaced by n_0 . Hence [3]

$$T = 4n_0 n_{co} / (n_0 + n_{co})^2. \quad (4-7)$$

This result holds approximately for graded-profile fibers as well, since $n(r) \cong n_{co}$. In practice $n_{co} \cong 1.5$, $n_0 \cong 1$, and thus a minimum of about 96% of source power is transmitted into the core. Throughout the rest of this chapter we neglect this slight loss, but it can be accounted for by replacing the intensity $I(\theta_0)$ of Eq. (4-1) by $TI(\theta_0)$.

DIFFUSE ILLUMINATION

We can now calculate the source power carried by bound rays when the fiber is illuminated by the diffuse source. In this part of the chapter we determine the total source power, the total bound-ray power and the radial distribution of bound-ray power over the core cross-section. Later in the chapter we show how to derive the distribution of power among the various bound-ray directions. We assume that the source of Fig. 4-3(a) is placed against the fiber endface in Fig. 4-4, and its surface covers at least the core cross-section. Only the portion of the source within the core cross-section can excite bound rays, so we ignore any effects due to the source outside of this region. The excitation of leaky rays by sources is examined in Chapter 8.

The element of power dP radiated into solid angle $d\Gamma$ by area dA of the source in the medium of refractive index n_0 is given by Eqs. (4-1) and (4-2). In Fig. 4-4, the angles (θ_0, θ_ϕ) are spherical polar angles relative to the normal QN and (r, ϕ) are polar coordinates relative to the fiber axis. Hence [4-6]

$$dP = I_0 \cos \theta_0 dA d\Gamma \quad dA = r dr d\phi; \quad d\Gamma = \sin \theta_0 d\theta_0 d\theta_\phi, \quad (4-8)$$

where the range of source-ray directions satisfies $0 \leq \theta_0 \leq \pi/2$, $0 \leq \theta_\phi \leq 2\pi$ and the range of positions on the endface satisfies $0 \leq r \leq \rho$, $0 \leq \phi \leq 2\pi$.

4-5 Total source power

The total power P_{tot} radiated by the source in all directions over the area of the core cross-section in Fig. 4-4 is obtained by integrating dP of Eq. (4-8) over the complete range of values of each of the four variables given above. Accordingly [6]

$$P_{tot} = \int_0^\rho r dr \int_0^{2\pi} d\phi \int_0^{\pi/2} d\theta_0 \int_0^{2\pi} I_0 r \sin \theta_0 \cos \theta_0 d\theta_\phi. \quad (4-9a)$$

The intensity is assumed to depend only on r , so on performing the remaining

integrations we obtain

$$P_{\text{tot}} = 2\pi^2 \int_0^\rho r I_0 dr. \quad (4-9b)$$

When the illumination is uniform, I_0 is constant and therefore

$$P_{\text{tot}} = \pi^2 \rho^2 I_0. \quad (4-10)$$

Only part of the total source power is transmitted to bound rays; the rest excites leaky rays, which is discussed in Chapter 8. If we denote the amount of source power transmitted to all bound rays by P_{br} , then the *source efficiency* \mathcal{E} is defined by

$$\mathcal{E} = P_{\text{br}}/P_{\text{tot}} = P_{\text{br}}/(\pi^2 \rho^2 I_0), \quad (4-11)$$

which ignores the slight power loss at the endface, discussed in Section 4-4. For weakly guiding fibers, we anticipate that \mathcal{E} will be small because of the narrow range of bound-ray directions.

4-6 Total bound-ray power

The amount of source power carried by bound rays, P_{br} , is found by integrating Eq. (4-8) over the complete ranges of values of ϕ , r and θ_ϕ given below Eq. (4-8), and the range of values of θ_0 corresponding to bound rays within the fiber, i.e. $0 \leq \theta_0 \leq \theta_m(r)$, where $\theta_m(r)$ was derived in Section 4-3. Hence

$$P_{\text{br}} = I_0 \int_0^{2\pi} d\phi \int_0^\rho r dr \int_0^{2\pi} d\theta_\phi \int_0^{\theta_m(r)} \sin \theta_0 \cos \theta_0 d\theta_0. \quad (4-12)$$

Substituting for $\theta_m(r)$ from Eq. (4-6) we obtain by straightforward integration

$$P_{\text{br}} = 2\pi^2 \frac{I_0}{n_0^2} \int_0^\rho r S(r) dr; \quad S(r) = n^2(r) - n_{\text{cl}}^2, \quad (4-13)$$

where $S(r)$ is the square of the local numerical aperture, or the *profile shape*, i.e. the variation of $n^2(r)$ above its uniform cladding value n_{cl}^2 . Apart from a factor $\pi I_0/n_0^2$ associated with the source intensity and source medium, P_{br} varies with the *profile volume* Ω , which we define to be the volume obtained by rotating the profile shape about the fiber axis, i.e.

$$P_{\text{br}} = \pi \frac{I_0}{n_0^2} \Omega; \quad \Omega = 2\pi \int_0^\rho r S(r) dr = 2\pi \int_0^\rho r \{n^2(r) - n_{\text{cl}}^2\} dr. \quad (4-14)$$

An immediate consequence of this definition is that *fibers with equal profile volumes carry identical total bound-ray power when illuminated by a diffuse source*. It also follows from Eq. (4-13) that *the bound-ray power density per unit area of cross-section at radius r is proportional to the profile shape*. If $P(r)$ denotes this quantity, then

$$\boxed{P(r) = \pi \frac{I_0}{n_0^2} S(r);} \quad P_{\text{br}} = \int_{A_{\text{co}}} P(r) dA, \quad (4-15)$$

where A_{co} is the core cross-sectional area. We now consider examples.

4-7 Example: Step and clad power-law profiles

The total bound-ray power excited on a step-profile fiber is obtained by setting $n(r) = n_{\text{co}}$ in Eq. (4-13). Hence

$$P_{\text{br}} = 2I_0(\pi\rho n_{\text{co}}/n_0)^2 \Delta = I_0(\pi\rho n_{\text{co}}/n_0)^2 \sin^2 \theta_c, \quad (4-16)$$

using the definitions at the front of the book. Thus P_{br} is proportional to the square of the numerical aperture of the fiber, which provides a measure of the light-gathering capacity. The source efficiency follows from Eqs. (4-11) and (4-16) as

$$\mathcal{E} = 2(n_{\text{co}}/n_0)^2 \Delta = (n_{\text{co}}/n_0)^2 \sin^2 \theta_c \cong (n_{\text{co}}/n_0)^2 \theta_c^2, \quad (4-17)$$

where the approximation applies to the weak-guidance, or paraxial approximation, when bound rays carry only a small fraction of source power since $\theta_c \ll 1$.

If we substitute the clad power-law profiles of Table 2-1, page 40, for $n(r)$ in Eq. (4-13), the total bound-ray power due to diffuse illumination is readily shown to be [6]

$$P_{\text{br}} = \frac{2q}{q+2} I_0 \frac{(\pi\rho n_{\text{co}})^2}{n_0^2} \Delta = \frac{q}{q+2} I_0 \frac{(\pi\rho n_{\text{co}})^2}{n_0^2} \sin^2 \theta_c, \quad (4-18)$$

and the corresponding expressions to Eq. (4-17) for the source efficiency are

$$\mathcal{E} = \frac{2q}{q+2} \frac{n_{\text{co}}^2}{n_0^2} \Delta = \frac{q}{q+2} \frac{n_{\text{co}}^2}{n_0^2} \sin^2 \theta_c \cong \frac{q}{q+2} \frac{n_{\text{co}}^2}{n_0^2} \theta_c^2. \quad (4-19)$$

Thus both P_{br} and \mathcal{E} are smaller than the corresponding expressions for the step profile by a factor of $q/(q+2)$. In particular, *the clad parabolic-profile fiber ($q = 2$) accepts only half as much bound-ray power as the step-profile fiber ($q = \infty$)*.

Equal-volume profiles

The clad power-law profiles defined in Table 2-1, page 40, do not have the same profile volume as the step profile. However, we can make these volumes equal by redefining the core radius for each value of the exponent. Accordingly we replace ρ by ρ_c , substitute $n(r)$ into Eq. (4-14), and equate Ω to the volume $\pi\rho^2(n_{\text{co}}^2 - n_{\text{cl}}^2)$ of the step profile. We

deduce that

$$\rho_e = \{(q+2)/q\}^{1/2} \rho. \quad (4-20)$$

The total bound-ray power on each fiber with the modified clad power-law profile is given by Eq. (4-18) with ρ replaced by ρ_e . If we then substitute the above result for ρ_e , we verify a result of Section 4-6, namely that the modified clad power-law profile fibers carry the same bound-ray power as the step-profile fiber when illuminated by a diffuse source.

4-8 Nonuniform illumination

So far we have assumed a uniform intensity I_0 over the source. Here we examine the effect of a nonuniform diffuse source on total bound-ray power, using the Gaussian distribution of Eq. (4-3) for intensity [6]. The total power emitted by the source is found by substituting Eq. (4-3) into Eq. (4-9b) with $\rho_s = \rho$, and gives

$$P_{\text{tot}} = \pi^2 \rho^2 A (1 - e^{-\alpha}) / \alpha. \quad (4-21)$$

When the fiber has a step profile, the total bound-ray power is given by Eq. (4-12) with I_0 replaced by A and a factor $\exp(-\alpha r^2 / \rho^2)$ introduced into the integrand of the radial integration. On evaluating the integrals we obtain

$$P_{\text{br}} = 2A \frac{(\pi \rho n_{\text{co}})^2}{n_0^2} \frac{1 - e^{-\alpha}}{\alpha} \Delta = A \frac{(\pi \rho n_{\text{co}})^2}{n_0^2} \frac{1 - e^{-\alpha}}{\alpha} \sin^2 \theta_c, \quad (4-22)$$

and consequently the source efficiency is

$$\mathcal{E} = \frac{P_{\text{br}}}{P_{\text{tot}}} = 2 \frac{n_{\text{co}}^2}{n_0^2} \Delta = \frac{n_{\text{co}}^2}{n_0^2} \sin^2 \theta_c, \quad (4-23)$$

which is unaltered from its value in Eq. (4-17) by the source nonuniformity.

Clad parabolic-profile fiber

This profile is given by the $q = 2$ clad parabolic-profile in Table 2-1, page 40. The total bound-ray power and source efficiency are obtained in an analogous manner to the step-profile expressions above. Hence

$$P_{\text{br}} = 2A \frac{(\pi \rho n_{\text{co}})^2}{n_0^2} \frac{e^{-\alpha} + \alpha - 1}{\alpha^2} \Delta; \quad \mathcal{E} = 2 \frac{n_{\text{co}}^2}{n_0^2} \frac{e^{-\alpha} + \alpha - 1}{\alpha (1 - e^{-\alpha})} \Delta. \quad (4-24)$$

Source efficiency is a minimum when $\alpha \rightarrow 0$, corresponding to a uniform source, and doubles as $\alpha \rightarrow \infty$, when only on-axis illumination occurs. However, although efficiency increases with increasing nonuniformity, bound-ray power decreases and is negligible as $\alpha \rightarrow \infty$.

COLLIMATED-BEAM ILLUMINATION

We consider the source of Section 4-2 which is so aligned that it emits a collimated beam at angle θ_0 to the fiber axis, as shown in Fig. 4-5. The collimated beam, as well as approximating the output of a laser, also provides insight into diffuse-source illumination, which can be regarded as a superposition of beams propagating at all angles. Only that part of the beam illuminating the core can excite bound rays, so we ignore any illumination of the cladding. It is intuitive that if the beam angle is too large then no bound rays will be excited. In fact, *bound rays are only excited if θ_0 does not exceed the maximum value of $\theta_m(r)$ over the core*, where $\theta_m(r)$ is defined by Eq. (4-6). We consider specific examples.

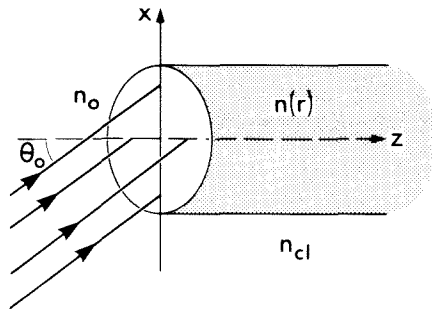


Fig. 4-5 Collimated beam incident at angle θ_0 to the fiber and parallel to the x - z plane.

4-9 Example: Step profile

The maximum incidence angle for bound rays, θ_m , is given by Eq. (4-6) with $n(r) = n_{co}$, i.e. $\sin \theta_m = (n_{co}/n_0) \sin \theta_c$, and is uniform over the core endface. Consequently, *only* bound rays are excited if $0 \leq \theta_0 < \theta_m$, and *no* bound rays are excited if $\theta_0 > \theta_m$. If the beam carries uniform power P_i per unit area of its cross-section, then the total incident power $P_{tot} = \pi \rho^2 P_i \cos \theta_0$. Accordingly, total bound-ray power and the source efficiency of Eq. (4-11) are given by

$$P_{br} = P_{tot} = \begin{cases} \pi \rho^2 P_i \cos \theta_0; & \mathcal{E} = \begin{cases} 1; & 0 \leq \theta_0 < \theta_m, \\ 0; & \theta_m < \theta_0 \leq \pi/2, \end{cases} \end{cases} \quad (4-25)$$

ignoring the slight loss of power at the endface. For weakly guiding fibers with $\theta_c \ll 1$, the range of beam angle for bound-ray excitation is small.

4-10 Example: Graded profiles

When the fiber has a graded profile which decreases monotonically from the axis to the interface, the maximum angle of incidence for exciting bound rays, i.e. $\theta_m(r)$ of Eq. (4-6), decreases from a maximum on-axis value $\sin \theta_m(0) = (n_{co}/n_o) \sin \theta_c$, to $\theta_m(\rho) = 0$ at the interface, as $n(r)$ decreases from n_{co} to n_{cl} . Accordingly, if $\theta_0 > \theta_m(0)$ no bound rays are excited, but if $0 \leq \theta_0 < \theta_m(0)$, bound rays are excited within a circle of radius r_{br} , where r_{br} is the solution of $\theta_0 = \theta_m(r_{br})$. Substituting into Eq. (4-6) and using as examples the clad power-law profiles of Table 2-1, page 40, we deduce that [7]

$$r_{br} = \rho \{1 - (n_o \sin \theta_0 / n_{co} \sin \theta_c)^2\}^{1/q}; \quad 0 \leq \theta_0 \leq \theta_m(0). \quad (4-26)$$

Outside of the circular region only leaky rays are excited, as discussed in Chapter 8. When $\theta_0 = 0$ and the beam is on axis, bound rays are excited over the whole core and propagate parallel to the fiber axis. If the beam carries uniform power P_i per unit cross-sectional area, then the total bound-ray power and source efficiency of Eq. (4-11) are given by

$$P_{br} = \begin{cases} \pi r_{br}^2 P_i \cos \theta_0; \\ 0; \end{cases} \quad \mathcal{E} = \begin{cases} r_{br}^2 / \rho^2; & 0 \leq \theta_0 \leq \theta_m, \\ 0; & \theta_m < \theta_0 \leq \pi/2, \end{cases} \quad (4-27)$$

where the factor $\cos \theta_0$ accounts for the beam direction.

LENS ILLUMINATION

In practice the cross-sectional area of a source can greatly exceed the size of the fiber core. By placing such a source against the endface, none of the light entering the cladding can excite bound rays, and consequently the source efficiency of Eq. (4-11) *decreases* as the source *increases* in size. However, if the light from the source is highly directed, as in the collimated beam, we can improve its efficiency by placing a lens between the source and the fiber. On the other hand, *the use of a lens cannot improve the efficiency of a diffuse source*, as we show in Section 4-14.

4-11 Collimated beam

Consider a source which emits a collimated beam of radius r_d . The beam can be focused onto the endface of the fiber at Q on the axis by introducing a thin lens of radius equal to the beam radius and focal length f , as shown in Fig. 4-6(a). All of the light from the source excites only bound rays provided the angle θ_d subtended by the lens at Q does not exceed the maximum angle of incidence $\theta_m(0)$ defined by Eq. (4-6). If for convenience we assume a step profile and set $n(0) = n_{co}$, then $\theta_m(0) = \sin^{-1} \{ (n_{co}/n_o) \sin \theta_c \}$. On setting $r_d = f \tan \theta_d$ in the inequality $\theta_d \leq \theta_m(0)$ and rearranging with the help of Eq. (37-7), we find that

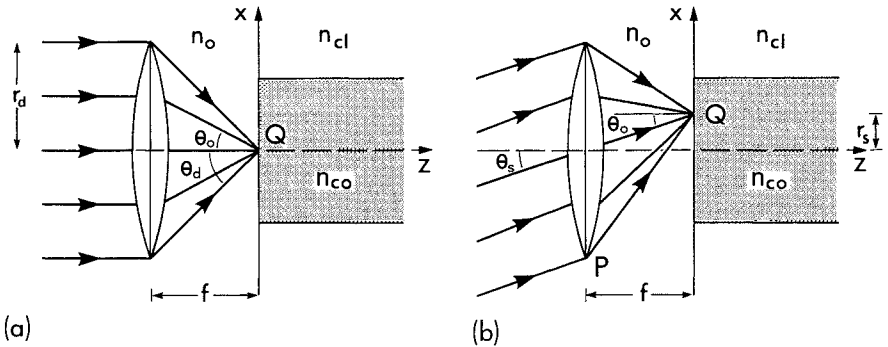


Fig. 4-6 On-axis lens focused onto the fiber endface for (a) an on-axis collimated beam and (b) a skew collimated beam.

the focal length must exceed a certain minimum. Thus

$$f \geq r_d \frac{\{(n_o/n_{co})^2 - \sin^2 \theta_c\}^{1/2}}{\sin \theta_c} \approx \frac{n_o}{n_{co}} \frac{r_d}{\theta_c}, \quad (4-28)$$

where the approximation applies to weakly guiding fibers with $\theta_c \ll 1$. The presence of the lens increases the power entering bound rays, and therefore the source efficiency, by a factor $(r_d/\rho)^2$ compared with direct illumination by the same source. In other words, all of the source power enters bound rays when Eq. (4-28) is satisfied. By symmetry, only meridional rays are excited at Q.

4-12 Example: Intensity distribution

It is useful to know the intensity distribution in the source medium at Q in Fig. 4-6(a). This can be used, for example, in the impulse response calculations at the end of the chapter. If the beam carries uniform power P_i per unit cross-sectional area, then the power dP arriving at Q between angles θ_0 and $\theta_0 + d\theta_0$ crosses an annular area of circumference $2\pi f \tan \theta_0$ and width $d(f \tan \theta_0) = (f/\cos^2 \theta_0) d\theta_0$ in the plane of the lens. Hence

$$dP = 2\pi f^2 (\tan \theta_0 / \cos^2 \theta_0) d\theta_0. \quad (4-29)$$

By symmetry, the intensity I per unit solid angle is given by $(1/2\pi) dP/d\theta_0$. If we include the spatial dependence on the endface relative to the polar coordinates in Fig. 4-4, then

$$I = \frac{\delta(r)}{2\pi r} \frac{f^2 P_i}{\cos^3 \theta_0}, \quad 0 \leq \theta_0 \leq \theta_d; \quad I = 0, \quad \theta_d < \theta_0 \leq \frac{\pi}{2}, \quad (4-30)$$

where δ is the Dirac delta function. For small values of θ_d the intensity is almost independent of θ_0 .

4-13 Example: Oblique incidence

The collimated beam makes angle θ_s with the fiber axis, as shown in Fig. 4-6(b), and the focal point Q is distance $r_s = f \tan \theta_s$ along the x -axis, assuming the beam direction is parallel to the x - z plane. Both meridional and skew rays are excited in the core, and all of these rays are bound provided that the largest angle of incidence, corresponding to the ray PQ in Fig. 4-6(b), does not exceed $\theta_m(r)$ of Eq. (4-6). If the fiber has a step profile, then $\theta_m(r) = \sin^{-1} \{ (n_{co}/n_0) \sin \theta_c \}$, and we can parallel the derivation of Eq. (4-28) to show that the focal length must satisfy

$$f \geq \frac{n_0}{n_{co}} \frac{r_d}{\theta_c} \left/ \left\{ 1 - \frac{n_0}{n_{co}} \frac{\theta_s}{\theta_c} \right\} \right.; \quad \theta_c \ll 1, \quad (4-31)$$

when the fiber is weakly guiding. Clearly $\theta_s < (n_{co}/n_0)\theta_c$, otherwise not all of the rays excited at Q are bound.

Intensity distribution

The intensity distribution on the fiber endface in the source medium has a similar form to the expression in Eq. (4-30) because the power density over the lens is uniform. We replace P_i by $P_i \cos \theta_s$, where P_i is the power per unit cross-sectional area of the beam, and $\delta(r)/r$ by $\delta(r - r_s)/r_s$, i.e. a translation from $r = 0$ to $r = r_s$ along the x -axis in Fig. 4-4. The asymmetry of the ray distribution about the normal at Q in Fig. 4-6(b) means that the upper limit on θ_0 varies with the polar angle ϕ in Fig. 4-4. Hence the intensity distribution is given by

$$I = \frac{\delta(r - r_s)}{2\pi r_s} \frac{f^2 P_i \cos \theta_s}{\cos^3 \theta_0}, \quad 0 \leq \theta_0 < \theta_d(\phi), \quad (4-32a)$$

and is otherwise zero, where $\theta_d(\phi)$ satisfies

$$f \tan \theta_d(\phi) = (r_d^2 - r_s^2 \sin^2 \phi)^{1/2} - r_s \cos \phi, \quad (4-32b)$$

as may be verified by geometry.

4-14 Diffuse source

A diffuse source of radius r_d is situated distance f from a fiber, as shown in Fig. 4-7(a). Each point on the surface of the source emits light in all possible directions. When these rays reach the plane of the fiber endface $z = 0$, the range of ray directions at each point on this plane is clearly reduced. In other words the *diffuse source of finite area in Fig. 4-7(a) can be replaced by a partially diffuse source of infinite extent which abuts the fiber in Fig. 4-7(b)*.

If a thin lens is inserted between the diffuse source and the fiber, this will modify the intensity distribution on $z = 0$. It is intuitive that by choosing a lens of radius equal to the source radius and focal length equal to the separation of the source and fiber, power will be concentrated about the fiber axis on the endface if the lens abuts the source as in Fig. 4-8. Furthermore, if the focal

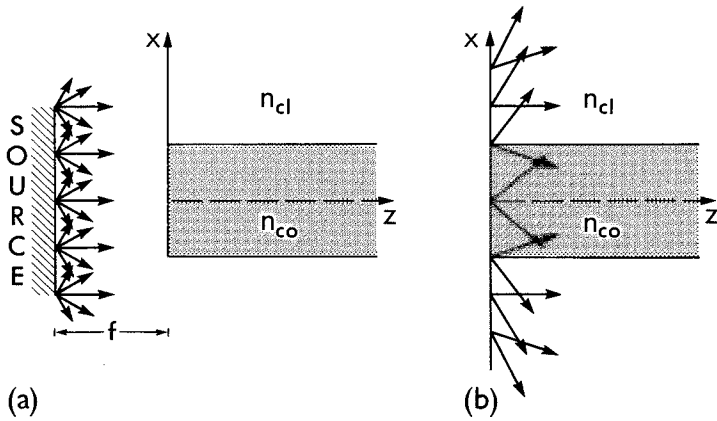


Fig. 4-7 A diffuse source of finite radius r_d distance f from the fiber in (a) is equivalent to a partially diffuse source of infinite extent abutting the fiber in (b).

length is large compared to both the core and source radii, then the angle θ_d subtended by the lens is small and the intensity across the core endface is nearly uniform. We investigate the accuracy of this approximation in the following section, by regarding the light emitted from the source as a superposition of collimated beams.

Optimum bound-ray power

With a view to optimizing bound-ray power, the focal length of the lens, and thus the separation of the source and the fiber, is chosen so that the angle θ_d

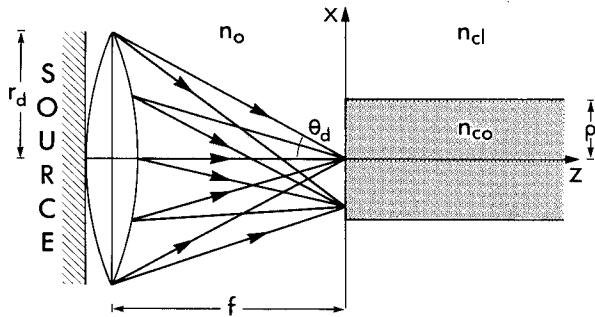


Fig. 4-8 On-axis lens is focused onto the fiber endface and abuts a diffuse or partially diffuse source.

subtended by the lens over the core endface is equal to the maximum angle of incidence for bound rays, assuming a step profile. If the fiber is weakly guiding, this condition follows from Eq. (4-6) as

$$\theta_d = \theta_m(0) \cong (n_{co}/n_0)\theta_c; \quad \theta_c \ll 1. \quad (4-33)$$

The amount of source power entering bound rays in this approximation is the product of the solid angle $\pi\theta_d^2$ subtended by the lens at each point on the interface, the core area $\pi\rho^2$ and the source intensity of Eq. (4-2) which has the approximately uniform value I_0 since θ_0 is small. Thus Eq. (4-33) gives

$$P_{br} = I_0 (\pi\rho n_{co}/n_0)^2 \theta_c^2, \quad (4-34)$$

which is identical to the corresponding expression in Eq. (4-16) for $\theta_c \ll 1$. Thus *a lens cannot improve the efficiency of a diffuse source for exciting bound-ray power.*

4-15 Example: Intensity distribution

Here we determine the intensity distribution on the core endface for the situation in Fig. 4-8, which enables us to verify the accuracy of the approximate expression for total bound-ray power derived in the previous section. We replace the diffuse source by an equivalent axially symmetric superposition of collimated beams, whose directions of propagation are defined by spherical polar angles θ and ϕ relative to the axial and azimuthal directions, respectively, where $0 \leq \theta \leq \pi/2$ and $0 \leq \phi \leq 2\pi$. We deduce from Eq. (4-8) that the power density P_i per unit cross-sectional area of beams with directions in the ranges θ to $\theta + d\theta$ and ϕ to $\phi + d\phi$ is given by

$$P_i d\theta d\phi = I_0 \sin \theta \cos \theta d\theta d\phi. \quad (4-35)$$

In Section 4-13 we showed that the angular dependence of the intensity distribution I on the endface for a single beam incident at angle θ_s to the lens is given by the second factor in Eq. (4-32a), i.e. by $f^2 P_i \cos \theta_s / \cos^3 \theta_0$, where $P_i \cos \theta_s$ is the beam power density. Accordingly we replace $P_i \cos \theta_s$ by the right side of Eq. (4-35) and deduce that I satisfies

$$I r dr d\phi = I_0 f^2 (\sin \theta \cos \theta / \cos^3 \theta_0) d\theta d\phi. \quad (4-36)$$

By geometry each beam is focused onto the endface at radius $r = f \tan \theta$. If we differentiate this expression and substitute for θ in Eq. (4-36), we obtain

$$I = \frac{I_0}{\cos^3 \theta_0} \frac{f^4}{(r^2 + f^2)^2}; \quad 0 \leq \theta_0 \leq \theta_d(\phi), \quad (4-37)$$

and $I = 0$ otherwise, where $\theta_d(\phi)$ is defined by Eq. (4-32b) with r_s replaced by r . When the total power arriving at the endface is also the total bound-ray power, we integrate Eq. (4-37) over the incident-ray angles θ_0 , θ_ϕ and the core cross-section. Here straightforward integration leads to

$$P_{br} = \int_0^\rho r dr \int_0^{2\pi} d\phi \int_0^{\theta_d(\phi)} \sin \theta_0 d\theta_0 \int_0^{2\pi} I d\theta_\phi = I_0 \frac{(\pi\rho r_d)^2}{\rho^2 + f^2}. \quad (4-38)$$

If $f \gg \rho$ we approximate the denominator by f^2 , set $r_d/f \cong \theta_d$ where θ_d is the angle subtended by the lens, and deduce from Eq. (4-33) that Eq. (4-38) reduces to Eq. (4-34) when the fiber is weakly guiding.

4-16 Partially diffuse source

In the last five sections we have shown how a lens, on the one hand can increase source efficiency for collimated beam illumination of a fiber, while, on the other hand, it is ineffective at increasing the efficiency of the diffuse source. If we couple these facts with the description of the diffuse source as a superposition of collimated beams, it is evident that the efficiency of a partially diffuse source can be increased by a lens. The situation is illustrated in Fig. 4-8. We assume the step-profile fiber is weakly guiding so that $\theta_c \ll 1$, and the focal length satisfies $f \gg \rho$ so that the angle subtended by the lens $\theta_d \cong r_d/f$ is small and, together with the intensity, is approximately uniform over the endface.

Under these conditions, maximum bound-ray power results when θ_d satisfies Eq. (4-33), i.e. $\theta_d \cong (n_{co}/n_o)\theta_c$, and all the light emitted from the source falls on the core endface when $f\theta_s \leq \rho$, where θ_s is the maximum angle of emission relative to the fiber axis. By combining these two relations, all source power excites bound modes provided $\theta_s \leq (\rho/r_d)(n_{co}/n_o)\theta_c$. Thus the maximum bound-ray power increases by a factor of $(r_d/\rho)^2$ compared to placing the source directly against the end of the fiber.

POWER DISTRIBUTION AMONG BOUND RAYS

In Section 4-6 we showed how to determine the total bound-ray power and the radial distribution of bound-ray power within the core of the fiber when illuminated by a uniform diffuse source which abuts the endface. Here we determine the distribution of source power among the bound-ray directions. This distribution can be conveniently described in terms of the ray invariants by defining a distribution function $F(\bar{\beta}, \bar{l})$ such that [6]

$$F(\bar{\beta}, \bar{l}) = \text{the power carried by all bound rays with invariants} \\ \text{in the ranges } \bar{\beta} \text{ to } \bar{\beta} + d\bar{\beta} \text{ and } \bar{l} \text{ to } \bar{l} + d\bar{l}. \quad (4-39)$$

The calculation of impulse response in this and later chapters is considerably simplified by using the distribution function.

4-17 Derivation of the distribution function

Our starting point is the expression for total bound-ray power of a uniform diffuse source given by Eq. (4-12). We perform the ϕ integration and transform

variables from the angles θ_0, θ_ϕ to the invariants $\bar{\beta}, \bar{l}$ through Eq. (4-5). Although $\bar{\beta}$ and \bar{l} are not orthogonal when used as integration variables, the Jacobian J gives the correct transformation. Thus we deduce from Eq. (37-129) that

$$\frac{\partial(\theta_0, \theta_\phi)}{\partial(\bar{\beta}, \bar{l})} = \frac{\bar{\beta}}{n_0^2} \frac{1}{\sin \theta_0 \cos \theta_0} \frac{\rho}{r} \frac{1}{g(r)^{1/2}}; \quad g(r) = n^2(r) - \bar{\beta}^2 - \bar{l}^2 \frac{\rho^2}{r^2}, \quad (4-40)$$

and consequently Eq. (4-12) is replaced by

$$P_{\text{br}} = 8\pi\rho \frac{I_0}{n_0^2} \int_0^\rho dr \int_{n_{\text{cl}}}^{n(r)} \bar{\beta} d\bar{\beta} \int_0^{\bar{l}_m(r, \bar{\beta})} \frac{d\bar{l}}{g(r)^{1/2}}, \quad (4-41a)$$

$$\bar{l}_m(r, \bar{\beta}) = \frac{r}{\rho} \{n^2(r) - \bar{\beta}^2\}^{1/2}, \quad (4-41b)$$

where the upper and lower limits on $\bar{\beta}$ correspond to $\theta_0 = 0$ and the maximum value of θ_0 for a ray to be bound, respectively. The same limits on \bar{l} correspond to $\theta_\phi = 0$ and $\theta_\phi = \pi/2$, respectively, and a factor of 4 is included to cover the complete range of values of θ_ϕ in Eq. (4-12).

Reordering of the integration

In order to determine $F(\bar{\beta}, \bar{l})$, we must move the r integration in Eq. (4-41) inside the $\bar{\beta}$ and \bar{l} integrals. We first reverse the order of the r and $\bar{\beta}$ integrals, whence

$$P_{\text{br}} = 8\pi\rho \frac{I_0}{n_0^2} \int_{n_{\text{cl}}}^{n_{\text{co}}} \bar{\beta} d\bar{\beta} \int_0^{r(\bar{\beta})} dr \int_0^{\bar{l}_m(r, \bar{\beta})} \frac{d\bar{l}}{g(r)^{1/2}}; \quad n(r(\bar{\beta})) = \bar{\beta}, \quad (4-42)$$

where the integration limits follow from Fig. 4-9(a), which plots a typical profile from its axial value to its value n_{cl} at the interface. The area involved in the two integrations is shown shaded. The upper limit $n(r)$ of the $\bar{\beta}$ integration in Eq. (4-41) is replaced by the upper limit $r(\bar{\beta})$ in the r integral of Eq. (4-42), where $r(\bar{\beta})$ is the solution of $n(r(\bar{\beta})) = \bar{\beta}$ for graded profiles and $r(\bar{\beta}) = \rho$ for the step profile.

We then reverse the order of the r and \bar{l} integrals, which leads to

$$P_{\text{br}} = 4\pi\rho \frac{I_0}{n_0^2} \int_{n_{\text{cl}}}^{n_{\text{co}}} d\bar{\beta} \int_0^{\bar{l}_{\text{max}}(\bar{\beta})} d\bar{l} \left\{ 2\bar{\beta} \int_{r_{\text{ic}}}^{r_{\text{tp}}} \frac{dr}{g(r)^{1/2}} \right\}, \quad (4-43)$$

where the integration limits are deduced from Fig. 4-9(b). It follows from the definitions in Eqs. (4-41) and (4-42) that the upper limits of the r and \bar{l} integrals in Eq. (4-42) are equal when $g(r) = 0$. A plot of the curve $g(r) = 0$ has the characteristic shape shown in Fig. 4-9(b) since $\bar{l} = 0$ at $r = 0$ and $r = r(\bar{\beta})$. The

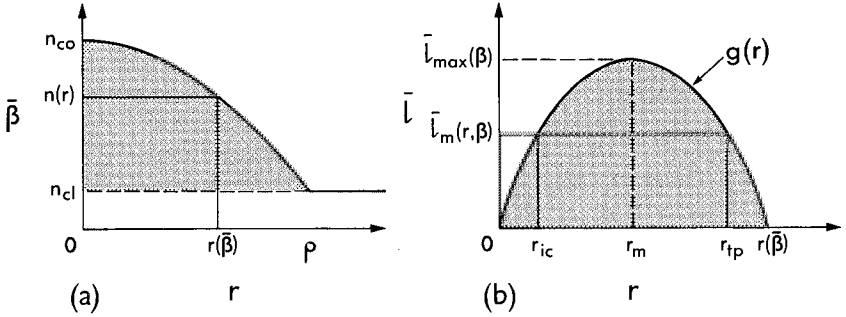


Fig. 4-9 Shaded areas denote the regions of integration for (a) the $\bar{\beta} - r$ plane and (b) the $\bar{l} - r$ plane.

upper limit $\bar{l}_m(r, \bar{\beta})$ on the \bar{l} integration in Eq. (4-42) determines both the lower and upper limits on the r integration in Eq. (4-43) at the intersections of the horizontal line with the curve $g(r) = 0$, i.e. at the *inner caustic* r_{ic} and the *turning-point caustic* r_{tp} , as is clear from Eq. (2-19). Finally, the upper limit $\bar{l}_{max}(\bar{\beta})$ on \bar{l} in Eq. (4-43) is the maximum value of \bar{l} along the curve $g(r) = 0$. Straightforward differentiation shows that

$$\bar{l}_{max}(\bar{\beta}) = \{n^2(r_m) - \bar{\beta}^2\}^{1/2} (r_m/\rho), \quad (4-44a)$$

where r_m is the corresponding value of r , which is the solution of

$$2\{n^2(r_m) - \bar{\beta}^2\} = -r_m(dn^2(r)/dr)_{r_m}. \quad (4-44b)$$

The expression within the curly brackets of Eq. (4-43) is identified with the ray half-period of Table 2-1, page 40. On recalling the definition of the distribution function from Eq. (4-39), we deduce from Eq. (4-43) that [7]

$$F(\bar{\beta}, \bar{l}) = (4\pi\rho I_0/n_0^2)z_p. \quad (4-45a)$$

Thus the distribution function for bound-ray power is proportional to the ray half-period. We give examples in Section 4-19 below.

Normalized distribution function

It is useful to define a normalized distribution function $\hat{F}(\bar{\beta}, \bar{l})$ corresponding to unit total bound-ray power entering the fiber. This quantity is the ratio of $F(\bar{\beta}, \bar{l})$ of Eq. (4-45a) to P_{br} of Eq. (4-14), whence

$$\hat{F}(\bar{\beta}, \bar{l}) = 4\rho z_p/\Omega, \quad (4-45b)$$

in terms of the profile volume Ω defined in Eq. (4-14).

4-18 Distribution function dependent on $\bar{\beta}$ only

In determining impulse response later in the chapter, we consider as examples the step and clad power-law profiles, for which transit times are independent of ray skewness, or \bar{l} . It is then useful to introduce a distribution function $G(\bar{\beta})$, dependent only on $\bar{\beta}$, which is the integral of $F(\bar{\beta}, \bar{l})$ over the range of values of \bar{l} , i.e. $G(\bar{\beta}) \bar{\beta}$ is the power carried by all rays with invariants $\bar{\beta}$ in the range $\bar{\beta}$ to $\bar{\beta} + d\bar{\beta}$. It is not necessary to know $F(\bar{\beta}, \bar{l})$, and therefore, z_p , to determine $G(\bar{\beta})$ explicitly. This is useful for the clad power-law profiles, since z_p is given analytically only for the parabolic profile. We deduce from Eq. (4-42) that

$$G(\bar{\beta}) = 8\pi\rho \frac{I_0}{n_0^2} \bar{\beta} \int_0^{r(\bar{\beta})} dr \int_0^{\bar{l}_m(r, \bar{\beta})} \frac{d\bar{l}}{g(r)^{1/2}}. \quad (4-46)$$

We transform variables from \bar{l} to w , where $\bar{l} = \bar{l}_m(r, \bar{\beta}) \sin w$, and note that the definitions in Eqs. (4-40) and (4-41) enables us to set $g(r) = \{\bar{l}_m^2(r, \bar{\beta}) - \bar{l}^2\} \rho^2 / r^2$. On integrating we find that

$$G(\bar{\beta}) = (2\pi^2 I_0 / n_0^2) \bar{\beta} r^2(\bar{\beta}); \quad n(r(\bar{\beta})) = \bar{\beta}. \quad (4-47a)$$

The normalized distribution function $\hat{G}(\bar{\beta})$, corresponding to unit total bound-ray power, is found by analogy with Eq. (4-45b) to be

$$\hat{G}(\bar{\beta}) = 2\pi \bar{\beta} r^2(\bar{\beta}) / \Omega, \quad (4-47b)$$

where Ω is the profile volume of Eq. (4-14), and $r(\bar{\beta}) = \rho$ for the step profile.

4-19 Example: Step and clad power-law profiles

The ray half-period for the step-profile fiber is given in Table 2-1, page 40, and the profile volume defined in Eq. (4-14) is $\Omega = \pi\rho^2(n_{co}^2 - n_{cl}^2)$. Accordingly the distribution functions of Eq. (4-45) for this profile are

$$F(\bar{\beta}, \bar{l}) = 8\pi\rho^2 \frac{I_0}{n_0^2} \bar{\beta} \frac{(n_{co}^2 - \bar{\beta}^2 - \bar{l}^2)^{1/2}}{n_{co}^2 - \bar{\beta}^2}; \quad \hat{F}(\bar{\beta}, \bar{l}) = \frac{8}{\pi} \frac{\bar{\beta}(n_{co}^2 - \bar{\beta}^2 - \bar{l}^2)^{1/2}}{(n_{co}^2 - n_{cl}^2)(n_{co}^2 - \bar{\beta}^2)}. \quad (4-48)$$

Similarly with $r(\bar{\beta}) = \rho$, the distribution functions of Eq. (4-47) give

$$G(\bar{\beta}) = 2\pi^2\rho^2 \frac{I_0}{n_0^2} \bar{\beta}; \quad \hat{G}(\bar{\beta}) = \frac{2\bar{\beta}}{n_{co}^2 - n_{cl}^2}. \quad (4-49)$$

The ranges of values of $\bar{\beta}$ and \bar{l} for bound rays are given by Eq. (2-8a).

In the case of the clad power-law profiles of Table 2-1, there is no general expression for the ray half-period for arbitrary values of the exponent q , and, with the exception of the parabolic profile ($q = 2$), $F(\bar{\beta}, \bar{l})$ cannot be given explicitly. However, the distri-

bution functions of Eq. (4-47) can be given explicitly. We deduce from Eqs. (4-47a) and (4-14) that

$$r(\bar{\beta}) = \rho \left\{ \frac{n_{\text{co}}^2 - \bar{\beta}^2}{n_{\text{co}}^2 - n_{\text{cl}}^2} \right\}^{1/q}; \quad \Omega = \pi \rho^2 \frac{2q}{q+2} (n_{\text{co}}^2 - n_{\text{cl}}^2), \quad (4-50)$$

which in turn leads to

$$G(\bar{\beta}) = 2\pi^2 \rho^2 \frac{I_0}{n_0^2} \bar{\beta} \left\{ \frac{n_{\text{co}}^2 - \bar{\beta}^2}{n_{\text{co}}^2 - n_{\text{cl}}^2} \right\}^{2/q}; \quad \hat{G}(\bar{\beta}) = \frac{q+2}{q} \frac{2\bar{\beta}}{n_{\text{co}}^2 - n_{\text{cl}}^2} \left\{ \frac{n_{\text{co}}^2 - \bar{\beta}^2}{n_{\text{co}}^2 - n_{\text{cl}}^2} \right\}^{2/q} \quad (4-51)$$

The range of values of $\bar{\beta}$ for bound rays is given by Eq. (2-24a).

Clad parabolic profile

The ray half-period is given in Table 2-1, whence we deduce from Eqs. (4-45) and (4-50) that

$$F(\bar{\beta}, \bar{l}) = 4\pi^2 \rho^2 \frac{I_0}{n_0^2} \frac{\bar{\beta}}{(n_{\text{co}}^2 - n_{\text{cl}}^2)^{1/2}}; \quad \hat{F}(\bar{\beta}, \bar{l}) = \frac{8\bar{\beta}}{(n_{\text{co}}^2 - n_{\text{cl}}^2)^{3/2}}, \quad (4-52)$$

which are independent of skewness.

Range of skew-ray invariants

We showed in Section 2-7 that bound rays on clad fibers have values of the invariant $\bar{\beta}$ which lie in the range of Eq. (2-24a). The corresponding range of values of \bar{l} satisfies $0 \leq \bar{l} \leq \bar{l}_{\text{max}}(\bar{\beta})$, where the upper limit is defined by Eq. (4-44). For the step profile $r_m = \rho$ and $\bar{l}_{\text{max}}(\bar{\beta}) = (n_{\text{co}}^2 - \bar{\beta}^2)^{1/2}$, while for the clad power-law profiles we substitute from Table 2-1 into Eq. (4-44) and find that

$$r_m = \rho \left\{ \frac{2}{q+2} \frac{n_{\text{co}}^2 - \bar{\beta}^2}{n_{\text{co}}^2 - n_{\text{cl}}^2} \right\}^{1/q}; \quad \bar{l}_{\text{max}}(\bar{\beta}) = q^{1/2} \left\{ \frac{2}{n_{\text{co}}^2 - n_{\text{cl}}^2} \right\}^{1/q} \left\{ \frac{n_{\text{co}}^2 - \bar{\beta}^2}{q+2} \right\}^{(q+2)/2q}, \quad (4-53)$$

which reduce to the step-profile expressions when $q \rightarrow \infty$.

IMPULSE RESPONSE

In the previous chapter we described pulse spreading by the maximum temporal width possible between the transit times of the slowest and fastest propagating rays, i.e. $t_{\text{max}} - t_{\text{min}}$. This description is very useful, since it gives an upper bound on pulse spreading for an arbitrary source of excitation. If the pulse shape is virtually rectangular, then, clearly, knowledge of the pulse width

is sufficient to describe the pulse. However, if the pulse shape differs greatly from rectangular we require the distribution of power within the pulse, or *impulse response*. Hence we show how to derive this distribution for an arbitrary source, and consider specific examples. We consider first the class of profiles which have transit times dependent on the invariant $\bar{\beta}$ only, and then arbitrary profiles which have transit times dependent on both invariants. The effects of material dispersion are briefly discussed.

4-20 Ray transit times dependent on $\bar{\beta}$ only

We consider pulses which have zero width at the beginning of the fiber, as in Chapter 3, but carry finite power described by the Dirac delta function. The response to any initial pulse of finite duration can then be found by convolution.

Derivation of the impulse response

The impulse response describes the distribution of power within the pulse when it reaches the end of the fiber, as a function of the transit time t , and is denoted by $Q(t)$. The power arriving between times t and $t + dt$ is then given by $Q(t)dt$. For convenience we assume unit total power in the pulse, i.e.

$$\int_{t_{\min}}^{t_{\max}} Q(t) dt = 1, \quad (4-54)$$

where t_{\max} and t_{\min} are the transit times of the slowest and fastest propagating rays. For the profiles considered in the examples, transit times are independent of skewness, or \bar{l} . Hence all rays with the same value of $\bar{\beta}$ arrive simultaneously at the end of the fiber after time $t(\bar{\beta})$. The power in these rays is described by the normalized distribution function $\hat{G}(\bar{\beta})$ introduced in Section 4-18. Accordingly the power arriving at the end of the fiber in rays with invariants in the range $\bar{\beta}$ to $\bar{\beta} + d\bar{\beta}$ is $\hat{G}(\bar{\beta})d\bar{\beta}$, where the spread $d\bar{\beta}$ is equivalent to a spread dt in transit times. We therefore deduce [6]

$$Q(t) = \hat{G}(\bar{\beta}) |d\bar{\beta}/dt|, \quad (4-55)$$

where the modulus sign is included since $Q(t)$ is positive by definition. The right side is expressed as a function of t by inverting the transit time relationship $t = t(\bar{\beta})$ to give $\bar{\beta} = \bar{\beta}(t)$. If the transit time is the same for two or more values of $\bar{\beta}$, then there will be two or more contributions to the right of Eq. (4-55), corresponding to these values of $\bar{\beta}$.

R.m.s. width

The r.m.s. (root mean square) width σ contains information about the power distribution within the pulse. This is useful when the pulse is no longer rectangular and cannot be described just by its overall width. To evaluate σ we define R_m to be the m th moment of the impulse response, whence we deduce from Eq. (4-55) that [6]

$$R_m = \int_{t_{\min}}^{t_{\max}} t^m Q(t) dt = \int_{n_{cl}}^{n_{co}} t^m(\bar{\beta}) \hat{G}(\bar{\beta}) d\bar{\beta}, \quad (4-56)$$

and $R_0 = 1$ because of the normalization of Eq. (4-54). The first moment R_1 gives the mean transit time \bar{t} weighted according to ray power, and the r.m.s. width σ requires the first and second moments. Thus

$$\bar{t} = R_1; \quad \sigma = (R_2 - R_1^2)^{1/2}. \quad (4-57)$$

We now consider specific examples assuming diffuse illumination.

4-21 Example: Step profile

The transit time for rays on a step-profile fiber is expressed in terms of $\bar{\beta}$ in Table 2-1, page 40, whence on inverting the relationship

$$t(\bar{\beta}) = zn_{co}^2/(c\bar{\beta}); \quad \bar{\beta}(t) = zn_{co}^2/(ct). \quad (4-58)$$

The distribution function $\hat{G}(\bar{\beta})$ for diffuse illumination is given by Eq. (4-49), and the impulse response follows from Eq. (4-55). Hence

$$Q(t) = \frac{2n_{co}^4}{n_{co}^2 - n_{cl}^2} \frac{z^2}{c^2 t^3} \cong 2 \frac{n_{co}^2}{\theta_c^2} \frac{z^2}{c^2 t^3}; \quad t_{\min} \leq t \leq t_{\max}, \quad (4-59)$$

and is otherwise zero, where t_{\min} and t_{\max} are defined in Eq. (3-1) and the approximation applies to weakly guiding fibers. Although $Q(t)$ varies inversely with the cube of the transit time, the actual variation in practice is very small. For example, when $n_{co} = 1.45$, $n_{cl} = 1.44$ and $z = 1$ km, $Q(t)$ decreases from 3.01×10^7 to 2.95×10^7 s⁻¹ as t increases from t_{\min} to t_{\max} . Hence the impulse response for the step profile is virtually rectangular. The mean transit time of Eq. (4-57) is found to be

$$\bar{t} = \frac{z}{c} \frac{2n_{co}^2}{n_{co} + n_{cl}} = \frac{1}{2}(t_{\min} + t_{\max}) - \frac{z}{2c} \frac{n_{co}}{n_{cl}} \frac{(n_{co} - n_{cl})^2}{n_{co} + n_{cl}}, \quad (4-60)$$

from which we deduce that \bar{t} is slightly closer to t_{\min} than t_{\max} , indicating that only fractionally more power travels in the faster rays propagating at smaller angles θ_z . Assuming weak guidance, the r.m.s. pulse width σ of Eq. (4-57) is readily shown to be approximately $(t_{\max} - t_{\min})/\sqrt{12}$.

4-22 Example: Clad power-law profiles

The transit time $t = t(\bar{\beta})$ for rays on clad power-law profile fibers is given in Table 2-1, page 40. Inverting this relationship we find that

$$\bar{\beta}(t) = \frac{q+2}{4} \frac{ct}{z} \pm \left\{ \left[\frac{ct}{z} \frac{q+2}{4} \right]^2 - \frac{q}{2} n_{co}^2 \right\}^{1/2}, \quad (4-61)$$

so that there are two different values of $\bar{\beta}$ for each value of t . For diffuse illumination we substitute $\hat{G}(\beta)$ of Eq. (4-51) into Eq. (4-55). The impulse response is then given by the term [6]

$$Q(t) = \frac{c}{z} \frac{(q+2)^2}{qn_{co}^2 \Delta} \frac{\bar{\beta}^3(t)}{|qn_{co}^2 - 2\bar{\beta}^2(t)|} \left\{ \frac{n_{co} - \bar{\beta}^2(t)}{2n_{co}^2 \Delta} \right\}^{2/q}, \quad (4-62)$$

when only one value of $\bar{\beta}(t)$ is involved, and by the sum of two such terms – one for each value of $\bar{\beta}(t)$ – when both values are involved. The range of t and the number of values of $\bar{\beta}(t)$ depend on q and are deduced from Eq. (3-7). Outside the range $Q(t)$ is zero. The qualitative shapes of the impulse response for all values of q are shown in Fig. 4-10. For practical values of n_{co} and n_{cl} , the impulse response of the clad parabolic profile is virtually rectangular. However, as the value of q increases or decreases from $q = 2$, the impulse response shape changes greatly from rectangular. In particular, when $q = q_{opt}$ – the optimum profile of Eq. (3-8) for minimum overall pulse spread – the impulse response is unbounded as $t \rightarrow t_{min}$. The total pulse power, of course, remains finite. For the clad parabolic profile, the mean transit time of Eq. (4-57) in the weak guidance approxima-

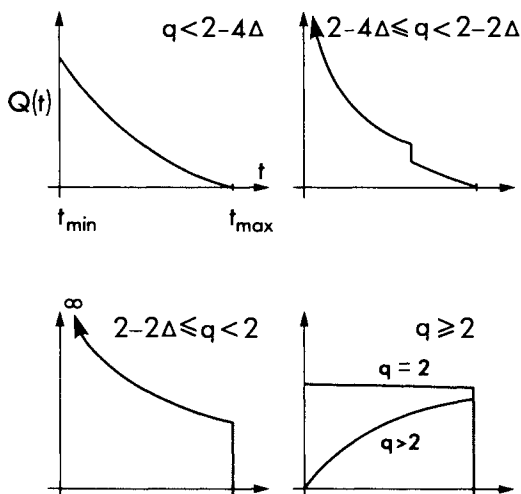


Fig. 4-10 Impulse response of Eq. (4-62) as a function of transit time t and exponent q of the clad power-law profiles [6]. The optimum profile is $q_{opt} = 2 - 2\Delta \cong 2 - \theta_c^2$.

tion $\theta_c \ll 1$ is given by

$$\bar{t} \cong (zn_{co}/c)(1 + \theta_c^4/16) = (t_{\max} + t_{\min})/2, \quad (4-63)$$

which correct to order θ_c^4 is the mean transit time, as may be verified from Eqs. (3-5) and (3-7). The r.m.s. width is $\sigma \cong (t_{\max} - t_{\min})/\sqrt{12}$.

4-23 Ray transit times dependent on both invariants

The transit time for an arbitrary profile depends in general on both ray invariants, i.e. $t = t(\bar{\beta}, \bar{l})$. Thus a group of rays, each ray having different values of $\bar{\beta}$ and \bar{l} , *can all have the same transit time* t . In Fig. 4-11(a) these rays lie along the contour $t(\bar{\beta}, \bar{l}) = t$ in the $\bar{\beta}$ - \bar{l} plane. Rays with common transit time $t + dt$ lie along the neighboring contour $t(\bar{\beta}, \bar{l}) = t + dt$. It then follows that the total power arriving at the end of the fiber between times t and $t + dt$ is carried by those rays in the shaded area between the two contours, denoted by dA . If we recall the normalized distribution function $\hat{F}(\bar{\beta}, \bar{l})$ for bound rays introduced in Section 4-17, then

$$Q(t) dt = \iint_{dA} \hat{F}(\bar{\beta}, \bar{l}) d\bar{\beta} d\bar{l}. \quad (4-64)$$

Analytically $Q(t)$ is found by dividing the right side by dt and taking the limit $dt \rightarrow 0$.

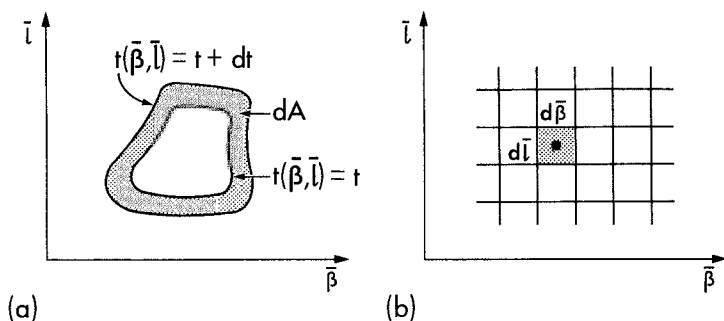


Fig. 4-11 (a) Rays with equal transit times lie on a contour in the \bar{l} - $\bar{\beta}$ plane, and (b) rectangular grid in the \bar{l} - $\bar{\beta}$ plane for numerical computation of impulse response.

Numerical determination of impulse response

Unfortunately, for virtually all profiles of practical interest, the integral in Eq. (4-64) cannot be expressed in simple form. Thus $Q(t)$ is determined numerically, and it is then more convenient to adopt a slightly different

approach [8]. Rather than search for contours of constant transit time, the $\bar{\beta}$ - \bar{l} plane is divided by a grid into small rectangles of sides $d\bar{\beta}$ and $d\bar{l}$, as shown in Fig. 4-11(b). The power $F(\bar{\beta}, \bar{l})d\bar{\beta}d\bar{l}$ of the rays within the rectangle is associated with a mean transit time $t(\bar{\beta}_c, \bar{l}_c)$ evaluated at the center of the rectangle. We now divide the range of transit times $t_{\max} - t_{\min}$ into a large number of intervals. Clearly $t(\bar{\beta}_c, \bar{l}_c)$ lies within one of these intervals. The power associated with $t(\bar{\beta}_c, \bar{l}_c)$ is then identified with that interval. If we repeat this for all the rectangles, the impulse response is approximated by the distribution of accumulated power within each interval. As the size of the rectangles and intervals decreases, the more closely the result approaches $Q(t)$. A complete discussion of this method can be found elsewhere [8].

4-24 Material dispersion

The inclusion of material dispersion leads to simple modifications of the expressions for impulse response in Sections 4-21 and 4-22. For the step profile, it is clear from Section 3-7 that $Q(t)$ still varies with $1/t^3$ as in Eq. (4-59), although the magnitude of $Q(t)$ and the range of t are modified to account for the dependence of n_{co} , n_{cl} and Δ on wavelength. Similar conclusions hold for the clad power-law profiles and results are presented elsewhere [6].

REFERENCES

1. Jackson, J. D. (1967) *Classical Electrodynamics*, Wiley, New York.
2. Born, M. and Wolf, E. (1970) *Principles of Optics*, Pergamon Press, Oxford.
3. Snyder, A. W. (1974) Leaky-ray theory of optical waveguides of circular cross-section. *Appl. Phys.*, **4**, 273-98.
4. Pask, C. and Snyder, A. W., (1974) Illumination of multimode optical fibres—leaky ray analysis. *Opto-electronics*, **6**, 297-304.
5. Albertin, F., Di Vita, P. and Vannuci, R. (1974) Geometrical theory of energy launching and pulse distortion in dielectric optical waveguides. *Opto-electronics*, **6**, 369-89.
6. Ankiewicz, A. and Pask, C. (1977) Geometric optics approach to light acceptance and propagation in graded index fibres. *Opt. Quant. Elect.*, **9**, 87-109.
7. Barrell, K. F. and Pask, C. (1979) Ray launching and observation in graded-index optical fibres. *J. Opt. Soc. Am.*, **69**, 294-300.
8. Barrell, K. F. and Pask, C. (1980) Pulse dispersion in optical fibres of arbitrary refractive-index profile. *Appl. Opt.*, **19**, 1298-1305.

Nonuniform fibers

Continuously varying nonuniformities	90
5-1 Ray transit time	91
5-2 Ray-path equations	91
5-3 <i>Example: Step-profile with variable core index</i>	92
Random nonuniformities	93
5-4 Reduction in pulse spread	93
Slowly varying fibers	94
5-5 Ray transit time	95
5-6 <i>Example: Clad power-law profiles</i>	97
5-7 Small-amplitude nonuniformities	98
5-8 <i>Example: Slight core-radius variations</i>	99
5-9 <i>Example: Slight exponent variations</i>	100
5-10 Adiabatic invariant	102
5-11 <i>Example: Step profile</i>	103
5-12 <i>Example: Clad power-law profiles</i>	104
5-13 Radiation loss	105
5-14 <i>Example: Variable core radius-step profile</i>	106
5-15 <i>Example: Variable core radius-clad power-law profiles</i>	107
Tapers and light concentration	107
5-16 Collimated-beam illumination	108
5-17 <i>Example: Parabolic taper</i>	108
5-18 <i>Example: Linear taper</i>	109
5-19 Diffuse-source illumination	110
5-20 Accuracy of the slow-variation approximation	111
Discontinuous nonuniformities and scatterers	112
5-21 Distribution of bound-ray power	113
5-22 <i>Example: Diffusion equation</i>	115
5-23 <i>Example: Rayleigh scattering</i>	116
References	118

In the first four chapters we assumed that optical waveguides are *uniform*, with refractive-index profiles and cross-sections which are unchanged along their

length. In practice, however, this need not be the case because of imperfections in manufacturing techniques and external stresses acting on fibers. Even an ideal nonabsorbing fiber made from optically transparent materials has an innate variation along its length due to the molecular granularity of matter. Accordingly we consider *nonuniform* fibers in this chapter, characterized by profiles and cross-sections which vary along their length. Nonuniformities are sometimes introduced intentionally to achieve particular pulse-spreading characteristics or for devices such as tapers.

Our purpose here is to investigate the effects of nonuniformities, particularly on pulse spreading. One result of practical importance is that pulse spreading can be *decreased* by nonuniformities, but always at the cost of a loss of pulse power due to radiation. We develop a simple theory for studying fibers that vary slowly along their length, as such fibers often occur in practice. In addition we investigate the light-concentrating properties of nonuniform fibers, e.g. tapers.

It is convenient to distinguish between two types of nonuniformity. The first type is associated with macroscopic nonuniformities which vary continuously, such as a variable core radius. In these cases the light power associated with a bound ray remains constant as the ray propagates, although the trajectory is modified by the nonuniformity. The second type is associated with discontinuous nonuniformities, such as tiny isolated scatterers. In this case light power associated with a bound ray incident on the scatterer is redistributed amongst all ray directions. We treat these two situations with different methods. However, if the fibers are sufficiently long, approximate statistical models can be introduced to describe the nonuniformities when they are randomly distributed along the fiber; this leads to similar conclusions for both cases.

CONTINUOUSLY VARYING NONUNIFORMITIES

We first consider fibers with nonuniformities which vary continuously with distance z along the fiber. A simple example of a step-profile fiber with varying

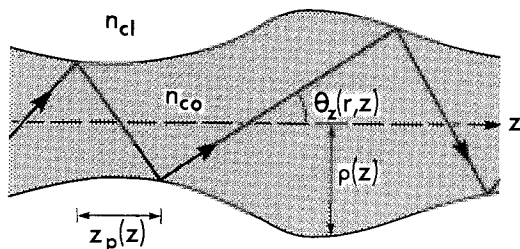


Fig. 5-1 Step-profile fiber with variable core radius, showing a bound-ray trajectory and the half-period $z_p(z)$, which varies between successive reflections.

core radius $\rho(z)$ is shown in Fig. 5-1. The trajectory of a bound ray is still a zig-zag, but the ray half-period, measured along the axis between successive reflections, is no longer constant. Continuity of the nonuniformity along the fiber ensures that, although the ray path can vary considerably from that of the uniform fiber, ray power is conserved along the modified path. For ray analysis to be valid, the nonuniformity must vary slowly over distances of the order of the wavelength of light, but may vary quite arbitrarily over a ray half-period.

5-1 Ray transit time

We assume a circular fiber with refractive-index profile $n(r, z)$. The local velocity of light is $c/n(r, z)$ and the transit time over length z of the fiber is therefore given by

$$t = \frac{1}{c} \int n(r, z) ds = \frac{1}{c} \int \frac{n(r, z) dz}{\cos \theta_z(r, z)} = \frac{1}{c} \int \frac{n^2(r, z) dz}{\bar{\beta}(z)}, \quad (5-1)$$

where ds is the differential element of distance along the ray path, and

$$\bar{\beta}(z) = n(r, z) \cos \theta_z(r, z) = n(r, z) \frac{dz}{ds}, \quad (5-2)$$

is the *ray function*, defined by analogy with the ray invariant of Eq. (2-16). The angle $\theta_z(r, z)$ is between the tangent to the path and the axial direction. We emphasize that the integrals must be evaluated along the path $r = r(z)$; this is a complicated procedure when the fiber varies along its length. Because of this variation with z , the ray function $\bar{\beta}(z)$ is no longer an invariant, i.e. $\bar{\beta}(z) \neq \bar{\beta}(0)$, as in the case of a uniform fiber, and the method for calculating transit time in Section 2-9 cannot be used. To determine $\bar{\beta}(z)$ we start with the ray-path equations.

5-2 Ray-path equations

If we replace $n(r)$ with $n(r, z)$ in Eq. (1-18), the component ray-path equations in the radial, azimuthal and axial directions are obtained by making the same replacement throughout Section 35-4, which leads to

$$\frac{d}{ds} \left\{ n(r, z) \frac{dr}{ds} \right\} - rn(r, z) \left(\frac{d\phi}{ds} \right)^2 = \frac{\partial n(r, z)}{\partial r}, \quad (5-3a)$$

$$\frac{d}{ds} \left\{ n(r, z) \frac{d\phi}{ds} \right\} + \frac{2n(r, z)}{r} \frac{d\phi}{ds} \frac{dr}{ds} = 0, \quad (5-3b)$$

$$\frac{d}{ds} \left\{ n(r, z) \frac{dz}{ds} \right\} = \frac{\partial n(r, z)}{\partial z}, \quad (5-3c)$$

respectively, where s is the distance along the path and (r, ϕ, z) are cylindrical polar coordinates oriented as in Fig. 2-1.

Ray function

If we eliminate ds between Eqs. (5-2) and (5-3c), the equation satisfied by the ray function $\bar{\beta}(z)$ is found to be

$$\frac{d\bar{\beta}^2(z)}{dz} = \frac{\partial n^2(r, z)}{\partial z} \bigg|_{r=r(z)}, \quad (5-4)$$

where $r(z)$ is evaluated along the ray path. The solution in terms of the initial value of $\bar{\beta}(z)$ at the beginning of the fiber is

$$\bar{\beta}^2(z) = \bar{\beta}^2(0) + \int_0^z \frac{\partial n^2(r, z)}{\partial z} \bigg|_{r=r(z)} dz, \quad (5-5)$$

where the integration is along the ray path. The determination of this path is complicated because of the variation in profile along the fiber.

Ray invariant \bar{l}

The circular symmetry of the fiber at each position z means that there is an invariant \bar{l} associated with the azimuthal direction. To determine \bar{l} we multiply Eq. (5-3b) by r^2 and integrate. Hence

$$\bar{l} = \frac{r^2}{\rho(0)} n(r, z) \frac{d\phi}{ds} = \frac{r}{\rho(0)} n(r, z) \sin \theta_z(r, z) \cos \theta_\phi(r, z), \quad (5-6)$$

is independent of both r and z , where $\theta_\phi(r, z)$ is the angle between the azimuthal direction and the tangent to the ray-path projection onto the fiber cross-section. The initial core radius $\rho(0)$ is included to ensure that \bar{l} is dimensionless and also reduces to the invariant of Eq. (2-17) for uniform fibers, when $n(r, z) = n(r)$ and $\rho(0) = \rho$.

Ray path

Both the transit time of Eq. (5-1) and $\bar{\beta}(z)$ of Eq. (5-5) require the ray path $r = r(z)$. This can be found from Eq. (5-3a). One simplification is to use the invariant \bar{l} of Eq. (5-6) to eliminate $d\phi/ds$.

5-3 Example: Step-profile with variable core index

For an arbitrary nonuniform fiber it is necessary to know the ray path $r = r(z)$ explicitly, in order to determine the transit time. However, the step-profile fiber of *constant core*

radius is an exception since it is not necessary to know the path. The core index $n(z)$ depends only on z and, consequently, the partial derivative in Eq. (5-4) becomes a total derivative. The solution is

$$\bar{\beta}^2(z) = \bar{\beta}^2(0) + n^2(z) - n^2(0), \quad (5-7a)$$

or in terms of the angle $\theta_z(z)$ the path makes with the fiber axis

$$n(z) \sin \theta_z(z) = n(0) \sin \theta_z(0), \quad (5-7b)$$

using Eq. (5-2). If we substitute for $\bar{\beta}(z)$ in Eq. (5-1) and set $n(r, z) = n(z)$, the transit time is given by a simple integral over z

$$t = \frac{1}{c} \int_0^z \frac{n^2(z) dz}{[n^2(z) + \bar{\beta}^2(0) - n^2(0)]^{1/2}}, \quad (5-8)$$

and is *independent of the ray path, apart from its initial direction.*

RANDOM NONUNIFORMITIES

Although it is not possible in general to give the transit time analytically, there are two cases of practical interest for which approximation methods are applicable—random nonuniformities and slowly varying nonuniformities—discussed, respectively, here and in later sections. When the fiber has nonuniformities that are randomly distributed along its length, we need only have knowledge of certain statistical averages of the ray path $r = r(z)$ and the associated ray function $\bar{\beta}(z)$ of Eq. (5-2) in order to determine the transit time from Eq. (5-1). In general this requires solving the ray equations by statistical methods, but in the case of the step profile this is unnecessary. For example, variations in core radius can be modelled through the random variable $\theta_z(z)$ in Eq. (5-1) by keeping $n(r, z) = n_{co}$ constant, while variations in core index $n(z)$ are modelled by the same random variable through Eq. (5-7b). The mean ray transit time and the r.m.s. fluctuation about the mean can then be calculated using standard statistical methods on Eq. (5-1). When the nonuniformities are sufficiently uncorrelated, simple physical reasoning provides the necessary insight, as we now show.

5-4 Reduction in pulse spread

Consider a fiber of length z within which the distribution of nonuniformities is sufficiently random, so that there is *no correlation between the direction of a ray at the beginning and end of the fiber*. We further assume that the fiber is illuminated by the diffuse source of Section 4-1, so that all bound rays are excited. Under these conditions, and after a sufficiently large number of ray half-periods, each ray path will have passed through all possible ray directions,

or, equivalently, taken all values of $\bar{\beta}(z)$ for bound rays. Consequently, the transit time for each bound ray excited by the source is approximately equal to the average transit time. This average time is proportional to the length z of the fiber because the transit times for all ray directions is proportional to z , as shown in Sections 2-5 and 2-9. However, because of the random nature of the nonuniformities, the fluctuation in transit times about this mean—measured by the r.m.s. value or variance—is known from statistics [1] to be proportional to the square root of the average transit time, and is thus proportional to $z^{1/2}$.

We recall from Chapter 3 that in the absence of nonuniformities the pulse spread is proportional to the fiber length z . Thus, *by introducing random nonuniformities the pulse has a slower ($z^{1/2}$) spread with distance*, provided that the fiber is sufficiently long for the statistical situation to be realized [1]. This result holds provided the nonuniformities are sufficiently large to enable a ray to take on *all* bound-ray directions, or values of $\bar{\beta}(z)$, as it propagates the length of the fiber. For example, on a step-profile fiber, the size of the nonuniformity must be sufficient to occasionally cause a ray to change direction by θ_c , where θ_c is the complement of the critical angle. The $z^{1/2}$ effect will not occur on slowly-varying fibers, for which there is only a slight change in $\bar{\beta}(z)$ over a ray half-period, as we discuss in Section 5-7 below. In such cases each output ray is correlated with an input ray direction because the mean fluctuation in the nonuniformities is zero.

There is also a penalty [2] for achieving reduced pulse spread, since some bound-ray power is inevitably lost to radiation. This occurs because the change in $\bar{\beta}(z)$ over a ray half-period can be sufficient to convert a bound ray into a tunneling or refracting ray—discussed in Section 2-7. The radiation loss is reduced when the nonuniformities result in predominantly forward-direction changes in ray direction, i.e. to higher values of $\bar{\beta}(z)$.

SLOWLY VARYING FIBERS

Here we examine a second case of practical importance for which the transit time can be evaluated approximately. We assume that *the change in the nonuniformity along the fiber is so slow that the refractive-index profile is virtually uniform, i.e. independent of z , over the distance z_p required for a ray to undergo a half-period, i.e. $z_p |\partial n(r, z) / \partial z| \ll 1$* . An example of a slowly varying fiber is shown in Fig. 5-2. The nonuniformities may be arbitrarily large, e.g. a tapered fiber whose core radius at one end is many multiples of the radius at the other end, provided the taper angle is everywhere small.

Approximate model

When the conditions for slow variation are satisfied, we can make an approximate model of the *nonuniform fiber* by dividing it into a series of *uniform*

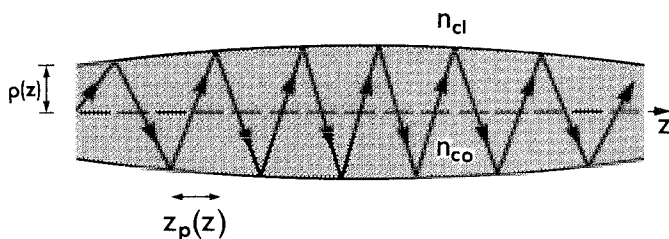


Fig. 5-2 Step-profile fiber of constant core and cladding indices with core radius $\rho(z)$ which varies slowly over a ray half-period $z_p(z)$.

sections, as shown in Fig. 5-3. Each section has length $z_p(z)$ equal to a ray half-period, core radius $\rho(z)$ and refractive-index profile $n(r, z)$, all evaluated, for convenience, at the midpoint z of the section.

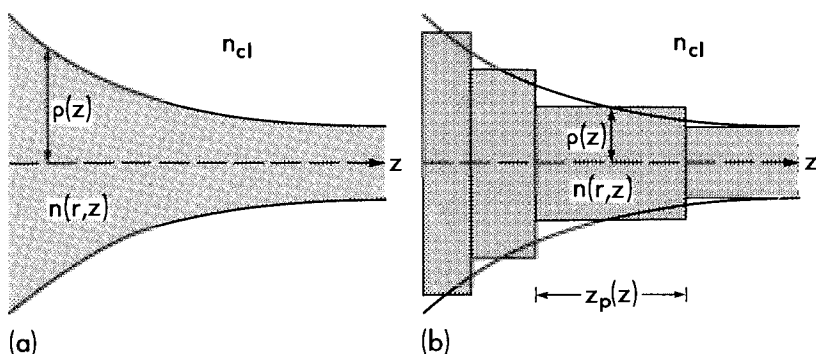


Fig. 5-3 (a) Fiber with core radius $\rho(z)$ and profile $n(r, z)$ which vary slowly with z , and (b) the approximate model comprising a series of uniform sections. The variation is exaggerated for clarity. Within each section the core radius and profile are independent of z .

5-5 Ray transit time

The transit time for the nonuniform fiber in Fig. 5-3(a) is the sum of the transit times for each uniform section in Fig. 5-3(b). If $t_p(z)$ denotes the transit time over the uniform section of length $z_p(z)$, then from Eq. (2-32) we have

$$t_p(z) = L_o(z)/c, \quad (5-9)$$

where c is the free-space speed of light, and $L_o(z)$ is the optical path length, which, by analogy with Eq. (2-27), has the definition

$$L_o(z) = 2 \int_{r_{ic}(z)}^{r_{ip}(z)} \frac{n^2(r, z) dr}{g(r, z)^{1/2}}; \quad g(r, z) = n^2(r, z) - \beta^2(z) - l^2 \frac{\rho^2(0)}{r^2}, \quad (5-10)$$

where z is the midpoint of the section, $\bar{\beta}(z)$ is defined by Eq. (5-5), \bar{l} is the invariant of Eq. (5-6) and $\rho(0)$ is the core radius at the beginning of the fiber. Clearly z remains fixed when performing the integration. We can approximate the sum over $t_p(z)$ by an integral if we set $z_p(z) \cong dz$. The overall transit time is then given by

$$t = \frac{1}{c} \int_0^z \frac{L_o(z)}{z_p(z)} dz, \quad (5-11)$$

where $z_p(z)$ is defined by analogy with Eq. (2-28) as

$$z_p(z) = 2\bar{\beta}(z) \int_{r_{ic}(z)}^{r_{ip}(z)} \frac{dr}{g(r, z)^{1/2}}, \quad (5-12)$$

in terms of $g(r, z)$ of Eq. (5-10) with z fixed at the midpoint value. The expression for t is a significant simplification of Eq. (5-1) since it is *not necessary to integrate along a ray path of the nonuniform fiber*, and requires only ray-path parameters.

Characteristic length scales

We can parallel the physical arguments leading to Eq. (5-11) by a more mathematical derivation. With reference to Fig. 5-2, we recognize that ray paths on slowly varying fibers are characterized by two length scales—one *fast* and one *slow*. The fast length scale is equal to the ray half-period $z_p(z)$, and the fiber is treated as if it is axially uniform over distance $z_p(z)$, while the slow scale characterizes nonuniformities which are significant only over distances large compared with a ray half-period. The radial variation in the refractive-index profile is much faster than the longitudinal variation so that the condition $|\partial n / \partial r| \gg |\partial n / \partial z|$ is satisfied. Hence, in deriving Eq. (5-11) we average out the rapid change in path direction over a ray half-period, *treating the fiber as axially uniform*. Mathematically this is equivalent to replacing the integrand in Eq. (5-1) by its average over a half-period. Thus

$$\left\langle \frac{n^2(r, z)}{\bar{\beta}(z)} \right\rangle = \frac{1}{\bar{\beta}(z)z_p(z)} \int_{z-z_p(z)/2}^{z+z_p(z)/2} n^2(r(\zeta), z) d\zeta, \quad (5-13)$$

where for clarity we use ζ to distinguish the axial distance along the locally uniform fiber from the distance z along the nonuniform fiber. It is crucial to appreciate that the integration is along the ray path $r = r(\zeta)$ of the uniform fiber. The displacement of this path from the fiber axis varies rapidly with ζ , whereas the profile varies slowly with z . In other words, z in both the argument of the integral and the remaining quantities on the right of Eq. (5-13) is held fixed when performing the integration. Finally, if we set $d\zeta/\bar{\beta}(z) = dr/g(r, z)^{1/2}$

by analogy with Eq. (2-21), we recover the integrand of Eq. (5-11) through Eq. (5-10).

Equation for the ray function

The expressions for $L_o(z)$ and $z_p(z)$ given by Eqs. (5-10) and (5-12) both depend on $\beta(z)$. Thus, to evaluate the transit time of Eq. (5-11), we require the solution of Eq. (5-4). The solution given by Eq. (5-5) requires knowledge of the ray path, but, if we use the fact that the fiber is slowly varying, we can average the right side of Eq. (5-4) over a half-period for reasons given below Eq. (5-13). Hence [3, 4]

$$\frac{d\bar{\beta}^2(z)}{dz} = \left\langle \frac{\partial n^2(r, z)}{\partial z} \right\rangle, \quad (5-14)$$

where the average is defined by analogy with Eq. (5-13). An alternative method for finding $\bar{\beta}(z)$ is given in Section 5-10 below.

5-6 Example: Clad power-law profiles

To illustrate the application of the above results, we consider the clad power-law profile fibers when ρ , Δ and n_{co} change slowly along the fiber, but the exponent q remains fixed. These profiles are defined by

$$n^2(r, z) = n_{co}^2(z) \{1 - 2\Delta(z)[r/\rho(z)]^q\}; \quad 0 \leq r \leq \rho(z), \quad (5-15a)$$

$$= n_{cl}^2 = n_{co}^2(z) \{1 - 2\Delta(z)\}; \quad \rho(z) \leq r < \infty. \quad (5-15b)$$

The ratio $L_o(z)/z_p$ is given by the ratio L_o/z_p , or ct/z , of Table 2-1, page 40, with $\bar{\beta}$ replaced by $\bar{\beta}(z)$, and n_{co} by $n_{co}(z)$. Hence the transit time of Eq. (5-11) becomes

$$t = \frac{1}{c(q+2)} \int_0^z \left\{ q \frac{n_{co}^2(z)}{\bar{\beta}(z)} + 2\bar{\beta}(z) \right\} dz. \quad (5-16)$$

To determine $\bar{\beta}(z)$, we find from Eq. (5-15) that in the core

$$\frac{\partial n^2(r, z)}{\partial z} = n^2 \frac{d}{dz} \ln \left(\frac{n_{co}^2 2\Delta}{\rho^q} \right) - n_{co}^2 \frac{d}{dz} \ln \left(\frac{2\Delta}{\rho^q} \right), \quad (5-17)$$

With the aid of Eq. (5-13) we deduce that over a ray half-period

$$\langle n^2(r, z) \rangle = \bar{\beta}(z) \frac{L_o(z)}{z_p(z)} = \frac{1}{q+2} \{ 2\bar{\beta}^2(z) + qn_{co}^2(z) \}. \quad (5-18)$$

Substituting Eqs. (5-17) and (5-18) into Eq. (5-14), we obtain a first order ordinary differential equation for $\bar{\beta}^2$ whose solution is [4]

$$\frac{n_{co}^2(z) - \bar{\beta}^2(z)}{n_{co}^2(0) - \bar{\beta}^2(0)} = \left[\frac{n_{co}^2(z) - n_{cl}^2(z)}{\rho(z)^q} \frac{\rho(0)^q}{n_{co}^2(0) - n_{cl}^2(0)} \right]^{2/(q+2)}. \quad (5-19)$$

This expression gives $\beta(z)$ for the clad parabolic profile when $q = 2$, and for the step profile when $q = \infty$. In the latter case we substitute for $\bar{\beta}(z)$ from Eq. (5-2) and rearrange to obtain

$$n_{co}(z)\rho(z)\sin\theta_z(z) = n_{co}(0)\rho(0)\sin\theta_z(0), \quad (5-20)$$

which is the generalization of Eq. (5-7b) for a variable core radius $\rho(z)$.

5-7 Small-amplitude nonuniformities

Nonuniformities on practical fibers tend to be of small amplitude in addition to being slowly varying. In such cases the determination of transit time, and hence pulse spread, is considerably simplified. Before considering specific characteristics of small-amplitude variations, we first recall from Section 5-4 that, when such variations are random and slowly varying, pulses cannot have the factor $z^{1/2}$ decrease in pulse width. This reduction requires each output ray direction at the end of the fiber to be uncorrelated with an input ray direction at the beginning of the fiber, and is incompatible with a fiber that varies slowly over a ray period. Indeed, the solution of Eq. (5-14) for $\bar{\beta}(z)$ and the adiabatic invariant of Section 5-10 explicitly express correlation between ray directions at the beginning and end of the fiber, regardless of any fiber variations, provided only that they are slowly varying.

In Chapter 3 we showed that on a uniform fiber, pulse spreading is proportional to distance z along the fiber. Accordingly, the only influence slowly varying nonuniformities can have on this result is to modify the coefficient multiplying z , in addition to changing the pulse shape and reducing pulse power by radiation. The latter is discussed in Section 5-13. However, as we show below, these effects tend to be small when the fiber variations are of small amplitude.

Expansion of the ray function

We assume that we can approximate the solution of Eq. (5-14) by expanding $\bar{\beta}(z)$ in powers of a small dimensionless ratio $\kappa(z)$, which is proportional to the amplitude of the nonuniformity. For reasons given below, we retain terms correct to second order and set

$$\bar{\beta}(z) = \bar{\beta}(0) + \bar{\beta}_1\kappa(z) + \bar{\beta}_2\kappa^2(z), \quad (5-21)$$

where $\bar{\beta}(0)$ is the value of $\bar{\beta}(z)$ at the beginning of the fiber, and $\bar{\beta}_1, \bar{\beta}_2$ are independent of z . The latter are determined by iterating Eq. (5-14). To lowest order in $\kappa(z)$ the right side of Eq. (5-14) is zero, corresponding to the uniform-fiber result $\bar{\beta}(z) = \bar{\beta}(0)$. The first-order correction $\bar{\beta}_1$ is obtained by equating

terms of order $\kappa(z)$ in Eq. (5-14) and integrating. Thus

$$\bar{\beta}_1(z) = \frac{1}{2\bar{\beta}(0)} \int_0^z \left\langle \frac{\partial n^2(r, z)}{\partial z} \right\rangle dz; \quad \bar{\beta}_1(0) = 0, \quad (5-22)$$

where the averaging procedure is explained below Eq. (5-13) and is performed correct to order $\kappa(z)$ with $\bar{\beta}(z)$ approximated by $\bar{\beta}(0)$ in the ray-path equation. The second-order correction is found similarly.

Transit time

The ray transit time along a slowly varying fiber is expressed by Eq. (5-11). We can expand $L_0(z)$ and $z_p(z)$ in powers of $\kappa(z)$ in a similar manner to Eq. (5-21). On substituting these expansions into Eq. (5-11), we obtain correct to second order

$$t = t_u + A\bar{\kappa} + B\bar{\kappa}^2, \quad (5-23)$$

where t_u is the transit time for a uniform fiber with $\bar{\beta}(z) = \bar{\beta}(0)$, and A, B are independent of z but involve fiber and ray-path parameters. The mean value of $\kappa(z)$ and the average value of $\kappa^2(z)$ over the fiber length are defined by

$$\bar{\kappa} = \frac{1}{z} \int_0^z \kappa(z) dz; \quad \bar{\kappa}^2 = \frac{1}{z} \int_0^z \kappa^2(z) dz. \quad (5-24)$$

Clearly we can always choose the parameters of the uniform fiber in such a way as to ensure that the mean value of the nonuniformities over the fiber length is zero. The correction to the transit time for the uniform fiber is then of second order, i.e. $A = 0$ in Eq. (5-23).

Pulse spread

Although the correction to ray transit time due to fiber nonuniformities is small, we recall from Chapter 3 that the pulse width on a weakly guiding fiber is also small. For example, the minimum pulse width of Eq. (3-9) for the optimum clad power-law profile is proportional to Δ^2 , or θ_c^4 . We investigated the effect of material dispersion on pulse spreading in Section 3-8; here we account for the effect of slight nonuniformities on the pulse minimum.

5-8 Example: Slight core-radius variations

We consider the clad power-law profiles of Table 2-1, page 40, when there is only a slight variation in core radius. Thus we set

$$\rho(z) = \rho_0 + \delta\rho(z); \quad |\delta\rho(z)| \ll \rho_0, \quad (5-25)$$

where ρ_0 is the core radius of the uniform fiber for which $\delta\bar{\rho} = 0$. The mean variation $\delta\bar{\rho}$ is defined by the first expression in Eq. (5-24) with $\kappa(z) = \delta\rho(z)/\rho_0$. To determine the terms in the expansion of $\bar{\beta}(z)$ in Eq. (5-21) with $\kappa(z) = \delta\rho(z)/\rho_0$, we can either use the iterative procedure based on Eq. (5-22), or simply expand the exact solution of Eq. (5-19), leading to

$$\bar{\beta}_1 = \frac{q}{q+2} \frac{n_{\text{co}}^2 - \bar{\beta}^2(0)}{\bar{\beta}(0)}; \quad \bar{\beta}_2 = -\frac{3q+2}{2(q+2)} \bar{\beta}_1 - \frac{\bar{\beta}_1^2}{2\bar{\beta}(0)}. \quad (5-26)$$

If we substitute into Eq. (5-16) with $n_{\text{co}}(z)$ replaced by n_{co} , then

$$t = t_u + \frac{z}{c} D \frac{\delta\rho^2}{\rho_0^2}; \quad D = \frac{qn_{\text{co}}^2\bar{\beta}_1^2 + (2\bar{\beta}^2(0) - qn_{\text{co}}^2)\bar{\beta}_2\bar{\beta}(0)}{(q+2)\bar{\beta}^3(0)}, \quad (5-27)$$

since $\delta\bar{\rho} = 0$. The transit time t_u for the uniform fiber is given in Table 2-1, page 40, with $\bar{\beta} = \bar{\beta}(0)$ and $\rho = \rho_0$, and $\delta\rho^2/\rho_0^2$ is defined by the second expression in Eq. (5-24) with $\kappa(z) = \delta\rho(z)/\rho_0$.

Pulse spread

The pulse spread for the uniform clad power-law profiles is discussed in Section 3-2. If we repeat the analysis using the transit time of Eq. (5-27) for the nonuniform fiber, we find that the minimum transit time t_{\min} occurs approximately at $\bar{\beta}(z) = \bar{\beta}_m$ of Eq. (3-6) and the maximum transit time t_{\max} occurs at $\bar{\beta}(z) = n_{\text{cl}}$. At the optimum profile exponent of Eq. (3-8), the pulse spread t_d of Eq. (3-9) for the weakly guiding fiber is modified by the slight nonuniformity and becomes[4]

$$t_{\max} - t_{\min} \cong t_d \{1 + 8(\delta\rho^2/\rho_0^2)\}; \quad q = q_{\text{opt}} \cong 2 - \theta_c^2. \quad (5-28)$$

Hence the increase in pulse width depends only on the amplitude of the non-uniformities and not on their spatial frequency. This can be best illustrated by considering a sinusoidally varying core radius defined by

$$\delta\rho(z) = \delta\rho_m \cos(z/z_s); \quad \delta\rho_m \ll \rho_0, \quad (5-29)$$

where z_s is the spatial period. Substitution into Eq. (5-28) gives

$$t_{\max} - t_{\min} \cong t_d \{1 + 4(\delta\rho_m/\rho_0)^2\}, \quad (5-30)$$

assuming $z \gg z_s$. Thus a 10% variation in core radius gives only a 4% increase in pulse width at the optimum profile.

5-9 Example: Slight exponent variations

We now consider the clad power-law profiles of Table 2-1, page 40, when only the exponent $q(z)$ varies slowly along the fiber [3-5]. The variation about some mean value

q_0 is slight, and we set

$$q(z) = q_0 + \delta q(z); \quad |\delta q(z)/q_0| \ll 1, \quad (5-31)$$

where q_0 is chosen so that $\delta q(z)$ has zero mean along the length of the fiber, i.e. $\overline{\delta q} = 0$. The solution of Eq. (5-14) is not known exactly in this situation, and must be found iteratively, as explained in Section 5-7, leading to the coefficients in Eq. (5-21), where $\kappa(z) = \delta q(z)/q_0$. By analogy with Eq. (5-16), the transit time is given by

$$t = \frac{n_{co}}{c} \int_0^z \frac{1}{q(z) + 2} \left\{ q(z) \frac{n_{co}}{\bar{\beta}(z)} + \frac{2\bar{\beta}(z)}{n_{co}} \right\} dz. \quad (5-32)$$

Substituting Eqs. (5-21) and (5-31), and recalling that $\overline{\delta q} = 0$, we find that, correct to second order, the result analogous to Eq. (5-27) is [4]

$$t = t_u + (C_3 + \Delta C_4) \overline{\delta q^2}, \quad (5-33)$$

where C_3 and C_4 are dimensionless constants involving $\bar{\beta}(0)$, n_{co} and q_0 .

Effective exponent

If the fiber is weakly guiding with a sufficiently small variation in profile, we can ignore the term ΔC_4 compared with C_3 in Eq. (5-33), which is equivalent to assuming $\bar{\beta}(z) = \bar{\beta}(0)$ in the ray-path equation to all orders in $\delta q(z)$ when iterating Eq. (5-14). If we make this assumption in Eq. (5-32) and introduce an *effective exponent* q_e defined by [3]

$$\frac{1}{2 + q_e} = \frac{1}{z} \int_0^z \frac{dz}{2 + q(z)}, \quad (5-34)$$

then the transit time is given by

$$t = \frac{z}{c} \frac{n_{co}}{2 + q_e} \left\{ \frac{2\bar{\beta}(0)}{n_{co}} + q_e(z) \frac{n_{co}}{\bar{\beta}(0)} \right\}. \quad (5-35)$$

This is identical in form to the uniform fiber transit time of Table 2-1, page 40, with $\bar{\beta} = \bar{\beta}(0)$ and q replaced by q_e . Thus a *slight variation in exponent on a slowly varying fiber in the weak-guidance approximation is equivalent to a uniform fiber with a different exponent*. If we substitute Eq. (5-31) into Eq. (5-34), we find that correct to second order

$$q_e = q_0 - \overline{\delta q^2} / \{2 + q_0\}, \quad (5-36)$$

since $\overline{\delta q} = 0$. Thus, only the amplitude of the variations in $q(z)$ affect pulse width. If we assume that $\delta q(z)$ has the sinusoidal variation

$$\delta q(z) = \delta q_m \cos(z/z_s); \quad \delta q_m \ll q_0, \quad (5-37)$$

where δq_m is the maximum value of $\delta q(z)$, then [4]

$$q_e = q_0 - \delta q_m^2 / 2(q_0 + 2), \quad (5-38)$$

provided $z \gg z_s$.

Pulse spread

We showed in Section 3-2 that the minimum pulse width on a uniform fiber with a clad power-law profile is acutely sensitive to small changes in exponent about the optimum profile. The effect of exponent nonuniformities on the optimum profile can be deduced by substituting q_{opt} of Eq. (3-8) into Eq. (5-36). Since the fiber is assumed weakly guiding, the effective exponent is

$$q_e \cong 2 - 2\Delta - \overline{\delta q^2}/4 \cong 2 - \theta_c^2 - \overline{\delta q^2}/4. \quad (5-39)$$

A deviation of $\pm \Delta$ in exponent about $q = q_{\text{opt}}$ in Fig. 3-3 causes a tenfold increase in pulse width. Consequently if $\overline{\delta q^2} = 4\Delta$ the same increase occurs. On the other hand, given that a fiber has slow exponent variations, we can use Eq. (5-39) to compensate for them. In other words, if $\overline{\delta q^2}$ is prescribed, the profile with exponent $q = 2 - 2\Delta + \overline{\delta q^2}/4$ suffers minimum pulse spread. Furthermore, as the profile height Δ decreases, the pulse spread becomes more vulnerable to nonuniformities. The spreading depends only on the amplitude of the nonuniformities and is independent of their spatial distribution, as long as they are slowly varying. Finally, we note that spreading is more sensitive to slight fractional variations in the profile exponent than to equivalent fractional variations in core radius, discussed in the previous example.

5-10 Adiabatic invariant

We now introduce an alternative approach to the description of slowly varying fibers which makes contact with other areas of physics.

When a fiber is uniform it is straightforward to determine ray paths, because $\bar{\beta}$ and \bar{l} are constant along a path. If the fiber is nonuniform, the invariant \bar{l} is defined by Eq. (5-6), provided the fiber remains circularly symmetric, but, in general, there is no equivalent generalization of the $\bar{\beta}$ invariant. However, if the nonuniformities change slowly over a ray half-period, then there is a parameter which is approximately constant along the fiber length, and thereby simplifies the determination of the ray-path parameters. We call this parameter the *adiabatic invariant*. The nonuniformities can become arbitrarily large provided only that this occurs over distances large compared with the ray half-period, e.g. a tapered fiber when the ratio of core radii at the ends is large, but the taper angle is everywhere small.

To derive this invariant, we recall from Section 5-5 that ray trajectories on slowly varying fibers are characterized by a short length scale equal to the half-period $z_p(z)$ and the length scale of the nonuniformities which is long compared with $z_p(z)$. If we average the ray-path equations of Eq. (5-3) over a half-period, we remove the rapid variation along the path. This leads to equations which describe the slow variation due to the nonuniformities, e.g. Eq. (5-6), which is exact, Eq. (5-14), and a similar equation corresponding to the average of Eq. (5-3a). From these equations it is possible to show that the parameter \bar{l} is nearly constant along a path extending the length of the fiber,

where

$$I = \int_{z_p(z)} n(r, z) \frac{dr}{ds} dr. \quad (5-40)$$

The integration is along the path over a half-period, ds is the element of length along the path, and the explicit z dependence in $n(r, z)$ and $z_p(z)$ is held fixed for evaluation of the integral. This is a well-known result of classical mechanics, where I is called the *adiabatic invariant* [6]. Discussions of ray propagation within the framework of classical mechanics are available elsewhere [7, 8]. We can put I into a more convenient form using Eq. (5-2) and the obvious generalization of Eq. (2-21) to slowly varying fibers to obtain

$$I = 2\bar{\beta}(z) \int_{r_{ic}(z)}^{r_{tp}(z)} \frac{dr}{dz} dr = 2 \int_{r_{ic}(z)}^{r_{tp}(z)} \left\{ n^2(r, z) - \bar{l}^2 \frac{\rho^2(0)}{r^2} - \bar{\beta}^2(z) \right\}^{1/2} dr, \quad (5-41)$$

where $r_{ic}(z)$ and $r_{tp}(z)$ are the the positions of the inner caustic and turning-point caustic. This invariant implicitly governs the variation in $\bar{\beta}(z)$. When evaluating the integral, the explicit dependence of $n(r, z)$, $\bar{\beta}(z)$, $r_{ic}(z)$ and $r_{tp}(z)$ on z is held fixed. To demonstrate the usefulness of this result we consider simple examples.

5-11 Example: Step profile

When the nonuniform fiber has a step profile, the core index $n(z)$ depends only on z , and the upper limit of integration $r_{tp}(z)$ in Eq. (5-41) is replaced by the core radius $\rho(z)$. If the path makes angle $\theta_z(z)$ with the axial direction, then with the help of Eq. (5-2) we have

$$I = 2 \int_{r_{ic}(z)}^{\rho(z)} \left\{ n^2(z) \sin^2 \theta_z(z) - \frac{\bar{l}^2 \rho^2(0)}{r^2} \right\}^{1/2} dr, \quad (5-42)$$

where $r_{ic}(z) = \bar{l}\rho(0)/\{n(z) \sin \theta_z(z)\}$. If we change variable from r to $x = r/r_{ic}(z)$, then

$$I = 2\bar{l}\rho(0) \int_1^{\rho(z)/r_{ic}(z)} \frac{(x^2 - 1)^{1/2}}{x} dx. \quad (5-43)$$

Since \bar{l} is an invariant for the circular fiber we deduce that $\rho(z)/r_{ic}(z)$ is also invariant, whence

$$n(z)\rho(z) \sin \theta_z(z) = n(0)\rho(0) \sin \theta_z(0), \quad (5-44)$$

which was derived directly from the ray-path equations in Eq. (5-20). We are reminded that this result applies only to rays whose half-period is small compared with the distance along the fiber in which there is a significant change in core index or radius. Consequently rays with $\theta_z(z) \cong 0$ are excluded, since $z_p(z) \rightarrow \infty$ as $\theta_z(z) \rightarrow 0$. The result is identical to the Abbe' sine law of geometric optics [7, 9]. If we substitute Eq. (5-44) into Eq. (5-2), then the variation in $\bar{\beta}(z)$ is given explicitly by

$$\bar{\beta}(z) = \{n^2(z) - [n^2(0) - \bar{\beta}^2(0)]\rho^2(0)/\rho^2(z)\}^{1/2}, \quad (5-45)$$

where $\bar{\beta}(0) = n(0) \cos \theta_z(0)$. When the core radius is uniform, i.e. $\rho(z) = \rho(0)$, Eqs. (5-45) and (5-44) reduce to Eqs. (5-7a) and (5-7b), respectively, which are both exact and are derived directly from Eq. (5-4) for $\bar{\beta}(z)$.

Slight nonuniformities

For fibers in which there is only a slight departure from the initial index and radius values, we set

$$n(z) = n(0) + \delta n(z); \quad \rho(z) = \rho(0) + \delta \rho(z), \quad (5-46)$$

where $|\delta n(z)| \ll n(0)$ and $|\delta \rho(z)| \ll \rho(0)$. Substituting into Eq. (5-45) and retaining only lowest-order terms, we obtain

$$\bar{\beta}(z) = \bar{\beta}(0) + \frac{n(0)}{\bar{\beta}(0)} \delta n(z) + \frac{n^2(0) - \bar{\beta}^2(0)}{\bar{\beta}(0)\rho(0)} \delta \rho(z). \quad (5-47)$$

This shows that when the fiber is weakly guiding, i.e. $\bar{\beta}(0) \cong n(0)$, small changes in core index have a much larger effect on $\bar{\beta}(z)$ than equivalent changes in core radius $\rho(z)$.

5-12 Example: Clad power-law profiles

We next consider nonuniform fibers with clad power-law profiles. These profiles have the form given by Eq. (5-15), with n_{co} , Δ and ρ dependent on z , but we assume the exponent q remains constant. Substituting into Eq. (5-41) we have

$$I = 2 \int_{r_{ic}(z)}^{r_{tp}(z)} \left\{ n_{co}^2(z) - \bar{\beta}^2(z) - \frac{l^2 \rho^2(0)}{r^2} - 2\Delta(z)n_{co}^2(z) \frac{r^q}{\rho(z)^q} \right\}^{1/2} dr. \quad (5-48)$$

We change the variable from r to x and define a parameter $h(z)$, where

$$r = \frac{x}{\{n_{co}^2(z) - \bar{\beta}^2(z)\}^{1/2}}; \quad h(z) = \frac{2\Delta(z)n_{co}^2(z)}{\rho(z)^q \{n_{co}^2(z) - \bar{\beta}^2(z)\}^{(q+2)/2}}. \quad (5-49)$$

The invariant then has the simpler form

$$I = 2 \int_{x_{ic}(z)}^{x_{tp}(z)} \left\{ 1 - \frac{l^2 \rho^2(0)}{x^2} - h(z)x^q \right\}^{1/2} dx, \quad (5-50)$$

where $x_{ic}(z) = \{n_{co}^2(z) - \bar{\beta}^2(z)\}^{1/2} r_{ic}(z)$ and similarly for $x_{ip}(z)$. Since $x_{ic}(z)$ and $x_{ip}(z)$ are roots of the integrand, they depend only on $\bar{l}\rho(0)$, $h(z)$ and q . Consequently the invariant I is a function of these three quantities, but as \bar{l} is an invariant and q is assumed constant, $h(z)$ must also be an invariant. On rearranging the equation $h(z) = h(0)$, we recover Eq. (5-19).

Slowly varying exponent

If we now allow the exponent q to vary with z , we can generate an invariant for meridional rays. We set $\bar{l} = x_{ic}(z) = 0$ and $q = q(z)$ in Eq. (5-50) and change the variable to $u = h(z)x^{q(z)}$, so that $x = x_{ip}(z)$ corresponds to $u = 1$. The resulting integral can be evaluated using Eqs. (37-104) and (37-105), and leads to the invariant

$$\frac{1}{h(z)^{1/q(z)}} \frac{\Gamma(1 + 1/q(z))}{\Gamma(3/2 + 1/q(z))} = \frac{1}{h(0)^{1/q(0)}} \frac{\Gamma(1 + 1/q(0))}{\Gamma(3/2 + 1/q(0))}, \quad (5-51)$$

where $h(z)$ is defined by Eq. (5-49) with $q = q(z)$.

5-13 Radiation loss

On a *uniform* fiber, a ray which is bound at the beginning of the fiber remains bound along the fiber. However, on a *nonuniform* fiber, a ray which is initially bound may become a leaky ray over part of its trajectory and lose power by radiation, if the variation in the parameter $\bar{\beta}(z)$ of Eq. (5-2) is sufficiently large. Otherwise it will remain a bound ray over the length of the fiber even though $\bar{\beta}(z)$ varies. Here we give a simple upper bound for the radiation loss.

Upper bound on power loss

Consider a nonuniform fiber with constant cladding index n_{cl} , but whose core radius $\rho(z)$ and profile $n(r, z)$ vary *arbitrarily* along its length. By analogy with Eq. (2-24a), rays which are bound at the beginning of the fiber have parameter values $\bar{\beta}(0)$ in the range $n_{cl} < \bar{\beta}(0) \leq n_{co}(0)$, where $n_{co}(z)$ is the maximum core index at position z . Some of these rays will subsequently have parameter values $\bar{\beta}(z)$ satisfying $\bar{\beta}(z) \leq n_{cl}$ and will radiate power along part of their trajectories, as illustrated in Fig. 5-4. The actual rate of power loss for an individual ray is discussed in Chapter 7. Here we give an upper bound on this loss by assuming *all* power is lost from rays which become leaky.

For convenience we assume excitation by a diffuse source. The total initial bound ray power, P_{br} , is then given by Eq. (4-13) with ρ and $n(r)$ replaced by $\rho(0)$ and $n(r, 0)$. We define \bar{P}_{br} to be the total power of rays which remain bound everywhere along the fiber, i.e. $\bar{\beta}(z) > n_{cl}$ for all z . The maximum power which

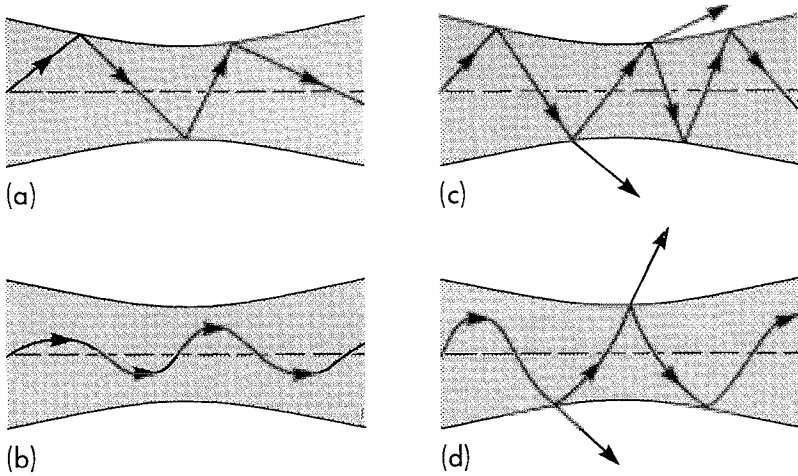


Fig. 5-4 Step- and graded-profile fibers whose core radius and profile vary along their length, showing (a), (b) a ray which remains bound, and (c), (d) a bound ray which becomes a leaky ray along part of its path.

can be radiated, P_{rad} , is then given by

$$P_{\text{rad}} = P_{\text{br}} - \bar{P}_{\text{br}}. \quad (5-52)$$

To determine \bar{P}_{br} we need to know how $\beta(z)$ varies along the fiber. If we assume the fiber is *slowly varying*, we can use the results of previous sections. We now determine P_{rad} for fibers with slow variations in core radius only.

5-14 Example: Variable core radius—step profile

Consider a step-profile fiber with core and cladding indices n_{co} and n_{cl} , when the core radius $\rho(z)$ is slowly varying. The angle $\theta_z(z)$ a ray makes with the axial direction at position z is related to the initial angle $\theta_z(0)$ by Eq. (5-44) with $n_{\text{co}}(z) = n_{\text{co}}(0) = n_{\text{co}}$. An initially bound ray may become a leaky ray only if the core radius decreases below its initial value $\rho(0)$. If the smallest radius anywhere along the fiber is ρ_{min} and z_m is the corresponding position, the ray direction at z_m is given by

$$\sin \theta_z(z_m) = \{\rho(0)/\rho_{\text{min}}\} \sin \theta_z(0). \quad (5-53)$$

Hence, by analogy with Eq. (2-6a), a ray is bound everywhere along the fiber if $\theta_z(z_m) < \theta_c$, where θ_c is defined by Eq. (2-5). Accordingly, only those rays on the endface with directions in the range

$$0 \leq \sin \theta_z(0) \leq \{\rho_{\text{min}}/\rho(0)\} \sin \theta_c, \quad (5-54)$$

satisfy this condition. To determine \bar{P}_{br} we observe that the total power in bound rays due to illumination by a diffuse source, as given by Eq. (4-61), varies with the square of

the core radius. Hence \bar{P}_{br} is proportional to ρ_m^2 and thus the maximum fraction of the total initial bound-ray power which can be lost to radiation is given by

$$P_{rad}/P_{br} = 1 - \rho_{min}^2/\rho^2(0) \cong 2\{1 - \rho_{min}/\rho(0)\}, \quad (5-55)$$

where P_{rad} is given by Eq. (5-52) and the approximation holds when $\rho_{min} \cong \rho(0)$.

5-15 Example: Variable core radius—clad power-law profiles

We next consider the clad power-law profiles of Table 2-1, page 40, when there is a slow variation in core radius $\rho(z)$ only. If the minimum radius occurs at z_m , then $\bar{\beta}(z_m)$ and $\bar{\beta}(0)$ are related by Eq. (5-19) with $\rho(z) = \rho_{min}$. A ray is everywhere bound if $\bar{\beta}(z_m) > n_{cl}$, and on the endface the corresponding range of $\bar{\beta}(0)$ satisfies

$$n_{co}^2[1 - 2\Delta\{\rho_{min}/\rho(0)\}^{2q/(q+2)}] < \bar{\beta}^2(0) \leq n_{co}^2(0). \quad (5-56)$$

To determine \bar{P}_{br} , we note that total bound-ray power due to a diffuse source is given by Eq. (4-18) and, like the step-profile above, is proportional to the square of core radius. Consequently, the maximum fraction of initial bound-ray power that can be radiated is given by Eq. (5-55) and is independent of the exponent q , i.e. independent of profile shape.

TAPERS AND LIGHT CONCENTRATION

It is often desirable to channel light from a source or fiber of comparatively large cross-section into a fiber of smaller cross-section as efficiently as possible. We discussed the use of lenses for this purpose in Chapter 4. Here we investigate how tapered fibers, such as the ones illustrated in Fig. 5-5, can concentrate light power. We first show how the light-concentrating properties

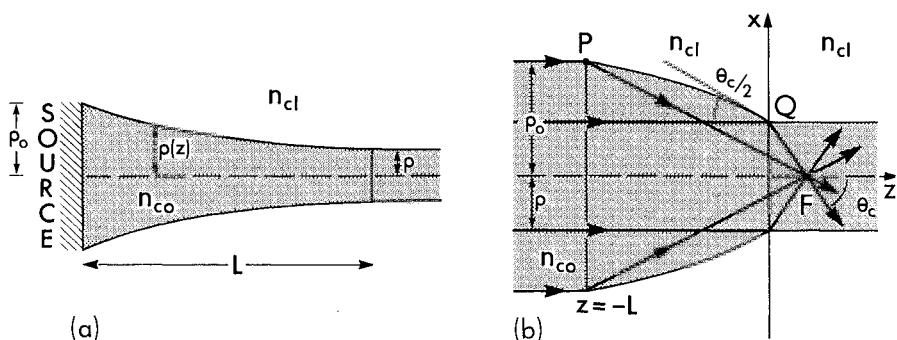


Fig. 5-5 Step-profile tapers, showing (a) a slowly-varying taper illuminated by a diffuse source and (b) a parabolic taper illuminated by an on-axis beam.

of linear and parabolic tapers of arbitrary taper angle can be determined simply and exactly using ray tracing. Since tapers are often slowly varying, i.e. the local taper angle is small, we use the approximate ray invariant of Section 5–11 to describe light concentration for otherwise arbitrary tapers. Direct comparison with the linear taper enables us to determine the accuracy of the slow-variation approximation. To illustrate the concepts involved as simply as possible, we consider only step-profile tapers and fibers with common core and cladding indices.

5–16 Collimated-beam illumination

When the core radius of a taper varies arbitrarily along its length, the slow-variation approximation is inaccurate, and we must determine the exact trajectory of each ray. In this regard it is simplest to consider meridional rays only. Thus we assume illumination by a collimated beam of radius ρ_0 equal to the radius at the beginning of the taper. Given the radii at each end of the taper and the complementary critical angle θ_c of the adjoining fiber, our main interest is to determine the minimum length of the taper which ensures that all the power incident on the taper is transmitted into bound rays of the fiber.

5–17 Example: Parabolic taper

An on-axis collimated beam enters a step-profile, parabolic taper at $z = -L$ in Fig. 5–5(b), where the core radius is ρ_0 . A step-profile fiber of core radius ρ abuts the end of the taper at $z = 0$. The core index of the fiber, taper and source medium is assumed to be n_{co} for convenience, and likewise the fiber and taper cladding index is n_{cl} . Each on-axis ray reflects from the parabolic interface so that the angles of incidence and reflection relative to the tangent to the interface are equal. It is a well-known property of the parabolic shape, that every reflected ray passes through the focus F as shown. Furthermore, the angle the reflected ray makes with the axis increases as the point of reflection moves closer to the end of the taper. Accordingly, given ρ_0 , ρ and θ_c , as defined inside the front cover, the minimum taper length L_{min} which ensures that all the light power entering the taper excites only bound rays of the fiber, corresponds to the reflected ray at Q making angle θ_c with the fiber axis, according to Eq. (2–6a). We then deduce from Snell's law that the angle between the incident ray and the tangent to the interface at Q is $\theta_c/2$. Relative to the axes in Fig. 5–5(b), the equation of the taper interface is readily shown to be

$$x^2 = \rho^2 - (\rho_0^2 - \rho^2)(z/L); \quad -L \leq z \leq 0. \quad (5-57)$$

If we impose the condition $dx/dz = -\tan(\theta_c/2)$ at $z = 0$, we deduce that

$$L_{min} = \frac{\rho_0^2 - \rho^2}{2\rho} \frac{1}{\tan(\theta_c/2)} \cong \frac{\rho_0^2 - \rho^2}{\rho\theta_c}, \quad (5-58)$$

where the approximation applies when the fiber is weakly guiding, i.e. $\theta_c \ll 1$.

5-18 Example: Linear taper

The parameters for the linear taper of Fig. 5-6(a) are identical with those of the previous example and the taper angle is Ω . We can determine very simply the minimum taper length for total power transmission when a meridional ray enters the taper at $z = -L$ and makes angle θ_0 with the axis. This result applies to both direct on-axis illumination by a collimated beam, i.e. $\theta_0 = 0$, and the inclusion of a lens, as discussed in Section 4-11, which transforms the on-axis beam into a cone of meridional rays at angle $\theta_0 > 0$.

Consider meridional rays incident at angle θ_0 over the taper cross-section at $z = -L$. All these rays will become bound rays of the fiber if the extreme ray incident on the taper interface at P in Fig. 5-6(a) becomes bound. Given ρ_0 , ρ and θ_c for the step profile, the shortest taper length satisfying this condition corresponds to the trajectory which meets the end of the fiber at Q, and after reflection crosses the fiber axis at angle θ_c . This means that the incident ray at Q makes angle $\theta_c + \Omega$ with the direction of the taper interface.

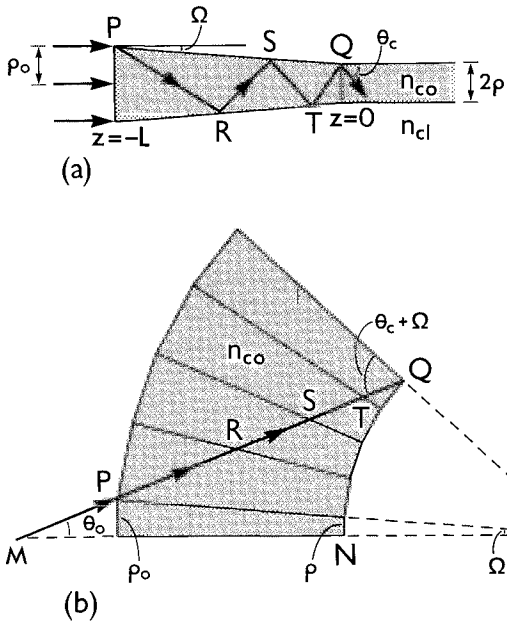


Fig. 5-6 (a) Step-profile linear taper with taper angle Ω and (b) the equivalent geometrical path.

Equivalent geometrical path

We require the geometry of the ray path between P and Q in Fig. 5-6(a) in order to determine the minimum taper length L_{min} . This is obtained by using an equivalent path in Fig. 5-6(b), which shows an arc of contiguous, identical tapers with common vertex

O. The length of path between successive reflections and the angles it makes with the taper interface at P, R, S, T and Q in Fig. 5-6(a) are identical to the corresponding values for the straight line path PRSTQ in Fig. 5-6(b) [9]. Thus PQ makes angle $\theta_c + \Omega$ with OQ, and by geometry $OQ = \rho_0 / \tan \Omega$, $OM = ON + L + \rho_0 / \tan \theta_0$. On applying the sine rule of Eq. (37-8) to triangle OQM, we deduce that Ω , and hence L_{\min} , are determined in terms of ρ , ρ_0 and θ_c by

$$L_{\min} = \frac{\rho_0 - \rho}{\tan \Omega}; \quad \frac{\rho \sin(\theta_c + \Omega)}{\rho_0 \sin \theta_0} = 1 + \frac{\tan \Omega}{\tan \theta_0}. \quad (5-59a)$$

The solution for Ω is obtained numerically, but if all the angles involved are small, there is an approximate solution given by

$$L_{\min} \cong (\rho_0 - \rho)^2 / (\theta_c \rho - \theta_0 \rho_0). \quad (5-59b)$$

For an on-axis beam $\theta_0 = 0$, in which case Eqs. (5-58) and (5-59b) show that the minimum length parabolic taper is longer than the corresponding linear taper by a factor $(\rho_0 + \rho) / (\rho_0 - \rho)$ provided the taper angle is small and the fiber is weakly guiding.

5-19 Diffuse-source illumination

An exact ray analysis of arbitrarily shaped tapers is complicated, especially if both meridional and skew rays are excited. However, provided that the taper is sufficiently slowly varying, i.e. the local taper angle is small, we can circumvent these difficulties by using the approximate invariant derived earlier in the chapter. To demonstrate this simplification, we assume that a diffuse source of radius ρ_0 equal to the initial taper radius abuts the step-profile taper in Fig. 5-5(a). The taper radius decreases to ρ in distance L and abuts a step-profile fiber of core radius ρ . For convenience the source medium, taper core and fiber core have common index n_{co} and likewise the common cladding index is n_{cl} .

A ray excited by the source makes angle $\theta_z(z)$ with the axis of the taper at position z . The ray will be a bound ray of the fiber provided $\theta_z(0) \leq \theta_c$, where $z = 0$ denotes the end of the taper. If the taper radius $\rho(z)$ decreases monotonically with increasing z , then the range of ray directions at the beginning of the taper $z = -L$ for which rays remain bound satisfies $0 \leq \theta_z(-L) \leq \theta_0$. These quantities are related by Eq. (5-20), provided the taper is slowly varying, and since the core index is uniform we deduce that the limiting ray directions satisfy

$$\rho_0 \sin \theta_0 = \rho(z) \sin \theta_z(z) = \rho \sin \theta_c. \quad (5-60)$$

Accordingly the relationship between the total bound-ray power entering the

fiber, P_{br} , and the total power, \bar{P}_{br} , of rays within $0 \leq \theta_z(-L) \leq \theta_c$ at the beginning of the taper follows by analogy with Eq. (5-55) as

$$P_{\text{br}} = (\rho^2/\rho_0^2)\bar{P}_{\text{br}}. \quad (5-61)$$

Since total bound-ray power is proportional to the core area in Eq. (4-16), and ρ^2/ρ_0^2 is the ratio of the core and source cross-sections, it is clear that there is no advantage in the arrangement in Fig. 5-5(a) over placing the source directly against the fiber. Thus, *when the source excites rays over a range of directions greater than that for bound rays within the fiber, it is not possible to increase the bound-ray power by use of a taper.* This is the identical conclusion reached in Section 4-14 when a lens is used to concentrate diffuse-source power.

Partially diffuse source

Now consider the situation in Fig. 5-5(a) when the diffuse source is replaced by a partially diffuse source which emits light only within the range of angles $0 \leq \theta_z(-L) \leq \theta_s$. If θ_s does not exceed θ_0 of Eq. (5-60), then *all of the source power goes into bound rays of the fiber*, and, compared with placing the source directly against the fiber, there is an increase in total bound-ray power by a factor ρ_0^2/ρ^2 through using a taper. This conclusion parallels the results of Section 4-16 for a lens and a partially diffuse source.

Arbitrary taper angle

Although the above conclusions are based on a slowly varying taper, it is possible to make more general statements about tapers whose radii vary arbitrarily. Instead of the complicated procedure of determining each ray path along the taper, the whole family of rays excited by the source is considered [10]. It is possible to show that, instead of Eq. (5-60), we have an inequality $\rho_0 \sin \theta_0 \leq \rho \sin \theta_c$. In other words, Eq. (5-61) is the upper limit to light concentration.

5-20 Accuracy of the slow-variation approximation

The approximate ray invariant for a slowly varying step-profile taper is expressed by Eq. (5-60). This relationship is accurate provided that the change $\delta\rho(z)$ in taper radius over the local ray half-period is small. If the taper and fiber are weakly guiding then $\theta_z(z) \ll 1$, and by generalizing the expression for z_p in Table 2-1, page 40, to slowly varying fibers, we deduce that $z_p(z) \cong 2\rho(z)/\theta_z(z)$ for meridional rays. In terms of the local taper angle $\Omega(z)$, the slow-variation

condition is equivalent to

$$\Omega(z) \cong \delta\rho(z)/z_p(z) \ll \rho(z)/z_p(z) \cong \theta_z(z)/2. \quad (5-62a)$$

Hence the ray angle must greatly exceed the taper angle everywhere along the taper if the relationship of Eq. (5-60) is to be accurate. Furthermore, although Eq. (5-60) does not give the minimum taper length L_{\min} , it can be estimated qualitatively by satisfying Eq. (5-62a) for each value of z . This criterion applies to the diffuse-source problem of the previous section.

Linear taper

We can quantify the accuracy of Eq. (5-60) for the linear taper of the previous section. At the minimum taper length of Eq. (5-59b) we deduce from Eq. (5-59a) that for meridional rays

$$2(\Omega/\theta_c) = 2\{\rho - (\theta_0/\theta_c)\rho_0\}/(\rho_0 - \rho). \quad (5-62b)$$

If $\rho_0 \gg \rho$, then $\Omega \ll \theta_c/2$ regardless of the value of θ_0 , which agrees qualitatively with Eq. (5-62a) when $\theta_z(z) = \theta_c$. However, if $\rho_0 \gtrsim \rho$ then $\theta_0 \cong 0$ and Eq. (5-62a) is not satisfied.

DISCONTINUOUS NONUNIFORMITIES AND SCATTERERS

We now turn attention to nonuniformities associated with abrupt, or discontinuous changes from the uniform cylindrical fiber, concentrating on the effects of small, isolated scatterers distributed throughout the core. The dimensions of each scatterer are assumed small compared with the wavelength of light. When a bound ray hits one of these scatterers, its power is redistributed, in general, in all directions, as shown in Fig. 5-7(a) for a step-profile fiber. The fraction of incident power scattered into a particular direction depends on the nature of the scatterer. Some power will be scattered into leaky rays, and the rest will be redistributed among bound rays. Since this occurs at each scatterer, it is clear that the initial power distribution will be modified along the fiber, some being lost as radiation. Obviously, the greater the density of scatterers the more rapidly this modification occurs.

When the scatterers are randomly distributed along the fiber, each ray entering the fiber is uncorrelated with each ray at the end of the fiber. These are the conditions, discussed in Section 5-4, which lead to a pulse spread proportional to $z^{1/2}$. Our purpose here is to derive an equation which describes the distribution of light intensity among the various ray directions [11]. This

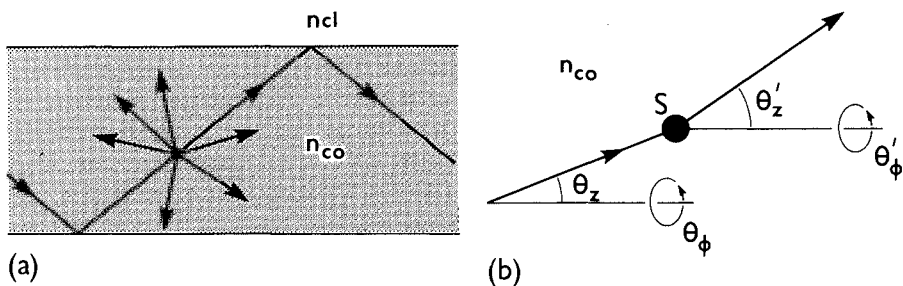


Fig. 5-7 (a) Scattering of bound-ray power in the core of a step-index fiber and (b) angular directions of incident and scattered rays at an isolated scatterer relative to the fiber axis.

equation reduces to a diffusion equation when the scattering is forward directed, as we show in Section 5-22.

5-21 Distribution of bound-ray power

Starting from the redistribution of ray power due to a ray incident on an isolated scatterer, we derive an integral equation which governs the distribution of bound-ray power when many scatterers are present in the fiber. For convenience we assume a step profile, but the derivation is readily extended to graded-profile fibers [11].

Scattering cross-section

Consider the isolated scatterer S in Fig. 5-7(b), and a ray incident on it. Scattering is usually described in terms of a differential scattering cross-section σ_d , which determines the distribution of scattered power when a *plane wave* is incident on the scatterer [12]. To relate σ_d to scattering in terms of rays, we recall our concept of a ray as a *local plane wave*, discussed in Section 35-3. We regard the local plane wave associated with the incident ray in Fig. 5-7(b) as part of an infinite plane wave propagating in the same direction. Accordingly we may set

$$\sigma_d = \frac{\text{ray power scattered per unit solid angle}}{\text{incident ray power per unit area}}. \quad (5-63)$$

The incident ray direction is defined by the angles θ_ϕ and θ_z relative to the azimuthal and axial directions, as indicated in Fig. 5-7(b), and each scattering direction by θ'_ϕ and θ'_z . Since σ_d depends only on the angle between the incident ray directions, $\sigma_d \equiv \sigma_d(\theta_\phi - \theta'_\phi, \theta_z - \theta'_z)$, in addition to any spatial dependence and its variation with the wavelength λ of the incident light.

Intensity distribution

We define an intensity distribution function I_s to be the ray power per unit solid angle of ray directions, per unit area of core cross-section, by analogy with Eq. (4-1). Accordingly, the power incident per unit area of the scatterer in Fig. 5-7(b) is $I_s/\cos\theta_z$, where θ_z is the angle between the incident ray and the axial direction. The power scattered into rays with directions θ'_ϕ, θ'_z is $\sigma_d I_s/\cos\theta_z$. If the density of scatterers per unit volume is N , then there are $NdAdz$ scatterers in a volume of length dz and cross-section dA . The total power scattered into rays with direction angles θ'_ϕ, θ'_z is given by

$$\frac{NdzdA}{\cos\theta_z} I_s \sigma_d(\theta_\phi - \theta'_\phi, \theta_z - \theta'_z), \quad (5-64)$$

per unit solid angle.

Governing equation

We define $I(\theta_\phi, \theta_z, z)$ to be the total power per unit solid angle of all rays with direction angles θ_ϕ, θ_z over the whole core cross-section at position z . Hence I is related to I_s by

$$I(\theta_\phi, \theta_z, z) = \int_0^\rho r dr \int_0^{2\pi} d\phi I_s(r, \phi, z, \theta_\phi, \theta_z), \quad (5-65)$$

where r and ϕ are cylindrical polar coordinates in the fiber cross-section. The equation satisfied by I is found by examining the components of power change over length dz . First, there is the total power scattered out of direction θ_ϕ, θ_z into all directions θ'_ϕ, θ'_z , including bound, tunneling and refracting rays. This power change is given by dP_s , where

$$dP_s = -\frac{Ndz}{\cos\theta_z} I \sigma_{\text{tot}}; \quad \sigma_{\text{tot}} = \int_0^{2\pi} d\theta'_\phi \int_0^\pi \sigma_d(\theta_\phi - \theta'_\phi, \theta_z - \theta'_z) \sin\theta'_z d\theta'_z. \quad (5-66)$$

The total scattering cross-section σ_{tot} is by definition independent of θ_ϕ and θ_z and we have assumed σ_d independent of position for simplicity. Second, there is a gain from power scattered into direction θ_ϕ, θ_z . Ignoring contributions from leaky rays, the total contribution is from bound rays, whose range of θ'_z values satisfies Eq. (2-6a). Thus the power gained, dP_g , is found by integrating Eq. (5-64) over the cross-section

$$dP_g = Ndz \int_0^{2\pi} d\theta'_\phi \int_0^{\theta_c} I(\theta'_\phi, \theta'_z, z) \sigma_d(\theta'_\phi - \theta_\phi, \theta'_z - \theta_z) \tan\theta'_z d\theta'_z. \quad (5-67)$$

The change in I is the sum of dP_s and dP_g . Assuming a weakly guiding fiber, then $\theta_z, \theta'_z \ll 1$, and I satisfies the integro-differential equation [11]

$$\frac{\partial I}{\partial z} + N\sigma_{\text{tot}}I = N \int_0^{2\pi} d\theta'_\phi \int_0^{\theta_c} I\sigma_d \theta'_z d\theta'_z, \quad (5-68)$$

where $I(\theta_\phi, \theta_z, 0)$ is prescribed at the beginning of the fiber. The total bound-ray power at any position is given by

$$P_{\text{br}}(z) = \int_0^{2\pi} d\theta_\phi \int_0^{\theta_c} I\theta_z d\theta_z, \quad (5-69)$$

in terms of the solution of Eq. (5-68).

Pulse propagation

The derivation of Eq. (5-68) assumes steady-state excitation. To describe pulse propagation, we must include the dependence of I on time. This is achieved by replacing $\partial/\partial z$ in Eq. (5-68) with the total derivative d/dz , where

$$\frac{d}{dz} = \frac{\partial}{\partial z} + \frac{dt}{dz} \frac{\partial}{\partial t} = \frac{\partial}{\partial z} + \frac{n_{\text{co}}}{c \cos \theta_z} \frac{\partial}{\partial t}, \quad (5-70)$$

from Eq. (2-12). Accordingly, Eq. (5-68) is replaced by [11]

$$\frac{\partial I}{\partial z} + \frac{n_{\text{co}}}{c \cos \theta_z} \frac{\partial I}{\partial t} + N\sigma_{\text{tot}}I = N \int_0^{2\pi} d\theta'_\phi \int_0^{\theta_c} I\sigma_d \theta'_z d\theta'_z. \quad (5-71)$$

We must not suppress the $1/\cos \theta_z$ multiplying the time derivative, since it is precisely this variation in θ_z that gives rise to ray dispersion, as we showed in Section 3-1. We give examples of the application of this result.

5-22 Example: Diffusion equation

Here we examine the effect of scatterers which concentrate scattered power into directions close to the incident-ray direction in Fig. 5-7(b). Under this condition virtually all bound-ray power is redistributed amongst bound rays, and a negligible fraction of total power is lost to radiation from those bound rays propagating at angles $\theta_z \cong \theta_c$. If χ is the angle between the incident-ray direction θ_ϕ, θ_z and the scattered-ray direction θ'_ϕ, θ'_z , then the differential scattering cross-section $\sigma_d(\chi)$ is highly peaked about $\chi = 0$. We model this dependence by the Gaussian distribution

$$\sigma = \sigma_0 \exp(-b\chi^2); \quad b \gg 1, \quad (5-72)$$

where σ_0 and b are constants. By geometry we deduce

$$\cos \chi = \cos \theta_z \cos \theta'_z + \sin \theta_z \sin \theta'_z \cos(\theta_\phi - \theta'_\phi), \quad (5-73)$$

so that in the region $\chi \cong 0$ we have approximately

$$\chi^2 \cong (\theta_z - \theta'_z)^2 + \theta_z^2 (\theta_\phi - \theta'_\phi)^2; \quad \theta_\phi \cong \theta'_\phi, \quad \theta_z \cong \theta'_z. \quad (5-74)$$

within the weak-guidance approximation. Since σ is highly peaked about $\theta_z = \theta'_z$, $\theta_\phi = \theta'_\phi$, we can extend the ranges of integration of θ'_ϕ and θ'_z to $(-\infty, \infty)$ without any significant loss in accuracy. Thus, Eq. (5-71) is replaced by

$$\frac{\partial I}{\partial z} + \frac{n_{co}}{c \cos \theta_z} \frac{\partial I}{\partial t} = N \sigma_0 \int_{-\infty}^{\infty} d\theta'_\phi \int_{-\infty}^{\infty} \exp(-b\chi^2) \{I(\theta'_\phi, \theta'_z, z) - I(\theta_\phi, \theta_z, z)\} \theta'_z d\theta'_z. \quad (5-75)$$

We write the terms in the curly brackets as $\{I(\theta'_\phi, \theta'_z, z) - I(\theta_\phi, \theta'_z, z)\} + \{I(\theta_\phi, \theta'_z, z) - I(\theta_\phi, \theta_z, z)\}$ and Taylor expand in powers of $\theta'_\phi - \theta_\phi$ and $\theta'_z - \theta_z$ about θ_ϕ and θ_z . Substituting for χ from Eq. (5-74) and using the integrals of Eq. (37-126), we find correct to order b^{-2} that

$$\boxed{\frac{\partial I}{\partial z} + \frac{n_{co}}{c \cos \theta_z} \frac{\partial I}{\partial t} = D \left\{ \frac{1}{\theta_z^2} \frac{\partial^2 I}{\partial \theta_\phi^2} + \frac{\partial^2 I}{\partial \theta_z^2} + \frac{2}{\theta_z} \frac{\partial I}{\partial \theta_z} \right\};} \quad D = \frac{\pi N \sigma_0}{4b^2}. \quad (5-76)$$

Hence, I satisfies a diffusion equation, where the diffusion coefficient D is constant, and is proportional to the density of scatterers. When I is independent of θ_ϕ , this equation has been derived to describe the continuum limit of nearest-neighbor coupling of modal power on weakly guiding, multimode fibers [13]. It is possible to derive the $z^{1/2}$ dependence on pulse r.m.s. width from this equation in the steady state as $z \rightarrow \infty$; details are presented elsewhere [14].

5-23 Example: Rayleigh scattering

We have already introduced the notion of an ideal fiber, free from absorption and all nonuniformities. In practice, however, fibers are made from materials which are slightly absorbing. Further, the molecular granularity of the materials gives rise to Rayleigh, or dipole, scattering. Here we examine propagation on a step-profile fiber, ignoring absorption, so that we can determine the effect of Rayleigh scattering in isolation [15].

In the weak-guidance approximation, the differential scattering cross-section σ_d and the total cross-section σ_{tot} have the forms [16]

$$\sigma_d(\chi) = \kappa(1 + \cos^2 \chi); \quad \sigma_{tot} = 16\pi\kappa/3; \quad \kappa \ll 1, \quad (5-77)$$

where χ is related to ray directions by Eq. (5-73). The constant κ determines the total scattered power and includes the λ^{-4} dependence on the wavelength of light. Since $\kappa \leq \sigma_d \leq 2\kappa$, it is clear that the scattering is close to isotropic. In particular, $\sigma_d \cong 2\kappa$ for all bound-ray directions. Accordingly, we can integrate out the θ_ϕ dependence in Eq. (5-71) by defining

$$G(\theta_z, z, t) = \int_0^{2\pi} I(\theta_\phi, \theta_z, z, t) d\theta_\phi. \quad (5-78)$$

Integration of Eq. (5-71) within the approximations $\theta_z, \theta'_z \ll 1$, leads to

$$\frac{\partial G}{\partial z} + \frac{n_{co}}{c \cos \theta_z} \frac{\partial G}{\partial t} + \alpha G = \frac{3\alpha}{4} \int_0^{\theta_c} G(\theta'_z, z, t) \theta'_z d\theta'_z, \quad (5-79)$$

where $\alpha = N\sigma_{tot}$. Given the initial form of G at $z = 0$, we can solve this equation by iteration for small values of α and θ_z .

On-axis beam

We assume that at $z = 0$ the pulse is composed of a uniform collimated beam of on-axis rays, with unit total power. Using Eqs. (5-69) and (5-78), we deduce that

$$G(\theta_z, 0, t) = \delta(t) \delta(\theta_z) / \theta_z; \quad P_{br}(0) = 1, \quad (5-80)$$

where δ is the Dirac delta function. The lowest order solution of Eq. (5-79) corresponds to $\alpha = 0$. Hence

$$G(\theta_z, z, t) = \delta(t - zn_{co}/c) \delta(\theta_z) / \theta_z. \quad (5-81)$$

In other words, when scattering is ignored, the pulse propagates unattenuated and undistorted along the fiber with speed c/n_{co} . To first order, we can consider the scattering effects due to the two terms in α in Eq. (5-79) separately. The term αG on the left of the equation gives rise to an overall attenuation of G by the factor $\exp(-\alpha z)$, while the term on the right accounts for dispersion. The contribution from the latter is found by substituting for G from Eq. (5-81), multiplying by $\exp(-\alpha z)$, and integrating with respect to z with $t = n_{co}z/c \cos \theta_z$. Putting the two contributions together we obtain correct to first order

$$G(\theta_z, z, t) = \left\{ \delta\left(t - \frac{zn_{co}}{c}\right) \frac{\delta(\theta_z)}{\theta_z} + \frac{3\alpha}{4} \frac{c}{n_{co}} \frac{\cos \theta_z}{1 - \cos \theta_z} \right\} \exp(-\alpha z), \quad (5-82)$$

for $(zn_{co}/c) < t < (zn_{co}/c \cos \theta_z)$, and $G = 0$ otherwise. The first term within the curly brackets represents the undistorted pulse and the second term the distribution of scattered power, while the overall attenuation is due to scattering into leaky rays. Secondary scattering from these rays back into bound rays is ignored in this description.

Attenuation of pulse power

The impulse response $Q(z, t)$ is the integral of G over all ray directions. Noting the limitations on Eq. (5-82), we deduce that for $(zn_{co}/c) < t < (zn_{co}/c \cos \theta_z)$ the impulse response is given by

$$Q(z, t) = \int_{\theta_m}^{\theta_c} G \theta_z d\theta_z \cong \exp(-\alpha z) \left\{ \delta\left(t - \frac{zn_{co}}{c}\right) + \frac{3\alpha}{2} \frac{c}{n_{co}} \ln\left(\frac{\theta_c}{\theta_m}\right) \right\}, \quad (5-83)$$

since $\theta_c \ll 1$, where $\cos \theta_m = zn_{co}/ct$ and $\theta_m \cong \sqrt{2(1 - zn_{co}/ct)^{1/2}}$. A plot of $Q(z, t)$ is shown in Fig. 5-8. Finally, the pulse power $P_{br}(z)$ is found by integrating the impulse

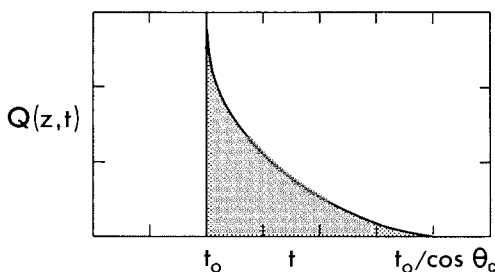


Fig. 5-8 Impulse response of Eq. (5-83) plotted as a function of t , where $t_0 = zn_{co}/c$ and $\theta_c = 0.1$ [15].

response with respect to time

$$P_{br}(z) = \int_0^{\infty} Q(z, t) dt. \quad (5-84)$$

However, it is simpler to replace $Q(z, t)$ by the integral over G in Eq. (5-83) and reverse the order of integration. Hence

$$P_{br}(z) = \int_0^{\theta_c} \theta_z d\theta_z \int_{zn_{co}/c}^{zn_{co}/c \cos \theta_z} G dt = \left\{ 1 + \frac{3\alpha}{8} \theta_c^2 z \right\} \exp(-\alpha z), \quad (5-85)$$

where, to lowest order, we have multiplied the term inside the curly brackets of Eq. (5-82) by the temporal pulse width $(zn_{co}/c)(1/\cos \theta_z - 1)$. Thus the result is valid only if z is not too large.

In conclusion, the effect of Rayleigh scatterers on an initially on-axis pulse is to redistribute power among all bound-ray directions and distort the pulse through ray dispersion. Simultaneously, power is lost from the pulse by scattering into radiation. The power loss is significant whenever the pulse spread is significant.

REFERENCES

1. Personick, S. D. (1971) Time dispersion in dielectric waveguides. *Bell Syst. Tech. J.*, **50**, 843-59.
2. Marcuse, D. (1972) Higher-order processes and the loss penalty of multimode operations. *Bell Syst. Tech. J.*, **51**, 1819-36.
3. Pask, C. (1980) Pulse propagation in optical fibres with index profile slowly varying along their length. *Opt. Quant. Elect.*, **12**, 281-90.
4. Ankiewicz, A., Love, J. D., Pask, C. and Snyder A. W. (1982) Slowly varying optical fibres. *J. Opt. Soc. Am.*, **72**, 198-203.
5. Marcuse, D. (1979) Multimode fiber with z -dependent α -value. *Appl. Opt.* **18**, 2229-31.
6. Landau, L. D., and Lifshitz, E. M. (1960) *Classical Mechanics*, Pergamon Press, Oxford, p. 154.

7. Marcuse, D. (1972) *Light Transmission Optics*, Van Nostrand, New York, p. 98.
8. Arnaud, J. A. (1976) *Beam and Fibre Optics*, Academic Press, New York.
9. Allan, W. B. (1973) *Fibre Optics Theory and Practice*, Plenum, New York, p. 21.
10. Winston, R. (1970) Light collection within the framework of geometric optics. *J. Opt. Soc. Am.*, **60**, 245–7.
11. Snyder, A. W., Mitchell, D. J. and Pask C. (1975) Pulse propagation in multimode optical fibres. *Electron. Lett.*, **11**, 275–6.
12. Jackson, J. D. (1962) *Classical Electrodynamics*, Wiley, New York, p. 489.
13. Gloge, D. (1972) Optical power flow in multimode fibers. *Bell Syst. Tech. J.*, **51**, 1767–83.
14. Marcuse, D. (1974) *Theory of Dielectric Optical Waveguides*, Academic Press, New York, p. 237.
15. Snyder, A. W. (1976) Pulse distortion in the ultimate multimode optical fibre. *Appl. Opt.*, **15**, 1290–4.
16. Jones, D. S. (1964) *The Theory of Electromagnetism*, Pergamon Press, Oxford, p. 510.

Material absorption

6-1 Absorbing media and attenuation	121
Absorption in the core	122
6-2 <i>Example: Uniformly absorbing core</i>	123
6-3 <i>Example: Nonuniformly absorbing core</i>	123
Absorption in the cladding	124
6-4 Evanescent fields	124
6-5 Power transmission coefficient	125
6-6 <i>Example: Step profile</i>	126
6-7 <i>Example: Graded profiles</i>	127
6-8 <i>Example: Clad parabolic profile</i>	129
6-9 <i>Example: Clad power-law profiles</i>	129
Absorption in both core and cladding	130
Influence of absorption on pulse shape	130
6-10 <i>Example: Step profile</i>	131
6-11 <i>Example: Clad parabolic profile</i>	133
References	133

The ray analysis thus far has assumed that fibers are nonabsorbing, and consequently bound rays will propagate indefinitely on an infinitely long uniform fiber. The materials which constitute the core and cladding of fibers used for communication purposes are, however, slightly absorbing. Thus, as a bound ray propagates, its power slowly attenuates due to absorption by the fiber, and, on a sufficiently long fiber, virtually all the initial power will be lost. The purpose of this chapter is to show how to calculate this attenuation and to determine how attenuation modifies pulse shape.

The power loss due to an absorbing core is described directly as an integrated effect along each ray path, and thus fits naturally into a treatment by classical geometric optics. On the other hand, the power loss due to an absorbing cladding cannot be described directly by geometric optics, because this loss occurs beyond the ray path where the ray power is zero, and must therefore be described by a different mechanism. The absorption of light power beyond the ray path is a diffraction, or wave, phenomenon since it

depends on the wavelength of the light in the core. Accordingly, *we must now build a wave effect into our ray description*. The philosophy behind the analysis uses a *building block* approach, whereby (i) we retain the ray trajectories of geometric optics, and (ii) describe the attenuation of ray power along the trajectory by a power attenuation coefficient [1,2].

For fibers with parameters of practical interest, the dominant effect of material absorption is the attenuation of total pulse power, together with a slight modification of pulse shape. The change in pulse shape is due to the fact that rays with larger inclinations to the fiber axis on step-profile fibers or with turning points closer to the interface of graded-profile fibers lose relatively more of their power to the cladding.

6-1 Absorbing media and attenuation

When a dielectric material is absorbing, it is mathematically convenient to describe absorption by ascribing an imaginary component to the refractive index at each position. Hence, for slight absorption, we have

$$n(r) = n^r(r) + in^i(r); \quad n^i(r) \ll n^r(r), \quad (6-1)$$

where superscripts r and i denote real and imaginary parts. Throughout this chapter we consider only circularly symmetric fibers, so that $n^r(r)$ and $n^i(r)$ are functions of the cylindrical polar radius r , or are constants. We shall also make use of the *power absorption coefficient* $\alpha(r)$. This is the fraction of power absorbed per unit length and is defined by

$$\alpha(r) = 4\pi n^i(r)/\lambda = 2kn^i(r), \quad (6-2)$$

where λ is the free-space wavelength. This coefficient is identical to the power attenuation coefficient for a plane wave propagating in an unbounded, uniform medium with uniform refractive index defined by Eq. (6-1) for a particular value of r . This may be verified by setting $n = n^r + in^i$ in Eq. (35-1a), whence the definition of power density in Eq. (35-2) gives rise to an attenuation factor $\exp(-2n^i \mathbf{k} \cdot \mathbf{r})$.

Power attenuation coefficient

To describe attenuation, we define $P(z)$ to be the power flowing within a narrow ray tube of rays, such as those illustrated in Fig. 4-1 and discussed at the beginning of Chapter 4. We then introduce the *power attenuation coefficient* $\gamma(z)$ of a ray defined by

$$\gamma(z) = -\frac{1}{P(z)} \frac{dP(z)}{dz}, \quad (6-3)$$

where $dP(z) < 0$ is the change in ray power due to absorption in distance dz along the fiber. Hence $\gamma(z)$ is the rate of power loss per unit length. On integrating, the power at any position is given in terms of the initial power

$P(0)$ by

$$P(z) = P(0) \exp \left\{ - \int_0^z \gamma(z) dz \right\}, \quad (6-4a)$$

when the power attenuation coefficient varies along the fiber, and by

$$P(z) = P(0) \exp \{ -\gamma z \}, \quad (6-4b)$$

when the power attenuation coefficient is constant. The first form is useful for slowly varying or bent fibers that are absorbing.

ABSORPTION IN THE CORE

We first consider fibers which have an absorbing core and a nonabsorbing cladding. In this case, the power absorption coefficient is zero in the cladding and in the core it is denoted by $\alpha_{co}(r)$, which is related to $n^i(r)$ through Eq. (6-2). The power absorbed over differential length ds of the ray path follows from the definition of $\alpha_{co}(r)$. It is also expressible in terms of the corresponding distance dz along the fiber by using the ray invariant $\bar{\beta}$ of Eq. (2-16), which is defined in terms of $n^r(r)$ instead of $n(r)$. Hence

$$-dP(z) = \alpha_{co}(r)P(z)ds = \{ \alpha_{co}(r)n^r(r)P(z)/\bar{\beta} \} dz, \quad (6-5)$$

where $r = r(s)$ and $z = z(s)$ are evaluated along the ray path in the middle expression, and similarly $r = r(z)$ in the right-hand expression. On comparing Eqs. (6-3) and (6-5) we obtain the power attenuation coefficient $\gamma_{co}(z)$ due to core absorption. Thus

$$\gamma_{co}(z) = \alpha_{co}(r)n^r(r)/\bar{\beta}, \quad (6-6)$$

where $r = r(z)$ along the path. We then deduce from Eqs. (6-3) to (6-5) that the ray power at distance z along the fiber is given by

$$P(z) = P(0) \exp \left\{ -\frac{1}{\bar{\beta}} \int_0^z \alpha_{co}(r)n^r(r) dz \right\} = P(0) \exp \left\{ - \int_0^z \alpha_{co}(r) ds \right\}, \quad (6-7)$$

where the integrands are evaluated along the ray path.

Cylindrical symmetry

The power absorption coefficient $\alpha_{co}(r)$ does not vary along a cylindrically symmetric fiber. Thus, provided z is large compared to the ray half-period z_p , we can make an accurate approximation to the integrals in Eq. (6-7) by

following the reasoning of Section 1-9. This leads to

$$P(z) = P(0) \exp(-\gamma_{co} z); \quad \gamma_{co} = \bar{\alpha}_{co} = \frac{1}{z_p} \int_0^{z_p} \alpha_{co}(r) ds, \quad (6-8)$$

where the constant γ_{co} is an *effective* power attenuation coefficient, defined by the average value $\bar{\alpha}_{co}$ of the power absorption coefficient over a half-period following the ray path.

6-2 Example: Uniformly absorbing core

When the power absorption coefficient is uniform, i.e. $\alpha_{co}(r) = \alpha_{co}$, the power attenuation coefficient of Eq. (6-6) is proportional to the real part of the profile. Ray power attenuates according to Eq. (6-8), which has the form

$$P(z) = P(0) \exp\{-\alpha_{co}(L_p/z_p)z\}, \quad (6-9)$$

where L_p is the path length of Eq. (2-26). For the step profile we deduce from Table 2-1, page 40, that $L_p/z_p = 1/\cos \theta_z$, and hence

$$P(z) = P(0) \exp\{-\alpha_{co} z / \cos \theta_z\}; \quad \alpha_{co} = 2kn_{co}^i, \quad (6-10)$$

where θ_z is the inclination of the ray path to the axial direction. Thus, although ray-power attenuation is independent of skewness, it increases with increasing θ_z . Consequently, bound rays propagating at the complementary critical angle θ_c suffer the highest attenuation.

Clad power-law profiles

The ratio L_p/z_p for the clad power-law profiles is given by Table 2-1, page 40, in the weak-guidance approximation. If we set $n = n^r(r) + in_{co}^i$, where $n^r(r)$ denotes the profile $n(r)$ of Table 2-1 and n_{co}^i is a constant, then [3]

$$P(z) = P(0) \exp\left\{-\frac{\alpha_{co}}{q+2} \left[(q+1)\frac{n_{co}^r}{\bar{\beta}} + \frac{\bar{\beta}}{n_{co}^r}\right]z\right\}; \quad \theta_c \ll 1, \quad (6-11)$$

where $\alpha_{co} = 2kn_{co}^i$ and n_{co}^r denotes the on-axis value of $n(r)$. This expression reduces to the step-profile result of Eq. (6-10) when $q \rightarrow \infty$, and is also independent of skewness. It is readily verified that the ray path which suffers highest attenuation is the one which just reaches the interface, i.e. when $\bar{\beta} = n_{cl} = n_{co}^r(1 - 2\Delta)^{1/2}$.

6-3 Example: Nonuniformly absorbing core

In general, the integration in Eq. (6-8) must be performed numerically when $\alpha_{co}(r)$ varies across the core. However, an analytical solution is possible for one case of practical interest [4], when the power absorption coefficient is proportional to the real

part of the profile, i.e.

$$\alpha_{co}(r) = \alpha_{co}(0)n^r(r)/n_{co}^r, \quad (6-12)$$

where n_{co}^r is the on-axis value of $n^r(r)$. The integral in Eq. (6-8) is proportional to the optical path length L_o of Eq. (2-26). Thus for clad power-law profiles we deduce from Table 2-1, page 40, that

$$P(z) = P(0) \exp \left\{ -\frac{\alpha_{co}(0)}{q+2} \left[q \frac{n_{co}^r}{\bar{\beta}} + 2 \frac{\bar{\beta}}{n_{co}^r} \right] z \right\}. \quad (6-13)$$

A second example with an analytical solution arises when the power absorption coefficient varies inversely with the profile, i.e.

$$\alpha_{co}(r) = \alpha_{co}(0)n^r(0)/n^r(r). \quad (6-14)$$

On substituting into Eq. (6-8) and using the invariant $\bar{\beta}$ of Eq. (2-16)—now defined in terms of $n^r(r)$ —to transform the integration to the z -direction, we find that the integral is proportional to the ray half-period. Hence

$$P(z) = P(0) \exp \{ -\alpha_{co}(0)n^r(0)z/\bar{\beta} \}, \quad (6-15)$$

and attenuation is independent of the variation in profile.

ABSORPTION IN THE CLADDING

Unlike core absorption, the power loss due to an absorbing cladding cannot be described directly by geometric optics, because this loss occurs beyond the ray path and is, therefore, a diffraction, or wave, effect dependent on the wavelength of the light in the core. This is the first occasion where we have to contend with wave effects and ray power. Our approach is to retain the ray paths of geometric optics and to assume that a ray loses power only at reflection or turning points. The rate of power loss is then simply related to the separation, or density, of reflection or turning points along the fiber. We determine the fraction of ray power lost at each reflection or turning point by treating the ray locally as a plane wave. Using the theory of local plane waves, it is then straightforward to derive expressions for power loss on step- and graded-profile fibers [1, 2]. For the step-profile fiber, the expression for power loss is identical to the expression first derived by Fresnel for plane-wave reflection from a planar interface [5]. Given the expressions for power loss at a reflection or turning point, the attenuation of ray power along the fiber due to cladding absorption requires only the separation, or density, of reflection or turning points, which is determined by geometric optics.

6-4 Evanescent fields

To gain insight into the mechanism responsible for cladding absorption, we treat the ray as a plane wave in localized regions about a reflection or turning

point. Such a view is justified for reasons discussed in Section 35-3. In the region beyond the ray path, i.e. beyond the interface within a step-profile fiber and beyond the turning point within a graded-profile fiber, the fields associated with the local plane waves become evanescent and decrease exponentially with increasing distance from the axis. This decrease is very rapid for virtually all rays, and varies exponentially with the inverse of the free-space wavelength λ of the light in the core, e.g. Eqs. (35-22a) and (35-32c) for step- and graded-profile waveguides. The fields are plotted qualitatively in Fig. 6-1. In the limit of classical geometric optics, $\lambda = 0$, the fields are zero beyond the ray path.

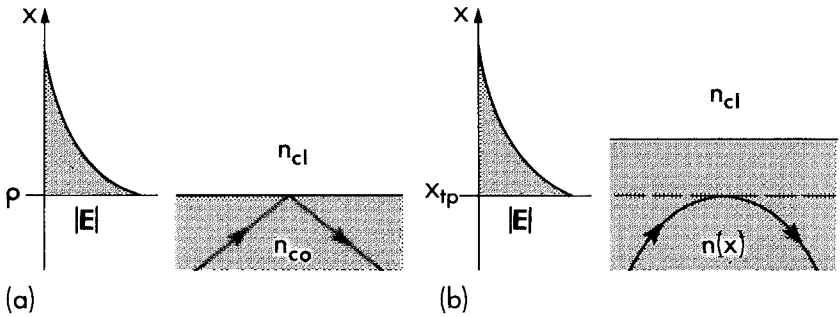


Fig. 6-1 The electric field intensity $|E|$ decreases exponentially beyond (a) the interface of a step-profile waveguide and (b) the turning-point caustic of a graded-profile waveguide.

6-5 Power transmission coefficient

For the finite values of λ for light, the evanescent fields lose some of their power to the absorbing cladding. This loss in turn leads to a loss of power from the ray path. Ray power flows along narrow ray tubes, as discussed at the beginning of Chapter 4, from which loss can occur only at reflection or turning points, i.e. at positions where there is an abrupt discontinuity in the tube or its cross-sectional area is zero. At these points, we express the loss in terms of a *power transmission coefficient* T , also known as a *loss coefficient*, defined by the dimensionless ratio

$$T = 1 - \frac{\text{power in the reflected ray}}{\text{power in the incident ray}}. \quad (6-16)$$

In other words a fraction T of ray power is transmitted across the interface or turning point to the evanescent field, as shown schematically in Fig. 6-2, and absorbed in the cladding.

The power attenuation coefficient γ_{cl} for cladding absorption is found either by averaging T over the ray half-period z_p between successive reflections or

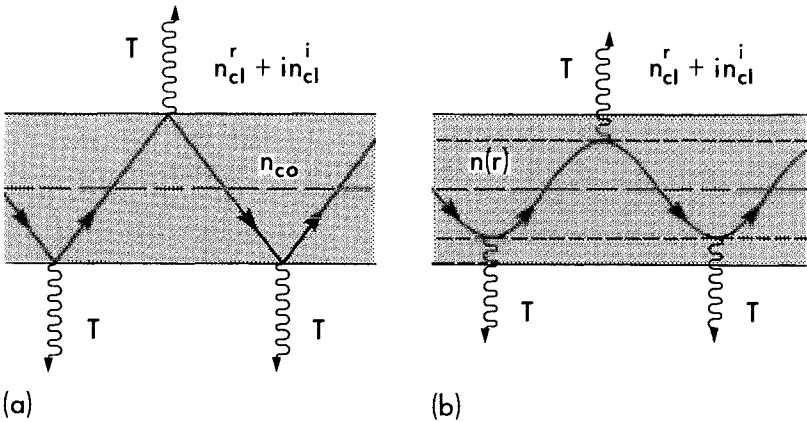


Fig. 6-2 Squiggly lines denote the fraction T of ray power lost to the absorbing cladding from a bound ray at (a) the reflection points on a step-profile waveguide and (b) the turning points of a graded-profile waveguide.

turning points, or by summing the loss at the N such points in unit length of the fiber. Either way we have

$$\gamma_{cl} = T/z_p = NT. \quad (6-17)$$

On a cylindrically symmetric fiber, the power attenuation coefficient is constant and is related to the power of a ray by Eq. (6-3) with γ replaced by γ_{cl} . If $P(0)$ is the ray power at the beginning of the fiber, then

$$P(z) = P(0) \exp(-\gamma_{cl} z). \quad (6-18)$$

To calculate γ_{cl} , we use the expressions for the ray half-period and the power transmission coefficient derived in Chapter 2 and Section 35-13, respectively. Examples are given below. In most cases of practical interest the cladding index is uniform, and we therefore assume $n_{cl} = n_{cl}^r + i n_{cl}^i$ is constant. The cladding power absorption coefficient α_{cl} is also constant, where by analogy with Eq. (6-2) we have

$$\alpha_{cl} = 4\pi n_{cl}^i / \lambda = 2k n_{cl}^i, \quad (6-19)$$

in terms of the free-space wavelength λ . A further simplification is possible by assuming the absorption is slight, i.e. $n_{cl}^i \ll n_{cl}^r$.

6-6 Example: Step profile

Consider a step-profile fiber with a nonabsorbing core of index n_{co} and radius ρ , and an absorbing cladding of index $n_{cl} = n_{cl}^r + i n_{cl}^i$. When n_{co} and n_{cl}^r are arbitrary, power

absorption depends on the polarization of the ray, i.e. on the orientation of the electric and magnetic fields in the local plane-wave description of Section 35-3, but if the fiber is weakly guiding, i.e. $n_{co} \cong n_{cl}^r$ this dependence is negligible. Under these conditions, a simple form of the power transmission coefficient is derived in Section 35-13. If we set $n_{co}^i = 0$ in Eq. (35-52), then

$$T = \frac{2}{\theta_c^2} \frac{\alpha_{cl}}{kn_{cl}^r} \frac{\pi/2 - \alpha}{\{\theta_c^2 - (\pi/2 - \alpha)^2\}^{1/2}}, \quad (6-20)$$

where α_{cl} is the power absorption coefficient of Eq. (6-19), the complementary critical angle $\theta_c \cong \{1 - (n_{cl}^r)^2/n_{co}^2\}^{1/2}$ and α is the angle between the ray path and the normal in Fig. 2-3. This expression is a limiting form of the Fresnel transmission coefficient of Eq. (35-24) for reflection at a planar interface between unbounded uniform media of refractive indices n_{co} and n_{cl} [5]. It depends only on α , regardless of whether the ray path is skew or meridional, and is accurate provided that $\pi/2 - \alpha$ is not too close to θ_c . In the weak-guidance approximation $\theta_c \ll 1$ and consequently Eq. (6-20) covers the narrow range of bound-ray directions satisfying $\pi/2 - \theta_c \lesssim \alpha < \pi/2$. Finally, we note that $T \rightarrow 0$ in the classical geometric optics limit $\lambda \rightarrow 0$, or $k = 2\pi/\lambda \rightarrow \infty$, thereby verifying that cladding absorption is a wavelength-dependent phenomenon.

Power attenuation coefficient

To obtain the power attenuation coefficient, we substitute Eq. (6-20) and Eq. (2-11) for z_p in Eq. (6-17). The angle α in the denominator of Eq. (6-20) is expressed in terms of the angles θ_z and θ_ϕ by Eq. (2-3). By setting $\pi/2 - \alpha \cong \sin(\pi/2 - \alpha) \cong \cos \alpha$, the numerator can be expressed similarly. Furthermore, we can use the definition of the fiber parameter inside the front cover to set $k = V/(\rho n_{co} \sin \theta_c) \cong V/(\rho n_{cl}^r \theta_c)$ since $\theta_c \ll 1$ and $n_{co} \cong n_{cl}^r$. If we put all these facts together, we deduce that the power attenuation coefficient is given by

$$\gamma_{cl} = \frac{\alpha_{cl}}{V} \left(\frac{\theta_z}{\theta_c} \right)^2 \frac{1}{\{1 - (\theta_z/\theta_c)^2 \sin^2 \theta_\phi\}^{1/2}}; \quad 0 \leq \theta_z < \theta_c. \quad (6-21)$$

This result is accurate for all bound rays, with the exception of those few rays whose directions are close to $\theta_z = \theta_c$ and $\theta_\phi = \pi/2$. For a fixed value of θ_z , attenuation is a maximum when the ray is meridional, i.e. $\theta_\phi = \pi/2$, and decreases with increasing skewness. Although a skew ray makes more reflections than a meridional ray over a given fiber length, this is more than offset by the smaller value of the transmission coefficient for skew rays.

6-7 Example: Graded profiles

We now consider a graded-profile fibre, with nonabsorbing core of index profile $n(r)$ and radius ρ , surrounded by a uniform cladding with index $n_{cl} = n_{cl}^r + in_{cl}^i$. For convenience, we also assume that $n(0)$ is the maximum profile value, denoted by n_{co} , and

that the fiber is weakly guiding, i.e. $n_{co} \cong n_{cl}^r$. Under these conditions, the power transmission coefficient is derived in Section 35-13, where Eq. (35-51) gives [2]

$$T = \frac{\alpha_{cl}}{2k} \frac{n_{co}}{\bar{\beta}^2 + \bar{l}^2 - (n_{cl}^r)^2} \exp \left\{ -2k \int_{r_{tp}}^{\rho} \left[\bar{\beta}^2 + \bar{l}^2 \frac{\rho^2}{r^2} - n^2(r) \right]^{1/2} dr \right\}, \quad (6-22)$$

in terms of the ray invariants $\bar{\beta}$ and \bar{l} of Table 2-1, page 40, which define the bound-ray path, and the radius of the turning-point caustic, r_{tp} , which denotes the farthest departure of the path from the fiber axis. This expression is valid for all bound rays, with the exception of those few rays whose turning points virtually coincide with the interface, i.e. $r_{tp} \cong \rho$, or, equivalently, $(\bar{\beta}^2 + \bar{l}^2)^{1/2} \cong n_{cl}^r$. Because of the exponential factor in Eq. (6-22), it is clear by comparison with Eq. (6-20) that *for most of the rays on graded-profile fibers, the fraction of power lost to the cladding is much smaller than for rays of step-profile fibers with the same values of $\bar{\beta}$ and \bar{l}* . This is attributable to the rapid decrease in the evanescent field amplitude between the turning point and the interface, which accounts for the exponential factor. Only those rays whose turning points are very close to the interface, i.e. $r_{tp} \cong \rho$, suffer absorption losses comparable with rays on the step-profile fiber. The power attenuation coefficient follows from Eq. (6-17), where we use the general expression of Eq. (2-28) for the ray half-period on graded profiles.

Linear approximation

The expression for the transmission coefficient given by Eq. (6-22) is unnecessarily complicated if we are only interested in rays which suffer significant loss of power over finite distances, as is often the case in practice. For such rays, the turning points are near the interface and we can evaluate the integral in Eq. (6-22) approximately by making a Taylor expansion about $r = r_{tp}$ of the expression in the square brackets within the exponent, and then retaining only the lowest order term. Thus

$$\bar{\beta}^2 + \bar{l}^2 \frac{\rho^2}{r^2} - n^2(r) \cong (r - r_{tp}) \left\{ - \frac{dn^2(r)}{dr} \bigg|_{\rho} - \frac{2\bar{l}^2}{\rho} \right\}, \quad (6-23)$$

since $r_{tp} \cong \rho$ and on substituting into Eq. (6-22) we obtain

$$T = \frac{\alpha_{cl}}{2k} \frac{n_{co}}{\bar{\beta}^2 + \bar{l}^2 - (n_{cl}^r)^2} \exp \left\{ - \frac{4}{3} k \rho \left[- \rho \frac{dn^2(r)}{dr} \bigg|_{\rho} - 2\bar{l}^2 \right]^{1/2} \times \left(1 - \frac{r_{tp}^2}{\rho^2} \right)^{3/2} \right\}, \quad (6-24)$$

which requires only the slope of the core profile at the interface.

6–8 Example: Clad parabolic profile

To determine the transmission coefficient of Eq. (6–22) for the clad parabolic profile of Table 2–1, page 40, we recall from Eq. (2–19) that the radii of the inner and turning-point caustics are roots of the integrand. Hence the integrand is expressible as

$$(n_{co}\theta_c/\rho)(r^2 - r_{ic}^2)^{1/2}(r^2 - r_{tp}^2)^{1/2}/r, \quad (6-25)$$

where r_{ic} and r_{tp} are given in terms of the ray invariants by Eq. (2–35). With the help of the integral in Eq. (37–123) we deduce that

$$T = \frac{\alpha_{cl}}{2k\beta^2 + \Gamma^2 - (n_{cl}^r)^2} \frac{n_{co}}{\exp(-k\rho n_{co}\theta_c g)}, \quad (6-26a)$$

where g is expressed in terms of the normalized radii $a = r_{tp}/\rho$ and $b = r_{ic}/\rho$ by

$$g = (1 - a^2)^{1/2}(1 - b^2)^{1/2} - \frac{a^2 + b^2}{2} \ln(p_+ p_-) - ab \ln \left\{ \frac{1 + p_+^2}{1 + p_-^2} \frac{a + b}{a - b} \right\}, \quad (6-26b)$$

and $p_{\pm} = \{(1 - a^2)^{1/2} + (1 - b^2)^{1/2}\}/(a \pm b)$. As the turning-point caustic approaches the interface, this expression reduces to the linear approximation of Eq. (6–24), in which case g of Eq. (6–26a) is given by

$$g = \frac{4\sqrt{2}}{3} \left\{ 1 - \left(\frac{\Gamma}{n_{co}\theta_c} \right)^2 \right\}^{1/2} \left(1 - \frac{r_{tp}^2}{\rho^2} \right)^{3/2}, \quad (6-27)$$

which is sufficient for many cases of practical interest.

Power attenuation coefficient

The ray half-period is given in Table 2–1, whence we deduce from Eqs. (6–17) and (6–26a) that the power attenuation coefficient can be expressed in the form

$$\gamma_{cl} = \frac{\alpha_{cl}}{2V\pi\beta} \frac{\theta_c^2}{\beta^2 + \Gamma^2 - (n_{cl}^r)^2} \frac{n_{co}^3}{\exp(-Vg)}, \quad (6-28)$$

where $V \cong k\rho n_{co}\theta_c$ and $\theta_c \cong \{1 - (n_{cl}^r)^2/n_{co}^2\}^{1/2}$. The form of g appropriate for the particular problem is taken from Eq. (6–26b) or (6–27).

6–9 Example: Clad power-law profiles

With the exception of the parabolic profile, the transmission coefficient of Eq. (6–22) cannot be expressed in closed form for the clad power-law profiles of Table 2–1, page 40. However, within the linear approximation, T is given by Eq. (6–24) with $-\rho dn^2(r)/dr|_p$ replaced by $qn_{co}^2\theta_c^2$, where $\theta_c \cong (2\Delta)^{1/2}$ in the weak-guidance approximation. Furthermore, the ray half-period is given explicitly only for the parabolic profile.

Step-profile limit

In the limit $q \rightarrow \infty$, the clad power-law profiles approach the step profile, but the graded-profile transmission coefficient of Eq. (6-24) does not approach the step-profile expression of Eq. (6-20). To demonstrate this fact, we substitute these profiles into Eq. (2-19) and determine r_{tp} . If we set $r_{tp} = \rho(1 - \epsilon)$ and retain only terms linear in ϵ , it is straightforward to show that

$$\frac{r_{tp}}{\rho} \approx 1 - \frac{\bar{\beta}^2 + \bar{l}^2 - (n_{cl}^r)^2}{2(n_{co}^2 q \Delta - \bar{l}^2)}, \quad (6-29)$$

assuming $n_{co}^2(1 - 2\Delta) = (n_{cl}^r)^2$. Thus $r_{tp} \rightarrow \rho$ as $q \rightarrow \infty$ for given values of $\bar{\beta}$ and \bar{l} , and the exponential factor in Eq. (6-24) approaches unity. It is then clear from Eq. (2-7a) that the remaining factors in Eq. (6-24) do not reduce to Eq. (6-20). The reason for this difference, as discussed in Section 35-11, is due to the method of derivation. We use local plane-wave results to derive the transmission coefficients for graded profiles. This requires the profile to vary slowly over a wavelength, but, as q increases, the profiles in Fig. 1-10 become progressively steeper until this requirement is violated and the transmission coefficients are no longer accurate.

ABSORPTION IN BOTH CORE AND CLADDING

When both the core and cladding materials of a fiber are absorbing, the power attenuation coefficient γ for a ray is given by the sum of the core and cladding absorption coefficients. Hence

$$\gamma(z) = \gamma_{co} + \gamma_{cl}, \quad (6-30)$$

and the power of the ray attenuates according to Eq. (6-4). This combination is justifiable because the attenuation coefficients are calculated over a differential length dz of the fiber. The core attenuation coefficient γ_{co} is determined by geometric optics following the ray path, as we showed earlier in the chapter. The cladding attenuation coefficient γ_{cl} is expressed in terms of the power transmission coefficient T for an absorbing cladding, *assuming that the core is nonabsorbing*.

INFLUENCE OF ABSORPTION ON PULSE SHAPE

When a fiber is very slightly absorbing, the absorption of ray power has no effect on ray transit times, so that the pulse width discussed in Chapter 3 is unaffected. However, the pulse shape, or impulse response, introduced in

Chapter 4, describes the distribution of power within a pulse, and this is modified by absorption. If the fiber is weakly guiding and there is little variation in absorption over the core, then, regardless of the profile, all bound rays suffer approximately the same attenuation $\exp(-\alpha_{co}z)$ in propagating distance z , as is clear from Eq. (6-10) when $\theta_z \ll 1$. Consequently, *pulse shape is not significantly affected by core absorption, although total pulse power is reduced by a factor of approximately $\exp(-\alpha_{co}z)$ [3].*

Cladding absorption

On the other hand, attenuation due to cladding absorption is sensitive to the particular ray path, as we showed in Sections 6-6 and 6-7. For rays satisfying $\theta_z \cong 0$ or $\bar{\beta} \cong n_{co}$ on step- or graded-profile fibers, respectively, attenuation is very small, but it increases rapidly as $\theta_z \rightarrow \theta_c$ or $\bar{\beta} \rightarrow n_{cl}$. The increase is most dramatic for meridional rays. If the pulse is excited with the diffuse source, the small values of θ_z mean that each bound ray initially carries about the same power. However, as the pulse propagates and disperses, the differing attenuation rates will modify the pulse shape. As we verify in the examples below, the rays with $\theta_z \cong 0$ or $\bar{\beta} \cong n_{co}$ are attenuated least and the rays with $\theta_z \cong \theta_c$ or $\bar{\beta} \cong n_{cl}$ are attenuated most. However, *unless cladding absorption is so severe as to remove virtually all pulse power, the effective narrowing of pulse r.m.s. width is insignificant compared with the spread due to ray dispersion.* For these reasons, we ignore core absorption and determine quantitatively the effect of a uniformly absorbing cladding in the following examples.

6-10 Example: Step profile

Consider a weakly guiding step-profile fiber with an absorbing cladding, described by the uniform power absorption coefficient α_{cl} of Eq. (6-19). A diffuse source excites pulses at $z = 0$. When $\alpha_{cl} = 0$, we recall from Eq. (4-55) that the impulse response $Q(t)$ depends only on the invariant $\bar{\beta}$, or equivalently on the ray angle θ_z , since the ray transit time is independent of skewness. However, when $\alpha_{cl} > 0$, the power attenuation coefficient γ_{cl} for each ray of the pulse is given by Eq. (6-21), and depends on both ray angles, or equivalently on both $\bar{\beta}$ and \bar{l} through Eq. (2-7a). Accordingly, the impulse response is now found from Eq. (4-64), where the distribution function $\hat{F}(\bar{\beta}, \bar{l})$ is multiplied by the factor $\exp(-\gamma_{cl}z)$ to account for absorption [6]. Since the ray transit time is independent of \bar{l} , we deduce from the prescription below Eq. (4-64) that

$$Q(t) = \left| \frac{d\bar{\beta}}{dt} \right| \int_0^{\bar{l}_{\max}(\bar{\beta})} \hat{F}(\bar{\beta}, \bar{l}) \exp(-\gamma_{cl}z) d\bar{l}, \quad (6-31)$$

where the distribution function $\hat{F}(\bar{\beta}, \bar{l})$ is given by Eq. (4-48), and $\bar{l}_{\max}(\bar{\beta}) = (n_{co}^2 - \bar{\beta}^2)^{1/2}$. The relationship $\bar{\beta} = \bar{\beta}(t)$ is found in Eq. (4-58), and the range of values of t for which

$Q(t)$ is nonzero is expressed by Eq. (4-59). The total power in the pulse at position z is given by

$$P_{br}(z) = \int_{n_{co}}^{n_{cl}} d\bar{\beta} \int_0^{\bar{\Gamma}_{max}(\bar{\beta})} \hat{F}(\bar{\beta}, \bar{\Gamma}) \exp(-\gamma_{cl} z) d\bar{\Gamma}, \quad (6-32)$$

or, equivalently, by the integral of $Q(t)$ over the range $t_{min} \leq t \leq t_{max}$.

The integrals in Eq. (6-31) are performed numerically [6], and the normalized impulse response is plotted in Fig. 6-3(a) for a fiber with parameters $V = 70$, $n_{co} = 1.5$ and $\Delta = 0.01$. As the imaginary part of the cladding refractive index increases, more power is lost from the slower rays propagating at larger angles to the fiber axis. The r.m.s. pulse width is only significantly reduced when either n_{cl}^i is large or the fiber is very long, and in either case there is a drastic reduction in total pulse power.

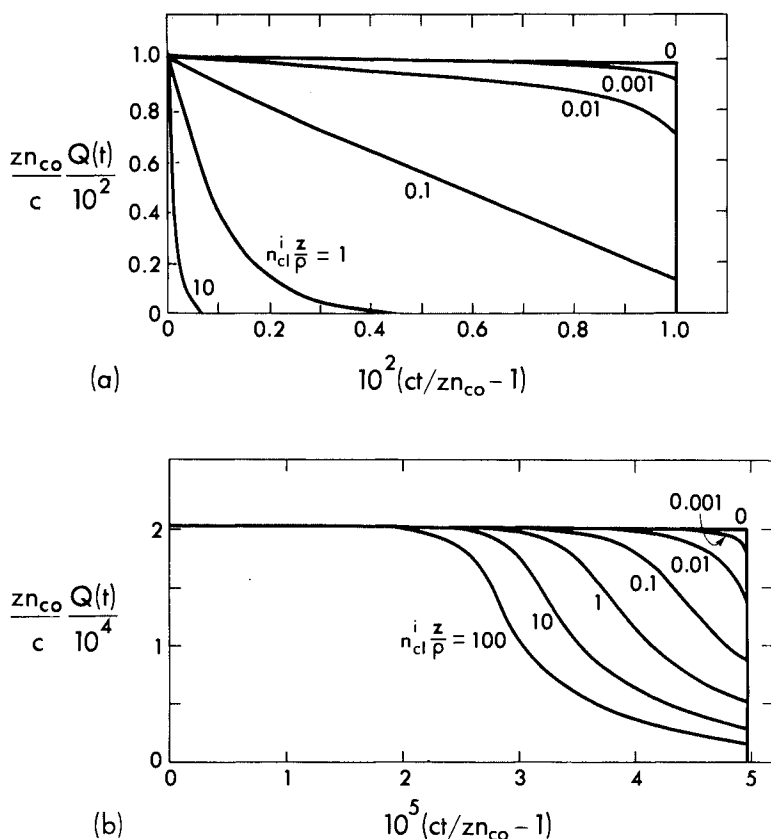


Fig. 6-3 The normalized impulse response for a fiber with an absorbing cladding and (a) a step profile or (b) a clad parabolic profile. Fiber parameters in both cases are $V = 70$, $\Delta = 0.01$ and $n_{co} = 1.5$. Curves are for differing values of the product $n_{cl}^i z / \rho$ [6].

6-11 Example: Clad parabolic profile

We can repeat the calculation of the previous example when the core has the clad parabolic profile given in Table 2-1, page 40. The impulse response and total power are given in Eqs. (6-31) and (6-32), except that $\hat{F}(\bar{\beta}, \bar{l})$ is now expressed by Eq. (4-52) and γ_{cl} by Eq. (6-28) using g of Eq. (6-27). The upper limit $\bar{l}_{\max}(\bar{\beta})$ of the integral is given by Eq. (4-53) with $q = 2$, and $\bar{\beta} = \bar{\beta}(t)$ by Eq. (4-61). When evaluating the impulse response, $Q(t)$ is given either by the integral in Eq. (6-31) or by the sum of two such terms for reasons explained below Eq. (4-61).

The integral in Eq. (6-31) is evaluated numerically [6], and Fig. 6-3(b) shows the normalized impulse response for a fiber with the same parameter values as for the step-profile above. The slowest propagating rays suffer the highest attenuation, but, compared with the step profile, the loss of pulse power for particular values of z and n_{cl}^2 is very much reduced. This is because only ray paths with turning points close to the interface are significantly attenuated, whereas all rays reach the interface of the step-profile fiber.

REFERENCES

1. Snyder, A. W. (1974) Leaky-ray theory of optical waveguides of circular cross section. *Appl. Phys.*, **4**, 273-98.
2. Snyder, A. W. and Love, J. D. (1976) Attenuation coefficient for rays in graded fibres with absorbing cladding. *Electron. Lett.*, **12**, 255-7.
3. Ankiewicz, A. and Pask, C. (1977) Geometric optics approach to light acceptance and propagation in graded index fibres. *Opt. Quant. Elect.*, **9**, 87-109.
4. Gloge, D. (1975) Propagation effects in optical fibres. *I.E.E.E. Trans. Microwave Theory Tech.*, **23**, 106-20.
5. Born, M. and Wolf, E. (1970) *Principles of Optics*, Pergamon Press, Oxford, p. 40.
6. Barrell, K. F. and Pask C. (1978) The effect of cladding loss in graded-index fibres. *Opt. Quant. Elect.*, **10**, 223-31.

Leaky rays

Refracting rays	135
7-1 Step-profile planar waveguide	136
7-2 Graded-profile planar waveguides	137
7-3 Step-profile fiber	138
7-4 Graded-profile fibers	140
Tunneling rays	140
7-5 Graded-profile fibers	141
7-6 Step-profile fiber	143
7-7 Attenuation of tunneling rays	145
7-8 <i>Example: Graded profiles</i>	145
7-9 <i>Example: Clad parabolic profile</i>	146
7-10 <i>Example: Step profile</i>	147
7-11 Transition from tunneling to refracting rays	148
7-12 Universal transmission coefficients	148
Noncircular and nonuniform fibers	149
7-13 Locally valid transmission coefficients	149
7-14 Interfaces and caustics of arbitrary curvature	149
Absorbing fibers	151
References	152

So far in our ray description of light propagation we have concentrated mainly on bound rays, which convey power without loss along nonabsorbing optical waveguides, and have assumed that refracting and tunneling rays are associated with a loss of power by radiation. In this chapter we describe the physical mechanisms of power loss by refraction or tunneling, and derive expressions for the rate of loss of power.

We recall from Chapters 1 and 2 that Snell's laws and the ray-path equation tell us that certain rays within the core of a waveguide will undergo refraction at the core-cladding interface. These are the *refracting rays*. The ray equation further tells us that other rays within the core of a fiber have an associated path in the cladding which extends indefinitely from some finite radial position beyond the core-cladding interface. These are the *tunneling rays* [1, 2]. In

addition to these rays, there are the *tunneling-refracting rays* which propagate on noncircular fibers [3]. These three types of rays are also described by the more general term *leaky rays*, since geometric optics indicates that each type will radiate power and attenuate, i.e. some power will be lost by radial transmission. However, geometric optics does not provide information on the rate of loss of power.

Radiation loss is a wave phenomenon which explains why it cannot be quantified by geometric optics. Thus, we again have a situation, similar to the cladding absorption of Chapter 6, where wave effects must be built into the ray treatment. Accordingly, we follow the strategy of Chapter 6, retain the ray paths of geometric optics and assume that ray power losses to radiation occur only at reflection or turning points. The rate of power loss is then simply related to the separation, or density, of reflection or turning points along the fiber. We determine the fraction of ray power lost at each reflection or turning point by treating the ray locally as a plane wave. Then, by using the theory of local plane waves, it is straightforward to derive expressions for radiation loss on step- and graded-profile waveguides [4, 5]. On step-profile planar waveguides, the expression for radiation loss from a refracting ray at each reflection from the interface is identical to the expression first derived by Fresnel for refraction of plane waves at a planar interface [6]. The derivation of the loss at reflection or turning points by local plane-wave theory is given in Chapter 35. Given this loss, the attenuation of ray power along the waveguide requires only the separation, or density, of reflection or turning points, which is determined by geometric optics.

When fibers are illuminated by sources which emit light over a wide range of directions, such as the diffuse source of Section 4-1, both bound and leaky rays will be excited. Sufficiently far along the fiber from the source each leaky ray will have radiated away virtually all of its power and bound rays will carry nearly all the remaining power in the fiber. However, in the intermediate region leaky rays – predominantly tunneling rays on circular fibers – can contribute significantly to total light power. This chapter prepares us for the analysis of the intermediate region to be discussed in the next chapter. We find that refracting rays and tunneling-refracting rays attenuate very rapidly, but tunneling rays may have arbitrarily low attenuation rates and behave almost as bound rays when the fiber parameter V is sufficiently large.

REFRACTING RAYS

In Chapters 1 and 2 we identified refracting rays within the cores of planar waveguides and circular fibers. The important feature of such rays is the bifurcation of the path at each reflection from the core-cladding interface. Here we determine the effect of this on power flow along the path. We consider the simplest example first to emphasize the concepts involved.

7-1 Step-profile planar waveguide

Refracting ray paths on the step-profile planar waveguide of core and cladding indices n_{co} and n_{cl} , and core half-width ρ were discussed in Section 1-2. Such a path is illustrated in Fig. 1-4(b), which shows the bifurcation at each reflection, one part being reflected back into the core and the other part being refracted into the cladding. Light power propagating along the path is similarly affected, and the power transmitted into the cladding is lost as radiation from the waveguide. This loss is conveniently described by a power transmission coefficient T , or loss coefficient, which has the same definition as Eq. (6-16), introduced to describe losses due to cladding absorption.

$$T = 1 - \frac{\text{power in the reflected ray}}{\text{power in the incident ray}}. \quad (7-1)$$

Thus a fraction of T of ray power is lost at each reflection. The ray power attenuation coefficient γ is found either by averaging T over a ray half-period z_p , between successive reflections, or by summing the loss at the N reflections in unit length of the fiber. Either way we have [7]

$$\gamma = \frac{T}{z_p} = NT, \quad (7-2)$$

and the ray power distance z along the fiber follows by analogy with Section 6-1. This is given by Eq. (6-4b) as

$$P(z) = P(0) \exp(-\gamma z), \quad (7-3)$$

assuming that γ is constant.

Power transmission coefficient

The transmission coefficient T is found by using the local plane-wave description of a ray. We regard the local plane wave as part of an infinite plane-wave incident on a planar interface between unbounded media, whose refractive indices coincide with the core and cladding indices n_{co} and n_{cl} of the waveguide, as shown in Fig. 1-3(b). For the step interface, T is identical to the Fresnel transmission coefficient for plane-wave reflection at a planar dielectric interface [6]. In the weak-guidance approximation, when $n_{co} \cong n_{cl}$, the transmission coefficient is independent of polarization, and is derived in Section 35-6. From Eq. (35-20) we have [7]

$$T = \frac{4 \sin \theta_z (\sin^2 \theta_z - \sin^2 \theta_c)^{1/2}}{\{\sin \theta_z + (\sin^2 \theta_z - \sin^2 \theta_c)^{1/2}\}^2}, \quad (7-4)$$

where θ_z is the angle between the ray and the axial direction, and θ_c is the complementary critical angle defined inside the front cover. This expression holds for all refracting rays with $\theta_c \leq \theta_z \leq \pi/2$.

Power attenuation coefficient

The ray half-period z_p for refracting rays is the same expression, used for bound rays, in Eq. (1-10). Substituting Eq. (7-4) into Eq. (7-2), the power attenuation coefficient is given by

$$\gamma = \frac{2 \sin^2 \theta_z}{\rho \cos \theta_z} \frac{(\sin^2 \theta_z - \sin^2 \theta_c)^{1/2}}{\{\sin \theta_z + (\sin^2 \theta_z - \sin^2 \theta_c)^{1/2}\}^2}. \quad (7-5)$$

As $\theta_z \rightarrow \pi/2$ attenuation becomes arbitrarily large and as $\theta_z \rightarrow \theta_c$ it can be arbitrarily small. In other words, if θ_z is sufficiently close to θ_c , a refracting ray can propagate for large distances along the planar waveguide before most of its power is lost to radiation.

7-2 Graded-profile planar waveguides

Consider a graded-profile planar waveguide whose core profile $n(x)$ decreases monotonically from the axis to the interface and takes the uniform value $n_{cl} = n(\rho)$ in the cladding. In Section 1-6 we showed that a refracting ray has the representative path illustrated in Fig. 1-7(b). Thus *all* ray power is transmitted across the interface and the power transmission coefficient of Eq. (7-1) satisfies $T = 1$. This conclusion is based on classical geometric optics which assumes that the wavelength is zero. However, for the finite values of λ for light, not all the ray power is transmitted and a fraction of the incident ray power is reflected back into the core *because of the abrupt change in the slope of the profile at the interface*, i.e. the change from $dn(x)/dx$ to zero at $x = \rho$. The situation is illustrated in Fig. 7-1(a), which shows the incident, reflected and transmitted rays all making the same angle θ_t with the interface. By analogy with Fig. 1-8, a refracting ray path along the waveguide has the characteristic shape shown in Fig. 7-1(b).

The transmission coefficient for reflection at the interface is derived in Section 35-9. Within the weak-guidance approximation, Eq. (35-36) gives [8]

$$T = 1 / \left\{ 1 + \left(\frac{\kappa}{8kn_{cl}^3 \sin^3 \theta_t} \right)^2 \right\}; \quad \kappa = - \left. \frac{dn^2(x)}{dx} \right|_{\rho-}, \quad (7-6a)$$

$$\cong 1 - \left(\frac{\kappa}{8kn_{cl}^3} \right)^2 \frac{1}{\sin^6 \theta_t}, \quad (7-6b)$$

which is valid for all transmission angles provided that θ_t is not too close to

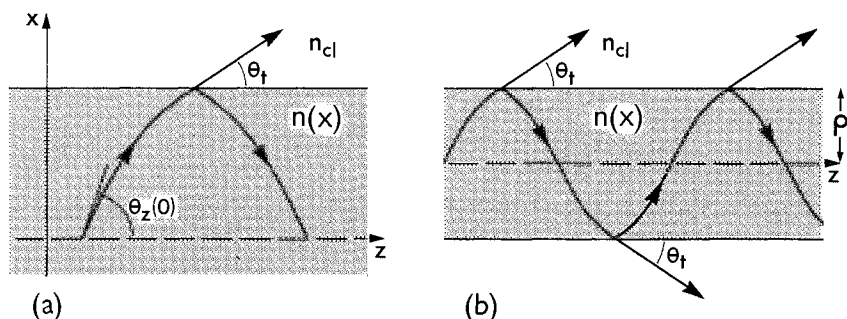


Fig. 7-1 (a) Incident, transmitted and reflected rays at a discontinuity in slope of a graded profile, and (b) the characteristic path of a refracting ray along a graded-profile planar waveguide.

$\theta_i = 0$. The derivative is evaluated on the core side of the interface, and Eq. (7-6b) holds when the second term is small compared with unity.

Clad parabolic profile

It follows from Table 2-1, page 40, that $\kappa = 4\Delta n_{co}^2/\rho$ for a fiber with this profile. Curve (ii) in Fig. 7-2(a) plots T of Eq. (7-6a) as a function of both θ_i and the angle $\theta_z(0)$ the path makes with the fiber axis in Fig. 7-1(a). For comparison we include curve (i), which is valid for small values of θ_i . Its derivation is given elsewhere [8]. Clearly the geometric optics result $T = 1$ is sufficient for all transmitted ray directions with the exception of very small values of θ_i . Conversely, a refracting ray with a sufficiently small value of θ_i , or, equivalently, $\bar{\beta} \lesssim n_{cl}$, can propagate for large distances along a graded-profile planar waveguide before most of its power is lost as radiation. The ray half-period for refracting rays is found by modifying Eq. (1-33) so that the limits of integration are $\pm \rho$, as is clear from Fig. 7-1(b). The attenuation coefficient then follows from Eqs. (7-2) and (7-6).

7-3 Step-profile fiber

On planar waveguides with the profiles discussed in the previous two sections, only bound and refracting rays can propagate. However, as we showed in Section 2-7, on fibers with the same profile forms, there are tunneling rays, in addition to bound and refracting rays. Here we derive expressions to describe refracting ray attenuation on fibers. Tunneling rays will be considered later below. These expressions are simple generalizations of the corresponding planar waveguide expressions given above, and account for both skew and meridional rays.

In Fig. 2-3, a skew refracting ray is incident on the curved interface of a step-

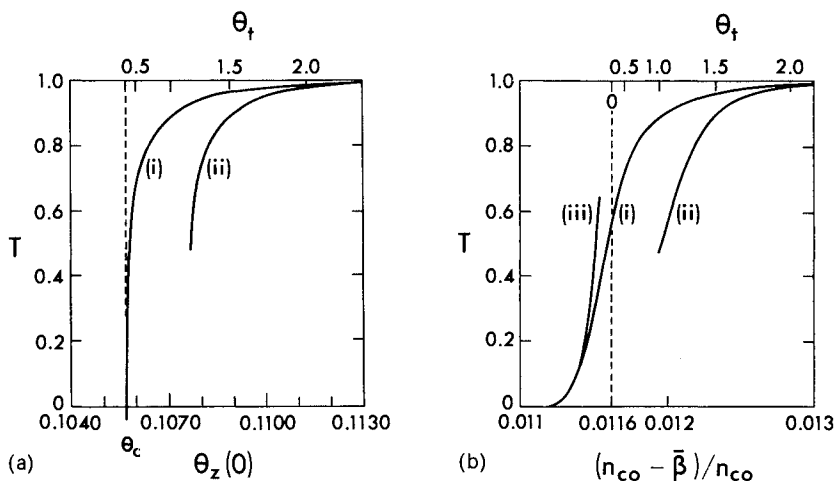


Fig. 7-2 (a) Power transmission coefficient T for refracting rays on a clad parabolic-profile planar waveguide with $\rho = 50 \mu\text{m}$, $\lambda = 1 \mu\text{m}$, $\Delta = 0.0056$, $n_{co} = 1.504$, $\theta_c = 0.106$ and $V = 50$. Curve (i) is found in Ref. [8], curve (ii) is given by Eq. (7-6), and θ_t is in degrees. Rays cut the axis at angle $\theta_z(0)$, and are bound for $0 \leq \theta_z(0) < \theta_c$. (b) Power transmission coefficient T for skew leaky rays with $\bar{T} = 0.032$ on a clad parabolic-profile fiber with the parameter values of (a). Curve (i) is found in Ref. [8], curve (ii) is given by Eqs. (7-6) and (7-9), and curve (iii) by Eq. (7-18). The angle θ_t is in degrees, and the dashed line corresponds to $\bar{\beta} = (n_{cl}^2 - \bar{T}^2)^{1/2}$. To the right of this line rays are refracting, and to the left are tunneling. For meridional rays ($\bar{T} = 0$), T is given by (a).

profile fiber at angle α to the normal. If α lies in the range of Eq. (2-6b) then the ray is a refracting ray. It is intuitive that if the core radius ρ is large compared with the wavelength of light in the core, λ/n_{co} , then the curved interface will appear locally plane to the ray. It then follows from Section 7-1, that the transmission coefficient T is given by the classical Fresnel coefficient of Eq. (35-50). The transmitted ray makes angle $\pi/2 - \theta_t$ with the normal, where θ_t is related to α by Snell's law, and to the angles θ_ϕ and θ_z by Eq. (2-3). Hence

$$n_{cl} \cos \theta_t = n_{co} \sin \alpha; \quad \sin \theta_t \cong (\sin^2 \theta_z \sin^2 \theta_\phi - \theta_c^2)^{1/2}, \quad (7-7)$$

where $n_{co} \cong n_{cl}$ and $\theta_c \cong (1 - n_{cl}^2/n_{co}^2)^{1/2} \ll 1$, assuming the fiber is weakly-guiding. Substituting into Eq. (35-50), we deduce from Eqs. (7-2) and (2-11) that the power attenuation coefficient is

$$\gamma = \frac{2 \sin^2 \theta_z}{\rho \cos \theta_z} \frac{(\sin^2 \theta_z \sin^2 \theta_\phi - \theta_c^2)^{1/2}}{\{\sin \theta_z \sin \theta_\phi + (\sin^2 \theta_z \sin^2 \theta_\phi - \theta_c^2)^{1/2}\}^2}. \quad (7-8)$$

For meridional rays, $\theta_\phi = \pi/2$, this reduces to Eq. (7-4) for the planar waveguide. A more rigorous analysis, which takes into account curvature of the interface, shows that the above expression is highly accurate for all refracting-ray directions except extremely close to the critical angle $\alpha_c = \pi/2 - \theta_c$ [9].

7-4 Graded-profile fibers

The refracting-ray transmission coefficient for skew rays on graded-profile fibers is given by Eq. (7-6) within the local plane-wave approximation, except that $\theta_t = \pi/2 - \alpha$, where α is the angle between the incident, reflected or transmitted rays and the normal at the interface. We deduce from Eqs. (2-14), (2-16) and (2-17) that

$$n_{cl} \sin \theta_t = (n_{cl}^2 - \bar{\beta}^2 - \bar{T}^2)^{1/2}, \quad (7-9)$$

where $\bar{\beta}$ and \bar{T} are the ray invariants and n_{cl} the uniform cladding index. When $\bar{T} = 0$ we recover the planar waveguide relationship, namely $\bar{\beta} = n_{cl} \cos \theta_t$.

Clad parabolic profile

We substitute Eq. (7-9) into Eq. (7-6) and plot T as a function of θ_t in Fig. 7-2(b) for a skew ray with $\bar{T} = 0.032$ on the clad parabolic profile fiber with the same parameters as Fig. 7-2(a). This generates curve (ii) provided θ_t is not too small, and curve (i), which is valid for small values of θ_t , is derived elsewhere [8]. The power attenuation coefficient follows from Eqs. (7-6) and (7-2), and the ray half-period is given by Eq. (2-28) with r_{tp} replaced by ρ in the limits of integration.

Skew and meridional rays

It follows from Eq. (7-8) and Fig. 7-2 that as $\theta_t \rightarrow 0$, the transmission coefficient $T \rightarrow 0$ *only for meridional rays*. For every skew ray, T approaches a finite limit as $\theta_t \rightarrow 0$, and, consequently, *virtually all skew refracting rays lose power very rapidly as they propagate*. Since meridional rays constitute a negligible fraction of refracting-ray directions, we conclude that, *in general, all refracting-ray power is rapidly lost over very short lengths of fiber* [10]. Those rays which can contribute significantly to total ray power over long distances along fibers are the tunneling rays, which we now discuss.

TUNNELING RAYS

In Section 2-7, we found from the ray-path equation of geometric optics, that there are certain rays within the core of a circular fiber which have an

associated ray path in the cladding which extends indefinitely from a position at a finite radial distance from the interface. This arrangement suggests that power is lost to radiation, and rays with this property are called tunneling rays because power appears to tunnel from the core into the cladding [1,2]. Tunneling rays do not exist on planar waveguides with the profiles discussed in Chapter 1. The mechanism for radiation loss by tunneling is a form of frustrated total internal reflection [11], caused in this instance by the curvature of the core-cladding interface. Here we describe the physical attributes of these rays and derive their power attenuation coefficient [5,12,13].

7-5 Graded-profile fibers

We first recall from Section 2-7 the discussion of tunneling ray paths on monotonic graded-profile fibers with minimum index n_{cl} in the cladding and maximum core index n_{co} on the axis. Part of the trajectory of a narrow tube of identical tunneling rays is illustrated in Fig. 7-3(a). Each ray touches the turning-point caustic at radius r_{tp} , where r_{tp} is the larger root of Eq. (2-19) in the core. The continuation of the path in the cladding originates at the radiation caustic, whose radius r_{rad} is given by Eq. (2-23). Since the cladding is uniform, the path is a straight line tangent to the caustic as shown.

A tunneling ray loses power each time it touches the turning-point caustic. The lost power reappears at the radiation caustic and is radiated away along the path in the cladding, as shown in Fig. 7-3(a). In the region between the two caustics, the local plane-wave fields associated with the tunneling ray are evanescent. The evanescent fields transfer power from the turning point to the radiation caustic across the darkly shaded region between the dashed lines of

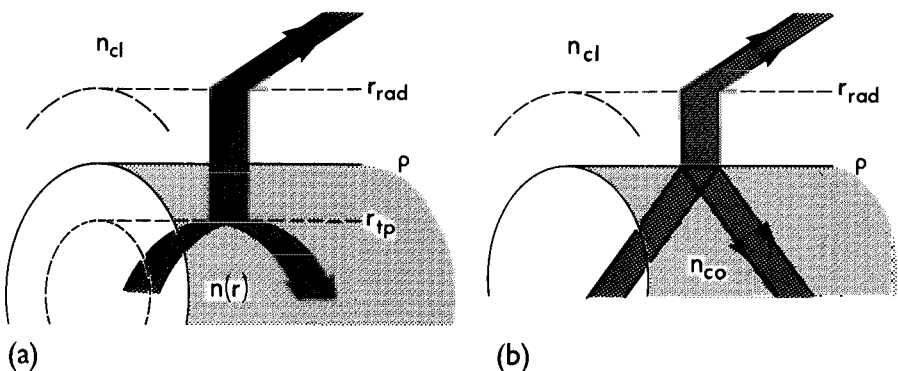


Fig. 7-3 (a) Tunneling ray on a graded-profile fiber. The turning-point caustic is at $r = r_{tp}$, the interface at $r = \rho$ and the radiation caustic at $r = r_{rad}$. (b) Tunneling ray on a step-profile fiber. The interface is at $r = \rho$ and the radiation caustic at $r = r_{rad}$.

Fig. 7–3(a), which connect the boundaries of the ray tubes. As light cannot be seen between the caustics, we refer to the transfer process as *electromagnetic tunneling*, or, simply, *tunneling*. On planar waveguides with the same form of profile, i.e. decreasing monotonically from the axis to the interface, there are no tunneling rays. Thus *tunneling on the fiber is due solely to curvature of the interface* for such profiles, which includes the step profile. Nevertheless, it is possible to propagate tunneling rays on planar waveguides by suitably choosing the profile. Such an example is the multilayered planar waveguide, discussed elsewhere [14].

Classification of leaky rays

The range of values of ray invariants for tunneling rays was established in Eq. (2–24c), and includes both graded and step profiles which decrease monotonically from the fiber axis to the interface

$$\bar{\beta}_{\min} \leq \bar{\beta} < n_{\text{cl}} \quad \text{and} \quad n_{\text{cl}}^2 - \bar{\beta}^2 \leq \bar{l}^2 \leq \bar{l}_{\max}^2(\bar{\beta}), \quad (7-10)$$

where $\bar{\beta}_{\min}$ and $\bar{l}_{\max}(\bar{\beta})$ depend on the profile. The two conditions cannot be satisfied by meridional rays ($\bar{l} = 0$), so every tunneling ray must be skew.

An alternative way of expressing these conditions, which provides a simple physical interpretation, is to examine the corresponding values of the radiation caustic radius r_{rad} . From Eq. (2–23) we have

$$r_{\text{rad}} = \rho \bar{l} / (n_{\text{cl}}^2 - \bar{\beta}^2)^{1/2}. \quad (7-11)$$

It is straightforward to show that at its minimum value $r_{\text{rad}} \rightarrow \rho$, when $\bar{\beta}^2 + \bar{l}^2 \rightarrow n_{\text{cl}}^2$, and at its maximum value $r_{\text{rad}} \rightarrow \infty$, when $\bar{\beta} \rightarrow n_{\text{cl}}$. Thus, every tunneling ray has a value of r_{rad} in the range $\rho < r_{\text{rad}} < \infty$. In the limit $r_{\text{rad}} \rightarrow \infty$, there is no path in the cladding and the tunneling ray becomes a bound ray. At the opposite extreme when $r_{\text{rad}} \rightarrow \rho$, the path in the cladding originates on the interface and $r_{\text{tp}} \rightarrow \rho$, as is clear from Eq. (2–19), so that the tunneling ray becomes a refracting ray. The delineation of ray types according to the values of r_{tp} and r_{rad} is summarized in Table 7–1.

Rotation of the transmitted ray

According to Snell's laws, when a ray is refracted at an interface, the incident ray, transmitted ray and normal are coplanar. However, this does not hold for tunneling rays. If we define a plane of incidence in Fig. 7–3(a) as the plane containing the normal, or radial direction, and the tangent to the ray path at the turning point, then the transmitted ray in the cladding does not lie in this plane [9]. To determine the direction of the path in the cladding, we recall that the azimuthal angle $\theta_{\phi}(r)$, defined by Eq. (2–14), is zero at the two caustics in Fig. 7–3(a) because the ray paths are perpendicular to the normal. The plane of

Table 7-1 Delineation of ray types according to the value of the radiation caustic radius r_{rad} in the cladding. The corresponding values of the turning-point caustic r_{tp} are included for step- and graded-profile fibers.

Ray type	r_{tp}		r_{rad}
	Step	Graded	
Bound	ρ	$0 \leq r_{\text{tp}} < \rho$	∞
Tunneling	ρ	$0 \leq r_{\text{tp}} < \rho$	$\rho < r_{\text{rad}} < \infty$
Refracting	ρ	ρ	ρ

incidence and the transmitted ray make angles $\theta_z(r_{\text{tp}})$ and $\theta_z(r_{\text{rad}})$, respectively, with the axial direction. By taking the ratio of the invariants defined by Eqs. (2-16) and (2-17), these angles satisfy

$$\frac{\bar{l}}{\bar{\beta}} = \frac{r_{\text{tp}}}{\rho} \tan \theta_z(r_{\text{tp}}) = \frac{r_{\text{rad}}}{\rho} \tan \theta_z(r_{\text{rad}}). \quad (7-12)$$

All tunneling rays are skew ($\bar{l} \neq 0$) and $r_{\text{rad}} > r_{\text{tp}}$. Hence $\theta_z(r_{\text{rad}}) < \theta_z(r_{\text{tp}})$ and the transmitted ray is rotated towards the fiber axis through angle $\theta_z(r_{\text{tp}}) - \theta_z(r_{\text{rad}})$, where from Eq. (7-12) we deduce that

$$\tan \{ \theta_z(r_{\text{tp}}) - \theta_z(r_{\text{rad}}) \} = \frac{\rho \bar{\beta} \bar{l} (r_{\text{rad}} - r_{\text{tp}})}{\rho^2 \bar{l}^2 + \bar{\beta}^2 r_{\text{rad}} r_{\text{tp}}}. \quad (7-13)$$

In the refracting-ray limit $r_{\text{rad}} \rightarrow r_{\text{tp}}$ and the rotation is zero, while in the bound-ray limit $r_{\text{rad}} \rightarrow \infty$, $\theta_z(r_{\text{rad}}) \rightarrow 0$ so the rotation is precisely $\theta_z(r_{\text{tp}})$. Thus, for sufficiently large values of r_{rad} , the transmitted ray direction is virtually parallel to the fiber axis.

7-6 Step-profile fiber

Tunneling-ray paths on step-profile fibers of core and cladding indices n_{co} and n_{cl} were discussed in Section 2-2. Part of the trajectory of a narrow tube of tunneling rays is shown in Fig. 7-3(b). The only difference from the trajectory of Fig. 7-3(a) for graded-profile fibers is that the core path reflects from the interface, rather than from the turning point. Consequently the local plane-wave fields are evanescent between $r = \rho$ and $r = r_{\text{rad}}$.

Classification of leaky rays

The range of values of invariants for leaky rays is given by Eq. (2-8). However, if we recall the ranges of ray angles for bound, refracting and tunneling rays in

Eq. (2-6), they can be conveniently represented pictorially as in Fig. 7-4. At P on the curved interface, bound-ray directions occupy the solid angle within a cone whose axis is parallel to the axial direction through P and whose angle θ_c is the complementary critical angle. Refracting-ray directions occupy the solid angle within a second half-cone of angle $\alpha_c = \pi/2 - \theta_c$ whose axis is along the normal, or radial direction, NP. The two half-cones touch along a common generator, and tunneling-ray directions occupy the solid angle between the cones, as shown. In terms of the value of r_{rad} , the delineation of ray types is the same as for graded profiles, and r_{tp} is replaced by ρ in Table 7-1

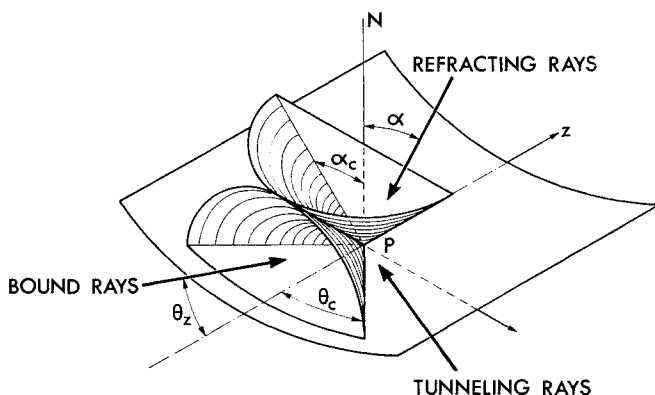


Fig. 7-4 Classification of rays on a step-profile fiber according to the angle of incidence at the interface.

Rotation of the transmitted ray

Tunneling rays on step-profile fibers undergo the rotation phenomenon discussed in Section 7-5. The cladding path rotates away from the plane of incidence of the incident ray and normal towards the axial direction. At the radiation caustic, $\theta_z(r_{\text{rad}})$ is given by Eq. (7-12), while $\bar{\beta} = n_{\text{co}} \cos \theta_z$ at the reflection point on the interface. Using Eq. (7-11) to replace r_{rad} , the rotation can be related to the difference $\theta_z - \theta_z(r_{\text{rad}})$, which satisfies

$$\tan \{ \theta_z - \theta_z(r_{\text{rad}}) \} = \frac{(n_{\text{co}}^2 - \bar{\beta}^2)^{1/2} - (n_{\text{cl}}^2 - \bar{\beta}^2)^{1/2}}{\bar{\beta}^2 + (n_{\text{cl}}^2 - \bar{\beta}^2)^{1/2} (n_{\text{co}}^2 - \bar{\beta}^2)^{1/2}} \bar{\beta}, \quad (7-14)$$

and is independent of ray skewness. In the limit of refracting rays, $\bar{\beta}^2 + \bar{l}^2 \rightarrow n_{\text{cl}}^2$ and $\theta_z(r_{\text{rad}}) \rightarrow \theta_z(\rho)$, where $\bar{\beta} = n_{\text{cl}} \cos \theta_z(\rho)$. The difference between θ_z and $\theta_z(\rho)$ is then consistent with the incident ray, refracted ray and normal being coplanar, i.e. Snell's law. In the limit $\bar{\beta} \rightarrow n_{\text{cl}}$, the rotation is precisely θ_z . Hence, when $r_{\text{rad}} \gg \rho$, radiation is nearly parallel to the fiber axis.

7-7 Attenuation of tunneling rays

The power of a tunneling ray at distance z along a fiber, $P(z)$, is given by Eq. (7-3) in terms of the power attenuation coefficient γ . The latter is related to the transmission coefficient T and the ray half-period by Eq. (7-2). The transmission coefficient determines the fraction of incident-ray power which is conveyed across the evanescent regions in Fig. 7-3 by tunneling. In contrast to refracting rays, the half-period z_p is given by the same expressions for bound rays in Table 2-1, page 40, and the values of $\bar{\beta}$ lie in the range of Eq. (2-24c) rather than Eq. (2-24a). Expressions for the transmission coefficient are derived within the local plane-wave approximation in Chapter 35. We now consider examples.

7-8 Example: Graded profiles

We consider weakly-guiding fibers whose profiles decrease monotonically from a maximum index n_{co} on the axis to the uniform cladding index n_{cl} at the interface. Within the local plane-wave approximation, the transmission coefficient for tunneling rays is given by Eq. (35-45) as [5,12,13]

$$T = \exp \left\{ -2k \int_{r_{ip}}^{r_{rad}} \left\{ \bar{\beta}^2 + \bar{l}^2 \frac{\rho^2}{r^2} - n^2(r) \right\}^{1/2} dr \right\}, \quad (7-15)$$

where $k = 2\pi/\lambda$, the free-space wavelength is λ and the ray invariants are defined in Table 2-1, page 40. The core radius is ρ , the turning-point caustic is the larger root of Eq. (2-19) and the radiation caustic is given by Eq. (2-23). This expression is valid provided r_{ip} and r_{rad} are not too close to one another. As the width $r_{rad} - r_{ip}$ of the evanescent region in Fig. 7-3(a) increases, T decreases very rapidly and approaches zero as $r_{rad} \rightarrow \infty$. Thus, tunneling rays can contribute significantly to total ray power over long distances, as we anticipated at the end of Section 7-4.

Weakly tunneling rays

Rays which have very small values of the transmission coefficient are known as weakly tunneling rays and, following the discussion above, have values of $r_{rad} \rightarrow \infty$, or, equivalently, $\bar{\beta} \lesssim n_{cl}$ according to Eq. (2-23). Thus the radiation caustic is much further from the interface than the turning-point caustic, i.e. $r_{rad} - \rho \gg \rho - r_{ip}$. In this situation, we can approximate r_{ip} by ρ in the lower limit of integration of Eq. (7-15), and generate an accurate expression for T for all weakly tunneling rays. Since $n(r) = n_{cl}$ in the cladding, we obtain with the help of Eq. (37-118) the explicit form

$$T = \exp \left\{ -2k\rho\bar{l} \left[\ln \{ p + (p^2 - 1)^{1/2} \} - \frac{(p^2 - 1)^{1/2}}{p} \right] \right\}, \quad (7-16a)$$

$$p = \frac{r_{rad}}{\rho} = \frac{\bar{l}}{(n_{cl}^2 - \bar{\beta}^2)^{1/2}}. \quad (7-16b)$$

This result is independent of the core profile, since it requires only the ray invariants describing the core path.

Linear approximation

Most tunneling rays have turning points and radiation caustics which are not far from the interface, i.e. $r_{\text{tp}} \cong \rho$, $r_{\text{rad}} \cong \rho$. We can then make an expansion about the interface by linearizing the expression within the square root of the integrand in Eq. (17-15) for $r < \rho$ and for $r > \rho$, respectively. This is carried out in Section 35-12 and leads to Eq. (35-48) where [5]

$$T = \exp \left\{ -\frac{2}{3} k \rho \frac{\kappa \rho n_{\text{cl}}^2}{\kappa \rho n_{\text{cl}}^2 - 2\bar{l}^2} \frac{(\bar{l}^2 + \bar{\beta}^2 - n_{\text{cl}}^2)^{3/2}}{n_{\text{cl}}(n_{\text{cl}}^2 - \bar{\beta}^2)} \right\}; \quad \kappa = -\frac{1}{n_{\text{cl}}^2} \frac{dn^2(r)}{dr} \bigg|_{\rho-}, \quad (7-17)$$

in terms of the slope of the profile on the core side of the interface. Rays satisfying the condition $r_{\text{tp}} \cong r_{\text{rad}}$ have transmission coefficients that are significantly larger than those for the weakly leaky rays described above.

Whichever of the above forms is used to derive the transmission coefficient, the power attenuation coefficient follows from Eq. (7-2), where the ray half-period is determined from the general expression of Eq. (2-28) for graded profiles.

7-9 Example: Clad parabolic profile

We can obtain the transmission coefficient of Eq. (7-15) in closed form for the clad parabolic profile of Table 2-1, page 40. In the exponent, the contribution to the integral from the cladding, i.e. $\rho \leq r \leq r_{\text{rad}}$, follows from Eq. (7-16), while the core contribution, i.e. $r_{\text{tp}} \leq r \leq \rho$ is deduced from the exponent of Eq. (6-26). Thus T is expressible as

$$T = \exp \{ -k \rho (n_{\text{co}} \theta_c I_1 + 2\bar{l} I_2) \}, \quad (7-18a)$$

where I_1 and I_2 are functions of the normalized radii of the caustics $a = r_{\text{tp}}/\rho$, $b = r_{\text{ic}}/\rho$ and $p = r_{\text{rad}}/\rho$ defined by

$$I_1 = (1 - a^2)^{1/2} (1 - b^2)^{1/2} - \frac{a^2 + b^2}{2} \ln(d_+ d_-) - ab \ln \left\{ \frac{1 + d_+^2}{1 + d_-^2} \frac{a + b}{a - b} \right\}, \quad (7-18b)$$

$$I_2 = \ln \{ p + (p^2 - 1)^{1/2} \} - (p^2 - 1)^{1/2} / p, \quad (7-18c)$$

where $d_{\pm} = \{ (1 - a^2)^{1/2} + (1 - b^2)^{1/2} \} / (a \pm b)$. The radii of the core caustics are given in terms of the ray invariants by Eq. (2-35) and the radius of the cladding caustic is given in Eq. (7-16). A plot of T against $1 - \bar{\beta}/n_{\text{co}}$ for a skew tunneling ray with $\bar{l} = 0.033$ is given by curve (iii) in Fig. 7-2(b). The vertical dashed line is the division between tunneling and refracting rays when $r_{\text{rad}} = r_{\text{tp}} = \rho$, or, equivalently, when $\bar{\beta} = (n_{\text{cl}}^2 - \bar{l}^2)^{1/2}$. As $\bar{\beta}$ increases above this value the transmission coefficient decreases rapidly, but very close

to this value Eq. (7-18) is invalid. The appropriate values of T in the latter case are given by curve (i), whose derivation is discussed elsewhere [8]. The ray half-period is given in Table 2-1, which together with Eq. (7-18) leads to the power attenuation coefficient through Eq. (7-2).

7-10 Example: Step profile

The transmission coefficient for tunneling rays on a weakly guiding, step-profile fiber with core and cladding indices n_{co} and n_{cl} is derived in Section 35-12 within the local plane-wave approximation. Thus Eq. (35-46a) gives [9,14]

$$T = |T_f| \exp \left\{ -2k \int_{\rho}^{r_{\text{rad}}} \left(\bar{\beta}^2 + \bar{T}^2 \frac{\rho^2}{r^2} - n_{cl}^2 \right)^{1/2} dr \right\}, \quad (7-19a)$$

where r_{rad} is given in Eq. (7-16) and T_f is the analytic continuation of the classical Fresnel transmission coefficient to angles less than the complementary critical angle θ_c of Fig. 1-3(b), i.e. to rays which would be bound on a planar waveguide. In terms of the ray invariants, Eq. (35-46c) gives

$$|T_f| = \frac{4}{n_{co}^2 - n_{cl}^2} (n_{co}^2 - \bar{\beta}^2 - \bar{T}^2)^{1/2} (\bar{\beta}^2 + \bar{T}^2 - n_{cl}^2)^{1/2}, \quad (7-19b)$$

where the ranges of values of $\bar{\beta}$ and \bar{T} for tunneling rays are in Eq. (2-8c). The factor $|T_f|$ accounts for the jump in profile at the interface, and the exponential factor is due to the evanescent field in the region between the interface and the radiation caustic. The integral in the exponent is evaluated using Eq. (37-118), so that the transmission coefficient has the closed form

$$T = |T_f| \exp \{ -2k\rho\bar{T} [\ln \{ p + (p^2 - 1)^{1/2} \} - (p^2 - 1)^{1/2}/p] \}, \quad (7-20)$$

where p is defined by Eq. (7-16b). Only rays whose radiation caustics are very close to the interface are inaccurately described by this expression.

It should be noted that Eq. (7-19) *cannot be deduced from the graded-profile result of Eq. (7-15) in the limit $r_{\text{tp}} \rightarrow \rho$* . As explained in Section 6-9, the local plane-wave derivation requires that the profile vary slowly over a distance equal to the wavelength of light. If the profile steepens and approaches the step profile, this condition is violated and Eq. (7-15) is no longer accurate [15].

Linear approximation

For those tunneling rays whose radiation caustics are not too far from the interface, we can obtain a simpler, approximate transmission coefficient by linearizing the expression within the square root of the integrand in Eq. (7-19a). This

is carried out in Section 35–12 and leads to Eq. (35–49b), where

$$T = |T_r| \exp \left\{ -\frac{2}{3} k \rho \frac{(\bar{\beta}^2 + \bar{l}^2 - n_{cl}^2)^{3/2}}{n_{cl}^2 - \bar{\beta}^2} \right\}, \quad (7-21)$$

where $|T_r|$ is defined by Eq. (7–19b).

7–11 Transition from tunneling to refracting rays

The transmission coefficients of Eqs. (7–15) and (7–19) apply to all tunneling rays on graded- and step-profile fibers, except in the limit where a tunneling ray becomes a refracting ray, i.e. when $r_{\text{rad}} \rightarrow \rho$. In this limit, the value of the transmission coefficient is relatively large compared to its value for tunneling rays close to the bound-ray limit, i.e. when $r_{\text{rad}} \rightarrow \infty$. Consequently, for certain excitation problems involving all or nearly all leaky-ray directions, the assumption that Eqs. (7–15) and (7–19) *hold for all tunneling rays* will introduce negligible error into the calculation of total ray power at positions sufficiently far along the fiber. This assumption is adopted in the following chapter when discussing spatial transients.

For situations where the above assumption cannot be adopted, expressions for the transmission coefficient in the transition region between tunneling and refracting rays are available [4, 8]. The values of T are plotted as curve (i) in Fig. 7–2(b) for a skew leaky ray with $\bar{l} = 0.033$ on a clad parabolic fiber. To the left of the vertical dashed line, the curve corresponds to tunneling rays and coincides with the local plane-wave expression of Eq. (7–18) as $\bar{\beta}$ increases [8]. Similarly, to the right of the vertical dashed line, the curve corresponds to refracting rays and coincides with the local plane-wave expression of Eq. (7–6) as $\bar{\beta}$ decreases. A similar transition occurs for skew leaky rays on a step-profile fiber [16].

7–12 Universal transmission coefficients

In earlier sections, we presented separate local plane-wave expressions for the transmission coefficients of refracting and tunneling rays on both step- and graded-profile fibers, and, in the previous section, indicated that a third expression is required to provide a transition between them. This description of leaky-ray attenuation not only gives physical insight into the differences between refracting and tunneling rays, but also leads to the simplest forms for T . Alternatively, we can use the method of uniform approximation [17] and derive a single expression for T that is valid for *all* leaky rays, i.e. refracting rays, tunneling rays and the transition. This expression, whilst lacking the simplicity of the above expressions, is of considerable benefit for computational purposes. Details of the derivation for graded and step profiles are given elsewhere [16].

NONCIRCULAR AND NONUNIFORM FIBERS

So far in this chapter we have considered leaky rays only on planar waveguides and circular fibers. Here we extend the analysis to leaky rays on noncircular fibers, such as elliptical fibers, and nonuniform fibers, such as bent fibers. We showed in Chapter 2 that noncircular fibers give rise to *tunneling–refracting rays*, where a ray loses power by tunneling at turning points along its trajectory and by refraction at the interface. Here we show that the concept of leaky rays is applicable to these more general waveguides provided the transmission coefficient depends only on the local geometry. We derive expressions for the transmission coefficients of tunneling rays which require only the two principal radii of curvature of the turning-point caustic or interface.

7–13 Locally valid transmission coefficients

The ray analysis of multimode fibers—regardless of their symmetry or uniformity properties—assumes that we can trace a ray path along the fiber, and that each time the path reflects from a caustic or interface at which power is lost, we can ascribe a transmission coefficient to predict the fraction of incident power radiated away. The ray path is defined by the direction of the local wave vector, as we show in Section 35–3, and thus, for consistency, *the transmission coefficient depends only on the local geometry*. This requirement is automatically satisfied on planar waveguides and circular fibers, because the transmission coefficient has the same value anywhere on the interface or turning-point caustic. There is also a set of noncircular profiles which has this property [18]. For an arbitrary cross-section, it is intuitive that if the radius of curvature of the interface or turning-point caustic is large compared with the wavelength of light, and if the radiation caustic is not too far from the interface, then the transmission coefficient will depend only on the local geometry. However, if the radiation caustic is very far from the interface, the transmission coefficient will depend on the geometry of the whole core cross-section, and, apart from the cases mentioned above, will not be locally valid. Only those tunneling leaky rays with extremely small attenuation coefficients have radiation caustics very far from the interface. Consequently, radiation loss from fibers of arbitrary cross-sections can be described by leaky ray transmission coefficients for many problems of practical interest. We now give these localized transmission coefficients.

7–14 Interfaces and caustics of arbitrary curvature

Following the above discussion, the loss of leaky-ray power on noncircular and nonuniform fibers is described by local transmission coefficients for

interfaces and turning-point caustics of arbitrary curvature, provided that the curvature is large compared to the wavelength, and the radiation caustic is not too far from the interface. These coefficients can be derived formally by expanding the fields in the neighborhood of the interface of turning-point caustic [4, 19]. However, for many problems of practical interest, it is sufficient to know the transmission coefficients for tunneling rays alone. These coefficients can be found either as a limit of the more general results [4, 19], or, intuitively, as a generalization of the coefficients for tunneling rays on circular fibers. The latter approach is adopted in Section 35-14.

There we show that the dependence of the transmission coefficients on the local geometry of a circular fiber involves only the radius of curvature $\bar{\rho}$ in the plane of incidence of the ray, i.e. the radius of curvature of the interface or turning-point caustic in the plane defined by the ray path or the tangent to the ray path, respectively, and the normal. We then claim that the locally valid transmission coefficients for interfaces or turning-point caustics of arbitrary curvature have the same functional dependence on $\bar{\rho}$. In these cases $\bar{\rho}$ depends on two principal radii of curvature instead of the single radius of curvature of the circular fiber.

Reflection at an interface – step profile

Consider an interface of arbitrary curvature between media of uniform refractive indices n_{co} and n_{cl} as shown in Fig. 7-5(a). Cartesian axes P_y and P_z lie in the tangent plane at P and are orthogonal to the normal, or radial, direction. Their orientation is such that the two principal radii of curvature, ρ_y and ρ_z , lie in the r - y and r - z planes, respectively. The local transmission

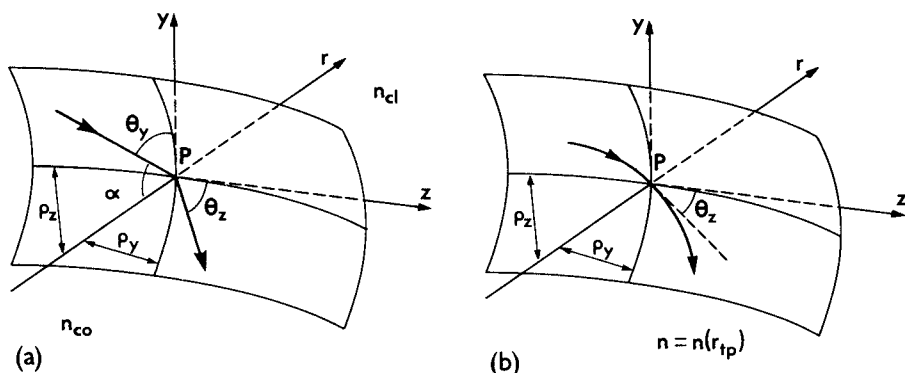


Fig. 7-5 (a) A ray path reflects from the arbitrarily curved interface between uniform media of refractive indices n_{co} and n_{cl} . (b) A ray path touches the arbitrarily curved surface $n = n(r_{tp})$ of the turning point caustic in a graded medium.

coefficient for a tunneling ray incident at angle α to the radial direction is derived in Section 35-14. We deduce from Eqs. (35-53) and (35-54) that [4]

$$T = |T_f| \exp \left\{ -\frac{2}{3} k \bar{\rho} n_{co} \frac{(\sin^2 \alpha - \sin^2 \alpha_c)^{3/2}}{\sin^2 \alpha} \right\}, \quad (7-22a)$$

where T_f is the analytic continuation of the Fresnel transmission coefficient, and

$$|T_f| = 4 \cos \alpha (\sin^2 \alpha - \sin^2 \alpha_c)^{1/2} / \cos^2 \alpha_c. \quad (7-22b)$$

The critical angle $\alpha_c = \sin^{-1} (n_{cl}/n_{co})$, and the radius of curvature in the plane of incidence at P is given by

$$\bar{\rho} = \rho_y \rho_z \sin^2 \alpha / (\rho_y \cos^2 \theta_z + \rho_z \cos^2 \theta_y), \quad (7-22c)$$

where θ_y and θ_z are the angles between the incident ray direction and the Py- and Pz-axes, respectively, in Fig. 7-5(a). The expression for T is valid provided that $k \bar{\rho} n_{co} \gg 1/\cos^3 \alpha$ [4,20].

Reflection at a caustic – graded media

A turning-point caustic of arbitrary curvature is illustrated in Fig. 7-5(b), and is defined by the surface $n = n(r_{tp})$, where r_{tp} is the position of the turning point in the radial direction. We assume that the turning point is not too far from the intersection of the radial axis with the interface at $r = \rho$, beyond which the profile is uniform, i.e. $n = n(\rho) = n_{cl}$. The tangent to the ray path at P lies in the tangent plane at P and makes angles $\pi/2 - \theta_z$ and θ_z with the y- and z-axes, respectively. Otherwise the notation is identical with Fig. 7-5(a). In this situation, the local transmission coefficient is given by Eq. (35-55) [19]

$$T = \exp \left\{ -\frac{2}{3} k \bar{\rho} n_{cl} \frac{\kappa \bar{\rho}}{\kappa \bar{\rho} - 2} \left[\frac{n^2(r_{tp})}{n_{cl}^2} - 1 \right]^{3/2} \right\}, \quad (7-23a)$$

where κ involves the profile slope at the interface and $\bar{\rho}$ of Eq. (35-56) is the radius of curvature in the plane of incidence. These are defined by

$$\kappa = \frac{1}{n_{cl}^2} \frac{dn^2(r)}{dr} \bigg|_{r=\rho-}; \quad \bar{\rho} = \frac{\rho_y \rho_z}{\rho_y \cos^2 \theta_z + \rho_z \sin^2 \theta_z}. \quad (7-23b)$$

The expression for T is valid provided that $k \bar{\rho} n_{co} \gg 1$ [19].

ABSORBING FIBERS

When a leaky ray propagates along a fiber that is absorbing, it is intuitive that the total attenuation is simply the sum of the power attenuation coefficients for

core absorption, cladding absorption and radiation loss. If these are denoted by γ_{co} , γ_{cl} and γ_{lr} , respectively, then the power of the ray distance z along the fiber is given by [21]

$$P(z) = P(0)\exp(-\gamma z); \quad \gamma = \gamma_{co} + \gamma_{cl} + \gamma_{lr}, \quad (7-24)$$

where γ_{lr} denotes the attenuation coefficient of Eq. (7-3), and the core and cladding absorption is related to γ_{co} and γ_{cl} in Chapter 6. The localized transmission coefficient for an absorbing cladding beyond an interface of arbitrary curvature can be derived in an analogous manner to Eq. (7-22) [22].

REFERENCES

1. Snyder, A. W. (1974) Leaky-ray theory of optical waveguides of circular cross-section. *Appl. Phys.*, **4**, 273-98.
2. Snyder, A. W. and Love, J. D. (1974) Tunnelling leaky rays on optical waveguides. *Opt. Commun.*, **12**, 326-8.
3. Love, J. D., Pask, C. and Winkler, C. (1979) Rays and modes on step-index multimode elliptical waveguides. *Micro waves, Opt. Acoust.*, **3**, 231-8.
4. Snyder, A. W. and Love, J. D. (1975) Reflection at a curved dielectric interface-electromagnetic tunnelling. *I.E.E.E. Trans. Microwave Theory Tech.* **23**, 134-41.
5. Snyder, A. W. and Love, J. D. (1976) Attenuation coefficient for tunnelling leaky rays in graded fibers. *Electron. Lett.*, **12**, 324-6.
6. Born, M. and Wolf, E. (1970) *Principles of Optics*, Pergamon Press, Oxford, p. 40.
7. Snyder, A. W. and Mitchell, D. J. (1974) Generalized Fresnel's laws for determining radiation loss from optical waveguides and curved dielectric structures. *Optik*, **40**, 438-59.
8. Love, J. D. and Winkler, C. (1978) Refracting leaky rays in graded-index fibers. *Appl. Opt.*, **17**, 2205-8.
9. Love, J. D. and Snyder, A. W. (1975) Fresnel's and Snell's laws for the multimode optical waveguide of circular cross-section. *J. Opt. Soc. Am.*, **65**, 1241-7.
10. Pask, C. (1975) On the neglect of refracting rays in optical power calculations. *Opt. Quant. Elect.*, **7**, 428-9.
11. Kapany, N. S. and Burke, J. J. (1972) *Optical Waveguides*, Academic Press, New York.
12. Stewart, W. J. (1975) Leaky modes in graded fibers. *Electron. Lett.*, **11**, 321-2.
13. Adams, M. J., Payne, D. N. and Sladen, F. M. E. (1975) Leaky rays on optical fibers of arbitrary (circularly symmetric) index profiles. *Electron. Lett.*, **11**, 238-40.
14. Love, J. D. and Winkler, C. (1977) Attenuation and tunnelling coefficients for leaky rays in multilayered optical waveguide. *J. Opt. Soc. Am.*, **67**, 1627-33.
15. Love, J. D. and Winkler, C. (1978) The step index limit of power law refractive index profiles for optical waveguides. *J. Opt. Soc. Am.*, **68**, 1188-91.
16. Love, J. D. and Winkler, C. (1978) A universal tunnelling coefficient for step- and graded-index multimode fibers. *Opt. Quant. Elect.*, **10**, 341-51.
17. Abramowitz, M. and Stegun, I. A. (1972) *Handbook of Mathematical Functions*, Dover, New York, p. 448.

18. Ramskov Hansen, J. J., Ankiewicz, A. and Adams, M. J. (1980) Attenuation of leaky modes in graded noncircular multimode fibers. *Electron Lett.*, **16**, 94–6.
19. Love, J. D. and Winkler, C. (1980) Generalized Fresnel power transmission coefficients for curved graded-index media. *I.E.E.E. Trans. Microwave Theory Tech.*, **28**, 689–94.
20. Jones, D. S. (1978) Electromagnetic tunnelling. *Quart. J. Mech. Appl. Math.*, **31**, 409–34.
21. Love, J. D. and Winkler, C. (1978) The effects of material absorption on ray power attenuation in multi-layered optical waveguides. *Opt. Quant. Elect.*, **10**, 383–92.
22. Love, J. D. and Snyder, A. W. (1975) Generalized Fresnel's laws for a curved absorbing interface. *J. Opt. Soc. Am.*, **65**, 1072–4.

Spatial transient

8-1	Spatial transient and spatial steady state	155
Radiation from fibers illuminated by a diffuse source		157
8-2	Leaky-ray excitation on step-profile fibers	157
8-3	Spatial transient for step-profile fibers	160
8-4	Leaky-ray excitation on graded-profile fibers	161
8-5	Spatial transient for clad parabolic-profile fibers	163
Generalized parameters		164
8-6	Generalized parameter for step-profile fibers	165
8-7	Generalized parameter for graded-profile fibers	166
8-8	<i>Example: Diffuse illumination of step-profile fibers</i>	167
8-9	<i>Example: Diffuse illumination of clad parabolic-profile fibers</i>	168
Pulse spread		169
8-10	<i>Example: Ray dispersion on step-profile fibers</i>	170
8-11	<i>Example: Ray dispersion on clad parabolic-profile fibers</i>	171
Noncircular fibers		172
Intensity distribution at the end of the fiber		173
8-12	<i>Example: Step-profile fiber</i>	174
8-13	<i>Example: Clad power-law profile fibers</i>	175
Radiation and absorption losses		176
8-14	<i>Example: Step-profile fiber</i>	177
8-15	<i>Example: Clad parabolic-profile fiber</i>	177
References		178

Our main concern in the first six chapters was with the behavior of bound rays, which propagate without loss of power on nonabsorbing fibers. Bound rays provide a complete description of light propagation on nonabsorbing fibers sufficiently far from the source, when virtually all leaky-ray power has been lost. We call this the *spatial steady state*. In this chapter our attention is

turned to the region intermediate between the source and the onset of the spatial steady state, where light propagation is described by the *spatial transient*.

8-1 Spatial transient and spatial steady state

Consider an ideal, nonabsorbing fiber of arbitrary profile and cross-section, illuminated by a source at its endface, as shown in Fig. 8-1. In general, the source excites both bound and leaky rays. The power in the bound rays propagates indefinitely along the fiber without loss. As each leaky ray propagates, its power attenuates exponentially according to Eq. (7-3), so that total leaky-ray power decreases very rapidly away from the source, as indicated schematically by the radiation in Fig. 8-1. Sufficiently far along the fiber, total leaky-ray power is arbitrarily small, but is only completely lost from the core when $z \rightarrow \infty$. For practical purposes, however, it is convenient to divide the fiber into two regions about $z = z_0$, so that for $z > z_0$ leaky-ray power is a prescribed, negligibly small fraction of total bound-ray power. Propagation in the region $z_0 < z < \infty$ is virtually in a spatial steady state, accurately described by bound rays alone. The region $0 \leq z < z_0$ corresponds to the spatial transient, where propagation is described by both bound and leaky rays.

We begin by determining the power exciting leaky rays on fibers illuminated by a diffuse source, and then show that the spatial transient is accurately and simply described in terms of a single dimensionless parameter which embraces all the physical quantities of the problem. The effect of leaky rays on pulse dispersion is also expressible in terms of this parameter. We then show how

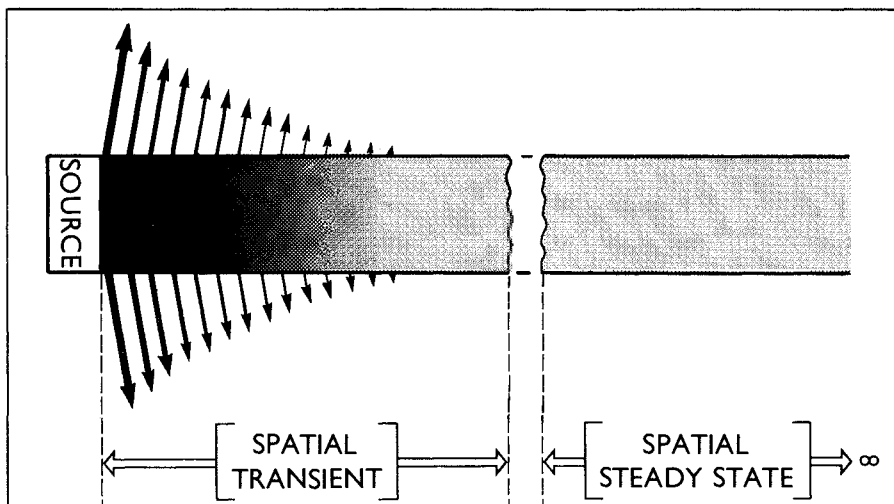


Fig. 8-1 Qualitative description of radiation loss along a fiber. Darker regions correspond to higher light intensity and thicker arrows to higher radiation losses.

leaky rays account for the black-band phenomenon on step-profile fibers, and a similar phenomenon on graded-profile fibers. Following a brief discussion of leaky-ray effects on asymmetric fibers, we conclude by examining the interplay of radiation and absorption losses.

Duration and characteristics of the spatial transient

The main objective in the first eleven sections is to determine an effective length, or duration, of the spatial transient, as well as pulse shape. Because the conclusions are both simple and important, we summarize them here for ready reference and also to provide perspective for their derivation.

The spatial transient on fibers is composed mainly of bound and tunneling rays, as refracting rays attenuate very rapidly [1,2]. Thus, except very close to the source, total light power in the core is the sum of the power of bound rays P_{br} and the power of tunneling rays $P_{tr}(z)$ at distance z along the fiber. Assuming a diffuse source, the powers of bound and tunneling rays are approximately equal at the beginning of a weakly guiding step-profile fiber, i.e. $P_{br} \cong P_{tr}(0)$ [3], while for a clad parabolic profile $P_{br} \cong 3P_{tr}(0)$ [4].

In Sections 4-21 and 4-22, we showed that the shape of the impulse response on step and clad parabolic profiles is virtually rectangular. This conclusion is valid only in the spatial steady state. In the spatial transient, the power in tunneling rays manifests itself by adding a tail to the pulse. The power in the tail is large close to the source but becomes negligible at the onset of the spatial steady state [5].

The duration z_0 of the spatial transient depends on wavelength, or, equivalently, on the fiber parameter V , since the attenuation of tunneling rays is a wavelength-dependent phenomenon. Taking z_0 to be the position where tunneling ray power has decreased by 90%, we shall show in Section 8-8 that [6, 7]

$$z_0 \cong (\rho/2\theta_c) \exp(V/2), \quad (8-1a)$$

for diffuse illumination of a step-profile fiber of core radius ρ , where V and θ_c are defined inside the front cover. For a typical multimode fiber with $\rho = 25 \mu\text{m}$, $\theta_c = 0.14$ and $V = 30$, we have $z_0 \cong 300 \text{ m}$, while for the same fiber with $V < 10$ the transient extends only a few centimeters. For a clad parabolic fiber, we shall show in Section 8-9 that the corresponding expression is [6, 7]

$$z_0 \cong (\pi\rho/\theta_c) \exp(V/2), \quad (8-1b)$$

so that the transient extends a factor of 2π further than for the step profile.

RADIATION FROM FIBERS ILLUMINATED BY A DIFFUSE SOURCE

In Sections 4-6 and 4-17 we discussed light-acceptance properties of fibers illuminated by a diffuse source by considering the power entering bound rays. Here we examine the power entering leaky rays and its variation along the fiber. For convenience we consider step and graded profiles separately.

8-2 Leaky-ray excitation on step-profile fibers

The diffuse source of Fig. 4-3(a) illuminates the endface of a step-profile fiber in Fig. 4-4. This source excites all tunneling and refracting rays, as well as bound rays. In order to determine the power entering the tunneling rays, we must first determine the distribution function.

Distribution function

In Section 4-17 we introduced the distribution function $F(\bar{\beta}, \bar{l})$ of Eq. (4-39) to describe the power carried by bound rays, and showed that for diffuse illumination it is proportional to the ray half-period, as expressed by Eq. (4-45a). Thus $F(\bar{\beta}, \bar{l})$ depends only on the ray path within the core. Since tunneling rays differ from bound rays only in their behavior in the cladding, we deduce that the distribution function for tunneling rays has the same functional form. If we follow the procedure in Section 4-17, this result can be obtained formally, starting from Eq. (4-41) with the limits on $\bar{\beta}$ and \bar{l} replaced by those in Eq. (8-4b) below. Thus, for the step profile, we have from Eq. (4-48) that

$$F(\bar{\beta}, \bar{l}) = \frac{8\pi\rho^2 I_0}{n_0^2} \frac{\bar{\beta}(n_{co}^2 - \bar{\beta}^2 - \bar{l}^2)^{1/2}}{n_{co}^2 - \bar{\beta}^2}, \quad (8-2a)$$

and Eq. (2-8c) gives the ranges of values of invariants for tunneling rays

$$0 \leq \bar{\beta} < n_{cl}; \quad (n_{cl}^2 - \bar{\beta}^2)^{1/2} \leq \bar{l} \leq (n_{co}^2 - \bar{\beta}^2)^{1/2}, \quad (8-2b)$$

where n_{co} and n_{cl} are the core and cladding indices, respectively.

It is often helpful to integrate out the dependence on skewness, i.e. \bar{l} . In Section 4-18 we introduced the distribution function $G(\bar{\beta})$, which is defined to be the integral of $F(\bar{\beta}, \bar{l})$ over the range of values of \bar{l} . For bound rays, $G(\bar{\beta})$ is given by Eq. (4.47a), and for tunneling rays, we integrate Eq. (8-2a) over the range of \bar{l} given by Eq. (8-2b). By making the following substitution

$\bar{l} = (n_{co}^2 - \bar{\beta}^2)^{1/2} \sin w$, straightforward integration leads to

$$G(\bar{\beta}) = 2\pi^2 \rho^2 \frac{I_0}{n_0^2} \bar{\beta} \left\{ 1 - \frac{2}{\pi} \sin^{-1} \left[\frac{(n_{cl}^2 - \bar{\beta}^2)^{1/2}}{(n_{co}^2 - \bar{\beta}^2)^{1/2}} \right] - \frac{2(n_{co}^2 - n_{cl}^2)^{1/2} (n_{cl}^2 - \bar{\beta}^2)^{1/2}}{n_{co}^2 - \bar{\beta}^2} \right\}, \quad (8-3)$$

for the range $0 \leq \bar{\beta} < n_{cl}$.

Invariants and power distribution on the endface

The range of values of invariants for bound rays at each point on the endface of a step-profile fiber is independent of position and is given by $n_{cl} < \bar{\beta} \leq n_{co}$. In the case of tunneling rays, however, this range varies across the endface, and can be obtained by simultaneously deriving the power $P(r)$ exciting tunneling rays at each point on the endface. We recall that Eq. (4-41) gives the total bound-ray power, and hence, by symmetry, the power entering bound rays at each point on the endface is given by the right side of Eq. (4-41a) with the radial integration omitted and a multiplicative factor $1/2\pi r$ included. In analogy, $P(r)$ is given by the same expression with the upper limit of the $\bar{\beta}$ integral and the lower limit of the l integral determined from Eq. (2-24c). Hence

$$P(r) = 4 \frac{I_0 \rho}{n_0^2 r} \int_{\bar{\beta}_{\min}(r)}^{n_{cl}} \bar{\beta} d\bar{\beta} \int_{(n_{cl}^2 - \bar{\beta}^2)^{1/2}}^{\bar{l}_m(r, \bar{\beta})} \frac{d\bar{l}}{g(r)}, \quad (8-4a)$$

where $g(r)$ and $\bar{l}_m(r, \bar{\beta})$ are defined in Eqs. (4-40) and (4-41b), respectively, with $n(r)$ replaced by n_{co} . Since the lower limit of the \bar{l} integral cannot exceed the upper limit, the $\bar{\beta}$ integral has the lower limit $\bar{\beta}_{\min}(r) \geq 0$, which is the value of $\bar{\beta}$ when the limits on \bar{l} are equal. Hence the ranges of invariant values for tunneling rays at radius r on the endface satisfy

$$\bar{\beta}_{\min}(r) \leq \bar{\beta} < n_{cl}; \quad (n_{cl}^2 - \bar{\beta}^2)^{1/2} \leq \bar{l} \leq \bar{l}_m(r, \bar{\beta}), \quad (8-4b)$$

$$\bar{\beta}_{\min}^2(r) = \max \left\{ 0, \frac{\rho^2 n_{cl}^2 - r^2 n_{co}^2}{\rho^2 - r^2} \right\}; \quad \bar{l}_m(r, \bar{\beta}) = \frac{r}{\rho} (n_{co}^2 - \bar{\beta}^2)^{1/2}, \quad (8-4c)$$

as may be verified. A schematic representation of these regions is presented in Fig. 8-2 for (a) $\bar{\beta}_{\min}(r) = 0$ and (b) $\bar{\beta}_{\min}(r) > 0$. Bound-ray invariants lie within the triangular areas and refracting-ray invariants lie within the hatched areas. These domains are subsets of the domains in Fig. 2-7(a) for the whole fiber.

Refracting rays

In Chapter 7 we showed that refracting rays attenuate so rapidly that they contribute significantly to total ray power only extremely close to the source.

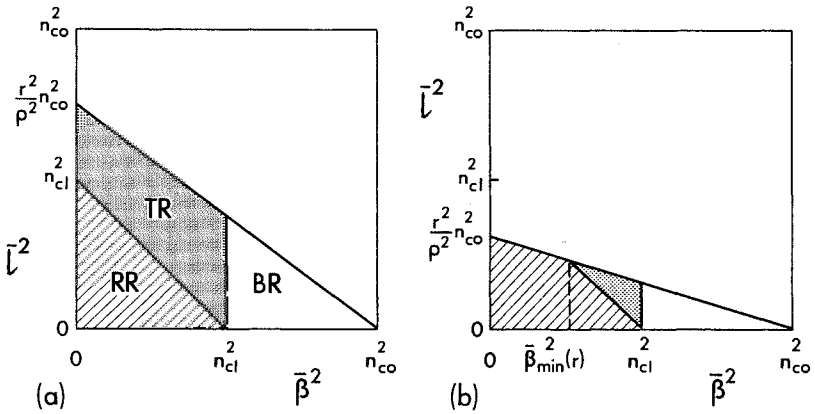


Fig. 8-2 Domains of ray invariants for bound rays (BR), tunneling rays (TR) and refracting rays (RR) at radius r on a step-profile fiber illuminated by a diffuse source. In (a) $r \geq \rho n_{cl}/n_{co}$ and $\bar{\beta}_{min}(r) = 0$, and in (b) $r < \rho n_{cl}/n_{co}$ and $\bar{\beta}_{min}(r) > 0$.

We can, therefore, ignore their presence when determining the spatial transient at distances along the fiber well away from the source. A quantitative analysis, based on a similar approach to that of the present section, fully justifies their omission [8].

Initial tunneling ray power

The total tunneling ray power excited on the endface, $P_{tr}(0)$, is found by integrating Eq. (8-3) over the range $0 \leq \bar{\beta} < n_{cl}$. This is facilitated by integrating the second term within the curly brackets by parts in order to remove the inverse sine function, and then amalgamating with the integral of the third term. The substitution $\bar{\beta} = n_{cl}(1 - w^2)^{1/2}$ reduces the combined integral to the form of Eq. (37-116). If we normalize with the total bound-ray power of Eq. (4-16) then

$$\frac{P_{tr}(0)}{P_{br}} = 1 - \frac{2}{\pi} \cot \theta_c + \frac{2}{\pi} \theta_c \frac{\cos 2\theta_c}{\sin^2 \theta_c}, \quad (8-5a)$$

$$\cong 1 - \frac{8}{3} \frac{\theta_c}{\pi}; \quad \theta_c \ll 1, \quad (8-5b)$$

where $\sin \theta_c = \{1 - n_{cl}^2/n_{co}^2\}^{1/2}$. In the weak-guidance limit, bound and tunneling ray powers are equal to lowest order in θ_c . However, total bound and tunneling ray powers are of order θ_c^2 smaller than the total power emitted

by the source, as is clear from Eq. (4-10). Consequently, virtually all diffuse source power excites refracting rays, which is rapidly radiated away from the core in a very short distance along the fiber.

8-3 Spatial transient for step-profile fibers

The extent of the spatial transient depends on the variation of total ray power along the fiber. We ignore refracting rays, for reasons given above, and define $P_s(z)$ to be the sum of bound and tunneling ray power at distance z . Bound-ray power is conserved along a nonabsorbing fiber, consequently

$$P_s(z) = P_{br} + P_{tr}(z); \quad P_s(0) = P_{br} + P_{tr}(0). \quad (8-6)$$

The ratio $P_s(z)/P_s(0)$ determines the radiation loss and the duration of the spatial transient. At distance z , the total tunneling ray power is obtained by integrating the product of the attenuation factor and the distribution function of Eq. (8-2a) over the range of invariants in Eq. (8-2b). Thus

$$P_{tr}(z) = \int_0^{n_{cl}} d\bar{\beta} \int_{(n_{cl}^2 - \bar{\beta}^2)^{1/2}}^{(n_{co}^2 - \bar{\beta}^2)^{1/2}} F(\bar{\beta}, \bar{l}) \exp\{-\gamma(\bar{\beta}, \bar{l})z\} d\bar{l}, \quad (8-7)$$

where the attenuation coefficient given by Eq. (7-2) is the ratio of the transmission coefficient of Eq. (7-20) and the ray half-period of Table 2-1, page 40. The integration is performed numerically and leads to the curves in Fig. 8-3(a), which plot $P_s(z)/P_s(0)$ of Eq. (8-6) against the normalized distance z/ρ along the fiber for various values of the fiber parameter V and $\theta_c = 0.1$ [9]. To help interpret these curves, we plot the initial distribution of bound and tunneling ray power in Fig. 8-3(b) as a function of $\bar{\beta}/n_{co}$ for the same value of θ_c . This uses the distribution of Eqs. (4-49) and (8-3) in the normalized form $n_o^2 G(\bar{\beta})/(2\pi^2 \rho^2 I_o n_{co})$. As $\bar{\beta}$ decreases from $\bar{\beta} = n_{co}$, bound-ray power remains virtually uniform, but tunneling-ray power decreases rapidly for $\bar{\beta} < n_{cl}$, i.e. for rays making larger angles θ_z with the fiber axis. Furthermore, the attenuation coefficient increases as θ_z increases. This means that rays with the smaller values of θ_z carry the major portion of tunneling-ray power and have the lowest attenuation. In the classical geometric optics limit $\lambda \rightarrow 0$, or, equivalently, $V \rightarrow \infty$, there is no attenuation, corresponding to the horizontal line in Fig. 8-3(a). As λ increases, or V decreases, total ray power at a given position z decreases, and as $z \rightarrow \infty$ only bound-ray power remains. In this limit we deduce from Eqs. (8-5) and (8-6) that provided $\theta_c \ll 1$

$$\frac{P_s(z)}{P_s(0)} \cong \frac{1}{2} + \frac{2}{3\pi} \theta_c; \quad z \rightarrow \infty. \quad (8-8)$$

The spatial transient can extend over considerable distances for larger values of V before approaching this limit. In other words, *bound rays alone are insufficient to describe propagation, even on long fibers, as $V \rightarrow \infty$.*

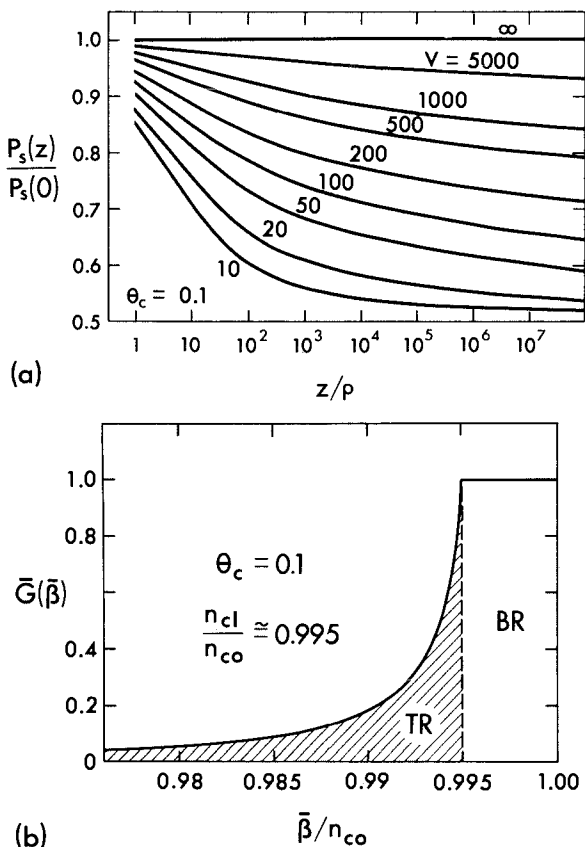


Fig. 8-3 (a) Fraction of initial bound- and tunneling-ray power remaining on a step-profile fiber illuminated by a diffuse source. (b) Distribution of bound-ray (BR) and tunneling-ray (TR) power as a function of $\bar{\beta}/n_{co}$ where $\bar{G}(\bar{\beta})$ denotes the normalized function $G(\bar{\beta})n_0^2/(2\pi^2\rho^2 I_0 n_{co})$.

8-4 Leaky-ray excitation on graded-profile fibers

Here we consider clad graded-profile fibers and parallel the discussion of Section 8-3, again ignoring refracting rays. We recall from Section 2-7 that the ranges of invariant values for tunneling rays depend on the profile, and are expressed by Eq. (2-24c). The upper limit on \bar{T} for the clad power-law profiles of Table 2-1, page 40, was obtained in Section 4-19, and Eq. (4-53) gives

$$\bar{T}_{\max}(\bar{\beta}) = q^{1/2} \left\{ \frac{2}{n_{co}^2 - n_{cl}^2} \right\}^{1/q} \left\{ \frac{n_{co}^2 - \bar{\beta}^2}{q+2} \right\}^{(q+2)/2q} \quad (8-9)$$

We showed in Section 8-2 that the minimum value of $\bar{\beta}$ follows by equating the upper and lower limits of \bar{l} , whence

$$\bar{\beta}_{\min} = \begin{cases} 0; & n_{\text{co}}^2 \geq n_{\text{cl}}^2(q+2)/q, \\ [n_{\text{cl}}^2 - (q/2)(n_{\text{co}}^2 - n_{\text{cl}}^2)]^{1/2}; & n_{\text{co}}^2 \leq n_{\text{cl}}^2(q+2)/q. \end{cases} \quad (8-10a)$$

For practical fibers $n_{\text{co}} \cong n_{\text{cl}}$ and $q \cong 2$, so that Eq. (8-10b) is normally satisfied, as we shall assume from hereon. The distribution of ray types in the $\bar{\beta}, \bar{l}$ plane is shown in Fig. 2-7(b).

Initial tunneling ray power

The range of values of the invariants for tunneling rays at each position on the endface are given by Eq. (8-4b), where, by paralleling the derivation of Eq. (8-4c) for the graded fiber, we now have

$$\bar{\beta}_{\min}^2(r) = \max \left\{ 0, \frac{\rho^2 n_{\text{cl}}^2 - r^2 n^2(r)}{\rho^2 - r^2} \right\}; \quad \bar{l}_m(r, \bar{\beta}) = \frac{r}{\rho} \{n^2(r) - \bar{\beta}^2\}^{1/2}, \quad (8-11)$$

and the power exciting tunneling rays at each position is expressed by Eq. (8-4a) in terms of these limits in the integrals.

Distribution function

We showed in Section 4-19 that the distribution function $F(\bar{\beta}, \bar{l})$ for both bound- and tunneling-ray power is given analytically for the clad parabolic profile fiber by Eq. (4-52), where

$$F(\bar{\beta}, \bar{l}) = 4\pi^2 \rho^2 \frac{I_0}{n_o^2} \frac{\bar{\beta}}{(n_{\text{co}}^2 - n_{\text{cl}}^2)^{1/2}}. \quad (8-12a)$$

If we integrate over the range $(n_{\text{cl}}^2 - \bar{\beta}^2)^{1/2} \leq \bar{l} \leq \bar{l}_{\max}(\bar{\beta})$ using Eq. (8-9) with $q = 2$, the distribution of tunneling-ray power corresponding to Eq. (8-3) for the step-profile fiber is given by

$$G(\bar{\beta}) = 2\pi^2 \rho^2 \frac{I_0}{n_o^2} \frac{\bar{\beta}}{n_{\text{co}}^2 - n_{\text{cl}}^2} \{n_{\text{co}}^2 - \bar{\beta}^2 - 2(n_{\text{co}}^2 - n_{\text{cl}}^2)^{1/2} (n_{\text{cl}}^2 - \bar{\beta}^2)^{1/2}\}, \quad (8-12b)$$

over the range $\bar{\beta}_{\min} \leq \bar{\beta} < n_{\text{cl}}$.

Initial tunneling-ray power

The total tunneling-ray power excited over the endface is obtained by integrating Eq. (8-12b) over the range of $\bar{\beta}$ with $\bar{\beta}$ given by Eq. (8-10b) for $q = 2$. If we normalize with the total bound-ray power of Eq. (4-18) for

$q = 2$, then

$$P_{tr}(0)/P_{br} = 1/3. \quad (8-13)$$

Accordingly, we deduce from this result and Eqs. (4-16), (4-18) and (8-5b) that *the diffuse source excites twice as much bound-ray power on a step-profile fiber as on a parabolic-profile fiber, while six times as much power goes into tunneling rays on a step-profile fiber as on a parabolic-profile fiber within the weak-guidance approximation.*

Clad power-law profiles

The ratio of initial tunneling-ray power to bound-ray power can be determined for the clad power-law profiles of Table 2-1, page 40. Details are presented elsewhere [4] and lead to

$$\frac{P_{tr}(0)}{P_{br}} = \frac{q+2}{q} \left\{ \frac{q+4}{q+2} - \sqrt{\pi} \frac{\Gamma[(q+2)/2]}{\Gamma[(q+3)/2]} \right\}, \quad (8-14)$$

where P_{br} is given by Eq. (4-18), and Γ is the gamma function defined by Eq. (37-104). This ratio increases monotonically from 0.288 at $q = 1$ to 0.333 at $q = 2$ and to 0.370 at $q = 3$. We emphasize that the step-profile result of Eq. (8-5a) is *not* the limit $q \rightarrow \infty$, since Eq. (8-14) assumes $\beta_{min} > 0$, whereas $\beta_{min} = 0$ for the step profile.

8-5 Spatial transient for clad parabolic-profile fibers

The situation is identical to that in Section 8-3, with the step profile replaced by the clad parabolic profile. The total tunneling-ray power, $P_{tr}(z)$, is given by Eq. (8-7) in terms of $F(\bar{\beta}, \bar{l})$ of Eq. (8-12a), with the upper limit of the \bar{l} integral and the lower limit of the $\bar{\beta}$ integral replaced by $\bar{l}_{max}(\bar{\beta})$ of Eq. (8-9) and $\bar{\beta}_{min}$ of Eq. (8-10b), respectively. The attenuation coefficient $\gamma(\bar{\beta}, \bar{l})$ is the ratio of the transmission coefficient of Eq. (7-18) and the ray half-period of Table 2-1, page 40. We evaluate Eq. (8-7) numerically, and plot the ratio $P_s(z)/P_s(0)$ of Eq. (8-6) in Fig. 8-4 as a function of the normalized distance z/ρ for various values of the fiber parameter V and $\theta_c = 0.1$ [10]. Each curve approaches 0.75 as $z/\rho \rightarrow \infty$, and the deviation from the classical geometric optics result at a given position increases with decreasing V . For sufficiently large V the spatial transient can persist for large distances. Thus, the characteristic behavior of Figs. 8-3(a) and 8-4 is similar, although the tunneling power ratio $P_{tr}(z)/P_{tr}(0)$ decreases more slowly on the clad parabolic fiber. This is in keeping with the fact that on graded-profile fibers the attenuation coefficients for rays with turning points well away from the interface are very much smaller than on step-profile fibers, where every ray reaches the interface.

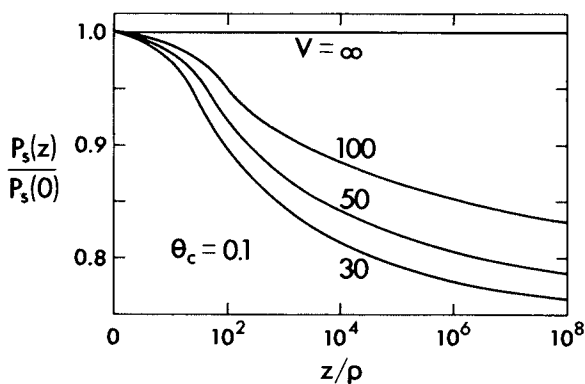


Fig. 8-4 Fraction of initial bound- and tunneling-ray power remaining on a clad parabolic-profile fiber illuminated by a diffuse source.

GENERALIZED PARAMETERS

If we extend the analysis of the spatial transient in Sections 8-3 and 8-5 to *arbitrary* sources of illumination and fiber profiles, the total tunneling-ray power will always be given by a double integral which differs from Eq. (8-7) only in the limits of integration. Consequently, the spatial transient depends on three dimensionless parameters associated with the fiber: the normalized distance z/ρ along the fiber, the fiber parameter V , and the complement of the critical angle θ_c . For each set of values of this triad the double integral must be evaluated numerically. However, it is possible to derive an approximate expression for the fraction of initial tunneling-ray power remaining within the core at position z , which depends on one parameter only, called the *generalized parameter* G . This parameter is a simple combination of z/ρ , V and θ_c , determined by the profile, and is derived from a qualitative examination of tunneling-ray attenuation coefficients.

Attenuation of tunneling-ray power

At distance z along a fiber, the initial power of each tunneling ray has been attenuated by the factor $\exp(-\gamma z)$ of Eq. (7-3), where γ is the power attenuation coefficient. The product γz for each ray depends on both the parameters ρ , θ_c , V of the fiber and the ray invariants $\bar{\beta}$, \bar{l} . If, for a particular ray, $\gamma z \gg 1$, then virtually all of its power has been lost to radiation, but if $\gamma z \ll 1$, the initial power has been nearly conserved along the fiber. In other words, the attenuation is effectively infinite or zero for the respective cases. We approximate the power of every tunneling ray by assuming it is either zero, if

$\gamma z \gtrsim 1$, or equal to the initial power if $\gamma z \lesssim 1$. The division between the two categories corresponds to $\gamma z \cong 1$ and leads to the combination of parameters of the fiber which defined the generalized parameter. The precise value of γz which defines the demarcation is obtained by expressing γz in dimensionless form as we show in the following examples.

8-6 Generalized parameter for step-profile fibers

The attenuation of tunneling-ray power in Eq. (7-3) depends on the product $\gamma(\bar{\beta}, \bar{l})z$, where the attenuation coefficient is the ratio of the transmission coefficient T to the ray half-period z_p . For the step profile, the latter is given in Table 2-1, page 40, and we use the linear approximation of Eq. (7-21) for T , which is an excellent approximation for all but the most weakly tunneling rays. If we express k in terms of the fiber parameter using the definition inside the front cover, then

$$\gamma(\bar{\beta}, \bar{l})z = \frac{2z}{\rho} \frac{n_{co}^2 - \bar{\beta}^2}{\bar{\beta}} \frac{(\bar{\beta}^2 + \bar{l}^2 - n_{cl}^2)^{1/2}}{n_{co}^2 - n_{cl}^2} \exp \left\{ -\frac{2V}{3} \frac{(\bar{\beta}^2 + \bar{l}^2 - n_{cl}^2)^{3/2}}{(n_{cl}^2 - \bar{\beta}^2)(n_{co}^2 - n_{cl}^2)^{1/2}} \right\}, \quad (8-15)$$

We rearrange this expression so that the term multiplying the exponential does not depend on V , z or ρ , and is dimensionless. The variation in $\gamma(\bar{\beta}, \bar{l})z$ will then be dominated by the exponential factor, where

$$\gamma(\bar{\beta}, \bar{l})z = \frac{n_{co} n_{co}^2 - \bar{\beta}^2}{\bar{\beta}} \frac{(\bar{\beta}^2 + \bar{l}^2 - n_{cl}^2)^{1/2}}{n_{co}^2 - n_{cl}^2} \frac{1}{(n_{co}^2 - n_{cl}^2)^{1/2}} \times \left(\exp \left\{ G - \frac{2}{3} \frac{(\bar{\beta}^2 + \bar{l}^2 - n_{cl}^2)^{3/2}}{(n_{cl}^2 - \bar{\beta}^2)(n_{co}^2 - n_{cl}^2)^{1/2}} \right\} \right)^V, \quad (8-16)$$

and the generalized parameter G is defined by [6, 7]

$$G = \frac{1}{V} \ln \left\{ 2\theta_c \frac{z}{\rho} \right\}, \quad (8-17)$$

where $\theta_c \cong (1 - n_{cl}^2/n_{co}^2)^{1/2}$ in the weak-guidance approximation.

As the fiber is multimoded, we can make quantitative statements about the value of $\gamma(\bar{\beta}, \bar{l})z$. When a tunneling ray has parameters $\bar{\beta}$ and \bar{l} which make the exponent of Eq. (8-16) positive, $\gamma(\bar{\beta}, \bar{l})z$ will be very large for nearly all such rays since $V \gg 1$. We approximate this high attenuation rate by setting $\gamma(\bar{\beta}, \bar{l})z = \infty$. Conversely, when the values of $\bar{\beta}$ and \bar{l} make the exponent of Eq. (8-16) negative, $\gamma(\bar{\beta}, \bar{l})z$ will be extremely small for nearly all such rays. The very low attenuation rate is approximated by setting $\gamma(\bar{\beta}, \bar{l})z = 0$. In other words, given z/ρ , V and θ_c , and hence G , we attribute either infinite or zero attenuation to each tunneling ray, depending on whether the values of $\bar{\beta}$ and \bar{l} make the

exponent of Eq. (8-16) positive or negative, respectively. The division between the two classes occurs when the exponent is zero, i.e. when $\bar{\beta}$ and \bar{l} satisfy

$$3G(n_{\text{cl}}^2 - \bar{\beta}^2)(n_{\text{co}}^2 - n_{\text{cl}}^2)^{1/2} = 2(\bar{\beta}^2 + \bar{l}^2 - n_{\text{cl}}^2)^{3/2}, \quad (8-18)$$

and lie within the tunneling-ray range in Eq. (2-8c).

8-7 Generalized parameter for graded-profile fibers

One of the simplest examples of a generalized parameter for graded-profile fibers is provided by the clad parabolic profile. The attenuation coefficient is the ratio of the transmission coefficient T to the ray half-period z_p of Table 2-1, page 40. We use the approximation of Eq. (7-16) for T and express k in terms of V through the relationship inside the front cover. Thus

$$\gamma(\bar{\beta}, \bar{l})z = \frac{n_{\text{co}}\theta_c z}{\pi\rho\bar{\beta}} \exp \left\{ -\frac{2V\bar{l}}{(n_{\text{co}}^2 - n_{\text{cl}}^2)^{1/2}} \left(\ln \{p + (p^2 - 1)^{1/2}\} - \frac{(p^2 - 1)^{1/2}}{p} \right) \right\}, \quad (8-19)$$

where $p = \bar{l}/(n_{\text{cl}}^2 - \bar{\beta}^2)^{1/2}$ and $\sqrt{2\Delta} \cong \theta_c$ assuming weak guidance. We rearrange this equation in a similar manner to Eq. (8-16) and obtain

$$\gamma(\bar{\beta}, \bar{l})z = \frac{n_{\text{co}}}{\bar{\beta}} \exp \left\{ G - \frac{2\bar{l}}{(n_{\text{co}}^2 - n_{\text{cl}}^2)^{1/2}} \left(\ln \{p + (p^2 - 1)^{1/2}\} - \frac{(p^2 - 1)^{1/2}}{p} \right) \right\}^V, \quad (8-20)$$

where the generalized parameter G is defined by [6, 7]

$$G = \frac{1}{V} \ln \left\{ \frac{\theta_c z}{\pi \rho} \right\}, \quad (8-21)$$

and $\theta_c \cong (1 - n_{\text{cl}}^2/n_{\text{co}}^2)^{1/2}$. The classification of tunneling rays according to whether the attenuation is effectively infinite or zero follows the discussion below Eq. (8-17). The division between the two classes is defined by values of $\bar{\beta}$ and \bar{l} satisfying

$$G(n_{\text{co}}^2 - n_{\text{cl}}^2)^{1/2} = 2\bar{l} \{ \ln [p + (p^2 - 1)^{1/2}] - (p^2 - 1)^{1/2}/p \}, \quad (8-22)$$

within the domain of Eq. (2-24c) for tunneling rays.

Clad power-law profiles

The generalized parameter for the remaining clad power-law profiles in Table 2-1, page 40, cannot be obtained so readily as there is no simple expression for the ray half-period. However, by suitably approximating the ray half-period and working with the transmission coefficient of Eq. (7-16) it may be

shown that [7]

$$G \cong \frac{1}{V} \ln \left\{ \frac{\theta_c}{\pi N(q) \rho} \frac{z}{\rho} \right\}; \quad N(q) = \frac{2}{q^{1/2}} \left\{ \frac{2}{2+q} \right\}^{1/q} \quad (8-23)$$

This reduces to the parabolic profile result of Eq. (8-21) for $q = 2$. We now consider applications of the generalized parameters.

8-8 Example: Diffuse illumination of step-profile fibers

Here we repeat the spatial transient calculation of Section 8-3 using the generalized parameter of Section 8-6. The total tunneling-ray power is given by Eq. (8-7), where now only those rays with effectively zero attenuation contribute. The values of $\bar{\beta}$ and \bar{l} for these rays must both satisfy Eq. (2-8c) and ensure that the right side of Eq. (8-18) is not smaller than the left side. Hence

$$\bar{l}(\bar{\beta}) \leq \bar{l} \leq \bar{l}_{\max}(\bar{\beta}) = (n_{co}^2 - \bar{\beta}^2)^{1/2}; \quad \bar{\beta}_g \leq \bar{\beta} \leq n_{cl}, \quad (8-24a)$$

where $\bar{l}(\bar{\beta})$ denotes the solution of Eq. (8-18), and $\bar{\beta}_g$ is found by setting $\bar{l}(\bar{\beta}) = \bar{l}_{\max}(\bar{\beta})$. This leads to

$$\bar{\beta}_g = n_{co} \left\{ 1 - \theta_c^2 \left(1 + \frac{2}{3G} \right) \right\}^{1/2} \cong n_{co} \left\{ 1 - \frac{\theta_c^2}{2} \left(1 + \frac{2}{3G} \right) \right\}, \quad (8-24b)$$

since $\theta_c \ll 1$. The integrand of Eq. (8-7) is zero unless $\bar{\beta}$ and \bar{l} satisfy Eq. (8-24a), when $\gamma z = 0$. If we normalize with the initial tunneling-ray power $P_{tr}(0)$, which is approximately equal to the bound-ray power P_{br} of Eq. (4-16) when $\theta_c \ll 1$, and substitute for the distribution function from Eq. (4-48), then

$$\frac{P_{tr}(z)}{P_{tr}(0)} = \frac{8}{\pi} \frac{1}{n_{co}^2 - n_{cl}^2} \int_{\bar{\beta}_g}^{n_{cl}} \frac{\bar{\beta} d\bar{\beta}}{n_{co}^2 - \bar{\beta}^2} \int_{\bar{l}(\bar{\beta})}^{\bar{l}_{\max}(\bar{\beta})} (n_{co}^2 - \bar{\beta}^2 - \bar{l}^2)^{1/2} d\bar{l}. \quad (8-25)$$

The \bar{l} integration is performed by setting $\bar{l} = (n_{co}^2 - \bar{\beta}^2)^{1/2} \sin s$. It is then convenient to change variable, from $\bar{\beta}$ to u , where $n_{co}^2 - \bar{\beta}^2 = u^2 (n_{co}^2 - n_{cl}^2)$, so that the final integral is a function of G alone

$$\frac{P_{tr}(z)}{P_{tr}(0)} = \frac{4}{\pi} \int_1^{u_g} u \{ \cos^{-1} w(u) - w(u) [1 - w^2(u)]^{1/2} \} du, \quad (8-26a)$$

where

$$u_g = \left\{ 1 + \frac{2}{3G} \right\}^{1/2}; \quad w(u) = \frac{1}{u} \left\{ u^2 - 1 + \left(\frac{3G}{2} (u^2 - 1) \right)^{2/3} \right\}^{1/2}. \quad (8-26b)$$

This integral is evaluated numerically and is given as a function of G by the solid curve in Fig. 8-5(a). The ratio of total power at position z to total initial power follows from Eqs. (8-6) and (4-16), and is plotted as the solid curve in Fig. 8-5(b). Direct numerical evaluation of the same ratio from Eq. (8-7) for sets of values of z/ρ , V and θ_c produces sets of points which all lie on or close to the dashed curve. The relatively small difference between the two curves confirms the accuracy of the generalized parameter method [6, 7].

Duration of the spatial transient

We can now quantify the duration of the spatial transient, as discussed in Section 8-1. If we assume that the spatial steady state begins when the tunneling-ray power has fallen to 10% of its initial value, then Fig. 8-5(a) shows that this corresponds to $G \cong 0.5$. We can then relate G to the duration of the spatial transient through Eq. (8-17), and deduce that

$$z_0 \cong (\rho/2\theta_c) \exp(V/2). \quad (8-27)$$

as given in Eq. (8-1a).

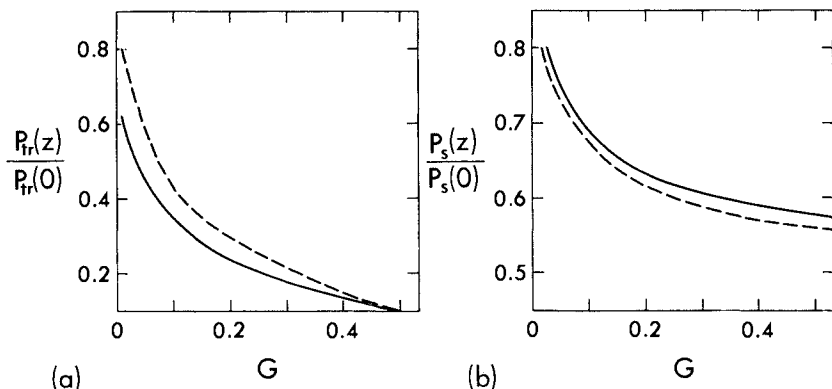


Fig. 8-5 (a) Fraction of initial tunneling-ray power remaining on a fiber illuminated by a diffuse source as a function of the generalized parameter G . The solid curve corresponds to the step profile and the dashed curve to the clad parabolic profile. (b) Fraction of initial bound- and tunneling-ray power remaining on the step profile. The solid curve is the exact numerical result and the dashed curve is the generalized parameter value.

8-9 Example: Diffuse illumination of clad parabolic-profile fibers

We use the generalized parameter of Eq. (8-21) to repeat the spatial transient calculation of Section 8-5. The development is similar to that of Section 8-8. The values of $\bar{\beta}$ and \bar{l} lie in the ranges given by Eq. (8-24a), except that $\bar{l}_{\max}(\bar{\beta})$ is given by Eq. (8-9) with $q = 2$, $\bar{l}(\bar{\beta})$ denotes the solution of Eq. (8-22), and $\bar{\beta}_g$ is the smallest value of $\bar{\beta}$ such that $\bar{l}(\bar{\beta}) = \bar{l}_{\max}(\bar{\beta})$. The initial tunneling-ray power is given by Eq. (8-13), and $F(\bar{\beta}, \bar{l})$ by Eq. (4-52). By analogy with Eq. (8-25), we obtain

$$\frac{P_{tr}(z)}{P_{tr}(0)} = \frac{24}{(n_{co}^2 - n_{cl}^2)^{3/2}} \int_{\bar{\beta}_g}^{n_{cl}} \bar{\beta} d\bar{\beta} \int_{\bar{l}(\bar{\beta})}^{\bar{l}_{\max}(\bar{\beta})} d\bar{l}. \quad (8-28)$$

It is helpful to change variables from $\bar{\beta}, \bar{l}$ to u, w where

$$u = \frac{n_{cl}^2 - \bar{\beta}^2}{n_{co}^2 - n_{cl}^2}; \quad w = \frac{\bar{l}}{(n_{co}^2 - n_{cl}^2)^{1/2}}, \quad (8-29a)$$

so that Eq. (8-28) is a function of G only expressed by

$$\frac{P_{\text{tr}}(z)}{P_{\text{tr}}(0)} = 12 \int_0^{u_g} du \int_{w(u)}^{(1+u)/2} dw = 6u_g + 3u_g^2 - 12 \int_0^{u_g} w(u) du, \quad (8-29b)$$

where $w(u)$ is the solution of the transformed equation corresponding to Eq. (8-22), i.e.

$$G = 2w(u) \ln [w(u) + \{w^2(u) - u\}^{1/2}] - w(u) \ln u - 2\{w^2(u) - u\}^{1/2}, \quad (8-30a)$$

and u_g is the solution of this equation when $\bar{l}(\bar{\beta}) = \bar{l}_{\text{max}}(\bar{\beta})$, or $w = (1 + u_g)/2$. Thus

$$2G = 2u_g - 2 - (1 + u_g) \ln u_g. \quad (8-30b)$$

Numerical evaluation of this integral leads to the dashed curve in Fig. 8-5(a). If the ratio of total power at position z to total initial power is calculated from Eqs. (8-6) and (4-18) with $q = 2$, then for practical values of G there is an error of the order of 1-2% compared with exact numerical evaluation of Eq. (8-7) [7].

Duration of the spatial transient

To quantify the duration of the spatial transient, we assume, as for the step profile, that the spatial steady state begins when tunneling-ray power has fallen to 10% of its initial value. This corresponds to $G \cong 0.5$ in Fig. 8-5(a), and we deduce from Eq. (8-21) that

$$z_0 \cong (\pi\rho/\theta_c) \exp(V/2). \quad (8-31)$$

Thus the spatial transient is a factor of 2π longer on the clad parabolic profile than on the step-profile fiber as anticipated in Eq. (8-1b).

In the present and previous sections we have demonstrated the considerable simplification which results from using generalized parameters to describe the spatial transient when a fiber is illuminated by a diffuse source. A similar simplification occurs when the generalized parameters are used to describe the spatial transient due to collimated-beam excitation [11].

PULSE SPREAD

In Chapter 3 we analysed pulse spread in terms of the variation in transit times between rays propagating at different angles $\theta_z(r)$ to the axial direction. Our analysis was limited to bound rays, whose directions lie in the range $0 \leq \theta_z(r) < \theta_c(r)$, where $\theta_c(r)$ is the local critical angle of Eq. (2-29). However, we assumed a diffuse source of illumination which also excites leaky rays propagating at angles in the range $\theta_c(r) \leq \theta_z(r) \leq \pi/2$. The transit time t for leaky rays propagating in a cross-sectional plane, i.e. $\theta_z(r) = \pi/2$, is infinite. Thus, when leaky rays are included, ray dispersion becomes very large compared with the dispersion due to bound rays alone. However, the majority of leaky rays which propagate at larger values of $\theta_z(r)$ attenuate extremely rapidly and in practice cannot be detected over long lengths of fiber. Since

these rays are responsible for nearly all of the increase in dispersion beyond that due to bound rays, it follows that the effective increase in pulse spread due to leaky rays is very much smaller.

We can quantify the leaky-ray contribution to ray dispersion by using the generalized parameter G of Sections 8-6 and 8-7 to divide the rays on the basis of their effective attenuation being infinite or zero. First we consider step-profile fibers and then power-law profiles; the effect is most significant for the optimum profile of Eq. (3-8).

8-10 Example: Ray dispersion on step-profile fibers

The dispersion due to bound rays on step-profile fibers is given by Eq. (3-3) in the weak-guidance approximation. If we include leaky rays, then only those tunneling rays with effectively zero attenuation are included. Since transit time is independent of skewness, i.e. independent of \bar{l} , this is equivalent to reducing the lower limit on $\bar{\beta}$ from n_{cl} to $\bar{\beta}_g$, defined by Eq. (8-24b). Thus the difference in transit times between the fastest, on-axis bound ray ($\bar{\beta} = n_{co}$) and the slowest tunneling ray ($\bar{\beta} = \bar{\beta}_g$) follows from Table 2-1, page 40, as [7]

$$t_d = \frac{z}{c} n_{co}^2 \left\{ \frac{1}{\bar{\beta}_g} - \frac{1}{n_{co}} \right\} \cong \frac{z}{c} n_{co} \Delta \left\{ 1 + \frac{2}{3G} \right\} \cong \frac{z}{c} \frac{n_{co}}{2} \left\{ 1 + \frac{2}{3G} \right\} \theta_c^2, \quad (8-32)$$

for $\Delta \ll 1$, and reduces to Eq. (3-3) when $G \rightarrow \infty$. Recalling the definition of G from Eq. (8-17) we see that Eq. (8-32) gives a simple indication of the effects of leaky rays on pulse width for given values of z/ρ , V and θ_c .

Pulse shape

Although tunneling rays can significantly increase pulse width, the distribution of power within the pulse, or impulse response, shows that for practical fibers, *very little power is conveyed by tunneling rays*. To see this, we follow the procedure used in Section 4-20 to determine the impulse response $Q(t)$ from the distribution function $\hat{G}(\bar{\beta})$. For bound rays $\hat{G}(\bar{\beta})$ is defined by Eq. (4-47b), and for tunneling rays with effectively zero attenuation it is proportional to the right side of Eq. (8-25) with the $\bar{\beta}$ integral suppressed. Since $\hat{G}(\bar{\beta})$ is continuous at $\bar{\beta} = n_{cl}$, we deduce that for tunnelling rays

$$G(\bar{\beta}) = \frac{4}{\pi} \frac{\bar{\beta}}{n_{co}^2 - n_{cl}^2} \{ \cos^{-1} w(u) - w(u) [1 - w^2(u)]^{1/2} \}; \quad \bar{\beta}_g \leq \bar{\beta} \leq n_{cl}, \quad (8-33)$$

where $w(u)$ is defined by Eq. (8-26b), $u = (n_{co}^2 - \bar{\beta}^2)^{1/2} / (n_{co}^2 - n_{cl}^2)^{1/2}$ and $\bar{\beta}_g$ is defined in Eq. (8-24b). We replace $\bar{\beta}$ by the transit time t through Eq. (4-58) and substitute into Eq. (4-55). The resulting expression is plotted in normalized form $Q(t)/Q(t_0)$ in Fig. 8-6(a) against $(t - t_0)/t_b$, where $t_0 = zn_{co}/c$ and $t_b = zn_{co}(n_{co} - n_{cl})/cn_{cl}$ is the bound-ray pulse width of Eq. (3-2) [5]. As G increases both the pulse width and the fraction of pulse power in tunneling rays decrease. When $G = -\infty$ all tunneling rays carry power, and when $G = \infty$ only bound rays carry power.

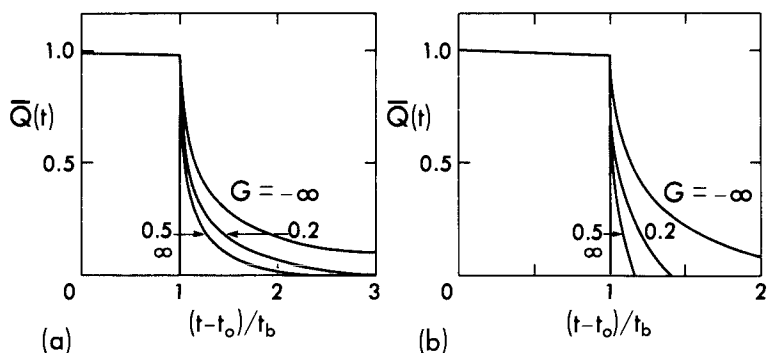


Fig. 8-6 Normalized impulse response $\bar{Q}(t) = Q(t)/Q(t_0)$ as a function of the normalized transit time $(t - t_0)/t_b$ for various values of the generalized parameter G . For (a) the step profile $t_b = zn_{co}(n_{co} - n_{cl})/cn_{cl}$, $t_0 = zn_{co}/c$ and for (b) the clad parabolic profile, $t_b = z(n_{co}^2 + n_{cl}^2)/2cn_{cl}$, $t_0 = zn_{co}/c$. When $G = -\infty$ all tunneling rays are included, and when $G = \infty$ only bound rays are included.

8-11 Example: Ray dispersion on clad parabolic-profile fibers

The effects of tunneling rays on pulse broadening and impulse response on clad power-law profile fibers can be found quantitatively following the approach of the previous section. A simple example is the clad parabolic profile, for which the effective pulse broadening follows from Table 2-1, page 40, as [5]

$$t_d = t(\bar{\beta}_g) - t(n_{co}) \cong \frac{z n_{co}}{c} \frac{\Delta^2}{2} (1 + u_g)^2 \cong \frac{z n_{co}}{c} \frac{\Delta^2}{8} (1 + u_g)^2 \theta_c^4, \quad (8-34)$$

when $\Delta \ll 1$. Here G is defined by Eq. (8-21), u_g by Eq. (8-30b) and $\bar{\beta}_g$ is given in terms of u_g by Eq. (8-29a). When $G \rightarrow \infty$, $u_g \rightarrow 0$ and t_d reduces to the bound ray result of Eq. (3-7a). The normalized dispersion $2ct_d/(z\Delta^2 n_{co})$ is plotted in Fig. 8-7. There is an increase in broadening of the order of 20 per cent for practical values of G in the range $0.3 \leq G \leq 0.5$.

Optimum profile

For the optimal profile with exponent q_{opt} of Eq. (3-8), the effective pulse broadening follows from Eq. (3-7) and Table 2-1, page 40, as [5]

$$t_d = t(\bar{\beta}_g) - t(\bar{\beta}_m) \cong \frac{z n_{co}}{c} \frac{\Delta^2}{8} (1 + 2u_g)^2 \cong \frac{z n_{co}}{c} \frac{\Delta^2}{32} (1 + 2u_g)^2 \theta_c^4, \quad (8-35)$$

where $\bar{\beta}_m$ is given by Eq. (3-6). Since $q_{opt} \cong 2$, we use the values of $\bar{\beta}_g$ and G for the parabolic profile. This is justified because of the weak dependence of G on q in

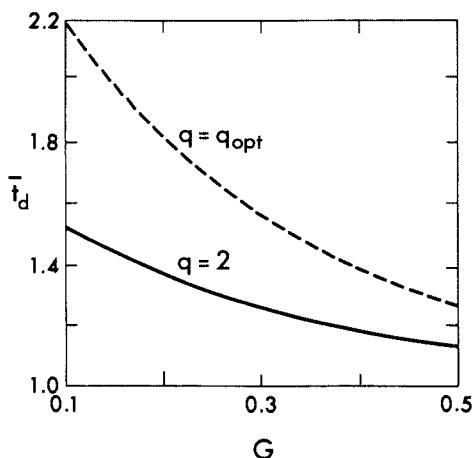


Fig. 8-7 Pulse width \bar{t}_d normalized to the bound-ray pulse width as a function of the generalized parameter G . The solid curve is for the clad parabolic profile, when $\bar{t}_d = 2ct_d/z\Delta^2n_{co}$, and the dashed curve is for the optimum profile, when $\bar{t}_d = 8ct_d/z\Delta^2n_{co}$.

Eq. (8-23). The normalized dispersion $8ct_d/(z\Delta^2n_{co})$ is plotted as the dashed curve in Fig. 8-7, and shows a 40–50% increase due to leaky rays. It is intuitive that leaky rays maximize the increase in pulse broadening for the optimum profile, because of the rapid variation in pulse width about q_{opt} in Fig. 3-3.

Impulse response

The impulse response for the clad parabolic profile can be found using the method of the previous section, and is plotted in Fig. 8-6(b) [5]. The fraction of pulse power in tunneling rays is much smaller than it is on the step profile. This is in keeping with the fact that the diffuse source excites only one-third as much tunneling-ray power on the parabolic profile fiber, as we showed in Section 8-4.

NONCIRCULAR FIBERS

The spatial transient on noncircular fibers can be determined by summing the power of leaky rays at each position z , but, in general, the noncircular cross-section makes the analysis very complicated. The paths no longer have the fixed periodicity of the axisymmetric fiber, so that, in particular, the ray half-period z_p will vary from reflection to reflection. In Chapter 2 we showed that a

leaky ray on a noncircular fiber may be either a tunneling ray or a refracting ray or a mixed tunneling-refracting ray. The latter behaves as either a tunneling or refracting ray at reflections from the turning-point caustic or interface. On fibers where only refracting or tunneling-refracting rays are excited, the spatial transient will be quite short compared with a circular fiber, because of the loss of a large fraction of a ray's power each time it refracts.

The power transmission coefficient T will generally vary along a leaky-ray path. It is therefore convenient to introduce an average attenuation coefficient $\bar{\gamma}$, so that the power $P(z)$ of the leaky ray will attenuate according to $P(z) = P(0) \exp(-\bar{\gamma}z)$. If T_i denotes the fraction of ray power lost at the i th reflection and z_{pi} is the corresponding half-period, then $\bar{\gamma} = \sum_i T_i / \sum_i z_{pi}$. Since T_i depends on the path parameters and on the fiber profile in the neighborhood of the caustic or interface, we employ the local transmission coefficients introduced in Section 7-14.

There is a general class of noncircular graded profiles where the fraction of power lost at each reflection does not vary, i.e. T is constant along a given ray path [12]. The power attenuation coefficient is then given by $T/\langle z_p \rangle$, where $\langle z_p \rangle$ is the average value of the ray half-period along the fiber.

When the asymmetry is slight, it is sometimes possible to simplify the above analysis by treating the noncircular fiber as a small perturbation of a circular fiber. Thus, for example, the ray invariant \bar{l} of the circular fiber can be replaced by an approximate invariant $\bar{l}(z)$ which varies very slowly along the noncircular fiber. The spatial transient on the elliptical, clad parabolic-profile fiber can be determined within this approximation. Details are given elsewhere [13].

INTENSITY DISTRIBUTION AT THE END OF THE FIBER

If a fiber is illuminated by a diffuse source, light power is distributed amongst all bound and leaky rays—both tunneling and refracting—at the beginning of the fiber. The power in each bound ray remains constant along the length of the fiber, but each leaky ray radiates power as it propagates. Here we consider the distribution of light intensity after it leaves the far end of the fiber and is viewed by a distant observer.

The observer at angle θ_0 to the fiber axis in Fig. 8-8 sees an elliptical beam of parallel rays originating on the core cross-section. If we ignore the small reflection losses from the fiber end, then the rays in the beam which correspond to bound rays on the fiber will have the same intensity as at the beginning of the fiber. However, the rays in the beam which correspond to leaky rays will have a lower intensity than at the beginning of the fiber. Accordingly the observer will see a pattern of lighter and darker areas on the fiber end. The shape of this

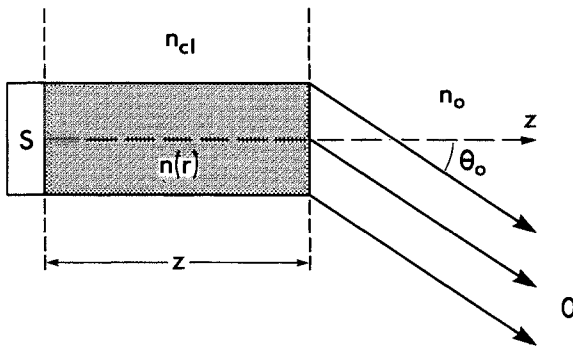


Fig. 8-8 A distant observer O at angle θ_o to the axis views the output from a fiber of length z , illuminated by a diffuse source S .

pattern depends on the refractive-index profile of the fiber, its length and θ_o . It is not necessary to determine the attenuation of each leaky ray; all we require is the distribution of rays over the core. We consider simple examples.

8-12 Example: Step-profile fiber

In Section 4-9 we determined the relationship between the angle of incidence θ_o of a collimated beam on a step-profile fiber and the types of rays excited in the core. Clearly this relationship is unaffected if we reverse the direction of propagation of every ray of the beam. We then have the situation in Fig. 8-8, with $n(r) = n_{co}$, and we can use the results of Section 4-9. Thus, if $0 \leq \theta_o < \theta_m$, where $n_o \sin \theta_m = n_{co} \sin \theta_c$ and $\sin \theta_c = \{1 - n_{cl}^2/n_{co}^2\}^{1/2}$, every ray of the emergent beam is bound and the whole core cross-section appears bright to the observer, as in Fig. 8-9(a). If $\theta_m < \theta_o \leq \pi/2$, then every ray of the beam is leaky. The division between tunneling and refracting rays is given by Eq. (2-24) as $\beta^2 + l^2 = n_{cl}^2$. If we substitute for the invariants from Eqs. (2-16) and (2-17)

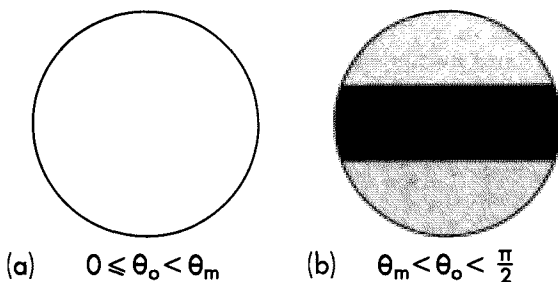


Fig. 8-9 Intensity pattern over the endface of a step-profile fiber, showing (a) a bright circle due to bound rays and (b) a dark band due to refracting rays, and lighter regions due to tunneling rays.

with $n(r) = n_{co}$, $\theta_z(r) = \theta_z$, and rearrange, we obtain

$$\frac{r}{\rho} \cos \theta_\phi(r) = \left\{ 1 - \frac{\sin^2 \theta_c}{\sin^2 \theta_z} \right\}^{1/2}; \quad n_{co} \sin \theta_z = n_0 \sin \theta_0. \quad (8-36)$$

We recall that $\theta_\phi(r)$ is the angle between the projection of the path onto the cross-section and the azimuthal direction in Fig. 2-4(c). Thus Eq. (8-36) denotes two straight lines a distance $2\rho \{1 - \sin^2 \theta_c / \sin^2 \theta_z\}^{1/2}$ apart, as shown in Fig. 8-9(b). The lines are parallel to the plane defined by the fiber axis and the beam direction.

The region between the two lines denotes refracting rays and the two regions on either side denote tunneling rays. Since refracting rays have attenuation coefficients which on average are much larger than those for tunneling rays, then provided the fiber is not too long, the observer will see a much darker region between the lines since virtually all refracting-ray power will have been radiated away. However, on average, tunneling rays will have lost little of their power and the observer will see a nearly uniform and relatively bright illumination in the two adjacent regions. The divisions between the lighter and darker regions will not be sharp, because tunneling and refracting rays in the neighborhood of $\bar{\beta}^2 + \bar{l}^2 = n_{cl}^2$, or $\alpha = \alpha_c$, will have nearly equal attenuation coefficients. This effect is known as the *black band phenomenon* [14, 15]. As the fiber length increases, the tunneling ray intensity diminishes and eventually the whole endface will appear dark.

8-13 Example: Clad power-law profile fibers

By repeating the argument at the beginning of the previous example, we can use the results of Section 4-10 to determine the beam pattern in Fig. 8-8 when the fiber has a clad power-law profile, as defined in Table 2-1, page 40. If $\theta_m(0) < \theta_0 \leq \pi/2$, where $\theta_m(0) = \theta_m$ defined above, the beam contains no bound rays, and if $0 \leq \theta_0 < \theta_m(0)$, bound rays alone occupy a circle of radius r_{br} on the fiber endface, defined by Eq. (4-26). If we ignore the ellipticity of the beam, due to viewing the endface obliquely, the observer will see a bright region within the dashed circles in Fig. 8-10. The division between tunneling and refracting rays is given by Eq. (2-24) as $\bar{\beta}^2 + \bar{l}^2 = n_{cl}^2$. If we substitute for the invariants from Eqs. (2-16) and (2-17) and for the profile, we find with the help of the relationship $n(r) \sin \theta_z(r) = n_0 \sin \theta_0$ that [11]

$$\left(\frac{r}{\rho}\right)^q - \frac{n_0^2 \sin^2 \theta_0}{n_{co}^2 - n_{cl}^2} \left(\frac{r}{\rho}\right)^2 \cos^2 \theta_\phi(r) + \frac{n_0^2 \sin^2 \theta_0}{n_{co}^2 - n_{cl}^2} - 1 = 0. \quad (8-37)$$

For the parabolic ($q = 2$) profile the curve is an ellipse. When $q < 2$ and $0 \leq \theta_0 < \theta_m$, this curve defines the boundary between the black regions, denoting refracting rays, and the hatched regions, denoting tunneling rays, in Fig. 8-10. We assume that the fiber length is not too large so that there is a sharp distinction between average refracting- and tunneling-ray intensities, as explained in the previous section, and between bound- and average tunneling-ray intensities. If $\theta_m \leq \theta_0 \leq \pi/2$ and $q \leq 2$, there is no solution to Eq. (8-37) and the beam contains only refracting rays, corresponding to the black circles in Fig. 8-10. When $q > 2$, the beam contains both tunneling and refracting rays unless the value of θ_0 exceeds the value of the solution of [11]

$$2n_0^2 \sin^2 \theta_0 = q(n_{co}^2 - n_{cl}^2), \quad (8-38)$$

when Eq. (8-37) has no solution and the beam contains only refracting rays.

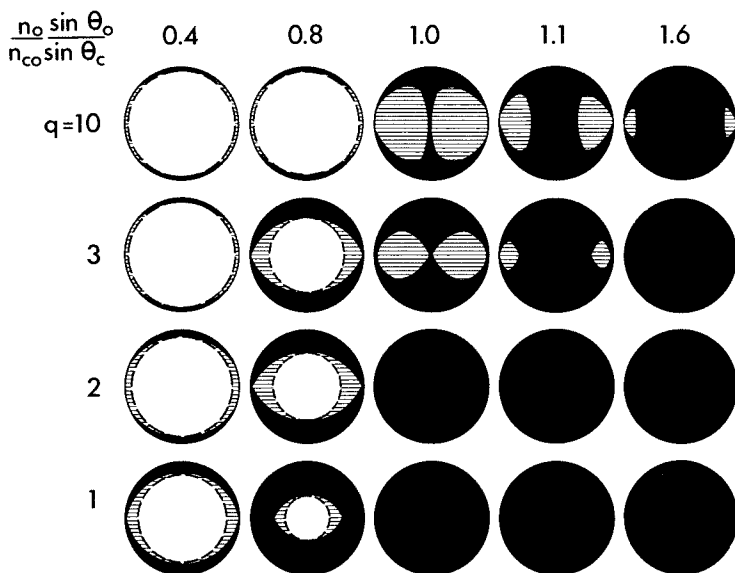


Fig. 8-10 Intensity patterns for the clad power-law profiles as a function of the exponent q and the angle of observation θ_0 . Black areas denote refracting rays, hatched areas tunneling rays and the white areas within the dashed circles bound rays.

RADIATION AND ABSORPTION LOSSES

So far in this chapter we have assumed that the fiber is nonabsorbing, and that all power loss is due solely to radiation from leaky rays. Here we examine the combined effects of loss due to radiation and material absorption. The most significant effect is that there is no longer a spatial steady state, since every bound ray loses power as it propagates. On a sufficiently long fiber, any power that is not lost by radiation will eventually be absorbed.

The power in each ray attenuates as $\exp(-\gamma z)$, where z is the distance along the fiber and γ is the power attenuation coefficient. For bound rays, Eq. (6-30) gives $\gamma = \gamma_{co} + \gamma_{cl}$, where γ_{co} and γ_{cl} are the attenuation coefficients describing core and cladding absorption, and for leaky rays, Eq. (7-24) gives $\gamma = \gamma_{co} + \gamma_{cl} + \gamma_{lr}$, where γ_{lr} is the leaky-ray attenuation coefficient. We ignore refracting rays because of their rapid attenuation, which is equivalent to assuming that $\gamma_{lr} = \infty$. The total ray power distance z along the fiber, $P_s(z)$, is found by integrating the distribution function of Eq. (4-45a), weighted by the attenuation factor, over all ray directions. Hence

$$P_s(z) = \int_0^{n_{co}} d\beta \int_0^{\Gamma_{\max}(\beta)} F(\beta, l) \exp(-\gamma z) dl, \quad (8-39)$$

where $I_{\max}(\beta)$ is defined in Eq. (2-24). We now consider examples when the illumination is due to a diffuse source.

8-14 Example: Step-profile fiber

On a step-profile fiber, the tunnelling-ray attenuation coefficient γ_{tr} is given by the ratio of the transmission coefficient of Eq. (7-19) to the ray half-period of Table 2-1, page 40. Assuming uniform core and cladding power absorption coefficients α_{co} and α_{cl} , the corresponding attenuation coefficients are given by Eqs. (6-10) and (6-21), where the angles θ_z and θ_ϕ are related to β and \bar{l} by Eq. (2-7). Numerical integration of Eq. (8-39) leads to the middle curve in Fig. 8-11(a) for the ratio $P_s(z)/P_s(0)$, where $V = 70$, $\theta_c = 0.1$, $\rho = 70 \mu\text{m}$, $\alpha_{co} = 5 \text{ dB/km}$ and $\alpha_{cl} = 50 \text{ dB/km}$ [16]. All ray power is lost after about 4 km. The top curve ignores radiation loss, which is equivalent to setting $\gamma_{tr} = 0$ in Eq. (8-39), and the dashed curves are for the nonabsorbing fiber, when $\gamma_{co} = \gamma_{cl} = 0$ in Eq. (8-39). The bottom curve includes only bound rays, i.e. $P_s(z) = P_{br}(z)$.

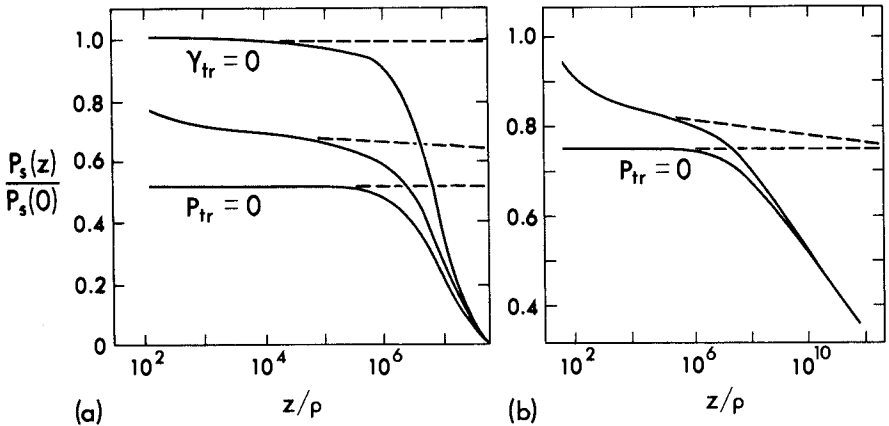


Fig. 8-11 The fraction of initial bound- and tunneling-ray power remaining on an absorbing fiber illuminated by a diffuse source, for (a) the step profile and (b) the clad parabolic profile. The bottom curves correspond to ignoring all tunneling-ray power and the top curve $\gamma_{tr} = 0$ in (a) corresponds to zero tunneling-ray attenuation. Dashed continuations of the curves are for the nonabsorbing fiber.

8-15 Example: Clad parabolic-profile fiber

On a clad parabolic-profile fiber, the tunneling-ray attenuation coefficient γ_{tr} is given by the ratio of Eq. (7-18) to the ray half-period z_p of Table 2-1, page 40. We assume a nonabsorbing core and uniformly absorbing cladding for which γ_{cl} is given by

Eqs. (6-26b) and (6-28). Numerical evaluation of Eq. (8-39) for a fiber with $V = 50$, $\theta_c = 0.14$ and $\alpha_{cl} = 100 \text{ dB/km}$ leads to the curves in Fig. 8-11(b) [10]. The characteristic behavior of the curves is similar to that for the step profile, but the effect of the cladding absorption is very much reduced because most ray paths have turning points well away from the interface.

REFERENCES

1. Snyder, A. W. (1974) Leaky-ray theory of optical waveguides of circular cross section. *Appl. Phys.*, **4**, 273-98.
2. Snyder, A. W. and Pask, C. (1975) Optical fibre: spatial transient and steady state. *Opt. Commun.*, **15**, 314-16.
3. Snyder, A. W., Mitchell, D. J. and Pask, C. (1974) Failure of geometric optics for analysis of circular optical fibres. *J. Opt. Soc. Am.*, **64**, 608-14.
4. Ankiewicz, A. and Pask, C. (1977) Geometric optics approach to light acceptance and propagation in graded-index fibres. *Opt. Quant. Elect.*, **9**, 87-109.
5. Ankiewicz, A. and Pask, C. (1978) Tunnelling rays in graded-index fibres. *Opt. Quant. Elect.*, **10**, 83-93.
6. Love, J. D. and Pask, C. (1976) Universal curves for power attenuation in ideal multimode fibres. *Electron. Lett.*, **12**, 252-3.
7. Pask, C. (1978) Generalized parameters for tunnelling ray attenuation in optical fibres. *J. Opt. Soc. Am.*, **68**, 110-16.
8. Pask, C. (1975) On the neglect of refracting rays in optical power calculations. *Opt. Quant. Elect.*, **7**, 428-9.
9. Pask, C. and Snyder, A. W. (1974) Illumination of multimode optical fibres - leaky ray analysis. *Opt. Quant. Elect.*, **6**, 297-304.
10. Barrell, K. F. and Pask, C. (1978) The effect of cladding loss in graded-index fibres. *Opt. Quant. Elect.*, **10**, 223-31.
11. Barrell, K. F. and Pask, C. (1979) Ray launching and observation in graded-index optical fibres. *J. Opt. Soc. Am.*, **69**, 294-300.
12. Ramkov Hansen, J. J., Ankiewicz, A. and Adams, M. J. (1980) Attenuation of leaky modes in graded noncircular multimode fibres. *Electron. Lett.*, **16**, 94-6.
13. Barrell, K. F. and Pask, C. (1980) Leaky ray correction factors for elliptical multimode fibres. *Electron. Lett.*, **16**, 580-1.
14. Potter, R. J. (1961) Transmission properties of optical fibres. *J. Opt. Soc. Am.*, **51**, 1079-89.
15. Kapany, N. S. (1967) *Fiber Optics*, Academic Press, New York.
16. Pask, C. and Snyder, A. W. (1976) Multimode optical fibres: interplay of absorption and radiation losses. *Appl. Opt.*, **15**, 1295-8.

Bends

Bent planar waveguides	180
9-1 Classification of rays on the bend	180
9-2 Attenuation of light power	181
9-3 <i>Example: Step profile</i>	182
9-4 <i>Example: Clad parabolic profile</i>	184
Bent fibers	185
9-5 <i>Example: Step and clad parabolic profiles</i>	187
References	188

In this chapter we study the radiation loss from optical waveguides due to bending. As we show from the ray-path equation, *there are no bound rays on bent waveguides*. Accordingly every ray is leaky and radiates power through the mechanisms of tunneling or refraction, as described in Chapter 7. In other words, total internal reflection on a straight waveguide is *frustrated* by bending. To calculate the radiation loss, we use geometric optics to determine the leaky-ray path within the core of the bent waveguide, and then attribute the appropriate power transmission coefficient to find the loss at turning or reflection points [1]. The total radiation loss is the sum of the losses along each leaky-ray path [2]. For practical multimode waveguides, we find that bending losses are negligible since the bend radius is generally enormous compared with the core dimensions [3, 4].

On bent planar waveguides, radiation loss is described by leaky rays which are either tunneling or refracting. Sufficiently far around the bend tunneling rays alone are adequate to determine the loss. The analysis is simplified by recognizing that propagation of rays on a bent planar waveguide is identical to propagation in the cross-section of a circular waveguide. Accordingly, the transmission coefficients are just particular cases of those for fibers [5].

A bent fiber can be thought of as a segment of a ring, or torus, and the leaky-ray paths are either refracting, tunneling or tunneling–refracting. Compared with the calculations for bent planar waveguides, the determination of radiation loss involves ray tracing in a more complicated core geometry and uses the localized transmission coefficients for interfaces or turning-point caustics defined by two radii of curvature, discussed in Sections 7–13 and 7–14. The situation is analogous to the determination of radiation loss from

noncircular fibers, as discussed in Chapter 8.

We first consider bent planar waveguides and show that all rays are leaky. Then we find their trajectories and attenuation.

BENT PLANAR WAVEGUIDES

In Fig. 9-1 a planar waveguide has a straight section of length d leading into a curved section of fixed radius R . A diffuse source S illuminates the waveguide at $z = 0$ and excites all bound and refracting rays. We assume d is sufficiently large for the spatial steady state to be reached. On the bend we need then consider only rays which are bound on the straight waveguide. Any ray which is leaky on the straight section has a much higher attenuation around the bend and can be neglected.

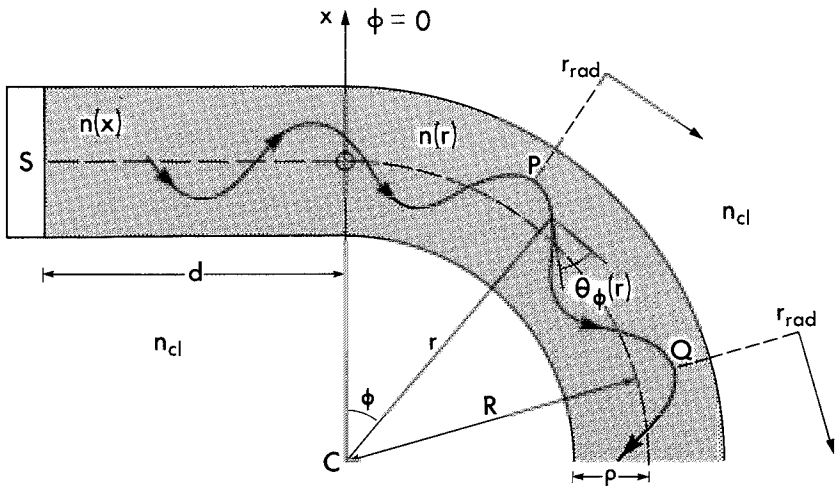


Fig. 9-1 A straight planar waveguide or fiber of length d is illuminated by a diffuse source S , and leads into a bend of radius R . The core half-width or radius is ρ .

9-1 Classification of rays on the bend

Here we show that all rays on the bent planar waveguide are leaky, regardless of the profile. We regard the bend as part of a circular fiber whose axis is orthogonal to the plane of the bend in Fig. 9-1 and passes through C . There are two interfaces at $r = R \pm \rho$, where r is the cylindrical radius from C , and we assume the core profile shape $n(r)$ is unaffected by bending, i.e. $n(r) = n(x)$, $r = x + R$. The azimuthal symmetry of the bend ensures that every ray follows a curved sinusoidal-like path. If the core is graded, the path has the

characteristic shape shown in Fig. 9-1, and if the core is uniform, the path has a similar zig-zag shape or a polygonal shape, as shown in Fig. 9-2(a). These paths lie in the cross-section of the fiber and thus the longitudinal ray invariant $\bar{\beta}$ satisfies $\bar{\beta} = 0$ for every ray.

Ray invariant for the bend

There is an invariant \bar{l}_b associated with each path around the bend. By analogy with Eq. (2-17), we set $\theta_z(r) = \pi/2$ and define

$$\bar{l}_b = \{r/(R + \rho)\} n(r) \cos \theta_\phi(r), \quad (9-1)$$

where $R + \rho$ is the radius of the outer interface and $\theta_\phi(r)$ is the angle between the tangent to the path and the azimuthal direction in Fig. 9-1. We relate \bar{l}_b to the invariant $\bar{\beta}_s$ on the straight waveguide, defined by $\bar{\beta}$ of Table 1-1, page 19 in terms of the profile $n(x)$ and the angle $\theta_z(x)$ between the path tangent and the axial direction. At the beginning of the bend $\theta_z(x) = \theta_\phi(r_0)$, where r_0 is the value of r at $\phi = 0$, so on the straight waveguide

$$\bar{\beta}_s = n(x) \cos \theta_z(x) = n(r_0) \cos \theta_\phi(r_0). \quad (9-2)$$

If we substitute from Eq. (9-1) with $r = r_0$, we deduce that on the bend

$$\bar{l}_b = \{r_0/(R + \rho)\} \bar{\beta}_s. \quad (9-3)$$

On the straight waveguide, bound-ray invariants satisfy $n_{cl} < \bar{\beta}_s \leq n_{co}$. Hence for any profile the values of \bar{l}_b are bounded by

$$n_{cl}(R - \rho)/(R + \rho) \leq \bar{l}_b \leq n_{co}, \quad (9-4)$$

since r_0 must lie between $R - \rho$ and $R + \rho$.

Radiation caustic on the bend

For a tunneling ray on the bend, the position of the radiation caustic r_{rad} and the paths in the cladding are shown in Fig. 9-1. The value of r_{rad} is given by Eq. (2-23) with $\bar{\beta} = 0$, $\bar{l} = \bar{l}_b$ and ρ replaced by $R + \rho$ for reasons given above

$$r_{rad} = (R + \rho) \bar{l}_b / n_{cl}. \quad (9-5)$$

Since \bar{l}_b of Eq. (9-4) is finite, r_{rad} must be finite and, therefore, *every ray on the bend is leaky*. Tunneling rays have $r_{rad} > R + \rho$ and refracting rays originate on the interface, i.e. $r_{rad} = R + \rho$. On a slight bend virtually all rays are tunneling rays.

9-2 Attenuation of light power

Every ray on the bend radiates power either by tunneling or by refraction. To describe the attenuation of the power in each ray, we follow the description of

Section 7-1, but replace z with the angular displacement ϕ in Fig. 9-1. If $P(\phi)$ is the power at angle ϕ and γ is the power attenuation coefficient, then, by analogy with Eq. (7-3), we have

$$P(\phi) = P(0) \exp(-\gamma\phi), \quad (9-6)$$

where $P(0)$ is the bound-ray power on the straight waveguide. To relate γ to the power transmission coefficient T of Eq. (7-1), we define ϕ_p to be the angular separation between successive turning points or reflections at which power is lost, e.g. ϕ_p is the angle between CP and CQ in Fig. 9-1. Then, by analogy with Eq. (7-2), we have

$$\gamma = T/\phi_p. \quad (9-7)$$

The total ray power $P_s(\phi)$ at angle ϕ around the bend is found by integrating Eq. (9-6) over all ray directions and over the core cross-section. If we assume weak guidance, the initial power $P(0)$ on the straight waveguide is virtually the same for all rays. Then by analogy with Eq. (4-12), and allowing for the planar geometry and ray attenuation, we have

$$P_s(\phi) = P(0) \int_{R-\rho}^{R+\rho} dr \int_{-\theta_c(r)}^{\theta_c(r)} \exp(-\gamma\phi) d\theta_z, \quad (9-8)$$

where $\theta_c(r) \ll 1$ is the complement of the local critical angle defined by Eq. (2-29) and referred to the centre of curvature. Since T and ϕ_p depend on profile, we consider specific examples.

9-3 Example: Step profile

On a bent step-profile planar waveguide, the ray paths follow straight lines between reflections from the inner and outer interfaces, as shown in Fig. 9-2(a). Path (i) reflects alternately from the inner and outer interfaces, and path (ii) reflects only from the outer interface and is known as a *whispering-gallery ray* [6]. For either path, the invariant of Eq. (9-1) reduces to

$$\bar{l}_b = n_{co} \cos \theta_\phi = \{(R-\rho)/(R+\rho)\} n_{co} \cos \theta'_\phi, \quad (9-9)$$

where θ_ϕ and θ'_ϕ are the angles between the path and the tangent to the outer or inner interface, respectively. Hence whispering-gallery rays satisfy

$$\cos \theta_\phi > (R-\rho)/(R+\rho). \quad (9-10)$$

Since $R \gg \rho$ in practice, only a few rays close to $\theta_\phi = 0$ satisfy this condition.

The delineation between tunneling and refracting rays on the bend is found by substituting Eq. (9-9) into Eq. (9-5), whence

$$r_{rad}/(R+\rho) = (n_{co}/n_{cl}) \cos \theta_\phi. \quad (9-11)$$

From the discussion of the radiation caustic in Section 9-1, we deduce that if $\theta_\phi > \theta_c$, where $\theta_c = \cos^{-1}\{n_{cl}/n_{co}\}$ is the complement of the critical angle, the ray refracts at the

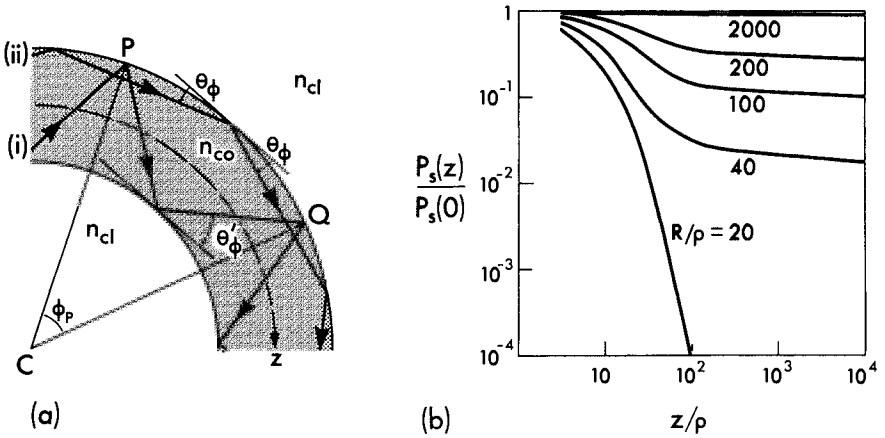


Fig. 9-2 (a) Ray paths on a bent step-profile planar waveguide and (b) the fraction of initial power remaining along the bend when $V = 50$ and $\theta_c = 0.1$.

outer interface, and if $\theta_\phi < \theta_c$ it tunnels. At the inner interface there is refraction if $\theta'_\phi > \theta_c$, but no power is lost if $\theta'_\phi < \theta_c$ since the interface is convex to the incident ray [5]. Since $\theta'_\phi < \theta_\phi$, according to Eq. (9-9), only a few rays refract at either or both interfaces. These rays correspond to bound rays on the straight waveguide with θ_z close to θ_c . Thus, virtually all rays on the bend are tunneling rays, which lose power only at the outer interface.

Power attenuation

To describe tunneling losses, we use the power transmission coefficient of Eq. (7-20) with $\bar{\beta} = 0$ and $\bar{l} = \bar{l}_b = n_{co} \cos \theta_\phi$. For refraction losses, we use the classical Fresnel coefficient of Eq. (7-4), with θ_z replaced by θ_i or θ'_i for the outer or inner interface, respectively. The angular separation ϕ_p of Eq. (9-7) for the paths (i) and (ii) in Fig. 9-2(a) is given, respectively, by

$$(i) \quad \phi_p = 2(\theta_\phi - \theta'_\phi); \quad (ii) \quad \phi_p = 2\theta_\phi, \quad (9-12)$$

if the rays lose power only at the outer interface. For rays which refract at the inner interface, $\phi_p = \theta_\phi - \theta'_\phi$. If $R \gg \rho$, we deduce from Eq. (9-9) that $\theta_\phi - \theta'_\phi \cong 2\rho/\theta_\phi R$ and the transition angle from path (i) to path (ii) occurs when $\theta_\phi \cong 2(\rho/R)^{1/2}$. The angle θ_ϕ is related to θ_z on the straight guide by Eqs. (9-2), (9-3) and (9-9), whence

$$\cos \theta_\phi = r_0 \cos \theta_z / (R + \rho). \quad (9-13)$$

Since $R - \rho \leq r_0 \leq R + \rho$, we deduce that $\theta_\phi \geq \theta_z$. Even though $\theta_z \ll 1$, we find that θ_ϕ can be very much larger than θ_z . Only when $R/\rho \rightarrow \infty$ can we assume $\theta_\phi \cong \theta_z$.

From the above information we calculate the attenuation coefficient of Eq. (9-7) and evaluate the total power numerically, using Eq. (9-8) with $\theta_c(r) = \theta_c$. The fraction of power remaining is plotted as a function of the normalized distance $z/\rho = R\phi/\rho$ along the bent waveguide axis in Fig. 9-2(b), for a waveguide with $V = 50$ and $\theta_c \cong \sqrt{2\Delta} = 0.1$ [2, 3]. As the normalized radius of curvature R/ρ decreases power is lost more rapidly. Each curve shows the same characteristic behavior. Initially, there is a *transition* region of rapid power loss, dominated by refracting rays and tunneling rays with the largest attenuation coefficients. The curves then become effectively straight, corresponding to a *steady state* region where power decreases exponentially with z/ρ . In this region, loss is described by tunneling rays alone. We also find that loss increases as θ_c decreases, for a fixed value of V . Most importantly, however, for practical values of bending radius, when $R/\rho \gtrsim 10^3$, bending losses are negligible.

9-4 Example: Clad parabolic profile

We again consider the situation in Fig. 9-1. The straight waveguide has the clad parabolic profile of Table 1-1, page 19, and on the bend the core profile is defined by

$$n^2(r) = n_{co}^2 \{1 - 2\Delta(r - R)^2/\rho^2\}, \quad (9-14)$$

relative to the axis C. Each path is labelled by the invariant \bar{T}_b of Eq. (9-1), which is related by Eq. (9-3) to the invariant $\bar{\beta}_s$ of the corresponding bound-ray path on the straight section.

It is clear from Eq. (9-1) that if $\bar{T}_b < n_{cl}$ the path reaches the outer interface of the bend and refracts. However, there are few such paths, corresponding to $\bar{\beta}_s \cong n_{cl}$. Each tunneling ray has an invariant in the range $n_{cl} < \bar{T}_b \leq n_{co}$, and follows the characteristic path shown in Fig. 9-3(a). This path makes angle $\theta_\phi(r)$ with the azimuthal, or z , direction, and lies between inner and turning-point caustics of radii r_{ic} and r_{tp} relative to the bend centre C. If we substitute Eq. (9-14) into Eq. (9-1) and set $\theta_\phi(r) = 0$, we find that r_{ic} and r_{tp} are roots of the quartic equation

$$(R + \rho)^2 \bar{T}_b^2 = r^2 n^2(r). \quad (9-15)$$

Compared with the straight waveguide, the effect of the bend is to displace the caustics towards the outer interface in Fig. 9-3(a).

Power attenuation

We assume that all power is lost from a refracting ray when it reaches the interface, i.e. $T = 1$. Tunneling rays lose power only at the turning-point caustic because the inner caustic is convex to the ray path. It is sufficiently accurate to use the linear approximation to the transmission coefficient given by Eq. (7-17), provided we set $\bar{\beta} = 0, \bar{T} = \bar{T}_b$ and replace ρ by $R + \rho$. On substituting for the profile from Eq. (9-14), we obtain

$$T = \exp \left\{ -\frac{2}{3} k(R + \rho) \left(\frac{\bar{T}_b^2}{n_{cl}^2} - 1 \right)^{3/2} \left/ \left(1 - \frac{\rho}{R + \rho} \frac{\bar{T}_b^2}{n_{co}^2 \theta_c^2} \right) \right. \right\}, \quad (9-16)$$

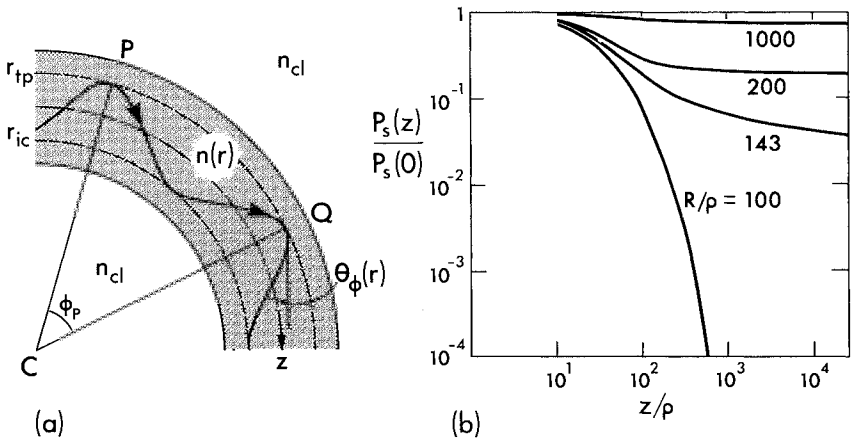


Fig. 9-3 (a) Ray path on a bent clad parabolic-profile planar waveguide and (b) the fraction of initial power remaining along the bend when $V = 50$ and $\theta_c = 0.1$.

where $2\Delta \cong \theta_c^2$. To determine the angular separation ϕ_p between successive outer turning points in Fig. 9-3(a), we note that when $R \gg \rho$, the corresponding axial distance is given approximately by twice the ray half-period z_p for the straight waveguide. If we replace $\bar{\beta}$ by \bar{l}_b in the expression for z_p in Table 2-1, page 40, and use the relation $R\phi_p = 2z_p$, we deduce that

$$\phi_p \simeq 2\pi\rho\bar{l}_b/R(n_{co}^2 - n_{cl}^2)^{1/2}. \quad (9-17)$$

The attenuation coefficient for each ray follows from Eq. (9-7), and, after changing variable in Eq. (9-8) from θ_z to $\bar{\beta} = n(x)\cos\theta_z$, the total power remaining is evaluated numerically. The fraction of power remaining is plotted in Fig. 9-3(b) as a function of the normalized distance $z/\rho = R\phi/\rho$ along the bent waveguide axis, assuming $V = 50$ and $\theta_c \cong (2\Delta)^{1/2} = 0.1$ [2, 4]. The characteristic behavior of each curve is similar to that in Fig. 9-2(b) for the step profile waveguide. However, for a given bending radius, the loss is greater for the parabolic profile. This increase arises because the displacement of the turning-point caustic towards the outer interface in Fig. 9-3(a) results in a higher loss compared with that for the corresponding path (with the same $\bar{\beta}$ value as the straight waveguide) in Fig. 9-3(b), whose angle of propagation increases from θ_z to θ_i . The major conclusion is that *bending losses are again negligible in practical waveguides*.

BENT FIBERS

As we discussed at the beginning of the chapter, the philosophy for finding bending loss is the same for planar waveguides and fibers. There is, of course, the geometrical complication that, by the addition of an extra dimension, rays

in general follow a three-dimensional helical-like path around the bent fiber. More importantly, however, each ray touches or reflects from surfaces now defined by two radii of curvature, and this requires the more general expressions for loss discussed in Section 7-14.

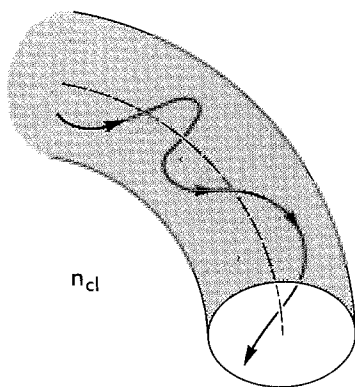


Fig. 9-4 Skew-ray path of varying half-period on a bent fiber.

Ray classification

The bent fiber is illustrated in Fig. 9-4 and can be thought of as a section of a ring or torus. Meridional rays propagate in the plane of the bend, defined by the bent fiber axis and the center of curvature C , and are identical to the rays on bent planar waveguides. In particular, they propagate along trajectories with fixed half-periods. All other rays are skew and, because of the asymmetry introduced by the bend, each skew ray propagates along a trajectory with a varying half-period, as shown in Fig. 9-4.

Attenuation of light power

As we showed for bent planar waveguides, all rays on a bent fiber are leaky. Meridional rays are either tunneling rays or refracting rays, and skew rays lose power at successive reflections or turning points either by tunneling or refraction. The latter are analogous to tunneling-refracting rays on non-circular fibers, discussed in Section 2-14.

With reference to Fig. 9-1, we assume that a diffuse source excites a sufficiently long straight fiber to enable the spatial steady state to be reached at the beginning of the bend. The analysis of ray paths around the bend depends on the profile. If the profile is a step, the trajectory is a straight line between successive reflections, involving the solution of cubic and quartic polynomial equations, whereas, if the profile is a clad parabola, a paraxial approximation is used [2].

The interface and turning-point caustic are curved surfaces. They are defined by two principal radii of curvature which depend on both the core radius ρ and the bend radius R . Under these conditions we use the localized transmission coefficients of Section 7-14 each time a ray loses power by tunneling. When power is lost by refraction, we employ the Fresnel coefficient of Eq. (35-50) for the step profile, and assume complete power loss for the clad parabolic profile, i.e. $T = 1$.

By analogy with Eq. (9-8), the total power at any position around the bend is given by a fourth order integration of the power in each ray over the core cross-section and all leaky-ray directions. The evaluation of this integral is complicated by the fact that, unlike meridional rays, the attenuation coefficient for a skew ray varies along its trajectory. This means the complete trajectory must be determined in order to correctly specify the attenuation.

9-5 Example: Step and clad parabolic profiles

The calculation of ray power along bent fibers with these profiles is based on the procedure described above. Here we present results, and refer elsewhere for details [2]. In Fig. 9-5 we plot the normalized power ratio $P_s(z)/P_s(0)$ against normalized distance z/ρ along the bent fiber axis for (a) a step profile, and (b) a clad parabolic profile. Here $P_s(0)$ denotes the total bound-ray power on the straight fiber. In both cases $V = 50$ and $\theta_c = 0.1$, and the values of R/ρ correspond to those for the bent planar waveguides in Figs. 9-2(b) and 9-3(b). The qualitative behavior of the curves in Fig. 9-5 is similar to that for the planar waveguides, but the loss of power in the transient region is not as severe, since only the relatively few rays close to the meridional plane have large losses. Beyond the transient the attenuation is higher than for the planar waveguide. This is because skew rays can pass through regions of high attenuation, although they may

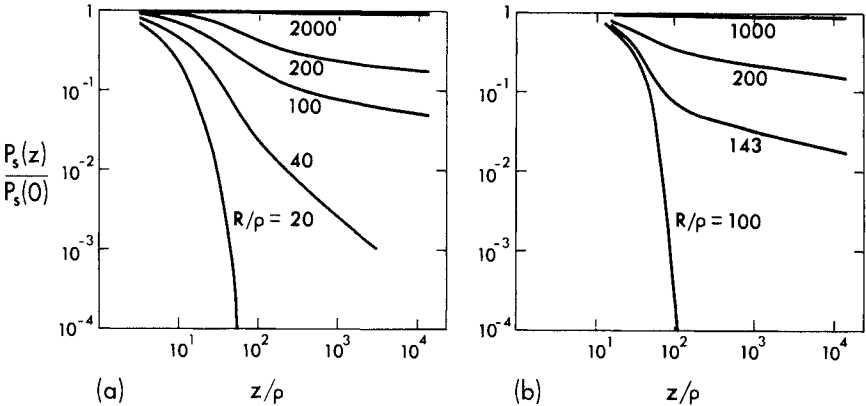


Fig. 9-5 The fraction of initial power remaining along a bent fiber when $V = 50$, $\theta_c = 0.1$ and the profile is (a) step and (b) clad parabolic.

initially have had a low attenuation. However, like the bent planar waveguides, *losses from bent fibers are negligible for practical values of bending radius.*

REFERENCES

1. Snyder, A. W. and Mitchell, D. J. (1974) Bending losses of multimoded optical fibres. *Electron. Lett.*, **10**, 11-12.
2. Winkler, C., Love, J. D. and Ghatak, A. K. (1979) Loss calculations in bent multimode optical waveguides. *Opt. Quant. Elect.* **11**, 173-83.
3. Love, J. D. and Winkler, C. (1978) Power attenuation in bent multimode step-index slab and fibre waveguides. *Electron. Lett.*, **14**, 32-4.
4. Winkler, C., Love, J. D. and Ghatak, A. K. (1978) Power attenuation in bent parabolic-index slab and fiber waveguides. *Electron. Lett.*, **14**, 570-1.
5. Snyder, A. W. and Mitchell, D. J. (1974) Generalized Fresnel's laws for determining radiation loss from optical waveguides and curved dielectric structures. *Optik*, **40**, 438-59.
6. Snyder, A. W. and Mitchell, D. J. (1974) Whispering-gallery rays within dielectric circles and spheres. *Electron. Lett.*, **10**, 16-17.

Diffraction phenomena

Diffraction of a light beam	190
10-1 Uniform and Gaussian beams	190
10-2 Light containment by a fiber	192
10-3 Applicability of geometric optics	193
Influence of diffraction on total internal reflection	194
10-4 Lateral shift	195
10-5 Transit time for the lateral shift	197
10-6 Lateral shift in planar waveguides	198
10-7 Preferred ray directions	200
Diffraction effects in arbitrary waveguides	201
References	202

In the first five chapters we described light propagation in optical waveguides using only geometric optics, and, therefore, ignored all wavelength-dependent phenomena. As we show in this chapter, such a description is accurate for waveguides of comparatively large core cross-section, i.e. multimode waveguides with $V \gg 1$. However, for waveguides with comparatively small core cross-sections and small values of V , the description of light propagation requires the electromagnetic theory approach of Part II. Our purpose here is to provide physical understanding for the failure of a geometric optics analysis when V is small and to anticipate new features of light propagation. *The cardinal assumption of all previous chapters is that light power propagates along the trajectories of geometric optics, determined by the ray-path equation.* Any deviation of this power flow from the geometric optics path is due solely to the wave nature of light, i.e. due to finite wavelength [1]. In this chapter we investigate the influence of wave effects on propagation using the simplest models possible. Before beginning, we are reminded that the deviation of power flow from the geometric optics path is often negligible in practical situations involving multimode waveguides and can be ignored as is done in Chapters 1 to 5. Nevertheless, when considering losses due to cladding absorption or curvature, wave effects cannot be ignored, however small, as they give rise to the mechanism of power attenuation. In Chapters 6 to 9 we account for such wave effects by using a transmission coefficient derived from

local plane-wave theory but we retain the *geometric optics trajectory*. This chapter is primarily concerned with the error in using the geometric optics trajectory in common with all previous chapters.

We first show qualitatively that, because of diffraction, it is impossible to confine light entirely within the core of any small- V waveguide. Thus, light must propagate in both the core and cladding if it is to be guided—a situation not described by classical geometric optics. By using the planar, step-profile waveguide, we can show quite simply how diffraction alters the classical ray picture of propagation. As a preliminary, we briefly review the diffraction of a beam propagating in free space, as this is the building block for the analysis.

DIFFRACTION OF A LIGHT BEAM

Within a geometric optics description, we would expect a finite beam of parallel rays to propagate indefinitely in a uniform medium without spreading. However, because of diffraction, the narrower the beam, the greater the spread in ray directions, and, consequently, the more the beam spreads out as it propagates. This is one reason why a guiding structure—the optical waveguide—is needed for long-distance transmission. To quantify this spread, we give a brief overview of the fundamental properties of beam diffraction, complemented by simple examples.

10-1 Uniform and Gaussian beams

In order to determine the diffraction of a beam, we decompose its electric field into plane-wave components by performing a two-dimensional Fourier transform. This decomposition is carried out in Section 36-3. The diffraction, or spreading, of the beam arises because these plane-wave components, or rays, propagate in different directions. The situation is analogous to diffraction by an aperture equal in area to the cross-section of the beam [2, 3]. As examples, we consider uniform and Gaussian beams of circular cross-section which propagate in the z -direction in a medium of uniform refractive index n . The beam fields are monochromatic with free-space wavelength λ , and the variation of the axisymmetric electric field amplitude $E(r)$ with cylindrical radius r is given in Table 10-1, where a and r_s are arbitrary scaling lengths. The diffraction-pattern amplitude $A(u)$ is the two-dimensional Fourier transform of $E(r)$ normalized to unity for on-axis waves ($u = 0$), where u gives the inclination θ_z of the diffraction waves to the z -axis. This transform is often called the Hankel transform, for which tables are available [4].

Beam transform

The transform of the Gaussian beam is Gaussian in shape, and the transform of the uniform beam is the cylindrical polar analogue of $\sin x/x$. It is also useful

Table 10–1 Beam fields and transforms. Electric field intensity $E(r)$ and diffraction pattern amplitude $A(u)$, where J_0 and J_1 are Bessel functions of order 0 and 1.

	Gaussian beam	Uniform beam
$E(r)$	$\exp \left(-(r/a)^2 \right)$	$1, \quad 0 \leq r < r_s$ $0, \quad r > r_s$
$A(u)$	$\exp \left\{ -(ua/2)^2 \right\}$	$\frac{2J_1(ur_s)}{ur_s}$
$u = \frac{2\pi n}{\lambda} \sin \theta_z$		$A(u) = \int_0^\infty E(r) J_0(ur) r \, dr \bigg/ \int_0^\infty E(r) r \, dr$

to note that the diffraction *intensity* pattern $A^2(u)$ of the uniform beam is nearly Gaussian for values of ur_s smaller than the first zero of $J_1(ur_s)$, and therefore can be expressed by

$$A^2(u) \cong \exp \left(-0.28(ur_s)^2 \right). \tag{10-1}$$

Conversely, a Gaussian beam with $a \cong 0.75r_s$ has nearly the same diffraction intensity pattern as the uniform beam of radius r_s . The situation is illustrated in Fig. 10–1. Clearly $A^2(u)$ is also approximately Gaussian for various smoothed-out beam profiles intermediate between the uniform and Gaussian cases, e.g. the profiles given by Eq. (15–9), so the results and conclusions for the Gaussian beam have wide applicability.

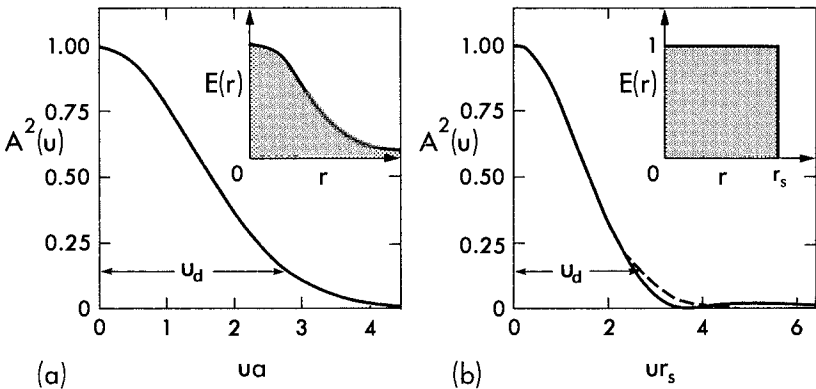


Fig. 10–1 Electric field amplitude $E(r)$ and diffraction intensity pattern $A^2(u)$ for (a) a Gaussian beam and (b) a uniform beam. The dashed curve is the Gaussian beam approximation of Eq. (10–1) for the uniform beam, and u_d is defined by Eq. (10–2).

Characteristic angular spread

It is helpful to describe the diffraction intensity pattern by a characteristic small angular spread θ_d in θ_z . We relate this spread to the corresponding value u_d of the transform variable when the diffraction pattern amplitude has fallen to $1/e$ of its peak value, i.e. $A(u_d) = 1/e$. This gives

$$u_d \cong 2/a; \quad \theta_d \cong \lambda/(\pi na), \quad (10-2a)$$

for the Gaussian beam, and

$$u_d \cong 2.7/r_s; \quad \theta_d \cong 0.43\lambda/nr_s, \quad (10-2b)$$

for the Gaussian approximation to the uniform beam in Eq. (10-1). As the characteristic beam radius r_s decreases, θ_d increases and light spreads more rapidly as it propagates in the z -direction. If $r_s(z)$ denotes the characteristic beam radius distance z along the beam, then by geometry $r_s(z)$ increases linearly with z , i.e. $r_s(z) = r_s(0) + z\theta_d$.

10-2 Light containment by a fiber

We can now provide insight into the role of diffraction in the propagation of light along fibers with comparatively small values of V , by using qualitative arguments involving beam diffraction and bound rays. Thus we consider a weakly guiding fiber of core radius ρ and otherwise arbitrary refractive-index profile. We assume that the electric field is x -polarized with amplitude $E(r)$ at radius r , and $E(r)$ has the Gaussian shape of Fig. 10-1(a). The light intensity S across the fiber also has a Gaussian dependence, since it is proportional to $E^2(r)$. Thus the electric field of the fiber is just the electric field of the Gaussian beam discussed in the previous section. This enables us to determine the scaling length a of Table 10-1 which is associated with maximizing the concentration of guided light within the fiber core. In Section 10-1 we showed that the beam has an innate spread θ_d in ray directions due to diffraction. Accordingly it is intuitive that the narrowest beam which maintains the light intensity distribution along the fiber has a diffraction spread which is equal to the complementary critical angle θ_c , since all rays propagating within this angle are bound. Hence with the definition of Eq. (10-2a), we deduce that

$$\theta_d = \theta_c; \quad a = \lambda/\pi n\theta_c, \quad (10-3)$$

where θ_c is defined inside the front cover, and the uniform index $n \cong n_{co}$. In the special case when the value of a coincides with the core radius ρ , we deduce from the definition of the fiber parameter inside the front cover that $V = 2$.

Whilst the above argument is only qualitative, it is important because it shows that *propagation involves a balance between the spread in ray directions due to diffraction and containment by the grading of the refractive-index profile.*

A measure of this balance is given by the fiber parameter. If we set $a = \rho$ in the definition of V , and substitute from Eq. (10–2a), we deduce that

$$V = 2\theta_c/\theta_d. \quad (10-4)$$

Thus, for multimode fibers with $V \gg 1$ we have $\theta_d \ll \theta_c$, and diffraction plays an insignificant part in light propagation. However, for fibers with $V < 2$ we have $\theta_d > \theta_c$, and light propagation is strongly influenced by diffraction. This helps explain why it is impossible to concentrate light power within small radius fibers, i.e. within fibers with $\rho \ll a$, where a is given by Eq. (10–3).

10–3 Applicability of geometric optics

The above discussion enables us to appreciate when geometric optics is valid for analysing propagation on optical waveguides. Classical applications of geometric optics, e.g. to ray tracing through a lens, require only that the refractive-index profile n be nearly uniform over a distance equal to the wavelength of light in the medium. For an optical waveguide this is satisfied when $\rho \gg \lambda/n$, where ρ is the core radius and λ is the free-space wavelength of light. However, because of diffraction, this condition is insufficient when considering optical waveguides, and is augmented by the requirement that *optical waveguides must be multimoded with $V \gg 1$ for geometric optics to be valid*, as we show below. Recalling the definition $V = 2\pi\rho n_{\text{co}}\theta_c/\lambda$ from inside the front cover, it is clear that $\rho n_{\text{co}}/\lambda$ can be arbitrarily large yet V may be small provided θ_c is sufficiently small. For example, a typical single-mode fiber with $V = 2.4$ and $\theta_c = 0.01$ has $\rho n_{\text{co}}/\lambda = 38$, yet the application of geometric optics, e.g. to pulse dispersion in Chapter 3, would be extremely inaccurate.

Diffraction limitation

According to geometric optics, all guided light follows the trajectories of bound rays, and is therefore *confined entirely within the fiber core*. However, because of diffraction, light confined to a region of radius ρ undergoes an angular spread θ_d , which by analogy with Eq. (10–2a) is proportional to $\lambda/\rho n_{\text{co}}$. Obviously geometric optics is a poor approximation unless θ_d is small compared to the angular width for bound-ray propagation given by Eq. (2–6a), i.e. unless $\theta_d \ll \theta_c$. Coupled with Eq. (10–4), this requirement leads to the condition $V \gg 1$.

Propagation in the cladding

We anticipate from the above discussion that light power must be distributed far into the cladding if it is to be guided by a low- V fiber, since the angular spread due to diffraction increases as the beam width decreases. This

contradicts the assumption of geometric optics that power is confined entirely within the core. Diffraction also accounts for the failure of geometric optics in the more familiar examples of the focal point of a lens and the caustics bounding ray trajectories along a fiber.

INFLUENCE OF DIFFRACTION ON TOTAL INTERNAL REFLECTION

We now consider the step-profile planar waveguide to give a quantitative example of how diffraction alters the classical geometric optics analysis for small values of the waveguide parameter V . In Chapter 1 we showed that bound rays in the core of this waveguide follow a zig-zag path, such as that in Fig. 1-4(a), and undergo total internal reflection at the core-cladding interfaces. We now re-examine this interpretation beginning with a closer examination of the mechanism of total internal reflection at a planar interface in order to better appreciate the physical mechanism for the penetration of light power into the cladding medium. This enables us to show how diffraction effects can be described within the ray picture.

Total internal reflection

When a plane wave undergoes total internal reflection at a planar interface between two semi-infinite, uniform dielectric media, as in Fig. 10-2, an evanescent field is set up in the rarer medium and the reflected wave differs in

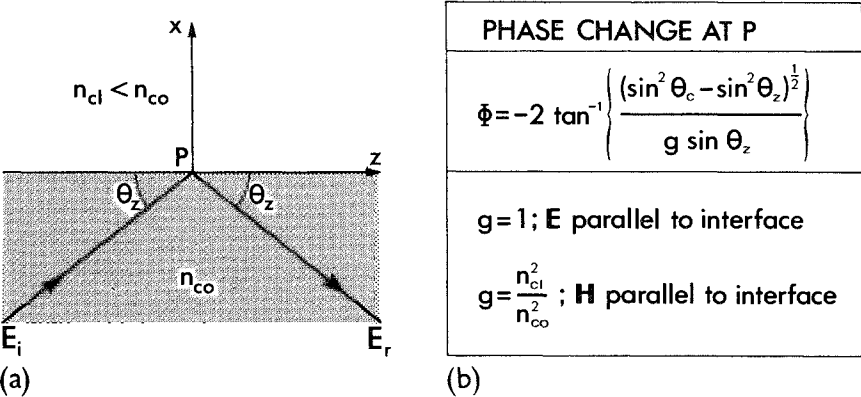


Fig. 10-2 Total internal reflection of a plane wave at a planar interface between semi-infinite media of refractive indices n_{co} and n_{cl} . When $n_{cl} \cong n_{co}$, the phase change ϕ is approximately independent of the direction of **E**, i.e. independent of polarization.

phase from the incident wave. The formulae are taken from Section 35-6. The ray analysis of the first nine chapters ignores phase and assumes that power flows only along the geometric optics trajectories within the denser medium. However, some of the power associated with the ray is carried by the evanescent field, so that 'total' internal reflection might be more accurately described by the ray path shown schematically in Fig. 10-3(a), which passes through the cladding. This path assumes a finite wavelength λ , whereas the path in Fig. 10-2(a) assumes $\lambda = 0$ and is based on Snell's law. We now investigate this question more closely by examining the influence of diffraction effects on total internal reflection.

10-4 Lateral shift

A plane wave is infinite in extent and therefore does not reveal the precise behavior of power flow along a ray occupying only a finite portion of space. For this reason we study the power flow in a beam which reflects from the planar dielectric interface in Fig. 10-3(b). We showed in Section 10-1 that the

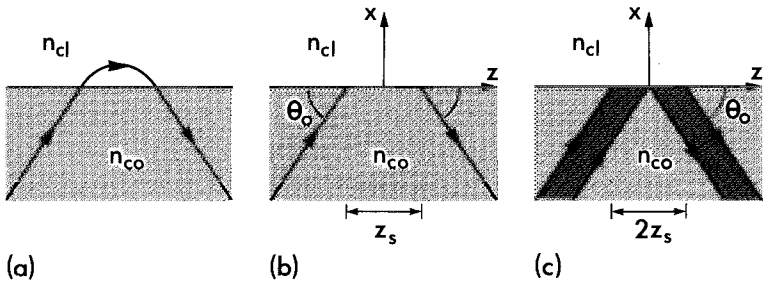


Fig. 10-3 (a) Schematic ray path in the cladding, (b) lateral shift z_s of a beam whose axis makes angle θ_0 with the interface, and (c) a beam incident at angle $\theta_0 \cong \theta_c$, whose shift is equal to its z -directed cross-section. The refractive indices on either side of the interface are n_{co} and $n_{cl} < n_{co}$.

beam is a superposition of a continuum of plane waves. If θ_z is the angle between the direction of propagation of one such wave and the interface, then the z -dependence of the incident and reflected electric field amplitudes of Section 35-6 is expressible as

$$E_i(z) = A \exp(i\beta z); \quad E_r(z) = A \exp(i\beta z + i\Phi(\theta_z)), \quad (10-5)$$

respectively, where A is a constant, $\beta = 2\pi n_{co} \cos \theta_z / \lambda$ and λ is the free-space wavelength of the beam. The change of phase upon reflection, $\Phi(\theta_z)$, depends generally on the polarization of the fields, but if $n_{co} \cong n_{cl}$ it is approximately independent of polarization, and is given in Fig. 10-2(b) with $g = 1$. As $\Phi(\theta_z)$

varies with θ_z , the plane-wave components of the beam undergo slightly different phase changes upon reflection. On summing the reflected waves, we obtain a reflected-beam field that differs from the incident-beam field on the basis of geometric optics. We now show that the beam shifts upon reflection.

Derivation of the shift

If the incident beam makes angle θ_0 with the interface, we know from Section 10-1 that the beam is characterized by a small spread θ_d about θ_0 in the direction of the waves comprising the beam. Thus we could expand $\Phi(\theta_z)$ in powers of $\theta_z - \theta_0$, but it is more convenient to expand in powers of $\beta - \beta_0$, where $\beta_0 = 2\pi n_{co} \cos \theta_0 / \lambda$. Hence to first order

$$\Phi(\beta) \cong \Phi(\beta_0) + (\beta - \beta_0)\Phi'(\beta_0), \quad (10-6)$$

where $\Phi'(\beta_0)$ denotes $\partial\Phi(\beta)/\partial\beta$ evaluated at β_0 . If we substitute into Eq. (10-5) the field of the reflected beam is expressible as

$$E_r(z) = C \exp\{i\beta[z + \Phi'(\beta_0)]\}, \quad (10-7)$$

where C is a constant independent of β . We can then interpret the term $\Phi'(\beta_0)$ as a shift z_s in the position of the reflected beam, as shown in Fig. 10-3(b). When $n_{co} \cong n_{cl}$, it follows that $\theta_0 \ll 1$ for total internal reflection. By differentiating the expression in Fig. 10-2 we find that

$$z_s = -\left. \frac{\partial\Phi}{\partial\beta} \right|_{\beta_0} = \frac{2}{kn_{co}\theta_0} \frac{1}{(\theta_c^2 - \theta_0^2)^{1/2}}, \quad (10-8)$$

where $k = 2\pi/\lambda$ and $\theta_c \cong \{1 - n_{cl}^2/n_{co}^2\}^{1/2}$. This shift is often called the *Goos-Hanchen shift*. Much of the extensive literature on this shift is reviewed in Ref. [5], and more recent studies include Refs. [6-10]. At optical frequencies the shift is very small, except for incidence close to $\theta_0 = \theta_c$. When $\theta_0 \cong \theta_c$ the incident beam penetrates deeply into the rarer medium.

Interpretation in terms of power flow

The above derivation is based on phase and does not show directly that the shift is due to light power propagating within the rarer medium. An explicit proof requires power arguments [6-10]. To illustrate the relationship between the shift and power flow, consider a finite section of a plane wave of width $z_s \sin \theta_0$, incident at angle θ_0 to the interface, as shown in Fig. 10-3(c). Because of the shift, the incident and reflected waves do not overlap, and thus all the power in the reflected wave must flow from the rarer to the denser medium. Indeed, it is straightforward to show that the total, z -directed power flow in the

rarer medium is exactly equal to the power in the incident and reflected waves when $\theta_0 \cong \theta_c$. Using the notation of Section 35-6, the latter is given by $(z_s/2)|A|^2 n_{co} (\epsilon_0/\mu_0)^{1/2}$ and the former is the integral of $(\bar{\Psi}_t^2/2)n_{cl}(\epsilon_0/\mu_0)^{1/2}$ of Eq. (35-22a) over $0 \leq x < \infty$. Using the relationship of Eq. (35-22b) between A and C , together with the approximations $(\sin^2 \theta_c - \sin^2 \theta_0)^{1/2} \ll \theta_0$, and $\theta_0 \cong \theta_c$ verifies the result.

10-5 Transit time for the lateral shift

We define a transit time t_s for the beam to transverse the shift z_s . The concept of transit time implies that we are considering a beam which exists for only a finite duration in time. This is dual to the concept of the shift, involving beams of finite (or nonuniform) extent in space. Hence the beam cannot be monochromatic, and has a small spread in frequency $\delta\omega$ about a central frequency ω_0 . The phase function $\Phi(\theta_z)$ depends on frequency through the relationship $\beta = 2\pi n_{co} \cos \theta_z/\lambda$. If we express λ in terms of ω using $\lambda\omega = 2\pi c$, where c is the free-space speed of light, then $\beta = \omega n_{co} \cos \theta_z/c$. We expand $\Phi(\omega)$ about ω_0 and, correct to first order, obtain

$$\Phi(\omega) = \Phi(\omega_0) + (\omega - \omega_0)\Phi'(\omega_0), \quad (10-9)$$

where $\Phi'(\omega_0)$ denotes $\partial\Phi(\omega)/\partial\omega$ evaluated at ω_0 . The beam fields contain the implicit time dependence $\exp(-i\omega t)$, and, by analogy with Eq. (10-7), the time variation of the reflected-beam field is expressible as

$$E_r(t) = D \exp\{i\omega[\Phi'(\omega_0) - t]\}, \quad (10-10)$$

where D is a constant independent of ω . We then identify $\Phi'(\omega_0)$ with the transit time t_s . Substituting for Φ from Fig. 10-2(b) with θ_z expressed in terms of β and ω , and recalling that $\theta_0, \theta_c \ll 1$, we obtain [9]

$$t_s = \left. \frac{\partial\Phi}{\partial\omega} \right|_{\omega_0} = \frac{n_{co}}{c} z_s \cos \theta_0, \quad (10-11)$$

where z_s is defined by Eq. (10-8).

It is interesting to note that the explicit form for the transit time in Eq. (10-11) can be determined directly from plane-wave theory. If we consider a plane wave incident as in Fig. 10-2, then the velocity with which power flows parallel to the interface in Fig. 10-3(b) is given by the z -directed group velocity $v_{gz} = d\omega/d\beta = c/(n_{co} \cos \theta_0)$, since $\beta = \omega n_{co} \cos \theta_0/c$. Hence $t_s = z_s/v_{gz}$, in agreement with Eq. (10-11).

In this and the previous section, we have assumed nondispersive media. If material dispersion is included, n_{co} and n_{cl} then depend on ω . The shift z_s is given explicitly by Eq. (10-8) provided we take into account that n_{co} and θ_c vary

with ω . However, the transit time t_s must be recalculated, starting from $\partial\Phi(\omega_0)/\partial\omega_0$ in Eq. (10-11) [9].

Summary

Taken together, Eqs. (10-8) and (10-11) describe the effect of diffraction on the path and transit time for a ray undergoing total internal reflection at a planar dielectric interface. The physical origin of the shift is due to light propagating in the rarer medium. Our next objective is to use this single-interface result, derived from plane-wave theory, as a building block to study the effect of diffraction on ray propagation in planar waveguides.

10-6 Lateral shift in planar waveguides

In Chapter 1, we describe propagation along step-profile planar waveguides in terms of bound rays traveling along zig-zag trajectories and undergoing total internal reflection at each interface. Here we show how this description is modified for small- V waveguides by including the lateral shift. By allowing for the lateral shift z_s at every reflection along a bound-ray path, the geometric optics path of Fig. 1-4(a) is replaced by the path shown in Fig. 10-4(a).

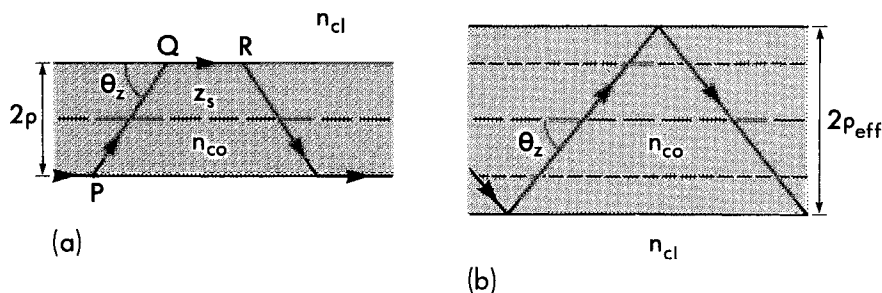


Fig. 10-4 The lateral shift z_s of the path in (a) is equivalent to an effective core half width p_{eff} in (b), for the step-profile planar waveguide.

Ray transit time

If we define t_{go} to be the geometric optics transit time over length z of waveguide, then Eq. (1-14) gives $t_{go} = zn_{co}/c \cos \theta_z$. The transit time t over the same length with the shift included is found by considering the half-period PQR in Fig. 10-4(a). Along PQR the transit time is given by $t_p + t_s$, where $t_p = 2pn_{co}/c \sin \theta_z$ is the transit time along PQ and t_s is the transit time across the shift z_s . The half-period is $z_p + z_s$, where z_p is the geometric optics half-period

of Eq. (1-10). Assuming $z \gg z_p + z_s$ we use the reasoning below Eq. (1-36) to deduce that t is accurately given by [9].

$$t = z(t_p + t_s)/(z_p + z_s). \quad (10-12)$$

Substituting from Eqs. (10-8) and (10-11) with $\theta_0 = \theta_z$ and rearranging [11]

$$t = t_{go} \left\{ 1 - \frac{\theta_z^2}{1 + V(\theta_c^2/\theta_z^2 - 1)^{1/2}} \right\}, \quad (10-13)$$

where $\theta_z \cong \theta_c \ll 1$. In other words, the consequence of the lateral shift is to *reduce the ray transit time from that of geometric optics*, i.e. the smaller the value of V , the greater the reduction. On the other hand, for large- V waveguides, only rays with $\theta_z \cong \theta_c$ have transit times that differ significantly from those of geometric optics. However, in practice, only a small fraction of the total source power is directed into rays with $\theta_z \cong \theta_c$ so that the determination of pulse width is well approximated by geometric optics for large- V waveguides.

Loss phenomena

In Chapters 6 to 9 we included the effects of power loss from the core due to cladding absorption and radiation by using a power transmission coefficient, T , derived from local plane-wave theory. In the case of cladding absorption, T is the well-known Fresnel transmission coefficient for total internal reflection by a plane wave from an absorbing dielectric interface discussed in Section 35-7. Thus, by using T , we have already accounted for the presence of light power in the cladding. However, we have not previously accounted for the shift, z_s , in the ray path that is associated with the mechanism for the light to penetrate into the cladding from the core. We confirm this relationship in Section 36-10 using simple power attenuation arguments. The shift has the same effect as decreasing the number of reflections. It therefore is convenient for analysis to preserve the zig-zag path of geometric optics and incorporate the effect of the lateral shift by replacing the core half-width, ρ , with an effective half-width ρ_{eff} . From the geometry of Fig. 10-4(b), it is obvious that [8, 9]

$$\frac{\rho_{\text{eff}}}{\rho} = 1 + \frac{z_s}{2\rho} \tan \theta_z = 1 + \frac{1}{V(1 - \theta_z^2/\theta_c^2)^{1/2}}, \quad (10-14)$$

where θ_z is the angle between the ray path and the waveguide axis, $V \cong k\rho n_{\text{co}} \theta_c$ and z_s is substituted from Eq. (10-8) with $\theta_0 = \theta_z \ll 1$.

Effective half-width

Thus, the effect of the lateral shift on cladding losses is equivalent to increasing the waveguide width. By substituting ρ_{eff} for ρ in the expressions for power attenuation derived in Chapters 6 to 9, we find that the original expressions

which ignore the lateral shift *overestimate* the loss. For example, to account for the effect of the lateral shift on cladding absorption, we replace V by $V\rho_{\text{eff}}/\rho$ in Eq. (6-21), taking $\theta_\phi = \pi/2$ so that the expression is applicable to the planar waveguide. The resulting expression for the power attenuation coefficient γ_{cl} is then found to approach α_{cl} as V decreases for $\theta_z \cong \theta_c$, where α_{cl} is the attenuation coefficient of a plane wave in a lossy cladding. If we ignore the lateral shift, then Eq. (6-21) shows that $\gamma_{\text{cl}} \rightarrow \infty$. Thus the expression for cladding absorption is highly inaccurate for low- V waveguides. It is also clear from Eq. (10-14) that only those rays with $\theta_z \cong \theta_c$ are effected by the lateral shift when $V \gg 1$. In practice, these rays normally carry an insignificant fraction of the total source power and can therefore be ignored.

Finally, we emphasize that the lateral shift is not the only manifestation of diffraction on the step-profile planar waveguide. Taken alone, it is insufficient for describing propagation on low- V waveguides. We next investigate another diffraction phenomenon to better appreciate the departure of electromagnetic theory from the ray methods of Part I.

10-7 Preferred ray directions

The geometric optics analysis of the excitation of the planar waveguide by sources assumes that power may enter any *bound* ray whose direction belongs to the continuum of directions defined by Eq. (1-5a). However, as a consequence of diffraction, power enters certain preferred directions only, and the smaller V , the smaller the number of preferred directions. If V is sufficiently small, then there is only one preferred direction and all bound rays propagate with the same transit time. As V increases, the number of preferred ray directions becomes sufficiently large that it can be accurately approximated by a continuum.

Consistency conditions

The diffraction phenomenon that gives rise to preferred ray directions is a consistency condition on the phase of the local plane waves constituting the ray path, and arises because of the symmetry properties of the waveguide, i.e. translational invariance along the waveguide. Thus, preferred ray directions are a consequence of the geometry of the complete waveguide unlike the lateral shift, which is a localized phenomenon manifested through the change in phase accompanying total internal reflection.

The determination of preferred ray directions for the step-profile planar waveguide follows by treating rays as local plane waves following the zig-zag trajectory of geometric optics in Fig. 10-5, and then examining their phase properties over a complete ray period $2z_p$ [12, 13]. Over the path ABCD the phase change comprises two parts. First there is the phase change along the

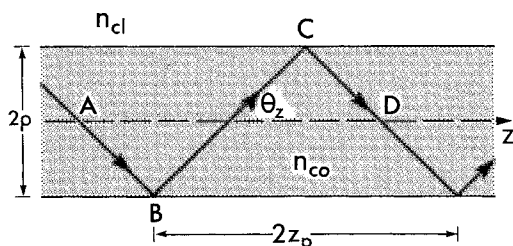


Fig. 10-5 Section of a bound-ray on a step-profile planar waveguide, showing the complete ray period $2z_p$.

path, which is the product of the path length $4\rho/\sin\theta_z$ and the local wavenumber kn_{co} , and second there is the phase change at B and C due to total internal reflection from the interfaces, given by Φ in Fig. 10-2(b). The translational invariance of the waveguide means that the change in phase due to the z -component of the local plane-wave vector at A progressing parallel to the waveguide axis a distance $2z_p$ to D, i.e. $(kn_{co} \cos\theta_z)(2z_p)$, should be equal to the phase change over the path to within an integer multiple of 2π . Hence

$$4k\rho n_{co}/\sin\theta_z + 2\Phi = 2kz_p n_{co} \cos\theta_z + 2n\pi, \quad (10-15)$$

where $n = 0, \pm 1, \dots$. We substitute for z_p from Table 1-1, page 19, and for Φ from Fig. 10-2(b), assuming weak guidance so that $g \cong 1$. Hence

$$\{\sin^2\theta_c - \sin^2\theta_z\}^{1/2} = \sin\theta_z \tan(V \sin\theta_z/\sin\theta_c), \quad (10-16)$$

when n is zero or an even integer, together with a similar expression when n is an odd integer. The important point here is that only certain ray directions, given by the solutions of the above equation for θ_z , can carry power. For $V < \pi/2$, only one such direction is possible. In Section 36-7, we show how the preferred ray directions for more general waveguides are obtained.

DIFFRACTION EFFECTS IN ARBITRARY WAVEGUIDES

We have shown two ways in which diffraction manifests itself on ray propagation in the step-profile planar waveguide—the lateral shift and preferred ray directions. It is clear, from all our discussions, that as V becomes smaller a significant fraction of power propagates in the cladding and thus the local behavior of rays which we exploited in Chapters 1 to 9 is lost. By incorporating two diffraction effects into the ray picture we have derived exact expressions for the *step-profile, planar* waveguide. If we further account for diffraction by the source, we could then determine the distribution of power among the preferred bound rays. The fields of this waveguide are given exactly by the superposition of the fields of just two plane waves as we show in Section

36–1. Hence it is not surprising that ray methods can be easily modified to obtain exact electromagnetic results. However, all other waveguides must be multimoded with $V \gg 1$ if ray, or local plane wave, methods are to be used. In other words, the nonuniformity of the core medium and the core cross-section introduces additional diffraction effects which, in general, are not easy to incorporate into a ray treatment when V is small. With the proviso that $V \gg 1$, it is possible to apply the concepts of lateral shift and preferred ray direction to any waveguide, but we know that such waveguides are already well approximated by the methods of Chapters 1 to 9. In general, the methods of Part II are most suitable for waveguides with small values of V .

REFERENCES

1. Sommerfeld, A. (1953) *Optics*, Academic Press, New York, chap. V.
2. Goodman, J (1968) *Fourier Optics*, McGraw-Hill, New York, p. 48 and chap. 4.
3. Johnson, C. C. (1965) *Field and Wave Electrodynamics*, McGraw-Hill, New York, p. 331.
4. Bracewell, R. N. (1978) *The Fourier Transform and Its Applications*, 2nd Edn, New York, pp. 244–50.
5. Lotsch, H. K. V. (1970) 'Beam displacement at total reflection: the Goos-Hänchen shift. *Optik*, **32**, 116–37, 189–204; 1971 **32**, 299–319, 553–69.
6. Renard, R. H. (1964) Total reflection: a new evaluation of the Goos-Hänchen shift. *J. Opt. Soc. Am.*, **54**, 1190–8.
7. Horowitz, B. R. and Tamir, T. (1971) Lateral displacement of light beam at a dielectric interface. *J. Opt. Soc. Am.*, **61**, 586–95.
8. Kapany, N. S. and Burke, J. J. (1972) *Optical Waveguides*, Academic Press, New York.
9. Kogelnik, H. and Weber, H. P. (1974) Rays, stored energy, and power flow in dielectric waveguides. *J. Opt. Soc. Am.*, **64**, 174–85.
10. Snyder, A. W. and Love, J. D. (1976) Goos-Hänchen shift. *Appl. Opt.*, **15**, 236–8.
11. White, I. A. and Pask, C. (1977) Effect of Goos-Hänchen shifts on pulse widths in optical waveguides. *Appl. Opt.*, **16**, 2353–5.
12. Love, J. D. and Snyder, A. W. (1976) Optical fiber eigenvalue equation: plane wave derivation. *Appl. Opt.*, **15**, 2121–5.
13. Tien, P. K. (1971) Light waves in thin films and integrated optics. *Appl. Opt.*, **10**, 2395–413.

PART II

Electromagnetic Analysis of Optical Waveguides

Introduction to Part II

In Part I, we described propagation within optical waveguides by classical geometric optics, together with a generalized Fresnel transmission coefficient to account for losses due to evanescent field effects, such as cladding absorption and radiation losses. As discussed in Chapter 10, this simple procedure is inaccurate unless the waveguide is multimoded, with the waveguide parameter obeying $V \gg 1$. Now, in Part II, we present an electromagnetic analysis of optical waveguides by solving Maxwell's equations. In general, these equations can be solved either by modal, i.e. eigenfunction methods, or by Green's function methods. Both of these methods are implemented, although most of Part II is devoted to modal analysis. The modal method, which is also common to metal waveguides [1–3], represents the electromagnetic field by a sum of solutions to Maxwell's source-free equations. In the Green's function approach, we first determine the field due to a point dipole at an arbitrary position and then, by linearly superposing the fields of a distribution of dipoles, we represent the field due to a specific source. The Green's function approach, which is common to antenna theory [2,3], is often more useful for determining radiation losses from optical waveguides, as we show in Chapters 21 and 23.

Spatial transient and spatial steady state

Only a portion of the total source power is guided without attenuation along an ideal, i.e. nonabsorbing, waveguide. The remaining portion is radiated. The portion that travels without attenuation is most conveniently represented by a class of modes, finite in number, here called *bound modes* analogous to the *bound rays* of Part I. There are various ways to represent the radiated portion, the most appropriate depending on the particular problem of interest. Sufficiently far from the source, the fields within the waveguide core are due mainly to bound modes, the remaining initial core power having been lost to radiation. Within this region, the waveguide fields are in what we call appropriately the *spatial steady state*, while in the region between the source and the steady-state region, the fields are in the *spatial transient*. The situation is depicted schematically in Fig. II–1, and is discussed for multimode waveguides in Chapter 8. As we show in Chapter 8, the duration of the spatial transient can be kilometres long for multimode fibers but is typically less than a centimetre for single-mode fibers.

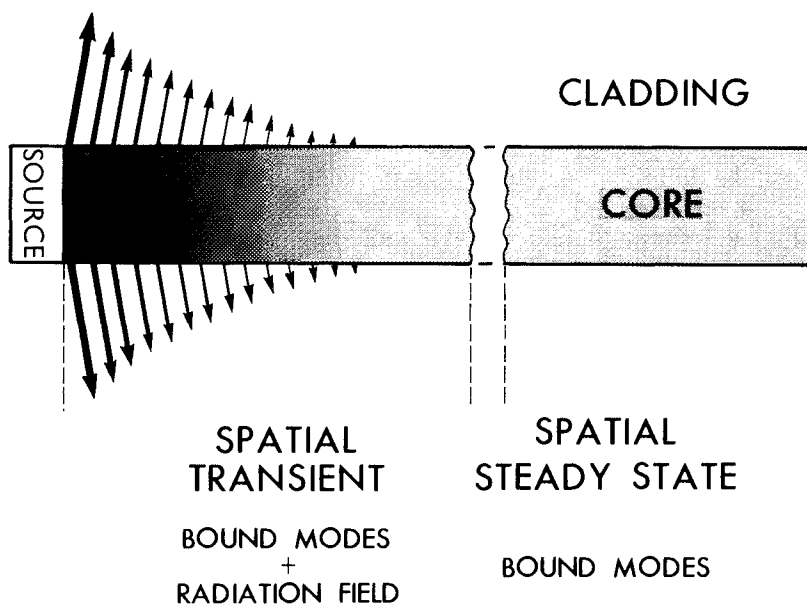


Fig. II-1 Qualitative representation of radiation from a waveguide excited by a source at its endface. Arrows denote power flow in the radiation fields and the darker shading denotes higher power densities in the core.

Fundamental modes

In Part II, we pay particular attention to single-mode waveguides that propagate *one* bound mode only—called the *fundamental mode*—since they are of great practical interest, both to the field of optical communications [4–6] and to the study of visual photoreceptors of animals [7,8]. At this point, we anticipate possible confusion associated with the nomenclature. When we refer to a waveguide that is *single* moded, we mean that it can propagate only the *two polarization states of the fundamental mode*. The adjective bound is usually omitted from this description.

Historical development

While the first theoretical investigation of optical fibers dates back to Hondros and Debye in 1910 [9], there was little subsequent interest until highly transparent materials became available in the late sixties and early seventies. The fabrication of optical fibers capable of transmitting light over distances of several kilometres stimulated rapid development of the theoretical analysis of their propagation properties. Whilst, in principle, Maxwell's equations de-

termine propagation characteristics exactly, such solutions can usually be determined only by numerical techniques. The elucidation of the underlying physical processes was considerably simplified by taking advantage of the slight variation in profile normally found in practical fibers used for long-distance communication. This led first to the *weak-guidance approximation*, which enabled Maxwell's equations to be replaced by the simpler scalar wave equation, and then the *Gaussian approximation*, which accurately quantifies virtually all aspects of propagation on arbitrary profile fibers in the simplest manner possible. Accordingly, much of Part II is concerned with the derivation and application of these approximations.

We begin in Chapter 11 by discussing the fundamental properties of bound modes on optical waveguides, in order to build from a strong foundation and to better appreciate the nature and limitations of the many approximations introduced later on. Chapter 12 discusses the few waveguides for which Maxwell's equations can be solved exactly. Then, in Chapters 13 to 19, approximation methods are given for finding the modes of various waveguides. Chapter 20 treats illumination, while Chapters 21 to 26 are primarily concerned with radiation from waveguides. In Chapters 27 and 28 we treat mode coupling, and in Chapter 29 we consider optical cross-talk between fibers. We also call attention to Part III, where extensive supplementary material is provided, from which many of the results of Part II are drawn.

REFERENCES

1. Collin, R. E. (1965) *Field Theory of Guided Waves*, McGraw-Hill, New York.
2. Johnson, C. C. (1965) *Field and Wave Electrodynamics*, McGraw-Hill, New York.
3. Felsen, L. B. and Marcuvitz, N. (1973) *Radiation and Scattering of Waves*, Prentice-Hall, Englewood Cliffs, N.J.
4. Miller, S. E., Marcatili, E. A. J. and Li, T. (1973) Research toward optical fiber transmission systems. *Proc. I.E.E.E.* **61**, 1703–51.
5. Gambling, W. A., Matsumura, H. and Ragdale, C. M. (1978) Loss mechanisms in practical single-mode fibers. *Proceedings of the Fourth European Conference on Optical Communication*, Genoa, Italy.
6. Gambling, W. A., Matsumura, H. and Ragdale, C. M. (1979) Mode dispersion, material dispersion and profile dispersion in graded-index, single-mode fibers. *Microwaves, Opt. Acoust.* **3**, 239–46.
7. Snyder, A. W. and Menzel, R. (eds.) (1975) *Photoreceptor Optics*, Springer-Verlag, Berlin.
8. Snyder, A. W. (1979) in *Handbook of Sensory Physiology*, Vol. VII/6A (ed. H. Autram), Springer-Verlag, Berlin, pp. 279–81.
9. Hondros, A. and Debye, P. (1910) Electromagnetic waves in dielectric waveguides. *Ann. Phys.*, **32**, 465–76.

Fundamental properties of modes

Electromagnetic representation of light propagation	209
11-1 Propagation constant and phase velocity	211
11-2 Symmetry properties of the field components	212
11-3 Field representation on nonabsorbing waveguides	212
11-4 Orthogonality relations and normalization	212
11-5 Orthonormal modes	214
Energy and power	214
11-6 Stored electric and magnetic energies	214
11-7 Power flow	215
11-8 Fraction of modal power in the core	216
11-9 Total guided power	216
11-10 Fraction of total power in the core	217
Group velocity	218
11-11 Group delay	219
Pulse spreading	219
11-12 Pulse spreading in single-mode fibers	220
Derivation and properties of the modal fields	220
11-13 Eigenvalue equation	221
11-14 Solution in terms of the longitudinal field components	222
11-15 Coupling of the field components	222
11-16 Hybrid nature of the modal fields	223
11-17 Propagation constant	226
Waveguide and modal parameters	226
11-18 Modal cutoff	228
11-19 Number of bound modes	229
11-20 Distortion parameter	229
11-21 Relationship with ray invariants	231
Absorbing waveguides	231
11-22 Power attenuation	232

Anisotropic waveguides	234
11-23 Uniform anisotropic medium	234
11-24 Anisotropic waveguides	235
References	237

The propagation of light along nonabsorbing optical waveguides in regions sufficiently far from any source of excitation, where the spatial steady state is reached, is most conveniently described by the bound modes of the waveguide. Bound modes are solutions of the source-free Maxwell equations, and, like the modes of vibration of a stretched membrane, are formed by resonance conditions in the waveguide cross-section. In the spatial steady state, bound modes are the building blocks for describing light propagation. The fields of the waveguide are represented by an expansion over these modes.

This chapter discusses the fundamental properties of bound modes on *ideal waveguides*, i.e. nonabsorbing, dielectric structures, uniform along their length. *The derivation of these results from Maxwell's equations is provided in Chapters 30 and 31.* Much of this chapter establishes definitions and conventions to be followed throughout the remainder of the book. While a thorough understanding is not mandatory at this stage, it is advisable to become familiar with Chapters 11, 30 and 31 before continuing, as this material is referred to frequently.

ELECTROMAGNETIC REPRESENTATION OF LIGHT PROPAGATION

A representative waveguide is illustrated in Fig. 11-1(a). The shaded region denotes the *core* with a cross-section of arbitrary shape. This is surrounded by the *cladding* which is assumed unbounded in extent. The surface between the

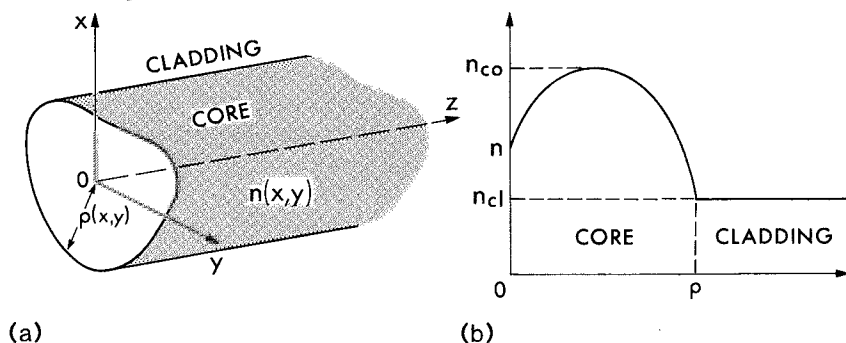


Fig. 11-1 (a) Nomenclature and coordinates for describing optical waveguides, and (b) a representative graded profile $n(x,y)$ which varies over the core and is uniform in the cladding, assumed unbounded.

core and cladding is called the *core-cladding interface* and lies at distance $\rho(x, y)$ from the axis of the waveguide. To describe the waveguide, we introduce cartesian axes aligned so that the z -axis coincides with the axis of the waveguide. The variation in refractive index over the waveguide cross-section is given by the profile $n(x, y)$, which takes real values for nonabsorbing waveguides.

All of the profiles appearing in this book fall into one of two classes. The first class consists of clad profiles which have a uniform value n_{cl} in the cladding, and an arbitrary variation in the core, such as the representative profile in Fig. 11-1(b). These profiles are characterized by a discontinuity in the profile or its slope at the core-cladding interface. The second class, as exemplified by the infinite parabolic profile, comprises profiles which vary smoothly over the infinite cross-section, and do not necessarily have a well-defined interface between core and cladding. For these profiles we define ρ to be a characteristic profile radius, which sets the rate at which the profile changes. We define

$\begin{aligned} n_{co} &= \text{maximum refractive index in the core} \\ n_{cl} &= \text{uniform cladding refractive index} \end{aligned}$	(11-1)
---	--------

where $n_{co} > n_{cl}$ for the waveguide to provide guidance.

Expansion of the fields

The electric and magnetic field vectors $\mathbf{E}(x, y, z)$ and $\mathbf{H}(x, y, z)$ are each separated into two parts, one part representing power that is guided without attenuation along the waveguide, the remaining part representing power that is radiated from the waveguide. The guided, or bound, portion is expressed as a finite sum of bound modes, which are the source-free solutions to Maxwell's equations for the waveguide. Electromagnetic modes can be regarded as transverse resonances of the fields of the waveguide, by analogy with the normal modes of vibration of a membrane fixed at its periphery. However, whereas the membrane has an infinite number of bound modes, an optical waveguide can only support a *finite* number of bound modes. Thus we set

$$\mathbf{E}(x, y, z) = \sum_j a_j \mathbf{E}_j(x, y, z) + \sum_j a_{-j} \mathbf{E}_{-j}(x, y, z) + \mathbf{E}_{rad}(x, y, z), \quad (11-2a)$$

$$\mathbf{H}(x, y, z) = \sum_j a_j \mathbf{H}_j(x, y, z) + \sum_j a_{-j} \mathbf{H}_{-j}(x, y, z) + \mathbf{H}_{rad}(x, y, z), \quad (11-2b)$$

where $j = 1, 2, \dots, M$. The first summation is over the *forward-propagating modes* which travel in the positive z -direction, and the second summation is over the *backward-propagating modes* which travel in the negative z -direction

of Fig. 11-1(a). The subscript *rad* denotes the *radiation fields*, and the constants a_j and a_{-j} are the *modal amplitudes*. The fields of the j th forward- and backward-propagating modes are \mathbf{E}_j , \mathbf{H}_j and \mathbf{E}_{-j} , \mathbf{H}_{-j} , respectively. It is a property of Maxwell's equations, Eq. (30-1), that the same modal amplitudes appear in both expansions. The values of a_j and a_{-j} depend on the source of excitation.

We now examine the properties of bound modes and their fields. These results are derived from Maxwell's equations in Chapters 30 and 31.

11-1 Propagation constant and phase velocity

The cylindrical symmetry, or translational invariance, of the waveguide enables us to express the modal fields in the separable form

$$\mathbf{E}_j(x, y, z) = \mathbf{e}_j(x, y) \exp(i\beta_j z); \quad \mathbf{H}_j(x, y, z) = \mathbf{h}_j(x, y) \exp(i\beta_j z), \quad (11-3)$$

where β_j is called the *propagation constant* or *eigenvalue* of the j th mode. Generally each mode has a unique value of β_j .

Throughout this book, all fields contain the implicit time dependence $\exp(-i\omega t)$, where ω is the angular frequency. If we combine the longitudinal and temporal variations, the modal fields vary as $\exp(i\beta_j z - i\omega t)$, and, consequently, each mode propagates along the waveguide with *phase velocity* $v_j = \omega/\beta_j$. To distinguish between modes with the same propagation constant that propagate in the forward and backward directions, we adopt the following convention. With reference to Eq. (11-2) we have

$$a_j \text{ forward-propagating} \quad \beta_j > 0, \quad (11-4a)$$

$$a_{-j} \text{ backward-propagating} \quad \beta_{-j} = -\beta_j < 0, \quad (11-4b)$$

$$j = 1, 2, \dots, M,$$

where M is the total number of forward-propagating or backward-propagating modes. Thus, for example, the phase velocity v_{pj} satisfies

$$v_{pj} = \frac{\omega}{\beta_j} = -\frac{\omega}{\beta_{-j}} = -v_{p-j}. \quad (11-5)$$

Given ω , the values of β_j are determined from an *eigenvalue equation*. This equation is a consistency condition, or transverse resonance condition, resulting from the requirements that the field solutions of the source-free Maxwell equations (i) are bounded everywhere, (ii) go to zero sufficiently fast at infinity and (iii) satisfy all boundary conditions at the core-cladding interface. The formulation of the eigenvalue equation is discussed in Section 11-13, and specific examples are given in the following chapter.

11-2 Symmetry properties of the field components

Relationships between the fields of forward- and backward-propagating modes will be used frequently. We obtain these relationships by first decomposing the fields of Eq. (11-3) into transverse and longitudinal components, denoted by subscripts t and z , so that

$$\mathbf{E}_j = \mathbf{e}_j(x, y) \exp(i\beta_j z) = \{\mathbf{e}_{tj}(x, y) + e_{zj}(x, y)\hat{\mathbf{z}}\} \exp(i\beta_j z), \quad (11-6a)$$

$$\mathbf{H}_j = \mathbf{h}_j(x, y) \exp(i\beta_j z) = \{\mathbf{h}_{tj}(x, y) + h_{zj}(x, y)\hat{\mathbf{z}}\} \exp(i\beta_j z), \quad (11-6b)$$

where $\hat{\mathbf{z}}$ is the unit vector parallel to the waveguide axis in Fig. 11-1(a). Under the convention of Eq. (11-4), the forward- and backward-propagating modes with the same propagation constant have subscripts j and $-j$, respectively, where $j > 0$. In Section 30-5, we show that the fields of the two modes are related in either of two ways. We adopt the convention of Eq. (30-11b), namely

$$\mathbf{e}_{-j} = \mathbf{e}_{tj} - e_{zj}\hat{\mathbf{z}}; \quad \mathbf{h}_{-j} = -\mathbf{h}_{tj} + h_{zj}\hat{\mathbf{z}}; \quad \beta_{-j} = -\beta_j. \quad (11-7)$$

This convention is also valid for absorbing waveguides, when the refractive-index profile $n(x, y)$ is complex. Absorbing waveguides are discussed later in the chapter.

11-3 Field representation on nonabsorbing waveguides

If the waveguide is nonabsorbing, so that the refractive index $n(x, y)$ is real, we show in Section 30-4 that, among various delineations, it is always possible to choose the field components of each bound mode to satisfy the convention

$$\mathbf{e}_{tj}, \mathbf{h}_{tj} \text{ pure real}; \quad e_{zj}, h_{zj} \text{ pure imaginary}, \quad (11-8)$$

where subscripts t and z denote transverse and longitudinal components. This representation helps simplify the physical interpretation of many results.

It is often necessary to use the complex conjugate of the fields of a mode. By combining Eqs. (11-7) and (11-8), these fields obey

$$\mathbf{e}_j^* = \mathbf{e}_{-j} = \mathbf{e}_{tj} - e_{zj}\hat{\mathbf{z}}; \quad \mathbf{h}_j^* = -\mathbf{h}_{-j} = h_{tj} - h_{zj}\hat{\mathbf{z}}; \quad \beta_j^* = -\beta_{-j} = \beta_j, \quad (11-9)$$

on a nonabsorbing waveguide, where $j > 0$ and $*$ denotes complex conjugate.

11-4 Orthogonality relations and normalization

In order to determine the amplitude a_j of a bound mode in the expansion of Eq. (11-2), we require an *orthogonality condition*. This condition is derived

from the reciprocity theorem of Maxwell's equations in Section 31-3. Assuming that the waveguide is nonabsorbing, the modal fields of the j th and k th forward-propagating modes obey the vector orthogonality condition of Eq. (31-14), where

$$\int_{A_\infty} \mathbf{e}_j \times \mathbf{h}_k^* \cdot \hat{\mathbf{z}} dA = \int_{A_\infty} \mathbf{e}_k^* \times \mathbf{h}_j \cdot \hat{\mathbf{z}} dA = 0; \quad j \neq k, \quad (11-10)$$

where A_∞ is the infinite cross-section, * denotes complex conjugate and $\hat{\mathbf{z}}$ is the unit vector parallel to the waveguide axis. Note that the scalar triple products in the integrands involve only the *transverse* components of the fields. When either or both modes are *backward-propagating*, it is simplest to re-express the fields \mathbf{e}_{-j} , \mathbf{h}_{-j} , \mathbf{e}_{-k} and \mathbf{h}_{-k} in terms of the fields of the corresponding forward-propagating modes through Eq. (11-7) and then apply the above conditions. This procedure is followed throughout the book wherever both forward- and backward-propagating modes are present. The modes of the nonabsorbing waveguide also obey the nonconjugated orthogonality relation given by Eq. (11-14) below, but the conjugated form is more useful for deriving quantities relating to modal power, as is evident in Section 11-7.

In Section 31-3 we show that each bound mode is orthogonal to the radiation field in Eq. (11-2). Hence Eq. (31-15) gives

$$\int_{A_\infty} \mathbf{e}_j \times \mathbf{H}_{\text{rad}}^* \cdot \hat{\mathbf{z}} dA = \int_{A_\infty} \mathbf{E}_{\text{rad}}^* \times \mathbf{h}_j \cdot \hat{\mathbf{z}} dA = 0, \quad (11-11)$$

where $j > 0$ and subscript rad denotes the radiation field.

We define the mode *normalization* N_j for nonabsorbing waveguides by

$$N_j = \frac{1}{2} \left| \int_{A_\infty} \mathbf{e}_j \times \mathbf{h}_j^* \cdot \hat{\mathbf{z}} dA \right|. \quad (11-12)$$

The modulus ensures that N_j is positive for all modes. In the case of backward-propagating modes, Eqs. (11-7) and (11-12) give $N_{-j} = N_j$. If we combine the orthogonality conditions, Eq. (11-10), with normalization, then for *two forward-propagating modes* we obtain [1]

$$\frac{1}{2} \int_{A_\infty} \mathbf{e}_j \times \mathbf{h}_k^* \cdot \hat{\mathbf{z}} dA = \frac{1}{2} \int_{A_\infty} \mathbf{e}_k^* \times \mathbf{h}_j \cdot \hat{\mathbf{z}} dA = \begin{cases} N_j & \text{if } j = k, \\ 0 & \text{if } j \neq k, \end{cases} \quad (11-13)$$

where $j, k > 0$. For two backward-propagating modes, or one backward-propagating mode and one forward-propagating mode, we use Eq. (11-7) to re-express the fields in terms of the fields of forward-propagating modes, and then apply Eq. (11-12).

Absorbing waveguides

The most general form of orthogonality holds for both absorbing and nonabsorbing waveguides, and has the form of Eq. (31-16) where

$$\int_{A_x} \mathbf{e}_j \times \mathbf{h}_k \cdot \hat{\mathbf{z}} dA = \int_{A_x} \mathbf{e}_k \times \mathbf{h}_j \cdot \hat{\mathbf{z}} dA = 0; \quad j \neq k. \quad (11-14)$$

Normalization and orthogonality to the radiation field are expressed by Eqs. (11-11) and (11-13) with the * suppressed. However, the conjugated relationships in Eq. (11-13) hold approximately for slightly absorbing media, as discussed later in the chapter.

11-5 Orthonormal modes

In some applications it is convenient to use modal fields that have unit normalization. Modes satisfying this condition are called *orthonormal* modes, and are constructed from modes with arbitrary normalization by setting

$$\hat{\mathbf{e}}_j = \frac{\mathbf{e}_j}{\sqrt{N_j}}, \quad \hat{\mathbf{h}}_j = \frac{\mathbf{h}_j}{\sqrt{N_j}}; \quad \hat{\mathbf{e}}_{-j} = \frac{\mathbf{e}_{-j}}{\sqrt{N_j}}, \quad \hat{\mathbf{h}}_{-j} = \frac{\mathbf{h}_{-j}}{\sqrt{N_j}}, \quad (11-15)$$

for forward- and backward-propagating modes, respectively. The orthogonality condition for *two forward-propagating orthonormal modes* is

$$\boxed{\frac{1}{2} \int_{A_x} \hat{\mathbf{e}}_j \times \hat{\mathbf{h}}_k^* \cdot \hat{\mathbf{z}} dA = \frac{1}{2} \int_{A_x} \hat{\mathbf{e}}_k^* \times \hat{\mathbf{h}}_j \cdot \hat{\mathbf{z}} dA = \begin{cases} 1 & \text{if } j = k, \\ 0 & \text{if } j \neq k. \end{cases}} \quad (11-16)$$

The fields of forward- and backward-propagating orthonormal modes are related by Eq. (11-7) with a \wedge introduced over each field component, and the orthogonality of backward-propagating orthonormal modes is handled by the procedure laid down below Eq. (11-10).

ENERGY AND POWER

The guided portion of the fields stores electromagnetic energy in the waveguide and transports power along the waveguide. A fraction of this energy is stored in the fields of each bound mode, and these fields also transport a portion of the total power. From a knowledge of the energy and power in each mode, we can deduce the total stored energy and power guided along the waveguide.

11-6 Stored electric and magnetic energies

Consider a nonabsorbing waveguide with a *nondispersive* refractive index, i.e. $n(x, y)$ is real and does not vary with wavelength λ . Let \mathcal{W}_{e_j} and \mathcal{W}_{h_j} be the

time-averaged, stored, *electric* and *magnetic energies* per unit length of waveguide for the j th forward-propagating mode, defined by

$$\mathcal{W}_{ej} = \frac{1}{4} |a_j|^2 \epsilon_0 \int_{A_\infty} n^2 |\mathbf{e}_j|^2 dA; \quad \mathcal{W}_{hj} = \frac{1}{4} |a_j|^2 \mu_0 \int_{A_\infty} |\mathbf{h}_j|^2 dA, \quad (11-17)$$

where a_j is the modal amplitude, A_∞ is the infinite cross-section and $|\mathbf{e}_j|^2 = \mathbf{e}_j \cdot \mathbf{e}_j^*$. The refractive-index profile is n , and ϵ_0 , μ_0 are the free-space dielectric constant and permeability, respectively. It follows from Eqs. (11-7) and (11-9) that the corresponding energies for the j th backward-propagating mode are also given by Eq. (11-17) with a_j replaced by a_{-j} . In Section 31-5, we show that stored energies are equal, i.e.

$$\mathcal{W}_{ej} = \mathcal{W}_{hj}; \quad \mathcal{W}_j = \mathcal{W}_{ej} + \mathcal{W}_{hj} = 2\mathcal{W}_{ej}, \quad (11-18)$$

where \mathcal{W}_j is the *total* stored energy per unit length of waveguide.

When the waveguide is *dispersive*, the permeability and dielectric constant vary with wavelength λ , i.e. $\epsilon = \epsilon(\lambda)$, $\mu = \mu(\lambda)$. In this case the total stored energy per unit length is given by [2]

$$\mathcal{W}_j = -\frac{\lambda^2}{4} |a_j|^2 \int_{A_\infty} \left\{ \epsilon_0 |\mathbf{e}_j|^2 \frac{d}{d\lambda} \left(\frac{n^2}{\lambda} \right) + |\mathbf{h}_j|^2 \frac{d}{d\lambda} \left(\frac{\mu}{\lambda} \right) \right\} dA. \quad (11-19)$$

In deriving this result, we have assumed the waveguide to be nonabsorbing. This ignores the intimate relation between dispersiveness and absorption, as expressed by the Kramers-Kronig relationships [2]. However, if we restrict this discussion to comparatively small absorption the correction to Eq. (11-19) due to absorption is a higher-order effect.

11-7 Power flow

When an optical waveguide is excited, each mode will, in general, carry power. The portion of source power exciting a particular mode depends on the nature of the source, and is discussed in Chapters 20 and 21. For nonabsorbing waveguides, *power* flows parallel to the waveguide axis and, for the j th mode, is distributed over the infinite cross-section with *density*, or *intensity*, S_j , given by the magnitude of the time-averaged Poynting vector. From Eqs. (11-3) and (11-8) we have

$$S_j = \frac{1}{2} |a_j|^2 \operatorname{Re} \{ \mathbf{E}_j \times \mathbf{H}_j^* \cdot \hat{\mathbf{z}} \} = \frac{1}{2} |a_j|^2 \mathbf{e}_j \times \mathbf{h}_j^* \cdot \hat{\mathbf{z}}, \quad (11-20)$$

where a_j is the modal amplitude and Re denotes real part. The *total power* in each mode is found by integrating S_j over the infinite cross-section A_∞ . For the

j th forward- and backward-propagating modes, we find from Eq. (11–9) that

$$P_j = \frac{1}{2}|a_j|^2 \int_{A_\infty} \mathbf{e}_j \times \mathbf{h}_j^* \cdot \hat{\mathbf{z}} dA, \quad (11-21a)$$

$$P_{-j} = -\frac{1}{2}|a_j|^2 \int_{A_\infty} \mathbf{e}_j \times \mathbf{h}_j^* \cdot \hat{\mathbf{z}} dA. \quad (11-21b)$$

Thus $P_j > 0$ represents power propagating in the positive z -direction in Fig. 11–1(a), and $P_{-j} < 0$ represents power propagating in the negative z -direction. In terms of the mode normalization of Eq. (11–12)

$$P_j = |a_j|^2 N_j; \quad P_{-j} = -|a_{-j}|^2 N_j, \quad (11-22a)$$

while for the orthonormal modes of Eq. (11–16)

$$P_j = |a_j|^2; \quad P_{-j} = -|a_{-j}|^2. \quad (11-22b)$$

11–8 Fraction of modal power in the core

The characteristically different forms of the refractive index in the core and cladding in Fig. 11–1(b) lead to distinctly different behavior of the waveguide fields in the two regions. However, we can often gain insight into the relative behavior of the fields in the two regions by examining the fraction of a mode's power that propagates within the core. We define a parameter η_j as

$$\eta_j = \frac{\text{power flow within the core}}{\text{total power flow of the mode}}. \quad (11-23)$$

For a nonabsorbing waveguide, we deduce from Eq. (11–21) that

$$\eta_j = \eta_{-j} = \frac{\frac{1}{2} \int_{A_{\text{co}}} \mathbf{e}_j \times \mathbf{h}_j^* \cdot \hat{\mathbf{z}} dA}{\frac{1}{2} \int_{A_\infty} \mathbf{e}_j \times \mathbf{h}_j^* \cdot \hat{\mathbf{z}} dA}, \quad (11-24)$$

where A_{co} is the core cross-section, and A_∞ is the infinite cross-section. This expression is also useful for describing slightly absorbing waveguides, discussed later in the chapter.

11–9 Total guided power

We define P_{tot} to be the *total, time-averaged power* propagating along an optical waveguide in the increasing z -direction of Fig. 11–1(a). In terms of the

total fields of Eq. (11-2), P_{tot} is given by the integrated Poynting vector over the infinite cross-section A_{∞}

$$P_{\text{tot}} = \frac{1}{2} \text{Re} \int_{A_{\infty}} \mathbf{E} \times \mathbf{H}^* \cdot \hat{\mathbf{z}} dA. \quad (11-25)$$

We can divide P_{tot} into the power of the guided, or bound, portion of the fields, P_{bd} , and the power of the radiation field, P_{rad} , so that

$$P_{\text{tot}} = P_{\text{bd}} + P_{\text{rad}}. \quad (11-26)$$

If we substitute Eqs. (11-2) and (11-3) into Eq. (11-25), apply the orthogonality condition, Eq. (11-13), and recall the definition of modal power from Eq. (11-21), we find from Eq. (11-26) that for a nonabsorbing waveguide

$$P_{\text{bd}} = \sum_{j=1}^M \{P_j + P_{-j}\} = \sum_{j=1}^M |a_j|^2 N_j - \sum_{j=1}^M |a_{-j}|^2 N_j, \quad (11-27)$$

where a_j and a_{-j} are the amplitudes of the j th forward- and backward-propagating modes, and N_j is the normalization of Eq. (11-12). Thus, the total guided power propagating in the positive z -direction is equal to the power in all forward-propagating modes minus the power in all backward-propagating modes. At any position along the waveguide, the power in the radiation field is the difference between P_{tot} and P_{bd} .

11-10 Fraction of total power in the core

The total power P_{tot} of Eq. (11-25) is the sum of the *total power in the core*, P_{co} , and the total power in the cladding, where

$$P_{\text{co}} = \frac{1}{2} \text{Re} \left\{ \int_{A_{\text{co}}} \mathbf{E} \times \mathbf{H}^* \cdot \hat{\mathbf{z}} dA \right\}. \quad (11-28)$$

In regions sufficiently far along the waveguide from any source of excitation, the radiation field within the core becomes negligible, and the total power of the fields within the core is given accurately by the bound modes in Eq. (11-2). However, P_{co} is still a complicated expression because *the bound modes are not orthogonal over any finite cross-section*. To see this, consider a situation in which only the forward-propagating modes are excited on a nonabsorbing waveguide. Substituting Eq. (11-2) into Eq. (11-28) and applying Eq. (11-3) gives

$$P_{\text{co}} = \frac{1}{2} \sum_j \sum_k a_j a_k^* \exp \{ i(\beta_j - \beta_k)z \} \int_{A_{\text{co}}} \mathbf{e}_j \times \mathbf{h}_k^* \cdot \hat{\mathbf{z}} dA, \quad (11-29)$$

where $j, k > 0$. Rearranging and employing the definitions of Eqs. (11-21a) and

(11-24) gives

$$P_{co} = \sum_j \eta_j P_j + \frac{1}{2} \sum_{j \neq k} a_j a_k^* \exp \{ i(\beta_j - \beta_k)z \} \int_{A_{co}} \mathbf{e}_j \times \mathbf{h}_k^* \cdot \hat{\mathbf{z}} dA, \quad (11-30)$$

which has a simple physical interpretation. The first summation adds up the fraction of each mode's power that is propagating within the core. The second summation represents the interference between different modes due to the nonorthogonality over the core. However, in many cases of practical importance, interference is a small effect and can be ignored [3].

GROUP VELOCITY

The power of a mode is transmitted along an optical waveguide at a speed given by the *group velocity* v_{gj} . This is to be distinguished from the phase velocity v_{pj} of Eq. (11-5), which determines the speed of a wave front along the waveguide [7]. Group velocity is defined by

$$v_{gj} = \frac{d\omega}{d\beta_j} = \frac{-2\pi c}{\lambda^2} \frac{d\lambda}{d\beta_j}, \quad (11-31)$$

where ω is the angular frequency implicit in the time dependence $\exp(-i\omega t)$ of the fields, λ is the free-space wavelength and β_j is the propagation constant of the j th mode. We can determine v_{gj} by differentiating the eigenvalue equation and substituting values for β_j . Alternatively, if the fields of the mode are prescribed, we show in Section 31-6 that Eq. (31-30) gives

$$v_{gj} = - \frac{\frac{1}{2} \int_{A_{co}} \mathbf{e}_j \times \mathbf{h}_j^* \cdot \hat{\mathbf{z}} dA}{(\lambda^2/4) \int_{A_{co}} \{ \epsilon_0 |\mathbf{e}_j|^2 (d/d\lambda) (n^2/\lambda) + |\mathbf{h}_j|^2 (d/d\lambda) (\mu/\lambda) \} dA}, \quad (11-32)$$

for nonabsorbing waveguides with permeability μ . This form takes account of material dispersion, i.e. n and μ depend on λ , but ignores absorption. For waveguides with no material dispersion, Eq. (11-32) can be replaced by Eq. (31-31), where

$$v_{gj} = \frac{(c\beta_j/2) \int_{A_{co}} \mathbf{e}_j \times \mathbf{h}_j^* \cdot \hat{\mathbf{z}} dA}{(k/2) \int_{A_{co}} n^2 \mathbf{e}_j \times \mathbf{h}_j^* \cdot \hat{\mathbf{z}} dA}. \quad (11-33)$$

If we compare the numerator and denominator of Eq. (11-32) with Eqs.

(11-19) and (11-21), we find that the group velocity of a mode is expressible as

$$v_{gj} = P_j / \mathcal{W}_j, \quad (11-34)$$

where P_j is the modal power and \mathcal{W}_j is the total stored energy per unit length of waveguide.

11-11 Group delay

It is common practice [4, 5] to refer to the *group delay time* τ_j per unit length of waveguide, rather than the group velocity v_{gj} , of a pulse, where

$$\tau_j = 1/v_{gj}. \quad (11-35)$$

The group delay for a waveguide of length z gives the *mean transit time* t_j . From Eq. (11-31) we have

$$t_j = \frac{z}{v_{gj}} = z\tau_j = z \frac{d\beta_j}{d\omega} = -z \frac{\lambda^2}{2\pi c} \frac{d\beta_j}{d\lambda}, \quad (11-36)$$

where c is the free-space speed of light. For modes which propagate only on multimode waveguides, t_j is equal to the ray transit time t of Chapter 3, as we demonstrate in Section 36-9.

PULSE SPREADING

When a pulse of light propagates along a waveguide, several effects contribute to distort its shape. First, different modes have different group delays, analogous to the transit times of different rays in Chapter 3. Thus, if the pulse is formed by more than one mode it will spread out as it propagates. This form of pulse spreading is called *intermodal dispersion*, and for multimode waveguides is analysed in Chapter 3 using classical geometric optics. On isotropic single-mode fibers of circular cross-section intermodal dispersion is exactly zero, as this fiber represents an exceptional case when the two fundamental modes—defined below Eq. 11-51—have identical group delays.

The second cause of pulse spreading has its origins in the small but finite bandwidth of the source of light transmission. This bandwidth is important because the group delay of each mode depends on wavelength, since both the refractive index of a dispersive medium depends on λ —*material dispersion*—and the propagation characteristics of a mode of the waveguide depend on λ —*waveguide dispersion*. The pulse spreading due to the combination of these two effects is known as *intramodal dispersion*, and, in practice, is dominated by the component due to material dispersion [5, 6].

11-12 Pulse spreading in single-mode fibers

We discussed pulse spreading in multimode waveguides in Chapter 3. Now we consider a single-mode fiber, assuming that both fundamental modes have the same mean transit time, as is the case on a circular fiber. Only intramodal dispersion is present, and the pulse spread is due to the spread δt_j in the mean transit time due to a given source, i.e. the slight spread $\delta\omega$ or $\delta\lambda$ in frequency or wavelength. Thus Eq. (11-36) gives

$$\delta t_j = z \frac{d^2 \beta_j}{d\omega^2} \delta\omega = -\frac{z}{2\pi c} \left\{ \lambda^2 \frac{d^2 \beta_j}{d\lambda^2} + 2\lambda \frac{d\beta_j}{d\lambda} \right\} \delta\lambda. \quad (11-37)$$

In general, the contributions to δt_j due to material and waveguide dispersion are not easily separated [5, 6]. Accordingly, we can only examine each in isolation from the other in special situations.

Material dispersion

To examine material dispersion in isolation, we disregard the light-guiding influence of the fiber and assume the mode is a z -directed plane wave, for which $\beta_j = 2\pi n(\lambda)/\lambda$ and the refractive index is spatially uniform. Substituting into Eq. (11-36) we find that

$$t_j = \frac{z}{c} n_g; \quad n_g = n(\lambda) - \lambda \frac{dn}{d\lambda}, \quad (11-38)$$

where n_g is the *group index* introduced in Section 1-5. Accordingly, the pulse spread is found from Eq. (11-38) to be

$$\delta t_g = -\frac{z}{c} \lambda \frac{d^2 n}{d\lambda^2} \delta\lambda, \quad (11-39)$$

which depends on the second derivative of n only.

Waveguide dispersion

The contribution to pulse spreading due to waveguide dispersion in isolation from material dispersion is found from Eq. (11-37) by assuming n is independent of λ . The form of δt_g depends on the refractive-index profile. Later, in Section 11-20, we express waveguide dispersion in terms of more convenient modal parameters.

DERIVATION AND PROPERTIES OF THE MODAL FIELDS

The electric and magnetic fields \mathbf{E}_j and \mathbf{H}_j of a bound mode are source-free solutions of Maxwell's equations, Eq. (30-1), or, equivalently, the vector wave

equations of Eq. (30–14). However these equations are complicated by the *vector* Laplacian ∇^2 , which in an arbitrary coordinate system couples the components of the field vectors. A considerable simplification is possible if we refer the components of \mathbf{E}_j and \mathbf{H}_j to *fixed cartesian directions*, since ∇^2 is replaced by the *scalar* Laplacian ∇^2 . In addition, the translational invariance of the fields, expressed by Eq. (11–3), leads to a further simplification of the vector wave equation, as we demonstrate in Section 30–7. From Eq. (30–18) we have

$$\{\nabla_t^2 + n^2 k^2 - \beta_j^2\} \mathbf{e}_j = -\{\nabla_t + i\beta_j \hat{\mathbf{z}}\} \{\mathbf{e}_{tj} \cdot \nabla_t \ln n^2\}, \quad (11-40a)$$

$$\{\nabla_t^2 + n^2 k^2 - \beta_j^2\} \mathbf{h}_j = -(\nabla_t \ln n^2) \times (\{\nabla_t + i\beta_j \hat{\mathbf{z}}\} \times \mathbf{h}_j), \quad (11-40b)$$

where β_j is the propagation constant, $n = n(x, y)$ is the refractive-index profile, $k = 2\pi/\lambda$ is the free-space wavenumber and λ is the free-space wavelength. As explained at the beginning of Chapter 30, we assume that the magnetic permeability takes the free-space value μ_0 throughout this book, unless otherwise stated. Relationships between n , k , λ and other electromagnetic parameters are given inside the back cover. An implicit time dependence $\exp(-i\omega t)$ is assumed in the field vectors, where ω is the angular frequency. The transverse Laplacian ∇_t^2 and the vector operator ∇_t are defined in Table 30–1, page 592. We emphasize that the fields have cartesian components, i.e.

$$\mathbf{e}_j = e_{xj} \hat{\mathbf{x}} + e_{yj} \hat{\mathbf{y}} + e_{zj} \hat{\mathbf{z}}; \quad \mathbf{h}_j = h_{xj} \hat{\mathbf{x}} + h_{yj} \hat{\mathbf{y}} + h_{zj} \hat{\mathbf{z}}, \quad (11-41)$$

where $\hat{\mathbf{x}}$, $\hat{\mathbf{y}}$ and $\hat{\mathbf{z}}$ are unit vectors parallel to the axes in Fig. 11–1(a), but *the spatial variation of these components is expressible in any cylindrically symmetric coordinate system*. Thus, for example, the component equations of Eq. (11–40) for planar waveguides and circular fibers are given by Eqs. (30–21) and (30–23), respectively.

11–13 Eigenvalue equation

The vector wave equations are a restatement of Maxwell's equations for an arbitrary profile shape. Subject to the requirements that the modal fields are everywhere bounded and decay sufficiently fast at large distances from the waveguide axis, these equations contain all the information necessary to determine the spatial dependence of the fields everywhere in the waveguide. Alternatively, the electric and magnetic fields can be generated by solving the same equations in regions where the profile is continuous, and matching at any discontinuities through the appropriate boundary conditions of Maxwell's equations. In either case, the formulation leads to a consistency condition for determining the modal propagation constants β_j , i.e. *an eigenvalue equation*.

As well as being the solution of an eigenvalue equation, the propagation constant is also an explicit function of the modal fields. For a nonabsorbing

waveguide, Eq. (31–23) gives

$$\beta_j = \left(\frac{\mu_0}{\varepsilon_0} \right)^{1/2} k \frac{\int_{A_\infty} n^2 \mathbf{e}_j \times \mathbf{h}_j^* \cdot \hat{\mathbf{z}} dA}{\int_{A_\infty} n^2 |\mathbf{e}_j|^2 dA}, \quad (11-42)$$

where A_∞ is the infinite cross-section and $|\mathbf{e}_j|^2 = \mathbf{e}_j \cdot \mathbf{e}_j^*$. Since the modal fields depend implicitly on β_j , this equation is an integral form of the eigenvalue equation for any profile.

11–14 Solution in terms of the longitudinal field components

It is not necessary to solve the vector wave equations for the transverse components of \mathbf{e}_j and \mathbf{h}_j once the longitudinal components e_{zj} and h_{zj} are known. In Section 30–3 we show how to determine the transverse components $\mathbf{e}_{\perp j}$ and $\mathbf{h}_{\perp j}$ in terms of the longitudinal components. From Eq. (30–6) we have

$$\mathbf{e}_{\perp j} = \frac{i}{n^2 k^2 - \beta_j^2} \left\{ \beta_j \nabla_{\perp} e_{zj} - \left(\frac{\mu_0}{\varepsilon_0} \right)^{1/2} k \hat{\mathbf{z}} \times \nabla_{\perp} h_{zj} \right\}, \quad (11-43a)$$

$$\mathbf{h}_{\perp j} = \frac{i}{n^2 k^2 - \beta_j^2} \left\{ \beta_j \nabla_{\perp} h_{zj} + \left(\frac{\varepsilon_0}{\mu_0} \right)^{1/2} k n^2 \hat{\mathbf{z}} \times \nabla_{\perp} e_{zj} \right\}, \quad (11-43b)$$

where $n = n(x, y)$, $k = 2\pi/\lambda$, ε_0 is the free-space dielectric constant and μ_0 is the free-space permeability. In Section 30–8 we show that the longitudinal field components satisfy a pair of coupled equations. These equations are given by Eq. (30–25) as

$$(\nabla_{\perp}^2 + p_j) e_{zj} - \frac{\beta_j^2}{p_j} \nabla_{\perp} e_{zj} \cdot \nabla_{\perp} \ln n^2 = - \left(\frac{\mu_0}{\varepsilon_0} \right)^{1/2} \frac{k \beta_j}{p_j} \hat{\mathbf{z}} \cdot (\nabla_{\perp} h_{zj} \times \nabla_{\perp} \ln n^2), \quad (11-44a)$$

$$(\nabla_{\perp}^2 + p_j) h_{zj} - \frac{n^2 k^2}{p_j} \nabla_{\perp} h_{zj} \cdot \nabla_{\perp} \ln n^2 = \left(\frac{\varepsilon_0}{\mu_0} \right)^{1/2} \frac{k n^2 \beta_j}{p_j} \hat{\mathbf{z}} \cdot (\nabla_{\perp} e_{zj} \times \nabla_{\perp} \ln n^2), \quad (11-44b)$$

where $p_j = n^2 k^2 - \beta_j^2$ and $n = n(x, y)$.

11–15 Coupling of the field components

The terms involving $\nabla_{\perp} \ln n^2$ in Eqs. (11–40) and (11–44) couple various field components. These terms describe polarization phenomena due to the waveguide structure, as we discuss in the following section. This presents a complication as far as obtaining analytical solutions is concerned, but is the mathematical basis for the hybrid nature of the modal fields to be discussed in

the next section. Prior to confronting the general case, we first discuss the step profile when both the core and cladding indices are uniform.

Step-profile waveguides and the scalar wave equation

For waveguides with a step-index profile, i.e. $n = n_{\text{co}}$ in the core and $n = n_{\text{cl}}$ in the cladding, all terms involving $\nabla_{\perp} \ln n^2$ in Eqs. (11–40) and (11–44) vanish within the core and cladding *but not on the core–cladding interface*. Consequently each *cartesian* field component of Eq. (11–40) satisfies a simplified equation *within* the core and cladding, e.g.

$$\{\nabla_{\perp}^2 + n^2 k^2 - \beta_j^2\} e_{zj} = 0. \quad (11-45)$$

This equation is sometimes referred to as the scalar wave equation. However, in this book we describe a field component as a solution of the scalar wave equation only if (i) it satisfies Eq. (11–45) for all values of x and y , including the interface, and consequently (ii) is continuous and has continuous first derivatives everywhere—see Section 33–1. This is not the case for any cartesian component of \mathbf{e}_j on a step-profile waveguide of arbitrary cross-sectional shape, since the $\nabla_{\perp} \ln n^2$ terms are nonzero at the interface. Thus, to solve for e_{zj} *everywhere*, we impose the boundary conditions of Maxwell's equations on the solutions of Eq. (11–45) derived in each homogeneous region. The component h_{zj} is derived similarly. Alternatively we can solve Eq. (11–44) with $\nabla_{\perp} \ln n^2$ terms retained. The transverse components then follow from Eq. (11–43).

The step-index profile is exceptional in that we can solve the vector wave equation analytically for certain cross-sections with the $\nabla_{\perp} \ln n^2$ terms included, but without directly confronting these terms. We can regard the step profile as a special case of a graded profile where all the grading occurs at a single interface. Thus, the step profile has the greatest influence on the polarization behavior of the fields.

TE modes

There are two exceptional cases when the $\nabla_{\perp} \ln n^2$ terms do not appear in the vector wave equations for the transverse fields. These occur for modes with $e_{zj} = 0$ everywhere on a planar waveguide and on a circularly symmetric fiber, and are called TE modes. In these two special cases, it is indeed true that the transverse electric field $\mathbf{e}_{\perp j}$ satisfies the scalar wave equation, Section 33–1, everywhere.

11–16 Hybrid nature of the modal fields

From the discussion of the previous section, we can infer certain properties about the composition of modal fields. Consider a metal waveguide comprising a perfectly conducting cladding and a core of uniform dielectric—thus

$\nabla_t \ln n^2 = 0$ in the core. The longitudinal-field equations of Eq. (11-44) reduce to the homogeneous equation of Eq. (11-45) for e_{zj} and h_{zj} . The modes of this system comprise two linearly independent sets [7], one with $h_{zj} = 0$ everywhere, called *transverse magnetic* (TM); the other with $e_{zj} = 0$ everywhere, called *transverse electric* (TE). However, on optical waveguides, the nonzero $\nabla_t \ln n^2$ terms in Eq. (11-44) mix e_{zj} and h_{zj} , so that the equations cannot, in general, be decoupled. Thus the TE and TM modes are, in general, no longer appropriate since neither $e_{zj} = 0$ nor $h_{zj} = 0$ are solutions. Accordingly, the modes of optical waveguides are, in general, hybrid having both e_{zj} and h_{zj} components. These hybrid modes are usually called *HE* and *EH* modes for reasons discussed elsewhere [8]. In special situations, depending on the geometry of the cross-section and the profile variation, the right side of Eq. (11-44) vanishes and some modes of optical waveguides can be purely TE or purely TM. The trivial example is the planar waveguide, when all modes can be expressed as either TE or TM modes. Another example is provided by modes with azimuthally symmetric fields on circular fibers. Apart from the trivial case of an infinite uniform medium, the modal fields are never TEM waves, i.e. waves with $e_{zj} = h_{zj} = 0$ everywhere.

Physical explanation of TE and TM modes

On planar waveguides, TE and TM modes correspond to the two possible polarization states of the electromagnetic field. This fact can be anticipated from total reflection of plane waves from a planar interface between two uniform semi-infinite dielectric media, as illustrated in Fig. 10-2. The phase of the reflected wave differs from the phase of the incident wave and depends on whether the electric field or the magnetic field is parallel to the interface. In each case the direction of the electric or magnetic fields is unaltered after reflection, so that either $e_{zj} = 0$ or $h_{zj} = 0$ is conserved, and the TE and TM modes do not mix. Thus, the origin of the difference between TE and TM modes on a planar waveguide is the polarization-dependent nature of plane-wave reflection. This dependence is fully contained within the $\nabla_t \ln n^2$ terms of the vector wave equation. The argument is easily generalized to include graded-index media, using the notion of local plane waves, as explained in Section 35-3.

On circular fibers, TE and TM modes with circularly symmetric fields can propagate in the same manner as on planar waveguides, because they have electric and magnetic fields, respectively, that are parallel to the interface. In terms of local plane waves, or rays, only meridional rays, i.e. those passing through the waveguide axis, can preserve $e_{zj} = 0$ or $h_{zj} = 0$ at every reflection. Thus only meridional rays can make up TE and TM modes on round waveguides, as illustrated in Fig. 11-2(a). This is consistent with the noncoupling of the fields of these modes in the vector wave equation.

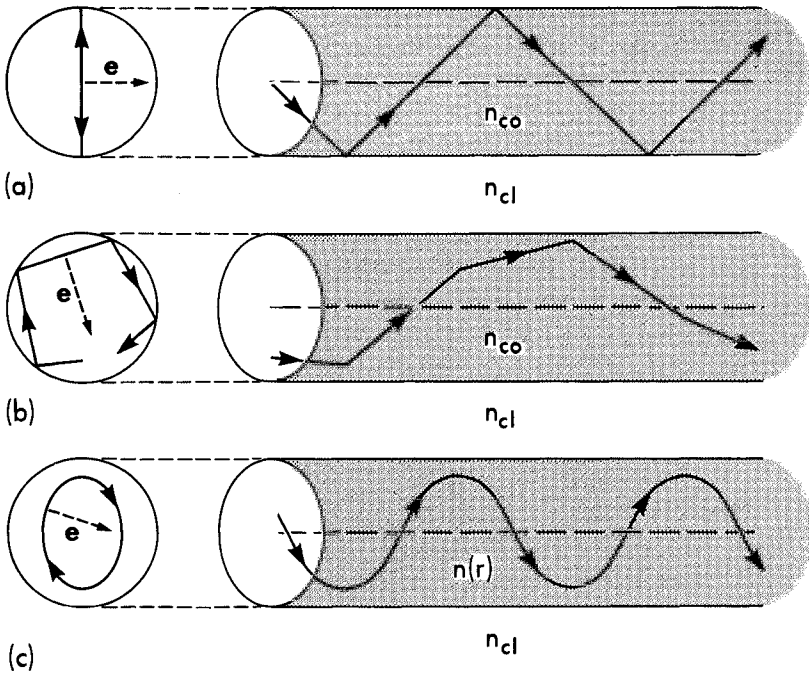


Fig. 11–2 The electric field vector is orthogonal to the ray, or local plane-wave direction. On the step-profile fiber, the direction of \mathbf{e} for (a) a meridional ray is parallel to a fixed direction, and for (b) a skew ray it changes direction at each reflection. On the parabolic-profile fiber the direction of \mathbf{e} changes continuously along the skew-ray path (c).

Whilst such a description in terms of rays is not strictly accurate for waveguides propagating one or a few modes, it nevertheless provides qualitative insight.

Physical explanation of hybrid modes

We can also use the local plane-wave interpretation to appreciate the origin of hybrid modes on a circular fiber. Consider a ray propagating in the core of the fiber. In general, the ray follows the helical or skew trajectory on step- or graded-index profiles, as shown in Figs. 11–2(b) and 11–2(c), respectively. If we follow the direction of the electric vector along a skew ray path using the local plane-wave description, we appreciate the impossibility of maintaining either $e_{zj} = 0$ or $h_{zj} = 0$ because the direction of propagation rotates along the ray trajectory. Consequently, a skew ray of necessity mixes TE and TM polarizations at each reflection, so that the corresponding modal fields couple

both e_{zj} and h_{zj} field components, consistent with the definition of hybrid modes. Conversely, all EH and HE modes are composed of skew rays.

The $\nabla_t \ln n^2$ term in the vector wave equation describes the rotation of the electric vector—see Eq. (35-8). Clearly the smaller $\nabla_t \ln n^2$, the greater the axial distance z which is required for the ray path to complete a full period. Consequently, regardless of how small the value of $\nabla_t \ln n^2$, the electric vector must eventually rotate through 360° . This phenomenon is described by the hybrid nature of the modes.

To summarize, *the waveguide structure has polarization properties by virtue of its cross-sectional geometry and refractive-index profile. These effects are built into the vector wave equation, Eq. (11-40), through the $\nabla_t \ln n^2$ terms, which are responsible for the hybrid modes. Ignoring these terms completely disregards polarization properties of the waveguide structure and leads to the scalar wave equation.*

11-17 Propagation constant

The value of the propagation constant β_j for each bound mode is found from the eigenvalue equation, discussed in Section 11-13. For a given free-space wavelength λ and refractive-index profile $n(x, y)$, only certain values of the propagation constant β_j are possible. By definition, a bound mode does not attenuate on a nonabsorbing waveguide, so that β_j is real. The range of values of β_j for bound modes can be derived on physical grounds. The refractive-index profile satisfies $n_{co} \geq n(x, y) \geq n_{cl}$, where n_{co} and n_{cl} are the maximum and minimum indices. Thus the minimum phase velocity is equal to the minimum speed of light within the waveguide, c/n_{co} . However, although it is possible for the phase velocity of a mode to exceed the maximum speed of light in the cladding, c/n_{cl} , this cannot occur without losing power to radiation. Accordingly, the phase velocity of a bound mode must lie between these limits. Using Eq. (11-5) and the relationships inside the back cover, we deduce that regardless of the profile variation and cross-sectional geometry

$$n_{cl} k < \beta_j \leq n_{co} k, \quad (11-46)$$

where $k = 2\pi/\lambda$.

WAVEGUIDE AND MODAL PARAMETERS

The modal fields of an optical waveguide depend on all of the physical quantities which define the waveguide, i.e. the parameters which describe the refractive-index profile and the cross-sectional geometry, together with the frequency or wavelength of the source of excitation. From these parameters,

we can form two dimensionless quantities. The *waveguide* or *fiber parameter* V is defined by

$$V = \frac{2\pi\rho}{\lambda} (n_{\text{co}}^2 - n_{\text{cl}}^2)^{1/2}, \quad (11-47)$$

where n_{co} and n_{cl} are the maximum and minimum values of refractive index in Fig. 11-1(b), and the free-space wavelength λ is combined with a typical linear dimension ρ in the core cross-section, e.g. the core radius of a fiber or the half-width of the planar waveguide. Next we define the *profile height parameter*

$$\Delta = \frac{1}{2} \left\{ 1 - \frac{n_{\text{cl}}^2}{n_{\text{co}}^2} \right\}. \quad (11-48)$$

Equivalent definitions of V and Δ are given inside the back cover.

A waveguide is said to be *multimoded* or *overmoded* if $V \gg 1$, when many bound modes can propagate. At the opposite extreme, when V is sufficiently small so that only the two polarization states of the fundamental mode can propagate, the waveguide is said to be *single-moded*. For example, the step-profile, circular fiber is single-moded when $V < 2.405$, as we show in Section 12-9.

For a waveguide of given cross-section and profile shape, the modal electric field can be normalized to depend parametrically on V , Δ and ρ only, i.e. $\mathbf{e}_j = \mathbf{e}_j(V, \Delta, \rho)$. The magnetic field \mathbf{h}_j then has the same parametric dependence, apart from a factor $n_{\text{co}} (\epsilon_0/\mu_0)^{1/2}$. This factor originates from the first Maxwell equation in Eq. (30-1a) by substituting for k in terms of V , ρ and Δ , and multiplying by ρ to make the operator $\nabla \times$ dimensionless. Further parameters are required to account for variations in cross-section, e.g. the eccentricity of an elliptical waveguide, and in profile shape, e.g. the exponent of the power-law profiles of Eq. (1-59).

Modal parameters

To facilitate description of the modal fields, we introduce dimensionless *modal parameters* U_j and W_j for the core and cladding defined by

$$U_j = \rho(k^2 n_{\text{co}}^2 - \beta_j^2)^{1/2}; \quad W_j = \rho(\beta_j^2 - k^2 n_{\text{cl}}^2)^{1/2}, \quad (11-49)$$

where $k = 2\pi/\lambda$, n_{co} is the maximum core index and n_{cl} is the uniform cladding index. The characteristic core half-width or radius is denoted by ρ . On nonabsorbing waveguides bound modes have real values of U_j and W_j . We deduce from Eq. (11-47) that the waveguide and modal parameters are related

by

$$V^2 = U_j^2 + W_j^2, \quad (11-50)$$

and the range of bound mode propagation constants in Eq. (11-46) is equivalent to

$$0 \leq U_j < V; \quad 0 < W_j \leq V, \quad (11-51)$$

for a given value of V . In solving the eigenvalue equation, it is usually more convenient to work with the dimensionless modal parameters rather than the un-normalized propagation constant. The *fundamental modes* are defined by the two smallest values of U_j , or, equivalently, the two largest values of β_j which satisfy the eigenvalue equation for the given value of V . On circular fibers these two values are equal.

The limit of small V

It follows from Eq. (11-47) that $V \rightarrow 0$ when $\lambda \rightarrow \infty$. Thus when $V = 0$ we have the electrostatic limit of the vector wave equation in Eq. (11-40a). In this limit $\nabla \times \mathbf{e}_{tj} = 0$, $\nabla \cdot (n^2 \mathbf{e}_{tj}) = 0$ and, therefore, \mathbf{e}_{tj} is expressible in terms of a scalar function $\Psi(x, y)$, where

$$\nabla_t^2 \Psi + \nabla_t \Psi \cdot \nabla_t \ln n^2 = 0; \quad \mathbf{e}_{tj} = \nabla_t \Psi. \quad (11-52)$$

The equation for Ψ reduces to Laplace's equation in the uniform cladding.

11-18 Modal cutoff

The lower limit $\beta_j = kn_{cl}$ of permissible values of the bound mode propagation constant in Eq. (11-46) is called *modal cutoff*. In the notation of Eqs. (11-49) and (11-50) modal cutoff, or just cutoff, is defined by

$$U_j = V; \quad W_j = 0. \quad (11-53)$$

The fundamental modes of all waveguides considered in this text are cut off when $V = 0$. At cutoff the phase velocity of the mode is equal to that of a z -directed plane wave in an unbounded medium of refractive index n_{cl} , but the modal fields are *not* TEM waves except in special cases. In general, a significant fraction of a mode's power can propagate within the core at cutoff, i.e. η_j of Eq. (11-24) is nonzero, and the group velocity v_{gj} differs from the phase velocity. Below cutoff, these modes propagate with loss and are the leaky modes of Chapter 24.

In the uniform cladding, the right side of the vector wave equation in Eq. (11-40a) vanishes, and the cutoff condition $\beta_j = kn_{cl}$ reduces the left side to Laplace's equation.

$$\nabla_t^2 \mathbf{e}_j = 0, \quad (11-54)$$

where ∇_t^2 is defined in Table 30–1, page 592. On circular fibers the transverse electric field of the fundamental mode is uniform in the cladding, and corresponds to the axially symmetric, bounded solution of this equation.

Far from cutoff

A mode is far from cutoff when $V \gg U_j$ or, equivalently, $\beta_j \cong kn_{co}$, leading to

$$W_j \cong V; \quad V \rightarrow \infty. \quad (11-55)$$

In this limit, all of a mode's power is concentrated in a finite region about the maximum core index, i.e. about $n = n_{co}$. For clad profiles this region is entirely within the core.

11–19 Number of bound modes

The exact number of bound modes which propagate on a waveguide can be found by counting the discrete solutions of the eigenvalue equation. In general this is a cumbersome procedure, but simple expressions are available for multimode waveguides with $V \gg 1$. Examples are given in Sections 36–12 and 36–13.

11–20 Distortion parameter

We discussed pulse spreading due to waveguide dispersion in Section 11–12. It is convenient to express the pulse spread δt_j of Eq. (11–37) in terms of the waveguide parameter V and the modal parameter U_j . Using the definitions inside the back cover, we first rewrite Eq. (11–37) in terms of the group velocity of Eq. (11–31) as

$$\delta t_j = -\frac{z}{v_{gj}^2} \frac{V dv_{gj}}{\omega dV} \delta \omega = \frac{z}{v_{gj}^2} \frac{V dv_{gj}}{\lambda dV} \delta \lambda = z \frac{V^2 d^2 \beta_j}{\omega^2 dV^2} \delta \omega. \quad (11-56)$$

From the group velocity definition of Eq. (11–31) it follows that

$$v_{gj} = \frac{c}{n_{co}(2\Delta)^{1/2}} \frac{dV}{d(\rho\beta_j)} = \frac{c}{n_{co}} \frac{(V^2 - 2\Delta y)^{1/2}}{V - \Delta y'}, \quad (11-57)$$

where $y = U_j^2$ and prime denotes differentiation with respect to V . Substituting Eq. (11–57) into (11–56), we obtain

$$\delta t_j = 2 \frac{z n_{co}}{c \omega} D V \Delta \delta \omega = -2 \frac{z n_{co}}{c \lambda} D V \Delta \delta \lambda, \quad (11-58)$$

Table 11-1 Properties of bound modes. Summary of bound-mode properties, dropping the subscript j when only one mode is involved. A nonabsorbing waveguide is assumed so that $\mathbf{e}_1, \mathbf{h}_1$ can be taken to be real and $\mathbf{e}_z, \mathbf{h}_z$ are then imaginary. The modal amplitude coefficient, a , is defined by Eq. (11-2).

Modal electric field	$\mathbf{E}(x, y, z) = \{ \mathbf{e}_1(x, y) + \hat{\mathbf{z}} e_z(x, y) \} \exp(i\beta z)$
Modal magnetic field	$\mathbf{H}(x, y, z) = \{ \mathbf{h}_1(x, y) + \hat{\mathbf{z}} h_z(x, y) \} \exp(i\beta z)$
Orthogonality $j \neq k$	$\int_{A_\infty} \mathbf{e}_j \times \mathbf{h}_k^* \cdot \hat{\mathbf{z}} dA = \int_{A_\infty} \mathbf{e}_k^* \times \mathbf{h}_j \cdot \hat{\mathbf{z}} dA = 0$
Normalization	$N = \frac{1}{2} \left \int_{A_\infty} \mathbf{e} \times \mathbf{h}^* \cdot \hat{\mathbf{z}} dA \right $
Orthonormal modes	$\hat{\mathbf{e}} = \frac{\mathbf{e}}{N^{1/2}}; \quad \hat{\mathbf{h}} = \frac{\mathbf{h}}{N^{1/2}}$
Power density or intensity	$S = \frac{1}{2} a ^2 \mathbf{e} \times \mathbf{h}^* \cdot \hat{\mathbf{z}}$
Modal power	$P = \frac{1}{2} a ^2 \int_{A_\infty} \mathbf{e} \times \mathbf{h}^* \cdot \hat{\mathbf{z}} dA$
Fraction of modal power in the core	$\eta = \frac{\frac{1}{2} \int_{A_{\text{co}}} \mathbf{e} \times \mathbf{h}^* \cdot \hat{\mathbf{z}} dA}{\frac{1}{2} \int_{A_\infty} \mathbf{e} \times \mathbf{h}^* \cdot \hat{\mathbf{z}} dA}$
Phase velocity	$v_p = \frac{\omega}{\beta} = \frac{1}{\mu_0} \frac{\int_{A_\infty} n^2 \mathbf{e} ^2 dA}{\int_{A_\infty} n^2 \mathbf{e} \times \mathbf{h}^* \cdot \hat{\mathbf{z}} dA}$
Group velocity (non-dispersive media)	$v_g = \frac{d\omega}{d\beta} = \frac{1}{\epsilon_0} \frac{\int_{A_\infty} \mathbf{e} \times \mathbf{h}^* \cdot \hat{\mathbf{z}} dA}{\int_{A_\infty} n^2 \mathbf{e} ^2 dA}$
Distortion parameter	$D(V, \Delta) = \frac{1}{(2\Delta)^{1/2}} \frac{d^2(\rho\beta)}{dV^2}$

where $D = D(V, \Delta)$ is a dimensionless distortion parameter defined by

$$D(V, \Delta) = \frac{1}{(2\Delta)^{1/2}} \frac{d^2(\rho\beta_j)}{dV^2} = \frac{1}{2n_{co}\Delta} \frac{d}{dV} \left(\frac{c}{v_{gj}} \right), \quad (11-59a)$$

$$= \frac{\Delta(2yy'' - y'^2) - (V^2 y'' - 2Vy' + 2y)}{2(V^2 - 2\Delta y)^{3/2}}. \quad (11-59b)$$

Consequently, pulse spreading due to waveguide dispersion is characterized by the product $DV\Delta$. In practice, the source frequency or wavelength is prescribed, whereas ρ and Δ are design parameters.

To summarize this part of the chapter, we have laid out inside the back cover physical quantities and waveguide parameters defining light propagation on a waveguide, together with bound-mode parameters. Table 11-1 summarizes the properties of bound modes.

11-21 Relationships with ray invariants

In Part I we used ray analysis to describe propagation on multimode waveguides with profiles that vary slowly over distances equal to the wavelength of light. Clearly we can also perform an electromagnetic analysis using the modes of this chapter, and, in Chapter 36, we demonstrate the equivalence of the two approaches. Throughout Part II, we frequently make contact with results in Part I, so it is useful to relate modal parameters to ray invariants. Thus, given the propagation constant β_j of a mode *which can propagate only on a multimode waveguide*, the longitudinal ray invariant is given by Eq. (36-2)

$$\bar{\beta} = \lambda\beta_j/2\pi, \quad (11-60)$$

where λ is the free-space wavelength of light. This relationship is independent of profile. In the special case of the step profile, we can express β_j and the modal parameters U_j, W_j in terms of the angle θ_z the ray path makes with the waveguide axis, as summarized in Table 36-1, page 695, with the subscript j omitted. Further relationships for circular fibers are discussed in Section 36-2.

ABSORBING WAVEGUIDES

When the materials constituting a waveguide are absorbing, the modal fields lose power as they propagate. The absorption process is described mathematically by attributing an imaginary part to the dielectric constant, or, equivalently, to the refractive index, as in Table 11-2. Thus the profile is now complex, leading to complex values for the propagation constant, as well as for

Table 11-2 Propagation on absorbing waveguides. Superscripts r and i denote real and imaginary parts, and Re denotes real part. For slightly absorbing waveguides the fields in the expression for γ can be approximated by the fields of the nonabsorbing waveguide.

Complex profiles	$\epsilon(x, y) = \epsilon^r(x, y) + i\epsilon^i(x, y); \quad n(x, y) = n^r(x, y) + in^i(x, y)$ $\epsilon^r = \epsilon_0 \{ (n^r)^2 - (n^i)^2 \}; \quad \epsilon^i = 2\epsilon_0 n^r n^i$
Modal parameters	$\beta = \beta^r + i\beta^i; \quad U_j = U_j^r + iU_j^i; \quad W_j = W_j^r + iW_j^i$
Modal fields	$\mathbf{E}_j = \mathbf{e}_j(x, y) \exp(i\beta_j^r z) \exp(-\beta_j^i z);$ $\mathbf{H}_j = \mathbf{h}_j(x, y) \exp(i\beta_j^r z) \exp(-\beta_j^i z)$
Modal power	$P_j(z) = P_j(0) \exp(-\gamma_j z); \quad \gamma_j = 2\beta_j^i$
Power attenuation coefficient	$\gamma_j = 2k \left(\frac{\epsilon_0}{\mu_0} \right)^{1/2} \frac{\int_{A_x} n^r n^i \mathbf{e}_j ^2 dA}{\text{Re} \left\{ \int_{A_x} \mathbf{e}_j \times \mathbf{h}_j^* \cdot \hat{\mathbf{z}} dA \right\}}$

the waveguide and modal parameters. Consequently, we can no longer use the representation of Section 11-3 in which the transverse fields are real.

11-22 Power attenuation

The imaginary part of the propagation constant, β_j^i , accounts for the attenuation factor $\exp(-\beta_j^i z)$ of the modal fields in Table 11-2. If $P_j(z)$ is the modal power distance z along the waveguide, then, by substituting these fields into Eq. (11-21a), we obtain the expression for power attenuation in terms of the *power attenuation coefficient* γ_j , and the initial power $P_j(0)$.

Uniform media

We first consider the trivial case of an infinite, uniform medium of constant refractive index $n = n^r + in^i$. The modal fields, which depend implicitly on time through the factor $\exp(-i\omega t)$, are the fields of a plane wave propagating in the z -direction with propagation constant $\beta_j = kn^r + ikn^i$, where $k = 2\pi/\lambda$. Thus the field amplitude attenuates as $\exp(-kn^i z)$, and the power attenuation coefficient $\gamma_j = 2\beta_j^i = 2kn^i$. The quantity $2kn^i$ defines the *power absorption coefficient* α , introduced in Eq. (6-2), and thus $\gamma_j = \alpha$ in this case.

Nonuniform media

The derivation of the power attenuation coefficient for a waveguide composed of arbitrary absorbing media is more involved. One approach is to derive the eigenvalue equation for the absorbing waveguide and look for the complex roots corresponding to the propagation constants of bound modes. In general, however, the roots must be determined numerically. Alternatively, we can express the power attenuation coefficient in terms of the modal fields in a manner analogous to Eq. (11-42) for the propagation constant on nonabsorbing waveguides, as we now show.

The power dP_j lost from the modal fields due to absorption over a differential length dz of the waveguide follows from the time-averaged Poynting vector theorem in Section 30-9, and is given by Eq. (30-28) with \mathbf{E} replaced by the modal field $a_j \mathbf{E}_j$. If \mathcal{V} denotes the volume between cross-sectional planes at z and $z + dz$, then

$$dP_j = -k(\epsilon_0/\mu_0)^{1/2} |a_j|^2 dz \int_{A_\infty} n^r n^i |\mathbf{E}_j|^2 dA, \quad (11-61)$$

where A_∞ is the infinite cross-section. A second expression is obtained by differentiating the expression for power in Table 11-2, whence

$$dP_j = -\gamma_j dz P_j(0) \exp(-\gamma_j z). \quad (11-62)$$

We substitute for \mathbf{E}_j in Eq. (11-61) from Table 11-2, and for $P_j(0)$ in Eq. (11-62) using the expression for P_j in Eq. (11-21a). If we then equate the two expressions for dP_j , we obtain the power attenuation coefficient

$$\gamma_j = 2k \left(\frac{\epsilon_0}{\mu_0} \right)^{1/2} \frac{\int_{A_\infty} n^r n^i |\mathbf{e}_j|^2 dA}{\text{Re} \left\{ \int_{A_\infty} \mathbf{e}_j \times \mathbf{h}_j^* \cdot \hat{\mathbf{z}} dA \right\}}, \quad (11-63)$$

where Re denotes real part, $*$ denotes complex conjugate and $\hat{\mathbf{z}}$ is the unit vector parallel to the waveguide axis. Remaining parameters are defined inside the back cover. We are reminded that the fields in this expression are those of the *absorbing* waveguide.

Weak absorption

When the waveguide is only slightly absorbing, as is normally the case in practice, we can obtain approximations to the power attenuation coefficient in explicit form. In one approach, the imaginary part of the propagation constant is determined by setting $\beta = \beta_j^r + i\beta_j^i$ in the eigenvalue equation for the absorbing waveguide, expanding in powers of β_j^i/β_j^r and retaining only terms

correct to first order. An alternative and more direct solution is to approximate \mathbf{e}_j and \mathbf{h}_j in Eq. (11-63) by treating the waveguide as if it were nonabsorbing. In fact, we can make this approximation in all calculations involving weakly absorbing waveguides, provided that we allow for the attenuation factor $\exp(-\beta_j z)$ in the fields \mathbf{E}_j and \mathbf{H}_j , and for the attenuation $\exp(-\gamma_j z)$ of modal power, as given in Table 11-2. Weakly absorbing waveguides are considered again in Chapters 13 and 18.

ANISOTROPIC WAVEGUIDES

In the previous sections we assumed the waveguides were constructed from isotropic material. We now consider waveguides constructed from anisotropic material. For perspective, we first treat plane-wave propagation in an unbounded, uniform anisotropic medium. Then we discuss the modes of anisotropic waveguides.

11-23 Uniform anisotropic medium

An isotropic medium has the property that the electric field vector \mathbf{E} produces a displacement vector $\epsilon_0 n^2 \mathbf{E}$ in the same direction, i.e. the refractive index is independent of the direction of \mathbf{E} . For a specific direction, plane waves can propagate in any state of polarization. Thus, in general, propagation in each direction can be described by two linearly polarized plane waves with their electric field vectors orthogonal to each other, but otherwise arbitrarily oriented.

An anisotropic material has an ordered arrangement of molecules and thus crystalline-like properties [2, 9, 10]. In particular, *the displacement vector is not, in general, parallel to \mathbf{E}* , i.e. the value of the refractive index depends on the direction of \mathbf{E} . A crystal has three mutually perpendicular *principal axes* such that, if the electric field is parallel to any one of them, the displacement vector is also parallel to the field. In this case, the description of propagation is no more complicated than for an isotropic medium, except that we must specify three values of n , corresponding to $\mathbf{D} = \epsilon_0 n_x^2 \mathbf{E}$ when \mathbf{E} is parallel to the x -axis, $\mathbf{D} = \epsilon_0 n_y^2 \mathbf{E}$ when \mathbf{E} is parallel to the y -axis and $\mathbf{D} = \epsilon_0 n_z^2 \mathbf{E}$ when \mathbf{E} is parallel to the z -axis. However, when \mathbf{E} is *not* parallel to a principal axis, it is necessary to express \mathbf{E} in terms of its components, so that

$$D_x = \epsilon_0 n_x^2 E_x; \quad D_y = \epsilon_0 n_y^2 E_y; \quad D_z = \epsilon_0 n_z^2 E_z, \quad (11-64)$$

and \mathbf{D} is no longer parallel to \mathbf{E} . The description of propagation is then considerably more complicated. In particular, for each direction of propagation, there are only two allowed directions of polarization for which a plane wave can propagate. These are the only modes of the crystalline-like medium.

Each mode can be expressed as a linearly polarized plane wave. The allowed polarization directions and the propagation constants for the two modes are found by solving three homogeneous linear equations in E_x , E_y , and E_z , which can be expressed as [2, 9]

$$\beta^2 \{ \mathbf{E} - (\hat{\mathbf{k}} \cdot \mathbf{E}) \hat{\mathbf{k}} \} = k^2 \mathbf{n}^2 \cdot \mathbf{E} = k^2 (n_x^2 E_x \hat{\mathbf{x}} + n_y^2 E_y \hat{\mathbf{y}} + n_z^2 E_z \hat{\mathbf{z}}), \quad (11-65)$$

where $\hat{\mathbf{k}}$ is the unit vector parallel to the direction of propagation of the plane wave, k is defined inside the back cover, and $\hat{\mathbf{x}}$, $\hat{\mathbf{y}}$, $\hat{\mathbf{z}}$ are the unit vectors parallel to the cartesian, or principal, axes. The solutions of Eq. (11-65) have the properties that $\hat{\mathbf{k}}$, \mathbf{D} and \mathbf{E} are coplanar, the direction of power flow differs from the direction of the wave vector, $\hat{\mathbf{k}}k$, and, in general, the value of the propagation constant β , for at least one of the two allowable directions, depends on the direction of propagation.

Axially directed plane wave

The description of propagation is considerably simplified in special cases. In particular, if the direction of propagation is along the z -axis, then one allowed mode is an x -polarized plane wave in a medium characterized by principal refractive index $n = n_x$, while the other allowed mode is a y -polarized plane wave in a medium characterized by principal refractive index $n = n_y$. If $n_x = n_y$, the crystal is called *uniaxial*, and if $n_x \neq n_y \neq n_z$ it is *biaxial*.

11-24 Anisotropic waveguides

The fundamental equations governing propagation in anisotropic waveguides are given in Section 30-10. In general, they are considerably more difficult to solve than the corresponding equations for the isotropic waveguide. From our discussion above it is intuitive that unless the three principal axes of the dielectric material are aligned with the geometrical axes of the waveguide in Fig. 11-1(a), the modes of the waveguide are very complicated. When the two sets of axes are so aligned, the TM modes of an anisotropic planar waveguide, characterized by principal refractive indices n_x , n_y and n_z , are elementary generalizations of the modes of the corresponding isotropic planar waveguide, while the TE modes are identical to the modes of the isotropic planar waveguide, characterized by $n = n_y$, assuming invariance along the y -direction. This is discussed further in Section 12-19. In analogy with the planar waveguide, the modes of a uniaxial fiber, characterized by principal refractive indices satisfying $n_x = n_y$, are also elementary generalizations of the modes of the isotropic fiber, and are discussed in Section 12-20. However, the modes of a *biaxial* crystalline fiber characterized by $n_x \neq n_y \neq n_z$ cannot be expressed in closed form. Indeed, this can be anticipated since the circular symmetry of the profile is broken by the anisotropy.

Propagation constant

The range of values of the propagation constant β_j for bound modes of clad anisotropic waveguides follows by generalizing the argument of Section 11–17 for isotropic waveguides. In particular, bound modes must satisfy $\beta_j > kn_{cl}^x$, assuming $n_{cl}^x > n_{cl}^y$, otherwise the x-polarized portion of the modal field will radiate because it travels faster than an x-polarized plane wave in the cladding. The cladding indices for x- and y-polarized light are n_{cl}^x and n_{cl}^y , respectively. Thus, the generalization of Eq. (11–46) to anisotropic waveguides is

$$kn_{cl}^x < \beta_j \leq kn_{co}^x, \quad (11-66)$$

assuming that $n_{co}^x > n_{co}^y$ and $n_{cl}^x > n_{cl}^y$, where n_{co}^x is the maximum value of the core index for x-polarized light. *More generally, the lower limit on β_j is set by the larger of n_{cl}^x, n_{cl}^y while the upper limit depends on the larger of n_{co}^x, n_{co}^y .*

In deriving Eq. (11–66), we assumed that the modal electric field has both x and y components. For the exceptional case of a planar anisotropic waveguide, the transverse modal field can be purely x- or y-polarized, as we showed in Section 12–19. In other words, the x- and y-polarized mode sets decouple, with the propagation constant of the x-polarized modes obeying Eq. (11–66), while the propagation constant of the y-polarized modes obeys Eq. (11–66) with superscript x replaced by y.

Weakly guiding, anisotropic waveguides

When the refractive indices of the waveguide core and cladding are approximately equal, regardless of the direction of \mathbf{E} , the waveguide is called *weakly guiding*. For such cases, the bound modes are composed of plane waves which are directed approximately along the waveguide axis. This simplifies the propagation characteristics, as anticipated from the discussion at the end of Section 11–23. The modes of such structures are discussed at the end of Chapter 13. Although the waveguide is weakly guiding, we emphasize that anisotropy can have a significant effect on propagation.

Waveguides with slight anisotropy

Waveguides that are nearly isotropic can be treated by the perturbation methods of Chapter 18. Weakly guiding waveguides are discussed in Section 18–9, and waveguides with arbitrarily varying refractive-index profiles are discussed in Section 18–21.

REFERENCES

1. Adler, R. B. (1952) Waves on inhomogeneous cylindrical structures. *Proc. I.R.E.*, **40**, 339–48.
2. Landau, L. D. and Lifshitz, E. M. (1960) *Electrodynamics of Continuous Media*. Pergamon Press, Oxford.
3. Snyder, A. W. and Pask, C. (1973) Incoherent illumination of an optical fiber. *J. Opt. Soc. Am.*, **63**, 806–12.
4. Miller, S. E. and Chynoweth, A. G. (eds.) (1979) *Optical Fiber Communications*, Academic Press, New York.
5. Dyott, R. B. and Stern, J. R. (1971) Group delay in fiber waveguides. *Electron Lett.*, **7**, 82–4.
6. Gambling, W. A., Matsumura, H. and Ragdale, C. M. (1979) Mode dispersion, material dispersion and profile dispersion in graded-index, single-mode fibers. *Microwaves, Opt. Acoust.*, **3**, 239–46.
7. Johnson, C. C. (1965) *Fields and Wave Electrodynamics*, McGraw-Hill, New York.
8. Snitzer, E. (1961) Cylindrical dielectric waveguide modes. *J. Opt. Soc. Am.*, **51**, 491–8.
9. Born, M. and Wolf, E. (1970) *Principles of Optics*, Pergamon Press, London, chap. XIV.
10. Stokes, A. R. (1963) *The Theory of Optical Properties of Inhomogeneous Materials*, E. & F. N. Spon, London, chap. 4.

Waveguides with exact solutions

12-1	Step-profile waveguides	239
	Step-profile planar waveguide	240
12-2	Modal fields	240
12-3	Propagation constants	241
12-4	Modal properties	245
12-5	Weakly guiding waveguide	246
12-6	Plane-wave decomposition of the modal fields	246
12-7	Asymmetric and multilayered waveguides	248
	Step-profile fiber	248
12-8	Modal fields	249
12-9	Propagation constants	252
12-10	Modal properties	254
12-11	Weakly guiding fiber	259
12-12	Plane-wave decomposition of the modal fields	262
12-13	Multilayered and elliptical fibers	262
	Graded-profile waveguides	263
12-14	<i>Example: TE modes on graded-profile planar waveguides</i>	263
12-15	<i>Example: TM modes on graded-profile planar waveguides</i>	267
12-16	<i>Example: TE modes on graded-profile fibers</i>	267
12-17	<i>Example: TM modes on graded-profile fibers</i>	269
12-18	<i>Example: Hybrid modes on a graded-profile fiber</i>	271
	Anisotropic waveguides	272
12-19	Step-profile planar waveguide	273
12-20	Step-profile uniaxial fiber	278
	References	279

The basic properties of bound modes on optical waveguides were given in the previous chapter. In this chapter we display these properties explicitly for those few profiles which have exact solutions of Maxwell's equations. Our primary objective is to derive analytical expressions for the modal vector fields, which contain all the polarization properties of the waveguide discussed in Section 11-16. We pay particular attention to fundamental modes, since these

are the only modes which can propagate on single-mode waveguides. As we consider only individual modes, we can drop the modal subscript. Thus the modal fields of Eq. (11-3) are now expressed as

$$\mathbf{E}(x, y, z) = \mathbf{e}(x, y) \exp(i\beta z); \quad \mathbf{H}(x, y, z) = \mathbf{h}(x, y) \exp(i\beta z), \quad (12-1)$$

where β is the propagation constant. The field components are solutions to the homogeneous vector wave equations of Eq. (30-14), where

$$\{\nabla_t^2 + n^2 k^2 - \beta^2\} \mathbf{e} = -(\nabla_t + i\beta \hat{\mathbf{z}}) \mathbf{e}_t \cdot \nabla_t \ln n^2, \quad (12-2a)$$

$$\{\nabla_t^2 + n^2 k^2 - \beta^2\} \mathbf{h} = \{(\nabla_t + i\beta \hat{\mathbf{z}}) \times \mathbf{h}\} \times \nabla_t \ln n^2, \quad (12-2b)$$

where $n = n(x, y)$ is the refractive-index profile, $k = 2\pi/\lambda$, and λ is the free-space wavelength. Subscript t denotes transverse component, and $\hat{\mathbf{z}}$ is the unit vector parallel to the waveguide axis. The vector operators ∇_t^2 and ∇_t are defined by Eqs. (37-38) and (37-33), respectively. For the profiles of planar and circularly symmetric fibers considered here, we work with the component equations of Eqs. (30-21) and (30-15), respectively. We begin with step-profile waveguides, since these are of practical interest and Maxwell's equations are straightforward to solve. Throughout the chapter we assume the free-space permeability μ_0 for every waveguide.

12-1 Step-profile waveguides

The step-profile waveguide has a core of uniform refractive index n_{co} , surrounded by a cladding of uniform refractive index n_{cl} , which is assumed unbounded. Thus the only variation in profile is a step, or jump, discontinuity at the core-cladding interface in Fig. 11-1(a). This profile has exact analytical solutions for the modal fields on planar waveguides, circularly symmetric fibers and elliptical fibers.

Solution of the vector wave equations

A general approach for finding the fields of step-profile waveguides is to solve the vector wave equations of Eq. (12-2) within the core and cladding regions, where the $\nabla_t \ln n^2$ terms are zero, and then use the boundary conditions of Maxwell's equations to determine the field amplitudes. This approach was discussed in Section 11-15, which emphasized that the $\nabla_t \ln n^2$ terms manifest themselves through the boundary conditions. We need solve only for the longitudinal components e_z and h_z in Eq. (12-2), since the transverse components are then given by Eq. (11-43). Accordingly, the equations satisfied by the longitudinal components *within* the core and cladding regions are given by Eq. (11-45) as

$$\{\nabla_t^2 + n^2 k^2 - \beta^2\} \Psi = 0, \quad (12-3)$$

where Ψ denotes e_z or h_z , and ∇_t^2 is defined in Table 30-1, page 592. The boundary conditions of Maxwell's equations, given below Eq. (30-1), require that \mathbf{h} and the tangential components of \mathbf{e} be continuous at the interface, and that the fields be everywhere finite. The solution for the modal fields is determined to within an arbitrary constant multiple. The value of this multiple, or modal amplitude, a_j , is determined by the amplitude of either the source of excitation or the prescribed waveguide fields.

STEP-PROFILE PLANAR WAVEGUIDE

The simplest example of a step-profile waveguide is the symmetric planar waveguide of Fig. 12-1 with profile

$$n(x) = n_{co}, \quad 0 \leq |x| < \rho; \quad n(x) = n_{cl}, \quad \rho < |x| < \infty, \quad (12-4)$$

where ρ is the core half-width. This is a two-dimensional waveguide, and by orienting cartesian axes as shown, the fields depend on x and z only, i.e.

$$\mathbf{E}(x, z) = \mathbf{e}(x) \exp(i\beta z); \quad \mathbf{H}(x, z) = \mathbf{h}(x) \exp(i\beta z). \quad (12-5)$$

The physical parameters of the waveguide and the free-space wavelength λ of the source of excitation are contained in the waveguide parameter V and the profile height parameter Δ defined inside the back cover.

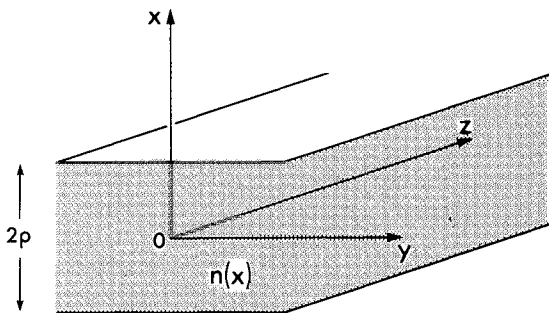


Fig. 12-1 Section of a planar waveguide, which is unbounded in the y - and z -directions. The core half-width is ρ and $n(x)$ is the refractive-index profile. The z -axis coincides with the waveguide axis midway between interfaces.

12-2 Modal fields

We follow the prescription for constructing the fields given in Section 12-1. Substituting Eq. (12-4) into Eq. (12-3) and referring to Table 30-1, page 592,

we deduce that

$$\left\{ \rho^2 \frac{d^2}{dx^2} + U^2 \right\} \Psi = 0; \quad 0 \leq |x| < \rho, \quad (12-6a)$$

$$\left\{ \rho^2 \frac{d^2}{dx^2} - W^2 \right\} \Psi = 0; \quad \rho < |x| < \infty, \quad (12-6b)$$

where the modal parameters U and W are defined by Eq. (11-49), and Ψ denotes e_z or h_z . Solutions which are everywhere bounded vary as $\sin(Ux/\rho)$ or $\cos(Ux/\rho)$ in the core and as $\exp(-W|x|/\rho)$ in the cladding. We explained in Section 11-16 why the modes of planar waveguides are expressible as either TE with $e_z = 0$ or as TM with $h_z = 0$. In either case the remaining longitudinal component is continuous across both interfaces and has the form given in Table 12-1. The nonvanishing transverse field components follow from Eq. (30-8). Continuity of h_x or h_y at $x = \pm \rho$ leads to the eigenvalue equations in Table 12-2, which in turn have been used to express the amplitude of each field component in the form given in Table 12-1. We assume that *within the core* $e_y = 1$ or $e_x = 1$ at $x = \rho$. Even and odd modes have transverse electric fields that are even or odd functions of x . On a nonabsorbing waveguide n_{co} and n_{cl} are real, and the fields obey the convention of Eq. (11-8), i.e. e_z, h_z are imaginary, and e_x, e_y, h_x, h_y are real. The complete spatial dependence of the fields follow from Eq. (12-5).

In the next section we show that U depends on V or on V and Δ . Thus, if we substitute for β and n_{co}^2/n_{cl}^2 , from inside the back cover, the parametric dependence of the electric fields in Table 12-1 involves the independent parameters V, Δ and ρ only, i.e. $\mathbf{e} = \mathbf{e}(V, \Delta, \rho)$ as discussed below Eq. (11-48). The magnetic fields depend on the same parameters, apart from the factor $n_{co}(\epsilon_0/\mu_0)^{1/2}$.

Alternative derivation

The derivation of the modal fields, given above, is based on the longitudinal components, for which the longitudinal components of the vector wave equation decouple on step-profile waveguides, as explained in Section 11-15. However, for the special case of the planar waveguide, the TE and TM mode fields can also be derived starting with e_y and h_y , respectively, as we show later in Sections 12-14 and 12-15.

12-3 Propagation constants

As noted above, continuity of the tangential fields at the interfaces gives rise to the eigenvalue equations. There are four eigenvalue equations corresponding

Table 12-2 (a) Modal properties of the step-profile planar waveguide. (b) Asymptotic forms of U . (a) The modal quantities N , η and v_g are calculated from Table 11-1, page 230, and (b) gives the asymptotic solutions of the eigenvalue equations in (a). All parameters are defined inside the back cover.

(a)

	<i>Even TE modes</i>	<i>Odd TE modes</i>	<i>Even TM modes</i>	<i>Odd TM modes</i>
Eigenvalue equation	$W = U \tan U$	$W = -U \cot U$	$n_{\text{co}}^2 W = n_{\text{cl}}^2 U \tan U$	$n_{\text{co}}^2 W = -n_{\text{cl}}^2 U \cot U$
Normalization	$N = \frac{\rho \beta}{2k} \left(\frac{\epsilon_0}{\mu_0} \right)^{1/2} \frac{V^2}{U^2} \frac{1+W}{W}$		$N = \frac{\rho k n_{\text{co}}^2}{2\beta} \left(\frac{\epsilon_0}{\mu_0} \right)^{1/2} \left\{ 1 + \frac{n_{\text{co}}^4 W^2}{n_{\text{cl}}^4 U^2} + \frac{n_{\text{co}}^2}{n_{\text{cl}}^2} \frac{V^2}{U^2 W} \right\}$	
Fraction of power in core	$\eta = 1 - \frac{U^2}{V^2(1+W)}$		$\eta = 1 - \frac{n_{\text{co}}^2 n_{\text{cl}}^2 U^2}{n_{\text{co}}^2 n_{\text{cl}}^2 V^2 + n_{\text{co}}^4 W^3 + n_{\text{cl}}^4 W U^2}$	
Group velocity	$v_g = \frac{c}{n_{\text{co}}^2} \frac{\beta}{k} \frac{1}{1 - 2\Delta(1 - \eta)}$			
Number of bound modes	$M_b = \text{Int} \left\{ \frac{4V}{\pi} \right\}$			

(b)

	TE _j modes	TM _j modes
Cutoff $U = V, W = 0$	$U = V = j \frac{\pi}{2}$	
Near cutoff $U \cong V, W \cong 0$	$U \cong V - \frac{V^3}{2} \quad (j = 0)$	$U \cong V - \frac{n_{\text{cl}}^4}{n_{\text{co}}^4} \frac{V^3}{2} \quad (j = 0)$
	$U \cong V - j \frac{\pi}{4} \left(V - j \frac{\pi}{2} \right)^2 \quad (j > 0)$	$U \cong V - \frac{n_{\text{cl}}^4}{n_{\text{co}}^4} j \frac{\pi}{4} \left(V - j \frac{\pi}{2} \right)^2 \quad (j > 0)$
$V = W = \infty$	$U = (j+1) \frac{\pi}{2}$	
Far from cutoff $V \cong W \gg 1$	$U \cong (j+1) \frac{\pi}{2} \left\{ 1 - \frac{1}{V+1} \right\}$	$U \cong (j+1) \frac{\pi}{2} \left\{ 1 - \frac{n_{\text{cl}}^2}{n_{\text{cl}}^2 + V n_{\text{co}}^2} \right\}$
Range of single-mode operation $0 < V < \frac{\pi}{2}$		

to even and odd TE and TM modes; these are given in Table 12-2. The solution of each equation for U leads to the propagation constant β through the relationship inside the back cover. Each value of β must lie in the range for bound modes $kn_{cl} < \beta \leq kn_{co}$.

The eigenvalue equations are transcendental and must be solved numerically. Plots of U as a function of V for the first eight modes of a waveguide with $\Delta = 0.32$ are presented in Fig. 12-2. We choose a relatively large difference between core and cladding indices to ensure that the TE and TM mode solutions are clearly distinguishable. Even and odd values of the subscript j refer to even and odd TE _{j} and TM _{j} modes, the value of j increasing with increasing U .

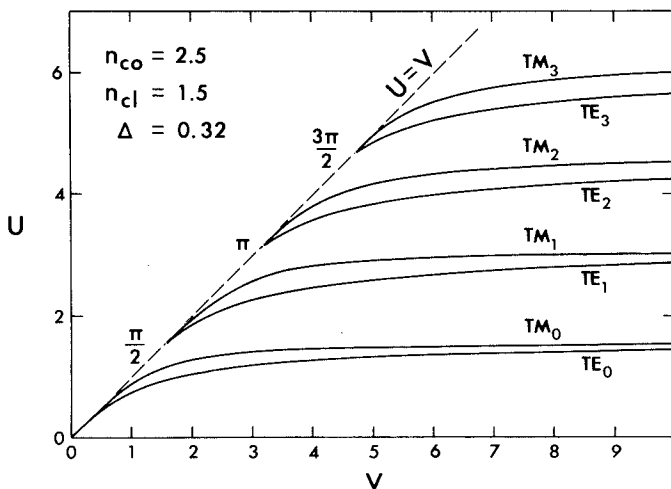


Fig. 12-2 Numerical solution of the eigenvalue equations of Table 12-2 for the first eight modes. The values along the dashed line are the cutoff values of U .

Cutoff and $V = \infty$

The cutoff values of U , discussed in Section 11-18, are found by setting $U = V$ in each eigenvalue equation. We deduce from Table 12-2 that $U = j\pi/2$ for both TE _{j} and TM _{j} modes. The fundamental TE₀ and TM₀ modes are not cut off. Consequently the waveguide is single moded if $0 < V < \pi/2$, when only these two modes can propagate. As $V \rightarrow \infty$ we deduce that $U \rightarrow (j+1)\pi/2$. Thus, for all modes, U increases by $\pi/2$ as V increases from cutoff to infinity. These results are included in Table 12-2.

Near to and far from cutoff

Approximations for U close to cutoff and far from cutoff are given in Table 12-2. Close to cutoff, U is expanded as a power series in $V - j\pi/2$ and coefficients of like powers are equated in the eigenvalue equation. Far from cutoff we differentiate the eigenvalue equation [1], e.g. for the even TE modes

$$\frac{dU}{dV} = \frac{U}{V} \frac{1}{1 + (V^2 - U^2)^{1/2}}, \quad (12-7)$$

and ignore the U dependence in the denominator since $V \gg U$. This leaves an integrable function from which we deduce the expression in Table 12-2. If we compare these approximations with the exact values of U in Fig. 12-2, the relative error increases in both the near-cutoff approximations as V increases, and in the far-from-cutoff approximation as V decreases. For the TE₀ mode the error in each approximation is 10.4 % at $V = 0.72$, while for the TM₀ mode the error is 25.2 % at $V = 1.26$.

12-4 Modal properties

If we substitute the modal fields of Table 12-1 into Table 11-1, page 230, we obtain the expressions for N , η and v_g in Table 12-2, noting that the area integrals in Table 11-1 reduce to single integrals over $-\infty < x < \infty$ for the planar waveguide. The parameters η and v_g in particular provide insight into propagation phenomena, as discussed below.

TM modes

If we substitute for W and n_{co}^2/n_{cl}^2 from inside the back cover, the eigenvalue equations for TM modes in Table 12-2 show that U depends on both V and Δ . The dependence on Δ is a manifestation of the polarization properties of the waveguide contained in the $\nabla_t \ln n^2$ terms in Eq. (12-2), or, equivalently, in the polarization-dependent property of plane-wave reflection from a planar interface, discussed in Section 11-16. The influence of waveguide polarization increases with Δ .

TE modes

If we substitute for W from inside the back cover, the eigenvalue equations for TE modes in Table 12-2 show that U depends only on V and is independent of Δ . Thus, U is insensitive to waveguide polarization, as anticipated in Section 11-15, and corresponds to the vanishing of the $\nabla_t \ln n^2$ terms in Eqs. (30-21b) and (31-21d) for e_y and h_x , respectively. Hence the transverse fields satisfy the scalar wave equation *everywhere including the interface*. In Section 33-1 we show that any solution of the scalar wave equation must be continuous

everywhere and have continuous first derivatives. From this fact we can derive the TE mode eigenvalue equations directly from Eq. (12-3) without recourse to the boundary conditions of Maxwell's equations. The longitudinal fields satisfy Eqs. (30-21c) and (30-21f) in which the $\nabla_t \ln n^2$ terms vanish everywhere *except at the interface*. Consequently e_z and h_z are *not* solutions of the scalar wave equation.

Near to and far from cutoff

As U approaches its cutoff value, $W \rightarrow 0$ and $\beta \rightarrow kn_{cl}$. We deduce from Table 12-2 that $\eta \rightarrow 0$, so that all of a mode's power is in the cladding, and $v_g \rightarrow c/n_{cl}$, i.e. the modal group velocity approaches the speed of light in the cladding. Furthermore, Table 12-1 shows that $e_z \rightarrow 0$, $h_z \rightarrow 0$, so that the modal fields are TEM at cutoff. We warn that the conclusions $\eta \rightarrow 0$ and the fields becoming TEM for *all* modes is specific to the planar waveguide.

Far from cutoff where $W \rightarrow V \rightarrow \infty$ and $\beta \rightarrow kn_{co}$, we deduce that $\eta \rightarrow 1$ and $v_g \rightarrow c/n_{co}$. Hence all modal power is in the core and the modal group velocity is equal to the speed of light in the core.

Number of modes

The total number of bound modes M_{bm} which can propagate on the step-profile planar waveguide is most simply found by counting solutions of the eigenvalue equations. Since the cutoff values of U in Fig. 12-1 are $\pi/2$ apart and there are two polarization states for each value of cutoff, we deduce that $M_{bm} = \text{Int}(4V/\pi)$, where Int denotes the largest integer not exceeding $4V/\pi$. Hence the number of modes depends only on V .

12-5 Weakly guiding waveguide

The waveguide is weakly guiding if $n_{co} \cong n_{cl}$ or, equivalently, if the profile height is small, i.e. $\Delta \ll 1$. The dependence of U on Δ in the TM mode eigenvalue equations of Table 12-2 is then slight. A further consequence is that the range of propagation constant values for bound modes, $kn_{cl} < \beta \leq kn_{co}$, becomes very narrow and $\beta \cong kn_{co} \cong V/\rho(2\Delta)^{1/2}$. It is then clear that the longitudinal fields in Table 12-1 are of order $\Delta^{1/2}$ times the order of the transverse fields. Hence the modal fields of the weakly guiding waveguide are nearly TEM waves, with only a weak dependence on the polarization properties of the waveguide.

12-6 Plane-wave decomposition of the modal fields

The core fields of each mode on a step-profile planar waveguide can be decomposed *exactly* into just two families of plane waves, as we show in

Section 36-1. Each plane wave, or ray, propagates at angle θ_z to the waveguide axis, where $\beta = kn_{\text{co}} \cos \theta_z$ and θ_z lies in the range of bound-ray directions $0 \leq \theta_z < \theta_c$ of Eq. (1-5(a)), where $\theta_c = \sin^{-1} \{1 - n_{\text{cl}}^2/n_{\text{co}}^2\}$ is the complement of the critical angle of geometric optics. If the waveguide is weakly guiding $\beta \cong kn_{\text{co}}$ and the rays are paraxial, i.e. $\theta_z \ll 1$. The discrete values of β correspond to the preferred ray directions discussed in Section 10-7.

Mode and ray transit times

The modal transit time t over length z of the waveguide follows from Eq. (11-36) as $t = z/v_g$. We denote the corresponding ray transit time expression in Table 1-1, page 19, by t_{go} . Substituting for group velocity from Table 12-2 and using the relationship between modal propagation constant β and ray invariant $\bar{\beta}$ in Table 36-1, page 695, we deduce

$$t = t_{\text{go}} \{1 - 2\Delta(1 - \eta)\}. \quad (12-8)$$

Thus the modal and ray transit times are equal only when $\eta \rightarrow 1$. This condition is satisfied only by those rays belonging to modes well above cutoff, i.e. when $V \gg U$, or, equivalently, when $\theta_z \ll \theta_c$. Hence t_{go} is inaccurate for arbitrary values of θ_z . This inaccuracy arises because the ray transit time ignores diffraction effects, which were discussed in Chapter 10. The step-profile planar waveguide is a special case, however, because *all* diffraction effects can be accounted for exactly by including the lateral shift at each reflection, together with recognizing the preferred ray directions. This was carried out in Section 10-6, and for rays, or local plane waves, whose electric field is polarized in the y -direction in Fig. 10-2, leads to the modified ray transit time of Eq. (10-13). If we use Table 36-1 to express θ_z and θ_c in terms of U , V and W and substitute η for TE modes from Table 12-2, we find that Eqs. (10-13) and (12-8) are identical since $\theta_z \cong \theta_c$. It is readily verified that the same conclusion holds for TM modes and local plane waves whose magnetic field is polarized in the y -direction of Fig. 10-2.

Material absorption

If the core and cladding materials of the waveguide are slightly absorbing, the ray power attenuation coefficient of Eq. (6-3) is identical to the modal power attenuation coefficient of Table 11-2, page 232, provided the lateral shift is included. Details are presented in Section 36-10.

Eigenvalue equations

It is possible to derive the eigenvalue equations of Table 12-2 directly from the trajectories of plane waves within the waveguide core by calculating the total

phase change along the trajectory and at reflections, and then imposing a simple consistency condition. This is demonstrated in Section 36-7.

12-7 Asymmetric and multilayered waveguides

The analysis so far has been applied to the symmetric planar waveguide. However, it is straightforward to generalize Eq. (12-6) to asymmetric waveguides when the refractive index has uniform but different values in the regions $x > \rho$ and $x < -\rho$ in Fig. 12-1 [2]. Similarly, if further layers are introduced parallel to $x = 0$ so that the waveguide is multilayered, the modal fields are constructed from the appropriate solutions of Eq. (12-6) in each layer, ensuring the tangential components are continuous at each interface.

STEP-PROFILE FIBER

The step-profile fiber is illustrated in Fig. 12-3. It has a circularly symmetric cross-section and refractive-index profile

$$n(r) = n_{co}, \quad 0 \leq r < \rho; \quad n(r) = n_{cl}, \quad \rho < r < \infty, \quad (12-9)$$

where ρ is the core radius. The modal fields depend, in general, on all three cylindrical polar coordinates r , ϕ , z and have the separable forms

$$\mathbf{E}(r, \phi, z) = \mathbf{e}(r, \phi) \exp(i\beta z); \quad \mathbf{H}(r, \phi, z) = \mathbf{h}(r, \phi) \exp(i\beta z). \quad (12-10)$$

The physical parameters of the fiber and the free-space wavelength λ of the source of excitation are contained in the fiber parameter V and the profile height parameter Δ defined inside the back cover.

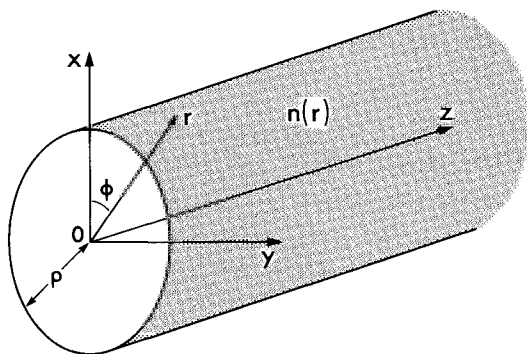


Fig. 12-3 Section of a circularly symmetric fiber, which is unbounded in the r - and z -directions. The core radius is ρ and $n(r)$ is the refractive-index profile. The z -axis coincides with the fiber axis of symmetry.

12-8 Modal fields

The construction of the fields follows the prescription given in Section 12-1. We substitute Eq. (12-9) into Eq. (12-3), and with reference to Table 30-1, page 592, deduce that if Ψ denotes e_z or h_z then Ψ satisfies

$$\left\{ \frac{\partial^2}{\partial R^2} + \frac{1}{R} \frac{\partial}{\partial R} + \frac{1}{R^2} \frac{\partial^2}{\partial \phi^2} + U^2 \right\} \Psi = 0; \quad 0 \leq R < 1, \quad (12-11a)$$

$$\left\{ \frac{\partial^2}{\partial R^2} + \frac{1}{R} \frac{\partial}{\partial R} + \frac{1}{R^2} \frac{\partial^2}{\partial \phi^2} - W^2 \right\} \Psi = 0; \quad 1 < R < \infty, \quad (12-11b)$$

where the normalized radius $R = r/\rho$, and U, W are defined inside the back cover. Separable solutions which are everywhere bounded vary as $J_\nu(UR)\cos(\nu\phi)$ or $J_\nu(UR)\sin(\nu\phi)$ in the core, and as $K_\nu(WR)\cos(\nu\phi)$ or $K_\nu(WR)\sin(\nu\phi)$ in the cladding, where ν is a positive integer or zero. The J_ν is the Bessel function of the first kind defined by Eq. (37-62), and K_ν is the modified Bessel function of the second kind, defined by Eq. (37-66). We explained in Section 11-16 why the modes of fibers are generally hybrid, being composed of linear combinations of TE and TM modes. They possess both e_z and h_z components, and are known as EH and HE modes. The functional forms of their fields are identical, but the values of U differ as we show in the next section. To construct the fields, we first choose longitudinal components which are continuous across the interface, i.e.

$$e_z = A \frac{J_\nu(UR)}{J_\nu(U)} f_\nu(\phi), \quad h_z = B \frac{J_\nu(UR)}{J_\nu(U)} g_\nu(\phi), \quad 0 \leq R < 1, \quad (12-12a)$$

$$e_z = A \frac{K_\nu(WR)}{K_\nu(W)} f_\nu(\phi), \quad h_z = B \frac{K_\nu(WR)}{K_\nu(W)} g_\nu(\phi), \quad 1 < R < \infty, \quad (12-12b)$$

where A and B are constants and f_ν, g_ν are defined in Table 12-3(a). The transverse components follow from Eq. (30-9), and by imposing continuity of the azimuthal components e_ϕ and h_ϕ at $R = 1$ we determine the ratio A/B and the eigenvalue equation of EH and HE modes in Table 12-4(a). Normally we would set $A = 1$. However, A is chosen for consistency with the weak-guidance results, as explained in Section 12-11. Thus, the fields have the forms in Table 12-3(a). Even and odd modes have radial electric field components which are even or odd functions of ϕ . A similar derivation for the axisymmetric TE and TM modes leads to the field components in Table 12-3(b) and the eigenvalue equations in Table 12-4(a). The notation is defined in Table 12-3(a). If the fiber is nonabsorbing, n_{co} and n_{cl} are real, and the fields obey the convention of Eq. (11-8), i.e. e_z, h_z are imaginary, and e_r, e_ϕ, h_r, h_ϕ are real. Repeating the discussion in Section 12-2, it is clear that \mathbf{e} and \mathbf{h} in Table 12-3 depend

Table 12-3 Field components of (a) HE_{vm} and EH_{vm} and (b) TE_{0m} and TM_{0m} modes of the step-profile fiber. The axes and coordinates are defined in Fig. 12-3, and $R = r/\rho$, where ρ is the core radius. Core and cladding refractive indices are n_{co} and n_{cl} , and all other parameters are defined inside the back cover.

(a)

Component	Core	Cladding
e_r	$-\frac{a_1 J_{v-1}(UR) + a_2 J_{v+1}(UR)}{J_v(U)} f_v(\phi)$	$-\frac{U a_1 K_{v-1}(WR) - a_2 K_{v+1}(WR)}{W} f_v(\phi)$
e_ϕ	$-\frac{a_1 J_{v-1}(UR) - a_2 J_{v+1}(UR)}{J_v(U)} g_v(\phi)$	$-\frac{U a_1 K_{v-1}(WR) + a_2 K_{v+1}(WR)}{W} g_v(\phi)$
e_z	$-\frac{iU J_v(UR)}{\rho\beta} \frac{f_v(\phi)}{J_v(U)}$	$-\frac{iU K_v(WR)}{\rho\beta} \frac{f_v(\phi)}{K_v(W)}$
h_r	$\left(\frac{\epsilon_0}{\mu_0}\right)^{1/2} \frac{kn_{co}^2}{\beta} \frac{a_3 J_{v-1}(UR) - a_4 J_{v+1}(UR)}{J_v(U)} g_v(\phi)$	$\left(\frac{\epsilon_0}{\mu_0}\right)^{1/2} \frac{kn_{co}^2}{\beta} \frac{U a_5 K_{v-1}(WR) + a_6 K_{v+1}(WR)}{K_v(W)} g_v(\phi)$
h_ϕ	$-\left(\frac{\epsilon_0}{\mu_0}\right)^{1/2} \frac{kn_{co}^2}{\beta} \frac{a_3 J_{v-1}(UR) + a_4 J_{v+1}(UR)}{J_v(U)} f_v(\phi)$	$-\left(\frac{\epsilon_0}{\mu_0}\right)^{1/2} \frac{kn_{co}^2}{\beta} \frac{U a_5 K_{v-1}(WR) - a_6 K_{v+1}(WR)}{K_v(W)} f_v(\phi)$
h_z	$-i\left(\frac{\epsilon_0}{\mu_0}\right)^{1/2} \frac{UF_2}{k\rho} \frac{J_v(UR)}{J_v(U)} g_v(\phi)$	$-i\left(\frac{\epsilon_0}{\mu_0}\right)^{1/2} \frac{UF_2}{k\rho} \frac{K_v(WR)}{K_v(W)} g_v(\phi)$

$f_v(\phi) = \begin{cases} \cos(v\phi), \\ \sin(v\phi), \end{cases}$	$g_v(\phi) = \begin{cases} -\sin(v\phi) & \text{even modes} \\ \cos(v\phi) & \text{odd modes} \end{cases}$
$a_1 = \frac{(F_2 - 1)}{2}; \quad a_3 = \frac{(F_1 - 1)}{2}; \quad a_5 = \frac{(F_1 - 1 + 2\Delta)}{2}$	
$a_2 = \frac{(F_2 + 1)}{2}; \quad a_4 = \frac{(F_1 + 1)}{2}; \quad a_6 = \frac{(F_1 + 1 - 2\Delta)}{2}$	
$F_1 = \left(\frac{UW}{V} \right)^2 \frac{b_1 + (1 - 2\Delta)b_2}{v}; \quad F_2 = \left(\frac{V}{UW} \right)^2 \frac{v}{b_1 + b_2}$	
$b_1 = \frac{1}{2U} \left\{ \frac{J_{v-1}(U)}{J_v(U)} - \frac{J_{v+1}(U)}{J_v(U)} \right\}$	
$b_2 = -\frac{1}{2W} \left\{ \frac{K_{v-1}(W)}{K_v(W)} + \frac{K_{v+1}(W)}{K_v(W)} \right\}$	

TM Modes

Component	Core	Cladding
e_r	$\frac{J_1(UR)}{J_1(U)}$	$\frac{n_{co}^2 K_1(WR)}{n_{cl}^2 K_1(WR)}$
e_z	$\frac{iU J_0(UR)}{\rho\beta J_1(U)}$	$\frac{-in_{co}^2 W K_0(WR)}{n_{cl}^2 \rho\beta K_1(W)}$
h_ϕ	$\left(\frac{\epsilon_0}{\mu_0} \right)^{1/2} \frac{kp^2 J_1(UR)}{\beta J_1(U)}$	$\left(\frac{\epsilon_0}{\mu_0} \right)^{1/2} \frac{kn_{co}^2 K_1(WR)}{\beta K_1(W)}$
$e_\phi = h_r = h_z = 0$		

TE Modes

Component	Core	Cladding
e_ϕ	$\frac{-J_1(UR)}{J_1(U)}$	$\frac{-K_1(WR)}{K_1(W)}$
h_r	$\left(\frac{\epsilon_0}{\mu_0} \right)^{1/2} \frac{\beta J_1(UR)}{k J_1(U)}$	$\left(\frac{\epsilon_0}{\mu_0} \right)^{1/2} \frac{\beta K_1(WR)}{k K_1(W)}$
h_z	$i \left(\frac{\epsilon_0}{\mu_0} \right)^{1/2} \frac{U J_0(UR)}{kp J_1(U)}$	$-i \left(\frac{\epsilon_0}{\mu_0} \right)^{1/2} \frac{W K_0(WR)}{kp K_1(W)}$
$e_r = e_z = h_\phi = 0$		

parametrically on V , Δ and ρ only, apart from the factor $n_{co}(\epsilon_0/\mu_0)^{1/2}$ in the magnetic field dependence.

12-9 Propagation constants

As noted above, continuity of the tangential field components at the fiber interface leads to the eigenvalue equations for the even and odd HE_{vm} and EH_{vm} modes, the TE_{0m} modes and the TM_{0m} modes in Table 12-4(a). Each mode is labelled by two subscripts. The first subscript v is the order, and the second subscript m denotes the m th root of the eigenvalue equation. The roots are ordered so that $m = 1$ corresponds to the root with the smallest value of U or, equivalently, to the largest value of β for a given value of v . Increasing values of m correspond to increasing values of U . The values of β for all modes lie within the range $kn_{cl} < \beta \leq kn_{co}$. If we follow the reasoning in Section 12-4, it is clear that the values of U depend on V , Δ and v for EH_{vm} and HE_{vm} modes, on V and Δ for TM_{0m} modes and on V alone for TE_{0m} modes. Further, the *transverse* fields of the TE_{0m} modes satisfy the scalar wave equation everywhere, including the interface, i.e. they are the polar equivalent of TE modes on the planar waveguide.

The eigenvalue equations are transcendental and must be solved numerically. Plots of U against V are presented in Fig. 12-4 for a fiber with $\Delta = 0.32$. The relatively large value of Δ helps distinguish between solutions. When $\Delta = 0$, or $n_{co} = n_{cl}$, the HE_{11} mode solution is given by the dashed curve.

Cutoff and $V = \infty$

Following the discussion in Section 11-18, the cutoff values of U are found by letting $U \rightarrow V$, $W \rightarrow 0$ in each eigenvalue equation in Table 12-4(a). Using the asymptotic form of $K_v(W)$ as $W \rightarrow 0$ in Eq. (37-86), the values of U at cutoff are given implicitly by the equations in Table 12-4(b). The even and odd HE_{11} modes are the fundamental modes, since they have the smallest value of U for all V and are not cut off. For finite values of V the modes with the smallest cutoff are the TE_{01} and TM_{01} modes; the value of U is given by the first zero of J_0 , i.e. $U \geq 2.405$. Hence the fiber is single-moded for $0 < V < 2.405$. As $V \rightarrow \infty$ the asymptotic forms of $K_v(W)$ for $W \rightarrow \infty$ in Eq. (37-88) lead to the implicit values of U in Table 12-4(b). The value of U for each mode increases monotonically with V , as is clear from Fig. 12-4.

Near to and far from cutoff

Approximations for U close to cutoff and far from cutoff can be derived, in particular, for the fundamental modes which are of importance for single-

Table 12–4 (a) Eigenvalue equations for the step-profile fiber. (b) Limiting values of the modal parameter U . (c) Fundamental modes. Parameters are defined inside the back cover.

(a)

HE _{vm} and EH _{vm} modes	$\left\{ \frac{J'_v(U)}{U J_v(U)} + \frac{K'_v(W)}{W K_v(W)} \right\} \left\{ \frac{J'_v(U)}{U J_v(U)} + \frac{n_{cl}^2}{n_{co}^2} \frac{K'_v(W)}{W K_v(W)} \right\} = \left(\frac{v\beta}{kn_{co}} \right)^2 \left(\frac{V}{U W} \right)^4$
Alternative form	$k^2 n_{co}^2 F_1 = \beta^2 F_2$
TE _{0m} modes	$\frac{J_1(U)}{U J_0(U)} + \frac{K_1(W)}{W K_0(W)} = 0$
TM _{0m} modes	$\frac{n_{co}^2 J_1(U)}{U J_0(U)} + \frac{n_{cl}^2 K_1(W)}{W K_0(W)} = 0$

(b)

Mode	Cutoff $W = 0, U = V$	$V = W = \infty$
TE _{0m} TM _{0m}	$J_0(U) = 0$	$J_1(U) = 0$
HE _{1m}	$J_1(U) = 0$	$J_0(U) = 0$
EH _{vm}	$J_v(U) = 0$	$J_{v+1}(U) = 0$
HE _{vm} ($v > 1$)	$\frac{U}{(v-1)} \frac{J_{v-2}(U)}{J_{v-1}(U)} = \frac{-2\Delta}{1-2\Delta}$	$J_{v-1}(U) = 0$

Range of single-mode operation $0 < V < 2.405$

(c)

$W \cong 1.123 \exp \left\{ \frac{-1 + \Delta}{V} \frac{J_0(V)}{J_1(V)} \right\}$	$V \ll 1$
$U \cong 2.405 \exp \left\{ -\frac{1 + \Delta}{V} \right\}$	$V \gg 1$

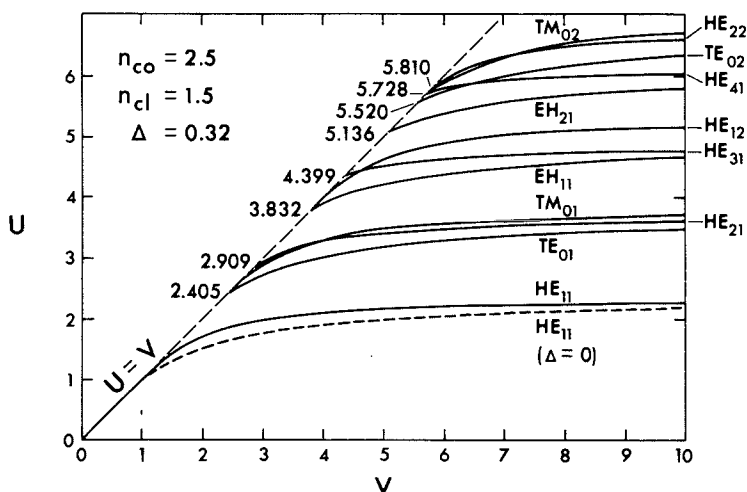


Fig. 12-4 Numerical solution of the eigenvalue equations of Table 12-4(a) for the first twelve modes. The values along the dashed line are the cutoff values of U , and the dashed curve is the fundamental mode solution for a fiber with $n_{co} = n_{cl}$ and V fixed.

mode fibers. We follow the technique described in Section 12-3 and derive an eigenvalue equation for dU/dV from the HE_{11} mode eigenvalue equation in Table 12-4(a). Far from cutoff [3] and close to cutoff [4], this leads to the expressions in Table 12-4(c). Similar expressions can be derived for other modes [3, 4]. If we compare the values of these expressions with the exact values of U in Fig. 12-4 for the HE_{11} modes, the relative error increases in the near-cutoff approximation as V increases, and in the far-from-cutoff approximation as V decreases. The error in each approximation is 8.1 per cent at $V = 1.4$.

12-10 Modal properties

If we substitute the modal fields of Table 12-3 into Table 11-1, page 230, we obtain the expressions for S_z , N , η and v_g in Table 12-5. The elemental area $dA = \rho^2 R dR d\phi$ and the integrals of Bessel functions together with recurrence relations are found in Chapter 37. We have plotted η in Fig. 12-5 for the first twelve modes, using the same parameter values as Fig. 12-4. The dashed curve gives the values of η for the HE_{11} mode when $\Delta = 0$, i.e. when $n_{co} = n_{cl}$.

Polarization of the modal fields

At any position in the fiber cross-section the modal electric field is expressible as a linearly polarized field, but since the field varies with position, the direction

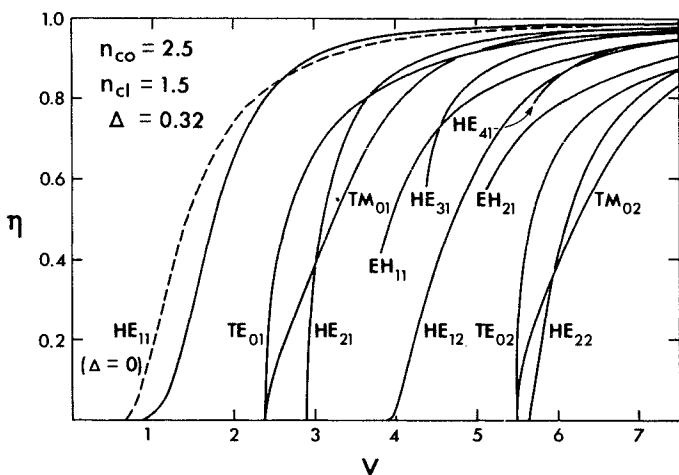


Fig. 12-5 The fraction of modal power residing in the core for each of the first twelve modes as a function of V . The dashed curve is for the fundamental modes when $n_{co} = n_{cl}$ and V fixed.

of the electric field changes over the cross-section as shown in Fig. 12-6. For the axisymmetric TE_{0m} or TM_{0m} modes the electric field lines are circles or lie in planes through the fiber axis, respectively.

Modal intensity patterns

The intensity S_z for EH and HE modes in Table 12-5 varies both radially and azimuthally. Only for the TE and TM modes is S_z axisymmetric, as exemplified by the TE_{01} and TM_{01} modes in Fig. 12-7, where darker shading denotes higher intensity. The intensity is zero on axis and has a maximum at $UR \cong 1.8$.

Near to and far from cutoff

Unlike the modes of the planar waveguide, only some of the modes of the fiber have zero power within the core at cutoff, i.e. $\eta = 0$ in Fig. 12-5. This includes the TE_{0m} , TM_{0m} , HE_{1m} and HE_{2m} modes, all other modes having $\eta > 0$ at cutoff. We then deduce from Table 12-5 that only modes with $\eta = 0$ have a group velocity at cutoff equal to the speed of light in the cladding c/n_{cl} . The remaining modes have $v_g < c/n_{cl}$.

Far from cutoff, all modes have their power concentrated in the core, i.e. $\eta \rightarrow 1$ as $V \rightarrow \infty$, and hence their group velocity approaches the speed of light in the core c/n_{co} .

Table 12-5 Modal properties of the step-profile fiber. All quantities except M_{bm} are calculated from Table 11-1, page 230. Parameters are defined in Table 12-3(a) and inside the back cover. The + and - refer to even and odd modes, $R = r/\rho$ and a is the modal amplitude.

		Core	Cladding
S_z	TE_{0m}	$\frac{ a ^2}{2} \left(\frac{\epsilon_0}{\mu_0} \right)^{1/2} \frac{\beta}{k} \frac{J_1^2(UR)}{J_1^2(U)}$	$\frac{ a ^2}{2} \left(\frac{\epsilon_0}{\mu_0} \right)^{1/2} \frac{\beta}{k} \frac{K_1^2(WR)}{K_1^2(W)}$
	TM_{0m}	$\frac{ a ^2}{2} \left(\frac{\epsilon_0}{\mu_0} \right)^{1/2} \frac{k n_{\infty}^2}{\beta} \frac{J_1^2(UR)}{J_1^2(U)}$	$\frac{ a ^2}{2} \left(\frac{\epsilon_0}{\mu_0} \right)^{1/2} \frac{k n_{\infty}^2}{\beta(1-2\Delta)} \frac{K_1^2(WR)}{K_1^2(W)}$
	EH_{vm} and HE_{vm}	$\frac{ a ^2}{2} \left(\frac{\epsilon_0}{\mu_0} \right)^{1/2} \frac{k n_{\infty}^2}{\beta J_v^2(U)} \left\{ a_1 a_3 J_{v-1}^2(UR) \right.$ $+ a_2 a_4 J_{v+1}^2(UR)$ $\left. \mp \frac{1 - F_1 F_2}{2} J_{v-1}(UR) J_{v+1}(UR) \cos(2v\phi) \right\}$	$\frac{ a ^2}{2} \left(\frac{\epsilon_0}{\mu_0} \right)^{1/2} \frac{k n_{\infty}^2}{\beta K_v^2(W)} \frac{U^2}{W^2} \left\{ a_1 a_5 K_{v-1}^2(WR) \right.$ $+ a_2 a_6 K_{v+1}^2(WR)$ $\left. \pm \frac{1 - 2\Delta - F_1 F_2}{2} K_{v-1}(WR) K_{v+1}(WR) \cos(2v\phi) \right\}$

$N = N_{\text{co}} + N_{\text{cl}}$	TE_{0m}	N_{co}		$\frac{\pi \rho^2}{2} \left(\frac{\varepsilon_0}{\mu_0} \right)^{1/2} \frac{\beta}{k} \left\{ 1 - \frac{J_0(U) J_2(U)}{J_1^2(U)} \right\}$	$-\frac{\pi \rho^2}{2} \left(\frac{\varepsilon_0}{\mu_0} \right)^{1/2} \frac{\beta}{k} \left\{ 1 - \frac{K_0(W) K_2(W)}{K_1^2(W)} \right\}$
	TM_{0m}	N_{cl}		$\frac{\pi \rho^2}{2} \left(\frac{\varepsilon_0}{\mu_0} \right)^{1/2} \frac{kn_{\text{co}}^2}{\beta} \left\{ 1 - \frac{J_0(U) J_2(U)}{J_1^2(U)} \right\}$	$-\frac{\pi \rho^2}{2} \left(\frac{\varepsilon_0}{\mu_0} \right)^{1/2} \frac{kn_{\text{co}}^2}{\beta(1-2\Delta)} \left\{ 1 - \frac{K_0(W) K_2(W)}{K_1^2(W)} \right\}$
	EH_{vm} and HE_{vm}			$\frac{\pi \rho^2}{2} \left(\frac{\varepsilon_0}{\mu_0} \right)^{1/2} \frac{kn_{\text{co}}^2}{\beta J_v^2(U)} [a_1 a_3 \{J_{v-1}^2(U)\} - J_v(U) J_{v-2}(U)] + a_2 a_4 \{J_{v+1}^2(U) - J_v(U) J_{v+2}(U)\}]$	$-\frac{\pi \rho^2}{2} \left(\frac{\varepsilon_0}{\mu_0} \right)^{1/2} \frac{kn_{\text{co}}^2}{\beta K_v^2(W) W^2} [a_1 a_5 \{K_{v-1}^2(W)\} - K_v(W) K_{v-2}(W)] + a_2 a_6 \{K_{v+1}^2(W) - K_v(W) K_{v+2}(W)\}]$
η	All	$\frac{N_{\text{co}}}{N_{\text{co}} + N_{\text{cl}}}$			
v_g	All	$\frac{c}{n_{\text{co}}^2} \frac{\beta}{k} \frac{1}{1-2\Delta(1-\eta)}$			
M_{bm}		$\text{Int} \left\{ \frac{V^2}{2} \right\}; \quad V \gg 1$			

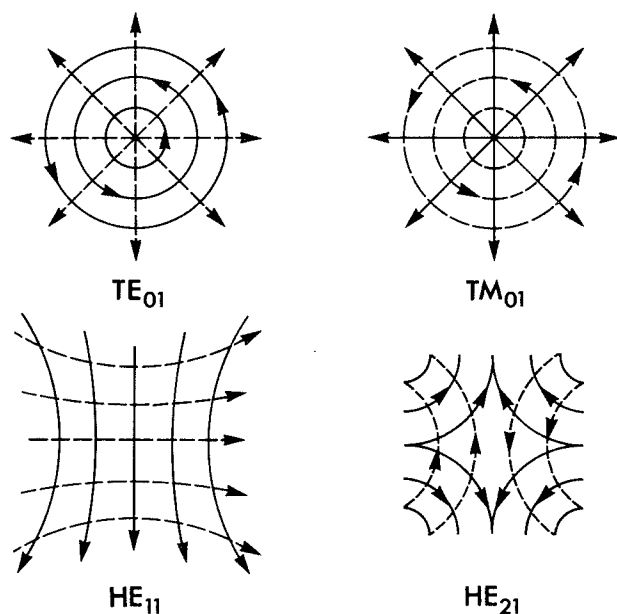


Fig. 12-6 The directions of the electric and magnetic field vectors, denoted by continuous and broken curves, for low order modes, showing the pattern in the cross-section of a step-profile fiber. When $n_{co} = n_{cl}$ and V is fixed, the fundamental mode-pattern becomes a rectangular grid.

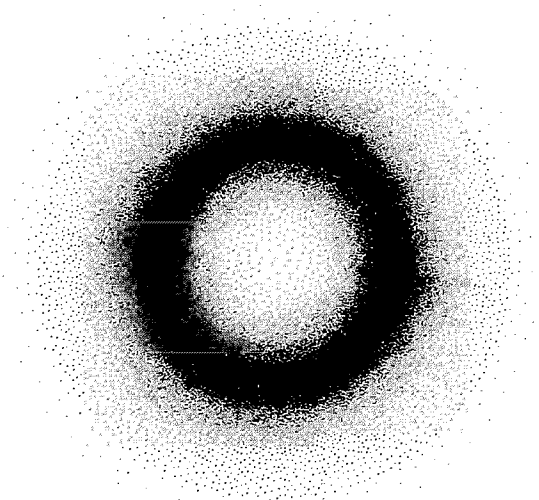


Fig. 12-7 Qualitative representation of light intensity over the core of the step-profile fiber for the axisymmetric TE_{01} and TM_{01} modes. Darker shading corresponds to higher intensity.

Number of modes

It is harder to count the number of bound mode solutions M_{bm} for the fiber, than it is for the planar waveguide, because the roots of the eigenvalue equations in Table 12-4(a) are now not uniformly spaced, even at cutoff. However, we show in Section 36-13 that, provided the fiber is multimoded with $V \gg 1$, $M_{\text{bm}} = \text{Int}(V^2/2)$, the smallest integer just exceeding $V^2/2$.

12-11 Weakly guiding fiber

The fiber is weakly guiding if $n_{\text{co}} \cong n_{\text{cl}}$ or, equivalently, if $\Delta \ll 1$. Under this condition, $\beta \cong kn_{\text{co}}$ and the eigenvalue equations of Table 12-4(a) have solutions virtually independent of Δ , i.e. insensitive to the polarization properties of the fiber. With k in terms of V , we have $\beta \cong V/\rho(2\Delta)^{1/2}$, which, combined with $\Delta \ll 1$ in Table 12-3, leads to $|\mathbf{e}_t| \gg |e_z|$, $|\mathbf{h}_t| \gg |h_z|$. Consequently the modes are nearly TEM waves [5].

Expansion of the exact modal fields

It is sometimes useful to know the first few terms in the expansion of the modal fields for $\Delta \ll 1$. As an illustration we consider the two fundamental modes because of their importance in single-mode fibers. Section 32-1 discusses these expansions at length, so it is sufficient to summarize results here. The lowest order fields and values of the modal parameters for the weakly guiding fiber are discussed at length in Chapters 13 and 14. The expansions are in powers of $\Delta^{1/2}$. Correct to third order, the even HE_{11} mode field expansions are

$$\mathbf{e} = \tilde{\mathbf{e}}_x \hat{\mathbf{x}} + \Delta^{1/2} e_z^{(1/2)} \hat{\mathbf{z}} + \Delta \{e_x^{(1)} \hat{\mathbf{x}} + e_y^{(1)} \hat{\mathbf{y}}\} + \Delta^{3/2} e_z^{(3/2)} \hat{\mathbf{z}}, \quad (12-13a)$$

$$\mathbf{h} = \tilde{\mathbf{h}}_y \hat{\mathbf{y}} + \Delta^{1/2} h_z^{(1/2)} \hat{\mathbf{z}} + \Delta \{h_x^{(1)} \hat{\mathbf{x}} + h_y^{(1)} \hat{\mathbf{y}}\} + \Delta^{3/2} h_z^{(3/2)} \hat{\mathbf{z}}, \quad (12-13b)$$

where $\hat{\mathbf{x}}$, $\hat{\mathbf{y}}$ and $\hat{\mathbf{z}}$ are unit vectors parallel to the axes in Fig. 12-3, a \sim denotes the weak-guidance, or zero-order, fields, and superscripts denote the order in Δ . Cartesian and cylindrical polar field components are related by Eq. (37-49). The coefficients of each power of Δ in Table 12-6 are obtained by expanding the exact fields of Table 12-3(a), for which we require the expansions of the modal parameters correct to order Δ , i.e.

$$U = \tilde{U} + \Delta U^{(1)}; \quad W = \tilde{W} + \Delta W^{(1)}, \quad (12-14)$$

where \tilde{U} and \tilde{W} are defined inside the back cover. If we substitute these expansions into the eigenvalue equation of Table 12-4(a) and equate powers of Δ , we obtain the eigenvalue equation satisfied by \tilde{U} and \tilde{W} and the expressions for $U^{(1)}$ and $W^{(1)}$ in Table 12-6. Relationships between the Bessel functions are given by Eqs. (37-72) and (37-73). The choice of normalization of the exact fields in Table 12-5 was made to ensure that $\tilde{e}_x = 1$ at the interface.

Table 12-6 Weak-guidance expansion of the even $HE_{1,1}$ mode fields of the step-profile fiber. Coefficients of the expansion of Eq. (12-13) correct to third order, where $k = r/\rho$ and parameters are defined inside the back cover.

	Core	Cladding
\tilde{e}_x	$\frac{J_0(\tilde{U}R)}{J_0(\tilde{U})}$	$\frac{K_0(\tilde{W}R)}{K_0(\tilde{W})}$
\tilde{e}_y	0	0
$e_z^{(1/2)}$	$-2^{1/2}i \frac{\tilde{U}}{V} \frac{J_1(\tilde{U}R)}{J_0(\tilde{U})} \cos \phi$	$-2^{1/2}i \frac{\tilde{W}}{V} \frac{K_1(\tilde{W}R)}{K_0(\tilde{W})} \cos \phi$
\tilde{h}_x	0	0
\tilde{h}_y	$n_{co} \left(\frac{\epsilon_0}{\mu_0} \right)^{1/2} \frac{J_0(\tilde{U}R)}{J_0(\tilde{U})}$	$n_{co} \left(\frac{\epsilon_0}{\mu_0} \right)^{1/2} \frac{K_0(\tilde{W}R)}{K_0(\tilde{W})}$
$h_z^{(1/2)}$	$-2^{1/2}in_{co} \left(\frac{\epsilon_0}{\mu_0} \right)^{1/2} \frac{\tilde{U}}{V} \frac{J_1(\tilde{U}R)}{J_0(\tilde{U})} \sin \phi$	$-2^{1/2}in_{co} \left(\frac{\epsilon_0}{\mu_0} \right)^{1/2} \frac{\tilde{W}}{V} \frac{K_1(\tilde{W}R)}{K_0(\tilde{W})} \sin \phi$
$e_x^{(1)}$	$-\frac{\tilde{U}\tilde{U}^{(1)}}{J_0(\tilde{U})} \left\{ J_0(\tilde{U}R) + \frac{2R}{\tilde{U}} J_1(\tilde{U}R) + J_2(\tilde{U}R) \cos 2\phi \right\}$	$\frac{\tilde{W}\tilde{W}^{(1)}}{K_0(\tilde{W})} \left\{ K_0(\tilde{W}R) - \frac{2R}{\tilde{W}} K_1(\tilde{W}R) - K_2(\tilde{W}R) \cos 2\phi \right\}$
$e_y^{(1)}$	$-\tilde{U}\tilde{U}^{(1)} \frac{J_2(\tilde{U}R)}{J_0(\tilde{U})} \sin 2\phi$	$\tilde{W}\tilde{W}^{(1)} \frac{K_2(\tilde{W}R)}{K_0(\tilde{W})} \sin 2\phi$

	Core	Cladding
$e_z^{(3/2)}$	$-\frac{2^{3/2}i\tilde{U}}{VJ_0(\tilde{U})}\left\{\frac{\tilde{U}^2}{2V^2}J_1(\tilde{U}R)+\tilde{U}^{(1)}RJ_0(\tilde{U}R)\right\}\cos\phi$	$-\frac{2^{3/2}\tilde{W}}{VK_0(\tilde{W})}\left\{\frac{\tilde{U}^2}{2V^2}K_1(\tilde{W}R)-\tilde{W}^{(1)}RK_0(\tilde{W}R)\right\}\cos\phi$
$h_x^{(1)}$	$n_{\text{co}}\left(\frac{\epsilon_0}{\mu_0}\right)^{1/2}\left\{\frac{\tilde{U}^2}{V^2}+\tilde{U}U^{(1)}\right\}\frac{J_2(\tilde{U}R)}{J_0(\tilde{U})}\sin 2\phi$	$n_{\text{co}}\left(\frac{\epsilon_0}{\mu_0}\right)^{1/2}\left\{\frac{\tilde{W}^2}{V^2}+\tilde{W}W^{(1)}\right\}\frac{K_2(\tilde{W}R)}{K_0(\tilde{W})}\sin 2\phi$
$h_y^{(1)}$	$-\frac{n_{\text{co}}}{J_0(\tilde{U})}\left(\frac{\epsilon_0}{\mu_0}\right)^{1/2}\left\{\frac{\tilde{U}U^{(1)}}{2}J_0(\tilde{U}R)+2\tilde{U}^{(1)}RJ_1(\tilde{U}R)\right. \\ \left.+\left(\frac{\tilde{U}^2}{V^2}+\tilde{U}U^{(1)}\right)J_2(\tilde{U}R)\cos 2\phi\right\}$	$-\frac{n_{\text{co}}}{K_0(\tilde{W})}\left(\frac{\epsilon_0}{\mu_0}\right)^{1/2}\left\{1-\tilde{W}W^{(1)}K_0(\tilde{W}R)+2\tilde{W}^{(1)}RK_1(\tilde{W}R)\right. \\ \left.+\left(\frac{\tilde{W}^2}{V^2}+\tilde{W}W^{(1)}\right)K_2(\tilde{W}R)\cos 2\phi\right\}$
$h_z^{(3/2)}$	$\frac{2^{3/2}in_{\text{co}}}{J_0(\tilde{U})}\left(\frac{\epsilon_0}{\mu_0}\right)^{1/2}\frac{\tilde{U}U^{(1)}}{V}\left\{\tilde{U}J_1(\tilde{U}R)-RJ_0(\tilde{U}R)\right\}\sin\phi$	$-\frac{2^{3/2}in_{\text{co}}}{K_0(\tilde{W})}\left(\frac{\epsilon_0}{\mu_0}\right)^{1/2}\frac{\tilde{W}W^{(1)}}{V}\left\{\tilde{W}K_1(\tilde{W}R)-RK_0(\tilde{W}R)\right\}\sin\phi$
Eigenvalue equation		$\tilde{U}\frac{J_1(\tilde{U})}{J_0(\tilde{U})}=\tilde{W}\frac{K(\tilde{W})}{K_0(\tilde{W})}; \quad \tilde{U}^2+\tilde{W}^2=V^2; \quad F_1\cong-1+2\Delta\left\{\tilde{U}U^{(1)}+\frac{\tilde{U}^2}{V^2}\right\}; \quad F_2\cong-1+2\Delta\tilde{U}U^{(1)}$
Modal corrections		$U^{(1)}=\frac{\tilde{U}\tilde{W}}{V^2}\frac{K_0(\tilde{W})}{K_1(\tilde{W})}; \quad W^{(1)}=-\frac{\tilde{U}^2}{V^2}\frac{K_0(\tilde{W})}{K_1(\tilde{W})}; \quad \tilde{U}U^{(1)}=-\tilde{W}W^{(1)}$

12–12 Plane-wave decomposition of the modal fields

Unlike the planar waveguide, the core fields of the fiber are not given by the superposition of two families of plane waves, and require a continuum representation as discussed in Section 36–2. However, if the fiber is multimoded, the higher-order modes, i.e. those modes with $U \gg 1$ or $v \gg 1$ in Table 12–3, can be accurately approximated by the superposition of plane waves propagating in four directions. Each plane wave, or ray, propagates at angle θ_z to the fiber axis, where $\beta = kn_{\text{co}} \cos \theta_z$, and its projection onto the core cross-section makes angle θ_ϕ with the azimuthal direction, where $v = kn_{\text{co}} r \sin \theta_z \times \cos \theta_\phi$. The range of bound-ray directions is given by Eq. (2–6a), where $\theta_c = \sin^{-1} (1 - n_{\text{cl}}^2/n_{\text{co}}^2)$ is the complement of the critical angle of geometric optics. Relationships between modal parameters, ray angles, and ray invariants are given in Table 36–1, page 592. On weakly guiding fibers $\beta \cong kn_{\text{co}}$ and the rays are paraxial, i.e. $\theta_z \ll 1$. The discrete values of β correspond to the preferred ray directions discussed in Section 10–7.

Mode and ray transit times

The expressions for group velocity in Tables 12–5 and 12–2 are identical, and consequently the modal transit time $t = z/v_g$ over length z of fiber is identical with the corresponding expression for the planar waveguide. Since the ray transit times t_{go} of Table 1–1, page 19, and Table 2–1, page 40, are also identical, it follows that t and t_{go} for the fiber are also related by Eq. (12–8), and are only equal when $\theta_z \ll \theta_c$, as discussed in Section 12–6. For angles $\theta_z \cong \theta_c$, the times differ because t_{go} neglects diffraction effects. Unlike the planar waveguide, diffraction effects are not fully accounted for by incorporating the lateral shift of Chapter 10. There are additional diffraction effects caused by the curvature of the fiber interface, since η depends on the azimuthal order v .

Eigenvalue equations

In Section 36–7 we show how to derive eigenvalue equations for higher-order modes on multimode fibers by applying a consistency condition on the phase change along the trajectory of each plane wave. These equations are the large order limit of the eigenvalue equations in Table 12–4(a).

12–13 Multilayered and elliptical fibers

The analysis of the step-profile fiber is readily extended to multilayered fibers with a uniform refractive index in each layer. An example of this is the W fiber, which has three layers with a smaller index in the centre layer than in the two adjacent layers [6]. The modal fields and eigenvalue equations for such structures are constructed from the appropriate solution of Eq. (12–11) in each layer, ensuring that the tangential fields are continuous at each interface.

If the interface of the step-profile fiber has an elliptical cross-section, the methods of Section 12-1 can be used to derive the modal fields and eigenvalue equations for *arbitrary* eccentricity. Unfortunately, it is difficult to gain insight into the effects of eccentricity because the field expressions involve infinite sets of Mathieu functions [7].

GRADED-PROFILE WAVEGUIDES

There are few known examples of graded profiles which lead to exact solutions of Maxwell's equations for the modal fields, and most of these are of little practical interest. The solutions are usually not expressible in terms of simple functions, but they do provide a useful check on numerical and approximate solutions. In the following examples we provide only a schematic derivation, listing profiles and the corresponding modal fields and eigenvalue equations. The derivations do not follow the approach of Section 12-1, as the longitudinal field components are coupled throughout the graded profile region. Instead, we start from the component equations of the vector wave equation of Eq. (30-14). The following set of examples provides a fairly comprehensive range of profiles with exact modal field solutions, but is by no means complete.

12-14 Example: TE modes on graded-profile planar waveguides

The planar waveguide of Fig. 12-1 has refractive-index profile $n(x)$, and the modal fields have the separable form of Eq. (12-5). Under these conditions there are consistent solutions of Maxwell's equations with $e_x = e_z = h_y = 0$ in Eq. (30-5). These are TE modes and e_y satisfies Eq. (30-21b). If we express the profile in the general form

$$n^2(X) = n_{co}^2 \{1 - 2\Delta f(X)\}; \quad X = x/\rho, \quad (12-15)$$

where $f(X) \geq 0$, then by substituting into Eq. (30-21b) and referring to the definitions inside the back cover we have

$$\left\{ \frac{d^2}{dX^2} + U^2 - V^2 f(X) \right\} e_y = 0, \quad (12-16)$$

and hence e_y satisfies the scalar wave equation. Remaining field components are given by Eq. (30-5) as

$$h_x = -\left(\frac{\varepsilon_0}{\mu_0}\right)^{1/2} \frac{\beta}{k} e_y; \quad h_z = -\left(\frac{\varepsilon_0}{\mu_0}\right)^{1/2} \frac{i}{k} \frac{de_y}{dx}. \quad (12-17)$$

In Table 12-7 we give profiles which lead to closed-form solutions for e_y and the corresponding eigenvalue equations. Each profile is symmetrical in x and is plotted in Fig. 12-8. The parameter ρ scales profiles (a) to (f), which do not have a well-defined interface, and the waveguide parameter is defined by $V = k\rho n_{co}(2\Delta)^{1/2}$. For each such profile, the eigenvalue equation is obtained by requiring that e_y be bounded everywhere, and that e_y and de_y/dx be continuous at $x = 0$. Profiles (a), (d) and (e) are unphysical

Table 12-7 TE modes of symmetric graded-profile planar waveguides. Parameters are defined inside the back cover. Prime denotes differentiation with respect to argument, and $X = x/\rho$. Even and odd refers to modes with e_y an even or odd function of x . In profile (b) n is a positive integer or zero, and p of profile (c) is not necessarily an integer. On profiles (a), (d) and (e) all modes are bound.

	Profile $n^2(X)$	Electric field e_y	Eigenvalue equation
(a)	$n_{co}^2 \{1 - 2\Delta X^2\}$	$\exp(-V X^2/2) H_n(X V^{1/2})$	$U = (2n+1)^{1/2} V^{1/2}$
(b)	$n_{co}^2 \{1 - 2\Delta \tanh^2 X\}$	$P_s^{n-s}(\tanh X)$; $s = \{(4V^2 + 1)^{1/2} - 1\}/2$	$U = \{V^2 - (s-n)^2\}^{1/2}$
(c)	$n_{co}^2 \{1 - 2\Delta[1 - \exp(-2 X)]\}$	$J_p(V \exp(- X))$ even	$J'_p(V) = 0$ even
		$(X/ X) J_p(V \exp\{- X \})$ odd	$J_p(V) = 0$ odd
(d)	$n_{co}^2 \{1 - 2\Delta \tan^2 X\}$ $-\pi/2 \leq X \leq \pi/2$	$\cos^a X \sum_{i=m}^n c_i \sin^2 X$ even: $m=0$ n, i even	$U = \{(n+a)^2 - V^2\}^{1/2}$
		$\frac{c_{i+2}}{c_i} = \frac{(n-i)(n+i+2a)}{(i+1)(i+2)}$ odd: $m=1$ n, i odd	$a = \{(4V^2 + 1)^{1/2} + 1\}/2$
(e)	$n_{co}^2 \{1 - 2\Delta X \}$	$\text{Ai}(\{ X V^2 - U^2\}/V^{4/3})$ even	$\text{Ai}'(-U^2/V^{4/3}) = 0$ even
		$(X/ X)\text{Ai}(\{ X V^2 - U^2\}/V^{4/3})$ odd	$\text{Ai}(-U^2/V^{4/3}) = 0$ odd

(f)	$n_{\infty}^2 \left\{ 1 - 2\Delta \left[1 - \frac{1}{(1 + X ^2)^2} \right] \right\}$	$F^{1/2} K_{iv}(WF)$	even	$K_{iv}(W) = -2W K'_{iv}(W)$	even	$v^2 = V^2 - 1/4$
		$(X/ X) F^{1/2} K_{iv}(WF)$	odd	$K_{iv}(W) = 0$	odd	$F = 1 + X $
(g)	$n_{\infty}^2 \{ 1 - 2\Delta X^2 \}$ $0 \leq X \leq 1$	$\exp(-V X^2/2) M_e(V X^2)/M_e(V)$	even	$2M'_e(V) - M_e(V) = -W$	even	$M_e(V X^2) = M \left(-\frac{U^2}{4V} + \frac{1}{4}, \frac{1}{2}, V X^2 \right)$
		$\exp(-V X^2/2) M_o(V X^2)/M_o(V)$	odd			
		$\exp(-W \{ X - 1 \} - V/2)$	even	$2M'_o(V) + M_o(V) = -W$	odd	
		$(X/ X) \exp(-W \{ X - 1 \} - V/2)$	odd	$M_o(V X^2) = M \left(\frac{U^2}{4V} + \frac{1}{4}, \frac{1}{2}, V X^2 \right)$		

since $n^2(x) \rightarrow -\infty$ as $x \rightarrow \pm\infty$ for the first two, or $x \rightarrow \pm\pi/2$ for the latter. However, provided V is large enough, modal power will be confined close to $x = 0$, and the effect of the profile for $|x| \gg \rho$ will be negligible.

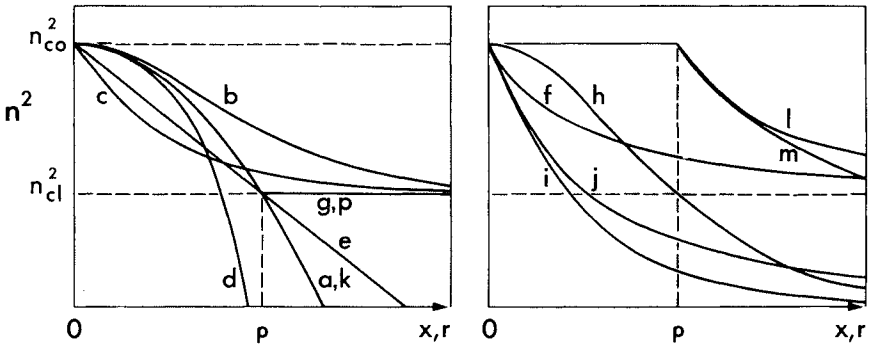


Fig. 12-8 Plots of the profiles in Tables 12-7 to 12-9 as a function of the transverse coordinate x for planar waveguides or the radius r for fibers, where ρ is the core half-width or core radius, respectively.

In Table 12-7, the field for the *infinite parabolic profile* (a) is in terms of the Hermite polynomial H_n of order $n \geq 0$ [8]. This is the solution of Eq. (12-16) after making the transformations $w = XV^{1/2}$ and $e_y = \exp(-w^2/2)g(w)$. Even and odd modes correspond to even and odd values of n , respectively. The fundamental mode has the largest value of β , i.e. $n = 0$, and from inside the back cover we deduce

$$e_y = \exp(-VX^2/2); \quad U = V^{1/2}. \quad (12-18)$$

The H_n are given explicitly in Eq. (37-107) for low-order modes. For the *hyperbolic tangent profile* (b), the transformation $w = \tanh X$ of Eq. (12-15) leads to Legendre's equation. The field is in terms of the associated Legendre function P_s^{n-s} , where s is not necessarily an integer, and even and odd values of $n \geq 0$ correspond to even and odd modes [9]. The transformation $w = V \exp(-|X|)$ of Eq. (12-16) for the *exponential profile* (c) generates Bessel's equation, and e_y varies with the Bessel function of the first kind, J_p , whose order p is determined implicitly by continuity at $x = 0$ [8]. The *tangent profile* (d) is only defined over a finite region. It is readily verified that the series for e_y satisfies Eq. (12-16) [10]. For the fundamental mode, $n = 0$, the field is

$$e_y = \cos^a X; \quad U = a^{1/2}. \quad (12-19)$$

The transformation $w = (V^2X - U^2)/V^{4/3}$ of Eq. (12-16) for the *linear profile* (e) gives Airy's equation, and e_y is expressed in terms of the Airy function of the first kind Ai [11]. The *inverse-square profile* (f) has e_y in terms of the modified Bessel function of the second kind K_{iv} of pure imaginary order [12]. This function satisfies an equation similar to Bessel's equation obtained by setting $w = (1 + X)W$ and $e_y = w^{1/2}g(w)$ in Eq. (12-16), where $W = (V^2 - U^2)^{1/2}$. Finally, the *clad-parabolic profile* (g) is an example of a composite profile, with the parabolic variation of (a) in the core and a uniform cladding index n_{cl} . Thus the profile is continuous at the interface. The transformations $w = XV^{1/2}$ and $e_y = \exp(-w^2/2)g(w)$ of Eq. (12-16) for the core lead to the even and odd mode fields in terms of the confluent hypergeometric functions denoted by $M_c(w^2)$

and $M_0(w^2)$, respectively [13]. In the cladding e_y varies as $\exp(-W|X|)$. Other composite profiles can be constructed in a similar manner from the profiles in Table 12-7.

12-15 Example: TM modes on graded-profile planar waveguides

There is a second set of consistent solutions of Maxwell's equations for planar waveguides with $e_y = h_x = h_z = 0$ in Eq. (30-5). These are TM modes, and the dimensionless form of Eq. (30-21e) for h_y is

$$\left\{ \frac{d^2}{dX^2} - \frac{dn^2}{dX} \frac{d}{dX} + U^2 - V^2 f(X) \right\} h_y = 0, \quad (12-20)$$

where $n = n(X)$, $X = x/\rho$ and $f(X)$ is defined by Eq. (12-15). One method of solving this equation is to first make the transformation $h_y = n(X)g(X)$ leading to [12]

$$\left\{ \frac{d^2}{dX^2} + U^2 - V^2 f(X) + \frac{1}{n} \frac{d^2 n}{dX^2} - \frac{2}{n^2} \left(\frac{dn}{dX} \right)^2 \right\} g = 0. \quad (12-21)$$

If we then impose the condition

$$\frac{1}{n} \frac{d^2 n}{dX^2} - \frac{2}{n^2} \left(\frac{dn}{dX} \right)^2 = A, \quad (12-22)$$

where A is a constant, Eq. (12-21) is identical with Eq. (12-16) provided we replace $U^2 + A$ by U^2 . Since e_z is continuous, we deduce from Eq. (30-5b) that both h_y and dh_y/dx are everywhere continuous. Apart from the step profile, there are three profiles satisfying Eq. (12-22) which lead to closed-form solutions of Eq. (12-21) and support bound modes. Each profile is plotted in Fig. 12-8, and is presented in Table 12-8 together with h_y and the corresponding eigenvalue equation. Profiles (h), (i) and (j) are special cases of profiles (b), (c) and (f), respectively, in Table 12-7 when $2\Delta = 1$ and the waveguide parameter $\bar{V} = k\rho n_{co}$. Remaining field components follow from Eq. (30-5) as

$$e_x = \left(\frac{\mu_0}{\epsilon_0} \right)^{1/2} \frac{\beta}{kn^2} h_y; \quad e_z = \left(\frac{\mu_0}{\epsilon_0} \right)^{1/2} \frac{i}{kn^2} \frac{dh_y}{dx}. \quad (12-23)$$

and Eq. (12-5) gives the complete spatial dependence of each TM mode.

The profiles in Table 12-8 satisfy $n(X) \rightarrow 0$ as $|X| \rightarrow \infty$. The value of A follows by substituting each profile into Eq. (12-22). The solution of Eq. (12-21) for profiles (h), (i) or (j) is obtained by analogy with the solution of Eq. (12-16) for profiles (b), (c) or (f), respectively, in Table 12-7.

12-16 Example: TE modes on graded-profile fibers

The circularly symmetric fiber of Fig. 12-3 has refractive-index profile $n(r)$, and the modal fields have the separable form of Eq. (12-10). If we examine Eq. (30-15), then there are consistent solutions of the vector wave equation provided the fields are independent of ϕ and $e_r = e_z = h_\phi = 0$. These are TE mode solutions, and e_ϕ satisfies Eq. (30-15b), which in normalized form reduces to

$$\left\{ \frac{d^2}{dR^2} + \frac{1}{R} \frac{d}{dR} - \frac{1}{R^2} + U^2 - V^2 f(R) \right\} e_\phi = 0, \quad (12-24)$$

Table 12-8 TM modes of symmetric graded-profile planar waveguide. Prime denotes differentiation with respect to argument, and $X = x/\rho$. Even and odd refers to modes with e_x an even or odd function of x . The parameters $\bar{V} = k\rho n_{\text{co}}$, $\bar{W} = \beta\rho$ and all other parameters are defined inside the back cover. In profile (h) n is a positive integer or zero, and p of profile (i) is not necessarily an integer.

	Profile $n^2(X)$	Magnetic field h_y	Eigenvalue equation	
(h)	$n_{\text{co}}^2 \operatorname{sech}^2 X$	$\operatorname{sech} X P_s^{n-1}(\tanh X)$; $s = \{(4\bar{V}^2 + 1)^{1/2} - 1\}/2$	$U = \{\bar{V}^2 + 1 - (n-s)^2\}^{1/2}$	
(i)	$n_{\text{co}}^2 \exp(-2 X)$	$\exp(- X) J_p(V \exp\{- X \})$ even	$J_p(\bar{V}) = -V J'_p(\bar{V})$ even	$U = (\bar{V}^2 + 1 - p^2)^{1/2}$
		$\{(X/ X) \exp(- X)\} J_p(V \exp\{- X \})$ odd	$J_p(\bar{V}) = 0$ odd	
(j)	$\frac{n_{\text{co}}^2}{(1 + X)^2}$	$F^{-1/2} K_{1v}(\bar{W} F)$ even	$K_{1v}(\bar{W}) = -2\bar{W} K'_{1v}(\bar{W})$ even	$v^2 = V^2 - 1/4$
		$(X/ X) F^{-1/2} K_{1v}(\bar{W} F)$ odd	$K_{1v}(\bar{W}) = 0$ odd	$F = 1 + X $

where $R = r/\rho$ and the profile is expressed as

$$n^2(R) = n_{co}^2 \{1 - 2\Delta f(R)\}. \quad (12-25)$$

Accordingly e_ϕ satisfies the scalar wave equation. Remaining field components follow from Eq. (30-5) as

$$h_r = -\left(\frac{\varepsilon_0}{\mu_0}\right)^{1/2} \frac{\beta}{k} e_\phi; \quad h_z = -\left(\frac{\varepsilon_0}{\mu_0}\right)^{1/2} \frac{i}{kr} \frac{d}{dr}(r e_\phi). \quad (12-26)$$

Profiles leading to closed-form solutions of Eq. (12-24) are plotted in Fig. 12-8, and are presented together with e_ϕ and the corresponding eigenvalue equations in Table 12-9.

For the *infinite parabolic profile* (k), the transformations $w = RV^{1/2}$ and $e_\phi = w \exp(-w^2/2)g(w)$ of Eq. (12-24) lead to an equation whose solution is the generalized Laguerre polynomial $L_n^{(1)}$ of order $n \geq 0$ [13]. Profile (l), the *clad inverse-square profile* comprises a uniform core and a cladding in which the profile varies with the inverse square of the cylindrical radius. The core field is in terms of the Bessel function of the first kind J_1 of order one and the cladding field is in terms of the modified Bessel function of the second kind K_{iv} of pure imaginary order. Next, the *clad inverse-linear profile* (m) is identical to profile (l) in the core, but has an inverse dependence on radius for its cladding profile. The cladding field is given by the Whittaker function $W_{v,1}$ [14]. Lastly, the *clad parabolic profile* (p) is equal to profile (k) in the core and has a uniform cladding index, so that there is continuity at the interface. The core field is in terms of the Whittaker function $M_{v,\mu}$ [13] and the cladding field varies with K_1 , the modified Bessel function of the second kind. We discuss TE modes on profile (m) in Section 12-18.

12-17 Example: TM modes on graded-profile fibers

There is a second set of solutions of Eq. (30-15) which are independent of ϕ . These are the TM modes, for which $e_\phi = h_r = h_z = 0$ and h_ϕ satisfies Eq. (30-15e). In normalized form this equation becomes

$$\left\{ \frac{d^2}{dR^2} + \left(\frac{1}{R} - \frac{2}{n} \frac{dn}{dR} \right) \frac{d}{dR} - \frac{2}{nR} \frac{dn}{dR} - \frac{1}{R^2} + U^2 - V^2 f(R) \right\} h_\phi = 0, \quad (12-27)$$

where $n = n(R)$, $R = r/\rho$ and $f(R)$ is defined by Eq. (12-25). Since e_z is continuous, it follows from Eq. (30-5c) that both h_ϕ and dh_ϕ/dr are everywhere continuous. Remaining field components follow from Eq. (30-5) as

$$e_r = \left(\frac{\mu_0}{\varepsilon_0}\right)^{1/2} \frac{\beta}{kn^2} h_\phi; \quad e_z = \frac{i}{r} \left(\frac{\mu_0}{\varepsilon_0}\right)^{1/2} \frac{1}{kn^2} \frac{d(rh_\phi)}{dr}. \quad (12-28)$$

To solve Eq. (12-27) we adopt the approach of Section 12-15 and set $h_\phi = n(R)g(R)$ whence

$$\left\{ \frac{d^2}{dR^2} + \frac{1}{R} \frac{d}{dR} - \frac{1}{R^2} + U^2 - V^2 f(R) + p(R) \right\} g = 0, \quad (12-29a)$$

where

$$p(R) = \frac{1}{n} \frac{d^2 n}{dR^2} - \frac{2}{n^2} \left(\frac{dn}{dR} \right)^2 - \frac{1}{nR} \frac{dn}{dR}. \quad (12-29b)$$

Table 12-9 TE modes on circularly-symmetric graded-profile fibers. Prime denotes differentiation with respect to argument, and $R = r/\rho$. In profile (k) n is a positive integer or zero.

	Profile $n^2(R)$	Electric field e_ϕ	Eigenvalue equation
(k)	$n_{co}^2 \{1 - 2\Delta R^2\}$	$R \exp(-VR^2/2) L_n^{(1)}(VR^2)$	$U = 2(n+1)^{1/2} V^{1/2}$
(l)	$n_{co}^2; \quad 0 \leq R \leq 1$ $n_{co}^2 \left\{ 1 - 2\Delta \frac{R^2 - 1}{R^2} \right\}; \quad R \geq 1$	$J_1(UR)/J_1(U)$	$U \frac{J'_1(U)}{J_1(U)} = W \frac{K'_{iv}(W)}{K_{iv}(W)}$
		$K_{iv}(WR)/K_{iv}(W)$	$v^2 = V^2 - 1$
(m)	$n_{co}^2; \quad 0 \leq R \leq 1$ $\frac{n_{co}^2}{R}; \quad 1 \leq R < \infty$	$J_1(UR)/J_1(U)$	$U \frac{J'_1(U)}{J_1(U)} = 2\beta\rho \frac{W'_{v,1}(2\beta\rho)}{W_{v,1}(2\beta\rho)} - \frac{1}{2}$
		$R^{-1/2} W_{v,1}(2\beta r)/W_{v,1}(2\beta\rho)$	$v = k^2 n_{co}^2 \rho / 2\beta$
(p)	$n_{co}^2 \{1 - 2\Delta R^2\}; \quad 0 \leq R < 1$ $n_{cl}^2 = n_{co}^2 \{1 - 2\Delta\}; \quad R \geq 1$	$M_{\kappa,\mu}(VR^2)/RM_{\kappa,\mu}(V)$	$2V \frac{M'_{\kappa,\mu}(V)}{M_{\kappa,\mu}(V)} = W \frac{K_0(W)}{K_1(W)}$
		$K_1(WR)/K_1(W)$	$\kappa = U^2/4V; \quad \mu = 1/2$

For the special class of profiles with a power-law variation, we have

$$n^2(R) = n_{co}^2 R^q; \quad p(R) = -q(4+q)/4R^2, \quad (12-30)$$

and Eq. (12-29a) becomes the scalar wave equation of Eq. (12-24) with the term $-1/R^2$ replaced by $-(2+q)^2/4R^2$. There are closed-form solutions supporting bound modes if $q = -2$ or $q = -1$. The inverse-square profile is discussed in the following section, and the $q = -1$ profile is the cladding portion of profile (m) in Fig. 12-8. Within the core the fields vary as $J_1(UR)$, where J_1 is the Bessel function of the first kind. In the cladding, $U^2 - V^2 f(R) = (k\rho n_{co})^2/R - (\rho\beta)^2$, and the transformation $w = 2\rho\beta R$, $g = y/R^{1/2}$ of Eq. (12-29a) lead to Whittaker's equation with solutions $W_{\kappa, 1/2}$ [13]. Hence

$$h_\phi = \frac{J_1(UR)}{J_1(U)}, \quad 0 \leq R \leq 1; \quad h_\phi = \frac{W_{\kappa, 1/2}(2\beta R)}{RW_{\kappa, 1/2}(2\beta\rho)}, \quad 1 \leq R < \infty, \quad (12-31a)$$

where $\kappa = \rho k^2 n_{co}^2 / 2\beta$, and the eigenvalue equation is

$$\frac{U J_0(U)}{J_1(U)} = 2\beta\rho \frac{W'_{\kappa, 1/2}(2\beta\rho)}{W_{\kappa, 1/2}(2\beta\rho)}, \quad (12-31b)$$

where prime denotes differentiation with respect to argument.

12-18 Example: Hybrid modes on a graded-profile fiber

If a fiber has the refractive-index profile (m) of Fig. 12-8, the fields of *every* mode are expressible in closed form [15]. This profile has a uniform core index n_{co} and an inverse-square variation in the cladding

$$n^2(R) = n_{co}^2, \quad 0 \leq R \leq 1; \quad n^2(R) = n_{co}^2/R^2, \quad 1 \leq R < \infty, \quad (12-32)$$

where $R = r/\rho$. By examining the azimuthal components of the vector wave equation in Eqs. (30-15b) and (30-15e), we find that in the cladding the equations decouple from the e_r and h_r terms, respectively. If we express the azimuthal field components in the separable forms

$$e_\phi = G(R)g_v(\phi); \quad h_\phi = \{F(R)/R\}f_v(\phi), \quad (12-33)$$

where f_v and g_v are defined in Table 12-3(a), we can reduce the two equations to dimensionless ordinary differential equations

$$\left\{ \frac{d^2}{dR^2} + \frac{1}{R} \frac{d}{dR} + \frac{\bar{V}^2 - v^2 - 1}{R^2} - \rho^2 \beta^2 \right\} G = 0, \quad (12-34a)$$

$$\left\{ \frac{d^2}{dR^2} + \frac{1}{R} \frac{d}{dR} + \frac{\bar{V}^2 - v^2}{R^2} - \rho^2 \beta^2 \right\} F = 0, \quad (12-34b)$$

where $\bar{V} = \rho k n_{co}$. Solutions bounded as $R \rightarrow \infty$ are

$$e_\phi = C \frac{K_{ip}(\rho\beta R)}{K_{ip}(\rho\beta)} g_v(\phi); \quad h_\phi = \frac{D}{R} \frac{K_{iq}(\rho\beta R)}{K_{iq}(\rho\beta)} f_v(\phi), \quad (12-35)$$

where C, D are constants, $p = (\bar{V}^2 - v^2 - 1)^{1/2}$, $q = (\bar{V}^2 - v^2)^{1/2}$, and K_{ip}, K_{iq} are modified Bessel functions of the second kind of pure imaginary order defined by Eq. (37-67). The remaining field components are expressible in terms of e_ϕ and h_ϕ only,

as may be shown by deriving a pair of equations similar to Eq. (30-6)[15]. Alternatively, it is readily verified that the source-free Maxwell equations of Eq. (30-1) are satisfied by substituting into Eq. (30-15)

$$e_r = \frac{f_v}{\kappa} \left\{ \left(\frac{\mu_0}{\varepsilon_0} \right)^{1/2} \rho^2 \beta k R F - v \frac{d(RG)}{dR} \right\}; \quad e_z = \frac{iRf_v}{\kappa} \left\{ \left(\frac{\mu_0}{\varepsilon_0} \right)^{1/2} \rho k \frac{dF}{dR} - \rho \beta v G \right\}, \quad (12-36a)$$

$$h_r = \frac{g_v}{\kappa} \left\{ v \frac{dF}{dR} - \left(\frac{\varepsilon_0}{\mu_0} \right)^{1/2} \frac{\beta}{k} \bar{V}^2 G \right\}; \quad h_z = \frac{ig_v}{\kappa} \left\{ \rho \beta v F - \left(\frac{\varepsilon_0}{\mu_0} \right)^{1/2} \frac{\bar{V}^2}{\rho k R} \frac{d(RG)}{dR} \right\}, \quad (12-36b)$$

where $G = CK_{ip}(\rho\beta R)/K_{ip}(\rho\beta)$, $F = DK_{iq}(\rho\beta R)/K_{iq}(\rho\beta)$ and $\kappa = \bar{V}^2 - v^2$.

The longitudinal fields e_z and h_z in the core are given by Eq. (12-12a) and the remaining components follow from Eq. (30-9). Continuity of the four tangential components at $R = 1$ lead to the eigenvalue equations

$$U \frac{J_0(U)}{J_1(U)} = \rho \beta \frac{K'_{iq}(\rho\beta)}{K_{iq}(\rho\beta)}; \quad U \frac{J_0(U)}{J_1(U)} = 1 + \rho \beta \frac{K'_{ip}(\rho\beta)}{K_{ip}(\rho\beta)}, \quad (12-37a)$$

for TE_{0m} and TM_{0m} modes, respectively, and to

$$\begin{aligned} & \left(\frac{\rho \beta v}{\bar{V}} \right)^2 \left\{ \rho \beta \frac{K'_{iq}(\rho\beta)}{K_{iq}(\rho\beta)} - U \frac{J'_v(U)}{J_v(U)} \right\} \left\{ 1 + \rho \beta \frac{K'_{ip}(\rho\beta)}{K_{ip}(\rho\beta)} - U \frac{J'_v(U)}{J_v(U)} \right\} \\ &= \left\{ \bar{V}^2 - v^2 - \rho^2 \beta^2 + U \frac{J'_v(U)}{J_v(U)} \rho \beta \frac{K'_{iq}(\rho\beta)}{K_{iq}(\rho\beta)} \right\} \\ &\times \left\{ \bar{V}^2 - v^2 - \rho^2 \beta^2 + U \frac{J'_v(U)}{J_v(U)} \left[1 + \rho \beta \frac{K'_{ip}(\rho\beta)}{K_{ip}(\rho\beta)} \right] \right\} \end{aligned} \quad (12-37b)$$

for the HE_{vm} and EH_{vm} modes, where prime denotes differentiation with respect to argument. A physically more realistic fiber with a continuous three-region profile, corresponding to uniform core, uniform cladding and an inverse-square transition between the two, is discussed elsewhere [15].

ANISOTROPIC WAVEGUIDES

In this part of the chapter, we consider waveguides constructed from anisotropic materials. General concepts for such waveguides were presented at the end of Chapter 11. We now quantify their properties by presenting results for the step-profile, planar, anisotropic waveguide [16, 17] and the step-profile, uniaxial fiber [18]. These results parallel those for the corresponding isotropic waveguides given earlier in this chapter. Accordingly, we assume familiarity with the derivations of the results in Tables 12-1 to 12-4.

The values of the core and cladding refractive indices of the anisotropic waveguide depend on the direction, or polarization, of the electric field \mathbf{E} . Assuming the principal axes are parallel to the waveguide axes, we have

Direction of \mathbf{E}	x -polarized	y -polarized	z -polarized
Core index	n_{co}^x	n_{co}^y	n_{co}^z
Cladding index	n_{cl}^x	n_{cl}^y	n_{cl}^z

(12–38)

where the z -axis lies along the waveguide axis, and the x - and y -axes are in the waveguide cross-section. For step-profile waveguides, the n 's are constants.

12–19 Step-profile planar waveguide

We now suppose that the planar waveguide of Fig. 12–1 has a step profile and is composed of anisotropic materials. The modal fields are either TE or TM, provided the principal axes are parallel to the cartesian axes, as discussed in Section 30–11.

TE modes

We show in Section 30–11 that the fields of the TE modes are found by solving the scalar wave equation of Eq. (30–32a) for e_y and relating the remaining nonzero components to e_y through Eq. (30–33). Since the fields of the isotropic waveguide can be derived in an identical manner from Eqs. (12–16) and (12–17), as explained in Sections 12–2 and 12–14, the fields of the anisotropic waveform are identical in form to those of the isotropic waveguide if we replace n_{co} and n_{cl} by n_{co}^y and n_{cl}^y throughout. This leads to the TE mode fields in Table 12–10, where U , V and W are defined in terms of n_{co}^y and n_{cl}^y . Similarly, the TE mode expressions in Table 12–11 are identical to those for the isotropic waveguide in Table 12–2, as may be verified by substituting the fields of Table 12–10 into the expressions for N and η in Table 11–1, page 230. The group velocity is found from Eq. (31–31) on replacing $n^2\mathbf{e}_t$ by $\mathbf{n}^2 \cdot \mathbf{e}_t = n_x^2e_x\hat{\mathbf{x}} + n_y^2e_y\hat{\mathbf{y}}$.

TM modes

The fields are constructed from the solution of Eq. (30–32b) for h_y and Eq. (30–33). This leads to the components in Table 12–10, where U , V and W are now defined in terms of n_{co}^x , n_{co}^z , n_{cl}^x and n_{cl}^z . The differences with the TM mode fields in Table 12–1 arise solely due to the changes in refractive-index values. This is evident from comparing Eqs. (30–32b) and (30–33) with Eq. (12–20) and (12–23), respectively. The eigenvalue equations in Table 12–11 follow by demanding continuity of e_z and h_y at the interfaces, and the remaining expressions follow from Table 11–1, with the exception of the group velocity, which is calculated from the modified form of Eq. (31–31).

	e_x		h_y		e_z	
	Core	Cladding	Core	Cladding	Core	Cladding
Even TM	$\frac{\cos(\kappa_{co} U X)}{\cos(\kappa_{co} U)}$	$\frac{(n_{co}^x)^2}{(n_d^x)^2} \frac{\exp(-\kappa_d W X)}{\exp(-\kappa_d W)}$	$\frac{k(n_{co}^x)^2}{\beta} \left(\frac{\epsilon_0}{\mu_0}\right)^{1/2} \frac{\cos(\kappa_{co} U X)}{\cos(\kappa_{co} U)}$	$\frac{k(n_{co}^x)^2}{\beta} \left(\frac{\epsilon_0}{\mu_0}\right)^{1/2} \frac{\exp(-\kappa_d W X)}{\exp(-\kappa_d W)}$	$\frac{-iW}{\rho\beta} \left(\frac{n_{co}^x}{n_d^x}\right)^2 \frac{\sin(\kappa_{co} U X)}{\sin(\kappa_{co} U)}$	$\frac{-iW}{\rho\beta} \left(\frac{n_{co}^x}{n_d^x}\right)^2 \frac{X \exp(-\kappa_d W X)}{ X \exp(-\kappa_d W)}$
Odd TM	$\frac{\sin(\kappa_{co} U X)}{\sin(\kappa_{co} U)}$	$\frac{(n_{co}^x)^2}{(n_d^x)^2} \frac{X}{ X } \frac{\exp(-\kappa_d W X)}{\exp(-\kappa_d W)}$	$\frac{k(n_{co}^x)^2}{\beta} \left(\frac{\epsilon_0}{\mu_0}\right)^{1/2} \frac{\sin(\kappa_{co} U X)}{\sin(\kappa_{co} U)}$	$\frac{k(n_{co}^x)^2}{\beta} \left(\frac{\epsilon_0}{\mu_0}\right)^{1/2} \frac{\exp(-\kappa_d W X)}{\exp(-\kappa_d W)}$	$\frac{-iW}{\rho\beta} \left(\frac{n_{co}^x}{n_d^x}\right)^2 \frac{\cos(\kappa_{co} U X)}{\cos(\kappa_{co} U)}$	$\frac{-iW}{\rho\beta} \left(\frac{n_{co}^x}{n_d^x}\right)^2 \frac{\exp(-\kappa_d W X)}{\exp(-\kappa_d W)}$
$h_x = h_z = e_y = 0 \quad \kappa_{co} = \frac{n_{co}^x}{n_{co}^z} \quad \kappa_{cl} = \frac{n_d^x}{n_d^z}$						

TE mode	$U = \rho[(kn_{co}^x)^2 - \beta^2]^{1/2}$	$W = \rho[\beta^2 - (kn_d^x)^2]^{1/2}$	$V = (U^2 + W^2)^{1/2} = k\rho[(n_{co}^x)^2 - (n_d^x)^2]^{1/2}$
TM mode	$U = \rho[(kn_{co}^x)^2 - \beta^2]^{1/2}$	$W = \rho[\beta^2 - (kn_d^x)^2]^{1/2}$	$V = (U^2 + W^2)^{1/2} = k\rho[(n_{co}^x)^2 - (n_d^x)^2]^{1/2}$

Table 12-11 Modal properties of the anisotropic step-profile planar waveguide. Eigenvalue equations and modal quantities N and η calculated from Table 11-1, page 230. These expressions parallel Table 12-2 for the isotropic waveguide. The group velocity is obtained from Eq. (31-31) with n_e replaced by $n^2 \cdot \mathbf{e}_i = n_x^2 \mathbf{e}_x \hat{\mathbf{x}} + n_y^2 \mathbf{e}_y \hat{\mathbf{y}}$.

	Even TE modes	Odd TE modes	Even TM modes	Odd TM modes
Eigenvalue equation	$W = U \tan U$	$W' = -U \cot U$	$W = \left(\frac{n_{\text{cl}}^x n_{\text{co}}^z}{n_{\text{co}}^x n_{\text{co}}^z} \right) U \tan(\kappa_{\text{co}} U)$	$W' = - \left(\frac{n_{\text{cl}}^x n_{\text{cl}}^z}{n_{\text{co}}^x n_{\text{co}}^z} \right) U \cot(\kappa_{\text{co}} U)$
Normalization	$N = \frac{\rho \beta}{2k} \left(\frac{\epsilon_0}{\mu_0} \right)^{1/2} \left(\frac{V}{U} \right)^2 \frac{1+W'}{W}$		$N = \frac{\rho k (n_{\text{co}}^x)^2}{2\beta} \left(\frac{\epsilon_0}{\mu_0} \right)^{1/2} \left\{ 1 + \left(\frac{W'}{U} \right)^2 \left(\frac{n_{\text{co}}^x n_{\text{co}}^z}{n_{\text{cl}}^x n_{\text{cl}}^z} \right)^2 + \frac{V^2}{U^2 W} \frac{(n_{\text{co}}^x)^2}{n_{\text{cl}}^x n_{\text{cl}}^z} \right\}$	
Fraction of power in core	$\eta = 1 - \frac{U^2}{V^2(1+W)}$		$\eta = 1 - \frac{\{(n_{\text{co}}^x)^2/n_{\text{cl}}^x n_{\text{cl}}^z\} U^2}{U^2 W + (n_{\text{co}}^x n_{\text{co}}^z/n_{\text{cl}}^x n_{\text{cl}}^z)^2 W^3 + ((n_{\text{co}}^x)^2/n_{\text{cl}}^x n_{\text{cl}}^z) V^2}$	
Group velocity	$v_g = \frac{c}{(n_{\text{co}}^y)^2} \frac{\beta}{k} \frac{1}{1-2\Delta_y(1-\eta)}$		$v_g = \frac{c}{(n_{\text{co}}^x)^2} \frac{\beta}{k} \frac{1}{1-2\Delta_x(1-\eta)}$	
Profile height parameter	$2\Delta_y = 1 - \left(\frac{n_{\text{cl}}^y}{n_{\text{co}}^y} \right)^2$		$2\Delta_x = 1 - \left(\frac{n_{\text{cl}}^x}{n_{\text{co}}^x} \right)^2$	

Table 12-12 Step-profile uniaxial fiber. Parameters not defined in the table are given inside the back cover. Prime denotes differentiation with respect to argument.

Longitudinal field equations

Core ($0 \leq r \leq \rho$)	Cladding ($\rho \leq r < \infty$)
$(\rho^2 \nabla_t^2 + \kappa_{\text{co}}^2 U^2) e_z = 0$	$(\rho^2 \nabla_t^2 - \kappa_{\text{cl}}^2 W^2) e_z = 0$
$(\rho^2 \nabla_t^2 + U^2) h_z = 0$	$(\rho^2 \nabla_t^2 - W^2) h_z = 0$

Eigenvalue equation

$$XY = \left\{ \frac{v\beta}{kn_{\text{co}}^t} \right\}^2 \left\{ \frac{V}{UW} \right\}^4$$

$$X = \frac{1}{U} \frac{J_v(U)}{J_v(U)} + \frac{1}{W} \frac{K_v(W)}{K_v(W)}$$

$$Y = \frac{\kappa_{\text{co}}}{U} \frac{J_v'(U)}{J_v(U)} + \frac{\kappa_{\text{cl}}}{W} \frac{K_v'(n_{\text{cl}}^t)}{K_v(n_{\text{co}}^t)} \frac{K_v(\kappa_{\text{cl}} W)}{K_v(\kappa_{\text{cl}} W)}$$

Modal and fiber parameters

$$U = \rho \{ (kn_{\text{co}}^t)^2 - \beta^2 \}^{1/2} \quad W = \rho \{ \beta^2 - (kn_{\text{cl}}^t)^2 \}^{1/2}$$

$$V = (U^2 + W^2)^{1/2} = k\rho \{ (n_{\text{co}}^t)^2 - (n_{\text{cl}}^t)^2 \}^{1/2}$$

$$\kappa_{\text{co}} = n_{\text{co}}^z / n_{\text{co}}^t \quad \kappa_{\text{co}} = n_{\text{cl}}^z / n_{\text{cl}}^t$$

Cutoff

$v = 0$	$J_0(U) = 0$ (TE mode)	$J_0(\kappa_{\text{co}} U) = 0$ (TM mode)
$v = 1$	$J_1(U) = 0$	$J_1(\kappa_{\text{co}} U) = 0$
$v \geq 2$	$J_{v-1}(U) J_v(\kappa_{\text{co}} U) + \kappa_{\text{co}} \left(\frac{n_{\text{co}}^t}{n_{\text{cl}}^t} \right)^2 J_v(U) J_{v-1}(\kappa_{\text{co}} U)$ $- \frac{(1 + \kappa_{\text{cl}}^2) U}{2(v-1)} J_v(\kappa_{\text{co}} U) J_v(U) = 0$	

Weakly guiding waveguides

When the anisotropic waveguide is weakly guiding, all six values of the refractive index in Eq. (12-38) are approximately equal, and thus $\kappa_{co} \cong \kappa_{cl} \cong 1$ in Table 12-10. Hence the only significant difference between TE and TM modes is in the definition of V . For the former, V depends on the difference $(n_{co}^y)^2 - (n_{cl}^y)^2$ and, for the latter, V depends on the difference $(n_{co}^x)^2 - (n_{cl}^x)^2$. Furthermore, TE and TM mode fields can be written down from a knowledge of the TE mode fields of the isotropic waveguide simply by replacing n_{co} , n_{cl} by n_{co}^y , n_{cl}^y or n_{co}^x , n_{cl}^x , respectively.

12-20 Step-profile uniaxial fiber

We now suppose that the fiber of Fig. 12-3 has a step profile and is composed of anisotropic materials. Furthermore, we assume the fiber is uniaxial, as discussed in Section 30-12, in which case it is characterized by

Direction of \mathbf{E}	x - or y -polarized	z -polarized
Core index	$n_{co}^t = n_{co}^x = n_{co}^y$	n_{co}^z
Cladding index	$n_{cl}^t = n_{cl}^x = n_{cl}^y$	n_{cl}^z

(12-39)

where all the indices are constants, and $n_{cl}^t < n_{co}^t$, $n_{cl}^z < n_{co}^z$. If we substitute into Eq. (30-34), the equations for the longitudinal field components can be expressed in analogous forms to Eq. (12-11) for the isotropic fiber, as shown in Table 12-12. The modal and waveguide parameters have the definitions given in the Table. We show in Section 30-13 that, once e_z and h_z are known, the transverse field components are determined from Eq. (30-9), provided we set $p = (kn_{co}^t)^2 - \beta^2$ for the core and $p = (kn_{cl}^t)^2 - \beta^2$ for the cladding. Thus, the method of construction for the modes of the anisotropic waveguide is identical to that of the isotropic waveguide, but the modal properties will differ.

Eigenvalue equation

Continuity of the four tangential field components e_ϕ , h_ϕ , e_z and h_z at the interface $r = \rho$ leads to the eigenvalue equation in Table 12-12. A study of its solutions shows that it is not possible to distinguish between HE and EH modes, unlike the isotropic fiber. In general, modes of the anisotropic fiber can have any combination of TE and TM components, except for the $v = 0$ modes, which may be pure TE or TM [18]. This can be appreciated by examining the cutoff of each mode.

Cutoff

At cutoff, $U = V = V_c$ and $W = 0$, as discussed in Section 11-18. The values of

V_c are given in Table 12-12 for each value of ν , and reduce to the values in Table 12-4 for the isotropic fiber when $\kappa_{co} = \kappa_{cl} = 1$. For the first TE and TM modes, the cutoff values are $V_c = 2.405$ and $V_c = 2.405 (n_{cl}^2/n_{co}^2)$, respectively. The $\nu = 1$ modes have a similar split, but for $\nu \geq 2$ there is no split, i.e. no clear distinction between HE and EH modes as there is for the isotropic fiber in Table 12-4.

REFERENCES

1. Snyder, A. W. and de la Rue, R. (1970) Asymptotic solution of eigenvalue equations for surface waveguide structures. *I.E.E.E. Trans. Microwave Theory Tech.*, **18**, 650-1.
2. Marcuse, D. (1974) *Theory of Dielectric Optical Waveguides*, Academic Press, New York, chap. 1.
3. Snyder, A. W. (1971) Approximate eigenvalues for a circular rod of arbitrary dielectric constant. *Electron. Lett.*, **7**, 105-6.
4. Marcuse, D. (1972) *Light Transmission Optics*, Van Nostrand, New York, p. 331.
5. Snyder, A. W. (1969) Asymptotic expressions for eigenfunctions and eigenvalues of a dielectric or optical waveguide. *I.E.E.E. Trans. Microwave Theory Tech.*, **17**, 1130-8.
6. Kawakami, S. and Nishida, S. (1974) Characteristics of a doubly clad optical fiber with a low-index inner cladding. *I.E.E.E. Trans. J. Quantum Electron.*, **10**, 879-87.
7. Yeh, C. (1962) Elliptical dielectric waveguides. *J. Appl. Phys.*, **33**, 3235-42.
8. Kogelnik, H. (1975) in *Integrated Optics* (ed. T. Tamir), Springer-Verlag, Berlin, pp. 53-61.
9. Landau, L. and Lifshitz, E. (1958) *Quantum Mechanics*, Pergamon Press, Oxford, p. 70.
10. Gordon, J. (1966) Optics of general guiding media. *Bell Syst. Tech. J.*, **46**, 321-32.
11. Ankiewicz, A. (1978) Comparison of wave and ray techniques for solution of graded index optical waveguide problems. *Opt. Acta*, **25**, 361-73.
12. Love, J. D. and Ghatak, A. K. (1979) Exact solutions for TM modes in graded index slab waveguides. *I.E.E.E. Trans. J. Quantum Electron.*, **15**, 14-16.
13. Abramowitz, M. and Stegun, I. A. (1965) *Handbook of Mathematical Functions*, Dover, New York.
14. Burman, R. (1968) Some electromagnetic wave functions for propagation along cylindrically stratified columns. *I.E.E.E. Trans. Microwave Theory Tech.*, **16**, 127-9.
15. Love, J. D. (1984) Exact, analytical solutions for modes on a graded-profile fiber. *Opt. Quant. Elect. (submitted)*.
16. Yamamoto, S., Koyamada, Y. and Makimoto, T. (1972) Normal-mode analysis of an anisotropic and gyrotropic thin-film waveguide for integrated optics. *J. Appl. Phys.*, **43**, 5090-7.
17. Ramaswamy, V. (1974) Ray model of energy and power flow in anisotropic film waveguides. *J. Opt. Soc. Am.*, **64**, 1313-20.
18. Kapany, N. S. and Burke, J. J. (1972) *Optical Waveguides*, Academic Press, New York, p. 141.

Weakly guiding waveguides

13-1	Polarization phenomena due to the waveguide structure	281
	Modes of weakly guiding waveguides	282
13-2	TEM wave approximation to the modes	283
13-3	Spatial dependence of the modal fields	283
	Vector direction of the modal fields	284
13-4	Fundamental and HE_{1m} modes of circular fibers	284
13-5	Fundamental modes of waveguides of arbitrary cross-section	285
13-6	Polarization corrections to the scalar propagation constant	286
13-7	Higher-order modes of circular fibers	287
13-8	Higher-order modes of waveguides of arbitrary cross-section	289
13-9	Higher-order modes of nearly circular fibers	289
	Modal properties of weakly guiding waveguides	290
13-10	Dependence of absorption on polarization	291
13-11	Higher-order polarization corrections	291
	Anisotropic weakly guiding waveguides	295
13-12	Modes of anisotropic waveguides	296
13-13	Single-mode single-polarization fibers	299
	Radiation leakage in anisotropic fibers	299
13-14	Leaky single-mode single-polarization fibers	299
	References	300

In Chapter 11 we discussed the fundamental properties of modes on optical waveguides. The vector fields of these modes are solutions of Maxwell's source-free equations or, equivalently, the homogeneous vector wave equations. However, we found in Chapter 12 that there are few known refractive-index profiles for which Maxwell's equations lead to exact solutions for the modal fields. Of these the step-profile is probably the only one of practical interest. Even for this relatively simple profile the derivation of the vector modal fields on a fiber is cumbersome. The objective of this chapter is to lay the foundations of an approximation method [1, 2], which capitalizes on the small

variation in refractive-index profile of fibers used for long-distance communications, i.e. $\Delta \ll 1$, where Δ is the profile height parameter of Eq. (11-48). The simplicity of this approximation method is that it relies on solutions of the scalar wave equation, rather than on vector solutions of the vector wave equation.

Optical waveguides with $\Delta \ll 1$, or, equivalently, $n_{co} \cong n_{cl}$, are called *weakly guiding*, although the terminology is somewhat misleading since both strong guidance and total containment of light within the core are possible when $\Delta \ll 1$. The modes of weakly guiding optical waveguides were first given for the step-index fibre [2], the term weak guidance was then coined [3] and additional insights followed later [4]. Subsequently the theory was generalized to waveguides of arbitrary cross-section [1].

13-1 Polarization phenomena due to the waveguide structure

In order to appreciate the approximations involved, we first consider some aspects of propagation to augment Section 11-16.

Uniform medium

Suppose the waveguide is composed of an unbounded uniform medium of refractive index n_{co} , i.e. effectively 'free space'. The modal fields are then found from Maxwell's equations to be the fields of transverse electromagnetic, or TEM, waves propagating in the z -direction parallel to the waveguide axis. Thus, the propagation constant $\beta = n_{co}k$, the longitudinal components satisfy $e_z = h_z = 0$, and the transverse electric and magnetic fields are related by

$$\mathbf{h}_t = \left(\frac{\epsilon_0}{\mu_0} \right)^{1/2} n_{co} \hat{\mathbf{z}} \times \mathbf{e}_t, \quad (13-1)$$

where $\hat{\mathbf{z}}$ is the unit vector parallel to the waveguide axis, and ϵ_0, μ_0 are defined inside the back cover. The propagation constant is independent of the orientation of \mathbf{e}_t , so *the waveguide has no polarization properties*. In this trivial example, it is obvious that each *cartesian* component of \mathbf{e}_t and \mathbf{h}_t obeys the *scalar wave equation* at all positions in space, since the right side of Eq. (11-40) is zero in a uniform medium.

Nonuniform media

We next consider a waveguide with a nonuniform refractive-index profile $n = n(x, y)$. The propagation constant now depends on the orientation of the electric field, and the modes are no longer TEM waves. In general the modal fields are not solutions of the scalar wave equation but obey the vector wave

equations of Eq. (11-40), where waveguide polarization effects are governed by the $\nabla_t \ln n^2$ terms. Exceptions are the TE modes of planar waveguides and fibers discussed in Sections 12-14 and 12-16. A simple example illustrating the polarization dependence of propagation due to the waveguide structure is that of a waveguide with a planar interface between uniform media of refractive indices n_{co} and n_{cl} . If a plane wave is incident on the interface from the medium of index n_{co} , as in Fig. 10-2, and suffers total internal reflection, the phase of the incident and reflected waves differ as shown in Fig. 10-2, and this difference increases as the difference between n_{co} and n_{cl} increases. This explains the difference between TE and TM modes on step-profile waveguides discussed in Section 11-16. In other words, the waveguide structure introduces polarization effects which give rise to the $\nabla_t \ln n^2$ terms in the vector wave equation.

Conversely, in the above example, the variation of the phase change with polarization of the plane wave electric field is small when the difference between n_{co} and n_{cl} is small, although the incident wave is still totally reflected. Thus, *if the refractive indices are nearly equal, the slight nonuniformity maintains total internal reflection, but the medium is virtually homogeneous as far as polarization effects are concerned.* Further, the fields associated with plane-wave reflection satisfy the scalar wave equation, as discussed in Section 35-6. With this perspective, we anticipate that waveguides of arbitrary refractive-index profile have some analogous simplification in the description of their modal fields, *provided only that the profile height parameter is small*, i.e. $\Delta \ll 1$, or $n_{co} \cong n_{cl}$.

We now show how to construct the modal fields of weakly guiding waveguides using simple physical arguments based on the above insight. These fields can also be formally derived by applying perturbation methods to Maxwell's equations, as we show in Chapter 32.

MODES OF WEAKLY GUIDING WAVEGUIDES

We start by recalling from Eq. (11-6) that the electric and magnetic fields \mathbf{E} and \mathbf{H} of individual bound modes of a waveguide are expressible as

$$\mathbf{E}(x, y, z) = \mathbf{e}(x, y) \exp(i\beta z) = (\mathbf{e}_t + \hat{\mathbf{z}}e_z) \exp(i\beta z), \quad (13-2a)$$

$$\mathbf{H}(x, y, z) = \mathbf{h}(x, y) \exp(i\beta z) = (\mathbf{h}_t + \hat{\mathbf{z}}h_z) \exp(i\beta z), \quad (13-2b)$$

where β is the propagation constant, and subscripts t and z denote transverse and longitudinal components, respectively. As we consider only individual modes in this chapter we omit the modal subscript. The representative waveguide in Fig. 11-1(a) has maximum index n_{co} and cladding index n_{cl} . If $n_{co} \cong n_{cl}$, it follows from the definition inside the back cover that

$$\Delta = \frac{1}{2} \left\{ 1 - \frac{n_{cl}^2}{n_{co}^2} \right\} \cong \frac{n_{co} - n_{cl}}{n_{co}}. \quad (13-3)$$

It is convenient to use the profile representation

$$n^2(x, y) = n_{co}^2 \{1 - 2\Delta f(x, y)\}, \quad (13-4)$$

where $f = 0$ at the maximum index and $f = 1$ in the cladding.

13-2 TEM wave approximation to the modes

The range of bound mode propagation constants in Eq. (11-46) is

$$kn_{cl} < \beta \leq kn_{co}. \quad (13-5)$$

Thus the variation in β on weakly guiding waveguides is very narrow, and for all modes we may assume

$$\beta \cong kn_{co} \cong kn_{cl}. \quad (13-6)$$

The modes must therefore be nearly TEM waves with $e_z \cong 0$, $h_z \cong 0$, and consequently the transverse fields obey Eq. (13-1) approximately. Hence by knowing only \mathbf{e}_t the modal fields are specified.

13-3 Spatial dependence of the modal fields

We showed above that the modes of weakly guiding waveguides are approximately TEM waves, with fields $\mathbf{e} \cong \mathbf{e}_t$, $\mathbf{h} \cong \mathbf{h}_t$ and \mathbf{h}_t related to \mathbf{e}_t by Eq. (13-1). In an exact analysis, the spatial dependence of $\mathbf{e}_t(x, y)$ requires solution of Maxwell's equations, or, equivalently, the vector wave equation, Eq. (11-40a). However, when $\Delta \ll 1$, polarization effects due to the waveguide structure are small, and the *cartesian* components of \mathbf{e}_t are approximated by solutions of the scalar wave equation. The justification in Section 13-1 is based on the fact that the waveguide is virtually homogeneous as far as polarization effects are concerned when $\Delta \ll 1$. As we showed in Section 11-16, these effects are contained in the $\nabla_t \ln n^2$ term of the vector wave equation. Hence, ignoring polarization effects altogether is equivalent to ignoring the $\nabla_t \ln n^2$ term in Eq. (11-40a). Accordingly if we set

$$\mathbf{e}_t(x, y) = e_x(x, y)\hat{\mathbf{x}} + e_y(x, y)\hat{\mathbf{y}}, \quad (13-7)$$

where $\hat{\mathbf{x}}$ and $\hat{\mathbf{y}}$ are unit vectors parallel to the cartesian axes in Fig. 11-1(a) and let Ψ denote e_x or e_y , then Ψ satisfies

$$\{\nabla_t^2 + k^2 n^2(x, y) - \beta^2\}\Psi = 0, \quad (13-8)$$

where $k = 2\pi/\lambda$, the free-space wavelength is λ , and ∇_t^2 is defined in Table 30-1, page 592. Although the cartesian components of \mathbf{e}_t satisfy Eq. (13-8), their spatial dependence can be determined in any cylindrical coordinate system,

e.g. in cylindrical polar coordinates $\mathbf{e}_t = \mathbf{e}_t(r, \phi)$ and ∇_t^2 is again given in Table 30-1.

We emphasize that in Eq. (13-8), $\tilde{\beta}$ denotes the propagation constant for the scalar wave equation, as distinct from the exact propagation constant β for the vector wave equation. In Section 33-1 we show that any solution of the scalar wave equation and its first derivatives are continuous everywhere. Together with the requirement that Ψ be bounded everywhere, this property leads to an eigenvalue equation for the allowed values of $\tilde{\beta}$.

Although Eqs. (13-7) and (13-8) determine the spatial dependence of $\mathbf{e}_t(x, y)$, they give no information about its polarization, i.e. its vector field direction. This direction must be determined from the polarization properties of the waveguide, or by its symmetry properties.

VECTOR DIRECTION OF THE MODAL FIELDS

We have now established that modes of weakly guiding waveguides are nearly TEM waves, and that the spatial dependence of $\mathbf{e}_t(x, y)$ is governed by the scalar wave equation. It remains only to specify the vector direction of $\mathbf{e}_t(x, y)$ as a function of position. In general, $\mathbf{e}_t(x, y)$ is comprised of both $e_x(x, y)$ and $e_y(x, y)$ components. The specific combination is dictated by the polarization properties of the waveguide, i.e. by the profile shape, and can usually be deduced from the symmetry of the waveguide cross-section. If we ignore waveguide polarization, then any linear combination is valid, but, as we show below, this will generally lead to significant errors.

First we consider fundamental modes and then higher-order modes. Like the exact propagation constant β , the scalar propagation constant $\tilde{\beta}$ is largest for fundamental modes. It is convenient to distinguish between fibers of circular cross-section and waveguides of arbitrary cross-section.

13-4 Fundamental and HE_{1m} modes of circular fibers

The fundamental and HE_{1m} modes of a fiber of circular cross-section are formed from the scalar wave equation solution with no azimuthal variation. Hence Ψ in Eq. (13-8) depends only on the radial position r . There is no preferred axis of symmetry in the circular cross-section. Thus, in this exceptional case, the transverse electric field can be directed so that it is everywhere parallel to one of an arbitrary pair of orthogonal directions. If we denote this pair of directions by x - and y -axes, as in Fig. 12-3, then there are two fundamental or HE_{1m} modes, one with its transverse electric field parallel to the x -direction, and the other parallel to the y -direction. The symmetry also requires that the scalar propagation constants of each pair of modes are equal.

Putting these facts together, we deduce from Eqs. (13-1) and (13-2) that [1, 2]

<i>x-polarized mode</i>	<i>y-polarized mode</i>	
$E_x = F_0(r) \exp(i\tilde{\beta}z)$	$E_y = F_0(r) \exp(i\tilde{\beta}z)$	(13-9a)
$H_y = \left(\frac{\epsilon_0}{\mu_0}\right)^{1/2} n_{co} E_x$	$H_x = -\left(\frac{\epsilon_0}{\mu_0}\right)^{1/2} n_{co} E_y$	(13-9b)

where $F_0(r)$ is an axisymmetric solution of Eq. (13-8), and all other field components are small. We give examples in the following chapter. Lastly, we emphasize that the description given by Eq. (13-9) is purely scalar, and contains no information about polarization properties of the fiber. The fundamental and HE_{1m} modes of circular fibers are exceptional in this regard; all other modes retain some polarization information as we show in Section 13-7.

LP designation for fundamental modes

The fundamental modes of *weakly guiding* circular fibers are sometimes designated LP_{01} modes [3] rather than HE_{11} modes. The nomenclature is intended to emphasize that the modal fields are everywhere polarized in the same direction, i.e. the fields are plane, or uniformly, polarized.

13-5 Fundamental modes of waveguides of arbitrary cross-section

If the cross-section is not circular, the transverse electric field is everywhere parallel to one of two orthogonal directions, denoted by axes x_0 and y_0 . We call these directions the *optical axes* of the waveguide cross-section. In many cases the optical axes are obvious from the symmetry of the cross-section, e.g. they are parallel to the major and minor axes of the elliptical cross-section, and are parallel to the x - or y -axis of the planar cross-section in Fig. 12-1. All information about the optical axes is contained within the $\nabla_t \ln n^2$ terms of the vector wave equations of Eq. (11-40). Because of the slight variation in the profile of a weakly guiding waveguide these terms are small, and the directions of the x_0 - and y_0 -axes can be found by perturbation methods for those cases when they are not obvious by inspection. This is discussed in Section 32-5. For convenience we shall assume that the x - and y -axes are aligned along the x_0 - and y_0 - directions.

The solution Ψ of Eq. (13-8) for the fundamental modes by definition has the largest value of $\tilde{\beta}$. Then, as for the circular fiber there are two modes associated with this solution, one polarized along the x -direction and the other polarized along the y -direction. Both modes have the same scalar propagation constant $\tilde{\beta}$, but, because the cross-section is not circular, we know the *exact*

propagation constants β_x and β_y of the two modes will differ. The difference is due to the polarization, or birefringence, properties of the waveguide, as manifested by the $\nabla_t \ln n^2$ terms in Eq. (11-40). In this sense propagation on noncircular waveguides is similar to propagation in anisotropic media, as discussed in Chapter 12. The small difference $\beta_x - \beta_y$ also leads to interference, or beating, between the fields of the two modes. More importantly, the transit time of the two fundamental modes will differ, and result in an extra component of pulse spreading on single-mode waveguides, in addition to the spreading due to material dispersion and waveguide dispersion in Section 11-12. Accordingly it is now necessary to determine the propagation constant of each mode more accurately than from the scalar wave equation. The polarization properties of the waveguide lead to small corrections $\delta\beta_x$ and $\delta\beta_y$ to $\tilde{\beta}$ for each mode, as we show in the next section. Collecting these facts, we deduce from Eqs. (13-1) and (13-2) that [1]

<i>x-polarized mode</i>	<i>y-polarized mode</i>	
$E_x = \Psi(x, y) \exp \{ i(\tilde{\beta} + \delta\beta_x)z \}$	$E_y = \Psi(x, y) \exp \{ i(\tilde{\beta} + \delta\beta_y)z \}$	(13-10a)
$H_y = \left(\frac{\epsilon_0}{\mu_0} \right)^{1/2} n_{co} E_x$	$H_x = - \left(\frac{\epsilon_0}{\mu_0} \right)^{1/2} n_{co} E_y$	(13-10b)

where $\Psi(x, y)$ is the solution of Eq. (13-8) with the largest value of β , and all other field components are small. We are reminded that the x - and y -axes are assumed parallel to the optical axes of the waveguide cross-section. We give examples in Chapter 16.

13-6 Polarization corrections to the scalar propagation constant

If we are to account for waveguide polarization properties in the propagation constant, we must add a correction $\delta\beta$ to the scalar propagation constant $\tilde{\beta}$. To determine $\delta\beta$ exactly we would have to solve the vector wave equation. However, the $\nabla_t \ln n^2$ term on the right of Eq. (11-40a) is small for weakly guiding waveguides, so we use simple perturbation methods in Section 32-4. From Eq. (32-24) we have

$$\delta\beta \cong \frac{\rho(2\Delta)^{3/2}}{2V} \frac{\int_{A_\infty} (\nabla_t \cdot \mathbf{e}_t) \mathbf{e}_t \cdot \nabla_t f(x, y) dA}{\int_{A_\infty} \mathbf{e}_t^2 dA}, \quad (13-11)$$

where $\Delta \ll 1$ is the profile height parameter, V the waveguide parameter, A_∞ the infinite cross-section and $f(x, y)$ is the variable part of the profile in Eq.

(13-4). For the step profile, $\nabla_t f(x, y)$ is a delta function at the interface, and $\delta\beta$ is given by Eq. (32-26), where

$$\delta\beta \cong \frac{\rho(2\Delta)^{3/2}}{2V} \oint_l (\nabla_t \cdot \mathbf{e}_t) \mathbf{e}_t \cdot \hat{\mathbf{n}} dl / \int_{A_\infty} \mathbf{e}_t^2 dA. \quad (13-12)$$

The contour l is along the interface and $\hat{\mathbf{n}}$ is the unit outward normal on l in the waveguide cross-section.

The polarization corrections $\delta\beta_x$ and $\delta\beta_y$ of Eq. (13-10) for the noncircular waveguide are given by Eq. (13-11) with $\mathbf{e}_t = \Psi(x, y)\hat{\mathbf{x}}$ and $\mathbf{e}_t = \Psi(x, y)\hat{\mathbf{y}}$, respectively, where $\hat{\mathbf{x}}$ and $\hat{\mathbf{y}}$ are unit vectors along the axes.

13-7 Higher-order modes of circular fibers

We now consider higher-order modes of fibers with circularly symmetric cross-sections and profiles. If we express ∇_t^2 in cylindrical polar coordinates r, ϕ as in Table 30-1, page 592, there are two separable solutions of Eq. (13-8) for each value of $\tilde{\beta}$. These are $\Psi = F_l(r) \cos l\phi$ and $\Psi = F_l(r) \sin l\phi$, where l is a positive integer and $F_l(r)$ satisfies the equation in Table 13-1. Because of symmetry, any pair of orthogonal x - and y -axes may be chosen as optical axes in the fiber cross-section. It also follows from symmetry that there are four possible directions for \mathbf{e}_t , depending on the particular combination of the two solutions of the scalar wave equation used in Eq. (13-7) [1, 2]. This is discussed further in Section 32-7. Hence, for each value of $l > 0$, there are four modes with the fields shown in Table 13-1. These combinations can also be derived without recourse to symmetry properties using the formal methods of Section 32-6. In general, this representation for \mathbf{e}_t is the simplest possible, for reasons explained in Section 32-8.

The four modes have the same scalar propagation constant $\tilde{\beta}$, but their exact propagation constants are not all equal. This can be anticipated from symmetry arguments [1] or from the example of the step-profile fiber in Chapter 12. Thus the higher-order modes of the circular fiber are analogous to the fundamental modes of noncircular waveguides, and, for reasons similar to those given in Section 13-5, we must incorporate polarization properties of the fiber through the small correction to $\tilde{\beta}$ for each mode. The polarization correction $\delta\beta_i$ for the i th mode in Table 13-1 is given by Eq. (13-11) with $\mathbf{e}_t = \mathbf{e}_{ti}$, and is expressible in terms of simple integrals in Table 14-1, page 304. Examples of modes on weakly guiding circular fibers are given in the following chapter.

LP designation for $l \geq 1$ modes

Unlike the fundamental and all other $l = 0$ modes, the fields of $l \geq 1$ modes are *not plane polarized*. Instead, due to fiber polarization effects, the direction of the field depends on the position in the fiber cross-section, as is clear from

Table 13-1 Bound-mode fields of weakly guiding waveguides. The form of the transverse electric field depends on the shape of the waveguide cross-section. Vector operators are defined in Table 30-1, page 592, and parameters are defined inside the back cover.

$\mathbf{E}(x, y, z) = \mathbf{e}(x, y) \exp \{i(\tilde{\beta} + \delta\beta)z\}$ $\mathbf{e}(x, y) \cong \mathbf{e}_t(x, y)$	$\mathbf{H}(x, y, z) = \mathbf{h}(x, y) \exp \{i(\tilde{\beta} + \delta\beta)z\}$ $\mathbf{h}(x, y) \cong \mathbf{h}_t(x, y) = \left(\frac{\epsilon_0}{\mu_0}\right)^{1/2} n_{co} \hat{\mathbf{z}} \times \mathbf{e}_t(x, y)$
$\{\nabla_t^2 + k^2 n^2(x, y) - \tilde{\beta}^2\} \mathbf{e}_t = 0$ $k = 2\pi/\lambda$	$n^2(x, y) = n_{co}^2 \{1 - 2\Delta f(x, y)\}$ $n_{cl}^2 = n_{co}^2 \{1 - 2\Delta\}$
$\delta\beta = \frac{(2\Delta)^{3/2}}{2\rho V} \frac{\int_{A_\infty} (\rho \nabla_t \cdot \mathbf{e}_t) \mathbf{e}_t \cdot \rho \nabla_t f dA}{\int_{A_\infty} \mathbf{e}_t^2 dA}$	

Noncircular cross-section

$$\mathbf{e}_{t1} = \Psi \hat{\mathbf{x}} \qquad \mathbf{e}_{t2} = \Psi \hat{\mathbf{y}}$$

$$\{\nabla_t^2 + k^2 n^2(x, y) - \tilde{\beta}^2\} \Psi = 0$$

Circular cross-section

$$\mathbf{e}_{t1} = F_l(r) \{\cos(l\phi) \hat{\mathbf{x}} - \sin(l\phi) \hat{\mathbf{y}}\} \qquad \mathbf{e}_{t2} = F_l(r) \{\cos(l\phi) \hat{\mathbf{x}} + \sin(l\phi) \hat{\mathbf{y}}\}$$

$$\mathbf{e}_{t3} = F_l(r) \{\sin(l\phi) \hat{\mathbf{x}} + \cos(l\phi) \hat{\mathbf{y}}\} \qquad \mathbf{e}_{t4} = F_l(r) \{\sin(l\phi) \hat{\mathbf{x}} - \cos(l\phi) \hat{\mathbf{y}}\}$$

$$\left\{ \frac{d^2}{dr^2} + \frac{1}{r} \frac{d}{dr} + k^2 n^2(r) - \frac{l^2}{r^2} - \tilde{\beta}^2 \right\} F_l = 0$$

Nearly circular cross-section

$$\mathbf{e}_{t1} = F_l(r) \{\cos(l\phi) \hat{\mathbf{x}} + a_- \sin(l\phi) \hat{\mathbf{y}}\} \qquad \mathbf{e}_{t2} = F_l(r) \{\cos(l\phi) \hat{\mathbf{x}} + a_+ \sin(l\phi) \hat{\mathbf{y}}\}$$

$$\mathbf{e}_{t3} = F_l(r) \{\sin(l\phi) \hat{\mathbf{x}} + a_+ \cos(l\phi) \hat{\mathbf{y}}\} \qquad \mathbf{e}_{t4} = F_l(r) \{\sin(l\phi) \hat{\mathbf{x}} + a_- \cos(l\phi) \hat{\mathbf{y}}\}$$

$$a_{\pm} = \Lambda \pm (1 + \Lambda^2)^{1/2} \qquad \Lambda = (\tilde{\beta}_e - \tilde{\beta}_o)/(\delta\beta_1 - \delta\beta_2)$$

Table 13–1. Accordingly, the LP designation of fundamental modes in Section 13–4 is *not applicable*. However, if we ignore all polarization properties of the fiber, then all four modes have the same propagation constant given by $\tilde{\beta}$, i.e. $\delta\beta_i = 0$. Then there is no constraint on the field directions and they can be expressed in a plane polarized form, e.g. $\mathbf{e}_{t1} = F_1(r) \cos(l\phi) \hat{\mathbf{x}}$ or $\mathbf{e}_{t1} = F_1(r) \times \exp(\pm il\phi) \hat{\mathbf{x}}$. Nevertheless, we emphasize that such a description will, in general, lead to significant errors, as discussed in Section 14–7, except for multimoded fibers where polarization effects of individual modes are masked and propagation is directly described by classical geometric optics as in Part I.

13–8 Higher-order modes of waveguides of arbitrary cross-section

The higher-order modes of waveguides with noncircular cross-sections are constructed from each pair of solutions $\Psi_e(x, y)$ and $\Psi_o(x, y)$ of Eq. (13–8) and their corresponding scalar propagation constants β_e and β_o . The transverse electric fields of these modes are polarized along the same optical axes as the fundamental modes of Section 13–5. There are two pairs of higher-order modes. Each pair has fields given by Eq. (13–10), with $\tilde{\beta}$ and $\Psi(x, y)$ replaced by $\tilde{\beta}_e$ and $\Psi_e(x, y)$ for one pair, and by $\tilde{\beta}_o$ and $\Psi_o(x, y)$ for the other pair. The polarization corrections $\delta\beta_{xe}$, $\delta\beta_{xo}$, $\delta\beta_{ye}$ and $\delta\beta_{yo}$ are obtained from Eq. (13–11) with the appropriate field substituted for \mathbf{e}_t .

13–9 Higher-order modes of nearly circular fibers

The forms for the transverse electric fields differ greatly between those for circular fibers in Table 13–1 and those for waveguides of arbitrary cross-section discussed above, as far as *higher-order modes* are concerned. Clearly there must be a transition region in which a nearly circular fiber starts to take on attributes of the perfectly circular fiber. Accordingly, the description of higher-order modes applies only when the cross-section is sufficiently noncircular. However, it turns out for weakly guiding fibers that only a slight asymmetry in the cross-section is necessary for the transition. In other words, the fields of fibers are almost uniformly polarized unless the cross-section is virtually circular. Provided Δ is sufficiently small, a nearly circular fiber has modal fields given by the noncircular case. If Δ and the asymmetry, e.g. the eccentricity of a slightly elliptical fiber, are of the same order, then there is a competition between the effects of noncircularity and weak guidance. Thus we need a description of the modal fields across the transition region.

In general the *spatial variation* of the modal fields of the slightly asymmetric fiber is similar to that of the modal fields of the circular fiber, but the fields are polarized along axes which we can take to be parallel to the optical axes of the circular fiber. When the symmetry of the circular cross-section is broken, the transverse electric fields are no longer given exactly by the symmetrical and

antisymmetrical combinations in Table 13-1 for the circular fiber. Instead, we assume the more general forms at the bottom of Table 13-1, where the constants a_{\pm} , as yet unknown, bridge the two extremes. At one extreme, when $a_{\pm} = \pm 1$, these forms reduce to the correct expressions for the circular fiber, and at the other extreme when $a_{+} \gg a_{-}$ or $a_{-} \gg a_{+}$, the forms reduce approximately to the expressions for waveguides of arbitrary cross-section given Section 13-8. The coefficients a_{\pm} are derived in Section 32-9 using simple perturbation methods, and for convenience are expressed in terms of the dimensionless parameter Λ defined in Table 13-1. This parameter is the ratio of $\hat{\beta}_e - \hat{\beta}_o$, which is a measure of the effect of noncircularity, to $\delta\beta_1 - \delta\beta_2$, which is a measure of the effect of polarization of the circular fiber. Examples of this transition are discussed quantitatively in Chapters 16 and 18.

MODAL PROPERTIES OF WEAKLY GUIDING WAVEGUIDES

Modes of weakly guiding waveguides obey the fundamental properties of modes delineated in Chapter 11, and mainly because of the approximate TEM nature of the modal fields, these properties have the simpler forms of Table 13-2. The expressions in the first column are in terms of the transverse electric field \mathbf{e}_t and apply to all weakly guiding waveguides. Those in the second column are for waveguides which are sufficiently noncircular that \mathbf{e}_t can be replaced by either of the two fields for noncircular waveguides in Table 13-1, while the third column is for circular fibers only, when \mathbf{e}_t is replaced by any one of the four linear combinations \mathbf{e}_{ti} for circular cross-sections in Table 13-1. We emphasize that Table 13-2 applies to all modes.

The first six expressions in the first column are obtained by substituting the fields at the top of Table 13-1 into the corresponding expressions in Table 11-1, page 230. Alternatively they can be derived directly from the scalar wave equation using the methods of Chapter 33 with Ψ replaced by \mathbf{e}_t , e.g. the proof of orthogonality in Section 33-2. The remaining expressions, with the exception of the distortion parameter, do not follow from the same simple substitution, since they require higher-order field corrections, even though these corrections do not appear explicitly in the final forms. It is easier to derive the expressions for the propagation constant and group velocity from the scalar wave equation in Sections 33-3 and 33-4, respectively. The expression for \tilde{U}^2 then follows from the definition of \tilde{U} in Eq. (13-14) and the profile representation at the top of Table 13-2. The expression for $d\tilde{U}/dV$ is obtained by paralleling the derivation of the group velocity, as described in Section 33-4. We have assumed that, in keeping with the convention of Section 11-3, both Ψ and $F_t(r)$ are real functions to ensure that the transverse modal fields are real on nonabsorbing waveguides.

13–10 Dependence of absorption on polarization

We showed in Section 11–22 that an absorbing waveguide attenuates the power of a mode as it propagates. The attenuation rate depends on the imaginary part of the propagation constant. The weak-guidance approximation applies to absorbing waveguides provided that both the real and imaginary parts $n^r(x, y)$ and $n^i(x, y)$ of the profile vary only slightly over the waveguide cross-section. The scalar propagation constant β is then complex, and its real and imaginary parts β^r and β^i are determined, in general, by numerical solution of the eigenvalue equation derived from the scalar wave equation. In practice, however, absorption is very small, and we can determine the power attenuation coefficient from the expression in Table 13–2 by taking Ψ to be the solution of Eq. (13–8) for the nonabsorbing waveguide.

We showed in Section 13–6 how to determine the polarization correction $\delta\beta$ to the scalar propagation constant $\tilde{\beta}$. On an absorbing waveguide, both the modal fields \mathbf{e}_t and the profile variation f are complex, and consequently Eq. (13–11) shows that $\delta\beta$ is complex. The imaginary part of $\delta\beta$ is usually small compared to the real part, but may be significant in the attenuation of modal power over long distances. This is the only situation we consider where \mathbf{e}_t cannot be treated as approximately real, since the ratio of imaginary to real parts of \mathbf{e}_t and f are comparable. In general, two distinct integrals must be evaluated for $\delta\beta^r$ and $\delta\beta^i$, but there are two special cases when some simplification is possible.

If the real and imaginary parts of $n(x, y)$ have the same spatial dependence, i.e. n^i/n^r is constant, then $\nabla_t \ln n^2 = \nabla_t \ln (n^r)^2$. Consequently, if $\delta\beta$ is known for the nonabsorbing waveguide with real profile n^r , then the complex value of $\delta\beta$ for the absorbing waveguide is given by the same expression provided $\tilde{\beta}$ is everywhere replaced by $\beta^r + i\beta^i$, as is clear from Eq. (13–11).

When the waveguide has a step profile, we can express $\delta\beta$ in terms of the line integral of Eq. (13–12). Allowing for arbitrary imaginary parts in the core and cladding indices, it is clear from the derivation in Section 32–4 that the real and imaginary parts of $\delta\beta$ are both proportional to the ratio of integrals in Eq. (13–12), where \mathbf{e}_t is now complex.

13–11 Higher-order polarization corrections

We have shown that the modes of weakly guiding waveguides are approximately TEM waves, with transverse field components \mathbf{e}_t and \mathbf{h}_t . However, the exact modal fields have longitudinal components. For the weakly guiding waveguide these components are very small, and are expressible approximately in terms of \mathbf{e}_t and \mathbf{h}_t . From Eq. (32–18) we have

$$e_z \cong \frac{i(2\Delta)^{1/2}}{V} (\rho \nabla_t \cdot \mathbf{e}_t); \quad h_z \cong \frac{i(2\Delta)^{1/2}}{V} (\rho \nabla_t \cdot \mathbf{h}_t). \quad (13-13)$$

Table 13-2 Properties of bound modes on weakly guiding waveguides. Parameters are defined inside the back cover. The modal amplitude a depends on the source of illumination, and A_{co} is the core cross-section. We assume \mathbf{e}_t , Ψ and F_t are real on nonabsorbing

		<i>Arbitrary waveguide</i>
Refractive-index profile		$n_{\text{co}}^2 \{1 - 2\Delta f(x, y)\}$
Orthogonality $j \neq k$		$\int_{A_{\infty}} \mathbf{e}_{ij} \cdot \mathbf{e}_{ik} \, dA = 0$
Normalization	\hat{N}	$\frac{n_{\text{co}}}{2} \left(\frac{\epsilon_0}{\mu_0} \right)^{1/2} \int_{A_{\infty}} \mathbf{e}_t^2 \, dA$
Intensity or power density	\hat{S}	$ a ^2 \frac{n_{\text{co}}}{2} \left(\frac{\epsilon_0}{\mu_0} \right)^{1/2} \mathbf{e}_t^2$
Modal power	\hat{P}	$ a ^2 \frac{n_{\text{co}}}{2} \left(\frac{\epsilon_0}{\mu_0} \right)^{1/2} \int_{A_{\infty}} \mathbf{e}_t^2 \, dA$
Fraction of power in the core	$\hat{\eta}$	$\int_{A_{\text{co}}} \mathbf{e}_t^2 \, dA \bigg/ \int_{A_{\infty}} \mathbf{e}_t^2 \, dA$
Power attenuation coefficient	$\hat{\gamma}$	$2k \int_{A_{\infty}} n^i \mathbf{e}_t^2 \, dA \bigg/ \int_{A_{\infty}} \mathbf{e}_t^2 \, dA$
Propagation constant	$\tilde{\beta}^2$	$\frac{\int_{A_{\infty}} \{ (k n \mathbf{e}_t)^2 - (\nabla_t \cdot \mathbf{e}_t)^2 \} \, dA}{\int_{A_{\infty}} \mathbf{e}_t^2 \, dA}$
Modal parameter	\tilde{U}^2	$\frac{\int_{A_{\infty}} \{ f V^2 \mathbf{e}_t^2 + (\rho \nabla_t \cdot \mathbf{e}_t)^2 \} \, dA}{\int_{A_{\infty}} \mathbf{e}_t^2 \, dA}$
Useful derivative	$\frac{d\tilde{U}}{dV}$	$\frac{\tilde{V}}{\tilde{U}} \int_{A_{\infty}} f \mathbf{e}_t^2 \, dA \bigg/ \int_{A_{\infty}} \mathbf{e}_t^2 \, dA$
Group velocity	\tilde{v}_g	$\frac{c \tilde{\beta}}{k} \int_{A_{\infty}} \mathbf{e}_t^2 \, dA \bigg/ \int_{A_{\infty}} n^2 \mathbf{e}_t^2 \, dA$
Distortion parameter	\tilde{D}	$-\frac{d^2}{dV^2} \left(\frac{\tilde{U}^2}{2V} \right)$

waveguides, and are approximately real on an absorbing waveguide if $n^i \ll n^r \cong n_{co}$. The equations satisfied by Ψ and F_l are in Table 13-1, and $F_l^{(j)}$, $F_l^{(k)}$ denote different solutions of the scalar wave equation for the same value of l . Vector operators are defined in Table 30-1, page 592.

<i>Noncircular waveguide</i>	<i>Circular fiber</i>
$n_{co}^2 \{1 - 2\Delta f(x, y)\}$	$n_{co}^2 \{1 - 2\Delta f(R)\}$
$\int_{A_\infty} \Psi_j \Psi_k dA = 0$	$\int_0^\infty F_l^{(j)} F_l^{(k)} R dR = 0$
$\frac{n_{co}}{2} \left(\frac{\epsilon_0}{\mu_0}\right)^{1/2} \int_{A_\infty} \Psi^2 dA$	$\pi \rho^2 n_{co} \left(\frac{\epsilon_0}{\mu_0}\right)^{1/2} \int_0^\infty F_l^2 R dR$
$ a ^2 \frac{n_{co}}{2} \left(\frac{\epsilon_0}{\mu_0}\right)^{1/2} \Psi^2$	$ a ^2 \frac{n_{co}}{2} \left(\frac{\epsilon_0}{\mu_0}\right)^{1/2} F_l^2$
$ a ^2 \frac{n_{co}}{2} \left(\frac{\epsilon_0}{\mu_0}\right)^{1/2} \int_{A_\infty} \Psi^2 dA$	$\pi \rho^2 a ^2 n_{co} \left(\frac{\epsilon_0}{\mu_0}\right)^{1/2} \int_0^\infty F_l^2 R dR$
$\int_{A_{co}} \Psi^2 dA \Big/ \int_{A_\infty} \Psi^2 dA$	$\int_0^1 F_l^2 R dR \Big/ \int_0^\infty F_l^2 R dR$
$2k \int_{A_\infty} n^i \Psi^2 dA \Big/ \int_{A_\infty} \Psi^2 dA$	$2k \int_0^\infty n^i F_l^2 R dR \Big/ \int_0^\infty F_l^2 R dR$
$\frac{\int_{A_\infty} \{(kn\Psi)^2 - (\nabla_t \Psi)^2\} dA}{\int_{A_\infty} \Psi^2 dA}$	$\frac{\int_0^\infty \left\{ (k\rho n F_l)^2 - \left(\frac{dF_l}{dR}\right)^2 - \left(l\frac{F_l}{R}\right)^2 \right\} R dR}{\rho^2 \int_0^\infty F_l^2 R dR}$
$\frac{\int_{A_\infty} \{fV^2 \Psi^2 + (\rho \nabla_t \Psi)^2\} dA}{\int_{A_\infty} \Psi^2 dA}$	$\frac{\int_0^\infty \left\{ \left(\frac{dF_l}{dR}\right)^2 + \left(\frac{l^2}{R^2} + V^2 f\right) F_l^2 \right\} R dR}{\int_0^\infty F_l^2 R dR}$
$\frac{V}{\bar{U}} \int_{A_\infty} f \Psi^2 dA \Big/ \int_{A_\infty} \Psi^2 dA$	$\frac{V}{\bar{U}} \int_0^\infty f F_l^2 R dR \Big/ \int_0^\infty F_l^2 R dR$
$\frac{c\hat{\beta}}{k} \int_{A_\infty} \Psi^2 dA \Big/ \int_{A_\infty} n^2 \Psi^2 dA$	$\frac{c\hat{\beta}}{k} \int_0^\infty F_l^2 R dR \Big/ \int_0^\infty n^2 F_l^2 R dR$
$-\frac{d^2}{dV^2} \left(\frac{\tilde{U}^2}{2V} \right)$	$-\frac{d^2}{dV^2} \left(\frac{\tilde{U}^2}{2V} \right)$

These small fields are rarely required, and in situations where they appear important, it is usually true that the transverse fields need to be known more accurately than in Table 13-1. It is possible to generate terms to higher and higher order for improved accuracy by expressing the modal fields as perturbation expansions in the small parameter Δ , but at the penalty of increasing complexity. This is described in Section 32-2.

Group velocity and distortion parameter

The expressions in Table 13-2 for the group velocity and distortion parameter are given in terms of solutions of the scalar wave equation. Given the polarization correction $\delta\beta$ to the scalar propagation constant, we can write down higher-order corrections to these expressions. This is facilitated by first defining the mode parameter \tilde{U} associated with the scalar propagation constant

$$\tilde{U} = \rho(k^2 n_{co}^2 - \tilde{\beta}^2)^{1/2}. \quad (13-14)$$

If δU denotes the polarization correction to \tilde{U} , then the exact mode parameter U and propagation constant β are well approximated by

$$U \cong \tilde{U} + \delta U; \quad \beta \cong \tilde{\beta} + \delta\beta, \quad (13-15)$$

and we show in Section 32-2 that the corrections are related by Eq. (32-11b), i.e.

$$\delta U = -\{\rho V / \tilde{U} (2\Delta)^{1/2}\} \delta\beta. \quad (13-16)$$

For the group velocity, we expand the second expression for v_g in Eq. (11-57) in powers of Δ and omit the modal subscript. We then substitute for U from Eq. (13-15) and note that δU is of order Δ according to Eqs. (13-11) and (13-16). Correct to second order in Δ we find

$$v_g = \tilde{v}_g + \delta v_g; \quad \tilde{v}_g = \frac{c}{n_{co}} \left\{ 1 + \Delta y \right\}, \quad (13-17a)$$

$$\delta v_g = \frac{c}{n_{co}} \Delta^2 \left\{ y^2 + \frac{\tilde{U}}{V^2} y - \frac{\tilde{U}^4}{2V^4} + 2 \frac{d}{dV} \left(\frac{\tilde{U}}{V} \frac{\delta U}{\Delta} \right) \right\}; \quad y = \frac{d}{dV} \left(\frac{\tilde{U}^2}{V} \right). \quad (13-17b)$$

The corresponding expansion of the distortion parameter follows from the second expression for D in Eq. (11-59a). Correct to first order in Δ we deduce

$$D = \tilde{D} + \delta D; \quad \tilde{D} = -\frac{d^2}{dV^2} \left(\frac{\tilde{U}^2}{2V} \right); \quad \delta D = \frac{\Delta}{2} \frac{d}{dV} \left\{ y^2 - \frac{n_{co}}{c} \frac{\delta v_g}{\Delta^2} \right\}, \quad (13-18)$$

where y is given by Eq. (13-17b).

ANISOTROPIC WEAKLY GUIDING WAVEGUIDES

We now generalize the theory of this chapter to include single-mode waveguides constructed from anisotropic material, as discussed in Section 11–23. Such waveguides have a variety of practical applications [5] and they also model the visual photoreceptor of animals [6, 7]. For perspective, we first review the anisotropic propagation characteristics due solely to waveguide geometry, i.e. due to the *structural anisotropy* of the waveguide. Then we discuss those additional polarization effects introduced by anisotropic material. Our main concern here is for waveguides that have significant material anisotropy, as very weak anisotropy can be treated directly by the perturbation methods of Section 18–9.

Structural anisotropy

A single-mode, isotropic waveguide propagates two fundamental modes with orthogonal polarization states. Unless the waveguide cross-section has circular symmetry, the propagation characteristics of the two modes differ. This difference is due to the geometry of the waveguide cross-section, i.e. due to *structural anisotropy*. The greater the departure from circular symmetry, the greater the structural anisotropy. Thus, for step profiles, structural anisotropy is maximum for planar waveguides. In the case of the step-profile planar waveguide, the physical mechanism for structural anisotropy is the polarization dependence of total internal reflection, summarized in Fig. 10–2, which manifests itself as a polarization-dependent lateral shift. We ignore this polarization dependence in Chapter 10, since only weakly guiding waveguides are considered.

Large index difference

When the core refractive index n_{co} greatly exceeds the refractive index n_{cl} of the cladding, i.e. $n_{cl}/n_{co} \rightarrow 0$ or, equivalently, $\Delta \rightarrow \frac{1}{2}$, structural anisotropy strongly influences propagation on planar waveguides. Consider, for example, the two fundamental modes, i.e. the first even TE and TM modes, of the step-profile planar waveguide. The fraction of power propagating in the core, η , is given by the expression in Table 12–2 for the two polarizations. When $V = 1.55$, we find that 80% of the TE mode's power propagates in the core for any value of Δ , whereas the value of η for the TM mode depends on Δ and $\eta \rightarrow 0$ as $\Delta \rightarrow \frac{1}{2}$, e.g. $\eta \cong 0.1$ when $\Delta \cong 0.495$. At the opposite extreme, when the difference in indices is small, the variation in η for the two fundamental modes is slight, e.g. a variation of only 1% when $\Delta \cong 0.05$. Thus, *structural anisotropy is insignificant in weakly guiding waveguides*, and manifests itself through the slight difference

in propagation constants, discussed in Section 13–5. On the other hand, material anisotropy can influence propagation on weakly guiding waveguides considerably as we now show.

Material anisotropy

Consider waveguides constructed from anisotropic or, equivalently, crystal-line material with the properties discussed in Section 11–23. For simplicity, we assume that the three principal axes of the dielectric medium are parallel to the three geometrical axes of the isotropic waveguide. The spatial variation of the refractive-index profile can differ for each polarization direction. For light polarized in the x -direction, the waveguide is characterized by the refractive-index profile $n_x(x, y)$ and associated parameters Δ_x and V_x , while for light polarized entirely in the y -direction it is characterized by the profile $n_y(x, y)$ and associated parameters Δ_y and V_y , where

x -polarized light	y -polarized light	
$2\Delta_x = 1 - (n_{cl}^x/n_{co}^x)^2$ $V_x = k\rho n_{co}^x (2\Delta_x)^{1/2}$	$2\Delta_y = 1 - (n_{cl}^y/n_{co}^y)^2$ $V_y = k\rho n_{co}^y (2\Delta_y)^{1/2}$	(13–19)

These parameters are generalizations of the definitions inside the back cover for isotropic waveguides. Thus n_{co}^x and n_{co}^y are the maximum values of the core index and n_{cl}^x and n_{cl}^y are the uniform values of the cladding index.

13–12 Modes of anisotropic waveguides

Now we modify the early sections of this chapter to include weakly guiding waveguides constructed from the anisotropic material discussed above, i.e. $n_{co}^x \cong n_{cl}^x \cong n_{co}^y \cong n_{cl}^y$. To do this, we first recall from Section 11–23 that the two axially directed, or z -directed modes of an unbounded, uniform anisotropic medium are TEM waves. One mode is polarized parallel to the x -axis, the other is polarized parallel to the y -axis, assuming the cartesian axes are the principal axes of the anisotropic medium. Next, we recall from Section 13–2 that the modes of weakly guiding, isotropic waveguides are also axially directed TEM waves. From Sections 13–4 and 13–5, we know that one fundamental mode is x -polarized and the other is y -polarized, where the x - and y -axes are the optical axes of the waveguide cross-section. For example, the optical axes are parallel to the major and minor axes of an elliptical cross-section, while they are any orthogonal pair of axes for the circular cross-section.

Circular cross-section

From the above discussion, it is intuitive that the two fundamental modes of an anisotropic fiber of circular cross-section must be polarized along the x and y principal axes, respectively. Hence the anisotropy breaks the geometrical circular symmetry of the fiber, and is analogous to the fiber of noncircular cross-section discussed in Section 13-5. Thus, the x -polarized mode 'sees' a fiber characterized by $n_x(x, y)$, Δ_x and V_x , while the y -polarized mode 'sees' a fiber characterized by $n_y(x, y)$, Δ_y and V_y , as illustrated in Fig. 13-1. The modes

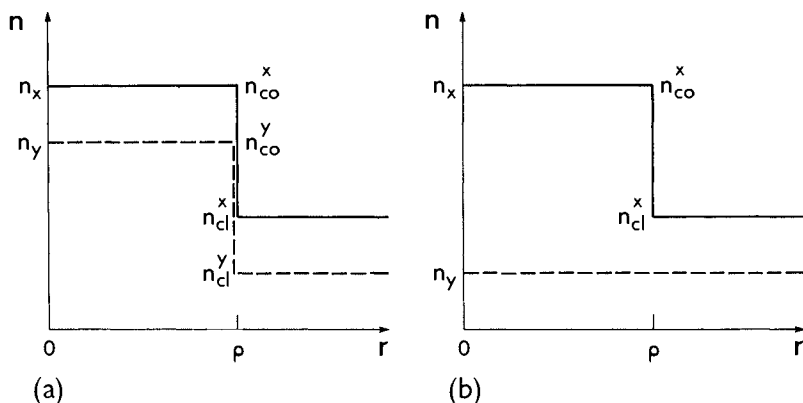


Fig. 13-1 Two examples of anisotropic fibers, each characterized by the profile n_x for x -polarized light and the profile n_y for y -polarized light.

are independent of $n_z(x, y)$ within the weak-guidance approximation because of their approximate TEM nature. Accordingly results for the isotropic weakly guiding fiber apply to the anisotropic fiber provided we replace $n(x, y)$, n_{co} , n_{cl} and Δ by the corresponding expressions in Eq. (13-19), and take the cartesian x and y axes in the cross-section to be parallel to the principal axes of the anisotropic dielectric material. Thus, for example, we deduce from Eq. (13-9), that the two fundamental modes have fields of the form

x -polarized	y -polarized	
$E_x = \Psi_x(r) \exp(i\tilde{\beta}_x z)$	$H_y = \Psi_y(r) \exp(i\tilde{\beta}_y z)$	(13-20)
$H_y = \left(\frac{\epsilon_0}{\mu_0}\right)^{1/2} n_{co}^x E_x$	$H_x = -\left(\frac{\epsilon_0}{\mu_0}\right)^{1/2} n_{co}^y E_y$	

where Ψ_x , $\tilde{\beta}_x$ and Ψ_y , $\tilde{\beta}_y$ are the fundamental solutions of the scalar wave equation of Eq. (13-8) with n replaced by n_x and n_y , respectively. Apart from

exceptional cases [8], the higher-order modes have fields with the same form as Eq. (13–20), since the anisotropy breaks the circular symmetry of the fiber cross-section. However, if the material anisotropy is *sufficiently* weak, i.e. $n_x(x, y) \cong n_y(x, y)$, then we have a situation similar to higher-order modes on a nearly circular fiber discussed in Section 13–9.

Polarization corrections

The small polarization correction to the scalar propagation constant $\tilde{\beta}$ due to *structural* anisotropy is given by Eq. (13–11). For an isotropic fiber of circular cross-section, the corrections for the two fundamental modes are identical, i.e. $\delta\beta_x = \delta\beta_y$. This is not the case for the anisotropic fiber, since the parameters in Eq. (13–19) depend on polarization. However, $|\delta\beta_x - \delta\beta_y|$ is small compared to the difference in propagation constants in Eq. (13–20), $|\tilde{\beta}_x - \tilde{\beta}_y|$, since the fiber is weakly guiding, and can be ignored.

Mathematical derivation

The results derived above by intuitive arguments can also be found by generalizing the perturbation method of Section 32–6. Starting from the vector wave equation for \mathbf{E} , given by Eq. (30–31), we recognize that the simplification in Section 30–13, leading to Eq. (30–35), applies to modes of weakly guiding anisotropic waveguides. Thus, as Eq. (30–35) has the identical form as its isotropic analogue, all perturbation results for the isotropic waveguide hold for the anisotropic waveguide provided the profile n is replaced by either n_x or n_y for the appropriate polarization state.

Noncircular cross-section

If the principal axes of the anisotropic material are parallel to the optical axes of a fiber of noncircular cross-section, it is intuitive that the two fundamental modes must also be polarized along these axes. We then have a situation identical to the circular cross-section, discussed above, except that $\Psi_x(r)$ in Eq. (13–20) is replaced by $\Psi_x(x, y)$ and $\Psi_y(r)$ by $\Psi_y(x, y)$. Thus, *all results for weakly guiding isotropic waveguides apply to weakly guiding anisotropic waveguides by following the simple substitution discussed above.*

We ignore the small polarization corrections to $\tilde{\beta}_x$ and $\tilde{\beta}_y$, given by Eq. (13–11), because $\tilde{\beta}_x \neq \tilde{\beta}_y$ for isotropic, noncircular waveguides. This is an accurate approximation, provided the material anisotropy is not so minute as to be comparable to the small contribution of order $\Delta^{3/2}$, due to the waveguide structure. The higher-order modes of the noncircular waveguide have the same form as the fundamental modes, except when the fiber is nearly circular, for reasons given in Section 13–9.

13–13 Single-mode single-polarization fibers

We showed in the discussion of structural anisotropy above, that the core index must *greatly exceed* the cladding index for the propagation characteristics of the two fundamental modes to differ significantly. Here we show that a *relatively small amount* of material anisotropy can dramatically influence propagation by removing one of the two possible polarization states of the fundamental mode. This results in a fiber that is truly single moded.

Consider a step profile fiber of circular cross-section whose refractive index profile, n_x , for x-polarized light is shown in Fig. 13–1(b). We assume that V_x is sufficiently small so no higher-order modes propagate. Thus, an x-polarized source will excite the fundamental mode with field E_x given by Eq. (13–20). To completely eliminate the y-polarized mode, we ensure that the refractive index profile, n_y , for y-polarized light does not provide guidance. The most direct way to achieve this is to let the core and cladding refractive indices be equal, so that $\Delta_y = 0$. An alternative method for removing the y-polarized mode is discussed below.

RADIATION LEAKAGE IN ANISOTROPIC FIBERS

The above description of anisotropic fibers treats each modal polarization state as if it were in isolation from the other. This is valid only when the modal fields are uniformly-polarized, which is never exactly the case for non-planar waveguides, as is clear from Section 11–15 and 11–16. Even on an isotropic weakly guiding fiber, the x-polarized modal field has a very small y-component of order Δ and the y-polarized modal field has a very small x-component, as we show in Section 12–11. Thus, a fraction of the power propagating in the x-polarized mode ‘sees’ something of the n_y profile and, analogously, the y-polarized mode ‘sees’ something of the n_x profile. In other words, there is a small amount of coupling between the two polarization states. We now show that the y-polarized mode of Fig. 13–1(a) will suffer radiation loss when the birefringence is sufficiently large. This radiation is due to polarization coupling and is anticipated from the discussion of Section 11–24, which specifies the minimum value of β for a mode to be bound to an anisotropic fiber.

13–14 Leaky, single-mode, single-polarization fibers

We now consider the fiber profile defined in Fig. 13–1(a). From the argument of Section 11–24, we know that radiation losses will occur to any mode with $\beta < kn_{cl}^x$, i.e. β will have an imaginary part. Thus, the ‘y’-polarized mode of Fig 13–1(a) will ‘leak’ as it propagates [9], if the birefringence is sufficiently high to satisfy $\beta_y < kn_{cl}^x$. When this occurs, some of the ‘y’-polarized mode ‘sees’ a

cladding index n_{cl}^x which is *higher* than β_y/k , so that guidance is not possible. Because the imaginary part of $\tilde{\beta}_y$ is small and the fiber is weakly guiding, the vector wave equation, Eq. (30-31), can be solved by perturbation methods to obtain the leakage rate [10]. Thus, depending on the fiber length and modal leakage rate, the fiber of Fig. 13-1(a) is effectively a single-moded, single-polarization waveguide [9, 11].

Following the above logic and Section 11-24, we can also appreciate that even the x-polarized mode of the profile of Fig. 13-1(b) will be leaky if the uniform profile index, n_y , is sufficiently greater than n_{cl}^x so that $\tilde{\beta}_x < kn_{cl}^y$.

REFERENCES

1. Snyder, A. W. and Young, W. R. (1978) Modes of optical waveguides. *J. Opt. Soc. Am.*, **68**, 297-309.
2. Snyder, A. W. (1969) Asymptotic expressions for eigenfunctions and eigenvalues of dielectric or optical waveguides. *I.E.E.E. Trans. Microwave Theory Tech.* **17**, 1130-8.
3. Gloge, D. (1971) Weakly guiding fibers. *Appl. Opt.*, **10**, 2252-8.
4. Arnaud, J. A. (1976) *Beam and Fiber Optics*, Academic Press, New York.
5. Kaminow, I. P. (1981) Polarization in optical fibers. *I.E.E.E. Trans. J. Quantum Electron.*, **17**, 15-22.
6. Snyder, A. W. (1974) Light absorption in visual photoreceptors. *J. Opt. Soc. Am.*, **64**, 216-30.
7. Snyder, A. W. (1979), in *Handbook of Sensory Physiology*, Vol. VII/6A (ed. H. Autrum), Springer-Verlag, Berlin, pp. 279-81.
8. A. W. Snyder and F. Rühl (1983) Novel polarization phenomena on anisotropic multimoded fibres. *Electron. Lett.*, **19**, 401-2.
9. A. W. Snyder and F. Rühl (1983) New single-mode single-polarization optical fiber. *Electron. Lett.*, **19**, 185-6.
10. A. W. Snyder and F. Rühl (1983) Single-mode, single-polarization fibers made of birefringence material. *J. Opt. Soc. Am.*, **73**, 1165-74.
11. M. P. Varnham, D. N. Payne, R. D. Birch and E. J. Tarbox (1983) Single polarisation operation of highly birefringent bow-tie optical fibers. *Electron. Lett.*, **19**, 246-7.

Circular fibers

Bound modes of circular fibers	301
14-1 Construction of the modal fields	302
14-2 Fundamental and HE_{1m} ($l = 0$) modes	303
14-3 Higher-order ($l \geq 1$) modes	306
14-4 <i>Example: Infinite parabolic profile</i>	306
14-5 <i>Example: Infinite power-law profiles</i>	309
Step-profile fiber	311
14-6 Fundamental and HE_{1m} ($l = 0$) modes	311
14-7 Higher-order ($l \geq 1$) modes	317
Clad graded-profile fibers	326
14-8 <i>Example: Closed-form solutions</i>	326
14-9 <i>Example: Clad power-law profiles</i>	326
14-10 Equal volume profiles	330
14-11 Fundamental mode for small V	333
References	334

We showed in the previous chapter how the modes of weakly guiding waveguides are constructed from solutions of the scalar wave equation. Here we consider fibers of circular cross-section and solve the scalar wave equation analytically for specific refractive-index profiles with axial symmetry. We pay particular attention to single-mode fibers and to the properties of the fundamental HE_{11} modes. One important observation for a general class of single-mode fibers with a power-law variation in core profile and a uniform cladding is that both the distribution of fundamental-mode power over the cross-section, and the maximum value of the fiber parameter V for single-mode operation depend primarily on the profile ‘volume’ and are relatively insensitive to profile shape. This volume is proportional to the integral over the core cross-section of the excess of the profile above its cladding value. Conversely, pulse dispersion on single-mode fibers depends principally on profile shape and is comparatively insensitive to the profile volume.

BOUND MODES OF CIRCULAR FIBERS

The circular fiber is illustrated in Fig. 14-1, which shows the cartesian and

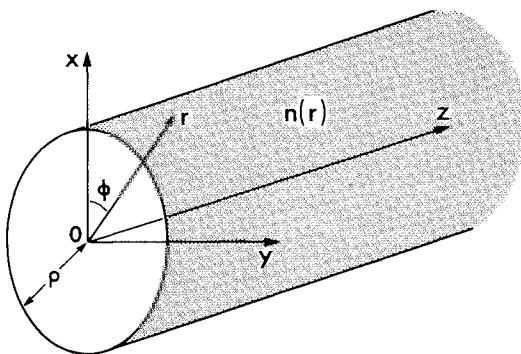


Fig. 14.1 Section of a circularly symmetric fiber, which is unbounded in the r - and z -directions. The core radius is ρ , the normalized radius $R = r/\rho$ and $n(r)$ is the refractive-index profile.

cylindrical polar coordinates used to describe the modes. For the refractive-index profile $n(r)$ we use the representation

$$n^2(R) = n_{co}^2 \{1 - 2\Delta f(R)\}; \quad R = r/\rho, \quad (14-1)$$

where n_{co} is the maximum index and $f(R) \geq 0$ specifies the profile variation. The radial coordinate r is normalized by ρ , which denotes either the core radius, when there is a uniform cladding, or a scaling length when there is no obvious interface. We define Δ to be the profile height parameter, or relative index difference, which satisfies $\Delta \ll 1$ for weakly guiding fibers. Hence from Eq. (11-48) we have

$$\Delta = \frac{1}{2} \left\{ 1 - \frac{n_{cl}^2}{n_{co}^2} \right\} \cong \frac{n_{co} - n_{cl}}{n_{co}}, \quad (14-2)$$

for fibers with a uniform cladding.

14-1 Construction of the modal fields

In Chapter 13 we showed that the modal fields of weakly guiding fibers have the general form

$\mathbf{E} \cong \mathbf{e}_t(x, y) \exp\{i(\tilde{\beta} + \delta\beta)z\}$	$\mathbf{H} \cong \mathbf{h}_t(x, y) \exp\{i(\tilde{\beta} + \delta\beta)z\}$
---	---

(14-3a)

$\mathbf{h}_t \cong n_{co}(\epsilon_0/\mu_0)^{1/2} \hat{\mathbf{z}} \times \mathbf{e}_t$
--

(14-3b)

The construction of \mathbf{e}_t for circular fibers is described in Sections 13-4 and 13-7, using physical arguments, and again in Sections 32-6 and 32-7, using

perturbation theory [1], where we show that it is necessary to solve the scalar wave equation, Eq. (13-8), to find \mathbf{e}_l . For a circular fiber, ∇_l^2 is given in Table 30-1, page 592, leading to solutions with the separable forms $\Psi = F_l(r)\cos l\phi$ and $\Psi = F_l(r)\sin l\phi$, where $l = 0, 1, \dots$, and $F_l(r)$ satisfies the ordinary differential equation

$$\left\{ \frac{d^2}{dr^2} + \frac{1}{r} \frac{d}{dr} + k^2 n^2(r) - \frac{l^2}{r^2} - \tilde{\beta}^2 \right\} F_l(r) = 0. \quad (14-4a)$$

It is convenient to make this equation dimensionless. To do this we take $n(R)$ from Eq. (14-1), set $R = r/\rho$ and use the definitions of \tilde{U} and V inside the back cover. This leads to

$$\left\{ \frac{d^2}{dR^2} + \frac{1}{R} \frac{d}{dR} - \frac{l^2}{R^2} + \tilde{U}^2 - V^2 f(R) \right\} F_l(R) = 0; \quad R = \frac{r}{\rho}. \quad (14-4b)$$

Continuity of F_l and dF_l/dR throughout the fiber leads to an eigenvalue equation for $\tilde{\beta}$ of each mode, as discussed in Section 33-1.

Given the solutions $F_l(R)$, we then determine the fields \mathbf{e}_{li} as discussed in Sections 13-4 and 13-7, and summarized in Table 13-1, page 288. We identify the fields of circular fibers in Table 14-1 using the conventional mode nomenclature of Section 11-16.

The left side of the table gives \mathbf{e}_{li} and \mathbf{h}_{li} , while the right side gives the small corrections due to polarization effects of the fiber structure. The $\delta\beta_l$ correction terms of Eq. (14-3a) are important for all but the HE_{1m} modes, for reasons discussed in Sections 13-4 and 13-7. These terms are found by substituting \mathbf{e}_{li} from Table 14-1 into the expression for $\delta\beta_l$ given in Table 13-1, page 288, and replacing dA by $\rho^2 R dR d\phi$. The longitudinal fields e_{zi} , h_{zi} are calculated from Eq. (13-13). For reasons given in Section 13-11, they are rarely required but are included for completeness.

14-2 Fundamental and HE_{1m} ($l = 0$) modes

The two fundamental, or HE_{11} , modes and all other pairs of HE_{1m} modes were discussed in Section 13-4. Each mode of a particular pair has a transverse electric field whose direction, or polarization, is parallel to one of an arbitrary pair of orthogonal directions in the fiber cross-section [1]. Thus, these modes are uniformly polarized. For convenience we take one mode to be x-polarized and the other y-polarized in Fig. 14-1. There is only one solution of the scalar wave equation for these modes, corresponding to $l = 0$ in Eq. (14-4). The transverse fields, given by Eq. (13-9) and repeated in Table 14-1, ignore all polarization properties of the fiber. For future reference, we give the transformation of the components of these fields from cartesian to polar

Table 14-1 Modal fields of weakly guiding circular fibers. Subscripts t and z denote transverse and longitudinal components. Unit vectors \hat{x} , \hat{y} and \hat{z} are parallel to the

i	Mode	\mathbf{e}_{ti}	\mathbf{h}_{ti}
-----	------	-------------------	-------------------

Fundamental HE_{11} and HE_{1m} ($l = 0$) modes

1	Even HE_{1m}	$\hat{x}F_0$	$n_{co}\left(\frac{\epsilon_0}{\mu_0}\right)^{1/2} \hat{y}F_0$
3	Odd HE_{1m}	$\hat{y}F_0$	$-n_{co}\left(\frac{\epsilon_0}{\mu_0}\right)^{1/2} \hat{x}F_0$

Higher-order modes ($l \geq 1$)

1	Even $\text{HE}_{l+1,m}$	$\{\hat{x} \cos(l\phi - \hat{y} \sin l\phi)\} F_l$	$n_{co}\left(\frac{\epsilon_0}{\mu_0}\right)^{1/2} \{\hat{x} \sin l\phi + \hat{y} \cos l\phi\} F_l$
2	TM_{0m} ($l = 1$)	$\{\hat{x} \cos \phi + \hat{y} \sin \phi\} F_1$	$-n_{co}\left(\frac{\epsilon_0}{\mu_0}\right)^{1/2} \{\hat{x} \sin \phi - \hat{y} \cos \phi\} F_1$
2	Even $\text{EH}_{l-1,m}$ ($l > 1$)	$\{\hat{x} \cos l\phi + \hat{y} \sin l\phi\} F_l$	$-n_{co}\left(\frac{\epsilon_0}{\mu_0}\right)^{1/2} \{\hat{x} \sin l\phi - \hat{y} \cos l\phi\} F_l$
3	Odd $\text{HE}_{l+1,m}$	$\{\hat{x} \sin l\phi + \hat{y} \cos l\phi\} F_l$	$-n_{co}\left(\frac{\epsilon_0}{\mu_0}\right)^{1/2} \{\hat{x} \cos l\phi - \hat{y} \sin l\phi\} F_l$
4	TE_{0m} ($l = 1$)	$\{\hat{x} \sin \phi - \hat{y} \cos \phi\} F_1$	$n_{co}\left(\frac{\epsilon_0}{\mu_0}\right)^{1/2} \{\hat{x} \cos \phi + \hat{y} \sin \phi\} F_1$
4	Odd $\text{EH}_{l-1,m}$ ($l > 1$)	$\{\hat{x} \sin l\phi - \hat{y} \cos l\phi\} F_l$	$n_{co}\left(\frac{\epsilon_0}{\mu_0}\right)^{1/2} \{\hat{x} \cos l\phi + \hat{y} \sin l\phi\} F_l$

$\left\{ \frac{d^2}{dR^2} + \frac{1}{R} \frac{d}{dR} - \frac{l^2}{R^2} + \tilde{U}^2 - V^2 f \right\} F_l = 0; \quad G_l^\pm = \frac{dF_l}{dR} \pm \frac{l}{R} F_l$
$\mathbf{e}_t = \hat{x}e_x + \hat{y}e_y = \hat{r}e_r + \hat{\phi}e_\phi$
$e_r = e_x \cos \phi + e_y \sin \phi \quad e_\phi = -e_x \sin \phi + e_y \cos \phi$
$e_x = e_r \cos \phi - e_\phi \sin \phi \quad e_y = e_r \sin \phi + e_\phi \cos \phi$

cartesian axes in Fig. 14-1. Parameters are defined inside the back cover.

e_{zi}	h_{zi}	$\delta\beta_i$
Fundamental HE₁₁ and HE_{1m} ($l = 0$) modes		
$i \frac{(2\Delta)^{1/2}}{V} G_0 \cos \phi$	$in_{co} \left(\frac{\epsilon_0}{\mu_0} \right)^{1/2} \frac{(2\Delta)^{1/2}}{V} G_0 \sin \phi$	I_1
$i \frac{(2\Delta)^{1/2}}{V} G_0 \sin \phi$	$-in_{co} \left(\frac{\epsilon_0}{\mu_0} \right)^{1/2} \frac{(2\Delta)^{1/2}}{V} G_0 \cos \phi$	I_1

Higher-order modes ($l \geq 1$)

$i \frac{(2\Delta)^{1/2}}{V} G_l^- \cos(l+1)\phi$	$in_{co} \left(\frac{\epsilon_0}{\mu_0} \right)^{1/2} \frac{(2\Delta)^{1/2}}{V} G_l^- \sin(l+1)\phi$	$I_1 - I_2$
$i \frac{(2\Delta)^{1/2}}{V} G_l^+$	0	$2(I_1 + I_2)$
$i \frac{(2\Delta)^{1/2}}{V} G_l^+ \cos(l-1)\phi$	$-in_{co} \left(\frac{\epsilon_0}{\mu_0} \right)^{1/2} \frac{(2\Delta)^{1/2}}{V} G_l^+ \sin(l-1)\phi$	$I_1 + I_2$
$i \frac{(2\Delta)^{1/2}}{V} G_l^- \sin(l+1)\phi$	$-in_{co} \left(\frac{\epsilon_0}{\mu_0} \right)^{1/2} \frac{(2\Delta)^{1/2}}{V} G_l^- \cos(l+1)\phi$	$I_1 - I_2$
0	$in_{co} \left(\frac{\epsilon_0}{\mu_0} \right)^{1/2} \frac{(2\Delta)^{1/2}}{V} G_l^+$	0
$i \frac{(2\Delta)^{1/2}}{V} G_l^+ \sin(l-1)\phi$	$in_{co} \left(\frac{\epsilon_0}{\mu_0} \right)^{1/2} \frac{(2\Delta)^{1/2}}{V} G_l^+ \cos(l-1)\phi$	$I_1 + I_2$

$$I_1 = \frac{(2\Delta)^{3/2}}{4\rho V} \int_0^\infty RF_l (dF_l/dR) (df/dR) dR \Big/ \int_0^\infty RF_l^2 dR$$

$$I_2 = \frac{l(2\Delta)^{3/2}}{4\rho V} \int_0^\infty F_l^2 (df/dR) dR \Big/ \int_0^\infty RF_l^2 dR$$

coordinates at the bottom of the left side. We are reminded that the fundamental-mode solution of Eq. (14-4) has the largest value of β , or, equivalently, the smallest value of U of the bound modes, and that $\delta\beta$ is the same for both even and odd modes.

14-3 Higher-order ($l \geq 1$) modes

The construction of the higher-order, or $l \geq 1$, modes of Table 14-1 is discussed in Section 13-7. For each $l \geq 1$, there are four modes. The far left column of Table 14-1 gives the value of i for the appropriate field e_{ti} of Table 13-1, page 288. These modes are not uniformly polarized, i.e. the direction of e_{ti} depends on the position in the fiber cross-section. The modes are labelled according to their hybrid characteristics, consistent with the labelling of the exact modes in Chapter 12. This may be verified by examining the limit $\Delta \rightarrow 0$ of the transverse fields of the step-profile fiber in Table 12-3, page 250[2]. The HE_{1m} modes of the previous section are a particular case of the $HE_{l+1,m}$ modes when $l = 0$.

We note that for each value of $l > 1$, two of the four modes have different values of $\delta\beta_i$, while the four $l = 1$ modes generally have three different values of $\delta\beta_i$. This is the reason why we cannot use a representation for the modal fields simpler than that in Table 14-1, such as the circularly polarized fields discussed in Section 32-8.

To summarize these two sections, the complete modal fields and corrected propagation constants for all bound modes of the weakly guiding circular fiber are given in Table 14-1. Consequently, for each profile considered below, we need only determine the solution $F_l(R)$ of Eq. (14-4).

14-4 Example: Infinite parabolic profile

Our first example has the refractive-index profile [3]

$$n^2(R) = n_{co}^2 \{1 - 2\Delta R^2\}; \quad R = r/\rho, \quad (14-5)$$

and is plotted as profile (k) in Fig. 12-8. Exact, closed-form solutions of Maxwell's equations are known only for TE modes, as we showed in Section 12-16. However, within the weak-guidance approximation, the scalar wave equation has closed-form solutions for all modes, from which we can derive simple expressions for the fields, propagation constants and properties of interest. These solutions are also the basis for the Gaussian approximation of Chapter 15. The parabolic profile is unphysical because $n^2(R) \rightarrow -\infty$ as $R \rightarrow \infty$. Also the weak-guidance approximation is accurate only for R sufficiently small to satisfy $n(R) \cong n(0)$. Both points can be overcome if the power of each mode is confined to a region within or close to $r = \rho$, and $\Delta \ll 1$. This constraint is discussed below. As the region increases in size, fiber polarization effects become important and the accuracy of the weak-guidance approximation decreases.

Table 14-2 Modes of the infinite parabolic-profile fiber. The vector modal fields are found by substitution into Table 14-1. Parameters are defined inside the back cover.

	$n^2(R) = n_{co}^2 \{1 - 2\Delta R^2\}; \quad R = \frac{r}{\rho}; \quad V = k\rho n_{co}(2\Delta)^{1/2}$	
	<i>Fundamental modes</i> ($l = 0, m = 1$)	<i>Higher-order modes</i> ($l \geq 0, m \geq 1$)
Radial dependence	$F_0 = \exp(-\frac{1}{2}VR^2)$ $G_0 = -VR \exp(-\frac{1}{2}VR^2)$	$F_l = R^l L_{m-1}^{(0)}(VR^2) \exp(-\frac{1}{2}VR^2)$
Eigenvalue equation	$\tilde{U} = (2V)^{1/2}$	$\tilde{U} = \{2V(2m + l - 1)\}^{1/2}$
Propagation constant	$\tilde{\beta} = \frac{V}{\rho(2\Delta)^{1/2}} \left\{ 1 - \frac{4\Delta}{V} \right\}^{1/2}$	$\tilde{\beta} = \frac{V}{\rho(2\Delta)^{1/2}} \left\{ 1 - \frac{4\Delta}{V}(2m + l - 1) \right\}^{1/2}$
Correction to propagation constant	$\delta\beta_1 = \delta\beta_3 = -\frac{(2\Delta)^{3/2}}{2\rho V}$ $\delta U_1 = \delta U_3 = \frac{\Delta}{\tilde{U}}$	$\delta\beta_1 = \delta\beta_3 = -\frac{l+1}{2\rho V}(2\Delta)^{3/2}$ $\delta\beta_2 = \delta\beta_4 = \frac{l-1}{2\rho V}(2\Delta)^{3/2}$
<i>Fundamental mode properties</i>		
$\tilde{N} = \frac{n_{co}}{2} \left(\frac{\epsilon_0}{\mu} \right)^{1/2} \frac{\pi\rho^2}{V}; \quad \tilde{\eta} = 1 - \exp(-V)$		
$\tilde{v}_g = \frac{c}{n_{co}}, \quad \delta v_g = -4 \frac{c}{n_{co}} \frac{\Delta^2}{V^2}; \quad \tilde{D} = 0, \quad \delta D = -\frac{4\Delta}{V^3}$		

<i>Specific forms for higher-order modes</i>		
l	m	$F_l(R)$
0	2	$(1 - VR^2) \exp(-\frac{1}{2}VR^2)$
0	3	$(1 - 2VR^2 + \frac{1}{2}V^2R^4) \exp(-\frac{1}{2}VR^2)$
1	1	$R \exp(-\frac{1}{2}VR^2)$
1	2	$R(2 - VR^2) \exp(-\frac{1}{2}VR^2)$
1	3	$R(3 - 3VR^2 + \frac{1}{2}V^2R^4) \times \exp(-\frac{1}{2}VR^2)$
2	1	$R^2 \exp(-\frac{1}{2}VR^2)$
2	2	$R^2(3 - VR^2) \exp(-\frac{1}{2}VR^2)$
2	3	$R^2(6 - 4VR^2 + \frac{1}{2}V^2R^4) \times \exp(-\frac{1}{2}VR^2)$
l	1	$R^l \exp(-\frac{1}{2}VR^2)$

Modal fields

If we set $f = R^2$ in Eq. (14-4) and make the transformations $w = VR^2$ and $F_l(R) = g_l(w)R^l \exp(-\frac{1}{2}VR^2)$, we obtain the equation [3]

$$\left\{ w \frac{d^2}{dw^2} + (l+1-w) \frac{d}{dw} + \frac{\tilde{U}^2}{4V} - \frac{l+1}{2} \right\} g_l = 0. \quad (14-6)$$

The solution which ensures F_l is everywhere bounded is the generalized Laguerre polynomial $L_{m-l}^{(l)}(w)$, where l and m are the modal subscripts appearing in Table 14-1. The general expression for F_l and specific forms for fundamental and low-order modes are presented in Table 14-2, from which the modal fields are determined by substituting into Table 14-1.

Propagation constants and polarization corrections

In solving Eq. (14-6) we simultaneously determine the eigenvalue equation which gives \tilde{U} , and thus the scalar propagation constant $\tilde{\beta}$, explicitly in terms of l , m and V in Table 14-2. There is no cutoff value of V for any mode, and consequently every mode may propagate for an arbitrary value of V . In fact, because $n^2(R) \rightarrow -\infty$ as $R \rightarrow \infty$, there are no radiation modes, and the totality of bound modes forms a complete set.

The polarization corrections $\delta\beta_i$ in Table 14-2 are found by setting $f = R^2$ in the integrals in Table 14-1. Using integration by parts in the numerator of I_1 , we have $I_1 = -(2\Delta)^{3/2}/2\rho V$ and $I_2 = -II_1$. We note that $\delta\beta = 0$ for both TE and TM modes. Thus, in this exceptional case, there are only two different values of the $\delta\beta_i$ for the four modes associated with F_l for $l \geq 1$. However, we can readily show from Eq. (32-22) that the next order correction to $\tilde{\beta}$ for TM modes is of order $(2\Delta)^{5/2}$, but the polarization corrections for TE modes are zero to all orders in Δ as the exact fields satisfy the scalar wave equation.

Fundamental modes ($l = 0$, $m = 1$)

The transverse fields of the fundamental modes have a Gaussian dependence on R , as is clear from Tables 14-1 and 14-2. By substituting F_0 into Table 13-2, page 292, we obtain simple expressions for quantities of interest, such as the normalization N . The fraction of power $\bar{\eta}$ within $0 \leq R \leq 1$ increases with increasing V and decreases with decreasing ρ , in keeping with the discussion in Chapter 10 on diffraction effects. Pulse propagation and spreading were discussed in Chapter 11. The transit time of a mode depends on its group velocity v_g , and within the weak-guidance approximation Table 14-2 shows that the group velocity \tilde{v}_g is just the on-axis speed of light c/n_{co} . The scalar distortion parameter \tilde{D} of Table 13-2 clearly vanishes, so that waveguide dispersion is a higher-order effect. If we include the polarization correction δU , we deduce from Eqs. (13-17) and (13-18) the corrections δv_g and δD in Table 14-2.

Condition for weak guidance

As discussed at the beginning of this example, the modal fields of the weak-guidance approximation are a good approximation to the exact fields of the fiber only under

certain restrictions. In addition to the requirement that $\Delta \ll 1$, we recall from Section 13-2 that $\beta \cong kn_{\infty}$. If we substitute for β and V from Table 14-2, we deduce that $V \gg 4\Delta$ for the fundamental modes. Even with this restriction, the modal fields are only accurate within the region of significant modal power flow.

Polarization corrections to the modal fields

The transverse fields of the fundamental modes in Table 14-1 contain no polarization effects due to the fiber. These effects are included in higher-order corrections through the expansions in Section 32-1. The second-order transverse electric field corrections satisfy the equation in Table 32-1, page 627. If we set $f = R^2$, substitute \mathbf{e}_{11} or \mathbf{e}_{13} from Table 14-1 for $\hat{\mathbf{e}}_i$ and take $\tilde{U}, U^{(1)} = \delta U/\Delta$ from Table 14-2, it is readily verified that the solutions for the second-order field are

$$\hat{\mathbf{r}}\Delta R^2 \exp(-\frac{1}{2}VR^2) \cos \phi \quad \text{and} \quad \hat{\mathbf{r}}\Delta R^2 \exp(-\frac{1}{2}VR^2) \sin \phi, \quad (14-7)$$

for the even and odd fundamental modes, respectively, where $\hat{\mathbf{r}}$ is the unit vector in the radial direction. These fields are by hypothesis small corrections to \mathbf{e}_{11} and \mathbf{e}_{13} , and consequently they are valid only in the region defined by $R \ll \Delta^{-1/2}$. This restriction arises because of the unphysical nature of the profile.

14-5 Example: Infinite power-law profiles

These profiles have the refractive-index distribution

$$n^2(R) = n_{\infty}^2 \{1 - 2\Delta R^q\}, \quad 0 < q < \infty; \quad R = r/\rho, \quad (14-8)$$

where q is a constant and the scaling radius ρ is such that $n(R) = n_{\text{cl}}$ when $R = 1$. Plots for various values of q are given in Fig. 14-2(a), including the parabolic profile ($q = 2$) discussed in the previous section. As $q \rightarrow 0$ the profiles approach $n(R) = n_{\text{cl}}$, an infinite uniform medium, and as $q \rightarrow \infty$ the profiles approach a step profile. For all q , the profiles are unphysical since $n^2(R) \rightarrow -\infty$ as $R \rightarrow \infty$. Consequently, the weak-guidance approximation is only accurate when the fiber parameter V is sufficiently large, for reasons discussed in the previous section. If we set $f = R^q$ in Eq. (14-4), there are no known closed-form solutions for F_l , with the exception of the parabolic profile.

Propagation constant

In Section 33-6 we use scaling arguments to show that for $l = 0$ modes, the parameter \tilde{U} is expressible in closed-form. From Eq. (33-27) we have [4]

$$\tilde{U} = \left[\frac{\Gamma(1/q + 1/2)(q+2)(2m-1)\pi^{1/2} V^{2/q}}{2\Gamma(1/q)} \right]^{q/(q+2)} = G(q)V^{2/(q+2)}, \quad (14-9)$$

for all HE_{1m} modes, where Γ is the gamma function of Eq. (37-104), m is the modal subscript in Table 14-1, and the scalar propagation constant $\tilde{\beta}$ is related to \tilde{U} inside the back cover.

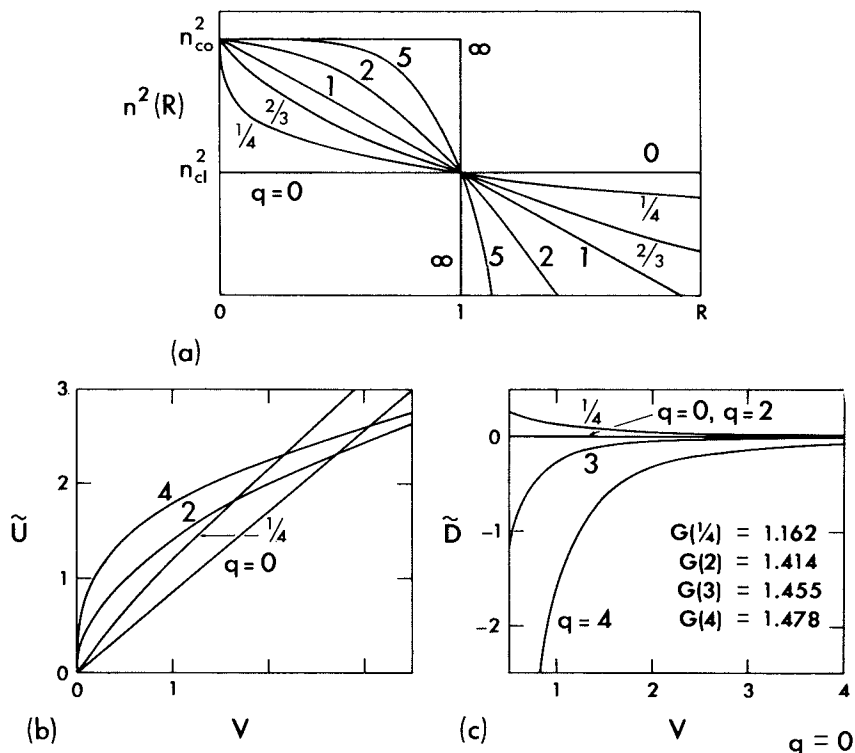


Fig. 14.2 Plots of (a) the infinite power-law profiles of Eq. (14-8), and (b), (c) the modal parameter \tilde{U} of Eq. (14-9) and the distortion parameter \tilde{D} of Eq. (14-11) respectively, for the fundamental mode on each profile.

Group velocity and waveguide dispersion

The power of a mode propagates at the group velocity. Substituting Eq. (14-9) into Eq. (13-17), we find that

$$\tilde{v}_g = \frac{c}{n_{\infty}} \left\{ 1 + \Delta \frac{2-q}{2+q} \frac{G^2(q)}{V^{2q/(q+2)}} \right\}, \quad (14-10)$$

where c is the free-space speed of light and $G(q)$ is defined by Eq. (14-9). Waveguide dispersion is described by the distortion parameter in Table 13-2. Substituting Eq. (14-9) we deduce that

$$\tilde{D} = q \frac{(2-q)}{(2+q)^2} G^2(q) V^{-(3q+2)/(q+2)}. \quad (14-11)$$

Thus waveguide dispersion is zero for the parabolic profile to this order. The next order correction is finite, as we showed in the previous section.

Condition for weak guidance

We discussed the accuracy of the weak-guidance approximation for the infinite parabolic profile in Section 14-4. If we impose the condition $\tilde{\beta} \cong kn_{\text{co}}$, we deduce from Eq. (14-9) and Table 14-2 that $V \gg \{G(q)\Delta^{1/2}\}^{(q+2)/q}$ for the infinite power-law profiles to be weakly guiding.

Fundamental modes

The values of \tilde{U} and \tilde{D} of Eqs. (14-9) and (14-11) are plotted against V for various values of q in Figs. 14-2(b) and 14-2(c) for the fundamental modes, i.e. $l = 0, m = 1$. The corresponding values of $G(q)$ are included in Fig. 14-2(c).

STEP-PROFILE FIBER

We now examine a profile of great practical interest. The step profile has a uniform core and a uniform cladding, and in terms of the profile representation of Eq. (14-1) is expressible as

$$n(R) = n_{\text{co}} \quad \text{or} \quad f = 0; \quad 0 \leq R < 1, \quad (14-12a)$$

$$n(R) = n_{\text{cl}} \quad \text{or} \quad f = 1; \quad 1 < R < \infty, \quad (14-12b)$$

where $R = r/\rho$ and ρ is the core radius. We assume $n_{\text{co}} \cong n_{\text{cl}}$, or, equivalently, $\Delta \ll 1$, so that the fiber is weakly guiding. The small overall variation in the profile means that there are no restrictions on the fiber parameter V , unlike the infinite profiles of the previous two sections. The modal fields can be found either from the exact fields of Chapter 12 by taking the limit $\Delta \rightarrow 0$, as shown in Section 12-11 [2], or by following the scalar description of Chapter 13. We adopt the latter course here [1]. In the following chapter, we use an approximation method to simplify description further.

14-6 Fundamental and HE_{1m} ($l = 0$) modes

The $l = 0$ solution of Eq. (14-4), $F_0(R)$, gives the radial dependence of the fundamental and remaining HE_{1m} modes. Substituting for f from Eq. (14-12) and normalizing so that $F_0 = 1$ at the interface $R = 1$, we find

$$F_0 = \frac{J_0(\tilde{U}R)}{J_0(\tilde{U})}, \quad 0 \leq R \leq 1; \quad F_0 = \frac{K_0(\tilde{W}R)}{K_0(\tilde{W})}, \quad 1 \leq R < \infty, \quad (14-13)$$

where J_0 is the Bessel function of the first kind and K_0 is the modified Bessel function of the second kind. The scalar mode parameters \tilde{U} and \tilde{W} for the core and cladding are defined inside the back cover, and are related to the fiber

parameter by

$$V^2 = \tilde{U}^2 + \tilde{W}^2; \quad V = k\rho(n_{\text{co}}^2 - n_{\text{cl}}^2)^{1/2}, \quad (14-14)$$

where $k = 2\pi/\lambda$ and λ is the free-space wavelength. The field components are obtained by substituting Eq. (14-13) into Table 14-1. Since we shall be referring to these components for the step-profile fiber frequently, they are included in Table 14-3 to provide a comprehensive summary of fundamental-mode properties.

Propagation constants and polarization corrections

The solution F_0 of Eq. (14-4) must be continuous and have a continuous derivative dF_0/dR at $R = 1$. Using the recurrence relations of Eq. (37-75) leads to the eigenvalue equation

$$\boxed{\tilde{U} \frac{J_1(\tilde{U})}{J_0(\tilde{U})} = \tilde{W} \frac{K_1(\tilde{W})}{K_0(\tilde{W})}}, \quad (14-15)$$

where \tilde{W} is related to \tilde{U} by Eq. (14-14). For a given value of V , this equation determines the value of \tilde{U} for each HE_{1m} mode that can propagate. The smallest value of \tilde{U} corresponds to the fundamental HE_{11} modes and increasing values of \tilde{U} correspond to increasing values of m . The propagation constant β is related to \tilde{U} in Table 14-3. Since Eq. (14-15) is transcendental, it must be solved numerically. Values of \tilde{U} and \tilde{W} for the range $1.05 \leq V \leq 4$ are given in Table 14-4 for the fundamental mode, and \tilde{U} is plotted against V in Fig. 14-3(a).

The polarization correction to the scalar propagation constant is given by Table 14-1 in terms of I_1 . In the numerator, the integral involves the profile derivative df/dR , which, by analogy with Eq. (32-13) for the general step profile, is given by the Dirac delta function $\delta(R-1)$. The integral in the denominator of I_1 is given in Table 14-6. Hence we deduce the expressions for $\delta\beta$ and δU in Table 14-3. We plot the ratio $\delta U/\tilde{U}$ in Fig. 14-3(b) for the fundamental mode. It has a maximum value of about 0.24 at $V \cong 2.25$. If we compare the corrected mode parameter $\tilde{U} + \delta U$ with the exact solution U of the fundamental mode eigenvalue equation in Table 12-4, page 253, we find that the maximum relative error occurs at the peak of the curve in Fig. 14-3(b), and has magnitude less than 0.005% for $\Delta = 0.005$, which rises to 0.07% and 0.5% for $\Delta = 0.045$ and $\Delta = 0.125$, respectively.

We now consider properties of the fundamental mode. The expressions in Table 14-3, e.g. normalization, are found by substituting F_0 into Table 13-2, page 292, and using the integrals of Eqs. (37-92) and (37-93).

Table 14-3 Fundamental and HE_{1m} modes of the weakly guiding step-profile fiber. Parameters are defined inside the back cover. Modal power is given by $|a|^2 N$, where a is the modal amplitude.

	<i>Even</i>	<i>Odd</i>
Transverse components	$e_x = F_0 \quad h_y = n_{co} \left(\frac{\epsilon_0}{\mu_0} \right)^{1/2} F_0$	$e_y = F_0 \quad h_x = -n_{co} \left(\frac{\epsilon_0}{\mu_0} \right)^{1/2} F_0$
Longitudinal components	$e_z = i \frac{(2\Delta)^{1/2}}{V} G_0 \cos \phi$ $h_z = i n_{co} \left(\frac{\epsilon_0}{\mu_0} \right)^{1/2} \frac{(2\Delta)^{1/2}}{V} G_0 \sin \phi$	$e_z = i \frac{(2\Delta)^{1/2}}{V} G_0 \sin \phi$ $h_z = -i n_{co} \left(\frac{\epsilon_0}{\mu_0} \right)^{1/2} \frac{(2\Delta)^{1/2}}{V} G_0 \cos \phi$
$F_0 = \frac{J_0(\tilde{U}R)}{J_0(\tilde{U})}, \quad 0 \leq R \leq 1$ $= \frac{K_0(\tilde{W}R)}{K_0(\tilde{W})}, \quad 1 \leq R < \infty$		$G_0 = -\tilde{U} \frac{J_1(\tilde{U}R)}{J_0(\tilde{U})}, \quad 0 \leq R \leq 1$ $= -\tilde{W} \frac{K_1(\tilde{W}R)}{K_0(\tilde{W})}, \quad 1 \leq R < \infty$
Eigenvalue equation	$\tilde{U} \frac{J_1(\tilde{U})}{J_0(\tilde{U})} = \tilde{W} \frac{K_1(\tilde{W})}{K_0(\tilde{W})}; \quad \tilde{U}^2 + \tilde{W}^2 = V^2; \quad \tilde{U}_\infty \cong 2.405$	
Range of single-mode operation $0 < V < 2.405$		

Propagation constant	$\tilde{\beta} = \frac{V}{\rho(2\Delta)^{1/2}} \left\{ 1 - 2\Delta \frac{\tilde{U}^2}{V^2} \right\}^{1/2}$
Polarization corrections	$\delta\beta = -\frac{(2\Delta)^{3/2}}{2\rho} \frac{\tilde{U}^2 \tilde{W}}{V^3} \frac{K_0(\tilde{W})}{K_1(\tilde{W})}; \quad \delta U = \Delta \frac{\tilde{U} \tilde{W}}{V^2} \frac{K_0(\tilde{W})}{K_1(\tilde{W})}$
Derivative of modal parameter	$\frac{d\tilde{U}}{dV} = \frac{\tilde{U}}{V} \left\{ 1 - \frac{K_0^2(\tilde{W})}{K_1^2(\tilde{W})} \right\}$
Normalization	$\tilde{N} = \frac{\pi \rho^2 n_{co}}{2} \left(\frac{\epsilon_0}{\mu_0} \right)^{1/2} \frac{V^2}{\tilde{U}^2} \frac{K_1^2(\tilde{W})}{K_0(\tilde{W})}$
Intensity	$\tilde{S} = \frac{ a ^2}{2} \left(\frac{\epsilon_0}{\mu_0} \right)^{1/2} n_{co} F_0^2$
Fraction of power in the core	$\tilde{\eta} = \frac{\tilde{U}^2}{V^2} \left\{ \frac{\tilde{W}^2}{\tilde{U}^2} + \frac{K_0^2(\tilde{W})}{K_1^2(\tilde{W})} \right\}$
Group velocity	$\tilde{v}_g = \frac{c}{n_{co}} \left\{ 1 + \Delta \frac{\tilde{U}^2}{V^2} (1 - 2\sigma^2) \right\}; \quad \sigma = \frac{K_0(\tilde{W})}{K_1(\tilde{W})}$
Distortion parameter	$\tilde{D} = 2 \frac{\tilde{U}^2 \tilde{W}}{V^3} \sigma \left\{ \frac{\tilde{U}^2}{\tilde{W}^2} \sigma^4 + \frac{\tilde{U}^2 - \tilde{W}^2}{\tilde{W}^3} \sigma^3 + \frac{\tilde{W}^2 - \tilde{U}^2}{\tilde{W}^2} \sigma^2 + \frac{3\sigma}{2\tilde{W}} - 1 \right\}$

Table 14-4 Values of fundamental-mode parameters for step-profile fibers. The expressions for these quantities are given in Table 14-3, with the exception of the depth of penetration, which is defined by Eq. (14-18).

V	\tilde{U}	\tilde{W}	$\frac{\delta U}{\Delta}$	$\left(\frac{\mu_0}{\epsilon_0}\right)^{1/2} \frac{N}{n_{\text{co}} \rho^2}$	$\tilde{\eta}$	$\frac{1}{\Delta} \left(\frac{n_{\text{co}} \tilde{b}_g}{c} - 1 \right)$	\tilde{D}	$\frac{d\tilde{U}}{dV}$	$\frac{r_{\text{pd}}}{\rho}$
4.00	1.907	3.516	0.370	8.890	0.949	-0.1262	-0.0123	0.106	1.293
3.95	1.902	3.462	0.372	8.749	0.948	-0.1274	-0.0122	0.108	1.297
3.90	1.896	3.408	0.374	8.610	0.946	-0.1286	-0.0120	0.110	1.301
3.85	1.890	3.354	0.376	8.472	0.944	-0.1298	-0.0119	0.113	1.306
3.80	1.885	3.300	0.378	8.335	0.943	-0.1310	-0.0117	0.116	1.310
3.75	1.879	3.245	0.378	8.200	0.941	-0.1320	-0.0115	0.119	1.315
3.70	1.873	3.191	0.380	8.067	0.939	-0.1322	-0.0112	0.122	1.319
3.65	1.867	3.137	0.382	7.935	0.936	-0.1344	-0.0109	0.124	1.325
3.60	1.860	3.082	0.384	7.806	0.934	-0.1354	-0.0106	0.127	1.330
3.55	1.854	3.027	0.386	7.678	0.932	-0.1364	-0.0101	0.131	1.335
3.50	1.847	2.973	0.388	7.552	0.929	-0.1374	-0.0097	0.134	1.341
3.45	1.841	2.918	0.390	7.427	0.927	-0.1384	-0.0091	0.137	1.347
3.40	1.834	2.863	0.390	7.304	0.924	-0.1392	-0.0085	0.141	1.352
3.35	1.827	2.808	0.392	7.184	0.921	-0.1400	-0.0078	0.144	1.359
3.30	1.819	2.753	0.394	7.064	0.918	-0.1408	-0.0070	0.148	1.365
3.25	1.812	2.698	0.394	6.947	0.915	-0.1414	-0.0061	0.152	1.372
3.20	1.804	2.643	0.396	6.832	0.912	-0.1420	-0.0051	0.156	1.378
3.15	1.796	2.588	0.398	6.719	0.909	-0.1424	-0.0040	0.160	1.386
3.10	1.788	2.532	0.398	6.607	0.905	-0.1428	-0.0027	0.165	1.394
3.05	1.780	2.477	0.400	6.498	0.901	-0.1430	-0.0013	0.169	1.401
3.00	1.771	2.421	0.400	6.390	0.897	-0.1432	-0.0002	0.174	1.409
2.95	1.762	2.366	0.402	6.286	0.893	-0.1430	0.0020	0.179	1.418
2.90	1.753	2.310	0.402	6.183	0.889	-0.1426	0.0039	0.184	1.427
2.85	1.744	2.254	0.402	6.082	0.884	-0.1422	0.0061	0.190	1.436
2.80	1.734	2.198	0.402	5.984	0.879	-0.1414	0.0085	0.196	1.446
2.75	1.724	2.143	0.402	5.889	0.874	-0.1404	0.0112	0.202	1.456
2.70	1.714	2.086	0.402	5.795	0.868	-0.1392	0.0142	0.208	1.467
2.65	1.704	2.030	0.402	5.700	0.862	-0.1376	0.0176	0.215	1.578
2.60	1.693	1.973	0.402	5.613	0.856	-0.1356	0.0213	0.221	1.490
2.55	1.681	1.917	0.400	5.532	0.849	-0.1332	0.0253	0.229	1.503
2.50	1.670	1.860	0.400	5.446	0.842	-0.1306	0.0300	0.236	1.516
2.45	1.658	1.804	0.398	5.367	0.835	-0.1274	0.0350	0.244	1.530
2.40	1.645	1.748	0.396	5.295	0.827	-0.1236	0.0406	0.253	1.544
2.35	1.633	1.690	0.394	5.218	0.818	-0.1192	0.0470	0.262	1.561
2.30	1.619	1.634	0.392	5.153	0.809	-0.1142	0.0539	0.271	1.577
2.25	1.605	1.577	0.390	5.090	0.800	-0.1084	0.0616	0.281	1.595
2.20	1.591	1.519	0.386	5.028	0.789	-0.1018	0.0703	0.291	1.614
2.15	1.576	1.462	0.382	4.974	0.779	-0.0944	0.0798	0.302	1.635
2.10	1.561	1.405	0.380	4.922	0.767	-0.0858	0.0906	0.314	1.657
2.05	1.545	1.347	0.374	4.877	0.754	-0.0762	0.103	0.326	1.681
2.00	1.528	1.290	0.368	4.841	0.741	-0.0652	0.116	0.339	1.706
1.95	1.511	1.233	0.362	4.808	0.726	-0.0530	0.130	0.353	1.733
1.90	1.493	1.175	0.354	4.785	0.711	-0.0392	0.147	0.368	1.764
1.85	1.474	1.118	0.346	4.771	0.694	-0.0236	0.164	0.384	1.796
1.80	1.454	1.061	0.338	4.768	0.677	-0.0064	0.184	0.400	1.832
1.75	1.434	1.003	0.328	4.773	0.658	0.0134	0.207	0.418	1.871

Table 14-4 (contd.)

V	\tilde{U}	\tilde{W}	$\frac{\delta U}{\Delta}$	$\left(\frac{\mu_0}{\epsilon_0}\right)^{1/2} \frac{N}{n_{\text{co}} \rho^2}$	$\tilde{\eta}$	$\frac{1}{\Delta} \left(\frac{n_{\text{co}} \tilde{v}_g}{c} - 1 \right)$	\tilde{D}	$\frac{d\tilde{U}}{dV}$	$\frac{r_{\text{pd}}}{\rho}$
1.70	1.413	0.945	0.318	4.793	0.637	0.0354	0.231	0.437	1.915
1.65	1.390	0.889	0.308	4.831	0.616	0.0594	0.257	0.456	1.962
1.60	1.367	0.832	0.294	4.885	0.592	0.0868	0.287	0.478	2.016
1.55	1.343	0.774	0.280	4.962	0.566	0.1176	0.320	0.501	2.077
1.50	1.317	0.718	0.266	5.068	0.539	0.1508	0.354	0.525	2.145
1.45	1.290	0.662	0.250	5.207	0.510	0.1882	0.392	0.551	2.222
1.40	1.262	0.606	0.234	5.389	0.479	0.230	0.432	0.578	2.311
1.35	1.232	0.552	0.216	5.623	0.447	0.274	0.473	0.606	2.475
1.30	1.201	0.498	0.1970	5.931	0.411	0.324	0.517	0.637	2.531
1.25	1.168	0.445	0.1776	6.327	0.375	0.376	0.558	0.669	2.672
1.20	1.134	0.393	0.1564	6.865	0.336	0.436	0.500	0.703	2.840
1.15	1.098	0.342	0.1354	7.582	0.296	0.498	0.635	0.738	3.048
1.10	1.060	0.294	0.1146	8.549	0.255	0.562	0.662	0.773	3.297
1.05	1.021	0.245	0.0924	10.01	0.211	0.632	0.678	0.811	3.635

Fraction of modal power within the core

This fraction is described by $\tilde{\eta}$ in Table 14-3, and is plotted against V in Fig. 14-3(a). Only for $V \ll 1$ is there negligible power in the core.

Distribution of modal power

The modal power flow along the fiber per unit cross-sectional area, or intensity, is given by the time-averaged Poynting vector \tilde{S} in Table 14-3, where a is the modal amplitude. To describe the change in this distribution with changes in V , we keep the total modal power P fixed, and define a normalized intensity $\hat{S} = \tilde{S}/P = \tilde{S}/|a|^2 \tilde{N}$. Hence

$$\hat{S} = \frac{1}{\pi} \left\{ \frac{\tilde{W}}{\rho V} \frac{J_0(\tilde{U}R)}{J_1(\tilde{U})} \right\}^2, \quad 0 \leq R \leq 1; \quad \hat{S} = \frac{1}{\pi} \left\{ \frac{\tilde{U}}{\rho V} \frac{K_0(\tilde{W}R)}{K_1(\tilde{W})} \right\}^2, \quad 1 \leq R < \infty, \quad (14-16)$$

using the eigenvalue equation in Table 14-3. The dimensionless ratio \hat{S}/\hat{S}_∞ is plotted as a function of R in Fig. 14-3(c) for various values of V , where \hat{S}_∞ is the value of \hat{S} when $R = 0$ and $V = \infty$. For the fundamental mode, we deduce from Table 14-5 that

$$\hat{S}_\infty = 1/\{\pi \rho^2 J_1^2(\tilde{U}_\infty)\}; \quad \tilde{U}_\infty \cong 2.405, \quad (14-17)$$

where \tilde{U}_∞ is the first root of J_0 . Only when $V = \infty$ is all modal power confined to the core. As V decreases, power flow becomes significant over a larger area which includes part of the cladding, and the maximum value of \hat{S} on axis is reduced.

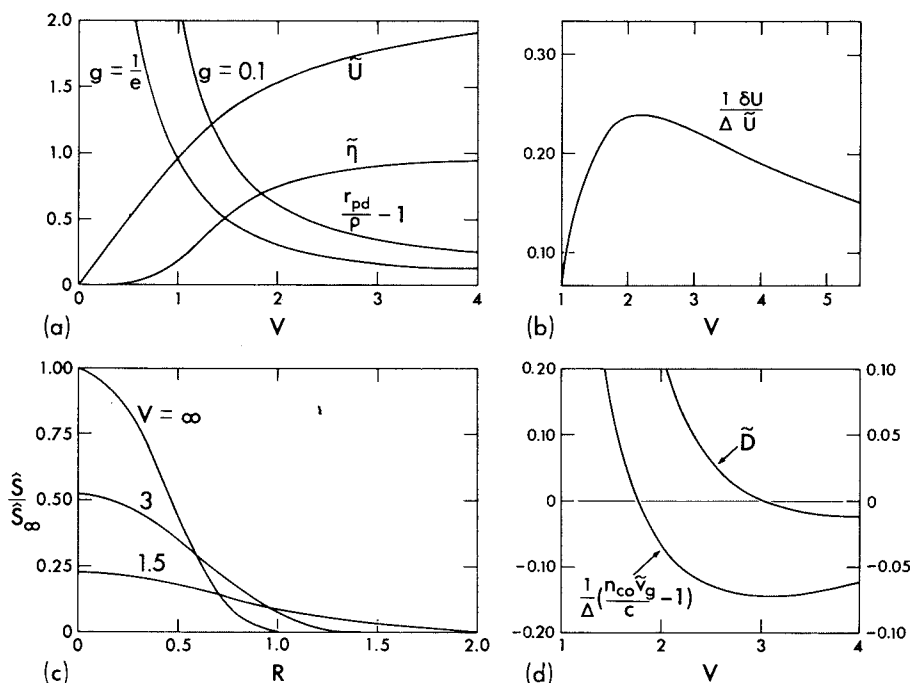


Fig. 14-3 Fundamental mode quantities for the step-profile fiber, showing (a) the modal parameter \tilde{U} , the fraction of power in the core $\tilde{\eta}$, and the depth of penetration r_{pd} , (b) the normalized polarization correction $\delta U/\Delta \tilde{U}$, (c) the normalized intensity distribution and (d) the normalized variation in group velocity relative to the left ordinate, and the distortion parameter \tilde{D} relative to the right ordinate. Numerical values are given in Table 14-4.

Depth of penetration of the field intensity

The fundamental-mode intensity in Fig. 14-3(c) can be significant well into the cladding. At sufficiently large distances from the axis it decreases exponentially with R , as is clear from Table 14-3 and Eq. (37-88). To quantify the size of this region, we define r_{pd} to be the distance from the fiber axis where S has fallen to a factor $g < 1$ of its value at the interface. Thus

$$K_0^2 (\tilde{W} r_{pd}/\rho) = g K_0^2 (\tilde{W}). \quad (14-18)$$

The normalized distance $(r_{pd}/\rho) - 1$ from the interface is a measure of the effective depth of penetration of the core field into the cladding. We plot this quantity as a function of V in Fig. 14-3(a), taking $g = e^{-1}$ for the lower curve and $g = 0.1$ for the upper curve. For example, when $V = 2.5$ we deduce from the $\tilde{\eta}$ curve that about 84% of total fundamental-mode power flows within the

core, and the intensity, or power density, falls by a factor of e^{-1} over a distance of approximately $\rho/2$ beyond the interface.

Pulse propagation and spreading

If V is below the cutoff value 2.405 of the second mode in Fig. 14-4, the fiber is single moded and only the even and odd fundamental modes can propagate. Both modes have the same propagation constant $\tilde{\beta}$. Consequently the group velocity \tilde{v}_g and the transit time of Eq. (11-36) are independent of polarization. In the weak-guidance approximation, the expression for \tilde{v}_g in Table 14-3 follows from Eq. (13-17), and is plotted against V in Fig. 14-3(d) as the dimensionless quantity $(n_{co}\tilde{v}_g - c)/c\Delta$.

Pulse spreading on single-mode fibers depends only on waveguide dispersion and material dispersion, as discussed in Section 11-12. The contribution to pulse spreading in the absence of material dispersion is proportional to the dimensionless distortion parameter introduced in Section 11-20. Using the definition \tilde{D} for weakly guiding fibers in Table 13-2, page 292, we are led to the expression in Table 14-3. Numerical values of D are given in Table 14-4 and are plotted in Fig. 14-3(d). There is zero waveguide dispersion at $V \cong 3$, which corresponds to the minimum group velocity value.

Approximate forms for large and small values of V

It is often useful to have approximations to the fundamental-mode properties in Table 14-3 when V is either large or small. These approximations are given in Table 14-5. The expressions for the modal parameters are the $\Delta \rightarrow 0$ limit of the expression in Table 12-4, page 253, where we have used the small argument expression of J_ν in Eq. (37-82). The remaining expressions in Table 14-5 are obtained from Table 14-3 by using the expansions of K_0 and K_1 in Eqs. (37-86) and (37-88) for small and large arguments, and assuming $\tilde{U} \cong V$ if V is small or $\tilde{W} \cong V$ if V is large. The accuracy of each approximation can be gauged by comparison with the exact values in Table 14-4 for $V = 1.05$ or $V = 4$. For intermediate values of V , an excellent approximation can be derived by assuming \tilde{W} is a linear function of V . This leads to [5].

$$\tilde{W} = 1.1428V - 0.996, \quad 1.5 \leq V \leq 2.5, \quad (14-19)$$

which is within 0.2% of the exact values over the range. However, derivatives of this expression do not usually lead to expressions for group velocity and the distortion parameter with the same accuracy [6].

14-7 Higher-order ($l \geq 1$) modes

The construction of the remaining modes of the fiber was described in Section 14-3. We give the solution F_l of Eq. (14-4) and the functions G_l^\pm in Table 14-6

Table 14-5 Fundamental-mode approximate forms. These forms are derived from the expressions in Table 14-3. Similar expressions can be derived for low-order HE_{1m} modes. Parameters are defined inside the back cover.

	<i>Small</i> $V \rightarrow 0$	<i>Large</i> $V \rightarrow \infty$
Modal Parameters	$\hat{U} \cong V$ $\hat{W} \cong 1.123 \exp\left(-\frac{2}{V^2}\right)$	$\hat{U} \cong 2.405 \exp\left(-\frac{1}{V}\right)$ $\hat{W} \cong V$
\hat{N}	$\frac{\pi \rho^2 n_{\text{co}}}{10} \left(\frac{\varepsilon_0}{\mu_0}\right)^{1/2} V^4 \exp\left(\frac{4}{V^2}\right)$	$\frac{\pi \rho^2 n_{\text{co}}}{2} \left(\frac{\varepsilon_0}{\mu_0}\right)^{1/2} \frac{V^2}{\hat{U}^2} \frac{\hat{W} + 1}{\hat{W}}$
$\frac{d\hat{U}}{dV}$	$1 - \frac{5.04}{V^4} \exp\left(-\frac{4}{V^2}\right)$	$\frac{\hat{U}}{V^2}$
$\hat{\eta}$	$1.261 \frac{V^2 + 2}{V^4} \exp\left(-\frac{4}{V^2}\right)$	$1 - \frac{\hat{U}^2}{V^3}$
\hat{v}_g	$\frac{c}{n_{\text{co}}} \left\{ 1 + \Delta \left[1 + \frac{4.492}{V^2} \exp\left(\frac{-2}{V^2}\right) \right] \right\}$	$\frac{c}{n_{\text{co}}} \left\{ 1 - \Delta \frac{\hat{U}^2}{V^2} \left(1 - \frac{2}{\hat{W}} \right) \right\}$

in terms of Bessel functions and modified Bessel functions of order l . The complete modal fields are obtained by substituting these expressions into Table 14-1. Mode parameters are defined inside the back cover.

Eigenvalue equations

Continuity of F_l and dF_l/dR at $R = 1$ leads to the eigenvalue equation for the values of U or \hat{W} . This operation, together with the recurrence relations of Eqs. (37-72) and (37-73), leads to the equation in Table 14-6. It is clear from Table 14-1, that if V and $l > 0$ are prescribed, each solution \hat{U} applies to all four even and odd $\text{HE}_{l+1,m}$ and $\text{EH}_{l-1,m}$ modes, the latter denoting the TM_{0m} and TE_{0m} modes when $l = 1$. Increasing values of \hat{U} correspond to increasing values of m . Numerical solution of the eigenvalue equation leads to the plots in Fig. 14-4 for low-order modes, including the HE_{1m} modes of the previous section. The modes and the values of l and m are shown in each plot.

Table 14-6 Modes of the weakly guiding step-profile fiber. The vector modal fields are found by substitution into Table 14-1. Modal power is given by $|a|^2 N$, where a is the modal amplitude. Parameters are defined inside the back cover.

$F_l = \frac{J_l(\tilde{U}R)}{J_l(\tilde{U})}, \quad 0 \leq R \leq 1; \quad F_l = \frac{K_l(\tilde{W}R)}{K_l(\tilde{W})}, \quad 1 \leq R < \infty$		$G_l^\pm = \pm U \frac{J_{l\pm 1}(U)}{J_l(U)}, \quad 0 \leq R \leq 1; \quad G_l^\pm = \pm \tilde{W} \frac{K_{l\pm 1}(\tilde{W})}{K_l(\tilde{W})}, \quad 1 \leq R < \infty$	
Eigenvalue equation	$\tilde{U} \frac{J_{l+1}(\tilde{U})}{J_l(\tilde{U})} = \tilde{W} \frac{K_{l+1}(\tilde{W})}{K_l(\tilde{W})};$	$\tilde{U}^2 + \tilde{W}^2 = V^2$	Derivative of modal parameter
Propagation constant	$\hat{\beta} = \frac{V}{\rho(2\Delta)^{1/2}} \left\{ 1 - 2\Delta \frac{\tilde{U}^2}{V^2} \right\}^{1/2};$	$V = k\rho n_{co}(2\Delta)^{1/2}$	Useful integral
Polarization corrections	$l \geq 0 \quad \delta\beta_1 = \delta\beta_3 = -\frac{(2\Delta)^{3/2} \tilde{W} \tilde{U}^2}{2\rho} \frac{K_l(\tilde{W})}{K_{l-1}(\tilde{W})}$	$\delta U_1 = \delta U_3 = \Delta \frac{\tilde{W} \tilde{U}}{V^2} \frac{K_l(\tilde{W})}{K_{l-1}(\tilde{W})}$	Normalization
	$l \geq 2 \quad \delta\beta_2 = \delta\beta_4 = -\frac{(2\Delta)^{3/2} \tilde{W} \tilde{U}^2}{2\rho} \frac{K_l(\tilde{W})}{K_{l+1}(\tilde{W})}$	$\delta U_2 = \delta U_4 = \Delta \frac{\tilde{W} \tilde{U}}{V^2} \frac{K_l(\tilde{W})}{K_{l+1}(\tilde{W})}$	Intensity
	$l = 1 \quad \delta\beta_2 = -\frac{(2\Delta)^{3/2} \tilde{W} \tilde{U}^2}{\rho} \frac{K_1(\tilde{W})}{K_2(\tilde{W})}$	$\delta U_2 = 2\Delta \frac{\tilde{W} \tilde{U}}{V^2} \frac{K_1(\tilde{W})}{K_2(\tilde{W})}$	Fraction of power in the core
	$l = 1 \quad \delta\beta_4 = 0$	$\delta U_4 = 0$	Group velocity
Cutoff $\tilde{U} = V, \quad \tilde{W} = 0$	$J_{l-1}(\tilde{U}) = 0$		Far from cutoff $\tilde{W} \cong V \rightarrow \infty$
		$J_l(\tilde{U}) = 0$	

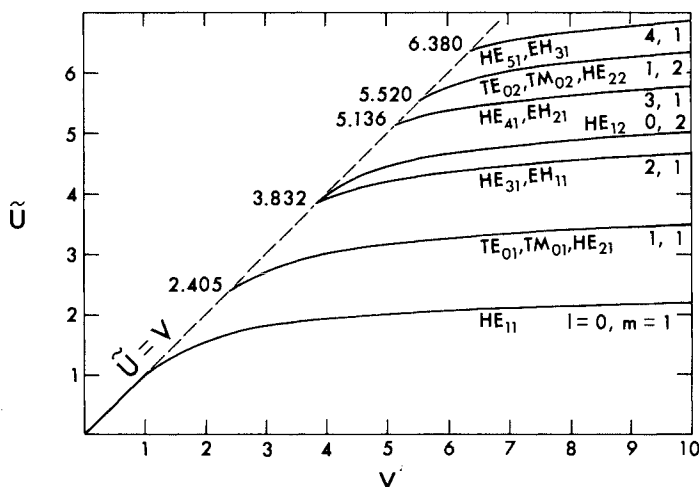


Fig. 14-4 Numerical solutions of the eigenvalue equation of Table 14-6, showing the mode labelling and the corresponding values of l and m . The values along the dashed line are the cutoff values V_c for each mode.

Mode cutoff

With the exception of the fundamental HE_{11} mode, every mode is cut off below a certain value of V and cannot propagate, as explained in Section 11-18. The cutoff value of \tilde{U} is the eigenvalue equation solution in the limit $\tilde{W} \rightarrow 0$. With the help of Eq. (37-86), we deduce that $J_{l-1}(\tilde{U}) = 0$ for all modes, including the HE_{1m} modes ($m > 1$) for which $J_1(\tilde{U}) = 0$. This leads to the cutoff values in Fig. 14-4, from which we find that the fiber is single-moded if $V < 2.405$, where $\tilde{U} = V \cong 2.405$ is the cutoff value of the $l = m = 1$ modes. When $\tilde{W} \cong \tilde{V} \rightarrow \infty$, we find from the eigenvalue equation and Eq. (37-88) that \tilde{U} satisfies $J_l(\tilde{U}) = 0$. It is readily verified that these limiting equations are the weak-guidance limit of the expressions in Table 12-4, page 253.

Polarization corrections

The corrections $\delta\beta_i$ to the scalar propagation constant are given in Table 14-1 in terms of I_1 and I_2 . In the numerator of each expression, the derivative df/dR is the Dirac delta function $\delta(R-1)$, as explained in Section 14-6, and the integral in the denominator is given in Table 14-6. This leads to the expressions for $\delta\beta_i$ and the corresponding δU_i in the same table. There is no correction for the TE_{0m} modes, whose fields satisfy the scalar wave equation exactly.

We plot the ratio $\delta U/\Delta\tilde{U}$ in Fig. 14-5(a) for the TM_{01} mode, which has a maximum value of approximately 0.22 when $V \cong 5$. If we compare the

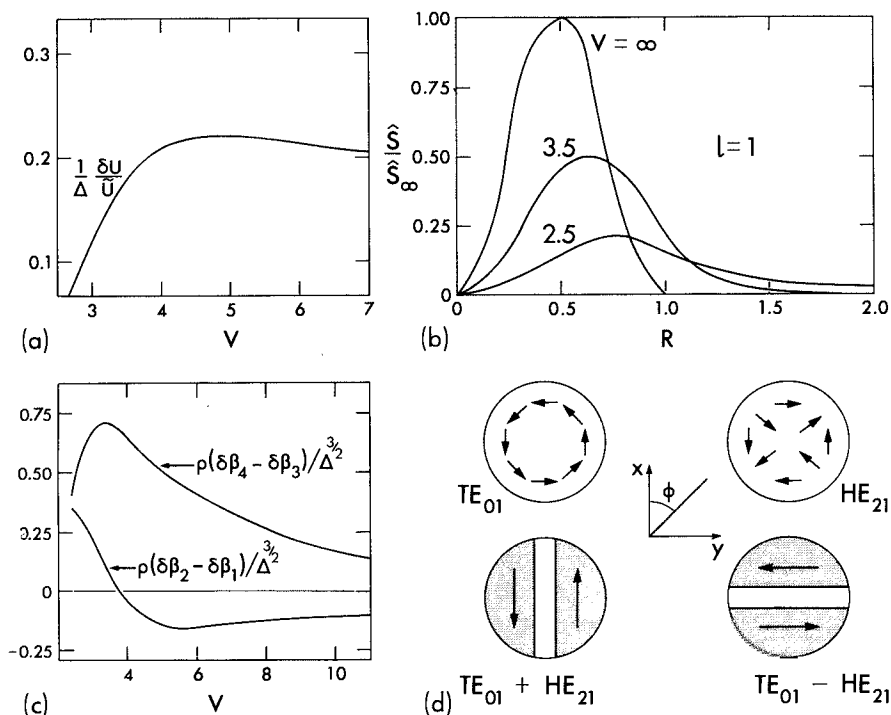


Fig. 14-5 Plots of $l = 1$ mode quantities for the step-profile fiber, showing (a) the normalized vector correction $\delta U/\Delta \tilde{U}$ for the TM_{01} mode, (b) the normalized intensity distribution, (c) the difference in vector corrections for the two pairs of $l = 1$ modes and (d) qualitative representation of the transverse electric field direction, denoted by arrows.

corrected mode parameter $\tilde{U} + \delta U$ with the exact value of U of the TM mode eigenvalue equation in Table 12-4, page 253, the maximum relative error is less than 0.005 % for $\Delta = 0.005$ and rises to 0.05 % and 0.41 % for $\Delta = 0.045$ and $\Delta = 0.125$, respectively.

Interference between modes

The finite propagation constant corrections $\delta\beta_i$ discussed above are responsible for interference effects between pairs of modes with the same scalar propagation constant. For example, suppose the odd HE_{21} and TE_{01} modes are excited with equal power and all other modes have zero power. If we erroneously ignore all polarization effects, then $\delta\beta_3 = \delta\beta_4 = 0$, and the total transverse electric field of the fiber follows from Table 14-1 as

$$\mathbf{E}_t = a\mathbf{e}_{i3}\exp(i\tilde{\beta}z) + a\mathbf{e}_{i4}\exp(i\tilde{\beta}z) = 2aF_l \sin\phi \exp(i\tilde{\beta}z)\hat{x}, \quad (14-20)$$

where a is the modal amplitude. Thus everywhere within the fiber, \mathbf{E}_t is linearly polarized parallel to the x -axis, as shown schematically in Fig. 14-5(d). The total transverse magnetic field $\mathbf{H}_t = n_{co}(\epsilon_0/\mu_0)^{1/2} \hat{\mathbf{z}} \times \mathbf{E}_t$ in the weak-guidance approximation. Consequently, the intensity distribution of Eq. (11-20) is expressible as

$$S = (n_{co}/2)(\epsilon_0/\mu_0)^{1/2} |\mathbf{E}_t|^2 = 2|a|^2 n_{co}(\epsilon_0/\mu_0)^{1/2} F_t^2 \sin^2 \phi. \quad (14-21)$$

Now consider the same fields with the correction $\delta\beta_3$ included, recalling that the correction for TE modes is zero. The analogous expression to Eq. (14-20) can be rearranged as

$$\mathbf{E}_t = 2aF_t \{ \hat{\mathbf{x}} \sin \phi \cos(\delta\beta_3 z/2) + i\hat{\mathbf{y}} \cos \phi \sin(\delta\beta_3 z/2) \} \exp\{i(\tilde{\beta} + \delta\beta_3/2)z\}. \quad (14-22)$$

Substitution into Eq. (14-21) now leads to

$$S = |a|^2 n_{co}(\epsilon_0/\mu_0)^{1/2} F_t^2 \{ \sin^2(\phi + \delta\beta_3 z/2) + \sin^2(\phi - \delta\beta_3 z/2) \}. \quad (14-23)$$

This expression has a simple interpretation. If, at distance z along the fiber, we rotate the intensity pattern of Eq. (14-21) clockwise through an angle $\delta\beta_3 z/2$ about the fiber axis, and superpose it on the same pattern rotated anticlockwise through angle $\delta\beta_3 z/2$, then Eq. (14-23) is the mean of the two superposed patterns. For example, when $\delta\beta_3 z = \pi$ the electric field is linearly polarized parallel to the y -axis in Fig. 14-5(d), and its amplitude depends on the difference between the TE_{01} and HE_{21} mode fields. The intensity pattern is given by rotating the pattern of Eq. (14-21) through $\pi/2$. Finally, the field of Eq. (14-22) becomes identical with Eq. (14-20) again over the beat length $z_b = 4\pi/\delta\beta_3$.

It is clear that the *difference* between propagation constant corrections is responsible for interference effects, and that as the difference increases, the more rapidly the field direction and intensity pattern change. To quantify these changes, the normalized quantities $\rho(\delta\beta_2 - \delta\beta_1)/\Delta^{3/2}$ and $\rho(\delta\beta_4 - \delta\beta_3)/\Delta^{3/2}$ are evaluated from the expressions in Table 14-6 for the $l = 1, m = 1$ modes, and are plotted against V in Fig. 14-5(c). When $V \cong 3.8$, the corrections $\delta\beta_1$ and $\delta\beta_2$ are equal, and consequently, any linear combination of the fields \mathbf{e}_{t1} and \mathbf{e}_{t2} of Table 14-1 constitutes a mode for this particular value of V . In Fig. 12-4, the plots of the *exact* mode parameter U for the TM_{01} and HE_{21} modes on a fiber with $\Delta = 0.32$ cross at $V \cong 3.4$.

Fraction of modal power within the core

The quantity $\tilde{\eta}$ is calculated from the expression in Table 14-6 using the values of U from Fig. 14-4, and is plotted in Fig. 14-6 for the first twelve modes. These curves are the weak-guidance limit of the curves in Fig. 12-5. The nonzero values of $\tilde{\eta}$ at cutoff are given in Table 14-7.

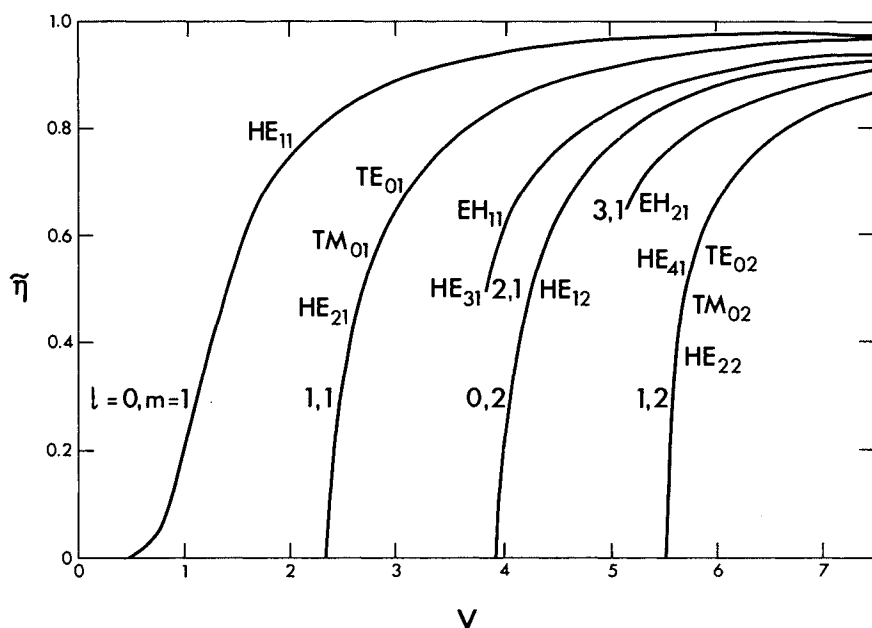


Fig. 14-6 The fraction of power residing in the core for the step-profile fiber, showing the mode labelling and the corresponding values of l and m . At cutoff, the values of $\tilde{\eta}$ are given in Table 14-7.

Distribution of modal power

We define a normalized intensity \hat{S} for $l = 0$ modes in the previous section. By analogy with Eq. (14-16), the corresponding expressions for $l > 1$ modes are expressible as

$$\hat{S} = -\frac{1}{\pi} \left(\frac{\tilde{W}}{\rho V} \right)^2 \frac{J_l(\tilde{U}R)}{J_{l-1}(\tilde{U})J_{l+1}(\tilde{U})}; \quad 0 \leq R \leq 1; \quad (14-24a)$$

$$\hat{S} = \frac{1}{\pi} \left(\frac{\tilde{U}}{\rho V} \right)^2 \frac{K_l(\tilde{W}R)}{K_{l-1}(\tilde{W})K_{l+1}(\tilde{W})}; \quad 1 \leq R < \infty, \quad (14-24b)$$

by using the eigenvalue equation in Table 14-6 and the recurrence relations of Eqs. (37-72) and (37-73). We plot the dimensionless ratio \hat{S}/\hat{S}_∞ in Fig. 14-5(b) for $l = 1$ modes, where \hat{S}_∞ is the maximum value of \hat{S} when $V = \infty$, i.e.

$$\hat{S}_\infty = J_1^2(\tilde{U}_\infty R_1) / \{ \pi \rho^2 J_2^2(\tilde{U}_\infty) \}. \quad (14-25)$$

Table 14-6 gives $\tilde{U}_\infty \cong 3.83$, the first zero of J_1 , and $\tilde{U}_\infty R_1 \cong 1.8$ corresponds to the first maximum of J_1 . As V increases, modal power is more tightly confined within the core region.

Approximate forms for low-order modes

Approximations for the properties of $l \geq 1$ modes at or near cutoff and far from cutoff are listed in Table 14-7. The expression for \tilde{U} close to its cutoff value V_c is derived in [7], and for $V \rightarrow \infty$ we use the differential equation technique of Section 12-3 [8] to express \tilde{U} in terms of its value \tilde{U}_∞ when $V = \infty$. The remaining expressions follow from Table 14-6 by using the asymptotic forms of the modified Bessel functions in Eqs. (37-86) and (37-88) for small and large arguments, respectively.

Table 14-7 Approximate forms for low-order $l \geq 1$ modes. These forms are derived from the expressions in Table 14-6, where U_∞ is the value of \tilde{U} when $V = \infty$.

	At or near cutoff V_c $\tilde{U} \cong V, \tilde{W} \cong 0$	Far from cutoff $\tilde{W} \cong V, V \gg \tilde{U}$
\tilde{U}	$\frac{1}{l} \{V + (l-1)V_c\}$	$\tilde{U}_\infty \left\{1 - \frac{2l}{V}\right\}^{1/2l}$
$\frac{K_{l-1}(\tilde{W})K_{l+1}(\tilde{W})}{K_l^2(\tilde{W})}$	$-2 \ln(0.89\tilde{W}) \quad (l=1)$ ----- $\frac{l}{l-1} \quad (l \geq 2)$	$1 + \frac{1}{V}$
$\frac{d\tilde{U}}{dV}$	$\frac{1}{l}$	$\frac{\tilde{U}_\infty}{V^2}$
\tilde{N}	$-\pi\rho^2 n_{co} \left(\frac{\epsilon_0}{\mu_0}\right)^{1/2} \ln(0.89\tilde{W}) \quad (l=1)$ ----- $\frac{\pi\rho^2 n_{co}}{2} \left(\frac{\epsilon_0}{\mu_0}\right)^{1/2} \frac{l}{l-1} \quad (l \geq 2)$	$\frac{\pi\rho^2 n_{co}}{2} \left(\frac{\epsilon_0}{\mu_0}\right)^{1/2} \frac{V}{\tilde{U}_\infty^2}$
$\tilde{\eta}$	$\frac{l-1}{l}$	$1 - \frac{\tilde{U}_\infty^2}{V^3}$
\tilde{v}_g	$\frac{c}{n_{co}} \left\{1 + \Delta \frac{2-l}{l}\right\}$	$\frac{c}{n_{co}} \left\{1 - \Delta \frac{\tilde{U}_\infty^2}{V^2}\right\}$

Asymptotic forms for high-order modes

High-order modes refers to modes which propagate only on fibers with $V \gg 1$, and thus satisfy $\tilde{U} \gg 1$ or $l \gg 1$. If we substitute the asymptotic forms of Eqs. (37-90) and (37-88) for the Bessel and modified Bessel functions into Table 14-6, we obtain the expressions listed in Table 14-8. The eigenvalue

Table 14-8 Asymptotic forms for high-order modes. These forms are derived from the expressions in Table 14-6. Parameters are defined inside the back cover.

Eigenvalue equation	$\tan \chi = \left\{ \frac{\tilde{W}^2 + l^2}{\tilde{U}^2 + l^2} \right\}^{1/2}; \quad \tilde{U} \gg 1, \quad \tilde{U} - l \gg l^{1/3}, \quad l \gg 1$	
	Large order in \tilde{U} $\tilde{U} \gg 1, \quad \tilde{U} - l \gg l^{1/3}$	Large order in l $l \gg 1$
$\frac{K_{l-1}(\tilde{W})K_{l+1}(\tilde{W})}{K_l^2(\tilde{W})}$	$\frac{\tilde{U}^2 \sin^2 \chi - l^2}{\tilde{W}^2 \cos^2 \chi}$	$1 + \frac{1}{(\tilde{W}^2 + l^2)^{1/2}}$
$\frac{d\tilde{U}}{dV}$	$\left(\frac{\tilde{U}}{V}\right) \frac{\tilde{U}^2 - l^2 - V^2 \cos^2 \chi}{\tilde{U}^2 \sin^2 \chi - l^2}$	$\frac{\tilde{U}}{V(\tilde{W}^2 + l^2)^{1/2}}$
\tilde{N}	$\frac{\pi \rho^2 n_{co}}{2} \left(\frac{\epsilon_0}{\mu_0}\right)^{1/2} \times$ $\left(\frac{V}{\tilde{U}\tilde{W}}\right)^2 \frac{\tilde{U}^2 \sin^2 \chi - l^2}{\tilde{W}^2 \cos^2 \chi}$	$\frac{\pi \rho^2 n_{co}}{2} \left(\frac{\epsilon_0}{\mu_0}\right)^{1/2} \times$ $\frac{V^2}{\tilde{U}^2} \left\{ 1 + \frac{1}{(\tilde{W}^2 + l^2)^{1/2}} \right\}$
$\tilde{\eta}$	$1 - \frac{\tilde{U}^2}{V^2} \frac{\tilde{U}^2 - l^2 - V^2 \cos^2 \chi}{\tilde{U}^2 \sin^2 \chi - l^2}$	$1 - \frac{\tilde{U}^2}{V^2 (\tilde{W}^2 + l^2)^{1/2}}$
\tilde{v}_g	$\frac{c}{n_{co}} \left\{ 1 + \Delta \frac{\tilde{U}^2}{V^2} \times \right.$ $\left. \frac{\tilde{U}^2 \sin^2 \chi - 2\tilde{W}^2 \cos^2 \chi - l^2}{\tilde{U}^2 \sin^2 \chi - l^2} \right\}$	$\frac{c}{n_{co}} \left\{ 1 - \Delta \frac{\tilde{U}^2}{V^2} \times \right.$ $\left. \left[1 - \frac{2}{(\tilde{W}^2 + l^2)^{1/2}} \right] \right\}$
$\chi = (\tilde{U}^2 - l^2)^{1/2} - l \cos^{-1}(l/\tilde{U}) - \pi/4$		

equation can also be derived directly from the scalar wave equation using the WKB methods or the local plane-wave theory described in Section 36–7.

CLAD GRADED-PROFILE FIBERS

In Sections 14–4 and 14–5 we considered graded-index fibers with infinite profiles. Now we investigate fibers with only a small variation in profile so that they are weakly guiding.

14–8 Example: Closed-form solutions

There are few clad profiles which lead to closed-form solutions of the scalar wave equation. These include profiles (l) and (p) of Fig. 12–8, which are defined in Table 12–9, p. 270. The fields and eigenvalue equations in Table 12–9 are for TE modes and thus depend on the $l = 1$ solution of Eq. (14–4). Accordingly, it is straightforward to generalize these solutions to arbitrary values of l . For profile (l) with a uniform core and graded cladding, we deduce that the solution of Eq. (14–4) is [9]

$$F_l = J_l(\tilde{U}R)/J_l(\tilde{U}), \quad 0 \leq R \leq 1; \quad F_l = K_{lv}(\tilde{W}R)/K_{lv}(\tilde{W}), \quad 1 \leq R < \infty, \quad (14-26a)$$

where $v = (V^2 - l^2)^{1/2}$, and the eigenvalue equation is

$$\tilde{U} J'_l(\tilde{U})/J_l(\tilde{U}) = \tilde{W} K'_{lv}(\tilde{W})/K_{lv}(\tilde{W}), \quad (14-26b)$$

where prime denotes differentiation with respect to argument, J_l is the Bessel function of the first kind and K_{lv} is the modified Bessel function of the second kind of pure imaginary order. The corresponding expressions for the clad-parabolic profile (p) are [10]

$$F_l = M_{\kappa, \mu}(VR^2)/RM_{\kappa, \mu}(V), \quad 0 \leq R \leq 1; \quad F_l = K_l(\tilde{W}R)/K_l(\tilde{W}), \quad 1 \leq R < \infty, \quad (14-27a)$$

where $\kappa = \tilde{U}^2/4V$, $\mu = l/2$ and

$$2VM'_{\kappa, \mu}(V)/fM_{\kappa, \mu}(V) - 1 = \tilde{W} K'_l(\tilde{W})/K_l(\tilde{W}), \quad (14-27b)$$

where $M_{\kappa, \mu}$ is the Whittaker function of the first kind. We can also solve the scalar wave equation for the clad-parabolic profile using a power-series expansion, as we show below.

14–9 Example: Clad power-law profiles

This class of profiles is defined by

$$n^2(R) = n_{co}^2\{1 - 2\Delta R^q\}, \quad 0 \leq R \leq 1; \quad R = r/\rho, \quad (14-28a)$$

$$= n_{cl}^2 = n_{co}^2\{1 - 2\Delta\}, \quad 1 \leq R < \infty; \quad 0 < q < \infty, \quad (14-28b)$$

where q is a constant. Plots are shown in Fig. 14–7(a) for various values of q , including

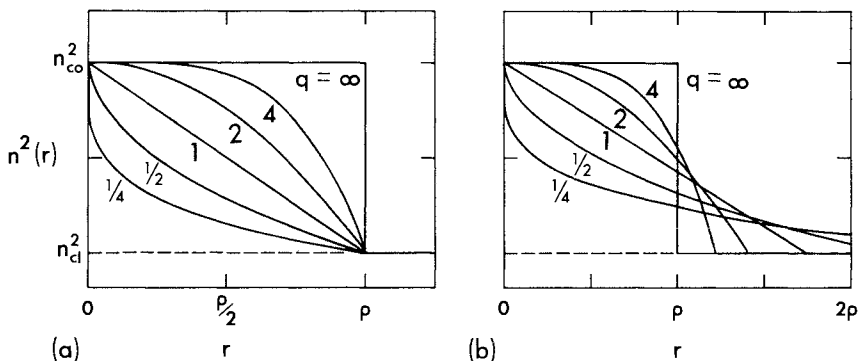


Fig. 14-7 Plots of (a) the clad power-law profiles and (b) the same profiles assuming equal profile volumes.

the clad parabolic profile ($q = 2$) and the step profile ($q = \infty$). In the weak-guidance approximation $n_{co} \cong n_{cl}$, or $\Delta \ll 1$. The scalar wave equation has the closed-form solution of Eq. (14-27a) for the clad parabolic profile, but we can generate an analytical solution for any rational value of q by using a power-series expansion [11, 12].

Power-series solution

For all practical purposes the exponent q is a rational number and can be represented by $q = p/s$, where p and s are relatively prime integers. Within the core, we make a change of variable $R = x^s$ in Eq. (14-4). Hence

$$\left\{ \frac{d^2}{dx^2} + \frac{1}{x} \frac{d}{dx} + \frac{s^2}{x^2} [\tilde{U}^2 x^{2s} - V^2 x^{2s+p} - l^2] \right\} F_l = 0. \quad (14-29)$$

The power series solution bounded at $R = x = 0$ is given by [12]

$$F_l = \sum_{n=0}^{\infty} a_n x^{n+ls} = \sum_{n=0}^{\infty} a_n R^{(l+n/s)}, \quad (14-30)$$

where the a_n are constants and a_0 is arbitrary. If we substitute into Eq. (14-29) and equate powers of x , we obtain the recurrence relations

$$a_{2ms} = -\frac{\tilde{U}^2}{4m(m+l)} a_{2ms-2s}; \quad m = 1, 2, \dots, \quad (14-31a)$$

for $n < 2s + p$, and

$$a_n = \frac{s^2}{n(n+2ls)} (V^2 a_{n-2s-p} - \tilde{U}^2 a_{n-2s}), \quad (14-31b)$$

for $n \geq 2s + p$. All remaining a_n are zero. The solution of Eq. (14-4) in the uniform cladding is proportional to $K_l(\tilde{W}R)$, the modified Bessel function of the second kind. If

we normalize so that $F_l = 1$ at $R = 1$, then

$$F_l = \frac{\sum_{n=0}^{\infty} a_n R^{(l+n/s)}}{\sum_{n=0}^{\infty} a_n}, \quad 0 \leq R \leq 1; \quad F_l = \frac{K_l(\tilde{W}R)}{K_l(\tilde{W})}, \quad 1 \leq R < \infty, \quad (14-32)$$

and \tilde{U}, \tilde{W} are defined inside the back cover.

Eigenvalue equation

Continuity of dF_l/dR at $R = 1$, together with the recurrence relation of Eq. (37-73), leads to the eigenvalue equation

$$\tilde{W} K_{l+1}(\tilde{W})/K_l(\tilde{W}) = - \sum_{n=0}^{\infty} n a_n / \left\{ s \sum_{n=0}^{\infty} a_n \right\}; \quad \tilde{U}^2 + \tilde{W}^2 = V^2. \quad (14-33)$$

The solution \tilde{U} for the fundamental mode ($l = 0, m = 1$) is plotted against V in Fig. 14-8(a) for various values of q . As V increases, the value of \tilde{U} approaches a finite limit only for the step profile. For all other profiles \tilde{U} is unbounded as $V \rightarrow \infty$. If we compare \tilde{U} with the analytical form of Eq. (14-9) for the infinite power-law profiles when $V = 8$, and use the values of $G(q)$ in Fig. 14-2(c), the error is less than 3.5% for the values of q shown. In other words, most of the fundamental-mode power is confined within the core, where the clad and infinite power-law profiles are identical, and the region beyond $R = 1$ has little effect.

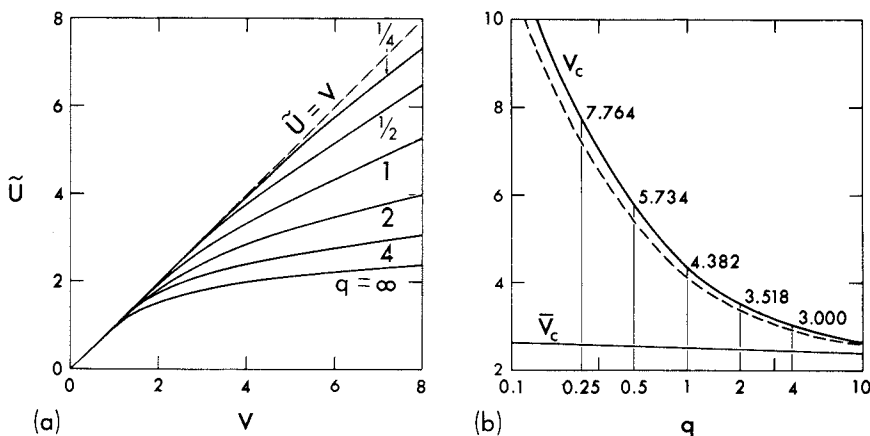


Fig. 14-8 (a) The modal parameter \tilde{U} for the fundamental mode of the clad power-law profiles and (b) the upper limit V_c on the range of single-mode operation given by the solid curve. The dashed curve is the analytic approximation of Eq. (14-45), and the solid curve \tilde{V}_c is the equal volume curve for the profiles of Fig. 14-7 (b).

Cutoff

The cutoff values V_c of the higher-order modes are the solutions of Eq. (14-33) when $\tilde{U} = V = V_c$ and $W = 0$. Using the asymptotic forms of Eq. (37-86) for the K_l when $\tilde{W} \rightarrow 0$, we deduce that V_c satisfies

$$\sum_{n=0}^{\infty} (n + 2ls) a_n = 0. \quad (14-34)$$

In Fig. 14-8(b) the solid curve gives V_c as a function of q for the modes with the smallest cutoff value, i.e. the $l = 1$, $m = 1$ or TE_{01} , TM_{01} , HE_{21} modes.

Intensity distribution

The intensity, or power flow density, \tilde{S} is defined in Table 13-2, page 292. To compare the intensity distribution of the fundamental mode on different profiles, we normalize \tilde{S} so that there is unit total power in the mode, i.e. $P = 1$. Using the definition of P in Table 13-2, the normalized intensity \hat{S} is defined by

$$\hat{S} = F_0^2 / \left\{ 2\pi\rho^2 \int_0^{\infty} F_0^2 R \, dR \right\}. \quad (14-35)$$

If we substitute for F_0 from Eq. (14-32) and use the integral in Eq. (37-93), then the integral in the denominator is expressible as

$$\int_0^{\infty} F_0^2 R \, dR = \frac{1}{2} \left\{ \frac{K_1^2(W)}{K_0^2(W)} - 1 \right\} + \sum_{m=0}^{\infty} \sum_{n=0}^{\infty} \frac{2sa_m a_n}{2s + m + n} / \left\{ \sum_{n=0}^{\infty} a_n \right\}^2. \quad (14-36)$$

We normalize with the core cross-sectional area and plot $\pi\rho^2 \hat{S}$ against R in Fig. 14-9(a) for various values of q with $V = 2.405$. For the step profile ($q = \infty$), S is then given in closed form by Eq. (14-16).

Distortion parameter

In the absence of material dispersion, pulse spreading on single-mode circular fibers is proportional to the distortion parameter \tilde{D} , as expressed by Eq. (13-18). To calculate this quantity for the clad power-law profiles, we first rearrange the definition as

$$\tilde{D} = -\frac{d\kappa}{dV} + \frac{\kappa}{V} - \frac{\tilde{U}^2}{V^3}; \quad \kappa = \frac{\tilde{U}}{V} \frac{d\tilde{U}}{dV}, \quad (14-37)$$

where κ is given in Table 13-2, page 292, in terms of integrals of F_0 of Eq. (14-32) over the cross-section. By differentiating this relationship with respect to V , we obtain

$$\frac{d\kappa}{dV} = 2 \int_0^{\infty} \{f - \kappa\} F_0 \frac{\partial F_0}{\partial V} R \, dR / \int_0^{\infty} F_0^2 R \, dR, \quad (14-38)$$

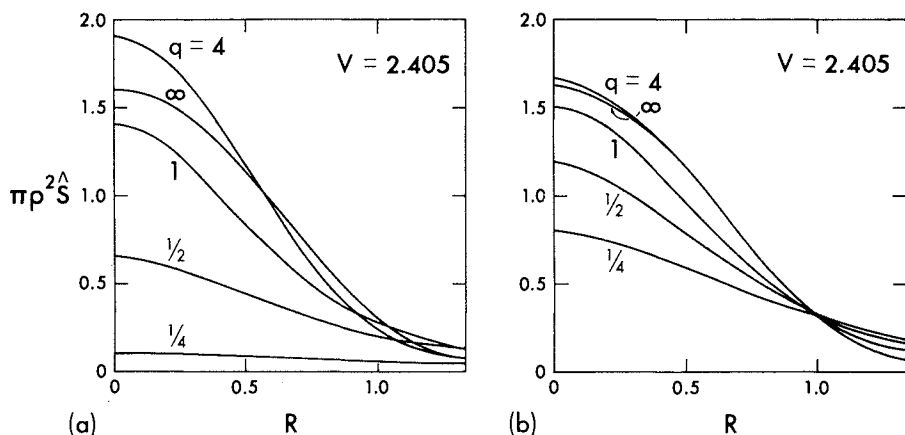


Fig. 14-9 (a) The normalized intensity distribution for the fundamental mode on clad power-law profiles assuming $V = 2.405$ and unit total power, and (b) the corresponding intensity distribution assuming the equal volume profiles of Fig. 14-7(b) with $V = \bar{V}_c = 2.405$.

and by differentiating Eqs. (14-32) and (14-31) with respect to V [13]

$$\frac{\partial F_0}{\partial V} = \left\{ \sum_{n=0}^{\infty} (R^{n/s} - F_0) b_n \right\} / \sum_{n=0}^{\infty} a_n; \quad b_n = \frac{da_n}{dV}, \quad (14-39)$$

where $b_0 = 0$ and the remaining b_n satisfy the recurrence relations

$$b_{2ms} = -\frac{1}{4m^2} \left\{ \tilde{U}^2 b_{2ms-2s} + 2V\kappa a_{2ms-2s} \right\}, \quad (14-40a)$$

if $n < 2s + p$, while for $n \geq 2s + p$

$$b_n = \frac{s^2}{n^2} \{ V^2 b_{n-2s-p} + 2V a_{n-2s-p} - \tilde{U}^2 b_{n-2s} - 2V\kappa a_{n-2s} \}, \quad (14-40b)$$

where the a_n are determined from Eq. (14-31). From this analysis, we calculate the plots of \bar{D} in Fig. 14-10(a) [13, 14]. We denote the value of V for which $\bar{D} = 0$ by V_d , and plot V_d as a function of the exponent in Fig. 14-10(b). When $\bar{D} = 0$ there is no waveguide dispersion. Hence only profiles with exponents in the range $2 < q < \infty$ can satisfy this condition. However, if we examine the cutoff values of V in Fig. 14-8(b), we deduce that a single-mode fiber will never have zero waveguide dispersion.

14-10 Equal volume profiles

The general profile $n(R)$ of a circular fiber has the form of Eq. (14-1). If we consider fibers with a uniform cladding of index n_{cl} , and recall the definition of

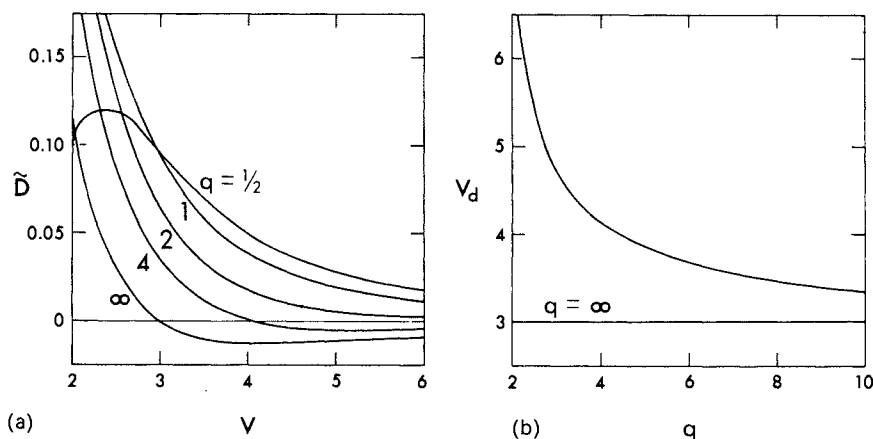


Fig. 14-10 (a) The distortion parameter for the fundamental modes of clad power-law profiles and (b) the values of the fiber parameter at which waveguide dispersion vanishes, the $q = \infty$ line corresponding to the value for the step profile.

Δ inside the back cover, we can express the profile as

$$n^2(R) = n_{cl}^2 \left\{ 1 + \frac{2\Delta}{1-2\Delta} (1-f) \right\}; \quad 0 \leq R \leq 1, \quad (14-41a)$$

$$= n_{cl}^2; \quad 1 \leq R < \infty. \quad (14-41b)$$

The function $1-f$ is the profile shape $S(r)$ introduced in Eq. (4-13), and is proportional to the excess or 'height' of $n^2(R)$ above its cladding value n_{cl}^2 . Now consider all clad profiles with the same value of Δ , and therefore the same value of n_{co} , and define an effective 'volume' Ω to be the integral of $1-f$ over the infinite cross-section of the fiber. This is identical to Eq. (4-14), whence

$$\Omega = \int_{A_\infty} (1-f) dA = 2\pi\rho^2 \int_0^\infty (1-f) R dR, \quad (14-42)$$

where ρ is the core radius or profile scaling length. *Equal volume profiles* have the same value of Ω , but, in general, will have differing core radii ρ .

The purpose of the equal volume concept is to normalize profiles with common values of n_{cl} and Δ in such a way as to separate effects which are dependent on profile shape from those which are almost independent of profile shape. To illustrate the idea we consider the profiles of the previous section.

Clad power-law profiles

The step profile ($q = \infty$) of core radius ρ is taken as a reference profile, which fixes the value of Ω in Eq. (14-42). We define ρ_e to be the core radius of the clad power-law profile with the same volume Ω . If we replace R by $R_e = r/\rho_e$ everywhere in Eq. (14-28) and substitute into Eq. (14-42), then,

$$\rho_e = \{(q+2)/q\}^{1/2} \rho. \quad (14-43)$$

The equal volume profiles are plotted in Fig. 14-7(b).

Cutoff

The cutoff value of V_c is plotted against q in Fig. 14-8(b). For the equal volume profiles the cutoff value for each profile is still given by V_c , although V_c is now proportional to ρ_e . If we define \bar{V}_c to be the corresponding cutoff value in terms of ρ , then Eq. (14-43) gives

$$\bar{V}_c = (\rho/\rho_e) V_c = \{q/(q+2)\}^{1/2} V_c. \quad (14-44)$$

The plot of \bar{V}_c in Fig. 14-8(b) is virtually flat for $q > 1$, with a difference at $q = 1$ of 5.1 per cent compared to $q = \infty$. In other words, \bar{V}_c is *virtually independent of profile shape in this range, and is well approximated by the step-profile value of 2.405*. On rearranging Eq. (14-44)

$$V_c \cong 2.405 \{(q+2)/q\}^{1/2}, \quad (14-45)$$

which corresponds to the dashed curve in Fig. 14-8(b).

Intensity distribution

The fundamental-mode intensity distribution is plotted in normalized form in Fig. 14-9(a), assuming $V = 2.405$ for each profile. If we consider the equal volume profiles, then for each profile we use the value of V given by Eq. (14-45). The corresponding value of \tilde{U} follows from Eq. (14-33) and plots of the normalized intensity $\pi\rho^2\hat{S}$ are given in Fig. 14-9(b). *For $q > 1$ the intensity distribution is almost independent of profile shape.*

Distortion parameter

We showed in the previous section that the distortion parameter \tilde{D} can have a zero for values of V of practical interest only if $q > 2$. Consequently, *the vanishing of waveguide dispersion depends primarily on profile shape.*

Arbitrary profiles

We have shown that clad power-law profiles of equal volume have a fundamental-mode intensity distribution and a maximum value V_c of the fiber

parameter for single-mode operation which are relatively insensitive to profile shape. By generalizing the above discussions to clad single-mode fibers of arbitrary profile shape and given V , a qualitative description of power distribution is given by the step-profile expression of Eq. (14-16) using a fiber parameter value \bar{V} given by

$$\bar{V} = V(\Omega/\pi)^{1/2} = V \left\{ 2 \int_0^\infty (1-f)R \, dR \right\}^{1/2}, \quad (14-46)$$

assuming the profile volumes of Eq. (14-42) are equal [15]. Similarly, by generalizing Eq. (14-45), a first estimate of V_c is given by

$$V_c = 2.405(\Omega/\pi)^{1/2} = 2.405 \left\{ 2 \int_0^\infty (1-f)R \, dR \right\}^{1/2}. \quad (14-47)$$

Both of these expressions assume common values of n_{cl} and Δ .

14-11 Fundamental mode for small V

On a weakly guiding clad fiber of otherwise arbitrary profile, the fraction of fundamental-mode power residing in the core becomes negligible as $V \rightarrow 0$. For the step profile, this is clear from the plot of $\bar{\eta}$ in Fig. 14-3(a). Simultaneously, the fields become nearly uniform over the core, as is evident from the intensity distributions in Fig. 14-3(c), and hence are comparatively insensitive to profile shape. Accordingly, we postulate that the fields depend primarily on the profile volume Ω of Eq. (14-42). It then follows from the discussion of the previous section that we can relate the fields of an arbitrary profile, with fiber parameter V , to the known fields of the step profile with fiber parameter \bar{V} through Eq. (14-46). Thus we replace V by \bar{V} in the small- V forms for the step-profile fiber listed in Table 14-5. The same conclusion can be derived more formally from the scalar wave equation, as we now show.

Derivation from the scalar wave equation

If the fiber parameter V for an arbitrary profile fiber decreases and Δ is fixed, then the wavelength λ increases, as is clear from the definition inside the back cover. When V is sufficiently small that $\lambda \gg \rho$, where ρ is the radius of the core, then the core electric field is given by the quasi-static approximation, as expressed in Eq. (11-52). Since the fiber is weakly-guiding we ignore the term in $\nabla_t \ln n^2$ and obtain Laplace's equation for the potential Ψ describing the transverse electric field

$$\nabla_t^2 \Psi = 0; \quad \mathbf{e}_t = \nabla_t \Psi, \quad (14-48)$$

where ∇_t^2 and ∇_t are defined in Table 30-1, page 592. The even and odd HE_{11} modes have separable solutions $R \cos \phi$ and $R \sin \phi$ of this equation which are bounded at $R = 0$. With reference to Fig. 14-1, $\Psi = x$ for the even mode and consequently $e_t = \hat{x}$ or $F_0 = 1$, where \hat{x} is the unit vector parallel to the x -axis. Hence the core field is uniform as discussed above.

In the cladding the scale length is always greater than λ unless $\lambda = \infty$. Since V is small, but finite, we must retain the scalar wave equation to describe the fields there. We use the integral form of this equation for \tilde{U}^2 given in Table 13-2, page 292, and set $l = 0$. It is convenient to rearrange this equation by setting $\tilde{U}^2 = V^2 - \tilde{W}^2$, and then put $f = 1$ in the cladding, with $F_0 \cong 1$ and $dF_0/dR \cong 0$ in the core, leading to

$$\tilde{W}^2 = \left\{ V^2 \int_0^1 (1-f)R \, dR - \int_1^\infty \left(\frac{dF_0}{dR} \right)^2 R \, dR \right\} / \left\{ \frac{1}{2} + \int_1^\infty F_0^2 R \, dR \right\}. \quad (14-49)$$

The first integral in the numerator is proportional to the profile volume Ω of Eq. (14-42), and in the cladding $F_0 = K_0(\tilde{W}R)/K_0(\tilde{W})$. Using the integrals in Eq. (37-93) and rearranging we deduce that

$$\tilde{W}^2/V^2 = (\Omega/\pi)K_0(\tilde{W})/K_2(\tilde{W}). \quad (14-50)$$

Substituting from Eq. (37-86) for the small W forms of the modified Bessel functions, and from Eq. (14-16), we obtain the explicit form

$$\tilde{W} \cong 1.123 \exp \{ -2\pi/\Omega V^2 \} = 1.123 \exp \{ -2/\bar{V}^2 \}. \quad (14-51)$$

For the step profile $f = 0$ and $\Omega = \pi$, so we recover the asymptotic form in Table 14-5.

REFERENCES

1. Snyder, A. W. and Young, W. R. (1978) Modes of optical waveguides. *J. Opt. Soc. Am.*, **68**, 297-309.
2. Snyder, A. W. (1969) Asymptotic expressions for eigenfunctions and eigenvalues of a dielectric or optical waveguide. *I.E.E.E. Trans. Microwave Theory Tech.* **17**, 1130-8.
3. Kurtz, C. N. and Streiffer, W. (1969) Guided waves in inhomogeneous focussing media, Part I: Formulation, solution for quadratic inhomogeneity. *I.E.E.E. Trans. Microwave Theory Tech.*, **17**, 11-15.
4. Pask, C. (1979) Exact expressions for scalar modal eigenvalues and group delays in power-law optical fibres. *J. Opt. Soc. Am.*, **69**, 1599-1603.
5. Rudolph, H. D. and Neumann, E. G. (1976) Approximations for the eigenvalues of the fundamental mode of a step index glass fiber waveguide. *Nachrichtentech. Z.*, **29**, 328-9.

6. Sammut, R. A. (1979) Analysis of approximations for the mode dispersion in monomode fibres. *Electron. Lett.*, **15**, 590–1.
7. Marcuse, D. (1972) *Theory of Dielectric Optical Waveguides*, Academic Press, New York.
8. Snyder, A. W. and de la Rue, R. (1970) Asymptotic solution of eigenvalue equations for surface waveguide structures. *I.E.E.E. Trans. Microwave Theory Tech.*, **9**, 650–1.
9. Love, J. D. (1984) Exact, analytical solutions for modes on a graded-profile fibre. *Opt. Quant. Elect.* (submitted).
10. Yamada, R. and Inabe, K. (1974) Guided waves in an optical square-law medium. *J. Opt. Soc. Am.*, **64**, 964–8.
11. Gambling, W. A., Payne, D. N. and Matsumura, H. (1977) Cut-off frequency in radially inhomogeneous single-mode fibre. *Electron. Lett.*, **13**, 139–40.
12. Love, J. D. (1979) Power series solutions of the scalar wave equation for cladded, power-law profiles of arbitrary exponent. *Opt. Quant. Elect.*, **11**, 464–6.
13. Love, J. D., Hussey, C. D., Snyder, A. W. and Sammut, R. A. (1982) Polarization corrections to mode propagation on weakly guiding fibres. *J. Opt. Soc. Am.*, **72**, 1583–91.
14. Snyder, A. W. and Sammut, R. A. (1978) Dispersion in graded, single-mode fibres. *Electron. Lett.*, **15**, 269–71.
15. Snyder, A. W. (1981) Understanding monomode optical fibres. *Proc. I.E.E.E.*, **69**, 6–13.

Gaussian approximation for circular fibers

Fundamental modes	337
15-1 Gaussian approximation	337
15-2 <i>Example: Gaussian profile</i>	342
15-3 <i>Example: Step profile</i>	344
15-4 <i>Example: Smoothed-out profiles</i>	345
15-5 Field far from the fiber axis	347
 Higher-order modes	 349
15-6 Approximations for the fields	349
15-7 <i>Example: Gaussian profile</i>	349
 Step-profile approximation	 350
15-8 Fundamental modes	350
15-9 Range of single-mode operation	352
 References	 353

The weak-guidance approximation, described in Chapter 13, greatly simplifies the determination of the modal fields of optical waveguides, because it depends on solutions of the scalar wave equation, rather than on vector solutions of Maxwell's equations. For circular fibers, with an arbitrary profile, the scalar wave equation must normally be solved by purely numerical methods. We discussed the few profiles that have analytical solutions in Chapter 14. These solutions, including those for profiles of practical interest such as the step and clad power-law profiles, are given in terms of special functions or by series expansions, which usually necessitate tables or numerical evaluation to reveal the physical attributes of the modes.

An exception is the infinite parabolic profile of Section 14-4. The fundamental-mode fields of Table 14-2, page 307, have the simple Gaussian dependence $\exp(-\frac{1}{2} V^2)$ and other modal properties have very elementary forms, from which their physical behavior is immediately apparent. To these facts we add the observation that the fundamental-mode intensity pattern – and hence the field distribution – for step and clad power-law profiles

in Fig. 14-9(a) is approximately Gaussian. Accordingly, we can take advantage of the simplicity of the Gaussian description and readily elucidate the physical attributes of a general profile by assuming that the fundamental-mode field distribution of an *arbitrary* profile can be approximated by *some* Gaussian function [1-3]. This observation together with a simple variational procedure is the basis of the *Gaussian approximation* presented here [4, 5]. The main purpose of this chapter is to show how to determine the Gaussian field for a particular profile. The propagation constant and other quantities of interest on single-mode fibers can then be accurately expressed by simple analytical functions [5].

In Section 14-10, we introduced the concept of profile volume. We showed in the case of clad power-law profiles of equal volume that some properties, such as the range of single-mode operation and the fundamental-mode intensity distribution are insensitive to profile shape, whereas other properties, such as waveguide dispersion, depend critically on profile shape. Within the Gaussian approximation, we can demonstrate directly the insensitivity of the intensity distribution to profile shape.

We also discuss generalizations of the Gaussian approximation to other low-order modes. Finally, we briefly describe the equivalent step-profile approximation [4], and compare it with the Gaussian approximation.

FUNDAMENTAL MODES

We begin with a brief review of the weak-guidance approximation for fundamental modes on circular fibers. In Sections 13-2 and 13-4, we showed that the two fundamental modes are virtually TEM waves, with transverse fields that are polarized parallel to one of a pair of orthogonal directions. The transverse field components for the x - and y -polarized HE_{11} modes are given by Eq. (13-9) relative to the axes of Fig. 14-1. The spatial variation $F_0(r)$ is the fundamental-mode solution ($l = 0$) of the scalar wave equation in Table 13-1, page 288. Hence

$$\left\{ \frac{d^2}{dr^2} + \frac{1}{r} \frac{d}{dr} + k^2 n^2(r) - \beta^2 \right\} F_0 = 0, \quad (15-1)$$

where $n(r)$ is the refractive-index profile, $k = 2\pi/\lambda$ and λ is the free-space wavelength. Throughout this chapter we consider only scalar quantities, and therefore the \sim denoting scalar quantities can be omitted.

15-1 Gaussian approximation

Our main objective is to find a good approximation for the field dependence $F_0(r)$ and the propagation constant β in Eq. (15-1). We know from examples

that F_0 has a maximum at $r = 0$ and decreases to zero as r increases and, for the profiles of Fig. 14-9(a), F_0 is approximately Gaussian. Hence we assume that F_0 can be approximated by

$$F_0(r) = \exp \left\{ -\frac{1}{2} \left(\frac{r}{r_0} \right)^2 \right\}, \quad (15-2)$$

where r_0 is the *spot size*. To determine r_0 , we use a simple variational method [4, 5]. If Eq. (15-2) is a good approximation to the solution of Eq. (15-1), it can be used as a trial function in a stationary expression for β . The value of r_0 then corresponds to the largest value of β [6]. We are reminded that, by definition, the fundamental mode has the largest value of the propagation constant β , or, equivalently, the smallest value of the modal parameter U .

To derive the stationary expression, we multiply Eq. (15-1) by rF_0 and use the identity

$$rF_0 \frac{d^2 F_0}{dr^2} + F_0 \frac{dF_0}{dr} = \frac{d}{dr} \left\{ rF_0 \frac{dF_0}{dr} \right\} - r \left\{ \frac{dF_0}{dr} \right\}^2, \quad (15-3)$$

to re-express the left side. We then integrate from $r = 0$ to $r = \infty$, noting that F_0 and dF_0/dr vanish exponentially at infinity, and rearrange to obtain [5]

$$\beta^2 = \frac{\int_0^\infty \left\{ k^2 n^2(r) F_0^2 - (dF_0/dr)^2 \right\} r dr}{\int_0^\infty r F_0^2 dr}, \quad (15-4)$$

where $k = 2\pi/\lambda$ and λ is the free-space wavelength. This is identical to the expression in Table 13-2, page 292, when $l = 0$. By using a stationary expression for β^2 , a first-order error between the Gaussian approximation to F_0 and the exact solution of Eq. (15-1) results in only a second-order error in β^2 . In other words, the approximation for β^2 given by substituting Eq. (15-2) into Eq. (15-4) is more accurate than the original approximation for F_0 .

We determine the spot size by substituting Eq. (15-2) into Eq. (15-4) and solving the equation

$$\partial \beta^2 / \partial r_0 = 0. \quad (15-5)$$

The propagation constant is found by substituting this solution back into Eq. (15-4). Knowing r_0 and β , the fields are specified by substituting into Table 15-1.

The analysis for finding r_0 and β is facilitated by working with the fiber and modal parameters V and U , since both are dimensionless and U is independent of the profile height parameter Δ . We substitute Eq. (15-2) and the profile

Table 15-1 Gaussian approximation for circular fibers. Gaussian approximation for the fundamental-mode fields of weakly guiding, circular fibers. Parameters are defined inside the back cover and coordinates are illustrated in Fig. 14-1

<i>Even HE₁₁ mode (x-polarized)</i>	<i>Odd HE₁₁ mode (y-polarized)</i>
$E_x = \exp \left\{ -\frac{1}{2} \frac{r^2}{r_0^2} \right\} \exp (i\beta z)$	$E_y = \exp \left\{ -\frac{1}{2} \frac{r^2}{r_0^2} \right\} \exp (i\beta z)$
$H_y = \left(\frac{\epsilon_0}{\mu_0} \right)^{1/2} n_{co} E_x$	$H_x = -\left(\frac{\epsilon_0}{\mu_0} \right)^{1/2} n_{co} E_y$
$n^2(R) = n_{co}^2 \{1 - 2\Delta f(R)\}; \quad V = k\rho n_{co} (2\Delta)^{1/2}; \quad R = \frac{r}{\rho}; \quad R_0 = \frac{r_0}{\rho}$	
<i>Variational equation for the propagation constant β</i>	
$U^2 = \frac{V^2}{2\Delta} - \rho^2 \beta^2 = \frac{1}{R_0^2} + V^2 \left\{ f(0) + \int_0^\infty \frac{df(R)}{dR} \exp \left\{ -\frac{R^2}{R_0^2} \right\} dR \right\}$	
<i>Equation for spot size r_0</i>	
$\frac{1}{V^2} = \int_0^\infty \frac{df(R)}{dR} R^2 \exp \left\{ -\frac{R^2}{R_0^2} \right\} dR; \quad r_0 = \rho R_0$	

representation of Table 15-1 into Eq. (15-4), perform the integration in the denominator, integrate by parts in the numerator and rearrange to obtain the expression for U^2 . If R_0 denotes the normalized spot size r_0/ρ , then Eq. (15-5) is equivalent to $\partial U^2 / \partial R_0 = 0$, and substitution of U^2 leads to the equation in Table 15-1.

Approximations for fundamental-mode quantities

If we substitute the Gaussian approximation of Eq. (15-2) into Table 13-2, page 292, we obtain the expressions in Table 15-2 for fundamental-mode quantities on an arbitrary profile. We have generalized the function η —the fraction of modal power within the core—and define $\eta(R)$ to be the fraction of modal power *within normalized radius* $R = r/\rho$. This is a more useful quantity for profiles with no well-defined core-cladding interface. The expressions for v_g and D follow from Eqs. (13-17) and (13-18). If for a particular profile the

Table 15-2 Gaussian approximation for fundamental-mode properties. Definitions are taken from Table 13-2, page 292, for modal quantities. The approximate

$n^2(R) = n_{co}^2 \{1 - 2\Delta f(R)\}; \quad R = \frac{r}{\rho}; \quad R_0 = \frac{r_0}{\rho};$		
Profile	Arbitrary	Gaussian
$f(R)$	—	$1 - \exp(-R^2)$
R_0	—	$\frac{1}{(V-1)^{1/2}}$
U	—	$(2V-1)^{1/2}$
$\frac{dU}{dV}$	$\frac{1}{UV} \left\{ U^2 - \frac{1}{R_0^2} \right\}$	$\frac{1}{(2V-1)^{1/2}}$
S	$\frac{ a ^2}{2} \left(\frac{\epsilon_0}{\mu_0} \right)^{1/2} n_{co} \exp \{ -(R^2/R_0^2) \}$	$\frac{ a ^2}{2} \left(\frac{\epsilon_0}{\mu_0} \right)^{1/2} n_{co} \exp \{ -(V-1)R^2 \}$
N	$\frac{\pi \rho^2 n_{co}}{2} \left(\frac{\epsilon_0}{\mu_0} \right)^{1/2} R_0^2$	$\frac{\pi \rho^2 n_{co}}{2} \left(\frac{\epsilon_0}{\mu_0} \right)^{1/2} \frac{1}{V-1}$
$\eta(R)$	$1 - \exp \{ -(R^2/R_0^2) \}$	$1 - \exp \{ -(V-1)R^2 \}$
v_g	$\frac{c}{n_{co}} \left\{ 1 + \frac{\Delta}{V^2} \left(U^2 - \frac{2}{R_0^2} \right) \right\}$	$\frac{c}{n_{co}} \left\{ 1 + \frac{\Delta}{V^2} \right\}$
D	$\frac{1}{V} \frac{d}{dV} \left\{ \frac{1}{VR_0^2} \right\}$	$\frac{1}{V^3}$
V_c	$2.405 \left\{ 2 \int_0^\infty (1-f)R dR \right\}^{1/2}$	2.405

cutoff value V_c is given by Eq. (14-47). Parameters are defined inside the back cover.

$V = k\rho n_{co}(2\Delta)^{1/2}; \quad \beta = \frac{1}{\rho} \left\{ \frac{V^2}{2\Delta} - U^2 \right\}^{1/2}$		
Profile	Step	Smoothed-out
$f(R)$	$0; \quad 0 \leq R < 1$ $1; \quad 1 < R < \infty$	$1 - \frac{1}{\Gamma(m+1)} \int_{(m+1)R^2}^{\infty} t^m e^{-t} dt$
R_0	$\frac{1}{\{2 \ln V\}^{1/2}}$	$\frac{1}{\{(m+1)[V^{2/(m+2)} - 1]\}^{1/2}}$
U	$\{1 + 2 \ln V\}^{1/2}$	$\{(m+2)V^{2/(m+2)} - (m+1)\}^{1/2}$
$\frac{dU}{dV}$	$\frac{1}{V\{1 + 2 \ln V\}^{1/2}}$	$\frac{V^{-m/(m+2)}}{\{(m+2)V^{2/(m+2)} - (m+1)\}^{1/2}}$
S	$\frac{ a ^2}{2} \left(\frac{\epsilon_0}{\mu_0} \right)^{1/2} n_{co} \exp(-2R^2 \ln V)$	$\frac{ a ^2}{2} \left(\frac{\epsilon_0}{\mu_0} \right)^{1/2} n_{co} \times$ $\exp[-(m+1)\{V^{2/(m+2)} - 1\}R^2]$
N	$\frac{\pi \rho^2 n_{co}}{4} \left(\frac{\epsilon_0}{\mu_0} \right)^{1/2} \frac{1}{\ln V}$	$\frac{\pi \rho^2 n_{co}}{2(m+1)} \left(\frac{\epsilon_0}{\mu_0} \right)^{1/2} \frac{1}{V^{2/(m+2)} - 1}$
$\eta(R)$	$1 - \exp(-2R^2 \ln V)$	$1 - \exp(-(m+1)\{V^{2/(m+2)} - 1\}R^2)$
v_g	$\frac{c}{n_{co}} \left\{ 1 + \frac{\Delta}{V^2} (1 - 2 \ln V) \right\}$	$\frac{c}{n_{co}} \left\{ 1 + \frac{\Delta}{V^2} [m+1 - mV^{2/(m+2)}] \right\}$
D	$\frac{2}{V^3} \{1 - \ln V\}$	$\frac{m+1}{V^3} \left\{ 1 - \left(\frac{m}{m+2} \right) V^{2/(m+2)} \right\}$
V_c	2.405	2.405

spot-size equation can be solved analytically, then every quantity in Table 15-2 can be given explicitly in terms of the fiber parameter.

Range of single-mode operation

One piece of information not provided by the Gaussian approximation is the upper value V_c of the fiber parameter for single-mode operation. In Section 14-10 we showed by example that the value of V_c depends primarily on the profile volume Ω of Eq. (14-42) and is relatively insensitive to profile shape. For clad profiles with the same maximum core index n_{co} and cladding index n_{cl} , an estimate for V_c is obtained by assuming that profiles with the same value of Ω have approximately the same value of V_c . This leads to Eq. (14-47), based on the step profile of volume Ω , which is included in Table 15-2.

The Gaussian approximation is of greatest use for profiles which do not have analytical solutions of the scalar wave equation. Our first example considers one such profile and demonstrates the accuracy of the Gaussian approximation by comparison with numerical solutions.

15-2 Example: Gaussian profile

The Gaussian refractive-index profile is illustrated in Fig. 15-1(a), and is defined by

$$n^2(R) = n_{co}^2 \{1 - 2\Delta(1 - \exp[-R^2])\}; \quad 0 \leq R < \infty, \quad (15-6)$$

where $R = r/\rho$, and hence $f(R) = 1 - \exp(-R^2)$. Thus $n(R)$ decreases smoothly from n_{co} to n_{cl} as R increases from 0 to ∞ . There is no well-defined interface, and the linear dimension ρ scales the profile. When $\rho \rightarrow 0$, the profile narrows to a spike about $R = 0$, and as $\rho \rightarrow \infty$ the profile becomes very flat. This profile is of practical interest, since it approximates the profiles of fibers whose core and cladding materials diffuse into one another during manufacture. It also leads to simple expressions for all characteristics of fundamental mode propagation.

Substituting Eq. (15-6) into the spot size equation in Table 15-1, we find that [4, 5]

$$r_0 = \rho/(V-1)^{1/2}. \quad (15-7)$$

The fact that this expression is physically meaningful only when $V > 1$ does not detract from a useful description of practical fibers. Fibers with $V \leq 1$ have little fundamental-mode power flowing close to the axis. The methods of Section 14-11 can be used to describe the small- V fiber.

If we substitute the spot size back into Table 15-1, we deduce the expressions for the propagation constant and modal parameter in Table 15-2, which in turn lead to the remaining expressions for fundamental-mode quantities.

Range of single-mode operation

The profile volume, defined by Eq. (14-42), is identical for the Gaussian profile of Eq.

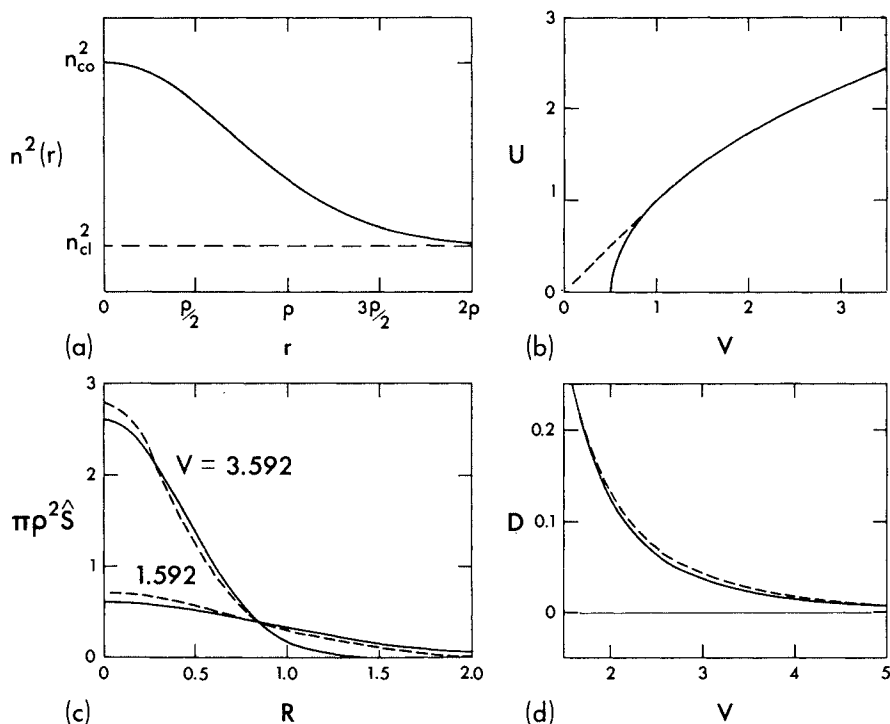


Fig. 15-1 (a) The Gaussian profile of Eq. (15-6), (b) the modal parameter U of Table 15-2 as a function of the fiber parameter, (c) the normalized intensity distribution $\pi\rho^2\hat{S}$ of Eq. (15-8) for $V = V_c \pm 1$, where $V_c = 2.592$ is the cutoff of the second mode, and (d) the distortion parameter of Table 15-2. In (b)–(d) the dashed curves denote numerical solution of the scalar wave equation [7].

(15-6) and the step profile of Eq. (14-12). Consequently the range of single-mode operation is the same for both profiles and $V_c \cong 2.405$. Using numerical methods [7], the exact value is found to be $V_c = 2.592$, so that the approximate value is in error by 7.2%.

Propagation constant

The propagation constant, expressed in terms of the mode parameter U , is plotted against V in Fig. 15-1(b), where the solid curve denotes the expression in Table 15-2, and the dashed curve is the exact solution. At $V = 1$ the error is 1.4%, rising to 1.8% at $V = 1.25$ and then steadily decreasing as V increases. For $V = V_c = 2.592$, the error is 0.6% [7].

Intensity distribution

We define \hat{S} to be the intensity distribution when there is unit power in the fundamental mode, i.e. $|a|^2 N = 1$, where a is the modal amplitude and N the normalization. If we normalize \hat{S} with the cross-sectional area within radius ρ , then Table 15-2 gives

$$\pi\rho^2\hat{S} = (V-1)\exp\{-R^2(V-1)\}, \quad (15-8)$$

which is plotted as the solid curve in Fig. 15-1(c) for $V = V_c + 1$ and $V = V_c - 1$. The dashed curved is the exact numerical solution. We note the characteristic behavior that as V decreases, power is distributed over an increasing area. This effect is described by the expression $\eta(R)$ in Table 15-2 for the fraction of power with radius r . If we keep this fraction fixed, then $r \propto \rho/(V-1)^{1/2}$, which increases rapidly as $V \rightarrow 1$.

Profile dimensions for maximum light concentration

We can determine the Gaussian profile for which the concentration of fundamental-mode power around the fiber axis will be maximized. In other words we find the value of ρ for which the spot size r_0 is a minimum. Noting that V is proportional to ρ , this minimum occurs when $r_0 = \rho$ and $V = 2$ in Eq. (15-7), whence $\rho = \lambda/\{\pi(n_{co}^2 - n_{cl}^2)^{1/2}\}$ from the definitions at the back of the book. In Section 10-2 we derived this result qualitatively by using physical arguments. At this value of r_0 , the intensity distribution and the profile have the same shape.

Group velocity and pulse spreading

If $0 < V < 2.592$ the fiber is single moded. The pulse transit time of Eq. (11-36) is inversely proportional to the group velocity, and pulse spreading due to waveguide dispersion is proportional to $V\Delta D = \Delta/V^2$, where D is the scalar distortion parameter. The expression for D in Table 15-2 is plotted as the solid curve in Fig. 15-1(d). Compared with the dashed curve, calculated numerically, the maximum relative error is 9.6% at $V = 2.9$, while at $V = V_c$ this error is 9.4%. There is no zero of waveguide dispersion.

15-3 Example: Step profile

The fundamental-mode properties of the weakly guiding, step-profile fiber were given in analytical form in the previous chapter, but, nevertheless, numerical solution of a transcendental eigenvalue equation is required. Within the Gaussian approximation the propagation constant is given explicitly, and all other modal properties have much simpler analytical forms, at the expense of only a slight loss of accuracy [4, 5].

The derivative df/dR for the profile of Eq. (14-12) is given by the Dirac delta function $\delta(R-1)$. Substitution into Table 15-1 leads to the spot size in Table 15-2 and the remaining modal quantities. The accuracy of these expressions can be judged by comparison with the numerical values in Table 14-4, page 314. If we differentiate the

spot-size expression, the core radius ρ for maximum light concentration close to the fiber axis occurs when $V = e^{1/2} \cong 1.65$ and $r_0 = \rho$. Using the definitions at the back of the book, this leads to $\rho \cong 0.83\lambda / \{\pi(n_{co}^2 - n_{cl}^2)^{1/2}\}$, which is 17% smaller than the corresponding expression for the Gaussian profile. Accordingly light is more confined by the step profile.

15-4 Example: Smoothed-out profiles

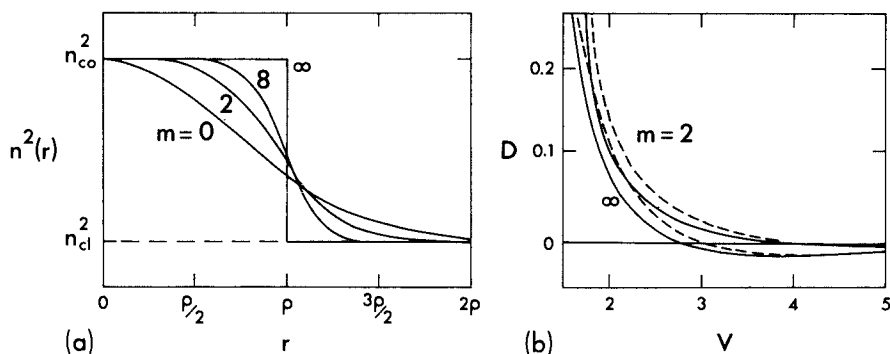


Fig. 15-2 (a) Plots of the smoothed-out profiles of Eq. (15-9), where $m = 0$ is the Gaussian profile and $m = \infty$ is the step profile, and (b) the solid curves are the approximation of Table 15-2 for the distortion parameter, while the dashed curves are numerical solutions of the scalar wave equation [7].

As our final example, we consider a continuum of profiles, illustrated in Fig. 15-2(a), which at one extreme reduces to the step profile and at the other extreme reduces to the Gaussian profile. These profiles are defined by [5]

$$n^2(R) = n_{co}^2 \{1 - 2\Delta f(R)\}; \quad f(R) = 1 - \frac{1}{\Gamma(m+1)} \int_{(m+1)R^2}^{\infty} t^m \exp(-t) dt, \quad (15-9)$$

where Γ is the gamma function, $m > -1$ is a constant and $R = r/\rho$. If m is a nonnegative integer, integration by parts leads to

$$f(R) = 1 - \exp\{-(m+1)R^2\} \sum_{n=0}^m \frac{(m+1)^n}{n!} R^{2n} \quad (15-10a)$$

$$= \exp\{-(m+1)R^2\} \sum_{n=m+1}^{\infty} \frac{(m+1)^n}{n!} R^{2n}. \quad (15-10b)$$

The Gaussian and step profiles correspond to $m = 0$ and $m = \infty$, respectively. For $R \ll 1$, expansion of the exponential function in Eq. (15-10) leads to $f(R) \cong (m+1)^m R^{2m+2}/m!$, which represents a set of power-law profiles similar to Eq. (14-28a).

Modal properties

If we substitute Eq. (15-9) into Table 15-1, we obtain the expressions in Table 15-2. The limits $m \rightarrow 0$ and $m \rightarrow \infty$ correspond to the forms for the Gaussian and step profiles. For $m \gg 1$ we can express quantities as a small perturbation of the step-profile results by setting $V^{2/(m+2)} = \exp\{2 - \ln V/(m+2)\}$, e.g.

$$\frac{\rho^2}{r_0^2} \cong 2 \ln V + \frac{2}{m} \ln V (\ln V - 1); \quad U^2 \cong 1 + 2 \ln V + \frac{2}{m} (\ln V)^2, \quad (15-11)$$

We show in Table 15-3 that there is only a very small error between the approximate and exact values of U for the fundamental mode, calculated at the exact cutoff V_c of single-mode operation for each profile [7]. The distortion parameter of Table 15-2 is plotted as the solid curves in Fig. 15-2(b) for the $m = 2$ and step profiles, together with the dashed curves for the exact values [7]. If V_d denotes the values of V for which there is no waveguide dispersion, i.e. $D = 0$, then

$$V_d \doteq \left\{ \frac{m+2}{m} \right\}^{(m+2)/2} \cong \exp \left\{ 1 + \frac{1}{m} \right\}; \quad m \gg 1. \quad (15-12)$$

Only for the Gaussian profile ($m = 0$) of Fig. 15-1(d) is there no zero of dispersion.

Table 15-3 Parameter values and relative errors for the smoothed-out profiles. Comparisons between approximate and exact values of the fundamental-mode parameter U when $V = V_c$, and between the exact value of V_c and the approximate value of Eq. (15-13).

m	U <i>exact</i>	U <i>Gaussian</i> <i>approx.</i>	<i>Relative</i> <i>error</i> (%)	V_c <i>exact</i>	V_c <i>Equal</i> <i>spot size</i>	<i>Relative</i> <i>error</i> (%)
0	2.034	2.045	-0.6	2.592	2.755	-6.3
2	1.818	1.826	-0.4	2.508	2.512	-0.2
4	1.758	1.766	-0.4	2.477	2.466	0.4
8	1.713	1.721	-0.5	2.451	2.437	0.6
16	1.683	1.694	-0.6	2.432	2.421	0.4
32	1.666	1.678	-0.7	2.420	2.413	0.3
∞	1.646	1.660	-0.8	2.405	2.405	0

Equal volume profiles

We showed in Section 14-10 that the fundamental mode intensity distribution and the maximum value of the fiber parameter for single-mode operation are relatively insensitive to profile shape, being strongly dependent on profile volume. On the other hand, waveguide dispersion is strongly dependent on profile shape. The Gaussian approximation, when applied to the smoothed-out profiles, provides an easy way to verify these general conclusions. These profiles all have the same profile volume, as may be verified by substituting Eq. (15-9) into Eq. (14-42), reversing the order of integration and recalling the definition of the gamma function in Eq. (37-104).

Intensity distribution and distortion parameters

The intensity distribution S in Table 15-2 varies exponentially with $-R^2/R_0^2$, where R_0 is the normalized spot size. At the extremes in profile shape, $1/R_0^2 = V - 1$ for the Gaussian profile ($m = 0$) and $1/R_0^2 = 2 \ln V$ for the step profile ($m = \infty$). If we use the cutoff values $V_c = 2.592$ for the former and $V_c = 2.405$ for the latter, it is readily verified that $1/R_0^2$ varies in value by about 9%, and thus S is relatively insensitive to profile shape. On the other hand, it is clear from either Table 15-2 or Eq. (15-12) that the distortion parameter depends on profile shape, i.e. on m .

Range of single-mode operation

If we assume that spot size is independent of profile shape when $V = V_c$, we can use the Gaussian approximation to check if the consequence of this assumption is consistent with the exact value of V_c . The normalized intensity is independent of profile shape only if the spot size has the same value r_0 for all profiles. Thus we set $V = V_c$ in the ratio $S/|a|^2 N$, as given by Table 15-2, and use the step profile with $V_c = 2.405$ as a reference profile which determines the value of r_0 . On rearranging

$$V_c = \left\{ 1 + \frac{1.755}{m+1} \right\}^{(m+2)/2} \cong 2.405 \exp \left\{ \frac{0.107}{m} \right\}, \quad m \rightarrow \infty. \quad (15-13)$$

Values of this expression are compared with the exact values of V_c in Table 15-3. There is negligible difference except for the Gaussian profile ($m = 0$), so spot size is indeed nearly independent of profile shape when $V = V_c$. This consistency check is a refinement of the approximation $V_c = 2.405$ for all equal-volume profiles given in Table 15-2.

15-5 Field far from the fiber axis

On clad fibers with profiles such as those considered in the previous three examples, the refractive index assumes a uniform value n_{cl} sufficiently far from

the fiber axis. In this region the solution of the scalar wave equation, Eq. (15-1), for the fundamental mode is $K_0(WR)$, where $R = r/\rho$ and K_0 is the modified Bessel function of the second kind. The mode parameter W is defined inside the back cover. When $WR \gg 1$, we find from Eq. (37-88) that K_0 varies as $R^{-1/2} \exp(-WR)$. Hence the Gaussian approximation, which varies as $\exp(-R^2/2R_0^2)$, is deficient in this region. The far, or evanescent, field is usually of minor importance, but an exception occurs in the case of cross-talk between fibers, which is discussed in Chapters 28 and 29. This phenomenon relies on coupling between the far fields of the fibers, and consequently, the evanescent behavior of these fields must be accurately known.

We can use the results of the Gaussian approximation to generate a more accurate expression for the far field [5, 8]. To do this, we substitute the profile representation of Table 15-1 into Eq. (15-1), rearrange, and write it in the dimensionless form

$$\left\{ \frac{d^2}{dR^2} + \frac{1}{R} \frac{d}{dR} - W^2 \right\} F_0 = -V^2(1-f)F_0, \quad (15-14)$$

where V is defined inside the back cover, and $f = 1$ when $n = n_{cl}$. Since $1-f$ is significant only in regions close to the fiber axis where the Gaussian approximation of Table 15-1 is accurate, we set $F_0 = \exp(-R^2/2R_0^2)$ on the right side. The resulting equation is solved by Green's function methods in Section 34-9, and the solution is given by the first integral in Eq. (34-42)

$$F_0(R) \cong V^2 K_0(WR) \int_0^\infty R' \{1-f(R')\} I_0(WR') \exp\left(-\frac{R'^2}{2R_0^2}\right) dR', \quad (15-15)$$

where I_0 is the modified Bessel function of the first kind.

Gaussian profile

If we substitute f , $W = (V^2 - U^2)^{1/2}$ and $R_0 = r_0/\rho$ for the Gaussian profile from Table 15-2, we find with the aid of Eq. (37-101) that

$$F_0(R) \cong V^2 K_0(WR) \int_0^\infty R' I_0(WR') \exp\left\{-\frac{V+1}{2} R'^2\right\} dR', \quad (15-16a)$$

$$= \frac{V^2}{V+1} K_0(\{V-1\}R) \exp\left\{\frac{1}{2} \frac{(V-1)^2}{V+1}\right\}. \quad (15-16b)$$

When $V = 2.5$ and $R > 1.5$, this approximation differs from the exact result by less than 4% [7].

HIGHER-ORDER MODES

The fundamental modes of the infinite parabolic profile fiber have a Gaussian spatial variation; it is the exact solution of the scalar wave equation. Thus, the essence of the Gaussian approximation is the approximation of the fundamental-mode fields of an arbitrary profile fiber by the fundamental-mode fields of *some* parabolic profile fiber, the particular profile being determined from the stationary expression for the propagation constant in Table 15-1. Clearly this approach can be generalized to apply to higher-order modes, by fitting the appropriate solution for the infinite parabolic profile [9].

15-6 Approximations for the fields

The spatial dependence of a general mode is approximated by the appropriately modified expressions in Table 14-2, page 307. Thus we have

$$F_l = (R/R_0)^l L_{m-1}^{(l)} (R^2/R_0^2) \exp(-R^2/2R_0^2), \quad (15-17)$$

where $L_{m-1}^{(l)}$ is the generalized Laguerre polynomial and the notation is defined in Table 15-1. To determine R_0 , we use the variational expression for U^2 in Table 13-2, page 292. Substituting Eq. (15-17) into the denominator and using Eq. (37-128), we obtain

$$U^2 = \frac{(m-1)!}{(l+m-1)!} \frac{2}{R_0^2} \int_0^\infty \left\{ \left(\frac{dF_l}{dR} \right)^2 + \left(\frac{l^2}{R^2} + V^2 f \right) F_l^2 \right\} R dR, \quad (15-18)$$

and the value of R_0 is found by solving the equation $\partial U^2 / \partial R_0 = 0$ for the minimum value of U^2 . To demonstrate the accuracy of the resulting approximations, we examine low-order modes of the Gaussian profile.

15-7 Example: Gaussian profile

We discussed the Gaussian approximation for the fundamental modes of this profile in Section 15-2. For all $m = 1$ modes, Eq. (15-17) reduces to

$$F_l = (R/R_0)^l \exp(-R^2/2R_0^2). \quad (15-19)$$

Substituting into Eq. (15-18), setting $f = 1 - \exp(-R^2)$ and using Eq. (37-126) we find

$$U^2 = \frac{l+1}{R_0^2} + V^2 \left\{ 1 - \frac{1}{(R_0+1)^{l+1}} \right\}, \quad (15-20)$$

and the equation for R_0 follows from Table 15-1

$$(1 + R_0^2)^{l+2} = V^2 R_0^4. \quad (15-21)$$

Apart from the $l = 0$ fundamental modes, there are analytical solutions for $l = 1$ and $l = 2$, when Eq. (15-21) reduces to a cubic and a quadratic polynomial, respectively. The solution for R_0 and U^2 are presented in Table 15-4 [9], together with the exact cutoff values [7]. If we compare the approximate and exact values of U , the error is less than 1.2% for the $l = m = 1$ modes if $V > 3$, and is less than 0.9% for the $l = 2, m = 1$ modes if $V > 4.5$. In both cases the error increases as V approaches V_c , because the field distribution F_l is a poor approximation to the spread-out fields of the Gaussian profile near cutoff.

STEP-PROFILE APPROXIMATION

This chapter is based on the concept that the modal field on a fiber of arbitrary profile can be well approximated by the corresponding modal field on another fiber of some specific profile shape, provided that the mode and fiber parameters are appropriately chosen. For example, the Gaussian approximation is based on a profile of infinite parabolic shape, and the spot size and propagation constant are determined by the equations in Table 15-1. An alternative approximation, based on the fundamental mode field of the step profile, is known as the *step-profile approximation* [4]. It is accurate over a larger region of space and a greater range of parameters than the Gaussian approximation, but with the penalty of a loss in simplicity.

15-8 Fundamental modes

With reference to Table 14-3, page 313, we assume that the fundamental-mode fields of an arbitrary profile fiber can be approximated by the fundamental-mode fields of some step-profile fiber, whose radial dependence is expressed by

$$F_0(\bar{R}) = \frac{J_0(\bar{U}\bar{R})}{J_0(\bar{U})}, \quad 0 \leq \bar{R} \leq 1; \quad F_0(\bar{R}) = \frac{K_0(\bar{W}\bar{R})}{K_0(\bar{W})}, \quad 1 \leq \bar{R} < \infty, \quad (15-22)$$

where $\bar{R} = r/\bar{\rho}$, and the parameters \bar{U} and \bar{W} are expressed in terms of \bar{V} through the eigenvalue equation

$$\bar{U} J_1(\bar{U})/J_0(\bar{U}) = \bar{W} K_1(\bar{W})/K_0(\bar{W}); \quad \bar{U}^2 + \bar{W}^2 = \bar{V}^2. \quad (15-23)$$

Thus, F_0 is uniquely determined once \bar{V} and $\bar{\rho}$ are specified.

Following the conceptual lead of Section 15-1, we substitute Eq. (15-22) into the variational expression for U^2 in Table 13-2, page 292, and set $l = 0$. With the help of the integrals of Eqs. (37-92) and (37-93), the eigenvalue equation in Table 14-6, page 319, and the recurrence relations of Eqs. (37-72) and (37-73) we find that [4]

$$U^2 = 2 \left\{ \frac{\bar{U}}{\bar{V}} \frac{K_0(\bar{W})}{K_1(\bar{W})} \right\}^2 \left\{ V^2 \int_0^\infty f(\bar{R}) F_0^2(\bar{R}) \bar{R} d\bar{R} + \frac{\rho^2}{\bar{\rho}^2} \frac{\bar{V}^2}{2} \right\}, \quad (15-24)$$

Table 15-4 Low-order modes of the Gaussian-profile fiber. Approximations for the spot size $r_0 = \rho R_0$ and propagation constant β , based on the variational solution of Eq. (15-18).

$n^2(R) = n_{co}^2 \{1 - 2\Delta(1 - \exp(-R^2))\}; \quad R = \frac{r}{\rho}; \quad R_0 = \frac{r_0}{\rho}; \quad V = k\rho n_{co}(2\Delta)^{1/2}$				
l	m	F_l	V_c	$R_0 = \frac{r_0}{\rho}$
0	1	$\exp\left\{-\frac{1}{2}\frac{R^2}{R_0^2}\right\}$	—	$\frac{1}{(V-1)^{1/2}} \quad (V > 1)$
1	1	$\frac{R}{R_0} \exp\left\{-\frac{1}{2}\frac{R^2}{R_0^2}\right\}$	2.592	$\left\{\frac{V^2}{3} - 1 + \frac{2V}{3}(V^2 - 6)^{1/2} \sin\left(\frac{\theta}{3} - \frac{\pi}{6}\right)\right\}^{1/2}$ $\tan \theta = \frac{\sqrt{27(27 - 4V^2)}}{(2V^4 - 18V^2 + 27)}$
2	1	$\frac{R^2}{R_0^2} \exp\left\{-\frac{1}{2}\frac{R^2}{R_0^2}\right\}$	4.339	$\frac{1}{2}\{\sqrt{V-4} - \sqrt{V-4}\}$
				$U^2 = \frac{V^2}{2\Delta} - \rho^2 \beta^2$
				$V^2 + \frac{1}{R_0^2} - \frac{1}{R_0^4}$
				$\frac{V^2}{2} + 3V - 3 + (V^2 - 4V)^{1/2} \left(2 - \frac{V}{2}\right)$

where $\bar{R} = r/\bar{\rho}$ and $V, f(\bar{R})$ for the arbitrary profile are defined inside the back cover. We seek the solution which minimizes U^2 with respect to variations in $\bar{\rho}$ and \bar{V} , by solving the simultaneous equations

$$\frac{\partial U^2}{\partial \bar{\rho}} = 0; \quad \frac{\partial U^2}{\partial \bar{V}} = 0. \quad (15-25)$$

In general these equations must be solved numerically. We refer elsewhere for details [4].

The Gaussian profile

If we use the step-profile approximation to determine the values of U for the fundamental modes of the Gaussian-profile fiber, then there is no limitation on the range of V , unlike the Gaussian approximation of Table 15-2. Furthermore, there is so little difference between the approximate and exact values of U , that a plot is indistinguishable from the dashed curve in Fig. 15-1(b). Plots of the intensity distribution calculated from the step-profile approximation are virtually coincident with the exact solution away from the fiber axis, particularly for small values of V , whereas the Gaussian approximation leads to a significant error, as is evident in the $V = 1.592$ plot of Fig. 15-1(c). The Gaussian approximation has a far field which decreases too rapidly, as explained in Section 15-5, whereas the choice of field in Eq. (15-22) ensures the correct far field behavior for $\bar{R} \gg 1$.

Although the step-profile approximation is more useful in these two situations, the solutions of Eqs. (15-24) and (15-25) must be obtained numerically. The corresponding equations of Table 15-1 for the Gaussian approximation have the simple, explicit forms of Table 15-2, and the far field is readily corrected, as we showed in Section 15-5.

15-9 Range of single-mode operation

The higher-order mode approximation of Section 15-6 is inadequate for determining the range of single-mode operation of arbitrary clad-profile fibers. At cutoff V_c of the $l = m = 1$ modes, the clad fiber fields satisfy Eq. (11-54) when $n(R) \cong n_{co}$, and thus have an R^{-1} radial dependence in cylindrical polar coordinates. The corresponding dependence of Eq. (15-17) is always exponential and is thus a poor approximation. To overcome this deficiency, we use the estimate for V_c in Table 15-2 based on equal profile volumes. However, a much more accurate value can be obtained within the step-profile approximation.

Cutoff of the second mode

It follows from the above discussion that the modal fields at cutoff V_c on an arbitrary profile fiber are approximated by the $l = m = 1$ modal fields of some

step-profile fiber at cutoff, i.e. $\bar{U} = \bar{V} = \bar{V}_c = 2.405$ and $\bar{W} = 0$. We deduce from Table 14-6, page 319, and Eq. (37-86) that as $\bar{W} \rightarrow 0$ the radial dependence of these fields is given by

$$F_1(\bar{R}) = \frac{J_1(\bar{V}_c \bar{R})}{J_1(\bar{V}_c)}, \quad 0 \leq \bar{R} \leq 1; \quad F_1(\bar{R}) = \frac{1}{\bar{R}}, \quad 1 \leq \bar{R} < \infty. \quad (15-26)$$

In the variational expression for U^2 given by Table 13-2, page 292, we set $U = V = V_c$, $l = 1$ and rearrange. Certain of the integrals can be evaluated from Eq. (15-26), Table 14-6 and Eqs. (37-91), (37-92), leading to [4]

$$V_c = 2.892 \frac{\rho^2}{\bar{\rho}^2} \left\{ \int_0^1 [1 - f(\bar{R})] \frac{J_1^2(\bar{V}_c \bar{R})}{J_1^2(\bar{V}_c)} \bar{R} d\bar{R} + \int_1^\infty \frac{[1 - f(\bar{R})]}{\bar{R}} d\bar{R} \right\}^{-1}. \quad (15-27)$$

The value of V_c is found by solving the equation $\partial V_c^2 / \partial \bar{\rho} = 0$ for $\bar{\rho}$ and substituting back into the above expression. This operation must be performed numerically for an arbitrary profile.

The Gaussian profile

If we use Eq. (15-27) to determine the range of single-mode operation for the Gaussian profile of Eq. (15-6), we find that $V_c \cong 2.62$. This differs from the exact value in Table 15-2 by only 1.2% [4, 7].

REFERENCES

1. Gambling, W. A. and Matsumura, H. (1977) Simple characterization factor for practical single-mode fibres. *Electron. Lett.*, **13**, 691-3.
2. Snyder, A. W. (1977) Acuity of compound eyes: physical limitation and design. *J. Comp. Physiol.*, **116**, 161-82.
3. Marcuse, D. (1978) Gaussian approximation of the fundamental modes of graded fibres. *J. Opt. Soc. Am.*, **68**, 103-9.
4. Snyder, A. W. and Sammut, R. A. (1979) Fundamental (HE_{11}) modes of graded optical fibers. *J. Opt. Soc. Am.*, **69**, 1663-71.
5. Snyder, A. W. (1981) Understanding monomode optical fibres. *Proc. I.E.E.E.*, **69**, 6-13.
6. Mathews, J. and Walker, R. L. (1965) *Mathematical Methods of Physics*, Benjamin, New York.
7. Anderssen, R. S., de Hoog, F. and Love, J. D. (1981) Modes of Gaussian profile optical fibres. *Opt. Quant. Elect.*, **13**, 217-24.
8. Snyder, A. W., Love, J. D. and Sammut, R. A. (1982) Green's function methods for perturbed optical fibres. *J. Opt. Soc. Am.*, **72**, 113-35.
9. Love, J. D. and Hussey, C. D. (1984) Variational approximations for modes of weakly guiding fibres, *Opt. Quant. Elect.* **16**.

Noncircular waveguides

16-1 Planar waveguides	354
Elliptical fiber of infinite parabolic profile	355
16-2 Fundamental modes	357
16-3 Higher-order modes	359
16-4 Nearly circular fibers	360
Noncircular profiles with analytical solutions	361
16-5 Homogeneous function profiles	361
16-6 Separable profiles	362
16-7 <i>Example: Infinite linear profile</i>	363
16-8 <i>Example: Double parabolic profile</i>	364
References	365

The general procedure for constructing the modes of weakly guiding, noncircular waveguides was laid down in Sections 13-5 and 13-8. Noncircular waveguides are of particular interest because of their birefringent propagation characteristics. In this chapter we examine waveguides whose refractive-index profiles admit *exact* analytical solutions of the scalar wave equation, and in Chapters 17 and 18 we discuss *approximate* solutions. We concentrate on the elliptical fiber with an infinite parabolic profile, since this leads to simple expressions for all modal quantities, including the propagation constant. Furthermore, we can readily demonstrate that only the slightest noncircularity is necessary for *all* modes of the noncircular fiber to be uniformly polarized in the cross-section. This profile is also the basis of the Gaussian approximation for noncircular fibers in Chapter 17.

16-1 Planar waveguides

The simplest example of a noncircular waveguide is the planar waveguide of Chapter 12, whose modes are either TE or TM, as explained in Section 11-16. For each TE mode the electric field lies in the cross-section and is uniformly polarized. Consequently the weak-guidance solution is identical to the exact solution for the field e_y and the propagation constant. Both satisfy the scalar wave equation of Eq. (12-16), and examples with analytical solutions are given in Table 12-7, page 264. Within the weak-guidance approximation the

transverse electric field e_x of each TM mode also satisfies Eq. (12-16), but the scalar propagation constant must be corrected for waveguide birefringence by using Eq. (13-11) for $\delta\beta$.

ELLIPTICAL FIBER OF INFINITE PARABOLIC PROFILE

The circular fiber of infinite parabolic profile was discussed in detail in Section 14-4. If the cross-section is deformed into elliptical shape, the profile is expressible as

$$n^2(x, y) = n_{co}^2 \left\{ 1 - 2\Delta \left[\frac{x^2}{\rho_x^2} + \frac{y^2}{\rho_y^2} \right] \right\}; \quad -\infty < x, y < \infty, \quad (16-1)$$

where ρ_x and ρ_y are length scales in the x - and y -directions, respectively. Contours of constant index are illustrated in Fig. 16-1. They form a set of concentric ellipses, i.e. each ellipse has the same eccentricity e , where

$$e = \{1 - \rho_y^2/\rho_x^2\}^{1/2}; \quad \rho_x > \rho_y. \quad (16-2)$$

For example, if $n = n_{cl}$, then the definition of Δ at the back of the book leads to the ellipse $(x/\rho_x)^2 + (y/\rho_y)^2 = 1$. To accommodate the two length scales ρ_x and ρ_y , we generalize the parameters for the circular fiber by introducing two fiber parameters V_x and V_y , and two modal parameters U_x and U_y , which are defined in Table 16-1.

The profile defined by Eq. (16-1) is unphysical, but by following the reasoning of Section 14-4, we see that the weak-guidance approximation is an

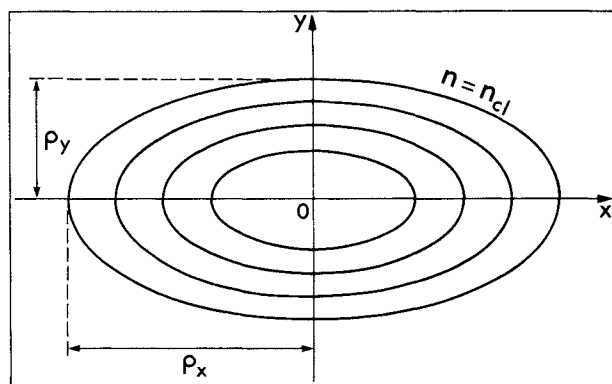


Fig. 16-1 Contours of constant refractive index for the elliptical fiber of infinite parabolic profile defined in Eq. (16-1).

Table 16-1 Fundamental modes of the elliptical fiber of infinite parabolic profile.
 Undefined parameters appear inside the back cover.

$n^2(x, y) = n_{co}^2 \left\{ 1 - 2\Delta \left(\frac{x^2}{\rho_x^2} + \frac{y^2}{\rho_y^2} \right) \right\}; \quad e = \left\{ 1 - \frac{\rho_y^2}{\rho_x^2} \right\}^{1/2}$		
$V_x = k\rho_x n_{co} (2\Delta)^{1/2}; \quad V_y = k\rho_y n_{co} (2\Delta)^{1/2}; \quad \frac{V_y}{V_x} = \frac{\rho_y}{\rho_x}; \quad k = \frac{2\pi}{\lambda}$		
$\hat{U}_x = \left\{ \frac{V_x^2}{2\Delta} - \rho_x^2 \hat{\beta}^2 \right\}^{1/2}; \quad \hat{U}_y = \left\{ \frac{V_y^2}{2\Delta} - \rho_y^2 \hat{\beta}^2 \right\}^{1/2}; \quad \frac{\hat{U}_y}{\hat{U}_x} = \frac{\rho_y}{\rho_x}$		
	<i>Even HE₁₁ mode</i> (x-polarized)	<i>Odd HE₁₁ mode</i> (y-polarized)
Transverse Fields	$E_x = \Psi(x, y) \exp \{ i(\beta + \delta\beta_x)z \}$ $H_y = \left(\frac{\epsilon_0}{\mu_0} \right)^{1/2} n_{co} E_x$	$E_y = \Psi(x, y) \exp \{ i(\hat{\beta} + \delta\beta_y)z \}$ $H_x = - \left(\frac{\epsilon_0}{\mu_0} \right)^{1/2} n_{co} E_y$
Scalar wave equation solution	$\Psi(x, y) = \exp \left\{ -\frac{1}{2} \left(\frac{V_x V_y}{\rho_x \rho_y} \right)^{1/2} \left[\frac{x^2}{\rho_x} + \frac{y^2}{\rho_y} \right] \right\}$	
Eigenvalue equation solution	$\hat{U}_x \hat{U}_y = V_x + V_y;$ $\hat{\beta} = kn_{co} \left\{ 1 - \frac{2\Delta}{(V_x V_y)^{1/2}} \left[\left(\frac{\rho_x}{\rho_y} \right)^{1/2} + \left(\frac{\rho_y}{\rho_x} \right)^{1/2} \right] \right\}^{1/2}$	
Polarization corrections	$\delta\beta_x = -\frac{(2\Delta)^{3/2}}{2\rho_x V_x}; \quad \delta U_x = \frac{\Delta}{\hat{U}_x}$	$\delta\beta_y = -\frac{(2\Delta)^{3/2}}{2\rho_y V_y}; \quad \delta U_y = \frac{\Delta}{\hat{U}_y}$
	$\beta_x = \hat{\beta} + \delta\beta_x$	$\beta_y = \hat{\beta} + \delta\beta_y$
Corrected modal parameters	$U_x = \hat{U}_x + \delta U_x$	$U_y = \hat{U}_y + \delta U_y$
Normalization	$N = \frac{\pi n_{co}}{2} \left(\frac{\epsilon_0}{\mu_0} \right)^{1/2} \frac{\rho_x \rho_y}{(V_x V_y)^{1/2}}$	
Birefringence	$\beta_x - \beta_y = \delta\beta_x - \delta\beta_y = \frac{e^2}{1 - e^2} \frac{(2\Delta)^{3/2}}{2\rho_x V_x}$	

accurate description of propagation provided that modal power is concentrated close to the fiber axis. This leads to a restriction on the range of values for V_x or V_y , as we show below.

16-2 Fundamental modes

The derivation of the transverse fields of the two fundamental modes on a weakly guiding, noncircular fiber was described in Section 13-5. These fields are given in Table 16-1 in terms of the solution $\Psi(x, y)$ of the scalar wave equation, which in cartesian coordinates has the form

$$\left\{ \frac{\partial^2}{\partial x^2} + \frac{\partial^2}{\partial y^2} + k^2 n^2(x, y) - \tilde{\beta}^2 \right\} \Psi = 0, \quad (16-3)$$

where $\tilde{\beta}$ is the scalar propagation constant and all other parameters are defined inside the back cover. If we substitute Eq. (16-1) into Eq. (16-3), it is readily verified that the fundamental-mode solution and eigenvalue equation are given by

$$\Psi = \exp \left\{ -\frac{1}{2} \left(\frac{V_x V_y}{\rho_x \rho_y} \right)^{1/2} \left[\frac{x^2}{\rho_x} + \frac{y^2}{\rho_y} \right] \right\}; \quad \tilde{U}_x \tilde{U}_y = V_x + V_y, \quad (16-4)$$

from which we obtain the propagation constant

$$\tilde{\beta} = kn_{co} \left\{ 1 - \frac{2\Delta}{(V_x V_y)^{1/2}} \left[\left(\frac{\rho_x}{\rho_y} \right)^{1/2} + \left(\frac{\rho_y}{\rho_x} \right)^{1/2} \right] \right\}^{1/2}, \quad (16-5)$$

which is the largest value of any mode. A detailed derivation is given in Section 16-3. The polarization corrections $\delta\beta_x$ and $\delta\beta_y$ for the x- and y-polarized modes differ because of the fiber noncircularity, discussed in Section 13-5. To determine the corrections we set $f(x, y) = (x/\rho_x)^2 + (y/\rho_y)^2$ in Eq. (13-11) and substitute either $\mathbf{e}_t = \Psi \hat{\mathbf{x}}$ or $\mathbf{e}_t = \Psi \hat{\mathbf{y}}$ from Eq. (16-4). This leads to the expressions in Table 16-1 for the corrected propagation constants $\beta_x = \tilde{\beta} + \delta\beta_x$ and $\beta_y = \tilde{\beta} + \delta\beta_y$. The small longitudinal field corrections are deduced from Eq. (13-13).

Distribution of modal power

The normalization expression in Table 16-1 follows from Eq. (16-4) and Table 13-2, page 292, and leads to the normalized intensity distribution \hat{S} , where

$$\hat{S} = \frac{S}{|a|^2 N} = \frac{1}{\pi} \frac{(V_x V_y)^{1/2}}{\rho_x \rho_y} \exp \left\{ -\left(\frac{V_x V_y}{\rho_x \rho_y} \right)^{1/2} \left[\frac{x^2}{\rho_x} + \frac{y^2}{\rho_y} \right] \right\}. \quad (16-6)$$

Hence contours of constant intensity form a set of concentric ellipses, whose eccentricity is smaller than that of the constant index contours.

Pulse propagation

Consider a pulse within which only the two fundamental modes are excited. Waveguide dispersion describes the spread in each mode, but because of ellipticity the spread for each polarization is different. In addition, the slight difference $\delta\beta_x - \delta\beta_y$ between corrected propagation constants implies the respective group velocities are unequal and consequently *there will be intermodal dispersion between the two modes*. Intermodal dispersion which relies on polarization difference is often referred to as a *birefringence* effect.

If we substitute Eq. (16-4) into Table 13-2, page 292, the group velocity for both modes within the scalar approximation is just the on-axis speed of light c/n_{co} . To incorporate the effects of the polarization corrections, we replace \bar{U} , V and $U^{(1)}$ by \bar{U}_x , V_x and $\delta U_x/\Delta$, respectively, in Eq. (13-17) and, correct to order Δ^2 , obtain

$$v_{gx} = \frac{c}{n_{co}} \left\{ 1 - \frac{\Delta^2}{2V_x^2} \left[4 + \left(\frac{\rho_x}{\rho_y} + 1 \right)^2 \right] \right\}, \quad (16-7)$$

for the x-polarized mode, while for the y-polarized mode v_{gy} is given by the same expression with the subscripts x and y interchanged. We describe waveguide dispersion through a generalization of the distortion parameter of Section 11-20, by defining $D_x(V, \Delta)$ through Eqs. (11-58) and (11-59) with V replaced by V_x . Correct to order Δ we deduce from Eqs. (16-7) and (13-18) that

$$D_x(V, \Delta) \cong -\frac{4\Delta}{V_x^3} \left\{ 1 + \frac{1}{8} \left(\frac{\rho_x}{\rho_y} - 1 \right) \left(\frac{\rho_x}{\rho_y} + 3 \right) \right\}, \quad (16-8)$$

for the x-polarized mode, together with a similar expression for $D_y(V, \Delta)$ with the subscripts interchanged.

Intermodal dispersion can be expressed in terms of the difference between the transit time t_x and t_y of the two modes over length z of fiber. Substituting Eqs. (16-2) and (16-7) into Eq. (11-36) gives for slight eccentricity

$$t_y - t_x \cong 2\Delta^2 \frac{zn_{co}}{c} \left\{ \frac{1}{V_y^2} - \frac{1}{V_x^2} \right\} = \frac{2e^2\Delta^2}{V_y^2} \frac{zn_{co}}{c}. \quad (16-9)$$

Hence, the y-polarized mode leads the x-polarized mode, and the effect increases with increasing eccentricity assuming V_y is fixed.

Polarization characteristics – birefringence

It follows from the above discussion that propagation of the two fundamental modes on the elliptical fiber is similar to plane-wave propagation in an anisotropic medium discussed in Section (11-23) [1]. In particular, the total transverse electric field E_t of the two modes is elliptically polarized and its direction changes with distance z along the fiber. On the other hand there is no

interference between the fields of the two modes and consequently the intensity pattern of the total field does not change along the fiber, i.e. the modes are plane polarized.

Condition for weak guidance

The weak-guidance approximation requires $\Delta \ll 1$ and $\tilde{\beta} \cong kn_{co}$, as discussed in Section 14-4, and this ensures that modal power is confined close to the fiber axis. We deduce from Eq. (16-5) that the fiber parameter V_x must be sufficiently large to satisfy

$$V_x \gg 2\Delta(1 + \rho_x/\rho_y). \quad (16-10)$$

For highly eccentric fibers $\rho_x \gg \rho_y$, which restricts the analysis to comparatively large values of V_x .

Polarization corrections to the modal fields

The first-order corrections to the transverse electric field are derived from the equation for $\mathbf{e}_t^{(1)}$ in Table 32-1, page 627, where $f = (x^2/\rho_x^2) + (y^2/\rho_y^2)$. For the x -polarized fundamental mode we set $\hat{\mathbf{e}}_t = \Psi \hat{\mathbf{x}}$, $U^{(1)} = \delta U_x/\Delta$ from Table 16-1 and replace ρ , U , V by ρ_x , U_x , V_x , respectively. It is readily verified that the solution is

$$\mathbf{e}_{tx}^{(1)} = \left\{ \frac{x}{\rho_x} \hat{\mathbf{x}} + \frac{4V_y}{V_x + V_y} \frac{y}{\rho_y} \hat{\mathbf{y}} \right\} \frac{x}{\rho_x} \Delta \Psi, \quad (16-11)$$

and the corresponding expression for \mathbf{e}_{ty} is obtained by interchanging x and y , including subscripts. By hypothesis $\mathbf{e}_{tx}^{(1)}$ and $\mathbf{e}_{ty}^{(1)}$ are small corrections to \mathbf{e}_{tx} and \mathbf{e}_{ty} and consequently are valid only in the region defined by $x \ll \rho_x/\Delta^{1/2}$, $y \ll \rho_y/\Delta^{1/2}$, respectively.

16-3 Higher-order modes

The procedure for constructing higher-order modes of noncircular fibers was established in Section 13-8. For each mode the transverse fields are identical in direction and form to the fundamental-mode fields of Table 16-1, except that Ψ now denotes the appropriate higher-order solution of the scalar wave equation of Eq. (16-3). Only when the fiber cross-section is sufficiently close to circular is this representation inappropriate, as explained in Section 13-9. We quantify this transition in the following section.

To determine Ψ , we substitute Eq. (16-1) into Eq. (16-3), make a change of variables, and express the solution in separable form, where

$$\Psi = F(w_x)G(w_y) \exp \left\{ -\frac{w_x^2 + w_y^2}{2} \right\}; \quad w_x = \frac{x}{\rho_x} V_x^{1/2}, \quad w_y = \frac{y}{\rho_y} V_y^{1/2}. \quad (16-12)$$

This leads to a pair of ordinary differential equations

$$\frac{d^2 F}{dw_x^2} - 2w_x \frac{dF}{dw_x} + \left\{ \frac{\tilde{U}_x^2}{2V_x} + \kappa - 1 \right\} F = 0, \quad (16-13a)$$

$$\frac{d^2 G}{dw_y^2} - 2w_y \frac{dG}{dw_y} + \left\{ \frac{\tilde{U}_y^2}{2V_y} - \kappa - 1 \right\} G = 0, \quad (16-13b)$$

where κ is the separation constant and parameters are defined in Table 16-1. The solutions of these equations which ensure Ψ is bounded as $|x|, |y| \rightarrow \infty$ are the Hermite polynomials H_n [2]. The factors multiplying F and G in Eq. (16-13) must be even positive integers or zero. Elimination of κ gives the eigenvalue equation. Hence

$$\Psi_{mn} = H_{m-1} \left(\frac{x}{\rho_x} V_x^{1/2} \right) H_{n-1} \left(\frac{y}{\rho_y} V_y^{1/2} \right) \exp \left\{ -\frac{1}{2} \left(\frac{V_x V_y}{\rho_x \rho_y} \right)^{1/2} \left(\frac{x^2}{\rho_x} + \frac{y^2}{\rho_y} \right) \right\}, \quad (16-14a)$$

$$\tilde{U}_x \tilde{U}_y = (2m-1)V_y + (2n-1)V_x, \quad (16-14b)$$

where $m, n = 1, 2, \dots$, and the propagation constant follows from the definitions in Table 16-1. The fundamental-mode solution of Eq. (16-4) corresponds to $m = n = 1$. We give the explicit forms of the Hermite polynomials in Eq. (37-107) for low-order modes. The polarization corrections $\delta\beta_x$ and $\delta\beta_y$ for each pair of modes corresponding to Ψ_{mn} are determined from Eq. (13-11).

16-4 Nearly circular fibers

We can use the elliptical fiber to quantify the transition from the uniformly polarized modes of the noncircular fiber to the modes of the circular fiber in Table 13-1, page 288, which was discussed qualitatively in Section 13-9. For this purpose we consider the modes corresponding to the Ψ_{21} and Ψ_{12} solutions, which are the successive lowest-order modes after the fundamental modes. Thus Eqs. (16-14) and (37-107) give to within constant multiples

$$\Psi_{21} = \frac{x}{\rho_x} \exp \left\{ -\frac{1}{2} \left(\frac{V_x V_y}{\rho_x \rho_y} \right)^{1/2} \left(\frac{x^2}{\rho_x} + \frac{y^2}{\rho_y} \right) \right\}; \quad \tilde{U}_x \tilde{U}_y = 3V_y + V_x, \quad (16-15a)$$

$$\Psi_{12} = \frac{y}{\rho_y} \exp \left\{ -\frac{1}{2} \left(\frac{V_x V_y}{\rho_x \rho_y} \right)^{1/2} \left(\frac{x^2}{\rho_x} + \frac{y^2}{\rho_y} \right) \right\}; \quad \tilde{U}_x \tilde{U}_y = V_y + 3V_x. \quad (16-15b)$$

In the circular limit $\rho_x \rightarrow \rho_y \rightarrow \rho$, $V_x \rightarrow V_y \rightarrow V$, and, relative to the coordinates in Fig. 14-1, $y/\rho = R \sin \phi$, $x/\rho = R \cos \phi$. Consequently Ψ_{21} and Ψ_{12} reduce

to the $l = 1$ solutions

$$\Psi_e = R \exp(-\frac{1}{2} VR^2) \cos \phi; \quad \Psi_o = R \exp(-\frac{1}{2} VR^2) \sin \phi, \quad (16-16)$$

respectively, obtained from Eq. (14-3) and Table 14-2, page 307. If $\tilde{\beta}_e$ and $\tilde{\beta}_o$ denote the scalar propagation constants associated with Ψ_{21} and Ψ_{12} , respectively, it follows from Eqs. (16-15) and (16-2) that for small eccentricity

$$\tilde{\beta}_e - \tilde{\beta}_o \cong \frac{\tilde{\beta}_e^2 - \tilde{\beta}_o^2}{2kn_{co}} \cong \frac{e^2}{\rho} \left(\frac{\Delta}{2}\right)^{1/2}; \quad \rho_x \cong \rho_y \cong \rho, \quad (16-17)$$

since $\tilde{\beta}_e, \tilde{\beta}_o \cong kn_{co}$ and $V_x/V_y = \rho_x/\rho_y$, $\tilde{U}_x/\tilde{U}_y = \rho_x/\rho_y$.

We show in Section 32-9, using perturbation theory, and in Section 13-9, using intuitive arguments, that the transition is described by the parameter Λ defined in Table 13-1, page 288. The difference $\delta\beta_1 - \delta\beta_2$ in the denominator follows from Table 14-2, page 307, with $l = 1$, and the numerator is given by Eq. (16-17). Hence

$$\Lambda \cong -e^2 V/4\Delta \cong -V\{1 - \rho_y/\rho_x\}/2\Delta. \quad (16-18)$$

When $|\Lambda| \ll 1$, the modal fields behave like the fields of the circular fiber, i.e. the linear combinations of Table 14-1, page 304, and when $|\Lambda| \gg 1$ the modal fields are uniformly polarized on the elliptical fiber. Since $\Delta \ll 1$ for a practical fiber, it is clear that only the slightest asymmetry is necessary for the modes to be uniformly polarized, and thus the circular fiber is an ideal which requires high precision to be realized.

NONCIRCULAR PROFILES WITH ANALYTICAL SOLUTIONS

Now we consider other noncircular waveguides with profiles which lead to analytical solutions of the scalar wave equation or to closed-form expressions for other modal properties.

16-5 Homogeneous function profiles

These profiles were introduced in Section 2-13 and have the form

$$n^2(x, y) = n_{co}^2 \{1 - 2\Delta f(x, y)\}, \quad -\infty < x, y < \infty, \quad (16-19a)$$

where $f(x, y)$ is a homogeneous function of degree q with the property that

$$f(\alpha x, \alpha y) = \alpha^q f(x, y). \quad (16-19b)$$

Using this property we can obtain analytical expressions for the propagation

constants of all modes. We substitute Eq. (16-19a) into Eq. (16-3) and multiply by ρ^2 , where ρ is a characteristic length in the noncircular cross-section. The scaling argument of Section 33-6 can then be repeated with obvious modification, and we deduce from Eq. (33-26)

$$\tilde{U} = G V^{2/(q+2)}, \quad (16-20)$$

where \tilde{U} and V are defined inside the back cover. The constant G depends on q and parameters describing the asymmetry, but is independent of V . For example, the elliptical profile of Eq. (16-1) together with $q = 2$, $\rho = \rho_x$ and Eq. (16-14b) leads to $G = \{2m - 1 + (2n - 1)(1 - e^2)^{1/2}\}^{1/2}$, where e is the eccentricity of Eq. (16-2).

Group velocity and waveguide dispersion

The functional dependence of \tilde{U} and V in Eq. (16-20) is identical to the dependence in Eq. (14-9) for the infinite power-law profiles on circular fibers, except that G is, in general, unknown. Since the profiles defined by Eq. (14-8) satisfy the homogeneity condition of Eq. (16-19b), it follows that the group velocity and distortion parameter for the asymmetric profiles are given by Eqs. (14-10) and (14-11). Eliminating G , we have

$$\tilde{v}_g = \frac{c}{n_{co}} \left\{ 1 + \Delta \frac{2-q}{2+q} \frac{\tilde{U}^2}{V^2} \right\}, \quad \tilde{D} = q \frac{(2-q)}{(2+q)^2} \frac{\tilde{U}^2}{V^3}, \quad (16-21)$$

and thus there is no waveguide dispersion on a $q = 2$ homogeneous profile.

16-6 Separable profiles

We introduced the class of separable profiles in Section 2-14. Each profile has a refractive-index distribution which is expressible as

$$n^2(x, y) = n_{co}^2 \{1 - 2\Delta[f(x) + g(y)]\}; \quad -\infty < x, y < \infty, \quad (16-22)$$

where $f(x)$ and $g(y)$ depend only on x and y , respectively. If we substitute into Eq. (16-3) and set $\Psi(x, y) = F(x)G(y)$, then the scalar wave equation can be replaced by the pair of ordinary differential equations

$$\rho^2 \frac{d^2 F}{dx^2} + \left\{ \frac{\tilde{U}^2}{2} - V^2 f(x) + \kappa \right\} F = 0, \quad (16-23a)$$

$$\rho^2 \frac{d^2 G}{dy^2} + \left\{ \frac{\tilde{U}^2}{2} - V^2 g(y) - \kappa \right\} G = 0, \quad (16-23b)$$

where κ is the separation constant and ρ is a length scale in the waveguide cross-section. The requirement that both F and G be everywhere bounded

leads to two relationships between U and κ . Eliminating κ we obtain the eigenvalue equation. The parabolic profile of Eq. (16-1) is one example of a separable profile, for which the scalar wave equation was solved in Section 16-3 using the procedure of this section. A second example is given below.

16-7 Example: Infinite linear profile

This profile varies linearly with both x and y , and is defined by

$$n^2(x, y) = n_{co}^2 \{1 - 2\Delta[|x/\rho_x| + |y/\rho_y|]\}; \quad -\infty < x, y < \infty, \quad (16-24)$$

where ρ_x and ρ_y are length scales. Contours of constant index comprise the diamond-shaped family in Fig. 16-2(a), and, recalling the definition of Δ , the index contour $n = n_{cl}$

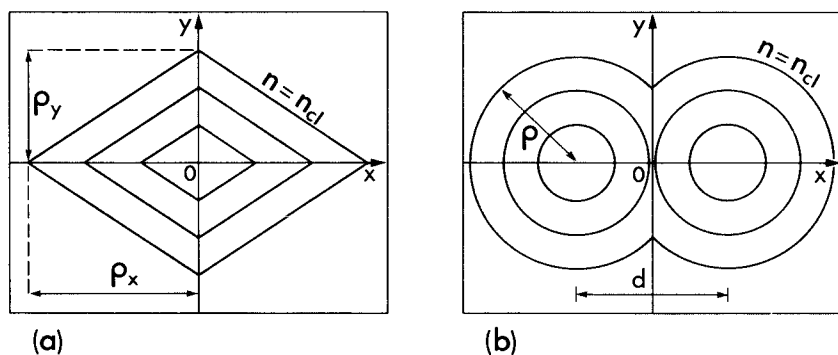


Fig. 16-2 Contours of constant refractive index for (a) the infinite linear profile of Eq. (16-24) and (b) the double parabolic fiber profile of Eq. (16-30), where d is the separation of the fiber centers.

satisfies $|x/\rho_x| + |y/\rho_y| = 1$. Since the profile is separable, the scalar wave equation solution is given by Eq. (16-23) with $f(x) = |x/\rho_x|$ and $g(y) = |y/\rho_y|$. By changing variables to

$$w_x = \frac{1}{V_x^{4/3}} \left\{ \frac{|x|}{\rho_x} V_x^2 - \frac{\tilde{U}_x^2}{2} - \kappa \frac{\rho_x^2}{\rho^2} \right\}; \quad w_y = \frac{1}{V_y^{4/3}} \left\{ \frac{|y|}{\rho_y} V_y^2 - \frac{\tilde{U}_y^2}{2} + \kappa \frac{\rho_y^2}{\rho^2} \right\}, \quad (16-25)$$

where parameters are defined in Table 16-1, we obtain the equations

$$\frac{d^2 F}{dw_x^2} - w_x F = 0; \quad \frac{d^2 G}{dw_y^2} - w_y G = 0, \quad (16-26)$$

and $\Psi = FG$. Hence, F and G both satisfy Airy's equation, and the solution which is everywhere bounded, is given by

$$\Psi = \pm \text{Ai}(w_x) \text{Ai}(w_y), \quad (16-27)$$

where Ai is the Airy function of the first kind [2]. The sign of Ψ may vary from quadrant to quadrant in Fig. 16-2(a) depending on the symmetry with respect to x and y . Continuity of Ψ , $\partial\Psi/\partial x$ and $\partial\Psi/\partial y$ along the axes in Fig. 16-2(a) leads to the eigenvalue equation. For example, the fundamental mode solution takes the + sign in every quadrant and leads to the eigenvalue equation

$$\frac{d\text{Ai}(w_x)}{dw_x} = 0, \quad x = 0; \quad \frac{d\text{Ai}(w_y)}{dw_y} = 0, \quad y = 0. \quad (16-28)$$

The largest value of the propagation constant is given by the first root of the Airy function derivative, namely $w_x \cong -1.018$ when $x = 0$, and $w_y \cong -1.018$ when $y = 0$ [2]. Substituting from Eq. (16-25) and eliminating κ , we obtain

$$\tilde{U}_x \tilde{U}_y = 1.018 \left\{ \left(\frac{\rho_x}{\rho_y} \right)^{1/3} + \left(\frac{\rho_y}{\rho_x} \right)^{1/3} \right\} (V_x V_y)^{2/3}, \quad (16-29)$$

in the notation of Table 16-1. The linear profile is also a homogeneous function profile, satisfying Eq. (16-19b) with $q = 1$. Consequently, Eq. (16-29) is identical to Eq. (16-20) with $q = 1$ and $\rho_x \rho_y = \rho^2$, and determines the parametric dependence of G on ρ_x and ρ_y .

16-8 Example: Double parabolic profile

The final example considers a profile which describes the refractive-index distribution for two parallel, infinite parabolic-profile fibers [3]. This profile is illustrated in Fig. 16-2(b) and is defined by

$$n^2(x, y) = n_{co}^2 \{1 - 2\Delta[(|x/\rho| - d/2\rho)^2 + (y/\rho)^2]\}; \quad -\infty < x, y < \infty, \quad (16-30)$$

where d is the separation of the fiber axes and ρ is a scaling length for both fibers. As the profile is separable, the scalar wave equation solution is obtained by setting $f(x) = (|x/\rho| - d/2\rho)^2$ in Eq. (16-23a) and $g(y) = (y/\rho)^2$ in Eq. (16-23b). The solution of the latter equation is found by analogy with Eq. (16-13b) to be

$$G = H_{n-1} \left(\frac{y}{\rho} V^{1/2} \right) \exp \left\{ -\frac{1}{2} \frac{y^2}{\rho^2} V \right\}; \quad 2n-1 = \frac{\tilde{U}^2}{2V} - \frac{\kappa}{V}, \quad (16-31)$$

where $n = 1, 2, \dots$, the parameters are defined at the back of the book, and H_{n-1} is the Hermite polynomial of order $n-1$ [2]. If we substitute for κ in Eq. (16-23a) and change variables to

$$w_+ = (2V)^{1/2} \frac{2x-d}{2\rho}, \quad x > 0; \quad w_- = (2V)^{1/2} \frac{2x+d}{2\rho}, \quad x < 0, \quad (16-32)$$

we obtain the equation

$$\frac{d^2 F}{dw^2} + \left\{ v + \frac{1}{2} - \frac{w^2}{4} \right\} F = 0; \quad v = \frac{\tilde{U}^2}{2V} - n, \quad (16-33)$$

where w denotes w_+ or w_- . This equation has a solution which is bounded as $x \rightarrow \pm \infty$

and is expressed in terms of the parabolic cylinder function D_v [2] by

$$F = D_v(w_+), \quad x > 0; \quad F = \pm D_v(-w_-), \quad x < 0, \quad (16-34)$$

where + and - signs refer to symmetric and antisymmetric modes, respectively. The solution Ψ of the scalar wave equation is then given by the product FG of Eqs. (16-31) and (16-34). Continuity of $\partial\Psi/\partial x$ at $x = 0$ for the symmetric modes and continuity of Ψ at $x = 0$ for the antisymmetric modes leads to the two eigenvalue equations

$$\left. \frac{dD_v}{dw} \right|_{w_0} = 0; \quad D_v(w_0) = 0, \quad (16-35)$$

respectively, where $w_0 = -(2V)^{1/2} d/2\rho$.

REFERENCES

1. Born, M. and Wolf, E. (1970) *Principles of Optics*, Pergamon Press, Oxford.
2. Abramowitz, M. and Stegun, I. A. (1965) *Handbook of Mathematical Functions*, Dover, New York.
3. Sharma, A., Khular, E., Thyagarajan, K. and Ghatak, A. K. (1979) Coupling of two parallel multimode parabolic index waveguides: an exact analysis in the weakly guiding approximation. *Opt. Commun.*, **30**, 166-9.

Gaussian approximation for noncircular fibers

Fundamental modes	366
17-1 The Gaussian approximation	367
17-2 <i>Example: Infinite power-law profiles</i>	369
Concentric elliptical fibers	369
17-3 Slight eccentricity	371
17-4 <i>Example: Step profile</i>	372
17-5 <i>Example: Gaussian profile</i>	373
References	373

The Gaussian approximation was introduced in Chapter 15 to provide simple, but accurate, analytical expressions for fundamental-mode quantities of interest on circular fibers of arbitrary profile. Here we show how to generalize this approximation and describe fundamental-mode propagation on weakly guiding fibers of arbitrary cross-section.

The basis of the Gaussian approximation for circular fibers is the observation that the fundamental-mode field distribution on an arbitrary profile fiber is *approximately* Gaussian. Coupled with the fact that the same field on an infinite parabolic-profile fiber is *exactly* Gaussian, the approximation fits the field of the arbitrary profile fiber to the field of an infinite parabolic-profile fiber. The optimum fit is found by the variational procedure described in Section 15-1. Now in Chapter 16, we showed that the fundamental-mode field distribution on an elliptical fiber with an infinite parabolic profile has a Gaussian dependence on both spatial variables in the cross-section. Accordingly, we fit the field of such a profile to the unknown field of the noncircular fiber of arbitrary profile by a similar variational procedure, as we show below [1, 2].

FUNDAMENTAL MODES

The two fundamental modes on a weakly guiding fiber of noncircular cross-

366

section are uniformly polarized parallel to the optical axes of the fiber, as we showed in Section 13-5. Their transverse fields have the forms given by Eq. (13-10), and repeated in Table 17-1, in terms of the fundamental solution $\Psi(x, y)$ of the scalar wave equation and the scalar propagation constant $\tilde{\beta}$. To correctly distinguish between the propagation constant of the two modes, we also need the polarization corrections $\delta\beta_x$ and $\delta\beta_y$ due to the waveguide structure. Our purpose is to provide simple analytical approximations for Ψ and $\tilde{\beta}$, and hence for $\delta\beta_x$ and $\delta\beta_y$.

17-1 The Gaussian approximation

By analogy with the fundamental-mode solution for the elliptical fiber of infinite parabolic profile given in Table 16-1, page 356, we assume that the solution $\Psi(x, y)$ of the scalar wave equation of Eq. (16-3) can be approximated by setting [1, 2]

$$\Psi(x, y) = \exp \left\{ -\frac{1}{2} \left(\frac{x^2}{a_x^2} + \frac{y^2}{a_y^2} \right) \right\}, \quad (17-1)$$

where a_x and a_y are spot sizes to be determined. We use this expression as a trial function in the stationary expression for the propagation constant in Table 13-2, page 292. The values of a_x and a_y correspond to the largest value of $\tilde{\beta}$ [3]. Relative to cartesian axes we have

$$\tilde{\beta}^2 = \frac{\int_{-\infty}^{\infty} \int_{-\infty}^{\infty} \{k^2 n^2(x, y) \Psi^2 - (\partial \Psi / \partial x)^2 - (\partial \Psi / \partial y)^2\} dx dy}{\int_{-\infty}^{\infty} \int_{-\infty}^{\infty} \Psi^2 dx dy}, \quad (17-2)$$

where $k = 2\pi/\lambda$ and λ is the free-space wavelength. The spot sizes are determined by substituting Eq. (17-1) into Eq. (17-2) and solving the pair of simultaneous equations

$$\frac{\partial \tilde{\beta}^2}{\partial a_x} = 0; \quad \frac{\partial \tilde{\beta}^2}{\partial a_y} = 0. \quad (17-3)$$

Substitution back into Eq. (17-2) gives the propagation constant and hence the scalar fields in Table 17-1. The corrections $\delta\beta_x$ and $\delta\beta_y$ then follow from Eq. (13-11).

The detailed analysis for finding a_x , a_y and $\tilde{\beta}$ is simplified by defining in Table 17-1 normalized coordinates X and Y , in terms of length scales ρ_x and ρ_y in the cross-section, fiber parameters V_x and V_y , mode parameters U_x and U_y , and normalized spot sizes A_x and A_y . The variational equation and spot-size equations follow directly from Eqs. (17-2) and (17-3) using integration by

Table 17-1 Gaussian approximation for fundamental modes of noncircular fibers. Parameters are defined inside the back cover and coordinates are illustrated in Fig. 16-1.

$n^2(x, y) = n_{co}^2 \{1 - 2\Delta f(X, Y)\}; \quad X = \frac{x}{\rho_x}; \quad Y = \frac{y}{\rho_y}; \quad e = \left\{1 - \frac{\rho_y^2}{\rho_x^2}\right\}^{1/2}$	
<p><i>Even HE₁₁ mode (x-polarized)</i></p> $E_x = \Psi(x, y) \exp\{i(\tilde{\beta} + \delta\beta_x)z\}$ $H_y = \left(\frac{\epsilon_0}{\mu_0}\right)^{1/2} n_{co} E_x$	<p><i>Odd HE₁₁ mode (y-polarized)</i></p> $E_y = \Psi(x, y) \exp\{i(\tilde{\beta} + \delta\beta_y)z\}$ $H_x = -\left(\frac{\epsilon_0}{\mu_0}\right)^{1/2} n_{co} E_y$
$\Psi(x, y) = \exp\left\{-\frac{1}{2}\left(\frac{X^2}{A_x^2} + \frac{Y^2}{A_y^2}\right)\right\}; \quad A_x = \frac{a_x}{\rho_x}; \quad A_y = \frac{a_y}{\rho_y}$	
$\delta\beta_x = -\frac{(2\Delta)^{3/2}}{2\rho_x V_x^3 A_x^4}$	$\delta\beta_y = -\frac{(2\Delta)^{3/2}}{2\rho_y V_y^3 A_y^4}$
$V_x = k\rho_x n_{co}(2\Delta)^{1/2}; \quad V_y = k\rho_y n_{co}(2\Delta)^{1/2}; \quad \frac{V_y}{V_x} = \frac{\rho_y}{\rho_x}; \quad k = \frac{2\pi}{\lambda}$	
<p>Variational equation for the propagation constant</p>	
$\tilde{U}_x \tilde{U}_y = \frac{V_x V_y}{\pi A_x A_y} \int_{-\infty}^{\infty} \int_{-\infty}^{\infty} f(X, Y) \exp\left\{-\frac{X^2}{A_x^2} - \frac{Y^2}{A_y^2}\right\} dX dY + \frac{1}{2} \left\{ \frac{\rho_y}{\rho_x A_x^2} + \frac{\rho_x}{\rho_y A_y^2} \right\}$	
$\tilde{U}_x = \left\{ \frac{V_x^2}{2\Delta} - \rho_x^2 \tilde{\beta}^2 \right\}^{1/2}; \quad \tilde{U}_y = \left\{ \frac{V_y^2}{2\Delta} - \rho_y^2 \tilde{\beta}^2 \right\}^{1/2}; \quad \frac{\tilde{U}_y}{\tilde{U}_x} = \frac{\rho_y}{\rho_x}$	
<p>Equations for spot sizes</p>	
$\frac{\pi}{V_x^2} = \frac{A_x}{A_y} \int_{-\infty}^{\infty} \int_{-\infty}^{\infty} X \frac{\partial f}{\partial X} \exp\left\{-\frac{X^2}{A_x^2} - \frac{Y^2}{A_y^2}\right\} dX dY$ $\frac{\pi}{V_y^2} = \frac{A_y}{A_x} \int_{-\infty}^{\infty} \int_{-\infty}^{\infty} Y \frac{\partial f}{\partial Y} \exp\left\{-\frac{X^2}{A_x^2} - \frac{Y^2}{A_y^2}\right\} dX dY$	

parts, and the propagation constant corrections from Eq. (13-11). To illustrate the method we consider a specific example.

17-2 Example: Infinite power-law profiles

We define a set of infinite power-law profiles for noncircular fibers relative to cartesian axes in the cross-section by

$$n^2(x, y) = n_{co}^2 \left\{ 1 - 2\Delta \left[\left| \frac{x}{\rho_x} \right|^q + \left| \frac{y}{\rho_y} \right|^q \right] \right\}; \quad -\infty < x, y < \infty, \quad (17-4)$$

where q is a positive constant. The parabolic profile ($q = 2$) and the linear profile ($q = 1$) are members of this set and were discussed in the previous chapter. Within the Gaussian approximation we set $f = |X|^q + |Y|^q$ in the spot-size equations of Table 17-1, and, with the help of the integral definition of Eq. (37-104), obtain a solution in terms of the gamma function

$$A_x = \left\{ \frac{\pi^{1/2}}{q\Gamma(q/2 + 1/2)V_x^2} \right\}^{1/(q+2)}; \quad A_y = \left\{ \frac{\pi^{1/2}}{q\Gamma(q/2 + 1/2)V_y^2} \right\}^{1/(q+2)}, \quad (17-5)$$

where the notation is defined in Table 17-1. Substitution back into the equation for the propagation constant leads to

$$\tilde{U}_x \tilde{U}_y = \frac{q+2}{2q} \left\{ \frac{q\Gamma(q/2 + 1/2)}{\pi^{1/2}} \right\}^{2/(q+2)} \left\{ \left(\frac{\rho_x}{\rho_y} \right)^{q/(q+2)} + \left(\frac{\rho_y}{\rho_x} \right)^{q/(q+2)} \right\} (V_x V_y)^{2/(q+2)}. \quad (17-6)$$

The power-law profiles satisfy Eq. (16-19b), and are therefore homogeneous function profiles. Consequently, the above expression is consistent with the more general result of Eq. (16-20). In the case of the infinite linear profile ($q = 1$), Eq. (17-6) reduces to the exact eigenvalue equation of Eq. (16-29), apart from a change in the multiplicative constant on the right from 1.018 to $3/(2\pi^{1/3}) \cong 1.024$, a relative error of 0.6%. This excellent agreement is independent of ρ_x and ρ_y , and demonstrates the accuracy of the Gaussian approximation for *arbitrary eccentricity*.

Birefringence depends on the difference $\delta\beta_x - \delta\beta_y$ between the corrected propagation constants of the two fundamental modes. We deduce from Table 17-1 and Eq. (17-5) that

$$\delta\beta_x - \delta\beta_y = \frac{(2\Delta)^{3/2}}{2\rho_x} \left[\left\{ \frac{q\Gamma(q/2 + 1/2)}{\pi^{1/2}} \right\}^4 V_x^{2-3q} \right]^{1/(q+2)} \left\{ \left[\frac{\rho_x}{\rho_y} \right]^{4q/(q+2)} - 1 \right\}, \quad (17-7)$$

which is identical to the expression in Table 16-1, page 356, for the parabolic profile ($q = 2$). For arbitrary q , birefringence increases with increasing eccentricity, i.e. with ρ_x fixed and ρ_y decreasing.

CONCENTRIC ELLIPTICAL FIBERS

In the cross-section of an elliptical fiber, contours of constant refractive index are closed ellipses. If the contours all have the same eccentricity, the fiber

profile is said to be *concentric*. The infinite parabolic profile of Fig. 16-1 is one such example. Any concentric fiber profile is expressible in the form

$$n^2(x, y) = n_{co}^2 \left\{ 1 - 2\Delta f \left(\frac{x^2}{\rho_x^2} + \frac{y^2}{\rho_y^2} \right) \right\}; \quad -\infty < x, y < \infty, \quad (17-8)$$

where f is an arbitrary function of the single variable $(x/\rho_x)^2 + (y/\rho_y)^2$. This representation leads to a simplification of the spot-size equations, as we show below, and, in the following section, we prove that *an elliptical fiber has the same scalar propagation constant as a circular fiber, provided the eccentricity is small and the profile volumes are equal*.

Spot-size equations

The elliptical cross-section is transformed to circular cross-section by making the change of coordinates

$$X = x/\rho_x = R \sin \phi; \quad Y = y/\rho_y = R \cos \phi. \quad (17-9)$$

The profile function of Eq. (17-8) becomes the profile function $f(R^2)$ for the circular fiber, and the spot-size equations of Table 17-1 are transformed to give

$$\frac{2\pi}{V_x^2} = \frac{A_x}{A_y} \int_0^\infty R^2 \frac{df}{dR} \exp(-aR^2) \int_0^{2\pi} (1 - \cos 2\phi) \exp(bR^2 \cos 2\phi) d\phi dR, \quad (17-10a)$$

$$\frac{2\pi}{V_y^2} = \frac{A_y}{A_x} \int_0^\infty R^2 \frac{df}{dR} \exp(-aR^2) \int_0^{2\pi} (1 + \cos 2\phi) \exp(bR^2 \cos 2\phi) d\phi dR, \quad (17-10b)$$

where a and b are constants defined by

$$a = \frac{A_x^2 + A_y^2}{2A_x^2 A_y^2}; \quad b = \frac{A_y^2 - A_x^2}{2A_x^2 A_y^2}. \quad (17-11)$$

The ϕ integration is expressible in terms of modified Bessel functions of the first kind through Eq. (37-64), and by adding and subtracting the resulting equations, we obtain, respectively

$$\frac{A_y}{A_x V_x^2} + \frac{A_x}{A_y V_y^2} = 2 \int_0^\infty R^2 \frac{df}{dR} \exp(-aR^2) I_0(bR^2) dR, \quad (17-12a)$$

$$\frac{A_y}{A_x V_x^2} - \frac{A_x}{A_y V_y^2} = -2 \int_0^\infty R^2 \frac{df}{dR} \exp(-aR^2) I_1(bR^2) dR. \quad (17-12b)$$

For arbitrary eccentricity these equations must generally be solved by numerical methods, but if the eccentricity is small an analytical solution can be found.

17-3 Slight eccentricity

To relate the elliptical fiber parameters to the circular fiber parameters, we assume the profile of Eq. (17-8) is clad and has the same profile volume Ω as the corresponding circular fiber. Substituting into Eq. (14-42) and integrating over the elliptical core $(x/\rho_x)^2 + (y/\rho_y)^2 \leq 1$, we find with the help of Eq. (17-9) that

$$\rho_x \rho_y = \rho^2, \quad (17-13)$$

regardless of the profile, where ρ is the core radius. For small eccentricity we then deduce from Table 17-1 that, correct to second order

$$\rho_x = \rho(1 + e^2/4); \quad \rho_y = \rho(1 - e^2/4); \quad V_x = V(1 + e^2/4); \quad V_y = V(1 - e^2/4), \quad (17-14)$$

where V is defined inside the back cover for the circular fiber.

If we compare Eqs. (17-1) and (15-2) in the limit $\rho_x = \rho_y = \rho$, then $A_x = A_y = R_0$ when $e = 0$, where R_0 is the normalized spot size of Table 15-1, page 339, for the fundamental modes of the circular fiber. For small eccentricity we set

$$A_x = R_0 \{1 + e^2 p_x\}; \quad A_y = R_0 \{1 + e^2 p_y\}. \quad (17-15)$$

Thus Eq. (17-11) can be approximated by

$$a = \{1 - e^2(p_x + p_y)\}/R_0^2; \quad b = e^2(p_y - p_x)/R_0^2. \quad (17-16)$$

The expansions of I_0 and I_1 for small argument follow from Eq. (37-85)

$$I_0(bR^2) \cong 1 + b^2 R^4/4; \quad I_1(bR^2) \cong bR^2/2. \quad (17-17)$$

We substitute Eqs. (17-14) to (17-17) into Eq. (17-12a) and equate powers of e^2 . To lowest order we recover the spot-size equation of Table 15-1, page 339, for the circular fiber, and to second order deduce that

$$p_x + p_y = 0; \quad a = 1/R_0^2. \quad (17-18)$$

If we set $\tilde{U}_x \tilde{U}_y = \tilde{U}^2$ in Table 17-1, the equation for the propagation constant is readily shown to be the corresponding equation in Table 15-1, apart from an integration by parts. Hence we deduce that, within the Gaussian approximation, *the elliptical fiber has the same scalar propagation constant for the fundamental modes as the corresponding circular fiber, provided that the profile volumes are equal and the eccentricity is small.*

If we substitute Eqs. (17-14) to (17-18) into Eq. (17-12b) and equate lowest-order terms, we find that

$$p_x = -p_y = -\frac{1}{4} \left[1 + \frac{V^2}{2R_0^2} \int_0^\infty R^4 \frac{df}{dR} \exp\left(-\frac{R^2}{R_0^2}\right) dR \right]^{-1}. \quad (17-19)$$

Thus, if the spot size for the circular fiber is known, the spot sizes for the

elliptical fiber are given explicitly to second order in eccentricity by substituting Eq. (17-19) into Eq. (17-15).

17-4 Example: Step profile

The step profile has uniform core and cladding indices n_{co} and n_{cl} , respectively, separated by the elliptical interface $(x/\rho_x)^2 + (y/\rho_y)^2 = 1$, relative to the axes in Fig. 16-1. The spot-size equations of Eq. (17-12) are expressed in terms of the profile function for the step-profile, circular fiber. Hence $df/dR = \delta(R-1)$, where δ is the Dirac delta function, and, on adding and subtracting Eqs. (17-12a) and (17-12b), we find that

$$A_y = A_x V_x^2 \{I_0 - I_1\} e^{-a}; \quad A_x = A_y V_y^2 \{I_0 + I_1\} e^{-a}, \quad (17-20)$$

where $I_0 = I_0(b)$, $I_1 = I_1(b)$ and remaining parameters are defined in Table 17-1. If we multiply these two expressions together and similarly divide them, express A_x and A_y in terms of a and b of Eq. (17-11) and rearrange, the resulting two equations decouple to give

$$a = -b \frac{(2-e^2)I_0 - e^2 I_1}{(2-e^2)I_1 - e^2 I_0} = \ln(V_x V_y) + \frac{1}{2} \ln(I_0^2 - I_1^2), \quad (17-21)$$

which holds for *arbitrary* eccentricity.

Planar waveguide limit

If we fix ρ_y and let $\rho_x \rightarrow \infty$, the elliptical fiber is transformed into the symmetric planar waveguide of Fig. 12-1. In this limit, the spot size $a_x \rightarrow \infty$, but the normalized spot size $A_x = a_x/\rho_x \rightarrow 0$. See, for example, the expression for A_x in Eq. (17-5). Hence both a and b of Eq. (17-11) become unbounded. If we substitute the asymptotic forms of Eq. (37-88) for the modified Bessel functions into the second equation in Eq. (17-20) and retain lowest-order terms, we deduce

$$A_y^2 \ln(2A_y V_y^2/\sqrt{\pi}) = 1. \quad (17-22)$$

It is readily verified, by repeating the derivation in Table 15-1, page 339, for planar waveguides, that the above expression is the spot-size equation for the Gaussian approximation to the fundamental modes of a step-profile, planar waveguide of core half-width ρ_y .

Small eccentricity

The solution of Eq. (17-21) for small eccentricity is given by Eqs. (17-15) and (17-19) with $df/dR = \delta(R-1)$ and $R_0 = (2 \ln V)^{-1/2}$, according to Table 15-2, page 340. Hence

$$A_x = \frac{1}{(2 \ln V)^{1/2}} \left\{ 1 - \frac{e^2}{4} \frac{1}{1 + \ln V} \right\}; \quad A_y = \frac{1}{(2 \ln V)^{1/2}} \left\{ 1 + \frac{e^2}{4} \frac{1}{1 + \ln V} \right\}, \quad (17-23)$$

and the birefringence follows from Table 17-1 as

$$\delta\beta_x - \delta\beta_y = \frac{e^2 (2\Delta)^{3/2}}{\rho} \frac{4}{V^3} \frac{(\ln V)^3}{1 + \ln V}; \quad V > 1, \quad (17-24)$$

correct to second order in eccentricity, where ρ and V are the core radius and fiber parameter for the circular fiber of equal profile volume to the elliptical fiber.

17-5 Example: Gaussian profile

On an elliptical fiber the Gaussian profile is defined by

$$n^2(x, y) = n_{co}^2 \left\{ 1 - 2\Delta \left[1 - \exp\left(-\frac{x^2}{\rho_x^2} - \frac{y^2}{\rho_y^2}\right) \right] \right\}; \quad -\infty < x, y < \infty. \quad (17-25)$$

We set $f = 1 - \exp(-R^2)$ for the corresponding circular profile in Eq. (17-12), and with the help of Eq. (37-102) find that the normalized spot sizes satisfy the coupled equations

$$A_x = \left(\frac{V_x^3}{V_x} \right)^{1/2} \frac{A_y^3}{1 + A_y^2}; \quad A_y = \left(\frac{V_y^3}{V_y} \right)^{1/2} \frac{A_x^3}{1 + A_x^2}. \quad (17-26)$$

Elimination of A_y leads to a quartic equation for A_x^2 , which has an explicit solution for arbitrary eccentricity [2]. The planar waveguide limit can be obtained by analogy with the previous example.

For small eccentricity, we substitute $R_0 = (V-1)^{-1/2}$ from Table 15-1, page 339, into Eq. (17-19) and deduce via Eq. (17-15) that

$$A_x = \frac{1}{(V-1)^{1/2}} \left\{ 1 - \frac{e^2}{4} \frac{V}{2V-1} \right\}; \quad A_y = \frac{1}{(V-1)^{1/2}} \left\{ 1 + \frac{e^2}{4} \frac{V}{2V-1} \right\}, \quad (17-27)$$

correct to second order, where ρ and V apply to the circular fiber of Gaussian profile with the same profile volume as the elliptical fiber. The birefringence expression then follows from Table 17-1

$$\delta\beta_x - \delta\beta_y = \frac{e^2 (2\Delta)^{3/2}}{\rho} \frac{(V-1)^3}{(2V-1)V^3}, \quad (17-28)$$

which is physically meaningful only when $V > 1$.

REFERENCES

1. Snyder, A. W. (1981) Understanding monomode optical fibers. *Proc. I.E.E.E.*, **69**, 6-13.
2. Love, J. D. and Hussey, C. D. (1984) Variational approximations for modes of noncircular waveguides. *Opt. Quant. Elect.* (submitted).
3. Mathews, J. and Walker, R. L. (1965) *Mathematical Methods of Physics*, Benjamin, New York.

Modes of perturbed fibers

Modes of weakly guiding perturbed fibers	375
18-1 Perturbation solution for isolated fibers	376
18-2 Polarization of the perturbed fields	377
18-3 Uniform changes in profile	377
18-4 <i>Example: Uniform changes in core and cladding indices</i>	378
18-5 <i>Example: Three-region fiber</i>	378
18-6 <i>Example: Change in core radius</i>	380
18-7 <i>Example: Isolated nonuniformity</i>	380
18-8 <i>Example: Absorbing fibers</i>	380
18-9 <i>Example: Anisotropic core</i>	381
18-10 <i>Example: Elliptical deformation</i>	382
18-11 Nonuniform changes in profile	387
 Modes of two parallel fibers	387
18-12 Fundamental modes of identical fibers	389
18-13 Cross-talk between identical fibers	391
18-14 <i>Example: Two step-profile fibers</i>	392
18-15 <i>Example: Double parabolic-profile waveguide</i>	394
18-16 Higher-order modes of identical fibers	395
18-17 <i>Example: Two step-profile fibers</i>	395
18-18 Fundamental modes of nonidentical fibers	397
18-19 <i>Example: Two step-profile fibers of similar core radii</i>	398
18-20 Cross-talk between nonidentical fibers	399
 Modes of perturbed fibers of arbitrary profile	399
18-21 Perturbation solution	400
18-22 <i>Example: Infinitesimal nonuniformity</i>	401
18-23 <i>Example: Change in core radius</i>	403
18-24 <i>Example: Elliptical deformation</i>	405
18-25 <i>Example: Absorbing fibers</i>	405
 References	405

So far in Part II we have considered waveguides and fibers whose cross-sectional geometry and profile variation allow the modal fields to be expressed

in exact or approximate analytical form. There are few exact solutions for arbitrary or weakly guiding waveguides, as is evident from Chapters 12, 14 and 16. However, when there is no known solution of the scalar wave equation, propagation on weakly guiding waveguides can be described analytically by the Gaussian approximation of Chapters 15 and 17, with only a slight loss in accuracy.

In this chapter, we consider both arbitrary and weakly guiding waveguides or fibers with cross-sections and profiles which differ only slightly, in some *perturbation* sense, from those of another fiber whose modal fields are known. For example, fibers that are slightly anisotropic, absorptive or elliptical, as well as composite waveguides consisting of two or more well-separated fibers, are perturbations of the circular fiber with an isotropic refractive-index profile. By taking advantage of the smallness of the perturbation, we can use approximation techniques to derive accurate expressions for the modes of the perturbed fiber in terms of the known modes of the unperturbed fiber.

Cylindrically symmetric perturbations

The perturbations discussed in this chapter do not vary with distance z along the fiber. Hence, the perturbed fiber is cylindrically symmetric, or translationally invariant, and its modes have all the properties described in Chapter 11. The perturbed fiber is characterized by a refractive-index profile $n(x, y)$ relative to cartesian axes in the cross-section, and the *unknown* electric and magnetic fields of one of its modes are expressed in the separable form of Eq. (11-6) as

$$\mathbf{E}(x, y, z) = \mathbf{e}(x, y) \exp(i\beta z); \quad \mathbf{H}(x, y, z) = \mathbf{h}(x, y) \exp(i\beta z), \quad (18-1)$$

where β is the propagation constant. The corresponding mode on the unperturbed fiber is characterized by the refractive-index profile $\bar{n}(x, y)$, and *known* fields with propagation constant $\bar{\beta}$, where

$$\bar{\mathbf{E}}(x, y, z) = \bar{\mathbf{e}}(x, y) \exp(i\bar{\beta} z); \quad \bar{\mathbf{H}}(x, y, z) = \bar{\mathbf{h}}(x, y) \exp(i\bar{\beta} z). \quad (18-2)$$

We omit the modal subscript since we shall be mainly concerned with only individual modes. In showing how \mathbf{e} , \mathbf{h} and β are expressed in terms of $\bar{\mathbf{e}}$, $\bar{\mathbf{h}}$ and $\bar{\beta}$, it is convenient to consider weakly guiding and arbitrary fibers separately.

MODES OF WEAKLY GUIDING PERTURBED FIBERS

When the perturbed and unperturbed fibers are weakly guiding, the variation in both profiles n and \bar{n} is small. The modal fields can then be constructed from solutions of the scalar wave equation, as described in Chapter 13. If Ψ and β denote the *unknown* solution and propagation constant for the perturbed fiber,

then they satisfy

$$\{\nabla_t^2 + k^2 n^2(x, y) - \beta^2\} \Psi = 0, \quad (18-3a)$$

while the *known* solution and propagation constant, $\bar{\Psi}$ and $\bar{\beta}$, for the unperturbed fiber satisfy

$$\{\nabla_t^2 + k^2 \bar{n}^2(x, y) - \bar{\beta}^2\} \bar{\Psi} = 0, \quad (18-3b)$$

where ∇_t^2 is the transverse Laplace operator, $k = 2\pi/\lambda$ and λ is the free-space wavelength. The \sim associated with scalar quantities in Chapter 13 is omitted here for clarity.

In order to express Ψ and β in terms of $\bar{\Psi}$ and $\bar{\beta}$, we use a reciprocal relationship between the two solutions. This relationship is derived directly from Eq. (18-3), as we show in Section 33-5, and is expressed by Eq. (33-20) as

$$\beta^2 - \bar{\beta}^2 = k^2 \int_{A_x} \{n^2 - \bar{n}^2\} \Psi \bar{\Psi} dA / \int_{A_x} \Psi \bar{\Psi} dA, \quad (18-4)$$

where A_∞ is the infinite cross-section, and for convenience Ψ and $\bar{\Psi}$ are assumed real. We first consider perturbations involving single fibers. Perturbations involving composite systems of two parallel fibers are discussed later.

18-1 Perturbation solution for isolated fibers

For slight perturbations, it is normally sufficient to assume that the transverse, or x, y dependence of the modal fields on the perturbed and unperturbed fibers is similar, i.e. $\mathbf{e} \cong \bar{\mathbf{e}}$, $\mathbf{h} \cong \bar{\mathbf{h}}$, and consequently $\Psi \cong \bar{\Psi}$. An exception is the calculation of the polarization corrections to the scalar propagation constant, discussed in the following section, for which higher-order corrections to Ψ are required. These can be obtained using either eigenfunction expansions, as outlined in Sections 33-9 and 33-10, or Green's functions, as discussed in Chapter 34.

It is usually inadequate to ignore the difference between the propagation constants β and $\bar{\beta}$. The longitudinal dependence of the perturbed fields in Eq. (18-1) involves the product βz . Thus a small error in β will eventually produce a significant error in the fields since z can be arbitrarily large. The perturbation correction to $\bar{\beta}$ is given by Eq. (18-4) with $\Psi = \bar{\Psi}$. Some simplification is possible within the weak-guidance approximation by setting $\beta^2 - \bar{\beta}^2 \cong 2kn_{\text{co}}(\beta - \bar{\beta})$ and $n^2 - \bar{n}^2 \cong 2n_{\text{co}}(n - \bar{n})$, assuming that n_{co} is the maximum value of refractive index on both perturbed and unperturbed fibers. Hence

$$\beta = \bar{\beta} + k \left\{ \int_{A_x} (n - \bar{n}) \bar{\Psi}^2 dA \right\} / \int_{A_x} \bar{\Psi}^2 dA, \quad (18-5)$$

where contributions to the integral in the numerator came from regions in which the perturbed and unperturbed fibers differ.

The description of the modal fields on the perturbed fiber will be complete once the polarization of the transverse components is specified.

18-2 Polarization of the perturbed fields

If the unperturbed fiber is noncircular, the transverse electric field of each mode is polarized parallel to one of the optical axes, x_0 or y_0 , as discussed in Sections 13-5 and 13-8. The directions of the optical axes on the perturbed fiber, which determine the polarization of the perturbed mode fields, are found either by inspection or by the formal methods of Section 32-5.

Perturbations which break circular symmetry

In many of the examples below, the unperturbed fiber has a circularly symmetric cross-section and profile. For perturbations which maintain this symmetry, the polarization of each mode is unchanged, and obeys the rules laid down in Sections 13-4 and 13-7. However, for perturbations which break circular symmetry, the modes are polarized along the optical axes x_0 and y_0 of the perturbed fiber. Only the fundamental and HE_{1m} modes remain plane polarized on the circular and noncircular fibers. If the perturbation is sufficiently small, the polarization of all other modes lies in the transition region between the circular and noncircular situations, as discussed in Section 13-9.

Polarization corrections to the propagation constant

The polarization corrections, $\delta\beta_x$ and $\delta\beta_y$, to the scalar propagation constant β for the x_0 - and y_0 -polarized modes on the perturbed, noncircular fiber are in general unequal, and their difference describes the anisotropic, or birefringent, nature of propagation. This is of basic interest for the two fundamental modes on single-mode fibers. The calculation of the corrections from the formula in Table 13-1, page 288, requires first-order corrections to the approximation $\Psi = \bar{\Psi}$. We derive these corrections for the slightly elliptical fiber in Section 18-10.

We now apply the results of this and the previous section to a variety of perturbation problems, to show their wide range of utility.

18-3 Uniform changes in profile

There is a class of problems, typified by the seven examples below, for which the fiber perturbation is equivalent to a change in refractive index by a constant

throughout the perturbation region. In this region the profile of the perturbed fiber is given by

$$n(x, y) = \bar{n}(x, y) + \delta n, \quad (18-6)$$

where δn is a constant. Substituting into Eq. (18-5) and recalling the definition of power density from Table 13-2, page 292, gives

$$\beta = \bar{\beta} + k\bar{\eta}_p \delta n, \quad (18-7a)$$

where $\bar{\eta}_p$ is the fraction of the unperturbed mode's total power flowing through the cross-sectional area A_p of the perturbation, i.e.

$$\bar{\eta}_p = \int_{A_p} \bar{\Psi}^2 dA / \int_{A_x} \bar{\Psi}^2 dA. \quad (18-7b)$$

Clearly, the greater the fractional power flow through the perturbation cross-section, the greater the difference between β and $\bar{\beta}$. Exact expressions for $\bar{\Psi}$ were given in Chapters 14 and 16 for various cross-sections and profiles, while the Gaussian approximation for $\bar{\Psi}$ on arbitrary profile fibers was given in Chapters 15 and 17.

18-4 Example: Uniform changes in core and cladding indices

When there is a uniform change δn_{co} in index over the core cross-section A_{co} of a graded-profile, clad fiber, we set $\bar{\eta}_p = \bar{\eta}$ and $\delta n = \delta n_{co}$ in Eq. (18-7), where $\bar{\eta}$ is the fraction of a mode's power flowing in the core, defined in Table 13-2, page 292. The fraction of power flowing in the cladding is $1 - \bar{\eta}$, so if, in addition to the core perturbation, there is a uniform change δn_{cl} in the cladding index, the perturbed propagation constant is given by

$$\beta = \bar{\beta} + k\{\bar{\eta} \delta n_{co} + (1 - \bar{\eta}) \delta n_{cl}\}, \quad (18-8)$$

where $k = 2\pi/\lambda$ and λ is the free-space wavelength. This result is independent of both the profile and the cross-sectional geometry. The polarization of the perturbed mode fields is determined from Section 18-2. Exact and approximate expressions for $\bar{\eta}$ are given in Chapters 14 and 15 for circular fibers.

18-5 Example: Three-region fiber

The unperturbed fiber is taken to be a clad, circular fiber with core profile $n(r)$ and radius ρ , and uniform cladding of index n_{cl} . A third region is then introduced beyond radius $\rho_0 > \rho$ with uniform refractive index $n_0 \cong n_{cl}$, as shown in Fig. 18-1(a). Provided $\delta n = n_0 - n_{cl}$ is sufficiently small, the perturbation is slight, and Eq. (18-7)

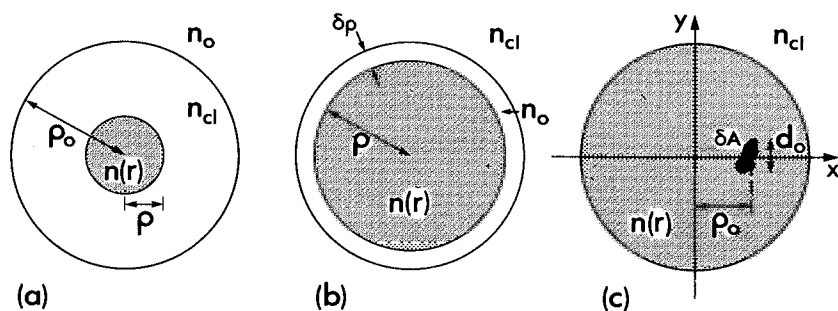


Fig. 18-1 Cross-section of a perturbed fiber, showing (a) three regions, (b) a thin layer at the core-cladding interface and (c) an isolated nonuniformity.

gives the perturbed propagation constant

$$\beta = \bar{\beta} + k\bar{\eta}_p(n_0 - n_{cl}), \quad (18-9)$$

where $\bar{\eta}_p$ is the fraction of the mode's power flowing through the region $r > \rho_0$.

To illustrate this result, consider the fundamental modes of the step-profile fiber. We substitute F_0 of Table 14-3, page 313, for $\bar{\Psi}$ in Eq. (18-7b) and assume ρ_0 is sufficiently large that $K_0(WR)$ can be replaced by the asymptotic form of Eq. (37-88). With the help of the integral in Table 14-6, page 319, we find that

$$\beta = \bar{\beta} + (n_0 - n_{cl}) \frac{\pi k}{2} \left(\frac{U}{WV} \right)^2 \frac{\exp(-2W\rho_0/\rho)}{K_1^2(W)}, \quad (18-10)$$

where parameters are defined inside the back cover.

Thin layer at the core-cladding interface

Another example of a three-region fiber is illustrated in Fig. 18-1(b). A thin concentric ring of width $\delta\rho$ and uniform refractive index n_0 is introduced at the interface of the unperturbed fiber. Hence $\delta n = n_0 - n_{cl}$ in this region, and the perturbed propagation constant follows from Eq. (18-7) as

$$\beta = \bar{\beta} + \delta\rho(n_0 - n_{cl})k\rho\bar{\Psi}^2(\rho) \bigg/ \int_0^\infty \bar{\Psi}^2 r dr, \quad (18-11)$$

where $\bar{\Psi}(\rho)$ is evaluated at the interface of the unperturbed fiber.

For the fundamental modes on a step-profile fiber, we set $\bar{\Psi} = F_0$ of Table 14-3, page 313, and evaluate the integral from Table 14-6, page 319. We obtain

$$\beta = \bar{\beta} + 2(n_0 - n_{cl})k \frac{\delta\rho}{\rho} \left\{ \frac{U}{V} \frac{K_0(W)}{K_1(W)} \right\}^2, \quad (18-12a)$$

where the K_i 's are modified Bessel functions of the second kind. A further simplification is possible if we employ the Gaussian approximation of Eq. (15-2) for F_0 . The spot size for the step profile is given in Table 15-2, page 340, and leads to

$$\beta = \bar{\beta} + 2(n_0 - n_{cl})k \frac{\delta\rho \ln V^2}{\rho V^2} \quad (18-12b)$$

provided $V > 1$.

18-6 Example: Change in core radius

Consider a step-profile fiber with core and cladding indices n_{co} and n_{cl} , and let the core radius change from ρ to $\rho + \delta\rho$. This perturbation is identical to the perturbation in Fig. 18-1(b) if we set $n_0 = n_{co}$. Hence, we deduce from Eq. (18-12) that the perturbed propagation constant is given by

$$\beta = \bar{\beta} + (2\Delta)^{1/2} \frac{\delta\rho}{\rho^2} \frac{U^2}{V} \frac{K_0^2(W)}{K_1^2(W)}, \quad (18-13a)$$

$$\cong \bar{\beta} + (2\Delta)^{1/2} \frac{\delta\rho \ln V^2}{\rho^2 V}; \quad V > 1, \quad (18-13b)$$

using the exact fields and the Gaussian approximation, respectively. Since $n_{co} \cong n_{cl}$ within the present approximation, we can set $n_{co}^2 - n_{cl}^2 \cong 2n_{co}(n_{co} - n_{cl})$ in the definitions of V and Δ .

18-7 Example: Isolated nonuniformity

Consider the circular fiber of arbitrary profile $n(r)$ in Fig. 18-1(c) with a small nonuniformity which remains unchanged along the length of the fiber. The nonuniformity has cross-sectional area δA , mean refractive index n_0 , and is located at distance ρ_0 from the fiber axis. For the fundamental modes, the perturbed propagation constant follows from Eq. (18-7) as

$$\beta = \bar{\beta} + k \delta A \{n_0 - n(\rho_0)\} \bar{\Psi}^2(\rho_0) \left/ 2\pi \int_0^\infty \bar{\Psi}^2 r dr \right., \quad (18-14)$$

since $\bar{\Psi}$ depends only on r . While this would appear to be a trivial example, the perturbation breaks the symmetry of the unperturbed fiber, and we must determine the polarization of the perturbed modes. From the discussion in Section 18-2 and the symmetry of the perturbed fiber, it is clear that the fundamental modes have a transverse electric field that is parallel to either the x - or y -axes in Fig. 18-1(c). We shall return to this problem later in the chapter when discussing arbitrary fibers.

18-8 Example: Absorbing fibers

A description of propagation on absorbing waveguides or fibers was given in Chapter 11. When absorption is slight, we can treat the absorbing fiber as a perturbation of the nonabsorbing fiber. Here we consider clad fibers of arbitrary cross-section on which

absorption is described by the addition of imaginary constants $i\delta n_{co}^i$ to the core profile $n(x, y)$ and $i\delta n_{cl}^i$ to the cladding index n_{cl} . Hence, δn in Eq. (18-7) is imaginary, and the correction to β is imaginary. If we denote the correction by β^i , then, by analogy with Eq. (18-8) we find

$$\beta^i = k \{ \bar{\eta} \delta n_{co}^i + (1 - \bar{\eta}) \delta n_{cl}^i \}, \quad (18-15)$$

where $\bar{\eta}$ is the fraction of the mode's power flowing within the core. We define power absorption coefficients $\alpha_{co} = 2k \delta n_{co}^i$ and $\alpha_{cl} = 2k \delta n_{cl}^i$ for the core and cladding. The power attenuation coefficient γ of Table 13-2, page 292 is then expressible as [1]

$$\gamma = \bar{\eta} \alpha_{co} + (1 - \bar{\eta}) \alpha_{cl}, \quad (18-16)$$

and the mode's power is reduced to $\exp(-\gamma z)$ of its original value after distance z .

Physical interpretation

It is clear from Table 13-2, page 292, that the *shape* of the intensity distribution S on an absorbing fiber *does not change* as the mode propagates, but its amplitude is reduced to $\exp(-\gamma z)$ of its original value everywhere in the cross-section after distance z . If the power absorption coefficient α is uniform over the whole cross-section, then $\gamma = \alpha$ and power lost by attenuation at any position is *exactly* equal to the power absorbed there. This special case corresponds to $\alpha = \alpha_{co} = \alpha_{cl}$ in Eq. (18-16), whence $\gamma = \alpha$. However, if α is not uniform, then power lost by attenuation and power absorbed will differ at an arbitrary point, and, consequently, there must be a flow of power within the cross-section. This corresponds to the general case $\alpha_{co} \neq \alpha_{cl}$ in Eq. (18-16), when power flows across the interface to maintain the shape of the intensity distribution. The direction of this flow depends on the relative values of α_{co} and α_{cl} . For example, if $\alpha_{cl} = 0$, power flows into the core.

18-9 Example: Anisotropic core

We discussed anisotropy and anisotropic waveguides at the end of Chapter 11, gave examples in Chapter 12 and considered weakly guiding anisotropic waveguides in Section 13-12. Here, we consider slightly anisotropic waveguides as a perturbation of the corresponding isotropic waveguide, concentrating on clad fibers with anisotropic cores. This situation is relevant to visual photoreceptors [2-4], and to crystalline core fibers [5].

Unbounded uniformly anisotropic medium

For perspective, we first consider a z -directed plane wave propagating in an unbounded, slightly anisotropic (birefringent) medium characterized by refractive index $n = \bar{n} + \delta n_x$, when the electric field is x -directed, and $n = \bar{n} + \delta n_y$, when the electric field is y -directed, where \bar{n} is the refractive index of the isotropic medium, and $\delta n_x, \delta n_y$ are constants. In an *isotropic* medium the plane wave can be polarized in any direction, but in the anisotropic medium there are only two polarizations, characterized

by differing propagation constants. One wave is x-polarized with propagation constant $\beta_x = k\bar{n} + k\delta n_x$, and the other is y-polarized with propagation constant $\beta_y = k\bar{n} + k\delta n_y$. If we also allow for anisotropic (dichroic) absorption the power absorption coefficient α is also polarization dependent. For convenience we assume that the principal axes of the real and imaginary parts of the refractive-index matrix describing the anisotropy are identical. The power absorption coefficients for the two polarizations are then given by

$$\alpha_x = 2k\delta n_x^i; \quad \alpha_y = 2k\delta n_y^i, \quad (18-17)$$

where $i\delta n_x^i$ and $i\delta n_y^i$ are small imaginary components associated with δn_x and δn_y , respectively.

Anisotropic fiber

It is clear from the above discussion that one of the fundamental modes of a circular fiber with an isotropic core is x-polarized with propagation constant β_x , and the other is y-polarized with propagation constant β_y . If $\bar{n}(x, y)$ is the profile of the isotropic fiber, then $n = \bar{n} + \delta n_x$ for the x-polarized mode and $n = \bar{n} + \delta n_y$ for the y-polarized mode. If the anisotropy is small and uniform, then δn_x and δn_y are constants. Accordingly we set $\delta n_{cl} = 0$ in Eq. (18-8) and replace δn_{co} by δn_x or δn_y to obtain [2, 3]

$$\beta_x = \bar{\beta} + k\bar{\eta}\delta n_x; \quad \beta_y = \bar{\beta} + k\bar{\eta}\delta n_y, \quad (18-18)$$

where $\bar{\eta}$ is the fraction of fundamental-mode power flowing in the core of the unperturbed fiber, and $\bar{\beta}$ is the unperturbed propagation constant. We can repeat the discussion of Section 18-8, and deduce from Eqs. (18-16) and (18-17) that the power attenuation coefficients for the two polarizations are

$$\gamma_x = \bar{\eta}\alpha_x; \quad \gamma_y = \bar{\eta}\alpha_y. \quad (18-19)$$

Thus the fiber has an identical influence on both anisotropy and absorption.

18-10 Example: Elliptical deformation

A step-profile, circular fiber with core and cladding indices n_{co} and n_{cl} is deformed into the slightly elliptical fiber of Fig. 18-2(a) in such a way that the core cross-sectional area is unchanged. If the semi-major and semi-minor axes of the elliptical fiber have lengths ρ_x and ρ_y , and e is the eccentricity, then

$$\rho_x\rho_y = \rho^2; \quad e = \{1 - \rho_y^2/\rho_x^2\}^{1/2} \leq 1, \quad (18-20)$$

where ρ is the radius of the circular fiber. The perturbation region consists of the four shaded regions in Fig. 18-2(a). As each area is very thin, we can approximate $\bar{\Psi}(r, \phi)$ by its value $\bar{\Psi}(\rho, \phi)$ on the circular interface, where r, ϕ are cylindrical polar coordinates as shown. Starting with the equation for the elliptical interface, $(x/\rho_x)^2 + (y/\rho_y)^2 = 1$, and transforming to polar coordinates, the radial width of the perturbation region

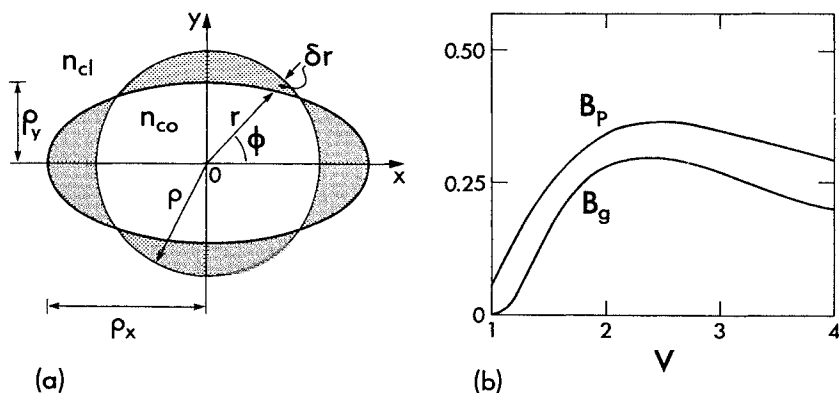


Fig. 18-2 (a) The elliptically deformed, step-profile fiber has the same core cross-sectional area as the circular fiber. (b) The normalized birefringence B_p of Eq. (18-25), together with the Gaussian approximation B_g of Eq. (17-24), are plotted as a function of the fiber parameter.

is $\delta r = (e^2 \rho / 4) \cos 2\phi$, correct to second order in eccentricity. Substituting into Eq. (18-7), the perturbed propagation constant is given by

$$\beta = \bar{\beta} + k(n_{co} - n_{cl})(\eta_x + \eta_y), \quad (18-21a)$$

where $\bar{\beta}$ is the propagation constant on the circular fiber, and η_x and η_y are defined by

$$\eta_x = e^2 \rho^2 \int_0^{\pi/4} \bar{\Psi}^2(\rho, \phi) \cos 2\phi \, d\phi \bigg/ \int_0^\infty \int_0^{2\pi} \bar{\Psi}^2(r, \phi) r \, d\phi \, dr, \quad (18-21b)$$

$$\eta_y = e^2 \rho^2 \int_{\pi/4}^{\pi/2} \bar{\Psi}^2(\rho, \phi) \cos 2\phi \, d\phi \bigg/ \int_0^\infty \int_0^{2\pi} \bar{\Psi}^2(r, \phi) r \, d\phi \, dr, \quad (18-21c)$$

and correspond to the shaded areas which cross the x - and y -axes, respectively.

Fundamental modes

For the fundamental modes on a circular fiber, $\bar{\Psi}$ is independent of ϕ . Consequently $\eta_x = -\eta_y$ and $\beta = \bar{\beta}$ in Eq. (18-21). In other words, *the propagation constants for the circular and elliptical fibers are identical for slight eccentricity, provided the core areas are equal* [6]. The latter condition is equivalent to requiring equal profile volumes, as is clear from Eq. (17-13). Hence the present result is consistent with the more general result of Section 17-3, which showed that, within the Gaussian approximation, $\beta = \bar{\beta}$ on an arbitrary, elliptical-profile fiber of slight eccentricity, provided the profile volumes are equal.

Fields of the elliptical fiber

The approximation $\Psi = \bar{\Psi}$ is inadequate for determining the vector corrections to the scalar propagation constant on the elliptical fiber. In Section 34-8 we use Green's functions to show that correct to second order in eccentricity Ψ is given by

$$\Psi = \frac{J_0(UR)}{J_0(U)} + e^2 \frac{W^2}{8} \frac{J_0(U)}{J_1(U)} \frac{K_2(W)}{K_0(W)} \frac{J_2(UR)}{J_1(U)} \cos 2\phi; \quad 0 \leq R \leq 1, \quad (18-22a)$$

$$= \frac{K_0(WR)}{K_0(W)} + e^2 \frac{W^2}{8} \frac{J_0(U)}{J_1(U)} \frac{J_2(U)}{J_1(U)} \frac{K_2(WR)}{K_0(W)} \cos 2\phi; \quad 1 \leq R < \infty. \quad (18-22b)$$

The J_i 's are Bessel functions of the first kind, the K_i 's are modified Bessel functions of the second kind, $R = r/\rho$, and U, W are defined inside the back cover. The first term on the right denotes the solution $\bar{\Psi}$ for the circular fiber, which is given by F_0 of Table 14-3, page 313. This result can also be derived by using the eigenfunction expansions of Sections 33-9 and 33-10 [7].

Birefringence

By symmetry the fundamental-mode fields of the elliptical fiber are polarized along the x - and y -axes in Fig. 18-2(a). On a step profile, the corrections $\delta\beta_x$ and $\delta\beta_y$ to the scalar propagation constant β can be obtained from Eq. (32-26) by setting $\hat{e}_1 = \Psi\hat{x}$ and $\hat{e}_1 = \Psi\hat{y}$, respectively, where \hat{x} and \hat{y} are unit vectors parallel to the axes. To second order in eccentricity, the birefringence is given by the line integral.

$$\delta\beta_x - \delta\beta_y = \frac{(2\Delta)^{3/2}}{4\pi V} \int_s \left\{ n_x \frac{\partial \Psi}{\partial x} - n_y \frac{\partial \Psi}{\partial y} \right\} \Psi ds \bigg/ \int_0^\infty \bar{\Psi}^2 r dr, \quad (18-23)$$

where s is the elliptical interface and $ds \cong \rho \{1 + \frac{1}{4}e^2 \cos(2\phi)\} d\phi$. The components of the unit outward normal on s parallel to the axes are n_x and n_y , where

$$n_x = (1 - e^2 \sin^2 \phi) \cos \phi; \quad n_y = (1 + e^2 \cos^2 \phi) \sin \phi, \quad (18-24)$$

to this order. We convert Eq. (18-23) to polar coordinates and substitute Eqs. (18-22) with $R = 1$ and (18-24). With the aid of the recurrence relations of Eqs. (37-72) and (37-73), Eq. (37-47) and the eigenvalue equation in Table 14-3, page 313, we obtain [8]

$$\delta\beta_x - \delta\beta_y = \frac{e^2}{\rho} \left(\frac{\Delta}{2} \right)^{3/2} \frac{W^2}{V^3} \left\{ UW^2 \frac{J_0^3(U)}{J_1^3(U)} + (U^2 - W^2) \frac{J_0^2(U)}{J_1^2(U)} + U^2 \right\}. \quad (18-25)$$

The normalized birefringence $B_p = (\delta\beta_x - \delta\beta_y)\rho/e^2\Delta^{3/2}$ is plotted in Fig. 18-2(b) against the circular fiber parameter V , using the values of U and W from Table 14-4, page 314. There is a peak at $V \cong 2.48$ when $d(\beta + \delta\beta_x)/dV = d(\beta + \delta\beta_y)/dV$, i.e. the two fundamental modes have the same group velocity. For comparison, we also plot the corresponding normalized quantity B_g , calculated from the Gaussian approximation of Eq. (17-24). This is given by the lower curve in Fig. 18-2(b), where there is a relative

difference of 19% at $V = 2.48$ and the peak is shifted to $V = 2.33$. Otherwise the two curves have the same characteristic shape.

The ' $l = 1$ ' mode set

We next consider the modes of the elliptical fiber which correspond to the $l = 1$ modes of the circular fiber. The two solutions of the scalar wave equation for the latter are given by

$$\bar{\Psi}_e = F_1(R) \cos \phi; \quad \bar{\Psi}_o = F_1(R) \sin \phi, \quad (18-26)$$

where F_1 is expressed in Table 14-6, page 319, and the propagation constants have the common value $\bar{\beta}$. There is no cancellation of integrals over the shaded areas in Fig. 18-2(a) as there was for the fundamental modes. Instead we deduce from Eq. (18-21) and the integral in Table 14-6 that

$$\eta_x + \eta_y = \pm \frac{e^2 U^2}{4 V^2} \frac{K_1^2(W)}{K_0(W)K_2(W)}, \quad (18-27)$$

where + and - signs refer to even and odd solutions, the K_i 's are modified Bessel functions of the second kind, and other parameters are defined inside the back cover. The propagation constants β_e and β_o on the elliptical fiber follow from Eq. (18-21a), and, in particular, their difference is given by

$$\beta_e - \beta_o = \frac{e^2 (2\Delta)^{1/2} U^2}{4 \rho V} \frac{K_1^2(W)}{K_0(W)K_2(W)}, \quad (18-28)$$

since $\Delta \cong (1 - n_{cl}/n_{co})$ within the weak-guidance approximation.

The nearly circular fiber

The polarization of the transverse electric field as the fiber changes from elliptical to circular cross-section is shown qualitatively in Fig. 18-3(a) for the four $l = 1$ modes. Here we examine the transition region between the two extremes, as discussed in Section 13-9. The transition is described quantitatively by the parameter Λ of Table 13-1, page 288. Substituting from Eq. (18-28) and Table 14-6, page 319, the absolute value of Λ is given by [9]

$$|\Lambda_{\pm}| = \frac{e^2 V^2}{8 \Delta} \left| 1 \mp \frac{W K_0(W)}{2 K_1(W)} \right|^{-1}, \quad (18-29)$$

where + and - signs denote $\delta\beta_1 - \delta\beta_2$ and $\delta\beta_3 - \delta\beta_4$, respectively, in the denominator of Λ . The fields follow from Table 13-1. Plots of the normalized parameters $2\Delta|\Lambda_{\pm}|/e^2$ appear in Fig. 18-3(b). The minimum values of $|\Lambda_+|$ and $|\Lambda_-|$ are approximately e^2/Δ , so that only a slight eccentricity is required for the elliptical modes to be linearly polarized, since $\Delta \ll 1$ on the weakly guiding fiber. When $V = 3.8$, there is no difference between $\delta\beta_1$ and $\delta\beta_2$, and $|\Lambda_+| = \infty$. At this special value, the linearly polarized modes

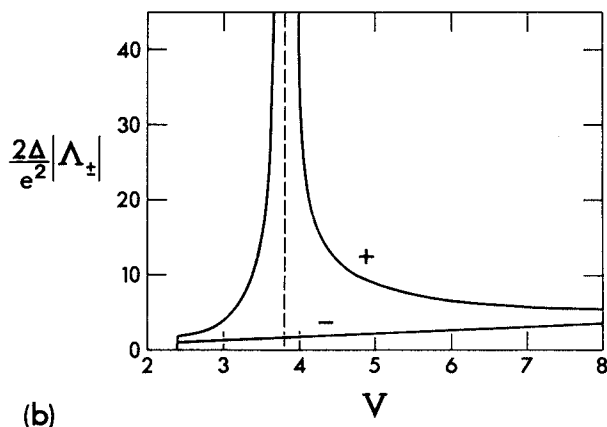
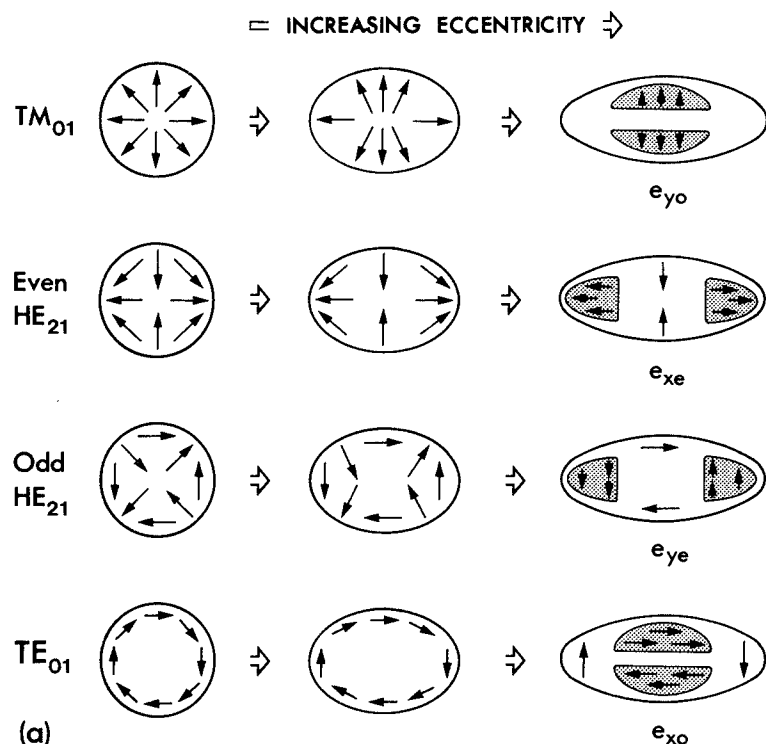


Fig. 18-3 (a) The transition of the $l = 1$ modes from the circular to elliptical fiber, where arrows denote the direction of the transverse electric field and the notation is defined by Eq. (32-42) and Fig. 32-1. (b) Plots of the normalized parameter $2\Delta|\Lambda \pm|/e^2$ of Eq. (18-29) as a function of fiber parameter. The modes are cut off at $V = 2.4$ and the vertical dashed line corresponds to $V = 3.8$.

are modes of both the elliptical and circular fibers, for reasons explained in Section 14-7.

18-11 Nonuniform changes in profile

When the perturbation is nonuniform, the difference between the perturbed and unperturbed refractive-index profiles varies with position, i.e.

$$n(x, y) = \bar{n}(x, y) + \delta n(x, y), \quad (18-30)$$

replaces Eq. (18-6). This complicates evaluation of the integral in the numerator of Eq. (18-5), and the simple interpretation of Eq. (18-7) no longer applies. However, some simplification is possible if we approximate $\bar{\Psi}$ by the Gaussian approximation of Chapters 15 and 17.

Consider, for example, a circular fiber which has a perturbation with the Gaussian dependence

$$\delta n(r) = \delta n(0) \exp\{-(r/a)^2\}; \quad |\delta n(r)| \ll n(r), \quad (18-31)$$

where a is a length scale. If we approximate $\bar{\Psi}^2$ by the Gaussian function $\exp(-r^2/r_0^2)$ for the fundamental modes, where r_0 is the spot size of Table 15-1, page 339, then we deduce from Eq. (18-5) with $n - \bar{n} = \delta n(r)$ that

$$\beta = \bar{\beta} + k \delta n(0) \frac{a^2}{a^2 + r_0^2}. \quad (18-32)$$

It remains to substitute the spot size. Examples are given in Table 15-2, page 340.

MODES OF TWO PARALLEL FIBERS

So far in this chapter we have examined perturbations which involve only a single fiber. Now we consider perturbations due to the introduction of a second fiber parallel to the first fiber. The composite two-fiber waveguide has the cross-section shown in Fig. 18-4. This waveguide is of practical interest, since it exhibits the phenomenon of optical cross-talk which is discussed below and in Chapter 29. We are primarily interested in pairs of identical, or nearly identical fibers, when, unlike the single-fiber perturbations discussed above, the fields of one fiber in isolation are not a good approximation to the fields of the composite waveguide. However, if the fibers are optically well separated, i.e. the contribution from one fiber to the field at the centre of the second fiber is small, and if they are also weakly guiding, then the fields of the composite waveguide are well approximated by a superposition of the fields of each fiber in isolation from the other. The restriction to weakly guiding fibers is more

than a convenient simplification. There is no known simple perturbation procedure for arbitrary index fibers, for reasons given in Section 18–21 below.

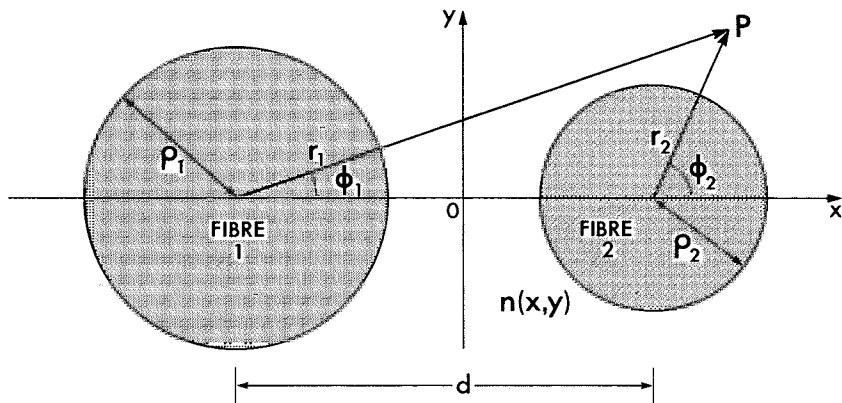


Fig. 18-4 Cross-section of the composite waveguide comprises two fibers of core radii ρ_1 and ρ_2 with refractive-index profile $n(x, y)$. The point P is defined by cylindrical polar coordinates r_1, ϕ_1 and r_2, ϕ_2 relative to the fiber axes, which are distance d apart.

Polarization and number of modes

On a single-fiber waveguide there are two orthogonally polarized fundamental modes whose fields are constructed from the fundamental solution of the scalar wave equation by the methods of Chapter 13. However, when two fibers are present, the symmetry of the composite waveguide doubles the number of modes which can propagate. Thus there are *two* fundamental solutions of the scalar wave equation, leading to two pairs of orthogonally polarized fundamental modes, i.e. *four* modes which are not generally cut off. Similarly, each set of four higher-order modes of the single fiber is replaced by a set of *eight* modes of the composite waveguide. Given each solution of the scalar wave equation for the composite waveguide, the polarization of the modal fields is determined by the methods of Chapter 13, i.e. either by symmetry or by perturbation methods.

Propagation constants

The propagation constants associated with the two fundamental-mode solutions of the scalar wave equation are generally distinct because of the

asymmetry of the composite waveguide. Hence we anticipate that the waveguide will exhibit characteristics similar to those of the anisotropic fiber of Section 18-9. In particular, *cross-talk can be explained by scalar theory alone*. Polarization corrections to the scalar propagation constants are required to distinguish between the two pairs of x - and y -polarized modes. However, as we show in Example 18-14 below, the length scale over which polarization corrections manifest themselves along the waveguide greatly exceeds that over which cross-talk is significant.

Notation

The composite waveguide has refractive-index profile $n(x, y)$ relative to the axes in Fig. 18-4, and its modal fields in Eq. (18-1) are expressed in terms of $\Psi(x, y)$ of Eq. (18-3a) through Table 13-1, page 288. In isolation, the unperturbed fiber 1 has refractive-index profile $\bar{n}_1(x, y)$ and scalar wave equation solution $\bar{\Psi}_1(x, y)$, relative to the axes in Fig. 18-4. The corresponding quantities for the perturbing fiber are $\bar{n}_2(x, y)$ and $\bar{\Psi}_2(x, y)$. We note that, in general, $n \neq \bar{n}_1 + \bar{n}_2$.

18-12 Fundamental modes of identical fibers

When the two fibers in Fig. 18-4 are identical and well separated, the symmetry of the composite waveguide dictates that the two fundamental solutions Ψ_+ and Ψ_- of the scalar wave equation are given approximately by [9]

$$\Psi_+ = \bar{\Psi}_1 + \bar{\Psi}_2; \quad \Psi_- = \bar{\Psi}_1 - \bar{\Psi}_2, \quad (18-33)$$

where $\bar{\Psi}_1$ and $\bar{\Psi}_2$ are the fundamental solutions for each fiber in isolation, referred to the common axes in Fig. 18-4. If these combinations are not obvious, they can be deduced from the perturbation theory in Section 18-18 below.

Propagation constants

The propagation constants associated with Ψ_+ and Ψ_- are β_+ and β_- , respectively, while $\bar{\beta}$ is the propagation constant common to $\bar{\Psi}_1$ and $\bar{\Psi}_2$. When the fiber separation is infinite, then $\beta_+ = \beta_- = \bar{\beta}$. For sufficiently large separation we set $\beta = \beta_{\pm}$, $\Psi = \Psi_{\pm}$, $\bar{n} = \bar{n}_1$, $\bar{\Psi} = \bar{\Psi}_1$ in Eq. (18-4) and use the simplifying approximations above Eq. (18-5) to obtain

$$\beta_{\pm} = \bar{\beta} + k \left\{ \int_{A_{\infty}} (n - \bar{n}_1) \bar{\Psi}_1 \Psi_{\pm} dA \right\} / \int_{A_{\infty}} \bar{\Psi}_1 \Psi_{\pm} dA, \quad (18-34)$$

where n denotes the composite profile, A_∞ is the infinite cross-section, $k = 2\pi/\lambda$ and λ is the free-space wavelength. Since the fibers are assumed to be electromagnetically well separated, we can simplify this expression by ordering the terms in the integrals. We substitute for Ψ_\pm from Eq. (18-33) and note that $\bar{\Psi}_2$ is exponentially small over the core of the unperturbed fiber. Thus the integral of $\bar{\Psi}_1\bar{\Psi}_2$ is negligible compared with the integral of $\bar{\Psi}_1^2$ in the denominator. In the numerator $n - \bar{n}_1$ vanishes over the core of the unperturbed fiber, so the dominant contribution to the integral comes from the core of the perturbing fiber 2. A similar argument applies to profiles with no well-defined interface. Hence Eq. (18-34) is well approximated by

$$\beta_\pm = \bar{\beta} \pm C; \quad C = k \left\{ \int_{A_x} (n - \bar{n}_1) \bar{\Psi}_1 \bar{\Psi}_2 dA \right\} / \int_{A_x} \bar{\Psi}_1^2 dA, \quad (18-35)$$

where $C \rightarrow 0$ exponentially with increasing separation.

Polarization corrections

The four fundamental modes of the two identical fibers are composed of pairs of symmetric and antisymmetric modes corresponding, respectively, to Ψ_+ and Ψ_- of Eq. (18-33). By symmetry the transverse electric fields are polarized parallel to either the x - or y -axes, as shown in Fig. 18-5. If subscripts x, y denote polarization and $+, -$ denote symmetry, then

$$e_{x+} = e_{y+} = \Psi_+; \quad e_{x-} = e_{y-} = \Psi_- \quad (18-36)$$

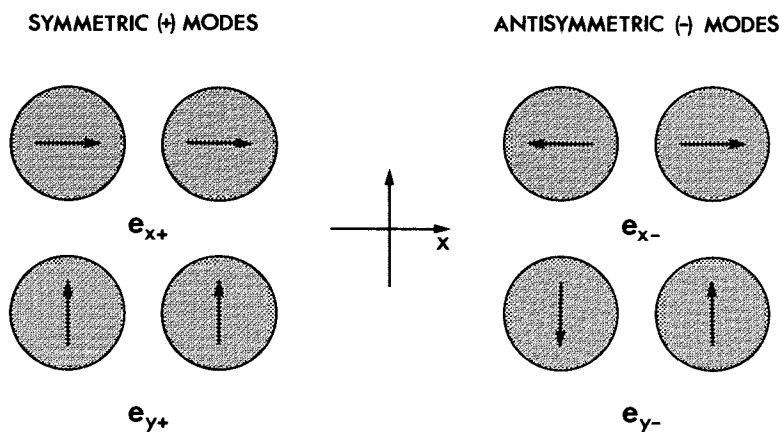


Fig. 18-5 Orientation of the transverse electric field for the four fundamental modes of a pair of identical fibers.

The corresponding polarization corrections $\delta\beta_{x+}$, $\delta\beta_{y+}$ and $\delta\beta_{x-}$, $\delta\beta_{y-}$ to the scalar propagation constants β_+ and β_- , respectively, are obtained by substituting the appropriate field into Eq. (13–11).

18–13 Cross-talk between identical fibers

Consider a composite waveguide consisting of two well-separated, identical fibers which, in isolation from one another, are single moded. The fundamental solutions, Ψ_{\pm} , and scalar propagation constants, β_{\pm} , for the composite waveguide were discussed in the previous section. Here we show that the phenomenon of *optical cross-talk*, whereby light initially in one fiber transfers to the other fiber during propagation, is a consequence of interference between the modal fields associated with the *scalar* solutions Ψ_+ and Ψ_- . We consider this problem again in Chapter 29.

We assume that only x -polarized modes are involved. Hence the magnitude E of the total transverse electric field is given everywhere by

$$E = b_+ \Psi_+ \exp(i\beta_+ z) + b_- \Psi_- \exp(i\beta_- z), \quad (18-37)$$

where b_+ and b_- are modal amplitudes. Because of the large separation, we may assume approximately that, at the endface $z = 0$ of the composite waveguide, the first fiber is illuminated with unit power and there is zero power in the neighborhood of the second fiber, i.e. $E = 0$. We deduce from Eq. (18–33) that $\Psi_+ \cong -\Psi_- \cong \bar{\Psi}_2$ close to the second fiber, whence at $z = 0$ Eq. (18–37) gives $b_+ \cong b_-$. For finite z , the field E_2 in the cross-section of the second fiber follows from Eqs. (18–37) and (18–35) as

$$E_2 = 2ib_+ \bar{\Psi}_2 \exp(i\bar{\beta}_2 z) \sin(Cz), \quad (18-38a)$$

and similarly the corresponding field for the first fiber is

$$E_1 = 2b_+ \bar{\Psi}_1 \exp(i\bar{\beta}_1 z) \cos(Cz). \quad (18-38b)$$

Power transfer and beat length

The power flow $P_1(z)$ or $P_2(z)$ in each fiber is obtained by integrating the intensity $(n_{co}/2)(\epsilon_0/\mu_0)^{1/2} |E_1|^2$ or $(n_{co}/2)(\epsilon_0/\mu_0)^{1/2} |E_2|^2$ over the infinite cross-section. Since by assumption $P_1(0) = 1$ and $P_2(0) = 0$, we deduce from Eq. (18–38) that

$$P_1(z) = \cos^2(Cz); \quad P_2(z) = \sin^2(Cz). \quad (18-39)$$

Thus power is conserved and unit total power flows along the composite waveguide. Furthermore, light power oscillates from one fiber to the other in a manner analogous to the behavior of a pair of coupled, identical pendulums.

If z_b denotes the *beat length*, i.e. the distance along the waveguide in which there is total transfer of power from one fiber to the other fiber and back again, then Eqs. (18-35) and (18-39) give

$$z_b = \frac{2\pi}{C} = \frac{4\pi}{\beta_+ - \beta_-}. \quad (18-40)$$

As the separation increases, $\beta_+ \rightarrow \beta_-$ and the beat length becomes exponentially large. The transfer of power is clearly a consequence of *interference*, or *beating*, between the fundamental mode fields in Eq. (18-37), and depends only on the difference between the *scalar* propagation constants. There is no need to consider polarization corrections to the propagation constants in order to study cross-talk on the composite waveguide.

18-14 Example: Two step-profile fibers

The composite waveguide consists of two identical, step-profile fibers of core radius $\rho = \rho_1 = \rho_2$ in Fig. 18-4 and center-to-center separation d . In isolation the fibers are single moded. Within each core $n = n_{co}$, and $n = n_{cl}$ in the surrounding medium, while $\bar{n}_1 = n_{co}$ over the core of the first fiber and $n_1 = n_{cl}$ elsewhere.

Beat length

To calculate C of Eq. (18-35) we note that $n - \bar{n}_1$ is nonzero only over the core of the second fiber, and that the integral in the denominator is proportional to the normalization N of Table 13-2, page 292. Expressions for $\bar{\Psi}_1$, $\bar{\Psi}_2$ and N are deduced from Table 14-3, page 313. If r_1 , ϕ_1 and r_2 , ϕ_2 denote cylindrical polar coordinates based on the fiber axes in Fig. 18-4, then

$$C = \frac{1}{\pi \rho^3} \left(\frac{\Delta}{2} \right)^{1/2} \frac{U^2}{V} \frac{K_0(W)}{K_1^2(W) J_0(U)} \int_0^{2\pi} \int_0^\rho r_2 K_0(W r_1 / \rho) J_0(U r_2 / \rho) dr_2 d\phi_2, \quad (18-41)$$

where parameters are defined inside the back cover and apply to either fiber, assuming $\Delta \cong 1 - n_{cl}/n_{co}$. We use the expansion of Eq. (37-81) to express $K_0(W r_1 / \rho)$ in terms of r_2 and ϕ_2 . The ϕ_2 integration reduces the expansion to a single term, which involves the modified Bessel function of the first kind $I_0(W r_2 / \rho)$, and the r_2 integration follows from Eq. (37-99). This introduces the factor $W J_0(U) I_1(W) + U J_1(U) I_0(W)$ which reduces to $J_0(U)/K_0(W)$ with the help of the eigenvalue equation in Table 14-3 and the Wronskian of Eq. (37-79). Hence we obtain

$$C = \frac{(2\Delta)^{1/2}}{\rho} \frac{U^2}{V^3} \frac{K_0(W d / \rho)}{K_1^2(W)} \cong \left\{ \frac{\pi \Delta}{W d \rho} \right\}^{1/2} \frac{U^2 \exp(-W d / \rho)}{V^3 K_1^2(W)}. \quad (18-42)$$

The approximate form follows from Eq. (37-88) and is no less accurate than the first

form since the fibers are assumed to be well separated electro-magnetically, i.e. $Wd/\rho \gg 1$. Substitution of Eq. (18-42) into Eq. (18-40) leads to the exponential dependence of beat length on separation as anticipated in the previous section. We return to this problem in more detail in Chapter 29.

Polarization corrections to the propagation constants

The scalar propagation constants β_+ and β_- for the fundamental modes of the composite waveguide are given by Eq. (18-35) in terms of the fundamental mode propagation constant $\bar{\beta}$ for either fiber in isolation and C of Eq. (18-42). We explained in Section 13-5 that polarization corrections are required to correctly distinguish between the propagation constants of each pair of fundamental modes associated with β_+ or β_- . To determine each correction, we substitute the approximate transverse electric field of Eq. (18-36) into Eq. (13-12), where l now denotes the interface of both fibers. Thus, in the notation of Section 18-12, and with the help of Eqs. (18-36) and (18-33), we obtain $\delta\beta_{x\pm}$ by setting

$$\mathbf{e}_t = \hat{\mathbf{x}}e_{x\pm} = \hat{\mathbf{x}}\Psi_{\pm} = \hat{\mathbf{x}}(\bar{\Psi}_1 \pm \bar{\Psi}_2), \quad (18-43)$$

where $\hat{\mathbf{x}}$ is the unit vector parallel to the x -axis in Fig. 18-4. We simplify Eq. (13-12) using arguments similar to those below Eq. (18-34). In the denominator the integral of the cross-term $\pm 2\bar{\Psi}_1\bar{\Psi}_2$ is exponentially small compared with the integral of $\bar{\Psi}_1^2 + \bar{\Psi}_2^2$, which is proportional to *twice* the normalization of the Table 14-3, page 313. By ignoring products of exponentially small terms, the integral in the numerator is expressible in terms of the coordinates of Fig. 18-4 giving

$$\delta\beta_{x\pm} = \frac{(2\Delta)^{3/2}}{2\pi} \frac{U^2}{V^3} \frac{K_0^2(W)}{K_1^2(W)} \int_0^{2\pi} \left\{ \bar{\Psi}_2 \frac{\partial \bar{\Psi}_2}{\partial x} \pm \frac{\partial}{\partial x} (\bar{\Psi}_1 \bar{\Psi}_2) \right\} \cos \phi_2 d\phi_2, \quad (18-44)$$

where Table 14-3, page 313, and Fig. 18-4 give

$$\bar{\Psi}_1 = \frac{K_0(Wr_1/\rho)}{K_0(W)}; \quad \bar{\Psi}_2 = \frac{K_0(Wr_2/\rho)}{K_0(W)}, \quad (18-45a)$$

$$\frac{\partial}{\partial x} = -\frac{\sin \phi_2}{\rho} \frac{\partial}{\partial \phi_2} + \cos \phi_2 \frac{\partial}{\partial r_2}, \quad (18-45b)$$

where $\partial/\partial r_2$ is evaluated on $r_2 = \rho$, and parameters are defined at the back of the book. We expand $K_0(Wr_1/\rho)$ in terms of r_2 and ϕ_2 through Eq. (37-81) and perform the integration to obtain

$$\begin{aligned} \delta\beta_{x\pm} = & -\frac{(2\Delta)^{3/2}}{2\rho} \frac{U^2 W K_0}{V^3 K_1} \left\{ 1 \pm \left(\frac{I_0}{K_0} - \frac{I_1}{K_1} \right) K_0(Wd/\rho) \right. \\ & \left. \pm \left(\frac{I_2}{K_0} - \frac{I_1}{K_1} \right) K_2(Wd/\rho) \right\}, \end{aligned} \quad (18-46)$$

where $I_l = I_l(W)$ and $K_l = K_l(W)$. Similarly $\delta\beta_{y\pm}$ is given by the same expression with the sign of $K_2(Wd/\rho)$ reversed. The common factor on the right is the polarization

correction for either fiber in isolation. Terms involving the fiber separation d arise from the interaction between fibers. As the fibers are well separated, some simplification is possible if we replace $K_0(Wd/\rho)$ and $K_2(Wd/\rho)$ by their asymptotic forms of Eq. (37-88).

The polarization corrections cause interference effects between pairs of fundamental modes with the same propagation constant. For example, if the modes associated with β_+ are excited, the difference between $\delta\beta_{x+}$ and $\delta\beta_{y+}$ accounts for the apparent rotation of the total transverse fields as they propagate [9]. This was examined in Section 14-7, and can be characterized by a beat length $4\pi/(\delta\beta_{x+} - \delta\beta_{y+})$. We can compare the cross-talk beat length of Eq. (18-40) with the rotation beat length. For large separation, Eqs. (18-40), (18-42) and (37-88) give

$$\left| \frac{\delta\beta_{x+} - \delta\beta_{y+}}{\beta_+ - \beta_-} \right| \cong 2\Delta W \{I_2(W)K_1(W) - I_1(W)K_0(W)\}. \quad (18-47)$$

Since $\Delta \ll 1$, cross-talk is the dominant effect regardless of separation.

18-15 Example: Double parabolic-profile waveguide

We next consider the fundamental modes of the double parabolic profile waveguide, which has the profile of Eq. (16-30), illustrated in Fig. 16-2(b). Despite the fact that such a waveguide is unphysical for the reasons given in Section 14-4, it provides the simplest perturbation problem for any two-fiber waveguide. The unperturbed fiber has the infinite parabolic profile

$$\bar{n}_1^2 = n_{co}^2 \{1 - 2\Delta[(x/\rho + d/2\rho)^2 + (y/\rho)^2]\}, \quad (18-48)$$

where ρ is the scaling length, and the perturbing fiber has the same profile except that the sign of d is reversed. By appropriately modifying the solution in Table 14-2, page 307, the fundamental-mode solution of the scalar wave equation for each fiber in isolation is given by

$$\bar{\Psi}_{1,2} = \exp \left\{ -\frac{V}{2} \left[\frac{(2x \pm d)^2}{4\rho^2} + \frac{y^2}{\rho^2} \right] \right\}, \quad (18-49)$$

where + and - refer to 1 and 2, respectively, and V is defined inside the back cover. To calculate C , we substitute Eqs. (16-30), (18-48) and (18-49) into Eq. (18-35), set $n - \bar{n}_1 \cong (n^2 - \bar{n}_1^2)/2n_{co}$, and deduce the integral in the denominator from the normalization expression in Table 14-2. Noting that $n^2 - \bar{n}_1^2$ is nonzero only for $x > 0$, straightforward integration over x and y leads to

$$C = \left(\frac{V\Delta}{2\pi} \right)^{1/2} \frac{d}{\rho^2} \exp \left\{ -\frac{V}{4} \frac{d^2}{\rho^2} \right\}; \quad d \gg \frac{2\rho}{V^{1/2}}, \quad (18-50)$$

since the fibers are assumed well separated. The Gaussian dependence of C on separation, instead of the simple exponential dependence of Eq. (18-42) for step-profile fibers, is a consequence of the infinite variation of the parabolic profile. The scalar

propagation constants follow from Eq. (18–35) and Table 14–2, and the polarization corrections can be simply determined from Eq. (13–11) by paralleling the derivation in the previous example.

Comparison with exact solution

We derived the exact solution of the scalar wave equation for the double parabolic profile in Section 16–8. The propagation constants for the fundamental modes are given implicitly by the eigenvalue equations of Eq. (16–35). If the normalized separation is sufficiently large to satisfy $d/\rho \gg 2/V^{1/2}$, it can be readily verified that the asymptotic forms of the parabolic cylinder functions lead to the perturbation solutions β_+ and β_- derived above. Similarly, the accuracy of the superposition approximation of Eq. (18–33) can also be shown. We refer elsewhere for details [10].

18–16 Higher-order modes of identical fibers

We showed in Section 14–3 that there are four modes associated with each value $l > 0$ on a circular fiber. If $\bar{\Psi}_1$ and $\bar{\Psi}_2$ denote the same scalar wave equation solution for one of these modes relative to identical fibers 1 and 2 in Fig. 18–4, then, by symmetry, the two corresponding perturbation solutions Ψ_+ and Ψ_- of the composite waveguide are given by Eq. (18–33). Thus the four modes of the circular fiber correspond to eight modes of the composite waveguide. According to Section 13–8, each higher-order mode has a transverse electric field which is uniformly polarized parallel to the x - or y -axis in Fig. 18–4, as is clear from symmetry. Only when the fiber separation is infinite do we recover the polarization patterns of the circular fiber, e.g. the transition in Fig. 18–6(a) for the mode which reduces to a superposition of two even HE_{21} modes. This transition was discussed qualitatively in Section 13–9. In the following example we show quantitatively how the transition depends on separation.

18–17 Example: Two step-profile fibers

The change from the uniformly polarized modes of the composite waveguide to the $l = 1$ patterns of the single fiber can be described quantitatively by Λ of Table 13–1, page 288. We take β_e and β_o to be the propagation constants for the even and odd scalar solutions

$$\Psi_{+e} = \bar{\Psi}_{1e} + \bar{\Psi}_{2e} = F_1(r_1/\rho) \cos \phi_1 + F_1(r_2/\rho) \cos \phi_2, \quad (18-51a)$$

$$\Psi_{+o} = \bar{\Psi}_{1o} + \bar{\Psi}_{2o} = F_1(r_1/\rho) \sin \phi_1 + F_1(r_2/\rho) \sin \phi_2, \quad (18-51b)$$

respectively, in the notation of Fig. 18–4, where $\rho = \rho_1 = \rho_2$ and F_1 is defined in Table

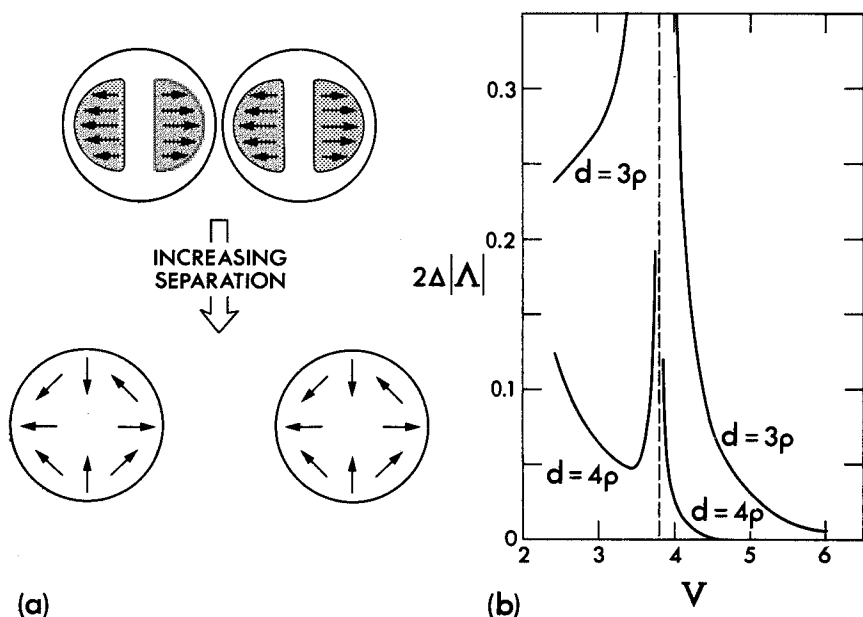


Fig. 18-6 (a) The transition of an $l = 1$ mode of the two-fiber waveguide to the superposition of two even HE_{21} modes, where arrows denote the direction of the transverse electric field. (b) Plots of the normalized parameter $2\Delta|\Lambda|$ of Eq. (18-53) as a function of the fiber parameter for various values of d/ρ . The mode is cut off at $V = 2.4$ and the vertical dashed line corresponds to $V = 3.8$.

14-6, page 319. To calculate β_e , it is adequate to use Eq. (18-35) with $\bar{\Psi}_1 = \bar{\Psi}_{1e}$, $\bar{\Psi}_2 = \bar{\Psi}_{2e}$, and similarly for β_o . By paralleling the development in Section 18-14, it is readily verified that

$$\beta_e - \beta_o = \frac{(2\Delta)^{1/2}}{\rho} \frac{U^2}{V^3} \frac{K_2(Wd/\rho)}{K_0(W)K_2(W)}. \quad (18-52)$$

Finally, by substituting from Table 14-6, we deduce from Table 13-1, page 288, that [9]

$$|\Lambda| = \frac{1}{2\Delta} \frac{K_2(Wd/\rho)}{K_1^2(W)} \left| 1 - \frac{W}{2} \frac{K_0(W)}{K_1(W)} \right|^{-1}. \quad (18-53)$$

The quantity $2\Delta|\Lambda|$ is plotted in Fig. 18-6(b) as a function of the parameter V for either fiber and for various values of the normalized separation d/ρ . Corresponding values of W are generated from the $l = 1$ eigenvalue equation in Table 14-6. The composite waveguide behaves as two fibers in isolation from one another if $\Lambda \rightarrow 0$. This occurs if the separation is large or $V \gg 1$. In the latter case, modal power is essentially confined to the fiber cores and the evanescent cladding field is very small. For $V = 3.8$, the modes of

the composite waveguides are uniformly polarized for arbitrary separation, for reasons explained in Sections 14-7 and 18-10.

18-18 Fundamental modes of nonidentical fibers

It is convenient to distinguish between pairs of distinctly different fibers, and pairs that are nearly identical.

Distinctly different fibers

Consider two parallel fibers which are significantly different from one another, e.g. the unequal core radii of Fig. 18-4. The fundamental solution of Eq. (18-33) for the composite waveguide is inappropriate because of the lack of symmetry. However, because of the dissimilarity it is intuitive that the fundamental-mode fields of the composite waveguide are just the corresponding fields of either fiber in isolation. Hence, provided the fibers are electromagnetically well separated, we have in the notation of Section 18-12

$$\Psi_+ = \bar{\Psi}_1, \quad \beta_+ = \bar{\beta}_1; \quad \Psi_- = \bar{\Psi}_2, \quad \beta_- = \bar{\beta}_2, \quad (18-54)$$

where $\bar{\beta}_1$ and $\bar{\beta}_2$ are the fundamental mode propagation constants for each fiber.

Nearly identical fibers

Clearly there must be a transition from the fundamental solutions of Eq. (18-54) to those of Eq. (18-33) as the fibers become similar. In the situation where the fibers are nearly identical, the fundamental-mode solutions of the composite waveguide may be expressed, for later comparison with Eq. (18-33), in the general form

$$\Psi_+ = \frac{\bar{\Psi}_1 + a_+ \bar{\Psi}_2}{(1 + a_+^2)^{1/2}}; \quad \Psi_- = \frac{\bar{\Psi}_1 + a_- \bar{\Psi}_2}{(1 + a_-^2)^{1/2}}, \quad (18-55)$$

using the notation of Section 18-12, and a_+ , a_- are constants. To determine the constants and the corresponding propagation constants β_+ and β_- , we set $\bar{\Psi} = \bar{\Psi}_1$, $\bar{\beta} = \bar{\beta}_1$, $\bar{n} = \bar{n}_1$ and $\Psi = \Psi_{\pm}$ of Eq. (18-55) in Eq. (18-4). The fibers are assumed to be well separated, so we can parallel the arguments leading from Eq. (18-34) to Eq. (18-35), and, with the help of the approximations above Eq. (18-5), obtain

$$\beta_{\pm} = \bar{\beta}_1 + a_{\pm} C_{12}, \quad (18-56a)$$

where β_{\pm} denotes β_+ or β_- , a_{\pm} denotes a_+ or a_- , and $C_{12} = C$ of Eq. (18-35).

A second equation is derived similarly by setting $\bar{\Psi} = \bar{\Psi}_2$, $\bar{\beta} = \bar{\beta}_2$ and $\bar{n} = \bar{n}_2$ in Eq. (18-4) with $\Psi = \Psi_{\pm}$ as before. This leads to

$$a_{\pm} \beta_{\pm} = a_{\pm} \bar{\beta}_2 + C_{21}, \quad (18-56b)$$

where C_{21} is given by C of Eq. (18-35) with subscripts interchanged. Elimination of a_{\pm} between these two equations gives the consistency condition for nontrivial solutions. Within the accuracy of Eq. (18-56) we can set $C_{12} \cong C_{21} \cong C$ since the fibers are nearly identical. Hence the propagation constants are given by

$$\beta_{\pm} = \frac{\bar{\beta}_1 + \bar{\beta}_2}{2} \pm \frac{C}{F}; \quad F = 1 / \left\{ 1 + \frac{(\bar{\beta}_1 - \bar{\beta}_2)^2}{4C^2} \right\}^{1/2}, \quad (18-57)$$

where $0 \leq F \leq 1$. Substitution of Eq. (18-57) into Eq. (18-56) gives

$$a_{\pm} = \frac{\bar{\beta}_2 - \bar{\beta}_1}{2C} \pm \frac{1}{F}. \quad (18-58)$$

When the fibers are identical $\bar{\beta}_1 = \bar{\beta}_2$, whence $F = 1$, $a_{\pm} = \pm 1$ and Eq. (18-55) reduces to Eq. (18-33) apart from an amplitude factor. If the fibers differ significantly $|\bar{\beta}_1 - \bar{\beta}_2| \gg 2C$, whence $F \rightarrow 0$, $a_{+} \rightarrow 0$, $a_{-} \rightarrow \infty$ and Eq. (18-55) reduces to Eq. (18-54). We recall from Eq. (18-35) that C decreases exponentially with increasing separation. Consequently, however slight the difference between fibers, $F \rightarrow 0$ provided the separation is large enough, and the fibers behave as if isolated from one another.

18-19 Example: Two step-profile fibers of similar core radii

Consider a composite waveguide consisting of two step-profile fibers of core radii ρ and $\rho + \delta\rho$, and common core and cladding indices n_{co} and n_{cl} . Using the notation of the previous section, the difference $\bar{\beta}_1 - \bar{\beta}_2$ in fundamental-mode propagation constants is given by $\beta - \bar{\beta}$ of Eq. (18-13a), and C follows from Eq. (18-42), assuming the fibers are well separated. Hence

$$\frac{\bar{\beta}_1 - \bar{\beta}_2}{2C} = \frac{\delta\rho}{\rho} \left(\frac{2Wd}{\pi\rho} \right)^{1/2} V^2 K_0^2(W) \exp(Wd/\rho), \quad (18-59)$$

where parameters are defined at the back of the book. For a separation $d = 4\rho$ and $V = 2.4$, we deduce from Table 14-4, page 314, that the value on the right is approximately $280 \delta\rho/\rho$. Hence for a 1% change in core radius, Eq. (18-57) gives $F \cong 0.3$.

18-20 Cross-talk between nonidentical fibers

The discussion of cross-talk in Section 18-13 can also be applied to a pair of nonidentical fibers, provided we use Eq. (18-55) in Eq. (18-37) instead of Eq. (18-33). We again assume the fibers are well separated and the first fiber is illuminated with unit power. The field in the neighborhood of the second fiber is zero at $z = 0$, and this leads to the requirement $a_+ b_+ = -a_- b_-$. Consequently the fields corresponding to Eq. (18-38) can be expressed as

$$E_1 = \frac{b_+}{a_-} \bar{\Psi}_1 \exp\{i(\bar{\beta}_1 + \bar{\beta}_2)z/2\} \left\{ (a_- - a_+) \cos\left(\frac{C}{F} z\right) + i(a_- + a_+) \sin\left(\frac{C}{F} z\right) \right\}, \quad (18-60a)$$

$$E_2 = 2ia_+ b_+ \bar{\Psi}_2 \exp\{i(\bar{\beta}_1 + \bar{\beta}_2)z/2\} \sin\left(\frac{C}{F} z\right). \quad (18-60b)$$

By analogy with Eq. (18-39) we find from Eqs. (18-57) and (18-58) that

$$P_1(z) = 1 - F^2 \sin^2\left(\frac{C}{F} z\right); \quad P_2(z) = F^2 \sin^2\left(\frac{C}{F} z\right). \quad (18-61)$$

Consequently the fraction of total power transferred between the two fibers is F^2 , and the beat length $z_b = 2\pi F/C$. Using the figures from the previous section a 1% difference in core radii of the two fibers results in a maximum exchange of 10% of total power. We consider this problem again in Chapter 29.

MODES OF PERTURBED FIBERS OF ARBITRARY PROFILE

All of the perturbation situations considered so far assume that (i) each fiber is weakly guiding, i.e. only a slight variation in profile, and (ii) the refractive index in the perturbation region is similar to the refractive index in the same region of the unperturbed fiber. Here we show that standard perturbation methods are generally inaccurate for describing the modal fields and propagation constants due to perturbations of fibers with arbitrary refractive-index profiles. The inaccuracy is due to polarization properties of the perturbation region. In certain special cases, alternative methods can be used, as described in the examples below.

Relationship between the modes of the perturbed and unperturbed fibers

We again consider perturbations which do not vary along the length of the fiber. The perturbed fiber with refractive-index profile $n(x, y)$ has unknown

modal fields and propagation constants expressed by Eq. (18-1). Similarly, the unperturbed fiber with *arbitrary* refractive-index profile $\bar{n}(x, y)$ has known modal fields and propagation constants expressed by Eq. (18-2). The two situations can be related exactly through Maxwell's equations, as we show in Section 31-7, and the analogous expression to Eq. (18-4) is given by Eq. (31-39). Dropping suffices we have

$$\beta = \bar{\beta} + k \left(\frac{\epsilon_0}{\mu_0} \right)^{1/2} \frac{\int_{A_\infty} (n^2 - \bar{n}^2) \mathbf{e} \cdot \bar{\mathbf{e}}^* dA}{\int_{A_\infty} \{ \mathbf{e} \times \bar{\mathbf{h}}^* + \bar{\mathbf{e}}^* \times \mathbf{h} \} \cdot \hat{\mathbf{z}} dA}, \quad (18-62)$$

where A_∞ is the infinite cross-section, $\hat{\mathbf{z}}$ is the unit vector parallel to the fiber axis, * denotes complex conjugate and remaining parameters are defined inside the back cover. This expression reduces to Eq. (18-4) when both perturbed and unperturbed fibers are weakly guiding, as may be verified from Table 13-1, page 288.

18-21 Perturbation solution

We consider perturbations for which β and $\bar{\beta}$ of Eq. (18-62) are similar. For convenience, we restrict attention to situations involving only a single fiber. Since $n^2 - \bar{n}^2$ can be arbitrarily large, the perturbation region must either be small or be located far from the fiber axis where the fields are exponentially small. For a sufficiently small perturbation region, the magnetic fields must be similar everywhere, i.e. $\mathbf{h} \cong \bar{\mathbf{h}}$, since Maxwell's equations require that \mathbf{h} be continuous across the boundaries of the perturbation region. However, this is not generally true of the electric fields. The condition $\mathbf{e} \cong \bar{\mathbf{e}}$ holds everywhere, *except within the perturbation region and possibly close to it*. This proviso arises because \mathbf{e} is a solution of Maxwell's equations and must therefore satisfy continuity of the normal component of $n^2 \mathbf{e}$ at a discontinuity in profile. We can best explain this by a simple example.

Step discontinuity

Consider an unperturbed fiber with the step profile of Fig. 18-7. The perturbed profile includes the narrow hatched region. Relative to the cylindrical polar directions in Fig. 14-1, the tangential, i.e. azimuthal and longitudinal components e_ϕ and e_z of the perturbed electric field are continuous across the interfaces at $r = r_1$ and $r = r_2$. Hence $e_z \cong \bar{e}_z$ and $e_\phi \cong \bar{e}_\phi$ *everywhere* including the perturbation region. However, since n changes abruptly from n_{cl} to n_0 at the interfaces, the normal, or radial, component e_r must be discontinuous to ensure continuity of $n^2 \mathbf{e}$. Consequently e_r differs from \bar{e}_r within the perturbation region, the difference

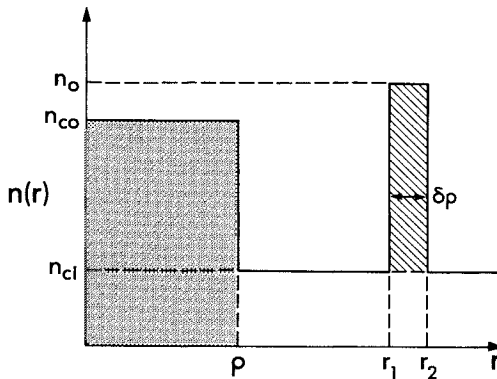


Fig. 18-7 The unperturbed step profile of core radius ρ has arbitrary core and cladding indices n_{co} and n_{cl} . A perturbation of width $\delta\rho \ll \rho$ and arbitrary index n_0 is introduced in the cladding.

increasing as the difference between n_0 and n_{cl} increases. Furthermore, even if $n_0 \cong n_{cl}$, it may be inadequate to assume $e_r \cong \bar{e}_r$ within the perturbation region, as we show in the first example below. A similar argument applies to continuous profiles with rapidly varying perturbations.

It follows from the above discussion that, in general, we may simplify only the denominator of Eq. (18-62) by assuming $\mathbf{e} \cong \bar{\mathbf{e}}$, $\mathbf{h} \cong \bar{\mathbf{h}}$ since the perturbation region gives only a negligibly small contribution to the integral. This leads to

$$\beta = \bar{\beta} + \frac{k}{2} \left(\frac{\epsilon_0}{\mu_0} \right)^{1/2} \frac{\int_{A_p} (n^2 - \bar{n}^2) \mathbf{e} \cdot \bar{\mathbf{e}}^* dA}{\int_{A_\infty} \bar{\mathbf{e}} \times \bar{\mathbf{h}}^* \cdot \hat{\mathbf{z}} dA}, \quad (18-63)$$

where A_p is the cross-section of the perturbation region. Thus, there is no perturbation expression for the arbitrary profile fiber that is analogous to Eq. (18-5) for weakly guiding fibers. This complicates the analysis because we have to find an approximation for the perturbed field \mathbf{e} in the perturbation region. There is no single, universal method for determining \mathbf{e} , and each case needs to be considered individually. We now consider examples.

18-22 Example: Infinitesimal nonuniformity

We reconsider the isolated nonuniformity of Section 18-7. The core profile and the refractive index n_0 of the nonuniformity in Fig. 18-1(c) are now arbitrary, and we assume that δA is sufficiently small that the largest linear dimension satisfies $d_0 \ll \lambda$,

where λ is the free-space wavelength. Under this condition, there is negligible spatial variation in the transverse dependence of the electric field *within* the perturbation region. Consequently, the longitudinal component of the perturbed field, which is continuous across the boundary of the perturbation region, satisfies $e_z \cong \bar{e}_z(\rho_0)$ within the perturbation region, where $x = \rho_0$, $y = 0$ locates the nonuniformity. On the other hand, the transverse electric field, which is discontinuous across the boundary, can be determined using the *quasi-static approximation*, i.e. the implicit time dependence $\exp(-i\omega t)$ is retained, but the transverse spatial dependence $\mathbf{e}_t(\rho_0)$ within the perturbation region is determined by Laplace's equation rather than by Maxwell's equations. The same conclusion can be obtained formally by multiplying the vector wave equation of Eq. (11-40a) by d_0^2 , setting $n = n_0$, and ignoring terms involving powers of d_0/λ . Accordingly, we need to solve the electrostatic problem for an infinitely long dielectric cylinder of uniform refractive index n_0 which is surrounded by a medium of uniform refractive index $\bar{n}(\rho_0)$ and is subjected to a constant transverse field $\bar{\mathbf{e}}_t(\rho_0)$. Solutions are available for elliptical and circular cross-sections [11,12]. For the circular cross-section

$$\mathbf{e}_t(\rho_0) = \frac{2\bar{n}^2(\rho_0)}{\bar{n}^2(\rho_0) + n_0^2} \bar{\mathbf{e}}_t(\rho_0). \quad (18-64)$$

Thus if n_0 and $\bar{n}(\rho_0)$ are sufficiently dissimilar, the perturbed and unperturbed fields can differ greatly within the perturbation region. Even if $n_0 \cong \bar{n}(\rho_0)$ we need to retain Eq. (18-64) without further approximation in order to describe correctly polarization effects due to the nonuniformity, e.g. the difference in fundamental-mode propagation constants.

Fundamental modes of the perturbed step-profile fiber

The direction of the fundamental-mode transverse electric field within the core of an arbitrary step-profile fiber is shown schematically in Fig. 12-6. When the nonuniformity of Fig. 18-1(c) is included, the symmetry of the circular fiber is broken. However, since the nonuniformity is infinitesimal, it is clear that the two fundamental-mode patterns are oriented as shown in Fig. 18-8. The propagation constants associated with Figs. 18-8(a) and 18-8(b) are β_x and β_y , respectively. If we substitute Eq. (18-64) into Eq. (18-63) and recall the normalization definition in Table 11-1, page 230, we obtain

$$\beta_x = \beta + (n_0^2 - n_{\infty}^2) \frac{\delta A}{4} \left(\frac{\epsilon_0}{\mu_0} \right)^{1/2} \frac{k}{N} \left\{ \frac{2n_0^2 |e_x(\rho_0)|^2}{n_0^2 + n_{\infty}^2} + |e_z(\rho_0)|^2 \right\}, \quad (18-65)$$

where n_{∞} is the unperturbed core index, and for clarity we omit the — from unperturbed quantities. Similarly, β_y is given by the same expression with e_x replaced by e_y . The components of \mathbf{e} are deduced from Table 12-3, page 250, by setting $v = 1$ and $R = \rho_0/\rho$. For components associated with β_x , we put $\phi = 0$ in the even HE_{11} mode fields and obtain

$$e_x = -\frac{a_1 J_0(U_0) + a_2 J_2(U_0)}{J_1(U)}; \quad e_z = -\frac{iU}{\rho\beta} \frac{J_1(U_0)}{J_1(U)}, \quad (18-66a)$$

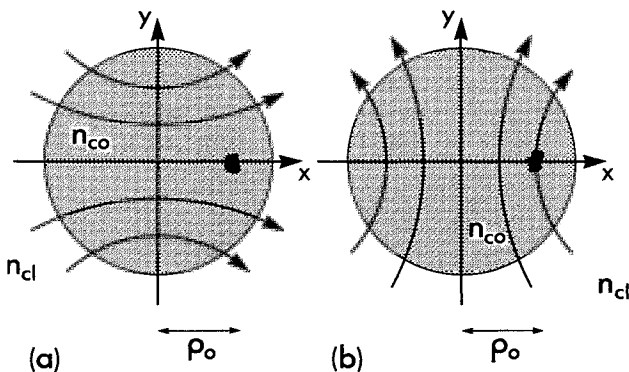


Fig. 18-8 Orientation of the transverse electric field for (a) the x -polarized and (b) the y -polarized fundamental modes on an arbitrary step-profile fiber with an isolated, small nonuniformity.

while for β_y we set $\phi = 0$ in the odd HE_{11} mode fields and get

$$e_y = \sqrt{-\frac{a_1 J_0(U_0) - a_2 J_2(U_0)}{J_1(U)}}; \quad e_z = 0, \quad (18-66b)$$

where $U_0 = U\rho_0/\rho$ and a_1, a_2 are defined in Table 12-3. Hence Eq. (18-65) leads to a measure of the asymmetry, or birefringence, given by

$$\beta_x - \beta_y = \frac{(n_0^2 - n_{co}^2)}{J_1^2(U)} \frac{\delta A}{4} \left(\frac{\epsilon_0}{\mu_0} \right)^{1/2} \frac{k}{N} \left\{ \frac{8a_1 a_2 n_0^2}{n_0^2 + n_{co}^2} J_0(U_0) J_2(U_0) + \frac{U^2}{\rho^2 \beta^2} J_1^2(U_0) \right\}, \quad (18-67)$$

for arbitrary values of n_0 and n_{co} . In the weak-guidance limit $n_0 \cong n_{co}$, and with the help of Tables 12-3, page 250, 12-6, page 260, and 14-3, page 313, the above expression reduces to

$$\beta_x - \beta_y = (2\Delta)^{1/2} \frac{n_0 - n_{co}}{n_{co}} \frac{\delta A}{\pi \rho^3} \frac{\tilde{U}^4}{V^3} \frac{K_0^2(\tilde{W})}{J_1^2(\tilde{U}) K_1^2(\tilde{W})} \left\{ J_1^2(\tilde{U}_0) - 2\tilde{W} \frac{K_0(\tilde{W})}{K_1(\tilde{W})} J_0(\tilde{U}_0) J_2(\tilde{U}_0) \right\}, \quad (18-68)$$

where $\tilde{U}_0 = \tilde{U}\rho_0/\rho$, and parameters are defined at the back of the book. It is clear from Table 12-6 that this result requires e_z correct to order $\Delta^{1/2}$ and e_t correct to order Δ . If we had used $\mathbf{e}_t \cong \bar{\mathbf{e}}_t$ in Eq. (18-63) instead of Eq. (18-64), we would not have obtained Eq. (18-68), even when $n_0 \cong n_{co}$.

18-23 Example: Change in core radius

The effect of a slight change $\delta\rho$ in the core radius ρ of a weakly guiding step-profile fiber was discussed in Section 18-6. Here we allow for an arbitrary difference between the

core and cladding indices n_{co} and n_{cl} . We recognize that this problem is superfluous because the known solution for the unperturbed fiber applies to *any* core radius. However, it is included to demonstrate very simply the basic idea involved. Unlike the previous example, the perturbation region width can be large compared with the wavelength λ , provided $\delta\rho \ll \rho$. The situation is shown in Fig. 18-9(a).

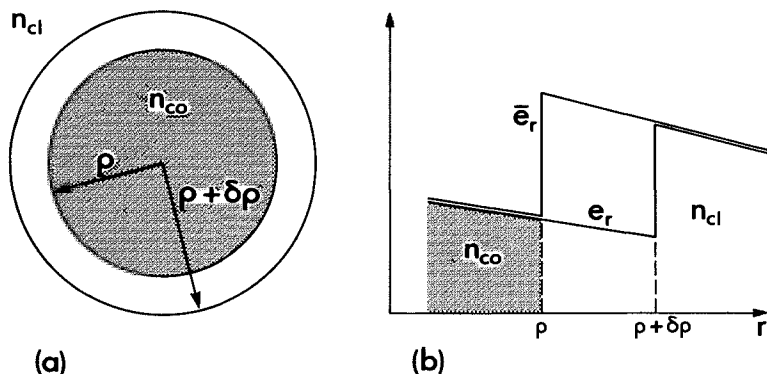


Fig. 18-9 (a) An arbitrary step-profile fiber is perturbed slightly by increasing its core radius from ρ to $\rho + \delta\rho$. (b) The radial component of the unperturbed and perturbed electric field across the perturbation region is given by \bar{e}_r and e_r , respectively.

The field \mathbf{e} in the perturbation region is expressible in terms of the field $\bar{\mathbf{e}}$ of the unperturbed fiber through the boundary conditions of Maxwell's equations. Hence both the longitudinal and azimuthal components of the unperturbed and perturbed fields must be continuous at $r = \rho$ and $r = \rho + \delta\rho$, respectively. Accordingly we set $e_z \cong \bar{e}_z(\rho)$, $e_\phi \cong \bar{e}_\phi(\rho)$ within the perturbation region. The radial component of the unperturbed field must satisfy continuity of $\bar{n}^2 \bar{e}_r$ at $r = \rho$. With reference to Fig. 18-9(b), this gives

$$n_{co}^2 \bar{e}_r(\rho_-) = n_{cl}^2 \bar{e}_r(\rho_+), \quad (18-69)$$

where subscripts $-$ and $+$ refer to the inner and outer sides of the interface. The perturbed component e_r is continuous across $r = \rho$ and satisfies $e_r(\rho_-) \cong \bar{e}_r(\rho_-)$ since $\delta\rho$ is small. Substitution into Eq. (18-69) leads to

$$e_r(r) \cong (n_{cl}/n_{co})^2 \bar{e}_r(\rho_+) \cong (n_{cl}/n_{co})^2 \bar{e}_r(r), \quad (18-70)$$

within the perturbation region. In other words, \mathbf{e} is given by the analytic continuation of the core field $\bar{\mathbf{e}}$ into the perturbation region. Since n and \bar{n} differ only within this region, the error in assuming $\mathbf{e} \cong \bar{\mathbf{e}}$ in Eq. (18-63) can be arbitrarily large. However, if $n_{co} \cong n_{cl}$, the approximation $\mathbf{e} \cong \bar{\mathbf{e}}$ is sufficient since the perturbation does not break circular symmetry, unlike the previous example. We can then recover the weak-guidance result of Eq. (18-13a), as may be readily verified.

18–24 Example: Elliptical deformation

We reconsider the slight elliptical deformation of Fig. 18–2(a). When the core and cladding indices of the step profile are arbitrary, the fields in the four perturbation regions can differ greatly from the fields of the circular fiber. If we apply the reasoning of the previous section, the perturbed field \mathbf{e} in the shaded areas which cross the x -axis is given by the analytic continuation of the *core* field $\bar{\mathbf{e}}$ of the circular fiber. Similarly, \mathbf{e} within the shaded areas which cross the y -axis is given by the analytic continuation of the *cladding* field $\bar{\mathbf{e}}$ of the circular fiber. With this substitution, Eq. (18–63) gives the appropriate propagation constant for the perturbed mode, provided the eccentricity is small. If we substitute the even and odd fundamental-mode fields from Table 12–3, page 250, into Eq. (18–63), then, with the help of Section 18–10 and Table 12–6, page 260, it is straightforward to recover Eq. (18–25) for the difference between perturbed propagation constants in the limit $n_{\text{co}} \cong n_{\text{cl}}$ [8].

18–25 Example: Absorbing fibers

On an arbitrary profile fiber which is slightly absorbing, it is sufficient to assume $\mathbf{e} \cong \bar{\mathbf{e}}$ in order to calculate the small imaginary correction to the propagation constant. We set $\beta = \bar{\beta} + \beta^i$, $n = \bar{n}^r + i\bar{n}^i$ in Eq. (18–63), where superscripts r and i denote real and imaginary parts and $\bar{n}^i \ll \bar{n}^r$. Using the definitions inside the back cover and in Table 11–2, page 232, we deduce that

$$\gamma = 2\beta^i = 2k \left(\frac{\epsilon_0}{\mu_0} \right)^{1/2} \frac{\int_{A_\infty} n^r n^i |\bar{\mathbf{e}}|^2 dA}{\int_{A_\infty} \bar{\mathbf{e}} \times \bar{\mathbf{h}}^* \cdot \hat{\mathbf{z}} dA}, \quad (18-71)$$

where γ is the power attenuation coefficient and the transverse field components of the unperturbed fiber are assumed real. This expression is identical to Eq. (11–63), which was derived from the Poynting vector theorem, since $\bar{\mathbf{e}}_t$ and $\bar{\mathbf{h}}_t$ are assumed real.

REFERENCES

1. Snyder, A. W. (1972) Power loss on optical fibers. *Proc. I.E.E.E.*, **60**, 757–8.
2. Snyder, A. W. and Menzel, R. (1975) *Photoreceptor Optics*, Springer-Verlag, New York.
3. Kirschfeld, K. and Snyder, A. W. (1976) Measurement of a photoreceptor's characteristic waveguide parameter. *Vision Res.*, **16**, 775–8.
4. Snyder, A. W. (1979), in *Handbook of Sensory Physiology*, VII/6A (ed. H. Autrum), Springer-Verlag, Berlin, pp. 279–81.
5. Kaminow, I. P. (1980) Polarization in optical fibers. *I.E.E.E. Trans. J. Quantum Electron.*, **17**, 15–22.
6. Tsuchiya, H. and Sakai, J. I. (1975) Characteristics of single-mode optical fiber with elliptical core. Technical group of the IECE Japan, OQE74-86.

7. Sammut, R. A., Hussey, C. D., Love, J. D. and Snyder, A. W. (1981) Modal analysis of polarization effects in weakly-guiding fibers. *I.E.E. Proc., Pt. H*, **128**, 173–87.
8. Love, J. D., Sammut, R. A. and Snyder, A. W. (1979) Birefringence in elliptically deformed optical fibers. *Electron. Lett.*, **15**, 615–16.
9. Snyder, A. W. and Young, W. R. (1978) Modes of optical waveguides. *J. Opt. Soc. Am.*, **68**, 297–309.
10. Thyagarajan, K., Kumar, A. and Ghatak, A. K. (1981) Perturbation analysis of the coupling between two cylindrical parabolic index waveguides. *Opt. Commun.*, **39**, 26–30.
11. Stratton, J. A. (1941) *Electromagnetic Theory*, McGraw-Hill, New York.
12. Smyth, W. R. (1941) *Static and Dynamic Electricity*, McGraw-Hill, New York.

Slowly varying waveguides

Local modes	407
19-1 Fields of local modes	408
19-2 Criterion for slow variation	409
19-3 <i>Example: Nonuniform core radius</i>	411
19-4 <i>Example: Twisted elliptical fibers</i>	412
Local modes of two nonuniform fibers	413
19-5 Fields of local modes	413
19-6 <i>Example: Cross-talk between identical fibers</i>	414
Tapered couplers	415
19-7 Local-mode propagation	416
19-8 Cross-talk	417
19-9 Criterion for slow variation	417
Local modes of bent fibers	418
Multimode fibers and rays	419
References	419

The previous chapter was concerned with perturbations due to nonuniformities which do not vary along the length of the fiber. However, fibers can also have nonuniformities which depend upon position along the fiber, e.g. variations in the core radius of a circular fiber or the twisting of the cross-section of an elliptical fiber. This chapter introduces a technique for describing propagation on such fibers with arbitrary profiles and arbitrarily large nonuniformities, *provided only that the nonuniformities change sufficiently slowly along the fiber*, as discussed below. Conceptually the method is the modal analogue of the ray analysis for slowly varying, multimode fibers in Chapter 5. However, our main interest here is in the application to single-mode fibers.

LOCAL MODES

Fibers which change along their length are not translationally invariant,

and therefore they cannot support the modes described in Chapter 11. Furthermore, there are, in general, no exact solutions of Maxwell's equations. However, if the fiber is slowly varying, it is intuitive that the modes of some unperturbed fiber are accurate approximations to the solution of Maxwell's equations within local regions. We call such approximate modes *local modes* in analogy with the local plane waves of Chapter 35. The characteristics of local modes can be best appreciated by deriving their fields.

19-1 Fields of local modes

The slowly varying fiber in Fig. 19-1(a) has the z -dependent refractive-index profile $n(x, y, z)$. To construct its local mode fields, we approximate the fiber by the series of cylindrical sections in Fig. 19-1(b) [1]. The profile is independent

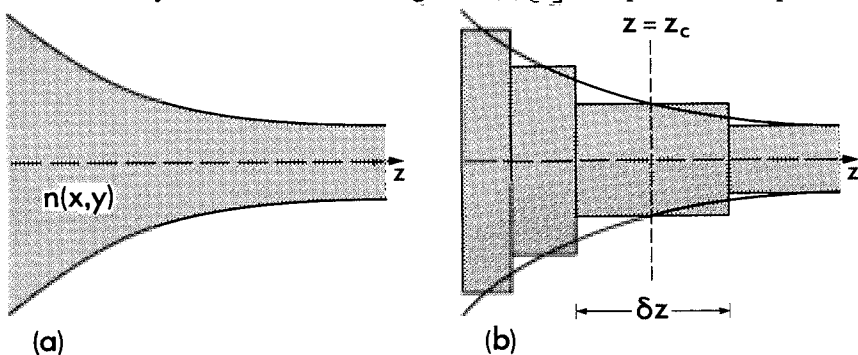


Fig. 19-1 (a) A nonuniform fiber varies along its length and has refractive-index profile $n(x, y, z)$ and (b) the approximate model is a series of sections, where z_c denotes the center of each section and δz is the length of a particular section.

of z within each section and is defined at the center $z = z_c$, where it coincides with the profile of the nonuniform fiber, i.e. $n = n(x, y, z_c)$. We approximate the fields within the *finite* section by the modal fields of an *infinitely long* fiber with profile $n(x, y, z_c)$. Clearly, this approximation is very accurate provided the length of the section δz is large compared with the biggest length scale for the fields, as discussed below. By analogy with Eq. (11-3), the fields of the j th local mode have the separable forms

$$\mathbf{E}_j = \mathbf{e}_j(x, y, \beta_j(z_c)) \exp \{i\beta_j(z_c)z\}; \quad \mathbf{H}_j = \mathbf{h}_j(x, y, \beta_j(z_c)) \exp \{i\beta_j(z_c)z\}, \quad (19-1)$$

within each section, where x and y are coordinates in the fiber cross-section. The \mathbf{e}_j and \mathbf{h}_j are solutions of the vector wave equations of Eq. (11-40) with $n = n(x, y, z_c)$, and the propagation constant $\beta_j(z_c)$, which is implicit in \mathbf{e}_j and \mathbf{h}_j , is determined from the eigenvalue equation.

Power and phase

Although the fields expressed by Eq. (19-1) vary as the profile varies from section to section, the power of a local mode must be conserved along the nonuniform fiber. This requirement is automatically satisfied if we use the orthonormal forms of Eq. (11-15) for the fields in each section, i.e. replace \mathbf{e}_j and \mathbf{h}_j by $\hat{\mathbf{e}}_j$ and $\hat{\mathbf{h}}_j$, respectively, in Eq. (19-1).

As a local mode propagates, its phase increases across each section by the product of $\beta_j(z_c)$ and the section length δz . Consequently, the phase at an arbitrary position along the nonuniform fiber is a sum of such products. However, the slow variation of the fiber means that the propagation constant $\beta_j(z_c)$ varies only slightly from one section to the next. Hence we can accurately approximate the phase sum by the integral $\int_0^z \beta_j(z) dz$. Likewise we can replace $\beta_j(z_c)$ by $\beta_j(z)$ in $\hat{\mathbf{e}}_j$ and $\hat{\mathbf{h}}_j$.

To summarize, the local-mode fields at position z are given by

$$\mathbf{E}_j = \hat{\mathbf{e}}_j(x, y, \beta_j(z)) \exp \left\{ i \int_0^z \beta_j(z) dz \right\}; \quad \mathbf{H}_j = \hat{\mathbf{h}}_j(x, y, \beta_j(z)) \exp \left\{ i \int_0^z \beta_j(z) dz \right\}, \quad (19-2)$$

where $\hat{\mathbf{e}}_j$, $\hat{\mathbf{h}}_j$ and $\beta_j(z)$ are determined from the prescription below Eq. (19-1) with $z_c = z$. Thus $\hat{\mathbf{e}}_j$ and $\hat{\mathbf{h}}_j$ depend implicitly on z through $\beta_j(z)$. This result can also be derived formally from Maxwell's equations, as we show in Chapter 28.

Our derivation of the local-mode fields is sometimes called the *adiabatic approximation*, since it assumes all changes in profile occur over such large distances that there is a negligible change in the power of the local mode [2]. Thus, although a local mode is an *excellent approximation* for a slowly varying fiber, it is not an *exact* solution. The small correction to the local-mode fields is determined by the methods of coupled local modes in Chapter 28 or by the induced current method of Section 22-10.

19-2 Criterion for slow variation

In nonuniform fibers many problems of practical interest can be easily solved by using local modes, as we demonstrate in the examples below. However, the local-mode fields will be an accurate approximation to the exact fields only if the nonuniformities vary sufficiently slowly along the fiber. Since the local-mode fields are constructed from the modal fields of the locally equivalent, cylindrically symmetric fiber, the appropriate slowness condition is determined by the largest distance over which the total field of the cylindrically symmetric fiber changes significantly due to phase differences between the various modes.

Beat length

We recall from Eqs. (11-2) and (11-3) that the total field on a cylindrically symmetric fiber can be represented by a summation of modes. It is then clear that the total field can undergo a significant change in a distance equal to the beat length, z_b , between a pair of modes. We need the largest beat length, which is given by

$$z_b = 2\pi/|\beta_1 - \beta_2|, \quad (19-3)$$

where β_1 and β_2 denote the two closest propagation constants. Hence the fiber nonuniformity must change over a distance large compared with z_b to ensure the accuracy of the local-mode solution. We note that z_b is much larger than the distance $2\pi/\beta_j$ necessary for a significant change in the phase of an individual mode.

Single-mode fibers

On a circular, nonuniform fiber that carries only the fundamental mode with propagation constant β_1 , the propagation constant β_2 in Eq. (19-3) refers to a packet of radiation modes. These modes are discussed in Chapter 25, and they constitute the radiation field. If the fiber has uniform cladding index n_{cl} , the radiation-mode propagation constant assumes all values in the range $0 \leq \beta_2 \leq kn_{cl}$, as do plane waves in an unbounded medium of index n_{cl} . Thus the *largest* value of z_b over which the field of the fundamental mode can change is given by Eq. (19-3) with $\beta_2 = kn_{cl}$. This is equivalent to assuming that the radiation is principally due to a z -directed plane wave and is therefore an overestimate in any practical problem. If we assume the fiber is weakly guiding, we can express this upper bound on z_b in terms of the parameters inside the back cover as

$$z_b = \frac{2\pi}{\bar{\beta} - kn_{cl}} \cong \frac{4\pi\rho}{(2\Delta)^{1/2}} \frac{V}{\bar{W}^2} \quad (19-4)$$

since $\bar{\beta} \cong kn_{co} \cong kn_{cl}$, where n_{co} is the maximum core index.

Multimode fibers

On a multimode fiber, the separation of modal propagation constants decreases as the fiber parameter V increases, and hence the slowness criterion of Eq. (19-3) gives $z_b \rightarrow \infty$ as $V \rightarrow \infty$. However, for the multimode-fiber problems of Chapters 1 to 9 this requirement is unnecessarily restrictive. We showed above that z_b arises from the phase difference between a pair of modes, whereas diffuse illumination of a fiber excites all modes, or, equivalently, all ray directions, and the importance of modal phase is de-emphasized. By ignoring phase, z_b is replaced by a distance we call the *modal half-period*. This is the

distance along the fiber associated with the flow of power within a mode and is contained implicitly within the eigenvalue equation. For modes which propagate only on multimode fibers, the modal half-period is identical to the ray half-period z_p of Section 5-5. On fibers which propagate only a few modes, the modal half-period generally is larger than the ray half-period, as may be anticipated from the discussion of the lateral shift in Section 10-6. For the step-profile planar waveguide, the modal half-period is the sum of z_p and z_s , as illustrated in Fig. 10-4(a).

Summary

Using the expressions derived above, we can give qualitative criteria for the validity of local-mode solutions on a nonuniform fiber with refractive-index profile $n(x, y, z)$. Over distance z_b , the change in profile varies as $(\partial n^2 / \partial z) z_b$, whence we deduce from Eqs. (19-3) and (19-4) that the slowness criteria are

$$\left| \frac{2\pi}{\beta_1 - \beta_2} \frac{1}{n^2} \frac{\partial n^2}{\partial z} \right| \ll 1; \quad \frac{4\pi\rho}{(2\Delta)^{1/2}} \frac{V}{\tilde{W}^2} \frac{1}{n^2} \left| \frac{\partial n^2}{\partial z} \right| \ll 1, \quad (19-5)$$

for weakly guiding fibers propagating two or more modes and one mode, respectively, where β_1 , β_2 , V and \tilde{W} are evaluated at position z .

While these criteria are only qualitative, they provide insight into the requisite slowness in variation along a fiber for a local mode to propagate without losing significant power. Later, in Chapter 28, we derive exact expressions for the slowness criterion from Maxwell's equations.

19-3 Example: Nonuniform core radius

Consider a clad fiber whose core radius $\rho(z)$ changes along its length, such as the taper in Fig. 19-1(a). For simplicity we assume the fiber is weakly guiding and has a step profile. As a particular local mode propagates, the fraction of its power within the core, $\eta(z)$, at each position z decreases as $\rho(z)$ decreases. This is evident from Fig. 14-3(c) since the local fiber parameter V is proportional to $\rho(z)$.

Absorbing core

If the core material is slightly absorbing with power absorption coefficient α_{co} , then Eq. (18-16) shows that the power attenuation coefficient is $\gamma(z) = \eta(z)\alpha_{co}$ at position z . The modal power $P(z)$ is found by replacing γ with $\gamma(z)$ in Eq. (11-62) and integrating to obtain

$$P(z) = P(0) \exp \left\{ -\alpha_{co} \int_0^z \eta(z) dz \right\} = P(0) \exp \{ -\alpha_{co} \eta_{av} z \}, \quad (19-6)$$

where η_{av} is the average value of $\eta(z)$ over length z of fiber. This result also applies to fibers where both the core radius and profile change slowly with z .

Slowness criterion

The above results will be accurate provided the fiber radius does not change significantly over a distance equal to the appropriate beat length in Eq. (19-5), i.e. $|\delta\rho/\rho(z)| \ll 1$ where $\delta\rho = z_b \, d\rho(z)/dz$. For a fiber supporting more than the fundamental mode z_b is given by Eq. (19-3), which leads to

$$|\Omega(z)| \ll |\hat{\beta}_1 - \hat{\beta}_2| \rho(z)/2\pi, \tag{19-7}$$

where $\Omega(z) \cong \tan \Omega(z) = d\rho(z)/dz$ is the local taper angle relative to the z -direction. The requirement that the ratio of the two sides of this inequality be constant suggests a taper shape along which the local mode is equally accurate everywhere. For a single-mode fiber, z_b of Eq. (19-4) gives

$$|\Omega(z)| \ll (2\Delta)^{1/2} \tilde{W}^2/4\pi V, \tag{19-8}$$

where parameters are defined inside the back cover and the value of \tilde{W} for each local value of V is found in Table 14-4, page 314. When this condition is satisfied, local fundamental modes can propagate with negligible radiation loss. However, if the taper angle is fixed and the index difference Δ is reduced, we anticipate that the fiber becomes more susceptible to radiation losses.

19-4 Example: Twisted elliptical fibers

Consider a single-mode, elliptical fiber whose refractive-index profile rotates along its length, as shown in Fig. 19-2. We recall from Section 13-5 that in the weak-guidance approximation one fundamental mode of the cylindrically symmetric, elliptical fiber is plane polarized with its transverse electric field parallel to the x -axis in Fig. 19-2(a) and has propagation constant $\tilde{\beta}_x$. The other fundamental mode's field is parallel to the y -axis and the propagation constant is $\tilde{\beta}_y$. It is intuitive that the two local fundamental modes propagate along the twisted fiber with their transverse electric fields parallel to the rotating x - and y -axes in Fig. 19-2(b), and have constant propagation constants $\tilde{\beta}_x$ and

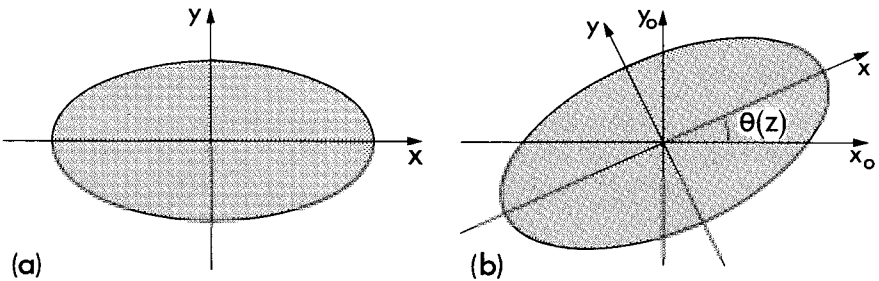


Fig. 19-2 The cross-section of an elliptical fiber rotates along its length. Axes x and y are fixed along the major and minor axes, and axes x_0 and y_0 are fixed in space.

$\tilde{\beta}_y$, respectively. Thus the only difference between the local modes and the corresponding modes of the translationally invariant fiber is the rotation of the field vectors to maintain alignment with the x - and y -axes at each position along the fiber. Similar arguments apply to twisted, anisotropic fibers.

Slowness criterion

The slowness criterion requires the twist be only slight over a distance equal to the beat length between the two fundamental modes in order for the above description to be accurate. By setting $\beta_1 = \tilde{\beta}_x$ and $\beta_2 = \tilde{\beta}_y$ in Eq. (19-5), the criterion is expressible as

$$|\tau(z)| \ll |\tilde{\beta}_x - \tilde{\beta}_y|/2\pi, \quad (19-9)$$

where $\tau(z) = (1/n^2)\partial n^2/\partial z$ defines the local rate of twist.

In the case of a step-profile fiber of slight eccentricity e and mean core radius ρ , it is clear from Fig. 18-2(b) that $\tilde{\beta}_x - \tilde{\beta}_y$ is of order $e^2(2\Delta)^{3/2}/10\rho$. If we define z_r to be the distance for the fiber to twist through a complete revolution, then Eq. (19-9) gives

$$z_r = 2\pi/|\tau(z)| \gg 40\pi^2\rho/\{e^2(2\Delta)^{3/2}\}. \quad (19-10)$$

For a typical single-mode fiber $e^2 \cong 0.5$, $2\Delta \cong 0.02$ and $\rho \cong 3 \mu\text{m}$, whence z_r must be a few metres to satisfy this condition.

LOCAL MODES OF TWO NONUNIFORM FIBERS

The local-mode concept also applies to slowly varying composite waveguides, such as the two identical fibers in Fig. 19-3(a) and the pairs of nonidentical fibers in Fig. 19-4, and is therefore a powerful method for studying the properties of nonuniform couplers.

19-5 Fields of local modes

The construction of the local-mode fields for the composite waveguide is straightforward. In analogy with Section 19-1, we first approximate the two fibers by the sections in Fig. 19-3(b). Thus each differential section is regarded as part of a composite waveguide consisting of two parallel, translationally invariant fibers with refractive-index profile evaluated at the center of the section. Assuming the fibers to be weakly guiding and sufficiently well separated, the fundamental-mode solutions and propagation constants for the scalar wave equation are given by Eqs. (18-33) and (18-34). If we parallel the discussion of Section 19-1, the local fundamental solutions $\bar{\Psi}_1(x, y, \bar{\beta}(z))$, $\bar{\Psi}_2(x, y, \bar{\beta}(z))$ and propagation constant $\bar{\beta}(z)$ of the scalar wave equation for each fiber in isolation depend on z . Consequently, the perturbation solutions Ψ_+ , β_+ and Ψ_- , β_- for the composite waveguide are z -dependent. The complete spatial dependence of the transverse electric field for the x - or y -

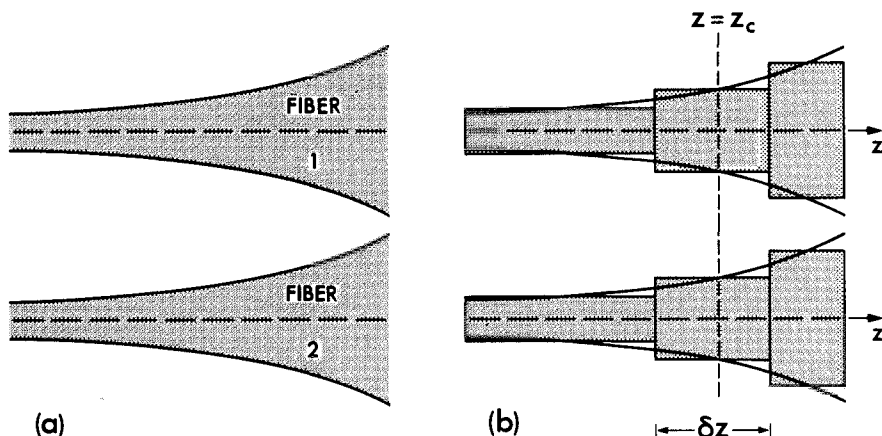


Fig. 19-3 (a) A composite waveguide comprising an identical pair of parallel, nonuniform fibers and (b) the approximate model consisting of a series of sections, where z_c denotes the center of each section and δz is the length of a particular section.

polarized local fundamental modes then follows from Eqs. (18-36) and (19-2) as

$$E_{\pm} = \Psi_{\pm}(x, y, z) \exp \left\{ i \int_0^z \beta_{\pm}(z) dz \right\}. \quad (19-11)$$

The same expression is applicable to nonidentical fibers, provided we replace Eqs. (18-33) and (18-34) by Eqs. (18-55) and (18-57), respectively, where the a_{\pm} of Eq. (18-58) now vary with z . Slowness criteria are discussed below.

19-6 Example: Cross-talk between identical fibers

One immediate consequence of using local modes for pairs of *identical*, slowly varying fibers is a simple description of power transfer due to cross-talk between fibers. If fiber 1 in Fig. 19-3(a) is initially illuminated with unit power and fiber 2 with zero power, the distribution of power along the composite waveguide is given by a simple modification to the corresponding problem for cylindrically symmetric fibers in Section 18-13. We replace $\bar{\beta}z$ and Cz by the integrals $\int_0^z \beta(z) dz$ and $\int_0^z C(z) dz$, where $C(z)$ is defined by Eq. (18-35) in terms of z -dependent quantities. Hence Eq. (18-39) is replaced by

$$P_1(z) = \cos^2 \left\{ \int_0^z C(z) dz \right\}; \quad P_2(z) = \sin^2 \left\{ \int_0^z C(z) dz \right\}. \quad (19-12)$$

Thus the two local fundamental modes interfere, and all power is transferred from one mode to the other mode and back again over a distance equal to the *local beat length* z_b ,

defined by

$$z_b = \frac{4\pi}{\beta_+(z) - \beta_-(z)} = \frac{2\pi}{C(z)}. \quad (19-13)$$

This description of cross-talk is accurate provided there is insignificant change in the fiber over distances large compared with z_b .

TAPERED COUPLERS

We now consider couplers consisting of pairs of nonidentical, single-mode fibers, such as those illustrated in Fig. 19-4. These couplers are of great practical importance [3], and their properties are readily explained in terms of local modes provided only that the couplers are sufficiently well separated and slowly varying.

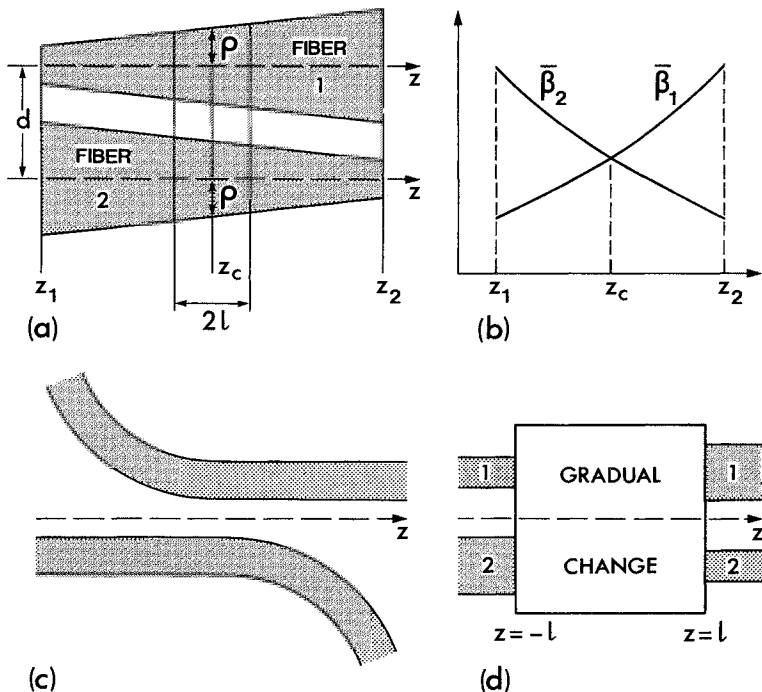


Fig. 19-4 (a) Two tapered fibers with equal core radii ρ at $z = z_c$, while at z_1 and z_2 the core radii are reversed. (b) Qualitative behavior of the local-mode propagation constants along fibers 1 and 2 of (a) in isolation. (c) Coupler consisting of bent fibers of constant core radius. (d) Schematic representation of an arbitrary tapered coupler consisting of fibers 1 and 2 of increasing and decreasing core radii, respectively.

19-7 Local-mode propagation

We examine the propagation of local fundamental modes along the composite waveguide, or coupler, in Fig. 19-4(a), which for simplicity consists of two parallel fibers with equal and opposite taper angles. It is clear from applying the results of Section 18-18 to each position z along the coupler, that, apart from a small region about $z = z_c$ where the core radii are virtually identical, the local modes of the coupler are essentially the local modes of each fiber in isolation. Suppose for instance the local fundamental solution Ψ_+ in Eq. (19-11) satisfies $\Psi_+ \cong \bar{\Psi}_1$ at $z = z_1$ in Fig. 19-4(a), where $\bar{\Psi}_1$ is the local fundamental solution for fiber 1 in isolation. Hence the local mode of the coupler is associated with the *smaller* of the core radii at $z = z_1$. The same local mode at $z = z_2$, where the core radii are reversed, by definition must be associated with the *smaller* core radius, i.e. that of fiber 2, and consequently $\Psi_+ \cong \bar{\Psi}_2$, where $\bar{\Psi}_2$ is the local fundamental solution for fiber 2 in isolation. In other words, *the fields of the Ψ_+ local mode switch from being concentrated around fiber 1 to being concentrated around fiber 2 as the mode propagates from z_1 to z_2 .* Similarly, the fields of the Ψ_- local mode switch from fiber 2 to fiber 1 as it propagates from z_1 to z_2 .

It is not necessary for the fibers to have the symmetry properties shown in Figs. 19-4(a) and (c). The description of the Ψ_+ and Ψ_- modes requires only that the core cross-section of one fiber, measured in the plane transverse to the z -axis, *decreases* slowly with z and the corresponding cross-section of the other fiber *increases* slowly with z , as shown schematically in Fig. 19-4(d). We discuss below how gradual these changes should be for the local-mode description to be accurate.

Mathematical description

The above conclusions, derived from physical arguments, can also be shown analytically. Following the discussion of Section 19-5, the expression for Ψ_+ at position z follows by analogy with Eqs. (18-55), (18-57) and (18-58). Hence

$$\Psi_+ = \frac{\bar{\Psi}_1 + a_+(z)\bar{\Psi}_2}{\{1 + a_+^2(z)\}^{1/2}}; \quad a_+(z) = \frac{\bar{\beta}_2(z) - \bar{\beta}_1(z)}{2C(z)} + \left\{ 1 + \frac{[\bar{\beta}_1(z) - \bar{\beta}_2(z)]^2}{4C^2(z)} \right\}^{1/2},$$

(19-14)

where $\bar{\beta}_1(z), \bar{\beta}_2(z)$ are the local-mode propagation constants for each fiber in isolation, and $C(z)$ is the z -dependent generalization of Eq. (18-35). At $z = z_1$ in Fig. 19-4(a) the core radii are sufficiently dissimilar that $\bar{\beta}_1(z_1) - \bar{\beta}_2(z_1) \gg C(z_1)$, assuming $C(z_1) > 0$, and hence Eq. (19-14) gives $a_+ \cong 0$ and $\Psi_+ \cong \bar{\Psi}_1$. It is clear from symmetry that the values of the propagation constants, which are plotted qualitatively in Fig. 19-4(b), are

reversed at $z = z_2$, but the coupling coefficient C is unchanged. Accordingly

$$\bar{\beta}_1(z_2) - \bar{\beta}_2(z_2) = -\{\bar{\beta}_1(z_1) - \bar{\beta}_2(z_1)\} \ll C(z_2) = C(z_1), \quad (19-15)$$

and we deduce from Eq. (19-14) that $a_+ \rightarrow \infty$ and $\Psi_+ \cong \bar{\Psi}_2$.

The switch in the local-mode fields from fiber 1 to fiber 2, or vice-versa, occurs in the region about $z = z_c$ where the core radii are virtually identical. This is evident from Eq. (18-55), since Ψ_+ and Ψ_- then depend on both $\bar{\Psi}_1$ and $\bar{\Psi}_2$.

19-8 Cross-talk

The simplicity of the local-mode description of propagation on couplers is evident in the analysis of cross-talk between the constituent fibers. If only fiber 1 is illuminated at $z \leq -l$ in Fig. 19-4(d), it is clear from the previous section that the Ψ_+ mode of Eq. (19-11) is excited and no power enters the Ψ_- mode. Consequently propagation is described entirely by the characteristics of the Ψ_+ mode, and thus all of its power is carried by fiber 2 for $z \geq l$. In other words, *there is essentially a 100% transfer of power from one fiber to the other on a tapered coupler, provided only that the slowness criterion below is satisfied.*

19-9 Criterion for slow variation

Following the reasoning of Section 19-2, the local-mode description of tapered couplers will be accurate provided the critical length $2l$ in Fig. 19-4(d) for complete power exchange between the component fibers is large compared with the local beat length z_b at $z = z_c$ in Fig. 19-4(a), where the fibers have equal core radius ρ , and center-to-center separation d . We showed in Section 18-13 that the beat length for identical fibers increases exponentially with separation. Since the expression for Ψ_+ and Ψ_- in Eq. (18-33) assume a sufficiently large separation, the accuracy of the local-mode description is acutely sensitive to separation.

The critical length $2l$ corresponds to a change $2\delta\rho$ in core radius of both fibers, assuming an equal and opposite taper angle Ω in the neighborhood of $z = z_c$. We then deduce from Eq. (19-13) the slowness criterion

$$\Omega = \frac{\delta\rho}{l} \ll \frac{\delta\rho}{\pi} \{\beta_+(z_c) - \beta_-(z_c)\} = 2 \frac{\delta\rho}{\pi} C(z_c). \quad (19-16)$$

When both fibers have a step profile, a difference of 1% in core radii is sufficient to reduce power transfer to 10% of total power, as shown in Section 18-20. Consequently $\delta\rho/\rho$ need be only a few per cent for the fibers to be effectively isolated, and as $C(z_c)$ is exponentially small, the taper angle, Ω , will be minute. Since $2l \gg z_b$, the critical length for total power transfer between tapered fibers is large compared with the beat length for total power transfer between

identical, translationally invariant fibers with core radius ρ . The accuracy of the local-mode description of couplers will be examined in Chapter 28.

LOCAL MODES OF BENT FIBERS

So far in this chapter it has been convenient to assume a direction of propagation for local modes fixed parallel to the z -axis of the fiber or composite waveguide. However, in the case of the bent fiber of Fig. 19-5(a), it is more appropriate to use the curved axis of the fiber as the direction of propagation. Then, by analogy with Section 19-1, the local-mode fields are constructed by approximating the bent fiber with the series of sections in Fig. 19-5(b). If the fiber profile and cross-section do not vary around the bend, the local-mode fields in the neighborhood of the fiber are just the fields of the straight fiber as given by Eq. (11-3) with βz replaced by $R\phi$, where R is the radius of the bend and ϕ is the angular displacement along the bend in Fig. 19-5. Clearly, the local modes so constructed will be a good approximation to the exact fields close to the fiber axis provided R is sufficiently large.

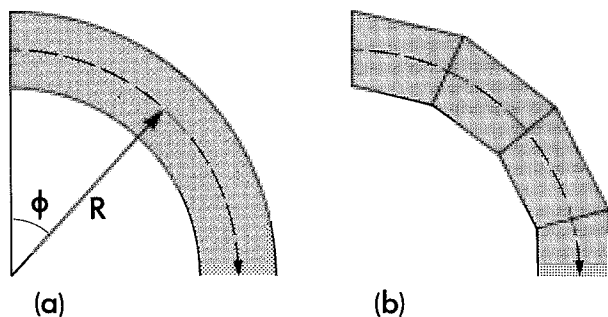


Fig. 19-5 (a) Bent fiber of radius R where ϕ is the angular displacement along the bend and (b) the equivalent sections.

Bent single-mode fibers

The slowness criterion for the local fundamental mode on a bent, single-mode fiber can be derived from the arguments of Section 19-2. Over the beat length z_b of Eq. (19-4), there must be negligible change in the angle ϕ , i.e. $z_b/R \ll 1$. Assuming weak guidance, this is equivalent to

$$R/\rho \gg 4\pi V / \{ (2\Delta)^{1/2} \tilde{W}^2 \}, \quad (19-17)$$

where ρ is the core radius and other parameters are defined at the back of the book. When this condition is satisfied, we anticipate that the local-mode fields accurately approximate the fields close to the fiber axis.

MULTIMODE FIBERS AND RAYS

At each position z along a nonuniform, multimode fiber, a high-order local mode is equivalent to a single family of rays, as is clear from Section 36-2. Each ray follows a path which changes slowly over the local half-period $z_p(z)$ of Eq. (5-12). This is the ray analogue of the multimode-fiber discussion in Section 19-2. Furthermore, the equivalence of mode and ray transit times, which is demonstrated in Section 36-9, is readily extended to slowly varying fibers, for which the transit time is given by Eq. (5-11).

The modal propagation constant $\beta(z)$ satisfies the local eigenvalue equation for each value of z . This equation has the plane-wave form of Eqs. (36-12) and (36-13) for high-order modes on step- and graded-profile fibers. Using the relationships between mode and ray parameters in Table 36-1, page 695, we find that the local eigenvalue equation has the form of the adiabatic invariant of Eq. (5-41).

Step-profile fiber

Consider the parameter U for a mode on a nonuniform, step-profile fiber of core index and radius $n(z)$ and $\rho(z)$, respectively. It is clear from Fig. 12-4 that U is constant as the fiber parameter $V \rightarrow \infty$, regardless of variations in the fiber provided they occur slowly. The relationships between U , β and θ_z in Table 36-1, apply at each position z , and hence

$$U = k\rho(z)n(z) \sin \theta_z(z) \quad (19-18)$$

is constant along the fiber, where $\theta_z(z)$ is the angle between the local ray direction and the fiber axis. Thus U/k is identical to the invariant derived either in Eq. (5-20) from the ray equation or in Eq. (5-44) from the adiabatic invariant.

REFERENCES

1. Snyder, A. W. (1965) Surface mode coupling along a tapered dielectric rod. *I.E.E.E. Trans. Antennas Propag.*, **13**, 821-2.
2. Jackson, J. D. (1964) *Electrodynamics*, Wiley, New York, p. 419.
3. Wilson, M. G. F. and Teh, G. A. (1975) Tapered optical couplers. *I.E.E.E. Trans. Microwave Theory Tech.*, **23**, 85-92.

Illumination, tilts and offsets

Mode launching	421
20-1 Modal amplitudes and power	422
Illumination of weakly guiding fibers	422
20-2 Fields at the endface	423
20-3 Fields of the illuminating beam	424
20-4 Gaussian and uniform beams	424
20-5 Modal amplitudes and power	425
Infinite parabolic-profile fiber	427
20-6 <i>Example: On-axis Gaussian beam</i>	427
20-7 <i>Example: Tilted Gaussian beam</i>	427
20-8 <i>Example: Offset Gaussian beam</i>	428
20-9 <i>Example: On-axis uniform beam</i>	428
20-10 <i>Example: Oblique plane wave</i>	429
Illumination of single-mode fibers	430
20-11 Junctions between fibers	430
Step-profile fibers	431
20-12 <i>Example: Tilted uniform beam</i>	431
20-13 <i>Example: On-axis uniform beam</i>	433
20-14 Comparison with geometric optics	434
Lens illumination	434
20-15 <i>Example: Infinite parabolic profile</i>	435
20-16 <i>Example: Gaussian approximation</i>	436
Diffuse illumination	436
20-17 <i>Example: Single-mode fibers</i>	437
20-18 <i>Example: Multimode fibers</i>	438
20-19 Error in the geometric optics analysis	439
References	440

In earlier chapters we established the properties of bound modes and showed

420

how to construct the fields. Now we consider the excitation of these modes when the endface of the fiber is illuminated by an external source, such as a beam of light. Not all of the source power incident on the endface is transformed into bound-mode power; part of it is reflected from the endface and part of it excites the radiation field of the fiber. The present chapter is concerned with the spatial steady state, as discussed in the Introduction to Part II. This state is realized sufficiently far along the fiber, where only bound modes are necessary to describe light propagation. We showed in Chapter 8 how illumination of multimode fibers can be described by simple ray methods. Here we are primarily concerned with fibers that propagate only one or a few modes.

MODE LAUNCHING

Consider the fiber of arbitrary profile and cross-section in Fig. 20-1(a) whose endface, i.e. the infinite cross-section at $z = 0$, is illuminated by an arbitrary light source. The amplitudes of the bound modes launched at the endface are easily determined whenever we specify either the total transverse electric field distribution \mathbf{E}_t at $z = 0$ or the corresponding magnetic field \mathbf{H}_t . We represent the fields of the fiber by an expansion over its modes and determine the modal amplitudes from orthogonality relations. However, the fields \mathbf{E}_t and \mathbf{H}_t are the sum of both the illuminating fields which are prescribed, and the fields reflected from the endface which are unknown. The exact determination of the latter is extremely complicated. Fortunately, a simple and accurate approximation can be used for weakly guiding fibers. We first give the general theory [1-4], then the approximation for weakly guiding fibers, followed by examples.

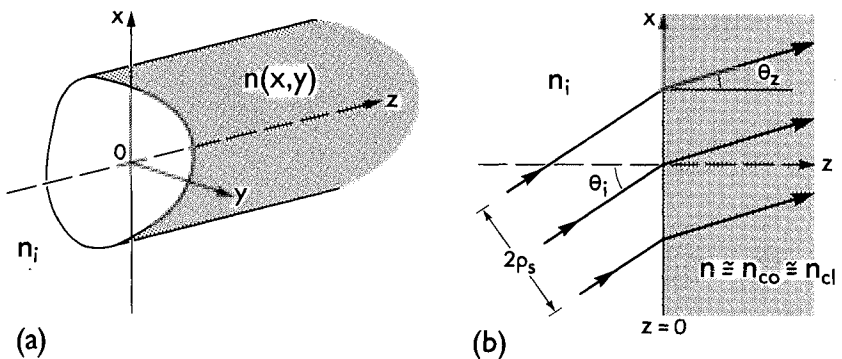


Fig. 20-1 (a) The endface $z = 0$ of a fiber of arbitrary profile and cross-sectional geometry and (b) refraction of a finite beam at the endface of a weakly guiding fiber.

20-1 Modal amplitudes and power

The total transverse fields of the fiber at its endface, \mathbf{E}_t and \mathbf{H}_t , can be represented by the transverse portion of the eigenfunction expansion of Eq. (11-2). Clearly only the forward-propagating modes are required. We use the representation of Eq. (11-6) for the bound-mode fields, and denote the transverse portions of the radiation fields at $z = 0$ by \mathbf{E}_{tr} and \mathbf{H}_{tr} . Continuity of the transverse fields at the endface requires that

$$\mathbf{E}_t(x, y) = \sum_j a_j \mathbf{e}_{tj}(x, y) + \mathbf{E}_{tr}(x, y), \quad (20-1a)$$

$$\mathbf{H}_t(x, y) = \sum_j a_j \mathbf{h}_{tj}(x, y) + \mathbf{H}_{tr}(x, y), \quad (20-1b)$$

for all values of x and y , where the constants a_j are the modal amplitudes and $j = 1, \dots, M$. We have assumed that the source is monochromatic, with the same implicit time dependence $\exp(-i\omega t)$ as the modal fields. For an arbitrary source, the right side of Eq. (20-1) must include a superposition over frequency.

We recall from Section 11-4 that each mode is orthogonal to the radiation field and all other bound modes. Assuming that the fiber is nonabsorbing, we take the cross product of Eq. (20-1a) with \mathbf{h}_{tk}^* , Eq. (20-1b) with \mathbf{e}_{tk}^* and integrate over the infinite cross-section A_∞ . We deduce from Eq. (11-13) that

$$a_j = \frac{1}{2N_j} \int_{A_\infty} \mathbf{E}_t \times \mathbf{h}_{tj}^* \cdot \hat{\mathbf{z}} dA = \frac{1}{2N_j} \int_{A_\infty} \mathbf{e}_{tj}^* \times \mathbf{H}_t \cdot \hat{\mathbf{z}} dA, \quad (20-2)$$

where $\hat{\mathbf{z}}$ is the unit vector parallel to the fiber axis, and $*$ denotes complex conjugate. The normalization N_j of Eq. (11-12) is real if we use the convention of Eq. (11-8) and chose the transverse fields to be real. The power P_j propagating in each mode is given by Eq. (11-22). Consequently, the total power P in the guided portion of the fields is

$$P = \sum_j P_j = \sum_j |a_j|^2 N_j, \quad (20-3)$$

where the summation is over all bound modes.

ILLUMINATION OF WEAKLY GUIDING FIBERS

In order to determine the modal amplitudes of Eq. (20-2), we must know either \mathbf{E}_t or \mathbf{H}_t at the fiber endface. In general, it is not possible to determine analytical expressions for these fields. However, the problem is much simpler when the fiber is weakly guiding [2], as we show below.

20-2 Fields at the endface

The small variation in the refractive-index profile of a weakly guiding fiber means that the fields \mathbf{E}_t and \mathbf{H}_t at the endface are approximately those at the boundary between two semi-infinite media of refractive indices n_i and $n(x, y) \cong n_{co} \cong n_{cl}$, as shown schematically in Fig. 20-1(b). Here n_i is the refractive index of the region $z < 0$ containing the source of illumination, and n_{co}, n_{cl} are, respectively, the maximum core and uniform cladding indices of the fiber. When the fiber is illuminated by a beam of diameter $2\rho_s$, the spread in angles due to the finite width of the beam can be ignored provided $2\rho_s \gg \lambda$, where λ is the free-space wavelength. Consequently, \mathbf{E}_t and \mathbf{H}_t are determined from the familiar expressions for plane-wave reflection from a dielectric interface. In this approximation we ignore small scattering effects due to the nonuniformity of the fiber profile over the endface, and assume the medium $z \geq 0$ has uniform refractive index n_{co} .

Refraction

Following the above discussion, the fields at the endface are the transmitted fields in Fig. 20-1(b) associated with the illuminating field. If the beam makes angle θ_i with the fiber axis, then it is refracted at $z = 0$ and makes angle θ_z with the fiber axis for $z > 0$ given by Snell's Law

$$n_i \sin \theta_i = n_{co} \sin \theta_z. \quad (20-4)$$

In practice $n_i < n_{co}$ so that $\theta_z < \theta_i$ and the beam refracts towards the fiber axis. The relationships between $\mathbf{E}_t, \mathbf{H}_t$ and the incident beam fields \mathbf{E}_i and \mathbf{H}_i are provided by the Fresnel reflection coefficients for plane-wave reflection at a dielectric interface, discussed in Section 35-6. In general, these coefficients depend on the polarization of the beam, but, if θ_i is small, they are independent of polarization and are given by Eq. (35-18) with n_{co} and n_{cl} replaced by n_i and n_{co} , respectively. Thus we deduce from Eqs. (35-1b), (35-15) and (35-17) that

$$\mathbf{E}_t(\theta_z) \cong \frac{2n_i}{n_i + n_{co}} \mathbf{E}_i(\theta_i); \quad \mathbf{H}_t(\theta_z) \cong \frac{2n_{co}}{n_i + n_{co}} \mathbf{H}_i(\theta_i), \quad (20-5)$$

where \mathbf{E}_i and \mathbf{H}_i are approximately transverse to the fiber axis when $\theta_i \ll 1$, i.e. when $\theta_i \cong \theta_z \cong \pi/2$ in Eq. (35-18).

Transmitted power

The fraction of beam power transmitted across the interface depends on the product of \mathbf{E}_t and \mathbf{H}_t , and is given by the Fresnel power transmission coefficient T of Eq. (35-21) with n_{co} and n_{cl} replaced by n_i and n_{co} , respectively.

Hence

$$T = 4n_i n_{co} / (n_i + n_{co})^2, \quad (20-6)$$

for $\theta_i \ll 1$. In other words only a fraction T of incident power crosses the endface.

From the form of Eq. (20-5), it is clear that we can solve Eq. (20-2) for a_j by first assuming $n_{co} = n_i$ and $\theta_z = \theta_i$ in Fig. 20-1(b), and then replacing the resultant expression for $a_j(\theta_i)$ by $T^{1/2} a_j(n_i \theta_i / n_{co})$. In practice, virtually all of the beam power is transmitted across the endface, since, for the usual case of an air-fiber interface, $n_i = 1$ and $n_{co} \cong 1.5$, leading to $T \cong 0.96$. *Throughout the rest of the chapter we shall assume $n_{co} = n_i$ and $\theta_z = \theta_i$.* Thus the transverse fields on the endface are those of the illuminating beam, i.e. $\mathbf{E}_t = \mathbf{E}_i$ and $\mathbf{H}_t = \mathbf{H}_i$. When $n_{co} \neq n_i$, our results may be corrected using the procedure described above.

20-3 Fields of the illuminating beam

We now consider illumination by light beams that are parallel to, or subtend only small angles θ_i to the axis of the fiber. The fields of the beam at the endface of the fiber have the form of a local plane wave whose wave vector is parallel to the direction of the beam. If the electric field, \mathbf{E}_i , is uniformly polarized parallel to the x -axis in Fig. 20-2(a) and the beam is parallel to the x - z plane, with a symmetric amplitude distribution $f(r)$, then

$$\mathbf{E}_i = E_x \hat{x} \cong \hat{x} f(r) \exp \{ i k n_i (x \theta_i + z) \} = \hat{x} f(r) \exp \{ i k n_i (\theta_i r \cos \phi + z) \}, \quad (20-7a)$$

$$\mathbf{H}_i = \left(\frac{\epsilon_0}{\mu_0} \right)^{1/2} n_i \hat{z} \times \mathbf{E}_i \cong H_y \hat{y}, \quad (20-7b)$$

where \hat{x} , \hat{y} and \hat{z} are unit vectors parallel to the axes in Fig. 20-2(a), and remaining parameters are defined inside the back cover. The total z -directed power in the beam, P_i , follows from Eq. (11-25) as

$$P_i = \pi n_i \left(\frac{\epsilon_0}{\mu_0} \right)^{1/2} \int_0^\infty r f^2(r) dr, \quad (20-8)$$

which allows for beams of finite or infinite width.

20-4 Gaussian and uniform beams

Later in the chapter we shall consider illumination by Gaussian and uniform beams. The *Gaussian beam* has an infinite width, and the radial distribution and

total power of Eq. (20-8) are given by

$$f(r) = \exp \left\{ -\frac{1}{2} \frac{r^2}{\rho_s^2} \right\}; \quad P_i = \frac{\pi}{2} \left(\frac{\varepsilon_0}{\mu_0} \right)^{1/2} n_i \rho_s^2, \quad (20-9)$$

respectively, where ρ_s is the spot size. If we consider a step-function radial distribution, then the *uniform beam* will carry the same power as the Gaussian beam provided its radius is equal to the spot size, i.e.

$$f(r) = \begin{cases} 1, & 0 \leq r < \rho_s; \\ 0, & \rho_s < r < \infty; \end{cases} \quad P_i = \frac{\pi}{2} \left(\frac{\varepsilon_0}{\mu_0} \right)^{1/2} n_i \rho_s^2, \quad (20-10)$$

which may be verified from Eq. (20-8).

20-5 Modal amplitudes and power

When the fiber is weakly guiding, the transverse fields \mathbf{e}_{ij} and \mathbf{h}_{ij} of each mode are simply related by Eq. (13-1). Assuming $n_{co} = n_i$ in Fig. 20-1(b), the fields at the endface are given by Eq. (20-7), subject to the modifications discussed in Section 20-2 when $n_{co} \neq n_i$. Thus we deduce from Eq. (13-1) and the first expression for a_j in Eq. (20-2) that

$$a_j = \int_{A_x} E_x e_{xj}^* dA \bigg/ \int_{A_x} |\mathbf{e}_{ij}|^2 dA, \quad (20-11)$$

where E_x is evaluated at $z = 0$, and e_{xj} is the x -component of \mathbf{e}_{ij} . If we use the second expression in Eq. (20-2), the resulting form for a_j is consistent with Eq. (20-11) only when the angle of incidence of the beam is small. This restriction is a consequence of assuming both $\mathbf{E}_t = \mathbf{E}_i$ and $\mathbf{H}_t = \mathbf{H}_i$ at the endface, whereas the exact expressions for \mathbf{E}_t and \mathbf{H}_t depend on the fiber structure [2]. However, the assumption is consistent with the intuitive statements at the end of Section 20-2. Hence Eq. (20-11) is *accurate for weakly guiding fibers illuminated by beams at a small angle to the fiber axis*. If either of these two conditions is relaxed, there is no comparable simple theory for determining a_j .

We note that Eq. (20-11) can be derived directly from the scalar wave equation. In the weak-guidance approximation, the fields \mathbf{e}_{ij} in Eq. (20-1a) satisfy the scalar wave equation. Consequently, the above result follows directly from the orthogonality condition of Eq. (33-5b).

The restriction $\theta_i \ll 1$ is of little practical concern for weakly guiding fibers. In terms of the local plane-wave vector, each bound mode field makes an angle θ_z with the fiber axis, and this angle lies within the range $0 \leq \theta_z < \theta_c$, where $\theta_c \cong \{1 - n_{cl}^2/n_{co}^2\}^{1/2}$ is the complementary critical angle. By hypothesis $n_{co} \cong n_{cl}$, whence both θ_c and θ_z are small.

Modal power

The power in each mode follows from Eq. (20-11) and Table 13-2, page 292. For fibers of arbitrary cross-section

$$P_j = \frac{n_{co}}{2} \left(\frac{\epsilon_0}{\mu_0} \right)^{1/2} \left| \int_{A_x} E_x e_{xj}^* dA \right|^2 / \int_{A_x} |e_{ij}|^2 dA, \quad (20-12)$$

while for fibers of circular cross-section, it is clear from Table 14-1, page 304, that

$$P_l = \frac{\rho^2 n_{co}}{4\pi} \left(\frac{\epsilon_0}{\mu_0} \right)^{1/2} \left| \int_0^\infty \int_0^{2\pi} E_x \Psi_l R dR d\phi \right|^2 / \int_0^\infty F_l^2(R) R dR, \quad (20-13)$$

where ρ is either the core radius or scaling length, Ψ_l denotes $F_l(R) \cos l\phi$ or $F_l(R) \sin l\phi$ and $F_l(R)$ satisfies the scalar wave equation, Eq. (14-4). By symmetry, the power excited in each mode of a circular fiber is independent of the polarization of the beam fields, and therefore does not depend on our choice of an x -polarized electric field in Eq. (20-7a). We now consider specific examples.

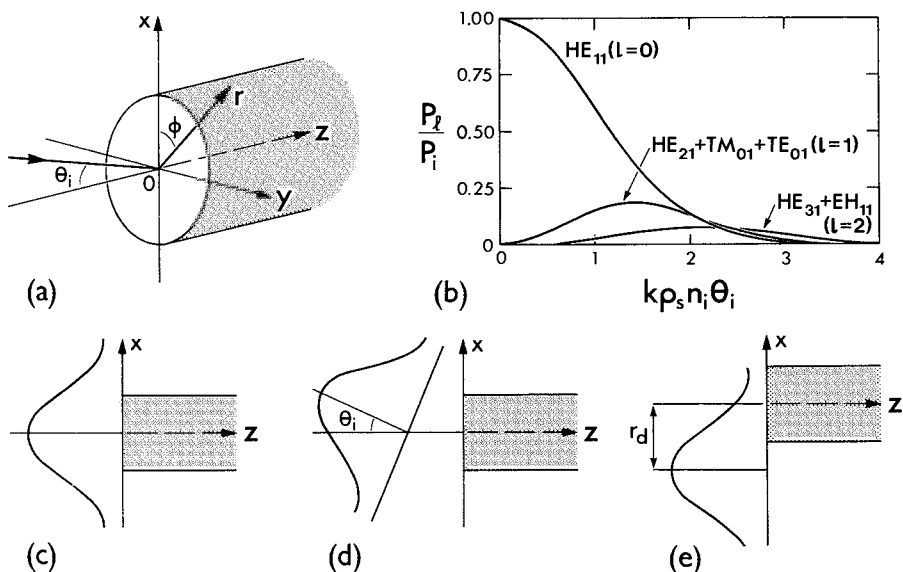


Fig. 20-2 (a) Coordinates for describing the fields of the beam incident on the endface and (b) the fraction of total power of a Gaussian beam entering the modes of an infinite parabolic-profile fiber as a function of the tilt angle θ_i . The orientation of the Gaussian beam is shown for (c) on-axis, (d) tilted and (e) offset illumination.

INFINITE PARABOLIC-PROFILE FIBER

This profile is the simplest example for determining the physical attributes of Gaussian-beam illumination [5-7], and is defined by

$$n^2(R) = n_{co}^2 \{1 - 2\Delta R^2\}; \quad 0 \leq R < \infty, \quad (20-14)$$

where $R = r/\rho$ and $\Delta \ll 1$. Although the profile becomes unphysical as $R \rightarrow \infty$, the discussion of Section 14-4 shows the weak-guidance approximation is valid provided the fiber parameter is large enough, e.g. $V \gg 4\Delta$ for the fundamental modes.

20-6 Example: On-axis Gaussian beam

When the Gaussian beam is at normal incidence, $\theta_i = 0$ in Fig. 20-2(c) and Eqs. (20-7a) and (20-9) show that the electric field on the endface reduces to $E_x = \exp(-r^2/2\rho_s^2)$, where ρ_s is the beam spot size. Thus E_x is independent of ϕ , and Eq. (20-13) shows that only the $l = 0$, or HE_{1m} , modes are excited. For the x-polarized fundamental mode, Table 14-2, page 307, gives $\Psi_0 = F_0 = \exp(-r^2/2r_0^2)$, where $r_0 = \rho/V^{1/2}$ is the mode spot size. If we substitute into Eq. (20-13) and take the ratio with Eq. (20-9), then the fraction of beam power entering the fundamental mode, assuming $n_i = n_{co}$, is

$$P_0/P_i = \{2\rho_s r_0 / (\rho_s^2 + r_0^2)\}^2. \quad (20-15)$$

Consequently, all beam power goes into the fundamental mode only when $r_0 = \rho_s$, i.e. when the beam and mode spot sizes are equal. The greater the departure of ρ_s from r_0 , the smaller the fraction of beam power entering the fundamental mode, as more power enters higher-order HE_{1m} modes.

20-7 Example: Tilted Gaussian beam

The situation is identical to that in the previous example, except the beam is now inclined at a small angle θ_i to the fiber axis, as shown in Fig. 20-2(d). The significant property of off-axis illumination is the excitation of modes with $l > 0$, in addition to the $l = 0$ modes. To account for the excitation of all modes, we use Eq. (37-80a) to expand the exponential dependence on ϕ in Eq. (20-7a) and obtain

$$\exp(ikn_i\theta_i r \cos\phi) = J_0(\kappa R) + 2 \sum_{l=1}^{\infty} i^l J_l(\kappa R) \cos l\phi, \quad (20-16)$$

where $\kappa = k\rho n_i\theta_i$ and J_l is the Bessel function of the first kind. If we substitute Eq. (20-7a) into Eq. (20-13) and divide by Eq. (20-9), we obtain the fraction of beam power

$$\frac{P_l}{P_i} = 2 \frac{\rho^2}{\rho_s^2} \left| \int_0^{\infty} F_l(R) J_l(\kappa R) \exp(-R^2 \rho^2 / 2\rho_s^2) R dR \right|^2 \bigg/ \int_0^{\infty} R F_l^2(R) dR, \quad (20-17)$$

assuming $n_i = n_{co}$. Note that only even order modes are excited, i.e. $\Psi_l = F_l(R) \cos l\phi$. If we consider only the lowest-order mode for each value of l , then Table 14–2, page 307, shows that $F_l(R) = (r/r_0)^l \exp(-r^2/2r_0^2)$ where $r_0 = \rho/V^{1/2}$ is the modal spot size. Substituting into Eq. (20–17) and applying Eqs. (37–100b) and (37–125) leads to

$$\frac{P_l}{P_i} = 4 \frac{(k\rho_s n_i \theta_i)^{2l}}{l!} \left\{ \frac{r_0 \rho_s}{r_0^2 + \rho_s^2} \right\}^{2l+2} \exp \left\{ -\frac{(k\rho_s n_i \theta_i r_0)^2}{r_0^2 + \rho_s^2} \right\}. \quad (20-18)$$

These ratios give the efficiency with which the Gaussian beam excited modes, as a function of the tilt angle θ_i . For each value of l , this efficiency is a maximum at angle $\bar{\theta}_i$ found by differentiating Eq. (20–18) with respect to θ_i . Thus

$$\bar{\theta}_i = l^{1/2} (r_0^2 + \rho_s^2)^{1/2} / (k\rho_s n_i r_0). \quad (20-19)$$

To illustrate these results, we plot P_l/P_i in Fig. 20–2(b) as a function of $k\rho_s n_i \theta_i$, assuming $r_0 = \rho_s$. As θ_i increases, less power enters the fundamental mode and power increases in each higher-order mode up to the optimum value $\bar{\theta}_i$.

20–8 Example: Offset Gaussian beam

In this case the Gaussian beam is incident normally on the endface, but the center of the beam is shifted a distance r_d along the x -axis in Fig. 20–2(e). Thus the fiber is illuminated asymmetrically, so less power enters the fundamental mode, and higher-order modes will be excited. In this situation, it is clear from Eqs. (20–7a) and (20–9) that on the endface

$$E_x = \exp \{ -[(x + r_d)^2 + y^2]/2\rho_s^2 \}, \quad (20-20)$$

relative to the coordinates in Fig. 20–2(a). If we express $F_0(R)$ of Table 14–2, page 307 in terms of cartesian coordinates and substitute into Eq. (20–13), we find with the help of Eqs. (37–127) and (20–9) that the fraction of beam power exciting the fundamental mode, when $n_i = n_{co}$, is given by

$$P_0/P_i = \{2\rho_s r_0/(\rho_s^2 + r_0^2)\}^2 \exp \{ -r_d^2/(r_0^2 + \rho_s^2) \}, \quad (20-21)$$

Thus the excitation efficiency decreases exponentially as the beam is displaced farther away from the fiber axis.

20–9 Example: On-axis uniform beam

If the Gaussian beam of Section 20–6 is replaced by the uniform beam of Section 20–4 with radius ρ_s , then we can parallel the derivation of Eq. (20–15) and deduce that the

fraction of beam power exciting the fundamental mode is

$$P_0/P_i = (2r_0/\rho_s)^2 \{1 - \exp(-\rho_s^2/2r_0^2)\}^2,$$

(20-22)

where $r_0 = \rho/V^{1/2}$. Thus, unlike the Gaussian-beam result of Eq. (20-15), not all of the power in the uniform beam can excite the fundamental mode, and higher-order HE_{1m} modes must be excited simultaneously. The maximum excitation efficiency for the HE_{11} mode is $P_0/P_i \cong 81\%$ when $\rho_s \cong 1.6r_0$.

The expressions for the fundamental-mode excitation efficiency P_0/P_i in this and the previous three examples are conveniently repeated together in Table 20-1.

Table 20-1 Excitation efficiency for the fundamental mode. These expressions are exact for the infinite parabolic-profile fiber when $r_0 = \rho/V^{1/2}$, and, within the Gaussian approximation, r_0 is the spot size of Eq. (20-24). Here ρ_s is the radius or spot size for the beam. P_i is the total beam power and P_0 is the power entering the fundamental mode.

Gaussian beam	
On axis	$\frac{P_0}{P_i} = 4 \frac{r_0^2 \rho_s^2}{(r_0^2 + \rho_s^2)^2}$
Tilted at angle θ_i to axis	$\frac{P_0}{P_i} = 4 \frac{r_0^2 \rho_s^2}{(r_0^2 + \rho_s^2)^2} \exp \left\{ - \frac{(kn_i \theta_i r_0 \rho_s)^2}{r_0^2 + \rho_s^2} \right\}$
Offset r_d from axis	$\frac{P_0}{P_i} = 4 \frac{r_0^2 \rho_s^2}{(r_0^2 + \rho_s^2)^2} \exp \left\{ - \frac{r_d^2}{r_0^2 + \rho_s^2} \right\}$
Uniform beam	
On axis	$\frac{P_0}{P_i} = 4 \frac{r_0^2}{\rho_s^2} \left\{ 1 - \exp \left(- \frac{1}{2} \frac{\rho_s^2}{r_0^2} \right) \right\}^2$
On axis with lens	$\frac{P_0}{P_i} = \frac{4}{(kn_i \theta_i r_0)^2} \left\{ 1 - \exp \left(- \frac{1}{2} [kn_i \theta_i r_0]^2 \right) \right\}^2$

20-10 Example: Oblique plane wave

Illumination by an infinite plane wave corresponds to the uniform beam in the limit $\rho_s \rightarrow \infty$. We can then repeat the calculation of Section 20-7 for oblique incidence at angle

θ_i to the fiber axis by suppressing the exponential term in Eq. (20-17). The result corresponding to Eq. (20-18) is readily shown to be

$$P_i = 2\pi r_0^2 n_i \left(\frac{\epsilon_0}{\mu_0} \right)^{1/2} \frac{(kr_0 n_i \theta_i)^{2l}}{l!} \exp\{-(kr_0 n_i \theta_i)^2\}, \quad (20-23)$$

assuming $f(r) = 1$ everywhere in Eq. (20-7a). When $\theta_i \rightarrow 0$, the power entering the fundamental mode is $2\pi r_0^2 n_i (\epsilon_0/\mu_0)^{1/2}$; this agrees with Eqs. (20-22) and (22-10) in the limit $\rho_s \rightarrow \infty$. The power density of the plane wave is $(n_i/2) (\epsilon_0/\mu_0)^{1/2}$, so that the incident power P_i is infinite.

ILLUMINATION OF SINGLE-MODE FIBERS

The efficiency with which beams excite the fundamental modes of circular fibers, with the fields of Eq. (13-9), is of particular interest when the fiber is single moded. In order to account for weakly guiding fibers of otherwise arbitrary profile, when analytical solutions of the scalar wave equation for $F_0(r)$ are not available, we use the Gaussian approximation of Chapter 15. The radial dependence of the fundamental-mode transverse fields is approximated in Eq. (15-2) by setting

$$F_0(r) = \exp(-r^2/2r_0^2). \quad (20-24)$$

The spot size, r_0 , depends on the particular profile shape. Examples, including the step and Gaussian profiles are given in Table 15-2, page 340. If we approximate $F_0(r)$ by Eq. (20-24), it follows that all of the results for fundamental-mode excitation of the infinite parabolic-profile fiber, derived earlier in this chapter, *apply equally to arbitrary profile fibers provided the appropriate expression for r_0 is substituted into Table 20-1.*

20-11 Junctions between fibers

A further consequence of the Gaussian approximation is a simple and accurate description of power loss at junctions between single-mode fibers. In practice, junctions are imperfect because of (a) mismatches between fibers, (b) tilts and (c) offsets, as illustrated in Fig. 20-3. If the incident, fundamental-mode fields of the fiber for $z < 0$ are described by the Gaussian approximation and have spot size ρ_s , i.e. $F_0(r) = \exp(-r^2/2\rho_s^2)$, then *each junction imperfection can be regarded as a Gaussian beam incident on the fiber in $z > 0$.* If we also use the Gaussian approximation for the latter, as described above, the fractional

power loss at the junction is given by $1 - P_0/P_i$, where we substitute the appropriate expression for P_0/P_i from Table 20-1.

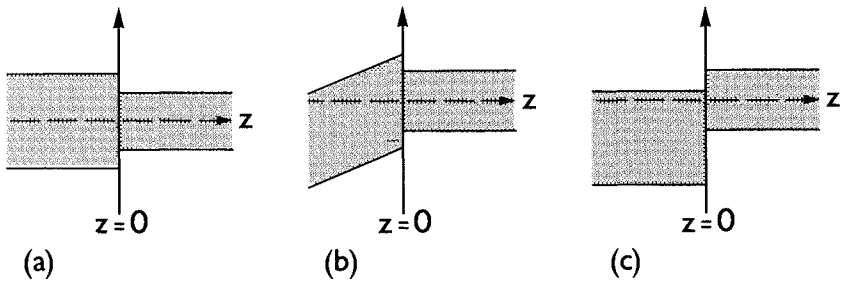


Fig. 20-3 Imperfections at a junction between two fibers due to (a) mismatch, (b) tilt or (c) offset.

STEP-PROFILE FIBERS

To complement our examples of beam illumination of the infinite parabolic-profile fiber, we now derive expressions for the efficiency of a uniform beam in exciting the modes of a weakly guiding, step-profile fiber.

20-12 Example: Tilted uniform beam

When the uniform beam of Section 20-4 is tilted at angle θ_i to the fiber axis, the analysis parallels Section 20-7 as far as Eq. (20-17), which becomes

$$\frac{P_l}{P_i} = 2 \frac{\rho_s^2}{\rho_s^2} \left| \int_0^{\rho_s/\rho} F_l(R) J_l(\kappa R) R \, dR \right|^2 \bigg/ \int_0^\infty F_l^2(R) R \, dR, \quad (20-25)$$

where $\kappa = k\rho n_i \theta_i$ in the notation of Fig. 20-2(a), and $F_l(R)$ is given in Table 14-6, page 319. Integrals of products of Bessel functions can be found in Eqs. (37-94) and (37-98); these together with the integral in Table 14-6 lead to [2]

$$\frac{P_l}{P_i} = 4 \frac{U^2}{V^2} \frac{K_l^2(W)}{K_{l-1}(W)K_{l+1}(W)} \left\{ \frac{\{UJ_{l+1}(U_s)J_l(\kappa_s) - \kappa J_l(U_s)J_{l+1}(\kappa_s)\}^2}{(U^2 - \kappa^2)J_l(U)} \right\}, \quad (20-26a)$$

for $\rho_s \leq \rho$, while for $\rho_s \geq \rho$ we find that

$$\frac{P_l}{P_i} = \left\{ \frac{2\rho}{\rho_s} \frac{U}{V} \right\}^2 \frac{K_l^2(W)}{K_{l-1}(W)K_{l+1}(W)} \left\{ \frac{UJ_{l+1}(U)J_l(\kappa) - \kappa J_l(U)J_{l+1}(\kappa)}{(U^2 - \kappa^2)J_l(U)} + \Lambda \right\}^2, \quad (20-26b)$$

$$\Lambda = \frac{\{\kappa K_l(W_s)J_{l+1}(\kappa_s) - WK_{l+1}(W_s)J_l(\kappa_s)\}\rho_s - \{\kappa K_l(W)J_{l+1}(\kappa) - WK_{l+1}(W)J_l(\kappa)\}\rho}{(W^2 + \kappa^2)\rho K_l(W)}, \quad (20-26c)$$

where $U_s = U\rho_s/\rho$, $W_s = W\rho_s/\rho$, $\kappa_s = \kappa\rho_s/\rho$ and for clarity we have omitted the \sim from U and W as defined at the back of the book. We are reminded that in the present approximation $n_i \cong n_{co} \cong n_{cl}$. If n_i differs significantly from the fiber indices, the corrections of Section 20-2 are required.

To illustrate these results, we consider a $V = 5$ fiber when the beam and core radii are equal, i.e. $\rho_s = \rho$. It is clear from Fig. 14-4 and the even symmetry of excitation about the x -axis that the x -polarized beam field of Eq. (20-7a) excites only the TM_{01} and even HE_{11} , HE_{12} , HE_{21} , HE_{31} , EH_{11} modes. In Fig. 20-4(a) we plot the ratios \bar{P}/P_i , where \bar{P}

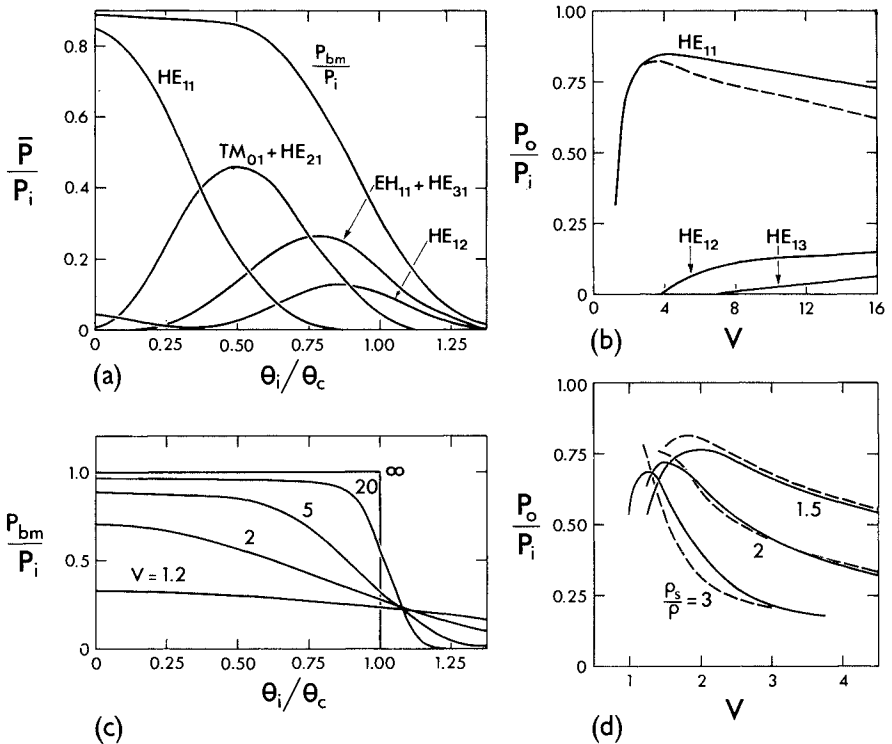


Fig. 20-4 (a) The fraction of total power in a uniform beam that excites modes of a step-profile fiber as a function of the tilt angle θ_i , where \bar{P} includes all modes with the same values of U in Fig. 14-4, and P_{bm} is the total excited power [2]. (b) Variation of the excitation efficiency with the fiber parameter for on-axis illumination, where solid curves denote the exact solution of Eq. (20-27c) and the dashed curve is the Gaussian approximation of Eq. (20-28a). (d) The corresponding curves for the fundamental mode for various ratios of beam to core radii calculated from Eqs. (20-27c) and (20-28b). (c) Plots of P_o/P_i for the fundamental mode and different ratios of beam to core radii.

is the total power in modes with the same value of U , and P_{bm}/P_i , where P_{bm} is the total power in all the modes, as a function of the normalized beam angle θ_i/θ_c . The angle $\theta_c \cong (2\Delta)^{1/2} \cong \{1 - n_{\text{cl}}^2/n_{\text{co}}^2\}^{1/2}$ is the complementary critical angle. As θ_i increases from zero, the power in the fundamental mode decreases, and higher-order modes are excited. However, the total bound-mode power decreases rapidly as more beam power radiates from the fiber.

Optimum inclination

For a given value of the fiber parameter V , there is an optimum inclination θ_i which maximizes the power entering a particular mode. In Fig. 20-4(a) these values of θ_i correspond to the peak values of \bar{P}/P_i . Now it is intuitive that maximum excitation should occur when θ_i is similar to the characteristic angle θ_z which the local plane-wave vector of the modal field makes with the fiber axis, as discussed in Section 36-2. Since θ_c and θ_z are small on a weakly guiding fiber, the relationship with the modal parameter U in Table 36-1, page 695, shows that $\theta_i/\theta_z \cong (\theta_i/\theta_c) (V/U)$. If we insert the values of θ_i/θ_c at the peaks in Fig. 20-4(a) and the corresponding values of V/U , from Fig. 14-4, we find that $\theta_i/\theta_z \cong 1$. A more rigorous analysis shows the peaks in Fig. 20-4(a) for all but the fundamental modes are proportional to $J_{l+1}(U)$ provided $V \gg U$ [2]. For the HE_{11} mode the maximum possible efficiency of 85% occurs when $\theta_i \cong 0$ and $V \cong 3.8$.

20-13 Example: On-axis uniform beam

If, in the previous example, the beam is on axis, then $\theta_i = \kappa = 0$ and, by symmetry, only the HE_{11} and HE_{12} modes are excited. Thus Eq. (20-26) reduces to [2]

$$\frac{P_0}{P_i} = \left\{ \frac{2}{V} \frac{K_0(W)}{K_1(W)} \frac{J_1(U_s)}{J_0(U)} \right\}^2; \quad \rho_s \leq \rho, \quad (20-27a)$$

$$= \left\{ \frac{2U}{VW_s} \right\}^2 \left\{ \frac{V^2}{U^2} - \frac{\rho_s K_1(W_s)}{\rho K_1(W)} \right\}^2; \quad \rho_s \geq \rho, \quad (20-27b)$$

using the same notation. When the beam and core radii are equal

$$P_0/P_i = (2W/UV)^2; \quad \rho_s = \rho, \quad (20-27c)$$

and if the beam radius is much larger than the core radius, Eq. (37-88) gives

$$P_0/P_i \cong (2\rho V/\rho_s UW)^2; \quad \rho_s \gg \rho. \quad (20-27d)$$

In this case, the power excited in each HE_{1m} mode varies with the ratio of core to beam cross-sectional areas.

Numerical results

The ratio P_0/P_i of Eq. (20-27c) is plotted as a function of V in Fig. 20-4(b) for the first three HE_{1m} modes. Cutoff values are $V = 3.832$ for the HE_{12} mode and $V = 7.016$ for

the HE_{13} mode. The peak efficiency of 85% for the HE_{11} mode occurs at $V = 3.8$, and the dashed curve is the Gaussian approximation of Table 20-1 with $\rho_s = \rho$ and $r_0 = \rho/(2 \ln V)^{1/2}$, giving

$$P_0/P_1 = (2/\ln V)(V-1)^2/V^2, \quad (20-28a)$$

which is indistinguishable from the exact expression for $V < 2.4$.

In Fig. 20-4(d) we show how an increase in beam radius affects the fraction of power exciting the fundamental mode, as calculated from Eq. (20-27b). For larger values of V , less power enters the HE_{11} mode as ρ_s increases. The dashed curves are the Gaussian approximation of Table 20-1 with $r_0 = \rho/(2 \ln V)^{1/2}$, i.e.

$$P_0/P_1 = (2\rho^2/\rho_s^2 \ln V) \{1 - \exp(-\rho_s^2 (\ln V)/\rho^2)\}^2, \quad (20-28b)$$

and are in good agreement with the exact values for $V > 2.4$.

When either the HE_{12} or HE_{13} mode is close to cutoff, a significant fraction of power propagates in the cladding, as is clear from Fig. 14-6. Thus a beam that is very much wider than the core can excite substantial power in a mode when that mode is close to cutoff, although most of this power propagates in the cladding. When the beam and core radii are equal, negligible power is launched into a particular mode unless that mode is well above cutoff, as exemplified by the HE_{12} and HE_{13} modes in Fig. 20-4(b).

20-14 Comparison with geometric optics

A useful comparison can be made with the geometric optics analysis of uniform-beam illumination of a multimode, step-profile fiber in Section 4-9. We assume the beam and core radii are equal, and ignore the effect of the endface. Then, if the beam angle satisfies $0 \leq \theta_i < \theta_c$, where θ_c is the complementary critical angle, all of the beam power entering the core excites bound rays and $P_{br}/P_i = 1$, where P_{br} denotes the total bound-ray power. However, when $\theta_i > \theta_c$ no power goes into bound rays and $P_{br}/P_i = 0$. A plot of P_{br}/P_i against normalized beam angle θ_i/θ_c corresponds to the $V = \infty$ curve in Fig. 20-4(c).

The corresponding modal calculation determines the fraction of beam power entering all bound modes that are excited for a given value of the waveguide parameter V . Thus P_{bm}/P_i is calculated by summing Eq. (20-26) with $\rho_s = \rho$ over all bound modes. As V increases, more bound modes are excited, but only when $V = \infty$ is there exact agreement with the ray analysis [8]. For finite values of V , the geometric optics analysis does not take into account spreading of the beam fields due to the diffraction at the fiber endface, as discussed in Chapter 10.

LENS ILLUMINATION

The presence of a lens in front of the endface of a fiber can increase the amount of power entering the bound modes. Consider the situation in Fig. 20-5 where a

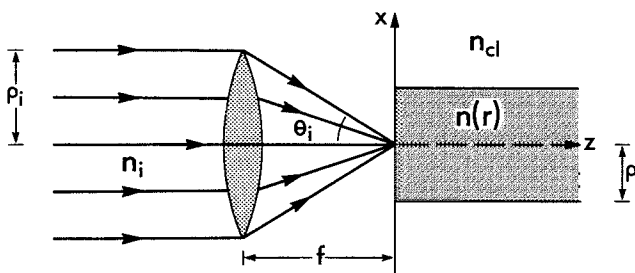


Fig. 20-5 On-axis lens illumination of a fiber assuming equal beam and lens radii. The focal point of the lens is on the endface.

uniform, on-axis beam of radius ρ_i passes through a convex lens, positioned so that its focus coincides with the center of the endface. The effect of the lens on the beam is to produce a far-field diffraction pattern in the focal plane due to a circular aperture equal in radius to the lens radius ρ_i . Assuming that the angle $2\theta_i$ subtended by the lens at the endface is small, then the polarization of the beam fields is only slightly changed on passing through the lens. We also assume that the power of the beam is conserved on passing through the lens. For comparative purposes, the total power in the incident beam is taken to be P_i of Eq. (20-10), which, with the aid of Eq. (37-91) and Table 13-2, page 292, determines the normalization of the far-field diffraction pattern of the lens at the endface [9]

$$E_x = \frac{\rho_i J_1(\kappa R)}{\rho R}; \quad \kappa = \kappa \rho n_i \theta_i, \quad R = \frac{r}{\rho}, \quad (20-29)$$

where J_1 is the Bessel function of the first kind, n_i is the refractive index of the beam medium and θ_i is the angle subtended by the lens, i.e. if f is the focal length $\theta_i \cong \rho_i/f$. The radial coordinate r is shown in Fig. 20-2(a) and ρ is the core radius or scaling length. We now consider examples.

20-15 Example: Infinite parabolic profile

Only the HE_{1m} modes are excited on the circular fiber, and the power in each mode is determined by substituting Eq. (20-29) into Eq. (20-13) and using the expressions for $F_i(R)$ in Table 14-2, page 307. For the fundamental mode the integral in the numerator of Eq. (20-13) is given by Eq. (37-100a), whence we deduce the excitation efficiency is [10]

$$P_0/P_i = (2/\Omega)^2 \{1 - \exp(-\Omega^2/2)\}^2; \quad \Omega = \kappa r_0 n_i \theta_i, \quad (20-30)$$

where $r_0 = \rho/V^{1/2}$ is the spot size. This expression is functionally identical to Eq. (20-22), and therefore the maximum excitation efficiency is 81 % when $\Omega \cong 1.6$. Thus we have the interesting conclusion that the maximum excitation efficiency for uniform-beam illumination of the fundamental mode on an infinite, parabolic-profile fiber is independent of the presence of the lens. However, if the beam power density is the same in both cases, the actual power P_0 in the fundamental mode when the lens is present can be arbitrary large compared to when no lens is present. In the first case, the beam and lens radius ρ_i and the focal length f are increased simultaneously so that θ_i remains fixed at its optimum value.

20-16 Example: Gaussian approximation

The expression in Eq. (20-30) for the fundamental-mode efficiency is also the result which we would obtain using the Gaussian approximation of Eq. (20-24) for an arbitrary profile. Thus we have a general expression for lens illumination. For example, Table 15-2, page 340, gives $r_0 = \rho/(2 \ln V)^{1/2}$ for the step profile, and at $V = 2.4$ the error between Eq. (20-30) and an exact analysis is less than 1 % [10].

DIFFUSE ILLUMINATION

So far in this chapter we have considered mode excitation due to a single beam directed at a particular angle to the fiber axis. Let us now consider the effect on mode excitation when the illumination is composed of a family of beams which differ in their angles of incidence at the endface, e.g. the source of diffuse illumination depicted in Fig. 20-6(a). Such sources are known as (partially)

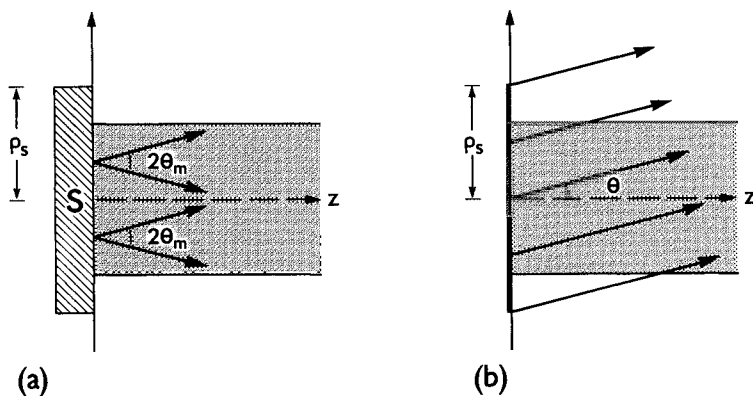


Fig. 20-6 (a) A diffuse source of radius ρ_s abuts the endface of a fiber. Each point on the source emits light within a cone of half angle θ_m . (b) The model of the source superposes beams making a variable angle θ with the fiber axis.

spatially incoherent sources, whereas the uniform and Gaussian beam used earlier in the chapter are approximately *spatially coherent*, i.e. all points on a cross-section of the beam have virtually the same phase, as on a plane-wave front, provided the angle of incidence is small.

The partially diffuse source in Fig. 20-6(a) is modelled as a superposition of (coherent) beams, one of which is shown in Fig. 20-6(b). There is a random relative phase between adjacent beams, and consequently, the total power P_s radiated by the source is found by summing the power in each beam. Assuming that the source is axisymmetric we have

$$P_s = 2\pi \int_0^{\theta_m} P(\theta) \sin \theta \, d\theta, \quad (20-31)$$

where $P(\theta)$ is the total power in the beam at angle θ to the fiber axis per unit angle. If P_j denotes the power excited in the j th mode, it is composed of the modal powers due to each incident beam. Hence

$$P_j = 2\pi \int_0^{\theta_m} P_j(\theta) \sin \theta \, d\theta, \quad (20-32)$$

where $P_j(\theta)$ is the power contributed to the mode by the beam incident at angle θ . Thus the efficiency with which the source excites the j th mode, assuming that each beam contains the same power, i.e. $P(\theta) = P$, is given by the ratio

$$\frac{P_j}{P_s} = \frac{1}{1 - \cos \theta_m} \int_0^{\theta_m} \frac{P_j(\theta)}{P} \sin \theta \, d\theta \cong \frac{2}{\theta_m^2} \int_0^{\theta_m} \frac{P_j(\theta)}{P} \theta \, d\theta, \quad (20-33)$$

where the second expression assumes $\theta_m \ll 1$. The ratio $P_j(\theta)/P$ is given by the ratio of Eq. (20-13) to P_i of Eq. (20-9) for circular fibers. Hence Eq. (20-33) confirms the intuitive suggestion that the modal power excited by a diffuse source is simply the modal power averaged over all the incident beams that compose the diffuse source. Thus, by knowing the modal excitation due to a beam at an arbitrary angle θ , we can determine the power due to diffuse illumination by superposition.

20-17 Example: Single-mode fibers

The partially diffuse source of Fig. 20-6(a) illuminates a single-mode fiber. We showed in Sections 20-7 and 20-12 that the fundamental mode is most efficiently excited by on-axis beams. Thus, it is intuitive that the more diffuse the source, i.e. the larger θ_m , the lower the efficiency of the source in exciting the fundamental mode. To demonstrate this behavior quantitatively, we consider a source with a Gaussian intensity

distribution over its cross-section which is modelled by a superposition of Gaussian beams. The Gaussian approximation is used for the fundamental-mode fields, whence $P_j(\theta)/P$ in Eq. (20-33) is given by P_0/P_i for a tilted Gaussian beam in Table 20-1 with θ_i replaced by θ . Straightforward integration leads to

$$\frac{P_0}{P_s} = \frac{4}{V^2} \frac{\theta_c^2}{\theta_m^2 r_0^2 + \rho^2} \left[1 - \exp \left\{ -V^2 \frac{\theta_m^2}{\theta_c^2} \frac{r_0^2}{r_0^2 + \rho^2} \right\} \right] \quad (20-34)$$

assuming equal source and core radii, i.e. $\rho_s = \rho$, where V is the fiber parameter, $\theta_c \cong (1 - n_{ci}^2/n_{co}^2)^{1/2}$ is the complementary critical angle, and $n_i \cong n_{co}$, neglecting the slight reflection loss from the endface. We plot P_0/P_s as a function of θ_m/θ_c for given values of V in Fig. 20-7(a). With reference to Table 15-2, page 340, the step profile (s) corresponds to $r_0 = \rho/(2 \ln V)^{1/2}$ and $V \cong 2.41$ at the cutoff of the second mode, the Gaussian profile (g) corresponds to $r_0 = \rho/(V-1)$ and $V \cong 2.59$ at the cutoff of the second mode, and the infinite parabolic profile (p) corresponds to $r_0 = \rho/V^{1/2}$ and $V = 3$, for which Eq. (20-34) is exact.

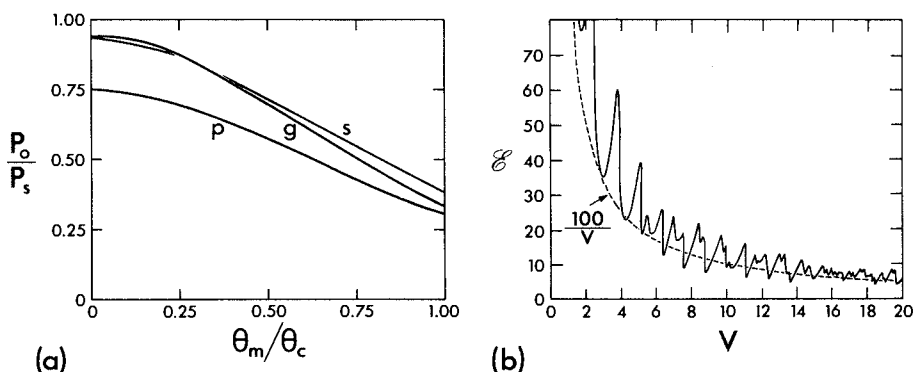


Fig. 20-7 (a) The fraction of power, calculated from Eq. (20-34), that enters the fundamental mode as a function of the angular spread θ_m of a diffuse source for step (s), Gaussian (g) and infinite parabolic (p) profile fibers. (b) The percentage error in the geometric optics analysis of totally incoherent illumination of a multimode fiber as a function of the fiber parameter. The solid curve is the exact result calculated from Eq. (20-39) and the dashed curve is the approximation of Eq. (20-41) [11].

20-18 Example: Multimode fibers

The total bound-mode power P_{bm} for a weakly guiding fiber of arbitrary cross-section and illuminated by a diffuse source is the sum of the power P_j of Eq. (20-32) for each

mode. If we assume that the source is spatially *totally incoherent*, i.e. $\theta_m = \pi/2$, then the radiation from each point of the source is independent of all other points, and the power P_j entering a mode follows from power considerations at each point. Thus P_j is given by Eq. (20–12) with the square of the modulus of the integral replaced by the integral of the square of the modulus of the integrand. However, this ignores the facts that each point emits light polarized in the x - and y -directions of Fig. 20–2(a) with equal probability, and that the source electric field has equal x - and y -components. Hence Eq. (20–12) must be reduced by a factor of 4 to give

$$P_j = \frac{n_{co}}{8} \left(\frac{\epsilon_0}{\mu_0} \right)^{1/2} \int_{A_{co}} |E_x|^2 |e_{xj}|^2 dA \Big/ \int_{A_{co}} |e_{ij}|^2 dA. \quad (20-35)$$

If the source is *uniform* and has a cross-section equal to the fiber core cross-section A_{co} , we find with the help of Table 13–2, page 292, that [11]

$$P_j = C \int_{A_{co}} |e_{xj}|^2 dA \Big/ \int_{A_{co}} |e_{ij}|^2 dA = C \eta_j, \quad (20-36)$$

where the constant $C = (n_{co} |E_x|^2 / 8) (\epsilon_0 / \mu_0)^{1/2}$, and η_j is the fraction of modal power in the core. This result states what is physically obvious from the outset, namely that an incoherent source excites each mode with the maximum efficiency possible, i.e. η_j . Accordingly the total bound mode power is given by

$$P_{bm} = \sum_{j=1}^M P_j = C \sum_{j=1}^M \eta_j, \quad (20-37)$$

where M is the number of bound modes.

On a multimode fiber, with fiber parameter $V \rightarrow \infty$, virtually all modes satisfy $\eta_j \cong 1$, and thus P_{bm} of Eq. (20–37) varies with the number of modes. We show in Section 36–13 that $M \cong V^2/2$ for the step-profile fiber, and, from the definition of V inside the back cover, P_{bm} is proportional to θ_c^2 , where θ_c is the complementary critical angle. Apart from normalization factors associated with total source power, this result agrees with the total bound-ray power P_{br} of Eq. (4–16), which assumes illumination by the Lambertian source of Eq. (4–2). Since $\theta_c \ll 1$ in the weak-guidance approximation, the intensity distribution for the Lambertian source is approximately independent of direction for bound rays. This is the ray equivalent of the diffuse source for propagation within θ_c .

20–19 Error in the geometric optics analysis

In the example above, we established the equivalence of the geometric optics and modal analysis for the total, guided power excited in a weakly guiding, step-profile fiber by a totally incoherent source when the fiber parameter $V \rightarrow \infty$. To determine the error in the geometric optics analysis when V is

finite, we start with the electromagnetic expression for the total bound-mode power P_{co} in the fiber core. We deduce from Eqs. (11-24) and (20-37) that

$$P_{\text{co}} = C \sum_{j=1}^M \eta_j^2, \quad (20-38)$$

where C is a constant and $M \cong V^2/2$. If \mathcal{E} is the error in the geometric optics expression P_{br} for bound-ray power, then since $\eta_j \rightarrow 1$ as $V \rightarrow \infty$

$$\mathcal{E} = \frac{P_{\text{br}} - P_{\text{co}}}{P_{\text{co}}} = \frac{V^2}{2} \left\{ \sum_{j=1}^m \eta_j^2 \right\}^{-1} - 1, \quad (20-39)$$

The density of eigenvalue equation solutions approaches a continuum as $V \rightarrow \infty$, so for finite V we can approximate the summation by an integral. We replace η_j by its asymptotic form for large V in Table 14-7, page 324. Although this form is a slight overestimate for higher-order modes, it nevertheless leads to a simple expression for \mathcal{E} . Hence

$$\sum_{j=1}^m \eta_j^2 \cong \int_0^{V^{2/2}} \left\{ 1 - \frac{U^2(\xi)}{V^3} \right\}^2 d\xi, \quad (20-40)$$

where the continuous variable ξ coincides with j at integral values. For a given value of V , the values of U satisfy $0 \leq U \leq V$ and are distributed approximately quadratically, i.e. $U^2 \cong 2\xi$. Substituting into Eq. (20-40) and retaining only lowest and first order terms in $1/V$, we deduce from Eq. (20-39) that [11]

$$\boxed{\mathcal{E} = 1/V.} \quad (20-41)$$

The percentage error $100/V$ is plotted in Fig. 20-7(b) as the dashed curve, together with the exact numerical value of \mathcal{E} calculated from Eq. (20-39).

REFERENCES

1. Snyder, A. W. (1966) Surface waveguide modes along a semi-infinite dielectric fiber excited by a plane wave. *J. Opt. Soc. Am.*, **56**, 601-10.
2. Snyder, A. W. (1969) Excitation and scattering of modes on a dielectric or optical fiber. *I.E.E.E., Trans. Microwave Theory Tech.*, **17**, 1138-44.
3. Cardama, A. and Kornhauser, E. T. (1975) Modal analysis of coupling problems in optical fibers. *I.E.E.E. Trans. Microwave Theory Tech.* **23**, 162-70.
4. Kapany, N. S. and Burke, J. J. (1972) *Optical Waveguides*, Academic Press, chap. 5.
5. Stern, J. R., Peace, M. and Dyott, R. B. (1970) Launching into optical-fiber waveguides. *Electron Lett.*, **6**, 160-2.
6. Marcuse, D. (1970) Excitation of the dominant mode of a round fiber by a Gaussian beam. *Bell Syst. Tech. J.*, **49**, 1695-1703.

7. Mostafavi, M., Itoh, T. and Mittra, R. (1975) Excitation of an optical fiber by a Gaussian beam. *Appl. Opt.*, **14**, 2190–3.
8. Snyder, A. W., Pask, C. and Mitchell, D. J. (1973) Light acceptance property of an optical fiber. *J. Opt. Soc. Am.*, **63**, 59–64.
9. Born, M. and Wolf, E. (1970) *Principles of Optics*, Pergamon Press, London.
10. Barrell, K. F. and Pask, C. (1979) Optical fiber excitation by lenses. *Opt. Acta*, **26**, 91–108.
11. Snyder, A. W. and Pask, C. (1973) Incoherent illumination of an optical fiber. *J. Opt. Soc. Am.*, **63**, 806.

Sources within fibers

Bound-mode excitation	442
21-1 Modal amplitudes and power	443
21-2 Weakly guiding fibers	444
21-3 <i>Example: Current dipole within an arbitrary fiber</i>	445
21-4 <i>Example: Transverse dipole within a weakly guiding fiber</i>	445
21-5 <i>Example: Longitudinal dipole within a weakly guiding fiber</i>	446
21-6 <i>Example: Tubular current sources</i>	447
 Radiation-field excitation	 448
21-7 Weakly guiding fibers	448
21-8 'Free-space' approximation	450
21-9 <i>Example: Dipole radiation</i>	451
21-10 <i>Example: Tubular-source radiation</i>	453
21-11 Radiation correction due to the fiber profile	455
21-12 Correction factor	455
21-13 <i>Example: Step profile</i>	456
21-14 <i>Example: Corrected tubular-source radiation</i>	458
 References	 459

In the previous chapter we examined the excitation of modes of a fiber by illumination of the endface with beams and diffuse sources, i.e. by sources external to the fiber. Here we investigate the power of bound modes and the power radiated due to current sources distributed within the fiber, as shown in Fig. 21-1. Our interest in such problems is mainly motivated by the following chapter, where we show that fiber nonuniformities can be modelled by current sources radiating within the uniform fiber. Thus, isolated nonuniformities radiate like current dipoles and surface roughness, which occurs at the core-cladding interface, can be modelled by a tubular current source.

BOUND-MODE EXCITATION

The fiber or waveguide in Fig. 21-1 has arbitrary refractive-index profile and cross-sectional geometry, and supports modes with the properties described in Chapter 11. Outside of the region occupied by currents, the total fields **E** and **H**

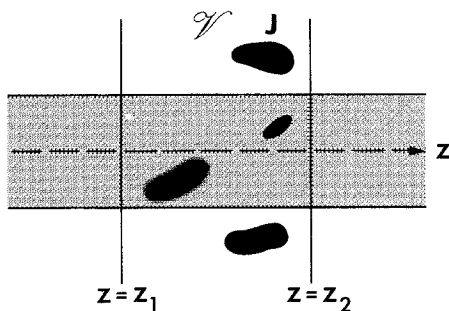


Fig. 21-1 The darker regions denote distributions of currents with density and direction \mathbf{J} . These currents are contained in volume \mathcal{V} between cross-sectional planes $z = z_1$ and $z = z_2$.

are expressible as a summation over all bound modes, together with a term representing the radiation field, given by Eq. (11-2). It is intuitive that in the region $z > z_2$ of Fig. 21-1 the fields must propagate in the increasing z -direction. Consequently, the fields consist of only the forward-propagating bound modes and the forward-propagating components $\mathbf{E}_{\text{rad}}^+$ and $\mathbf{H}_{\text{rad}}^+$ of the radiation field. Similarly, when $z < z_1$ only the backward-propagating bound modes and the backward-propagating components $\mathbf{E}_{\text{rad}}^-$ and $\mathbf{H}_{\text{rad}}^-$ of the radiation field are involved. Combining Eqs. (11-2) to (11-4), the total fields are expressible as

$$\mathbf{E}(x, y, z) = \sum_j a_j \mathbf{e}_j(x, y) \exp(i\beta_j z) + \mathbf{E}_{\text{rad}}^+(x, y, z); \quad z > z_2, \quad (21-1a)$$

$$= \sum_j a_{-j} \mathbf{e}_{-j}(x, y) \exp(-i\beta_j z) + \mathbf{E}_{\text{rad}}^-(x, y, z); \quad z < z_1, \quad (21-1b)$$

$$\mathbf{H}(x, y, z) = \sum_j a_j \mathbf{h}_j(x, y) \exp(i\beta_j z) + \mathbf{H}_{\text{rad}}^+(x, y, z); \quad z > z_2, \quad (21-1c)$$

$$= \sum_j a_{-j} \mathbf{h}_{-j}(x, y) \exp(-i\beta_j z) + \mathbf{H}_{\text{rad}}^-(x, y, z); \quad z < z_1, \quad (21-1d)$$

where $j = 1, \dots, M$ and the $a_{\pm j}$ are the modal amplitudes. In the region $z_1 \leq z \leq z_2$, the $a_{\pm j}$ depend on z through Eqs. (31-35) and (31-36).

21-1 Modal amplitudes and power

The current sources in Fig. 21-1 launch power into bound modes, and thus specify the modal amplitudes. Expressions for these amplitudes are derived from Maxwell's equations in Chapter 31. We find from Eqs. (31-35) and

(31-36) together with Eq. (11-7) that [1]

$$a_j = -\frac{1}{4N_j} \int_{\mathcal{V}} (\mathbf{e}_{tj} + e_{zj}\hat{\mathbf{z}})^* \cdot \mathbf{J} \exp(-i\beta_j z) d\mathcal{V}; \quad z > z_2, \quad (21-2a)$$

$$a_{-j} = \frac{1}{4N_j} \int_{\mathcal{V}} (\mathbf{e}_{tj} - e_{zj}\hat{\mathbf{z}})^* \cdot \mathbf{J} \exp(i\beta_j z) d\mathcal{V}; \quad z < z_1, \quad (21-2b)$$

where \mathcal{V} is the volume occupied by currents in Fig. 21-1, $\mathbf{e}_j = \mathbf{e}_{tj} + e_{zj}\hat{\mathbf{z}}$, subscripts t and z denote transverse and longitudinal components, respectively, and $\hat{\mathbf{z}}$ is the unit vector parallel to the fiber axis. The normalization N_j is defined in Table 11-1, page 230. If the fiber is nonabsorbing, the conjugated fields are expressible in terms of the unconjugated fields through Eq. (11-9).

The power in each mode is given by Eq. (11-22) as

$$P_j = |a_j|^2 N_j; \quad P_{-j} = |a_{-j}|^2 N_j, \quad (21-3)$$

where the power P_j in the forward-propagating mode flows in the increasing z -direction of Fig. 21-1, and the power P_{-j} in the backward-propagating mode flows in the decreasing z -direction. The total power excited in bound modes is given by

$$P_{\text{bm}} = \sum_j (P_j + P_{-j}) = \sum_j (|a_j|^2 + |a_{-j}|^2) N_j. \quad (21-4)$$

The efficiency with which each mode is excited, is found by dividing $P_{\pm j}$ by the total power emitted by the sources, P_{tot} .

21-2 Weakly guiding fibers

When the fiber is weakly guiding, the approximations of Chapter 13 can be used to simplify Eq. (21-2). If for convenience we assume a circular fiber with current sources parallel to the x -axis in the cross-section, then we deduce from Tables 13-2, page 292, and 14-1, page 304, and Eq. (21-3) that the power in each mode is given by

$$P_{\pm l} = \frac{1}{16\pi\rho^2 n_{\text{co}}} \left(\frac{\mu_0}{\epsilon_0} \right)^{1/2} \left| \int_{\mathcal{V}} J_x e_{xl} \exp(\mp i\tilde{\beta}_l z) d\mathcal{V} \right|^2 \bigg/ \int_0^\infty R F_l^2(R) dR,$$

(21-5)

where $e_{xl} = F_l \cos l\phi$ or $e_{xl} = F_l \sin l\phi$, the scalar propagation constants $\tilde{\beta}_l$ and F_l are solutions of the scalar wave equation, Eq. (14-4), and remaining parameters are defined inside the back cover. The same expression can be derived directly from the scalar wave equation using the analysis at the end of Chapter 33. When the current sources are parallel to the fiber axis, the

corresponding result is

$$P_{\pm l} = \frac{1}{16\pi\rho^2 n_{\text{co}}} \left(\frac{\mu_0}{\epsilon_0} \right)^{1/2} \left| \int_{\mathcal{V}} J_z e_{zl} \exp(\mp i\beta_l z) d\mathcal{V} \right|^2 \bigg/ \int_0^\infty R F_l^2(R) dR, \quad (21-6)$$

where e_{zl} denotes the appropriate form of e_{zi} in Table 14–1. To illustrate these results we now consider some simple examples.

21–3 Example: Current dipole within an arbitrary fiber

The vector current density \mathbf{J} for a point current dipole of length d , small compared with a wavelength, and located at position (r_d, ϕ_d, z_d) in Fig. 12–3 is given by

$$\mathbf{J}(r, \phi, z) = \frac{\delta(r - r_d)}{r_d} \delta(\phi - \phi_d) \delta(z - z_d) \mathbf{I}, \quad (21-7)$$

where δ is the Dirac delta function, and \mathbf{I} is the vector current on the dipole which contains the implicit time dependence $\exp(-i\omega t)$ and gives the direction of \mathbf{J} . Substitution of Eq. (21–7) into Eq. (21–2) gives the modal amplitudes, and the modal power excited by the dipole is then found from Eq. (21–3). Provided the modal fields are known exactly, this calculation is also exact, e.g. the step-profile fiber of Table 12–3, page 250. However, because there are few such solutions available, we consider instead the power excited in the fundamental modes of weakly guiding fibers, since we can use the Gaussian approximation to describe the modal fields of otherwise arbitrary profiles.

21–4 Example: Transverse dipole within a weakly guiding fiber

The dipole is oriented parallel to the x -axis in the fiber cross-section, as shown in Fig. 21–2(a). Consequently the y -polarized fundamental modes are not excited and equal power P_0 enters the forward- and backward-propagating x -polarized modes. Substituting Eq. (21–7) into Eq. (21–5) we obtain

$$P_0 = \frac{|Id|^2}{16\pi\rho^2 n_{\text{co}}} \left(\frac{\mu_0}{\epsilon_0} \right)^{1/2} F_0^2(r_d/\rho) \bigg/ \int_0^\infty R F_0^2(R) dR, \quad (21-8)$$

where F_0 is the fundamental solution of the scalar wave equation. For the step profile we can substitute the exact expression for F_0 from Table 14–3, page 313, while for an arbitrary profile we replace F_0 by the Gaussian approximation of Eq. (15–2), leading to

$$P_0 = \frac{|Id|^2}{8\pi r_0^2 n_{\text{co}}} \left(\frac{\mu_0}{\epsilon_0} \right)^{1/2} \exp \left\{ -\frac{r_d^2}{r_0^2} \right\}, \quad (21-9)$$

where r_0 is the spot size for the particular profile. This expression, which is exact for the infinite parabolic profile of Section 14–4 if we set $r_0 = \rho/V^{1/2}$, shows that fundamental-mode power is greatest for an on-axis dipole and decreases exponentially with increasing distance from the axis.

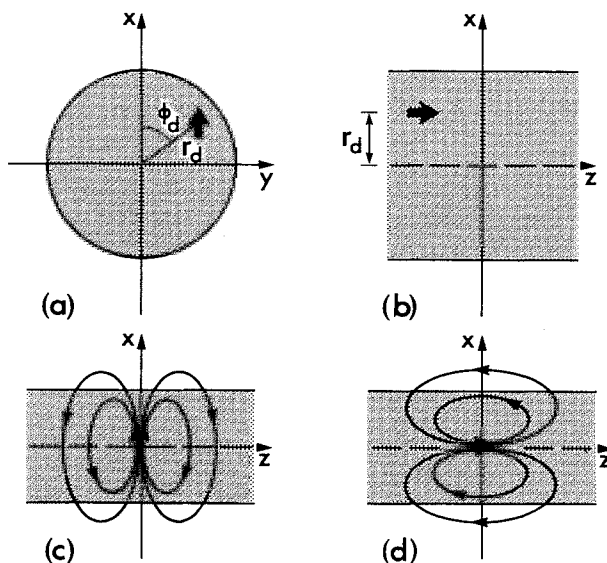


Fig. 21-2 A current dipole is located at radius r_d and azimuthal angle ϕ_d in the fiber cross-section so that its direction is parallel to (a) the x -axis and (b) the z -axis. The direction along contours of constant electric field amplitude for the two cases, when $r_d = 0$, are shown in (c) and (d), respectively, which ignore the slight effect of the fiber.

21-5 Example: Longitudinal dipole within a weakly guiding fiber

In this case the dipole is oriented parallel to the fiber axis, as shown in Fig. 21-2(b). On substituting Eq. (21-7) into Eq. (21-6) and referring to Table 14-1, page 304, we find that both x - and y -polarized fundamental modes are excited, with powers P_{0x} and P_{0y} , respectively, in the forward- and backward-propagating modes, where

$$\frac{P_{0x}}{\cos^2 \phi_d} = \frac{P_{0y}}{\sin^2 \phi_d} = \frac{\Delta |Id|^2}{8\pi V^2 n_{co}} \left(\frac{\mu_0}{\epsilon_0} \right)^{1/2} \left\{ \frac{dF_0}{dr} \Big|_{r_d} \right\}^2 \Big/ \int_0^\infty R F_0^2(R) dR, \quad (21-10)$$

and parameters are defined at the back of the book. Within the Gaussian approximation of Eq. (15-2), the corresponding expression is

$$\boxed{\frac{P_{0x}}{\cos^2 \phi_d} = \frac{P_{0y}}{\sin^2 \phi_d} = \frac{\Delta |Id\rho|^2}{4\pi V^2 r_0^4 n_{co}} \left(\frac{\mu_0}{\epsilon_0} \right)^{1/2} \frac{r_d^2}{r_0^2} \exp \left\{ -\frac{r_d^2}{r_0^2} \right\}}, \quad (21-11)$$

where r_0 is the spot size for the particular profile, e.g. Table 15-2, page 340. For the step and infinite parabolic profiles, Eqs. (21-10) and (21-11) are exact if we substitute for F_0 from Table 14-3, page 313, and set $r_0 = \rho/V^{1/2}$, respectively. We deduce from Eq. (21-11) that the on-axis dipole excites zero power, while the dipole at $r_d = r_0$ excites maximum power. Furthermore, the power of the bound mode due to the z -directed

dipole is of order Δ smaller than that due to the x -directed dipole. This is obvious from the radiation patterns of Figs. 21-2(c) and 21-2(d) for the two cases, which show the direction and constant amplitude contours of the dipole electric field \mathbf{E} when $r_d = 0$. Close to the fiber axis, where the fundamental-mode field is essentially transverse and has its peak value, the z -directed dipole field is parallel to the axis, whereas the transverse dipole has a transverse field.

21-6 Example: Tubular current sources

The modelling of nonuniform fibers by current sources in the following chapter leads to the *tubular current source*. This source, which is depicted in Fig. 21-3, consists of a current distribution of density \mathbf{J} on the cylindrical surface, or tube, $r = r_0$ defined by [2]

$$\mathbf{J} = \hat{\mathbf{n}} g(z) \frac{\delta(r - r_0)}{2\pi r_0} \cos l(\phi - \phi_0); \quad -L \leq z \leq L, \quad (21-12)$$

where ϕ_0 is a fixed azimuthal angle, l is a positive integer or zero and δ is the Dirac delta function. The unit vector $\hat{\mathbf{n}}$ gives the direction and $g(z)$ specifies the current variation along the fiber. If we regard the source as a superposition of current dipoles, it includes the previous two examples as special cases.

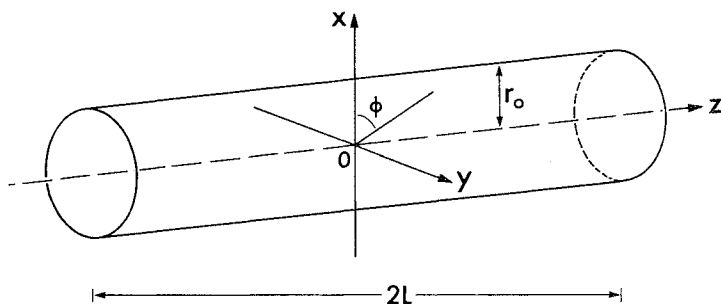


Fig. 21-3 A tubular current source of length $2L$ and radius r_0 carries the distribution \mathbf{J} of Eq. (21-12) on its surface.

We are primarily interested in sinusoidal distributions on arbitrarily long tubes when the currents are parallel to a fixed direction, i.e.

$$g(z) = \exp(iCz) \sin \Omega z; \quad L \rightarrow \infty, \quad (21-13)$$

and $\hat{\mathbf{n}} = \hat{\mathbf{x}}$ or $\hat{\mathbf{n}} = \hat{\mathbf{z}}$, where C, Ω are constants and $\hat{\mathbf{x}}, \hat{\mathbf{z}}$ are unit vectors parallel to the axes in Fig. 21-3. If we substitute Eqs. (21-12) and (21-13) into Eq. (21-5) or Eq. (21-6), then the power excited in the forward- or backward-propagating modes is proportional to $|I_+|^2$ or $|I_-|^2$, respectively, where

$$I_{\pm} = \int_{-L}^L \exp\{i(C \mp \beta_l)z\} \sin \Omega z \, dz = i \left\{ \frac{\sin(C \mp \beta_l - \Omega)L}{C \mp \beta_l - \Omega} - \frac{\sin(C \mp \beta_l + \Omega)L}{C \mp \beta_l + \Omega} \right\}, \quad (21-14)$$

and the \sim is omitted for clarity. These integrals are negligibly small except close to resonance. In other words, sources satisfying $\Omega \cong |C - \beta_l|$ excite significant power in forward-propagating modes, and sources satisfying $\Omega \cong |C + \beta_l|$ excite significant power in backward-propagating modes. Hence

$$|I_{\pm}|^2 \cong L^2; \quad \Omega \cong |C \pm \beta_l|, \quad (21-15)$$

provided the tube is sufficiently long.

RADIATION-FIELD EXCITATION

So far in this chapter we have determined the power excited in bound modes by a current source. This power is guided indefinitely by the fiber. The remaining portion of the total power emitted by the source radiates from the fiber. There are two general methods for determining the radiation field. One is the modal approach of Chapter 25, where the radiation field is expanded in terms of radiation modes. In this chapter we follow the Green's function approach which first investigates the radiation due to a point dipole and then linearly superimposes dipoles to form arbitrary current sources. Because the waveguide is weakly guiding, most of the source power radiates from the structure with only a small fraction directed into bound-mode power. Consequently, in the first approximation, the radiated power is that due to a source within an unbounded cladding medium. For this reason we appeal to the well-known methods of antenna theory which are ideally suited to such problems. The effect of the fiber structure is then determined as a small correction to the 'free-space' radiation result.

21-7 Weakly guiding fibers

When a current source is located within a clad fiber of arbitrary profile, the determination of the radiation field is extremely complicated. However, if the fiber is weakly guiding the determination is greatly simplified [2]. It is intuitive that when the variation in the refractive-index profile is small, the source radiates as if it were located in a virtually uniform, infinite medium of refractive index equal to the cladding index n_{cl} . The problem is then analogous to the radiation from an antenna in free space. Consequently, we can borrow from standard antenna theory, and couch the solution to radiation from the weakly guiding fiber in terms of the electromagnetic vector potential \mathbf{A} [3-5].

Vector potential representation of the fields

In Section 34-3 we show how the classical, free-space representation of the radiation fields in terms of the vector potential \mathbf{A} is modified by the presence of

the fiber. The electric and magnetic components \mathbf{E} and \mathbf{H} of the radiation field are related to the vector potential by Eq. (34-13). Hence

$$\mathbf{E} = \frac{ik}{(\mu_0 \epsilon_0)^{1/2}} \left\{ \mathbf{A} + \frac{1}{k^2 n_{cl}^2} \nabla (\nabla \cdot \mathbf{A}) \right\}; \quad \mathbf{H} = \frac{1}{\mu_0} \nabla \times \mathbf{A}, \quad (21-16)$$

where n_{cl} is the uniform cladding refractive index, and ϵ_0 and μ_0 are the free-space dielectric constant and permeability. The free-space wavenumber k is related inside the back cover to the angular frequency ω of the implicit time dependence $\exp(-i\omega t)$ of \mathbf{E} , \mathbf{H} , \mathbf{A} and \mathbf{J} below. In the weak-guidance approximation, the vector potential $\mathbf{A} = \mathbf{A}(x, y, z)$ satisfies Eq. (34-14)

$$\{\nabla^2 + k^2 n^2\} \mathbf{A} = -\mu_0 \mathbf{J}, \quad (21-17)$$

where $n = n(x, y)$ is the fiber profile, $\mathbf{J} = \mathbf{J}(x, y, z)$ is the prescribed current distribution and ∇^2 is the scalar Laplacian of Eq. (37-36). This equation assumes *the scalar components of \mathbf{A} are referred to fixed cartesian directions*, although the spatial dependence is expressible in an arbitrary coordinate system. The major differences between the present formulation and the usual free-space representation are the dependence on profile in Eq. (21-17) and the introduction of the factor $1/n_{cl}^2$ in Eq. (21-16).

Sufficiently far into the cladding, the fields due to all sources are locally plane. As we discuss in Section 34-4, expressions for the far fields are then readily shown to be [3-5]

$$\mathbf{E} = -\frac{ik}{(\mu_0 \epsilon_0)^{1/2}} \hat{\mathbf{r}} \times (\hat{\mathbf{r}} \times \mathbf{A}); \quad \mathbf{H} = \frac{ik n_{cl}}{\mu_0} \hat{\mathbf{r}} \times \mathbf{A} = n_{cl} \left(\frac{\epsilon_0}{\mu_0} \right)^{1/2} \hat{\mathbf{r}} \times \mathbf{E}, \quad (21-18)$$

from which the Poynting vector \mathbf{S} and total radiated power P_{rad} follow

$$\mathbf{S} = \frac{c^2 k^2 n_{cl}}{2} \left(\frac{\epsilon_0}{\mu_0} \right)^{1/2} |\hat{\mathbf{r}} \times \mathbf{A}|^2 \hat{\mathbf{r}}; \quad P_{rad} = \frac{c^2 k^2 s^2 n_{cl}}{2} \left(\frac{\epsilon_0}{\mu_0} \right)^{1/2} \int_{S_\infty} |\hat{\mathbf{r}} \times \mathbf{A}|^2 d\Omega, \quad (21-19)$$

where c is the free-space speed of light, S_∞ is the spherical surface $r = \infty$ and Ω is the solid angle. The unit vector $\hat{\mathbf{r}}$ is parallel to the radial vector \mathbf{r} of Fig. 21-4 and $s = |\mathbf{r}|$ is the spherical radius.

To summarize this section, the problem of determining radiation due to a given current distribution within a weakly guiding fiber is reduced to the

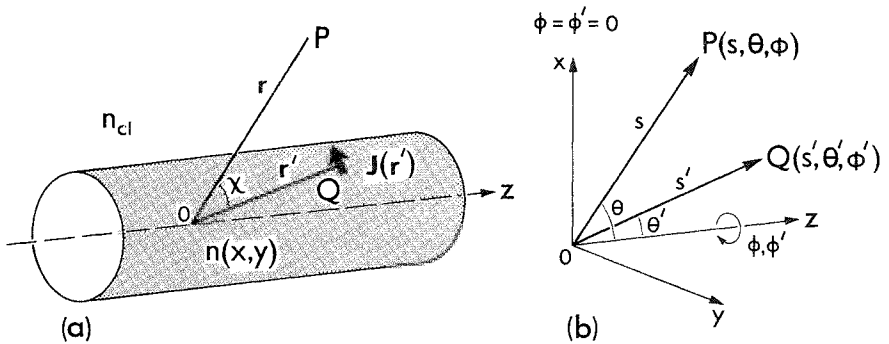


Fig. 21-4 (a) Vector notation for describing the far field at P due to current density \mathbf{J} at Q and (b) the spherical polar coordinates of P and Q relative to the fiber axis.

solution of Eq. (21-17) for the vector potential, from which the radiation is described by Eqs. (21-18) and (21-19).

21-8 'Free-space' approximation

In the present context, we refer to the '*free-space*' approximation, when a weakly guiding fiber is replaced by an unbounded, uniform medium of refractive index n_{cl} [2, 6]. This approximation ignores the slight variation in the fiber profile, which we discuss in Section 21-12.

For weakly guiding fibers, it is intuitive that only radiation in directions close to the fiber axis can differ significantly from radiation in free space. This is consistent with the fact that excitation of bound modes is poor unless the source directs energy along the fiber. It may be helpful to think in terms of ray propagation, where only rays making angles θ_z with the axis within the complementary critical angle θ_c are bound and do not radiate. Since $\theta_c \cong (1 - n_{cl}^2/n_{co}^2)^{1/2}$ and $n_{co} \cong n_{cl}$, then $\theta_c \ll 1$ and only paraxial rays fall into this category. Consequently, if we consider the total power radiated, it is clear that only sources with highly directed, paraxial radiation will give an answer significantly different from the 'free-space' solution. In almost all cases of practical interest, radiated power is accurately described by the 'free-space' approximation. We demonstrate the accuracy of this approximation in Section 21-13.

Radiation field and radiated power

The far-field expression for the vector potential in the 'free-space' approximation is derived in Sections 34-3 and 34-4, where Eqs. (34-15) and (34-19)

give

$$\mathbf{A} = \frac{\mu_0}{4\pi s} \mathbf{M} \exp(iks n_{cl}); \quad \mathbf{M} = \int_{\mathcal{V}} \mathbf{J}(\mathbf{r}') \exp(-iks' n_{cl} \cos \chi) d\mathcal{V}'. \quad (21-20)$$

The integral is over the volume \mathcal{V}' occupied by currents, \mathbf{r}' is the position vector of the current distribution $\mathbf{J}(\mathbf{r}')$ in Fig. 21-4(a), $s = |\mathbf{r}|$ and $s' = |\mathbf{r}'|$ are spherical radii and χ is the angle between \mathbf{r} and \mathbf{r}' . If (s, θ, ϕ) are spherical polar coordinates oriented in Fig. 21-4(b) so that the azimuthal angle ϕ about the z -axis coincides with the x -axis at $\phi = 0$, then we deduce from Eqs. (21-19) and (21-20) that

$$\mathbf{S} = \frac{k^2 n_{cl}}{32\pi^2 s^2} \left(\frac{\mu_0}{\epsilon_0} \right)^{1/2} \{ |M_\theta|^2 + |M_\phi|^2 \} \hat{\mathbf{r}}, \quad (21-21a)$$

$$P_{\text{rad}} = \frac{k^2 n_{cl}}{32\pi^2} \left(\frac{\mu_0}{\epsilon_0} \right)^{1/2} \int_0^{2\pi} \int_0^\pi \{ |M_\theta|^2 + |M_\phi|^2 \} \sin \theta d\theta d\phi, \quad (21-21b)$$

where M_θ and M_ϕ are the components of \mathbf{M} in the θ - and ϕ -directions at P. We now use these expressions to calculate the radiation from the examples in Sections 21-4 to 21-6.

21-9 Example: Dipole radiation

Within the free-space approximation, the total power radiated by the current dipole of Sections 21-4 and 21-5 is independent of both the position and orientation of the dipole. Thus, for simplicity, we can assume the dipole is parallel to the z -axis at the origin in Fig. 21-4. Substituting Eq. (21-7) into Eq. (21-20), we deduce that the vector potential has only a z -component. Hence

$$A_z = (\mu_0 Id / 4\pi s) \exp \{ iks n_{cl} \}; \quad M_\theta = -Id \sin \theta, \quad M_\phi = 0. \quad (21-22)$$

The nonzero far-field components follow from Eq. (21-18) as

$$E_\theta = -\frac{ik}{(\mu_0 \epsilon_0)^{1/2}} A_z \sin \theta; \quad H_\phi = -\frac{ik n_{cl}}{\mu_0} A_z \sin \theta, \quad (21-23a)$$

and Eq. (21-21) leads to the radial power flow and total radiated power

$$\mathbf{S} = \frac{|Id|^2 k^2 n_{cl}}{32\pi^2 s^2} \left(\frac{\mu_0}{\epsilon_0} \right)^{1/2} \sin^2 \theta \hat{\mathbf{r}}, \quad P_{\text{rad}} = \frac{|Id|^2 k^2 n_{cl}}{12\pi} \left(\frac{\mu_0}{\epsilon_0} \right)^{1/2}, \quad (21-23b)$$

where parameters are defined inside the back cover.

Excitation efficiency

We can now determine the efficiency with which a current dipole excites the fundamental modes for various profiles. For a dipole at radius r_d from the axis in the core of a step-profile fiber, Eqs. (21-8), (21-10), (21-23b) and Table 14-3, page 313, show that the efficiency P_o/P_{rad} is given by

$$3\Delta \frac{\tilde{W}^2}{V^4} \frac{J_0^2(\tilde{U}r_d/\rho)}{J_1^2(\tilde{U})} \quad \text{and} \quad 6\Delta^2 \frac{\tilde{U}^2 \tilde{W}^2}{V^6} \frac{J_1^2(\tilde{U}r_d/\rho)}{J_1^2(\tilde{U})}, \quad (21-24)$$

for the x - and z -directed dipoles, respectively, where we have used the eigenvalue equation and the approximation $n_{\text{co}} \cong n_{\text{cl}}$. In the latter case, P_o denotes the power in both x - and y -polarized modes. We plot the ratios $P_o/\Delta P_{\text{rad}}$ and $P_o/\Delta^2 P_{\text{rad}}$ for the x - and z -directed dipoles, respectively, as a function of the normalized radius r_d/ρ in Fig. 21-5(a) for a fiber with $V = 2.4$, using the values of \tilde{U} and \tilde{W} in Table 14-4, page 314. As r_d/ρ increases, the excitation efficiency for the x -directed dipole decreases, since the transverse field of the fundamental mode decreases away from the axis, whereas the excitation efficiency for the z -directed dipole increases as the longitudinal field increases.

Within the Gaussian approximation, the expressions corresponding to those in Eq.

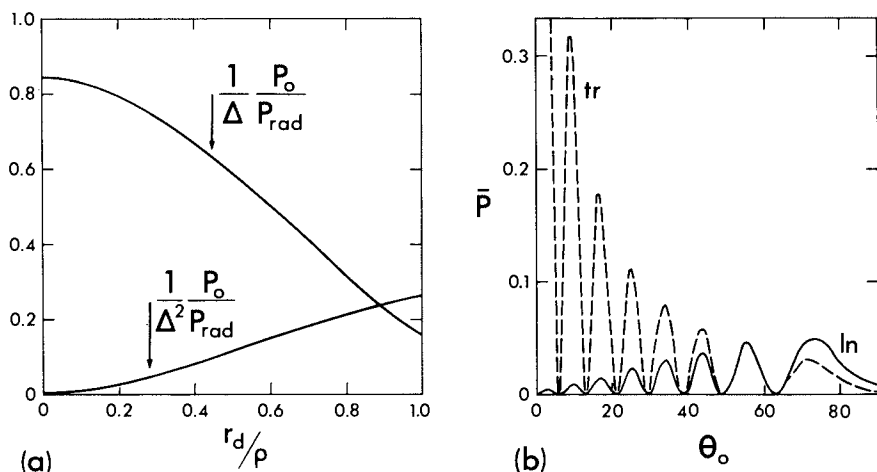


Fig. 21-5 (a) Excitation efficiency of the fundamental modes plotted as the normalized ratios $P_o/\Delta P_{\text{rad}}$ and $P_o/\Delta^2 P_{\text{rad}}$ for x - and z -directed dipoles, respectively. (b) Normalized radiation power \bar{P} as a function of the radiation angle θ_0 for an axisymmetric tubular source for the longitudinal (ln) case of Eq. (21-31) and the transverse (tr) case of Eq. (21-32).

(21-24) follow from Eqs. (21-9), (21-11) and (21-23b) as, respectively,

$$\frac{3\Delta}{V^2} \frac{\rho^2}{r_0^2} \exp\left\{-\frac{r_d^2}{r_0^2}\right\} \quad \text{and} \quad \frac{6\Delta^2}{V^4} \frac{\rho^4}{r_0^4} \frac{r_d^2}{r_0^2} \exp\left\{-\frac{r_d^2}{r_0^2}\right\}, \quad (21-25)$$

where r_0 is the spot size given in Table 15-2, page 340, for various profiles.

21-10 Example: Tubular-source radiation

The tubular current source was described in Section 21-6, where we showed that it is ineffective in exciting bound modes unless either of the resonance conditions of Eq. (21-15) is satisfied. A similar conclusion holds for the radiation fields. If the tube length $2L$ is large compared to the spatial period $2\pi/\Omega$, where Ω is the frequency in Eq. (21-13), it is intuitive that power will be radiated essentially at a fixed angle to the fiber axis. This is also a consequence of Floquets' theorem [7]. However, unlike the current dipole, radiation now depends on the orientation of the currents on the tube.

Longitudinally directed currents

Within the 'free-space' radiation approximation of Section 21-8, the vector \mathbf{M} of Eq. (21-20) has only one component, M_z , when the currents on the tube of Fig. 21-3 are everywhere parallel to the fiber axis. To calculate M_z , we apply the relationship $\hat{\mathbf{f}} \cdot \hat{\mathbf{f}}' = \cos \chi$ to Fig. 21-4(b), where $\hat{\mathbf{f}}$ and $\hat{\mathbf{f}}'$ are unit vectors along OP and OQ, respectively, to deduce the identity

$$s' \cos \chi = r_0 \sin \theta \cos(\phi - \phi') + z \cos \theta, \quad (21-26)$$

where $r_0 = s' \sin \theta'$ and $z = s' \cos \theta'$ on the tube. Substituting into Eq. (21-20), together with Eqs. (21-12) and (21-13) for $\mathbf{J}(\mathbf{r}')$, we deduce that

$$M_z = \frac{1}{2\pi} \int_{-L}^L \sin \Omega z \exp\{i(C - kn_{cl} \cos \theta)z\} dz \int_0^{2\pi} \cos l(\phi' - \phi_0) \times \\ \exp\{-ikr_0 n_{cl} \sin \theta \cos(\phi - \phi')\} d\phi'. \quad (21-27)$$

We use Eq. (37-62) to express the ϕ' integration in terms of the Bessel function of the first kind

$$M_z = (-i)^{l-1} J_l(kr_0 n_{cl} \sin \theta) \cos l(\phi - \phi_0) \left\{ \frac{\sin(\chi - \Omega)L}{\chi - \Omega} - \frac{\sin(\chi + \Omega)L}{\chi + \Omega} \right\}. \quad (21-28)$$

where $\chi = C - kn_{cl} \cos \theta$. As $L \rightarrow \infty$, the first and second terms inside the curly brackets are peaked about $\chi = \Omega$ and $\chi = -\Omega$, respectively. The applications in the following chapter satisfy $C + \Omega > kn_{cl}$, and consequently only the first term is significant. If θ_0 denotes the value of θ at the peak, then

$$\theta_0 = \cos^{-1} \{ (C - \Omega)/kn_{cl} \}; \quad 0 \leq \theta_0 \leq \pi. \quad (21-29)$$

By setting $M_\theta = -M_z \sin \theta$, $M_\phi = 0$ in Eq. (21-21a), we deduce from the spatial dependence of the Poynting vector that the power radiated by the tube propagates predominantly at angle θ_0 to the fiber axis.

Radiated power

In calculating total radiation power, we ignore the second term inside the curly brackets of Eq. (21-28), and, because of the rapid oscillation of $\sin(\chi - \Omega)L$ when $\theta \neq \theta_0$, we can make an accurate simplification by setting $\theta = \theta_0$ in the remaining factors. Hence, by setting $M_\theta = -M_z \sin \theta$, $M_\phi = 0$ in Eq. (21-21b) we find that

$$P_{\text{rad}} = \frac{kL}{32\pi^2} \left(\frac{\mu_0}{\epsilon_0} \right)^{1/2} \sin^2 \theta_0 J_l^2(kr_0 n_{\text{cl}} \sin \theta_0) \int_{x_-}^{x_+} \frac{\sin^2 x}{x^2} dx \int_0^{2\pi} \cos^2 l(\phi - \phi_0) d\phi, \quad (21-30)$$

where $x = (C - kn_{\text{cl}} \cos \theta - \Omega)L$, and $x_{\pm} = (C \pm kn_{\text{cl}} - \Omega)L$. As $L \rightarrow \infty$, both x_+ and x_- are well separated, and we let $x_+ \rightarrow \infty$, $x_- \rightarrow -\infty$. Thus Eq. (37-111) leads to

$$P_{\text{rad}} = \frac{kL}{32} \left(\frac{\mu_0}{\epsilon_0} \right)^{1/2} (1 + \delta_{l,0}) \sin^2 \theta_0 J_l^2(kr_0 n_{\text{cl}} \sin \theta_0), \quad (21-31)$$

where the Kronecker delta $\delta_{l,0} = 1$ if $l = 0$ and is zero otherwise. Hence radiated power varies linearly with tube length, whereas bound-mode power increases with the square of tube length, as is clear from Eq. (21-15).

Transversely directed currents

The tube currents are now taken to be parallel to the x -axis in Fig. 21-4(b), and have the same spatial distribution as for the longitudinal case. Accordingly, the vector \mathbf{M} of Eq. (21-20) has only one component M_x which is identical in magnitude to M_z of Eq. (21-28), and consequently radiation is again directed at angle θ_0 to the fiber axis, as defined in Eq. (21-29). Total radiated power is found by setting $M_\theta = M_x \cos \theta_0 \cos \phi$, $M_\phi = -M_x \sin \phi$ in Eq. (21-21b) and otherwise paralleling the derivation of Eq. (21-31). We obtain [2]

$$P_{\text{rad}} = \frac{kL}{32} \left(\frac{\mu_0}{\epsilon_0} \right)^{1/2} D_l(\theta_0) J_l^2(kr_0 n_{\text{cl}} \sin \theta_0), \quad (21-32a)$$

assuming $\phi_0 = 0$. The factor D_l is defined by

$$D_0 = 1 + \cos^2 \theta_0; \quad D_1 = \frac{1}{4}(1 + 3 \cos^2 \theta_0); \quad D_l = \frac{1}{2}(1 + \cos^2 \theta_0), \quad l \geq 2. \quad (21-32b)$$

In Fig. 21-5(b) we plot the normalized power $\bar{P} = 32P_{\text{rad}} (\epsilon_0/\mu_0)^{1/2}/kL$ of Eqs. (21-31) and (21-32) as a function of the radiation direction θ_0 for an axisymmetric source ($l = 0$), assuming that $r_0 = \rho$, $V = 2.4$ and $\Delta = 0.005$, and consequently that $k\rho n_{\text{cl}} \cong 24$. The peaks in these curves are due to resonances in the cross-section of the tube.

21-11 Radiation correction due to the fiber profile

In the two examples above, we determined the power radiated from current sources within a fiber by ignoring the variation in profile and assuming an unbounded medium of uniform refractive index n_{cl} . Now we determine the correction to the 'free-space' result due to the variation in profile [2]. As the fiber is assumed to be weakly guiding, it is intuitive that the correction is small except when the radiation is directed predominantly close to the axis, i.e. $\theta_0 \cong 0$. Thus we anticipate that the 'free-space' results are, in general, highly accurate.

To determine radiation from sources within weakly-guiding fibers, we must solve Eq. (21-17) for the vector potential. However, if the 'free-space' solution for the particular problem is known, we need only determine the modification due to the fiber profile. The 'free-space' solution is the solution of Eq. (21-17) when $n(x, y) = n_{\text{cl}}$ everywhere. The solution to Eq. (21-17) as $n(x, y)$ varies, can then be built from a linear superposition of *exact* solutions for the tubular source of Fig. 21-3 with the current distribution given by Eqs. (21-12) and (21-13). Consequently, we need only determine the solution of Eq. (21-17) for one tubular source. For simplicity, we restrict attention to tubes of circular cross-section.

21-12 Correction factor

We denote the known, 'free-space' electric field due to the tubular source in Fig. 21-3 by $\mathbf{E}_{\text{fs}}(s, \theta, \phi)$ where s, θ, ϕ are spherical polar coordinates defined in Fig. 21-4(b). If $\mathbf{E}(s, \theta, \phi)$ denotes the corrected field due to the fiber profile, then within the weak-guidance approximation, the polarization properties of \mathbf{E} are approximately the same as those of \mathbf{E}_{fs} . If the fiber profile is axisymmetric, it is intuitive that the slight change in the direction of radiation depends only on θ . If this is not obvious, it may be helpful to think of a ray description, which, although not accurate for low- V fibers, gives a useful qualitative insight. Within the 'free-space' approximation, rays propagate along straight lines everywhere, whereas the variation in core profile gives rise to refraction which changes the direction of these lines in the cladding. Consequently, we set [2]

$$\mathbf{E}(s, \theta, \phi) = C_l(\theta) \mathbf{E}_{\text{fs}}(s, \theta, \phi), \quad (21-33)$$

where $C_l(\theta)$ is the *correction factor* due to the profile. A formal derivation of this result is given in Section 34-6. The correction factor is independent of the polarization of the fields and is derived from the inhomogeneous scalar wave equation in Section 34-6. Thus Eq. (34-26) gives

$$C_l(\theta) = \Psi_l / \Psi_l^{\text{fs}}, \quad (21-34a)$$

in terms of the solution, Ψ_l , of Eq. (34-25), where

$$\{\nabla_t^2 + k^2 n^2(r) - \beta^2\} \Psi_l = b \frac{\delta(r - r_0)}{r_0} \cos l(\phi - \phi_0), \quad (21-34b)$$

and the corresponding solution Ψ_l^{fs} when $n(r) = n_{\text{cl}}$ everywhere. This equation is based on the current distribution of Eqs. (21-12) and (21-13) when all currents are parallel to a fixed direction. The Laplacian is defined in Table 30-1, page 592, $n(r)$ is the axisymmetric profile, $\beta = kn_{\text{cl}} \cos \theta$, r_0 is the tube radius and δ is the Dirac delta function. Procedures for solving Eq. (21-34) are given in Section 34-7. We now consider a simple example and its application.

21-13 Example: Step profile

When the tubular source of radius r_0 in Fig. 21-3 is located within the core or at the core-cladding interface of a step-profile fiber of radius ρ , the solution of Eq. (21-34) is derived in Section 34-7 and is given by Eq. (34-32) as [2]

$$C_l(\theta) = \frac{J_l(Ur_0/\rho) W_l(Q, Q)}{J_l(Qr_0/\rho) W_l(U, Q)}, \quad (21-35)$$

where J_l is the Bessel function of the first kind and

$$W_l(U, Q) = U J_{l+1}(U) H_l^{(1)}(Q) - Q J_l(U) H_{l+1}^{(1)}(Q); \quad W_l(Q, Q) = 2i/\pi, \quad (21-36)$$

since $W_l(Q, Q)$ is proportional to the Wronskian of Eq. (37-77). The $H_l^{(1)}$ are Hankel functions of the first kind, and remaining parameters are related to θ by

$$Q = k\rho n_{\text{cl}} \sin \theta = (U^2 - V^2)^{1/2}; \quad V = k\rho n_{\text{co}} (2\Delta)^{1/2}, \quad (21-37)$$

where V is the fiber parameter, $k = 2\pi/\lambda$ and λ is the free-space wavelength.

Physical interpretation

The correction factor can be given a simple physical interpretation by decomposing C into two factors C_d and C_r such that

$$C_l(\theta) = C_d(\theta) C_r(\theta); \quad C_d(\theta) = \frac{J_l(Ur_0/\rho)}{J_l(Qr_0/\rho)}; \quad C_r(\theta) = \frac{W_l(Q, Q)}{W_l(U, Q)}. \quad (21-38)$$

If we substitute Eqs. (21-33) and (21-38) into Eq. (21-20), the magnitude S of the Poynting vector—which determines the far-field radiation pattern—is given by

$$S = |C_l(\theta)|^2 S_{fs} = |C_d(\theta)|^2 |C_r(\theta)|^2 S_{fs}, \quad (21-39)$$

where S_{fs} is the magnitude of the corresponding 'free-space' Poynting vector.

The factor $C_d(\theta)$ accounts for a change in the direction of flow of radiated power. To a distant observer this results in a shift in the apparent origin of the radiation. In ray terms, this is equivalent to refraction at the core-cladding interface, as expressed by Snell's law of Eq. (35-4), i.e. the change from U to Q in the argument of the Bessel function. The factor $C_r(\theta)$ is associated with resonances in the fiber cross-section, which are related to the excitation of leaky modes as explained in Section 24-21. If the tube and core radii differ, the resonance peaks for the current source and fiber occur at different values of θ . For the special case of equal tube and core radii the peaks virtually coincide, as is evident from Figs. 21-5(b) and 21-6(a). The latter plots $|C_r(\theta)|^2$ as a function of θ for the symmetric ($l = 0$) tube when $V = 2.4$ [2]. The maxima in the $\Delta = 5 \times 10^{-3}$ and $\Delta = 5 \times 10^{-5}$ curves correspond to $\theta = \theta_c \cong 5.7$ and $\theta = \theta_c \cong 0.57$, where $\theta_c \cong (2\Delta)^{1/2}$ is the complementary critical angle. Only when $\theta < \theta_c$ does $|C_r|$ differ greatly from unity, and $C_r \rightarrow 0$ as $\theta \rightarrow 0$ when the source power is transmitted by bound modes. Thus, for a diffuse source radiating in all directions, the total power radiated is virtually indistinguishable from the 'free-space' expression, since $S \cong S_{fs}$ for all but a negligible range of directions.

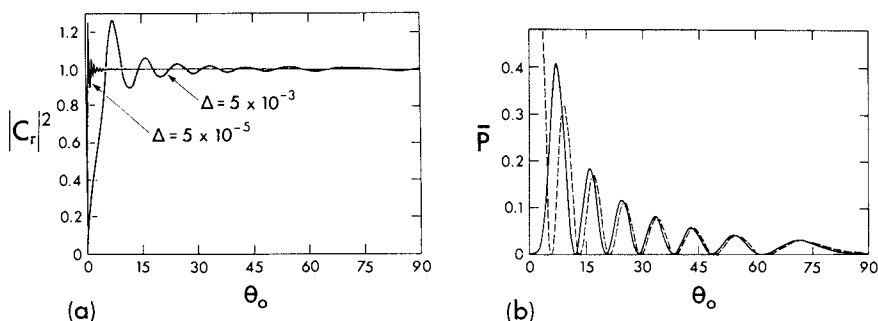


Fig. 21-6 (a) Plots of the factor $|C_r(\theta)|^2$ of Eq. (21-38) as a function of the radiation angle θ_0 for an axisymmetric source within a step-profile fiber. (b) Normalized power \bar{P} as a function of the radiation angle θ_0 for an axisymmetric tubular source coinciding with the interface of a step-profile fiber. The solid curve is calculated from Eq. (21-41b) and the 'free-space' dashed curve from Eq. (21-32).

Dipole radiation

We can quantify the correction to the 'free-space' radiated power in the case of an on-axis dipole parallel to the x -axis. If we integrate the product $|C(\theta)|^2 S$ of Eqs. (21-38)

and (21-23b) over all directions, with $l = r_0 = 0$, the corrected expression for total radiated power differs from the 'free-space' result of Eq. (21-23b) by less than 0.1 % when $V = 2.4$ and $\Delta < 0.01$.

Graded profiles

The same general interpretation of the correction factor for step-profile fibers also holds for clad, graded-profile fibers that are weakly guiding. Profiles leading to exact solutions of Eq. (21-35) are discussed in Chapter 14, while the WKB solution of the homogeneous scalar wave equation of Eq. (35-44) can often be used to determine the correction factor for other profiles [2, 8].

21-14 Example: Corrected tubular-source radiation

We showed in section 21-10 that the radiation from a tubular source with the current distribution of Eq. (21-13) is directed at the angle θ_0 of Eq. (21-29) relative to the fiber axis. Consequently, the total power P radiated from a tube of length $2L$ and radius $r_0 \leq \rho$ within a step-profile fiber is given by [2]

$$P = |C_l(\theta_0)|^2 P_{\text{rad}}, \quad (21-40)$$

where P_{rad} is the 'free-space' radiated power. Thus we deduce from Eqs. (21-35), (21-31) and (21-32) that

$$P = \frac{kL}{16} \left(\frac{\mu_0}{\varepsilon_0} \right)^{1/2} (1 + \delta_{l,0}) \sin^2 \theta_0 \left| \frac{W_l(Q_0, Q_0)}{W_l(U_0, Q_0)} \right|^2 J_l^2(U_0 r_0 / \rho), \quad (21-41a)$$

when the currents are parallel to the fiber axis, and

$$P = \frac{kL}{32} \left(\frac{\mu_0}{\varepsilon_0} \right)^{1/2} D_l(\theta) \left| \frac{W_l(Q_0, Q_0)}{W_l(U_0, Q_0)} \right|^2 J_l(U_0 r_0 / \rho), \quad (21-41b)$$

when the currents are parallel to the x -axis in the fiber cross-section. The D_l are defined by Eq. (21-32b), and W_l by Eq. (21-36) with U and Q replaced by U_0 and Q_0 , where the latter are related to θ_0 by Eq. (21-37) with $\theta = \theta_0$.

A plot of the normalized power $\bar{P} = 32P (\varepsilon_0/\mu_0)^{1/2} / kL$ of Eq. (21-41b) as a function of θ_0 is given by the solid curve in Fig. 21-6(b) for a tube with $r_0 = \rho$ and $l = 0$ within a fiber with $V = 2.4$ and $\Delta = 0.005$. The dashed curve is the corresponding 'free-space' solution of Eq. (21-32). As we explained in the previous section, the factor $C_a(\theta_0)$ of Eq. (21-38) is associated with a change in the direction of radiation, which can be seen in a shift in position of the peaks as θ_0 decreases, while the factor $C_r(\theta_0)$ is associated with resonances in the fiber cross-section; these affect the magnitude of the peaks.

REFERENCES

1. Adler, R. B. (1952) Waves on inhomogeneous cylindrical structures. *Proc. I.R.E.*, **40**, 339-48.
2. Snyder, A. W. (1980) Weakly guiding fibers. *J. Opt. Soc. Am.*, **70**, 405-11.
3. Ramo, S., Whinnery, J. R. and Van Duzer, T. (1965) *Fields and Waves in Communication Electronics*, Wiley, New York, sect. 12.04.
4. Jones, D. S. (1964) *Theory of Electromagnetism*, Pergamon Press, Oxford.
5. Papas, C. H. (1965) *Theory of Electromagnetic Wave Propagation*, McGraw-Hill, New York, sect. 2.2.
6. Snyder, A. W. (1970) Radiation losses due to variations of radius on dielectric or optical fibers. *I.E.E.E. Trans. Microwave Theory Tech.* **18**, 608-15.
7. Brouillon, L. (1946) *Wave Propagation in Periodic Structures; electric fitters and lattice structures*, McGraw Hill, New York.
8. Hussey, C. D. (1983) Radiation from graded-index single-mode fibers. *I.E.E. Pt H.* **130**, 225-9.

Nonuniform fibers

Induced-current representation of nonuniformities	460
22-1 Arbitrary nonuniformities	461
22-2 Slight nonuniformities	462
Radiation losses from the fundamental mode	463
22-3 <i>Example: Isolated nonuniformity</i>	463
22-4 <i>Example: Random distribution of nonuniformities</i>	464
22-5 <i>Example: Sinusoidally perturbed interface</i>	465
Bound-mode power redistribution	467
22-6 Single-mode fibers of arbitrary profile	467
22-7 Weakly guiding single-mode fibers	469
22-8 <i>Example: Isolated nonuniformity</i>	469
22-9 <i>Example: Sinusoidally perturbed interface</i>	470
Slowly varying arbitrary nonuniformities	470
22-10 Induced-current representation for local modes	471
22-11 Redistribution of guided power	471
References	472

When light propagates along a fiber and impinges on nonuniformities due to imperfections in the fiber, some of its power is scattered, as shown schematically in Fig. 22-1(a). Part of the scattered power is distributed into forward- and backward-propagating modes, while the remainder is radiated. For multimode fibers, the distribution of scattered power is best treated by the ray methods of Chapter 5. Here we are primarily interested in fibers that propagate only one or a few modes. We treat the nonuniformities of the perturbed fiber as induced current sources within the unperturbed fiber. The results of the previous chapter can then be used to describe excitation of bound modes and the radiation field [1-3].

INDUCED-CURRENT REPRESENTATION OF NONUNIFORMITIES

Here we show how nonuniformities within a fiber can be represented as current sources induced by the electric field. The nonuniformities of the

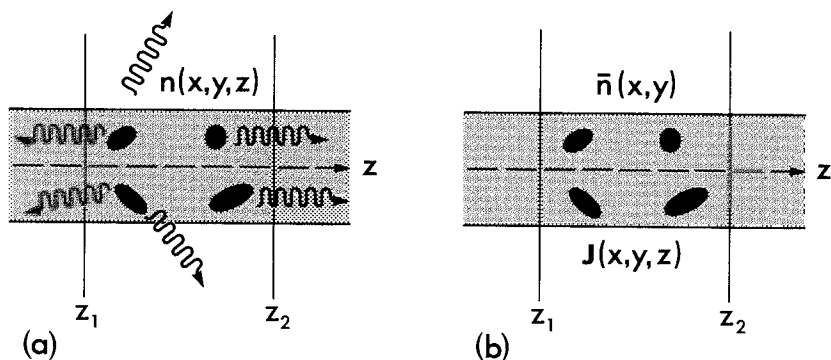


Fig. 22-1 (a) Darkly shaded regions denote nonuniformities which scatter incident light power into bound modes and radiation. The profile of the perturbed fiber is $n(x, y, z)$. (b) Darkly shaded regions denote corresponding induced currents with distribution $\mathbf{J}(x, y, z)$ within the unperturbed fiber of profile $\bar{n}(x, y)$.

perturbed fiber in Fig. 22-1(a) account for the z -dependence of its refractive-index profile $n(x, y, z)$. The total electric and magnetic fields, $\mathbf{E}(x, y, z)$ and $\mathbf{H}(x, y, z)$, are related by the source-free Maxwell equations everywhere within the perturbed fiber. In particular, we have from Eq. (30-1a) that

$$\nabla \times \mathbf{H} = -i(\epsilon_0/\mu_0)^{1/2} kn^2 \mathbf{E}, \quad (22-1)$$

where parameters are defined at the back of the book. The refractive-index profile of the same fiber in the absence of nonuniformities is denoted by $\bar{n}(x, y)$, and on rearranging the right side of Eq. (22-1) we can set

$$\nabla \times \mathbf{H} = i(\epsilon_0/\mu_0)^{1/2} k(\bar{n}^2 - n^2) \mathbf{E} - i(\epsilon_0/\mu_0)^{1/2} k\bar{n}^2 \mathbf{E}. \quad (22-2)$$

If we compare this equation with the corresponding equation in Eq. (30-1a) *in the presence of currents*, the first term on the right can be identified with a fictitious current \mathbf{J} whose direction and density is given by

$$\mathbf{J} = i(\epsilon_0/\mu_0)^{1/2} k(\bar{n}^2 - n^2) \mathbf{E}. \quad (22-3)$$

We regard \mathbf{J} as an *induced current density* set up by the nonuniformities. In other words, the fields of the perturbed fiber in Fig. 22-1(a) are identical to the fields of the unperturbed fiber of Fig. 22-1(b) in the presence of a current source whose distribution is specified by Eq. (22-3).

22-1 Arbitrary nonuniformities

The induced current source of Eq. (22-3) is nonzero only within regions occupied by nonuniformities, and is fully specified if the total electric field \mathbf{E} is

known. However, \mathbf{E} is the sum of the *known* incident field and the *unknown* scattered field which depends on the polarizability of the nonuniformity. For an arbitrary nonuniformity, there is no general expression available for the scattered field, and consequently Eq. (22-3), together with Eq. (30-1), is generally no easier to solve than the source-free Maxwell equations for the perturbed fiber. An exception is the infinitesimal nonuniformity consisting of a sphere of uniform index n and radius small compared with the wavelength of light. The field in its interior is given by the quasi-static approximation, as explained in Section 18-22, whence we deduce from standard electrostatic theory [4]

$$\mathbf{E} \cong 3\bar{n}^2 \bar{\mathbf{E}} / (n^2 + 2\bar{n}^2), \quad (22-4)$$

where \bar{n} and $\bar{\mathbf{E}}$ are the index value and electric field of the unperturbed fiber at the position of the sphere. The induced-current representation can also be used to calculate slight losses from local modes on fibers with slowly varying, arbitrary nonuniformities, as we show in Section 22-10.

22-2 Slight nonuniformities

When the nonuniformities are slight, the profiles of the perturbed and unperturbed fibers are similar, i.e. $n \cong \bar{n}$, then Eq. (22-3) leads to a considerable simplification in the determination of the fields with only minimal loss in accuracy [1-3, 5-7]. For convenience, we consider arbitrary and weakly guiding fibers separately.

Arbitrary fibers

For such fibers the variation in both n and \bar{n} is arbitrary and in regions occupied by nonuniformities $n \cong \bar{n}$. To lowest order we set $\mathbf{E} \cong \bar{\mathbf{E}}$ in Eq. (22-3) whence the induced current is well approximated by

$$\mathbf{J} = i(\epsilon_0/\mu_0)^{1/2} k (\bar{n}^2 - n^2) \bar{\mathbf{E}}.$$

(22-5)

Consequently, the induced current is specified in terms of the known field of the unperturbed fiber. Although this approximation ignores slight polarization effects due to nonspherical scatterers, it is accurate for spherical scatterers, so that $\mathbf{E} \cong \bar{\mathbf{E}}$ in Eq. (22-4), and can be used, for example, to show some of the power of an incident, even fundamental mode is scattered into the odd fundamental mode. The electric fields of the two modes are not orthogonal to one another, and are coupled by the nonuniformity, as we show in Section 22-8. However, if both modes are excited equally or if there is a random distribution of nonuniformities, the scattering process averages out and there is no significant redistribution of power between them.

Weakly guiding fibers

When the fiber is weakly guiding and $n \cong \bar{n}$, the fields are approximately transverse, as explained in Chapter 13, and the lowest-order approximation is $\mathbf{E} \cong \bar{\mathbf{E}}_t$, where t denotes transverse component. Hence Eq. (22-3) becomes

$$\mathbf{J} = i (\epsilon_0 / \mu_0)^{1/2} k (\bar{n}^2 - n^2) \bar{\mathbf{E}}_t, \quad (22-6)$$

which ignores all polarization effects due to nonuniformities since the transverse fields of all modes are orthogonal in the weak-guidance approximation. In particular, the odd, or y -polarized, fundamental mode cannot be excited by the even, or x -polarized, fundamental mode, unlike the arbitrary fiber discussed above. If we substitute from Eq. (13-9a), into Eq. (22-6) the induced current for an incident, x -polarized fundamental mode on a circular fiber is

$$\mathbf{J} = i a_1 (\epsilon_0 / \mu_0)^{1/2} k (\bar{n}^2 - n^2) F_0 \exp(i\tilde{\beta}z) \hat{\mathbf{x}}, \quad (22-7)$$

where a_1 is the modal amplitude, $F_0(R)$ is the fundamental solution of the scalar wave equation, Eq. (14-4), $\hat{\mathbf{x}}$ is the unit vector parallel to the x -axis in Fig. 14-1 and $\tilde{\beta}$ is the scalar propagation constant.

RADIATION LOSSES FROM THE FUNDAMENTAL MODE

To demonstrate the usefulness of the induced-current representation, we determine, through examples, the power radiated from the fundamental mode of a weakly guiding circular fiber due to slight nonuniformities of various kinds.

22-3 Example: Isolated nonuniformity

Consider a small nonuniformity of volume $\delta \mathcal{V}$ and uniform refractive index n located at radius r_d in the fiber cross-section. An incident, x -polarized fundamental mode sets up an induced current given by Eq. (22-7) with $R = R_d = r_d / \rho$ and $\bar{n} = \bar{n}(r_d)$, where ρ is the core radius. Within the 'free-space' approximation of Section 21-8, the total power radiated, P_{rad} , is independent of polarization of the mode and is obtained by replacing $I d$ with $a_1 (\epsilon_0 / \mu_0)^{1/2} k (\bar{n}^2 - n^2) F_0 \delta \mathcal{V}$ in Eq. (21-23b). The fraction of incident power P_i radiated follows from Table 13-2, page 292 as

$$\frac{P_{\text{rad}}}{P_i} = \frac{1}{48\pi^2} \left\{ \frac{V^2 \bar{n}^2 - n^2}{\Delta} \frac{\delta \mathcal{V}}{\rho^3} F_0(R_d) \right\}^2 \bigg/ \int_0^\infty F_0^2(R) R dR, \quad (22-8)$$

where the fiber parameter V is defined inside the back cover, and we have assumed that $\bar{n} \cong n_{\text{co}} \cong n_{\text{cl}}$. If the nonuniformity is located within the core of a step-profile fiber, we

deduce from the integral and $l = 0$ eigenvalue equation in Table 14-6, page 319, that

$$\frac{P_{\text{rad}}}{P_i} = \frac{1}{24\pi^2} \left\{ \frac{V\tilde{W}}{\Delta} \frac{n_{\text{co}}^2 - n^2}{n_{\text{co}}^2} \frac{\delta\mathcal{V}}{\rho^3} \frac{J_0(\tilde{U}r_d/\rho)}{J_1(\tilde{U})} \right\}^2, \quad (22-9)$$

where parameters are defined inside the back cover. This ratio can be given explicitly in terms of V if we approximate $F_0(R)$ in Eq. (22-8) by the Gaussian approximation of Eq. (15-2) and Table 15-2, page 340.

22-4 Example: Random distribution of nonuniformities

Consider a fiber with small nonuniformities distributed at random throughout the fiber with number density M per unit volume. The total power radiated from length dz of fiber is just the sum of the power P_{rad} radiated by each nonuniformity. If $P(z)$ is the modal power at position z along the fiber, and M is sufficiently large, it follows that

$$dP(z) = - \left\{ \int_{A_\infty} MP_{\text{rad}} dA \right\} dz, \quad (22-10)$$

where A_∞ is the infinite cross-section, and P_{rad} is related to the incident power by Eq. (22-8) with P_i replaced by $P(z)$. We denote the right side of Eq. (22-8) by $C(R_d)$, substitute into Eq. (22-10) and integrate to obtain

$$P(z) = P(0)\exp(-\gamma z); \quad \gamma = \int_{A_\infty} MC dA, \quad (22-11)$$

assuming M and C are independent of z . The initial power in the mode is $P(0)$ and γ is the power attenuation coefficient.

Uniform core distribution

Consider a step-profile fiber of core index n_{co} with a uniform density M_{co} of nonuniformities of equal volume $\delta\mathcal{V}_{\text{co}}$ and index \tilde{n}_{co} . The factor C is given by the right side of Eq. (22-8), whence we deduce from Eqs. (22-11), Table 13-2, page 292, and the $l = 0$ integral and eigenvalue equation of Table 14-6, page 319, that the attenuation coefficient for the fundamental mode is

$$\gamma = 2\pi M_{\text{co}} \rho^2 \int_0^1 C(R_d) R_d dR_d = \frac{M_{\text{co}} \rho^2}{24\pi} \left\{ \frac{V^2}{\Delta} \frac{n_{\text{co}}^2 - \tilde{n}_{\text{co}}^2}{n_{\text{co}}^2} \frac{\delta\mathcal{V}_{\text{co}}}{\rho^3} \right\}^2 \eta, \quad (22-12)$$

where η is the fraction of modal power in the core. The definition of the fiber parameter in terms of wavelength λ at the back of the book shows that γ is proportional to λ^{-4} , which is the wavelength dependence of Rayleigh scattering [8].

Uniform core and cladding distributions

If the above situation is generalized to include a distribution of nonuniformities in the cladding with uniform density M_{cl} , volume $\delta\mathcal{V}_{cl}$ and index \bar{n}_{cl} , it is straightforward to show that Eq. (22-12) is replaced by

$$\gamma = \eta\alpha_{co} + (1 - \eta)\alpha_{cl}, \quad (22-13)$$

where α_{co} and α_{cl} describe bulk losses in the core and cladding materials [8]. The coefficient α_{co} is defined by comparing Eq. (22-12) with the first term on the right of Eq. (22-13), and α_{cl} follows by replacing the subscript co by cl everywhere.

22-5 Example: Sinusoidally perturbed interface

Consider a step-profile fiber with an interface which is sinusoidally deformed along its length $2L$, as shown in Fig. 22-2(a). If $\rho(z)$ is the core radius at position z , then

$$\rho(z) = \rho + \delta\rho \sin(\Omega z), \quad (22-14)$$

where ρ is the unperturbed radius, Ω is the spatial frequency and the perturbation is slight, i.e. $\delta\rho \ll \rho$. The effect of the deformed interface on an x -polarized fundamental

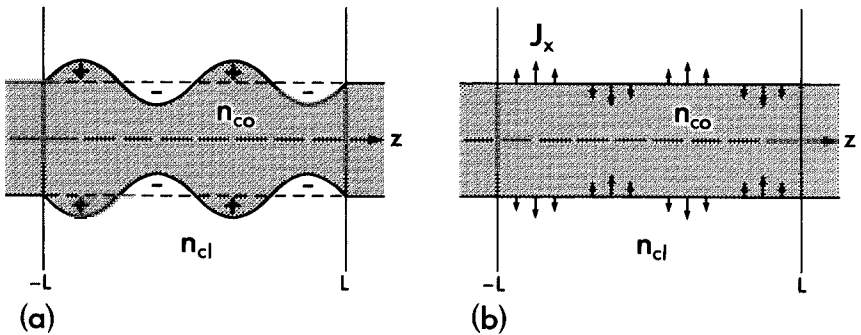


Fig. 22-2 (a) Step-profile fiber of core and cladding indices n_{co} and n_{cl} whose interface is sinusoidally deformed between $z = -L$ and $z = L$, and (b) the equivalent distribution of x -directed currents on the interface of the unperturbed fiber.

mode is expressible in terms of induced currents. By examining Fig. 22-2(a), the difference $\bar{n}^2 - n^2$, where \bar{n} and n are the unperturbed and perturbed profiles, varies as $\pm(n_{cl}^2 - n_{co}^2)$ in the shaded areas marked \pm and is zero elsewhere. Since $\delta\rho$ is small, we can assume the currents are located on the interface. Substituting into Eq. (22-7)

$$J_x = -ia(\epsilon_0/\mu_0)^{1/2}k(n_{co}^2 - n_{cl}^2)\delta\rho \sin(\Omega z) \exp(i\beta z) \bar{\delta}(r - \rho), \quad (22-15)$$

where $\bar{\delta}$ is the Dirac delta function, the \sim is omitted from scalar quantities and $F_0(1) = 1$

on the interface. Thus, with reference to Fig. 21-3, the deformed interface is replaced by the unperturbed fiber excited by a tubular source coincident with the interface and carrying x -directed current, as shown in Fig. 22-2(b), proportional in magnitude to Eqs. (21-12) and (21-13) with $r_0 = \rho$, $l = 0$ and $C = \beta$. Accordingly, we can appeal to the results in Sections 21-10 and 21-14.

When the length of the deformed section of fiber is sufficiently large, radiation is directed predominantly at the angle θ_0 of Eq. (21-30). The power radiated will be negligible unless $0 < \theta_0 < \pi$, which, by setting $C = \beta$, is equivalent to the spatial frequency of the sinusoid lying in the range

$$\beta - kn_{cl} < \Omega < \beta + kn_{cl}. \quad (22-16)$$

It is useful to know the characteristic length of interface roughness which causes radiation loss. From the definitions inside the back cover, weakly guiding fibers obey $\rho(\beta - kn_{cl}) \cong W^2(\Delta/2)^{1/2}/V$. Thus, we deduce from Eq. (22-16) that roughness with a ripple period, $2\pi/\Omega$, greater than about 0.5 mm will cause negligible radiation loss on a fiber with $V \cong 2.4$, $\rho \cong 5 \mu\text{m}$ and $\Delta \cong 0.005$, taking W from Table 14-4, page 314.

Radiated power

The total power radiated from the deformity when the fiber has a step profile, is proportional to Eq. (21-41b) with $l = 0$ and $r_0 = \rho$. On comparing Eqs. (22-15) and (21-12), we deduce the proportionality factor for the current source, and on taking the square of the modulus we find that

$$P_{\text{rad}} = |a_1|^2 \frac{\pi^2}{8} \left(\frac{\epsilon_0}{\mu_0} \right)^{1/2} \left(\frac{\delta\rho}{\rho} \right)^2 \frac{L}{k} V^4 (1 + \cos^2 \theta_0) \left| \frac{W_0(Q_0, Q_0)}{W_0(U_0, Q_0)} \right|^2 J_0^2(U_0), \quad (22-17a)$$

where V is the fiber parameter defined inside the back cover, and

$$W_0(U_0, Q_0) = U_0 J_1(U_0) H_0^{(1)}(Q_0) - Q_0 J_0(U_0) H_1^{(1)}(Q_0); \quad W_0(Q_0, Q_0) = 2i/\pi, \quad (22-17b)$$

$$Q_0 = k\rho n_{cl} \sin \theta_0 = (U_0^2 - V^2)^{1/2}; \quad \cos \theta_0 = (\beta - \Omega)/kn_{cl}. \quad (22-17c)$$

The J_l 's and $H_l^{(1)}$'s are Bessel and Hankel functions of the first kind.

Modal attenuation

The power $P(z)$ of the fundamental mode distance z along the sinusoid in Fig. 22-2 attenuates because of the radiation loss. If we subdivide the deformity into lengths dz which are short compared with L , but long enough for the above analysis to be valid, the change in modal power over distance dz is given by

$$dP(z) = -(P_{\text{rad}}/2L)dz = -(P_{\text{rad}}/2NL|a_1|^2)P(z)dz, \quad (22-18)$$

using the relationship $P(z) = |a_1|^2 N$ of Eq. (11-22), where a_1 is the modal amplitude and N is the normalization. On integrating Eq. (22-18) we obtain

$$P(z) = P(-L) \exp \{ -\gamma(z+L) \}; \quad \gamma = P_{\text{rad}}/2NL|a_1|^2, \quad (22-19)$$

where γ is the power attenuation coefficient and the sinusoid begins at $z = -L$. Substituting for N and using the eigenvalue equation in Table 14-3, page 313, we deduce from Eq. (22-17) that

$$\gamma = \frac{\pi}{8\rho} \left(\frac{\delta\rho}{\rho} \right)^2 (2\Delta)^{1/2} VW^2 \left\{ \frac{J_0(U)}{J_1(U)} \right\}^2 (1 + \cos^2 \theta_0) \left| \frac{W_0(Q_0, Q_0)}{W_0(U_0, Q_0)} \right|^2 J_0^2(U_0), \quad (22-20)$$

where the modal parameters U and W are defined inside the back cover. Apart from a normalization factor, the variation of γ with Ω is given in Fig. 21-6(b) by the solid curve as a function of θ_0 of Eq. (22-17d). Except for small angles, the correction factor can be ignored.

BOUND-MODE POWER REDISTRIBUTION

In addition to scattering into radiated power, nonuniformities generally redistribute power amongst all bound modes, both forward- and backward-propagating, including the incident mode. Here we use the induced current representation to calculate the power in each mode.

22-6 Single-mode fibers of arbitrary profile

On a circular fiber which propagates only the fundamental modes, scattered power that is not radiated can only be directed into the forward- and backward-propagating, even and odd fundamental modes. If the forward-propagating, even HE_{11} mode is incident on the nonuniformities in Fig. 22-1(a), then the *bound* portion of the total electric field is given by

$$\bar{\mathbf{E}} = \bar{a}_1 \mathbf{e}_1 \exp(i\beta z), \quad (22-21a)$$

on the unperturbed fiber, and on the perturbed fiber by

$$\bar{\mathbf{E}} = \{ (\bar{a}_1 + a_1) \mathbf{e}_1 + a_2 \mathbf{e}_2 \} \exp(i\beta z) + \{ a_{-1} \mathbf{e}_{-1} + a_{-2} \mathbf{e}_{-2} \} \exp(-i\beta z), \quad (22-21b)$$

where β is the common propagation constant, subscripts 1 and 2 denote the forward-propagating even and odd modes, and negative subscripts denote the corresponding backward-propagating modes. The amplitude \bar{a} of the incident mode is everywhere constant, while outside the region occupied by non-

uniformities in Fig. 22-1, the remaining amplitudes are constant. We deduce from Eq. (11-27) that the total power P_+ of the forward-propagating modes in the region $z > z_2$ is given by

$$P_+ = \{|\bar{a}_1 + a_1|^2 + |a_2|^2\}N \cong \bar{P}_1 + 2\text{Re}(\bar{a}_1 a_1^*)N, \quad (22-22a)$$

where \bar{P}_1 is the power of the incident mode, N is the common normalization, Re denotes real part and $*$ denotes complex conjugate. The approximation ignores higher-order terms in a_1 and a_2 which are both small compared to \bar{a}_1 when the nonuniformities are slight. Similarly, the total power P_- in the backward-propagating modes in the region $z < z_1$ is given by

$$P_- = \{|a_{-1}|^2 + |a_{-2}|^2\}N, \quad (22-22b)$$

where a_{-1} and a_{-2} are small compared with \bar{a}_1 .

Induced-current representation

We treat the nonuniformities as induced currents within the fiber of Fig. 22-1(b). On substituting Eq. (22-21a) into Eq. (22-5), the distribution is given by

$$J = i\bar{a}_1 (\epsilon_0/\mu_0)^{1/2} k(\bar{n}^2 - n^2) \mathbf{e} \exp(i\beta z), \quad (22-23)$$

where \bar{n} and n are the profiles of the unperturbed and perturbed fibers, respectively. This approximation ignores the polarization of non-spherical nonuniformities, as explained in Section 22-2. The unknown amplitudes in Eq. (22-21) are then found by substituting Eq. (22-23) into Eq. (21-2). Using the above notation, we obtain

$$\begin{aligned} a_j &= -\frac{i}{4} \frac{k\bar{a}_1}{N} \left(\frac{\epsilon_0}{\mu_0}\right)^{1/2} \int_{\mathcal{V}} (\bar{n}^2 - n^2) \mathbf{e}_1 \cdot (\mathbf{e}_{tj} + e_{zj} \hat{\mathbf{z}})^* d\mathcal{V}; \quad z > z_2, \\ a_{-j} &= \frac{i}{4} \frac{k\bar{a}_1}{N} \left(\frac{\epsilon_0}{\mu_0}\right)^{1/2} \int_{\mathcal{V}} (\bar{n}^2 - n^2) \mathbf{e}_1 \cdot (\mathbf{e}_{tj} - e_{zj} \hat{\mathbf{z}})^* \exp(2i\beta z) d\mathcal{V}; \quad z < z_1, \end{aligned} \quad (22-24)$$

where $j = 1$ or 2 , subscripts t and z denote transverse and longitudinal components, \mathbf{z} is the unit vector parallel to the fiber axis and \mathcal{V} is the volume between planes $z = z_1$ and $z = z_2$ in Fig. 22-1.

Multimode fibers

The above analysis is readily generalized to describe the redistribution of power due to slight nonuniformities within multimode fibers by including all

forward- and backward-propagating bound modes of the fiber in Eq. (22-21). However, when the incident field is due to illumination of the fiber by a diffuse source, the ray methods of Chapter 5 are more appropriate.

22-7 Weakly guiding single-mode fibers

We claimed in Section 22-2 that there is negligible coupling between the two polarizations of the fundamental mode due to slight nonuniformities on a weakly guiding fiber. Thus, in the first approximation the incident even, or x -polarized, mode excites power in only the forward- and backward-propagating modes with the same polarization. Hence Eq. (22-21) is replaced by

$$\bar{\mathbf{E}} = \bar{a}_1 F_0 \exp(i\tilde{\beta}z) \hat{\mathbf{x}}; \quad \mathbf{E} = \{(\bar{a} + a_1) \exp(i\tilde{\beta}z) + a_{-1} \exp(-i\tilde{\beta}z)\} F_0 \hat{\mathbf{x}}, \quad (22-25)$$

where $F_0 = F_0(R)$ is the fundamental solution of the scalar wave equation, Eq. (14-4), β is the corresponding scalar propagation constant and $\hat{\mathbf{x}}$ is the unit vector parallel to the x -axis in the fiber cross-section. We set $\bar{\mathbf{E}}_t = \bar{\mathbf{E}}$ in Eq. (22-6), and with the aid of Eqs. (33-64c) and (33-65a) deduce that

$$a_1 = -\frac{i}{4} \frac{k\bar{a}_1}{\tilde{N}} \left(\frac{\epsilon_0}{\mu_0} \right)^{1/2} \int_{\mathcal{V}} (\bar{n}^2 - n^2) F_0^2 d\mathcal{V}; \quad z > z_2, \quad (22-26a)$$

$$a_{-1} = \frac{i}{4} \frac{k\bar{a}_1}{\tilde{N}} \left(\frac{\epsilon_0}{\mu_0} \right)^{1/2} \int_{\mathcal{V}} (\bar{n}^2 - n^2) F_0^2 \exp(2i\tilde{\beta}z) d\mathcal{V}; \quad z < z_1 \quad (22-26b)$$

where \tilde{N} is the scalar normalization of Table 13-2, page 292, F_0 is real for a nonabsorbing fiber and we have set $\tilde{\beta} \cong kn_{\text{co}}$, $\Psi_0 = F_0$.

22-8 Example: Isolated nonuniformity

We now examine the scattering of power into bound modes when an x -polarized HE_{11} mode is incident on an isolated nonuniformity within a single-mode, step-profile fiber. Within the weak-guidance approximation, we deduce from Eq. (22-26) and Table 14-3, page 313, that

$$\dot{a}_1 = -a_{-1} \exp(-2i\tilde{\beta}z_d) = -\frac{i}{2\pi} \frac{n_{\text{co}}^2 - n^2}{n_{\text{co}}^2} \frac{\delta\mathcal{V}}{\rho^3} \frac{\bar{a}_1}{(2\Delta)^{1/2}} \frac{\tilde{W}^2}{V} \frac{J_0^2(\tilde{U}r_d/\rho)}{J_1^2(\tilde{U})}. \quad (22-27)$$

The nonuniformity has volume $\delta\mathcal{V}$ and index n , and is located at $r = r_d$, $z = z_d$. Remaining parameters are defined inside the back cover. If we substitute into Eq. (22-22) and note that a_1/\bar{a}_1 is pure imaginary, we find that equal power is scattered into the forward- and backward-propagating fundamental modes. However, the fraction of incident power scattered is minute since it is proportional to the square of both the volume of the nonuniformity and the difference in indices.

Polarization coupling

The weak guidance approximation, given above, ignores the slight polarization coupling due to nonuniformities. Such effects can be calculated for spherical scatterers as explained in Section 22-2. We then use the polarization corrections to the HE_{11} fields given in Section 12-11. Substituting these into Eq. (22-24) leads to expressions for $a_{\pm 2}$ of order Δ , arising from second-order corrections to \mathbf{e}_{ij} and first-order expressions for e_{zj} . Hence, for an incident x-polarized mode, the power scattered into the y-polarized (odd) mode is of order Δ^2 smaller than the power scattered into the x-polarized (even) mode.

22-9 Example: Sinusoidally perturbed interfaces

Radiation from the sinusoidally perturbed interface of a weakly guiding, step-profile fiber was discussed in Section 22-5 in terms of the induced current of Eq. (22-15). When the fiber is single moded, power is scattered into both forward- and backward-propagating x-polarized fundamental modes from the incident mode. Following the discussion of Section 22-5, we set

$$\bar{n}^2 - n^2 = -(n_{\text{co}}^2 - n_{\text{cl}}^2) \delta \rho \sin(\Omega z) \bar{\delta}(r - \rho), \quad (22-28)$$

in Eq. (22-26) and let \mathcal{V} be the volume between $z = z_1 = -L$ and $z = z_2 = L$ in Fig. 22-2(b). We find that $a_1 = 0$ and hence no power is scattered into the forward-propagating mode within this approximation. By analogy with Eq. (21-15), negligible power is scattered into the backward-propagating mode unless the resonance condition $\Omega \cong 2\beta$ is satisfied, in which case

$$a_{-1} \cong \bar{a}_1 \frac{L \delta \rho}{\rho} (2\Delta)^{1/2} \frac{\tilde{W}^2 J_0^2(\tilde{U})}{V J_1^2(\tilde{U})}, \quad (22-29)$$

using the normalization expression in Table 14-3, page 313. Hence the fraction of incident power so scattered increases quadratically with the length of the non-uniformity, but becomes invalid for arbitrarily large values of L since the induced current of Eq. (22-7) assumes the fields of the perturbed and unperturbed fibers are virtually equal. However, we show in Chapter 27 that the solution in this situation can be obtained using coupled-mode theory. The resonance condition requires the spatial period $2\pi/\Omega$ of the sinusoid to be comparable with the wavelength of light.

SLOWLY VARYING ARBITRARY NONUNIFORMITIES

So far in this chapter we have discussed power redistribution due to slight perturbations of fibers that are translationally invariant. Here we show how the induced-current representation can be used to determine power redistribution and radiation losses from fibers with arbitrary nonuniformities, provided only that the nonuniformities vary slowly along the fiber.

22–10 Induced-current representation for local modes

In Chapter 19 we introduced the concept of local modes to describe propagation on fibers with arbitrary nonuniformities. It is clear from the method of construction in Section 19–1 that the local-mode fields are an accurate approximation to the exact fields of the fiber provided the nonuniformities vary sufficiently slowly with z , as discussed in Section 19–2. Nevertheless, the local-mode fields are not an exact solution of Maxwell's equations, and the slight error can be described by induced currents.

We recall from Fig. 19–1 that the l th local mode is constructed using a superposition of cylindrical sections which approximate the fiber. The profile within each section is given by $\bar{n}(x, y) = n(x, y, z_c)$, where $n(x, y, z)$ is the profile of the perturbed fiber and z_c is the center of the section. Similarly, the exact electric field, \mathbf{E}_l , is approximated by the field, $\bar{\mathbf{E}}_l = \mathbf{e}_l(x, y) \exp(i\beta_l z)$, of an infinitely long section with profile \bar{n} . Since $\mathbf{E}_l \cong \bar{\mathbf{E}}_l$ and $\mathbf{n} \cong \bar{\mathbf{n}}$, we make a Taylor expansion of n about \bar{n} and deduce from Eq. (22–3) that correct to first order, the induced current is given by

$$\mathbf{J} = -i(\epsilon_0/\mu_0)^{1/2} k \hat{\mathbf{e}}_l \exp(i\beta_l z) (z - z_c) \partial n^2 / \partial z \Big|_{z_c}, \quad (22-30)$$

where the derivative is evaluated at the center of the section, and $\hat{\mathbf{e}}_l$ is the orthonormal field.

The philosophy for determining power loss is analogous to the construction of the local-mode fields in Section 19–1. We determine the loss from each section in terms of \mathbf{J} , sum the loss from each section and then approach a continuum limit.

22–11 Redistribution of guided power

Here we examine the excitation of other local modes by the l th local mode. We start by determining the contribution da_j to the amplitude of the j th forward-propagating local mode due to the induced current of Eq. (22–30) within one section. If we re-express Eq. (21–2a) in terms of the orthonormal modes of Section 11–5, then

$$da_j = -\frac{1}{4} \int_{z_c - \delta z}^{z_c + \delta z} \int_{A_\infty} \hat{\mathbf{e}}_j^* \cdot \mathbf{J} \exp(-i\beta_j z) dA dz, \quad (22-31)$$

for $z > z_c + \delta z$, where $2\delta z$ is the length of the section. Substituting from Eq. (22–30), we find that da_j is expressible as the product of two integrals

$$da_j = \frac{ik}{4} \left(\frac{\epsilon_0}{\mu_0} \right)^{1/2} \int_{z_c - \delta z}^{z_c + \delta z} (z - z_c) \exp\{i(\beta_l - \beta_j)z\} dz \int_{A_\infty} \hat{\mathbf{e}}_j^* \cdot \hat{\mathbf{e}}_l \frac{\partial n^2}{\partial z} \Big|_{z_c} dA. \quad (22-32)$$

The second integral depends on the two modes involved, whence it is convenient to define constants C_{jl} by

$$C_{jl} = \frac{k}{4} \left(\frac{\epsilon_0}{\mu_0} \right)^{1/2} \frac{1}{\beta_j - \beta_l} \int_{A_x} \hat{\mathbf{e}}_j^* \cdot \hat{\mathbf{e}}_l \frac{\partial n^2}{\partial z} dA; \quad j \neq l, \quad (22-33)$$

evaluated at $z = z_c$. On performing the z integration and rearranging, we find that Eq. (22-32) is expressible as the sum of two terms

$$da_j = -2 \delta z C_{jl} \exp \{i(\beta_l - \beta_j)z_c\} \cos \{(\beta_l - \beta_j) \delta z\} + db_j, \quad (22-34a)$$

$$db_j = -\frac{iC_{jl}}{\beta_l - \beta_j} \{ \exp [i(\beta_l - \beta_j)(z_c + \delta z)] - \exp [i(\beta_l - \beta_j)(z_c - \delta z)] \}. \quad (22-34b)$$

The first and second exponents in db_j are evaluated at the left-hand and right-hand ends of the section, respectively. Now consider the corresponding terms for the adjacent section to the right of the section in Fig. 19-1 (b), with centre z'_c and length $2 \delta z'$. The minute variation in the fiber means that we can neglect the changes in β_l and β_j . Consequently the term $\exp \{i(\beta_l - \beta_j)(z_c + \delta z)\}$ in db_j must cancel with the term $-\exp \{i(\beta_l - \beta_j)(z'_c - \delta z')\}$ in db'_j , since $z'_c = z_c + \delta z + \delta z'$. Hence, if we sum da_j of Eq. (22-34a) over all sections, there is no contribution from the db_j . We then parallel Section 19-1, by replacing z_c , β_l , β_j with z , $\beta_l(z)$, $\beta_j(z)$, respectively, and setting $dz = 2 \delta z$, to obtain, in the limit

$$a_j(z) = - \int_0^z C_{jl}(z) \exp \left\{ i \int_0^z [\beta_l(t) - \beta_j(t)] dt \right\} dz, \quad (22-35)$$

for the amplitude of the j th local mode at position z , where $C_{jl}(z)$ is now the z -dependent function defined by Eq. (22-33) in terms of $\beta_j(z)$, $\beta_l(z)$, $\hat{\mathbf{e}}_j(x, y, \beta_j(z))$, $\hat{\mathbf{e}}_l(x, y, \beta_l(z))$ and $n(x, y, z)$. Using this result, we determine the accuracy of the local-mode description in Chapter 28.

Radiation modes

Excitation of the local radiation modes, described in Chapter 28, is expressible by Eq. (22-35) provided we replace the j th local mode by the j th local radiation mode throughout the above analysis.

REFERENCES

1. Snyder, A. W. (1969) Scattering due to irregularities on dielectric or optical fibers. *I.E.E. Electron. Lett.*, **5**, 271-72.

2. Snyder, A. W. (1969) Excitation and scattering of modes on a dielectric or optical fibre. *I.E.E.E. Trans. Microwaves Theory Tech.* **17**, 1138–44.
3. Snyder, A. W. (1970) Radiation losses due to variations of radius on dielectric or optical fibers. *I.E.E.E. Trans. Microwaves Theory Tech.* **18**, 608–15.
4. Stratton, J. A. (1941) *Electromagnetic Theory*, McGraw-Hill, New York.
5. White, I. A. and Snyder, A. W. (1977) Radiation from dielectric optical waveguides. *Appl. Opt.*, **16**, 1470–2.
6. Marcuse, D. (1975) Radiation losses of the HE_{11} mode of a fiber with sinusoidally perturbed core boundary. *Appl. Opt.*, **14**, 3021–25.
7. Rawson, E. G. (1974) Analysis of scattering from fiber waveguides with irregular core surfaces. *Appl. Opt.*, **13**, 2370–7.
8. Jones, D. S. (1964) *Theory of Electromagnetism*, Pergamon Press, Oxford.

Bends

Bends of constant radius	474
23-1 Physical mechanism of radiation loss	474
23-2 Radiation model	475
23-3 Weakly guiding fibers	476
23-4 Radiation from a bent antenna	477
23-5 <i>Example: Step profile</i>	479
23-6 <i>Example: Graded profiles</i>	479
23-7 Radiation from bent fibers	480
23-8 <i>Example: Step profile</i>	481
23-9 <i>Example: Graded profiles</i>	482
Transition losses	483
23-10 Bends of different radii	483
23-11 Microbends	485
23-12 Tilts and offsets	485
References	485

This chapter is mainly concerned with the power radiated from single-mode fibers due to bending. We first consider losses from bends of constant radius, and then examine losses due to random, but slight, curvature along the fiber, commonly known as *microbends*. Bending losses for multimode fibers are described by the ray methods of Chapter 9.

BENDS OF CONSTANT RADIUS

Before establishing our model for the calculation of radiation loss, it may be helpful to understand the physical processes involved.

23-1 Physical mechanism of radiation loss

On a straight fiber of arbitrary profile, the modal field at every point in the cross-section propagates parallel to the fiber axis with the same phase velocity, so that planes of constant phase are orthogonal to the axis. However, if the fiber is bent into a planar arc of constant radius, as shown in Fig. 23-1(a), it is

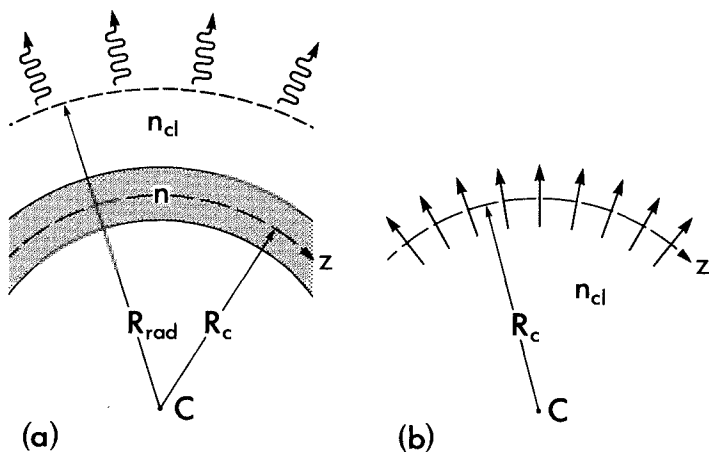


Fig. 23-1 (a) Section of a fiber bent into an arc of radius R_c . The core profile has index n , and n_{cl} is the uniform cladding index. (b) The fiber and its fields are approximated by induced currents \mathbf{J} denoted by the arrows in the volume occupied by the fiber core.

intuitive that the fields and phase fronts rotate about the center of curvature of the bend with constant angular velocity. Consequently, the phase velocity parallel to the fiber axis must increase linearly with distance from the center of curvature C . Since the fiber has a uniform cladding and the phase velocity cannot exceed the local speed of light, there will be a certain radius, R_{rad} , in the plane of the bend beyond which the phase velocity cannot remain in step, and the fields in this region must therefore become radiative, as shown qualitatively in Fig. 23-1(a). Close to and within the core, the fields are accurately described by a local mode, as discussed in Chapter 19, providing the radius of curvature is sufficiently large.

23-2 Radiation model

To calculate the power radiated from the bend, it is sufficient to use an approximate model of the fiber consisting of a current-carrying antenna of *infinitesimal thickness* which radiates in an infinite medium of index equal to the cladding index n_{cl} , i.e. the 'free-space' approximation of Section 21-8. The far-field formulae of antenna theory, as expressed by Eq. (21-21), can then be applied to calculate the radiation, once the current on the antenna is specified.

The antenna current is obtained in two stages [1, 2]. Firstly, we recognize that the fiber and its modal fields are together identical to a distribution of currents \mathbf{J} in a uniform medium of index n_{cl} , as shown qualitatively in Fig. 23-1(b). This equivalence is readily deduced by paralleling the discussion at the beginning of Chapter 22 and rearranging Maxwell's equations in the

manner of Eqs. (22-1) to (22-3) with \bar{n} replaced by n_{cl} . This leads to the distribution

$$\mathbf{J} = i(\epsilon_0/\mu_0)^{1/2} k(n_{cl}^2 - n^2)\mathbf{E}, \quad (23-1)$$

where n is the profile and \mathbf{E} the *exact* field of the fiber. Clearly \mathbf{J} is nonzero only within the volume corresponding to the fiber core. We can approximate \mathbf{E} by the local-mode field, i.e. by the field of a uniform fiber in local regions, provided the bending radius is large enough to satisfy Eq. (19-17).

The second stage takes advantage of the large ratio of bend to core radii and the fact that, for the problems considered in this chapter, the direction of \mathbf{J} does not vary over the cross-section. We then suppose that the distribution of currents throughout the core cross-section is concentrated on the fiber axis, resulting in a line current \mathbf{I}_a defined by

$$\mathbf{I}_a = \hat{\mathbf{n}} \int_{A_{co}} J dA, \quad (23-2)$$

where J is the magnitude of \mathbf{J} in Eq. (23-1), A_{co} is the core cross-sectional area and $\hat{\mathbf{n}}$ is a unit vector parallel to a fixed direction in the fiber cross-section.

Using this formulation, we calculate the radiation from the bent fiber in Section 23-4 by treating it as if it were a wire of negligible thickness located along the fiber axis and carrying the current of Eq. (23-2). This calculation isolates the dominant contribution to radiation loss. The accuracy of the thin-wire approximation is established in Section 23-7, where the effect of the finite cross-section of the fiber is included.

23-3 Weakly guiding fibers

We are primarily interested in radiation from the fundamental modes of bent, single-mode fibers. Within the weak-guidance approximation, the power radiated is insensitive to polarization, since $R \gg \rho$. Thus we can conveniently assume that the transverse electric field is parallel to the Z -axis in Fig. 23-2(a), i.e. orthogonal to the plane of the bend. Close to and within the core, the magnitude of the electric field on the bend is given by $a_1 F_0(R) \exp(i\beta z)$, using the local-mode approximation, where a_1 is the modal amplitude, $F_0(R)$ is the fundamental solution of the scalar wave equation in Table 14-3, page 313, and β is the scalar propagation constant. For clarity, we omit the \sim from scalar quantities. The coordinate z is the distance along the bent fiber axis in Fig. 23-2(a) and r is the usual cylindrical radius in Fig. 23-2(b). Substituting into Eq. (23-1) and using the fiber parameter and profile variation definitions inside the back cover, the equivalent current distribution is given by

$$\mathbf{J} = I \exp(i\beta z) \hat{\mathbf{z}}; \quad I = -ia_1 n_{co} \frac{V}{\rho} \left(\frac{2\Delta\epsilon_0}{\mu_0} \right)^{1/2} \{1 - f(R)\} F_0(R), \quad (23-3)$$

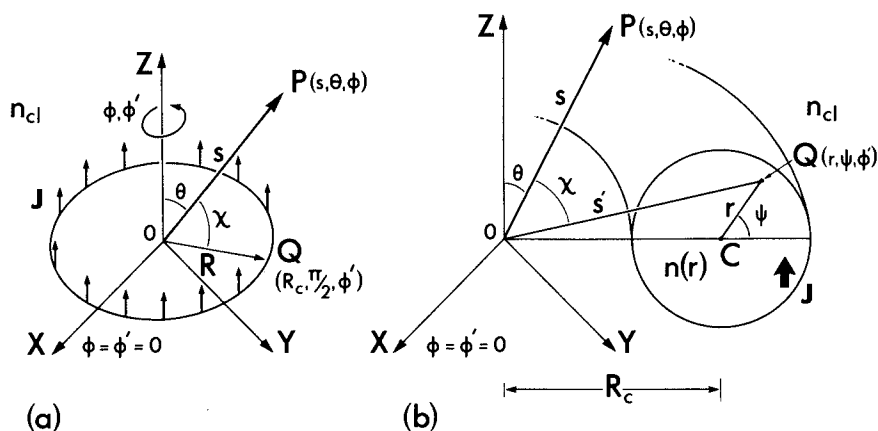


Fig. 23-2 (a) Orientation of cartesian axes $OXYZ$ and spherical polar coordinates (s, θ, ϕ) , (s', θ', ϕ') relative to a circular wire of radius R_c in an unbounded, uniform medium of refractive index n_{cl} . Arrows denote the Z -directed currents \mathbf{J} . (b) The wire is replaced by a bent fiber whose core cross-section is described by coordinates (r, ψ, ϕ) .

where $I = -i|\mathbf{J}|$, and $\hat{\mathbf{Z}}$ is the unit vector parallel to the Z -axis in Fig. 23-2(a). Consequently the antenna current of Eq. (23-2) is expressible as

$$\mathbf{I}_a = I_c \exp(i\beta z) \hat{\mathbf{Z}}; \quad I_c = -2\pi i a_1 n_{co} \rho V \left(\frac{2\Delta\epsilon_0}{\mu_0} \right)^{1/2} \int_0^\infty \{1 - f(R)\} F_0(R) R dR, \quad (23-4)$$

where $I_c = -i|\mathbf{I}_a|$, $R = r/\rho$ and ρ is the core radius.

23-4 Radiation from a bent antenna

The fundamental mode on a weakly guiding, bent fiber has been replaced by an antenna, or thin wire, carrying the current distribution of Eq. (23-4). Because the currents are orthogonal to the antenna, it may be helpful to think of them as a continuous distribution of Z -directed current dipoles. To calculate the power radiated, we assume, for simplicity, that the antenna is a closed loop of radius R_c , as shown in Fig. 23-2(a). If (s', θ', ϕ') are spherical polar coordinates describing the loop relative to the Z -axis, then Eq. (23-4) leads to the complete spatial distribution of the currents

$$I_c \{ \delta(s' - R_c) / R_c \} \delta(\theta' - \pi/2) \exp(i\beta R_0 \phi') \hat{\mathbf{Z}}, \quad (23-5)$$

where δ is the Dirac delta function and $z = R_c \phi'$ is the distance along the antenna from the X -axis. To calculate the power radiated, we follow the 'free-

space' formulation of Section 21-7 in terms of the vector potential. The far-field point P in Fig. 23-2(a) is described by spherical polar coordinates (s, θ, ϕ) as shown, and on substituting Eq. (23-5) into Eq. (21-20) with $s' = R_c$, we deduce that the vector \mathbf{M} has only the Z-component

$$M_z = I_c R_c \int_0^{2\pi} \exp \{ i R_c [\beta \phi' - k n_{cl} \sin \theta \cos (\phi - \phi')] \} d\phi', \quad (23-6)$$

where the relationship $\cos \chi = \sin \theta \cos (\phi - \phi')$ follows by geometry. On setting $\beta \phi' = -\beta (\phi - \phi') + \beta \phi$, comparison with Eq. (37-61) shows that the integral is well approximated by

$$|M_z| = 2\pi R_c |I_c| |J_v(k R_c n_{cl} \sin \theta)|; \quad v = \beta R_c, \quad (23-7)$$

provided $v \gg 1$. If v is an integer this expression is exact. The total radiated power follows from setting $M_\theta = -M_z \sin \theta$, $M_\phi = 0$ in Eq. (21-21b). On rearranging and setting $n_{co} \cong n_{cl}$, we obtain

$$P_{\text{rad}} = \frac{\pi}{8} \frac{R_c^2}{\rho^2} \left(\frac{\mu_0}{\epsilon_0} \right)^{1/2} \frac{V^2 |I_c|^2}{n_{co} \Delta} \int_0^\pi J_v^2(k R_c n_{cl} \sin \theta) \sin^3 \theta d\theta. \quad (23-8)$$

The integral can be evaluated asymptotically since both v and $k R_c$ are large. We replace the Bessel function by Eq. (37-90), since its order is larger than its argument, whence the integral reduces to

$$\frac{1}{\pi R_c} \int_0^{\pi/2} \frac{\sin^3 \theta}{(\beta^2 - k^2 n_{cl}^2 \sin^2 \theta)^{1/2}} \exp \left\{ -\frac{2}{3} \frac{\beta R_c}{\sin^3 \theta} \left[\frac{\beta^2}{k^2 n_{cl}^2} - \sin^2 \theta \right]^{3/2} \right\} d\theta. \quad (23-9)$$

The major contribution comes from values of θ close to $\pi/2$. Hence we can use Laplace's method to determine the asymptotic value of the integral, which is deduced by comparison with Eq. (37-131). Substituting into Eq. (23-8) and normalizing with the initial-mode power $P(0) = |a_1|^2 N$, where N is the normalization, we deduce that

$$\frac{P_{\text{rad}}}{P(0)} = \frac{\pi^{1/2}}{32} \left| \frac{I_c}{a_1} \right|^2 \left(\frac{R_c}{\rho} \right)^{1/2} \left(\frac{\mu_0}{\epsilon_0} \right)^{1/2} \frac{V^2 n_{co}}{W^{3/2} N \Delta} \exp \left\{ -\frac{4 R_c}{3 \rho} \frac{\Delta W^3}{V^2} \right\}, \quad (23-10)$$

where parameters are defined at the back of the book, and I_c is given by Eq. (23-4).

Power attenuation coefficient

The ratio $P_{\text{rad}}/P(0)$ is the fraction of power radiated from the entire loop in Fig. 23-2(a), and ignores attenuation of local-mode power along the antenna.

The fractional power loss per unit length, or power attenuation coefficient γ , is found by dividing Eq. (23-10) by the length of the loop $2\pi R_c$. Since γ is independent of z , the power at any position along the loop is found by analogy with Section 22-4 to be given by

$$P(z) = P(0) \exp(-\gamma z); \quad \gamma = P_{\text{rad}} / \{2\pi R_c P(0)\}. \quad (23-11)$$

If we substitute Eqs. (23-4) and (23-10) together with the normalization definition of Table 13-2, page 292, into Eq. (23-11), the fundamental-mode attenuation coefficient for an arbitrary, weakly guiding fiber is given by

$$\gamma = \left(\frac{\pi V^8}{16\rho R_c W^3} \right)^{1/2} \exp \left\{ -\frac{4 R_c \Delta W^3}{3 \rho V^2} \right\} \left[\int_0^\infty \{1-f\} F_0 R dR \right]^2 / \int_0^\infty F_0^2 R dR, \quad (23-12)$$

in terms of the profile function f and the fundamental solution F_0 of the scalar wave equation. The dominant feature of this expression is the exponential dependence on the ratio of bend to core radii. Since $R_c \gg \rho$, the attenuation coefficient is extremely small, and is relatively insensitive to the quantity multiplying the exponential.

23-5 Example: Step profile

The thin-wire approximation to radiation from the fundamental mode on a bent step-profile fiber is given in terms of the power attenuation coefficient of Eq. (23-12) by setting $f = 0$ over $0 \leq R < 1$ and $f = 1$ elsewhere. The $l = 0$ integral and eigenvalue equation in Table 14-6, page 319, together with the integral of Eq. (37-91), lead to

$$\gamma = \frac{\pi^{1/2}}{2\rho} \left(\frac{\rho}{R_c} \right)^{1/2} \frac{V^2 W^{1/2}}{U^2} \exp \left\{ -\frac{4 R_c W^3 \Delta}{3 \rho V^2} \right\}, \quad (23-13)$$

where values of U and W are to be found in Table 14-4, page 314.

23-6 Example: Graded profiles

We can use the Gaussian approximation for clad, graded-profile fibers. Thus F_0 is given by Eq. (15-2) and $W = (V^2 - U^2)^{1/2}$ by Table 15-2, page 340, in terms of the spot size. For example, the attenuation coefficient for the fundamental mode on a bent Gaussian-profile fiber is given by

$$\gamma = \frac{\pi^{1/2}}{2\rho} \left(\frac{\rho}{R_c} \right)^{1/2} \frac{V^4}{(V+1)^2 (V-1)^{1/2}} \exp \left\{ -\frac{4 R_c (V-1)^3}{3 \rho V^2} \Delta \right\}, \quad (23-14)$$

assuming $V > 1$. A similar expression can be derived in terms of the fiber parameter for the step profile.

23-7 Radiation from bent fibers

The thin-wire approximation of Section 23-2 superposes the equivalent core currents of the bent fiber onto its axis. Thus the results of Section 23-4 *ignore effects due to the finite core cross-section*. Here we derive the power attenuation coefficient of the fundamental mode allowing for the volume distribution of currents, and thus determine corrections to the above results [1-3]. However, we show below that the additional effect due to the finite cross-section can usually be ignored since the attenuation coefficient is exponentially small.

To describe the fiber cross-section, we introduce polar coordinates r and ψ , as shown in Fig. 23-2(b), whence (r, ψ, ϕ') form a set of orthogonal coordinates with metric coefficients $(1, r, R_c + r \cos \psi)$, respectively. We can then parallel the derivation in Section 23-4 and substitute the equivalent currents of Eq. (23-3) into Eq. (21-21). Assuming the fiber forms a closed ring, the analogous expression to Eq. (23-6) is

$$M_z = \int_0^\infty I r dr \int_0^{2\pi} (R_c + r \cos \psi) d\psi \int_0^{2\pi} \exp \{i(\beta z - k s' n_{cl} \cos \chi)\} d\phi', \quad (23-15)$$

where by geometry $z = (R_c + r \cos \psi)\phi'$ and χ satisfies

$$s' \cos \chi = (R_c + r \cos \psi) \sin \theta \cos (\phi - \phi') + r \cos \theta \sin \psi. \quad (23-16)$$

By analogy with Eq. (23-7), the ϕ' integration leads to

$$M_z = 2\pi R_c \int_0^\infty I r dr \int_0^{2\pi} J_v(k n_{cl} \{R_c + r \cos \psi\} \sin \theta) \times \\ \exp(-ikr n_{cl} \sin \psi \cos \theta) d\psi, \quad (23-17)$$

since $R_c \gg r \cos \psi$ and $v = \beta(R_c + r \cos \psi) \cong \beta R_c \gg 1$. The argument of the Bessel function is always smaller than its order, and consequently we use the Debye approximation of Eq. (37-90), where

$$J_v(z) \cong \frac{\exp \{ (v^2 - z^2)^{1/2} - v \cosh^{-1}(v/z) \}}{(2\pi)^{1/2} (v^2 - z^2)^{1/4}}; \quad z = k n_{cl} \sin \theta (R_c + r \cos \psi). \quad (23-18)$$

This expression is dominated by the exponential dependence and is therefore sensitive to slight changes in the argument of the exponential. Accordingly, we make a Taylor expansion of the argument of the exponential about $z_0 = k R_c n_{cl} \sin \theta$ in the small parameter $k r n_{cl} \sin \theta \cos \psi$, and retain terms correct to first order. On rearranging Eq. (23-18), we obtain

$$J_v(z) \cong J_v(k R_c n_{cl} \sin \theta) \exp \{ r \cos \psi (\beta^2 - k^2 n_{cl}^2 \sin^2 \theta)^{1/2} \}, \quad (23-19)$$

since $R_c \gg r \cos \psi$. Substitution into Eq. (23-17) leads to

$$M_z \cong 2\pi R_c J_v(kR_c n_{cl} \sin \theta) \int_0^\infty I_r dr \int_0^{2\pi} \exp\{WR \cos(\psi + i\delta)\} d\psi, \quad (23-20)$$

where $R = r/\rho$, the parameter W is defined inside the back cover and $\delta = \sinh^{-1}(\{k\rho n_{cl} \cos \theta\}/W)$. Using Eq. (37-65), the ψ integral is $2\pi I_0(WR)$, where I_0 is the modified Bessel function of the first kind. Thus M_z has the same dependence on θ as in Eq. (23-7), and hence the ratio of total power radiated to initial power is given by the product of Eq. (23-10) and the *area factor*, i.e. the square of the ratio of Eq. (23-20) to Eq. (23-7). If we denote the area factor by A , we deduce from Eqs. (23-3) and (23-4) that

$$A = \left\{ \int_0^\infty [1 - f(R)] F_0(R) I_0(WR) R dR \right\}^2 / \int_0^\infty [1 - f(R)] F_0(R) R dR. \quad (23-21)$$

Thus the attenuation coefficient is given by the product of A and Eq. (23-12).

Dependence on index difference

It is intuitive that bending losses from weakly guiding fibers should be higher than for fibers with larger index differences, since the latter are more effective in guiding modal power around the bend. The quantitative dependence of loss on the relative index difference is identical for the actual fiber and the thin-wire antenna, and is given by the exponential variation with Δ in Eq. (23-12). Thus, although weakly guiding fibers are more susceptible to bending loss, the fraction of mode power radiated is negligible unless the ratio of bend to core radii takes impractically small values, as is clear from Fig. 23-3 below. We now consider examples.

23-8 Example: Step profile

In Eq. (23-21) we set $f = 0$ over $0 \leq R < 1$ and $f = 1$ elsewhere, and substitute for F_0 from Table 14-3, page 313. The integrals follow from Eqs. (37-92) and (37-99). With the help of the eigenvalue equation in Table 14-3 and the Wronskian of Eq. (37-79), the area factor is expressible as

$$A = [U^2 / \{WV^2 K_1(W)\}]^2. \quad (23-22)$$

For a fiber with $V = 2.4$, we find from Table 14-4, page 314, that $A \cong 1.9$. The product of A and Eq. (23-13) gives the attenuation coefficient for the fundamental mode on a bent, step-profile fiber [1-3]

$$\gamma = \frac{\pi^{1/2}}{2\rho} \left(\frac{\rho}{R_c} \right)^{1/2} \frac{U^2}{V^2 W^{3/2}} \frac{1}{K_1^2(W)} \exp \left\{ -\frac{4 R_c W^3 \Delta}{3 \rho V^2} \right\}. \quad (23-23)$$

The normalized coefficient $\gamma\rho$ is plotted as a function of Δ for various values of R_c/ρ in Fig. 23-3(a) for a fiber with $V = 2.4$. Unless Δ is minute or R_c/ρ is impractically small, the area factor of Eq. (23-22) can be ignored in calculating the attenuation coefficient, since the latter is exponentially small.

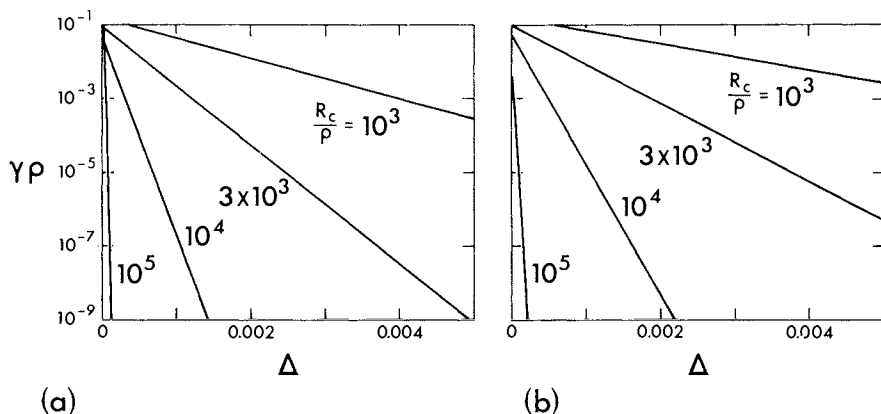


Fig. 23-3 (a) The normalized attenuation coefficient $\gamma\rho$ of Eq. (23-23) as a function of Δ for various values of the normalized bending radius R_c/ρ when the fiber has a step profile. (b) The corresponding results for a Gaussian-profile fiber calculated from Eq. (23-25).

23-9 Example: Graded profiles

We can evaluate the area factor for graded-profile fibers within the Gaussian approximation. We replace F_0 with Eq. (15-2) and W with $(V^2 - U^2)^{1/2}$, taken from Table 15-2, page 340. Thus for the Gaussian profile, the area factor follows from Eq. (37-101) as

$$A = \exp \left\{ (V-1)^2 / (V+1) \right\}; \quad V > 1. \quad (23-24)$$

At the cutoff $V \cong 2.6$ of the second mode, $A \cong 2$. The product of A and Eq. (23-14) leads to the fundamental-mode attenuation coefficient

$$\gamma = \frac{\pi^{1/2}}{2\rho} \left(\frac{\rho}{R_c} \right)^{1/2} \frac{V^4}{(V+1)^2 (V-1)^{1/2}} \exp \left\{ \frac{(V-1)^2}{V+1} - \frac{4}{3} \frac{R_c}{\rho} \frac{(V-1)^3}{V^2} \Delta \right\}. \quad (23-25)$$

The normalized coefficient $\gamma\rho$ is plotted against Δ for various values of R_c/ρ in Fig. 23-3(b) for a fiber with $V = 2.6$. Here ρ is the scaling length for the profile in Eq. (15-6). As was the case for the step profile, the area factor can be ignored in determining the order of the radiation loss from practical fibers, since it is exponentially small.

TRANSITION LOSSES

In addition to the radiation loss associated with bending of a fiber, there is a *transition loss* due to abrupt changes in curvature, as occur at the cross-sectional plane AA' of the fibers in Fig. 23-4. As we show below, there is a mismatch between the fields on AA', and, consequently, the incident field on one side excites both the local modes and the radiation field on the other side. The power in the radiation field accounts for the transition loss [4-6].

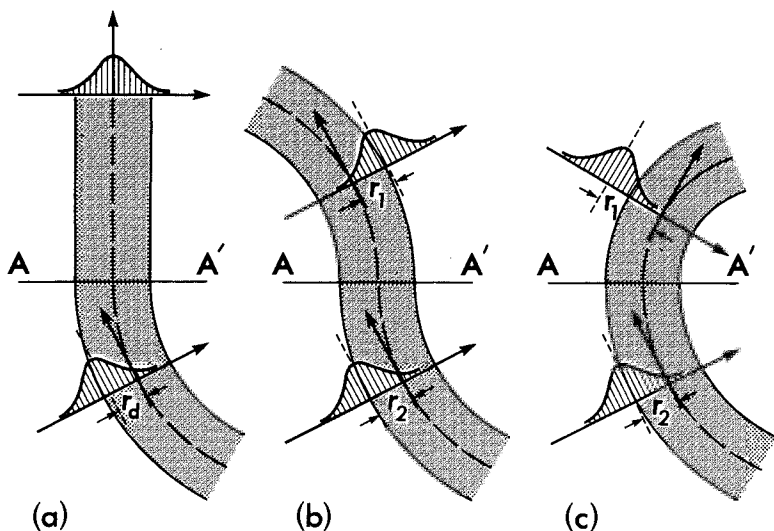


Fig. 23-4 The shift in the Gaussian-shaped fundamental mode electric field distribution from the fiber axis shown qualitatively from (a) a bend, (b) bends of opposite curvature and (c) a change in bend radius.

23-10 Bends of different radii

In order to calculate the radiation due to an abrupt change in curvature, we need to know the modal fields of the bent fiber more accurately than the local-mode approximation described in Chapter 19. The latter assumes the fields in any cross-section of the bent fiber are identical to the fields of the straight fiber, so that there is no mismatch, regardless of curvature. In Section 36-15 we show that the predominant effect of curvature on the fundamental mode is to shift the field distribution radially outwards in the plane of the bend a distance r_d from the fiber axis, as shown in Fig. 23-4(a). For an arbitrary profile,

Eq. (36-56) gives the shift within the Gaussian approximation in terms of the spot size r_0 of Eq. (15-2)

$$r_d = \frac{V^2 \rho^2}{2\Delta R_c} \left(\frac{r_0}{\rho} \right)^4; \quad R_c \gg \rho, \quad (23-26)$$

where R_c is the radius of the bend, and remaining parameters are defined at the back of the book.

Straight and curved sections

The transition loss for Fig. 23-4(a) is due to the mismatch over AA' between the fields of the straight section and the offset fields of the curved section. We use the Gaussian approximation of Eq. (15-2) to describe the radial distribution of the fundamental-mode fields relative to the fiber axis and obtain

$$F_0 = \exp \{ -r^2/2r_0^2 \}; \quad F_0 = \exp \{ -(r-r_d)^2/2r_0^2 \}, \quad (23-27)$$

respectively, where r_d is the shift of Eq. (23-26). The situation on AA' is then identical to incidence of an offset Gaussian beam, as discussed in Section 20-8. Assuming the fiber is single moded, the fraction of incident-mode power which remains bound is given by Eq. (20-21) with $\rho_s = r_0 + r_d$. Hence the fraction of power radiated, or transition loss, is given by

$$1 - \frac{P_0}{P_i} \cong 1 - \exp \left\{ -\frac{r_d^2}{2r_0^2} \right\} \cong \left(\frac{\rho}{R_c} \right)^2 \left(\frac{r_0}{\rho} \right)^6 \frac{V^4}{8\Delta^2}, \quad (23-28)$$

since $r_d \ll r_0$. This result applies for incidence at AA' from either direction.

Two curved sections

Consider two curved sections of a fiber with radii R_1 and R_2 , such as those shown in Fig. 23-4(b) and (c). The fundamental-mode shift r_1 or r_2 for each section is calculated from Eq. (23-26) with R_c replaced by R_1 or R_2 , respectively. On AA', the relative shift r_d also depends on the angle χ between the planes containing each bend according to

$$r_d = (r_1^2 + r_2^2 - 2r_1 r_2 \cos \chi)^{1/2}. \quad (23-29)$$

When the bends lie in the same plane, $r_d = r_1 + r_2$ if the bends are in the opposite sense ($\chi = \pi$), as in Fig. 23-4(b), or $r_d = |r_1 - r_2|$ if the bends are in the same sense ($\chi = 0$), as in Fig. 23-4(c). Hence the relative shift and fraction of power radiated follow from Eqs. (23-26) and (23-28) as

$$r_d = \frac{|R_1 \pm R_2|}{R_1 R_2} \frac{\rho^2 V^2}{2\Delta} \left(\frac{r_0}{\rho} \right)^4; \quad 1 - \frac{P_0}{P_i} \cong \left\{ \frac{R_1 \pm R_2}{R_1 R_2} \right\}^2 \frac{\rho^2 V^4}{8\Delta^2} \left(\frac{r_0}{\rho} \right)^6, \quad (23-30)$$

for the two cases, respectively, independent of the direction of incidence at AA'.

23–11 Microbends

When the fiber has a large number of random bends of arbitrary radii of curvature and lengths, the radiation is uncorrelated, so we can add the power losses from transitions and from bends. Thus the total microbending loss along the length of the fiber is the sum of the power radiated from each bend and from each transition. Provided the ratio of bend to core radii is large, as is the case in practice, we can use the expressions developed in this chapter. For large bending radii, transition loss dominates pure bending loss because of the exponential dependence in Eq. (23–12). Further results are to be found elsewhere [7, 8].

When the microbending is of sufficiently small amplitude, it is equivalent to a form of interface roughness, and the methods of Section 22–5 then apply. We find that the radiation losses are significant only when Ω is in the range given by Eq. (22–16), assuming the fiber interface meanders sinusoidally about a straight path.

23–12 Tilts and offsets

In Section 20–11, we showed that the fraction of fundamental-mode power transmitted between contiguous fibers in the presence of mismatches in profile, tilts or offsets is given by the appropriate expression for P_o/P_i in Table 20–1, page 429, in terms of the spot sizes for the Gaussian approximation on each fiber. The transition loss, or fraction of power radiated, in each situation is given by $1 - P_o/P_i$, provided the fibers are single moded.

Reflected power

The transition losses discussed in Section 23–10 do not account for power reflected into backward-propagating modes from junctions or changes in bending radius. In Section 20–2, we showed that negligible power is reflected from the endface of a weakly guiding fiber, and consequently, we are justified in ignoring reflection losses.

REFERENCES

1. Snyder, A. W., White, I. A. and Mitchell, D. J. (1975) Radiation from bent optical waveguides. *Electron. Lett.*, **11**, 332–3.

2. White, I. A. (1979) Radiation from bends in optical waveguides: the volume-current method. *Microwaves, Opt. Acoust.*, **3**, 186–8.
3. White, I. A. (1977) Radiation losses in dielectric optical waveguides. Ph.D. Thesis, The Australian National University.
4. Gambling, W. A., Matsumura, H. and Ragdale, C. M. (1978) Field deformation in a curved single-mode fibre. *Electron. Lett.*, **14**, 130–2.
5. Gambling, W. A., Payne, D. N. and Matsumura, H. (1976) Radiation from curved single-mode fibres. *Electron. Lett.*, **12**, 567–9.
6. Marcuse, D. (1976) Field deformation and loss caused by curvature of optical fibres. *J. Opt. Soc. Am.*, **66**, 311–20.
7. Gambling, W. A., Matsumura, H. and Ragdale, C. M. (1979) Curvature and microbending losses in single-mode optical fibres. *Opt. Quant. Elect.*, **11**, 43–59.
8. Sakai, J. I. (1980) Microbending loss evaluation in arbitrary-index single-mode optical fibers. *I.E.E.E. J. Quant. Elec.*, **16**, 36–49.

CHAPTER 24

Leaky modes

24-1	Radiation close to the axis	488
24-2	Heuristic derivation	489
24-3	Leaky modes and space-wave representation of radiation	490
Characteristics of leaky modes		490
24-4	Modal parameters	491
24-5	Modal fields	491
24-6	Radiation caustic	492
24-7	Classification of leaky modes	492
24-8	Plane-wave decomposition	494
24-9	Weakly guiding waveguides	494
24-10	Number of leaky modes	494
Power and attenuation		495
24-11	Intuitive physical description	495
24-12	Guided and radiated power	496
24-13	Fraction of guided power in the core	497
24-14	Power attenuation coefficient	498
Orthogonality and normalization		499
24-15	Orthogonality relations	500
24-16	Normalization	500
24-17	Excitation and perturbation problems	501
Solution of the eigenvalue equation		502
24-18	<i>Example: Analytical solution for the step-profile fiber</i>	502
24-19	<i>Example: Numerical solution for the step-profile fiber</i>	504
24-20	<i>Example: Step-profile planar waveguide</i>	506
Applications of leaky modes		507
24-21	<i>Example: Far-field radiation pattern</i>	508
24-22	<i>Example: Sinusoidal line source</i>	509
24-23	<i>Example: On-axis sinusoidal nonuniformity</i>	510
References		512
		487

In Chapters 21 to 23 we were mainly concerned with the *total* power radiated by sources and fiber nonuniformities, rather than the distribution of radiation throughout the fiber. This distribution describes the *spatial transient* between the source of excitation of the radiation fields and the *spatial steady state* further along the fiber, where essentially only bound modes propagate. The spatial transient and the spatial steady state were discussed in Section 8-1, and for a source on the endface, the situation is depicted schematically in Fig. 8-1. Within the region of the spatial transient, both bound modes and the radiation fields are necessary to fully describe light propagation. The duration of the spatial transient depends on the degree to which the fiber retains radiation from the source prior to its eventual escape, or leakage, from the core. The purpose of this chapter is to introduce a class of modes, called *leaky modes*, to describe the portion of the radiation field which travels *comparatively long distances along and close to the fiber axis*.

We shall mainly be concerned with fibers that propagate only one or a few modes. The spatial transient of multimode fibers was examined in Chapter 8, using the leaky rays of Chapter 7. We recall from Eq. (8-1) that the duration of the spatial transient along the fiber increases exponentially with the fiber parameter V . For example, a step-profile fiber with $V = 50$ and $\theta_c \cong \sqrt{(2\Delta)} = 0.1$ has a spatial transient over a distance of approximately $10^{11}\rho$, where ρ is the core radius, whereas a fiber with the same value of Δ , but with $V = 2.4$ has a spatial transient of approximately 17ρ . Although Eq. (8-1) is not precise for such a small value of V , it does show that the spatial transient plays only a minor role in describing light propagation along low- V fibers which propagate only one or a few modes, although the transient can be important when the fiber length is short, as in some visual photoreceptors [1, 2]. Nevertheless, it is important to appreciate the properties of leaky modes, since they not only provide a good approximation for describing the spatial transient of low- V fibers, but the physical properties of an individual leaky mode provide a simple description of the loss mechanism for the fiber.

24-1 Radiation close to the axis

The main objective of this chapter is to approximate that portion of the radiation field which propagates within or near the core for comparatively large distances from the source of excitation. The fiber is then effectively guiding some of the radiated power over finite distances. It is intuitive that within and close to the core, the fields which describe this radiation must have almost the same representation as the fields which describe the guided, bound-mode power. The only difference between the two representations is due to the attenuation of the radiation fields along the axis as power is lost into the cladding. Thus we anticipate that the guided portion of the radiation fields can be described approximately by leaky modes, i.e. by modes which are similar to bound modes near and within the core, but have a complex propagation

constant to account for the attenuation in the direction of propagation.

The description of leaky modes comes from several logical approaches. We begin with a heuristic argument and follow with the detailed mathematical formulation which applies to waveguides of arbitrary cross-section and profile. For clarity, we omit modal subscripts when discussing an individual leaky mode.

24-2 Heuristic derivation

We saw in Chapter 11 that the propagation constant β of a bound mode is given by an eigenvalue equation, provided the waveguide parameter V is *above* the cutoff value V_c for that mode. If we now investigate this solution for values of V *below* the cutoff value V_c , we find that β becomes complex and the modal fields possess the attributes of leaky modes described above.

We could have anticipated this by examining the modal properties of particular waveguides. For example, compare the fraction η of bound-mode power within the core of the step-profile, planar waveguide with the same fraction for the step-profile fiber. It is clear from Table 12-2, page 243, that $\eta \rightarrow 0$ for *every mode of the planar waveguide* as V approaches the cutoff value V_c , i.e. $U = V = V_c, W = 0$. However, in Fig. 12-5, $\eta > 0$ at cutoff for *every mode of the fiber*, with the exception of the TE_{0m} , TM_{0m} , HE_{1m} and HE_{2m} modes. Thus, there is a significant difference between the modes of the two waveguides close to cutoff. As a mode of the planar waveguide approaches cutoff, all of its power resides in the cladding, whereas a substantial fraction of power remains within the core of the fiber at cutoff, excepting the above-mentioned modes.

Propagation below cutoff

Now consider on the fiber endface a source which excites only the HE_{31} mode at its cutoff $V_c = 4.399$, assuming $\Delta = 0.32$. This mode propagates unattenuated along the fiber with approximately 60% of its power within the core, according to Fig. 12-5. If we increase the wavelength λ of the source infinitesimally so that V is just below V_c , then the propagation characteristics of the fiber have changed only infinitesimally, yet the exact electromagnetic analysis shows that all the power in this mode is ultimately radiated. Close to or within the core, the radiation field can be approximated by the fields of the bound HE_{31} mode. However, the eigenvalue equation shows that the propagation constant β has an infinitesimal, imaginary part and it gives rise to an infinitesimal attenuation coefficient. Physically, the attenuation coefficient accounts for the gradual spread of power away from the core as the leaky mode propagates, and, as we show in Section 24-14, the imaginary part of β can be identified directly with the rate at which guided power of the leaky mode is radiated.

The above example provides additional justification for our intuitive belief

that the portion of the radiation fields propagating along and close to the fiber axis can be approximated by bound modes below cutoff. Perhaps the most convincing evidence is the experimental observation [3, 4] of mode patterns for fibers with values of the fiber parameter V below the cutoff, V_c , of each mode. Although leaky modes on planar waveguides have been understood for some time [5-9], it is only recently that leaky modes of the type exemplified by the HE_{31} mode have been described [10-19].

24-3 Leaky modes and space-wave representation of radiation

The radiation fields of an optical waveguide can be determined either by modal methods or by Green's function methods, as discussed in Chapters 25 and 34. In Chapter 26, we show how, starting from either representation, the total radiation fields \mathbf{E}_{rad} and \mathbf{H}_{rad} can be expressed *exactly* as a sum of leaky modes together with a *space-wave* contribution \mathbf{E}_{sw} and \mathbf{H}_{sw} . Thus

$$\mathbf{E}_{\text{rad}} = \sum_{j=1}^{M_{\text{lm}}} \{a_j \mathbf{E}_j + a_{-j} \mathbf{E}_{-j}\} + \mathbf{E}_{\text{sw}}; \quad \mathbf{H}_{\text{rad}} = \sum_{j=1}^{M_{\text{lm}}} \{a_j \mathbf{H}_j + a_{-j} \mathbf{H}_{-j}\} + \mathbf{H}_{\text{sw}},$$

(24-1)

where the a_j and a_{-j} are modal amplitudes of the forward- and backward-propagating modes, respectively, and M_{lm} is the number of forward- or backward-propagating leaky modes, discussed in Section 24-10. The modal fields \mathbf{E}_j , \mathbf{H}_j , \mathbf{E}_{-j} and \mathbf{H}_{-j} , are the fields of the bound modes of Eq. (11-3) evaluated below the cutoff, V_c , of each mode, while the space-wave fields represent the remaining portion of the radiation fields. The power associated with the space-wave fields *rapidly* propagates away from the waveguide.

At large distances from the waveguide axis, the space-wave fields represent the entire radiation fields, while at the other extreme, the radiation field far from the source and close to or within the core is represented approximately by the leaky-mode fields. An exception to this is the very special situation when the power of the source of excitation is highly directed at the complementary critical angle, θ_c , of geometric optics. Under these circumstances, the radiation fields propagate along the core-cladding interface for comparatively long distances. We include this radiation, which is discussed in Chapter 26, within the space-wave contribution to Eq. (24-1), since it is not contained within the core by the transverse resonance mechanism satisfied by the leaky modes, i.e. the eigenvalue equation.

CHARACTERISTICS OF LEAKY MODES

We now examine the properties of leaky modes on nonabsorbing, clad fibers of arbitrary profile and cross-section. Later, in Section 24-20, we briefly discuss the leaky modes of planar waveguides.

24-4 Modal parameters

Since leaky modes are bound modes below cutoff, they have fields which are functionally identical to those of bound modes. However, the modal parameters appearing in the fields are now complex. If superscripts r and i denote real and imaginary parts, then we define

$$\beta = \beta^r + i\beta^i; \quad U = U^r + iU^i; \quad W = W^r + iW^i, \quad (24-2)$$

where U and W are related to β and the waveguide parameter V , as inside the back cover. The range of bound-mode propagation constants is given by Eq. (11-46). Consequently, the leaky-mode propagation constant satisfies

$$0 \leq \beta^r < kn_{cl} \quad \text{or} \quad U^r > V. \quad (24-3)$$

In Section 24-10, we show that there is only a finite number of leaky modes. Just below cutoff, W is almost pure imaginary, so it is convenient to introduce a new modal parameter Q defined by

$$Q = \rho(k^2 n_{cl}^2 - \beta^2)^{1/2} = iW = (U^2 - V^2)^{1/2}, \quad (24-4)$$

and included at the back of the book. Thus Q is almost real just below cutoff. The signs of the parts of the complex parameters satisfy

$$\beta^r, \beta^i, U^r, Q^r, \text{ positive; } U^i, W^r, W^i, Q^i, \text{ negative,} \quad (24-5)$$

for forward-propagating modes.

24-5 Modal fields

If we substitute Eq. (24-2) into Eq. (11-3), the functional dependence of the leaky-mode fields is given by

$$\mathbf{E}(x, y, z) = \mathbf{e}(x, y) \exp(i\beta^r z) \exp(-\beta^i z), \quad (24-6a)$$

$$\mathbf{H}(x, y, z) = \mathbf{h}(x, y) \exp(i\beta^r z) \exp(-\beta^i z), \quad (24-6b)$$

where \mathbf{e} and \mathbf{h} depend on the complex modal parameters. The spatial dependence of \mathbf{e} and \mathbf{h} in the uniform cladding of an arbitrary fiber is identical to the dependence for the step profile in Table 12-3, page 250, apart from a change in the constant factor in each component. The radial dependence involves the modified Bessel function of the second kind $K_\nu(WR)$ where $R = r/\rho$. Since W is almost pure imaginary just below cutoff, we use the transformations of Eqs. (24-4) and (37-71) to replace K_ν by the Hankel function $H_\nu^{(1)}(QR)$ of the first kind, whose argument is almost pure real. Thus, for example, the spatial variation of the longitudinal field components of the even modes is proportional to

$$H_\nu^{(1)}(QR) \cos(\nu\phi) \exp(i\beta z). \quad (24-7)$$

At large distances from the fiber such that $QR \gg v$, we can replace the Hankel function by its asymptotic form of Eq. (37-87). If we include the implicit time dependence, Eq. (24-7) is proportional to

$$(1/R^{1/2}) \cos(v\phi) \exp \left[i \left\{ QR + \beta z - (2v + 1) \frac{\pi}{4} - \omega t \right\} \right]. \quad (24-8)$$

The expression within the curly brackets represents a wave propagating away from the fiber. The direction of propagation determines the direction of the power radiating from the leaky mode. In the cladding this direction makes angle θ_z with the fiber axis, whence, we deduce from Eqs. (24-8) and (24-4) that

$$\cos \theta_z = \beta^r / k n_{cl}; \quad \tan \theta_z = Q^r / \rho \beta^r, \quad (24-9)$$

where n_{cl} is the uniform cladding index.

24-6 Radiation caustic

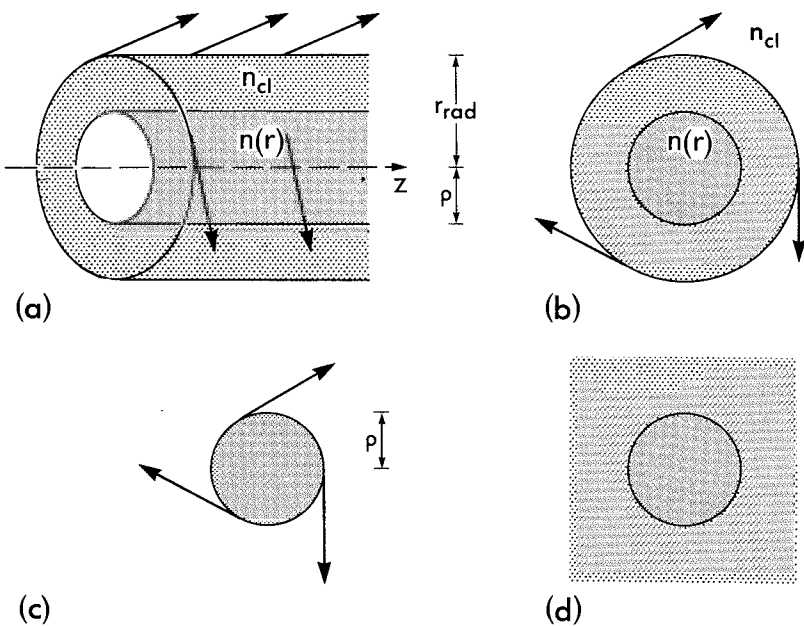
The fields of leaky modes are characterized by a distinct change in their physical behavior sufficiently far from the fiber axis. We define a radius r_{rad} in the cladding at which the order and the real part of the argument of the Hankel function in Eq. (24-7) are equal, assuming high-order modes with $v \gg 1$. Hence

$$r_{rad} = v\rho/Q^r; \quad r \geq \rho, \quad (24-10)$$

where ρ is the core radius. The behavior of the fields in the regions $\rho < r < r_{rad}$ and $r_{rad} < r < \infty$ follows by substituting Eqs. (37-90) and (37-87) for the asymptotic forms of the Hankel function into Eq. (24-7). Between the interface and the surface $r = r_{rad}$, the fields are evanescent, and decrease with increasing radius, while beyond r_{rad} the fields are oscillatory or wavelike and power propagates in the direction given by Eq. (24-9). Accordingly, we identify r_{rad} with the apparent position from which radiation originates. We call this position the *radiation caustic*. The situation is depicted in Fig. 24-1(a). Within the core and the region $\rho \leq r < r_{rad}$, the leaky mode appears like a bound mode, but for $r > r_{rad}$ power is radiated. We emphasize that r_{rad} is sharply defined as the actual origin of radiation only for high-order modes.

24-7 Classification of leaky modes

Where the radiation caustic lies at a finite distance beyond the interface, the modal fields in the region $\rho < r < r_{rad}$ are evanescent and the direction of power flow, as determined by the Poynting vector, is parallel to the fiber axis. Since power is lost at r_{rad} , and because the fields at every position within $0 \leq r < r_{rad}$ attenuate at the same rate, part of the power radiated must originate within the core. The physical mechanism whereby core power is



(b)	TUNNELING LEAKY MODES	$\rho < r_{rad} < \infty$
(c)	REFRACTING LEAKY MODES	$r_{rad} = \rho$
(d)	BOUND MODES	$r_{rad} = \infty$

Fig. 24-1 Leaky mode radiation from a clad fiber originates on the radiation caustic of radius r_{rad} and propagates away at angle θ_z to the axis. Shaded regions denote the core and dotted regions denote evanescent fields in the cladding. A tunneling leaky mode is depicted in (a) and (b), a refracting leaky mode in (c) and a bound mode in (d). The table classifies modes according to the value of r_{rad}

transmitted across the evanescent region is known as *tunneling*, or *frustrated total reflection*, as already discussed in Chapter 7 in terms of rays. Hence leaky modes with values of r_{rad} satisfying $\rho < r_{rad} < \infty$, are referred to as *tunneling leaky modes* [13–15]. It is intuitive that the larger r_{rad} the smaller the modal attenuation, since, when $r_{rad} = \infty$, the evanescent fields extend indefinitely into the cladding and the leaky mode becomes a bound mode.

If the radiation caustic coincides with the interface, then $r_{rad} = \rho$ and, in keeping with the ray nomenclature of Chapter 7, we refer to such modes with

no evanescent region in the cladding as *refracting leaky modes*. The range of values of r_{rad} for bound and leaky modes, together with the evanescent field depth, are shown qualitatively in Fig. 24–1.

24–8 Plane-wave decomposition

We show in Section 36–2 how the fields of high-order bound modes on the step-profile fiber can be decomposed into families of plane waves, or rays, each ray propagating with the same characteristic angles θ_z and θ_ϕ in the core of the fiber. This decomposition also applies to the fields of leaky modes in the core, and verifies that tunneling leaky modes are composed of tunneling leaky rays and refracting leaky modes are composed of refracting leaky rays [11]. The connection between the modal parameters v and β^r and the ray invariants T and β is given in Table 36–1, page 695, provided β is replaced by β^r .

24–9 Weakly guiding waveguides

In Chapter 13, we showed how to construct the bound-mode fields of weakly guiding fibers, starting from solutions of the scalar wave equation. The transverse electric fields \mathbf{e}_t of leaky modes have the same functional form as the bound-mode field \mathbf{e}_t of Table 13–1, page 288, provided the propagation constant $\tilde{\beta}$ and the modal parameters U and \tilde{W} are replaced by the complex forms corresponding to Eq. (24–2). We introduce the modal parameter \tilde{Q} which is defined by analogy with Eq. (24–4). For forward-propagating modes, the signs of the real and imaginary parts of these parameters obey the same rules as the exact parameters in Eq. (24–5).

The corresponding transverse magnetic field \mathbf{h}_t is no longer related to \mathbf{e}_t by the expression in Table 13–1, since β^r satisfies the same range of values as β^r in Eq. (24–3) and thus may differ significantly from kn_{co} . Instead, we use a simplified form of Eq. (30–5b) for arbitrary values of $\tilde{\beta}$. We show in subsequent sections that solutions of the eigenvalue question for leaky modes satisfy $|\tilde{\beta}| \cong kn_{\text{co}}$. This arises because $\tilde{\beta}^i$ rapidly increases as V decreases below cutoff, V_c and offsets the decrease in β^r . Accordingly, the longitudinal fields of Eqs. (30–5c) and (30–5d) are of order $1/\rho\tilde{\beta}$, or $\Delta^{1/2}/V$, times the transverse fields and can be ignored. Thus Eq. (30–5b) can be well approximated by setting

$$\mathbf{h}_t = (\epsilon_0/\mu_0)^{1/2} (\tilde{\beta}/k) \hat{\mathbf{z}} \times \mathbf{e}_t, \quad (24-11)$$

where $\hat{\mathbf{z}}$ is the unit vector parallel to the fiber axis.

24–10 Number of leaky modes

We derive expressions in Section 36–13 for the number M_{lm} of leaky modes which can propagate on an arbitrary multimode fiber with $V \gg 1$. The numbers of tunneling leaky modes M_{lm} and refracting leaky modes M_{rm} on a

step-profile fiber follow from Eqs. (36-45) and (36-42)

$$M_{\text{tm}} \cong \frac{V^2}{2} \left\{ 1 + \frac{(2\Delta)^{12}}{3\pi} \right\}; \quad \Delta \ll 1, \quad (24-12a)$$

$$M_{\text{rm}} = M_{\text{lm}} - M_{\text{tm}} \cong \frac{V^2}{2} \left\{ \frac{1}{2\Delta} - \frac{2}{\pi} \left(\frac{2}{\Delta} \right)^{1/2} \right\}, \quad (24-12b)$$

where the smallest integer just exceeding the right side is implied, and Δ is defined inside the back cover. These expressions include all even and odd HE and EH modes, as well as the TE and TM modes. The number of bound modes M_{bm} is given by Eq. (36-41), whence the total number of modes is

$$M_{\text{tot}} = M_{\text{bm}} + M_{\text{tm}} + M_{\text{rm}} = M_{\text{bm}} + M_{\text{lm}} = V^2/4\Delta, \quad (24-13)$$

The numbers of bound and of tunneling modes are approximately equal when $\Delta \ll 1$.

POWER AND ATTENUATION

Leaky modes are a useful concept if we can apply them to problems as easily as bound modes. This is facilitated by the development of a sound, physical description of the power and attenuation of leaky modes [11, 13]. As there is no formal definition of leaky-mode power, we present an intuitive description.

24-11 Intuitive physical description

Using the attributes of leaky modes discussed above, we can gain further insight into the structure of each mode [13]. Consider a tunneling leaky mode on length L of a fiber as shown in Fig. 24-2(a). The mode is excited at $z = 0$ and as it propagates we assume that radiation originates from the radiation caustic of Section 24-6. The guided portion of the leaky mode's power is assumed to lie in the region $0 \leq r < r_{\text{rad}}$. At $z = L$, the radiation flowing through each point of the cross-sectional plane can be identified with its point of origin on $r = r_{\text{rad}}$. Thus radiation at $r = r_0$ originates from $z = 0$, and at $r = r_1$ from $z = z_1$, as shown. As the guided leaky-mode power attenuates along the fiber, the radiation fields at r_0 on $z = L$ are greater than at r_1 , since more power is available for radiation at $z = 0$ than at $z = z_1$. Thus we can anticipate that the field of a leaky mode beyond $r = r_{\text{rad}}$ increases with radial distance up to $r = r_0$ where it reaches a maximum. Beyond r_0 the field vanishes. Within $r = r_{\text{rad}}$, the leaky-mode fields appear like bound-mode fields, apart from a complex propagation constant which accounts for the attenuation along the fiber. It may be helpful to note that this attenuation is qualitatively identical to the attenuation caused by an absorbing medium occupying the region $r > r_{\text{rad}}$.

The increase in the radiation field intensity for $r > r_{\text{rad}}$ can be seen in the

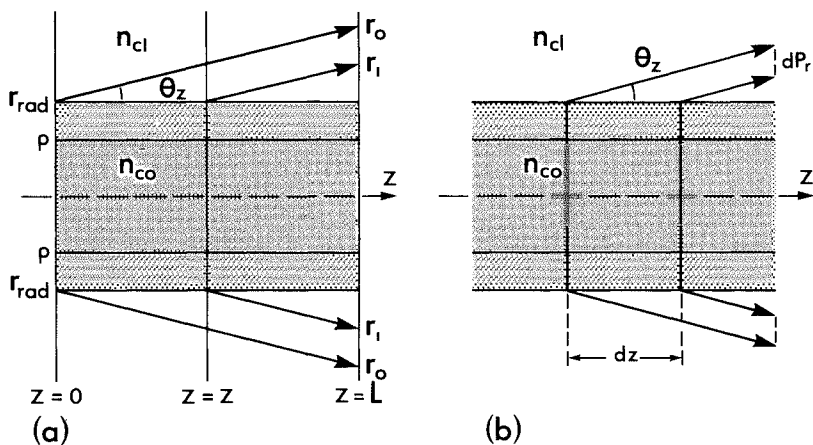


Fig. 24-2 (a) Intuitive description of power flow on a fiber when a leaky mode is excited at $z = 0$ and (b) a differential section of length dz of a step-profile fiber, showing the element of leaky-mode power dP_r lost to radiation.

asymptotic field expression of Eq. (24-8). If we fix z and allow r to increase, then, according to Eq. (24-5), there is an increase in field amplitude varying as $(1/R^{1/2}) \exp(|Q^i|R)$.

24-12 Guided and radiated power

The power flow in Fig. 24-2(a) is composed of two distinct parts: a guided portion which occupies the core and the evanescent region within radius r_{rad} , and a radiated portion propagating at angle θ_z , defined by Eq. (24-9), and occupying part of the region $r > r_{rad}$. If we define $P_g(z)$ to be the total guided power at position z , the Eqs. (11-21a) and (24-6) give

$$P_g(z) = \frac{|a|^2}{2} \exp(-2\beta^i z) \operatorname{Re} \left\{ \int_{A_{rad}} \mathbf{e} \times \mathbf{h}^* \cdot \hat{\mathbf{z}} dA \right\} \quad (24-14)$$

where a is the modal amplitude, Re denotes real part, A_{rad} is the cross-sectional area within $r = r_{rad}$, $*$ denotes complex conjugate and $\hat{\mathbf{z}}$ is the unit vector parallel to the fiber axis. Similarly, we define $P_r(z)$ to be the total radiated power flowing over the cross-sectional plane at position z . Hence

$$P_r(z) = \frac{|a|^2}{2} \exp(-2\beta^i z) \operatorname{Re} \left\{ \int_{A(z)} \mathbf{e} \times \mathbf{h}^* \cdot \hat{\mathbf{z}} dA \right\}, \quad (24-15)$$

where $A(z)$ is the annular area between r_{rad} and $r_0 = r_{rad} + z \tan \theta_z$.

It follows from these definitions that $P_r(z)$ accounts for all the guided power lost as radiation in distance z along the fiber. Initially, no guided power is

transferred to radiated power, but as $z \rightarrow \infty$ all guided power is transferred to radiated power. Hence

$$P = P_g(z) + P_r(z) = P_g(0) = P_r(\infty), \quad (24-16)$$

since the total leaky-mode power P is constant along the fiber. The initial guided power is determined by the source of excitation in Section 24-17.

Extrapolation of bound-mode power

The radiation and guided portions of leaky-mode power are presented as intuitive concepts, since the demarcation provided by r_{rad} is only meaningful for higher-order modes, and the definition of θ_z assumes the attenuation is small. Nevertheless, as $r_{\text{rad}} \rightarrow \infty$ and the attenuation becomes very small, we anticipate that $P_g(z)$ will have the same functional form as the power of a bound mode with W replaced by $-iQ$, apart from the factor $\exp(-2\beta^i z)$. In other words, just below cutoff the guided power of a leaky mode is the extrapolation of bound-mode power, as may be verified by evaluating Eq. (24-14) for a particular fiber and then taking the limit $\beta^i \rightarrow 0$.

Step-profile fiber

In the case of weakly guiding, step-profile fibers, the power of a bound mode is given by $P = |a|^2 N$, where the normalization is defined in Table 14-6, page 319. Setting $W = -iQ$ and applying the transformation of Eq. (37-71) yields

$$P_g(z) = \frac{\pi}{2} |a|^2 \rho^2 n_{\text{co}} \left(\frac{\epsilon_0}{\mu_0} \right)^{1/2} \frac{V^2}{U^2} \frac{H_{l+1}^{(1)}(Q) H_{l-1}^{(1)}(Q)}{\{H_l^{(1)}(Q)\}^2} \exp(-2\beta^i z), \quad (24-17)$$

where the \sim is omitted and $H_l^{(1)}$ is a Hankel function of the first kind. Since P_g is real, the right side is evaluated in the limit $Q \cong Q^r \rightarrow 0$, when, to lowest order, the Hankel functions are pure imaginary and $U \cong U^r$.

24-13 Fraction of guided power in the core

In Section 11-8 we defined η as the fraction of modal power propagating within the waveguide core. Although there is no formal definition of η for leaky modes, we can provide an intuitive expression by adopting the description of the previous section and setting

$$\eta = \frac{\text{power flow within the core}}{\text{power flow within the radiation caustic}} = \frac{\text{Re} \left\{ \int_{A_{\text{co}}} \mathbf{e} \times \mathbf{h}^* \cdot \hat{\mathbf{z}} \, dA \right\}}{\text{Re} \left\{ \int_{A_{\text{rad}}} \mathbf{e} \times \mathbf{h}^* \cdot \hat{\mathbf{z}} \, dA \right\}}, \quad (24-18)$$

where the notation is defined in Section 24-12.

Step-profile fiber

On the weakly guiding, step-profile fiber, the form of η immediately below cutoff is obtained from Table 14-6, page 319, by analogy with Eq. (24-17). Hence

$$\eta = \frac{U^2}{V^2} \left\{ \frac{[H_l^{(1)}(Q)]^2}{H_{l-1}^{(1)}(Q)H_{l+1}^{(1)}(Q)} - \frac{Q^2}{U^2} \right\}, \quad (24-19)$$

where the \sim is omitted from scalar quantities.

24-14 Power attenuation coefficient

Our intuitive description of a leaky mode in Section 24-12 ensures that total power is conserved as the mode propagates. This property emphasizes the idea that the power attenuation coefficient γ represents the rate of power loss from the guided portion of the fields to the radiation portion of the same fields, namely

$$P_g(z) = P_g(0)\exp(-\gamma z); \quad \gamma = 2\beta^i. \quad (24-20)$$

As the mode propagates, power originally confined to the guided portion spreads throughout an increasing domain to occupy the region $r_{\text{rad}} < r \leq r_0$ at $z = L$ in Fig. 24-2(a). This concept enables us to derive an expression for the power attenuation coefficient [13].

Step-profile fiber

For convenience and simplicity, we use the weakly guiding, step-profile fiber as an example. Consider a differential section of the fiber of length dz , as shown in Fig. 24-2(b). This section is sufficiently short that only a small $dP_r(z)$ is lost to radiation from the radiation caustic. The power attenuation coefficient then satisfies

$$dP_r(z) = \gamma P_g(z) dz, \quad (24-21)$$

where P_r and P_g are defined by Eqs. (24-15) and (24-14). To evaluate $dP_r(z)$, we note that the power leaving the surface $r = r_{\text{rad}}$ is contained between two conical surfaces making angle θ_z of Eq. (24-9) with the axis. If r' is the mean radius of these surfaces at position z , we deduce from Eqs. (11-20a) and (24-16) that

$$dP_r(z) = \pi |a|^2 \frac{r'}{\rho} \frac{Q^r}{\beta^r} \{ \text{Re}(\mathbf{e} \times \mathbf{h}^* \cdot \hat{\mathbf{z}})_{r=r'} \} \exp(-2\beta^i z) dz, \quad (24-22)$$

where a is the leaky-mode amplitude and the scalar product is evaluated at $r = r'$. It follows from Table 14-6, page 319, Eqs (24-11) and

(37-71) that

$$\operatorname{Re}(\mathbf{e} \times \mathbf{h}^* \cdot \hat{\mathbf{z}})_{r=r'} = \left(\frac{\epsilon_0}{\mu_0} \right)^{1/2} \frac{\beta^r}{k} |\mathbf{e}_t|^2 = \left(\frac{\epsilon_0}{\mu_0} \right)^{1/2} \frac{\beta^r}{k} \left| \frac{H_1^{(1)}(Qr'/\rho)}{H_1^{(1)}(Q)} \right|^2, \quad (24-23)$$

where $H_1^{(1)}$ is the Hankel function of the first kind. Since $dP_r(z)$ must be independent of r' , it is convenient to let $r' \rightarrow \infty$ and use the asymptotic form of Eq. (37-87) for $H_1^{(1)}(Qr'/\rho)$. Substituting Eqs. (24-17), (24-22) and (24-23) into Eq. (24-21), we finally obtain [13]

$$\gamma = \frac{4(\Delta)^{1/2}}{\pi} \frac{(U^r)^2}{\rho} \frac{1}{V^3 |H_{1-1}^{(1)}(Q^r) H_{1+1}^{(1)}(Q^r)|}, \quad (24-24)$$

where we have set $U \cong U^r$ and $Q \cong Q^r$. Later, in Section 24-18 we confirm that this result, based on an intuitive physical description of leaky modes, is consistent with the formal electromagnetic solution for small values of γ .

Comparison with leaky rays

The attenuation of leaky rays on multimode fibers is discussed in Section 7-1. For higher-order modes, it is intuitive that there should be good agreement between the leaky-mode and corresponding leaky-ray attenuation coefficients. We discuss this agreement both qualitatively and quantitatively in Section 36-11 for step-profile planar waveguides and fibers.

ORTHOGONALITY AND NORMALIZATION

The total fields of an optical waveguide are expressible as a summation over discrete bound and leaky modes, together with the space-wave fields. This representation is formally identical to the expansion of Eq. (11-2). If we consider only forward-propagating modes, then

$$\mathbf{E} = \sum_{j=1}^{M_{\text{bm}}} a_j \mathbf{e}_j \exp(i\beta_j z) + \sum_{k=1}^{M_{\text{lm}}} b_k \mathbf{e}_k \exp(i\beta_k^r z) \exp(-\beta_k^i z) + \mathbf{E}_{\text{sw}}, \quad (24-25a)$$

$$\mathbf{H} = \sum_{j=1}^{M_{\text{bm}}} a_j \mathbf{h}_j \exp(i\beta_j z) + \sum_{k=1}^{M_{\text{lm}}} b_k \mathbf{e}_k \exp(i\beta_k^r z) \exp(-\beta_k^i z) + \mathbf{H}_{\text{sw}}, \quad (24-25b)$$

where M_{bm} and M_{lm} are the numbers of bound and leaky modes, and $\mathbf{E}_{\text{sw}}, \mathbf{H}_{\text{sw}}$ denote the space-wave fields. To determine the modal amplitudes b_k of the leaky modes due to illumination of the endface of the waveguide, we require

orthogonality relationships between leaky modes, bound modes and the space wave, and an expression for the normalization of each leaky mode.

24–15 Orthogonality relations

The orthogonality relations of Section 11–4 for bound modes are invalid for leaky modes. This is evident from Eq. (24–8), which shows that the fields grow as $\exp(|Q^i|r/\rho)$ as $r \rightarrow \infty$. Such fields do not obey the orthogonality condition of Eq. (11–10) which involves integration over the infinite cross-section of the waveguide, since this requires that the fields vanish as $r \rightarrow \infty$. However, it is possible to construct an orthogonality condition by integrating in the complex r plane [20–22]. We assume r has a sufficiently large imaginary part to offset the exponential growth of the leaky mode with the largest value of Q^i . The contour in the complex r plane can be chosen so that bound and leaky modes are orthogonal to one another and to the space-wave fields. Consequently, the orthogonality condition for two leaky modes is functionally identical with Eq. (11–14), provided the infinite cross-section A_∞ is replaced by A'_∞ , where A'_∞ denotes the real cross-section of the waveguide for finite r and becomes complex as $r \rightarrow \infty$. Thus

$$\frac{1}{2} \int_{A'_\infty} \mathbf{e}_j \times \mathbf{h}_k \cdot \hat{\mathbf{z}} dA = \frac{1}{2} \int_{A'_\infty} \mathbf{e}_k \times \mathbf{h}_j \cdot \hat{\mathbf{z}} dA = 0; \quad j \neq k. \quad (24-26)$$

The leaky-mode fields have the same functional form as the bound-mode fields, but the modal parameters and propagation constants are complex.

We emphasize that leaky modes do not obey the power orthogonality of Eq. (11–13). This is because $\mathbf{e}_j \times \mathbf{h}_k^*$ is not an analytic function and thus cannot be continued into the complex plane as is necessary for the above generalization.

24–16 Normalization

It follows from the discussion in the previous section that the normalization N of each leaky mode is defined by

$$N = \frac{1}{2} \int_{A'_\infty} \mathbf{e} \times \mathbf{h} \cdot \hat{\mathbf{z}} dA, \quad (24-27)$$

where A'_∞ is the complex cross-section defined above and $\hat{\mathbf{z}}$ is the unit vector parallel to the waveguide axis. We emphasize that, for the implementation of the orthogonality relations and the determination of N , it is not necessary to know the details of A'_∞ . The important point is that A'_∞ ensures that all leaky-mode fields vanish infinitely far from the waveguide. Because $\mathbf{h}_l^* = \mathbf{h}_l$ for bound modes on nonabsorbing structures, as discussed in Section 11–3, N has

the same functional form for both leaky and bound modes. This can be found by integrating the leaky-mode fields over the infinite cross-section A'_∞ . Care must be exercised in evaluating N , since the arguments of \mathbf{e} and \mathbf{h} are complex.

Step-profile fiber

To illustrate the above point, consider a weakly guiding, step-profile fiber, whose leaky mode fields are given by Eq. (24-6) together with Tables 14-1, page 304, and 14-6, page 319. For example, within the core, the z -directed power density is

$$\mathbf{e} \times \mathbf{h} \cdot \hat{\mathbf{z}} = \left(\frac{\varepsilon_0}{\mu_0} \right)^{1/2} \frac{\beta}{k} \left\{ \frac{J_1(UR)}{J_1(U)} \right\}^2, \quad (24-28)$$

after using Eq. (24-11). For weakly leaky modes, $\beta \cong kn_{\text{co}}$, so that Eq. (24-28) has the same functional form as bound modes. Thus, N also has the same functional form as bound modes given by Table 14-6, with W replaced by $-iQ$. With the aid of Eq. (37-71), this leads to

$$N = \frac{\pi \rho^2 n_{\text{co}}}{2} \left(\frac{\varepsilon_0}{\mu_0} \right)^{1/2} \frac{V^2}{U^2} \frac{H_{l-1}^{(1)}(Q) H_{l+1}^{(1)}(Q)}{\{H_l^{(1)}(Q)\}^2}, \quad (24-29)$$

where $H^{(1)}$ is the Hankel function of the first kind, and the \sim is omitted.

Bound- and leaky-mode power

We emphasize that the definition of N given by Eq. (24-27) is formally correct for leaky modes of *arbitrary* attenuation. However, although the power of a bound mode on a nonabsorbing fiber is directly related to normalization in Eq. (11-22), there is no corresponding expression for the power of a leaky mode. The leaky-mode power P of Eq. (24-16) is an *intuitive* concept for understanding leaky modes. Only for weakly leaky modes can we express power in terms of normalization using Eq. (11-22). However, if we are only concerned with the power in the core, then Eq. (11-28) applies rigorously to both bound and leaky modes.

24-17 Excitation and perturbation problems

As we now have orthogonality relations and normalization expressions for leaky modes, results which were derived for bound modes in earlier chapters can simply be extended to apply to leaky modes. These include the perturbation expressions of Chapter 18, the modal amplitudes due to illumination in Chapter 20, and the excitation and scattering effects of current sources in Chapters 21 to 23. We give an example of leaky-mode excitation by a source in Section 24-23.

SOLUTION OF THE EIGENVALUE EQUATION

So far we have presented all the properties necessary for understanding the physical attributes of leaky modes, and for determining their excitation. All these properties, though, require a knowledge of the complex propagation constant β for each leaky mode. The solution of the eigenvalue equation for values of V below cutoff must, in general, be performed numerically. Only for weakly leaky modes when V is close to cutoff are analytical solutions available [13]. We now consider examples.

24-18 Example: Analytical solution for the step-profile fiber

The eigenvalue equation for bound modes of the weakly guiding, step-profile fibre is given in Table 14-6, page 319. We change parameter from W to $-iQ$, apply the transformation of Eq. (37-71) and omit the $-$ to obtain

$$U \frac{J_{l+1}(U)}{J_l(U)} = Q \frac{H_{l+1}^{(1)}(Q)}{H_l^{(1)}(Q)}; \quad Q^2 = U^2 - V^2, \quad (24-30)$$

where J_l and $H_l^{(1)}$ are Bessel and Hankel functions of the first kind, and U , Q are complex below cutoff $V = V_c$ for each mode, with the exception of the fundamental mode which is not cut off. Here we derive analytical approximations for the mode parameters just below cutoff, when U and Q are approximately real with small imaginary parts. These approximations also provide accurate starting values for the exact numerical solution in the following section.

Real parts of U and Q

The real part of U just below cutoff for all modes with $l \geq 1$ is given approximately by extrapolating the expression in Table 14-7 to $V \lesssim V_c$, whence the real part of Q follows from Eq. (24-30) as $Q^r \cong (\{U^r\}^2 - V^2)^{1/2}$. Such an extrapolation is less useful for higher-order $\text{HE}_{1,m}$ modes ($l = 0, m > 1$) since there is a discontinuity in U at the cutoff of each mode, as we show in the next section.

Imaginary parts of U and Q

The components U^i and Q^i of the mode parameters can be found from a perturbation solution of the eigenvalue equation. We define a function G by

$$G(U) = U \frac{J_{l+1}(U)}{J_l(U)} - Q \frac{H_{l+1}^{(1)}(Q)}{H_l^{(1)}(Q)}, \quad (24-31)$$

where $U = U^r + iU^i$. Just below cutoff, U^i is small compared to U^r , so we make a Taylor expansion of G about U^r and retain terms correct to first order only. Since U is a

solution of Eq. (24-30), we obtain, on rearrangement,

$$U^i = iG(U^r) \left/ \frac{dG}{dU} \right|_{U=U^r}. \quad (24-32)$$

We differentiate Eq. (24-31) with respect to U and apply the recurrence relations of Eq. (37-72). Using Eq. (24-30) to express the Bessel functions in terms of the Hankel functions leads to

$$\frac{dG}{dU} \bigg|_{U=U^r} = \frac{V^2}{U^r} \frac{H_{l-1}^{(1)}(Q^r) H_{l+1}^{(1)}(Q^r)}{\{H_l^{(1)}(Q^r)\}^2}; \quad Q^r = \{(U^r)^2 - V^2\}^{1/2}. \quad (24-33)$$

Close to cutoff, Q^r is small and the Hankel functions are dominated by their imaginary components. Thus the derivative is virtually real, and, since U^i is real by definition, we require the imaginary component $\text{Im}\{G(U^r)\}$ of Eq. (24-31). The latter involves only Hankel functions and, by setting $H_l^{(1)} = J_l + iY_l$, where Y_l is the Bessel function of the second kind, we find, with the aid of the Wronskian of Eq. (37-76b), that

$$\text{Im}\{G(U^r)\} = (2/\pi)(1/|H_l^{(1)}(Q^r)|^2). \quad (24-34)$$

Within the accuracy of the perturbation solution, we substitute Eq. (24-34) and the modulus of Eq. (24-33) into Eq. (24-32) to obtain [13]

$$U^i = -\frac{2}{\pi} \frac{U^r}{V^2} \frac{1}{|H_{l-1}^{(1)}(Q^r) H_{l+1}^{(1)}(Q^r)|}; \quad Q^i = U^i \frac{U^r}{Q^r}, \quad (24-35)$$

where Q^i follows from Eq. (24-30).

Power attenuation coefficient

To obtain the power attenuation coefficient, we equate the imaginary components in the definition of U inside the back cover, i.e. $U^i U^r = -\rho^2 \beta^i \beta^r$. On the weakly guiding fiber, $\beta^r \cong kn_{\text{co}} = V/\rho(2\Delta)^{1/2}$ just below cutoff, whence we deduce from Eqs. (24-20) and (24-35) that

$$\gamma = 2\beta^i = \frac{4}{\pi} \frac{(2\Delta)^{1/2}}{\rho} \frac{(U^r)^2}{V^3} \frac{1}{|H_{l-1}^{(1)}(Q^r) H_{l+1}^{(1)}(Q^r)|}, \quad (24-36)$$

which is identical to Eq. (24-24) which was derived from intuitive power conservation arguments. Very close to cutoff, the asymptotic forms of the Hankel function for small argument in Eqs. (37-83) and (37-84) lead to the simpler forms

$$U^i \cong -\pi(U^r - V), \quad l = 0; \quad U^i = -\pi(V_c - V)/|\ln 2V(V_c - V)|, \quad l = 1, \quad (24-37a)$$

$$U^i \cong -\frac{2\pi}{V} \frac{1}{l!(l-2)!} \left\{ \frac{l-1}{2l} V_c(V_c - V) \right\}^l, \quad l \geq 2; \quad \gamma \cong -\frac{2(2\Delta)^{1/2}}{\rho} \frac{U^i}{V}, \quad (24-37b)$$

using $U^r \cong U$ in the expression for in Table 14-7, page 324, and noting that $U^r \cong V \cong V_c$ in these approximations.

24-19 Example: Numerical solution for the step-profile fiber

The exact numerical solution of Eq. (24-30) for the real and imaginary parts of U and Q is facilitated by using Table 14-7, page 324, and Eq. (24-37) as initial estimates for values of U immediately below cutoff. As V decreases, the solution can then be found by using a Newton-Raphson iteration, which makes a Taylor expansion of G of Eq. (24-31) about a known zero and then truncates the expansion after two terms [21]. Using this method, U^r and $-U^i$ are plotted against V in Fig. 24-3(a) for the $\text{HE}_{l+1,1}$ and $\text{EH}_{l-1,1}$ modes for $l = 1, 2, \dots, 6$. The fundamental HE_{11} mode ($l = 0$), which is not cut off, is included for comparison. Bound-mode solutions correspond to the solid curves above cutoff. The dashed curves originating at cutoff $V = V_c$ for each mode denote the tunneling leaky-mode solution for U^r and U^i , when the radiation caustic is at a finite distance from the interface. The solid continuation of each curve denotes the refracting leaky-mode solution, when the radiation caustic coincides with the interface. We are reminded that this delineation is somewhat artificial for low-order modes, as the position of the radiation caustic is not well defined.

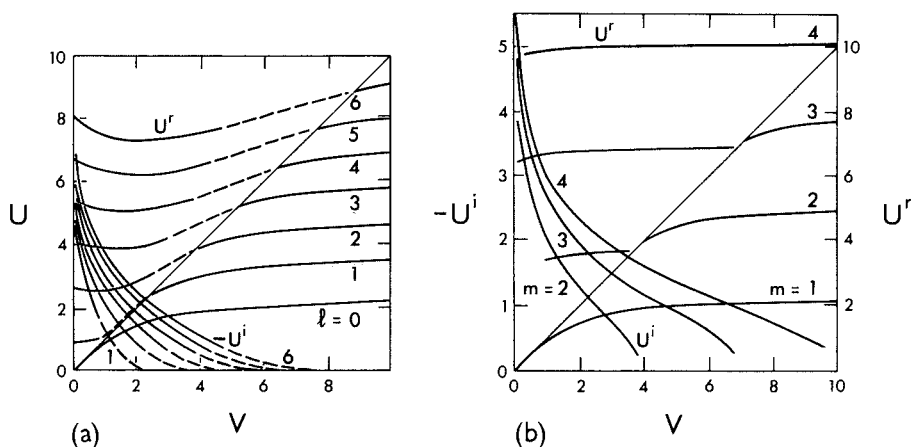


Fig. 24-3 Plots of U^r and $-U^i$ against V for (a) the $\text{HE}_{l+1,1}$ and $\text{EH}_{l-1,1}$ modes, $l = 1, \dots, 6$, and (b) the HE_{1m} modes, $m = 2, 3, 4$, of a weakly guiding step-profile fiber [21]. The thin diagonal line denotes cutoff $U^r = V$.

The second set of curves, in Fig. 24-3(b), give U^r and $-U^i$ for the HE_{1m} modes ($l = 0$) with $m = 2, 3$ and 4, including the fundamental mode ($m = 1$) for comparison. Below cutoff each mode becomes a refracting leaky mode; there is no tunneling leaky-mode region as in Fig. 24-3(a). These curves exhibit a feature that is peculiar to the HE_{1m} modes; immediately below cutoff, there is no leaky mode solution of the eigenvalue equation [19], as indicated by the breaks in the curves for U^r . This discontinuity is associated with the discontinuity in r_{rad} for these modes, which changes from $r_{\text{rad}} = \infty$

for bound modes immediately above cutoff to $r_{\text{rad}} = \rho$ immediately below cutoff for refracting leaky modes.

Attenuation coefficient

The leaky mode eigenvalue equation of Eq. (24-30) and its solutions U^r , U^i are independent of Δ , but the corresponding attenuation coefficient is very sensitive to the value of Δ . If we equate real and imaginary components of U^2 using the definition at the back of the book, eliminate β^r and substitute the solution of the resulting quadratic equation for $(\beta^i)^2$ into Eq. (24-20), then

$$\gamma = \frac{\sqrt{2}}{\rho} \left\{ \left[\left\{ \frac{V^2}{2\Delta} - (U^r)^2 + (U^i)^2 \right\}^2 + 4(U^r U^i)^2 \right]^{1/2} - \frac{V^2}{2\Delta} + (U^r)^2 - (U^i)^2 \right\}^{1/2}. \quad (24-38)$$

It is readily verified that $\gamma \rightarrow 0$ as $\Delta \rightarrow 0$. Plots of the normalized attenuation coefficient $\gamma\rho$ corresponding to the values of U^i in Fig. 24-3 are given in Fig. 24-4 for a fiber with $\Delta = 0.005$. Each curve shows how a leaky mode can have an arbitrarily small attenuation coefficient if V is sufficiently close to cutoff. Such a leaky mode can propagate for considerable distances, giving rise to a prolonged spatial transient. In the case of the refracting leaky modes which correspond to the solid curves in Fig. 24-4(a), even the smallest attenuation coefficient has a relatively high value, so that these modes rapidly disappear along the fiber. For a given value of V , attenuation increases as l increases.

These properties of leaky-mode attenuation coefficients are consistent with the attenuation of the family of leaky rays in Chapter 7, which comprise the mode. This is discussed in Section 36-11.

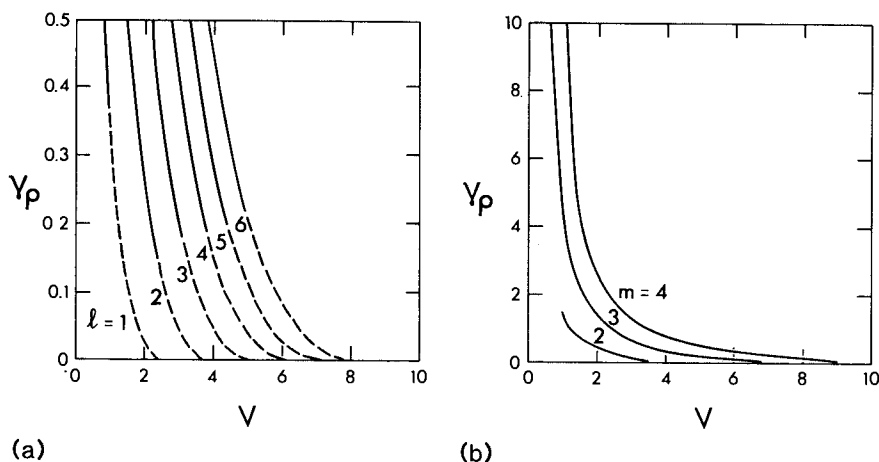


Fig. 24-4 The normalized power attenuation coefficient, $\gamma\rho$, plotted against V for the modes of Fig. 24-3, assuming $\Delta = 0.005$ in Eq. (24-38) [21].

Fraction of power in the core

The fraction of leaky-mode power propagating within the fiber core is given by Eq. (24-19). Using this definition and taking the real part of the quotient of Hankel functions, we plot η as a function of V in Fig. 24-5 for the modes of Fig. 24-3(a). The solid curves denote bound modes and the dashed curves denote tunneling leaky modes. All refracting leaky modes have $\eta = 1$ since $r_{\text{rad}} = \rho$ and $A_{\text{rad}} = A_{\text{co}}$.

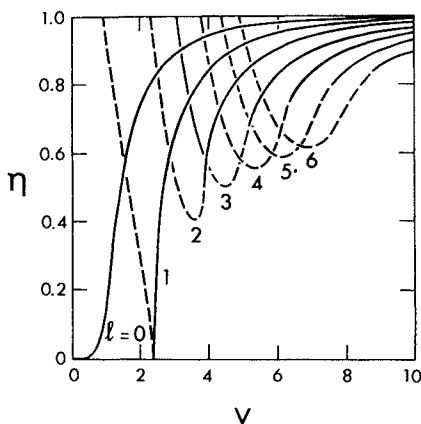


Fig. 24-5 The fraction of power within the core plotted against V for the modes of Fig. 24-3(a) [21].

Accuracy of the weak-guidance approximation

The accuracy of the leaky-mode solutions presented above for the weakly guiding fiber, can be determined by comparing them with the corresponding solutions for the step-profile fiber of arbitrary core and cladding indices, using the exact eigenvalue equations of Table 12-4, page 253, below cutoff [21]. We find that the values of U^r and U^i do not differ significantly from the exact solution as Δ varies, provided $\Delta \lesssim 0.01$ and the mode is not too far below cutoff.

24-20 Example: Step-profile planar waveguide

The eigenvalue equations for leaky TE and TM modes on the step-profile planar waveguide in the weak-guidance approximation are obtained by setting $W = -iQ$ in the TE mode eigenvalue equations of Table 12-2, page 243. Hence

$$Q = iU \tan U, \quad \text{even modes;} \quad Q = -iU \cot U, \quad \text{odd modes,} \quad (24-39)$$

where parameters are defined inside the back cover. The solution of these equations is

found by numerical methods similar to those of the previous section. Plots of U^r and $-U^i$ against V for the first five modes—including the fundamental, or first even, mode—are shown in Fig. 24-6(a), where the solid curves above cutoff correspond to bound modes. Immediately below cutoff, there is no leaky-mode solution in a region extending from $V = V_c$ down to the kink, or discontinuity in slope of the curve. Within this region W is pure real and negative, and hence the modal fields grow exponentially in the cladding with increasing distance from the waveguide axis, as is clear from Table 12-1, page 243. These solutions are neither leaky- nor bound-mode solutions, and have no role in the representation of the total fields in Eq. (24-1). For the first odd mode, the region extends from $V = V_c$ to $V = 0$. The remaining modes become refracting leaky modes as V is further reduced.

In Fig. 24-6(b), we plot the normalized attenuation coefficient $\gamma\rho$ of Eq. (24-38) for the modes of Fig. 24-6(a) on a waveguide with $\Delta = 0.005$. It is clear that attenuation can be arbitrarily small by an appropriate choice of V for a particular mode, leading to a prolonged spatial transient.

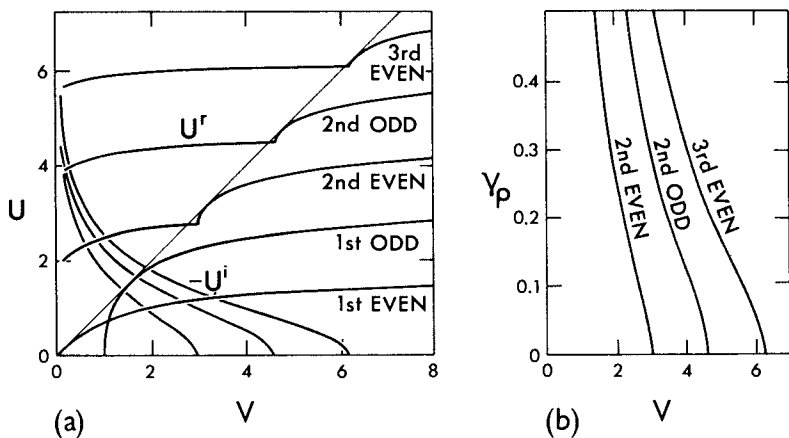


Fig. 24-6 (a) Plots of U^r and $-U^i$ against V for the even and odd TE and TM modes of a weakly guiding, step-profile, planar waveguide and (b) the corresponding normalized power attenuation coefficient, assuming $\Delta = 0.005$. The thin diagonal line denotes cutoff $U^r = V$.

APPLICATIONS OF LEAKY MODES

In the remainder of the chapter, we show by examples, how leaky modes can be used to determine both the qualitative and quantitative behavior of the radiation fields of fibers.

24-21 Example: Far-field radiation pattern

We showed in Sections 21-8 and 21-11 that when the fiber profile is included the far-field radiation pattern due to sources within a weakly guiding fiber can be described by a correction factor to the 'free-space' pattern. The correction factor is, in turn, expressible as a product of two factors, $C_d(\theta)$ and $C_r(\theta)$, as we showed for the step-profile fiber in Section 21-13. By examining the definitions in Eqs. (21-38) and (21-36b), we find that $C_r(\theta)$ is inversely proportional to $G(U)$ of Eq. (24-31), provided U and Q are defined in terms of θ by Eq. (21-37). Consequently, as θ varies, the peak values of $|C_r(\theta)|$ occur at the minima of $|G(U)|$. Now $G(U)$ vanishes only at a leaky-mode solution of the eigenvalue equation of Eq. (24-30); in these cases U is not real. Since Eq. (21-37) requires U to be real, we deduce that $|G(U)|$ has small but finite minima when U is approximately equal to the real part of the leaky-mode solution. Thus the peaks in $|C_r(\theta)|$ correspond to the finite minima of $|G(U)|$ and, therefore, to the excitation of leaky modes, i.e. to resonances in the fiber cross-section, as illustrated in Fig. 21-6(a).

Dipole radiation

To give a simple example, consider the z -directed current dipole of Section 21-9 when located on the axis of a step-profile fiber. The angular dependence of the 'free-space' radiation pattern of Eq. (21-24b) is proportional to $\sin^2 \theta$, where θ is the angle between the field point and the fiber axis. In this situation, we set $r_0 = 0$ and thus $C_d(\theta) = 1$ in Eq. (21-39), whence the radiation pattern in the presence of the fiber varies as

$$|C_r(\theta)|^2 \sin^2 \theta. \quad (24-40)$$

The qualitative plots in Fig. 24-7 show the 'free-space' pattern as the dashed curve and Eq. (24-40) as the solid curve. Assuming the fiber is single moded, the peaks correspond

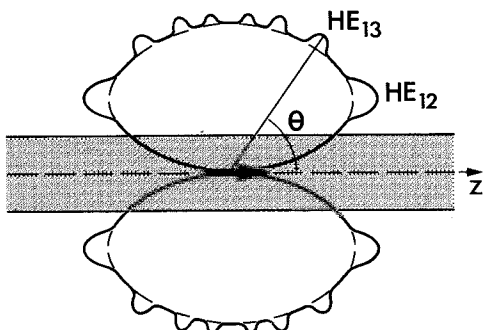


Fig. 24-7 Peaks in the far-field radiation pattern of a current dipole on the axis of a step-profile fiber correspond to leaky-mode resonances. The dashed curve is the 'free-space' pattern.

to excitation of the $\text{HE}_{12}, \text{HE}_{13}, \dots$ leaky modes as θ increases. The symmetry of the problem ensures that only HE_{1m} modes are excited. Furthermore, it is clear from Eq. (21-37) and the definition of Q at the back of the book that the angle θ subtended by each peak coincides with the leaky-mode angle θ_z of Eq. (24-9), which gives the direction of radiated power flow in the cladding. Consequently, we have a simple way of determining the directions of radiation peaks in the far field from a knowledge of the leaky-mode propagation constants. However, these peaks need to be distinguished from peaks arising in the 'free-space' radiation pattern in more complicated situations.

Close to and within the core, the radiation fields are composed of both leaky modes and a space wave, as expressed by Eq. (24-1). Thus, only when the source excites mainly leaky modes is the radiation field given approximately by the leaky-mode fields. This is the case at each peak in Fig. 24-7. We next consider a source which is efficient in exciting individual leaky modes.

24-22 Example: Sinusoidal line source

Consider a weakly guiding, step-profile fiber which contains a sinusoidal line source of length $2L$ on its axis, directed parallel with the x -axis in the fiber cross-section. The magnitude J_x of the distribution is assumed to be given by the tubular source of Eqs. (21-13) and (21-14) with $l = 0$ and $r_0 \rightarrow 0$. Hence

$$J_x = \{\delta(r - r_0)/2\pi r_0\} \exp(iCz) \sin(\Omega z); \quad -L \leq z \leq L, \quad (24-41)$$

where the notation is defined in Section 21-6. By symmetry, only the even, or x -polarized HE_{1m} modes are excited. The amplitude $a_j(z)$ of each leaky mode is given by Eqs. (31-35) and (31-36) with the infinite cross-section A_∞ replaced by the complex cross-section A'_∞ of Section 24-15 and the normalization calculated in the manner described in Section 24-16. Thus the forward-propagating mode amplitudes in the region $-L \leq x \leq L$ are given by

$$a_j(z) = -\frac{1}{4N_j} \int_{-L}^z \int_{A'_\infty} e_{xj}^* J_x \exp(-i\beta_j^i z) \exp(\beta_j^i z) dA dz, \quad (24-42)$$

where e_{xj} and $\beta = \beta_j^i + i\beta_j^r$ are scalar quantities associated with the eigenvalue equation of Eq. (24-30). If we substitute for J_x from Eq. (24-41) and assume that L is sufficiently large, then, by analogy with Eq. (21-16), strong excitation of the j th forward-propagating leaky mode occurs when the propagation constant satisfies

$$\Omega \cong |\beta_j^r - C|; \quad \beta_j^r \gg \beta_j^i. \quad (24-43)$$

In which case, we deduce, by analogy with Eq. (21-15), that

$$a_j(z) = \frac{i}{8} \frac{e_{xj}^*(0)}{N_j} \frac{\exp(\beta_j^i z) - \exp(-\beta_j^i L)}{\beta_j^i}; \quad -L \leq z \leq L, \quad (24-44)$$

where $e_{xj}(0)$ is evaluated on the axis. The corresponding leaky-mode fields follow from Eqs. (24-6) and (24-11) as

$$E_{xj} = \frac{i}{8} \frac{e_{xj}^*(0)}{N_j} \frac{1 - \exp\{-\beta_j^i(z+L)\}}{\beta_j^i} e_{xj} \exp(i\beta_j^r z); \quad H_{yj} = \frac{\beta_j}{k} \left(\frac{\epsilon_0}{\mu_0} \right)^{1/2} E_{xj}. \quad (24-45)$$

If we let $L \rightarrow \infty$, the field amplitudes $|E_x|$ and $|H_y|$ are effectively independent of z provided $z \gg 1/\beta_j^i$. This steady state solution occurs when the power flow into the leaky mode from the current source is exactly equal to the power flow from the leaky mode into the radiation field. The steady state amplitude, though, depends on the strength of the source. We are reminded from Section 24-16 that there is no expression for leaky-mode power in terms of the modal amplitude corresponding to the bound-mode expression of Eq. (11-22).

24-23 Example: On-axis sinusoidal nonuniformity

In Section 22-5 we determined the attenuation of the fundamental mode on a weakly guiding, step-profile fiber due to radiation from a sinusoidal perturbation of the interface, using 'free-space' antenna methods and correction factors. Here we consider the situation when the radiation field is well approximated by a single leaky mode, which can be realized by having an on-axis sinusoidal nonuniformity of the form of Eq. (22-14). The azimuthal symmetry ensures that only HE_{1m} leaky modes are excited. Further, the direction of radiation should coincide with the direction of the leaky-mode radiation [23]. If we represent the nonuniformity and the incident fundamental-mode fields by the induced current method, as in Section 22-5, the direction condition is satisfied by setting $C = \beta_1$ in Eq. (24-43), whence

$$\Omega \cong |\beta_j^i - \beta_1|; \quad \beta_j^i \gg \beta_1, \quad (24-46)$$

where subscript 1 denotes the fundamental mode. By analogy with Eq. (22-15), the induced current is x-directed, and has the value

$$J_{x1} = -i\delta\rho \left(\frac{\epsilon_0}{\mu_0} \right)^{1/2} \frac{(2\Delta)^{1/2}}{n_{co}} \frac{V}{J_0(U_1)} \frac{\bar{\delta}(r-r_0)}{r_0} \exp(i\beta_1 z) \sin(\Omega z), \quad (24-47)$$

since $F_0(0) = 1/J_0(U_1)$. For convenience we assume unit initial mode amplitude, and the limit $r_0 \rightarrow 0$ is implied. Following the analysis of the previous section, the leaky-mode amplitude is given by Eq. (24-44) normalized by the ratio of the right side of Eq. (24-47) to that of Eq. (24-41). Hence

$$a_j(z) = C_{1j} \frac{\exp(\beta_j^i z) - \exp(-\beta_j^i L)}{\beta_j^i}; \quad C_{1j} = \delta\rho \frac{\pi}{4} \frac{n_{co}}{N_j} \left(\frac{\epsilon_0}{\mu_0} \right)^{1/2} \frac{(2\Delta)^{1/2}}{J_0(U_j^*)} \frac{V}{J_0(U_1)}, \quad (24-48)$$

where N_j is the leaky-mode normalization of Section 24-16, $e_{xj}(0)$ is given in Table 14-3, page 313, and $-L \leq z \leq L$.

Attenuation of fundamental-mode power

We cannot determine directly radiation from the fundamental mode using Eq. (24-48), as there is no general definition of leaky-mode power in terms of $a_j(z)$. However, we can

use the known leaky-mode amplitude to calculate the change in the fundamental-mode amplitude, $a_1(z)$, from its initial value $a_1(0) = 1$, and hence the corresponding power attenuation. We regard the leaky-mode field, together with the nonuniformity, as an induced current, J_{xj} , on the uniform fiber. By analogy with Eq. (24-47), we deduce that

$$J_{xj} = -i\delta\rho\left(\frac{\varepsilon_0}{\mu_0}\right)^{1/2} \frac{(2\Delta)^{1/2}}{n_{co}} \frac{V}{J_0(U_j)} \frac{\bar{\delta}(r-r_0)}{r_0} a_j(z) \exp(i\beta_j^r z - \beta_j^i z) \sin(\Omega z). \quad (24-49)$$

We differentiate Eq. (24-42) with respect to z , interchange the subscripts 1 and j , and substitute the above expression for J_{xj} . The expressions e_{x1} and N_1 for the fundamental mode are given in Table 14-3, page 313, and the integral follows from Table 14-6, page 319. This leads to

$$\frac{da_1(z)}{dz} = -2iC_{j1} a_j(z) \exp\{i(\beta_j - \beta_1)z\} \sin(\Omega z), \quad (24-50)$$

where C_{j1} is given by Eq. (24-48) with subscripts reversed. We deduce from Eqs. (11-22) and (24-49) that the power $P_1(z)$ in the fundamental mode satisfies

$$\frac{dP_1(z)}{dz} = N_1 \frac{d}{dz} \{a_1(z) a_1^*(z)\} \cong 4N_1 \sin(\Omega z) \operatorname{Im}[C_{j1} a_j(z) \exp\{i(\beta_j - \beta_1)z\}], \quad (24-51)$$

since $a_1(z) \cong 1$. Substituting from Eq. (24-48) and rearranging gives

$$\begin{aligned} \frac{dP_1(z)}{dz} = 2N_1 \frac{1 - \exp\{(-z+L)\beta_j^i\}}{\beta_j^i} \operatorname{Re}[C_{1j} C_{j1} \{ \exp[i(\beta_j^r - \Omega - \beta_1)z] \\ - \exp(i[\beta_j^r + \Omega - \beta_1]z) \}], \end{aligned} \quad (24-52)$$

where Re denotes real part. We assume the nonuniformity is sufficiently long that the exponential dependence on L can be ignored, i.e. $2L \gg 1/\beta_j^i$. The resonance condition of Eq. (24-46) shows that the first term inside the curly brackets reduces to unity and the second term represents an oscillation at twice the ripple frequency. Since $L \gg \pi/\Omega$, we average the right side of Eq. (24-51) over a period and obtain

$$\gamma = \frac{dP_1(z)}{dz} \cong \frac{2}{\beta_j^i} \operatorname{Re}[C_{1j} C_{j1}]$$

(24-53)

for the fundamental-mode power attenuation coefficient.

Equivalence with antenna methods and the correction factor

When the j th leaky mode is just below its cutoff value $V = V_c$, the attenuation coefficient of Eq. (24-53) agrees with the corresponding expression derived by the 'free-space' approximation and correction factor for the fiber profile. For the on-axis source, it is clear by setting $r_0 = 0$ in Eqs. (22-15) and (21-38) that the attenuation coefficient is

given by analogy with Eq. (22-20) as

$$\gamma = \frac{\pi}{8\rho} \left(\frac{\delta\rho}{\rho} \right)^2 \frac{VW_1^2(2\Delta)^{1/2}}{J_1^2(U_1)} (1 + \cos^2 \theta_z) \left| \frac{W_0(Q_j^i, Q_j^i)}{W_0(U_j^i, Q_j^i)} \right|, \quad (24-54)$$

in terms of the fundamental- and leaky-mode parameters used above. We substitute for $W_0(Q_j^i, Q_j^i)$ from Eq. (22-17b) and deduce from Eq. (24-9) that $\cos \theta_z \cong 1$ since $\beta_j^i \cong kn_{cl}$ just below cutoff. It is clear from Eqs. (22-17b) and (24-31) that $W_0(U_j^i, Q_j^i)$ is proportional to $G(U_j^i)$, which is evaluated from Eq. (24-32) and (24-33). Hence

$$\gamma = \frac{1}{\pi\rho} \left(\frac{\delta\rho}{\rho} \right)^2 \frac{(2\Delta)^{1/2}}{V^3} \left\{ \frac{W_1}{U_j^i} \frac{U_j^i}{J_1(U_1)J_0(U_j^i)} \frac{|H_0^{(1)}(Q_j^i)|}{|H_1^{(1)}(Q_j^i)|^2} \right\}. \quad (24-55)$$

One factor of $1/U_j^i$ is expressed through Eq. (24-35) and the other factor through the relationship $U_j^i U_j^i = -\rho^2 \beta_j^i \beta_j^i \cong -k\rho^2 n_{cl} \beta_j^i = -\rho V \beta_j^i / (2\Delta)^{1/2}$. We approximate U and Q by U_j^i and Q_j^i , respectively, in the eigenvalue equation of Eq. (24-30), i.e. $G(U_j^i) \cong 0$ in Eq. (24-31). Thus Eq. (24-55) reduces to

$$\gamma = \frac{\Delta}{\rho^2 \beta_j^i} \left\{ \frac{\delta\rho}{\rho} \frac{W_1}{V} \frac{Q_j^i}{J_1(U_1)J_1(U_j^i)} \right\}^2. \quad (24-56)$$

In Eq. (24-53), we substitute for C_{1j} and C_{j1} from Eq. (24-48) with $U_j^* \cong U_j^i$. The normalization N_j is given by Eq. (24-29) and N_1 follows from Table 14-3, page 313. Using the condition $G(U_j^i) \cong 0$ to express the Hankel functions in terms of Bessel functions leads to Eq. (24-56). We are reminded that this equivalence holds only for the leaky-mode radiation direction of Eq. (24-9).

REFERENCES

1. Snyder A. W. and Menzel R. (eds) (1975) *Photoreceptor Optics*, Springer-Verlag, Berlin.
2. Snyder, A. W. (1978) *Handbook of Sensory Physiology*, Vol. VII/6A (ed. H. Autrum), Springer-Verlag, Berlin, pp. 279-81.
3. Snitzer, E. (1961) in *Advances in Quantum Electronics*, Columbia University Press, New York, p. 360.
4. Stewart, W. J. (1975) *Proceedings of the First European Conference on Optical Communication*, London.
5. Collin, R. E. (1960) *Field Theory of Guided Waves*, McGraw-Hill, New York, chap. 11.
6. Collin, R. E. and Zucher, F. J. (eds) (1969) *Antenna Theory*, Part II, McGraw-Hill, New York.
7. Kapany, N. S. and Burke, J. J. (1972) *Optical Waveguides*, Academic Press, New York.
8. Felsen, L. B. and Marcuvitz, N. (1973) *Radiation and Scattering of Waves*, McGraw-Hill, New York.
9. Tamir, T. (1973) Inhomogeneous wave types at planar structures. III. Leaky waves. *Optik*, **38**, 269-97.

10. Snyder, A. W. and Mitchell, D. J. (1973) Leaky rays cause failure of geometric optics on optical fibres. *Electron. Lett.*, **9**, 437–8.
11. Snyder, A. W. and Mitchell, D. J. (1974) Leaky rays on circular optical fibers *J. Opt. Soc. Am.*, **69**, 599–607.
12. Snyder, A. W., Mitchell, D. J. and Pask, C. (1974) Failure of geometric optics for analysis of circular optical fibers. *J. Opt. Soc. Am.*, **64**, 608–14.
13. Snyder, A. W. and Mitchell, D. J. (1974) Leaky mode analysis of circular optical waveguides. *Opto-electronics*, **6**, 287–96.
14. Snyder, A. W. (1974) Leaky-ray theory of optical waveguides of circular cross section. *Appl. Phys.* **4**, 273–98.
15. Snyder, A. W. and Love, J. D. (1974) Tunnelling leaky modes on optical waveguides. *Opt. Commun.*, **12**, 326–8.
16. Snyder, A. W. and Pask, C. (1975) Optical fibre: spatial transient and spatial steady state. *Opt. Commun.*, **15**, 314–16.
17. Adams, M. J., Payne, D. N. and Sladen, F. M. E. (1975) Leaky rays on optical fibres of arbitrary (circularly symmetric) index profiles. *Electron. Lett.*, **11**, 328–40.
18. Stewart, W. J. (1975) Leaky modes on graded fibres. *Electron. Lett.*, **11**, 321–2.
19. Sammut, R. and Snyder A. W. (1976) Leaky modes on a dielectric waveguide-orthogonality and excitation. *Appl. Opt.*, **15**, 1040–4.
20. Shevchenko, V. V. (1974) The expansion of the fields in open waveguides in proper and improper modes. *Radio Phys. Quantum Electron.*, **14**, 972–7.
21. Sammut, R. and Snyder, A. W. (1975) Leaky modes on circular optical waveguides. *Appl. Opt.*, **15**, 477–82.
22. Marcuse, D. (1974) *Theory of Dielectric Optical Waveguides*, Academic Press, New York.
23. Sammut, R. A. and Snyder, A. W. (1979) Radiation from optical waveguides: leaky mode interpretation. *Electron. Lett.*, **15**, 58–9.

Radiation modes

General properties	515
25-1 Representation of the modal fields	515
25-2 Propagation constant	516
25-3 Radiation-field expansion	517
25-4 Orthogonality and normalization	517
25-5 Power of the radiation field	518
25-6 Excitation of radiation modes	519
'Free-space' radiation modes	520
25-7 <i>Example: Solution in cylindrical polar coordinates</i>	521
Construction of the radiation modes	523
25-8 <i>Example: Step-profile fiber</i>	524
Weakly guiding waveguides	526
25-9 Spatial dependence of the fields	526
25-10 Vector direction of the radiation-mode fields	526
25-11 <i>Example: Step-profile fiber</i>	528
Radiation from sources in 'free space'	530
25-12 <i>Example: Dipole radiation</i>	530
25-13 <i>Example: Tubular-source radiation</i>	531
Radiation from sources within fibers	532
25-14 <i>Example: Dipole within a step-profile fiber</i>	532
25-15 <i>Example: Tubular source within a step-profile fiber</i>	533
25-16 Effect of a finite cladding	533
References	533

The total electromagnetic fields of an optical waveguide can be expressed as the sum of two components. One component, expressible as a summation over bound modes, describes the spatial steady state, where energy is guided indefinitely along a nonabsorbing waveguide. The second component is the radiation field, which describes the spatial transient. In Chapter 24 we

discussed leaky modes which describe a *portion* of the total radiation field, in particular the portion far from the source and sufficiently close to or within the fiber core. Thus, taken on their own, leaky modes are often sufficient for describing the radiation field for many situations of practical interest. The remaining portion of the radiation field is included in the space wave, as indicated in Eq. (24-1). At positions far from the source, this contribution is conveniently determined by the methods of the following chapter. In general, however, it is easier to calculate the total radiation field directly, particularly in situations where the leaky-mode power is only a small fraction of the total radiated power within the fiber core.

There are two general methods for solving Maxwell's equations for the total radiation field. The Green's function method, described in Chapter 34, was applied in Chapters 21 and 23 to finding the far field and calculating radiated power. The second method uses a modal, or eigenfunction, approach, which describes the radiation fields in terms of *radiation modes*, in a manner analogous to the bound-mode description of the guided fields. Both methods have their inherent advantages, and the choice depends on the particular problem. Whilst the modal approach determines the radiation fields *everywhere* in the waveguide, the Green's function method is often better suited for determining the far-field radiation.

This chapter shows how radiation modes are used to construct the *total* radiation fields. We first establish the general properties of radiation modes on arbitrary waveguides and then parallel Chapter 13 with a discussion of radiation modes on weakly guiding waveguides. Finally, we give examples of the application of radiation modes to complement the Green's function solutions given in earlier chapters.

GENERAL PROPERTIES

Radiation modes, like bound modes, obey nearly all of the general properties presented in Chapter 11. As we show below, the essential difference between bound and radiation modes is that there is no eigenvalue equation for radiation modes because of the relaxation of the boundary condition that the fields are evanescent as $r \rightarrow \infty$. Furthermore, at large distances from the waveguide, their fields are oscillatory, or wavelike, and do not have the evanescent behavior of the bound-mode fields [1, 2].

25-1 Representation of the modal fields

The electric field \mathbf{E}_j and magnetic field \mathbf{H}_j of an individual radiation mode are solutions to Maxwell's equations in the absence of sources. Because of the

cylindrical symmetry, or translational invariance, of the waveguide, they have the same representation as Eq. (11-6) for bound modes, except that the propagation constant β no longer has a discrete value. Hence

$$\mathbf{E}_j(x, y, z) = \mathbf{e}_j(x, y) \exp(i\beta z) = \{\mathbf{e}_{tj}(x, y) + e_{zj}(x, y)\hat{\mathbf{z}}\} \exp(i\beta z), \quad (25-1a)$$

$$\mathbf{H}_j(x, y, z) = \mathbf{h}_j(x, y) \exp(i\beta z) = \{\mathbf{h}_{tj}(x, y) + h_{zj}(x, y)\hat{\mathbf{z}}\} \exp(i\beta z), \quad (25-1b)$$

where $j = 1, 2, \dots, \infty$, subscripts t and z denote transverse and longitudinal components and $\hat{\mathbf{z}}$ is the unit vector parallel to the waveguide axis. If we include the implicit time dependence $\exp(-i\omega t)$, then Eq. (25-1) represents a forward-propagating mode, since we always take $\beta > 0$. The corresponding backward-propagating mode has fields \mathbf{E}_{-j} and \mathbf{H}_{-j} , which are related to the forward-propagating fields by Eq. (11-7). On nonabsorbing waveguides, the convention of Section 11-3 could be applied to radiation modes. However, choosing the transverse components \mathbf{e}_{tj} and \mathbf{h}_{tj} to be real leads to unnecessary complexity in representing the fields of the mode in later sections. Thus, for convenience \mathbf{e}_{tj} and \mathbf{h}_{tj} are generally complex.

25-2 Propagation constant

We recall from Section 11-17 that the propagation constants β_j for bound modes are found from an eigenvalue equation and, for a clad waveguide, form a *discrete* set of values within the range of Eq. (11-46). The propagation constant β for each radiation mode is *continuous* and can take any value within certain ranges. If the propagation constant is real and satisfies $0 \leq \beta < kn_{cl}$, then we have a *propagating* radiation mode, and if the real and imaginary parts of β satisfy $\beta^r = 0$ and $0 < \beta^i < \infty$, respectively, then we have an *evanescent* mode. The propagating modes transport power and the evanescent modes describe stored energy close to the source of excitation. In Table 25-1 we delineate the spectrum of values of the propagation constant and modal parameters for the various modes.

Table 25-1 Ranges of values of the propagation constant β and the modal parameters U and Q for modes of a clad fiber. Superscripts r and i denote real and imaginary parts, and subscript j denotes the discrete values for bound modes.

	β	U	Q
Bound modes	$kn_{cl} < \beta_j \leq kn_{co}$	$0 \leq U_j < V$	$Q_j^r = 0; Q_j^i > 0$
Radiation modes	$0 \leq \beta < kn_{cl}$	$V < U \leq k\rho n_{co}$	$0 < Q \leq k\rho n_{cl}$
Evanescent modes	$\beta^r = 0; \beta^i > 0$	$k\rho n_{co} < U < \infty$	$k\rho n_{cl} < Q < \infty$

25–3 Radiation-field expansion

The discrete set of bound-mode propagation constants means that the fields of the waveguide in the spatial steady state are given by the finite sum over all bound modes in Eq. (11–2). In contrast, each radiation and evanescent mode can take any of the continuum of propagation-constant values given in Table 25–1, and thus an integration over all values of β is necessary. However, like bound modes, the total radiation field requires a summation over the subscript j of Eq. (25–1) to account for the transverse fields of different modes. However, rather than use β as the continuum variable, when β is real for radiation modes and imaginary for evanescent modes, we use instead the modal parameter Q , defined below, in order to simplify the notation. We take β to be the positive root of the inverse relation whence

$$Q = \rho(k^2 n_{cl}^2 - \beta^2)^{1/2}; \quad \beta = \beta(Q) = (k^2 n_{cl}^2 - Q^2/\rho^2)^{1/2}. \quad (25-2)$$

Thus Q is always real and positive for both radiation and evanescent modes.

The total radiation fields of the waveguide are then given by

$$\mathbf{E}_{\text{rad}}(x, y, z) = \sum_j \int_0^\infty a_j(Q) \mathbf{e}_j(x, y, Q) \exp\{i\beta(Q)z\} dQ, \quad (25-3a)$$

$$\mathbf{H}_{\text{rad}}(x, y, z) = \sum_j \int_0^\infty a_j(Q) \mathbf{h}_j(x, y, Q) \exp\{i\beta(Q)z\} dQ, \quad (25-3b)$$

in terms of the forward-propagating radiation modes and corresponding evanescent modes, together with a similar expression for the backward-propagating radiation modes and corresponding evanescent modes with j and β replaced by $-j$ and $-\beta$, respectively. The $a_j(Q)$ are the modal amplitudes. Integration over the range $0 < Q \leq k\rho n_{cl}$ accounts for the radiation modes, and over $k\rho n_{cl} < Q < \infty$ accounts for the evanescent modes.

25–4 Orthogonality and normalization

In Section 11–4, we showed that each bound mode is orthogonal to every other bound mode and to all radiation modes. The orthogonality properties of radiation modes are derived in Section 31–3. On a nonabsorbing waveguide, the j th and k th forward-propagating radiation modes obey

$$\int_{A_\infty} \mathbf{e}_j(Q) \times \mathbf{h}_k^*(Q') \cdot \hat{\mathbf{z}} dA = \int_{A_\infty} \mathbf{e}_k^*(Q') \times \mathbf{h}_j(Q) \cdot \hat{\mathbf{z}} dA = 0, \quad (25-4)$$

valid for all Q if $j \neq k$, and valid for $Q \neq Q'$ if $j = k$.

where A_∞ is the infinite cross-section, * denotes complex conjugate and \hat{z} is the unit vector parallel to the waveguide axis. We emphasize that orthogonality holds when $j = k$ provided the values of Q and Q' differ. In other words, a radiation mode is orthogonal to itself for different values of the propagation constant.

The normalization, $N_j(Q)$, for the j th forward-propagating radiation mode on a nonabsorbing waveguide is defined by

$$\frac{1}{2} \int_{A_\infty} \mathbf{e}_j(Q) \times \mathbf{h}_j^*(Q') \cdot \hat{z} dA = N_j(Q) \delta(Q - Q'), \quad (25-5)$$

where δ is the Dirac delta function. The normalization integral is unbounded when $Q = Q'$, so to identify the functional form of N_j , the integral is factorized using a definition of the delta function, e.g. Eq. (37-108). We account for the unphysical nature of this normalization in the following section.

Orthonormal radiation modes

The fields $\hat{\mathbf{e}}_j$ and $\hat{\mathbf{h}}_j$ of an *orthonormal* radiation mode have the same definition in terms of the normalization $N_j(Q)$ as the bound-mode fields of Eq. (11-15). Any two modes j and k satisfy the orthonormality condition

$$\frac{1}{2} \int_{A_\infty} \hat{\mathbf{e}}_j(Q) \times \hat{\mathbf{h}}_k^*(Q') \cdot \hat{z} dA = \frac{1}{2} \int_{A_\infty} \hat{\mathbf{e}}_k^*(Q') \times \hat{\mathbf{h}}_j(Q) \cdot \hat{z} dA = \delta(Q - Q') \delta_{jk}, \quad (25-6)$$

where δ_{jk} is the Kronecker delta, i.e. $\delta_{jk} = 1$ if $j = k$ and $\delta_{jk} = 0$ otherwise.

Backward-propagating radiation modes

By analogy with Section 11-4, the orthogonality, normalization and orthonormality relations satisfied by backward-propagating radiation modes are obtained from Eqs. (25-4) to (25-6) by applying the convention of Eq. (11-7).

25-5 Power of the radiation field

The total, time-averaged power flow of the radiation field parallel to the waveguide axis has magnitude P_{rad} . This follows from Eq. (11-25) as

$$P_{\text{rad}} = \frac{1}{2} \text{Re} \left\{ \int_{A_\infty} \mathbf{E}_{\text{rad}} \times \mathbf{H}_{\text{rad}}^* \cdot \hat{z} dA \right\}, \quad (25-7)$$

where Re denotes real part. Substituting for the fields from Eq. (25-3) and

interchanging the order of integration and summation gives

$$P_{\text{rad}} = \frac{1}{2} \text{Re} \left\{ \int_0^\infty dQ \int_0^\infty dQ' \chi(Q, Q') \int_{A_{\infty}} \mathbf{e}_j(Q) \times \mathbf{h}_k^*(Q') \cdot \hat{\mathbf{z}} dA \right\}, \quad (25-8a)$$

$$\chi(Q, Q') = \exp[i\{\beta(Q) - \beta(Q')\}z] \sum_j \sum_k a_j(Q) a_k^*(Q'). \quad (25-8b)$$

The orthogonality conditions of Eq. (25-4) and the normalization of Eq. (25-5) lead to

$$P_{\text{rad}} = \sum_j \int_0^{k\rho_{\text{ncI}}} |a_j(Q)|^2 N_j(Q) dQ, \quad (25-9)$$

for the power propagating in the positive z -direction on a nonabsorbing waveguide. There is no contribution from the evanescent modes, which do not propagate.

The right side of Eq. (25-9) is independent of z and hence P_{rad} is constant along the waveguide. This is also true of the total guided power P_{bd} of Eq. (11-27), which is the total power of all bound modes, and, consequently, radiated power is determined in analogy with guided power. Individual radiation modes, like bound modes, propagate energy parallel to the waveguide axis. The total power radiated is the summed power of individual radiation modes, as expressed by Eq. (25-9). However, because of interference between the fields of different radiation modes, including the same mode with different values of the propagation constant, the continuum of modes, expressed by the integral in Eq. (25-9), represents the expected behavior of the total radiation field, i.e. a flow of power away from the waveguide. Clearly, an individual radiation mode is not physically meaningful and is only a convenient building block for describing radiation mathematically.

25-6 Excitation of radiation modes

Given a source of excitation, either at the waveguide endface or within the waveguide, the modal amplitudes $a_j(Q)$ of radiation modes are found by analogy with the bound-mode amplitudes a_j .

Illumination of the endface

When the endface of a waveguide is illuminated, we assume that the transverse fields $\mathbf{E}_t(x, y)$ and $\mathbf{H}_t(x, y)$ at $z = 0$ are prescribed. The portion of these fields which excites the radiation fields in Eq. (20-1) is expressible in terms of

radiation and evanescent modes by Eq. (25-3) with $z = 0$. Hence

$$\mathbf{E}_{\text{tr}}(x, y) = \sum_j \int_0^\infty a_j(Q) \mathbf{e}_{\text{tj}}(Q) dQ; \quad \mathbf{H}_{\text{tr}}(x, y) = \sum_j \int_0^\infty a_j(Q) \mathbf{h}_{\text{tj}}(Q) dQ. \quad (25-10)$$

We form the scalar cross product with $\mathbf{h}_{\text{tj}}^*(Q')$ in the first equation, and with $\mathbf{e}_{\text{tj}}^*(Q')$ in the second equation. Applying the orthogonality condition of Eq. (25-4), we obtain the expressions analogous to Eq. (20-2) as

$$a_j(Q) = \frac{1}{2N_j(Q)} \int_{A_x} \mathbf{E}_{\text{tj}} \times \mathbf{h}_{\text{tj}}^*(Q) \cdot \hat{\mathbf{z}} dA, \quad (25-11a)$$

$$a_j^*(Q) = \frac{1}{2N_j(Q)} \int_{A_x} \mathbf{e}_{\text{tj}}^*(Q) \times \mathbf{H}_{\text{t}} \cdot \hat{\mathbf{z}} dA, \quad (25-11b)$$

in terms of the normalization of Eq. (25-5).

Sources within the waveguide

If current sources with density \mathbf{J} are present within the waveguide, the radiation field is given by the second summation in Eq. (31-32), since the amplitudes of the radiation and evanescent modes are z -dependent within the region occupied by currents. Outside of this region the modal amplitudes are constant. We deduce from Eq. (31-37) that

$$a_{\pm j}(Q) = \mp \frac{1}{4N_j(Q)} \int_{\mathcal{V}} \{ \mathbf{e}_{\text{tj}}(Q) \pm e_{zj}(Q) \hat{\mathbf{z}} \}^* \cdot \mathbf{J} \exp \{ \mp i\beta(Q)z \} d\mathcal{V}, \quad (25-12)$$

where \mathcal{V} is the volume between $z = z_1$ and $z = z_2$. Upper and lower signs refer to the forward- and backward-propagating modes in $z > z_2$ and $z < z_1$, respectively, otherwise $a_{\pm j}(Q) = 0$.

'FREE-SPACE' RADIATION MODES

In order to apply radiation modes, we must show how to construct their fields and normalization from Maxwell's equations for a specific waveguide. This is facilitated if we first construct the '*free-space*' modes, i.e. the radiation modes of an unbounded medium of uniform refractive index n_{cl} [1]. The 'free-space' modes are easier to construct than the radiation modes of a waveguide, and

they exhibit all the general properties discussed above. They fully describe radiation from sources in ‘free space’, and are an alternative description to the ‘free-space’ antenna methods of Chapter 21. Furthermore, the radiation modes of a waveguide must reduce to the ‘free-space’ modes when the variation in profile vanishes.

Construction of the modes

To ensure that ‘free-space’ modes exhibit cylindrical symmetry, we treat the medium as a ‘waveguide’ with a uniform core of infinite cross-section and index n_{cl} . The most elementary modes are TE and TM whose longitudinal fields satisfy $e_{zj}^f = 0$ and $h_{zj}^f = 0$, respectively, where superscript f denotes ‘free space’. To construct the remaining field components, we recall from Section 11–15 that the nonvanishing longitudinal field component satisfies Eq. (11–45) *everywhere* in a uniform medium. Thus

$$(\rho^2 \nabla_t^2 + Q^2)h_{zj}^f = 0; \quad (\rho^2 \nabla_t^2 + Q^2)e_{zj}^f = 0, \quad (25-13)$$

for TE and TM modes, respectively, where Q is defined inside the back cover. Given solutions which are everywhere bounded, the transverse field components follow from Eq. (30–6).

25–7 Example: Solution in cylindrical polar coordinates

We construct the ‘free-space’ modes in the cylindrical polar coordinate system (r, ϕ, z) , choosing the z -direction as the direction of propagation, in order to relate to the radiation modes of circular fibers discussed in subsequent sections. The operator ∇_t^2 is defined in Table 30–1, page 592, and hence Eq. (25–13) has solutions which are everywhere bounded and are proportional to either $J_\nu(QR) \cos(\nu\phi)$ or $J_\nu(QR) \sin(\nu\phi)$, where J_ν is the Bessel function of the first kind, ν is a positive integer or zero, $R = r/\rho$, and ρ is a scaling length, e.g. the core radius of a step-profile fiber. The transverse components follow from Eq. (30–9) and the complete fields for TE and TM polarizations are listed in Table 25–2. The full spatial dependence is given by Eq. (25–1). In this instance it is convenient to choose e_j^f and h_j^f to satisfy the convention of Eq. (11–8), i.e. *real transverse and imaginary longitudinal components*.

Normalization

The derivation of the normalization expressions in Table 25–2 is best determined by example. We use the odd, $\nu = 1$, TE mode and deduce from Eq. (37–75) that the left side of Eq. (25–5) is expressible as

$$2\pi\rho^2 \frac{\beta}{k} \left(\frac{\epsilon_0}{\mu_0} \right)^{1/2} \int_0^\infty J_1(QR) J_1(Q'R) R \, dR. \quad (25-14)$$

Table 25-2 Free-space modes in cylindrical polar-coordinates. Prime denotes differentiation with respect to argument, and parameters are defined inside the back cover.

	<i>TE modes</i>	<i>TM modes</i>
e_{rj}^f	$\frac{2v}{QR} J_v(QR) f_v(\phi)$	$-2J'_v(QR) f_v(\phi)$
$e_{\phi j}^f$	$2J'_v(QR) g_v(\phi)$	$-\frac{2v}{QR} J_v(QR) g_v(\phi)$
e_{xj}^f	$J_{v+1}(QR) f_{v+1}(\phi) + J_{v-1}(QR) f_{v-1}(\phi)$	$J_{v+1}(QR) f_{v+1}(QR) - J_{v-1}(QR) f_{v-1}(QR)$
e_{yj}^f	$-J_{v+1}(QR) g_{v+1}(\phi) + J_{v-1}(QR) g_{v-1}(\phi)$	$-J_{v+1}(QR) g_{v+1}(\phi) - J_{v-1}(QR) g_{v-1}(\phi)$
e_{zj}^f	0	$2i \frac{Q}{\beta \rho} J_v(QR) f_v(\phi)$
h_{rj}^f	$-2 \left(\frac{\epsilon_0}{\mu_0} \right)^{1/2} \frac{\beta}{k} J'_v(QR) g_v(\phi)$	$2 \left(\frac{\epsilon_0}{\mu_0} \right)^{1/2} \frac{kv n_{cl}^2}{RQ\beta} J_v(QR) g_v(\phi)$
$h_{\phi j}^f$	$2 \left(\frac{\epsilon_0}{\mu_0} \right)^{1/2} \frac{v\beta}{RQk} J_v(QR) f_v(\phi)$	$-2 \left(\frac{\epsilon_0}{\mu_0} \right)^{1/2} \frac{kn_{cl}^2}{\beta} J'_v(QR) f_v(\phi)$
h_{zj}^f	$2i \left(\frac{\epsilon_0}{\mu_0} \right)^{1/2} \frac{Q}{k\rho} J_v(QR) g_v(\phi)$	0
N_j	$2\pi\rho^2 \left(\frac{\epsilon_0}{\mu_0} \right)^{1/2} \frac{\beta}{kQ} \times \begin{cases} 1; & v > 0 \\ 2; & v = 0 \end{cases}$	$2\pi\rho^2 \left(\frac{\epsilon_0}{\mu_0} \right)^{1/2} \frac{kn_{cl}^2}{\beta Q} \times \begin{cases} 1; & v > 0 \\ 2; & v = 0 \end{cases}$
$f_v(\phi) = \begin{cases} \cos(v\phi); \\ \sin(v\phi); \end{cases} \quad g_v(\phi) = \begin{cases} -\sin(v\phi); & \text{even modes} \\ \cos(v\phi); & \text{odd modes} \end{cases}$		

By definition, we are interested *only* in the case when $Q = Q'$. The singular behavior of the integral comes from the asymptotic forms of Eq. (37-87) for Bessel functions of large argument. Substitution into Eq. (25-14) gives

$$\frac{\rho^2 \beta}{Q k} \left(\frac{\epsilon_0}{\mu_0} \right)^{1/2} \int_0^\infty \{ \exp[i(QR - 3\pi/4)] + \exp[-i(QR - 3\pi/4)] \} \times \\ \{ \exp[i(Q'R - 3\pi/4)] + \exp[-i(Q'R - 3\pi/4)] \} dR. \quad (25-15)$$

Only terms involving the difference $Q - Q'$ in the exponent contribute to the singularity. Neglecting all other terms, we deduce from Eq. (25-5) that

$$\frac{\rho^2 \beta}{Q k} \left(\frac{\epsilon_0}{\mu_0} \right)^{1/2} \int_{-\infty}^\infty \exp[i(Q - Q')R] dR = N_j(Q) \delta(Q - Q'), \quad (25-16)$$

in terms of the Dirac delta function of Eq. (37-108), leading to the normalization expression in Table 25-2.

CONSTRUCTION OF THE RADIATION MODES

The radiation modes of a waveguide must reduce to the 'free-space' modes described above when there is no variation in the refractive-index profile, i.e. $n = n_{cl}$ everywhere or $V = 0$. Accordingly, one approach in constructing the radiation modes is to modify the 'free-space' modes and express the radiation-mode fields as the sum of the 'free-space' fields and the fields scattered by the waveguide profile [1]

$$\mathbf{e}_j = \mathbf{e}_j^f + \mathbf{e}_j^s, \quad \mathbf{h}_j = \mathbf{h}_j^f + \mathbf{h}_j^s, \quad (25-17a)$$

where superscripts f and s denote 'free-space' and scattered fields, respectively. This decomposition is exact, and enables the radiation modes to be formed in an intuitive way. Furthermore, such a construction ensures that the radiation modes have the same orthogonality and normalization as the corresponding 'free-space' modes [1]. Thus

$$\frac{1}{2} \int_{A_\infty} \mathbf{e}_j(Q) \times \mathbf{h}_j^*(Q') \cdot \hat{\mathbf{z}} dA = \frac{1}{2} \int_{A_\infty} \mathbf{e}_j^f(Q) \times \mathbf{h}_j^f(Q')^* \cdot \hat{\mathbf{z}} dA = N_j(Q) \delta(Q - Q').$$

(25-17b)

In the following section we verify this for the step-profile fiber. A general proof for arbitrary structures is available [3]. Radiation modes corresponding to 'free-space' TE modes ($e_{zj}^f = 0$) are called ITE modes, and those corresponding to 'free-space' TM modes ($h_{zj}^f = 0$) are called ITM modes [1].

Analytical solutions

The radiation-mode fields are solutions of the same equations satisfied by the bound-mode fields, so that whenever an exact solution exists for bound modes, a corresponding solution for radiation modes exists. We showed in Chapter 12 that, for waveguides with arbitrary variation in profile, there are few known profiles for which exact solutions of Maxwell's equations can be obtained analytically. Even in these cases, the expressions for the radiation-mode fields are generally more complex than those for the bound-mode fields. In the following section we consider the step-profile fiber. The radiation-mode fields of the step-profile planar waveguide can be derived similarly.

Plane-wave decomposition

The complete spatial variation of each radiation mode is given by Eq. (25-1), and the range of values of the propagation constant satisfies $0 \leq \beta < kn_{\text{cl}}$. For a particular value of β , the modal fields can be regarded as a Fourier superposition of the fields of a family of plane waves, all inclined at angle θ_z to the waveguide axis. In the uniform cladding, θ_z is related to β by

$$\beta = kn_{\text{cl}} \cos \theta_z, \quad (25-18)$$

and consequently, the range of values of θ_z satisfies $0 \leq \theta_z < \pi/2$.

25-8 Example: Step-profile fiber

The radiation-mode fields of the step-profile fiber are constructed in the same manner as the bound-mode fields of Section 12-8. Away from the core-cladding interface, the longitudinal components satisfy

$$(\rho^2 \nabla_t^2 + U^2) e_{zj} = 0; \quad (\rho^2 \nabla_t^2 + U^2) h_{zj} = 0; \quad 0 \leq R < 1, \quad (25-19a)$$

$$(\rho^2 \nabla_t^2 + Q^2) e_{zj} = 0; \quad (\rho^2 \nabla_t^2 + Q^2) h_{zj} = 0; \quad 1 < R < \infty. \quad (25-19b)$$

where ρ is the core radius, U and Q are defined at the back of the book and ∇_t^2 is defined in Table 30-1, page 592. The choice of e_{zj} and h_{zj} must satisfy the decomposition indicated in Eq. (25-17) into free-space and scattered parts. This is satisfied by the expressions in Table 25-3 where a_v , b_v , c_v^s and d_v^s are constants to be determined, and c_v^f and d_v^f are the 'free-space' constants obtained from Table 25-2. The Hankel function of the first-kind, $H_v^{(1)}$, ensures that the scattered fields correspond to an outward-travelling wave as $R \rightarrow \infty$.

We use Eq. (30-9) for the transverse-field components and determine the constants from continuity of e_{zj} , h_{zj} , $e_{\phi j}$ and $h_{\phi j}$ at the interface. With the aid of the Wronskian of Eq. (37-77) this leads to the expressions in Table 25-3 for the ITE and ITM modes. The orthogonality and normalization of each radiation mode is identical to the corresponding 'free-space' normalization of Table 25-2 for reasons given above. Alternatively, we can parallel the derivation of $N_j(Q)$ in Section 25-7 using the radiation-mode fields.

Quantitative form of the fields

Radiation modes with $\beta \ll kn_{\text{cl}}$, i.e. $\theta_z \cong \pi/2$, are composed of plane waves at near normal incidence to the core-cladding boundary so that they are only weakly influenced by the core. Thus, radiation modes with $\beta \ll kn_{\text{cl}}$ are approximately free-space modes with $\mathbf{e}_j \cong \mathbf{e}_j^f$ and $\mathbf{h}_j \cong \mathbf{h}_j^f$. The implicit conditions discussed below in Section 25-11 help facilitate this limiting condition. At the other extreme, when $\beta \cong kn_{\text{cl}}$, i.e. $\theta_z \cong 0$, the plane waves that form a radiation mode are at near grazing incidence and are significantly influenced by the fiber core.

Table 25–3 Radiation modes of the step-profile fiber. The transverse fields follow from Eq. (30–9). Prime denotes differentiation with respect to argument, and parameters are defined inside the back cover.

	Core	Cladding
e_{zj}	$a_v J_v(UR) f_v(\phi)$	$\{c_v^f J_v(QR) + c_v^s H_v^{(1)}(QR)\} f_v(\phi)$
h_{zj}	$b_v J_v(UR) g_v(\phi)$	$\{d_v^f J_v(QR) + d_v^s H_v^{(1)}(QR)\} g_v(\phi)$
$f_v(\phi) = \begin{cases} \cos(v\phi); \\ \sin(v\phi); \end{cases} \quad g_v(\phi) = \begin{cases} -\sin(v\phi); & \text{even modes} \\ \cos(v\phi); & \text{odd modes} \end{cases}$		

	ITE modes	ITM modes
a_v	$-\frac{4}{\pi} \frac{\beta}{kn_{co}^2} \frac{v}{k\rho} \frac{V^2}{U^2 Q^3} \frac{1}{J_v(U) H_v^{(1)}(Q) M_v}$	$-\frac{4}{\pi} \frac{n_{cl}^2}{n_{co}^2} \frac{1}{\beta \rho Q} \frac{F_v}{J_v(U) H_v^{(1)}(Q) M_v}$
b_v	$-\frac{4}{\pi} \left(\frac{\epsilon_0}{\mu_0}\right)^{1/2} \frac{1}{Q k \rho} \frac{G_v}{J_v(U) H_v^{(1)}(Q) M_v}$	$-\frac{4}{\pi} \frac{n_{cl}^2}{n_{co}^2} \left(\frac{\epsilon_0}{\mu_0}\right)^{1/2} \frac{v}{k\rho} \frac{V^2}{U^2 Q^3} \frac{1}{J_v(U) H_v^{(1)}(Q) M_v}$
c_v^f	0	$2i \frac{Q}{\beta \rho}$
c_v^s	$-\frac{4}{\pi} \frac{\beta}{kn_{co}^2} \frac{v}{k\rho} \frac{V^2}{U^2 Q^3} \frac{1}{\{H_v^{(1)}(Q)\}^2 M_v}$	$-2i \frac{Q}{\beta \rho} \frac{J_v(Q)}{H_v^{(1)}(Q)} \frac{A_v}{M_v}$
d_v^f	$2i \left(\frac{\epsilon_0}{\mu_0}\right)^{1/2} \frac{Q}{\rho k}$	0
d_v^s	$-2i \left(\frac{\epsilon_0}{\mu_0}\right)^{1/2} \frac{Q}{\rho k} \frac{J_v(Q)}{H_v^{(1)}(Q)} \frac{B_v}{M_v}$	$-\frac{4}{\pi} \frac{n_{cl}^2}{n_{co}^2} \left(\frac{\epsilon_0}{\mu_0}\right)^{1/2} \frac{v}{\rho k} \frac{V^2}{U^2 Q^3} \frac{1}{\{H_v^{(1)}(Q)\}^2 M_v}$
N_j	$\frac{2\pi\rho^2}{Q} \left(\frac{\epsilon_0}{\mu_0}\right)^{1/2} \frac{\beta}{k} \times \begin{cases} 1; & v > 0 \\ 2; & v = 0 \end{cases}$	$\frac{2\pi\rho^2}{Q} \left(\frac{\epsilon_0}{\mu_0}\right)^{1/2} \frac{kn_{cl}^2}{\beta} \times \begin{cases} 1; & v > 0 \\ 2; & v = 0 \end{cases}$

$F_v = \frac{J'_v(U)}{U J_v(U)} - \frac{H_v^{(1)'}(Q)}{Q H_v^{(1)}(Q)}; \quad G_v = \frac{J'_v(U)}{U J_v(U)} - \frac{n_{cl}^2}{n_{co}^2} \frac{H_v^{(1)'}(Q)}{Q H_v^{(1)}(Q)}$	
$A_v = M_v - \frac{2i}{\pi} \frac{n_{cl}^2}{n_{co}^2} \frac{F_v}{Q^2 J_v(Q) (H_v^{(1)})'(Q)}; \quad B_v = M_v - \frac{2i}{\pi} \frac{G_v}{Q^2 J_v(Q) H_v^{(1)}(Q)}$	
$M_v = \left(\frac{v\beta}{kn_{co}}\right)^2 \left(\frac{V}{UQ}\right)^4 - F_v G_v$	

WEAKLY GUIDING WAVEGUIDES

In Chapter 13 we showed how the bound-mode fields of weakly guiding waveguides can be constructed from solutions of the scalar wave equation. With slight modification, the same procedure applies to the radiation-mode fields as well [4]. However, while the bound modes are approximately TEM waves because $\beta \cong kn_{co} \cong kn_{cl}$, the radiation modes are not close to being TEM waves since β can take any value in the range $0 \leq \beta < kn_{cl}$.

25–9 Spatial dependence of the fields

The discussion of bound modes in Section 13–3 applies equally to radiation modes on weakly guiding waveguides, except that the fields are no longer predominantly perpendicular to the waveguide axis. However, the cartesian components of the transverse electric field e_{ij} of Eq. (13–7) are still solutions of the scalar wave equation. Thus, if Ψ_j denotes e_{xj} or e_{yj} , then

$$\{\nabla_t^2 + k^2 n^2(x, y) - \beta^2(Q)\}\Psi = 0, \quad (25-20)$$

where $\beta(Q)$ is now the continuous propagation constant for radiation modes. The solution for Ψ_j can be constructed by paralleling the construction of the radiation modes for arbitrary waveguides. Thus, by analogy with Eq. (25–17a), we express Ψ_j as the sum of a ‘free-space’ part and a scattered part

$$\Psi_j = \Psi_j^f + \Psi_j^s, \quad (25-21)$$

where Ψ_j^f is the solution of Eq. (25–20) when $n = n_{cl}$ everywhere, i.e.

$$\{\rho^2 \nabla_t^2 + Q^2\}\Psi_j^f = 0, \quad (25-22)$$

in terms of Q of Eq. (25–2). Thus Ψ_j reduces to Ψ_j^f when $\Delta = 0$, i.e. when $V = 0$. Expressions for Ψ_j^f and Ψ_j are derived in Section 25–11 for the step-profile fiber.

25–10 Vector direction of the radiation-mode fields

In Chapter 13 we used the polarization properties of the waveguide to determine the direction of e_{ij} and the correction $\delta\beta_j$ to the scalar propagation constant $\tilde{\beta}_j$. However, the propagation constant β for radiation modes takes any value in the range $0 \leq \beta < kn_{cl}$ and is therefore a continuous variable independent of waveguide polarization. Consequently, higher-order correc-

tions to e_{xj} and e_{yj} would be required to incorporate polarization properties of the waveguide. We recall that the polarization effects for bound modes are only significant over large distances along the waveguide. In the case of the radiation field these effects are even smaller, since radiation power does not remain close to the waveguide axis for such large distances. Accordingly, we ignore all polarization effects of the waveguide on radiation modes. Consequently, the appropriate combination of e_{xj} and e_{yj} forming \mathbf{e}_{Uj} need only satisfy the orthogonality properties of the radiation-mode fields.

Orthogonality and normalization

Within the weak-guidance approximation, the remaining components of the radiation-mode fields \mathbf{e}_j and \mathbf{h}_j are expressible in terms of \mathbf{e}_{Uj} by omitting all terms involving $\nabla_t \ln n^2$ in Eq. (30–5). Hence

$$e_{zj} = \frac{i}{\beta} \nabla_t \cdot \mathbf{e}_{Uj}; \quad h_{zj} = \frac{i}{\beta} \nabla_t \cdot \mathbf{h}_{Uj}, \quad (25-23a)$$

$$\mathbf{h}_{Uj} = \left(\frac{\epsilon_0}{\mu_0} \right)^{1/2} \frac{\beta}{k} \hat{\mathbf{z}} \times \left\{ \mathbf{e}_{Uj} - \frac{1}{\beta^2} \nabla_t (\nabla_t \cdot \mathbf{e}_{Uj}) \right\}, \quad (25-23b)$$

where $\hat{\mathbf{z}}$ is the unit vector parallel to the waveguide axis, the vector operators are defined in Table 30–1, page 592, and remaining parameters appear inside the back cover. Thus, unlike the corresponding bound-mode field, the transverse magnetic field does not satisfy the scalar wave equation. Using these expressions, we show in Section 32–11 that the orthogonality relations of Eq. (25–4) and the normalization of Eq. (25–5), reduce, respectively, to

$$\int_{A_x} \mathbf{e}_j(Q) \cdot \mathbf{e}_k^*(Q') dA = 0; \quad Q \neq Q' \quad \text{if } j \neq k, \quad (25-24a)$$

$$\frac{1}{2} \left(\frac{\epsilon_0}{\mu_0} \right)^{1/2} \frac{\beta(Q)}{k} \int_{A_x} \mathbf{e}_j(Q) \cdot \mathbf{e}_j^*(Q') dA = N_j(Q) \delta(Q - Q'). \quad (25-24b)$$

We note that the *total* electric field is required, whereas the corresponding bound-mode relations of Eqs. (33–5b) and (33–6) involve only the *transverse* component.

'Free-space' orthogonality and normalization

The combination of e_{xj} and e_{yj} which satisfies Eq. (25–24a) is not unique. However, when Ψ_j is constructed according to Eq. (25–21), the orthogonality of the free-space modes, like the normalization, automatically ensures orthogonality of the corresponding radiation modes [4]. This may be verified

for the example below. Thus it is simpler and more convenient to construct \mathbf{e}_{ij} so that the 'free-space' portion of the fields are polarized with either $e_{zj} = 0$ or $h_{zj} = 0$, i.e. ITE and ITM modes. Since every *cartesian* component of the fields satisfies the scalar wave equation *exactly* in 'free space', the fields in Table 25-2, which were constructed from the *longitudinal* components, can equally be constructed starting with Eq. (25-22) and the *transverse* components of the electric field. In other words, by transforming the radial and azimuthal components of \mathbf{e}_{ij} in Table 25-2 to cartesian components, we immediately determine the combination of e_{xj} and e_{yj} . This is the procedure adopted below.

25-11 Example: Step-profile fiber

To construct the radiation modes of a weakly guiding, step-profile fiber of core and cladding indices n_{co} and n_{cl} , we start with the 'free-space' solution of Eq. (25-22). When ∇^2 is expressed in cylindrical polar coordinates using Table 30-1, page 592, the only solutions which are everywhere bounded are the even and odd pair

$$\Psi_l^e = J_l(QR) \cos(l\phi); \quad \Psi_l^o = J_l(QR) \sin(l\phi), \quad (25-25)$$

where J_l is the Bessel function of the first kind, $R = r/\rho$, the core radius is ρ and l is a non-negative integer. The next step is to incorporate the scattered fields through Ψ_l^s , as in Eq. (25-21). Since Ψ_l^s must represent an outgoing wave as $r \rightarrow \infty$, and $\Psi_l = \Psi_l^e + \Psi_l^s$ must be bounded at $r = 0$, we deduce from Eq. (25-20) that these requirements are satisfied by

$$\Psi_l^e = p_l J_l(UR) \cos(l\phi); \quad 0 \leq R < 1, \quad (25-26a)$$

$$= \{J_l(QR) + q_l H_l^{(1)}(QR)\} \cos(l\phi); \quad 1 \leq R < \infty, \quad (25-26b)$$

together with a similar expression for Ψ_l^o with $\cos(l\phi)$ replaced by $\sin(l\phi)$. Here $H_l^{(1)}$ is the Hankel function of the first kind and U is defined at the back of the book. Since Ψ_l^e satisfies the scalar wave equation, both Ψ_l^e and $\partial\Psi_l^e/\partial R$ are continuous on $R = 1$. This determines the constants p_l and q_l , which with the help of the Wronskian of Eq. (37-77), have the forms given in Table 25-4.

If e_{xl} and e_{yl} are the cartesian components of \mathbf{e}_{tl} , then, as explained in the previous section, the linear combinations of Ψ_l^e and Ψ_l^o forming e_{xl} or e_{yl} are obtained by comparison with the x - and y -components of the 'free-space' field \mathbf{e}_{ij} of Table 25-2. Using Eq. (37-49) to transform the radial and azimuthal components, and the recurrence relations of Eq. (37-72) for the Bessel functions, we obtain the combinations for even and odd ITE and ITM modes in Table 25-4. The method of construction ensures that these modes have the same normalization as the 'free-space' modes and the exact radiation modes of Table 25-3.

Sometimes it is useful to know the normalization of the *scalar* radiation modes, as discussed in Section 33-7. By substituting from Table 25-4 into Eq. (33-31), we obtain, in an analogous manner to the normalization in Table 25-2, the scalar normalization

$$F_l(Q) = \int_{A_{\infty}} |\Psi_l^e|^2 dA = \int_{A_{\infty}} |\Psi_l^o|^2 dA = \frac{\pi\rho^2}{Q}. \quad (25-26c)$$

Table 25-4 Radiation modes of the weakly guiding step-profile fiber. Parameters are defined inside the back cover, and vector operators are defined in Table 30-1, page 592.

$\Psi_l^e = p_l J_l(UR) \cos(l\phi); \quad 0 \leq R \leq 1$ $= \{J_l(QR) + q_l H_l^{(1)}(QR)\} \cos(l\phi); \quad 1 \leq R < \infty$ $\Psi_l^o = \Psi_l^e \tan(l\phi)$	
$p_l = \frac{2i}{\pi} \{U J_{l+1}(U) H_l^{(1)}(Q) - Q J_l(U) H_{l+1}^{(1)}(Q)\}^{-1}$ $q_l = i \frac{\pi}{2} p_l \{U J_{l+1}(U) J_l(Q) - Q J_l(U) J_{l+1}(Q)\}$	
ITE	ITM
$\mathbf{e}_{tl} = (\Psi_{l+1}^e + \Psi_{l-1}^e) \hat{\mathbf{x}} + (\Psi_{l+1}^o - \Psi_{l-1}^o) \hat{\mathbf{y}}$ <p style="text-align: center;">(even)</p> $\mathbf{e}_{tl} = (\Psi_{l+1}^o + \Psi_{l-1}^o) \hat{\mathbf{x}} - (\Psi_{l+1}^e - \Psi_{l-1}^e) \hat{\mathbf{y}}$ <p style="text-align: center;">(odd)</p>	$\mathbf{e}_{tl} = (\Psi_{l+1}^e - \Psi_{l-1}^e) \hat{\mathbf{x}} + (\Psi_{l+1}^o + \Psi_{l-1}^o) \hat{\mathbf{y}}$ <p style="text-align: center;">(even)</p> $\mathbf{e}_{tl} = (\Psi_{l+1}^o - \Psi_{l-1}^o) \hat{\mathbf{x}} - (\Psi_{l+1}^e + \Psi_{l-1}^e) \hat{\mathbf{y}}$ <p style="text-align: center;">(odd)</p>
$\mathbf{h}_{tl} = \left(\frac{\epsilon_0}{\mu_0} \right)^{1/2} \frac{\beta}{k} \hat{\mathbf{z}} \times \left\{ \mathbf{e}_{tl} - \frac{1}{\beta^2} \nabla_t (\nabla_t \cdot \mathbf{e}_{tl}) \right\}$ $e_{zl} = \frac{i}{\beta} \nabla_t \cdot \mathbf{e}_{tl}; \quad h_{zl} = \frac{i}{\beta} \nabla_t \cdot \mathbf{h}_{tl}$	
$N_l = \frac{2\pi\rho^2}{Q} \left(\frac{\epsilon_0}{\mu_0} \right)^{1/2} \frac{\beta}{k} \times \begin{cases} 1; & l > 0 \\ 2; & l = 0 \end{cases}$	$N_l = \frac{2\pi\rho^2}{Q} \left(\frac{\epsilon_0}{\mu_0} \right)^{1/2} \frac{kn_{cl}^2}{\beta} \times \begin{cases} 1; & l > 0 \\ 2; & l = 0 \end{cases}$

We emphasize that $F_l(Q)$ should not be confused with the normalization N_l of Table 25-4 for the radiation modes of the weakly guiding fiber. The latter is used in this chapter.

Implicit conditions

The fields in Table 25-4 are the weak-guidance limit of the exact fields of Table 25-2. In this limit, the fiber parameter V is fixed and $n_{co} \rightarrow n_{cl}$. However, we find that certain implicit conditions must be used in order to correctly reproduce the weakly guiding fiber fields [5]. One of the following conditions must hold: either

$$\beta \cong kn_{cl}; \quad \beta\rho \rightarrow \infty \text{ as } \Delta \rightarrow 0, \quad (25-27a)$$

with U and Q arbitrary, or

$$U \cong Q; \quad U \rightarrow \infty \text{ as } \Delta \rightarrow 0. \quad (25-27b)$$

The domains of validity in β overlap, since $\beta \geq 0$ in the second case. As Δ decreases with V constant, the second condition holds for a larger range of values of β , until, when $\Delta = 0$, it holds for all values of β except $\beta = kn_{cl}$.

RADIATION FROM SOURCES IN 'FREE SPACE'

In this first set of examples, we determine radiation from sources in 'free space', using the 'free-space' radiation modes, and compare the results with the antenna methods of Chapter 21.

25-12 Example: Dipole radiation

An x -directed current dipole of strength I and length d is located in an infinite uniform medium of refractive index n_{cl} at the origin of coordinates, as shown in Fig. 25-1(a). The current can be represented by

$$J_x = Id \delta(r - r_d) \delta(z) / 2\pi r_d, \quad (25-28)$$

in the limit $r_d \rightarrow 0$, where δ is the Dirac delta function. The dipole excites 'free-space' modes, and, by substituting Eq. (25-28) into Eq. (25-12), the amplitude of each mode is given by

$$a_{\pm j}(Q) = \mp \frac{Id}{8\pi N_j(Q)} \int_0^{2\pi} e_{xj}(Q) d\phi, \quad (25-29)$$

where upper and lower signs refer to forward- and backward-propagating modes in the regions $z > 0$ and $z < 0$, respectively, and e_{xj} is evaluated at $r = 0$. We deduce from

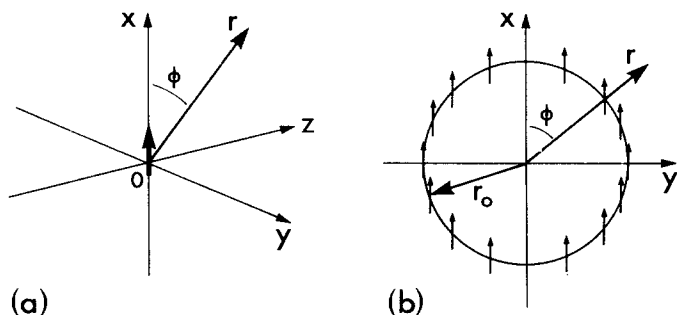


Fig. 25-1 (a) A current dipole of strength I and length d is located at the origin of coordinates and is parallel to the x -direction. (b) Cross-section of the tubular source showing the orientation of axes and the current direction parallel to the x -axis.

Table 25-2 that only the $v = 1$ even TE and TM modes are excited. Denoting these modes by $j = 1$ and $j = 2$, respectively, then, at $r = 0$, it is clear that $e_{x1} = 1$ and

$e_{x2} = -1$. Substitution into Eq. (25-29) yields

$$a_{\pm 1} = \mp \frac{Id}{4N_1(Q)}; \quad a_{\pm 2} = \pm \frac{Id}{4N_2(Q)}, \quad (25-30)$$

for the four excited modes.

Fields of the dipole

If we substitute Eq. (25-30) and the fields of Table 25-2 into Eq. (25-3), the dipole fields are given exactly by integration over two modes for $z \geq 0$ and $z \leq 0$. Asymptotic evaluation of these integrals for $r \rightarrow \infty$, together with a transformation from cylindrical to spherical polar coordinates, leads to the far fields of Eqs. (21-23) and (21-24a).

Radiated power

The total power radiated by the dipole is found by substituting Eq. (25-30) and the normalizations of Table 25-2 into Eq. (25-9). Allowing for forward- and backward-propagating modes

$$P_{\text{rad}} = \frac{|Id|^2}{16\pi\rho^2} \left(\frac{\mu_0}{\epsilon_0} \right)^{1/2} \int_0^{k\rho n_{\text{cl}}} \left\{ \frac{k}{\beta(Q)} + \frac{\beta(Q)}{kn_{\text{cl}}^2} \right\} Q \, dQ, \quad (25-31)$$

whence, by making the transformation $Q = k\rho n_{\text{cl}} \sin \theta_z$, $\beta = kn_{\text{cl}} \cos \theta_z$, it is readily verified that we recover the expression in Eq. (21-24b), which was derived using far-field antenna methods.

25-13 Example: Tubular-source radiation

Consider a tubular source, as described in Section 21-6, of length $2L$ and radius r_0 , which carries x -directed currents with magnitude

$$J_x = \delta(r - r_0) \cos(l\phi) \sin(\Omega z) \exp(iCz)/2\pi r_0, \quad (25-32)$$

where l is a positive integer or zero, and the tube is aligned as shown by the cross-section of Fig. 25-1(b) so that $\phi_0 = 0$ in Eq. (21-13). The tube is embedded in a uniform medium of refractive-index n_{cl} , and thus its radiation field can be described in terms of 'free-space' modes relative to the z -axis in Fig. 21-3. Substitution of Eq. (25-32) into Eq. (25-12) gives the modal amplitudes

$$a_{\pm j}(Q) = \mp \frac{1}{8\pi N_j(Q)} \int_0^{2\pi} e_{xj}(Q) \cos(l\phi) \, d\phi \int_{-L}^L \sin(\Omega z) \exp[i\{C \mp \beta(Q)\}z] \, dz, \quad (25-33)$$

where e_{xj} is evaluated on $r = r_0$. We deduce from Table 25-2 that only the even TE and TM modes with $v = l + 1$ and $v = l - 1$ are excited when $l \geq 1$, and when $l = 0$ only the even $v = 1$ modes are excited. We showed in Section 21-6 that the z integration is only significant if $\Omega \cong |C - \beta(Q)|$. Assuming $\beta(Q) \cong C - \Omega$, only forward-propagating modes are involved, which is equivalent to retaining the upper signs in Eq. (25-33) and the first term within the curly brackets of Eq. (21-15). We then deduce from Table 25-2

that

$$a_{l-1} = a_{l+1} = \frac{kn_{cl}}{\beta(Q)} G_l; \quad a_{l-1} = a_{l+1} = \frac{\beta(Q)}{kn_{cl}} G_l, \quad (25-34a)$$

for the TE and TM modes, respectively, when $l \geq 2$, and where

$$G_l = \frac{iQ}{16\pi\rho^2 n_{cl}} \left(\frac{\mu_0}{\epsilon_0} \right)^{1/2} \frac{\sin \{C - \beta(Q) - \Omega\} L}{C - \beta(Q) - \Omega} J_l(Qr_0/\rho). \quad (25-34b)$$

The radiated power in the four modes is found by substituting Eq. (25-34) into Eq. (25-9). Hence

$$P_{rad} = \frac{1}{64\pi\rho^2 n_{cl}} \left(\frac{\mu_0}{\epsilon_0} \right)^{1/2} \int_0^{k\rho n_{cl}} J_l^2(Qr_0/\rho) \frac{\sin^2 \{C - \beta(Q) - \Omega\} L}{\{C - \beta(Q) - \Omega\}^2} \left\{ \frac{\beta(Q)}{kn_{cl}} + \frac{kn_{cl}}{\beta(Q)} \right\} Q dQ. \quad (25-35)$$

To evaluate the integral we set $Q = k\rho n_{cl} \sin \theta_z$ and $\beta = kn_{cl} \cos \theta_z$, and, by following the discussion of Section 21-10, use the fact that the major contribution comes from around $\theta_z \cong \theta_0$ of Eq. (21-30). Thus

$$P_{rad} = \frac{kL}{64\pi} \left(\frac{\mu_0}{\epsilon_0} \right)^{1/2} (1 + \cos^2 \theta_0) J_l^2(kr_0 n_{cl} \sin \theta_0) \int_{x_-}^{x_+} \frac{\sin^2 x}{x^2} dx, \quad (25-36)$$

where $x = \{C - \beta(Q) - \Omega\} L$, $x_+ = (C - \Omega)L$ and $x_- = (C - kn_{cl} - \Omega)L$. By analogy with the x integration in Eq. (21-31), we deduce that Eq. (25-36) reduces to the far-field antenna result of Eq. (21-33a) when $l \geq 2$. The derivation for the cases $l = 0$ and $l = 1$ is similar.

RADIATION FROM SOURCES WITHIN FIBERS

We now examine how radiation from the point dipole and the tubular source is modified by the presence of a fiber. In order to relate the results to the correction factor of Section 21-12, the fiber is assumed to be weakly guiding.

25-14 Example: Dipole within a step-profile fiber

We determine the correction to the radiation from the current dipole of Section 25-12, when located on the axis of a weakly guiding, step-profile fiber. If the z -axis of Fig. 25-1(a) coincides with the axis of the fiber, we can repeat the analysis of Section 25-12 using the weakly guiding radiation modes instead of the 'free-space' modes. The on-axis fields e_{x1} and e_{x2} , and consequently the modal amplitudes of Eq. (25-30) are multiplied by the factor p_0 defined in Table 25-4. Thus the total radiated power of Eq. (25-31) must allow for the additional factor $|p_0|^2$ in the integrand, and in terms of the variable θ_z defined below Eq. (25-31), we obtain

$$P_{rad} = \frac{|kId|^2 n_{cl}}{32\pi} \left(\frac{\mu_0}{\epsilon_0} \right)^{1/2} \int_0^\pi \sin \theta_z (1 + \cos^2 \theta_z) |p_0|^2 d\theta_z. \quad (25-37)$$

We deduce from Table 25-4, Eqs. (21-36b) and (21-38) that

$$p_0 = W_0(Q, Q)/W_0(U, Q) = C_r(\theta). \quad (25-38)$$

Consequently Eq. (25–37) is identical with the angular integral of the product of the far-field of Eq. (21–24b) in ‘free space’ and the correction factor $C_0(\theta)$ of Eq. (21–36a) for an on-axis source within the fiber, as discussed in Section 21–13.

25–15 Example: Tubular source within a step-profile fiber

A tubular source of radius r_0 is located symmetrically within the core of a weakly guiding, step-profile fiber, i.e. $0 \leq r_0 \leq \rho$, where ρ is the core radius. To account for the fiber profile, we repeat the analysis of Section 25–13 using the weakly guiding radiation modes of Table 25–4 instead of the ‘free-space’ modes of Table 25–2. The modal amplitudes of Eq. (25–34a) are replaced by

$$a_{l-1} = a_{l+1} = p_l G_l \frac{J_l(Ur_0/\rho)}{J_l(Qr_0/\rho)} \frac{kn_{cl}}{\beta(Q)}; \quad a_{l-1} = -a_{l+1} = p_l G_l \frac{J_l(Ur_0/\rho)}{J_l(Qr_0/\rho)} \frac{\beta(Q)}{kn_{cl}}, \quad (25-39)$$

for the TE and TM modes, respectively, where $l \geq 2$ and G_l is defined by Eq. (25–34b). Accordingly, the final expression for radiated power is found to be identical with Eq. (21–41b) when p_l is expressed in terms of Eq. (21–36b).

25–16 Effect of a finite cladding

Throughout the chapter we have determined radiation fields on the assumption that the cladding is unbounded. However, in practice, fibers have a cladding of finite thickness as shown qualitatively by Fig. I–1 in the Introduction to Part I. When the cladding thickness is large, it has a negligible effect on the bound-mode fields, which decrease exponentially in the cladding. However, some of the radiated power will be reflected from the interface between the cladding and the jacket. We can regard the combined core and cladding regions of a single-mode fiber as the core of a multimode fiber. Consequently, the ray methods of Part I are applicable, and the power transmission coefficients of Chapters 6 and 7 can be used to determine the fraction of power entering the jacket. Reflected power is lost to the jacket at subsequent reflections in an analogous manner to the rays of Part I.

REFERENCES

1. Snyder, A. W. (1971) Continuous mode spectrum of a circular dielectric rod. *I.E.E.E. Trans. MTT*, **19**, 720–7.
2. Marcuse, D. (1974) *Theory of Dielectric Optical Waveguides*, Academic Press, New York. The radiation modes derived here are not orthogonal, and lead to errors.
3. Sammut, R. A. (1982) Orthogonality and normalization of radiation modes in dielectric waveguides. *J. Opt. Soc. Am.*, **72**, 1335–37.
4. Snyder, A. W. and Sammut, R. A. (1979) Radiation modes of optical waveguides. *Electron. Lett.*, **15**, 4–5.
5. Snyder, A. W. (1980) Weakly guiding optical fibres. *J. Opt. Soc. Am.*, **70**, 405–11.

Decomposition of the radiation field

Integral representation and decomposition	535
26-1 Singularities of the integrand	535
26-2 Transformation of the integration variable	537
26-3 Steepest descent path	537
Leaky-mode contribution to the radiation field	538
Space-wave contribution to the radiation field	539
References	541

The last five chapters have shown how the radiation fields of an optical waveguide can be represented in different ways. In Chapter 24, we introduced the notion of leaky modes to describe the bulk of the radiation field close to the waveguide axis at distances sufficiently far from the source of excitation. The remaining portion of the radiation field corresponds to a space wave, as defined in Eq. (24-1). The same radiation field can also be represented either by an expansion over radiation modes, as we showed in Chapter 25, or by a superposition of the fields of point dipole sources, using the Green's function techniques for waveguides described in Chapters 21 and 34. In this chapter, we show how to find the space-wave component of the radiation field by formally decomposing either representation into leaky modes and a space wave.

The radiation-mode and point-dipole representations of the radiation field are formally identical. For fibers, the former representation involves an integration over the parameter Q , as in Eq. (25-3), and the latter makes an equivalent integration over the angle θ of Fig. 21-4. The evanescent modes have a pure imaginary propagation constant β which corresponds to real values of Q . Thus, although β may have an imaginary part, Q is always real. We show that, by deforming the path of integration from the real Q -axis into the complex Q -plane, we can decompose the radiation field into: (i) a finite sum of leaky-mode fields, corresponding to contributions from discrete, complex poles; and (ii) a space-wave field, corresponding to the value of the integral along its path in the complex plane. With a view to evaluating the space-wave field asymptotically, at large distances from the source of excitation,

we use the steepest descent path for the integration path in the complex Q -plane [1].

INTEGRAL REPRESENTATION AND DECOMPOSITION

In the following discussion, we use the modal expressions of Eq. (25-3) to represent the radiation field. Since the analysis applies equally to the magnetic or electric fields, we need only consider the latter. Further, we use the weak-guidance approximation for simplicity and when we require an example, we refer to the step-profile fiber for any functional dependence. Thus

$$\mathbf{E}_{\text{rad}}(x, y, z) = \sum_j \int_0^\infty a_j(Q) \mathbf{e}_j(x, y, Q) \exp\{i\beta(Q)z\} dQ, \quad (26-1)$$

where the $a_j(Q)$ are modal amplitudes and β is related to Q inside the back cover. Integration over the range $0 \leq Q < k\rho n_{\text{cl}}$ corresponds to forward-propagating radiation modes, and over the range $k\rho n_{\text{cl}} < Q < \infty$ corresponds to evanescent radiation modes which decrease exponentially with increasing z .

When the source of excitation is specified, either as a current distribution \mathbf{J} within the fiber, or as illuminating fields \mathbf{E}_t and \mathbf{H}_t over the endface, the $a_j(Q)$ are given explicitly by Eqs. (25-12) and (25-11), respectively. In either case, we substitute the expression for $a_j(Q)$ into Eq. (26-1), and take advantage of the symmetry properties of the integrand to extend the range of integration to $Q = -\infty$. For the step-profile fiber, each cartesian, or scalar component, of the field is proportional to an integral I of the form

$$I(x, y, z) = \sum_l \int_{-\infty}^\infty \frac{f_l(x, y, Q)}{W_l(U, Q)} \exp\{i\beta(Q)z\} dQ, \quad (26-2)$$

as is clear from Sections 25-14 and 25-15. The integration is along the real Q -axis, f_l is a prescribed function which is analytic throughout the complex Q -plane with the property that $f_l \sim \exp(iQr/\rho)$ as $r \rightarrow \infty$, and $W_l(U, Q)$ is defined by Eq. (21-36b).

We have intentionally omitted the details in progressing from Eq. (26-1) to Eq. (26-2) because of their algebraic complexity. Since we only want to show the formal procedure for decomposing the radiation field, such details are counter-productive from a pedagogical point of view, and are to be found elsewhere [1-3]. Similarly, the approach from the Green's function representation to integrals of the form of Eq. (26-2) is available in Refs. [3, 4].

26-1 Singularities of the integrand

We now examine the singularities of the integrand of Eq. (26-2) in the complex Q -plane, with a view to deforming the path of integration away from the real

Q -axis. Integrals of this form are discussed in standard texts [1, 3]. The poles of the integral are the zeros of the eigenvalue equation of Eq. (24-30). Bound modes correspond to Q having zero real part and positive imaginary part, as is clear from Eq. (24-4), and correspond to the crosses on the imaginary Q -axis in Fig. 26-1 (a). Leaky modes correspond to the complex zeros of $W_l(U, Q)$, for which $Q^r > 0$ and $Q^i < 0$ according to Eq. (24-5), where superscripts r and i denote real and imaginary parts. Hence leaky-mode poles lie in the fourth quadrant of Fig. 26-1 (a).

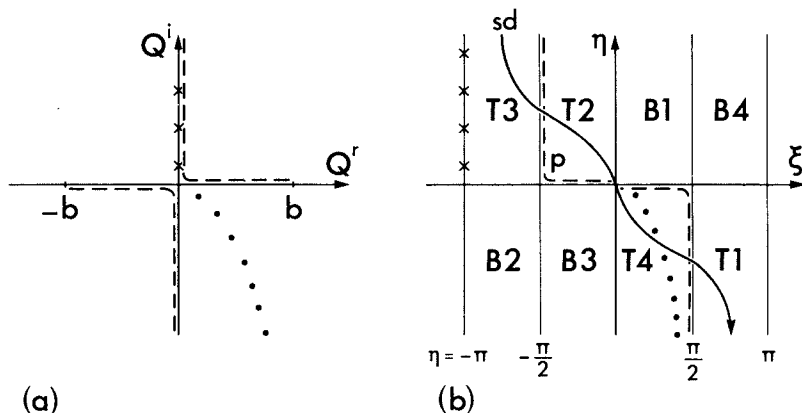


Fig. 26-1 (a) The complex Q -plane showing branch points at $\pm b$, where $b = k\rho n_{cl}$, and the dashed curves corresponding to the branch cuts. Bound- and leaky-mode poles are denoted by cross and dots, respectively. (b) The complex Ψ -plane, where the rectangular regions T1-T4 and B1-B4 correspond to the quadrants of the top and bottom Riemann sheets of the cut Q -plane in (a). The dashed curve p corresponds to the branch cuts and sd is the steepest-descent path.

Branch cuts

The relationship between the propagation constant, β , and Q is

$$\rho^2 \beta^2(Q) = (k\rho n_{cl})^2 - Q^2, \quad (26-3)$$

whence there are branch points at $\beta = 0$, or $Q = \pm k\rho n_{cl}$. These are to do with the fact that in satisfying the conditions on the radiation-mode fields as $r \rightarrow \infty$, we must specify a particular choice of signs for β and Q . The branch cuts may be chosen arbitrarily, as long as they do not cut the path of integration along the real Q -axis. In Fig. 26-1 (a), we choose the cuts so that, on the top sheet, $\beta^i \geq 0$, and on the bottom sheet, $\beta^i < 0$. Thus, forward-propagating bound and leaky modes lie on the top sheet. There are poles on the lower sheet, but these correspond to modes that grow in the direction of propagation. For a

nonabsorbing fiber, the branch cuts may be chosen to lie along the real and imaginary Q -axes. As the bound-mode poles also lie along the imaginary Q -axis, it is convenient to introduce a slight absorption into the cladding to clearly distinguish the position of poles and branch lines. The latter are then defined by

$$Q^r Q^i = k^2 \rho^2 n_{cl}^r n_{cl}^i; \quad n_{cl} = n_{cl}^r + i n_{cl}^i, \quad (26-4)$$

through equating imaginary components of Eq. (26-3).

Armed with a description of the singularities of the integrand of Eq. (26-2) in the complex Q -plane, we could now distort the path of integration from the real Q -axis. However, as can be seen from Fig. 26-1 (a), it would be necessary to evaluate integrals around branch cuts. To avoid this, we introduce a transformation that removes the branch cuts.

26-2 Transformation of the integration variable

A simple change of variable enables us to remove the branch cuts in Fig. 26-1 (a), and make the integrand in Eq. (26-2) single-valued. Hence we set

$$Q = k \rho n_{cl} \sin \Psi; \quad \beta = k n_{cl} \cos \Psi; \quad \Psi = \xi + i \eta, \quad (26-5)$$

whence the upper and lower sheets in the complex Q -plane map into the complex Ψ -plane in Fig. 26-1 (b), and the poles map into the appropriate regions. The real axis in the Q -plane becomes the contour p , comprising the ξ -axis for $-\pi/2 \leq \xi \leq \pi/2$ together with the lines $\xi = -\pi/2$, $\eta \geq 0$ and $\xi = \pi/2$, $\eta \leq 0$. Thus Eq. (26-2) becomes

$$I(x, y, z) = k \rho n_{cl} \sum_l \int_p \frac{f_l(x, y, Q, (\Psi))}{W_l(U(\Psi), Q(\Psi))} \exp(ikz n_{cl} \cos \Psi) \cos \Psi d\Psi, \quad (26-6)$$

evaluated along the contour p , where $U(\Psi) = \{V^2 + Q^2(\Psi)\}^{1/2}$. Now that the branch cuts have been removed, it is clear that, by suitably deforming the contour p , the contribution from the leaky-mode poles can be extracted from the integrals in Eq. (26-6). When this is carried out in detail, it is found that the analytical forms of the bound and leaky modes are identical. Consequently, the leaky-mode fields derived in Chapter 24 are identical to those derived here. Furthermore, the expressions for the modal amplitudes $a_j(Q)$ are exactly those discussed in Section 24-17 [2]. However, an integral along the deformed path remains. This is the space-wave contribution.

26-3 Steepest descent path

With a view to evaluating the space wave asymptotically at large distances from the source, we distort the path of integration p in Fig. 26-1(b) along the

steepest descent contour [1], denoted by sd. Thus Eq. (26-6) is replaced by

$$I(x, y, z) = \sum_j \mathcal{R}_j(x, y) \exp(i\beta_j z) + \sum_l \int_{sd} g_l(x, y, z, \Psi) d\Psi, \quad (26-7)$$

where $\mathcal{R}_j \exp(i\beta_j z)$ is the residue at *each leaky-mode pole* enclosed by the distorted path, and g_l denotes the integrand in Eq. (26-6). To determine the contribution from the steepest descent contour, we recall that g_l varies asymptotically as $\exp(i\{Qr/\rho + \beta z\})$ for $r \rightarrow \infty$. If we introduce dimensionless polar coordinates (τ, θ) which describe the radial and longitudinal displacements according to

$$r = \rho\tau \sin \theta; \quad z = \rho\tau \cos \theta; \quad \tau = \{r^2 + z^2\}^{1/2}/\rho, \quad (26-8)$$

then, recalling the definition of Ψ in Eq. (26-5), the function g_l contains a factor $\exp\{ik\rho n_{cl}\tau \cos(\Psi - \theta)\}$ as $r \rightarrow \infty$. Thus, there is a saddle point at $\Psi = \theta$, and the steepest descent path sd is found by requiring that the phase, or real part of $\tau \cos(\Psi - \theta)$ remains constant. Hence [2]

$$\cos(\xi - \theta) \cosh \eta = 1, \quad (26-9)$$

corresponding to the path shown in Fig. 26-1(b). *Only those leaky-mode poles lying between p and sd contribute to the first summation in Eq. (26-7).* If (ξ_q, η_q) are the coordinates of the q th leaky-mode pole, then the inequalities

$$\cos(\xi_q - \theta) \cosh \eta_q \leq 1; \quad \cos \xi_q \sinh \eta_q < 0, \quad (26-10)$$

must be satisfied for the pole to contribute. We now examine in more detail the leaky-mode and space-wave components.

LEAKY-MODE CONTRIBUTION TO THE RADIATION FIELD

The above decomposition complements our intuitive description of leaky modes in Chapter 24, and shows formally that *the fields of leaky modes have the same analytical forms as bound-mode fields. Each leaky mode is associated with a transverse resonance in the fiber cross-section, specified by the eigenvalue equation $W_l(U, Q) = 0$. Leaky modes only contribute to the radiation field within an angular sector of the (r, z) -plane of Fig. 26-2.* Consider the q th leaky-mode pole with coordinates (ξ_q, η_q) which lies between the steepest descent path sd and the path p in Fig. 26-1(b). In this case ξ_q and η_q satisfy the inequalities in Eq. (26-10). As r and z vary, the angle θ defined by Eq. (26-10) will vary and the steepest descent path defined by Eq. (26-9) will be continuously modified. Clearly, there is a maximum angle θ_q for which Eq. (26-10) is only just satisfied, when the leaky-mode pole lies on the steepest descent path. In this case,

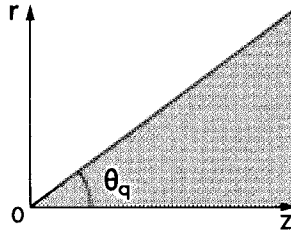


Fig. 26-2 The q th leaky mode contributes to the radiation field only within the shaded region. Outside this region the mode becomes part of the space wave.

$\cos(\xi_q - \theta_q)\cosh \eta_q = 1$, and by equating real parts in Eq. (26-5) with $\Psi = \zeta_q + i\eta_q$ and eliminating η_q , we find that for weakly leaky modes

$$\theta_q \cong \tan^{-1} \left\{ \frac{Q_q^r}{\rho \beta_q^r} \right\}, \quad (26-11)$$

where Q_q^r and β_q^r are the real parts of Q and β evaluated at the pole, and the imaginary parts have been ignored. In other words the q th leaky mode only contributes to the radiation field within the angular sector $0 \leq \theta \leq \theta_q$ in Fig. 26-2. When $\theta > \theta_q$, the leaky mode ceases to contribute to the summation in Eq. (26-7) and becomes part of the space wave. This result is consistent with our intuitive description of weakly leaky modes in Section 24-11, where we showed that the leaky-mode fields occupy an angular region bounded by a value of θ_z , given by Eq. (24-9) which is identical to the value of θ_q above.

Leaky modes play no role in representing the radiation fields at large radial distances from the fiber, i.e. as $r \rightarrow \infty$, z finite. Furthermore, as leaky modes attenuate exponentially along the fiber, their contribution to the radiation field at large distances along the fiber is negligible, i.e. as $z \rightarrow \infty$. We recall from Chapter 8 that this distance may be enormous, since leaky modes on multimode fibers can have very small attenuation rates. As we show below, except in certain rare cases, leaky modes provide a good approximation to the radiation field within and close to the core and sufficiently far from the source of excitation whenever the radiation field is significant.

SPACE-WAVE CONTRIBUTION TO THE RADIATION FIELD

There is no closed-form expression for the space wave at an arbitrary position in the (r, z) -plane. However, at large distances from the source of excitation, it can be represented by an integral along the path of steepest descent. The integral can then be evaluated asymptotically by the method of steepest

descent [1, 3, 5]. Thus at large radial distances from the fiber, when $r \rightarrow \infty$ and z is fixed, the space-wave fields vary as $r^{-1/2}$, due to the saddle point contribution along the steepest descent path [1, 3, 4]. This is the well-known far-field dependence of a radiating line source.

The space-wave contribution to the radiation field close to or within the core at large distances from the source, when $z \rightarrow \infty$ and $r \sim \rho$, is found by setting $\theta = 0$ in Eq. (26-9), so that the steepest descent path is defined by $\cos \xi \times \cosh \eta = 1$, or $\beta^r = kn_{cl}$ in Eq. (26-5). In this case, there is no saddle point contribution, but the next term in the expansion along the steepest descent path shows that the space-wave fields decay as $z^{-3/2}$ [6, 7]. Such attenuation is known to be a diffraction effect associated with the energy creeping along the interface between two dielectric media [3]. In the case of two semi-infinite media, this wave is called a *lateral wave* [3]. Thus, in the case of the fiber, the space wave is associated with an *interface wave*, as shown schematically in Fig. 26-3. It is well known that the interface wave is significantly excited only when the source S is highly directed at the complementary critical angle θ_c . Hence, apart from such exceptional cases, leaky modes describe the radiation field close to and within the core at large distances from the source, whenever the radiation field is significant.

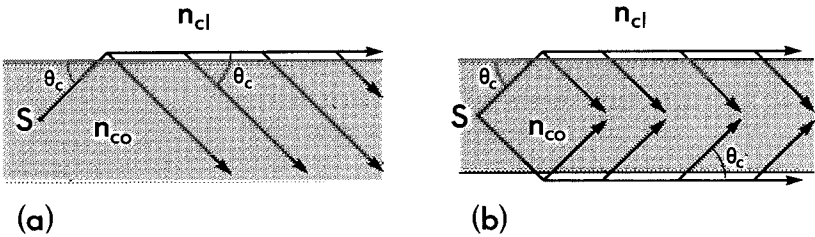


Fig. 26-3 Schematic representation of (a) a lateral wave at a planar interface between semi-infinite media of refractive indices n_{co} and $n_{cl} < n_{co}$ and (b) an interface wave on a step-profile fiber.

Summary

To summarize, at sufficiently large distances from a source within a waveguide, only the space wave, which has an $r^{-1/2}$ -dependence as $r \rightarrow \infty$, contributes to the far-field radiation. At large distances from the source and close to or within the waveguide core, the $r^{-1/2}$ -behavior is modified by the presence of the waveguide. The main contribution to the radiation then comes from energy that creeps along the interface in the form of an interface wave decaying as $z^{-3/2}$ as $z \rightarrow \infty$. However, the source must be highly directed if the interface wave is to transport significant power. In contrast, leaky modes describe

energy that is distributed throughout the core and close to it, and describe the radiation field whenever it is significant. Near to the source, both leaky modes and the space wave are significant and both must be included to correctly describe the radiation fields.

REFERENCES

1. Carrier, G. F., Krook, M. and Pearson, C. E. (1966) *Functions of a Complex Variable*, McGraw-Hill, New York.
2. Sammut, R. A. (1975) *The theory of unbound modes on circular dielectric waveguides*. Ph.D. Thesis, The Australian National University.
3. Felsen, L. B. and Marcuvitz, N. (1973) *Radiation and Scattering of Waves*, Prentice-Hall, Englewood Cliffs, N.J.
4. Collin, R. E. (1960) *Field Theory of Guided Waves*, McGraw-Hill, New York, pp. 485–506.
5. Morse, P. M. and Feshbach, H. (1953) *Methods of Theoretical Physics*, McGraw-Hill, New York.
6. Tamir, T. and Oliner, A. A. (1963) Guided complex waves. *Proc. I.E.E.*, **110**, 310–34.
7. Tamir, T. and Felsen, L. B. (1965) On lateral waves in slab configurations and their relation to other wave types. *I.E.E.E. Trans. Antennas Propag.*, **13**, 410–22.

Mode coupling

Coupled mode theory	542
27-1 Coupled mode equations	543
27-2 Weakly guiding fibers	543
27-3 <i>Example: Weak power transfer</i>	545
Strong power transfer	545
Sinusoidal perturbations	546
27-4 <i>Example: Two forward-propagating modes</i>	547
27-5 <i>Example: One forward- and one backward-propagating mode</i>	550
References	552

There are several methods for determining the fields of a perturbed waveguide, and the simplest approach depends on the form of the perturbation. If the perturbation is slight and does not vary along the waveguide, we use the perturbation methods of Chapter 18 to construct the modes of the waveguide. On the other hand, if the perturbation is arbitrary but varies slowly along the waveguide, we employ the local modes of Chapter 19. Here we are mainly concerned with *slight perturbations* which *vary arbitrarily* along a single fiber. The method of analysis is known as *coupled mode theory*, or *z-dependent perturbation theory*. Coupled mode theory is particularly useful when a slight perturbation has a large effect on the distribution of modal power, e.g. when a resonance condition causes a large exchange of power between the modes of the unperturbed fiber. Apart from such exceptional situations, slight perturbations have only a small effect on power exchange, and are adequately described by the induced current method of Chapter 22. Our main interest here is to describe resonant coupling on fibers which propagate only one or a few modes. The effects of *z-dependent perturbations* on multimode fibers are more easily described by the ray methods of Chapter 5.

COUPLED MODE THEORY

A fiber with *z-dependent nonuniformities* is no longer cylindrically symmetric and therefore cannot support individual modes of the unperturbed fiber.

Nevertheless, the fields of the perturbed fiber at position z can be described by a superposition of the fields of the complete set of bound and radiation modes of the unperturbed fiber. An individual mode of the set does not satisfy Maxwell's equations for the perturbed fiber, and hence the perturbed fields must generally be distributed between all modes of the set. This distribution varies with position along the fiber and is described by a set of *coupled mode equations*, which determine the amplitude of every mode [1-3].

27-1 Coupled mode equations

The set of coupled mode equations is obtained by substituting the modal expansion for the fields of the perturbed fiber into Maxwell's equations, and leads to an infinite set of coupled, first-order differential equations for the z -dependent amplitude of each mode. This set is a reformulation of Maxwell's equations and thus describes the fields of the perturbed fiber exactly. However there is generally no advantage in such a reformulation, since the coupled equations are intractable and have no known analytical solution. Nevertheless, when only two modes are involved, simple perturbation solutions are possible. For this to occur, it is intuitive that the modal fields of the unperturbed fiber must be a good approximation to the modal fields of the perturbed fiber, *including the perturbation region. This is possible only when the refractive-index profiles of the perturbed and unperturbed fibers differ slightly throughout the fiber*, for reasons explained in Section 18-21. Because there are few problems involving *arbitrary* profile fibers which can be solved when this condition is satisfied, we instead specialize our formulation to *weakly guiding* fibers and *ignore all polarization effects* due to the fiber structure. The inclusion of polarization effects, however slight, is complicated, as we showed in Section 18-21.

27-2 Weakly guiding fibers

The unperturbed fiber has refractive-index profile $\bar{n}(x, y)$ and the perturbed fiber has z -dependent nonuniformities described by $n(x, y, z)$. Both fibers are weakly guiding and we assume $\bar{n} \cong n \cong n_{cl}$ everywhere. For reasons given in the previous section, we ignore all polarization effects and work solely with solutions of the scalar wave equation. For convenience we assume the electric field is x -polarized and set

$$E_x(x, y, z) = \sum_{j=1}^M \{b_j(z) + b_{-j}(z)\} \Psi_j(x, y), \quad (27-1)$$

where $b_j(z)$ and $b_{-j}(z)$ contain the amplitude and phase-dependence of the forward- and backward-propagating scalar modes, respectively, M is the number of forward-propagating modes and $\Psi_j(x, y)$ is the solution of the

scalar wave equation of Eq. (13-8). In the present notation, this equation becomes

$$\{\nabla_t^2 + k^2 \bar{n}^2(x, y) - \tilde{\beta}_j^2\} \Psi_j = 0. \quad (27-2)$$

The scalar propagation constant $\tilde{\beta}_j$ is determined from the eigenvalue equation. We have ignored the continuum of radiation modes in Eq. (27-1) since we shall be considering coupling between bound modes only.

The set of coupled mode equations satisfied by the modal amplitudes can be derived directly from the scalar wave equation for the perturbed fiber, as we show in Section 33-11, or may be regarded as the weak-guidance limit of the corresponding equations for arbitrary profile fibers, derived in Section 31-11. The latter approach leads to

$$\frac{db_j}{dz} - i\tilde{\beta}_j b_j = i \sum_{l=1}^M D_{jl} \{b_l + b_{-l}\}, \quad (27-3a)$$

for the j th forward-propagating mode, and

$$\frac{db_{-j}}{dz} + i\tilde{\beta}_j b_{-j} = -i \sum_{l=1}^M D_{jl} \{b_l + b_{-l}\}, \quad (27-3b)$$

for the j th backward-propagating mode, where the D_{jl} are z -dependent coupling coefficients defined as the weak-guidance limit of Eq. (31-50a). Thus, we ignore longitudinal field components, replace $\hat{e}_{ij} \cdot \hat{e}_{il}$ by $\Psi_j \Psi_l$ and, on noting the difference in normalization between Eqs. (31-45a) and (27-1), deduce that

$$D_{jl}(z) = \frac{k}{2n_{co}} \int_{A_x} (n^2 - \bar{n}^2) \Psi_j \Psi_l dA \bigg/ \int_{A_x} \Psi_j^2 dA. \quad (27-4)$$

The fiber is assumed nonabsorbing so that the Ψ_j are real, and A_x is the infinite cross-section. In subsequent sections we examine those special situations where an analytical solution of the coupled mode equations can be found.

Power of the perturbed fields

The total bound-mode power at each position along the perturbed fiber is found by summing the power in each bound mode using the expressions in Table 13-2, page 292, with a replaced by $b_{\pm j}(z)$. Hence the power flowing in the positive z -direction is given by

$$P_{bd}(z) = \sum_{j=1}^M |b_j(z)|^2 \tilde{N}_j, \quad (27-5)$$

where \tilde{N}_j is the normalization. The power flowing in the negative z -direction is given by the same expression with $b_j(z)$ replaced by $b_{-j}(z)$.

27-3 Example: Weak power transfer

When only a small fraction of the total power of the perturbed fiber is transferred between modes, the coupled mode equations can be solved iteratively. The solution of the first iteration is then identical to the induced-current solution of Chapter 22. To demonstrate this equivalence, we assume that only the l th forward-propagating mode of the unperturbed fiber is excited at $z = 0$ of the perturbed fiber. To lowest order we ignore coupling to all other modes, whence the solution of Eq. (27-3a) is

$$b_l(z) = b_l(0) \exp(i\tilde{\beta}_l z); \quad b_j(z) = 0, \quad j \neq l. \quad (27-6)$$

where $b_l(0)$ determines the total initial power. The first order iteration is obtained by substituting Eq. (27-6) for the $b_{\pm l}$ on the right side of Eq. (27-3). This leads to

$$\frac{db_{\pm j}}{dz} \mp i\tilde{\beta}_j b_{\pm j} = \pm iD_{jl} b_l(0) \exp(i\tilde{\beta}_l z); \quad j \neq l. \quad (27-7)$$

The solution satisfying $b_{\pm j}(0) = 0, j \neq l$, is readily shown to be

$$b_{\pm j} = \pm ib_l(0) \exp(\pm i\tilde{\beta}_j z) \int_0^z D_{jl} \exp i\{\tilde{\beta}_l \mp \tilde{\beta}_j\}z \, dz; \quad j \neq l. \quad (27-8)$$

If we now solve the same problem by regarding the l th mode on the perturbed fiber as an induced current within the unperturbed fiber, we replace \mathbf{E}_l by $b_l(0)\Psi_l \exp(i\tilde{\beta}_l z)$ in Eq. (22-6) and deduce that the x -directed current has magnitude

$$J_x = i(\epsilon_0/\mu_0)^{1/2} k(\bar{n}^2 - n^2) b_l(0) \Psi_l \exp(i\tilde{\beta}_l z). \quad (27-9)$$

In Eq. (27-8) we substitute for D_{jl} from Eq. (27-4) and express the integrand in terms of J_x . If we set $b_{\pm j}(z) = a_{\pm j}(z) \exp(\pm i\tilde{\beta}_j z)$ and define \mathcal{V} to be the volume between planes at $z = 0$ and z , we obtain

$$a_{\pm j} = \mp \frac{1}{2n_{co}} \left(\frac{\mu_0}{\epsilon_0} \right)^{1/2} \int_{\mathcal{V}} \Psi_j J_x \exp(\mp i\tilde{\beta}_j z) \, d\mathcal{V} \bigg/ \int_{A_{\infty}} \Psi_j^2 \, dA. \quad (27-10)$$

With the help of Table 13-2, page 292, it is readily verified that this is the weak-guidance limit of Eq. (21-2), and, consequently, *the first iteration of the coupled mode equations is identical to the induced-current solution.*

STRONG POWER TRANSFER

Under certain resonance conditions, a small perturbation of the fiber leads to the transfer of a large proportion of total power between only two modes of the complete set of modes of the unperturbed fiber, e.g. resonant coupling on a sinusoidally deformed fiber as discussed below. The coupled mode equations describe arbitrary power transfer exactly, whereas the induced-current method of Chapter 22 is inaccurate, since it assumes only a slight transfer of total mode power. If we ignore the weak power transfer to all other modes, the set of coupled mode equations reduces to just two equations for the resonant modes.

We assume the fiber is weakly guiding and use the results of Section 27-2 to distinguish between two cases.

Two forward-propagating modes

When coupling occurs resonantly between forward-propagating modes with propagation constants $\tilde{\beta}_1, \tilde{\beta}_2$ and modal amplitudes $b_1(z), b_2(z)$, respectively, Eq. (27-3) reduces to

$$\frac{db_1}{dz} - i(\tilde{\beta}_1 + D_{11})b_1 = iD_{12}b_2, \quad (27-11a)$$

$$\frac{db_2}{dz} - i(\tilde{\beta}_2 + D_{22})b_2 = iD_{21}b_1, \quad (27-11b)$$

where the coupling coefficients are defined by Eq. (27-4). The *self-coupling coefficients* are D_{11}, D_{22} and the *cross-coupling coefficients* D_{12}, D_{21} satisfy $\tilde{N}_2 D_{21} = \tilde{N}_1 D_{12}$, in terms of the normalization of Table 13-2, page 292.

One forward- and one backward-propagating mode

Coupling between a forward- and a backward-propagating mode is described by Eq. (27-11) with b_2 replaced by b_{-2} and the sign of its derivative reversed. In the special case when the backward-propagating mode has propagation constant $-\tilde{\beta}_1$, the coupled equations become

$$\frac{db_1}{dz} - i(\tilde{\beta}_1 + D_{11})b_1 = iD_{11}b_{-1}, \quad (27-12a)$$

$$\frac{db_{-1}}{dz} + i(\tilde{\beta}_1 + D_{11})b_{-1} = -iD_{11}b_1. \quad (27-12b)$$

In more general situations where strong coupling occurs between several distinct pairs of modes, we can apply Eqs. (27-11) or (27-12) to each such pair. To illustrate the use of the coupled equations, we consider resonant coupling between pairs of modes on a sinusoidally deformed fiber.

SINUSOIDAL PERTURBATIONS

A weakly guiding fiber of refractive-index profile $\bar{n}(x, y)$ carries a sinusoidal nonuniformity of small amplitude. The profile of the perturbed fiber is assumed to have the form

$$n^2(x, y, z) = \bar{n}^2(x, y) + \delta n^2(x, y) \sin(\Omega z), \quad (27-13)$$

where $|\delta n^2| \ll \bar{n}^2$ and Ω is the spatial frequency. It is intuitive that strong coupling will take place between two bound modes of the unperturbed fiber when their propagation constants satisfy the resonant, or synchronous, condition. If we omit the \sim from scalar quantities hereon, this condition is given by

$$|\beta_1 - \beta_2| = \Omega. \quad (27-14)$$

For two forward-propagating bound modes this difference cannot exceed $k(n_{co} - n_{cl})$ on a clad fiber. Hence $\Omega \lesssim (V/\rho)(\Delta/2)^{1/2}$, which is approximately $1.2 \times 10^4 \text{ m}^{-1}$ for a fiber with $V = 2.4$, $\Delta = 0.005$ and $\rho = 10 \mu\text{m}$. We now quantify the resonant coupling for two different situations.

27-4 Example: Two forward-propagating modes

The coupled equations for the amplitudes of the two modes are given by Eq. (27-11). If we substitute Eq. (27-13) into Eq. (27-4), each coupling coefficient can be factorized according to

$$D_{ji}(z) = \bar{D}_{ji} \sin(\Omega z); \quad \bar{D}_{ji} = \frac{k}{2n_{co}} \int_{A_\infty} \delta n^2 \Psi_j \Psi_i dA \bigg/ \int_{A_\infty} \Psi_j^2 dA, \quad (27-15)$$

where \bar{D}_{ji} is a constant independent of z . In order to derive the approximate solution below, we first express the coupled equations in dimensionless form. The modal amplitudes are transformed to new functions X and Y by

$$X(z) = b_1(z) N_1^{1/2} \exp(-i\beta_1 z); \quad Y(z) = b_2(z) N_2^{1/2} \exp(-i\beta_2 z), \quad (27-16a)$$

where N_1 and N_2 are the mode normalizations, and a new variable θ is introduced, which satisfies

$$\theta = \kappa z/2; \quad \kappa = (\bar{D}_{12} \bar{D}_{21})^{1/2}. \quad (27-16b)$$

Dimensionless parameters are then defined by

$$\sigma = \frac{2}{\kappa}(\Omega - \beta_1 + \beta_2); \quad \tau = \frac{2}{\kappa}(\beta_1 - \beta_2); \quad s_1 = \frac{\bar{D}_{11}}{\kappa}; \quad s_2 = \frac{\bar{D}_{22}}{\kappa}. \quad (27-16c)$$

We substitute Eqs. (27-15) and (27-16) into Eq. (27-11) and obtain

$$\begin{aligned} \frac{dX}{d\theta} &= \{\exp(i\sigma\theta) - \exp(-i[\sigma + 2\tau]\theta)\}Y \\ &\quad + s_1 \{\exp(i[\sigma + \tau]\theta) - \exp(-i[\sigma + \tau]\theta)\}X, \end{aligned} \quad (27-17a)$$

$$\begin{aligned} \frac{dY}{d\theta} &= \{\exp(i[\sigma + 2\tau]\theta) - \exp(-i\sigma\theta)\}X \\ &\quad + s_2 \{\exp(i[\sigma + \tau]\theta) - \exp(-i[\sigma + \tau]\theta)\}Y. \end{aligned} \quad (27-17b)$$

Although these equations do not have a simple analytical solution, we can obtain an asymptotic solution for large spatial frequencies [4]. At low frequencies, when the sinusoid varies slowly along the fiber, we can use the local-mode description of Chapters 19 and 28.

Asymptotic solution

Since the amplitude of the sinusoid is small, it is clear from Eqs. (27-15) and (27-16) that the length scale $1/\bar{D}_{12}$ over which significant power coupling can take place between modes is large compared with the beat length $2\pi/|\beta_1 - \beta_2| \cong 2\pi/\Omega$, whence we deduce from Eq. (27-16) that $|\tau| \gg 1$ and $|\tau| \gg |\sigma|$. Thus the exponential terms involving $\sigma + \tau$ and $\sigma + 2\tau$ in Eq. (27-17) oscillate more rapidly than the corresponding terms in σ alone. Accordingly the solution consists of a slow-scale variation in θ , which is independent of τ , on which is superposed a fast-scale variation in θ . The amplitude of the fast-scale corrections is of order $1/\tau$, as may be deduced by integrating either equation by parts and ordering the θ dependence. If subscript 0 denotes the slow-scale solution, then [4]

$$\frac{dX_0}{d\theta} = Y_0 \exp(i\sigma\theta); \quad \frac{dY_0}{d\theta} = -X_0 \exp(-i\sigma\theta). \quad (27-18)$$

If the first mode has unit power and the second mode zero power at $z = 0$, then the solution satisfying $X_0 = 1, Y_0 = 0$ at $\theta = 0$ is readily shown to be

$$X_0 = \left\{ \cos\left(\frac{\theta}{F}\right) - \frac{i}{2} \sigma F \sin\left(\frac{\theta}{F}\right) \right\} \exp(i\sigma\theta/2), \quad (27-19a)$$

$$Y_0 = -F \sin\left(\frac{\theta}{F}\right) \exp(-i\sigma\theta/2); \quad F = 1 / \left\{ 1 + \frac{\sigma^2}{4} \right\}^{1/2}. \quad (27-19b)$$

The corresponding fields follow from Eqs. (27-1) and (27-16).

Power distribution along the fiber

The power in each mode follows from Eqs. (27-5) and (27-16) as

$$P_1(z) = 1 - F^2 \sin^2(\theta/F); \quad P_2(z) = F^2 \sin^2(\theta/F), \quad (27-20)$$

which conserves the initial power along the fiber. Thus the maximum power transfer, F^2 , is very sensitive to the value of σ in Eq. (27-19b), which in turn is proportional to the difference between Ω and $\beta_1 - \beta_2$ in Eq. (27-16c). Plots of $P_2(z)$ as a function of θ for various values of σ are given by the curves in Fig. 27-1(a). At resonance $\sigma = 0, F = 1$ and complete power transfer occurs, whereas at $\sigma = 2$ and $\sigma = 5$ only 50% and 14% power transfer occurs, respectively. It also follows from Eq. (27-20) that the distance over which maximum power transfer occurs decreases with decreasing F . Finally, when the maximum power transfer is small, the solution to the problem may require the involvement of other modes, in which case the weak power transfer solution of Section 27-3 is appropriate.

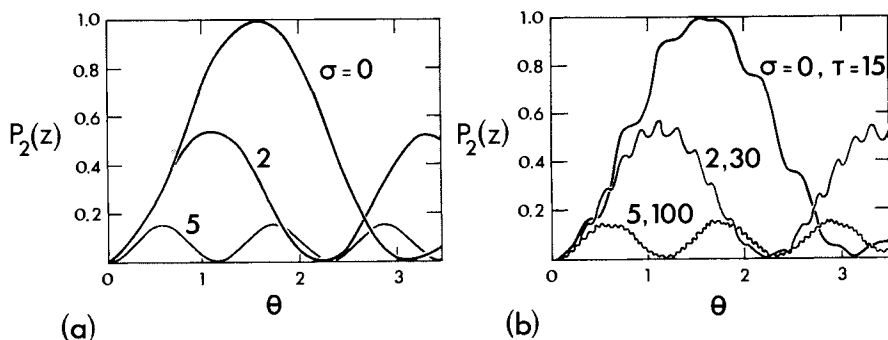


Fig. 27-1 The power $P_2(z)$ excited in the second mode due to resonant coupling with the first mode, which carries unit initial power on a fiber with a slight sinusoidal nonuniformity. The slow-scale solution (a) is given by Eq. (27-20) in terms of θ of Eq. (27-16b), and the fast-scale solution (b) is given by Eq. (27-25).

Higher-order corrections

The corrections to the slow-scale solution of the coupled mode equations, due to fast-scale variations in τ , can be included by iterating Eq. (27-17). To determine the first correction, we set

$$X = X_0 + X_1; \quad Y = Y_0 + Y_1, \quad (27-21)$$

where $|X_1| \ll |X_0|$, $|Y_1| \ll |Y_0|$, and substitute into Eq. (27-17). The slow-scale equations of Eq. (27-18) are subtracted out and we set $X = X_0, Y = Y_0$ in the remaining terms on the right side. Hence

$$\frac{dX_1}{d\theta} = -Y_0 \exp \{ i(\sigma + 2\tau)\theta \} + 2is_1 X_0 \sin(\sigma + \tau)\theta, \quad (27-22a)$$

$$\frac{dY_1}{d\theta} = X_0 \exp \{ i(\sigma + 2\tau)\theta \} + 2is_2 Y_0 \sin(\sigma + \tau)\theta. \quad (27-22b)$$

The slow-scale solutions are held fixed during integration, and, consequently, the solution satisfying $X_1 = Y_1 = 0$ at $z = \theta = 0$ is [4]

$$X_1 = -\frac{iY_0}{\sigma + 2\tau} \exp \{ -i(\sigma + 2\tau)\theta \} + \frac{2is_1 X_0}{\sigma + \tau} \{ 1 - \cos(\sigma + \tau)\theta \}, \quad (27-23a)$$

$$Y_1 = \frac{iX_0}{\sigma + 2\tau} \{ 1 - \exp \{ i[\sigma + 2\tau]\theta \} \} - \frac{2is_2 Y_0}{\sigma + \tau} \cos(\sigma + \tau)\theta, \quad (27-23b)$$

where X_0 and Y_0 are given by Eq. (27-19). Within the present approximation, the power

in each mode is given by

$$P_1(z) = |X_0|^2 + 2 \operatorname{Re}(X_0 X_1^*); \quad P_2(z) = |Y_0|^2 + 2 \operatorname{Re}(Y_0 Y_1^*), \quad (27-24)$$

where Re and $*$ denote real part and complex conjugate, respectively. If we substitute Eqs. (27-19) and (27-23) into Eq. (27-24), the self-coupling terms denoted by the real parameters s_1 and s_2 do not contribute to modal power. Thus the power in the second mode is [4]

$$P_2(z) = F^2 \sin^2(\theta/F) \left\{ 1 - \frac{2}{\tau} \sin(\tau + \sigma/2)\theta \times \left[\sigma \sin(\tau + 3\sigma/2)\theta + \frac{\cot(\theta/F)}{F} \cos(\tau + 3\sigma/2)\theta \right] \right\} \quad (27-25)$$

assuming $|\tau| \gg |\sigma|$. Plots of $P_2(z)$ are given by the curves in Fig. 27-1(b), which show the higher frequency oscillation about the slow-scale curves. There is negligible difference between the solid curves and the exact numerical solution of Eq. (27-17).

27-5 Example: One forward- and one backward-propagating mode

Coupling, in the special case of resonance between a forward-propagating mode and the corresponding backward-propagating mode, is described by Eq. (27-12). We substitute the factorized coupling coefficient of Eq. (27-15) and make analogous transformations to Eq. (27-16) defined by

$$X(z) = b_1(z) N^{1/2} \exp(-i\beta_1 z); \quad Y(z) = b_{-1}(z) N^{1/2} \exp(i\beta_1 z), \quad (27-26a)$$

$$\theta = \frac{\bar{D}_{11}}{2} z; \quad \sigma = \frac{2}{\bar{D}_{11}} (\Omega - 2\beta_1); \quad \tau = \frac{4\beta_1}{\bar{D}_{11}}, \quad (27-26b)$$

to obtain the coupled equations in the dimensionless form

$$\begin{aligned} \frac{dX}{d\theta} &= \{ \exp(i\sigma\theta) - \exp(-i[\sigma + 2\tau]\theta) \} Y \\ &\quad + \{ \exp(i[\sigma + \tau]\theta) - \exp(-i[\sigma + \tau]\theta) \} X, \quad (27-27a) \\ \frac{dY}{d\theta} &= \{ \exp(-i\sigma\theta) - \exp(i[\sigma + 2\tau]\theta) \} X \\ &\quad - \{ \exp(i[\sigma + \tau]\theta) - \exp(-i[\sigma + \tau]\theta) \} Y. \quad (27-27b) \end{aligned}$$

By paralleling the discussion of the previous section we have $|\tau| \gg 1$ and $|\tau| \gg |\sigma|$, whence the slow-scale equations are

$$\frac{dX_0}{d\theta} = Y_0 \exp(i\sigma\theta); \quad \frac{dY_0}{d\theta} = X_0 \exp(-i\sigma\theta). \quad (27-28)$$

The solution at or close to resonance $\sigma = 0$ involves functions which grow or decay

exponentially with θ . Consequently, the only solution which is bound as $\theta \rightarrow \infty$ and satisfies $X_0 = 1$ at $\theta = 0$ is

$$X_0 = \exp(i\sigma\theta/2) \exp(-\kappa\theta); \quad Y_0 = \frac{i\sigma - 2\kappa}{2} \exp(-i\sigma\theta/2) \exp(-\kappa\theta), \quad (27-29)$$

where $\kappa = (1 - \sigma^2/4)^{1/2}$ and $|\sigma| < 2$. We then deduce from Eqs. (27-5) and (27-26) that both modes carry the same power

$$P_1(z) = P_{-1}(z) = \exp(-\kappa \bar{D}_{11} z); \quad 0 \leq z < \infty, \quad (27-30)$$

propagating in opposite directions. This result is consistent with the physical description of the situation. The amplitude of the forward-propagating mode decreases with increasing z as power is continually lost to the backward-propagating mode. Consequently, as the backward-propagating mode travels in the decreasing z -direction it picks up all the power lost by the forward-propagating mode, and its power must increase as z decreases. The rate of power transfer between the two modes depends on σ and has maximum value $\bar{D}_{11} \exp(-\bar{D}_{11} z)$ at resonance $\sigma = 0$. As $|\sigma|$ increases this rate decreases rapidly until at $|\sigma| = 2$ it might appear that power transfer ceases since $\kappa = 0$. However, it is then necessary to include the fast-scale corrections to determine the actual power transfer. For $|\sigma| > 2$ the solutions for X_0 and Y_0 are given by Eq. (27-19) with $F = (\sigma^2/4 - 1)^{1/2}$.

Weak power transfer

In Section 22-9, we determined the power scattered into the backward-propagating fundamental mode when a forward-propagating fundamental mode is incident on the sinusoidally perturbed interface of a step-profile, weakly guiding fiber of length $2L$. The solution given by Eq. (22-29) is only valid when the power loss from the forward-propagating mode is slight. The solution in Eq. (27-29) is also inappropriate since it assumes an infinitely long fiber. If we formulate the problem of Section 22-9 in the notation of this section, we require a solution of Eq. (27-28) satisfying $X_0 = 1$ at $z = \theta = 0$ and $Y_0 = 0$ at $z = 2L$, or $\theta = \theta_L = \bar{D}_{11} L$. The solution satisfying the resonant condition is readily shown to be

$$X_0 = \cosh \theta - \sinh \theta \tanh \theta_L; \quad Y_0 = \sinh \theta - \cosh \theta \tanh \theta_L, \quad (27-31)$$

which reduces to the solution in Eq. (27-29) when $L \rightarrow \infty$. For weak power transfer, $\theta_L \ll 1$, in which case the amplitude of the backward-propagating mode at $z = \theta = 0$ is proportional to $-\theta_L$. If we substitute for δn^2 from Eqs. (22-28) and (27-13) into the definition of \bar{D}_{11} in Eq. (27-15) and recall that $\Psi_1 = 1$ on $r = \rho$ and the integral in the denominator follows from Table 14-6, page 319, it is straightforward to show that the ratio of a_{-1} to \bar{a}_1 in Eq. (22-29) is identical to $-\theta_L$.

REFERENCES

1. Snyder, A. W. (1972) Coupled-mode theory for optical fibers. *J. Opt. Soc. Am.*, **62**, 1267–77.
2. Marcuse, D. (1973) Coupled mode theory for round optical fibers. *Bell Syst. Tech. J.*, **52**, 817–18.
3. Marcuse, D. (1974) *Theory of Dielectric Optical Waveguides*, Academic Press, New York, p. 101.
4. Snyder, A. W. and Davies, O. J. (1970) Asymptotic solution of coupled mode equations for sinusoidal coupling. *Proc. I.E.E.E.*, **58**, 168–9.

Local-mode coupling

Coupled local-mode theory	553
28-1 Coupled local-mode equations	554
28-2 Weak power transfer	556
28-3 Slow variation condition	556
28-4 <i>Example: Step-profile fiber of nonuniform radius</i>	557
28-5 <i>Example: Twisted elliptical fiber</i>	558
 Local radiation modes	 560
28-6 <i>Example: Step-profile taper</i>	562
 Composite waveguides	 563
28-7 <i>Example: Tapered couplers</i>	564
28-8 <i>Example: Identical fibers</i>	565
 References	 566

In the previous chapter we introduced coupled mode theory to describe propagation on waveguides with *slight* perturbations which vary *arbitrarily* with distance along the waveguide. Here we consider waveguides with *arbitrarily* large nonuniformities, but with the proviso that they vary *slowly* along the length of the waveguide. We introduced the concept of local modes for studying such waveguides in Chapter 19. The use of local modes is an excellent approximation provided any change from cylindrical symmetry occurs sufficiently slowly. Even so, a local mode is not an exact solution of Maxwell's equations and, as it propagates, small amounts of power are lost by coupling to the radiation field or to other local modes. The principal purpose of this chapter is to show how to determine this loss.

However, before we begin, we emphasize that coupled local-mode theory is particularly useful in situations when there is a large transfer of power between local modes. Apart from such exceptional situations, power transfer is slight and the induced-current methods of Sections 22-10 and 22-11 are sufficient.

COUPLED LOCAL-MODE THEORY

The exact fields of an arbitrarily perturbed waveguide are expressible as a superposition of local-mode fields and the radiation field, and, provided the

waveguide is slowly varying, the power in each local mode remains virtually constant as the mode propagates. Nevertheless, there will be an exchange of power, however slight, between each local mode and the radiation field, because an individual local mode is not an exact solution of Maxwell's equations. This is described by a set of *coupled local-mode equations*, which determine the amplitude of each local and radiation mode.

28-1 Coupled local-mode equations

The expansion of the exact fields is described by

$$\mathbf{E}_t(x, y, z) = \sum_j \{b_j(z) + b_{-j}(z)\} \hat{\mathbf{e}}_{tj}(x, y, \beta_j(z)), \quad (28-1a)$$

$$\mathbf{H}_t(x, y, z) = \sum_j \{b_j(z) - b_{-j}(z)\} \hat{\mathbf{h}}_{tj}(x, y, \beta_j(z)), \quad (28-1b)$$

where subscript t denotes transverse component, $\hat{\cdot}$ denotes orthonormality and the $b_j(z)$ describe the modal amplitude and phase. The local-mode propagation constant, and hence the local-mode fields, vary with distance z along the fiber according to the prescription of Section 19-1. Negative subscripts denote backward-propagating modes, and the summation implicitly includes radiation modes.

There are essentially two methods for deriving the equations satisfied by the $b_j(z)$. The more physical approach is to divide the fiber into a series of differential sections, one of which is shown in Fig. 31-2, and then consider the change in each modal amplitude across each section [1]. Details are given in Section 31-16. Alternatively, we substitute Eq. (28-1) into Maxwell's equations and use the orthogonality conditions for local modes to derive the set of coupled local-mode equations [2, 3]. This approach is presented in Section 31-14, and leads to Eq. (31-65)

$$\frac{db_j}{dz} - i\beta_j b_j = \sum_l \{C_{jl}b_l + C_{j-l}b_{-l}\}, \quad (28-2a)$$

$$\frac{db_{-j}}{dz} + i\beta_j b_{-j} = -\sum_l \{C_{-jl}b_l + C_{-j-l}b_{-l}\}, \quad (28-2b)$$

for the j th forward- and backward-propagating local modes, respectively. The C_{jl} are coupling coefficients defined by

$$C_{jl} = \frac{1}{4} \int_{A_x} \left\{ \hat{\mathbf{h}}_j \times \frac{\partial \hat{\mathbf{e}}_l}{\partial z} - \hat{\mathbf{e}}_j \times \frac{\partial \hat{\mathbf{h}}_l}{\partial z} \right\} \cdot \hat{\mathbf{z}} dA, \quad j \neq l; \quad C_{jj} = 0, \quad (28-3)$$

where A_∞ is the infinite cross-section and \hat{z} is the unit vector parallel to the waveguide axis. When $l \rightarrow -l$ or $j \rightarrow -j$, we apply the field symmetries of Eq. (11-7). We are reminded that β_j , \hat{e}_j , \hat{h}_j and C_{jl} depend on z . The coupling coefficients can be expressed in an alternative form, as we show in Section 31-15 [4], leading to Eq. (31-70). Thus

$$C_{jl} = \frac{k}{4} \left(\frac{\epsilon_0}{\mu_0} \right)^{1/2} \frac{1}{\beta_j - \beta_l} \int_{A_x} \hat{e}_j^* \cdot \hat{e}_l \frac{\partial n^2}{\partial z} dA, \quad j \neq l; \quad C_{jj} = 0, \quad (28-4)$$

where * denotes complex conjugate and parameters are defined inside the back cover.

In Section 27-1 we showed that in applying the coupled mode equations there is an intrinsic restriction to weakly guiding waveguides. *This restriction does not occur in the application of the coupled local-mode equations.* A general solution of the coupled local-mode equations is derived for weak power transfer in the following section, and the radiation modes are discussed later in the chapter.

Total guided power

The local-mode fields are orthonormal, and consequently the total guided power propagating in the positive z -direction follows from Eqs. (11-16), (11-27) and (28-1) as

$$P_{\text{gd}}(z) = \sum_{j=1}^M |b_j(z)|^2, \quad (28-5)$$

where M is the number of forward-propagating local bound modes at position z . Replacing b_j by b_{-j} gives the guided power propagating in the negative z -direction.

Weakly guiding waveguides

In the special case of weakly guiding waveguides, when the variation in profile over any cross-sectional plane is slight, we can ignore all polarization properties of the waveguide, and express the fields and coupling coefficients in terms of solutions of the scalar wave equation. This is equivalent to ignoring the longitudinal components of the fields and expressing \hat{h}_{lj} in terms of \hat{e}_{lj} through Eq. (13-1). Alternatively, the coupled local-mode equations and the two forms of the coupling coefficients can be derived directly from the scalar wave equation, as we demonstrate in Sections 33-12 and 33-13.

28-2 Weak power transfer

The coupled local-mode equations can be solved approximately when only a small fraction of the total power of the perturbed waveguide is transferred between modes. We show that the first-order solution is identical to the induced-current solution of Chapter 22. For convenience we assume that only the l th forward-propagating local mode is excited at $z = 0$. To lowest order we ignore coupling to all other modes. The solution of Eq. (28-2) is then

$$b_l(z) = b_l(0) \exp \left\{ i \int_0^z \beta_l(z) dz \right\}; \quad b_j(z) = 0, \quad j \neq l. \quad (28-6)$$

The equation for the first-order solution is obtained by substituting Eq. (28-6) into the right side of Eq. (28-2), whence

$$\frac{db_{\pm j}(z)}{dz} \pm i\beta_j b_{\pm j}(z) = \pm b_l(0) C_{\pm jl}(z) \exp \left\{ i \int_0^z \beta_l(z) dz \right\}, \quad (28-7)$$

for $j \neq l$. The solution satisfying the initial condition $b_{\pm j}(0) = 0$ is

$$b_{\pm j}(z) = \pm b_l(0) \left(\exp \left\{ \pm i \int_0^z \beta_j(z) dz \right\} \right) \int_0^z C_{\pm jl}(z) \exp(i\overline{\delta\beta}z) dz, \quad (28-8a)$$

where $\overline{\delta\beta}$ is the average value of the accumulated difference in propagation constants along the waveguide, and is defined by

$$\overline{\delta\beta}(z) = \frac{1}{z} \int_0^z \{ \beta_l(z) \mp \beta_j(z) \} dz. \quad (28-8b)$$

If we substitute the coupling coefficient of Eq. (28-4) into Eq. (28-8a) and assume $b_l(0) = 1$, the resulting expression for $b_{\pm j}$ is identical with that of Eq. (22-35). The latter was derived using induced currents to represent the slight mismatch between the local-mode fields and the exact fields of the waveguide. Thus we deduce *the equivalence of the first iteration of the coupled local-mode equation and the induced-current representation.*

28-3 Slow variation condition

An important application of the solution of the coupled local-mode equations for weak power transfer determines how slowly a waveguide must vary along its length in order that an individual local mode can propagate with negligible variation in its power. If we assume the l th local mode alone is initially excited with unit power, i.e. $b_l(0) = 1$, then the fraction of power excited in the j th

forward-propagating mode follows from Eqs. (28-5) and (28-8a) as

$$P_j(z) = \left(\int_0^z C_{jl}(z) \exp(i\delta\beta z) dz \right) \left(\int_0^z C_{jl}(z) \exp(-i\delta\beta z) dz \right); \quad j \neq l, \quad (28-9)$$

where C_{jl} is real if we adopt the convention of Eq. (11-8). Since the waveguide is slowly varying, it follows from Eqs. (28-4) and (28-8b) that C_{jl} and $\delta\beta$ are also slowly varying, but the exponential term in Eq. (28-9) oscillates rapidly. Consequently, we integrate Eq. (28-9) by parts and drop the term involving $(dC_{jl}/dz)/\delta\beta$ [4]. On rearranging the solution, we have for $j \neq l$

$$P_j(z) \cong F^2(z) + F^2(0) - 2F(z)F(0) \cos(\delta\beta z); \quad F(z) = C_{jl}(z)/\delta\beta, \quad (28-10)$$

where F is proportional to the ratio of the cross-coupling length $1/C_{jl}$ and the average beat length $2\pi/\delta\beta$. Thus a local mode propagates with negligible power loss provided $|F(z)| \ll 1$ everywhere along the waveguide, i.e. *provided the coupling length is large compared to the local beat length*. In Eq. (28-4), C_{jl} is most sensitive to the change in profile with z , whence we conclude that the requirement $|F(z)| \ll 1$ is equivalent to our intuitive criterion of Section 19-2, i.e. the nonuniformity must change over a distance that is large compared to the local beat length.

The fraction of power coupled to the backward-propagating modes is given by Eq. (28-10), provided we replace β_j by $-\beta_j$ in Eq. (28-8b) and \hat{e}_j by \hat{e}_{-j} in Eq. (28-4). For weakly guiding waveguides, when the longitudinal fields may be neglected, it is clear that power exciting these modes is negligible compared to the power coupled into the forward-propagating modes. Similar conclusions apply for coupling to the radiation modes, which are discussed later in this chapter.

In general, the local-mode propagation constants are contained implicitly within the local eigenvalue equation, and their precise values must be obtained numerically. However, analytical expressions can be derived for the coupling coefficients, as we show in the example below.

28-4 Example: Step-profile fiber of nonuniform radius

The refractive-index profile $n^2(r, z)$ for a step-profile fiber with nonuniform core radius $\rho(z)$ is everywhere expressible as

$$n^2(r, z) = n_{co}^2 \{1 - 2\Delta H(r - \rho(z))\}, \quad (28-11)$$

where the Heaviside step function satisfies $H(x) = 1$ if $x > 0$ and $H(x) = 0$ otherwise. Consequently the coupling coefficient of Eq. (28-4) vanishes everywhere except on the interface. We distinguish between two situations.

Weakly guiding fiber

In this situation the longitudinal field components are ignored and the transverse components of the electric field are continuous across the interface. The derivative of the profile in the integrand of Eq. (28-4) is given in terms of the Dirac delta function by

$$\frac{\partial n^2}{\partial z} = 2n_{co}^2 \Delta \frac{d\rho}{dz} \delta(r - \rho(z)). \quad (28-12)$$

Consequently the coupling coefficient is given by [4]

$$C_{ji} = \frac{k}{4} \left(\frac{\epsilon_0}{\mu_0} \right)^{1/2} \frac{n_{co}^2 \Delta}{\beta_j - \beta_i} \frac{d\rho^2}{dz} \int_0^{2\pi} (\hat{\mathbf{e}}_{ij} \cdot \hat{\mathbf{e}}_{il})_{r=\rho(z)} d\phi. \quad (28-13)$$

Expressions for $\hat{\mathbf{e}}_j$ and $\hat{\mathbf{e}}_{il}$ are deduced from Tables 14-1, page 304, and 14-6, page 319, by replacing ρ with $\rho(z)$. The azimuthal integral involves products of trigonometrical functions and consequently only coupling between modes of the same order will occur. If we substitute the resulting expression into Eq. (28-10) and require $|F| \ll 1$, it is straightforward to show that the intuitive criterion of Eq. (19-7) for the validity of the local-mode description is modified by factors which take into account the fiber profile and accumulated changes along the fiber.

Arbitrary profile height

When Δ is arbitrary, the determination of C_{ji} is complicated by the fact that the radial components of $\hat{\mathbf{e}}_j$ and $\hat{\mathbf{e}}_i$ are discontinuous across the interface. We circumvent this difficulty by recognizing that $n^2 \hat{e}_{rj}$ and $n^2 \hat{e}_{ri}$ are continuous across the interface, and rearrange the integrand in Eq. (28-4) as

$$\hat{\mathbf{e}}_j^* \cdot \hat{\mathbf{e}}_i \frac{\partial n^2}{\partial z} = (\hat{e}_{\phi j}^* \hat{e}_{\phi i} + \hat{e}_{zj}^* \hat{e}_{zi}) \frac{\partial n^2}{\partial z} - (n^2 \hat{e}_{rj}^*) (n^2 \hat{e}_{ri}) \frac{\partial}{\partial z} \left(\frac{1}{n^2} \right), \quad (28-14a)$$

where the z -derivative in the second expression on the right is obtained in an analogous manner to Eq. (28-12) by setting

$$\frac{1}{n^2} = \frac{1}{n_{co}^2} \left\{ 1 + \frac{2\Delta}{1 - 2\Delta} H(r - \rho(z)) \right\}. \quad (28-14b)$$

Consequently C_{ji} is given by Eq. (28-13) with the integrand replaced by

$$\left\{ \hat{e}_{\phi j}^* \hat{e}_{\phi i} + \hat{e}_{zj}^* \hat{e}_{zi} + \left(\frac{n^2}{n_{co}^2} \hat{e}_{rj}^* \right) \left(\frac{n^2}{n_{ci}^2} \hat{e}_{ri} \right) \right\}_{r=\rho(z)} \quad (28-15)$$

Expressions for $\hat{\mathbf{e}}_j$ and $\hat{\mathbf{e}}_i$ are deduced from Tables 12-3, page 250, and 12-5, page 256, with ρ replaced by $\rho(z)$. The azimuthal integral involves products of trigonometrical functions and coupling only occurs between modes with the same order v .

28-5 Example: Twisted elliptical fiber

Consider a weakly guiding fiber whose elliptical cross-section rotates along its length,

as shown in Fig. 19-2. The local-mode description of the two fundamental modes was given in Section 19-4. We assume that the x - and y -polarized modes have power 1 and 0, respectively, at $z = 0$. The transverse electric fields $\hat{\mathbf{e}}_{t1}$ and $\hat{\mathbf{e}}_{t2}$ are parallel to the major and minor axes, respectively, and the common scalar propagation constant is β .

Weak power transfer

When the rate of twisting is sufficiently small, there is only slight transfer of power from the x - to the y -polarized mode. This can be calculated using the analysis of Section 28-3. We first evaluate the coupling coefficient C_{12} using Eq. (28-3). Relative to unit vectors $\hat{\mathbf{x}}$ and $\hat{\mathbf{y}}$ parallel to the rotating x - and y -axes, the nonzero field components for the two modes are given by

$$\hat{\mathbf{e}}_{t1} = \frac{\Psi}{N^{1/2}} \hat{\mathbf{x}}; \quad \hat{\mathbf{e}}_{t2} = \frac{\Psi}{N^{1/2}} \hat{\mathbf{y}}; \quad \hat{\mathbf{h}}_{ti} = \left(\frac{\epsilon_0}{\mu_0} \right)^{1/2} n_{co} \hat{\mathbf{z}} \times \hat{\mathbf{e}}_{ti}. \quad (28-16)$$

where Ψ is the fundamental solution of the scalar wave equation, N is the normalization defined in Table 13-2, page 292, $\hat{\mathbf{z}}$ is the unit vector parallel to the fiber axis and remaining parameters are defined at the back of the book. The next step is to relate the directions of the rotating axes to the fixed axes. Thus if \mathbf{x}_0 and \mathbf{y}_0 are unit vectors parallel to the x_0 - and y_0 -axes in Fig. 19-2, then

$$\hat{\mathbf{x}} = \hat{\mathbf{x}}_0 \cos \theta(z) + \hat{\mathbf{y}}_0 \sin \theta(z); \quad \hat{\mathbf{y}} = -\hat{\mathbf{x}}_0 \sin \theta(z) + \hat{\mathbf{y}}_0 \cos \theta(z), \quad (28-17)$$

where the angle of twist $\theta(z)$ is related to the rate of twist $\tau(z)$ by

$$\theta(z) = \int_0^z \tau(z) dz. \quad (28-18)$$

We substitute Eq. (28-16) into Eq. (28-3), differentiate Eq. (28-17) and recall the definition of N to obtain successively

$$C_{12}(z) = -\frac{n_{co}}{2} \left(\frac{\epsilon_0}{\mu_0} \right)^{1/2} \int_{A_x} \hat{\mathbf{e}}_{t1} \cdot \hat{\mathbf{p}} \frac{\partial \hat{\mathbf{e}}_{t2}}{\partial z} dA = \frac{n_{co}}{2} \left(\frac{\epsilon_0}{\mu_0} \right)^{1/2} \frac{\tau}{N} \int_{A_x} \Psi^2 dA = \tau(z). \quad (28-19)$$

In order to determine the ratio F of Eq. (28-10), we need the difference between the propagation constants $\beta_x = \beta + \delta\beta_x$ and $\beta_y = \beta + \delta\beta_y$ for the two modes, as these take into account polarization properties of the elliptical fiber. Consequently, the local, or fundamental, modes of the twisted fiber propagate with negligible exchange of power provided $|F| \ll 1$. Since the propagation constants are independent of z , this is equivalent to requiring that the length over which the fibers twist through 2π is large compared to the beat length, or

$$|\tau(z)| \ll |\beta_x - \beta_y|, \quad (28-20)$$

which, apart from the factor of 2π is identical to the intuitive criterion of Eq. (19-9). For a step-profile fiber of small eccentricity, the difference $\beta_x - \beta_y$ is given by Eq. (18-25).

Strong power transfer

If the rate of twist is no longer small, there will be significant coupling from the x -polarized local mode to the y -polarized local mode and to the radiation field, assuming the fiber is single moded. The solution in this case requires the complete set of coupled local-mode equations, including the radiation modes, and is generally intractable. However, one situation in which the problem becomes tractable arises when resonant coupling occurs between the two local modes. The length scale for significant power transfer from one mode to the other is the half beat length $\pi/|\beta_x - \beta_y|$. This corresponds to a rotation of the fiber through $\pi/2$, for which the length scale is $\pi/2\tau$. Accordingly the resonance condition is

$$|2\tau| = |\beta_x - \beta_y|. \quad (28-21)$$

When this condition is satisfied, we can neglect coupling between the local modes and the radiation field, and the coupled local-mode equations of Eq. (28-2a) reduce to [5]

$$\frac{db_1}{dz} - i\beta_x b_1 = \tau b_2; \quad \frac{db_2}{dz} - i\beta_y b_2 = -\tau b_1 \quad (28-22)$$

using the coupling coefficient of Eq. (28-19), where τ , β_x and β_y are independent of z . If we eliminate b_1 or b_2 between the two equations, the solution satisfying $b_1 = 1$, $b_2 = 0$ at $z = 0$ is readily shown to be

$$b_1(z) = \left\{ \cos\left(\frac{\tau}{F}z\right) + i\frac{\beta_x - \beta_y}{2\tau} F \sin\left(\frac{\tau}{F}z\right) \right\} \exp\left\{ i\frac{\beta_x + \beta_y}{2} z \right\}, \quad (28-23a)$$

$$b_2(z) = -F \sin\left(\frac{\tau}{F}z\right) \exp\left\{ i\frac{\beta_x + \beta_y}{2} z \right\}, \quad (28-23b)$$

$$F = 1 \left/ \left\{ 1 + \frac{(\beta_x - \beta_y)^2}{4\tau^2} \right\}^{1/2} \right. \quad (28-23c)$$

The corresponding power in each mode follows from Eq. (28-5) as

$$P_1(z) = 1 - F^2 \sin^2(\tau z/F); \quad P_2(z) = F^2 \sin^2(\tau z/F). \quad (28-24)$$

Thus a fraction F^2 of the total power is exchanged between the two modes and the beat length is $2\pi F/\tau$. At the resonance of Eq. (28-21), $F^2 = 1/2$, and 50 per cent power transfer occurs. We emphasize that the solution, Eq. (28-23), is only accurate at, or very close to, resonance. This situation minimizes the power loss to radiation and to the backward-propagating fundamental mode.

LOCAL RADIATION MODES

The coupled local-mode equations discussed in Section 28-1 implicitly include coupling to the radiation field. In keeping with the concept of local modes,

which describe the flow of guided power along the slowly varying waveguide, we define a set of *local radiation modes* to describe the radiation field and thus the power radiated from the waveguide. The form of the fields of each local radiation mode is identical to that of the local modes, except that the continuous propagation constant $\beta(Q)$ is independent of z . Hence

$$\mathbf{E}_j(x, y, z) = \hat{\mathbf{e}}_j(x, y, z) \exp(i\beta(Q)z); \quad \mathbf{H}_j(x, y, z) = \hat{\mathbf{h}}_j(x, y, z) \exp(i\beta(Q)z), \quad (28-25)$$

where $\hat{\mathbf{e}}_j$ and $\hat{\mathbf{h}}_j$ are the orthonormal fields defined in Section 25-4, and their z dependence arises from the construction of the fields at each position along the waveguide, as described in Section 19-1.

Coupled local-mode equations

The inclusion of the local radiation modes in Eq. (28-1) follows by analogy with the coupled mode equations derived in Section 31-11. For example, the amplitude and phase dependence $b_j(z, Q)$ of the j th forward-propagating local radiation mode satisfies the coupled local-mode equation

$$\frac{db_j}{dz} - i\beta(Q)b_j = \sum_l \{C_{jl}(Q)b_l + C_{j-l}(Q)b_{-l}\}, \quad (28-26)$$

where the right side implicitly includes an integration over Q' of the remaining local radiation modes as in Eq. (31-51a). The z -dependent coupling coefficients $C_{jl}(Q)$ are given by either Eq. (28-3) or Eq. (28-4) with β_j replaced by $\beta(Q)$.

Total radiated power

The total radiated power propagating away from the waveguide is given by analogy with Eqs. (28-5) and (25-9) as

$$P_{\text{rad}} = \sum_j \int_0^{k_{\rho n_{\text{cl}}}} |b_j(Q)|^2 dQ, \quad (28-27)$$

for the forward-propagating modes, and by the same expression with b_j replaced by b_{-j} for the backward-propagating modes.

Weak power transfer

By analogy with Eq. (28-8), the weak power transfer solution of Eq. (28-26) is

$$b_j(Q) = b_l(0) \exp\{i\beta(Q)z\} \int_0^z C_{jl}(Q) \exp(i\overline{\delta\beta}z) dz, \quad (28-28)$$

where $\overline{\delta\beta}$ is defined by Eq. (28-8b) with β_j replaced by $\beta(Q)$, and it is assumed

that only the l th local mode is excited initially. To illustrate the use of this result, we consider a simple example below. Further, it is clear from the discussion below Eq. (28-8b) that the above expression can be derived using the induced-current representation of Section 22-10, provided we replace the j th local mode by the j th local radiation mode throughout Section 22-11.

28-6 Example: Step-profile taper

Consider the step-profile tapers of Fig. 28-1, whose ends have fixed core radii ρ_0 and ρ_L but otherwise are of arbitrary, slowly decreasing radius. We are primarily interested in radiation loss when a local mode approximates the fundamental mode on the taper, but the analysis is easily modified to describe losses from higher-order local modes. This also provides criteria for the accuracy of the local-mode description.

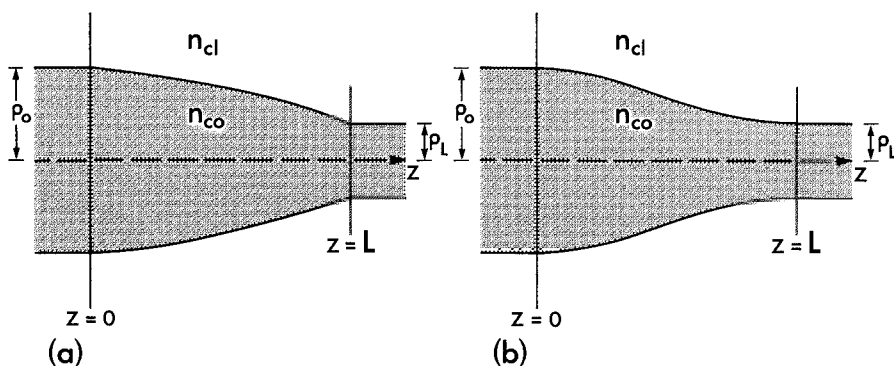


Fig. 28-1 Step-profile tapers occupy the region between fibers of core radii ρ_0 and ρ_L at $z = 0$ and $z = L$, respectively. In (a) the taper slope is discontinuous at its ends, and in (b) the taper merges smoothly into the fibers at both ends.

Weak power transfer

We denote the fundamental and local radiation modes by subscripts 1 and j , respectively. Assuming unit initial power in the fundamental mode, we deduce from Eqs. (28-27) and (28-28) that the total power excited in the j th mode is given by

$$P_j = \int_0^{k\rho n_{cl}} |G(Q)|^2 dQ; \quad G(Q) = \int_0^L C(z) \exp(i\delta\beta z) dz, \quad (28-29)$$

where $C(z)$ denotes the z -dependent $C_{j1}(Q)$. The integral for $G(Q)$ can be evaluated asymptotically. To cater for both tapers, we integrate twice by parts. If we set

$\delta\beta = \delta\beta(z) = \beta_1(z) - \beta(Q)$, this leads to

$$G(Q) = iG_0 + G_1 - \int_0^L \exp(i\overline{\delta\beta}z) \frac{d}{dz} \left\{ \frac{1}{\overline{\delta\beta}} \frac{d}{dz} \left(\frac{C}{\overline{\delta\beta}} \right) \right\} dz, \quad (28-30a)$$

$$G_0 = \frac{C(0)}{\overline{\delta\beta}(0)} - \frac{C(L) \exp(i\overline{\delta\beta}L)}{\overline{\delta\beta}(L)}, \quad (28-30b)$$

$$G_1 = \frac{\exp(i\overline{\delta\beta}L)}{\overline{\delta\beta}(L)} \frac{d}{dz} \left(\frac{C}{\overline{\delta\beta}} \right) \bigg|_L - \frac{1}{\overline{\delta\beta}(0)} \frac{d}{dz} \left(\frac{C}{\overline{\delta\beta}} \right) \bigg|_0, \quad (28-30c)$$

where $\overline{\delta\beta}$ is evaluated at $z = L$ in G_0 and G_1 . The length scale for the slow variation in $C/\overline{\delta\beta}$ is of order L . Accordingly, if we assume $L\overline{\delta\beta} \gg 1$, i.e. the taper length is large compared with the mean beat length $2\pi/\overline{\delta\beta}$, then G_1 is of order $1/L\overline{\delta\beta}$ times G_0 , and the integral is of order $1/(L\overline{\delta\beta})^2$ times G_0 and is ignored. It is clear from the expression for the coupling coefficient in Eq. (28–13) that $C(0)$ and $C(L)$ are nonzero in the case of the taper in Fig. 28–1(a), and consequently $G(Q)$ is well approximated by G_0 . However, in the case of the taper in Fig. 28–1(b), $C(0) = C(L) = 0$ and $G_0 = 0$, so that $G(Q)$ must be approximated by G_1 .

Radiated power

For simplicity we assume that there is a sufficiently large change in radius on the taper to ensure that $|\delta\beta(L)| \ll |\delta\beta(0)|$. We can then ignore terms in $\delta\beta(0)$ in Eq. (28–30b), and, on substituting into Eq. (28–27) obtain

$$P_j = \int_0^{k\rho n_{cl}} \left| \frac{C(L)}{\overline{\delta\beta}(L)} \right|^2 dQ; \quad P_j = \int_0^{k\rho n_{cl}} \left| \frac{L}{\overline{\delta\beta}(L)^2} \left(\frac{dC}{dz} \right)_L \right|^2 dQ, \quad (28-31)$$

for the tapers of Figs. 28–1(a) and 28–1(b), respectively. In other words the radiated power originates predominantly from the region close to the narrower end of the taper. If we substitute the coupling coefficient of Eq. (28–13) into Eq. (28–31), we deduce that the power radiated from the taper of Fig. 28–1(a) varies with the square of the slope at $z = L$. Thus if the taper is linear with constant slope, P_j is proportional to L^{-2} , where L is the length of the taper. Similarly, the power radiated from the taper of Fig. 28–1(b) involves the radius of curvature of the taper at $z = L$, but is an order of magnitude smaller. In both cases, the integration over Q is complicated by the dependence of the radiation field in the coupling coefficient, i.e. $\hat{e}_j(Q)$, and the quantitative value of P_j must be obtained numerically. Nevertheless, the slowness requirement that $L|\beta(Q) - \beta_1| \ll 1$ is consistent with the intuitive criterion of Eq. (19–7).

COMPOSITE WAVEGUIDES

The coupling of local modes on composite waveguides, such as two parallel, slowly varying fibers, is described by the results of this chapter, provided we

know the local-mode fields for the composite system. We showed in Section 19-7 how these fields could be described by a superposition of the local-mode fields of each fiber in isolation, assuming the fibers are sufficiently well separated. In the following, we investigate the accuracy of the composite-mode description of propagation by determining the coupling between the fundamental local modes.

28-7 Example: Tapered couplers

Propagation along slowly varying, tapered couplers of the type illustrated in Fig. 28-2(a) can be described by the local modes of the composite waveguide, as discussed in

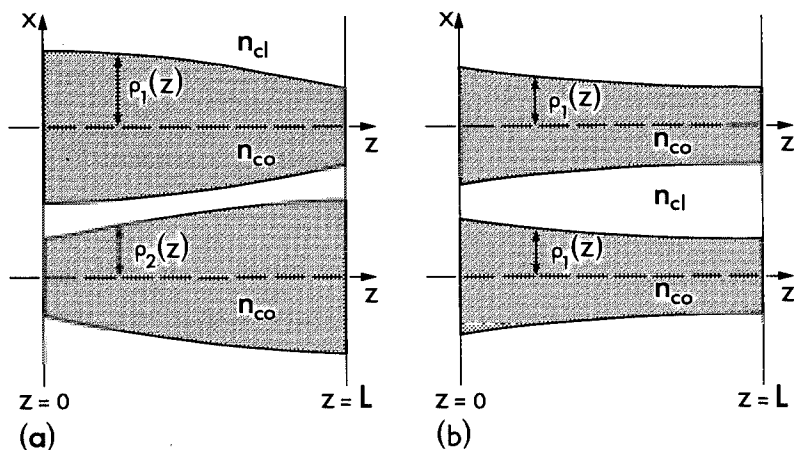


Fig. 28-2 Examples of (a) a tapered coupler of core index n_{co} and core radii $\rho_1(z)$ and $\rho_2(z)$ in a uniform cladding of index n_{cl} and (b) two identical fibers.

Section 19-7. Within the weak-guidance approximation, the fundamental solution Ψ_+ of the scalar wave equation is given by Eq. (19-14), and the second fundamental solution Ψ_- follows likewise. Hence

$$\Psi_{\pm} = \frac{\bar{\Psi}_1 + a_{\pm} \bar{\Psi}_2}{(1 + a_{\pm}^2)^{1/2}}; \quad a_{\pm} = -\frac{\chi}{2} \pm \left\{ 1 + \frac{\chi^2}{4} \right\}^{1/2}; \quad \chi = \frac{\bar{\beta}_1 - \bar{\beta}_2}{C}, \quad (28-32)$$

where $\bar{\Psi}_1$, $\bar{\beta}_1$ and $\bar{\Psi}_2$, $\bar{\beta}_2$ are the z -dependent local-mode solution and propagation constant, respectively, for each fiber in isolation, and C is the z -dependent generalization of Eq. (18-35). If we assume step-profile tapers, then $n - \bar{n}_1 = 0$ everywhere except over the core A_{co2} of the second taper, where $n - \bar{n}_1 = n_{co} - n_{cl}$. In terms of the normalization of Table 13-2, page 292, this leads to

$$C(z) = \frac{k \Delta n_{co}^2}{2 \bar{N}_1} \left(\frac{\epsilon_0}{\mu_0} \right)^{1/2} \int_{A_{co2}} \bar{\Psi}_1 \bar{\Psi}_2 dA, \quad (28-33)$$

since $n_{co}^2 - n_{cl}^2 \cong 2n_{co}(n_{co} - n_{cl})$. At the beginning of the coupler, $z = 0$, only the Ψ_+ mode is excited and has amplitude $b_+(0)$. The amplitude $b_-(z)$ of the Ψ_- mode, to which there is only weak power transfer, is given by Eq. (28-8) with j and l replaced by $-$ and $+$, respectively. The coupling coefficient follows from Eq. (28-4), and, for convenience, is expressed as

$$C_{-+}(z) = \frac{k}{4} \frac{\Delta n_{co}^2}{\beta_- - \beta_+} \left(\frac{\epsilon_0}{\mu_0} \right)^{1/2} \frac{I(z)}{N_+^{1/2} N_-^{1/2}}; \quad I(z) = -\frac{1}{\Delta n_{co}^2} \int_{A_z} \Psi_+ \Psi_- \frac{\partial n^2}{\partial z} dA, \quad (28-34)$$

where β_+ , N_+ and β_- , N_- are the propagation constant and normalization for the Ψ_+ and Ψ_- modes, respectively. By analogy with Eqs. (28-12) and (28-13)

$$I(z) = \frac{d\rho_1^2}{dz} \int_0^{2\pi} (\Psi_+ \Psi_-)_{r_1=\rho_1} d\phi_1 + \frac{d\rho_2^2}{dz} \int_0^{2\pi} (\Psi_+ \Psi_-)_{r_2=\rho_2} d\phi_2, \quad (28-35)$$

where ρ_1, ρ_2 are the core radii at position z , the azimuthal angles are relative to the fiber axes in Fig. 28-2(a), and r_1, r_2 are the cylindrical radii. We deduce from Eq. (28-32) that

$$\Psi_+ \Psi_- = (\bar{\Psi}_1^2 - \chi \bar{\Psi}_1 \bar{\Psi}_2 - \bar{\Psi}_2^2)/(4 + \chi^2)^{1/2}, \quad (28-36)$$

and, on ignoring exponentially small terms, it is clear that we need retain only $\bar{\Psi}_1^2$ and $-\bar{\Psi}_2^2$, respectively, in the integrand of the first and second integrals on the right of Eq. (28-35). Recalling from Table 14-3, page 313, that $\bar{\Psi}_1 = 1$ on $r_1 = \rho_1$ and $\bar{\Psi}_2 = 1$ on $r_2 = \rho_2$, we obtain

$$(4 + \chi^2)^{1/2} I(z) = 2\pi \frac{d}{dz} (\rho_1^2 - \rho_2^2) = 2 \frac{d}{dz} (A_{co1} - A_{co2}), \quad (28-37)$$

where A_{coi} denotes the core area of fiber i . We recall from Eq. (18-35) that $\beta_+ - \beta_- = 2C$, set $N_+ \cong N_- \cong \bar{N}_1 + \bar{N}_2$ for large separation, and substitute Eqs. (28-33) and (28-37) into Eq. (28-34) to obtain

$$C_{-+} = \frac{\pi \bar{N}_1}{\bar{N}_1 + \bar{N}_2} \frac{d}{dz} (\rho_2^2 - \rho_1^2) \left/ \left\{ (4 + \chi^2)^{1/2} \int_{A_{co2}} \bar{\Psi}_1 \bar{\Psi}_2 dA \right\} \right. \quad (28-38)$$

The power $P_-(z)$ in the Ψ_- mode is given by Eq. (28-10) with $F = C_{-+}/\delta\beta$, where $\delta\beta = 2\bar{C}$ and \bar{C} denotes the mean value of $C(z)$ over the taper length. Since the integrals in C_{-+} and \bar{C} decreases exponentially with increasing separation, it is clear that $P_-(z)$ will be small only if the taper angle is minute. In other words, *for a given taper angle the local-mode description is acutely sensitive to separation*, as anticipated in Section 19-9.

28-8 Example: Identical fibers

The analysis of the previous section also applies to the special case of identical fibers, such as those illustrated in Fig. 28-2(b). At each position along the composite waveguide $\rho_1 = \rho_2$ and $\beta_1 = \beta_2$, whence Eq. (28-32) and (28-37) show that $\chi = I(z) = 0$. In other words *there is no coupling to the Ψ_- mode* within the accuracy of the analysis. This is also obvious from symmetry arguments. Consequently coupling only occurs with higher-order local or radiation modes with the symmetry properties of Ψ_+ .

REFERENCES

1. Snyder, A. W., (1965) Surface mode coupling along a tapered dielectric rod. *I.E.E.E. Trans. Antennas Propag.*, **13**, 821–2.
2. Snyder, A. W. (1970) Coupling of modes on a tapered dielectric cylinder. *I.E.E.E. Microwaves Theory Tech.*, **18**, 383–92.
3. Marcuse, D. (1974) *Theory of Dielectric Optical Waveguides*, Academic Press, New York, p. 106.
4. Snyder, A. W. (1971) Mode propagation in a nonuniform cylindrical medium. *I.E.E.E. Trans. Microwaves Theory Tech.* **19**, 402–3.
5. McIntyre, P. and Snyder, A. W., (1978) Light propagation in twisted anisotropic media: application to photoreceptors. *J. Opt. Soc. Am.*, **68**, 149–57.

Cross-talk

29-1	Alternative descriptions of cross-talk	568
Two parallel fibers		568
29-2	Derivation of the coupled equations	569
29-3	Identical and nearly identical fibers	570
29-4	<i>Example: Identical step-profile fibers</i>	572
29-5	<i>Example: Identical Gaussian-profile fibers</i>	573
29-6	<i>Example: Slightly unequal step-profile fibers</i>	574
29-7	<i>Example: Slightly absorbing fibers</i>	574
29-8	<i>Example: Multimode fibers</i>	575
Two slowly varying fibers		575
29-9	Derivation of the coupled equations	576
29-10	Solution of the coupled equations	576
29-11	<i>Example: Identical fibers</i>	578
29-12	<i>Example: Tapered couplers</i>	578
Arrays of fibers		579
29-13	<i>Example: Periodic illumination of infinite arrays</i>	579
29-14	<i>Example: Absorption in infinite arrays</i>	581
29-15	<i>Example: Single-fiber illumination in an infinite array</i>	582
29-16	<i>Example: Finite polygonal arrays</i>	583
References		584

In this chapter we study the phenomenon of *optical cross-talk* between pairs and between arrays of cylindrically symmetric or slowly varying fibers. Cross-talk arises because the fields of a fiber extend indefinitely into the cladding and interact with any other fiber which may be present. This interaction excites the fields of the second fiber, which in turn interact with the fields of the first fiber. Consequently there will be an exchange of power between the two fibers as the fields propagate. The amount of cross-talk, or power exchange, depends on the overlap of the fields of the two fibers. In ray language, cross-talk is associated with frustrated internal reflection or, equivalently, optical tunneling.

Cross-talk problems are of interest in the design of optical couplers, or

switches [1]. In biological applications, the maximum density of visual photoreceptors in the retinae of animals may be limited by cross-talk [2, 3].

29-1 Alternative descriptions of cross-talk

Cross-talk can be described directly in terms of the modes of the composite waveguide. Thus, for example, cross-talk between a pair of identical fibers manifests itself by the interference, or beating, of the composite modes. Alternatively, cross-talk can be described in terms of the modes which propagate along each fiber in isolation from the other fibers. The coupling of power between these modes must clearly give the same cross-talk as the first method. We present the second approach in this chapter, since the first approach has already been described in Chapters 18 and 19.

While the analysis of cross-talk in terms of the coupling between modes of individual fibers is formally exact, *our ability to analyse such problems is restricted to weakly guiding fibers which are sufficiently well separated*, for reasons given in Section 18-21. The former restriction is equivalent to ignoring all polarization effects due to the composite waveguide structure, and the latter restriction ensures that a simple superposition solution is accurate.

TWO PARALLEL FIBERS

We begin by examining propagation along, and power transfer between, two parallel, cylindrically symmetric fibers, such as those illustrated in Fig. 29-1,

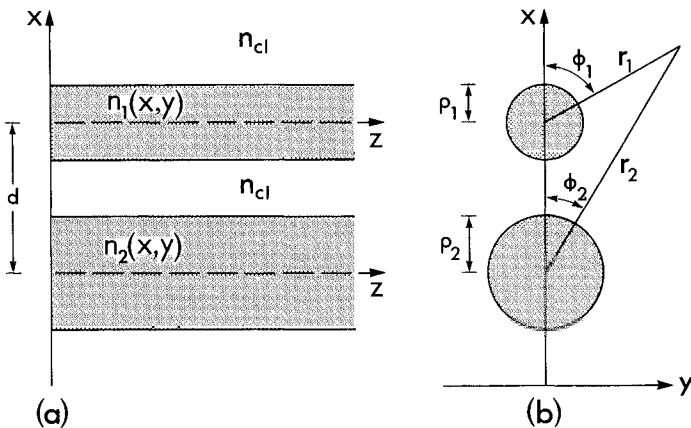


Fig. 29-1 (a) Two parallel fibers of core index and radius n_1, ρ_1 and n_2, ρ_2 , respectively, are surrounded by a uniform cladding of index n_{cl} . The axes are distance d apart. (b) Cylindrical polar coordinates r_1, ϕ_1 and r_2, ϕ_2 relative to the fiber axes.

and show that within the restrictions of the previous section, cross-talk depends on the solution of two coupled equations. The fiber cores are assumed to be surrounded by an unbounded, uniform cladding medium, which, in practice, can be realized by the use of an index-matching fluid.

29-2 Derivation of the coupled equations

The two fibers in Fig. 29-1 have core refractive-index profiles $\bar{n}_1(x, y)$ and $\bar{n}_2(x, y)$, referred to a common set of axes, and a uniform cladding of index n_{cl} . For convenience we assume both fibers are single moded in isolation of each other, and, within the weak-guidance approximation, we work with the x -polarized fundamental modes. Hence if N_1 and N_2 are the normalizations of Table 13-2, page 292, we set

$$E_{x1}(x, y, z) = a_1(z) \bar{\Psi}_1(x, y) \exp(i\bar{\beta}_1 z) / N_1^{1/2} = b_1(z) \bar{\Psi}_1(x, y) / N_1^{1/2}, \quad (29-1a)$$

$$E_{x2}(x, y, z) = a_2(z) \bar{\Psi}_2(x, y) \exp(i\bar{\beta}_2 z) / N_2^{1/2} = b_2(z) \bar{\Psi}_2(x, y) / N_2^{1/2}, \quad (29-1b)$$

where the modal amplitudes are z -dependent to account for the coupling. The fundamental solution of the scalar wave equation and propagation constant are $\bar{\Psi}_1, \bar{\beta}_1$ and $\bar{\Psi}_2, \bar{\beta}_2$ for each fiber in isolation, and $b_1(z), b_2(z)$ contain all the z -dependence for each fiber. We omit the \sim from scalar quantities for clarity.

We define $n(x, y)$ as the profile of the composite waveguide, i.e. $n = \bar{n}_1$ over the core of the first fiber, $n = \bar{n}_2$ over the core of the second fiber and $n = n_{cl}$ elsewhere, and let Ψ denote the corresponding solution of the scalar wave equation. The second fiber is regarded as a perturbation of the first fiber, in which case the equation satisfied by $b_1(z)$ is deduced from Eq. (31-49), by setting $k = 1$, and replacing \mathbf{E} and $\hat{\mathbf{e}}_k^*$ by Ψ and $\bar{\Psi}_1 / N_1^{1/2}$, respectively, in the weak-guidance limit, where N_1 is the normalization and we assume non-absorbing fibers. Hence [4]

$$\frac{db_1}{dz} - i\bar{\beta}_1 b_1 = \frac{i}{4} \frac{k}{N_1^{1/2}} \left(\frac{\epsilon_0}{\mu_0} \right)^{1/2} \int_{A_\infty} (n^2 - \bar{n}_1^2) \Psi \bar{\Psi}_1 dA, \quad (29-2)$$

where A_∞ is the infinite cross-section of the composite waveguide.

Solution using coupled mode equations

To solve Eq. (29-2) we need to know Ψ . An expression could be obtained by expanding Ψ over the complete set of $\bar{\Psi}_j$ for the bound and radiation modes of the first fiber, and this would, of course, lead to the infinite set of coupled mode equations derived in Section 33-11. The disadvantage of this description is that each mode of the first fiber by itself is a poor approximation to the field within the second fiber. Consequently large numbers of modes are required for accuracy, and the set of coupled equations is then intractable.

Superposition solution

It is intuitive that the fields of the composite waveguide are well approximated by a linear combination of the fundamental-mode fields of each fiber in isolation, provided the two fibers are optically well separated and are not too dissimilar. Accordingly we set

$$\Psi(x, y, z) = b_1(z) \bar{\Psi}_1(x, y)/N_1^{1/2} + b_2(z) \bar{\Psi}_2(x, y)/N_2^{1/2} \quad (29-3)$$

for the solution of the scalar wave equation of the composite waveguide. Substitution into Eq. (29-2) leads to one coupled equation. A second equation is obtained similarly by treating the first fiber as a perturbation of the second fiber. Hence [4]

$$\frac{db_1}{dz} - i(\bar{\beta}_1 + \bar{C}_{11})b_1 = i\bar{C}_{12}b_2, \quad (29-4a)$$

$$\frac{db_2}{dz} - i(\bar{\beta}_2 + \bar{C}_{22})b_2 = i\bar{C}_{21}b_1, \quad (29-4b)$$

where the C_{ij} are coupling coefficients defined by

$$C_{ij} = \frac{1}{4} \frac{k}{(N_i N_j)^{1/2}} \left(\frac{\epsilon_0}{\mu_0} \right)^{1/2} \int_{A_\infty} (n^2 - \bar{n}_i^2) \bar{\Psi}_i \bar{\Psi}_j dA; \quad i, j = 1, 2, \quad (29-5)$$

and are therefore constants independent of z . Since the fibers are assumed to be well separated, $\bar{\Psi}_i$ is exponentially small over the core of fiber j , and consequently both C_{12} and C_{21} are minute compared with $\bar{\beta}_1$ and $\bar{\beta}_2$. Furthermore, $n^2 - \bar{n}_j^2$ vanishes over the core of fiber j , and hence the self-coupling coefficients C_{11} and C_{22} are negligible compared with the cross-coupling coefficients. The former are usually ignored, although they are readily included in the solution of Eq. (29-4) by redefining $\bar{\beta}_1$ and $\bar{\beta}_2$ to include C_{11} and C_{22} , respectively.

29-3 Identical and nearly identical fibers

Although the cross-coupling coefficients may be arbitrarily small, a large fraction of total power of the composite waveguide can transfer between the two fibers under resonant conditions. Indeed, if this is not the case, then Eq. (29-3) is inadequate and coupling to the backward-propagating fundamental modes and to the radiation fields of both fibers must be included. Resonance occurs when the fibers are identical or nearly identical, in which case we deduce from Eq. (29-5) that

$$C_{12} \cong C_{21} \cong C \cong \frac{1}{4} \frac{k}{N_1} \left(\frac{\epsilon_0}{\mu_0} \right)^{1/2} \int_{A_\infty} (n^2 - \bar{n}^2) \bar{\Psi}_1 \bar{\Psi}_2 dA. \quad (29-6)$$

Substituting into Eq. (29-4) and ignoring C_{11} and C_{22} for reasons given above, we can eliminate b_1 or b_2 and obtain a second-order differential equation with constant coefficients. The solution satisfying $b_1(z) = b_1(0)$ and $b_2(z) = b_2(0)$ at $z = 0$ is readily shown to be

$$b_1(z) = \left\{ b_1(0) \cos\left(\frac{C}{F}z\right) + iF \left[b_2(0) + \frac{\bar{\beta}_1 - \bar{\beta}_2}{2C} b_1(0) \right] \sin\left(\frac{C}{F}z\right) \right\} \exp(i\beta_a z), \quad (29-7a)$$

$$b_2(z) = \left\{ b_2(0) \cos\left(\frac{C}{F}z\right) + iF \left[b_1(0) - \frac{\bar{\beta}_1 - \bar{\beta}_2}{2C} b_2(0) \right] \sin\left(\frac{C}{F}z\right) \right\} \exp(i\beta_a z), \quad (29-7b)$$

where β_a is the average of the two propagation constants, and

$$\beta_a = \frac{\bar{\beta}_1 + \bar{\beta}_2}{2}; \quad F = 1 / \left\{ 1 + \frac{(\bar{\beta}_1 - \bar{\beta}_2)^2}{4C^2} \right\}^{1/2} \quad (29-8)$$

Thus the amplitude of each mode varies sinusoidally along the waveguide.

Power transfer between modes

The power in each mode follows from Eqs. (11-22) and (29-1) as

$$P_1(z) = |b_1(z)|^2; \quad P_2(z) = |b_2(z)|^2 \quad (29-9)$$

Substitution from Eq. (29-7) leads to

$$P_1(z) = P_1(0) + F^2 \left\{ P_2(0) - P_1(0) + \frac{\bar{\beta}_1 - \bar{\beta}_2}{C} [P_1(0)P_2(0)]^{1/2} \right\} \sin^2\left(\frac{C}{F}z\right), \quad (29-10a)$$

$$P_2(z) = P_2(0) + F^2 \left\{ P_1(0) - P_2(0) - \frac{\bar{\beta}_1 - \bar{\beta}_2}{C} [P_1(0)P_2(0)]^{1/2} \right\} \sin^2\left(\frac{C}{F}z\right), \quad (29-10b)$$

in terms of the initial powers. We have assumed that both $b_1(0)$ and $b_2(0)$ are real to ensure the two modes are in phase at $z = 0$. When unit power is

launched only in the first mode, then $P_1(0) = 1$, $P_2(0) = 0$ and [5]

$$P_1(z) = 1 - F^2 \sin^2\left(\frac{C}{F}z\right); \quad P_2(z) = F^2 \sin^2\left(\frac{C}{F}z\right). \quad (29-11)$$

Hence a fraction F^2 of total power is transferred from one fiber to the other fiber and back in the beat length $z_b = 2\pi F/C$ along the waveguide. *Only when the fibers are identical is complete power transfer achieved*, and since C is very small compared with $\bar{\beta}_1$ or $\bar{\beta}_2$, *the fibers must be virtually identical for F^2 to be significant*; otherwise the accuracy of the analysis is reduced for reasons given above.

The results of this section are identical to those of Sections 18-13 and 18-20, as expressed by Eqs. (18-39) when $F = 1$ and Eq. (18-61) for $F < 1$, which were derived using the composite modes of the two-fiber waveguide. Furthermore, F of Eq. (29-8) and C of Eq. (29-6) are identical to Eqs. (18-57) and (18-35), respectively, provided we set $n^2 - \bar{n}^2 \cong 2n_{co}(n - \bar{n}_1)$ in the latter. We now consider examples to quantify the amount of cross-talk.

29-4 Example: Identical step-profile fibers

The solution given by Eq. (29-11) depends only on the coupling coefficient since $F = 1$ for identical fibers. We derived an expression for C in Section 18-14 assuming a step profile. The normalized coefficient $\rho C/(2\Delta)^{1/2}$ is plotted against the normalized separation d/ρ for various values of the common fiber parameter V in Fig. 29-2(a). For example, the beat length $z_b = 2\pi/C$ is approximately $2.8 \times 10^4 \rho$ for $V = 2.4$, $\Delta = 0.005$ and $d/\rho = 4$. Given V , the value of C increases with decreasing separation as the fields

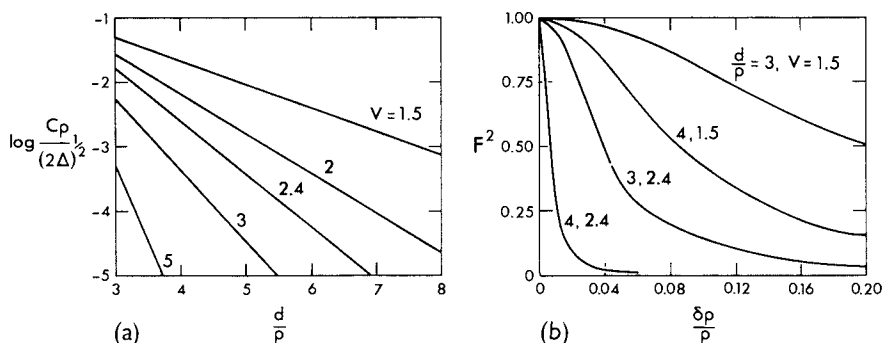


Fig. 29-2 (a) Normalized coupling coefficient of Eq. (18-42) as a function of the normalized separation d/ρ for a pair of identical step-profile fibers. (b) Fraction of total power transferred between step-profile fibers with slight difference $\delta\rho$ in their core radii.

overlap more. For fixed separation, C increases with decreasing V as more fundamental-mode power spreads into the cladding around the two fibers.

29-5 Example: Identical Gaussian-profile fibers

When each fiber in isolation has a Gaussian refractive-index profile, we can determine the coupling coefficient using the Gaussian approximation of Chapter 15 for the fundamental modes. The profile for the composite waveguide is given in terms of the radial coordinates of Fig. 27-1(b) by

$$n^2 = n_{co}^2 \left\{ 1 - 2\Delta \left[1 - \exp\left(-\frac{r_1^2}{\rho^2}\right) - \exp\left(-\frac{r_2^2}{\rho^2}\right) \right] \right\}, \quad (29-12)$$

where $\rho = \rho_1 = \rho_2$ is the scaling length, and the profile \bar{n}_1^2 is given by the same expression with the term in r_2 omitted. By examining the integrand in Eq. (29-6) it is clear that the dominant contribution to the coupling coefficient comes from a region close to the axis of the second fiber. Hence

$$C = \frac{(2\Delta)^{1/2}}{4} \frac{V \rho n_{co}}{N_1} \left(\frac{\epsilon_0}{\mu_0} \right)^{1/2} \int_0^\infty \int_0^{2\pi} \bar{\Psi}_1 \bar{\Psi}_2 \exp(-R_2^2) R_2 d\phi_2 dR_2, \quad (29-13)$$

where $R_2 = r_2/\rho$ and V is the common fiber parameter. We use the Gaussian approximation of Eq. (15-2) and Table 15-2, page 340, for $\bar{\Psi}_2$ close to the r_2 axis, and the far-field approximation of Eq. (15-16) for $\bar{\Psi}_1$, i.e.

$$\bar{\Psi}_1 = \frac{V^2}{V+1} \exp\left\{ \frac{(V-1)^2}{2(V+1)} \right\} K_0(\{V-1\}R_1); \quad \bar{\Psi}_2 = \exp\left\{ -\frac{V-1}{2} R_2^2 \right\}, \quad (29-14)$$

where $R_1 = r_1/\rho$. Together with the normalization of Table 15-2, we substitute into Eq. (29-13) and use the addition formula of Eq. (37-81) to express K_0 in terms of R_2 and ϕ_2 . Only the $p=0$ term of the addition formula remains after performing the ϕ_2 integration, whence

$$C = \frac{(2\Delta)^{1/2}}{\rho} V^3 \frac{V-1}{V+1} \exp\left\{ \frac{(V-1)^2}{2(V+1)} \right\} K_0(\{V-1\}d/\rho) G, \quad (29-15a)$$

where the integral G is expressible in closed form using Eq. (37-101)

$$G = \int_0^\infty I_0(\{V-1\}R_2) \exp\left\{ -\frac{V+1}{2} R_2^2 \right\} R_2 dR_2 = \frac{1}{V+1} \exp\left\{ \frac{(V-1)^2}{2(V+1)} \right\}. \quad (29-15b)$$

Finally we replace K_0 by its asymptotic form of Eq. (37-88), since $(V-1)d/\rho \gg 1$ when the fibers are optically well separated, and obtain

$$C = \left(\frac{\pi\Delta}{d\rho} \right)^{1/2} V^3 \frac{(V-1)^{1/2}}{(V+1)^2} \exp\left\{ (V-1) \left[\frac{V-1}{V+1} - \frac{d}{\rho} \right] \right\}. \quad (29-16)$$

When $V = 2.6$, $\Delta = 0.005$ and $d/\rho = 4$, the beat length $z_b \cong 1.7 \times 10^4 \rho$. This is approximately six times larger than the result for step-profile fibers with the same separation at cutoff of the second mode, and is due to the exponentially small difference $n^2 - \bar{n}^2$ for the Gaussian profile compared with $n_{co}^2 - n_{cl}^2$ for the step profile.

29-6 Example: Slightly unequal step-profile fibers

When the two fibers of Section 29-4 have slight differences δn_{co} and $\delta \rho$ in their core indices and radii, respectively, the fundamental-mode propagation constants are no longer equal and differ by a small amount $\delta\beta = \bar{\beta}_1 - \bar{\beta}_2$. The corresponding miniscule change in the fields has negligible effect on the coupling coefficient, but the value of $\delta\beta$ strongly affects the fraction of total power transferred between the fibers, as is clear from Eqs. (29-8) and (29-11).

Without loss of generality, we assume that fiber 1 has core index and radius $n_{co} + \delta n_{co}$ and $\rho + \delta\rho$, respectively, and consequently the contributions to $\delta\beta$ are given by $\beta - \bar{\beta}$ of Eq. (18-8) with $\delta n_{cl} = 0$ and Eq. (18-13a). We substitute for $\bar{\eta}$ from Table 14-3, page 313, and express k in terms of the fiber parameter V . On rearranging we obtain [5]

$$\delta\beta = \frac{1}{\rho} \frac{U^2}{V} \frac{1}{(2\Delta)^{1/2}} \left\{ \left(\frac{W^2}{U^2} + \frac{K_0^2(W)}{K_1^2(W)} \right) \frac{\delta n_{co}}{n_{co}} + 2\Delta \frac{K_0^2(W)}{K_1^2(W)} \frac{\delta\rho}{\rho} \right\}, \quad (29-17)$$

where the $-$ is omitted from scalar quantities. Hence we can offset, say, an increase in n_{co} by a decrease in ρ so that $\delta\beta = 0$ and total power transfer still occurs. For example, when $V = 2.4$ we deduce from Table 14-4, page 314, that this occurs when

$$\delta\rho/\rho \cong -(1.4/\Delta) (\delta n_{co}/n_{co}). \quad (29-18)$$

Since $\Delta \ll 1$ for the weakly guiding fibers, a small index change has a far greater effect than the same fractional change in radius.

When $\delta\beta$ is due to radius variations only, it follows from Eqs. (29-8) and (18-42) that the fraction of total power transferred between the fibers is

$$F^2 = 1 / \left\{ 1 + \frac{WV^4}{2\pi} K_0^4(W) \frac{d}{\rho} \exp \left(2W \frac{d}{\rho} \right) \left(\frac{\delta\rho}{\rho} \right)^2 \right\}. \quad (29-19)$$

This is plotted in Fig. 29-2(b) as a function of $\delta\rho/\rho$ for various values of V and d/ρ .

29-7 Example: Slightly absorbing fibers

When the fibers in Fig. 29-1 are absorbing, the refractive-index profile of each fiber and of the composite waveguide has the complex form given in Table 11-2, page 232. The fundamental-mode propagation constant for each fiber in isolation is also complex, so we set

$$\bar{\beta}_1 = \beta_1^r + i\beta_1^i, \quad \gamma_1 = 2\beta_1^i; \quad \bar{\beta}_2 = \beta_2^r + i\beta_2^i, \quad \gamma_2 = 2\beta_2^i, \quad (29-20)$$

where superscripts r and i denote real and imaginary parts, and γ_1, γ_2 are the corresponding power attenuation coefficients. Coupling between the absorbing fibers is described by Eqs. (29-4) in terms of the complex coupling coefficients of Eq. (29-5), and both β_a and F are complex in the solution given by Eq. (29-7).

If absorption is the dominant process, then C/F in the arguments of Eq. (29-7) is almost pure imaginary, and little or no coupling of power between the fibers occurs before all initial power is absorbed. On the other hand, when the fibers are only slightly absorbing, then C and F are approximately real and Eq. (29-7) differs from the solution

for nonabsorbing fibers by an overall attenuation factor $\exp\{-(\beta_1^i + \beta_2^i)z/2\}$. Thus the power in each fiber corresponding to the conditions of Eq. (29-11) is given by [6]

$$P_1(z) = \left\{1 - F^2 \sin^2\left(\frac{C}{F}z\right)\right\} \exp(-\gamma_a z); \quad P_2(z) = F^2 \sin^2\left(\frac{C}{F}z\right) \exp(-\gamma_a z), \quad (29-21)$$

where $\gamma_a = (\gamma_1 + \gamma_2)/2$ is the mean power attenuation coefficient for the two fibers.

29-8 Example: Multimode fibers

So far the discussion of cross-talk has assumed single-mode fibers with coupling between the fundamental modes. However, the solution of Section 29-3 is more general, because strong coupling can occur between every identical pair of modes on two equal multimode fibers. Even if the fibers differ, strong coupling can occur between different modes, since the propagation constant of, say, a TE_{0m} mode on one fiber may be close or equal to the propagation constant of a HE_{1m} mode on the other fiber.

Consider two parallel, weakly guiding fibers with identical step profiles, core radius ρ and axis separation d . A linearly polarized, uniform beam is focused onto the axis of one fiber and consequently only the HE_{1m} modes are excited. The same modes are then excited on the second fiber by coupling. Quantitative analysis then shows that the power P_2 excited in the second fiber is given by [7].

$$\frac{P_2(z)}{P_1(0)} = \frac{1}{2} \left\{1 - \frac{\sin L}{L}\right\}; \quad L = \frac{\theta_m^2}{\theta_c} \left(\frac{8\rho}{\pi dV}\right)^{1/2} \frac{z}{\rho} \exp\left\{-\frac{d-2\rho}{\rho}V\right\}, \quad (29-22)$$

where $P_1(0)$ is the total power entering the first fiber, V and θ_c are the fiber parameter and complementary critical angle defined inside the front cover and $\theta_m \leq \theta_c \leq 1$ is the angle subtended by the lens. If the fibers are long enough, an equilibrium situation is reached when the fibers carry equal power. However, this length is enormous unless the fibers are very close together. For example, if $\theta_c = 0.2$, $\rho = 7.5 \mu\text{m}$ and $V = 150$, the equilibrium length is about 1 m for touching fibers ($d = 2\rho$), and exceeds 100 m when $d = 2.04\rho$. Furthermore, if the core radii differ by only 0.1%, negligible power is transferred.

TWO SLOWLY VARYING FIBERS

To complement the analysis of cross-talk between cylindrically symmetric fibers, we now consider pairs of fibers which vary slowly along their length, such as the identical fibers of Fig. 19-3(a) and the tapered coupler of Fig. 19-4(a). Propagation along these systems was described in Chapter 19 using the local modes of the *composite* waveguide. Our purpose here is to describe cross-talk in terms of the coupling of the local modes of each fiber *in isolation* of the other.

29–9 Derivation of the coupled equations

If the fibers are sufficiently slowly varying, we can approximate the field of each fiber in isolation by a local mode, as described in Section 19–1. Cross-talk can then be determined by coupling between the local modes of each fiber. For convenience we retain the assumptions made for the cylindrically symmetric fibers, so that the slowly varying fibers are single moded, weakly guiding and optically well separated. Accordingly the analogous expressions to Eq. (29–1) are now

$$E_{x1} = a_1(z)\bar{\Psi}_1(x, y, \bar{\beta}_1(z)) \exp \left\{ i \int_0^z \beta_1(z) dz \right\} / N_1(z)^{1/2} \quad (29-23a)$$

$$= b_1(z)\bar{\Psi}_1 / N_1(z)^{1/2}, \quad (29-23b)$$

$$E_{x2} = a_2(z)\bar{\Psi}_2(x, y, \bar{\beta}_2(z)) \exp \left\{ i \int_0^z \beta_2(z) dz \right\} / N_2(z)^{1/2} \quad (29-23c)$$

$$= b_2(z)\bar{\Psi}_2 / N_2(z)^{1/2}, \quad (29-23d)$$

where $\bar{\beta}_1$ and $\bar{\beta}_2$ are slowly varying with z .

The coupled local-mode equations of Section 31–14 apply to local modes of the *same* fiber, and are therefore inappropriate for describing coupling between modes of the two fibers, for reasons given in Section 29–2. Instead we can generalize the derivation of the coupled equations of Eq. (29–4) to slowly varying fibers, and deduce that [8]

$$\frac{db_1}{dz} - i\bar{\beta}_1(z)b_1 = iC(z)b_2, \quad (29-24a)$$

$$\frac{db_2}{dz} - i\bar{\beta}_2(z)b_2 = iC(z)b_1, \quad (29-24b)$$

where b_1 and b_2 are defined by Eq. (29–23), $C(z)$ is the generalization of Eq. (29–6) when $N_1, n, \bar{n}, \bar{\Psi}_1$ and $\bar{\Psi}_2$ are z dependent, and we have ignored self-coupling terms for reasons given at the end of Section 29–2.

29–10 Solution of the coupled equations

To solve Eqs. (29–24) for the amplitude of the fundamental local mode on each fiber, we anticipate that propagation on the composite structure will occur at the average of the local phase velocities. Accordingly we make the substitution

$$b_j(z) = g_j(z) \exp \left\{ \frac{i}{2} \int_0^z (\bar{\beta}_1 + \bar{\beta}_2) dz \right\}, \quad (29-25)$$

where $j = 1$ or 2 , and obtain the coupled equations

$$\frac{dg_1}{dz} + i\frac{\bar{\beta}_2 - \bar{\beta}_1}{2}g_1 = iCg_2; \quad \frac{dg_2}{dz} - i\frac{\bar{\beta}_2 - \bar{\beta}_1}{2}g_2 = iCg_1. \quad (29-26)$$

On eliminating g_2 , we deduce that g_1 satisfies

$$\frac{d^2g_1}{dz^2} + \frac{d \ln C}{dz} \frac{dg_1}{dz} + i\left\{\frac{i}{2}C \frac{d}{dz} \left(\frac{\bar{\beta}_2 - \bar{\beta}_1}{C}\right) + C^2 + \frac{(\bar{\beta}_2 - \bar{\beta}_1)^2}{4}\right\}g_1 = 0. \quad (29-27)$$

We ignore the derivatives of $\bar{\beta}_1$, $\bar{\beta}_2$ and C compared with the remaining terms, since $\bar{\beta}_1$, $\bar{\beta}_2$ and C are slowly varying, and consequently g_1 satisfies the harmonic equation

$$\frac{d^2g_1}{dz^2} + \frac{C^2}{F^2}g_1 = 0; \quad F = 1/\left\{1 + \frac{(\bar{\beta}_1 - \bar{\beta}_2)^2}{4C^2}\right\}^{1/2}, \quad (29-28)$$

where F , and thus C/F , are slowly varying functions of z . The solutions of this equation are given within the WKB approximation by Eq. (35–29), whence

$$g_1 = p_+(z)I_+ + p_-(z)I_-; \quad I_{\pm} = \exp\left\{\pm i \int_0^z \frac{C}{F} dz\right\}, \quad (29-29)$$

where p_+ and p_- are arbitrary, slowly varying functions of z . The corresponding expressions for b_1 and b_2 follow from Eqs. (29–25) and (29–24), respectively, and we ignore derivatives of p_+ and p_- in the latter. Accordingly

$$b_1 = (p_+I_+ + p_-I_-)I_a; \quad b_2 = (a_+p_+I_+ + a_-p_-I_-)I_a, \quad (29-30)$$

where the slowly varying functions a_+ , a_- and the integral are defined by

$$a_{\pm}(z) = \frac{\bar{\beta}_2 - \bar{\beta}_1}{2C} \pm \frac{1}{F}; \quad I_a = \exp\left\{\frac{i}{2} \int_0^z (\bar{\beta}_1 + \bar{\beta}_2) dz\right\}, \quad (29-31)$$

at each position along the composite waveguide.

Power conservation

The solution of Eq. (29–30) must satisfy the requirement that the total power $P_1(z) + P_2(z)$ of the local modes is the same everywhere along the system. On substituting Eq. (29–30) into Eq. (29–9), we deduce that the functional forms of p_+ and p_- are given by

$$p_+(z) = B_+/\{1 + a_+^2(z)\}^{1/2}; \quad p_-(z) = B_-/\{1 + a_-^2(z)\}^{1/2}, \quad (29-32)$$

where B_+ and B_- are constants independent of z . Hence finally

$$b_1(z) = \left\{ \frac{B_+}{(1+a_+^2)^{1/2}} I_+ + \frac{B_-}{(1+a_-^2)^{1/2}} I_- \right\} I_a, \quad (29-33a)$$

$$b_2(z) = \left\{ \frac{a_+ B_+}{(1+a_+^2)^{1/2}} I_+ + \frac{a_- B_-}{(1+a_-^2)^{1/2}} I_- \right\} I_a, \quad (29-33b)$$

where I_{\pm} and I_a are defined by Eqs. (29–29) and (29–31). The corresponding power in each fiber follows from Eq. (29–9) as

$$P_1(z) = \frac{B_+^2}{1+a_+^2} + \frac{B_-^2}{1+a_-^2} + \frac{2B_+ B_-}{(1+a_+^2)^{1/2} (1+a_-^2)^{1/2}} \cos \left\{ 2 \int_0^z \frac{C}{F} dz \right\}, \quad (29-34a)$$

$$P_2(z) = \frac{a_+^2 B_+^2}{1+a_+^2} + \frac{a_-^2 B_-^2}{1+a_-^2} - \frac{2B_+ B_-}{(1+a_+^2)^{1/2} (1+a_-^2)^{1/2}} \cos \left\{ 2 \int_0^z \frac{C}{F} dz \right\}, \quad (29-34b)$$

since $a_+ a_- = -1$, as is clear from Eqs. (29–28) and (29–31). We have assumed that B_+ and B_- are real to ensure the modes have the same phase at $z = 0$.

29–11 Example: Identical fibers

When the two slowly varying fibers are identical, as in Fig. 19–3(a), then $\bar{\beta}_1 = \bar{\beta}_2$, and Eqs. (29–28) and (29–31) show that $F = 1$ and $a_{\pm} = \pm 1$. The solution of Eq. (29–33) satisfying $b_1(0) = 1$ and $b_2(0) = 0$ is $B_+ = B_- = 1/\sqrt{2}$, whence Eq. (29–34) gives the power at each position along the fibers as [8]

$$P_1(z) = \cos^2 \left\{ \int_0^z C(z) dz \right\}; \quad P_2(z) = \sin^2 \left\{ \int_0^z C(z) dz \right\}, \quad (29-35)$$

which is identical to the result derived in Section 19–6, using the composite local modes of the two-fiber waveguide.

29–12 Example: Tapered couplers

Consider a tapered coupler, such as the one illustrated in Fig. 19–4(a), and assume that only the first fiber carries unit initial power, i.e. $b_1(0) = 1$ and $b_2(0) = 0$. We can simplify the solution of Eq. (29–34) by using the fact that the fibers are optically well

separated, i.e. $\bar{\beta}_1 \gg |C|$, $\bar{\beta}_2 \gg |C|$. Furthermore, the fibers are sufficiently dissimilar that $\bar{\beta}_1 \gg \bar{\beta}_2$ at $z = 0$. It then follows from Eqs. (29-28) and (29-31) that $F \cong 0$, $a_+ \cong 0$ and $|a_-| \gg 1$, which merely verifies our initial conditions expressed by

$$P_1(0) \cong B_+^2 \cong 1; \quad P_2(0) \cong B_-^2 \cong 0. \quad (29-36)$$

Hence the power distribution between the two fibers along the length of the coupler follows from Eq. (29-34) as

$$P_1(z) = \frac{1}{1 + a_+^2}; \quad P_2(z) = \frac{a_+^2}{1 + a_+^2} = 1 - P_1(z). \quad (29-37)$$

In the central region of the coupler where the fibers are virtually identical, it follows that $F \cong a_+ \cong 1$, and each fiber carries half the total power. At the end of the taper, $z = L$, the dissimilarity between the fibers is the reverse of that at $z = 0$, and thus $\bar{\beta}_2 \gg \bar{\beta}_1$. In this case $F \cong 0$ and $a_+ \gg 1$, so that Eq. (29-37) reduces to $P_1(L) \cong 0$, $P_2(L) \cong 1$. In other words, *all of the power initially in the first fiber has transferred to the second fiber*, which is the conclusion reached in Section 19-7 using the composite local modes of the coupler.

ARRAYS OF FIBERS

When an arbitrary number of parallel, single-mode fibers forms an array, an equal number of coupled equations is required to describe cross-talk, since each fiber requires one equation to describe the coupling of its fundamental-mode fields with the fundamental-mode fields of all the other fibers in the array. We assume that power exchange between these modes is the predominant effect. In general, the set of coupled equations is intractable but, for some cases of practical interest, the symmetry of the array together with the symmetry of the illumination enables cross-talk to be described by pairs of coupled equations, which are simply related to the coupled equations studied in Sections 29-2 and 29-9. Thus the solution for two parallel, cylindrically symmetric or slowly varying fibers is the building block for constructing solutions to more complicated arrays. To demonstrate the idea we now consider examples.

29-13 Example: Periodic illumination of infinite arrays

Consider an infinite array of parallel, single-mode fibers which are identical and uniformly spaced. We assume the fibers are weakly guiding and have an otherwise arbitrary refractive-index profile. At the beginning of the array, $z = 0$, alternate fibers are illuminated with power $P_1(0)$ or $P_2(0) < P_1(0)$, denoted by + or -, respectively, in the examples of Fig. 29-3. The periodic illumination means that the amplitudes $b_1(z)$ and $b_2(z)$ of the fundamental-mode fields, defined in Eq. (29-1), are the same for every

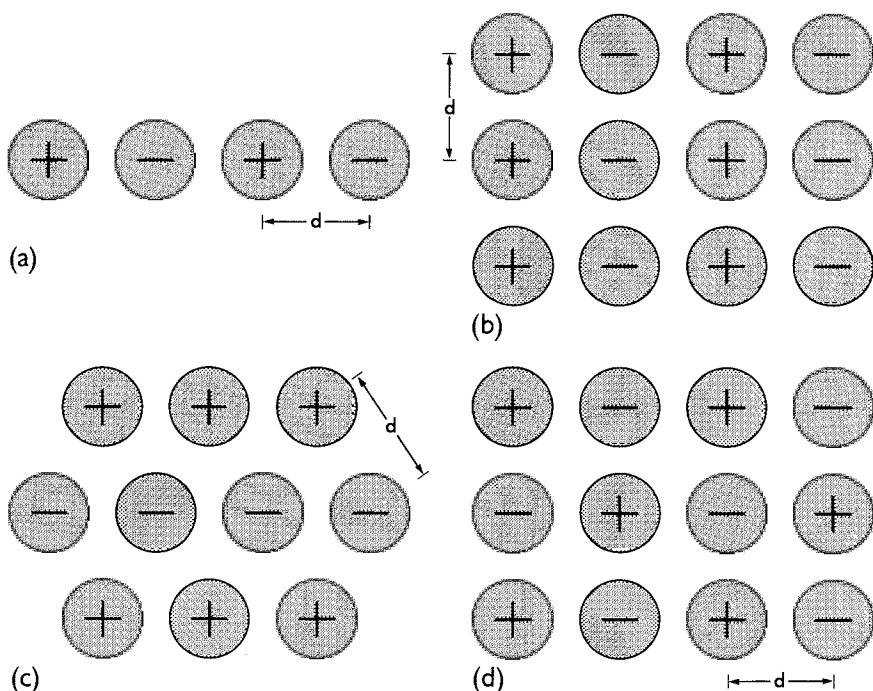


Fig. 29-3 Sections of infinite arrays of fibers illuminated alternatively with power $+$ and $-$. The arrays are (a) one-dimensional, (b) columnar, (c) hexagonal and (d) chess board.

fiber illuminated with power $P_1(0)$ and $P_2(0)$, respectively, i.e. $b_1(z)$ applies to every '+' fiber and $b_2(z)$ to every '-' fiber.

We can determine the modal amplitudes quite simply provided we assume that the fiber spacing is sufficiently large to ignore all but nearest-neighbor coupling. We are reminded that the coupling coefficient of Eq. (29-6) decreases exponentially with increasing separation. Nearest-neighbor coupling involves only fibers with different illumination, since two fibers with the same illumination clearly exchange no power. Consequently the solution for $b_1(z)$ and $b_2(z)$ is given by Eq. (29-7) with $\bar{\beta}_1 = \bar{\beta}_2 = \bar{\beta}$, i.e. $F = 1$ and $\beta_a = \bar{\beta}$, and C replaced by a weighted coupling coefficient to account for all nearest-neighbor fibers which interact, e.g. the number of '+'s adjacent to each '-' in Fig. 29-3. If $C(d)$ denotes the coupling coefficient between two fibers with center-to-center separation d , then the appropriate weighted coupling coefficient D for each of the arrays in Fig. 29-3 is given by

$$(a) \ 2C(d); \ (b) \ 2C(d) + 4C(\sqrt{2}d); \ (c) \ 4C(d); \ (d) \ 4C(d). \quad (29-38)$$

It is now evident that, by similar reasoning, coupling between one fiber and *all* other fibers of the array can be reduced to one pair of coupled equations in terms of a

weighted coupling coefficient which is a generalization of Eq. (29-38). However, nearest-neighbor coupling is a very accurate approximation and is adequate for most purposes.

Power in each fiber

The power in fibers with + or - illumination follows Eq. (29-10) by setting $\bar{\beta}_1 = \bar{\beta}_2$, $F = 1$ and replacing C by D . Hence

$$P_1(z) = P_1(0) \cos^2(Dz) + P_2(0) \sin^2(Dz), \quad (29-39a)$$

$$P_2(z) = P_1(0) \sin^2(Dz) + P_2(0) \cos^2(Dz). \quad (29-39b)$$

The values of D in Eq. (29-38) show that cross-talk is greater in an array than for two fibers with the same separation. Furthermore, the beat length varies inversely with D and therefore maximum power transfer occurs over a shorter distance in arrays.

29-14 Example: Absorption in infinite arrays

In addition to cross-talk, we can also take into account the effects of absorption in arrays. This is useful in the study of visual photoreceptors, which in many animals are absorbing fibers, often single moded and weakly guiding [2, 3]. The image encoded by a photoreceptor array is determined by the distribution of absorbed light across the array. Here we examine the image deterioration due to cross-talk when the photoreceptors have the alternate illumination of Fig. 29-3.

We assume a uniform power absorption coefficient α throughout the array, in which case the power attenuation coefficient γ for each fiber satisfies $\gamma = \alpha$, as we showed in Section 18-8. Thus, by analogy with Eq. (29-21), the power in each fiber is given by the product of $P_1(z)$ or $P_2(z)$ of Eq. (29-39) with $\exp(-\alpha z)$. We define $P_+(z)$ and $P_-(z)$ to be the power absorbed over length z of fibers with illumination + and -, respectively. If there were no cross-talk, then $P_+(z) \rightarrow P_1(0)$ and $P_-(z) \rightarrow P_2(0)$ as $z \rightarrow \infty$, i.e. each fiber of the array would absorb all of the power illuminating it. However, because of cross-talk, this situation is degraded. If we define a normalized difference in absorption by

$$\delta N(z) = \{P_+(z) - P_-(z)\} / \{P_1(0) - P_2(0)\}, \quad (29-40)$$

then $\delta N(z) \rightarrow 1$ as $z \rightarrow \infty$ without cross-talk. To determine the degradation, we consider a differential length dz of the array, and deduce from Eq. (11-62), Table 11-2, page 232, and Table 13-2, page 292, that

$$dP_+(z) - dP_-(z) = \alpha \{P_1(z) - P_2(z)\} \exp(-\alpha z) dz, \quad (29-41)$$

since $n^f \cong n_{\infty}$ everywhere. Thus for length L of the array

$$\delta N(L) = \frac{\alpha}{P_1(0) - P_2(0)} \int_0^L \{P_1(z) - P_2(z)\} \exp(-\alpha z) dz. \quad (29-42)$$

Substituting from Eq. (29-39) and using Eq. (37-114), we deduce that

$$\delta N(L) = \frac{1}{1 + 4D^2/\alpha^2} \{1 - [\cos(2DL) - (2D/\alpha)\sin(2DL)]\exp(-\alpha L)\}, \quad (29-43)$$

where the value of D is given by Eq. (29-38), and the parameter $2D/\alpha$ is proportional to the ratio of the absorption length $1/\alpha$ to the beat length $2\pi/D$. Hence $\delta N(L) \rightarrow 1/(1 + 4D^2/\alpha^2)$ as $L \rightarrow \infty$ for arbitrary values of $2D/\alpha$. On the other hand if L is finite and the absorption length is large compared to the beat length, i.e. $2D/\alpha \gg 1$, we deduce that $\delta N(L) \ll 1$ and the degradation due to cross-talk is severe.

29-15 Example: Single-fiber illumination in an infinite array

Consider an infinite, one-dimensional array of identical, single-mode fibers which are weakly guiding. They are labelled by $n = -\infty, \dots, -1, 0, 1, \dots, \infty$, as shown in Fig. 29-4(a). Only the center fiber $n = 0$ is illuminated with unit power at $z = 0$. As its fundamental mode propagates, power will be coupled to the fundamental modes of the neighboring fibers $n = \pm 1$. These two fibers in turn couple to the $n = \pm 2$ fibers and to the $n = 0$ fiber, and so on. Thus power is distributed over an increasing number of fibers farther into the array.

To model this process, we assume nearest-neighbor coupling only and ignore losses to the radiation field. There is a coupled mode equation for each fiber, which relates the fundamental-mode amplitude $b_n(z)$ of the n th fiber to the corresponding amplitudes $b_{n-1}(z)$ and $b_{n+1}(z)$ of the $(n-1)$ th and $(n+1)$ th fibers, where $b_n(z)$ is defined by analogy with Eq. (29-1). The cross-coupling coefficient between adjacent fibers is given by C of Eq. (29-6), and by generalizing Eq. (29-4a) to include coupling to adjacent fibers, then [9]

$$\frac{db_n}{dz} - i\beta b_n = iC(b_{n-1} + b_{n+1}); \quad -\infty < n < \infty, \quad (29-44)$$

where β is the fundamental-mode propagation constant, self-coupling is omitted and by symmetry $b_{-n} = b_n$. If we rearrange these equations as

$$2 \frac{d}{d(2Cz)} \{i^{-n} b_n \exp(-i\beta z)\} = \{i^{-(n-1)} b_{n-1} \exp(-i\beta z)\} - \{i^{-(n+1)} b_{n+1} \exp(-i\beta z)\}, \quad (29-45)$$

and compare with the recurrence relation of Eq. (37-72a), we find that the solution satisfying $b_0(0) = 1$ and $b_n(0) = 0$, $n \neq 0$, is given by

$$b_n(z) = i^n J_n(2Cz) \exp(i\beta z), \quad (26-46)$$

where J_n is the Bessel function of the first kind. The power $P_n(z)$ in each fiber of the array follows from Eq. (29-9) as

$$P_n(z) = P_{-n}(z) = J_n^2(2Cz). \quad (29-47)$$

We deduce from Eq. (37-87) that the maximum power in any fiber varies as $1/z$ when $z \rightarrow \infty$.

29-16 Example: Finite polygonal arrays

We now examine propagation along arrays consisting of a finite number of weakly guiding, single-mode fibers. The fibers are located at the n vertices of a regular, closed polygon, as illustrated by the triangular ($n = 3$) and hexagonal ($n = 6$) cases in Figs. 29-4(b) and (c), while another fiber—not necessarily identical to the surrounding fibers—is located at the center of the polygon. For arbitrary illumination, the description of cross-talk between any pair of fibers of the polygon is complicated. However, if the fields of all the surrounding fibers are taken together, propagation along the polygon can be described by one pair of coupled equations, similar to Eq. (29-4) [4,5].

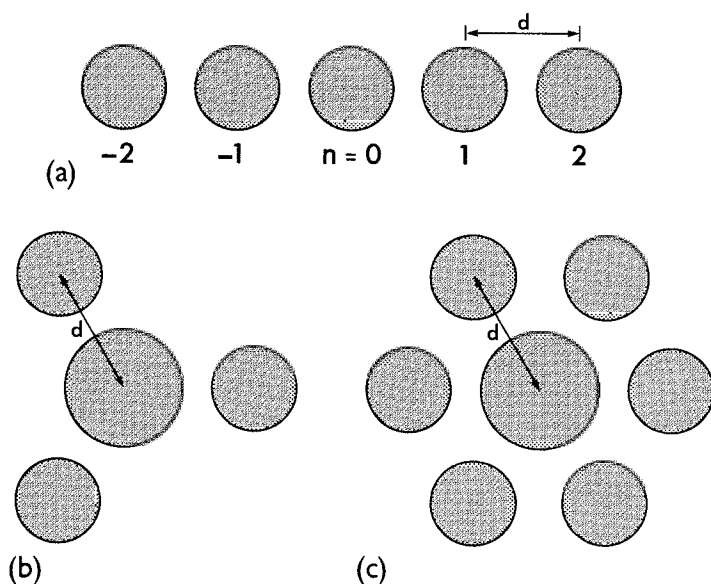


Fig. 29-4 (a) Infinite, one-dimensional array of fibers labelled by n and with center-to-center separation d . (b) and (c) are finite polygonal arrays for the triangular ($n = 3$) and hexagonal ($n = 6$) cores. The central fiber is not necessarily identical to the surrounding fibers, and the center-to-center separation between the central and surrounding fibers is d .

We ignore radiation losses and include only nearest-neighbor coupling. The central fiber is denoted by subscript 0 and the surrounding fibers by subscripts $1, 2, \dots, n$, and the center-to-center separation from the central fiber to each surrounding fiber is d . By analogy with Eq. (29-1), the amplitude of the fundamental-mode fields on the n th fiber is denoted by $b_n(z)$. If we omit self-coupling and generalize Eq. (29-4a) to include cross-coupling between the central fiber and the n surrounding fibers, then $b_0(z)$ satisfies

$$\frac{db_0}{dz} - i\beta_0 b_0 = iC_{01} \sum_{j=1}^n b_j, \quad (29-48)$$

where β_0 is the fundamental-mode propagation constant for the central fiber and C_{01} is the coupling coefficient between the central fiber and any surrounding fiber, evaluated from Eq. (29-6). For each surrounding fiber, we include coupling only to the central and adjacent fibers, whence

$$\frac{db_j}{dz} - i\beta_1 b_j = iC_{12}(b_{j+1} + b_{j-1}) + iC_{01}b_0, \quad (29-49)$$

for $j = 1, 2, \dots, n$, where C_{12} is the coupling coefficient between adjacent surrounding fibers and β_1 is the fundamental-mode propagation constant. Note that $b_{j+1} \rightarrow b_1$ when $j = n$ and $b_{j-1} \rightarrow b_n$ when $j = 1$. The next step is to sum Eq. (29-49) over all values of j , which leads to

$$\left\{ \frac{d}{dz} - i\beta_1 \right\} \sum_{j=1}^n b_j = 2iC_{12} \sum_{j=1}^n b_j + inC_{01}b_0, \quad (29-50)$$

for $n \geq 3$. When $n = 2$, the central and surrounding fibers are colinear, and consequently coupling between the outer fibers is negligible. Finally, we introduce the transformations

$$a_0 = \frac{1}{n^{1/2}} \sum_{j=1}^n b_j; \quad C = n^{1/2}C_{01}; \quad \beta_2 = \beta_1 + 2C_{12}, \quad (29-51)$$

which reduces Eqs. (29-48) and (29-50) to

$$\frac{da_0}{dz} - i\beta_0 a_0 = iCa_0; \quad \frac{da_0}{dz} - i\beta_2 a_0 = iCb_0. \quad (29-52)$$

The solution is then given by Eq. (29-7) with appropriate change of notation.

Symmetrical illumination

In the special case where the surrounding fibers are illuminated equally, then $b_1 = b_2 = \dots = b_n$ and the power $P_0(z)$ in the central fiber and the total power $P_1(z)$ in the surrounding fibers are given by Eq. (29-10) in terms of

$$F = 1/\{1 + (\beta_0 - \beta_1 - 2C_{12})^2/4C^2\}^{1/2}. \quad (29-53)$$

Consequently complete power transfer between the central and surrounding fibers can occur only if they differ sufficiently so that $\beta_0 = \beta_1 + 2C_{12}$. Since C_{12} is exponentially small, only a slight difference between the fibers is required to satisfy this condition.

REFERENCES

1. Kapany, N. S. and Burke, J. J. (1972) *Optical Waveguides*, Academic Press, New York, chap. 7.
2. Snyder, A. W. and Menzel, R. (eds) (1975) *Photoreceptor Optics*, Springer-Verlag, Berlin, p. 50.

3. Snyder, A. W. (1979) *Handbook of Sensory Physiology*, Vol. VII/6A (ed. K. Autrum), Springer-Verlag, Berlin, pp. 279–81.
4. Snyder, A. W. (1972) Coupled-mode theory for optical fibers. *J. Opt. Soc. Am.*, **62**, 1267–77.
5. McIntyre, P. and Snyder, A. W. (1973) Power transfer between optical fibers. *J. Opt. Soc. Am.*, **63**, 1518–27.
6. McIntyre, P. (1975) Crosstalk in absorbing optical fibers. *J. Opt. Soc. Am.*, **65**, 810–13.
7. Snyder, A. W. and McIntyre, P. (1976) Crosstalk between light pipes. *J. Opt. Soc. Am.*, **66**, 877–82.
8. McIntyre, P. and Snyder, A. W. (1974) Power transfer between nonparallel and tapered optical fibers. *J. Opt. Soc. Am.*, **64**, 285–8.
9. Jones, A. L. (1965) Coupling of optical fibers and scattering in fibers. *J. Opt. Soc. Am.*, **55**, 261–9.

PART III

Supplementary Materia.

Introduction to Part III

The presentation of the analysis in Parts I and II attempts, where possible, to provide basic physical insight, which is quantified with simple, worked examples. Now, in Part III, we augment this approach with a more rigorous mathematical foundation, which also includes important background material necessary to assist in the development of ideas in the preceding chapters.

Maxwell's equations

30-1	Fields of translationally invariant waveguides	591
30-2	Relationships between field components	591
30-3	Transverse fields in terms of the longitudinal fields	592
30-4	Fields of nonabsorbing waveguides	593
30-5	Forward- and backward-propagating fields	593
Vector wave equations		594
30-6	Cartesian components of the fields	595
30-7	Homogeneous vector wave equations	595
30-8	Equations for the longitudinal field components	597
Absorbing media		597
30-9	Absorbed power	597
Anisotropic media		598
30-10	Vector wave equations	598
30-11	Planar waveguides	598
30-12	Uniaxial waveguides	599
30-13	Polarization parallel to a principal axis	600
References		600

In this chapter we lay down the fundamental equations for an electromagnetic analysis of optical waveguides. From these equations we deduce elementary properties of the fields. The material presented here is used throughout Parts II and III, although it is abstracted mainly in Chapter 11 when discussing properties of bound modes.

The spatial dependence of the electric field $\mathbf{E}(x, y, z)$ and the magnetic field $\mathbf{H}(x, y, z)$ of an optical waveguide is determined by Maxwell's equations. *We assume an implicit time dependence $\exp(-i\omega t)$ in the field vectors, current density \mathbf{J} and charge density σ .* The dielectric constant $\epsilon(x, y, z)$ is related to the refractive index $n(x, y, z)$ by $\epsilon = n^2 \epsilon_0$, where ϵ_0 is the dielectric constant of free space. For the nonmagnetic materials which normally constitute an optical waveguide, the magnetic permeability μ is very nearly equal to the free-space value μ_0 . Thus for convenience *we assume $\mu = \mu_0$ throughout this book unless otherwise stated.* Under these conditions, Maxwell's equations are expressible in the form [1]

$$\nabla \times \mathbf{E} = i(\mu_0/\epsilon_0)^{1/2} k \mathbf{H}; \quad \nabla \times \mathbf{H} = \mathbf{J} - i(\epsilon_0/\mu_0)^{1/2} k n^2 \mathbf{E}, \quad (30-1a)$$

$$\nabla \cdot (n^2 \mathbf{E}) = \sigma/\epsilon_0; \quad \nabla \cdot \mathbf{H} = 0, \quad (30-1b)$$

using rationalized MKS units, where $k = 2\pi/\lambda$ is the free-space wavenumber, and λ is

the wavelength of light in free space. Relationships between n , k , ϵ_0 , μ_0 and other electromagnetic quantities are given inside the back cover.

In regions free of charges and currents, the boundary conditions satisfied by the fields across an interface between media of differing refractive index are: (i) continuity of the magnetic field and the component of the electric field *tangential* to the interface; and (ii) continuity of the *normal* component of the displacement vector $\epsilon_0 n^2 \mathbf{E}$.

30-1 Fields of translationally invariant waveguides

If a waveguide has a refractive-index profile that does not vary with distance z along the waveguide, i.e. $n = n(x, y)$, then the waveguide is *translationally invariant*. The electric and magnetic fields of the waveguide are expressible as a superposition of fields with the separable form [2]

$$\mathbf{E}(x, y, z) = \mathbf{e}(x, y)\exp(i\beta z); \quad \mathbf{H}(x, y, z) = \mathbf{h}(x, y)\exp(i\beta z), \quad (30-2)$$

where β is the propagation constant and the axes are oriented as in Fig. 11-1(a). The corresponding forms for the cylindrical polar coordinates shown in Fig. 12-3 are

$$\mathbf{E}(r, \phi, z) = \mathbf{e}(r, \phi)\exp(i\beta z); \quad \mathbf{H}(r, \phi, z) = \mathbf{h}(r, \phi)\exp(i\beta z). \quad (30-3)$$

We decompose these fields into longitudinal and transverse components, parallel to and orthogonal to the waveguide axis, respectively, and denoted by subscripts z and t , where

$$\mathbf{E} = (\mathbf{e}_t + e_z \hat{\mathbf{z}})\exp(i\beta z); \quad \mathbf{H} = (\mathbf{h}_t + h_z \hat{\mathbf{z}})\exp(i\beta z), \quad (30-4)$$

and $\hat{\mathbf{z}}$ is the unit vector parallel to the waveguide axis.

30-2 Relationships between field components

If we substitute the field representation of Eq. (30-4) into the source-free Maxwell equations, i.e. Eq. (30-1) with $\mathbf{J} = 0$, $\sigma = 0$, and compare longitudinal and transverse components, we deduce

$$\mathbf{e}_t = -\left(\frac{\mu_0}{\epsilon_0}\right)^{1/2} \frac{1}{kn^2} \hat{\mathbf{z}} \times \{\beta \mathbf{h}_t + i \nabla_t h_z\}, \quad (30-5a)$$

$$\mathbf{h}_t = \left(\frac{\epsilon_0}{\mu_0}\right)^{1/2} \frac{1}{k} \hat{\mathbf{z}} \times \{\beta \mathbf{e}_t + i \nabla_t e_z\}, \quad (30-5b)$$

$$e_z = i \left(\frac{\mu_0}{\epsilon_0}\right)^{1/2} \frac{1}{kn^2} \hat{\mathbf{z}} \cdot \nabla_t \times \mathbf{h}_t = \frac{i}{\beta} \{\nabla_t \cdot \mathbf{e}_t + (\mathbf{e}_t \cdot \nabla_t) \ln n^2\}, \quad (30-5c)$$

$$h_z = -i \left(\frac{\epsilon_0}{\mu_0}\right)^{1/2} \frac{1}{k} \hat{\mathbf{z}} \cdot \nabla_t \times \mathbf{e}_t = \frac{i}{\beta} \nabla_t \cdot \mathbf{h}_t, \quad (30-5d)$$

where $n = n(x, y)$ and $k = 2\pi/\lambda$. The vector operators are defined in Table 30-1, and vector identities are given in Section 37-2.

Table 30-1 Vector and scalar operators. Decomposition of vector and scalar operators into transverse and longitudinal components, where Ψ and \mathbf{A} are separable scalar and vector functions. The unit vectors \hat{x} , \hat{y} , \hat{z} , \hat{r} and $\hat{\phi}$ are parallel to the coordinate directions in Fig. 12-3.

$\Psi = \psi(x, y)\exp(i\beta z)$	$\mathbf{A} = \mathbf{a}(x, y)\exp(i\beta z)$
$\nabla\Psi = \nabla_t\Psi + i\beta\Psi\hat{z}$	$\nabla\cdot\mathbf{A} = \nabla_t\cdot\mathbf{A}_t + i\beta A_z$
$\nabla_t\Psi = \hat{x}\frac{\partial\Psi}{\partial x} + \hat{y}\frac{\partial\Psi}{\partial y}$ $= \hat{r}\frac{\partial\Psi}{\partial r} + \hat{\phi}\frac{1}{r}\frac{\partial\Psi}{\partial\phi}$	$\nabla_t\cdot\mathbf{A}_t = \frac{\partial A_x}{\partial x} + \frac{\partial A_y}{\partial y}$ $= \frac{1}{r}\frac{\partial}{\partial r}(rA_r) + \frac{1}{r}\frac{\partial A_\phi}{\partial\phi}$
$\nabla^2\Psi = \nabla_t^2\Psi - \beta^2\Psi$	$\nabla\times\mathbf{A} = \nabla_t\times\mathbf{A}_t + i\beta\hat{z}\times\mathbf{A}_t - \hat{z}\times\nabla_t A_z$
$\nabla_t^2\Psi = \frac{\partial^2\Psi}{\partial x^2} + \frac{\partial^2\Psi}{\partial y^2}$ $= \frac{1}{r}\frac{\partial}{\partial r}\left\{r\frac{\partial\Psi}{\partial r}\right\} + \frac{1}{r^2}\frac{\partial^2\Psi}{\partial\phi^2}$	$\nabla_t\times\mathbf{A}_t = \hat{z}\left\{\frac{\partial A_y}{\partial x} - \frac{\partial A_x}{\partial y}\right\}$ $= \hat{z}\left\{\frac{1}{r}\frac{\partial}{\partial r}(rA_\phi) - \frac{1}{r}\frac{\partial A_r}{\partial\phi}\right\}$

30-3 Transverse fields in terms of the longitudinal fields

If we eliminate \mathbf{e}_t or \mathbf{h}_t from Eqs. (30-5a) and (30-5b), we can express the transverse fields in terms of the longitudinal fields [2]

$$\mathbf{e}_t = \frac{i}{k^2 n^2 - \beta^2} \left\{ \beta \nabla_t e_z - \left(\frac{\mu_0}{\epsilon_0} \right)^{1/2} k \hat{z} \times \nabla_t h_z \right\}, \quad (30-6a)$$

$$\mathbf{h}_t = \frac{i}{k^2 n^2 - \beta^2} \left\{ \beta \nabla_t h_z + \left(\frac{\epsilon_0}{\mu_0} \right)^{1/2} k n^2 \hat{z} \times \nabla_t e_z \right\}, \quad (30-6b)$$

where $n = n(x, y)$ and $k = 2\pi/\lambda$. These expressions are particularly useful for constructing the modal fields of step-profile waveguides in Chapters 12 and 25, when the wavenumber is related to the modal parameters inside the back cover by

$$n^2 k^2 - \beta^2 = \begin{cases} k^2 n_{co}^2 - \beta^2 = U^2/\rho^2, & \text{core,} \\ k^2 n_{cl}^2 - \beta^2 = -W^2/\rho^2, & \text{cladding,} \end{cases} \quad (30-7a)$$

$$(30-7b)$$

where n_{co} and n_{cl} are the core and cladding refractive indices.

Planar waveguides

The cartesian components of Eq. (30-6) for planar waveguides with refractive-index

profile $n(x)$ are

$$e_x = \frac{i}{p} \left\{ \beta \frac{\partial e_z}{\partial x} + \left(\frac{\mu_0}{\varepsilon_0} \right)^{1/2} k \frac{\partial h_z}{\partial y} \right\}; \quad e_y = \frac{i}{p} \left\{ \beta \frac{\partial e_z}{\partial y} - \left(\frac{\mu_0}{\varepsilon_0} \right)^{1/2} k \frac{\partial h_z}{\partial x} \right\}, \quad (30-8a)$$

$$h_x = \frac{i}{p} \left\{ \beta \frac{\partial h_z}{\partial x} - \left(\frac{\varepsilon_0}{\mu_0} \right)^{1/2} kn^2 \frac{\partial e_z}{\partial y} \right\}; \quad h_y = \frac{i}{p} \left\{ \beta \frac{\partial h_z}{\partial y} + \left(\frac{\varepsilon_0}{\mu_0} \right)^{1/2} kn^2 \frac{\partial e_z}{\partial x} \right\}, \quad (30-8b)$$

where $p = k^2 n^2 - \beta^2$ and $n = n(x)$.

Circular fibers

The radial and azimuthal components of Eq. (30-6) for circular fibers with refractive-index profile $n(r)$ are

$$e_r = \frac{i}{p} \left\{ \beta \frac{\partial e_z}{\partial r} + \left(\frac{\mu_0}{\varepsilon_0} \right)^{1/2} k \frac{\partial h_z}{\partial \phi} \right\}; \quad e_\phi = \frac{i}{p} \left\{ \beta \frac{\partial e_z}{\partial \phi} - \left(\frac{\mu_0}{\varepsilon_0} \right)^{1/2} k \frac{\partial h_z}{\partial r} \right\}, \quad (30-9a)$$

$$h_r = \frac{i}{p} \left\{ \beta \frac{\partial h_z}{\partial r} - \left(\frac{\varepsilon_0}{\mu_0} \right)^{1/2} kn^2 \frac{\partial e_z}{\partial \phi} \right\}; \quad h_\phi = \frac{i}{p} \left\{ \beta \frac{\partial h_z}{\partial \phi} + \left(\frac{\varepsilon_0}{\mu_0} \right)^{1/2} kn^2 \frac{\partial e_z}{\partial r} \right\}, \quad (30-9b)$$

where $p = k^2 n^2 - \beta^2$ and $n = n(r)$.

30-4 Fields of nonabsorbing waveguides

The fields of the waveguide can have arbitrary normalization, so that in general \mathbf{e} and \mathbf{h} are complex. However, on a nonabsorbing waveguide, the refractive index n is real, and Eq. (30-5) shows that it is consistent to choose the components of \mathbf{e} and \mathbf{h} so that *either* the transverse components are real and the longitudinal components are imaginary *or* the transverse components are imaginary and the longitudinal components are real. We adopt the former convention throughout this book, so that

$$\mathbf{e}_t, \mathbf{h}_t \text{ real}; \quad e_z, h_z \text{ imaginary.} \quad (30-10)$$

The fields \mathbf{E} and \mathbf{H} of Eq. (30-4) do not obey this convention.

30-5 Forward- and backward-propagating fields

When the propagation constant β is positive, the fields of the waveguide propagate in the positive z -direction in Fig. 11-1(a). Under the transformation $\beta \rightarrow -\beta$, the backward-propagating fields are simply related to the forward-propagating fields. If we denote forward and backward by $+$ and $-$ superscripts, then we deduce from Eq. (30-5) that there are two possibilities. Either

$$\mathbf{e}^- = -\mathbf{e}_t^+ + e_z^+ \hat{\mathbf{z}}; \quad \mathbf{h}^- = \mathbf{h}_t^+ - h_z^+ \hat{\mathbf{z}}, \quad (30-11a)$$

or

$$\mathbf{e}^- = \mathbf{e}_t^+ - e_z^+ \hat{\mathbf{z}}; \quad \mathbf{h}^- = -\mathbf{h}_t^+ + h_z^+ \hat{\mathbf{z}}. \quad (30-11b)$$

We adopt the latter convention throughout. The relationships of Eqs. (30-10) and

(30-11b) both hold for nonabsorbing waveguides, so by combining them we deduce

$$\mathbf{e}^- = (\mathbf{e}^+)^*; \quad \mathbf{h}^- = (-\mathbf{h}^+)^*, \quad (30-12)$$

where * denotes complex conjugate.

VECTOR WAVE EQUATIONS

If we eliminate either the electric or magnetic fields from Maxwell's equations in Eq. (30-1a), we obtain the inhomogeneous vector wave equations

$$\{\nabla^2 + n^2 k^2\} \mathbf{E} = -\nabla(\mathbf{E}_t \cdot \nabla_t \ln n^2) - i \left(\frac{\mu_0}{\varepsilon_0} \right)^{1/2} \left\{ k \mathbf{J} + \frac{1}{k} \nabla \left(\frac{\nabla \cdot \mathbf{J}}{n^2} \right) \right\}, \quad (30-13a)$$

$$\{\nabla^2 + n^2 k^2\} \mathbf{H} = (\nabla \times \mathbf{H}) \times \nabla_t \ln n^2 - \nabla \times \mathbf{J} - \mathbf{J} \times \nabla_t \ln n^2, \quad (30-13b)$$

where $n = n(x, y)$, $k = 2\pi/\lambda$, and ∇^2 is defined by Eq. (37-30). We emphasize that ∇^2 is a *vector* operator, not to be confused with the *scalar* operator ∇^2 . If the scalar components of \mathbf{E} and \mathbf{H} are referred to the directions defined by an arbitrary coordinate system, then ∇^2 couples the components, e.g. Eq. (30-15) below in the case of cylindrical polar coordinates.

When there are no sources present, i.e. $\mathbf{J} = 0$, the fields with the separable form of Eq. (30-4) satisfy the *homogeneous* vector wave equations

$$\{\nabla_t^2 + n^2 k^2 - \beta^2\} \mathbf{e} = -(\nabla_t + i\beta \hat{\mathbf{z}}) \mathbf{e}_t \cdot \nabla_t \ln n^2, \quad (30-14a)$$

$$\{\nabla_t^2 + n^2 k^2 - \beta^2\} \mathbf{h} = \{(\nabla_t + i\beta \hat{\mathbf{z}}) \times \mathbf{h}\} \times \nabla_t \ln n^2, \quad (30-14b)$$

where $n = n(x, y)$, $k = 2\pi/\lambda$, and the vector operator ∇_t^2 is defined in Eq. (37-30).

Circular fibers

If we refer the component equations of Eq. (30-14) to the radial, azimuthal and longitudinal directions defined by the cylindrical polar coordinates r, ϕ, z in Fig. 12-3, i.e. $\mathbf{e} = (e_r, e_\phi, e_z)$, $\mathbf{h} = (h_r, h_\phi, h_z)$, and assume a symmetric refractive index profile $n(r)$, we find

$$\nabla_t^2 e_r - \frac{2}{r^2} \frac{\partial e_\phi}{\partial \phi} + \frac{\partial}{\partial r} \left\{ e_r \frac{d \ln n^2}{dr} \right\} - \frac{e_r}{r^2} + \{n^2 k^2 - \beta^2\} e_r = 0, \quad (30-15a)$$

$$\nabla_t^2 e_\phi + \frac{1}{r} \left\{ \frac{d \ln n^2}{dr} + \frac{2}{r} \right\} \frac{\partial e_r}{\partial \phi} - \frac{e_\phi}{r^2} + \{n^2 k^2 - \beta^2\} e_\phi = 0, \quad (30-15b)$$

$$\nabla_t^2 e_z + i\beta \frac{d \ln n^2}{dr} e_r + \{n^2 k^2 - \beta^2\} e_z = 0, \quad (30-15c)$$

$$\nabla_t^2 h_r - \frac{2}{r^2} \frac{\partial h_\phi}{\partial \phi} - \frac{h_r}{r^2} + \{n^2 k^2 - \beta^2\} h_r = 0, \quad (30-15d)$$

$$\nabla_t^2 h_\phi - \frac{1}{r} \frac{d \ln n^2}{dr} \frac{\partial}{\partial r} (r h_\phi) + \frac{1}{r} \left\{ \frac{d \ln n^2}{dr} + \frac{2}{r} \right\} \frac{\partial h_r}{\partial \phi} - \frac{h_\phi}{r^2} + \{n^2 k^2 - \beta^2\} h_\phi = 0, \quad (30-15e)$$

$$\nabla_t^2 h_z + \frac{d \ln n^2}{dr} \frac{\partial h_z}{\partial r} - i\beta \frac{d \ln n^2}{dr} h_r + \{n^2 k^2 - \beta^2\} h_z = 0, \quad (30-15f)$$

where $n = n(r)$ and the transverse Laplace operator ∇_t^2 is defined in Table 30-1.

30–6 Cartesian components of the fields

As emphasized above, the vector operator ∇^2 couples the field components in an arbitrary coordinate system. However, if the field vectors have components referred to fixed cartesian directions, this coupling does not occur and the vector operator ∇^2 is replaced by the scalar Laplacian ∇^2 . Thus, if we set

$$\mathbf{E} = E_x \hat{x} + E_y \hat{y} + E_z \hat{z}; \quad \mathbf{H} = H_x \hat{x} + H_y \hat{y} + H_z \hat{z}, \quad (30-16)$$

in Eq. (30-13a), where \hat{x} , \hat{y} and \hat{z} are unit vectors parallel to the axes in Fig. 11-1(a), we obtain

$$\{\nabla^2 + n^2 k^2\} \mathbf{E} = -\nabla \{ \mathbf{E}_t \cdot \nabla_t \ln n^2 \} - i \left(\frac{\mu_0}{\epsilon_0} \right)^{1/2} \left\{ k \mathbf{J} + \frac{1}{k} \nabla \left(\frac{\nabla \cdot \mathbf{J}}{n^2} \right) \right\}, \quad (30-17a)$$

$$\{\nabla^2 + n^2 k^2\} \mathbf{H} = (\nabla \times \mathbf{H}) \times \nabla_t \ln n^2 - \nabla \times \mathbf{J} - \mathbf{J} \times \nabla_t \ln n^2, \quad (30-17b)$$

where ∇^2 is defined by Eq. (37-36), and $n = n(x, y)$. We note that although the field components are in fixed cartesian directions, the spatial variation of the components is expressible in any cylindrical coordinate system, e.g. Eq. (30-23) below in the case of cylindrical polar coordinates.

30–7 Homogeneous vector wave equations

If we work with the cartesian field components of Eq. (30-16) and the separable fields of Eq. (30-4), then in source-free regions Eq. (30-17) reduces to the homogeneous vector wave equations with transverse and longitudinal components given by

$$\{\nabla_t^2 + n^2 k^2 - \beta^2\} \mathbf{e}_t = -\nabla_t (\mathbf{e}_t \cdot \nabla_t \ln n^2), \quad (30-18a)$$

$$\{\nabla_t^2 + n^2 k^2 - \beta^2\} e_z = -i\beta \mathbf{e}_t \cdot \nabla_t \ln n^2, \quad (30-18b)$$

$$\{\nabla_t^2 + n^2 k^2 - \beta^2\} \mathbf{h}_t = (\nabla_t \times \mathbf{h}_t) \times \nabla_t \ln n^2, \quad (30-18c)$$

$$\{\nabla_t^2 + n^2 k^2 - \beta^2\} h_z = (\nabla_t h_z - i\beta \mathbf{h}_t) \cdot \nabla_t \ln n^2, \quad (30-18d)$$

where $n = n(x, y)$, $k = 2\pi/\lambda$, the transverse fields are defined by

$$\mathbf{e}_t = e_x \hat{x} + e_y \hat{y}; \quad \mathbf{h}_t = h_x \hat{x} + h_y \hat{y}, \quad (30-19)$$

and the operators ∇_t^2 , ∇_t are defined in Table 30-1.

Planar waveguides

On a planar waveguide with refractive-index profile $n(x)$, the separable fields have the spatial dependence

$$\mathbf{E}(x, z) = \mathbf{e}(x) \exp(i\beta z); \quad \mathbf{H}(x, z) = \mathbf{h}(x) \exp(i\beta z). \quad (30-20)$$

The component equations of Eq. (30-18) are then

$$\frac{d^2 e_x}{dx^2} + \frac{d}{dx} \left\{ e_x \frac{d \ln n^2}{dx} \right\} + (n^2 k^2 - \beta^2) e_x = 0, \quad (30-21a)$$

$$\frac{d^2 e_y}{dx^2} + \{n^2 k^2 - \beta^2\} e_y = 0, \quad (30-21b)$$

$$\frac{d^2 e_z}{dx^2} + i\beta \frac{d \ln n^2}{dx} e_x + \{n^2 k^2 - \beta^2\} e_z = 0, \quad (30-21c)$$

$$\frac{d^2 h_x}{dx^2} + \{n^2 k^2 - \beta^2\} h_x = 0, \quad (30-21d)$$

$$\frac{d^2 h_y}{dx^2} - \frac{d \ln n^2}{dx} \frac{dh_y}{dx} + \{n^2 k^2 - \beta^2\} h_y = 0, \quad (30-21e)$$

$$\frac{d^2 h_z}{dx^2} + \frac{d \ln n^2}{dx} \left\{ i\beta h_x - \frac{dh_z}{dx} \right\} + \{n^2 k^2 - \beta^2\} h_z = 0, \quad (30-21f)$$

where $n = n(x)$ and $k = 2\pi/\lambda$.

Circular fibers

On a circular fiber with axisymmetric refractive-index profile $n(r)$, the separable fields have the form of Eq. (30-3), where

$$\mathbf{e}(r, \phi) = e_x(r, \phi) \hat{\mathbf{x}} + e_y(r, \phi) \hat{\mathbf{y}} + e_z(r, \phi) \hat{\mathbf{z}}, \quad (30-22a)$$

$$\mathbf{h}(r, \phi) = h_x(r, \phi) \hat{\mathbf{x}} + h_y(r, \phi) \hat{\mathbf{y}} + h_z(r, \phi) \hat{\mathbf{z}}, \quad (30-22b)$$

The component equations of Eq. (30-18) are then

$$\{\nabla_t^2 + n^2 k^2 - \beta^2\} e_x + \frac{\partial}{\partial x} \left[\{e_x \cos \phi + e_y \sin \phi\} \frac{d \ln n^2}{dr} \right] = 0, \quad (30-23a)$$

$$\{\nabla_t^2 + n^2 k^2 - \beta^2\} e_y + \frac{\partial}{\partial y} \left[\{e_x \cos \phi + e_y \sin \phi\} \frac{d \ln n^2}{dr} \right] = 0, \quad (30-23b)$$

$$\{\nabla_t^2 + n^2 k^2 - \beta^2\} e_z + i\beta \{e_x \cos \phi + e_y \sin \phi\} \frac{d \ln n^2}{dr} = 0, \quad (30-23c)$$

$$\{\nabla_t^2 + n^2 k^2 - \beta^2\} h_x + \left\{ \frac{\partial h_y}{\partial x} - \frac{\partial h_x}{\partial y} \right\} \sin \phi \frac{d \ln n^2}{dr} = 0, \quad (30-23d)$$

$$\{\nabla_t^2 + n^2 k^2 - \beta^2\} h_y - \left\{ \frac{\partial h_y}{\partial x} - \frac{\partial h_x}{\partial y} \right\} \cos \phi \frac{d \ln n^2}{dr} = 0, \quad (30-23e)$$

$$\begin{aligned} \{\nabla_t^2 + n^2 k^2 - \beta^2\} h_z + \left[\left\{ i\beta h_x - \frac{\partial h_z}{\partial x} \right\} \cos \phi \right. \\ \left. + \left\{ i\beta h_y - \frac{\partial h_z}{\partial y} \right\} \sin \phi \right] \frac{d \ln n^2}{dr} = 0, \end{aligned} \quad (30-23f)$$

where $n = n(r)$, $k = 2\pi/\lambda$ and ∇_t^2 is defined in Table 30–1. The cartesian operators are related to the polar operator by Eq. (37–47)

$$\frac{\partial}{\partial x} = \cos \phi \frac{\partial}{\partial r} - \frac{\sin \phi}{r} \frac{\partial}{\partial \phi}; \quad \frac{\partial}{\partial y} = \sin \phi \frac{\partial}{\partial r} + \frac{\cos \phi}{r} \frac{\partial}{\partial \phi}, \quad (30-24)$$

and the cartesian and polar coordinates are oriented as in Fig. 12–3. The solution of Eq. (30–23) for \mathbf{e} and \mathbf{h} is identical to the solution of Eq. (30–15), since the fields are independent of the choice of coordinates.

30–8 Equations for the longitudinal field components

The longitudinal components e_z and h_z in Eqs. (30–18b) and (30–18d) depend on the transverse fields \mathbf{e}_t and \mathbf{h}_t . If we use Eq. (30–6) to express \mathbf{e}_t and \mathbf{h}_t in terms of e_z and h_z , we obtain the coupled equations

$$\{\nabla_t^2 + p\}e_z - \frac{\beta^2}{p}\nabla_t e_z \cdot \nabla_t \ln n^2 = -\left(\frac{\mu_0}{\epsilon_0}\right)^{1/2} \frac{k\beta}{p} \hat{\mathbf{z}} \cdot (\nabla_t h_z \times \nabla_t \ln n^2), \quad (30-25a)$$

$$\{\nabla_t^2 + p\}h_z - \frac{n^2 k^2}{p}\nabla_t h_z \cdot \nabla_t \ln n^2 = \left(\frac{\epsilon_0}{\mu_0}\right)^{1/2} \frac{kn^2 \beta}{p} \hat{\mathbf{z}} \cdot (\nabla_t e_z \times \nabla_t \ln n^2), \quad (30-25b)$$

where $p = k^2 n^2 - \beta^2$, $n = n(x, y)$ and $k = 2\pi/\lambda$.

ABSORBING MEDIA

Maxwell's equations apply directly to absorbing media by allowing the refractive index to be complex, as explained in Chapter 11. Here we show how to determine the electromagnetic power that is absorbed.

30–9 Absorbed power

Poynting's vector theorem can be derived from Maxwell's equations as a consequence of power conservation. It shows that the time-averaged power produced by a distribution of currents with density \mathbf{J} within volume \mathcal{V} is given by [1]

$$P = -\frac{1}{2} \int_{\mathcal{V}} \mathbf{J} \cdot \mathbf{E}^* d\mathcal{V}, \quad (30-26)$$

where the time dependence $\exp(-i\omega t)$ is implicit in \mathbf{J} and \mathbf{E} . We can then use the induced-current representation of Chapter 22 to determine the power absorbed due to material absorption. Using the notation of that chapter, we let n be the refractive index of the absorbing medium and denote the refractive index of the corresponding nonabsorbing medium by \bar{n} . The effects of absorption can then be described by the induced current \mathbf{J} of Eq. (22–3), where

$$\mathbf{J} = i(\epsilon_0/\mu_0)^{1/2} k(\bar{n}^2 - n^2)\mathbf{E}, \quad (30-27)$$

and \mathbf{E} is the electric field of the absorbing medium. If the real and imaginary parts of the

refractive index for the absorbing medium are n^r and n^i , then we set $n = n^r + in^i$, $\bar{n} = n^r$ and substitute the resulting expression into Eq. (30–26). The power lost from the fields is found to be

$$P = -k \left(\frac{\epsilon_0}{\mu_0} \right)^{1/2} \int_{\mathcal{V}} n^r n^i |\mathbf{E}|^2 d\mathcal{V}. \quad (30-28)$$

This expression is exact, provided the electric field in the absorbing medium is known exactly.

ANISOTROPIC MEDIA

Here we generalize Maxwell's equations and the associated wave equations to describe propagation in anisotropic materials [3]. The generalization follows by recognizing that the displacement vector, \mathbf{D} , is not, in general, parallel to the electric field \mathbf{E} . Instead, it obeys the relationship

$$\mathbf{D} = \epsilon_0 \mathbf{n}^2 \cdot \mathbf{E}, \quad (30-29)$$

where \mathbf{n}^2 is a *tensor* with nine components, i.e. the components of \mathbf{D} are given by $D_i = \epsilon_0 n_{ik}^2 E_k$, where $i, k = 1, 2$ or 3 and summation over k is implied. These components depend on the particular reference axes. For simplicity, we assume the cartesian axes are aligned parallel to the principal axes of the anisotropic medium, as discussed in Section 11–23. The tensor then has only diagonal components n_{11}^2 , n_{22}^2 and n_{33}^2 ; all other components are zero. For convenience, we denote these components by n_x^2 , n_y^2 and n_z^2 , respectively.

30–10 Vector wave equations

Maxwell's equations for a source-free, anisotropic medium are

$$\nabla \times \mathbf{E} = i(\mu_0/\epsilon_0)^{1/2} k \mathbf{H}; \quad \nabla \times \mathbf{H} = -i(\epsilon_0/\mu_0)^{1/2} k \mathbf{n}^2 \cdot \mathbf{E}, \quad (30-30a)$$

$$\nabla \cdot (\mathbf{n}^2 \cdot \mathbf{E}) = 0; \quad \nabla \cdot \mathbf{H} = 0, \quad (30-30b)$$

where parameters are defined inside the back cover. If we take $\nabla \times$ of the equations in Eq. (30–30a), eliminate either \mathbf{H} or \mathbf{E} , and apply the vector identities of Eqs. (37–30) and (37–31), we obtain the vector wave equations for the *cartesian* components of the fields

$$\nabla^2 \mathbf{E} + k^2 \mathbf{n}^2 \cdot \mathbf{E} = \nabla(\nabla \cdot \mathbf{E}); \quad \nabla \times \{ \mathbf{n}^{-2} \cdot (\nabla \times \mathbf{H}) \} = k^2 \mathbf{H}, \quad (30-31)$$

where \mathbf{n}^{-2} is a diagonal tensor with components n_x^{-2} , n_y^{-2} and n_z^{-2} . These equations are analogous to Eq. (30–17) for a source-free ($\mathbf{J} = 0$), isotropic medium. Because $\mathbf{n}^2 \cdot \mathbf{E}$ is not parallel to \mathbf{E} , it is not possible, in general, to express the $\nabla(\nabla \cdot \mathbf{E})$ term in Eq. (30–31) in an analogous manner to the term $-\nabla(\mathbf{E}_t \cdot \nabla_t \ln n^2)$ in Eq. (30–17a). However, simplifications of the vector wave equations are possible in special cases, as we now show.

30–11 Planar waveguides

If the waveguide has planar symmetry, i.e. is uniform in both the y - and z -directions of Fig. 12–1, and the principal axes of the materials constituting the waveguide are parallel

to the cartesian axes, then the structure supports TE or TM modes. By analogy with the TE and TM modes of isotropic waveguides, discussed in Sections 12–14 and 12–15, respectively, the electric field of each TE mode and the magnetic field of each TM mode have only y -components. If we use the representation of Eq. (30–20) and substitute into the first equation in Eq. (30–31), we obtain

$$\left\{ \frac{d^2}{dx^2} + k^2 n_y^2 - \beta^2 \right\} e_y = 0, \quad (30-32a)$$

where $n_y = n_y(x)$. Thus the electric fields of the TE modes obey the scalar wave equation. Similarly, the second equation in Eq. (30–31) leads to

$$\left\{ \frac{d^2}{dx^2} - \frac{d \ln n_z^2}{dx} \frac{d}{dx} + k^2 n_z^2 - \beta^2 \right\} h_y = 0, \quad (30-32b)$$

for the TM modes, where $n_z = n_z(x)$. If n_z is constant across the waveguide, then h_y satisfies the scalar wave equation. The remaining components follow from Maxwell's equations, Eq. (30–30a), and, by analogy with Eqs. (12–17) and (12–23), we have

TE modes	TM modes
$h_x = -\frac{\beta}{k} \left(\frac{\epsilon_0}{\mu_0} \right)^{1/2} e_y$	$e_x = \frac{\beta}{k n_x^2} \left(\frac{\mu_0}{\epsilon_0} \right)^{1/2} h_y$
$h_z = -\frac{i}{k} \left(\frac{\epsilon_0}{\mu_0} \right)^{1/2} \frac{de_y}{dx}$	$e_z = \frac{i}{k n_z^2} \left(\frac{\mu_0}{\epsilon_0} \right)^{1/2} \frac{dh_y}{dx}$
$e_x = e_z = h_y = 0$	$h_x = h_z = e_y = 0$

(30–33)

where parameters are defined inside the back cover.

30–12 Uniaxial waveguides

The principal refractive indices of a uniaxial anisotropic waveguide satisfy $n_x = n_y \neq n_z$, and, if the z -direction is parallel to the waveguide axis, the vector wave equations can be simplified. The longitudinal components of Eq. (30–31) are readily shown to be

$$\{ \nabla_t^2 + k^2 n_z^2 - \beta^2 (n_z/n_t)^2 \} e_z = -i\beta (\mathbf{e}_t \cdot \nabla_t \ln n_t^2), \quad (30-34a)$$

$$\{ \nabla_t^2 + k^2 n_t^2 - \beta^2 \} h_z = (\nabla_t h_z - i\beta \mathbf{h}_t) \cdot \nabla_t \ln n_t^2, \quad (30-34b)$$

where $n_t = n_x = n_y$. These equations reduce to Eqs. (30–18b) and (30–18d), respectively, for the isotropic waveguide, i.e. when $n = n_t = n_z$.

The transverse field components can be expressed in terms of e_z and h_z by replacing n with n_t in Eq. (30–6), as may be readily verified. Thus, for example, the radial and

azimuthal field components of a circular fibre with $n_t = n_t(r)$ are given by Eq. (30-9) with $p = k^2 n_t^2 - \beta^2$.

30-13 Polarization parallel to a principal axis

Under special conditions, discussed at the end of Chapter 13, it is possible for a mode to propagate with its electric field virtually parallel to either the x - or y -axis in the waveguide cross-section, assuming these are the principal axes. In such cases the displacement vector is parallel to the electric field, and, using the field representation of Eq. (30-4), the cartesian components of the transverse field, \mathbf{e}_t , satisfy the transverse component of the vector wave equation of Eq. (30-31)

$$(\nabla_t^2 + k^2 n_t^2 - \beta^2) \mathbf{e}_t = -\nabla_t(\mathbf{e}_t \cdot \nabla_t \ln n_t^2), \quad (30-35)$$

where $n_t = n_x$, $\mathbf{e}_t = e_x \hat{\mathbf{x}}$ for the x -polarized modes, and $n_t = n_y$, $\mathbf{e}_t = e_y \hat{\mathbf{y}}$ for the y -polarized modes. The unit vectors $\hat{\mathbf{x}}$ and $\hat{\mathbf{y}}$ are parallel to the axes. Apart from the fact that the values of n_t differ for the two polarizations, this equation is identical to Eq. (30-18a) for isotropic waveguides.

REFERENCES

1. Stratton, J. A. (1941) *Electromagnetic Theory*, McGraw-Hill, New York.
2. Adler, R. B. (1952) Waves on inhomogeneous cylindrical structures. *Proc. I.R.E.*, **40**, 339-48.
3. Born, M. and Wolf, E. (1970) *Principles of Optics*, Pergamon Press Oxford, chap. XIV.

Modal methods for Maxwell's equations

Reciprocity theorem	602
31-1 Conjugated form	602
31-2 Unconjugated form	604
31-3 Mode orthogonality	604
31-4 Integral expressions for the propagation constant	606
31-5 Stored electric and magnetic energies	607
31-6 Phase and group velocities	607
Mode excitation by current sources	608
Modal methods for z-independent nonuniformities	610
31-7 Propagation constants	610
31-8 Modal fields	611
31-9 Modal amplitudes	612
31-10 Slightly perturbed waveguides	612
Modal methods for z-dependent nonuniformities	613
31-11 Coupled mode equations	613
31-12 Physical derivation	615
Local modes	616
31-13 Fields of z -dependent waveguides	616
31-14 Coupled local-mode equations	617
31-15 Alternative form of the coupling coefficients	619
31-16 Physical derivation of the coupled equations	620
References	621

There are two general methods for solving Maxwell's equations or, equivalently, the inhomogeneous vector wave equations. One method uses the Green's function approach of Chapter 34, while the other uses eigenfunction, or modal, methods. The purpose of this chapter is to lay the foundations of the modal approach, by deriving the basic properties of modes and showing how they are used to represent the fields of optical waveguides. Consequently the contents of this chapter are mainly mathematical, and supplement the summary of modal properties presented in Chapters 11, 25 and 28. The modes considered here are exact solutions of Maxwell's equations. In

Chapter 33 we parallel the results of this chapter for the modes of weakly guiding waveguides, starting from solutions of the scalar wave equation.

We begin by deriving an important integral relationship between two field solutions of Maxwell's equations, the *reciprocity theorem*. In its two-dimensional form, this theorem is ideal for deriving the properties of modes of translationally invariant waveguides. It has diverse application, ranging from proof of orthogonality and derivation of modal amplitudes due to current sources, to formulation of coupled mode equations, as well as providing stationary expressions for the propagation constant and group velocity.

There are two forms of the reciprocity theorem—conjugated and unconjugated—depending on whether the conjugated or unconjugated forms of the fields are employed. Throughout Part II, we have consistently used the conjugated reciprocity theorem, which provides a simple physical interpretation in terms of power flow. Although results derived from the conjugated form usually assume a nonabsorbing waveguide, the effects of material absorption on practical waveguides are normally so small that they can be treated as a perturbation of the nonabsorbing waveguide.

RECIPROCITY THEOREM

The derivation of the conjugated or unconjugated reciprocity theorems requires two distinct electromagnetic situations: one characterized by refractive-index profile n , current density \mathbf{J} and electric and magnetic fields \mathbf{E} and \mathbf{H} ; while the other is characterized by \bar{n} , $\bar{\mathbf{J}}$, $\bar{\mathbf{E}}$ and $\bar{\mathbf{H}}$. All vector quantities contain the implicit time dependence $\exp(-i\omega t)$, where ω is the angular frequency. The refractive-index profiles n and \bar{n} may depend on all three spatial variables, but the permeability is taken to have the free-space value μ_0 unless otherwise stated.

31-1 Conjugated form

We define a vector function \mathbf{F}_c by

$$\mathbf{F}_c = \mathbf{E} \times \bar{\mathbf{H}}^* + \bar{\mathbf{E}}^* \times \mathbf{H}, \quad (31-1)$$

where $*$ denotes complex conjugate. The unbarred fields satisfy Maxwell's equations of Eq. (30-1), and the barred fields satisfy the conjugated forms of these equations

$$\nabla \times \bar{\mathbf{E}}^* = -i \left(\frac{\mu_0}{\epsilon_0} \right)^{1/2} k \bar{\mathbf{H}}^*; \quad \nabla \times \bar{\mathbf{H}}^* = \bar{\mathbf{J}}^* + i \left(\frac{\epsilon_0}{\mu_0} \right)^{1/2} k (\bar{n}^*)^2 \bar{\mathbf{E}}^*, \quad (31-2)$$

where μ_0 , ϵ_0 and k are real. Using the vector identity of Eq. (37-28) we deduce that

$$\nabla \cdot \mathbf{F}_c = -i \left(\frac{\epsilon_0}{\mu_0} \right)^{1/2} k \{ (\bar{n}^*)^2 - n^2 \} \mathbf{E} \cdot \bar{\mathbf{E}}^* - (\bar{\mathbf{E}}^* \cdot \mathbf{J} + \mathbf{E} \cdot \bar{\mathbf{J}}^*). \quad (31-3)$$

The two-dimensional form of the divergence theorem of Eq. (37-56) for \mathbf{F}_c is

$$\int_A \nabla \cdot \mathbf{F}_c dA = \frac{\partial}{\partial z} \int_A \mathbf{F}_c \cdot \hat{\mathbf{z}} dA + \oint_l \mathbf{F}_c \cdot \hat{\mathbf{n}} dl, \quad (31-4)$$

where A is an arbitrary cross-sectional area of the waveguide, and \hat{z} is the unit vector parallel to the z -axis. The line integral is along the boundary of A , and \hat{n} is the unit outward normal on l in the plane of A . This result is valid for both continuous and discontinuous profiles. Along a step discontinuity the scalar product $\mathbf{F}_c \cdot \hat{n}$ depends only on the components of the fields orthogonal to the direction of \hat{n} , as is clear from Eq. (31-1). The boundary conditions of Maxwell's equations given at the beginning of Chapter 30 then show that $\mathbf{F}_c \cdot \hat{n}$ is continuous across the discontinuity. Consequently, there are no additional contributions to the line integral from discontinuities within A .

For optical waveguides, we take A to be the infinite cross-section A_∞ . The line integral is then over the circle $r = \infty$, where r is the cylindrical radius, and, if either or both of the barred and unbarred fields represent bound modes, then \mathbf{F}_c vanishes as $r \rightarrow \infty$, since bound-mode field amplitudes fall off exponentially. Thus we drop the line integral in Eq. (31-4) and obtain the conjugated form of the reciprocity theorem

$$\frac{\partial}{\partial z} \int_{A_\infty} \mathbf{F}_c \cdot \hat{z} dA = \int_{A_\infty} \nabla \cdot \mathbf{F}_c dA, \quad (31-5)$$

where \mathbf{F}_c is defined by Eq. (31-1), and $\nabla \cdot \mathbf{F}_c$ is given by Eq. (31-3). The result is valid for arbitrary refractive-index profiles, including those with material absorption, when n is complex.

Leaky and radiation modes

In the case of leaky modes, we showed in Section 24-15 that, by allowing r to take complex values, the leaky-mode fields decay faster than $r^{-1/2}$ as $|r| \rightarrow \infty$ [1]. If \mathbf{F}_c is composed of the radiation-mode fields discussed in Chapter 25, then the line integral in Eq. (31-4) is rapidly oscillating as $r \rightarrow \infty$, since the fields of any cylindrical structure will vary as $\exp\{iQr/\rho\}/\sqrt{r}$ for large r , as is clear from Section 25-8. Thus, the line integral is difficult to interpret, as well as being hard to evaluate exactly for a given structure. However, by taking the line integral to be zero, we obtain the correct properties of radiation modes. In Chapter 25, we show that one method of constructing radiation modes is to consider the bound modes of a metal clad waveguide in the limit when the waveguide cross-section becomes infinite. At the metal boundary, the tangential electric field vanishes, so that $\mathbf{F}_c \cdot \hat{n}$ vanishes, and the line integral is identically zero. Alternatively, we can start from the fact that an individual radiation mode, although well defined mathematically, is unphysical, since it carries an infinite amount of power. Only by superposing a continuum of radiation modes can the physical fields of a waveguide be correctly represented. Thus, although the line integral in Eq. (31-4) is not interpretable when \mathbf{F}_c is composed of the fields of individual radiation modes, it is clear that the integral will vanish as soon as a large number of rapidly oscillating functions are superposed, forming a continuum in the far field $r \rightarrow \infty$ [2]. A rigorous mathematical derivation uses the limit point at infinity property of the transverse vector wave equation [3]. Thus we can drop the line integral for both leaky and radiation modes, and all modes obey the conjugated reciprocity theorem of Eq. (31-5).

Line integral formulation

We can reformulate Eq. (31-5) so that the *area* integral on the right is replaced by a *line* integral. To do this, we define A_p to be the cross-sectional area either occupied by currents or in which $\bar{n}^* \neq n$. If we set $A = A_\infty - A_p$, then the left side of Eq. (31-4) is zero, as is clear from Eq. (31-3). The line integral on the right is evaluated along the contour $l = l_\infty + l_p$, where l_p is the perimeter of A_p . Since the integral along l_∞ vanishes for reasons given above, we deduce that

$$\frac{\partial}{\partial z} \int_{A_\infty - A_p} \mathbf{F}_c \cdot \hat{\mathbf{z}} dA = - \oint_{l_p} \mathbf{F}_c \cdot \hat{\mathbf{n}} dl, \quad (31-6)$$

which is formally identical to Eq. (31-5).

31-2 Unconjugated form

The second form of the reciprocity theorem relates the barred and unbarred fields of the previous section through the vector function \mathbf{F} , where

$$\mathbf{F} = \mathbf{E} \times \bar{\mathbf{H}} - \bar{\mathbf{E}} \times \mathbf{H}. \quad (31-7)$$

We deduce from Eqs. (30-1) and (37-28) that

$$\nabla \cdot \mathbf{F} = i \left(\frac{\epsilon_0}{\mu_0} \right)^{1/2} k (\bar{n}^2 - n^2) \mathbf{E} \cdot \bar{\mathbf{E}} + \bar{\mathbf{E}} \cdot \mathbf{J} - \mathbf{E} \cdot \bar{\mathbf{J}}. \quad (31-8)$$

The derivation then follows that of the previous section, with \mathbf{F} replacing \mathbf{F}_c in Eq. (31-4), and leads to the unconjugated form of the reciprocity theorem

$$\frac{\partial}{\partial z} \int_{A_\infty} \mathbf{F} \cdot \hat{\mathbf{z}} dA = \int_{A_\infty} \nabla \cdot \mathbf{F} dA, \quad (31-9)$$

where \mathbf{F} is defined by Eq. (31-7) and $\nabla \cdot \mathbf{F}$ is given by Eq. (31-8).

31-3 Mode orthogonality

The first application of the conjugated form of the reciprocity theorem demonstrates orthogonality of bound, radiation and leaky modes of nonabsorbing waveguides. Consider two modes propagating in the forward direction with propagation constants β_j and β_k . The subscripts j and k may refer to two different bound modes, but, in the case of radiation modes, may refer to the same mode with different values of the continuous propagation constant β . We set

$$\mathbf{E} = \mathbf{e}_j \exp(i\beta_j z); \quad \mathbf{H} = \mathbf{h}_j \exp(i\beta_j z); \quad \bar{\mathbf{E}} = \mathbf{e}_k \exp(i\beta_k z); \quad \bar{\mathbf{H}} = \mathbf{h}_k \exp(i\beta_k z), \quad (31-10)$$

and $\mathbf{J} = \bar{\mathbf{J}} = 0$. The two modes belong to the same waveguide, which we assume is nonabsorbing, i.e. $\bar{n}^* = n$. Substituting Eqs. (31-1) and (31-10) into Eq. (31-5) gives

$$(\beta_j - \beta_k) \int_{A_\infty} \{ \mathbf{e}_j \times \mathbf{h}_k^* + \mathbf{e}_k^* \times \mathbf{h}_j \} \cdot \hat{\mathbf{z}} dA = 0, \quad j \neq k, \quad (31-11)$$

where A_∞ is the infinite cross-section, and $\hat{\mathbf{z}}$ is the unit vector parallel to the waveguide axis. Now consider a second pair of modes, consisting of the same forward-propagating j th mode, and the k th backward-propagating mode with fields

$$\bar{\mathbf{E}} = \mathbf{e}_{-k} \exp(-i\beta_k z); \quad \bar{\mathbf{H}} = \mathbf{h}_{-k} \exp(-i\beta_k z). \quad (31-12)$$

We relate these fields to the fields of the forward-propagating mode through Eq. (11-7), and from Eqs. (31-1) and (31-5) deduce

$$(\beta_j + \beta_k) \int_{A_\infty} \{\mathbf{e}_j \times \mathbf{h}_k^* - \mathbf{e}_k^* \times \mathbf{h}_j\} \cdot \hat{\mathbf{z}} dA = 0, \quad (31-13)$$

since only transverse field components are involved. The orthogonality relations follow by adding and subtracting Eqs. (31-11) and (31-13) to obtain

$$\int_{A_\infty} \mathbf{e}_j \times \mathbf{h}_k^* \cdot \hat{\mathbf{z}} dA = \int_{A_\infty} \mathbf{e}_k^* \times \mathbf{h}_j \cdot \hat{\mathbf{z}} dA = 0; \quad j \neq k, \quad (31-14)$$

which holds for all forward-propagating modes – bound or radiation – *on nonabsorbing waveguides*. In particular, each bound mode is orthogonal to all radiation modes, and, therefore, to the total radiation fields \mathbf{E}_{rad} and \mathbf{H}_{rad} of the waveguide. Hence

$$\int_{A_\infty} \mathbf{e}_j \times \mathbf{H}_{\text{rad}}^* \cdot \hat{\mathbf{z}} dA = \int_{A_\infty} \mathbf{E}_{\text{rad}}^* \times \mathbf{h}_j \cdot \hat{\mathbf{z}} dA = 0. \quad (31-15)$$

For the leaky modes of Chapter 24, orthogonality is expressed by Eq. (31-14) if A_∞ is replaced by the complex cross-section A'_∞ , as discussed in Section 24-15.

Unconjugated form of orthogonality

We can repeat the above derivation, employing the unconjugated reciprocity theorem of Eq. (31-9). The corresponding expression to Eq. (31-14) is readily shown to be

$$\int_{A_\infty} \mathbf{e}_j \times \mathbf{h}_k \cdot \hat{\mathbf{z}} dA = \int_{A_\infty} \mathbf{e}_k \times \mathbf{h}_j \cdot \hat{\mathbf{z}} dA = 0, \quad j \neq k, \quad (31-16)$$

which is valid for *both absorbing and nonabsorbing waveguides*. For nonabsorbing waveguides, Eqs. (31-14) and (31-16) are identical, since the transverse field components are real under the convention of Eq. (11-8).

Orthogonality of radiation modes

The above results also show that both conjugated and unconjugated orthogonality apply to radiation modes on nonabsorbing waveguides, provided only that the propagation constants differ, i.e. $Q \neq Q'$ in the notation of Eqs. (25-2) and (25-4). The same conclusion can be reached by considering each radiation mode as the limit of a bound mode on a metal clad waveguide, when the cross-section becomes infinite. Within the metal waveguide, bound modes satisfy both conjugated and unconjugated orthogonality, so that this property is carried over to the radiation modes. If the core of

the metal waveguide is unfilled, this limiting procedure demonstrates the orthogonality of free-space radiation modes. When the dielectric waveguide occupies the core of the metal clad waveguide, the same procedure provides proof of the orthogonality of the radiation modes of the dielectric waveguide.

31-4 Integral expressions for the propagation constant

Another form of the reciprocity theorem leads to explicit forms for the bound-mode propagation constant. We parallel the derivation of Section 31-1 with F_c replaced by G_c , where

$$G_c = E \times \bar{H}^*, \quad (31-17)$$

and assume that $n = \bar{n}$, $J = \bar{J} = 0$. With the help of Eqs. (30-1) and (37-28), we deduce that

$$\nabla \cdot G_c = ik \left\{ \left(\frac{\mu_0}{\epsilon_0} \right)^{1/2} H \cdot \bar{H}^* - \left(\frac{\epsilon_0}{\mu_0} \right)^{1/2} (n^2)^* E \cdot \bar{E}^* \right\}. \quad (31-18)$$

Replacing F_c by G_c in Eq. (31-5) leads to

$$\frac{\partial}{\partial z} \int_{A_\infty} E \times \bar{H}^* \cdot \hat{z} dA = ik \int_{A_\infty} \left\{ \left(\frac{\mu_0}{\epsilon_0} \right)^{1/2} H \cdot \bar{H}^* - \left(\frac{\epsilon_0}{\mu_0} \right)^{1/2} (n^2)^* E \cdot \bar{E}^* \right\} dA. \quad (31-19)$$

The unbarred and barred fields are those of the forward- and backward-propagating modes with propagation constant β_j . Thus we set

$$E = e_j \exp(i\beta_j z); \quad H = h_j \exp(i\beta_j z), \quad (31-20a)$$

$$\bar{E} = e_{-j} \exp(-i\beta_j z); \quad \bar{H} = h_{-j} \exp(-i\beta_j z). \quad (31-20b)$$

Substituting into Eq. (31-19) and applying Eq. (11-7) gives

$$\beta_j = \frac{k}{2} \int_{A_\infty} \left\{ \left(\frac{\mu_0}{\epsilon_0} \right)^{1/2} h_j^2 + \left(\frac{\epsilon_0}{\mu_0} \right)^{1/2} (n^2)^* e_j^2 \right\} dA \Big/ \int_{A_\infty} e_j \times h_j^* \cdot \hat{z} dA, \quad (31-21)$$

which is valid for absorbing waveguides. The identity [4]

$$k \int_{A_\infty} n^2 e_j \times h_j^* \cdot \hat{z} dA = \frac{\beta_j}{2} \int_{A_\infty} \left\{ \left(\frac{\mu_0}{\epsilon_0} \right)^{1/2} |h_j|^2 + \left(\frac{\epsilon_0}{\mu_0} \right)^{1/2} n^2 |e_j|^2 \right\} dA, \quad (31-22)$$

leads to a second expression for nonabsorbing waveguides

$$\beta_j = k \left(\frac{\mu_0}{\epsilon_0} \right)^{1/2} \int_{A_\infty} n^2 e_j \times h_j^* \cdot \hat{z} dA \Big/ \int_{A_\infty} n^2 |e_j|^2 dA, \quad (31-23)$$

where $|e_j|^2 = e_j \cdot e_j^*$ and we have used the equality of stored electric and magnetic energies of Eq. (11-18).

31–5 Stored electric and magnetic energies

The time-averaged, electric and magnetic energies \mathcal{W}_{e_j} and \mathcal{W}_{h_j} are defined by Eq. (11–17). On a nonabsorbing, nondispersive waveguide, these two expressions are equal. This is deduced by setting $\bar{\mathbf{E}} = \mathbf{E}$ and $\bar{\mathbf{H}} = \mathbf{H}$ in Eq. (31–19). The integral on the left side is independent of z , whence

$$\frac{\epsilon_0}{4} \int_{A_\infty} n^2 |\mathbf{e}_j|^2 dA = \frac{\mu_0}{4} \int_{A_\infty} |\mathbf{h}_j|^2 dA, \quad (31-24)$$

using Eq. (31–20) for the fields.

31–6 Phase and group velocities

The phase and group velocities of a mode along the waveguide are defined by

$$v_{pj} = \frac{\omega}{\beta_j} = \frac{2\pi c}{\lambda \beta_j}; \quad v_{gj} = \frac{d\omega}{d\beta_j} = -\frac{2\pi c}{\lambda^2} \frac{d\lambda}{d\beta_j}, \quad (31-25)$$

respectively, where the angular frequency ω is related to wavelength λ inside the back cover. We can express v_{pj} in terms of the modal fields through the expressions for β_j in Section 31–4. Here we derive analogous expressions for v_{gj} which allow for material dispersion, when n and μ may vary with wavelength, i.e. $n = n(\lambda)$ and $\mu = \mu(\lambda)$, in addition to the spatial variation of n .

Generalized reciprocity theorem

To obtain the group velocity, we need a generalized reciprocity theorem which allows for variations in the frequency ω of the implicit time dependence of the fields. We let \mathbf{E} and \mathbf{H} be the fields of the j th mode at wavelength λ . These fields satisfy the source-free Maxwell equations, and if we allow for variations in the permeability μ , they have the form

$$\nabla \times \mathbf{E} = 2\pi ic \frac{\mu}{\lambda} \mathbf{H}; \quad \nabla \times \mathbf{H} = -2\pi ic \epsilon_0 \frac{n^2}{\lambda} \mathbf{E}, \quad (31-26)$$

where c is the free-space speed of light. If $\bar{\mathbf{E}}$ and $\bar{\mathbf{H}}$ denote the fields at wavelength $\bar{\lambda}$, they satisfy Eq. (31–26) with \mathbf{E} , \mathbf{H} , λ , μ and n replaced by $\bar{\mathbf{E}}$, $\bar{\mathbf{H}}$, $\bar{\lambda}$, $\bar{\mu} = \mu(\bar{\lambda})$ and $\bar{n} = n(\bar{\lambda})$, respectively. Substituting into Eq. (31–1) and using Eq. (37–28), we find that for nonabsorbing waveguides

$$\nabla \cdot \mathbf{F}_c = 2\pi ic \left\{ \left(\frac{n^2}{\lambda} - \frac{\bar{n}^2}{\bar{\lambda}} \right) \epsilon_0 \mathbf{E} \cdot \bar{\mathbf{E}}^* + \left(\frac{\mu}{\lambda} - \frac{\bar{\mu}}{\bar{\lambda}} \right) \mathbf{H} \cdot \bar{\mathbf{H}}^* \right\}. \quad (31-27)$$

The fields are expressed in separable form

$$\mathbf{E} = \mathbf{e}_j \exp(i\beta_j z); \quad \mathbf{H} = \mathbf{h}_j \exp(i\beta_j z); \quad \bar{\mathbf{E}} = \bar{\mathbf{e}}_j \exp(i\bar{\beta}_j z); \quad \bar{\mathbf{H}} = \bar{\mathbf{h}}_j \exp(i\bar{\beta}_j z). \quad (31-28)$$

On substituting Eqs. (31-1), (31-27) and (31-28) into Eq. (31-5), we deduce

$$\frac{(\beta_j - \bar{\beta}_j)}{2\pi c} \int_{A_x} \{ \mathbf{e}_j \times \bar{\mathbf{h}}_j^* + \bar{\mathbf{e}}_j^* \times \mathbf{h}_j \} \cdot \hat{\mathbf{z}} dA \\ = \int_{A_x} \left\{ \left(\frac{n^2}{\lambda} - \frac{\bar{n}^2}{\bar{\lambda}} \right) \epsilon_0 \mathbf{e}_j \cdot \bar{\mathbf{e}}_j^* + \left(\frac{\mu}{\lambda} - \frac{\bar{\mu}}{\bar{\lambda}} \right) \mathbf{h}_j \cdot \bar{\mathbf{h}}_j^* \right\} dA. \quad (31-29)$$

We divide both sides by $\lambda - \bar{\lambda}$, take the limit $\bar{\lambda} \rightarrow \lambda$ and substitute into Eq. (31-25). Hence $\lambda - \bar{\lambda} \rightarrow d\lambda$, $\beta_j - \bar{\beta}_j \rightarrow d\beta_j$ and

$$v_{gj} = - \frac{\frac{1}{2} \int_{A_x} \mathbf{e}_j \times \mathbf{h}_j^* \cdot \hat{\mathbf{z}} dA}{\frac{\lambda^2}{4} \int_{A_x} \{ \epsilon_0 |\mathbf{e}_j|^2 (d/d\lambda) (n^2/\lambda) + |\mathbf{h}_j|^2 (d/d\lambda) (\mu/\lambda) \} dA}, \quad (31-30)$$

assuming the waveguide is nonabsorbing. If, in addition, the waveguide is not dispersive, we can combine Eq. (31-30) with Eq. (31-23) and set $\mu = \mu_0$ to give

$$v_{gj} = \frac{c\beta_j}{k} \int_{A_x} \mathbf{e}_j \times \mathbf{h}_j^* \cdot \hat{\mathbf{z}} dA \Big/ \int_{A_x} n^2 \mathbf{e}_j \times \mathbf{h}_j^* \cdot \hat{\mathbf{z}} dA, \quad (31-31)$$

where we have used Eq. (31-24). The generalization of Eq. (31-31) to anisotropic waveguides, discussed at the end of Chapters 11 and 30, is found by replacing $n^2 \mathbf{e}_j \times \mathbf{h}_j^*$ by $\mathbf{n}^2 \cdot \mathbf{e}_j \times \mathbf{h}_j^*$, where \mathbf{n}^2 is the refractive index tensor.

MODE EXCITATION BY CURRENT SOURCES

Here we determine the amplitudes of bound and radiation modes excited by a prescribed distribution of currents \mathbf{J} , which occupy a volume \mathcal{V} between the planes $z = z_1$ and $z = z_2$ of a waveguide, as shown in Fig. 31-1. The total fields everywhere in the waveguide are expanded in terms of the complete set of forward- and backward-propagating modes

$$\mathbf{E} = \sum_j \{ a_j(z) \mathbf{e}_j \exp(i\beta_j z) + a_{-j}(z) \mathbf{e}_{-j} \exp(-i\beta_j z) \} + \sum_j \int_0^\infty \{ a_j(z, Q) \mathbf{e}_j(Q) \\ \times \exp[i\beta(Q)z] + a_{-j}(z, Q) \mathbf{e}_{-j}(Q) \exp[-i\beta(Q)z] \} dQ, \quad (31-32a)$$

$$\mathbf{H} = \sum_j \{ a_j(z) \mathbf{h}_j \exp(i\beta_j z) + a_{-j}(z) \mathbf{h}_{-j} \exp(-i\beta_j z) \} + \sum_j \int_0^\infty \{ a_j(z, Q) \mathbf{h}_j(Q) \\ \times \exp[i\beta(Q)z] + a_{-j}(z, Q) \mathbf{h}_{-j}(Q) \exp[-i\beta(Q)z] \} dQ, \quad (31-32b)$$

where the modal amplitudes depend on z only within \mathcal{V} , and are constant or zero elsewhere. In Eq. (31-1) the unbarred fields are given by Eq. (31-32), and the barred fields are equal to the fields of the j th forward-propagating bound mode on the source-

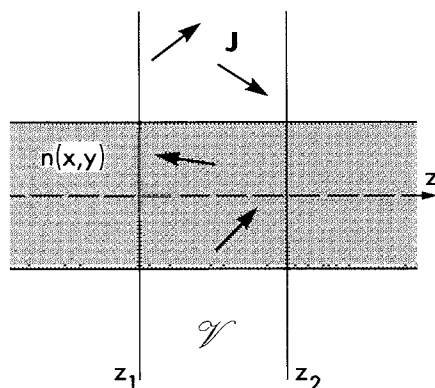


Fig. 31-1 A prescribed distribution of currents with density \mathbf{J} occupies volume \mathcal{V} between transverse planes $z = z_1$ and $z = z_2$ of the waveguide. Outside of \mathcal{V} there are no currents.

free waveguide, i.e. $\bar{\mathbf{J}} = 0$, $\bar{n} = n$, and

$$\bar{\mathbf{E}} = \mathbf{e}_j \exp(i\beta_j z); \quad \bar{\mathbf{H}} = \mathbf{h}_j \exp(i\beta_j z). \quad (31-33)$$

Substituting \mathbf{F}_c into Eq. (31-5) and using the orthogonality condition of Eq. (31-14), we find

$$\frac{da_j(z)}{dz} = -\frac{1}{4N_j} \int_{A_\infty} \mathbf{e}_j^* \cdot \mathbf{J} \exp(-i\beta_j z) dA, \quad (31-34)$$

where N_j is the normalization of Eq. (11-12). Integrating and imposing the condition that there are no forward-propagating modes in $z \leq z_1$, we obtain

$$a_j(z) = 0; \quad z \leq z_1, \quad (31-35a)$$

$$= -\frac{1}{4N_j} \int_{z_1}^z \int_{A_\infty} \mathbf{e}_j^* \cdot \mathbf{J} \exp(-i\beta_j z) dA dz; \quad z_1 \leq z \leq z_2, \quad (31-35b)$$

$$= -\frac{1}{4N_j} \int_{\mathcal{V}} \mathbf{e}_j^* \cdot \mathbf{J} \exp(-i\beta_j z) d\mathcal{V}; \quad z \geq z_2. \quad (31-35c)$$

The corresponding expressions for $a_{-j}(z)$ are obtained by following the same procedure, but using the fields of the j th backward-propagating mode in Eq. (31-33). This leads to

$$a_{-j}(z) = \frac{1}{4N_j} \int_{\mathcal{V}} \mathbf{e}_{-j}^* \cdot \mathbf{J} \exp(i\beta_j z) d\mathcal{V}; \quad z \leq z_1, \quad (31-36a)$$

$$= \frac{1}{4N_j} \int_z^{z_2} \int_{A_\infty} \mathbf{e}_{-j}^* \cdot \mathbf{J} \exp(i\beta_j z) dA dz; \quad z_1 \leq z \leq z_2, \quad (31-36b)$$

$$= 0; \quad z \geq z_2. \quad (31-36c)$$

By using the appropriate radiation-mode fields in Eq. (31-33), we deduce

$$a_j(z, Q) = -\frac{1}{4N_j(Q)} \int_{\mathcal{V}} \mathbf{e}_j^*(Q) \cdot \mathbf{J} \exp \{ -i\beta(Q)z \} d\mathcal{V}; \quad z \geq z_2, \quad (31-37a)$$

$$a_{-j}(z, Q) = \frac{1}{4N_j(Q)} \int_{\mathcal{V}} \mathbf{e}_{-j}^*(Q) \cdot \mathbf{J} \exp \{ i\beta(Q)z \} d\mathcal{V}; \quad z \leq z_1, \quad (31-37b)$$

for forward- and backward-propagating radiation modes, where the normalization $N_j(Q)$ is defined by Eq. (25-5). The forms of the amplitudes in the other regions of Fig. 31-1 are deduced by analogy with Eqs. (31-35) and (31-36). We can also derive surface integral expressions for the modal amplitudes by using Eq. (31-6) instead of Eq. (31-5).

MODAL METHODS FOR Z-INDEPENDENT NONUNIFORMITIES

When the modal fields and propagation constants for one waveguide are known, we can use the reciprocity theorem to determine the modal fields and propagation constants of modes on any other waveguide. The second waveguide is equivalent to the first waveguide with a translationally invariant, or z -independent, nonuniformity. The relationships derived below are exact, and form the basis for the perturbation analysis in Section 31-10 when the waveguides are similar.

31-7 Propagation constants

Let $\bar{\mathbf{E}}, \bar{\mathbf{H}}$ and $\bar{\beta}_k$ be the *known* fields and propagation constant of the k th mode on a waveguide with refractive-index profile \bar{n} , and let \mathbf{E}, \mathbf{H} and β_j be the *unknown* fields and propagation constant of the j th mode on a waveguide with refractive-index profile n . We assume that the modes on either waveguide have distinct values of $\bar{\beta}_k$ or β_j , and set

$$\mathbf{E} = \mathbf{e}_j \exp(i\beta_j z); \quad \mathbf{H} = \mathbf{h}_j \exp(i\beta_j z); \quad (31-38a)$$

$$\bar{\mathbf{E}} = \bar{\mathbf{e}}_k \exp(i\bar{\beta}_k z); \quad \bar{\mathbf{H}} = \bar{\mathbf{h}}_k \exp(i\bar{\beta}_k z). \quad (31-38b)$$

Substituting Eqs. (31-1) and (31-38) into Eq. (31-5) and applying Eq. (31-3) gives

$$\beta_j = \bar{\beta}_k + k \left(\frac{\epsilon_0}{\mu_0} \right)^{1/2} \frac{\int_{A_\infty} (n^2 - \bar{n}^2) \mathbf{e}_j \cdot \bar{\mathbf{e}}_k^* dA}{\int_{A_\infty} \{ \mathbf{e}_j \times \bar{\mathbf{h}}_k^* + \bar{\mathbf{e}}_k^* \times \mathbf{h}_j \} \cdot \hat{\mathbf{z}} dA}, \quad (31-39)$$

provided there are no sources. Both waveguides have free-space permeability μ_0 , and the first waveguide is nonabsorbing, i.e. \bar{n} is real. This expression is also stationary with respect to variations in the barred quantities [5, 6].

Line integral expression

An alternative expression to Eq. (31-39) is found by substituting into Eq. (31-6) instead of Eq. (31-5), and leads to

$$\beta_j - \bar{\beta}_k = -i \frac{\oint_{l_p} \{\mathbf{e}_j \times \bar{\mathbf{h}}_k^* + \bar{\mathbf{e}}_k^* \times \mathbf{h}_j\} \cdot \hat{\mathbf{n}} \, dl}{\int_{A_\infty - A_p} \{\mathbf{e}_j \times \bar{\mathbf{h}}_k^* + \bar{\mathbf{e}}_k^* \times \mathbf{h}_j\} \cdot \hat{\mathbf{z}} \, dA}, \quad (31-40)$$

where A_p is the area of cross-section in which $n \neq \bar{n}$ and l_p is the perimeter of A_p . The unit outward vector $\hat{\mathbf{n}}$ lies on l_p in the plane of A_p .

31-8 Modal fields

The transverse fields of the j th mode on the second waveguide can be found formally by using an eigenfunction expansion over the complete set of forward- and backward-propagating modes of the first waveguide. Thus we set

$$\mathbf{e}_{tj} = \sum_k \{a_k + a_{-k}\} \bar{\mathbf{e}}_{tk} + \sum_k \int_0^\infty \{a_k(Q) + a_{-k}(Q)\} \bar{\mathbf{e}}_{tk}(Q) \, dQ, \quad (31-41a)$$

$$\mathbf{h}_{tj} = \sum_k \{a_k - a_{-k}\} \bar{\mathbf{h}}_{tk} + \sum_k \int_0^\infty \{a_k(Q) - a_{-k}(Q)\} \bar{\mathbf{h}}_{tk}(Q) \, dQ, \quad (31-41b)$$

where a_k and $a_k(Q)$ are the amplitudes of the forward-propagating bound and radiation modes respectively, while a_{-k} and $a_{-k}(Q)$ are the amplitudes of the corresponding backward-propagating modes. The backward-propagating fields are related to the forward-propagating fields by Eq. (11-7). The longitudinal field e_{zj} is found by substituting Eq. (31-41b) into Eq. (30-5c) and noting that \bar{e}_{zk} and \bar{h}_{tk} are also related by Eq. (30-5c). Similarly h_{zj} follows from Eqs. (31-41a) and (30-5d). Hence

$$e_{zj} = \frac{\bar{n}^2}{n^2} \left\{ \sum_k \{a_k - a_{-k}\} \bar{e}_{zk} + \sum_k \int_0^\infty \{a_k(Q) - a_{-k}(Q)\} \bar{e}_{zk}(Q) \, dQ \right\}, \quad (31-42a)$$

$$h_{zj} = \sum_k \{a_k + a_{-k}\} \bar{h}_{zk} + \sum_k \int_0^\infty \{a_k(Q) + a_{-k}(Q)\} \bar{h}_{zk}(Q) \, dQ, \quad (31-42b)$$

assuming the waveguides have free-space permeability μ_0 . It is important to note that in the derivation of e_{zj} and h_{zj} , we have carried the vector operator $\nabla \cdot \mathbf{x}$ through the integration over the radiation modes. This is permissible if the first derivatives of \mathbf{h}_{tk} and \mathbf{e}_{tk} are continuous [7]. The modal fields of waveguides with continuous dielectric profiles satisfy this condition. However, for step profiles, Eq. (31-42) is not valid unless correctly interpreted in a certain limiting sense, as discussed in Section 31-10. Alternatively, e_{zj} and h_{zj} can be found from the second equations in Eqs. (30-5c) and (30-5d) once \mathbf{e}_{tj} and \mathbf{h}_{tj} are known.

31–9 Modal amplitudes

The modal amplitudes in Eq. (31–41) are determined by substituting the expansions into the denominator of Eq. (31–39) and applying the orthogonality condition of Eq. (31–14) to the barred fields. Only the k th forward- and backward-propagating modes contribute to give [8]

$$a_k = \frac{k}{4\bar{N}_k(\beta_j - \bar{\beta}_k)} \left(\frac{\epsilon_0}{\mu_0} \right)^{1/2} \int_{A_\infty} (n^2 - \bar{n}^2) \mathbf{e}_j \cdot \bar{\mathbf{e}}_k^* dA, \quad (31-43a)$$

$$a_{-k} = -\frac{k}{4\bar{N}_k(\beta_j + \bar{\beta}_k)} \left(\frac{\epsilon_0}{\mu_0} \right)^{1/2} \int_{A_\infty} (n^2 - \bar{n}^2) \mathbf{e}_j \cdot \bar{\mathbf{e}}_{-k}^* dA, \quad (31-43b)$$

for the bound modes, where the normalization \bar{N}_k is defined by Eq. (11–12) in terms of $\bar{\mathbf{e}}_k$ and $\bar{\mathbf{h}}_k$, and $\bar{\mathbf{e}}_{-k}^*$ is related to $\bar{\mathbf{e}}_k$ by Eq. (11–9). For the radiation modes, the orthogonality condition of Eq. (25–4) for the barred fields leads to

$$a_k(Q) = \frac{k}{4\bar{N}_k(Q)\{\beta_j - \bar{\beta}(Q)\}} \left(\frac{\epsilon_0}{\mu_0} \right)^{1/2} \int_{A_\infty} (n^2 - \bar{n}^2) \mathbf{e}_j \cdot \bar{\mathbf{e}}_k^*(Q) dA, \quad (31-43c)$$

$$a_{-k}(Q) = -\frac{k}{4\bar{N}_k(Q)\{\beta_j + \bar{\beta}(Q)\}} \left(\frac{\epsilon_0}{\mu_0} \right)^{1/2} \int_{A_\infty} (n^2 - \bar{n}^2) \mathbf{e}_j \cdot \bar{\mathbf{e}}_{-k}^*(Q) dA, \quad (31-43d)$$

where the normalization $\bar{N}_k(Q)$ is defined by Eq. (25–5) in terms of $\bar{\mathbf{e}}_k(Q)$ and $\bar{\mathbf{h}}_k(Q)$, and $\bar{\mathbf{e}}_{-k}^*(Q)$ is related to $\bar{\mathbf{e}}_k(Q)$ by Eq. (11–7). Note that Eq. (11–9) is inapplicable since our choice of radiation-mode fields does not satisfy the convention of Eq. (11–8), as explained in Section 25–1.

The derivation of Eq. (31–43) relies on Eq. (31–39), which means that an extra condition is required to determine the propagation constant β_j and the modal amplitudes. The latter are only determined to within an arbitrary normalization constant. This condition is provided by, for example, the eigenvalue equation for the second waveguide, expressed in integral form by Eq. (31–23). Substitution of the expansions of Eqs. (31–41) and (31–42) into Eqs. (31–23) and (31–43) leads to an infinite set of nonlinear, coupled equations for the modal amplitudes. There is no general solution to this set of equations, but it is sometimes possible to solve them when the second waveguide is only a slight perturbation of the first waveguide.

31–10 Slightly perturbed waveguides

We can obtain analytical solutions of Eq. (31–43) for the modal amplitudes when the two waveguides are similar, i.e. when one waveguide is a slight perturbation of the other waveguide and the perturbation does not vary along its length. However, for reasons explained in Section 18–21, *the refractive-index profiles of the two waveguides must be similar throughout the perturbation region*. This is a fundamental restriction on perturbation methods, and is equivalent to requiring that

$$\mathbf{e}_{ij} \cong \bar{\mathbf{e}}_{ij}; \quad \mathbf{h}_{ij} \cong \bar{\mathbf{h}}_{ij}, \quad (31-44)$$

everywhere, including the perturbation region. With this proviso, it is clear from Eqs. (31-39) and (31-41a) that $\beta_j \cong \beta_j$ and $a_j \cong 1$. The remaining modal amplitudes are found by iteration, i.e. by replacing β_j by β_j and e_j by \bar{e}_j in Eq. (31-43), providing $k \neq j$ in Eq. (31-43a). Thus, first-order corrections to Eq. (31-44) involve all radiation modes and all but the j th bound mode.

Discontinuous profiles

As pointed out in Section 31-8, the radiation-mode contribution to e_{zj} and h_{zj} in Eq. (31-42) is valid only for continuous profiles, but e_{zj} and h_{zj} can be found directly from the second equations in Eq. (30-5c) and (30-5d) once \mathbf{e}_{tj} and \mathbf{h}_{tj} are known. For a discontinuous profile, we will also obtain the correct results for e_{zj} and h_{zj} , provided we interpret the fields of Eq. (31-42) as the limit of a continuous, or smoothed-out, profile. However, it is crucial that the size of the region in which the smoothing occurs be much smaller than the perturbation region.

MODAL METHODS FOR Z-DEPENDENT NONUNIFORMITIES

Here we describe propagation along waveguides with nonuniformities that vary with distance z along the waveguide, i.e. the waveguides are no longer translationally invariant. The description employs the complete set of bound and radiation modes of the unperturbed, translationally invariant waveguide and leads to a set of linear, coupled mode equations for the z -dependence of the modal fields.

31-11 Coupled mode equations

The two waveguides have free-space permeability μ_0 , the translationally invariant refractive-index profile is $\bar{n}(x, y)$, and the profile of the perturbed waveguide is $n(x, y, z)$. For convenience we use the orthonormal modes of Sections 11-5 and 25-4, and set

$$\mathbf{E}_t = \sum_j \{b_j(z) + b_{-j}(z)\} \hat{\mathbf{e}}_{tj} + \sum_j \int_0^\infty \{b_j(z, Q) + b_{-j}(z, Q)\} \hat{\mathbf{e}}_{tj}(Q) dQ, \quad (31-45a)$$

$$\mathbf{H}_t = \sum_j \{b_j(z) - b_{-j}(z)\} \hat{\mathbf{h}}_{tj} + \sum_j \int_0^\infty \{b_j(z, Q) - b_{-j}(z, Q)\} \hat{\mathbf{h}}_{tj}(Q) dQ, \quad (31-45b)$$

where \mathbf{E}_t and \mathbf{H}_t are the *total* transverse fields of the perturbed waveguide. The $b_j(z)$ and $b_j(z, Q)$ contain *all* the z -dependence of the forward-propagating bound and radiation modes, i.e. the phase dependence and the variation of the modal amplitude with z , and $b_{-j}(z)$ and $b_{-j}(z, Q)$ correspond to the backward-propagating modes. We have employed Eq. (11-7) to relate the fields of backward- and forward-propagating modes. The power in each bound mode at any position is given by $|b_j(z)|^2$. By repeating the derivation leading to Eq. (31-42), the longitudinal fields of the perturbed waveguide

are given by

$$E_z = \frac{\bar{n}^2}{n^2} \left\{ \sum_j \{b_j(z) - b_{-j}(z)\} \hat{e}_{zj} + \sum_j \int_0^\infty \{b_j(z, Q) - b_{-j}(z, Q)\} \hat{e}_{zj}(Q) dQ \right\}, \quad (31-46a)$$

$$H_z = \sum_j \{b_j(z) + b_{-j}(z)\} \hat{h}_{zj} + \sum_j \int_0^\infty \{b_j(z, Q) + b_{-j}(z, Q)\} \hat{h}_{zj}(Q) dQ, \quad (31-46b)$$

provided $n(x, y, z)$ is everywhere continuous, for reasons given in Section 31-10. In Eqs. (31-1) and (31-3), we set the barred fields equal to the fields of the k th forward-propagating bound mode, i.e.

$$\bar{\mathbf{E}} = \hat{\mathbf{e}}_k \exp(i\beta_k z); \quad \bar{\mathbf{H}} = \hat{\mathbf{h}}_k \exp(i\beta_k z). \quad (31-47)$$

Assuming the waveguide is nonabsorbing, we find from Eq. (31-5) that

$$\begin{aligned} \frac{\partial}{\partial z} \int_{A_\infty} \{ \mathbf{E}_t \times \hat{\mathbf{h}}_{tk}^* + \hat{\mathbf{e}}_{tk}^* \times \mathbf{H}_t \} \cdot \hat{\mathbf{z}} \exp(-i\beta_k z) dA \\ = i \left(\frac{\epsilon_0}{\mu_0} \right)^{1/2} k \int_{A_\infty} (n^2 - \bar{n}^2) \mathbf{E} \cdot \hat{\mathbf{e}}_k^* \exp(-i\beta_k z) dA. \end{aligned} \quad (31-48)$$

Substituting Eq. (31-45) on the left side, applying the orthogonality conditions of Eqs. (11-16) and (25-6) and relating the forward- and backward-propagating modal fields through Eq. (11-9), we find

$$\frac{db_k}{dz} - i\beta_k b_k = \frac{i}{4} \left(\frac{\epsilon_0}{\mu_0} \right)^{1/2} k \int_{A_\infty} (n^2 - \bar{n}^2) \mathbf{E} \cdot \hat{\mathbf{e}}_k^* dA. \quad (31-49)$$

Substituting for \mathbf{E} from Eqs. (31-45a) and (31-46a) leads to the coupled equation for the k th forward-propagating, bound mode [9]

$$\begin{aligned} \frac{db_k}{dz} - i\beta_k b_k = i \sum_l \left\{ [C_{kl} b_l + C_{k-l} b_{-l}] \right. \\ \left. + \int_0^\infty [C_{kl}(Q) b_l(Q) + C_{k-l}(Q) b_{-l}(Q)] dQ \right\}, \end{aligned} \quad (31-50a)$$

where the coupling coefficients are given by

$$C_{kl} = \frac{k}{4} \left(\frac{\epsilon_0}{\mu_0} \right)^{1/2} \int_{A_\infty} (n^2 - \bar{n}^2) \left\{ \hat{\mathbf{e}}_{tk}^* \cdot \hat{\mathbf{e}}_{tl} + \frac{\bar{n}^2}{n^2} \hat{e}_{zk}^* \hat{e}_{zl} \right\} dA, \quad (31-50b)$$

$$C_{kl}(Q) = \frac{k}{4} \left(\frac{\epsilon_0}{\mu_0} \right)^{1/2} \int_{A_\infty} (n^2 - \bar{n}^2) \left\{ \hat{\mathbf{e}}_{tk}^* \cdot \hat{\mathbf{e}}_{tl}(Q) + \frac{\bar{n}^2}{n^2} \hat{e}_{zk}^* \hat{e}_{zl}(Q) \right\} dA, \quad (31-50c)$$

The amplitude b_{-k} of the k th backward-propagating mode is given by the same equations, provided we replace b_k by b_{-k} , β_k by $-\beta_k$, k by $-k$, and \hat{e}_{zk}^* by $-\hat{e}_{zk}^*$.

The coupled equations for the radiation-mode amplitudes follow the same

derivation, provided Eq. (31-47) is replaced by the fields of the k th forward-propagating radiation mode of the unperturbed waveguide. Thus [9]

$$\frac{db_k(Q)}{dz} - i\beta(Q)b_k(Q) = i \sum_l \left\{ [C_{kl}(Q)b_l + C_{k-l}(Q)b_{-l}] + \int_0^\infty [C_{kl}(Q, Q')b_l(Q') + C_{k-l}(Q, Q')b_{-l}(Q')] dQ' \right\}, \quad (31-51a)$$

where the coupling coefficients are given by

$$C_{kl}(Q) = \frac{k}{4} \left(\frac{\epsilon_0}{\mu_0} \right)^{1/2} \int_{A_x} (n^2 - \bar{n}^2) \left\{ \hat{\mathbf{e}}_{ik}^*(Q) \cdot \hat{\mathbf{e}}_{il} + \frac{\bar{n}^2}{n^2} \hat{\mathbf{e}}_{zk}^*(Q) \hat{\mathbf{e}}_{zl} \right\} dA, \quad (31-51b)$$

$$C_{kl}(Q, Q') = \frac{k}{4} \left(\frac{\epsilon_0}{\mu_0} \right)^{1/2} \int_{A_x} (n^2 - \bar{n}^2) \left\{ \hat{\mathbf{e}}_{ik}^*(Q) \cdot \hat{\mathbf{e}}_{il}(Q') + \frac{\bar{n}^2}{n^2} \hat{\mathbf{e}}_{zk}^*(Q) \hat{\mathbf{e}}_{zl}(Q') \right\} dA. \quad (31-51c)$$

For backward-propagating radiation modes, the set of coupled equations is given by the above equation if $b_k(Q)$ is replaced by $b_{-k}(Q)$, $\beta(Q)$ by $-\beta(Q)$, k by $-k$, and $\hat{\mathbf{e}}_k$ by $\hat{\mathbf{e}}_{-k}$.

The sets of coupled, integro-differential equations of Eqs. (31-50) and (31-51) are an exact restatement of Maxwell's equations for waveguides with *continuous* profiles. This restriction follows because we have used the expansions of Eq. (31-46). However, the coupled mode equations also apply to *discontinuous* profiles if we adopt the smoothing procedure described in Section 31-10. *The coupled mode equations can be solved by perturbation analysis, provided $n \cong \bar{n}$, for reasons given in Section 31-10.*

31-12 Physical derivation

The coupled mode equations of the previous section can be derived intuitively. This also provides insight into the physical mechanism of the coupling process. Consider a differential section of the perturbed waveguide of length dz , as shown in Fig. 31-2, and its effect on the k th forward-propagating bound mode. The z dependence of the fields, $b_k(z)$ of Eq. (31-45), is expressible as

$$b_k(z) = a_k(z) \exp(i\beta_k z), \quad (31-52)$$

where $a_k(z)$ is the modal amplitude and $\beta_k z$ the phase. The change in $b_k(z)$ over the section is given by

$$db_k(z) = i\beta_k b_k(z) dz + da_k(z) \exp(i\beta_k z), \quad (31-53)$$

where the first term on the right accounts for the change in phase. The change $da_k(z)$ in amplitude arises from the nonuniformity and thus all modes contribute to it. To determine this contribution, we replace the nonuniformities within the section in Fig. 31-2 by the induced current \mathbf{J} , discussed in Chapter 22. From Eq. (22-3) we

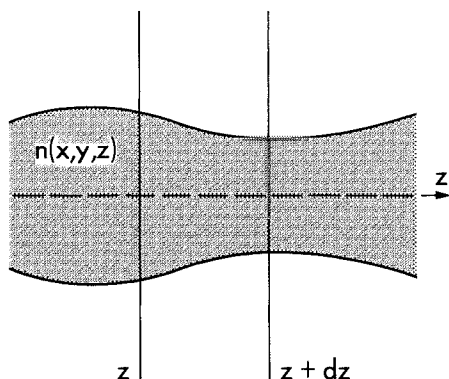


Fig. 31-2 A differential section of a nonuniform waveguide occupies the differential volume between transverse planes at z and $z + dz$.

have

$$\mathbf{J} = i \left(\frac{\epsilon_0}{\mu_0} \right)^{1/2} k (\bar{n}^2 - n^2) \mathbf{E}, \quad (31-54)$$

where n and \bar{n} are the profiles of the perturbed and unperturbed waveguides, and \mathbf{E} is the total electric field of the *perturbed* waveguide. We then treat \mathbf{J} as a source within the *unperturbed* waveguide. The contribution to $da_k(z)$ follows from Eq. (31-34) as

$$da_k(z) = -\frac{dz}{4} \int_{A_x} \mathbf{e}_k^* \cdot \mathbf{J} \exp(-i\beta_k z) dA, \quad (31-55)$$

since $N_k = 1$ for the orthonormal fields. If we substitute this result into Eq. (31-53), express \mathbf{J} in terms of the expansions of Eqs. (31-45a) and (31-46a) through Eq. (31-54), and recall the coupling coefficients of Eqs. (31-50b) and (31-50c), we arrive at the coupled mode equations of Eq. (31-50a).

LOCAL MODES

In Chapter 19 we introduced local modes to describe the fields of waveguides with large nonuniformities that vary slowly along their length. As an individual local mode is only an approximation to the exact fields, it couples power with other local modes as it propagates. Our purpose here is to derive the set of coupled equations which determines the amplitude of each mode [10]. First, however, we require the relationships satisfied by the fields of such waveguides.

31-13 Fields of z -dependent waveguides

On a waveguide that is not translationally invariant, the refractive-index profile varies with distance z along the waveguide, i.e. $n = n(x, y, z)$. Consequently we can no longer

express the exact fields \mathbf{E} and \mathbf{H} in the separable form of Eq. (30-4). However, we can still decompose the fields into transverse and longitudinal components

$$\mathbf{E} = \mathbf{E}_t + E_z \hat{\mathbf{z}}; \quad \mathbf{H} = \mathbf{H}_t + H_z \hat{\mathbf{z}}, \quad (31-56)$$

where each component depends on z . The vector operator ∇ is defined by

$$\nabla = \nabla_t + \hat{\mathbf{z}} \partial / \partial z, \quad (31-57)$$

where ∇_t is defined in Table 30-1, page 592. Substituting Eq. (31-56) into the source-free Maxwell equations of Eq. (30-1) and equating components

$$\mathbf{E}_t = \frac{i}{kn^2} \left(\frac{\mu_0}{\epsilon_0} \right)^{1/2} \hat{\mathbf{z}} \times \left\{ \frac{\partial \mathbf{H}_t}{\partial z} - \nabla_t H_z \right\}; \quad E_z = \frac{i}{kn^2} \left(\frac{\mu_0}{\epsilon_0} \right)^{1/2} \hat{\mathbf{z}} \cdot (\nabla_t \times \mathbf{H}_t), \quad (31-58a)$$

$$\mathbf{H}_t = -\frac{i}{k} \left(\frac{\epsilon_0}{\mu_0} \right)^{1/2} \hat{\mathbf{z}} \times \left\{ \frac{\partial \mathbf{E}_t}{\partial z} - \nabla_t E_z \right\}; \quad H_z = -\frac{i}{k} \left(\frac{\epsilon_0}{\mu_0} \right)^{1/2} \hat{\mathbf{z}} \cdot (\nabla_t \times \mathbf{E}_t). \quad (31-58b)$$

Eliminating longitudinal components and using Eq. (37-27) leads to

$$\mathbf{E}_t = \frac{1}{kn^2} \left\{ i \left(\frac{\mu_0}{\epsilon_0} \right)^{1/2} \hat{\mathbf{z}} \times \frac{\partial \mathbf{H}_t}{\partial z} + \frac{1}{k} \nabla_t \times (\nabla_t \times \mathbf{E}_t) \right\}, \quad (31-59a)$$

$$\mathbf{H}_t = -\frac{1}{k} \left\{ i \left(\frac{\epsilon_0}{\mu_0} \right)^{1/2} \hat{\mathbf{z}} \times \frac{\partial \mathbf{E}_t}{\partial z} - \frac{1}{k} \nabla_t \times \left(\frac{\nabla_t \times \mathbf{H}_t}{n^2} \right) \right\}, \quad (31-59b)$$

where parameters are defined inside the back cover.

31-14 Coupled local-mode equations

For convenience we only include bound modes in our derivation; radiation modes are readily incorporated by analogy with the coupled mode equations of Section 31-11. We express the total transverse field of the perturbed waveguide as an expansion over the complete set of forward- and backward-propagating local modes

$$\mathbf{E}_t = \sum_j \{ b_j(z) + b_{-j}(z) \} \hat{\mathbf{e}}_{tj}(x, y, \beta_j(z)), \quad (31-60a)$$

$$\mathbf{H}_t = \sum_j \{ b_j(z) - b_{-j}(z) \} \hat{\mathbf{h}}_{tj}(x, y, \beta_j(z)), \quad (31-60b)$$

where $\hat{\mathbf{e}}_{tj}$ denotes orthonormality, and $b_j(z)$ describes both the modal amplitude and phase dependence, i.e.

$$b_{\pm j}(z) = a_{\pm j}(z) \exp \left\{ \pm i \int_0^z \beta_j(z) dz \right\}. \quad (31-61)$$

The local propagation constant is $\beta_j(z)$, and the fields of each mode satisfy Eq. (31-59) at each position z along the fiber, i.e. the implicit dependence of $\hat{\mathbf{e}}_{tj}$ and $\hat{\mathbf{h}}_{tj}$ on z is ignored

when differentiating. Thus

$$\hat{\mathbf{e}}_{vj} = -\frac{1}{kn^2} \left\{ \left(\frac{\mu_0}{\varepsilon_0} \right)^{1/2} \beta_j \hat{\mathbf{z}} \times \hat{\mathbf{h}}_{vj} - \frac{1}{k} \nabla_t \times (\nabla_t \times \hat{\mathbf{e}}_{vj}) \right\}, \quad (31-62a)$$

$$\hat{\mathbf{h}}_{vj} = \frac{1}{k} \left\{ \left(\frac{\varepsilon_0}{\mu_0} \right)^{1/2} \beta_j \hat{\mathbf{z}} \times \hat{\mathbf{e}}_{vj} + \frac{1}{k} \nabla_t \times \left(\frac{\nabla_t \times \hat{\mathbf{h}}_{vj}}{n^2} \right) \right\}. \quad (31-62b)$$

The total transverse fields of the waveguide satisfy Eq. (31-59) exactly, so by substituting Eq. (31-60) and simplifying with Eq. (31-62) we deduce

$$\sum_j \left\{ (b_j - b_{-j}) \hat{\mathbf{z}} \times \frac{\partial \hat{\mathbf{h}}_{vj}}{\partial z} - i\beta_j (b_j + b_{-j}) \hat{\mathbf{z}} \times \hat{\mathbf{h}}_{vj} + \left(\frac{db_j}{dz} - \frac{db_{-j}}{dz} \right) \hat{\mathbf{z}} \times \hat{\mathbf{h}}_{vj} \right\} = 0, \quad (31-63a)$$

$$\sum_j \left\{ (b_j + b_{-j}) \hat{\mathbf{z}} \times \frac{\partial \hat{\mathbf{e}}_{vj}}{\partial z} - i\beta_j (b_j - b_{-j}) \hat{\mathbf{z}} \times \hat{\mathbf{e}}_{vj} + \left(\frac{db_j}{dz} + \frac{db_{-j}}{dz} \right) \hat{\mathbf{z}} \times \hat{\mathbf{e}}_{vj} \right\} = 0. \quad (31-63b)$$

Local modes are locally orthonormal and thus satisfy Eq. (11-16). We dot multiply Eq. (31-63a) with $\hat{\mathbf{e}}_{ik}$, Eq. (31-63b) with $\hat{\mathbf{h}}_{ik}$ and integrate over the infinite cross-section. Assuming a nonabsorbing waveguide, $\hat{\mathbf{e}}_{ik} = \hat{\mathbf{e}}_{ik}^*$, $\hat{\mathbf{h}}_{ik} = \hat{\mathbf{h}}_{ik}^*$ whence

$$\frac{db_j}{dz} - \frac{db_{-j}}{dz} - i\beta_j (b_j + b_{-j}) = -\frac{1}{2} \sum_k (b_k - b_{-k}) \int_{A_x} \hat{\mathbf{e}}_j \times \frac{\partial \hat{\mathbf{h}}_k}{\partial z} \cdot \hat{\mathbf{z}} dA, \quad (31-64a)$$

$$\frac{db_j}{dz} + \frac{db_{-j}}{dz} - i\beta_j (b_j - b_{-j}) = \frac{1}{2} \sum_k (b_k + b_{-k}) \int_{A_x} \hat{\mathbf{h}}_j \times \frac{\partial \hat{\mathbf{e}}_k}{\partial z} \cdot \hat{\mathbf{z}} dA, \quad (31-64b)$$

where the subscript t is dropped since only transverse components of the fields contribute to the integrals. Adding and subtracting gives [10, 11]

$$\frac{db_j}{dz} - i\beta_j b_j = \sum_k \{ C_{jk} b_k + C_{j-k} b_{-k} \}, \quad (31-65a)$$

$$\frac{db_{-j}}{dz} + i\beta_j b_{-j} = -\sum_k \{ C_{-jk} b_k + C_{-j-k} b_{-k} \}, \quad (31-65b)$$

where the C_{jk} are coupling coefficients defined by

$$C_{jk} = \frac{1}{4} \int_{A_x} \left\{ \hat{\mathbf{h}}_j \times \frac{\partial \hat{\mathbf{e}}_k}{\partial z} - \hat{\mathbf{e}}_j \times \frac{\partial \hat{\mathbf{h}}_k}{\partial z} \right\} \cdot \hat{\mathbf{z}} dA, \quad j \neq k; \quad C_{jj} = 0, \quad (31-65c)$$

and C_{jj} vanishes because it is proportional to the z -derivative of the unit normalization. When $k \rightarrow -k$ or $j \rightarrow -j$, we use the field symmetries of Eq. (11-7).

31-15 Alternative form of the coupling coefficients

The coupling coefficients of Eq. (31-65c) are expressible in a more compact form, as we show here. Combining the field components of Eq. (31-58) and substituting the fields for the j th forward-propagating local mode of Eq. (19-2), we have

$$-i \left(\frac{\epsilon_0}{\mu_0} \right)^{1/2} k n^2 \hat{\mathbf{e}}_j = \nabla_t \times \hat{\mathbf{h}}_j + i \beta_j \hat{\mathbf{z}} \times \hat{\mathbf{h}}_j, \quad (31-66a)$$

$$i \left(\frac{\mu_0}{\epsilon_0} \right)^{1/2} k \hat{\mathbf{h}}_j = \nabla_t \times \hat{\mathbf{e}}_j + i \beta_j \hat{\mathbf{z}} \times \hat{\mathbf{e}}_j, \quad (31-66b)$$

ignoring the implicit z -dependence in $\hat{\mathbf{e}}_j$ and $\hat{\mathbf{h}}_j$. We multiply the conjugate of Eq. (31-66a) with $\hat{\mathbf{e}}'_k$ and the conjugate of Eq. (31-66b) with $\hat{\mathbf{h}}'_k$, where prime denotes $\partial/\partial z$, and subtract to obtain

$$ik \left\{ \left(\frac{\mu_0}{\epsilon_0} \right)^{1/2} \hat{\mathbf{h}}_j^* \cdot \hat{\mathbf{h}}'_k + \left(\frac{\epsilon_0}{\mu_0} \right)^{1/2} n^2 \hat{\mathbf{e}}_j^* \cdot \hat{\mathbf{e}}'_k \right\} = \hat{\mathbf{e}}'_k \cdot \nabla_t \times \hat{\mathbf{h}}_j^* - \hat{\mathbf{h}}'_k \cdot \nabla_t \times \hat{\mathbf{e}}_j^* + i \beta_j \{ \hat{\mathbf{e}}_j^* \times \hat{\mathbf{h}}'_k - \hat{\mathbf{h}}_j^* \times \hat{\mathbf{e}}'_k \} \cdot \hat{\mathbf{z}}. \quad (31-67)$$

A second equation is obtained from Eq. (31-66) by replacing the subscript j with k , and differentiating both equations with respect to z . We then multiply the first equation by $\hat{\mathbf{e}}_j^*$, the second by $\hat{\mathbf{h}}_j^*$ and subtract to obtain

$$\begin{aligned} -ik \left\{ \left(\frac{\mu_0}{\epsilon_0} \right)^{1/2} \hat{\mathbf{h}}_j^* \cdot \hat{\mathbf{h}}'_k + \left(\frac{\epsilon_0}{\mu_0} \right)^{1/2} n^2 \hat{\mathbf{e}}_j^* \cdot \hat{\mathbf{e}}'_k \right\} - i \left(\frac{\epsilon_0}{\mu_0} \right)^{1/2} k \frac{\partial n^2}{\partial z} \hat{\mathbf{e}}_j^* \cdot \hat{\mathbf{e}}_k \\ = \hat{\mathbf{e}}_j^* \cdot \nabla_t \times \hat{\mathbf{h}}'_k - \hat{\mathbf{h}}_j^* \cdot \nabla_t \times \hat{\mathbf{e}}'_k - i \frac{d\beta_k}{dz} \{ (\hat{\mathbf{z}} \times \hat{\mathbf{e}}_k) \cdot \hat{\mathbf{h}}_j^* \\ - (\hat{\mathbf{z}} \times \hat{\mathbf{h}}_k) \cdot \hat{\mathbf{e}}_j^* \} - i \beta_k \{ \hat{\mathbf{e}}_j^* \times \hat{\mathbf{h}}'_k - \hat{\mathbf{h}}_j^* \times \hat{\mathbf{e}}'_k \} \cdot \hat{\mathbf{z}}. \end{aligned} \quad (31-68)$$

If we add Eqs. (31-67) and (31-68) and integrate over the infinite cross-section, the local-mode orthogonality condition of Eq. (11-16) shows that the terms multiplying $d\beta_k/dz$ vanish. Using Eq. (37-28), the four terms involving ∇_t are expressible as

$$\int_{A_\infty} \nabla_t \cdot \{ \hat{\mathbf{h}}_j^* \times \hat{\mathbf{e}}'_k - \hat{\mathbf{e}}_j^* \times \hat{\mathbf{h}}'_k \} dA. \quad (31-69)$$

The two-dimensional divergence theorem of Eq. (37-55) shows that the area integral is identical to a line integral at infinity, and this vanishes since the fields and their derivatives decrease to zero exponentially. If we assume the waveguide is nonabsorbing, so that $\hat{\mathbf{e}}_i$ and $\hat{\mathbf{h}}_i$ may be taken to be real, it follows that [12]

$$C_{jk} = \left(\frac{\epsilon_0}{\mu_0} \right)^{1/2} k \frac{1}{4\beta_j - \beta_k} \int_{A_\infty} \hat{\mathbf{e}}_j^* \cdot \hat{\mathbf{e}}_k \frac{\partial n^2}{\partial z} dA, \quad (31-70)$$

where the coupling coefficient is defined by Eq. (31-65c).

31-16 Physical derivation of the coupled equations

The set of coupled equations for local modes can be derived intuitively, using a differential section of the nonuniform fiber [12]. Here we give a brief description of the method. A section of fiber of length dz is shown in Fig. 31-2. The j th forward-propagating local mode is incident on the section at z with amplitude $a_j(z)$. The variation in $b_j(z)$ of Eq. (31-61) across the section is given by

$$db_j = i\beta_j b_j dz + da_j \exp \left\{ i \int_0^z \beta_j(z) dz \right\}. \quad (31-71)$$

The first term on the right accounts for the change in phase, and the second term for the change in amplitude. To determine the contribution to da_j , we examine the reflected and transmitted fields when the k th forward-propagating local mode is incident on the section.

The total transverse electric field is continuous across the section, i.e. $\mathbf{E}_t = \mathbf{E}'_t$, where \mathbf{E}_t is composed of the fields of the k th forward-propagating and all backward-propagating local modes at z , while \mathbf{E}'_t is composed of the fields of all forward-propagating local modes at $z + dz$. Hence

$$a_k \hat{\mathbf{E}}_{tk} + \sum_i a_{-i} \hat{\mathbf{E}}_{ti} = \sum_i a'_i \hat{\mathbf{E}}'_{ti}, \quad (31-72)$$

where $\hat{\mathbf{E}}$ denotes the electric field of the orthonormal local mode, including its phase dependence, negative subscripts denote backward-propagating local modes and $\hat{\mathbf{E}}_{t-i} = \hat{\mathbf{E}}_{ti}$. We cross-multiply with $(\mathbf{H}_j)^*/2$ and integrate over the infinite cross-section. The orthonormality condition of Eq. (11-16) leads to

$$a'_j = \frac{a_k}{2} \int_{A_x} \hat{\mathbf{E}}_k \times \hat{\mathbf{H}}_j^* \cdot \hat{\mathbf{z}} dA + \sum_i \frac{a_{-i}}{2} \int_{A_x} \hat{\mathbf{E}}_{-i} \times \hat{\mathbf{H}}_j^* \cdot \hat{\mathbf{z}} dA, \quad (31-73)$$

assuming a nonabsorbing waveguide. To first order in dz , the magnetic field at $z + dz$ is related to the field at z by

$$\hat{\mathbf{H}}'_j = \hat{\mathbf{H}}_j + \frac{\partial \hat{\mathbf{H}}_j}{\partial z} dz. \quad (31-74)$$

Substituting into Eq. (31-73) and applying Eq. (11-16) leads to

$$a'_j = a_k D_{kj} dz + a_{-j} + \sum_i a_{-i} D_{-ij} dz; \quad j \neq k, \quad (31-75a)$$

$$a'_j = a_j(1 + D_{jj} dz) + a_{-j} + \sum_i a_{-i} D_{-ij} dz; \quad j = k, \quad (31-75b)$$

where

$$D_{ij} = \frac{1}{2} \int_{A_x} \hat{\mathbf{E}}_i \times \frac{\partial \hat{\mathbf{H}}_j^*}{\partial z} \cdot \hat{\mathbf{z}} dA; \quad D_{-ij} = D_{ij}. \quad (31-75c)$$

A second pair of equations is generated in a similar manner, using continuity of the transverse magnetic field, i.e. $\mathbf{H}_t = \mathbf{H}'_t$. The corresponding expression to Eq. (31-72) is

$$a_k \hat{\mathbf{H}}_{tk} - \sum_i a_{-i} \hat{\mathbf{H}}_{ti} = \sum_i a'_i \hat{\mathbf{H}}'_{ti} \quad (31-76)$$

since $\hat{\mathbf{H}}_{t-i} = -\hat{\mathbf{H}}_i$. Using orthonormality and expanding $\hat{\mathbf{E}}'_j$ in a similar manner to Eq. (31-74), we find

$$a'_j = -a_k F_{kj} dz - a_{-j} - \sum_i a_{-i} F_{-ij} dz; \quad j \neq k, \quad (31-77a)$$

$$a'_j = a_j(1 - F_{jj} dz) - a_{-j} - \sum_i a_{-i} F_{-ij} dz; \quad j = k, \quad (31-77b)$$

where

$$F_{ij} = \frac{1}{2} \int_{A_\infty} \hat{\mathbf{H}}_i \times \frac{\partial \hat{\mathbf{E}}_j^*}{\partial z} \cdot \hat{\mathbf{z}} dA; \quad F_{-ij} = -F_{ij}. \quad (31-77c)$$

By differentiating Eq. (11-16) with respect to z we deduce that $D_{ij} = F_{ji}$, and by adding corresponding equations in Eqs. (31-75) and (31-77) we find

$$2a'_j = a_k(D_{kj} - D_{jk}) dz + \sum_i a_{-i}(D_{-ij} - D_{j-i}) dz; \quad j \neq k, \quad (31-78a)$$

$$2a'_j = 2a_j + \sum_i a_{-i}(D_{-ij} - D_{j-i}) dz; \quad j = k. \quad (31-78b)$$

From Eqs. (31-61), (31-65c), (31-75c) and (31-77c) it is readily verified that Eq. (31-78) is equivalent to

$$(a'_j - a_j) \exp \left\{ i \int_0^z \beta_j(z) dz \right\} = \left\{ C_{jk} b_k + \sum_i C_{j-i} b_{-i} \right\} dz. \quad (31-79)$$

If we sum over k all contributions to a'_j from every forward-propagating mode, set $a'_j - a_j = da_j$ in Eq. (31-71) and divide by dz , we arrive at the coupled equations of Eq. (31-65).

REFERENCES

1. Sammut, R. and Snyder, A. W. (1976) Leaky modes on a dielectric waveguide: orthogonality and excitation. *Appl. Opt.*, **15**, 1040-4.
2. Marcuse, D. (1973) *Light Transmission Optics*, Van Nostrand, New York, p. 323.
3. Friedman, B. (1956) *Principles and Techniques of Applied Mathematics*, Wiley, New York, pp. 230-50.
4. Brown, J. M. (1966) Electromagnetic momentum associated with waveguide modes. *Proc. I.E.E.*, **113**, 27-34.
5. Mathews, J. and Walker, R. L. (1965) *Mathematical Methods of Physics*, Benjamin, New York.
6. Rumsey, V. H. (1954) Reaction concept in electromagnetic theory. *Phys. Rev.*, **94**, 1483-91.
7. Whittaker, E. T. and Watson, G. N. (1969) *A Course of Modern Analysis*, Cambridge, London, p. 67.
8. Snyder, A. W. (1970) Mode propagation in optical waveguides. *Electron. Lett.*, **6**, 561-2.

9. Snyder, A. W. (1972) Coupled-mode theory for optical fibers. *J. Opt. Soc. Am.*, **62**, 1267–77.
10. Snyder, A. W. (1969) Coupling of modes on a tapered dielectric cylinder. *I.E.E.E. Trans. Microwave Theory Tech.*, **18**, 650–1.
11. Snyder, A. W. (1965) Surface mode coupling along a tapered dielectric rod. *I.E.E.E. Trans. Antennas and Propagation*, **13**, 821–2.
12. Snyder, A. W. (1971) Mode propagation in a non-uniform cylindrical medium. *I.E.E.E. Trans. Microwave Theory Tech.*, **19**, 402–3.

Weak-guidance approximation

Vector wave equation	623
32-1 Expansion of the bound-mode fields	624
32-2 Governing equations for the field expansions	626
32-3 Physical interpretation of the limit $\Delta \rightarrow 0$	627
32-4 Propagation constants	628
 Vector direction of the bound-mode fields	 630
32-5 Waveguides with noncircular cross-sections	630
32-6 Fibers with circular cross-sections	632
32-7 Symmetry properties of higher-order modes on circular fibers	633
32-8 Alternative representation for modes on circular fibers	635
32-9 Fibers with nearly circular cross-sections	635
32-10 Higher-order corrections to the modal fields	636
 Vector wave equation with sources	 637
 Radiation modes	 638
32-11 Orthogonality and normalization	638
 References	 639

In Chapter 13 we showed how to construct the fields of bound modes on weakly guiding waveguides using simple physical arguments, and then, in Chapter 25, we extended the method to include radiation modes. To complement the physical approach, we now give the formal mathematical derivation using perturbation theory on the vector wave equation.

VECTOR WAVE EQUATION

The electric and magnetic fields of a mode of an arbitrary waveguide are expressible in the separable forms of Eqs. (11-3) and (11-6)

$$\mathbf{E}(x, y, z) = \mathbf{e}(x, y) \exp(i\beta z) = \{\mathbf{e}_t + e_z \hat{\mathbf{z}}\} \exp(i\beta z), \quad (32-1a)$$

$$\mathbf{H}(x, y, z) = \mathbf{h}(x, y) \exp(i\beta z) = \{\mathbf{h}_t + h_z \hat{\mathbf{z}}\} \exp(i\beta z), \quad (32-1b)$$

where β is the propagation constant, $\hat{\mathbf{z}}$ is the unit vector parallel to the waveguide axis and subscripts t and z denote transverse and longitudinal components. We drop the modal subscript as only individual modes are considered in this chapter, and assume

that \mathbf{e}_t and \mathbf{h}_t have components relative to fixed cartesian axes, i.e.

$$\mathbf{e}_t = e_x \hat{\mathbf{x}} + e_y \hat{\mathbf{y}}; \quad \mathbf{h}_t = h_x \hat{\mathbf{x}} + h_y \hat{\mathbf{y}}, \quad (32-2)$$

where $\hat{\mathbf{x}}$ and $\hat{\mathbf{y}}$ are unit vectors parallel to the axes in Fig. 11-1(a). Under this condition \mathbf{e} obeys the vector wave equation of Eq. (11-40a), and its transverse component satisfies Eq. (30-18a)

$$\{\nabla_t^2 + k^2 n^2 - \beta^2\} \mathbf{e}_t = -\nabla_t \{\mathbf{e}_t \cdot \nabla_t \ln n^2\}, \quad (32-3)$$

where $n = n(x, y)$ is the refractive-index profile, $k = 2\pi/\lambda$ and λ is the free-space wavelength. The operators are defined in Table 30-1, page 592. All other components of \mathbf{e} and \mathbf{h} are obtained from \mathbf{e}_t using the relationships in Eq. (30-5).

Parametric dependence of the fields

We discussed the parametric dependence of the modal fields in Chapter 11, and showed that the electric field always depends on the waveguide parameter V and the profile height parameter Δ , both of which are dimensionless. Hence

$$\mathbf{e} = \mathbf{e}(V, \Delta), \quad (32-4)$$

where V and Δ are defined inside the back cover. We emphasize that these parameters are taken to be independent of one another.

32-1 Expansion of the bound-mode fields

If the waveguide is weakly guiding, there is only a slight variation in its profile and $\Delta \ll 1$. We then assume that we can express the transverse electric field \mathbf{e}_t as a power series in Δ , treating V and Δ as independent parameters [1-3]. Thus

$$\mathbf{e}_t(V, \Delta) = \tilde{\mathbf{e}}_t + \Delta \mathbf{e}_t^{(1)} + \Delta^2 \mathbf{e}_t^{(2)} + \dots, \quad (32-5)$$

where superscripts denote the order in Δ and the coefficient of each order depends only on V . The $\tilde{}$ denotes the solution when $\Delta = 0$.

It is convenient to express the vector wave equation in dimensionless form. In terms of the profile representation

$$n^2(x, y) = n_{co}^2 \{1 - 2\Delta f(x, y)\}, \quad (32-6)$$

where n_{co} is the maximum index value and $f \geq 0$, the waveguide and modal parameters U and V defined inside the back cover, and a linear dimension ρ in the waveguide cross-section, we can re-express Eq. (32-3) as

$$\{\rho^2 \nabla_t^2 + U^2 - V^2 f\} \mathbf{e}_t = -\rho \nabla_t \{\mathbf{e}_t \cdot \rho \nabla_t \ln n^2\}. \quad (32-7)$$

The expansion of U is assumed to be

$$U(V, \Delta) = \tilde{U} + \Delta U^{(1)} + \dots; \quad \tilde{U} = \rho(k^2 n_{co}^2 - \tilde{\beta}^2)^{1/2}, \quad (32-8)$$

where \tilde{U} is the value of U when $\Delta = 0$ and $\tilde{\beta}$ is the corresponding propagation constant. If we substitute this expansion into the relationship between U and the exact

propagation constant β given inside the back cover, express kn_{co} in terms of V and Δ , and make a binomial expansion, then

$$\beta = \frac{V}{\rho} \frac{1}{(2\Delta)^{1/2}} \left\{ 1 - 2\Delta \frac{U^2}{V^2} \right\}^{1/2}, \quad (32-9a)$$

$$= \frac{V}{\rho} \frac{1}{(2\Delta)^{1/2}} - \frac{\tilde{U}^2}{\rho V} \left(\frac{\Delta}{2} \right)^{1/2} - \frac{\tilde{U}^4 + 4\tilde{U} V^2 U^{(1)}}{\rho V^3} \left(\frac{\Delta}{2} \right)^{3/2} + \dots, \quad (32-9b)$$

By making a similar expansion of $\tilde{\beta}$ in terms of \tilde{U} through inverting the relationship in Eq. (32-8), we find that β and $\tilde{\beta}$ are related by

$$\beta = \tilde{\beta} - 4 \frac{\tilde{U} U^{(1)}}{\rho V} \left(\frac{\Delta}{2} \right)^{3/2}, \quad (32-10)$$

correct to order $\Delta^{3/2}$. In the notation of Chapter 13, the first corrections to $\tilde{\beta}$ and \tilde{U} are denoted by $\delta\beta$ and δU , respectively. Thus we deduce from Eqs. (32-8) and (32-10)

$$\beta \cong \tilde{\beta} + \delta\beta; \quad \delta\beta = - \frac{\tilde{U} \delta U}{\rho V} (2\Delta)^{1/2} = - \frac{4\tilde{U} U^{(1)}}{\rho V} \left(\frac{\Delta}{2} \right)^{3/2}, \quad (32-11a)$$

$$U \cong \tilde{U} + \delta U; \quad \delta U = U^{(1)} \Delta = - \{ \rho V / \tilde{U} (2\Delta)^{1/2} \} \delta\beta. \quad (32-11b)$$

To expand the $\nabla_t \ln n^2$ term in Eq. (32-7), we substitute from Eq. (32-6)

$$\nabla_t \ln n^2 = \nabla_t \ln (1 - 2\Delta f) = -2\Delta \nabla_t f - 2\Delta^2 \nabla_t f^2 - \dots \quad (32-12)$$

For the special case of the step profile, when $n = n_{\text{co}}$ in the core and $n = n_{\text{cl}}$ in the cladding, the definition of Δ inside the back cover leads to

$$f = H; \quad \nabla_t \ln n^2 = -2\Delta \delta \hat{s} + \dots, \quad (32-13)$$

where H is the step function, i.e. $H = 0$ in the core and $H = 1$ in the cladding, and δ is the Dirac delta function, which is nonzero only along the interface. The unit outward vector \hat{s} is on the interface in the waveguide cross-section.

Remaining field components

Given the transverse electric field \mathbf{e}_t , the remaining field components are expressible in terms of \mathbf{e}_t through the component equations of Eq. (30-5). If we use the definition of the waveguide parameter inside the back cover to express k in terms of V and Δ , then

$$e_z = \frac{i}{\rho\beta} \{ \rho \nabla_t \cdot \mathbf{e}_t + (\mathbf{e}_t \cdot \rho \nabla_t) \ln n^2 \}, \quad (32-14a)$$

$$\mathbf{h}_t = n_{\text{co}} \left(\frac{\varepsilon_0}{\mu_0} \right)^{1/2} \frac{(2\Delta)^{1/2}}{V} \hat{\mathbf{z}} \times \{ \rho \beta \mathbf{e}_t + i \rho \nabla_t e_z \}, \quad (32-14b)$$

$$h_z = -in_{\text{co}} \left(\frac{\varepsilon_0}{\mu_0} \right)^{1/2} \frac{(2\Delta)^{1/2}}{V} \left(\hat{\mathbf{z}} \cdot \rho \nabla_t \times \mathbf{e}_t \right) = \frac{i}{\rho\beta} \left(\rho \nabla_t \cdot \mathbf{h}_t \right), \quad (32-14c)$$

where ρ is a characteristic linear dimension in the waveguide cross-section. The terms in the expansion of these components are obtained in the following section.

32-2 Governing equations for the field expansions

Here we systematically determine the equations satisfied by the terms in the expansion of \mathbf{e}_t and show how to obtain the corresponding terms in the remaining field components. We substitute Eqs. (32-5), (32-8) and (32-12) into Eq. (32-7) and equate terms with the same power of Δ .

Zeroth order

To lowest order in Δ we find that $\tilde{\mathbf{e}}_t$ satisfies Eq. (32-7) with $\Delta = 0$, i.e.

$$\{\rho^2 \nabla_t^2 + \tilde{U}^2 - V^2 f\} \tilde{\mathbf{e}}_t = 0. \quad (32-15)$$

This is the scalar wave equation with properties discussed in Section 33-1, i.e. $\tilde{\mathbf{e}}_t$ and its first derivatives are everywhere continuous. The lowest-order term in the expansion of the transverse magnetic field \mathbf{h}_t is denoted by $\tilde{\mathbf{h}}_t$. If we substitute the expansions of Eqs. (32-5) and (32-9) into Eq. (32-14b) and note that the lowest-order term in the expansion of e_z is of order $\Delta^{1/2}$, as we show below, then

$$\tilde{\mathbf{h}}_t = n_{co} \left(\frac{\epsilon_0}{\mu_0} \right)^{1/2} \hat{\mathbf{z}} \times \tilde{\mathbf{e}}_t. \quad (32-16)$$

Hence $\tilde{\mathbf{h}}_t$ also satisfies the scalar wave equation. The corresponding lowest-order terms in the expansion of the longitudinal components e_z and h_z are obtained by substituting Eqs. (32-5), (32-9) and (32-12) into Eqs. (32-14a) and (32-14c), and are therefore of order $\Delta^{1/2}$. If superscripts denote the order in Δ , then

$$e_z^{(1/2)} = i \frac{2^{1/2}}{V} (\rho \nabla_t \cdot \tilde{\mathbf{e}}_t); \quad h_z^{(1/2)} = -i \frac{2^{1/2}}{V} \left(\frac{\epsilon_0}{\mu_0} \right)^{1/2} n_{co} \hat{\mathbf{z}} \cdot (\rho \nabla_t \times \tilde{\mathbf{e}}_t). \quad (32-17)$$

Unlike the transverse components $\tilde{\mathbf{e}}_t$ and $\tilde{\mathbf{h}}_t$, the longitudinal components are not solutions of the scalar wave equation.

First order

The first-order correction $\mathbf{e}_t^{(1)}$ satisfies the inhomogeneous equation in Table 32-1, which is obtained by equating powers of Δ in Eq. (32-7). Likewise the corrections $\mathbf{h}_t^{(1)}$, $e_z^{(3/2)}$ and $h_z^{(3/2)}$ are found by equating powers of Δ in Eq. (32-14b) and powers of $\Delta^{3/2}$ in Eqs. (32-14a) and (32-14c).

Summary

If we put the above results together, the fields of bound modes on weakly guiding waveguides have the expansions

$$\mathbf{e} = \tilde{\mathbf{e}}_t + \Delta^{1/2} e_z^{(1/2)} \hat{\mathbf{z}} + \Delta \mathbf{e}_t^{(1)} + \Delta^{3/2} e_z^{(3/2)} \hat{\mathbf{z}} + \dots, \quad (32-18a)$$

$$\mathbf{h} = \tilde{\mathbf{h}}_t + \Delta^{1/2} h_z^{(1/2)} \hat{\mathbf{z}} + \Delta \mathbf{h}_t^{(1)} + \Delta^{3/2} h_z^{(3/2)} \hat{\mathbf{z}} + \dots, \quad (32-18b)$$

Table 32-1 Governing equations for modal field expansions. Equations for the lowest and first-order transverse electric fields of a weakly guiding waveguide. Remaining field components correct to order $\Delta^{3/2}$ are given explicitly in terms of the solutions of the two equations.

$$\begin{aligned}
 &\{\rho^2 \nabla_t^2 + \tilde{U}^2 - V^2 f\} \tilde{\mathbf{e}}_t = 0 \\
 &\{\rho^2 \nabla_t^2 + \tilde{U}^2 - V^2 f\} \mathbf{e}_t^{(1)} = 2\rho \nabla_t \{\tilde{\mathbf{e}}_t \cdot \rho \nabla_t f\} - 2\tilde{U} U^{(1)} \tilde{\mathbf{e}}_t \\
 \\
 &\tilde{\mathbf{h}}_t = n_{\infty} \left(\frac{\epsilon_0}{\mu_0} \right)^{1/2} \hat{\mathbf{z}} \times \tilde{\mathbf{e}}_t; \quad e_z^{(1/2)} = i \frac{2^{1/2}}{V} \rho \nabla_t \cdot \tilde{\mathbf{e}}_t \\
 &h_z^{(1/2)} = i \frac{2^{1/2}}{V} \rho \nabla_t \cdot \tilde{\mathbf{h}}_t = -i 2^{1/2} \frac{n_{\infty}}{V} \left(\frac{\epsilon_0}{\mu_0} \right)^{1/2} \hat{\mathbf{z}} \cdot \rho \nabla_t \times \tilde{\mathbf{e}}_t \\
 &\mathbf{h}_t^{(1)} = n_{\infty} \left(\frac{\epsilon_0}{\mu_0} \right)^{1/2} \hat{\mathbf{z}} \times \left\{ \mathbf{e}_t^{(1)} - \frac{\tilde{U}^2}{V^2} \tilde{\mathbf{e}}_t - \frac{2}{V^2} \rho \nabla_t (\rho \nabla_t \cdot \tilde{\mathbf{e}}_t) \right\} \\
 &e_z^{(3/2)} = i \frac{2^{1/2}}{V} \left\{ \rho \nabla_t \cdot \mathbf{e}_t^{(1)} + \frac{\tilde{U}^2}{V^2} \rho \nabla_t \cdot \tilde{\mathbf{e}}_t - 2\tilde{\mathbf{e}}_t \cdot \rho \nabla_t f \right\} \\
 &h_z^{(3/2)} = -i 2^{1/2} \frac{n_{\infty}}{V} \left(\frac{\epsilon_0}{\mu_0} \right)^{1/2} \hat{\mathbf{z}} \cdot \rho \nabla_t \times \mathbf{e}_t^{(1)} = \frac{i 2^{1/2}}{V} \left\{ \rho \nabla_t \cdot \mathbf{h}_t^{(1)} + \frac{\tilde{U}^2}{2V^2} \rho \nabla_t \cdot \tilde{\mathbf{h}}_t \right\}
 \end{aligned}$$

where $\tilde{\mathbf{e}}_t$ and $\mathbf{e}_t^{(1)}$ satisfy the equations in Table 32-1, and remaining coefficients are given explicitly in terms of $\tilde{\mathbf{e}}_t$ and $\mathbf{e}_t^{(1)}$. An example of this expansion is given in Table 12-6, page 260, for the fundamental mode of the step-profile fiber. We discuss the propagation constant in Section 32-4, and in later sections we show how to construct the modal fields from the solutions of the scalar wave equation.

32-3 Physical interpretation of the limit $\Delta \rightarrow 0$

The first terms $\tilde{\mathbf{e}}_t$ and $\tilde{\mathbf{h}}_t$ in the expansions of Eq. (32-18) are the exact fields only when $\Delta = 0$, or, equivalently, when $n_{\infty} = n_{cl}$. Although V and Δ are treated as *independent* parameters in the expansions, the definition of V inside the back cover involves Δ . Consequently, when $\Delta = 0$, we must set $\lambda = 0$ so that in the limit $\Delta \rightarrow 0$, $\lambda \rightarrow 0$ the waveguide parameter remains finite and *arbitrary*. When $\lambda = 0$, Eq. (32-9) requires that $\beta = \infty$, which means that the fields of the $n_{\infty} = n_{cl}$ waveguide are strictly unphysical. However, when Δ and λ are small, but nonvanishing, and β is large, but finite, the fields and propagation constants of the $n_{\infty} = n_{cl}$ waveguide are excellent approximations for determining the modal fields and propagation constants of the weakly guiding waveguide, as we showed in Chapter 13.

Despite the fact that $\tilde{\mathbf{e}}_t$ is a highly accurate approximation to the exact transverse field, some readers may be disturbed that this approximation is based on the unphysical model of the $n_{\infty} = n_{cl}$ waveguide [2]. However, this situation is analogous to the well accepted point dipole approximation of real physical dipoles. Recall that the

electrostatic potential of a dipole can be expressed in terms of two independent parameters: the dipole moment $p = Qd$; and the separation d between two charges of equal and opposite strengths $\pm Q$. If d is sufficiently small, then the potential at a field point $\phi(p, d) \cong \phi(p, 0)$, where $\phi(p, 0)$ is the potential of a point dipole, when $d = 0$. A point dipole is unphysical because $Q = \infty$ to maintain the finite, but arbitrary, value of p . Nevertheless, the fields of a physical dipole, for $d \neq 0$, are well approximated by those of the point dipole, $d = 0$. The parameters p , d and Q of the dipole play the roles of V , Δ and λ^{-1} , respectively, of the optical waveguide.

At first sight the scalar wave equation of Eq. (13-8), which is expressed in terms of $\tilde{\beta}$, may appear ill-defined when $\Delta \rightarrow 0$ and $\tilde{\beta} \rightarrow \infty$. However, this equation is identical to Eq. (32-15), which is expressed in terms of \tilde{U} . Since $\tilde{\beta}$ must lie within the range given inside the back cover, we deduce that \tilde{U} must lie within the range $0 \leq \tilde{U} < V$. Consequently, as $\Delta \rightarrow 0$ and V remains fixed, \tilde{U} remains finite even when $\Delta = 0$. Thus both Eqs. (13-8) and (32-15) are well defined in this limit.

32-4 Propagation constants

In Section 32-2 we derived an expansion for the bound-mode fields of weakly guiding waveguides. The terms in this expansion depend in turn on the expansion of the modal parameter U in Eq. (32-8). Here we show how to find these terms.

Scalar propagation constant

The lowest order term \tilde{U} appears in the scalar wave equation of Eq. (32-15). In Section 33-1 we show that for the scalar wave equation, the solution and its first derivatives must be everywhere continuous, and therefore bounded. This leads to an eigenvalue equation for the allowable values of \tilde{U} . In general this equation is transcendental and must be solved numerically, as is clear from the examples in Chapter 14. Given \tilde{U} , the value of the scalar propagation constant $\tilde{\beta}$ is obtained from the relationship inside the back cover.

The modal fields depend on the product βz in Eq. (32-1), where β is the exact propagation constant. Since z can be arbitrarily large, we determine higher-order corrections to the scalar propagation constant $\tilde{\beta}$ so that our approximate expressions for the fields are accurate over finite distances along the waveguide. These corrections take into account polarization effects due to the waveguide.

Relationship between exact and scalar propagation constants

In order to correct the scalar propagation constant, we first derive a relationship between the scalar field $\tilde{\mathbf{e}}_t$ and propagation constant $\tilde{\beta}$, derived from the scalar wave equation, and the exact field \mathbf{e}_t and propagation constant β derived from the vector wave equation. Thus, from Eqs. (32-15) and (32-3) we have

$$\{\nabla_t^2 + k^2 n^2 - \tilde{\beta}^2\} \tilde{\mathbf{e}}_t = 0, \quad (32-19a)$$

$$\{\nabla_t^2 + k^2 n^2 - \beta^2\} \mathbf{e}_t = -\nabla_t \{\mathbf{e}_t \cdot \nabla_t \ln n^2\}, \quad (32-19b)$$

where $n = n(x, y)$. We dot multiply Eq. (32-19a) with \mathbf{e}_t , Eq. (32-19b) with $\tilde{\mathbf{e}}_t$, subtract

and integrate over the infinite cross-section A_∞ to obtain [2]

$$\beta^2 - \tilde{\beta}^2 = \int_{A_\infty} \hat{\mathbf{e}}_t \cdot \nabla_t \{ \mathbf{e}_t \cdot \nabla_t \ln n^2 \} dA \Big/ \int_{A_\infty} \hat{\mathbf{e}}_t \cdot \mathbf{e}_t dA, \quad (32-20)$$

where terms involving ∇_t^2 vanish. To see this, we transform the area integral over these terms into a line integral using the identity of Eq. (37-57)

$$\int_{A_\infty} \{ \hat{\mathbf{e}}_t \cdot \nabla_t^2 \mathbf{e}_t - \mathbf{e}_t \cdot \nabla_t^2 \hat{\mathbf{e}}_t \} dA = \oint_{l_\infty} \{ \hat{\mathbf{e}}_t \nabla_t \cdot \mathbf{e}_t - \mathbf{e}_t \nabla_t \cdot \hat{\mathbf{e}}_t \} \cdot \hat{\mathbf{n}} dl, \quad (32-21)$$

where l_∞ is the perimeter of A_∞ and $\hat{\mathbf{n}}$ is the unit outward normal on l_∞ in the plane of A_∞ . Because the fields of bound modes and their first derivatives decay exponentially to zero at large distances from the waveguide, the line integral vanishes.

The integrand in the numerator of Eq. (32-20) is of the form $\hat{\mathbf{e}}_t \cdot \nabla_t \Psi$, where Ψ is a scalar function. Using the vector identity of Eq. (37-26), this can be replaced by $\nabla_t \cdot (\Psi \hat{\mathbf{e}}_t) - \Psi \nabla_t \cdot \hat{\mathbf{e}}_t$. The area integral over $\nabla_t \cdot (\Psi \mathbf{e}_t)$ is transformed into a line integral, using Eq. (37-55), which vanishes for the same reason that Eq. (32-21) vanishes. If we recall the definitions of U and \tilde{U} from the inside the back cover, we finally obtain the alternative form

$$\tilde{\beta}^2 - \beta^2 = \frac{U^2 - \tilde{U}^2}{\rho^2} = \int_{A_\infty} (\nabla_t \cdot \hat{\mathbf{e}}_t) \mathbf{e}_t \cdot \nabla_t \ln n^2 dA \Big/ \int_{A_\infty} \hat{\mathbf{e}}_t \cdot \mathbf{e}_t dA, \quad (32-22)$$

which is *exact* and holds for any profile, step or graded.

TE mode propagation constants

We recall from Chapters 11 and 12 that modes with $e_z = 0$ everywhere are TE modes. Table 32-1 shows that the term $\nabla_t \cdot \hat{\mathbf{e}}_t$ in Eq. (32-22) is proportional to $e_z^{(1/2)}$ on weakly guiding waveguide. Consequently $\nabla_t \cdot \hat{\mathbf{e}}_t = 0$, and the scalar propagation constant is identical to the exact propagation constant. This is in keeping with Chapter 12, where we showed that the exact TE mode fields are derivable from the scalar wave equation.

Perturbation correction to the scalar propagation constant

Here we determine the first correction to $\tilde{\beta}$. This was denoted by $\delta\beta$ in Chapter 13 and was shown to be of order $\Delta^{3/2}$ in Eq. (32-11a). If we rearrange the left side of Eq. (32-22) and substitute Eqs. (32-9) and (32-11a), then to lowest order in Δ

$$\tilde{\beta}^2 - \beta^2 = -(\beta - \tilde{\beta})(\beta + \tilde{\beta}) = -(V/\rho)(2/\Delta)^{1/2} \delta\beta. \quad (32-23)$$

Similarly we substitute Eqs. (32-12) and (32-18a) into the right side of Eq. (32-22) and retain only lowest-order terms. On equating with Eq. (32-23) we have

$$\left[\delta\beta = \frac{(2\Delta)^{3/2}}{2\rho V} \int_{A_\infty} (\rho \nabla_t \cdot \hat{\mathbf{e}}_t) \hat{\mathbf{e}}_t \cdot \rho \nabla_t f dA \Big/ \int_{A_\infty} \hat{\mathbf{e}}_t^2 dA \right] \quad (32-24)$$

The corresponding expression for δU follows from Eq. (32-11b) as

$$\delta U = -\frac{\Delta}{U} \int_{A_x} (\rho \nabla_t \cdot \hat{\mathbf{e}}_t) \hat{\mathbf{e}}_t \cdot \rho \nabla_t f \, dA \bigg/ \int_{A_x} \hat{\mathbf{e}}_t^2 \, dA, \quad (32-25)$$

where \hat{U} is the solution of the eigenvalue equation for the scalar wave equation.

Perturbation correction for the step-profile

In the case of a step-profile waveguide, the $\nabla_t \ln n^2$ term in Eq. (32-22) is given by the weighted delta function of Eq. (32-13), and Eqs. (32-24), (32-25) reduce to

$$\delta\beta = -\frac{(2\Delta)^{1/2}}{\rho V} \hat{U} \delta U = \frac{(2\Delta)^{3/2}}{2V} \oint_l (\rho \nabla_t \cdot \hat{\mathbf{e}}_t) \hat{\mathbf{e}}_t \cdot \hat{\mathbf{n}} \, dl \bigg/ \int_{A_x} \hat{\mathbf{e}}_t^2 \, dA, \quad (32-26)$$

where the line integral is along the interface in the waveguide cross-section, and $\hat{\mathbf{n}}$ is the unit outward normal on l .

VECTOR DIRECTION OF THE BOUND-MODE FIELDS

We showed by physical arguments in Chapter 13 and by perturbation methods above that the spatial dependence of the transverse electric field \mathbf{e}_t of a weakly guiding waveguide is given approximately by solutions of the scalar wave equation. Since we are concerned only with scalar wave equation solutions from hereon, we adopt the notation of Chapter 13 and drop the \cdot used in earlier sections of this chapter. In general, \mathbf{e}_t is a linear combination of solutions of the scalar wave equation, each solution having two orthogonal polarization states [2]. The vector direction \mathbf{e}_t was found by simple physical arguments in Chapter 13; here we show how the direction can be determined by perturbation theory, paralleling each of the cases considered in Chapter 13.

32-5 Waveguides with noncircular cross-sections

When the cross-section of the waveguide is noncircular, there is only one solution Ψ of the scalar wave equation for each discrete value of the scalar propagation constant β in Eq. (13-8). The direction of \mathbf{e}_t , as expressed by Eq. (13-7), then takes the general form

$$\mathbf{e}_t = (a\hat{\mathbf{x}} + b\hat{\mathbf{y}})\Psi, \quad (32-27)$$

where a and b are constants. There are two possible values for a/b corresponding to two orthogonally polarized modes. We determine these values using a perturbation relation for weakly guiding waveguides similar to that of Eq. (32-24). This relation is derived by replacing \mathbf{e}_t by \mathbf{s}_t in Eq. (32-22), where \mathbf{s}_t denotes either $\Psi \hat{\mathbf{x}}$ or $\Psi \hat{\mathbf{y}}$ and Ψ satisfies Eq. (13-8). Thus

$$\delta\beta = \frac{(2\Delta)^{3/2}}{2\rho V} \int_{A_x} (\rho \nabla_t \cdot \mathbf{s}_t) \mathbf{e}_t \cdot \rho \nabla_t f \, dA \bigg/ \int_{A_x} \mathbf{s}_t \cdot \mathbf{e}_t \, dA. \quad (32-28)$$

This expression relates the correction $\delta\beta$ to the scalar propagation constant to the correct linear combination in Eq. (32-27). To determine, $\delta\beta$ and the ratio a/b , we

generate two equations by substituting for \mathbf{e}_t from Eq. (32-27) and setting; (i) $\mathbf{s}_t = \Psi \hat{\mathbf{x}}$; and (ii) $\mathbf{s}_t = \Psi \hat{\mathbf{y}}$. This gives, respectively

$$a\{D_{xx} - \delta\beta\} + bD_{xy} = 0; \quad aD_{yx} + b\{D_{yy} - \delta\beta\} = 0, \quad (32-29)$$

where the D 's are defined by

$$D_{pq} = \frac{(2\Delta)^{3/2}}{2\rho V} \int_{A_x} (\rho \nabla_t \cdot \Psi \hat{\mathbf{p}}) \Psi \hat{\mathbf{q}} \cdot \rho \nabla_t f dA \bigg/ \int_{A_x} \Psi^2 dA, \quad (32-30)$$

and $\hat{\mathbf{p}}, \hat{\mathbf{q}}$ denote either $\hat{\mathbf{x}}$ or $\hat{\mathbf{y}}$. Thus Eq. (32-29) is quadratic in a/b with solutions [2]

$$\delta\beta = \{D_{yy} + D_{xx} \pm [(D_{yy} - D_{xx})^2 + 4D_{xy}^2]^{1/2}\}/2, \quad (32-31a)$$

$$a/b = \{D_{xx} - D_{yy} \pm [(D_{yy} - D_{xx})^2 + 4D_{xy}^2]^{1/2}\}/2D_{xy}, \quad (32-31b)$$

where we have set $D_{xy} = D_{yx}$.

Proof of the identity $D_{xy} = D_{yx}$

The property $D_{xy} = D_{yx}$ follows from the scalar wave equation. We replace $\hat{\mathbf{e}}_t$ by Ψ in Eq. (32-15) and define the operator \mathcal{L} by

$$\mathcal{L}\Psi = \{\rho^2 \nabla_t^2 + \tilde{U}^2 - V^2 f\} \Psi = 0. \quad (32-32)$$

By differentiating with respect to x and y we obtain, respectively,

$$\mathcal{L} \frac{\partial \Psi}{\partial x} = V^2 \Psi \frac{\partial f}{\partial x}; \quad \mathcal{L} \frac{\partial \Psi}{\partial y} = V^2 \Psi \frac{\partial f}{\partial y}. \quad (32-33)$$

If we multiply the first equation by $\partial \Psi / \partial y$, the second equation by $\partial \Psi / \partial x$ and substitute into Eq. (32-30), we deduce that

$$D_{xy} - D_{yx} = \frac{\rho^3 (2\Delta)^{3/2}}{2V^3} \int_{A_x} \left\{ \frac{\partial \Psi}{\partial x} \nabla_t^2 \frac{\partial \Psi}{\partial y} - \frac{\partial \Psi}{\partial y} \nabla_t^2 \frac{\partial \Psi}{\partial x} \right\} dA \bigg/ \int_{A_x} \Psi^2 dA. \quad (32-34)$$

By analogy with Eq. (32-21), the right side can be transformed into a line integral which vanishes, since Ψ and its first derivatives decrease exponentially to zero at large distances from the waveguide axis, and we obtain the desired result.

If we substitute the two values of a/b of Eq. (32-31b) into Eq. (32-27), and take the scalar product of the two expressions for \mathbf{e}_t , the expression vanishes and consequently the two fields are orthogonal.

Determination of the optical axes

In Section 13-5 we used physical arguments to show that the transverse electric field must be polarized along the optical axes of the weakly guiding waveguide. If $\hat{\mathbf{x}}_0$ and $\hat{\mathbf{y}}_0$ are unit vectors parallel to the optical axes, then the two polarizations are expressible as

$$\mathbf{e}_t = \Psi \hat{\mathbf{x}}_0; \quad \mathbf{e}_t = \Psi \hat{\mathbf{y}}_0, \quad (32-35)$$

where Ψ is the scalar wave equation solution of Eq. (13-8). If we compare these

expressions with Eq. (32-27), we deduce that the directions of the optical axes are given by

$$\hat{\mathbf{x}}_0 = \frac{\hat{\mathbf{x}} + a_+ \hat{\mathbf{y}}}{(1 + a_+^2)^{1/2}}; \quad \hat{\mathbf{y}}_0 = \frac{\hat{\mathbf{x}} + a_- \hat{\mathbf{y}}}{(1 + a_-^2)^{1/2}} \quad (32-36)$$

where a_+ and a_- denote the values a/b corresponding to the $+$ and $-$ signs on the right of Eq. (32-31b). Usually these directions are obvious from the symmetries of the waveguide.

The results of this section apply to all fundamental and higher-order modes on weakly guiding waveguides of arbitrary cross-section, and parallel the results of Sections 13-5 and 13-8 derived by physical arguments. In addition they apply to the fundamental modes of fibers with circular cross-sections, discussed in the next section.

32-6 Fibers with circular cross-sections

The solutions of the scalar wave equation for a fiber of circular cross-section and refractive-index profile $n(r)$ have the separable forms

$$\Psi = F_l(R) \cos(l\phi); \quad \Psi = F_l(R) \sin(l\phi), \quad (32-37)$$

where $R = r/\rho$, and $F_l(R)$ satisfies the ordinary differential equation

$$\left\{ \frac{d^2}{dR^2} + \frac{1}{R} \frac{d}{dR} + \tilde{U}^2 - \frac{l^2}{R^2} - V^2 f(R) \right\} F_l = 0, \quad (32-38)$$

as we showed at the beginning of Chapter 14. The profile representation and other parameters are defined inside the back cover.

Fundamental and HE_{1m} modes

These are the only modes on a circular fiber for which there is a single solution of the scalar wave equation given the value of $\hat{\beta}$, or, equivalently, \tilde{U} , and correspond to $l = 0$ in Eq. (32-37). Consequently, the direction of \mathbf{e}_l is described by the analysis of the previous section. If we set $\Psi = F_0(R)$ in Eq. (32-30), it is straightforward to show that $D_{xx} = D_{yy}$ and $D_{xy} = 0$. The values of a/b in Eq. (32-31b) are then indeterminate, so that \mathbf{e}_l can be taken to be parallel to any pair of orthogonal directions, as we showed in Section 13-4.

Higher-order modes

The fiber of circular cross-section is unique because the scalar wave equation has two solutions for each value of $\hat{\beta}$ for its higher-order modes, corresponding to Eq. (32-37) with $l \geq 1$. Thus the direction of \mathbf{e}_l , as expressed by Eq. (13-7), takes the form

$$\mathbf{e}_l = F_l \left[\{a \cos(l\phi) + b \sin(l\phi)\} \hat{\mathbf{x}} + \{c \cos(l\phi) + d \sin(l\phi)\} \hat{\mathbf{y}} \right], \quad (32-39)$$

where a , b , c and d are constants. There are four sets of values for these constants, corresponding to two pairs of orthogonally polarized modes. We determine the equations for the constants in an analogous manner to Section 32-5. Thus we substitute

Eq. (32-39) into Eq. (32-28) and generate four equations corresponding to: (i) $s_t = F_l \cos(l\phi)\hat{x}$; (ii) $s_t = F_l \sin(l\phi)\hat{x}$; (iii) $s_t = F_l \cos(l\phi)\hat{y}$; and (iv) $s_t = F_l \sin(l\phi)\hat{y}$. If the area integrals are expressed in cylindrical polar coordinates (r, ϕ) , then $dA = \rho^2 R dR d\phi$ where $R = r/\rho$, and the range of integration is $0 \leq R < \infty$, $0 \leq \phi < 2\pi$. The ϕ integration is readily performed and the four equations are, respectively,

$$a \delta\beta = aI_1 + dI_2; \quad b \delta\beta = bI_1 - cI_2, \quad (32-40a)$$

$$c \delta\beta = cI_1 - bI_2; \quad d \delta\beta = dI_1 + aI_2, \quad (32-40b)$$

when $l > 1$, and when $l = 1$ we obtain

$$2a \delta\beta = (3a + d)I_1 + (a + 3d)I_2; \quad 2b \delta\beta = (b + c)(I_1 - I_2), \quad (32-40c)$$

$$2c \delta\beta = (b + c)(I_1 - I_2); \quad 2d \delta\beta = (a + 3d)I_1 + (3a + d)I_2, \quad (32-40d)$$

respectively. The factors I_1 and I_2 are defined by

$$I_1 = \frac{(2\Delta)^{3/2}}{4\rho V} \frac{\int_0^\infty R F_l (dF_l/dR) (df/dR) dR}{\int_0^\infty R F_l^2 dR}; \quad I_2 = \frac{l(2\Delta)^{3/2}}{4\rho V} \frac{\int_0^\infty F_l^2 (df/dR) dR}{\int_0^\infty R F_l^2 dR}. \quad (32-40e)$$

The four independent solutions of these equation and the corresponding transverse fields in Table 13-1, page 288, are

$$\mathbf{e}_{11}: a = -d = 1, b = c = 0; \quad \mathbf{e}_{12}: a = d = 1, b = c = 0, \quad (32-41a)$$

$$\mathbf{e}_{13}: b = c = 1, a = d = 0; \quad \mathbf{e}_{14}: b = -c = 1, a = d = 0. \quad (32-41b)$$

The corrections $\delta\beta_i$ to the scalar propagation constant are given in terms of I_1 and I_2 in Table 14-1, page 304. It is clear that \mathbf{e}_{11} and \mathbf{e}_{13} , and \mathbf{e}_{12} and \mathbf{e}_{14} are orthogonally polarized pairs of modes.

32-7 Symmetry properties of higher-order modes on circular fibers

The combination of solutions of the scalar wave equation for the transverse fields of weakly guiding fibers of circular cross-section are given in Table 13-1, page 288. As we showed in the previous section, these combinations can be derived using perturbation theory. In this section we show how the combinations can be deduced using only symmetry arguments [2]. We start with the four vector solutions constructed from the solutions of the scalar wave equation with the common propagation constant β , and denote them by

$$\mathbf{e}_{xe} = F_l(R) \cos(l\phi)\hat{x}; \quad \mathbf{e}_{xo} = F_l(R) \sin(l\phi)\hat{x}, \quad (32-42a)$$

$$\mathbf{e}_{ye} = F_l(R) \cos(l\phi)\hat{y}; \quad \mathbf{e}_{yo} = F_l(R) \sin(l\phi)\hat{y}, \quad (32-42b)$$

where $l \geq 1$ and $F_l(R)$ is the solution of Eq. (32-38).

A circular fiber is unchanged by rotation about its axis. Hence, if a mode of the fiber is rotated in a similar manner, it must remain a mode with the same propagation constant,

although not necessarily the same mode. For example, if the field pattern \mathbf{e}_{xe} for $l = 1$ is arbitrarily rotated, it will then be represented by a linear combination of all four patterns in Fig. 32-1(a). However, if \mathbf{e}_{xe} is to be a modal field of the fiber, all four fields in Eq. (32-42) must have the same corrected propagation constant β . Since the four corrections for $l \geq 1$ in Table 14-1, page 304, are not all equal, we deduce that none of the fields in Eq. (32-42) represents a mode of the fiber.

To form the correct linear combination, we combine those modes which have the same properties under a rotation by 90° and under reflections in the x - and y -axes. It may help at this point to consider a specific example, say the $l = 1$ mode shown in Fig. 32-1(b). Thus, \mathbf{e}_{xe} is combined with \mathbf{e}_{yo} because one rotates into the other, while \mathbf{e}_{xo} is combined with \mathbf{e}_{ye} because one rotates into minus the other. Taking symmetric and antisymmetric combinations leads to the transverse fields of the four modes of the weakly guiding fiber in Table 13-1, page 288. These combinations can be shown to be consistent with the symmetry properties of the fiber. The patterns \mathbf{e}_{t2} and \mathbf{e}_{t4} of Fig. 32-1(b) are unchanged by reflection in the fiber axis and by rotation through an arbitrary angle, consistent with their being modal fields of the fiber. However, under arbitrary rotation and reflections \mathbf{e}_{t1} changes into a pattern which is a linear combination of \mathbf{e}_{t1} and \mathbf{e}_{t3} . Symmetry demands that this new combination is also a mode, which in turn requires that \mathbf{e}_{t1} and \mathbf{e}_{t3} have identical propagation constants. This is evident from Table 14-1, page 304, since $\delta\beta_1 = \delta\beta_3$.

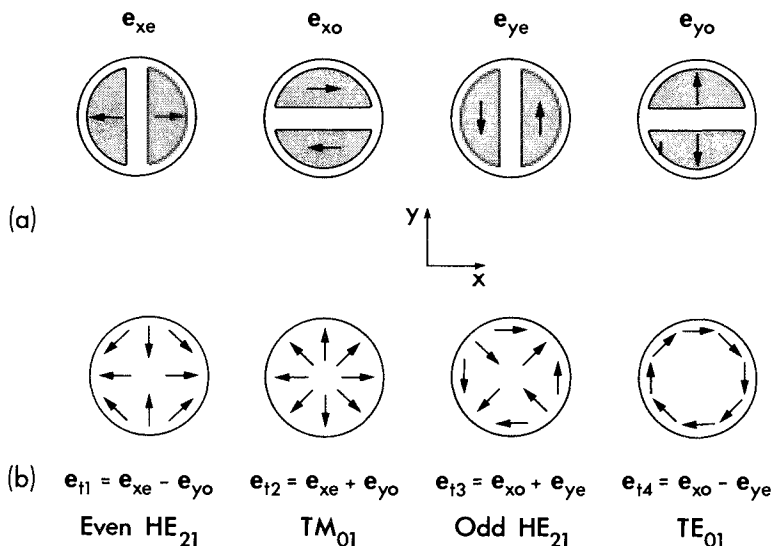


Fig. 32-1 (a) Qualitative representation of the transverse electric fields defined in Eq. (32-42), for the $l = 1$ modes in the core of a circular fiber. Shading corresponds to higher field intensity. (b) Combinations of the fields in (a) which constitute $l = 1$ modal fields. Arrows show the transverse electric field direction.

32–8 Alternative representation for modes on circular fibers

Our discussions of weakly guiding circular fibers both in this chapter, and in Chapters 13 and 14, have tacitly assumed that the combinations in Table 13–1, page 288, form the most basic set of modes for describing approximate solutions of the vector wave equation. For example, we might have considered the set of four right- and left-handed, circularly polarized fields which have the complex forms

$$\mathbf{e}_{1a} = (\hat{\mathbf{x}} + i\hat{\mathbf{y}})F_l(R)\exp(il\phi); \quad \mathbf{e}_{1b} = (\hat{\mathbf{x}} - i\hat{\mathbf{y}})F_l(R)\exp(il\phi), \quad (32-43a)$$

$$\mathbf{e}_{1c} = \mathbf{e}_{1a}^*, \quad \mathbf{e}_{1d} = \mathbf{e}_{1b}^*, \quad (32-43b)$$

where * denotes complex conjugate, and $F_l(R)$ is the real solution of Eq. (32–38). Let us now investigate if this even simpler set of fields can be modes of the vector wave equation in the weak-guidance approximation. We begin by observing that the modal fields of Table 13–1 are related to Eq. (32–43) by

$$\mathbf{e}_{11} = \text{Re}(\mathbf{e}_{1a}); \quad \mathbf{e}_{12} = \text{Re}(\mathbf{e}_{1b}); \quad \mathbf{e}_{13} = \text{Im}(\mathbf{e}_{1a}); \quad \mathbf{e}_{14} = \text{Im}(\mathbf{e}_{1b}), \quad (32-44)$$

where Re and Im denote real and imaginary parts. If each of the fields of Eq. (32–43) is an approximate solution of the vector wave equation of Eq. (32–3) with corrected propagation constant $\beta + \delta\beta_l$, then by equating real parts and imaginary parts, it is clear that the real and imaginary parts of each field are also solutions with the same propagation constant β . Thus, in particular, Re (\mathbf{e}_{1a}) and Im (\mathbf{e}_{1a}) have the same propagation constants for all $l \geq 0$, corresponding to $\delta\beta_1 = \delta\beta_3$ in Table 14–1, page 304. However, this is generally not true for Re (\mathbf{e}_{1b}) and Im (\mathbf{e}_{1b}) , since for $l = 1$ the corrections $\delta\beta_2$ and $\delta\beta_4$ for TE_{0m} and TM_{0m} modes differ. Consequently, the representation of Eq. (32–43) applies to all modes of a circular fiber with the exception of the TE_{0m} and TM_{0m} modes. In the case of the infinite parabolic profile, we show in Table 14–2, page 307, that $\delta\beta_2 = \delta\beta_4$ for the $l = 1$ modes, but not if higher-order corrections are included.

32–9 Fibers with nearly circular cross-sections

We discussed higher-order modes of fibers with nearly circular cross-sections in Section 13–9, and showed that the transverse electric field must take the forms given at the bottom of Table 13–1, page 288. These forms are in terms of the solutions of the scalar wave equation of Eq. (32–37) and unknown constants a_+ and a_- . When the cross-section is exactly circular, the two solutions of Eq. (32–37) have the same propagation constant. However, if the cross-section is only near to circular, the two solutions of the scalar wave equation have similar but distinct propagation constants $\hat{\beta}_e$ and $\hat{\beta}_o$, as discussed in Section 13–8.

The values of a_+ and a_- , and the corrections $\delta\beta_e$ and $\delta\beta_o$ to the scalar propagation constants $\hat{\beta}_e$ and $\hat{\beta}_o$, respectively, are directly related. These relationships are found by a procedure similar to that of Section 32–5. In Eq. (32–28), we set $\mathbf{e}_l = \mathbf{e}_{11}$ or $\mathbf{e}_l = \mathbf{e}_{12}$ from Table 13–1, and generate four equations by setting: (i) $\delta\beta = \delta\beta_e$, $\mathbf{s}_l = F_l \cos(l\phi) \hat{\mathbf{x}}$; and (ii) $\delta\beta = \delta\beta_o$, $\mathbf{s}_l = F_l \sin(l\phi) \hat{\mathbf{y}}$. Within the approximations made above, it is sufficient to take f to be the profile of the circular fiber in calculating $\nabla_l f$. Then, by analogy with the

derivation of Eq. (32-40), we obtain

$$\delta\beta_e = I_1 + aI_2; \quad a\delta\beta_o = I_2 + aI_1 \quad l > 1, \quad (32-45a)$$

$$2\delta\beta_e = (3+a)I_1 + (1+3a)I_2; \quad 2a\delta\beta_o = (3+a)I_2 + (1+3a)I_1, \quad l = 1, \quad (32-45b)$$

where a denotes a_+ or a_- , and I_1, I_2 are defined by Eq. (32-40e). With reference to Table 14-1, page 304, the solution of these equations is expressible in terms of the corrections $\delta\beta_1$ and $\delta\beta_2$ for the circular fiber as [2]

$$a_{\pm} = \Lambda \pm (1 + \Lambda^2)^{1/2}; \quad \Lambda = (\hat{\beta}_e - \hat{\beta}_o) / (\delta\beta_1 - \delta\beta_2); \quad l \geq 1. \quad (32-46)$$

The corrections for the noncircular fiber are found by substituting a_{\pm} into Eq. (32-45). If we repeat the calculation with $\mathbf{e}_l = \mathbf{e}_{l3}$ or $\mathbf{e}_l = \mathbf{e}_{l4}$, we obtain an identical expression for a_{\pm} , except that $\delta\beta_1 - \delta\beta_2$ is replaced by $\delta\beta_3 - \delta\beta_4$ in Eq. (32-46).

32-10 Higher-order corrections to the modal fields

For virtually all applications to weakly guiding waveguides in Part II, it is sufficient to know the lowest order modal fields $\hat{\mathbf{e}}_l$ and $\hat{\mathbf{h}}_l$. These fields with the \sim omitted were discussed at length in the previous five sections. We showed in Section 32-2 that the first corrections are the longitudinal fields $e_z^{(1/2)}$ and $h_z^{(1/2)}$, which are given explicitly in terms of $\hat{\mathbf{e}}_l$ and $\hat{\mathbf{h}}_l$ in Table 32-1. However, as pointed out in Section 13-11, for those problems in which $e_z^{(1/2)}$ and $h_z^{(1/2)}$ appear important, it is usually true that the first order corrections $\mathbf{e}_l^{(1)}$ and $\mathbf{h}_l^{(1)}$ are also required. The first-order corrections $\mathbf{h}_l^{(1)}$, $e_z^{(3/2)}$ and $h_z^{(3/2)}$ in Table 32-1 are given explicitly once the solution of the equation for $\mathbf{e}_l^{(1)}$ is known. The correction $U^{(1)}$ appearing in this equation is calculated from the lowest-order solution using Eqs. (32-11b) and (32-25). There are two general methods of solution, using either eigenfunction expansions of Green's functions.

Eigenfunction solution

In the eigenfunction approach, the component equations of the equation for $\mathbf{e}_l^{(1)}$ in the x - and y -directions are solved separately by expressing the cartesian components $e_x^{(1)}$ and $e_y^{(1)}$ in terms of complete sets of discrete eigenfunctions Ψ_j and continuous eigenfunctions $\Psi_j(Q)$ of the scalar wave equation, where Ψ_j satisfies Eq. (13-8), $\Psi_j(Q)$ satisfies Eq. (25-20) and Q is defined inside the back cover [4]. For example, we set

$$e_x^{(1)} = \sum_j a_j \Psi_j + \sum_j \int_0^\infty a_j(Q) \Psi_j(Q) dQ, \quad (32-47)$$

where a_j and $a_j(Q)$ are amplitude coefficients. This expansion is substituted into the x -component equation

$$\{\rho^2 \nabla_l^2 + \tilde{U}^2 - V^2 f\} e_x^{(1)} = 2\rho^2 \frac{\partial}{\partial x} \{\hat{\mathbf{e}}_l \cdot \nabla_l f\} - 2\tilde{U} U^{(1)} \tilde{e}_x, \quad (32-48)$$

where \tilde{e}_x is the x -component of $\hat{\mathbf{e}}_l$. The amplitude coefficients are then found by using the orthogonality properties of the eigenfunctions, discussed in Section 33-2.

Green's function solution

The solution for $\mathbf{e}_t^{(1)}$ is given directly in terms of the Green's function $G(\mathbf{r}, \mathbf{r}')$ for the scalar wave equation, where \mathbf{r} and \mathbf{r}' are position vectors in the waveguide cross-section [5], and

$$\{\rho^2 \nabla^2 + \tilde{U}^2 - V^2 f\} G = \rho^2 \delta(x - x') \delta(y - y'), \quad (32-49)$$

where δ is the Dirac delta function. Hence

$$\mathbf{e}_t^{(1)} = \int_{A_\infty} G(\mathbf{r}, \mathbf{r}') \mathbf{g}(\mathbf{r}') dA', \quad (32-50)$$

where A_∞ is the infinite cross-section, $\mathbf{r} = (x, y)$, $\mathbf{r}' = (x', y')$, and \mathbf{g} denotes the right side of the equation for $\mathbf{e}_t^{(1)}$ in Table 32–1.

For certain profiles there are more direct methods for determining $\mathbf{e}_t^{(1)}$. In Table 14–2, page 307, the solution for $\mathbf{e}_t^{(1)}$ is found using separation of variables and the solution of ordinary differential equations. For the clad power-law profiles of Section 14–8, we show that the solutions of the scalar wave equation are expressible as power-series expansions. The cartesian components of $\mathbf{e}_t^{(1)}$ can then be determined as power-series expansions [6].

As we showed in Chapter 13, all modes of waveguides with noncircular cross-sections and the fundamental modes of circular fibers are uniformly polarized, i.e. the field lines form an orthogonal mesh of straight lines over the cross-section. The higher-order field corrections account for a slight curvature of the field lines, and the electric and magnetic fields will in general no longer be exactly orthogonal.

VECTOR WAVE EQUATION WITH SOURCES

When current sources are present within a waveguide, the total fields are related to the currents through Maxwell's equations, or, equivalently, through the inhomogeneous vector wave equations. The cartesian components E_x , E_y and E_z of the total electric field \mathbf{E} satisfy Eq. (30–17a)

$$\{\nabla^2 + k^2 n^2\} \mathbf{E} = -\nabla \{ \mathbf{E}_t \cdot \nabla_t \ln n^2 \} - \frac{i}{k} \left(\frac{\mu_0}{\epsilon_0} \right)^{1/2} \left\{ k^2 \mathbf{J} + \nabla \left(\frac{\nabla \cdot \mathbf{J}}{n^2} \right) \right\}, \quad (32-51)$$

where $\mathbf{J} = \mathbf{J}(x, y, z)$ is the volume current density due to sources, $n = n(x, y)$, ∇^2 is the scalar Laplacian of Eq. (37–36), and remaining quantities are defined inside the back cover. We recall from Section 11–16 that the terms involving $\nabla_t \ln n^2$ are responsible for describing the polarization properties of the waveguide. If the waveguide is weakly guiding, then the variation in profile is small, and it is intuitive that polarization effects are small. The approximate form of Eq. (32–51) in this case is obtained by ignoring all terms which involve the derivative of the profile and replacing n by n_∞ on the right side. Hence [7]

$$\{\nabla^2 + k^2 n^2\} \mathbf{E} = -i \left(\frac{\mu_0}{\epsilon_0} \right)^{1/2} \left\{ k \mathbf{J} + \frac{\nabla(\nabla \cdot \mathbf{J})}{k n_\infty^2} \right\}. \quad (32-52)$$

This equation ignores all polarization properties of the waveguide, and, apart from the spatial dependence of the profile on the left side, is identical to the usual free-space description of current sources in which n is replaced by a uniform index [8]. Thus we must retain both terms on the right side. We discuss solutions of this equation in the following two chapters.

RADIATION MODES

We showed how to determine the radiation modes of weakly guiding waveguides in Sections 25–9 and 25–10, starting with the transverse electric field \mathbf{e}_t , which is constructed from solutions of the scalar wave equation. However, unlike bound modes, the corresponding magnetic field \mathbf{h}_t of Eq. (25–23b) does not satisfy the scalar wave equation. This means that the orthogonality and normalization of the radiation modes differ in form from that of the bound modes in Table 13–2, page 292, as we now show.

32–11 Orthogonality and normalization

Consider two distinct radiation modes with electric fields $\mathbf{e}_j = \mathbf{e}_j(Q)$ and $\mathbf{e}_k = \mathbf{e}_k(Q')$, and form the triple scalar product $\mathbf{e}_j \times \mathbf{h}_k^* \cdot \hat{\mathbf{z}}$, where $*$ denotes complex conjugate and $\hat{\mathbf{z}}$ is the unit vector parallel to the waveguide axis. This product requires only the transverse components of the fields. Thus, if we substitute for \mathbf{h}_{tk} using Eq. (25–23b) and rearrange using Eqs. (37–24) and (25–23a), then

$$\mathbf{e}_j \times \mathbf{h}_k^* \cdot \hat{\mathbf{z}} = \left(\frac{\epsilon_0}{\mu_0} \right)^{1/2} \frac{\beta(Q)}{k} \left\{ \mathbf{e}_{tj} \cdot \mathbf{e}_{tk}^* - \frac{i}{\beta} \mathbf{e}_{tj} \cdot \nabla_t e_{zk}^* \right\}. \quad (32-53)$$

We integrate over the infinite cross-section of the waveguide and use the identity in Eq. (37–26) to re-express the second term inside the curly brackets. Hence

$$\frac{1}{2} \int_{A_\infty} \mathbf{e}_j \times \mathbf{h}_k^* \cdot \hat{\mathbf{z}} dA = \frac{1}{2} \left(\frac{\epsilon_0}{\mu_0} \right)^{1/2} \frac{\beta(Q)}{k} \int_{A_\infty} \left\{ \mathbf{e}_{tj} \cdot \mathbf{e}_{tk}^* + \frac{i}{\beta} e_{zk}^* \nabla_t \cdot \mathbf{e}_{tj} - \frac{i}{\beta} \nabla_t \cdot (\mathbf{e}_{tj} e_{zk}^*) \right\} dA. \quad (32-54)$$

The two-dimensional divergence theorem of Eq. (37–55) shows that the integral over the third term inside the curly brackets is identical to a line integral along the perimeter of A_∞ . We then ignore this integral for reasons given in Section 31–1. Finally, we use Eq. (25–23a) to express $\nabla_t \cdot \mathbf{e}_{tj}$ in terms of e_{zj} , whence

$$\frac{1}{2} \int_{A_\infty} \mathbf{e}_j \times \mathbf{h}_k^* \cdot \hat{\mathbf{z}} dA = \frac{1}{2} \left(\frac{\epsilon_0}{\mu_0} \right)^{1/2} \frac{\beta(Q)}{k} \int_{A_\infty} \mathbf{e}_j(Q) \cdot \mathbf{e}_k^*(Q') dA. \quad (32-55)$$

Thus the orthogonality condition of Eq. (25–4) reduces to Eq. (25–24a) for the weakly guiding waveguide, and similarly the definition of normalization in Eq. (25–5) is replaced by Eq. (25–24b).

REFERENCES

1. Snyder, A. W. (1969) Asymptotic expressions for eigenfunctions and eigenvalues of dielectric or optical waveguides. *I.E.E.E. Trans. Microwaves Theory Tech.* **17**, 1130–8.
2. Snyder, A. W. and Young, W. R. (1978) Modes of optical waveguides. *J. Opt. Soc. Am.*, **68**, 297–309.
3. Tjaden, D. L. A. (1978) First-order correction to 'weak-guidance' approximation in fibre optics theory. *Philips J. Res.*, **33**, 103–12.
4. Sammut, R. A., Hussey, C. D., Love, J. D. and Snyder, A. W. (1981) Modal analysis of polarization effects in weakly-guiding fibres. *I.E.E. Proc.*, **128**, 173–87.
5. Snyder, A. W. and Love, J. D. (1982) Green's function methods for analyzing optical fibre perturbations. *J. Opt. Soc. Am.* **72**, 1131–35.
6. Love, J. D., Hussey, C. D., Snyder, A. W. and Sammut, R. A. (1982) Polarization corrections to mode propagation on weakly guiding fibres. *J. Opt. Soc. Am.*, **72**, 1583–91.
7. Snyder, A. W. (1980) Weakly guiding optical fibres. *J. Opt. Soc. Am.*, **70**, 405–11.
8. Ramo, S., Whinnery, J. R. and Van Duzer, T. (1965) *Fields and Waves in Communications Electronics*, Wiley, New York.

Modal methods for the scalar wave equation

33-1	The scalar wave equation	641
Bound modes of the scalar wave equation		641
33-2	Orthogonality and normalization	641
33-3	Integral expressions for the propagation constant	643
33-4	Phase and group velocities	643
33-5	Reciprocity relations	644
33-6	Analytical expressions for propagation constants	645
Radiation modes of the scalar wave equation		646
33-7	Orthogonality and normalization	647
33-8	Leaky modes	647
Modal methods for z-independent nonuniformities		648
33-9	Modal fields and propagation constants	648
33-10	Slightly perturbed waveguides	648
Modal methods for z-dependent nonuniformities		649
33-11	Coupled mode equations	649
Local modes		651
33-12	Coupled local-mode equations	651
33-13	Alternative form for the coupling coefficients	652
Mode excitation by current sources		653
References		655

In Chapter 11 we presented the fundamental properties of modes of optical waveguides. These properties were derived from Maxwell's equations in Chapters 30 and 31. Then, for the weakly guiding waveguides discussed in Chapter 13, we presented simplified expressions for these properties in Chapter 32, as summarized in Table 13-2. The corresponding simplification for radiation-mode properties was given in Chapter 25. There are two ways in which these simplified expressions can be obtained. One way is to take the limit $\Delta \rightarrow 0$ of the exact expressions holding V constant. Alternatively, we can recognize from the outset that the transverse electric field \mathbf{e}_t of a mode of the weakly guiding waveguide satisfies the scalar wave equation, and thus derive the modal properties by studying properties of the solutions of the scalar wave equation. In this chapter we follow the second and more direct approach. We emphasize that the

polarization effects due to the waveguide structure, discussed in Chapter 13, are neglected here.

33-1 The scalar wave equation

We showed in Section 13-3 that the cartesian components of the transverse electric field are solutions of the scalar wave equation. If Ψ denotes either component of Eq. (13-7), and $\tilde{\beta}$ is the scalar propagation constant, then

$$\{\nabla_t^2 + k^2 n^2(x, y) - \tilde{\beta}^2\} \Psi = 0, \quad (33-1)$$

where $n(x, y)$ is the profile, $k = 2\pi/\lambda$, λ is the free-space wavelength and ∇_t^2 is defined in Table 30-1, page 592. As we show below, the solution Ψ of the scalar wave equation and its first derivatives are everywhere continuous and are therefore bounded. This leads to an eigenvalue equation for the allowed values of $\tilde{\beta}$.

Continuity properties

The continuity properties of Eq. (33-1) follow by *reductio ad absurdum*. Suppose Ψ is not continuous, so that somewhere it has a step, or jump in value. The first derivatives will then contain a singularity described by the Dirac delta function, and the second derivatives will contain the derivative of the delta function. Since the profile $n(x, y)$ contains, at most, a step discontinuity, it is clear that Eq. (33-1) cannot be satisfied. Consequently Ψ must be continuous. A similar argument is used to prove that the first derivatives are also continuous. It is not necessary that the second derivatives be continuous. For example, if $n(x, y)$ is a step profile, then at least one of the second derivatives of Ψ must be discontinuous. Finally, since \mathbf{e}_t is constructed from solutions of the scalar wave equation, it must have the same continuity properties as Ψ .

BOUND MODES OF THE SCALAR WAVE EQUATION

Here we derive the modal properties of weakly guiding waveguides, starting from solutions of the scalar wave equation.

33-2 Orthogonality and normalization

Let Ψ_j and Ψ_k denote two distinct solutions of Eq. (33-1) with propagation constants $\tilde{\beta}_j$ and $\tilde{\beta}_k$. We assume that the waveguide is nonabsorbing, and, in keeping with the convention of Section 11-3, we can then choose Ψ_j and Ψ_k to be real. Hence

$$\{\nabla_t^2 + k^2 n^2 - \tilde{\beta}_j^2\} \Psi_j = 0; \quad \{\nabla_t^2 + k^2 n^2 - \tilde{\beta}_k^2\} \Psi_k = 0, \quad (33-2)$$

where $n = n(x, y)$. Multiplying the first equation by Ψ_k , the second equation by Ψ_j , subtracting and integrating over the infinite cross-section A_∞ yields

$$(\tilde{\beta}_j^2 - \tilde{\beta}_k^2) \int_{A_\infty} \Psi_j \Psi_k dA = \int_{A_\infty} \{\Psi_k \nabla_t^2 \Psi_j - \Psi_j \nabla_t^2 \Psi_k\} dA. \quad (33-3)$$

The two-dimensional Green's theorem of Eq. (37-58) converts the right side of this equation into the line integral

$$\oint_{l_\infty} \{\Psi_k \nabla_t \Psi_j - \Psi_j \nabla_t \Psi_k\} \cdot \hat{n} dl, \quad (33-4)$$

where l_∞ is the perimeter of A_∞ and \hat{n} is the unit outward vector on l_∞ in the plane of A_∞ . This integral vanishes because the bound-mode solutions and their first derivatives decrease exponentially to zero at infinity. Consequently, we deduce from Eq. (33-3) that all bound modes of weakly guiding waveguides satisfy

$$\int_{A_\infty} \Psi_j \Psi_k dA = 0; \quad j \neq k, \quad (33-5a)$$

which includes backward-propagating modes with propagation constants $\tilde{\beta}_{-j} = -\tilde{\beta}_j$ and $\tilde{\beta}_{-k} = -\tilde{\beta}_k$, using the convention of Eq. (11-4). If \mathbf{e}_{ij} and \mathbf{e}_{ik} denote solutions of the scalar wave equation constructed from Eq. (13-7) with propagation constants $\tilde{\beta}_j$ and $\tilde{\beta}_k$, respectively, we can repeat the above proof in vector language and obtain

$$\int_{A_\infty} \mathbf{e}_{ij} \cdot \mathbf{e}_{ik} dA = 0; \quad j \neq k. \quad (33-5b)$$

We recall from Table 11-1, page 230, that orthogonality of the exact modal fields is expressed in terms of the vector product $\mathbf{e}_{ij} \times \mathbf{h}_{ik}^* \cdot \hat{z}$. The expression for \mathbf{h}_i in Table 13-1, page 288, shows that this product is proportional to $\mathbf{e}_{ij} \cdot \mathbf{e}_{ik}^*$ on a weakly guiding waveguide. Since \mathbf{e}_i is real on a nonabsorbing waveguide, we deduce from Eq. (33-5) that, for bound modes, scalar and vector orthogonality are equivalent in the weak-guidance approximation.

Normalization

It is convenient to describe normalization of solutions of the scalar wave equation in terms of the vector normalization N in Table 11-1, page 230. By repeating the above argument, it follows that

$$\tilde{N} = \frac{1}{2} \left| \int_{A_\infty} \mathbf{e} \times \mathbf{h}^* \cdot \hat{z} dA \right| = \frac{n_{co}}{2} \left(\frac{\epsilon_0}{\mu_0} \right)^{1/2} \int_{A_\infty} \mathbf{e}_t^2 dA. \quad (33-6)$$

Substituting from Table 13-1, page 288, we deduce that for waveguides of noncircular cross-section and for circular fibers

$$\boxed{\tilde{N} = \frac{n_{co}}{2} \left(\frac{\epsilon_0}{\mu_0} \right)^{1/2} \int_{A_\infty} \Psi^2 dA;} \quad \boxed{\tilde{N} = \pi n_{co} \left(\frac{\epsilon_0}{\mu_0} \right)^{1/2} \int_0^x r F_1^2(r) dr,} \quad (33-7)$$

respectively, for all fundamental and higher-order modes.

33-3 Integral expressions for the propagation constant

In Section 11-13 we showed that the exact propagation constant is given explicitly in terms of integrals over the vector modal fields. Here we derive the analogous expression for the scalar propagation constant in terms of scalar solutions of the scalar wave equation. Starting with Eq. (33-1), we multiply by Ψ and integrate over the infinite cross-section A_∞ to obtain

$$\tilde{\beta}^2 \int_{A_\infty} \Psi^2 dA = k^2 \int_{A_\infty} n^2 \Psi^2 dA + \int_{A_\infty} \Psi \nabla_t^2 \Psi dA. \quad (33-8)$$

The second integral on the right is transformed, using the two-dimensional form of the divergence theorem in Eq. (37-55), and the identity in Eq. (37-26). Thus

$$\int_{A_\infty} \Psi \nabla_t^2 \Psi dA = \oint_{l_\infty} \Psi (\nabla_t \Psi) \cdot \hat{n} dl - \int_{A_\infty} (\nabla_t \Psi)^2 dA, \quad (33-9)$$

where l_∞ is the perimeter of A_∞ , and \hat{n} is the unit outward normal on l_∞ in the plane of A_∞ . The line integral vanishes since Ψ and its first derivatives decay exponentially to zero at infinity. Combining Eqs. (33-8) and (33-9) then gives

$$\boxed{\tilde{\beta}^2 = \frac{\int_{A_\infty} \{k^2 n^2 \Psi^2 - (\nabla_t \Psi)^2\} dA}{\int_{A_\infty} \Psi^2 dA}}, \quad (33-10)$$

where $n = n(x, y)$. This equation is an integral form of the eigenvalue equation for the scalar wave equation, discussed in Section 33-1. It is also a stationary expression with respect to changes in Ψ [1, 2]. Further, if we examine the corresponding expression for the exact propagation constant in Eq. (31-21), we find that in the weak-guidance limit Eq. (33-10) cannot be derived simply by approximating \mathbf{e} and \mathbf{h} by \mathbf{e}_t and \mathbf{h}_t of Table 13-1, page 288. In other words it is necessary to retain higher-order terms in the expansion of Eq. (32-18).

33-4 Phase and group velocities

The phase and group velocities of a bound-mode solution of the scalar wave equation are defined by

$$\tilde{v}_p = \frac{\omega}{\tilde{\beta}} = \frac{2\pi c}{\lambda \tilde{\beta}}; \quad \tilde{v}_g = \frac{d\omega}{d\tilde{\beta}} = -\frac{2\pi c}{\lambda^2} \frac{d\lambda}{d\tilde{\beta}}, \quad (33-11)$$

respectively, where the angular frequency ω and free-space wavelength λ are related at the back of the book. We can express \tilde{v}_p in terms of the solution Ψ of Eq. (33-1) through Eq. (33-10). Here we derive analogous expressions for \tilde{v}_g . Alternatively, \tilde{v}_g can be found by differentiating the scalar wave equation eigenvalue equation. In addition to the spatial variation in profile, we allow for material dispersion when n and μ vary with wavelength, i.e. $n = n(\lambda)$ and $\mu = \mu(\lambda)$, as explained in Section 31-6.

We denote the solution of Eq. (33-1) at wavelength λ by $\Psi(\lambda)$ and $\tilde{\beta}(\lambda)$. Since

$k = 2\pi/\lambda$, we deduce that

$$\{\nabla_t^2 + 4\pi^2 n^2(\lambda)/\lambda^2\}\Psi(\lambda) = \tilde{\beta}^2(\lambda)\Psi(\lambda). \quad (33-12)$$

The same solution at wavelength $\bar{\lambda}$ satisfies

$$\{\nabla_t^2 + 4\pi^2 n^2(\bar{\lambda})/\bar{\lambda}^2\}\Psi(\bar{\lambda}) = \tilde{\beta}^2(\bar{\lambda})\Psi(\bar{\lambda}). \quad (33-13)$$

We multiply Eq. (33-12) by $\Psi(\bar{\lambda})$, Eq. (33-13) by $\Psi(\lambda)$, subtract and integrate over the infinite cross-section A_∞ to obtain

$$\{\tilde{\beta}^2(\lambda) - \tilde{\beta}^2(\bar{\lambda})\} \int_{A_\infty} \Psi(\lambda)\Psi(\bar{\lambda}) dA = 4\pi^2 \int_{A_\infty} \left\{ \frac{n^2(\lambda)}{\lambda^2} - \frac{n^2(\bar{\lambda})}{\bar{\lambda}^2} \right\} \Psi(\lambda)\Psi(\bar{\lambda}) dA + I, \quad (33-14)$$

where I is the integral

$$\int_{A_\infty} \{\Psi(\bar{\lambda})\nabla_t^2 \Psi(\lambda) - \Psi(\lambda)\nabla_t^2 \Psi(\bar{\lambda})\} dA. \quad (33-15)$$

This integral is transformed into a line integral at infinity, through the two-dimensional Green's theorem of Eq. (37-58), and vanishes since $\Psi(\lambda)$ and $\Psi(\bar{\lambda})$ and their first derivatives vanish exponentially. If we then divide both sides of Eq. (33-14) by $\lambda - \bar{\lambda}$ and take the limit $\bar{\lambda} \rightarrow \lambda$ we find

$$\tilde{v}_g = -2 \frac{\tilde{\beta}}{k} \frac{c}{\lambda^3} \int_{A_\infty} \Psi^2 dA \Big/ \int_{A_\infty} \Psi^2 \frac{d}{d\lambda} \left(\frac{n^2}{\lambda^2} \right) dA. \quad (33-16)$$

For waveguides with no material dispersion this reduces to

$$\tilde{v}_g = c \frac{\tilde{\beta}}{k} \int_{A_\infty} \Psi^2 dA \Big/ \int_{A_\infty} n^2 \Psi^2 dA. \quad (33-17)$$

In the weak-guidance limit, it is clear from Table 13-1, page 288, that the group velocity of Eq. (31-31) for the exact fields reduces to Eq. (33-17).

Derivative of the modal parameter

It is useful to be able to express the modal derivative $d\tilde{U}/dV$ in terms of the solution of the scalar wave equation. This can be obtained by paralleling the derivation of the group velocity given above, but starting with Eq. (32-15) instead of Eq. (33-12) and assuming a nondispersive medium. In this case \tilde{U} and V , but not f , vary with wavelength, and it is straightforward to show that the analogous result to Eq. (33-17) is given by $d\tilde{U}/dV$ in Table 13-2, page 292. A detailed derivation can be found elsewhere [3].

33-5 Reciprocity relations

Starting with the scalar wave equation, we can derive a reciprocal relation between modes of different waveguides. Let Ψ and β be the field and propagation constant of a

mode on one weakly guiding waveguide, characterized by refractive-index profile $n = n(x, y)$, and let $\bar{\Psi}$ and $\bar{\beta}$ be the field and propagation constant of a mode on a second weakly guiding waveguide, characterized by refractive-index profile $\bar{n} = \bar{n}(x, y)$. For clarity we omit the \sim on the scalar propagation constants. Both modes obey the scalar wave equation, whence from Eq. (33-1) we have

$$\{\nabla_t^2 + k^2 n^2 - \beta^2\} \Psi = 0; \quad \{\nabla_t^2 + k^2 \bar{n}^2 - \bar{\beta}^2\} \bar{\Psi} = 0. \quad (33-18)$$

We multiply the first equation by $\bar{\Psi}$, the second equation by Ψ , subtract, and integrate over the infinite cross-section A_x to obtain

$$(\beta^2 - \bar{\beta}^2) \int_{A_x} \Psi \bar{\Psi} dA = k^2 \int_{A_x} (n^2 - \bar{n}^2) \Psi \bar{\Psi} dA + \int_{A_x} \{\bar{\Psi} \nabla_t^2 \Psi - \Psi \nabla_t^2 \bar{\Psi}\} dA. \quad (33-19)$$

Using Eq. (37-58), the second integral on the right is converted into a line integral at infinity, which vanishes since Ψ , $\bar{\Psi}$ and their derivatives decay exponentially to zero for bound modes. Hence

$$\beta^2 - \bar{\beta}^2 = k^2 \int_{A_x} (n^2 - \bar{n}^2) \Psi \bar{\Psi} dA \bigg/ \int_{A_x} \Psi \bar{\Psi} dA. \quad (33-20)$$

This expression is the weak-guidance limit of Eq. (31-39), as may be verified by setting $\beta^2 - \bar{\beta}^2 \cong 2kn_{co}(\beta - \bar{\beta})$ and substituting for the fields from Table 13-1, page 288. It is also stationary with respect to variations in the barred quantities [1, 2].

Line integral expression

It is also possible to obtain a relationship between modes of different waveguides in terms of a line integral. To do this, we replace A_x in Eq. (33-19) by $A_x - A_p$, where A_p is the cross-sectional area within which $n(x, y) \neq \bar{n}(x, y)$. The first integral on the right is then zero, and we again convert the second integral on the right into a line integral, as above, along $l_x + l_p$, where l_p is the perimeter of A_p . The integral along l_x is zero and we are left with

$$\beta^2 - \bar{\beta}^2 = \oint_{l_p} \{\bar{\Psi} \nabla_t \Psi - \Psi \nabla_t \bar{\Psi}\} \cdot \hat{n} dl \bigg/ \int_{A_x - A_p} \Psi \bar{\Psi} dA, \quad (33-21)$$

as may be verified from Eq. (37-58), where \hat{n} is the unit outward normal on l_p in the plane of A_x . This expression is the weak-guidance limit of Eq. (31-40), as may be readily verified.

33-6 Analytical expressions for propagation constants

There are few known refractive-index profiles which have closed-form solutions of the scalar wave equation, as discussed in Section 14-8, and even fewer profiles which have analytical expressions for the propagation constants as well. However, in the case of the infinite power-law profiles on circular fibers, we can derive closed-form expressions for

the propagation constants, although we cannot obtain closed-form expressions for the scalar wave equation solutions, with the exception of the infinite parabolic profile of Table 14-2, page 307. These profiles are defined by

$$n^2(R) = n_{co}^2 \{1 - 2\Delta R^q\}, \quad R \geq 0, q > 0, \quad (33-22)$$

where $R = r/\rho$ and the notation is defined inside the back cover. For circular fibers, the solutions of Eq. (33-1) are given by Eq. (32-37) in terms of $F_l(R)$. We substitute Eq. (33-22) into Eq. (32-38), whence

$$\left\{ \frac{d^2}{dR^2} + \frac{1}{R} \frac{d}{dR} - \frac{l^2}{R^2} + \tilde{U}^2 - V^2 R^q \right\} F_l = 0. \quad (33-23)$$

If we make the scaling transformation $R \rightarrow aR$, this becomes [4]

$$\left\{ \frac{d^2}{dR^2} + \frac{1}{R} \frac{d}{dR} - \frac{l^2}{R^2} + a^2 \tilde{U}^2 - V^2 a^{q+2} R^q \right\} F_l = 0. \quad (33-24)$$

Given l and q , the modal parameter \tilde{U} depends only on the waveguide parameter V , i.e. $\tilde{U} = \tilde{U}(V)$. Since the value of \tilde{U} must be the same in both equations, we deduce that \tilde{U} satisfies the functional equation

$$a\tilde{U}(V) = \tilde{U}(Va^{(q+2)/2}). \quad (33-25)$$

This equation has the solution

$$\tilde{U} = G V^{2/(2+q)}, \quad (33-26)$$

where G is a constant that depends on l and q , but is independent of V . We can determine G when $l = 0$ by noting that Eq. (33-26) must hold when $V \rightarrow \infty$. In this limit, expressions for \tilde{U} are derived in Section 36-8 by using WKB methods. On comparing Eqs. (33-26) and (36-19) we obtain G , whence [4]

$$\tilde{U} = \left[\frac{\Gamma(1/q + 1/2)(q+2)(2m-1)\pi^{1/2} V^{2/q}}{2\Gamma(1/q)} \right]^{q/(q+2)}, \quad (33-27)$$

where $m = 1, 2, \dots$ labels the modes, as in Table 14-1, page 304. If we express V in terms of ω and \tilde{U} in terms of $\tilde{\beta}$ through the definitions inside the back cover, then the corresponding group velocity expression follows from Eq. (33-11).

$$\tilde{v}_g = \frac{c}{n_{co}} (q+2) \left/ \left\{ \frac{2\tilde{\beta}}{kn_{co}} + q \frac{kn_{co}}{\tilde{\beta}} \right\} \right., \quad (33-28)$$

where $\tilde{\beta}$ is given through \tilde{U} by Eq. (33-27).

RADIATION MODES OF THE SCALAR WAVE EQUATION

The scalar wave equation has both scalar bound and scalar radiation modes. The bound modes are analogous to the elements of a Fourier series, while the radiation modes can be viewed as the elements of a Fourier integral. Both are necessary to form a complete set of modes for representing an arbitrary field. The radiation modes are characterized

by the scalar field $\Psi(Q)$ and propagation constant $\beta(Q)$ which satisfy the scalar wave equation

$$\{\nabla_t^2 + k^2 n^2(x, y) - \beta^2(Q)\} \Psi(Q) = 0. \quad (33-29)$$

Thus, the discrete values of $\tilde{\beta}$ for the bound modes of Eq. (33-1) are replaced by a continuum of values for $\beta(Q)$. We explained in Chapter 25 why it is more convenient to work with the radiation mode parameter Q , which is defined inside the back cover. We are also reminded that both the electric and magnetic transverse fields, \mathbf{e}_t and \mathbf{h}_t , of the vector bound modes of weakly guiding waveguides are solutions of the scalar wave equation. However, only $\mathbf{e}_t(Q)$ of the vector radiation modes satisfies the scalar wave equation, as we showed in Chapter 25.

33-7 Orthogonality and normalization

The continuum of scalar radiation modes satisfying Eq. (33-29) is treated in an analogous manner to the vector radiation modes of a waveguide. To determine the orthogonality condition, we repeat the derivation of Section 33-2 with Ψ_j and Ψ_k replaced by $\Psi_j(Q)$ and $\Psi_k(Q')$. Then, by paralleling the discussion of Section 31-1, we claim that the correct orthogonality properties are obtained by taking the line integral in Eq. (33-4) to be zero. Hence

$$\int_{A_x} \Psi_j(Q) \bar{\Psi}_k^*(Q') dA = 0, \quad Q \neq Q'. \quad (33-30)$$

Note that this implies orthogonality between identical radiation modes with different values of Q , i.e. when $j = k$.

We define $F_j(Q)$ to be the normalization of each scalar radiation mode, given by

$$F_j(Q) \delta(Q - Q') = \int_{A_x} \Psi_j(Q) \bar{\Psi}_j^*(Q') dA, \quad (33-31)$$

where δ is the Dirac delta function. We emphasize that $F_j(Q)$ should not be confused with the normalization $N_j(Q)$ for the vector radiation modes defined by Eq. (25-5). In general there is no simple relationship between the two expressions.

33-8 Leaky modes

The radiation field of the scalar wave equation can be represented by the continuum of scalar radiation modes discussed above, or by a discrete summation of scalar leaky modes and a space wave. This is clear by analogy with the discussion of vector radiation and leaky modes for weakly guiding waveguides in Chapters 25 and 26. Scalar leaky modes have solutions Ψ of Eq. (33-1) below their cutoff values when $\tilde{\beta}$ becomes complex. Many of the properties of bound modes derived in this chapter also apply to leaky modes. For example, the orthogonality condition of Eq. (33-5a) applies to leaky modes, provided only that the cross-sectional area A_x is replaced by the complex area A'_x of Section 24-15 to ensure that the line integral of Eq. (33-4) vanishes.

MODAL METHODS FOR Z-INDEPENDENT NONUNIFORMITIES

When the complete set of solutions of the scalar wave equation are known for one waveguide, they can be used to represent a scalar mode of any other waveguide. The second waveguide represents a translationally invariant, or z -independent, perturbation of the first waveguide. This is a particularly useful representation when the two waveguides differ only slightly.

33–9 Modal fields and propagation constants

Let Ψ_j and β_j be the unknown field and the propagation constant of the j th mode of the second waveguide, whose refractive-index profile is $n(x, y)$. We express Ψ_j as an eigenfunction expansion over the complete set of bound solutions $\bar{\Psi}_k$ and radiation solutions $\bar{\Psi}_k(Q)$ of the first waveguide with profile $\bar{n}(x, y)$. Hence

$$\Psi_j(x, y) = \sum_k a_k \bar{\Psi}_k(x, y) + \sum_k \int_0^\infty a_k(Q) \bar{\Psi}_k(x, y, Q) dQ, \quad (33-32)$$

where a_k and $a_k(Q)$ are modal amplitudes to be determined, and $\bar{\Psi}_k, \bar{\Psi}_k(Q)$ satisfy Eqs. (33–1), (33–29), respectively, with n and $\hat{\beta}$ replaced by \bar{n} and $\bar{\beta}$. For clarity we omit the \sim on scalar quantities. We substitute Eq. (33–32) into Eq. (33–20) and set $\Psi = \Psi_j$, $\bar{\Psi} = \bar{\Psi}_k$, $\beta = \beta_j$ and $\bar{\beta} = \bar{\beta}_k$. Using the orthogonality conditions of Eqs. (33–5a) and (33–30) we find that

$$a_k = \frac{k^2}{\beta_j^2 - \bar{\beta}_k^2} \frac{1}{F_k} \int_{A_x} (n^2 - \bar{n}^2) \Psi_j \bar{\Psi}_k dA, \quad (33-33a)$$

$$a_k(Q) = \frac{k^2}{\beta_j^2 - \bar{\beta}_k^2(Q)} \frac{1}{F_k(Q)} \int_{A_x} (n^2 - \bar{n}^2) \Psi_j \bar{\Psi}_k(Q) dA, \quad (33-33b)$$

where F_k and $F_k(Q)$ are scalar normalizations defined by

$$F_k = \int_{A_x} \bar{\Psi}_k^2 dA; \quad F_k(Q) \delta(Q - Q') = \int_{A_x} \bar{\Psi}_k(Q) \bar{\Psi}_k(Q') dA, \quad (33-33c)$$

and δ is the Dirac delta function. To fully determine the modal amplitudes, we need an equation for β_j . Following the discussion of Section 31–9, this condition is provided by Eq. (33–10) and leads to an infinite set of nonlinear coupled equations. Although there is no general solution to this set of equations, a perturbation solution is possible when the waveguides are similar.

33–10 Slightly perturbed waveguides

The procedure described in the previous section is formally exact, but does not lead to explicit expressions for Ψ_j and β_j . However, when the second waveguide is only a slight perturbation of the first waveguide, we can obtain a solution of Eq. (33–33) by iteration.

To lowest order it is clear that

$$\Psi_j \cong \bar{\Psi}_j; \quad \beta_j \cong \bar{\beta}_j, \quad (33-34)$$

and consequently $a_j \cong 1$ in Eq. (33-32). The next order corrections are found by setting $\beta_j = \bar{\beta}_j$ and $\Psi_j = \bar{\Psi}_j$ in Eq. (33-33), and $\beta = \beta_j$, $\bar{\beta} = \bar{\beta}_j$, $\Psi = \bar{\Psi} = \bar{\Psi}_j$ in Eq. (33-20). Hence

$$a_k = \frac{k^2}{\bar{\beta}_j^2 - \bar{\beta}_k^2} \frac{1}{F_k} \int_{A_x} (n^2 - \bar{n}^2) \bar{\Psi}_j \bar{\Psi}_k dA; \quad \beta_j^2 = \bar{\beta}_j^2 + \frac{k^2}{F_k} \int_{A_x} (n^2 - \bar{n}^2) \bar{\Psi}_j^2 dA, \quad (33-35)$$

together with an analogous expression for $a_k(Q)$. This method has been used to determine the modes of a slightly elliptical fiber in terms of the modes of a circular fiber. Details are given elsewhere [5].

MODAL METHODS FOR Z-DEPENDENT NONUNIFORMITIES

When a waveguide has nonuniformities which vary with distance z along its length, propagation can be described by a set of coupled equations based on the complete set of modes of the scalar wave equation. This description ignores all polarization properties of the waveguide, and is equivalent to the total transverse electric field remaining parallel to a fixed direction. Here we show how to derive this set of equations, starting from the scalar wave equation.

33-11 Coupled mode equations

Let $\bar{n}(x, y)$ and $n(x, y, z)$ be the refractive-index profiles of the uniform and nonuniform waveguides. Within the weak-guidance approximation, the field $\Phi(x, y, z)$ of the nonuniform waveguide satisfies the three-dimensional scalar wave equation, which is expressible as

$$\left\{ \nabla_t^2 + k^2 n^2(x, y, z) + \frac{\partial^2}{\partial z^2} \right\} \Phi = 0, \quad (33-36)$$

where ∇_t^2 is defined in Table 30-1, page 592, $k = 2\pi/\lambda$ and λ is the free-space wavelength. We express Φ as a summation over the complete set of scalar bound and radiation modes

$$\Phi = \sum_l a_l(z) \Psi_l(x, y) + \sum_l \int_0^\infty a_l(z, Q) \Psi_l(x, y, Q) dQ, \quad (33-37)$$

where $a_l(z)$ and $a_l(z, Q)$ contain all the z dependence for both the forward- and backward-propagating modes, and $\bar{\Psi}_l$ and $\bar{\Psi}_l(Q)$ satisfy Eqs. (33-1) and (33-29)

$$\{\nabla_t^2 + k^2 \bar{n}^2(x, y) - \beta_l^2\} \Psi_l = 0; \quad \{\nabla_t^2 + k^2 \bar{n}^2(x, y) - \beta_l^2(Q)\} \Psi_l(Q) = 0. \quad (33-38)$$

For clarity we omit the \sim from the scalar quantities. We substitute Eq. (33-37) into

Eq. (33-36) and use Eq. (33-38) to eliminate terms in $\nabla_t^2 \Psi_l$. Multiplying by Ψ_k and integrating over the infinite cross-section, we deduce from the orthogonality condition of Eq. (33-5a) that

$$\frac{d^2 a_k}{dz^2} + \beta_k^2 a_k = i \sum_l \left\{ D_{kl} a_l + \int_0^\infty D_{kl}(Q) a_l(Q) dQ \right\}, \quad (33-39a)$$

together with an analogous expression for $a_k(Q)$. The D_{kl} and $D_{kl}(Q)$ are coupling coefficients defined by

$$D_{kl} = ik^2 \int_{A_x} (n^2 - \bar{n}^2) \Psi_k \Psi_l dA \Big/ \int_{A_x} \Psi_k^2 dA, \quad (33-39b)$$

where $D_{kl}(Q)$ is defined by the same expression with $\Psi_l(Q)$ replacing Ψ_l . Thus the coefficients are functions of z . Once the solution for a_k is known, the amplitudes d_k and d_{-k} of the forward- and backward-propagating modes are determined by examining the z dependence of a_k in the relationship

$$a_k = d_k \exp(i\beta_k z) + d_{-k} \exp(-i\beta_k z). \quad (33-40)$$

It may be helpful to refer to the analogous procedure below Eq. (33-63), where the modal amplitudes due to current sources are determined.

Relationship with coupled mode equations for arbitrary waveguides

In Section 31-11 we derived sets of coupled mode equations to describe propagation along arbitrary waveguides with nonuniformities, based on the exact modes of a uniform waveguide. If we examine the weak-guidance limit of these equations, it is clear that, for example, Eq. (31-50a) is unchanged, but the coupling coefficients of Eqs. (31-50b) and (31-50c) are modified. We ignore terms in \hat{e}_{zk} , which are of higher order than terms in \hat{e}_{tk} , and, allowing for orthonormalization through Table 11-1, page 230, and Eq. (33-7), we deduce that

$$C_{kl} \cong D_{kl}/(2ikn_{co}); \quad C_{kl}(Q) \cong D_{kl}(Q)/(2ikn_{co}). \quad (33-41)$$

The next step is to differentiate Eq. (31-50a) with respect to z and, in the resulting expression, use Eq. (31-50a) to express db_k/dz in terms of b_k . If, for simplicity, we omit coupling to the radiation modes, then we have

$$\frac{d^2 b_k}{dz^2} + \beta_k^2 b_k = -\beta_k \sum_l C_{kl} (b_l + b_{-l}) + \chi, \quad (33-42a)$$

$$\chi = i \sum_l \left\{ (b_l + b_{-l}) \frac{dC_{kl}}{dz} + C_{kl} \left(\frac{db_l}{dz} + \frac{db_{-l}}{dz} \right) \right\}, \quad (33-42b)$$

since $C_{k-l} = C_{kl}$ in the weak-guidance limit. We derive a second equation, similarly, starting with the equation corresponding to Eq. (31-50a) for b_{-k} , and obtain

$$\frac{d^2 b_{-k}}{dz^2} + \beta_k^2 b_{-k} = -\beta_k \sum_l C_{kl} (b_l + b_{-l}) - \chi, \quad (33-43)$$

since $C_{-kl} = C_{k-l} = C_{kl}$. In the weak-guidance limit $\beta_k \cong kn_{co}$. Consequently, if we add Eqs. (33-42a) and (33-43) with β_k on the right replaced by kn_{co} , set $a_k = b_k + b_{-k}$, and

substitute from Eq. (33-41), then

$$\frac{d^2 a_k}{dz^2} + \beta_k^2 a_k = -2kn_{co} \sum_l C_{kl} a_l = i \sum_l D_{kl} a_l, \quad (33-44)$$

which is identical to Eq. (33-39a).

LOCAL MODES

Local modes were introduced in Chapter 28 to simplify the description of propagation on waveguides with large nonuniformities which vary slowly along their length. We derived the coupled local-mode equation for arbitrary waveguides in Section 31-14. Here we derive the coupled equations for local modes of the scalar wave equation. As in Section 33-11, our derivation ignores all polarization properties of the waveguide.

33-12 Coupled local-mode equations

On a weakly guiding, nonuniform waveguide the total scalar field $\Phi(x, y, z)$ satisfies the three-dimensional scalar wave equation, as expressed by Eq. (33-36). We express Φ as a summation over orthonormal local modes

$$\Phi = \sum_k a_k \hat{\Psi}_k = \sum_k a_k(z) \Psi_k(x, y, \beta_k(z)) \left/ \left\{ \int_{A_x} \Psi_k^2(x, y, \beta_k(z)) dA \right\}^{1/2} \right., \quad (33-45)$$

which implicitly includes radiation modes. The $a_k(z)$ include the z -dependence of both the forward- and backward-propagating modes. By analogy with the discussion in Section 19-1, the scalar local-mode field Ψ_k satisfies the two-dimensional wave equation at each position z along the waveguide

$$\{\nabla_t^2 + k^2 n^2(x, y, z) - \beta_k^2(z)\} \Psi_k = 0, \quad (33-46)$$

where $n(x, y, z)$ is the refractive-index profile of the nonuniform waveguide, and we have omitted the z on scalar quantities. We substitute Eq. (33-45) into Eq. (33-36) and use Eq. (33-46) to eliminate terms in $\nabla_t^2 \Psi_k$. Thus the resulting expression becomes

$$\sum_k \left\{ \frac{d^2 a_k}{dz^2} + \beta_k^2 a_k \right\} \hat{\Psi}_k = - \sum_k \left\{ 2 \frac{da_k}{dz} \frac{\partial \hat{\Psi}_k}{\partial z} + a_k \frac{\partial^2 \hat{\Psi}_k}{\partial z^2} \right\}. \quad (33-47)$$

We multiply by $\hat{\Psi}_j$, integrate over the infinite cross-section and apply the orthogonality condition of Eq. (33-5a), which is valid at each position z along the waveguide. Hence

$$\frac{d^2 a_j}{dz^2} + \beta_j^2 a_j = \sum_k \left\{ D_{jk} \frac{da_k}{dz} + E_{jk} a_k \right\}, \quad (33-48a)$$

where the D_{jk} and E_{jk} are coupling coefficients defined by

$$D_{jk} = -\frac{2}{\chi} \int_{A_x} \Psi_j \frac{\partial \Psi_k}{\partial z} dA; \quad E_{jk} = -\frac{1}{\chi} \int_{A_x} \Psi_j \frac{\partial^2 \Psi_k}{\partial z^2} dA, \quad (33-48b)$$

$$\chi = \left\{ \int_{A_x} \Psi_j^2 dA \int_{A_x} \Psi_k^2 dA \right\}^{1/2}, \quad (33-48c)$$

and are therefore functions of z . Like the solution of the coupled mode equations of Eq. (33–39a), once the solution a_j of Eq. (33–48a) is known, the amplitudes d_k and d_{-k} of the forward- and backward-propagating local modes are determined from the relationship

$$a_j = d_j \exp \left\{ i \int_0^z \beta_j(z) dz \right\} + d_{-j} \exp \left\{ -i \int_0^z \beta_j(z) dz \right\}, \quad (33-49)$$

by examining the z -dependence of a_j .

Relationship with the coupled local-mode equations for arbitrary waveguides

We derived the set of coupled local-mode equations for arbitrary waveguides in Section 31–14. In the weak-guidance approximation, the modal fields in the coupling coefficients of Eq. (31–65c) have only transverse components. If we use Table 13–1, page 288, to relate these components to the corresponding normalized solutions of the scalar wave equation of Eq. (33–45), we find with the help of Eq. (33–48b) that

$$C_{jk} = -C_{-j-k} \cong D_{jk}/2; \quad C_{j-k} = C_{-jk} \cong 0. \quad (33-50)$$

By analogy with Eqs. (33–42) and (33–43), the weak-guidance limit of the coupled local-mode equations of Eq. (31–65) is expressible as

$$\frac{d^2 b_j}{dz^2} + \beta_j^2 b_j = i\beta_j \sum_k C_{jk} b_k + \chi_+, \quad (33-51a)$$

$$\frac{d^2 b_{-j}}{dz^2} + \beta_j^2 b_{-j} = -i\beta_j \sum_k C_{jk} b_{-k} + \chi_-, \quad (33-51b)$$

where

$$\chi_{\pm} = \sum_k \left\{ b_{\pm k} \frac{dC_{jk}}{dz} + C_{jk} \frac{db_{\pm k}}{dz} \right\} \pm i b_{\pm j} \frac{d\beta_j}{dz}. \quad (33-51c)$$

In the weak-guidance limit, $\beta_j \cong kn_{co} = V/\rho(2\Delta)^{1/2}$, and thus $\beta_j \rightarrow \infty$ as $\Delta \rightarrow 0$. Furthermore, we deduce from Eq. (31–61) that to lowest order $db_{\pm k}/dz \cong \pm i\beta_k b_{\pm k}$. Consequently, the right side of Eqs. (33–51a) and (33–51b) are dominated by the first term in β_j and by the term $db_{\pm k}/dz$ in the definition of χ_{\pm} . Accordingly, if we neglect the remaining terms, add Eqs. (33–51a) and (33–51b), and set $a_j = b_j + b_{-j}$, then

$$\frac{d^2 a_j}{dz^2} + \beta_j^2 a_j = i k n_{co} \sum D_{jk} (b_k - b_{-k}). \quad (33-52)$$

We deduce from Eqs. (33–49) and (31–61) that $da_k/dz \cong i\beta_k (b_k - b_{-k})$ in the limit $\Delta \rightarrow 0$. Since $\beta_k \cong kn_{co}$ for all modes, we deduce that Eqs. (33–52) and (33–48a) are equivalent.

33–13 Alternative form for the coupling coefficients

Here we parallel Section 31–15 and derive an alternative form for the scalar coupling coefficients of Eq. (33–48). We differentiate Eq. (33–46) for Ψ_k with respect to z and

obtain

$$\{\nabla_t^2 + k^2 n^2 - \beta_k^2\} \frac{\partial \Psi_k}{\partial z} + \left\{ k^2 \frac{\partial n^2}{\partial z} - \frac{d\beta_k^2}{dz} \right\} \Psi_k = 0. \quad (33-53)$$

We multiply this equation by Ψ_j , Eq. (33-46) by $\partial \Psi_j / \partial z$ and subtract to give

$$\begin{aligned} \left\{ \frac{\partial \Psi_j}{\partial z} \nabla_t^2 \Psi_k - \Psi_j \nabla_t^2 \frac{\partial \Psi_k}{\partial z} \right\} + (k^2 n^2 - \beta_k^2) \left\{ \Psi_k \frac{\partial \Psi_j}{\partial z} - \Psi_j \frac{\partial \Psi_k}{\partial z} \right\} \\ = \left\{ k^2 \frac{\partial n^2}{\partial z} - \frac{d\beta_k^2}{dz} \right\} \Psi_j \Psi_k. \end{aligned} \quad (33-54a)$$

A second equation is generated by reversing the roles of Ψ_j and Ψ_k , giving

$$\begin{aligned} \left\{ \frac{\partial \Psi_k}{\partial z} \nabla_t^2 \Psi_j - \Psi_k \nabla_t^2 \frac{\partial \Psi_j}{\partial z} \right\} + (k^2 n^2 - \beta_j^2) \left\{ \Psi_j \frac{\partial \Psi_k}{\partial z} - \Psi_k \frac{\partial \Psi_j}{\partial z} \right\} \\ = \left\{ k^2 \frac{\partial n^2}{\partial z} - \frac{d\beta_j^2}{dz} \right\} \Psi_j \Psi_k. \end{aligned} \quad (33-54b)$$

We add the two equations and integrate over the infinite cross-section A_∞ . Terms involving ∇_t^2 are transformed into a line integral along the perimeter of A_∞ , by using Green's identity of Eq. (37-58). This integral vanishes since Ψ_j and Ψ_k and their first derivatives are exponentially small at large distances from the waveguide. The orthogonality condition of Eq. (33-5a) shows that terms in $d\beta_j^2/dz$ and $d\beta_k^2/dz$ vanish, since $j \neq k$. Rearranging the remaining terms and recalling Eq. (33-50) we deduce

$$C_{jk} = \frac{k^2}{\beta_j^2 - \beta_k^2} \int_{A_\infty} \frac{\partial n^2}{\partial z} \Psi_j \Psi_k dA \cong \frac{1}{2n_\infty} \frac{k}{\beta_j - \beta_k} \int_{A_\infty} \frac{\partial n^2}{\partial z} \Psi_j \Psi_k dA, \quad (33-55)$$

since $\beta_j + \beta_k \cong 2kn_\infty$ when $\Delta \ll 1$. This expression is identical to the weak-guidance limit of the coupling coefficient of Eq. (31-70) if we allow for the orthonormality of Table 11-1, page 230, and the normalization of Eq. (33-7).

MODE EXCITATION BY CURRENT SOURCES

In Chapter 32 we derived the governing equation which relates the total electric field \mathbf{E} of a weakly guiding waveguide to current sources of density \mathbf{J} within the waveguide. Using the waveguide parameter definition inside the back cover, Eq. (32-52) is expressible as

$$\{\nabla^2 + k^2 n^2(x, y)\} \mathbf{E} = -ik \left(\frac{\mu_0}{\epsilon_0} \right)^{1/2} \left\{ \mathbf{J} + \frac{2\Delta}{V^2} \rho \nabla (\rho \nabla \cdot \mathbf{J}) \right\}, \quad (33-56)$$

where ∇^2 is defined by Eq. (37-36), $k = 2\pi/\lambda$, λ is the free-space wavelength and \mathbf{E} is referred to cartesian components. In considering the excitation of bound modes, we ignore the second term inside the curly brackets on the right, regardless of how rapidly

\mathbf{J} may vary, by taking Δ to be sufficiently small. The transverse fields of the weakly guiding waveguide are specified once we know the solution of Eq. (33-56) for \mathbf{E}_t . This solution involves only the transverse current distribution \mathbf{J}_t . The longitudinal current distribution J_z is related to \mathbf{E}_t through the longitudinal field E_z , which involves higher-order effects not considered here. Accordingly Eq. (33-56) reduces to

$$\{\nabla^2 + k^2 n^2(x, y)\} \mathbf{E}_t = -ik(\mu_0/\epsilon_0)^{1/2} \mathbf{J}_t. \quad (33-57)$$

As all polarization effects due to the waveguide are ignored, we can decompose \mathbf{E}_t into cartesian components and solve the two inhomogeneous wave equations for these components separately.

Determination of the scalar fields

Let $\Phi(x, y, z)$ and $J(x, y, z)$ denote either E_x and J_x or E_y and J_y in the component equations of Eq. (33-57). Then by analogy with Eq. (33-36), the equation for Φ may be written as

$$\left\{ \nabla_t^2 + k^2 n^2(x, y) + \frac{\partial^2}{\partial z^2} \right\} \Phi = -ik \left(\frac{\mu_0}{\epsilon_0} \right)^{1/2} J. \quad (33-58)$$

We expand Φ over the complete set of scalar bound modes

$$\Phi = \sum_k \{a_k(z) \exp(i\beta_k z) + a_{-k}(z) \exp(-i\beta_k z)\} \Psi_k = \sum_k A_k(z) \Psi_k, \quad (33-59)$$

where $a_k(z)$ and $a_{-k}(z)$ are the z -dependent amplitudes of the k th forward- and backward-propagating modes, respectively, and $A_k(z)$ denotes all the z dependence associated with Ψ_k . The scalar radiation modes are omitted for simplicity. Each scalar function Ψ_k satisfies

$$\{\nabla_t^2 + k^2 n^2(x, y) - \beta_k^2\} \Psi_k = 0. \quad (33-60)$$

Substituting Eq. (33-59) into Eq. (33-58) and using Eq. (33-60) to eliminate terms in $\nabla_t^2 \Psi_k$ leads to

$$\sum_k \left\{ \frac{d^2 A_k}{dz^2} + \beta_k^2 A_k \right\} \Psi_k = -ik \left(\frac{\mu_0}{\epsilon_0} \right)^{1/2} J. \quad (33-61)$$

We multiply by Ψ_j , integrate over the infinite cross-section and use the orthogonality condition of Eq. (33-5a). This leads to

$$\frac{d^2 A_j}{dz^2} + \beta_j^2 A_j = g_j; \quad g_j = -ik \left(\frac{\mu_0}{\epsilon_0} \right)^{1/2} \int_{A_x} \Psi_j J dA \Big/ \int_{A_x} \Psi_j^2 dA, \quad (33-62)$$

where g_j is a function of z . This is an inhomogeneous, second-order, ordinary differential equation which can be solved by standard techniques, such as variation of parameters. The solution is

$$A_j = -\frac{i}{2\beta_j} \left\{ \int_{z_1}^z g_j(t) \exp\{i\beta_j(z-t)\} dt + \int_z^{z_2} g_j(t) \exp\{i\beta_j(t-z)\} dt \right\}, \quad (33-63)$$

where z_1 and z_2 are constants. We assume that the current distribution occupies the volume between cross-sectional planes $z = z_1$ and $z = z_2$ of the waveguide in Fig. 31-1. Consequently by comparing Eqs. (33-63) and (33-59) we deduce that the amplitude coefficients are given by

$$a_j = 0; \quad z \leq z_1, \quad (33-64a)$$

$$= -\frac{i}{2\beta_j} \int_{z_1}^z g_j(t) \exp(-i\beta_j t) dt; \quad z_1 \leq z \leq z_2, \quad (33-64b)$$

$$= -\frac{i}{2\beta_j} \int_{z_1}^{z_2} g_j(t) \exp(-i\beta_j t) dt; \quad z \geq z_2, \quad (33-64c)$$

for forward-traveling modes, and for backward traveling modes, by

$$a_{-j} = -\frac{i}{2\beta_j} \int_{z_1}^{z_2} g_j(t) \exp(i\beta_j t) dt; \quad z \leq z_1, \quad (33-65a)$$

$$= -\frac{i}{2\beta_j} \int_z^{z_2} g_j(t) \exp(i\beta_j t) dt; \quad z_1 \leq z \leq z_2, \quad (33-65b)$$

$$= 0; \quad z \geq z_2, \quad (33-65c)$$

where g_j is defined in Eq. (33-62). The corresponding expressions for the modes of arbitrary waveguides are given by Eqs. (31-35) and (31-36). If we take the limit $\Delta \rightarrow 0$ of these expressions and substitute for the normalization from Eq. (33-7), they reduce to the above expressions since $\beta_j \cong kn_{co}$ and Ψ_j is assumed to be real.

REFERENCES

1. Mathews, J. and Walker, R. L. (1965) *Mathematical Methods of Physics*, Benjamin, New York, pp. 315-23.
2. Morse, P. M. and Feshbach, H. (1953) *Methods of Theoretical Physics*, McGraw-Hill, New York, p. 1112.
3. Love, J. D., Hussey, C. D., Snyder, A. W. and Sammut, R. A. (1982) Polarization corrections to mode propagation on weakly guiding fibres. *J. Opt. Soc. Am.*, **72**, 1583-91.
4. Pask, C. (1979) Exact expressions for scalar modal eigenvalue and group delays in power-law optical fibres. *J. Opt. Soc. Am.*, **69**, 1599-1603.
5. Sammut, R. A., Hussey, C. D., Love, J. D. and Snyder, A. W. (1981) Modal analysis of polarization effects in weakly-guiding fibres. *I.E.E. Proc.*, **128**, 173-87.

Green's function methods

Fields of arbitrary current distributions	656
34-1 Derivation from the reciprocity theorem	657
34-2 Vector potential representation for arbitrary fibers	658
34-3 Vector potential representation for weakly guiding fibers	659
34-4 'Free-space' Green's function	660
34-5 Tubular sources within weakly guiding fibers	660
34-6 Correction factor	661
34-7 <i>Example: Step profile</i>	662
 Perturbation problems	663
34-8 <i>Example: Slightly elliptical fibers</i>	663
34-9 <i>Example: Far-field corrections</i>	664
 References	665

In the previous three chapters we described the solution of Maxwell's equations for the total electromagnetic field of arbitrary and weakly guiding fibers in terms of the bound and radiation modes of the fiber. The need to use a superposition of all these modes is not always the most straightforward procedure, particularly in the case of single-mode fibers when only the fundamental mode is of interest. Here we provide background information on the alternative method of Green's functions [1-3] to supplement their application to the perturbation problems of Chapter 18 and to the radiation problems for the current sources of Chapter 21. In the latter, the method is equivalent to first calculating the fields due to a single point current dipole and then constructing the fields of the current distribution by superposition. For an arbitrary distribution, however, this may be no easier than using an eigenfunction expansion. In other words, the advantages in using either Green's functions or eigenfunction expansions depends on the particular problem in question.

FIELDS OF ARBITRARY CURRENT DISTRIBUTIONS

In Chapter 31, we used the reciprocity theorem of Maxwell's equations to express the amplitudes of the modes of an arbitrary fiber in terms of a prescribed current distribution. We now use this theorem to show how the total fields due to this distribution can be constructed by linearly superposing the fields of point current dipoles.

34-1 Derivation from the reciprocity theorem

Consider two distinct electromagnetic situations within a fiber. In the first situation, an arbitrary current distribution \mathbf{J} gives rise to electric and magnetic fields \mathbf{E} and \mathbf{H} , and in the second situation, a point current dipole $\bar{\mathbf{J}}$ results in fields $\bar{\mathbf{E}}$ and $\bar{\mathbf{H}}$. All six electromagnetic quantities include the implicit time dependence $\exp(-i\omega t)$. The arbitrary location and orientation of the dipole is expressed by

$$\bar{\mathbf{J}} = \delta(\mathbf{r} - \mathbf{r}') \{ \bar{J}_x \hat{\mathbf{x}} + \bar{J}_y \hat{\mathbf{y}} + \bar{J}_z \hat{\mathbf{z}} \}, \quad (34-1)$$

where $\bar{J}_x, \bar{J}_y, \bar{J}_z$ are arbitrary, \mathbf{r}' and \mathbf{r} are position vectors for the field point and dipole, respectively, the $\hat{\mathbf{x}}, \hat{\mathbf{y}}, \hat{\mathbf{z}}$ are unit vectors parallel to cartesian axes with the z -axis along the fiber axis and δ is the Dirac delta function. We relate the two situations by the three-dimensional form of the conjugated reciprocity theorem. Assuming the fiber is nonabsorbing, so that its profile n is real, and substituting Eq. (34-1) into Eq. (31-3), we obtain

$$\mathbf{V} \cdot \mathbf{F}_c = -(\bar{\mathbf{E}}^* \cdot \mathbf{J} + \mathbf{E} \cdot \bar{\mathbf{J}}^*), \quad (34-2)$$

where $*$ denotes complex conjugate, $n = \bar{n}$ and \mathbf{F}_c is defined by Eq. (31-1). If we integrate over \mathbf{r}' -space and apply the divergence theorem of Eq. (37-55), the left side is transformed into a surface integral at infinity, which vanishes as the fields in \mathbf{F}_c disappear sufficiently rapidly for $|\mathbf{r}'| \rightarrow \infty$. Thus we are left with

$$E_x \bar{J}_x^* + E_y \bar{J}_y^* + E_z \bar{J}_z^* = - \int_{\mathcal{V}'} \bar{\mathbf{E}}^*(\mathbf{r}, \mathbf{r}') \cdot \mathbf{J}(\mathbf{r}') d\mathcal{V}' \quad (34-3)$$

where the left side is evaluated at $\mathbf{r}' = \mathbf{r}$ and \mathcal{V}' is the volume occupied by current sources. The component E_x is found by setting $\bar{J}_x = 1, \bar{J}_y = \bar{J}_z = 0$, so that $\bar{\mathbf{E}}$ is the field at position \mathbf{r} due to an x -directed dipole of unit strength at position \mathbf{r}' . A similar procedure applies to E_y and E_z , and by setting $\mathbf{E} = E_x \hat{\mathbf{x}} + E_y \hat{\mathbf{y}} + E_z \hat{\mathbf{z}}$, we finally obtain

$$\mathbf{E}(\mathbf{r}) = - \int_{\mathcal{V}'} \bar{\mathbf{E}}^*(\mathbf{r}, \mathbf{r}') : \mathbf{J}(\mathbf{r}') d\mathcal{V}', \quad (34-4)$$

where $\bar{\mathbf{E}}$ is called the *dyadic Green's function*, and the $:$ indicates the dyadic product defined below. It is clear that $\bar{\mathbf{E}}$ has nine components to distinguish the contributions to each component of \mathbf{E} from the x -, y -, and z -directed dipoles of strengths J_x, J_y and J_z at position \mathbf{r}' . If $\bar{E}_{xx}, \bar{E}_{xy}$ and \bar{E}_{xz} are the components of $\bar{\mathbf{E}}$ which denote the total contributions to E_x from the J_x, J_y and J_z components of the source, respectively, then

$$E_x = - \int_{\mathcal{V}'} (\bar{E}_{xx}^* J_x + \bar{E}_{xy}^* J_y + \bar{E}_{xz}^* J_z) d\mathcal{V}', \quad (34-5)$$

together with similar expressions for E_y and E_z .

Calculation of the current dipole fields

Once the fields of the point dipole within the fiber are known, the electric field due to the prescribed current distribution is determined from Eq. (34-4), and the corresponding

magnetic field follows from Eq. (30-1a). To determine the dipole fields, we could use a modal expansion, such as Eq. (31-32), and evaluate the modal amplitudes from Eqs. (31-35) to (31-37). This is carried out in Section 25-14 for an on-axis dipole. However, it would be simpler to determine the fields of the current distribution directly using the same modal expansion. Alternatively, we could solve the inhomogeneous vector wave equation of Eq. (30-13a) with \mathbf{J} given by Eq. (34-1), but, in general, solution of this equation is complicated because of coupling between components of the electric field due to the $\nabla_t \ln n^2$ term. The problem becomes tractable for the step-profile fiber since the $\nabla_t \ln n^2$ term vanishes everywhere except at the interface, and Eq. (30-13) can be solved in terms of the longitudinal field components as explained in Section 11-15. Even in this special case the derivation of the dipole fields and the total fields is cumbersome [4].

The above discussion relates to fibers of arbitrary profiles. If we restrict attention to weakly guiding fibers, the Green's function approach can be greatly simplified. To appreciate this simplification, we first set up the vector potential representation for the fields of arbitrary profile fibers and then specialize it to weakly guiding fibers.

34-2 Vector potential representation for arbitrary fibers

The solution of Maxwell's equations for the total fields of an arbitrary profile fiber can be expressed in terms of the familiar vector potential \mathbf{A} , taken within the Lorentz gauge. The standard derivation of this representation assumes a uniform medium [5, 6], but it is readily modified as follows to account for the graded medium of the fiber.

Regardless of profile variation, the divergence condition of Eq. (30-1b) for the magnetic field is satisfied by setting

$$\mathbf{H} = (1/\mu_0) \nabla \times \mathbf{A}, \quad (34-6)$$

where μ is the free-space permeability. Substituting into Eq. (30-1a) gives

$$\nabla \times \mathbf{E} = \{ik/(\mu_0 \epsilon_0)^{1/2}\} \nabla \times \mathbf{A}, \quad (34-7)$$

which has the general solution

$$\mathbf{E} = ik\mathbf{A}/(\mu_0 \epsilon_0)^{1/2} + \nabla \chi, \quad (34-8)$$

where χ is an arbitrary scalar function of position, and \mathbf{E} , \mathbf{H} , \mathbf{A} and χ contain the implicit time dependence $\exp(-i\omega t)$. The angular frequency ω is related to the other parameters inside the back cover. We substitute Eqs. (34-6) and (34-8) into the second Maxwell equation in Eq. (30-1a) and use the vector identity of Eq. (37-30) to obtain

$$\{\nabla^2 + k^2 n^2\} \mathbf{A} = \nabla(\nabla \cdot \mathbf{A}) - \mu_0 \mathbf{J} + ikn^2 (\mu_0 \epsilon_0)^{1/2} \nabla \chi, \quad (34-9)$$

where $n = n(x, y)$ is the fiber profile. The components of \mathbf{A} are referred to fixed cartesian directions, so that we can replace the vector Laplacian ∇^2 by the scalar Laplacian, as explained in Section 30-6. If we now choose

$$\chi = i(\nabla \cdot \mathbf{A})/\{kn^2 (\mu_0 \epsilon_0)^{1/2}\}, \quad (34-10)$$

then Eq. (34-9) is replaced by

$$\{\nabla^2 + k^2 n^2\} \mathbf{A} = -\mu_0 \mathbf{J} + (\nabla \cdot \mathbf{A}) \nabla_t \ln n^2.$$

(34-11)

The electric field follows from Eqs. (34-8) and (34-10) as

$$\mathbf{E} = \frac{ik}{(\mu_0 \epsilon_0)^{1/2}} \left\{ \mathbf{A} + \frac{1}{k^2} \nabla \left(\frac{\nabla \cdot \mathbf{A}}{n^2} \right) \right\}. \quad (34-12)$$

When the profile is everywhere constant, Eqs. (34-11) and (34-12) reduce to the familiar results for a uniform medium [5, 6].

34-3 Vector potential representation for weakly guiding fibers

When the fiber is weakly guiding, the vector potential representation of its fields is considerably simplified, since we can ignore all terms involving $\nabla_t \ln n^2$ for reasons given below Eq. (32-51). Consequently Eqs. (34-6) and (34-12) are replaced by [7]

$$\mathbf{H} = \frac{1}{\mu_0} \nabla \times \mathbf{A}; \quad \mathbf{E} = \frac{ik}{(\mu_0 \epsilon_0)^{1/2}} \left\{ \mathbf{A} + \frac{1}{k^2 n_{cl}^2} \nabla (\nabla \cdot \mathbf{A}) \right\}, \quad (34-13)$$

and from Eq. (34-11) the cartesian components of \mathbf{A} satisfy

$$\{\nabla^2 + k^2 n^2\} \mathbf{A} = -\mu_0 \mathbf{J}. \quad (34-14)$$

We have set $n \cong n_{cl}$ in Eq. (34-13) to be consistent with the 'free-space' approximation of the following section. These equations now differ from the standard equations for a uniform medium [5, 6], only in the dependence of \mathbf{A} on the fiber profile in the left side of Eq. (34-14).

Solution for the vector potential

Each cartesian component of the vector potential satisfies a scalar equation. Hence, the solution of Eq. (34-14) for each component is expressible in terms of the same scalar Green's function, and by superposition this leads to

$$\mathbf{A}(\mathbf{r}) = \mu_0 \int_{\mathcal{V}'} G(\mathbf{r}, \mathbf{r}') \mathbf{J}(\mathbf{r}') d\mathcal{V}', \quad (34-15)$$

where \mathcal{V}' is the volume occupied by current sources, and \mathbf{r} and \mathbf{r}' are the position vectors of the field point and source, respectively. The Green's function is given by the solution to

$$\{\nabla^2 + k^2 n^2\} G(\mathbf{r}, \mathbf{r}') = -\delta(\mathbf{r} - \mathbf{r}'), \quad (34-16)$$

with appropriate boundary conditions, where δ is the Dirac delta function.

We are principally interested in determining only the radiation, or far field. As explained in Section 21-8, radiation from sources within weakly guiding fibers is nearly identical to radiation in 'free space', i.e. in an unbounded medium of uniform refractive

index n_{cl} . Accordingly we first solve Eq. (34–16) with $n = n_{cl}$ everywhere and then correct for the presence of the fiber.

34–4 ‘Free-space’ Green’s function

In a medium of uniform refractive index n_{cl} , the solution of Eq. (34–16) is well known to be [1–3]

$$G(\mathbf{r}, \mathbf{r}') = \frac{\exp\{ikn_{cl}|\mathbf{r} - \mathbf{r}'|\}}{4\pi|\mathbf{r} - \mathbf{r}'|}, \quad (34-17)$$

where $|\mathbf{r} - \mathbf{r}'|$ is the distance between the field point and the source position. If we restrict attention to the far field, then $|\mathbf{r}| \gg |\mathbf{r}'|$, and by using the identity

$$|\mathbf{r} - \mathbf{r}'| = \{s^2 + s'^2 - 2ss' \cos \chi\}^{1/2} \quad (34-18)$$

to expand Eq. (34–17), where $s = |\mathbf{r}|$, $s' = |\mathbf{r}'|$ and χ is the angle between \mathbf{r} and \mathbf{r}' , as in Fig. 21–4(b), the dominant terms are [7]

$$G(\mathbf{r}, \mathbf{r}') = \frac{\exp\{iksn_{cl}\}}{4\pi s} \exp\{-iks'n_{cl} \cos \chi\}. \quad (34-19)$$

Substitution into Eq. (34–15) leads to the far-field expression for \mathbf{A} , as expressed by Eq. (21–20). Furthermore, sufficiently far from all currents where $s \gg s'$, we deduce from Eq. (34–19) that $\nabla \cong ikn_{cl}\hat{\mathbf{r}}$, where $\hat{\mathbf{r}}$ is the unit vector parallel to \mathbf{r} in Fig. 21–4(a). Consequently Eqs. (21–18) and (21–19) follow from Eq. (21–16) and the definition of the Poynting vector $\mathbf{S} = \frac{1}{2} \text{Re}(\mathbf{E} \times \mathbf{H}^*)$, where Re denotes real part and $*$ complex conjugate.

34–5 Tubular sources within weakly guiding fibers

Having set up the formalism for the calculation of ‘free-space’ radiation from current sources, we now account for the effect of the fiber on the radiation fields. We could proceed by solving Eq. (34–16) for a given profile, which leads to the fields through Eqs. (34–15) and (34–13). However, rather than superpose the far fields of point sources, we prefer to determine the Green’s function for the tubular source introduced in Section 21–6 and illustrated in Fig. 21–3 [7]. The advantage of the tubular source is that it has the same geometrical symmetry as the circular fiber. Furthermore, an arbitrary current source can be described either by a distribution of dipoles or by a complete set of tubular sources. Here we examine the latter approach.

Arbitrary source distributions

The current distribution carried by a tubular source is defined by Eq. (21–12) in the notation of Fig. 21–3 to be

$$\mathbf{J} = \hat{\mathbf{n}}g(z) \frac{\delta(r - r_0)}{2\pi r_0} \cos l(\phi - \phi_0); \quad -L \leq z \leq L, \quad (34-20)$$

where $2L$ is the length of fiber occupied by the distribution and l is a positive integer or zero. For convenience we assume the unit vector \hat{n} is parallel to a fixed direction. We can express an arbitrary current distribution as a superposition of tubular sources through integrations over r_0 , ϕ_0 and a summation over l . To account for the longitudinal dependence expressed by $g(z)$, we Fourier transform the current distribution, vector potential and fields with respect to the propagation constant β of the fiber. If subscript l denotes a particular tube, then for example

$$\bar{E}_l(\beta) = \int_{-\infty}^{\infty} E_l \exp(-i\beta z) dz; \quad E_l(z) = \frac{1}{2\pi} \int_{-\infty}^{\infty} \bar{E}_l \exp(i\beta z) d\beta, \quad (34-21)$$

where $\bar{}$ denotes the transform. The transform variables are related to one another by the transform of Eq. (34-13), obtained by replacing E , H and A by \bar{E}_l , \bar{H}_l and \bar{A}_l , respectively, and setting $\nabla = \nabla_t + i\beta \hat{z}$, where ∇_t is the transverse gradient operator of Table 30-1, page 592, and \hat{z} is the unit vector parallel to the fiber axis. Similarly, if we substitute Eq. (34-20) into the transform of Eq. (34-14), we obtain

$$\{\nabla_t^2 + k^2 n^2 - \beta^2\} \bar{A}_l = -\mu_0 \bar{g} \frac{\delta(r-r_0)}{2\pi r_0} \cos l(\phi - \phi_0) \hat{n}, \quad (34-22)$$

where \bar{g} is the transform of g , ∇_t^2 is the transverse Laplace operator of Table 30-1, and $n = n(r)$ is the fiber profile. Thus, the effect of the fiber on the 'free-space' radiation fields is reduced to the solution of this simple equation. We are reminded that this description ignores all polarization effects due to the weakly guiding fiber since terms involving $\nabla_t \ln n^2$ have been discarded.

34-6 Correction factor

The radiation fields of the tubular source depend on the solution of Eq. (34-22) for the cartesian components of \bar{A}_l . Nevertheless, we can make a general deduction about these fields regardless of the fiber profile [7]. First consider the 'free-space' solution when $n = n_{cl}$ everywhere. The spatial dependence of \bar{A}_l at radius r outside of the tube is proportional to

$$H_1^{(1)}(Qr/\rho) \cos l(\phi - \phi_0); \quad Q = \rho \{k^2 n_{cl}^2 - \beta^2\}^{1/2}, \quad (34-23)$$

in cylindrical polar coordinates. The $H_1^{(1)}$ is the Hankel function of the first kind, which together with the implicit time dependence $\exp(-i\omega t)$ represents an outward traveling wave as $r \rightarrow \infty$. If we now allow for the presence of the fiber then $n(r)$ in Eq. (34-22) varies in the core, but $n = n_{cl}$ everywhere in the cladding. Consequently the spatial variation of \bar{A}_l in the far field is again proportional to Eq. (34-23), but *the constant of proportionality will be different*. If we denote the 'free-space' solution of Eq. (34-22) by \bar{A}_l^{fs} , then the solution in the presence of the fiber is expressible as

$$\bar{A}_l = C_l(\beta) \bar{A}_l^{fs}, \quad (34-24)$$

where C_l is identical to the correction factor of Eq. (21-34), which was derived from intuitive, physical arguments in Section 21-11. If, for convenience, we assume that \hat{n} in Eq. (34-22) is parallel to the x -axis in the fiber cross-section, \bar{A}_l then has only an x -

component which we denote by Ψ_l . Thus Ψ_l satisfies the inhomogeneous scalar wave equation

$$\left\{ \frac{\partial^2}{\partial r^2} + \frac{1}{r} \frac{\partial}{\partial r} + \frac{1}{r^2} \frac{\partial^2}{\partial \phi^2} + k^2 n^2 - \beta^2 \right\} \Psi_l = b \frac{\delta(r-r_0)}{r_0} \cos l(\phi - \phi_0), \quad (34-25)$$

in cylindrical polar coordinates, where $b = -\mu_0 \bar{g}/2\pi$. If Ψ_l^{fs} denotes the 'free-space' solution when $n = n_{\text{cl}}$ everywhere, then the correction factor of Eq. (34-24) for the tube is given by the ratio

$$C_l = \Psi_l / \Psi_l^{\text{fs}}; \quad r > \rho, \quad (34-26)$$

evaluated in the cladding.

Arbitrary source distributions

We can now construct the total fields due to an arbitrary current distribution within the fiber. For an individual tube, the electric and magnetic fields are linearly related to the vector potential. Thus the relationships corresponding to Eq. (34-24) are

$$\bar{\mathbf{E}}_l = C_l \bar{\mathbf{E}}_l^{\text{fs}}; \quad \bar{\mathbf{H}}_l = C_l \bar{\mathbf{H}}_l^{\text{fs}}. \quad (34-27)$$

Substitution into Eq. (34-21) leads to the inverse transform \mathbf{E}_l , and by superposing tubes the total electric field is given by

$$\mathbf{E}(r, \phi, z) = \frac{1}{2\pi} \sum_{l=0}^{\infty} \int_{-\infty}^{\infty} \exp(i\beta z) d\beta \int_0^{\infty} C_l r_0 dr_0 \int_0^{2\pi} \bar{\mathbf{E}}_l^{\text{fs}} d\phi_0, \quad (34-28)$$

where C_l depends, in general, on both r_0 and ϕ_0 , as well as on β .

34-7 Example: Step profile

Here we derive the correction factor for a tubular source in the core of a weakly guiding, step-profile fiber. The solution of Eq. (34-25) is expressible as

$$\psi_l = p \frac{J_l(UR)}{J_l(U)} \cos l(\phi - \phi_0); \quad 0 \leq r < r_0, \quad (34-29a)$$

$$= \left\{ q \frac{J_l(UR)}{J_l(U)} + s \frac{H_l^{(1)}(UR)}{H_l^{(1)}(U)} \right\} \cos l(\phi - \phi_0); \quad r_0 < r \leq \rho, \quad (34-29b)$$

$$= t \frac{H_l^{(1)}(QR)}{H_l^{(1)}(Q)} \cos l(\phi - \phi_0); \quad \rho \leq r < \infty, \quad (34-29c)$$

where p, q, s, t are constants to be determined, the J_l and $H_l^{(1)}$ are Bessel and Hankel functions of the first kind, respectively, U and Q are related to β inside the back cover, $R = r/\rho$ and r_0, ρ are the tube and core radii, respectively. At the interface $r = \rho$, both Ψ_l and $\partial\Psi_l/\partial r$ are continuous, and over the tube $r = r_0$ only Ψ_l is continuous. The fourth boundary condition relates the discontinuity in $\partial\Psi_l/\partial r$ across $r = r_0$ to the right side of Eq. (34-25). If we multiply this equation by r , integrate over the small interval

$r_0 - \delta r < r < r_0 + \delta r$, and recall that Ψ_l is continuous, we deduce that

$$\lim_{\delta r \rightarrow 0} \left[\frac{\partial \Psi_l}{\partial r} \right]_{r_0 - \delta r}^{r_0 + \delta r} = \frac{b}{r_0} \cos l(\phi - \phi_0). \quad (34-30)$$

When applied to Eq. (34-29), these four conditions and the Wronskian of Eq. (37-77) lead to the solution

$$\Psi_l = b \frac{J_l(Ur_0/\rho)}{W_l(U, Q)} H_l^{(1)}(QR) \cos l(\phi - \phi_0); \quad r > \rho, \quad (34-31a)$$

$$W_l(U, Q) = QJ_l(U)H_l^{(1)'}(Q) - UH_l^{(1)}(Q)J_l'(U), \quad (34-31b)$$

where prime denotes differentiation with respect to argument. The corresponding 'free-space' solution Ψ_l^{fs} is given by the same expression, providing we replace U by Q throughout, and the correction factor of Eq. (34-26) becomes

$$C_l = \frac{J_l(Ur_0/\rho)}{J_l(Qr_0/\rho)} \frac{W_l(Q, Q)}{W_l(U, Q)}, \quad (34-32)$$

where $W_l(Q, Q)$ is the Wronskian of Eq. (37-77). A similar expression can be derived when the tube is in the cladding, i.e. $r_0 > \rho$.

PERTURBATION PROBLEMS

Green's functions can also be used to solve inhomogeneous, scalar, differential equations which arise in perturbation problems for weakly guiding fibers. We seek the solution $\Psi = \Psi(\mathbf{r})$ of the equation

$$\{\nabla_t^2 + k^2 n^2 - \beta^2\} \Psi = \chi, \quad (34-33)$$

where $\chi = \chi(\mathbf{r})$ is a prescribed function of position \mathbf{r} in the fiber cross-section, $n = n(\mathbf{r})$ is the profile, and ∇_t^2 is defined in Table 30-1, page 592. If $G = G(\mathbf{r}, \mathbf{r}')$ denotes the Green's function for this equation, then, subject to suitable boundary conditions, G satisfies

$$\{\nabla_t^2 + k^2 n^2 - \beta^2\} G = \delta(\mathbf{r} - \mathbf{r}'), \quad (34-34)$$

where δ is the Dirac delta function and \mathbf{r}' is a fixed position. The solution of Eq. (34-33) is then given by [1-3]

$$\Psi(\mathbf{r}) = \int_{\mathcal{V}'} G(\mathbf{r}, \mathbf{r}') \chi(\mathbf{r}') d\mathcal{V}', \quad (34-35)$$

where \mathcal{V}' is the volume within which χ is nonzero. To illustrate this technique, we consider examples.

34-8 Example: Slightly elliptical fibers

We used perturbation methods in Section 18-10 to determine the modal properties of a slightly eccentric, step-profile fiber. This description requires the fundamental solution

Ψ of the scalar wave equation of Eq. (18-3a) for the perturbed fiber. To lowest order $\Psi = \bar{\Psi}$, where $\bar{\Psi}$ is the known fundamental solution for the scalar wave equation of Eq. (18-3b). The first-order correction is obtained by rearranging Eq. (18-3a) as [8]

$$\{\nabla_t^2 + k^2 \bar{n}^2 - \beta^2\} \Psi = k^2 \{\bar{n}^2 - n^2\} \Psi, \quad (34-36)$$

where \bar{n} is the profile of the *circular* fiber and β is the propagation constant for the *elliptical* fiber. The right side vanishes everywhere except in the four shaded regions of Fig. 18-2(a). Within these narrow regions we can set $\Psi \cong \bar{\Psi}$ and approximate the right side by a delta function on the interface $r = \rho$ weighted by $k^2 (\bar{n}^2 - n^2) \delta r$, where δr is the width of the region given below Eq. (18-20). Hence Eq. (34-36) is replaced by

$$\{\nabla_t^2 + k^2 \bar{n}^2 - \beta^2\} \Psi = -\frac{e^2 V^2}{4 \rho} \delta(r - \rho) \cos 2\phi, \quad (34-37)$$

since $\bar{\Psi} = 1$ on $r = \rho$ in Table 14-3, page 313, and $\bar{n} = n_{cl}$, $n = n_{co}$ in the shaded regions crossing the x -axis in Fig. 18-2(a). By analogy with the solution of Eq. (34-25) in Section 34-7, we set

$$\Psi = p \frac{J_2(UR)}{J_2(U)} \cos 2\phi, \quad 0 \leq R \leq 1; \quad \Psi = q \frac{K_2(WR)}{K_2(W)} \cos 2\phi, \quad 1 \leq R < \infty, \quad (34-38)$$

where $R = r/\rho$. The constants p and q are determined from continuity of Ψ at $r = \rho$ and an analogous condition to Eq. (34-30) with $l = 2$, $r_0 = \rho$ and $b = -e^2 V^2/4$. With the aid of the eigenvalue equation in Table 14-3 and the recurrence relations of Eqs. (37-72) and (37-73), we find that the perturbation solution correct to order e^2 is given by Eq. (18-22).

34-9 Example: Far-field corrections

In Section 15-5, we showed how to derive the far field of a weakly guiding fiber from a knowledge of the Gaussian approximation to the fundamental mode. As explained below Eq. (15-14), this requires solution of

$$\left\{ \frac{d^2}{dR^2} + \frac{1}{R} \frac{d}{dR} - W^2 \right\} F_0 = -V^2 (1-f) \exp \left\{ -\frac{R^2}{2R_0^2} \right\}, \quad (34-39)$$

where $R = r/\rho$, $R_0 = r_0/\rho$ and W is defined inside the back cover. The spot size, assumed prescribed, is r_0 , and f is the profile variation of Eq. (14-1). Using standard methods [1-3], such as variation of parameters, the solution of

$$\left\{ \frac{d^2}{dR^2} + \frac{1}{R} \frac{d}{dR} - W^2 \right\} G = -\delta(R - R'), \quad (34-40)$$

for the Green's function $G(R, R')$ is readily shown to be [8]

$$G(R, R') = -K_0(WR)I_0(WR')R'; \quad 0 \leq R' \leq R, \quad (34-41a)$$

$$= -I_0(WR)K_0(WR')R'; \quad R \leq R' < \infty, \quad (34-41b)$$

where I_0 and K_0 are modified Bessel functions of the first and second kinds,

respectively. Accordingly the solution of Eq. (34-39) can be written down by analogy with Eqs. (34-34) and (34-35) as

$$F_0(R) = -K_0(WR) \int_0^R I_0(WR') \chi(R') R' dR' - I_0(WR) \int_R^\infty K_0(WR') \chi(R') R' dR', \quad (34-42)$$

where $\chi(R')$ denotes the right side of Eq. (34-39) with R replaced by R' . In the far field, $R \rightarrow \infty$ and $f \rightarrow 1$ on a clad fiber. Hence F_0 is dominated by the first integral, and by letting the limit of integration $R \rightarrow \infty$, we obtain Eq. (15-15).

REFERENCES

1. Morse, P. and Feshbach, H. (1953) *Methods of Mathematical Physics*, McGraw-Hill, New York, chap. 7.
2. Friedman, B. (1956) *Principles and Techniques of Applied Mathematics*, Wiley, New York, chaps. 3 and 4.
3. Mathews, J. and Walker, R. L. (1964) *Mathematical Methods of Physics*, Benjamin, New York, chap. 9.
4. Yip, G. L. (1970) Launching efficiency of the HE_{11} surface wave mode on a dielectric rod. *I.E.E.E. Trans. Microwave Theory Tech.*, **18**, 1033-41.
5. Papas, C. H. (1965) *Theory of Electromagnetic Wave Propagation*, McGraw-Hill, New York, chap. 2.2.
6. Ramo, S. Whinnery, J. R. and Van Duzer, T. (1965) *Fields and Waves in Communications Electronics*, Wiley, New York, sect. 12.04.
7. Snyder, A. W. (1980) Weakly guiding optical fibers. *J. Opt. Soc. Am.*, **70**, 405-11.
8. Snyder, A. W., Love, J. D. and Sammut, R. A. (1982) Green's function methods for analyzing optical fiber perturbations. *J. Opt. Soc. Am.*, **72**, 1131-35.

Rays and local plane waves

Local plane waves	666
35-1 Uniform media	667
35-2 Snell's laws	668
35-3 Slowly varying media	668
35-4 Component equations of the ray-path equation	670
Local plane-wave description of loss phenomena	671
35-5 Power transmission and attenuation coefficients	672
35-6 Planar interfaces	673
35-7 Planar interfaces between absorbing media	675
35-8 WKB solutions of the scalar wave equation	676
35-9 Planar caustics and tunneling	678
35-10 Planar caustics and absorbing media	680
35-11 Continuous and discontinuous profiles	682
35-12 Circular interfaces and caustics	683
35-13 Circular interfaces, caustics and absorbing media	686
35-14 Interfaces and caustics defined by two radii of curvature	687
35-15 Fields in the neighborhood of caustics	689
References	690

The behavior of the total electromagnetic fields of a multimode waveguide, whose waveguide parameter satisfies $V \gg 1$, can be described by the ray approach of Part I. There we expressed propagation along the waveguide in terms of a continuous superposition of rays, with power flowing along the trajectories determined by the classical laws of geometric optics. Now in this chapter we deduce the behavior of individual rays and the associated power flow, starting from the local plane-wave nature of electromagnetic fields in uniform and graded media.

In the following chapter we deduce the ray description of the total electromagnetic fields by summing the fields of the many modes of a multimode waveguide. This is less direct than the ray approach, because it requires knowing properties of individual modes—such as the *eigenvalue equation* for determining the propagation constant—which introduce both algebraic and conceptual complications to problems which can be solved directly by a ray analysis. Furthermore, the modal nature of the total fields of multimode waveguides is rarely observed [1] and is therefore somewhat of an abstraction.

LOCAL PLANE WAVES

When the refractive index n is everywhere constant in an unbounded medium, the electromagnetic fields can be expressed as individual *plane waves*. If we now suppose

that n is nearly constant and changes slowly over a distance equal to the wavelength of light, it is intuitive that the fields at each point are those of a *local plane wave*, except when diffraction, or wavelength-dependent, effects are significant, as at caustics or focal points. Using this simple notion, we derive the basic properties of local plane waves in Section 35-3. Alternatively, we can adopt a formal approach. This assumes each field component has a spatial dependence of the form $\exp \{i\Psi(x, y, z)\}$ which is substituted into Maxwell's equations. The slow-variation condition is expressible as $\lambda |\nabla \ln n^2| \ll 1$, where λ is the free-space wavelength, and leads to the equations governing local plane-wave propagation, including the ray-path, or eikonal, equation of Eq. (1-18). This derivation is fully described elsewhere [2-4] and need not be repeated here. Since our intuitive approach is based on wave propagation in uniform media, we first summarize the governing results, including Snell's laws.

35-1 Uniform media

The electric and magnetic fields \mathbf{E} and \mathbf{H} of a plane wave in an infinite medium of uniform refractive index n have the forms [5]

$$\mathbf{E}(\mathbf{r}) = \mathbf{E}_0 \exp(in\mathbf{k} \cdot \mathbf{r}); \quad \mathbf{H}(\mathbf{r}) = \mathbf{H}_0 \exp(in\mathbf{k} \cdot \mathbf{r}), \quad (35-1a)$$

where \mathbf{E}_0 and \mathbf{H}_0 are constant vectors, \mathbf{r} is the position vector and the time dependence $\exp(-i\omega t)$ is implicit. The wave vector $\mathbf{k} = k\hat{\mathbf{k}}$, where $\hat{\mathbf{k}}$ is the unit vector parallel to the propagation direction, $k = 2\pi/\lambda$ and λ is the free-space wavelength. The vectors \mathbf{E}_0 and \mathbf{H}_0 are orthogonal to one another and to $\hat{\mathbf{k}}$, and are related by

$$\mathbf{H}_0 = n(\epsilon_0/\mu_0)^{1/2} \hat{\mathbf{k}} \times \mathbf{E}_0, \quad (35-1b)$$

where parameters are defined inside the back cover.

Power flow

The intensity, or power density, S has magnitude and direction determined by the time-averaged Poynting vector. Thus we deduce from Eq. (35-1b) that

$$\mathbf{S} = \frac{1}{2} \text{Re} \{ \mathbf{E}(\mathbf{r}) \times \mathbf{H}^*(\mathbf{r}) \} = \frac{n}{2} \left(\frac{\epsilon_0}{\mu_0} \right)^{1/2} |\mathbf{E}_0|^2 \hat{\mathbf{k}}, \quad (35-2)$$

where Re denotes real part and $*$ complex conjugate. Hence power flows in the direction of propagation. Further, light energy is transported along rays whose direction is given by the wave vector, and power is conserved within a *ray tube*, i.e. a tube of parallel rays of differential cross-section dA illustrated in Fig. 35-2(a), since $|\mathbf{S}|dA$ is constant along the tube. Along each ray or ray tube, there is an accumulation of phase which is expressible as

$$n\mathbf{k} \cdot \mathbf{r} = nk\hat{\mathbf{k}} \cdot \mathbf{r} = \frac{2\pi n}{\lambda} L_p = \frac{2\pi}{\lambda} L_o, \quad (35-3)$$

where L_p and L_o are the *geometric* and *optical path lengths*, respectively.

35-2 Snell's laws

The reflection and transmission of a plane wave, or ray, which is incident on a planar interface between two semi-infinite, uniform media is determined by *Snell's Laws* [2]. In Fig. 35-1, the refractive indices of the medium of incidence and the second medium are n_{co} and $n_{cl} < n_{co}$, respectively, and the *critical angle* $\alpha_c = \sin^{-1}(n_{cl}/n_{co})$. We denote the angles of incidence, reflection and transmission, or refraction, relative to the normal QN by α_i , α_r and α_t , respectively. The incident, reflected and transmitted, or refracted, rays and the normal are *coplanar*.

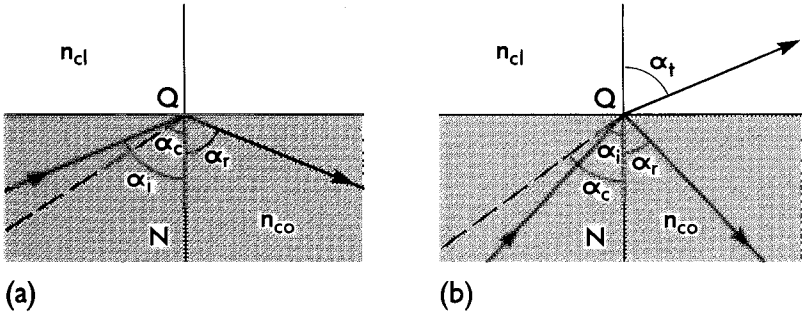


Fig. 35-1 Reflection at a planar interface between unbounded regions of refractive indices n_{co} and $n_{cl} < n_{co}$, showing (a) total internal reflection and (b) partial reflection and refraction.

If $\alpha_i > \alpha_c$, the incident ray in Fig. 35-1(a) undergoes *total internal reflection* and $\alpha_r = \alpha_i$, but if $\alpha_i < \alpha_c$ there is partial reflection and partial transmission, or refraction, as shown in Fig. 35-1(b), and the angles satisfy

$$\alpha_i = \alpha_r; \quad n_{co} \sin \alpha_i = n_{cl} \sin \alpha_t. \quad (35-4)$$

For the planar waveguides of Chapter 1 it is convenient to express these laws in terms of the complementary angles of incidence, reflection and transmission, i.e. $\theta_z = \pi/2 - \alpha_i = \pi/2 - \alpha_r$ and $\theta_t = \pi/2 - \alpha_t$. The *complementary critical angle* $\theta_c = \pi/2 - \alpha_c$ is used throughout the book.

35-3 Slowly varying media

The expressions given in Section 35-1 for a uniform medium can be generalized in an intuitive manner provided the refractive index $n(r)$ varies slowly over distance equal to the wavelength of light. Thus the accumulated phase of Eq. (35-3) becomes the integrated quantity

$$\int_p n \mathbf{k} \cdot d\mathbf{r} = \frac{2\pi}{\lambda} \int_p n ds, \quad (35-5)$$

where s is the distance along the ray path p , which is now curved because of the grading of the medium. Accordingly, the fields along the path are given by Eq. (35-1a) with

in $\mathbf{k} \cdot \mathbf{r}$ replaced by Eq. (35-5) and E_0, H_0 are now slowly varying functions of position. Hence the fields are locally plane and

$$\mathbf{E}(\mathbf{r}) = \mathbf{E}_0(\mathbf{r}) \exp \left\{ i \int_p n \mathbf{k} \cdot d\mathbf{r} \right\}; \quad \mathbf{H}(\mathbf{r}) = \mathbf{H}_0(\mathbf{r}) \exp \left\{ i \int_p n \mathbf{k} \cdot d\mathbf{r} \right\}. \quad (35-6a)$$

The tangent to p gives the direction of the local wave vector \mathbf{k} and power flow, and hence the spatial variation of the unit vector $\hat{\mathbf{k}}(\mathbf{r})$. Thus the appropriate generalization of Eq. (35-1b) is

$$\mathbf{H}_0(\mathbf{r}) = n(\mathbf{r}) (\epsilon_0/\mu_0)^{1/2} \hat{\mathbf{k}}(\mathbf{r}) \times \mathbf{E}_0(\mathbf{r}). \quad (35-6b)$$

For a given profile, the path p is determined from the ray-path, or eikonal equation, as we showed in Chapters 1 and 2.

Power flow

If we construct a ray tube from the curved ray paths, as shown in Fig. 35-2(b), then by definition the power flowing within the tube is conserved, i.e. $\mathbf{S}(\mathbf{r}) \cdot \hat{\mathbf{k}}(\mathbf{r}) dA(\mathbf{r})$ is constant along the tube, where $dA(\mathbf{r})$ is the elemental cross-sectional area and $\mathbf{S}(\mathbf{r})$ is given by Eq. (35-2) with n, \mathbf{E}_0 and $\hat{\mathbf{k}}$ replaced by $n(\mathbf{r}), \mathbf{E}_0(\mathbf{r})$ and $\hat{\mathbf{k}}(\mathbf{r})$, respectively.

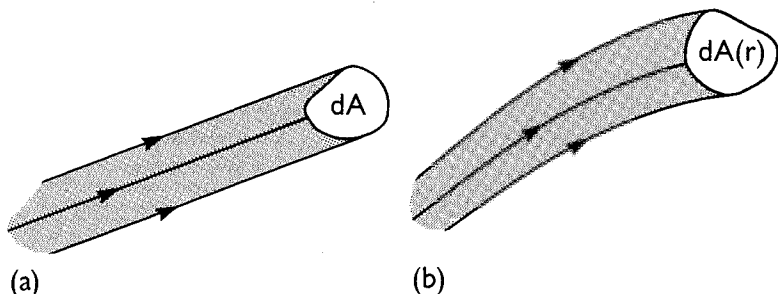


Fig. 35-2 Ray tubes of (a) constant cross-section dA in a uniform medium and (b) varying cross-section $dA(\mathbf{r})$ in a graded medium.

Hence $n(\mathbf{r}) |\mathbf{E}_0(\mathbf{r})|^2 dA(\mathbf{r})$ is constant along the tube, and, if \mathbf{r}_0 denotes a fixed position along the tube, the spatial dependence of the electric field for a local plane wave propagating in a graded medium follows from Eq. (37-6a) as

$$\mathbf{E}(\mathbf{r}) = \mathbf{E}_0(\mathbf{r}_0) \left\{ \frac{n(\mathbf{r}_0) dA(\mathbf{r}_0)}{n(\mathbf{r}) dA(\mathbf{r})} \right\}^{1/2} \exp \left\{ i \int_{\mathbf{r}_0}^{\mathbf{r}} n \mathbf{k} \cdot d\mathbf{r} \right\}, \quad (35-7)$$

where \mathbf{r} is any position on the path. The magnetic field is given by the same expression with $\mathbf{E}_0(\mathbf{r}_0)$ replaced by $\mathbf{H}_0(\mathbf{r}_0)$, and $\mathbf{H}_0(\mathbf{r}_0)$ is expressible in terms of $\mathbf{E}_0(\mathbf{r}_0)$ through Eq. (35-6b).

Polarization

We define the unit vector $\hat{\mathbf{E}}_0(\mathbf{r}) = \mathbf{E}_0(\mathbf{r})/|\mathbf{E}_0(\mathbf{r})|$ in the direction of the electric field to be the *polarization vector*. In a uniform medium this direction is fixed, but in a slowly

varying medium it changes direction as the local plane wave propagates according to [2,4]

$$\frac{d\hat{\mathbf{E}}_0}{ds} = -\frac{1}{2}\hat{\mathbf{k}}(r)\{\hat{\mathbf{E}}_0 \cdot \nabla \ln n^2(\mathbf{r})\}. \quad (35-8)$$

We recall that a term involving $\nabla \ln n^2$ appears in the vector wave equation of Eq. (11-40), and has the geometrical interpretation discussed in Section 11-16. However, we usually ignore both phase and polarization effects in weakly guiding, *multimode* fibers and treat propagation as a scalar phenomenon, because they are usually masked due to multiple reflections by the many rays propagating within the fiber. However, on weakly guiding fibers which propagate one or a few modes, polarization effects are often important over large distances, as discussed in Chapter 13.

Summary

When the refractive-index profile is slowly varying, the fields of the medium behave locally as a bundle of rays, with each ray transporting energy along the geometric optics trajectory. Thus phenomena of major interest on multimode waveguides, such as pulse propagation, pulse spreading and illumination can be described using the ray-tracing methods of classical geometric optics. This is the basis of Chapters 1 to 5. Because we ignore the small effects due to diffraction, *these phenomena are independent of wavelength in the ray description*. However, for reasons discussed in Section 10-3, it is necessary that the waveguide be multimoded with $V \gg 1$, for a ray description to be accurate.

35-4 Component equations of the ray-path equation

The construction of ray paths within the core of the step-profile waveguides of Chapters 1 and 2 is based on straight-line trajectories, which are solutions of the ray-path equation of Eq. (1-18) in a uniform medium. When the core is graded, the cartesian component equations of the ray-path equation follow directly, as in Eqs. (1-19) and (2-49). Here we derive the corresponding component equations in directions defined by the cylindrical polar coordinates (r, ϕ, z) of Fig. 2-1, for application to fibers with graded profiles $n(r)$ in Chapter 2, and, by simple generalization, to slowly varying fibers with profiles $n(r, z)$ in Chapter 5.

The position vector in Eq. (1-18) is expressed as

$$\mathbf{r} = r\hat{\mathbf{r}} + z\hat{\mathbf{z}}, \quad (35-9a)$$

where $\hat{\mathbf{r}}$ and $\hat{\mathbf{z}}$ are unit vectors in the radial and longitudinal directions, respectively. We use the chain rule and the spatial derivatives of the unit vectors in Eq. (37-54) to obtain the derivative along the path

$$\frac{d\mathbf{r}}{ds} = \hat{\mathbf{r}} \frac{dr}{ds} + r \frac{d\hat{\mathbf{r}}}{ds} + \hat{\mathbf{z}} \frac{dz}{ds} = \hat{\mathbf{r}} \frac{dr}{ds} + r\hat{\phi} \frac{d\phi}{ds} + \hat{\mathbf{z}} \frac{dz}{ds}, \quad (35-9b)$$

where $\hat{\phi}$ is the unit vector in the azimuthal direction. By repeating this procedure

$$\frac{d}{ds} \left\{ n(r) \frac{dr}{ds} \right\} = \hat{r} A_r + \hat{\phi} A_\phi + \hat{z} \frac{d}{ds} \left\{ n(r) \frac{dz}{ds} \right\}, \quad (35-10a)$$

$$A_r = \frac{d}{ds} \left\{ n(r) \frac{dr}{ds} \right\} - rn(r) \left(\frac{d\phi}{ds} \right)^2; \quad A_\phi = \frac{d}{ds} \left\{ rn(r) \frac{d\phi}{ds} \right\} + n(r) \frac{dr}{ds} \frac{d\phi}{ds}. \quad (35-10b)$$

If we equate like components in Eq. (1-18), with $n(\mathbf{r}) = n(r)$ on the right side, we obtain the component equations given in Eq. (2-13). Similarly, if we replace $n(r)$ by $n(r, z)$ on both sides of Eq. (1-18) we obtain the component equations given in Eq. (5-3).

LOCAL PLANE-WAVE DESCRIPTION OF LOSS PHENOMENA

The local plane wave, or ray, description of propagation introduced above enables us to determine directly absorption losses *along each path*, as we showed in Chapter 6, but it cannot tell us immediately how ray power is lost due to attenuation of the local plane-wave fields *beyond the path*, as occurs when the cladding is absorbing or a bent waveguide radiates. These losses are usually negligible over a short length of waveguide, since the fields beyond the path are evanescent and their amplitudes decrease exponentially away from the path. Nevertheless, they accumulate with distance along the waveguide and eventually become significant.

In the following sections we derive transmission, or loss, coefficients to account for such loss mechanisms. These transmission coefficients, taken together with the trajectories of classical geometric optics, fully describe propagation along multimode waveguides, as we showed in Chapter 6 to 9. All the graded-profile waveguides considered in Part I have *refractive-index profiles which are nearly uniform over a distance equal to the wavelength of light*. Similarly, *all curved interfaces and caustic surfaces are nearly planar over the same distance*. Consequently, *the electromagnetic fields have plane-wave characteristics in local regions*, except immediately adjacent to a caustic where there is a rapid transition from the wavelike behavior of the local plane-wave fields to the evanescent behavior beyond the ray path. Accordingly we approximate the fields of a waveguide by the local plane wave discussed in Section 35-3 and we treat rays as local plane waves:

Building blocks

As we show below, we need solve only two simple electromagnetic problems which serve as building blocks for determining the transmission coefficients for *any multimode waveguide*. The problems are:

- (i) *Plane-wave incidence at a planar interface*. This classical problem is the building block solution which determines the transmission coefficient for all step-profile waveguides;

- (ii) *Local plane-wave incidence at a planar caustic.* This problem is the building block solution from which we can determine the transmission coefficient for all graded-profile waveguides.

The delineation applies both to leaky rays and to bound rays on waveguides with an absorbing cladding.

Weak-guidance approximation

To simplify the algebra, and remain consistent with Chapters 6 to 9, we determine the transmission coefficients for weakly guiding waveguides only. This means that the expressions we derive are independent of the direction of the incident electric field.

35-5 Power transmission and attenuation coefficients

We showed in Section 35-3 that power flows within ray tubes along the core of the waveguide. The total power within a tube can change only at a *reflection* from an interface, when the tube direction changes abruptly, as in Fig. 35-3(a), or in the neighborhood of a *turning point*, or *caustic*, when the cross-sectional area $dA = 0$, as in Fig. 35-4(a). In order to describe power losses associated with the evanescent fields of the local plane wave in the cladding beyond the ray path, we retain the geometric optics path in the core and introduce a *power transmission, or loss, coefficient* T defined by

$$T = 1 - \frac{\text{power in the reflected ray}}{\text{power in the incident ray}}, \quad (35-11)$$

which gives the fraction of ray power lost at a reflection or turning point. The *power attenuation coefficient* γ is the rate of power loss per unit length of waveguide, found by averaging T over the distance between successive reflection or turning points, and is given by

$$\gamma = T/z_p = NT, \quad (35-12)$$

where z_p is the ray half-period and N is the number of reflection or turning points per unit length of waveguide, as illustrated in Figs. 1-5 and 1-9.

Ray power

We denote the power within the ray tube distance z along the waveguide by $P(z)$. Over a differential length dz , it follows from Eq. (35-12) that

$$dP(z) = -\gamma P(z) dz = -NTP(z) dz, \quad (35-13)$$

and the initial power $P(0)$ is attenuated exponentially according to

$$P(z) = P(0) \exp(-\gamma z) \quad \text{or} \quad P(z) = P(0) \exp \left\{ - \int_0^z \gamma(z) dz \right\}, \quad (35-14)$$

depending, respectively, on whether the waveguide is translationally invariant or varies along its length. We showed how to determine z_p and N in Chapters 1, 2 and 5; our main

purpose in the rest of this chapter is to use local plane-wave theory to determine T and hence γ .

35-6 Planar interfaces

We begin by considering plane-wave incidence at a planar interface with a view towards determining the transmission coefficient for planar, step-profile waveguides. This classical problem is treated in most texts on electromagnetic theory, but, nevertheless, we repeat the derivation because we require its generalization for graded media and also because the analysis is specialized to weakly guiding waveguides.

Consider two semi-infinite media of refractive indices n_{co} and $n_{cl} < n_{co}$, separated by the planar interface $x = 0$ in Fig. 35-3(a). A ray, or plane wave, is incident on the interface from the denser medium at angle θ_z to the z -direction. Plane wave reflection in this situation is well-known and the power transmission coefficient of Eq. (35-11) is identical to the classical Fresnel coefficient [2].

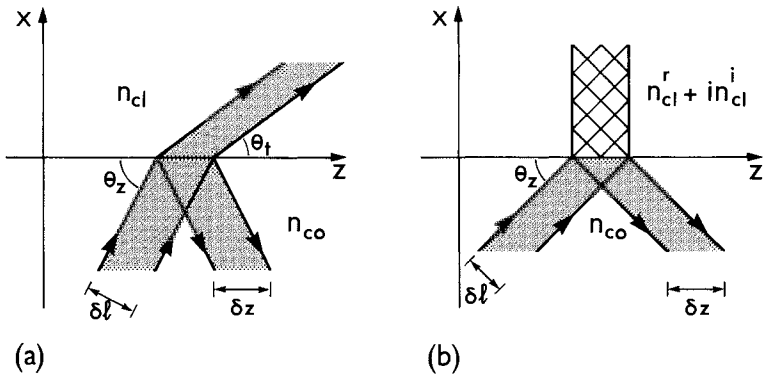


Fig. 35-3 (a) Partial reflection and refraction at a planar interface. The shading denotes power flow within the ray tubes. (b) Hatching denotes power absorption when a ray reflects from the planar interface of an absorbing medium.

Scalar approximation

We are interested in the special case when $n_{co} \cong n_{cl}$. In this limit, the well-known classical expressions are independent of polarization phenomena, i.e. the transmission coefficients are independent of the electric field direction. Thus, neglecting all polarization effects, the fields are then solutions of the scalar wave equation rather than Maxwell's equation. This is important because solutions of the scalar wave equation have the simple property discussed in Section 33-1. For convenience we take the electric field to be in the y -direction parallel to the interface. Hence

$$E_y = \Psi(x) \exp(i\beta z); \quad \beta = k n_{co} \cos \theta_z, \quad (35-15)$$

where β is the z -component of the incident wave vector, the implicit time dependence $\exp(-i\omega t)$ is assumed, and $\Psi(x)$ satisfies the scalar wave equation

$$\left\{ \frac{d^2}{dx^2} + k^2 n^2(x) - \beta^2 \right\} \Psi = 0, \quad (35-16)$$

where $n(x) = n_{co}$ for $x < 0$, $n(x) = n_{cl}$ for $x > 0$, $k = 2\pi/\lambda$, and λ is the free-space wavelength. If we denote the solutions for the incident and reflected fields in $x < 0$ by superscripts i and r , respectively, then

$$\Psi^i = A \exp(ikn_{co}x \sin \theta_z); \quad \Psi^r = B \exp(-ikn_{co}x \sin \theta_z), \quad (35-17a)$$

using Eq. (35-15), where A and B are constants. We recall from Snell's laws of Section 35-2 that power is transmitted across the interface only if $\theta_z > \theta_c$, where θ_c is the complementary critical angle defined inside the back cover. When this condition is satisfied, refraction occurs at the interface in Fig. 35-3(a) and the solution of Eq. (35-16) in $x > 0$, denoted by superscript t , has the form

$$\Psi^t = C \exp(ikn_{cl}x \sin \theta_t); \quad n_{cl} \cos \theta_t = n_{co} \cos \theta_z, \quad (35-17b)$$

where C is a constant and θ_t , the angle between the refracted ray and the z -direction, is related to θ_z by Snell's law. To determine B and C , we recall from Section 33-1 that any solution of the scalar wave equation and its first derivatives must be continuous everywhere. Hence $\Psi^i + \Psi^r$ and Ψ^t and the corresponding x -derivatives are continuous at $x = 0$, leading to

$$\frac{B}{A} = \frac{n_{co} \sin \theta_z - n_{cl} \sin \theta_t}{n_{co} \sin \theta_z + n_{cl} \sin \theta_t}, \quad \frac{C}{A} = \frac{2n_{co} \sin \theta_z}{n_{co} \sin \theta_z + n_{cl} \sin \theta_t}, \quad (35-18)$$

valid for $\theta_c \leq \theta_z \leq \pi/2$. Close to normal incidence we deduce that

$$C/A \cong 2n_{co}/(n_{co} + n_{cl}); \quad \theta_t \cong \pi/2, \quad (35-19)$$

which is the coefficient used to relate the fields in Section 20-2.

Power transmission, or Fresnel, coefficients

The ray tubes formed by the incident and reflected rays in Fig. 35-3(a) have the same z -directed cross-section, and, since Ψ is complex, the power density in each varies as $|\Psi|^2$, as is clear from Table 13-2, page 292. We deduce from Eqs. (35-11) and (35-18) that the transmission coefficient is given by $1 - |B/A|^2$ for $\theta_c \leq \theta_z \leq \pi/2$, leading to the Fresnel coefficient

$$T = \frac{4n_{co}n_{cl} \sin \theta_z \sin \theta_t}{(n_{co} \sin \theta_z + n_{cl} \sin \theta_t)^2} = \frac{4 \sin \theta_z (\sin^2 \theta_z - \sin^2 \theta_c)^{1/2}}{(\sin \theta_z + \{\sin^2 \theta_z - \sin^2 \theta_c\}^{1/2})^2}, \quad (35-20)$$

with the aid of Eq. (35-17b), where $\sin \theta_c = \{1 - n_{cl}^2/n_{co}^2\}^{1/2}$. The generalization to a cylindrical interface requires only a change in the angles defining T , as discussed in Section 35-12. The limiting form close to normal incidence is obtained by setting $\theta_z \cong \theta_t \cong \pi/2$, and close to the complementary critical angle, i.e. $\theta_z \cong \theta_c$, the

corresponding form follows from Eq. (35-17b). We obtain, respectively,

$$T \cong \frac{4n_{co}n_{cl}}{(n_{co} + n_{cl})^2}, \quad \theta_z \cong \pi/2; \quad T \cong 4 \left\{ 1 - \frac{\theta_c^2}{\theta_z^2} \right\}^{1/2}, \quad \theta_z \gtrsim \theta_c, \quad (35-21)$$

since $\theta_c \ll 1$ when $n_{co} \cong n_{cl}$.

Evanescent fields

When the incident ray is totally reflected, no power crosses the interface. Thus the fields in $x > 0$ are evanescent and Eq. (35-17b) is replaced by

$$\Psi' = C \exp(-\Omega k n_{co} x); \quad \Omega = (\sin^2 \theta_c - \sin^2 \theta_z)^{1/2}, \quad (35-22a)$$

and the expressions corresponding to Eq. (35-18) are now

$$\frac{B}{A} = \frac{\sin \theta_z - i\Omega}{\sin \theta_z + i\Omega}; \quad \frac{C}{A} = \frac{2 \sin \theta_z}{\sin \theta_z + i\Omega}. \quad (35-22b)$$

Furthermore, there is a change of phase Φ at the interface between the fields of the incident and reflected waves, i.e. $B = A \exp(i\Phi)$ at $x = 0$, whence

$$\Phi = -2 \tan^{-1} \left\{ \frac{(\sin^2 \theta_c - \sin^2 \theta_z)^{1/2}}{\sin \theta_z} \right\} \cong -2 \tan^{-1} \left\{ \frac{\theta_c^2}{\theta_z^2} - 1 \right\}^{1/2}, \quad (35-23)$$

since $0 \leq \theta_z \leq \theta_c \ll 1$.

35-7 Planar interfaces between absorbing media

When the media in Fig. 35-3(a) are absorbing, the refractive indices take the complex forms $n_{co} = n_{co}^r + i n_{co}^i$, $n_{cl} = n_{cl}^r + i n_{cl}^i$, where superscripts denote real and imaginary parts. The corresponding solutions of the scalar wave equation are given by Eqs. (35-17a), with n_{co} complex, and (35-22a), with $\sin^2 \theta_c$ replaced by the complex quantity $1 - n_{cl}^2/n_{co}^2$. Then, by paralleling the analysis of the previous section, we find that, for all values of θ_z , the power transmission coefficient is generally nonzero, and is expressible as

$$T = \frac{4 \sin \theta_z \operatorname{Re}(n_{cl}^2/n_{co}^2 - \cos^2 \theta_z)^{1/2}}{|\sin \theta_z + \{n_{cl}^2/n_{co}^2 - \cos^2 \theta_z\}^{1/2}|^2}; \quad 0 \leq \theta_z \leq \pi/2, \quad (35-24)$$

where Re denotes real part. Thus, rays which would be totally reflected if the media were nonabsorbing, now suffer a change in power on reflection. If the absorption is weak, i.e. $n_{co}^i \ll n_{co}^r$, $n_{cl}^i \ll n_{cl}^r$, $0 \leq \theta_z \leq \theta_c$ with θ_z not too close to θ_c , Eq. (35-24) is well approximated by

$$T = \frac{4}{(\theta_c^2 - \theta_z^2)^{1/2}} \frac{\theta_z}{\theta_c^2} \left\{ \frac{n_{cl}^i}{n_{cl}^r} - \frac{n_{co}^i}{n_{co}^r} \right\}. \quad (35-25)$$

In the special case when $n_{cl}^i = 0$ and $n_{co}^i > 0$, we note that $T < 0$, i.e. power is lost from

the nonabsorbing medium to the absorbing medium. Although the ray then *gains* power on reflection, this power is subsequently lost to absorption along its path. Within a waveguide, the appropriate attenuation coefficient γ is the sum of the attenuation coefficient γ_{co} for absorption in the core and γ_{cl} for power exchange with the cladding, as expressed by Eq. (6–30).

Alternative derivation

We now provide an alternative derivation for cladding absorption because it is easily generalized to include graded media. The derivation assumes that the core medium is lossless, $n_{\text{co}}^i = 0$, and the cladding medium is only slightly lossy, i.e. $n_{\text{cl}}^i \gg n_{\text{cl}}^r$. The ray tube formed by the incident and reflected rays in Fig. 35–3(b), which would constitute total reflection if $n_{\text{cl}}^i = 0$, is extended indefinitely into the region $x > 0$ to form the hatched tube shown in Fig. 35–3(b). It is intuitive that the total power absorbed from the evanescent fields within the hatched region is equal to the power lost by the incident ray, and consequently the transmission coefficient is given by the ratio of the absorbed to incident powers [6].

If the incident tube in Fig. 35–2(b) has width δl then the width δz of the hatched region is approximately $\delta l / \theta_z$, assuming $\theta_z \leq \theta_c \ll 1$. Since the medium is weakly absorbing, the total absorbed power, P_{abs} , is well approximated by integrating $|dP|$ of Table 13–2, page 292, over the hatched region with $|\mathbf{E}_j|$ replaced by $|\Psi^t|$ of Eq. (35–22) for the nonabsorbing medium. Hence with $n_{\text{co}} \cong n_{\text{cl}}^r$ we find

$$P_{\text{abs}} = kn_{\text{cl}}^i n_{\text{co}} \delta z \left(\frac{\epsilon_0}{\mu_0} \right)^{1/2} \int_0^\infty |\Psi^t|^2 dx = \frac{|C|^2 n_{\text{cl}}^i}{(\theta_c^2 - \theta_z^2)^{1/2}} \frac{\delta l}{2\theta_z} \left(\frac{\epsilon_0}{\mu_0} \right)^{1/2}, \quad (35-26)$$

since $\Omega \cong (\theta_c^2 - \theta_z^2)^{1/2}$. The power P_{inc} in the incident ray tube follows from Table 13–2 and Eq. (35–17a) as $(\delta l/2) |A|^2 n_{\text{co}} (\epsilon_0/\mu_0)^{1/2}$. On substituting from Eq. (35–22b) for C/A in the ratio $P_{\text{abs}}/P_{\text{inc}}$, we deduce that the expression for the transmission coefficient is identical to Eq. (35–25) with $n_{\text{co}}^i = 0$.

35–8 WKB solutions of the scalar wave equation

In the following two sections we extend the notions of the last two sections to graded media. Before doing so, it is helpful to provide some preliminary results. We recall the discussion of Section 35–3, where we showed that the solutions of Maxwell's equations can be approximated by local plane waves when the refractive-index profile varies slowly over a distance equal to the wavelength of light. Such solutions—known as asymptotic solutions—can be derived by either physical intuition or mathematical procedures. If we specialize our discussion to weakly guiding waveguides, electromagnetic propagation in this situation is also described by local plane waves, but the fields depend on solutions of the scalar wave equation rather than on Maxwell's equations, i.e. they describe phenomena which are independent of the direction of the electric field. Thus the solution of the scalar wave equation for local plane waves can be derived by the same intuitive reasoning given in Section 35–3.

Local plane-wave derivation

The tangent to the ray paths in the regions $x < x_{\text{tp}}$ and $x > x_{\text{rad}}$ of the medium with refractive-index profile $n(x)$ in Fig. 35-4(a) makes angle $\theta_z(x)$ with the z -direction. The propagation constant β is the component of the local wave vector $\mathbf{k}(x)$ in the z -direction. If the component in the x -direction is denoted by $k_x(x)$, then

$$\mathbf{k}(x) = [k_x(x), \beta] = [kn(x) \sin \theta_z(x), kn(x) \cos \theta_z(x)]. \quad (35-27)$$

The ray tube in Fig. 35-4(a) is bounded by identical rays displaced distance δz parallel to the z -axis, and therefore has width $\delta l(x) = \delta z \sin \theta_z(x)$. If we replace $n(\mathbf{r})dA(\mathbf{r})$ by $n(x)\delta l(x)$ in Eq. (35-7) and set $d\mathbf{r} = (dx, dz)$, then it follows from Eq. (35-27) that the local plane-wave solutions of the scalar wave equation have the forms

$$\frac{1}{\{n(x) \sin \theta_z(x)\}^{1/2}} \exp \left\{ \pm i \int^x kn(x) \sin \theta_z(x) dx \right\} \exp(i\beta z), \quad (35-28)$$

where the $+$ and $-$ signs denote propagation towards the positive and negative x directions, respectively. We drop the z -dependence and replace $\theta_z(x)$ by β through Eq. (35-27). Thus the solutions of Eq. (35-16) are

$$\Psi(x) = \frac{1}{\{k^2 n^2(x) - \beta^2\}^{1/4}} \exp \left\{ \pm i \int^x \{k^2 n^2(x) - \beta^2\}^{1/2} dx \right\}, \quad (35-29)$$

where the factors outside and inside the exponential account for power conservation and accumulated phase, respectively. This *oscillatory-type* solution is accurate in regions where $kn(x) - \beta \gg 1$, and is frequently referred to as *the WKB asymptotic solution of the scalar wave equation* [7].

When the condition $\beta - kn(x) \gg 1$ is satisfied, the WKB solution of the scalar wave equation is an *evanescent-type* solution given by [7]

$$\Psi(x) = \frac{1}{\{\beta^2 - k^2 n^2(x)\}^{1/4}} \exp \left\{ - \int^x \{\beta^2 - k^2 n^2(x)\}^{1/2} dx \right\}, \quad (35-30)$$

where for later application we note that $\beta^2 - k^2 n^2(x)$ is expressible as $|k^2 n^2(x) - \beta^2|$.

Ray caustics

The positions of the ray caustics in Fig. 35-4(a) are given by Eq. (1-26) in terms of the ray invariant $\bar{\beta}$. If we replace $\bar{\beta}$ with the propagation constant β through the relationship in Table 36-1, page 695, then x_{tp} and x_{rad} satisfy

$$kn(x_{\text{tp}}) = \beta; \quad kn(x_{\text{rad}}) = \beta, \quad (35-31)$$

respectively. In the immediate neighborhood of these caustics there is a rapid transition from the oscillatory behavior of Eq. (35-29) to the evanescent behavior of Eq. (35-30) and neither of the WKB solutions are valid. However, it is not necessary to know the detailed dependence of the scalar wave equation solution in this region in

order to link the two solutions. Connection formulae are available which relate the WKB solutions to one another [7], and are used below.

35-9 Planar caustics and tunneling

In this section we generalize the analysis of plane-wave incidence at a planar interface, and consider the incidence of local plane waves at a caustic in a slowly varying graded medium. Our goal is the derivation of the power transmission coefficient for tunneling rays.

Consider a medium whose continuous refractive-index profile $n(x)$ varies slowly over a distance equal to a wavelength. A ray path in the region $x < 0$ of Fig. 35-4(a) touches the turning-point caustic at $x = x_{tp}$. When there is no path in the region beyond the caustic, the ray is totally reflected from the caustic and no power is lost, i.e. $T = 0$. However, if a transmitted ray originates at the radiation caustic $x = x_{rad}$, then optical tunneling occurs, as described in Chapter 7, and power is lost from the path at x_{tp} to the path at x_{rad} . If the local plane-wave fields have propagation constant β , then the values of x_{tp} and x_{rad} are determined by Eq. (35-31).

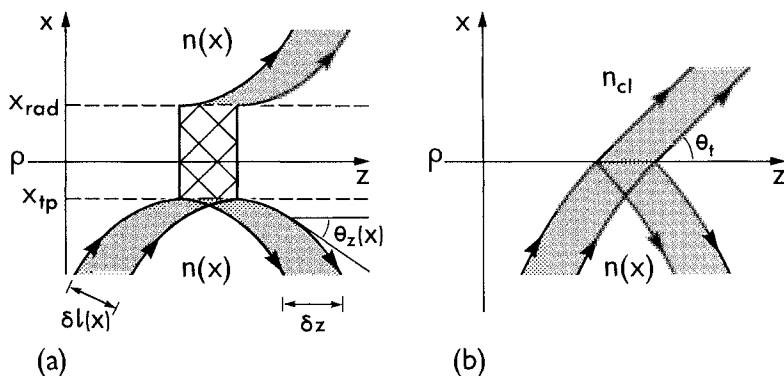


Fig. 35-4 (a) A tunneling ray in a graded medium is partially reflected at the turning-point caustic and partially transmitted at the radiation caustic. The shading denotes power flow within the ray tubes and the hatching indicates the region in which the fields are evanescent. (b) Partial reflection and transmission at an interface between graded and uniform media.

WKB solutions

In terms of the x -component of the local wave vector of Eq. (35-27) and the WKB solutions of Eq. (35-29), the solutions of the scalar wave equation for the incident, reflected and transmitted local plane waves, respectively, are expressible as

$$\Psi^i = \frac{A}{\{k_x(x)\}^{1/2}} \exp \left\{ -i \int_x^{x_{tp}} k_x(x) dx \right\}; \quad \Psi^r = \frac{B}{\{k_x(x)\}^{1/2}} \exp \left\{ i \int_x^{x_{tp}} k_x(x) dx \right\}$$

(35-32a)

in the region $x < x_{\text{tp}}$, and in the region $x > x_{\text{rad}}$

$$\Psi^i = \frac{C}{\{k_x(x)\}^{1/2}} \exp \left\{ i \int_{x_{\text{rad}}}^x k_x(x) dx \right\}, \quad (35-32b)$$

where A , B and C are constants related to the amplitudes of the corresponding fields. The fields in the region $x_{\text{tp}} < x < x_{\text{rad}}$ are evanescent and decrease exponentially as x increases. If Ψ^e denotes the solution of the scalar wave equation, we deduce from Eq. (35-30) that

$$\Psi^e = \frac{F}{|k_x(x)|^{1/2}} \exp \left\{ - \int_{x_{\text{tp}}}^x |k_x(x)| dx \right\}, \quad (35-32c)$$

where $k_x(x)$ is pure imaginary and F is a constant.

Connection formulae

The link between the ray tubes at the caustics is denoted by the hatched region of width δz in Fig. 35-4(a). Power lost by the incident ray at x_{tp} tunnels through this region and enters the transmitted ray at x_{rad} . At and close to the caustics, local plane-wave theory is inadequate, but, provided the caustics are not too close together, it is not necessary to know the fields in these regions in order to determine the transmission coefficient. We can link the solutions in Eq. (35-32) using the connection formulae of WKB theory, which are available in standard texts [7]. Hence

$$B = A \exp(-i\pi/2); \quad F = A; \quad C = F \exp \left\{ - \int_{x_{\text{tp}}}^{x_{\text{rad}}} |k_x(x)| dx \right\}. \quad (35-33)$$

The first expression exhibits the well-known phenomenon that there is a decrease of $\pi/2$ in phase when a ray touches a caustic; this is not plane-wave phenomenon.

Transmission coefficient for tunneling rays

Given Ψ^i , the power P_{inc} in the incident ray tube can be calculated from Table 13-2, page 292, and Eq. (35-32a) as the product of the tube width and intensity, leading to

$$P_{\text{inc}} = \frac{1}{2} \left(\frac{\epsilon_0}{\mu_0} \right)^{1/2} \delta l(x) n(x) |\Psi^i|^2 = \left(\frac{\epsilon_0}{\mu_0} \right)^{1/2} \frac{|A|^2 \delta z}{2k}, \quad (35-34)$$

since $\delta l(x) = \delta z \sin \theta_z(x)$ and $k_x(x) = kn(x) \sin \theta_z(x)$. Similarly, the power P_{tr} in the transmitted ray tube is given by the same expression with A replaced by C . The power transmission coefficient of Eq. (35-11) in this case is given by the ratio $P_{\text{tr}}/P_{\text{inc}}$. If we express $k_x(x)$ in terms of the ray invariant $\bar{\beta}$ through Eq. (35-27) and the relationship in Table 36-1, page 695, we obtain [8]

$$T = \exp \left\{ - 2k \int_{x_{\text{tp}}}^{x_{\text{rad}}} [\bar{\beta}^2 - n^2(x)]^{1/2} dx \right\}. \quad (35-35)$$

If the wavelength $\lambda \rightarrow 0$, then $k \rightarrow \infty$ and $T \rightarrow 0$. This confirms that tunneling is a wavelength-dependent phenomenon.

Frustrated total internal reflection

Tunneling losses from rays propagating along planar waveguides is expressed by Eq. (35–35) in terms of the positions of the planar caustic in the core and cladding. In planar geometry tunneling is due to *frustrated total internal reflection* [2]. Since the profile values at the caustics are equal by definition, i.e. $n(x_{\text{tp}}) = n(x_{\text{rad}}) = \bar{\beta}$, *tunneling can only occur on planar waveguides if there is a dip in the profile between caustics*. Although we have not considered such profiles in Part I, one reason for giving Eq. (35–35) is to show how to derive the transmission coefficient in the simplest geometry possible. A second reason is that the generalization of Eq. (35–35) to circular geometry is then straightforward, as we show below in Section 35–12.

Refracting rays

Clad planar waveguides with continuous graded profiles have an abrupt change in profile slope at the core–cladding interface, e.g. the clad parabolic profile of Fig. 1–10. As discussed in Section 7–2, the discontinuity in profile slope is responsible for the reflection of ray power from the interface. The situation is illustrated in Fig. 35–4(b), where the medium $x \geq \rho$ has uniform refractive index n_{cl} and the medium $x \leq \rho$ has a graded profile $n(x)$ such that $n(0) = n_{\text{cl}}$. The incident and reflected rays are represented by the expressions in Eq. (35–32a) with $x_{\text{tp}} = \rho$, and the transmitted ray by the first expression in Eq. (35–17b). Continuity of $\Psi^i + \Psi^r$ and Ψ^t and the corresponding first derivatives at $x = \rho$ determine B and C in terms of A . The derivative of $k_x(x)$ is obtained by first expressing $k_x(x)$ in terms of $n(x)$ and $\bar{\beta}$ through Eq. (35–27), and we note that $k_x(\rho) = kn_{\text{cl}} \sin \theta_t$. By forming the combination $1 - |B/A|^2$, we deduce that the transmission coefficient is [9]

$$T = 1 / \left\{ 1 + \left(\frac{\kappa}{8kn_{\text{cl}}^3 \sin^3 \theta_t} \right)^2 \right\}, \quad \kappa = - \left. \frac{dn^2(x)}{dx} \right|_{\rho-}, \quad (35-36a)$$

$$\cong 1 - \left(\frac{\kappa}{8kn_{\text{cl}}^3} \right)^2 \frac{1}{\sin^6 \theta_t}, \quad (35-36b)$$

where the approximation is valid when the second term is small compared to unity. The derivative is evaluated on the core side of the interface. As the wavelength $\lambda \rightarrow 0$, then $k \rightarrow \infty$ and $T \rightarrow 1$. In other words all the power of the incident ray crosses the interface in the classical geometric optics limit, as was assumed in Chapters 1 and 2.

35–10 Planar caustics and absorbing media

In this section we generalize the procedure given in the second half of Section 35–7 to apply to graded media. Thus we consider the situation Fig. 35–5(a) which has application to planar waveguides with a nonabsorbing core and an absorbing cladding. The medium $x > \rho$ is uniform and slightly absorbing with refractive index $n_{\text{cl}} = n_{\text{cl}}^r + in_{\text{cl}}^i$, where $n_{\text{cl}}^i \ll n_{\text{cl}}^r$, and the medium $x < \rho$ is graded and nonabsorbing with refractive-index profile $n(x)$ satisfying $n(\rho) = n_{\text{cl}}^r$. A ray, which would be totally reflected if $n_{\text{cl}}^i = 0$, touches the caustic $x = x_{\text{tp}}$. By analogy with Fig. 35–3(b), we extend the ray tube beyond the caustic, as shown in Fig. 35–5(a). The evanescent fields are denoted by

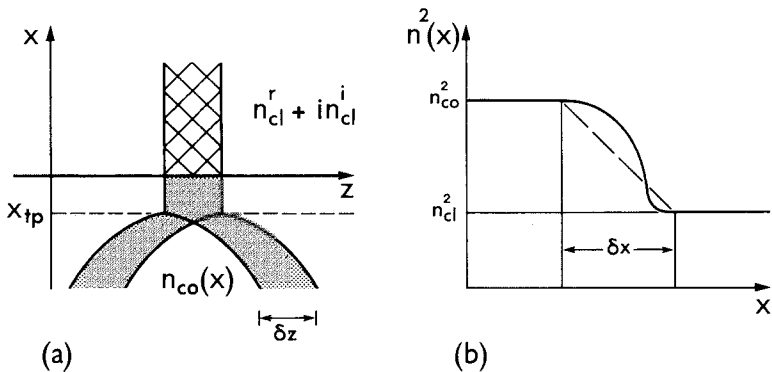


Fig. 35-5 (a) A ray reflects from the turning-point caustic and part of the power flow, shown shaded, is absorbed in the hatched region. (b) Graded profiles showing an arbitrary variation as the solid curve and a linear variation as the dashed curve.

Ψ^t of Eq. (35-32c) with $F = A$. For $x \geq \rho$ the function $|k_x(x)| = |k_x(\rho)| \cong \{\beta^2 - k^2(n_{cl}^r)^2\}^{1/2}$ is constant, whence we deduce that

$$\Psi^t = A \frac{\exp\{-(x-\rho)|k_x(\rho)|\}}{|k_x(\rho)|^{1/2}} \exp\left\{-\int_{x_{tp}}^{\rho} |k_x(x)| dx\right\}. \quad (35-37)$$

The power absorbed from the evanescent field in the hatched region of Fig. 35-5(a) is given by the first expression in Eq. (35-26). On substituting for Ψ^t we obtain

$$P_{abs} = \frac{|A|^2}{2} \frac{k^2 n_{co} n_{cl}^i \delta z}{\beta^2 - k^2 (n_{cl}^r)^2} \left(\frac{\epsilon_0}{\mu_0}\right)^{1/2} \exp\left\{-2 \int_{x_{tp}}^{\rho} |k_x(x)| dx\right\}. \quad (35-38)$$

The ratio of P_{abs} to P_{inc} of Eq. (35-34) gives the transmission coefficient. We express β in terms of the ray invariant $\bar{\beta}$ using the relationship in Table 36-1, page 695, and n_{cl}^i in terms of the power absorption coefficient α_{cl} of Eq. (6-19). Hence

$$T = \frac{\alpha_{cl}}{2k \bar{\beta}^2 - (n_{cl}^r)^2} \frac{n_{co}}{\bar{\beta}^2 - (n_{cl}^r)^2} \exp\left\{-2k \int_{x_{tp}}^{\rho} [\bar{\beta}^2 - n^2(x)]^{1/2} dx\right\}, \quad (35-39a)$$

which applies to all bound rays with the exception of the small number which have turning-point caustics virtually coincident with the interface. If the core medium $x < \rho$ is also absorbing, we superpose the power attenuation coefficients for core and cladding absorption, as expressed by Eq. (6-30).

Linear approximation

Only those rays with turning-point caustics not too far from the interface suffer significant power loss, i.e. when $x_{tp} \cong \rho$ in Fig. 35-5(a). By analogy with Eq. (6-23), we

can then make a Taylor expansion of the expression in the integrand of Eq. (35-39a) about $x = x_{tp}$, and by paralleling the derivation of Eq. (6-24) we deduce that relative to the interface $x = \rho$ of the waveguide

$$T = \frac{\alpha_{cl}}{2k\bar{\beta}^2 - (n_{cl}^r)^2} \exp \left\{ -\frac{4}{3}k\rho \left[-\rho \frac{dn^2(x)}{dx} \right]_{\rho^-} \right\} \left(1 - \frac{x_{tp}^2}{\rho^2} \right)^{3/2}, \quad (35-39b)$$

where the derivative is evaluated on the core side of the interface.

35-11 Continuous and discontinuous profiles

Our derivation of the transmission coefficient in earlier sections has considered graded and step profiles separately. This division is necessary because the local plane-wave, or WKB, solution of the scalar wave equation for a continuous graded profile does not approach the solution for a step profile, when the grading is concentrated at the interface. Consider, for example, the clad power-law profiles in the neighborhood of $x = \rho$ in Fig. 1-10. As q increases, the profile steepens and violates the requirement that $n(x)$ vary slowly over a distance equal to a wavelength of light. This is why the transmission coefficient for a graded profile given by Eq. (35-35) does not reduce to the step-profile expression of Eq. (35-20) as the turning-point caustic approaches the interface, i.e. $x_{tp} \rightarrow \rho$ in Fig. (35-4a).

However, if we knew the *exact* solution of the scalar wave equation for a graded profile, we would recover the step-profile results in the appropriate limit. The step profile is indistinguishable from any number of graded profiles, as typified by the solid curve in Fig. 35-5(b), with the property that the variation from uniform index n_{co} to uniform index n_{cl} occurs over a distance δx which is much smaller than the wavelength of light. Accordingly, we can model a step discontinuity by any graded profile with this behavior, and if we take the limit $\delta x \rightarrow 0$ of the transmission coefficient for the graded profile, we will recover the Fresnel expression of Eq. (35-20). This has been verified in the case when the profile variation is linear—denoted by the dashed line in Fig. 35-5(b)—and the solutions of the scalar wave equation are expressible in terms of Airy functions [10].

Graded profiles with a step discontinuity

The transmission coefficient of Eq. (35-35) for tunneling rays assumes a continuous profile. If we introduce a step discontinuity at the interface $x = \rho$, in Fig. 35-4(a), and assume that the fields on either side remain evanescent, it may be shown that the effect of the discontinuity is to multiply the transmission coefficient by an extra factor $|T_f|$, so that [11]

$$T = |T_f| \exp \left\{ -2k \int_{x_{tp}}^{x_{rad}} \{ \bar{\beta}^2 - n^2(x) \}^{1/2} dx \right\}, \quad (35-40a)$$

$$T_f = \frac{4(n_+^2 - \bar{\beta}^2)^{1/2} (n_-^2 - \bar{\beta}^2)^{1/2}}{\{ (n_+ - \bar{\beta}^2)^{1/2} + (n_- - \bar{\beta}^2)^{1/2} \}^2}, \quad (35-40b)$$

where n_+ and n_- are the values of $n(x)$ at the top and bottom of the step, and T_l is the *analytical continuation* of the Fresnel expression of Eq. (35-20), since the square roots within the expression are imaginary.

35-12 Circular interfaces and caustics

The derivations given above for the transmission coefficients are directly applicable to planar multimode waveguides. With minor modifications they also apply to multimoded fibers of *circular* cross-section, where rays are incident at cylindrical interfaces and caustics. This requires the cylindrical surfaces to appear planar over distances comparable with the wavelength of light. The dependence of the transmission coefficients of Eqs. (35-35) and (35-39a) on profile is always through the combination $k\{\bar{\beta}^2 - n^2(x)\}^{1/2}$. In regions where rays propagate this is the transverse component $k_x(x)$ of the local wave vector as expressed by Eq. (35-27) and in the region where the fields are evanescent it is given by $|k_x(x)|$. Because of the circular symmetry of the fiber, it is intuitive that we can extend the planar results to cylindrical geometry simply by replacing $k_x(x)$ with $k_r(r)$, where $k_r(r)$ is the radial component of the local wave vector in regions where rays propagate, and is defined by

$$k_r(r) = kn(r)\cos\alpha(r) = \left\{k^2 n^2(r) - \beta^2 - \frac{v^2}{r^2}\right\}^{1/2} = k\left\{n^2(r) - \bar{\beta}^2 - \bar{l}^2 \frac{\rho^2}{r^2}\right\}^{1/2}, \quad (35-41)$$

where $n(r)$ is the fiber profile, $\alpha(r)$ is the angle between the wave vector and the radial direction and v is the azimuthal order. Relationships between $\alpha(r)$, $\bar{\beta}$ and \bar{l} are given by Eqs. (2-14), (2-16) and (2-17), and between β , v , $\bar{\beta}$ and \bar{l} are listed in Table 36-1, page 695.

Solution of the scalar wave equation

The above procedure must of course give results identical to solving the scalar wave equation asymptotically, in analogy with Section 35-8. Accordingly we solve this equation analytically using the WKB approximation and then show that the solutions are identical to the intuitive local plane-wave solutions of Section 35-3. The most general situation for a fiber of radius ρ with graded core index $n(r)$ and uniform cladding index $n_{cl} = n(\rho)$ is illustrated in Fig. 35-6. A tunneling ray is incident on the turning-point caustic of radius r_{tp} and the transmitted ray originates on the radiation caustic at radius r_{rad} in the cladding. Because of the azimuthal and longitudinal symmetry, we seek solutions of the scalar wave equation of the form

$$\chi(r, \phi, z) = \Psi(r) \exp(iv\phi) \exp(i\beta z), \quad (35-42)$$

in cylindrical polar coordinates (r, ϕ, z) relative to the fiber axis, where β is the propagation constant and v is the azimuthal order. The function $\Psi(r)$ satisfies

$$\left\{ \frac{d^2}{dr^2} + \frac{1}{r} \frac{d}{dr} + k^2 n^2(r) - \frac{v^2}{r^2} - \beta^2 \right\} \Psi = 0, \quad (35-43a)$$

which can be solved by first making the change of variable $w = \ln r$. This leads to the

Transmission coefficient for tunneling rays in graded-profile fibers

If we replace x by r , $\delta l(x)$ by $\delta A(r)$ and $k_x(x)$ by $k_r(r)$ throughout Section 35-9, the derivation of the power transmission, or tunneling, coefficient for the circular fiber is identical to that for the planar waveguide. Accordingly we deduce from Eqs. (35-35) and (35-41) that [6]

$$T = \exp \left\{ -2k \int_{r_{tp}}^{r_{rad}} \left[\bar{\beta}^2 + \bar{\Gamma}^2 \frac{\rho^2}{r^2} - n^2(r) \right]^{1/2} dr \right\}, \quad (35-45)$$

provided that r_{tp} and r_{rad} are not too close together.

Transmission coefficient for tunneling rays in step-profile fibers

The corresponding result for a step-profile fiber can also be obtained from Section 35-9 by making the change in notation defined above Eq. (35-45), and, in addition, setting $x_{tp} = \rho$ in Eqs. (35-32) and (35-33), and $n(x) = n_{co}$ in Eq. (35-32a). We use the connecting formula of Eq. (35-33) to express C in terms of F , and then express F in terms of A by imposing continuity of $\Psi^i + \Psi^r$ and Ψ^e and their first derivatives at $x = \rho$. This leads to [12, 13]

$$T = |T_f| \exp \left\{ -2k \int_{\rho}^{r_{rad}} \left[\bar{\beta}^2 + \bar{\Gamma}^2 \frac{\rho^2}{r^2} - n_{cl}^2 \right]^{1/2} dr \right\}, \quad (35-46a)$$

where T_f is the analytic continuation of the Fresnel coefficient defined by

$$T_f = \frac{4(n_{co}^2 - \bar{\Gamma}^2 - \bar{\beta}^2)^{1/2} (n_{cl}^2 - \bar{\Gamma}^2 - \bar{\beta}^2)^{1/2}}{\{ (n_{co}^2 - \bar{\Gamma}^2 - \bar{\beta}^2)^{1/2} + (n_{cl}^2 - \bar{\Gamma}^2 - \bar{\beta}^2)^{1/2} \}^2}. \quad (35-46b)$$

For a tunneling ray, the first root in the numerator is real and the second root is pure imaginary. Consequently

$$|T_f| = \frac{4}{n_{co}^2 - n_{cl}^2} (n_{co}^2 - \bar{\Gamma}^2 - \bar{\beta}^2)^{1/2} (\bar{\Gamma}^2 + \bar{\beta}^2 - n_{cl}^2)^{1/2}. \quad (35-46c)$$

This result is a particular case of Eq. (35-40) in cylindrical geometry, when there are local plane-wave fields on one side of the interface and evanescent fields on the other.

Linear approximation

When the caustics are not too far from the core-cladding interface, the integrals in Eqs. (35-45) and (35-46a) can be evaluated approximately. For example, the contribution from the core over the range $r_{tp} \leq r \leq \rho$ is obtained by linearizing the expression within the square brackets of the integrand by making a Taylor expansion about $r = \rho$ and retaining only the first two terms. Hence we set

$$\bar{\beta}^2 + \bar{\Gamma}^2 \frac{\rho^2}{r^2} - n^2(r) \cong \bar{\beta}^2 + \bar{\Gamma}^2 - n_{cl}^2 + \frac{\rho - r}{\rho} \left\{ 2\bar{\Gamma}^2 + \frac{dn^2(r)}{dr} \right\} \bigg|_{\rho-}. \quad (35-47)$$

On performing the integration, there is no contribution from the lower limit of integration because the left side of the above equation is zero at $r = r_{tp}$. Thus

$$\int_{r_{tp}}^{\rho} \left[\bar{\beta}^2 + \bar{l}^2 \frac{\rho^2}{r^2} - n^2(r) \right]^{1/2} dr \cong \frac{2}{3} \rho \frac{(\bar{\beta}^2 + \bar{l}^2 - n_{cl}^2)^{3/2}}{\kappa \rho n_{cl}^2 - 2\bar{l}^2}; \quad \kappa = - \frac{1}{n_{cl}^2} \frac{dn^2(r)}{dr} \Big|_{r=\rho-}, \quad (35-48a)$$

in terms of the slope of the core profile at the interface. Similarly, the contribution to the integral from the cladding is given by

$$\int_{\rho}^{r_{rad}} \left[\bar{\beta}^2 + \bar{l}^2 \frac{\rho^2}{r^2} - n_{cl}^2 \right]^{1/2} dr \cong \frac{2}{3} \frac{\rho}{\bar{l}^2} (\bar{\beta}^2 + \bar{l}^2 - n_{cl}^2)^{1/2}, \quad (35-48b)$$

and the transmission coefficient follows from Eq. (35-45) as

$$T \cong \exp \left\{ - \frac{2}{3} k \rho \frac{\kappa \rho n_{cl}^2}{\kappa \rho n_{cl}^2 - 2\bar{l}^2} \frac{(\bar{\beta}^2 + \bar{l}^2 - n_{cl}^2)^{3/2}}{n_{cl}^2 - \bar{\beta}^2} \right\}, \quad (35-49a)$$

where κ is defined by Eq. (45-48a) and $\bar{l}^2 \cong n_{cl}^2 - \bar{\beta}^2$ since $r_{rad} \cong \rho$. A similar approximation can be made for the step-profile fiber, whence we deduce from Eqs. (35-46) and (35-48b) that

$$T \cong |T_f| \exp \left\{ - \frac{2}{3} k \rho \frac{(\bar{\beta}^2 + \bar{l}^2 - n_{cl}^2)^{3/2}}{n_{cl}^2 - \bar{\beta}^2} \right\}, \quad (35-49b)$$

where $|T_f|$ is given by Eq. (35-46c), and $\bar{l} \cong n_{cl}^2 - \bar{\beta}^2$ in this approximation. This ensures $T \rightarrow 0$ as $\bar{\beta} \rightarrow n_{cl}$, i.e. the limit of bound rays.

Refracting rays

Within the core of a step-profile fiber, we use the Fresnel coefficient to describe the fraction of power lost by rays which undergo refraction at the interface. In Fig. 35-1(b), the incident and transmitted rays make angles α_i and α_t , respectively, with the normal, or radial, direction. If we ignore polarization, then Eq. (35-20) is replaced by

$$T = \frac{4n_{co}n_{cl}\cos\alpha_i\cos\alpha_t}{(n_{co}\cos\alpha_i + n_{cl}\cos\alpha_t)^2}; \quad n_{co}\sin\alpha_i = n_{cl}\sin\alpha_t. \quad (35-50)$$

The corresponding expression for graded profiles is discussed in Section 7-3.

35-13 Circular interfaces, caustics and absorbing media

The transmission coefficient for tunneling rays within a graded profile is given by Eq. (35-45), and is a simple generalization of the corresponding planar-waveguide expression in Eq. (35-35). It should then be evident from the discussion of the previous section and the derivation in Section 35-9, that the transmission coefficient for a nominally bound ray propagating within a graded-profile fiber with a nonabsorbing core and a slightly absorbing cladding is given by the corresponding generalization of

Eq. (35-39). Hence

$$T = \frac{\alpha_{cl}}{2k} \frac{n_{co}}{\beta^2 + l^2 - (n_{cl}^r)^2} \exp \left\{ -2k \int_{r_{tp}}^{\rho} \left[\beta^2 + l^2 \frac{\rho^2}{r^2} - n^2(r) \right]^{1/2} dr \right\}, \quad (35-51)$$

where $n_{cl} = n_{cl}^r + in_{cl}^i$ is the cladding index. The corresponding expression valid within the linear approximation is derived in Section 6-7 and expressed by Eq. (6-24).

Step-profile fibers

The appropriate expression for the transmission coefficient when a nominally bound ray propagates within a step-profile fiber with slightly absorbing core and cladding is obtained from Eq. (35-25) by referring the ray direction to the normal, or radial, direction in Fig. 35-1(a), i.e. by replacing θ_z by $\pi/2 - \alpha_i$. Hence

$$T = \frac{4}{\theta_c^2 \{ \theta_c^2 - (\pi/2 - \alpha_i)^2 \}^{1/2}} \left\{ \frac{n_{cl}^i}{n_{cl}^r} - \frac{n_{co}^i}{n_{co}^r} \right\}, \quad (35-52)$$

provided $\pi/2 - \alpha_i$ is not too close to θ_c .

35-14 Interfaces and caustics defined by two radii of curvature

In general, the concept of a power transmission coefficient for leaky rays propagating along waveguides of arbitrary profile and cross-section is meaningful only if the transmission coefficient is determined by the local geometry. Thus, in Section 7-13 we introduced the concept of locally valid transmission coefficients to describe ray power losses in waveguides where the curvature of the interface or caustic changes along the path, e.g. noncircular fibers and bent fibers. The transmission coefficient is locally valid provided the turning point or interface and the radiation caustic are not too far apart, otherwise the transmitted power depends on the macroscopic shape of the waveguide and a local description is inaccurate.

Reflection at an interface - step profile

We first consider the interface in Fig. 35-7(a) between media of uniform refractive indices n_{co} and n_{cl} . The y - and z -axes at P on the interface are in the principal planes of curvature, and the corresponding principal radii of curvature are ρ_y and ρ_z . A ray reflects at P, making angles α_i , θ_y , and θ_z with the normal, y - and z -directions, respectively. The transmission coefficient for tunneling rays can then be written down from a knowledge of the corresponding transmission coefficient for a circular interface, derived in Section 35-12.

Tunneling rays whose radiation caustics are not too far from the interface of a circular fiber have a transmission coefficient given by Eq. (35-49b). We replace the ray invariants in the exponent by their definitions of Eq. (2-7) in terms of the angles shown

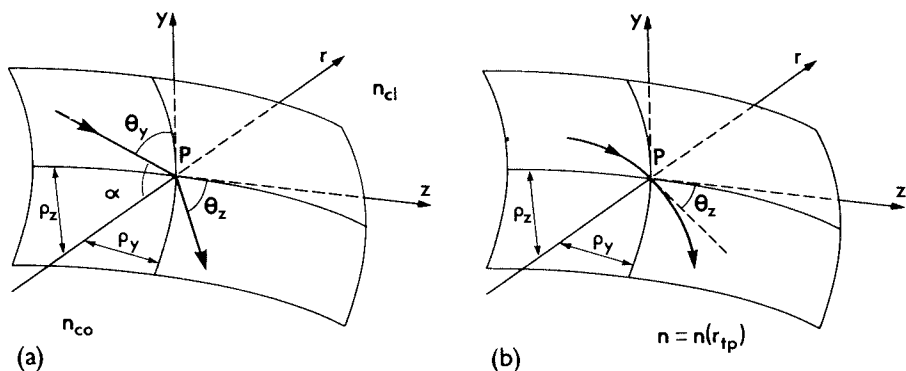


Fig. 35-7 (a) A ray path reflects from an arbitrarily curved interface between uniform media of refractive indices n_{co} and n_{cl} . (b) In a graded medium the ray path touches the arbitrarily curved surface $n = n(r_{ip})$ which defines the turning-point caustic.

in Fig. 2-3, and obtain

$$T = |T_r| \exp \left\{ -\frac{2}{3} k \bar{\rho} n_{co} \frac{(\sin^2 \alpha - \sin^2 \alpha_c)^{3/2}}{\sin^2 \alpha} \right\}; \quad \bar{\rho} = \rho \frac{\sin^2 \alpha}{\sin^2 \theta_z \cos^2 \theta_\phi}, \quad (35-53)$$

where $\alpha_c = \sin^{-1}(n_{cl}/n_{co})$ is the critical angle. It also follows from Eqs. (2-7) and (35-46c) that $|T_r|$ depends only on α and α_c . With the help of Euler's theorem [14], we show in Section 37-5 that $\bar{\rho}$ is the radius of curvature of the interface in the plane defined by the incident ray and the normal, i.e. the plane of incidence. Thus, for a given wavelength, the transmission coefficient is fully determined by the ray direction relative to the normal and $\bar{\rho}$. We now assert that this also holds for the more general situation in Fig. 35-7(a). In other words the transmission coefficient is given by Eq. (35-53), and the radius of curvature in the plane of incidence is now given by Eq. (37-135) as [12]

$$\bar{\rho} = \frac{\rho_y \rho_z \sin^2 \alpha}{\rho_y \cos^2 \theta_z + \rho_z \cos^2 \theta_y}, \quad (35-54)$$

which reduces to the expression for the circular interface when $\rho_z \rightarrow \infty$. This assertion may be verified formally by straightforward analysis [12, 15] which also shows that Eq. (35-53) is valid provided $k \bar{\rho} n_{co} \gg 1/\cos^3 \alpha$.

Reflection at a caustic – graded media

A similar result applies to a graded medium, where the situation is illustrated in Fig. 35-7(b) using the notation of Fig. 35-7(a). A ray touches the turning-point caustic at P and the tangent to the path there, which lies in the plane of the caustic, makes angles θ_z and $\pi/2 - \theta_z$ with the z- and y-directions, respectively. The surface of constant index $n(r) = n(r_{ip})$ has principal radii of curvature ρ_y and ρ_z .

Within the linear approximation, tunneling rays on graded-profile circular fibers with turning-point and radiation caustics which are not too far from the interface have the transmission coefficient given by Eq. (35-49a). If the ray invariants are $\bar{\beta}$ and \bar{I} , then it is clear from Eqs. (2-17), (2-19) and Fig. 35-7(b) that $\bar{\beta}^2 + \bar{I}^2 \cong n^2(r_{\text{tp}})$ and $\bar{I} \cong n(r_{\text{tp}}) \sin \theta_z$, since $r_{\text{tp}} \cong \rho$, whence

$$T = \exp \left\{ -\frac{2}{3} k \bar{\rho} n_{\text{cl}} \frac{\kappa \bar{\rho}}{\kappa \bar{\rho} - 2} \left[\frac{n^2(r_{\text{tp}})}{n_{\text{cl}}^2} - 1 \right]^{3/2} \right\}; \quad \bar{\rho} = \frac{\rho}{\sin^2 \theta_z}, \quad (35-55)$$

since $n(r_{\text{tp}}) \cong n_{\text{co}} \cong n_{\text{cl}}$. In Section 37-5 we use Euler's theorem [14] to show that $\bar{\rho}$ is the radius of curvature of the interface in the plane defined by the tangent to the ray path at the turning point and the radial direction, i.e. the plane of incidence. We now claim that Eq. (35-55) holds for the situation in Fig. 35-7(b), when the radius of curvature in the plane of incidence is given by Eq. (37-134) as

$$\bar{\rho} = \frac{\rho_y \rho_z}{\rho_y \cos^2 \theta_z + \rho_z \sin^2 \theta_z}. \quad (35-56)$$

The general result expressed by Eq. (35-55) can be derived formally [16], and is valid provided $k \bar{\rho} n_{\text{co}} \gg 1$.

35-15 Fields in the neighborhood of caustics

The fields of a waveguide in the neighborhood of the turning-point or radiation caustics do not have the simple plane-wave or evanescent behavior of the WKB solutions of Section 35-7. This is why the expressions for the transmission coefficient derived earlier in the chapter are not valid as these caustics approach one another. In most practical situations this limit is of little consequence since a large fraction of ray power is lost at each reflection and the ray attenuates very rapidly along the waveguide. However, it is convenient to have expressions for computational purposes, such as the bent fiber calculations of Chapter 9, which are uniformly valid for any value of the transmission coefficient, regardless of whether the leaky ray is a tunneling or refracting ray.

Solution of the scalar wave equation

By ignoring polarization, the fields of a fiber depend on the solution of the scalar wave equation, as represented by Eq. (35-43a). In the neighborhood of, say, the turning-point caustic, we linearize the second term within the curly brackets of the transformed equation given by Eq. (35-43b). Hence

$$k_r^2(w) \exp(2w) \cong (w - w_{\text{tp}}) \left[\frac{d}{dw} \{k_r^2(w) \exp(2w)\} \right]_{w_{\text{tp}}}, \quad (35-57)$$

since $k_r(w_{\text{tp}}) = 0$ by definition, and $w_{\text{tp}} = \ln r_{\text{tp}}$. If we substitute this into Eq. (35-43b) and change variable, then

$$\left\{ \frac{d^2}{d\zeta^2} - \zeta \right\} \Psi = 0; \quad \zeta = -(w - w_{\text{tp}}) \left[\frac{d}{dw} \{k_r^2(w) \exp(2w)\} \right]_{w_{\text{tp}}}^{1/3}, \quad (35-58)$$

and Ψ satisfies Airy's equation [17], with the general solution

$$\Psi(\zeta) = C \text{Ai}(\zeta) + D \text{Bi}(\zeta), \quad (35-59)$$

where Ai and Bi are Airy functions of the first and second kinds, and C and D are constants. A similar expression applies in the neighborhood of the radiation caustic. The constants are determined by matching the asymptotic forms of the solution well away from the caustics, i.e. in the limit $\zeta \rightarrow \pm \infty$, to the local plane-wave fields and satisfying continuity of Ψ and its first derivative at the interface [4,9]. The transmission coefficient for rays whose turning-point and radiation caustics are close together is constructed from Eq. (35-59), and it may be shown to reduce to the tunneling-ray expression of Eq. (35-49a) in one limit and to the refracting-ray expression of Eq. (35-36) in the other limit [9].

Uniform approximations

Following the above discussion, there are three forms of the transmission coefficient which, respectively, apply to tunneling rays, refracting rays and the transition from tunneling to refracting rays. This is inconvenient for computational purposes involving many ray directions, and can be avoided by using the method of *uniform approximations* to solve the scalar wave equation [17]. The three forms are replaced by a single expression which is uniformly valid for all leaky rays [18].

REFERENCES

1. Stewart, W. J. (1975) *Proceedings of the First European Conference on Optical Communication*, London.
2. Born, M. and Wolf, E. (1975) *Principles of Optics*, Pergamon Press, Oxford.
3. Jones, D. S. (1964) *The Theory of Electromagnetism*, Pergamon Press, New York.
4. Felsen, L. B. and Marcuvitz, N. (1973) *Radiation and Scattering of Waves*, Prentice-Hall, Englewood Cliffs, N.J.
5. Johnson, C. C. (1965) *Field and Wave Electrodynamics*, McGraw-Hill, New York.
6. Snyder, A. W. and Love, J. D. (1976) Attenuation coefficient for rays in graded fibers with absorbing cladding. *Electron. Lett.*, **12**, 255-7.
7. Mathews, J. and Walker, R. L. (1965) *Mathematical Methods of Physics*, Benjamin, New York.
8. Snyder, A. W. and Love, J. D. (1976) Attenuation coefficient for tunnelling leaky rays in graded fibers. *Electron. Lett.*, **12**, 324-6.
9. Love, J. D. and Winkler, C. (1978) Refracting leaky rays in graded-index fibers. *Appl. Opt.*, **17**, 2205-8.
10. Love, J. D. and Winkler, C. (1978) The step index limit of power law refractive index profiles for optical waveguides. *J. Opt. Soc. Am.*, **68**, 1188-91.
11. Love, J. D. and Winkler, C. (1977) Attenuation and tunneling coefficients for leaky rays in multilayered optical waveguides. *J. Opt. Soc. Am.*, **67**, 1627-33.
12. Snyder, A. W. and Love, J. D. (1975) Reflection at a curved interface—electromagnetic tunneling. *I.E.E.E. Trans. Microwave Theory Tech.*, **23**, 134-41.
13. Love, J. D. and Winkler, C. (1978) The effects of material absorption on ray power attenuation in multi-layered optical waveguides. *Opt. Quant. Elect.*, **10**, 383-92.

14. Korn, G. A. and Korn, T. M. (1968) *Mathematical Handbook for Scientists and Engineers*, McGraw-Hill, New York.
15. Jones, D. S. (1978) Electromagnetic tunnelling. *Quart. J. Mech. Appl. Math.*, **31**, 409–34.
16. Love, J. D. and Winkler, C. (1980) Generalized Fresnel power transmission coefficients for curved graded-index media. *I.E.E.E. Trans. Microwave Theory Tech.*, **28**, 689–94.
17. Abramowitz, M. and Stegun, I. (1964) *Handbook of Mathematical Functions*, Dover, New York.
18. Love, J. D. and Winkler, C. (1978) A universal tunnelling coefficient for step- and graded-index multimode fibers. *Opt. Quant. Elect.*, **10**, 341–51.

Rays and asymptotic modal methods

Ray decomposition of a mode	693
36-1 Step-profile planar waveguide	693
36-2 Step-profile fiber	693
36-3 Free-space decomposition	695
 Asymptotic modal description of propagation	696
36-4 Modal fields	696
36-5 Propagation constants	697
36-6 Step-profile planar waveguide	697
36-7 Infinite parabolic-profile fiber	698
36-8 Infinite power-law profiles	699
36-9 Transit times	700
36-10 Absorbing waveguides	700
36-11 Leaky modes and leaky rays	703
 Number of modes on multimode fibers	704
36-12 Step-profile planar waveguide	704
36-13 Step-profile fiber	705
 Field shift on bent fibers	706
36-14 Derivation of the effective profile	706
36-15 <i>Example: Gaussian approximation</i>	707
 References	708

In the previous chapter we discussed intuitive notions concerning the propagation of rays, or local plane waves, to complement the ray description of propagation along multimode waveguides in Part I. An alternative description is provided by the modal methods of Part II. A discrete superposition of the fields of a large number of modes is required, in general, to describe the total fields of a multimode waveguide, and as a result the role of individual modes becomes obscured. This is consistent with a continuous superposition of rays. We emphasize that the asymptotic modal analysis involves an unnecessary intermediate step—the eigenvalue equation. This equation introduces conceptual complications and in general can only be solved by numerical methods.

The main purpose of this chapter is to demonstrate the equivalence of the ray and asymptotic modal descriptions of multimode waveguides. We begin by deriving the asymptotic relationship between a mode of the waveguide and the equivalent family of

rays, or local plane waves, and then reverse the situation by showing how the mode can be constructed from local plane waves using simple consistency conditions.

RAY DECOMPOSITION OF A MODE

The fields of a mode within regions of an arbitrary waveguide where rays can propagate is expressible, in general, as a superposition of local plane wave fields over all ray directions. A noted exception is the step-profile planar waveguide discussed below, for which only two ray directions are involved. This apart, modes which can propagate *only* on multimode waveguides are asymptotically equivalent to a *single* family of rays, each ray having the same propagation characteristics, e.g. common values of the ray invariants $\bar{\beta}$ and \bar{T} on a circular fiber, as we show for the step-profile fiber below.

36-1 Step-profile planar waveguide

The trigonometrical dependence of the core fields for the modes of the step-profile planar waveguide in Table 12-1, page 242, can be decomposed into two components. For example, the electric field for the even TE modes is expressible as

$$e_y = \{ \exp(iUx) + \exp(-iUx) \} / 2 \cos U = e_y^+ + e_y^-, \quad (36-1)$$

where suffices + and - correspond to positive and negative exponents. Relative to the cartesian axes in Fig. 12-1, we define plane-wave vectors with components

$$\mathbf{k}^\pm = (\pm U/\rho, 0, \beta) = kn_{co} (\pm \sin \theta_z, 0, \cos \theta_z) = k (\pm \{n_{co}^2 - \bar{\beta}^2\}^{1/2}, 0, \bar{\beta}), \quad (36-2)$$

where θ_z is the angle between the direction of propagation and the waveguide axis, and remaining parameters are defined inside the covers. With the help of the eigenvalue equation in Table 12-2, page 243, we deduce from Table 12-1 that

$$\mathbf{h}^\pm = \left(\frac{\varepsilon_0}{\mu_0} \right)^{1/2} \frac{1}{k} \mathbf{k}^\pm \times \mathbf{e}^\pm; \quad \mathbf{e}^\pm \cdot \mathbf{h}^\pm = 0, \quad (36-3)$$

and each triad $(\mathbf{e}^+, \mathbf{h}^+, \mathbf{k}^+)$, $(\mathbf{e}^-, \mathbf{h}^-, \mathbf{k}^-)$ consists of mutually orthogonal vectors. Thus the fields at any position P in the core are a superposition of the fields of two plane waves propagating towards and away from the axis at angle θ_z , as indicated in Fig. 36-1(a). The same interpretation applies to all the remaining modes in Table 12-1, as may be verified.

36-2 Step-profile fiber

In contrast to the planar waveguide, the core fields of the circular fiber, which are given in terms of Bessel functions in Table 12-3, page 250, do not represent a single family of rays [1]. However, the fields of higher-order modes, which have $U \gg 1$, are asymptotically equivalent to a single family. To demonstrate this, we first use the recurrence relations of Eq. (37-72) to express $J_{v \pm 1}$ in Table 12-3 in terms of J_v and its derivative. Then, provided $U \gg 1$ and $U - v \gg v^{1/3}$, we can substitute the far Debye approximations of Eq. (37-89). The azimuthal dependence on $\sin(v\phi)$ or $\cos(v\phi)$ is

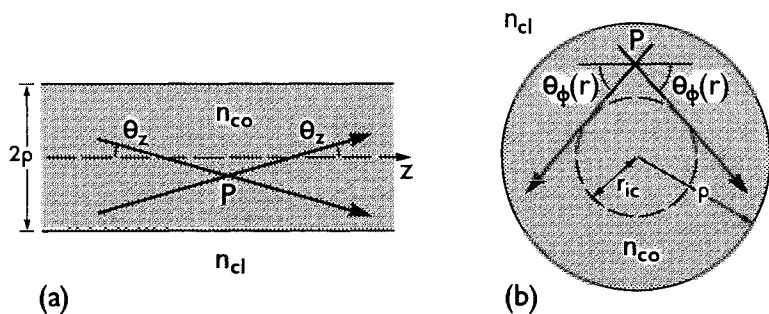


Fig. 36-1 Local plane wave decomposition of the modal fields within (a) the core of a step-profile planar waveguide and (b) the core cross-section of a step-profile fiber.

decomposed in an analogous manner to Eq. (36-1). If suffices + and - denote field variations $\exp(\pm i\nu\phi)$, respectively, then

$$e_r^\pm = f \left\{ 1 \pm i \frac{\nu F_2}{g^2} \right\} \exp(\pm i\chi), \quad (36-4a)$$

$$h_r^\pm = f n_{co}^2 \frac{k}{\beta} \left(\frac{\epsilon_0}{\mu_0} \right)^{1/2} \left\{ i F_1 \mp \frac{\nu}{g^2} \right\} \exp(\pm i\chi), \quad (36-4b)$$

$$e_\phi^\pm = f \left\{ \frac{\nu}{g^2} \mp i F_2 \right\} \exp(\pm i\chi), \quad (36-4c)$$

$$h_\phi^\pm = f n_{co}^2 \frac{k}{\beta} \left(\frac{\epsilon_0}{\mu_0} \right)^{1/2} \left\{ i \frac{\nu F_1}{g^2} \pm 1 \right\} \exp(\pm i\chi), \quad (36-4d)$$

$$e_z^\pm = -f \frac{R U^2}{\beta \rho g^2} \exp(\pm i\chi), \quad (36-4e)$$

$$h_z^\pm = -i f \left(\frac{\epsilon_0}{\mu_0} \right)^{1/2} \frac{U^2 R F_2}{\rho g^2} \exp(\pm i\chi), \quad (36-4f)$$

where F_1 and F_2 are defined in Table 12-3 and are related in Table 12-4, page 253. The functions f and g are given by

$$f = ig / \{ (2\pi)^{1/2} U R J_\nu(U) \}; \quad g = (U^2 R^2 - \nu^2)^{1/4}. \quad (36-4g)$$

If we include the z -dependence of Eq. (12-10), then the accumulated phase follows as

$$\chi + \beta z = (U^2 R^2 - \nu^2)^{1/2} - \nu \cos^{-1}(\nu/UR) - \pi/4 + \nu\phi + \beta z. \quad (36-4h)$$

We define plane-wave vectors \mathbf{k}^\pm with components relative to the radial, azimuthal and longitudinal directions in Fig. 12-3 given by

$$\mathbf{k}^\pm = \{ \pm (U^2 R^2 - \nu^2)^{1/2} / R\rho, \nu / R\rho, \beta \}, \quad (36-5a)$$

$$= k n_{co} \{ \pm \cos \alpha(r), \sin \theta_z \cos \theta_\phi(r), \cos \theta_z \}, \quad (36-5b)$$

$$= k \{ \pm (n_{co}^2 - \bar{\beta}^2 - \bar{l}^2 / R^2)^{1/2}, \bar{l} / R, \bar{\beta} \}, \quad (36-5c)$$

where θ_z and $\alpha(r)$ are angles between the direction of propagation and the longitudinal and radial directions at P in Fig. 36-1(b) distance r from the axis, and $\theta_\phi(r)$ is the angle between the azimuthal direction and the projection of the wave vectors onto the fiber cross-section. These relationships follow from generalizations of Eq. (2-7) and the relationships in Table 36-1 between β , v and the ray invariants. Consequently, it is readily verified that the fields of Eq. (36-4) satisfy the relationships of Eq. (36-3). The modal fields at P are asymptotically equivalent to the superposition of the fields of two plane waves propagating towards and away from the interface at angle $\alpha(r)$ to the radial direction.

Table 36-1 Ray and modal parameters for step-profile fibers and planar waveguides. Parameters are defined at the front and back of the book.

$\beta = \frac{2\pi}{\lambda} \bar{\beta} = k\bar{\beta} = kn_{co} \cos \theta_z$ $= \frac{V \cos \theta_z}{\rho \sin \theta_c}$	$v = \frac{2\pi}{\lambda} \rho \bar{l} = k\rho \bar{l} = krn_{co} \sin \theta_z \cos \theta_\phi$ $= U \frac{r}{\rho} \cos \theta_\phi$
$U = k\rho n_{co} \sin \theta_z = k\rho(n_{co}^2 - \bar{\beta}^2)^{1/2}$ $= V \frac{\sin \theta_z}{\sin \theta_c} = \frac{V}{\sin \theta_c} \left\{ 1 - \frac{\bar{\beta}^2}{n_{co}^2} \right\}^{1/2}$	$W = k\rho n_{co} (\sin^2 \theta_c - \sin^2 \theta_z)^{1/2} = k\rho(\bar{\beta}^2 - n_{cl}^2)^{1/2}$ $= V \left\{ 1 - \frac{\sin^2 \theta_z}{\sin^2 \theta_c} \right\}^{1/2} = \frac{V}{\tan \theta_c} \left\{ \frac{\bar{\beta}^2}{n_{cl}^2} - 1 \right\}^{1/2}$
$Q^r = k\rho n_{co} (\sin^2 \theta_z - \sin^2 \theta_c)^{1/2} = V \left\{ \frac{\sin^2 \theta_z}{\sin^2 \theta_c} - 1 \right\}^{1/2}$ $= k\rho(n_{cl}^2 - \bar{\beta}^2)^{1/2} = \frac{V}{\tan \theta_c} \left\{ 1 - \frac{\bar{\beta}^2}{n_{cl}^2} \right\}^{1/2}$	

When $\alpha(r) = \pi/2$, it follows from Eq. (36-5) that all rays touch the cylindrical surface of radius $r_{ic} = \rho v/U$ in Fig. 36-1(b). This is the inner caustic, introduced in Section 2-2. We deduce that only the TE_{0m} and TM_{0m} modes ($v = 0$) are composed of meridional rays, since $r_{ic} = 0$, and all HE_{vm} and EH_{vm} modes are composed of skew rays. We are reminded that all modes are composed of paraxial rays in the weak-guidance approximation.

36-3 Free-space decomposition

In the special case of free space, i.e. an unbounded, uniform medium of refractive-index n , any solution of Maxwell's equations is expressible as a continuous superposition of plane waves, or rays, propagating in all directions. Thus, for example, if the electric field is everywhere parallel to the x -direction on the infinite surface $z = 0$ and has the spatial distribution $E(x, y)$, then [2]

$$E(x, y) = \frac{1}{4\pi^2} \int_{-\infty}^{\infty} \int_{-\infty}^{\infty} S(k_x, k_y) \exp\{i(k_x x + k_y y)\} dk_x dk_y, \quad (36-6)$$

where $k_x = kn \cos \theta_x$ and $k_y = kn \cos \theta_y$ are the x - and y -components, respectively, of the plane-wave vector $n\mathbf{k}$, which has magnitude $nk = n|\mathbf{k}| = 2\pi n/\lambda$ and makes angles θ_x and θ_y with the x - and y -directions. The free-space wavelength is λ . The inverse relationship gives

$$S(k_x, k_y) = \int_{-\infty}^{\infty} \int_{-\infty}^{\infty} E(x, y) \exp\{-i(k_x x + k_y y)\} dx dy, \quad (36-7)$$

where $S(k_x, k_y)$ is the angular spectrum of plane waves.

Cylindrical waves

We can transform Eqs. (36-6) and (36-7) to cylindrical geometry by replacing (x, y) with cylindrical polar coordinates (r, ϕ) through Eq. (37-46), and defining u to be the radial component of $n\mathbf{k}$. If the wave vector makes angle θ_z with the z direction, then we deduce from Eq. (37-49) that

$$k_x x + k_y y = nkr \sin \theta_z = ur. \quad (36-8)$$

If the prescribed field is circularly symmetric, i.e. $E = E(r)$, then we deduce from Eq. (36-6) and the definition in Eq. (37-62) that [3]

$$E(r) = \int_0^{\infty} S(u) J_0(ur) r dr, \quad (36-9)$$

where J_0 is the Bessel function of order zero. Similarly, we find that Eq. (36-7) gives the symmetrical angular spectrum

$$S(u) = 2\pi \int_0^{\infty} E(r) J_0(ur) r dr. \quad (36-10)$$

It is convenient to normalize the spectral function for comparative purposes in Section 10-1. Accordingly we define

$$A(u) = \frac{S(u)}{S(0)} = \int_0^{\infty} E(r) J_0(ur) r dr / \int_0^{\infty} E(r) r dr, \quad (36-11)$$

so that $A(0) = 1$.

ASYMPTOTIC MODAL DESCRIPTION OF PROPAGATION

In this part of the chapter, we give an asymptotic description of propagation on weakly guiding waveguides using modes, and demonstrate the equivalence of this description with the ray, or local plane-wave, description of Part I. The specialization to weakly guiding waveguides is done for simplicity of presentation and not for fundamental reasons.

36-4 Modal fields

The fields of modes of weakly guiding waveguides are constructed from solutions of the scalar wave equation, as explained in Chapter 13. However, when the waveguide

parameter is large, i.e. $V \gg 1$, the solutions of the scalar wave equation for those modes which can propagate only on multimode waveguides are well approximated by the WKB solutions [4]. We showed in Sections 35–8 and 35–12 that the WKB solutions are identical to the local plane-wave solutions. Accordingly, the fields of high-order modes are asymptotically identical to the fields of local plane waves. This is precisely the equivalence in the modal decomposition of the examples in Sections 36–1 and 36–2, which take into account both the spatial dependence and direction of the modal fields. Furthermore, the summed effect of the asymptotic fields of a large number of modes approaches an integral over the continuum of fields as $V \rightarrow \infty$. This integral is identical to the integral over the continuum of local plane-wave fields, or rays. We demonstrated this limit for a particular example in Section 20–19.

36–5 Propagation constants

The modal propagation constants are determined by the eigenvalue equation, which is derived by solving the scalar wave equation, as explained in Section 33–1. However, for high-order modes, the eigenvalue equation can be obtained asymptotically, *without knowledge of the scalar wave equation solutions*. We recall that, on a multimode waveguide, the modal fields are only significant in the part of the core where they have an oscillatory behavior. Since the fields are effectively zero outside this region, it is intuitive that there should be an integral number of oscillations in the fields across the region. We show in the examples below how this simple criterion leads to the eigenvalue equation.

The same asymptotic form of the eigenvalue equation can also be derived using local plane waves. This approach imposes a consistency condition on the accumulated phase change following the ray path over a ray half-period, and is demonstrated in the following examples.

36–6 Step-profile planar waveguide

Consider a step-profile planar waveguide of core and cladding indices n_{co} and n_{cl} respectively. The propagation constant β is the z -component of the local plane-wave vector, which has magnitude kn_{co} . Accordingly, the transverse component is given by $(k^2 n_{\text{co}}^2 - \beta^2)^{1/2} = U/\rho$ in terms of the mode parameter. The fields are oscillatory everywhere between the interfaces at $x = \pm \rho$ in Fig. 12–1. If we allow for a phase change Φ due to both interfaces, where Φ is given by Eq. (35–23), then the condition that the field has an integral number of oscillations in the cross-section is equivalent to

$$\int_{-\rho}^{\rho} \frac{U}{\rho} dx + \Phi = N\pi; \quad N = 0, \pm 1, \dots \quad (36-12)$$

If we express Φ in terms of the waveguide and mode parameters, using the relationships at the back of the book, and rearrange, we obtain the eigenvalue equations for the even and odd TE modes in Table 12–2, page 243, when N is even or odd, respectively. Thus, in this special case, the condition expressed by Eq. (36–12) is exact for all modes.

Local plane-wave derivation

In Section 10–7, we demonstrated how a simple phase consistency argument, based on the translational invariance of the planar waveguide, leads to preferred ray, or local

plane-wave, directions. If we express the angles in Eq. (10-16) in terms of modal and waveguide parameters, using the relationships at the back of the book, it is readily verified that Eq. (10-16) is identical to the eigenvalue equation for the TE modes in Table 12-2. Thus, the preferred ray directions correspond to the discrete values of the modal propagation constant.

36-7 Infinite parabolic-profile fiber

Here we parallel the two derivations of the eigenvalue equation, given in the previous section, for a fiber with the infinite parabolic profile of Eq. (14-5). We recall from Chapter 2 that the ray, or local plane-wave, trajectory lies between the inner and turning-point caustics of radii r_{ic} and r_{ip} , respectively. Accordingly, the modal fields are oscillatory only between these two radial positions. The analogous condition to Eq. (36-12), that there be an integral number of oscillations between the two caustics, is

$$\int_{r_{ic}}^{r_{ip}} k_r(r) dr - \frac{\pi}{2} = m\pi; \quad m = 0, \pm 1, \dots, \quad (36-13a)$$

where $k_r(r)$ is the radial component of the local plane-wave vector at radius r , and the term $-\pi/2$ accounts for the phase change at a caustic. If we substitute the middle expression for $k_r(r)$ in Eq. (35-41), replace k and β by the fiber and mode parameters V and U , respectively, and set $v = l$, then

$$\int_{r_{ic/p}}^{r_{ip/p}} \left\{ U^2 - V^2 R^2 - \frac{l^2}{R^2} \right\}^{1/2} dR = \left(m + \frac{1}{2} \right) \pi, \quad (36-13b)$$

where $R = r/p$. We note that the limits of integration are roots of the integrand, and by setting $R^2 = A + B \sin \theta$, where $A = U^2/2V^2$ and $B = (U^4/4V^4 - l^2/V^2)^{1/2}$, the integral is given by Eq. (37-113). On rearranging

$$U^2 = 2V(2m + l - 1)^{1/2}; \quad l = 0, 1, \dots; m = 1, 2, \dots, \quad (36-14)$$

which is the eigenvalue equation given in Table 14-2, page 307. The ranges of values of l and m ensure that U is real. Thus our asymptotic eigenvalue equation holds for all modes of the infinite parabolic profile fiber.

Local plane-wave derivation

The path of a ray within the parabolic-profile fiber was discussed in Section 2-10. Over a distance along the fiber equal to the half-period, z_p , the path, shown in Fig. 36-2(a), starts at P on the turning-point caustic, touches the inner caustic at T and meets the turning-point caustic again at Q. Relative to the fiber axis, the path between P and Q rotates through π radians in the fiber cross-section, as shown in Fig. 36-2(b).

Following the conceptual lead of Section 10-7, the eigenvalue equation is obtained by imposing a consistency condition, arising from the translational and rotational symmetry properties of the fiber, on the accumulated phase change along the path from P to Q [5]. There are two components to the accumulated phase. The first component is the integral of the amplitude of the local plane-wave vector, $k(r)$, along the path. Since $k(r) = kn(r)$, this integral is proportional to the optical path length, L_o , of Eq. (2-26). The second component is the decrease in phase when the path touches the caustics, and

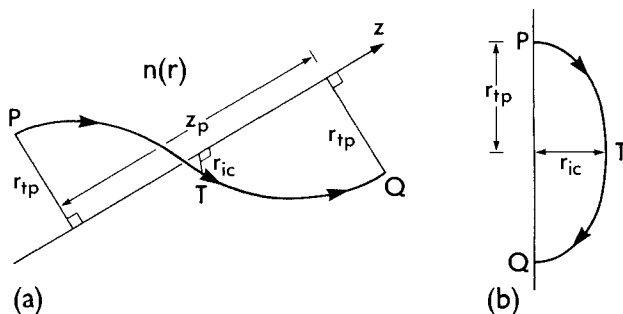


Fig. 36-2 Ray path on an infinite parabolic profile fiber, showing (a) the helical path between successive turning points and (b) the projection of the path onto the fiber cross-section.

is made up of a loss $\pi/2$ at the inner caustic and a loss of $\pi/2$ because the path begins and ends on the turning-point caustic. Thus the accumulated phase change is $kL_o - \pi$.

The path in Fig. 36-2(a) is invariant under a translation z_p parallel to the axis and a rotation π about the axis. Thus the associated phase change comprises

$$z_p k(r_{tp}) n(r_{tp}) \cos \theta_z(r_{tp}) + \pi r_{tp} k(r_{tp}) n(r_{tp}) \sin \theta_z(r_{tp}), \quad (36-15)$$

where $k(r_{tp}) n(r_{tp}) \cos \theta_z(r_{tp})$ is the component of the local plane-wave vector at Q parallel to the fiber axis, and $k(r_{tp}) n(r_{tp}) \sin \theta_z(r_{tp})$ is the component in the azimuthal direction. The ray path makes angle $\theta_z(r_{tp})$ with the z -direction at Q. If we recall the definition of the ray invariants $\bar{\beta}$ and \bar{l} in Table 2-1, page 40, set $r = r_{tp}$ and $\theta_\phi(r_{tp}) = 0$, then Eq. (36-15) is equivalent to $k(z_p \bar{\beta} + \pi \rho \bar{l})$. The consistency condition requires that this expression differ from the accumulated phase along the path by an even multiply of π . Hence

$$kL_o - \pi = k(z_p \bar{\beta} + \pi \rho \bar{l}) + 2m\pi; \quad m = 0, \pm 1, \dots \quad (36-16)$$

We substitute for L_o and z_p from Table 2-1 for the infinite parabolic profile, and express $\bar{\beta}$ and \bar{l} in terms of β and v , using the relationships in Table 36-1. Straightforward rearrangement in terms of the fiber and mode parameters leads to Eq. (36-14). A similar analysis of ray paths within the core of a step-profile fiber leads to the asymptotic form of the eigenvalue equation in Table 14-8, page 325 [5].

36-8 Infinite power-law profiles

When a fiber has any of the set of infinite power-law profiles defined by Eq. (14-8), we can derive the asymptotic eigenvalue equation for all axisymmetric modes, for which $l = 0$. Thus, if we substitute Eq. (14-8) into Eq. (36-13a), set $l = 0$ and $r_{ic} = 0$, then the analogous equation to Eq. (36-14) is

$$\int_0^{r_{tp}/\rho} (U^2 - V^2 R^q)^{1/2} dR = \left(m - \frac{1}{2}\right) \pi; \quad m = 0, \pm 1, \dots \quad (36-17)$$

If we make the substitution $R = (xU^2/V^2)^{1/q}$, then we obtain

$$\frac{U^{(q+2)/q}}{qV^{2/q}} \int_0^1 (1-x)^{1/2} x^{(1-q)/q} dx = \left(m - \frac{1}{2}\right) \pi. \quad (36-18)$$

The integral is expressible in terms of the beta function of Eq. (37–104), which is related to the gamma function through Eq. (37–105). On rearranging

$$U = \left[\frac{(2m-1)\pi^{1/2} (q+2)\Gamma(1/q+1/2) V^{2/q}}{2\Gamma(1/q)} \right]^{q/(q+2)} \quad (36-19)$$

This holds for all $l = 0$ modes of the infinite power-law profiles, and in particular for the parabolic profile ($q = 2$), when Eq. (36–19) reduces to Eq. (36–14).

36–9 Transit times

The transit time of a mode over length z of a fiber is given in terms of the group velocity v_g by Eq. (11–36), with the modal subscript omitted for convenience. Here we show that if we use the asymptotic form of the eigenvalue equation, as expressed by Eq. (36–13a), to calculate the group velocity, then the modal transit time is identical to the ray transit time [4]. This identity holds also when the fiber materials are dispersive [6].

We substitute the middle expression for $k_r(r)$ of Eq. (35–41) into Eq. (36–13a), replace $n(r)$ by $n(r, \lambda)$ to include material dispersion, and set $k = 2\pi/\lambda$. The resulting equation is differentiated with respect to λ . Although the limits of integration depend on λ , they do not contribute to the derivative of the integral because the integrand is zero at both caustics. On rearranging the remaining terms, we have

$$\frac{d\beta}{d\lambda} = -\frac{k^2}{\lambda\beta} \int_{r_{ic}}^{r_{ip}} \frac{nn_g dr}{k_r(r)^{1/2}} \bigg/ \int_{r_{ic}}^{r_{ip}} \frac{dr}{k_r(r)^{1/2}}, \quad (36-20)$$

where n_g is the group index of Eq. (2–33a). We express $k_r(r)$ in terms of ray invariants through Eq. (35–4), and, from Table 36–1, set $\beta = k\bar{\beta}$. The integral in the denominator of Eq. (36–20) is proportional to the ray half-period of Eq. (2–28), and the integral in the numerator is proportional to the optical path length of Eq. (2–33b). Hence, the transit time over distance z follows from Eqs. (11–31) and (11–36) as

$$t = \frac{z}{v_g} = -\frac{z\lambda^2}{2\pi c} \frac{d\beta}{d\lambda} = \frac{z}{c} \frac{L_m}{z_p}, \quad (36-21)$$

which is identical to the ray transit time of Eq. (2–33b).

36–10 Absorbing waveguides

In this section we compare the attenuation of modal power due to slightly absorbing media with the corresponding attenuation of ray power. For simplicity we consider a step-profile planar waveguide of core width 2ρ , and, if superscripts r and i denote real and imaginary parts, the core and cladding refractive indices are $n_{co} = n_{co}^r + in_{co}^i$ and $n_{cl} = n_{cl}^r + in_{cl}^i$, respectively, where $n_{co}^i \ll n_{co}^r$, $n_{cl}^i \ll n_{cl}^r$. The modal propagation constant is complex, $\beta = \beta^r + i\beta^i$, and is the solution of the eigenvalue equations in Table 12–2, page 243. Under these conditions, there are two methods for determining absorption. One method is to use the perturbation result of Eq. (18–16), which is valid for slightly absorbing waveguides, where η is taken from Table 12–2 for the TE modes. The other method is to solve the eigenvalue equation in Table 12–2 by a perturbation expansion. Since the two methods give the same result, we follow only the second method here. If

we consider even TE modes, then

$$W = U \tan U; \quad W = W^r + iW^i; \quad U = U^r + iU^i. \quad (36-22)$$

Equating terms of lowest order, we have

$$W^r = U^r \tan U^r. \quad (36-23)$$

The small imaginary parts of U and W are found by equating the imaginary parts of Eq. (36-22). Using Eqs. (37-3), (37-5) and (37-6) for the expansion of $\tan(U^r + iU^i)$ and setting $\tan(iU^i) \cong iU^i$, we find correct to first order

$$U^r W^i = \{W^r (W^r + 1) + (U^r)^2\} U^i. \quad (36-24)$$

We relate the modal parameters to the propagation constants by equating real and imaginary parts in the definitions inside the back cover and retaining only the lowest-order terms in each case. In terms of the core and cladding power absorption coefficients, α_{co} and α_{cl} , defined in Eqs. (6-10) and (6-19), respectively, and the power attenuation coefficient γ of Table 11-2, page 232, we obtain

$$U^r = \rho \{ (kn_{co}^r)^2 - (\beta^r)^2 \}^{1/2}; \quad 2U^r U^i = \rho^2 (kn_{co}^r \alpha_{co} - \beta^r \gamma), \quad (36-25a)$$

$$W^r = \rho \{ (\beta^r)^2 - (kn_{cl}^r)^2 \}^{1/2}; \quad 2W^r W^i = \rho^2 (\beta^r \gamma - kn_{cl}^r \alpha_{cl}). \quad (36-25b)$$

The waveguide parameter and the complement of the critical angle in this situation are defined in terms of the real parts of the profile by

$$V = k\rho \{ (n_{co}^r)^2 - (n_{cl}^r)^2 \}^{1/2}; \quad \cos \theta_c = n_{cl}^r / n_{co}^r. \quad (36-26)$$

If we substitute Eqs. (36-25) and (36-26) into Eq. (36-24) and rearrange, the power attenuation coefficient is given by

$$\gamma = \frac{kn_{co}^r}{\beta^r} \frac{(U^r)^2 (\cos \theta_c) \alpha_{cl} + W^r (V^2 + W^r) \alpha_{co}}{V^2 (1 + W^r)}, \quad (36-27)$$

provided the absorption is slight.

Attenuation of ray power

To relate the modal attenuation coefficient to the ray attenuation coefficient, we express the right side of Eq. (36-27) in terms of ray quantities. The real part of the propagation constant is related to the angle θ_z the ray path makes with the waveguide axis in Fig. 36-3 by replacing n_{co} with n_{co}^r in the relationship in Table 36-1. Similarly, the waveguide parameter is related to θ_c through Eq. (36-26). Since the waveguide is assumed to be weakly guiding, both θ_z and θ_c are small, and, for simplicity, we make the approximations

$$\beta \cong kn_{co}^r; \quad V \cong k\rho n_{co}^r \theta_c. \quad (36-28a)$$

The corresponding approximations in Eq. (36-25) are

$$U^r \cong k\rho n_{co}^r \theta_z; \quad W^r \cong k\rho n_{co}^r (\theta_c^2 - \theta_z^2)^{1/2}. \quad (36-28b)$$

If we substitute Eq. (36-28) into Eq. (36-27) and rearrange, we find

$$\gamma = \alpha_{co} + \frac{T}{z_p + s}, \quad (36-29)$$

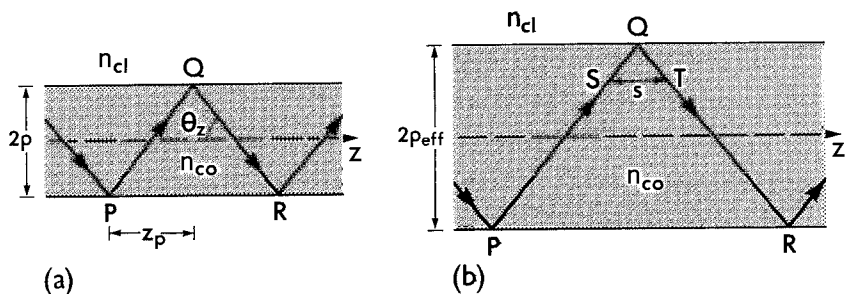


Fig. 36-3 (a) Ray path within the core of width 2ρ of an absorbing, step-profile planar waveguide and (b) the effective core width $2\rho_{\text{eff}}$ allowing for the lateral shift s .

where z_p is the half-period of Eq. (1-10), T is the transmission coefficient of Eq. (35-25) and s is the lateral shift of Eq. (10-8). Within the present approximation, these quantities have the forms

$$z_p \cong \frac{2\rho}{\theta_z}; \quad T \cong \frac{2\rho}{V} \frac{\theta_z}{\theta_c} \frac{\alpha_{\text{cl}} - \alpha_{\text{co}}}{(\theta_c^2 - \theta_z^2)^{1/2}}; \quad s = \frac{2\rho}{V} \frac{\theta_c}{\theta_z} \frac{1}{(\theta_c^2 - \theta_z^2)^{1/2}}, \quad (36-30)$$

as may be verified.

Multimode waveguides

For modes which propagate only on the planar waveguide when it is multimoded, $V \gg 1$, and the term involving s in Eq. (36-29) can be neglected, provided $\theta_z \neq \theta_c$. Furthermore, the contribution to γ from the component of T involving α_{co} is negligible compared with the first term on the right of Eq. (36-29) since $V \gg 1$, and is therefore neglected. Hence

$$\gamma = \alpha_{\text{co}} + T/z_p = \gamma_{\text{co}} + \gamma_{\text{cl}}. \quad (36-31)$$

With reference to the ray path in Fig. 36-3(a), the first term on the right is the power attenuation coefficient γ_{co} for the uniformly absorbing core, as expressed by Eq. (6-10) with $\theta_z \ll 1$. Similarly, T/z_p is the power attenuation coefficient γ_{cl} for the uniformly absorbing cladding, as expressed by Eq. (6-17) and assuming $\theta_z, \theta_c \ll 1$. The sum of the two expressions shows that the ray and modal power attenuation coefficients are identical.

Low- V waveguides

When V is small, only low-order modes can propagate. The term in s in Eq. (36-29) is retained to account for diffraction effects, as discussed in Section 10-4, and the complete expression for T in Eq. (36-30) is now required. However, we can still give a simple physical interpretation. We recall from Section 10-6 that the effect of the lateral shift is to increase the ray half-period from z_p to $z_p + s$, corresponding to the addition ST to the path in Fig. 36-3(b). If we introduce an effective core half-width, ρ_{eff} , as

shown, and replace the ray path PSTR by the zig-zag path PQR, then Eq. (36-29) describes attenuation along the new path [1].

We justify this claim by noting that the core absorption is independent of path since θ_z is small and is therefore unaffected by the path modification. Further, the denominator in the second term on the right of Eq. (36-29), $z_p + s$, is precisely the ray half-period for the new path, i.e. the axial projection of PQ. Finally, the component of the transmission depending on α_{co} accounts for a slight exchange of power from the cladding to the core. This exchange arises because of the difference in the core and cladding absorption coefficients.

36-11 Leaky modes and leaky rays

In Section 24-18, we derived the power attenuation coefficient for tunneling leaky modes on a step-profile, weakly guiding fiber. Here we show that, for higher-order modes, Eq. (24-36) is equivalent to the power attenuation coefficient of the corresponding skew tunneling rays. The argument of the Hankel functions in Eq. (24-36) is smaller than the order. Furthermore, we assume that l is sufficiently large that the order of both Hankel functions may be taken to be approximately l . Under these conditions, we can use the approximate forms of Eq. (37-90), and for simplicity we approximate χ by the middle expression in Eq. (37-90b). Hence

$$\gamma \cong 2 \frac{(2\Delta)^{1/2}}{\rho} \frac{(U^r)^2}{V^3} \{l^2 - (Q^r)^2\}^{1/2} \exp \left\{ -\frac{2[l^2 - (Q^r)^2]^{3/2}}{3(Q^r)^2} \right\}. \quad (36-32)$$

If we replace v , U and Q by l , U^r and Q^r , respectively, in the relationships with ray invariants in Table 36-1, then

$$\gamma \cong \frac{2}{\rho} \frac{n_{co}^2 - \bar{\beta}^2}{n_{co}^2 - n_{cl}^2} \frac{(\bar{\beta}^2 + \bar{l}^2 - n_{cl}^2)^{1/2}}{n_{co}} \exp \left\{ -\frac{2}{3} k\rho \frac{(\bar{l}^2 + \bar{\beta}^2 - n_{cl}^2)^{3/2}}{\bar{\beta}^2 - n_{cl}^2} \right\}. \quad (36-33)$$

The corresponding ray power attenuation coefficient follows from Eqs. (7-2) and (7-19) as

$$\gamma = \frac{T}{z_p} = \frac{|T_f|}{z_p} \exp \left\{ -\frac{2}{3} k\rho \frac{(\bar{l}^2 + \bar{\beta}^2 - n_{cl}^2)^{3/2}}{\bar{\beta}^2 - n_{cl}^2} \right\}. \quad (36-34)$$

If we substitute for $|T_f|$ from Eq. (7-19b) and for z_p from Table 2-1, page 40, and note that $\bar{\beta} \cong n_{co}$ in the weak-guidance approximation, it is readily verified that the mode and ray attenuation coefficients are identical [7]. A similar, analytical comparison can be made for refracting leaky modes and rays on the step-profile planar waveguide [8].

Numerical comparison

The expression for the modal power attenuation coefficient used above is derived by perturbation methods from the eigenvalue equation for the step-profile fiber. We can quantify the agreement between the modal and ray power attenuation coefficients by solving the eigenvalue equation numerically for the complex values of the propagation constant. This solution was discussed in Section 24-19. We find that there is good agreement for those modes with the smallest attenuation coefficients, while, for modes

with larger attenuation coefficients, the inclusion of a lateral shift for leaky rays and the use of a refined model for calculating the ray power attenuation coefficient also leads to good agreement. Details are presented elsewhere [9,10].

NUMBER OF MODES ON MULTIMODE WAVEGUIDES

We can derive simple, asymptotic expressions for the number of bound and leaky modes which can propagate on multimode waveguides. Since $V \gg 1$, most of the modes propagate well above their cutoff $V = V_c$, and their fields in the cladding are evanescent and decrease sufficiently rapidly beyond the interface that we need consider only the core fields. We appeal to a modification of a method frequently used in quantum electrodynamics, that of determining the density of modes in a two-dimensional box [11]. The total number of modes, M_{tot} , both bound and leaky, is found by integrating over the core cross-section, A_{co} , and the corresponding area, A_k in two-dimensional wavenumber space. Thus [12]

$$M_{\text{tot}} = 2 \int_{A_{\text{co}}} dx dy \int_{A_k} \frac{dk_x}{2\pi} \frac{dk_y}{2\pi} = \frac{1}{2\pi^2} A_{\text{co}} A_k, \quad (36-35)$$

which allows for the two possible polarization states of each mode, e.g. TE or TM on a planar waveguide. Examples are given below. We assume that Eq. (36-35), and subsequent equations, implicitly assume that the number of modes is the smallest integer just exceeding the right side. The numbers of bound or leaky modes are found by appropriately restricting the ranges of values of k_x and k_y , as we show below [13].

36-12 Step-profile planar waveguide

The total number of modes which can propagate on a planar waveguide is given by the one-dimensional analogue of Eq. (36-35). If the core half-width is ρ and the refractive index is n_{co} , then at any position in the cross-section the values of k_x lie between $-kn_{\text{co}}$ and kn_{co} . Hence

$$M_{\text{tot}} = 2 \int_{-\rho}^{\rho} dx \int_{-kn_{\text{co}}}^{kn_{\text{co}}} \frac{dk_x}{2\pi} = \frac{4}{\pi} \frac{V}{(2\Delta)^{1/2}}, \quad (36-36)$$

in terms of the waveguide parameter. The number of bound modes, M_{bm} , is given by the same expression as M_{tot} , provided the limits of integration on k_x are reduced to $\pm kn_{\text{co}} \sin \theta_c$, where θ_c is the complementary critical angle. Thus

$$M_{\text{bm}} = \frac{1}{\pi} \int_{-\rho}^{\rho} \int_{-kn_{\text{co}} \sin \theta_c}^{kn_{\text{co}} \sin \theta_c} dk_x = \frac{4}{\pi} V. \quad (36-37)$$

It is clear from the spacing of the cutoff values of V in Fig. 12-2 that this result holds for all values of V . Tunneling leaky modes do not propagate on planar waveguides, and the number, M_{rm} , of refracting leaky modes is the difference between the total number of modes and the number of bound modes

$$M_{\text{rm}} = M_{\text{tot}} - M_{\text{bm}} = \frac{4}{\pi} V \left\{ \frac{1}{(2\Delta)^{1/2}} - 1 \right\}. \quad (37-38)$$

Since $\Delta \ll 1$, it is clear that the number of bound modes on the weakly guiding waveguide is only a small fraction of the total number of modes.

36-13 Step-profile fiber

If θ_z and θ_ϕ are spherical polar angles relative to the axis of a fiber with axisymmetric refractive-index profile $n(r)$, where r is the cylindrical radius, then the cartesian components of the wave vector in the fiber cross-section are

$$k_x = kn(r) \sin \theta_z \cos \theta_\phi; \quad k_y = kn(r) \sin \theta_z \sin \theta_\phi. \quad (36-39)$$

With the help of the Jacobian of Eq. (37-129), the expression for the total number of modes in Eq. (36-35) is transformed into

$$M_{\text{tot}} = \frac{k^2}{\pi} \int_0^\rho n^2(r) r dr \int_0^{\pi/2} d\theta_z \int_0^{2\pi} \sin \theta_z \cos \theta_z d\theta_\phi. \quad (36-40)$$

We set $n(r) = n_{\text{co}}$ and deduce M_{tot} for the step-profile fiber. The number of bound modes, M_{bm} , is given by Eq. (36-40) provided the upper limit of integration on θ_z is replaced by θ_c . Hence, in terms of the definitions of the fiber parameters inside the back cover, we obtain

$$M_{\text{tot}} = \frac{V^2}{4\Delta}; \quad M_{\text{bm}} = \frac{V^2}{2}. \quad (36-41)$$

The number of tunneling and refracting leaky modes, M_{lm} , is therefore

$$M_{\text{lm}} = M_{\text{tot}} - M_{\text{bm}} = \frac{V^2}{2} \left\{ \frac{1}{2\Delta} - 1 \right\}. \quad (36-42)$$

The delineation between tunneling and refracting modes follows from the corresponding delineation between tunneling and refracting rays in Eq. (2-6), i.e. when $\alpha = \alpha_c = \pi/2 - \theta_c$ on the core-cladding interface. Thus Eq. (2-3) leads to

$$\sin \theta_c = \sin \theta_z \sin \theta_\phi. \quad (36-43)$$

If M_{lm} denotes the number of tunneling leaky modes, then we deduce from Eqs. (36-40) and (2-6) that

$$M_{\text{lm}} = \frac{V^2}{\pi\Delta} \int_{\theta_c}^{\pi/2} d\theta_z \int_0^{\bar{\theta}_\phi} \sin \theta_z \cos \theta_z \sin^2 \theta_\phi d\theta_\phi, \quad (36-44)$$

where $\bar{\theta}_\phi = \sin^{-1} \{\sin \theta_c / \sin \theta_z\}$, and the factor $\sin^2 \theta_\phi$ arises from the circular shape [13]. On performing the θ_ϕ integration and making the transformation $w = \sin \theta_z / \sin \theta_c$, we deduce with the aid of Eq. (37-113b) that

$$M_{\text{lm}} \cong \frac{V^2}{2} \left\{ 1 + \frac{(2\Delta)^{1/2}}{3\pi} \right\}, \quad (36-45)$$

assuming $\Delta \ll 1$. The number of refracting leaky modes is $M_{\text{lm}} - M_{\text{lm}}$.

Clad power-law profiles

The number of bound modes which can propagate on a multimode, clad power-law profile fiber is obtained from Eq. (36-40) by substituting for $n(r)$ from Table 2-1, page

40, and replacing the upper limit of the θ_z integration with the complement of the local critical angle $\theta_c(r)$ of Eq. (2-29). Thus

$$M_{bm} = 2k^2 \int_0^\rho n^2(r)r dr \int_0^{\theta_c(r)} \sin \theta_z \cos \theta_z d\theta_z = \frac{V^2}{2} \frac{q}{q+2}. \quad (36-46)$$

Thus, for example, the clad parabolic-profile fiber has only half the number of bound modes as the step-profile fiber.

FIELD SHIFT ON BENT FIBERS

In Section 23-10, we discussed the shift of the modal fields due to bending of a fiber. If the bending radius is large compared to the core radius, we can use perturbation methods to describe this shift. We show that the effect of the bend can be described by a straight fiber with an effective refractive-index profile [14]. The fields of the bent fiber can then be found by solving the scalar wave equation for the straight fiber with the effective profile.

36-14 Derivation of the effective profile

The situation is illustrated in Fig. 36-4. A straight section of a weakly guiding fiber leads into a bend of uniform radius R_c . The fundamental mode has propagation constant β and has an x -polarized electric field, where the x -axis is parallel to the plane of the bend. Thus, on the straight fiber

$$\mathbf{E} = F_0(r) \exp(i\beta z) \hat{\mathbf{x}}, \quad (36-47)$$

where $\hat{\mathbf{x}}$ is the unit vector parallel to the x -axis, z is the distance along the fiber, r is the cylindrical radius and $F_0(r)$ is the fundamental solution of the scalar wave equation of Eq. (14-4). On the bend, it is clear that the same field must have an angular dependence of the form $\exp(i\kappa\theta)$, where κ is a constant and θ is the angular displacement around the bend relative to the x -axis in Fig. 36-4. If z now denotes the distance along the bent fiber, i.e. along a curve of constant radius about the axis of the bend through C, then we

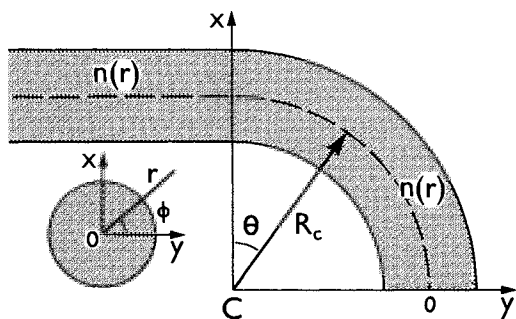


Fig. 36-4 A fiber of refractive-index profile $n(r)$ is bent into an arc of constant radius R_c . Polar coordinates (r, ϕ) describe the fiber cross-section relative to 0, where the $C0y$ -axis is parallel to the plane of the bend.

can define a local propagation constant $\hat{\beta}$ through the relationship

$$\exp(i\kappa\theta) = \exp(i\hat{\beta}z), \quad (36-48)$$

assuming $z = 0$ at $\theta = 0$. If r and ϕ are polar coordinates in the cross-section of the bent fiber, as shown in Fig. 36-4, then by geometry

$$z = (R_c + r \cos \phi)\theta. \quad (36-49)$$

On the fiber axis at the beginning of the bend we must have $\hat{\beta} = \beta$. Substituting Eq. (36-49) into Eq. (36-48), we deduce that $\kappa = \beta R_c$, and hence

$$\hat{\beta} = \frac{\beta R_c}{R_c + r \cos \phi} \cong \beta \left\{ 1 - \frac{r}{R_c} \cos \phi \right\}, \quad (36-50)$$

since, by assumption, $R_c \gg r$. We are reminded that the fundamental-mode fields are significant only in the region close to the fiber axis.

The local propagation constant can be regarded as a modified propagation constant which accounts for the bend. In other words, we can determine the field of the bent fiber approximately, by solving the scalar wave equation for the straight fiber, but with β replaced by $\hat{\beta}$. In cylindrical polar coordinates (r, ϕ, z) , this substitution from Eq. (36-50) into Eq. (14-4), together with a rearrangement of the equation, leads to

$$\left\{ \frac{\partial^2}{\partial r^2} + \frac{1}{r} \frac{\partial}{\partial r} + \frac{1}{r^2} \frac{\partial^2}{\partial \phi^2} + k^2 n_c^2 - \beta^2 \right\} G_0 = 0, \quad (36-51)$$

where we have used the weak-guidance approximation $\beta \cong kn_{co}$. The effective refractive-index profile, n_c , is related to the profile $n(r)$ of the straight fiber by [14]

$$n_c^2 = n^2(r) + 2n_{co}^2(r/R_c) \cos \phi, \quad (36-52)$$

assuming $R_c \gg r$. Thus the effective profile involves the superposition of a linear profile to account for the bend. The field shift due to the bend is found by comparing the solution G_0 of Eq. (36-51) with the corresponding solution F_0 for the straight fiber.

36-15 Example: Gaussian approximation

We can solve Eq. (36-51) for an arbitrary profile, $n(r)$, if we approximate the fundamental-mode fields with the Gaussian approximation of Chapter 15. The solution of the scalar wave equation for the straight fiber is given in terms of the spot size r_0 for the particular profile by Eq. (15-2). To solve Eq. (36-51), we set

$$G_0 = \{1 + A(r/R_c) \cos \phi\} F_0; \quad F_0 = \exp(-r^2/2r_0^2), \quad (36-53)$$

where A is a constant, and ignore terms of order $(r/R_c)^2$. Since F_0 is the approximate solution of Eq. (14-4) when $l = 0$, we deduce from a comparison of terms of order r/R_c in Eq. (36-51), that $A = (kr_0 n_{co})^2$. In terms of the fiber parameter defined inside the back cover, this is equivalent to $A = r_0^2 V^2 / 2\Delta\rho^2$. Hence the electric field on the bent fiber is in the radial direction and is given approximately by

$$\mathbf{E} = \hat{\mathbf{R}} \left\{ 1 + \frac{r_0^2 V^2}{2\Delta\rho^2} \frac{r}{R_c} \cos \phi \right\} \exp\left(-\frac{r^2}{2r_0^2}\right) \exp(i\beta R_c \theta), \quad (36-54)$$

where $\hat{\mathbf{R}}$ is the unit radial vector parallel to the plane of the bend.

Shift in the peak field

The peak value of the electric field amplitude, $|\mathbf{E}|$, is shifted outwards by the bend from its axial position on the straight fiber. We quantify this shift in the plane of the bend, $\phi = 0$. The second term within the curly brackets of Eq. (36-54) is small compared with unity, and thus the two terms are well approximated by $\exp\{(r_0^2 V^2/2\Delta\rho^2)(r/R_c)\cos\phi\}$. Substituting into Eq. (36-47), we obtain, correct to order r/R_c within the exponent

$$\mathbf{E} = \hat{\mathbf{R}} \exp\left\{-\frac{1}{2r_0^2}\left(r - \frac{V^2}{2\Delta} \frac{r_0^4}{R_c\rho^2}\right)^2\right\} \exp(i\beta R_c\theta), \quad (36-55)$$

where V is the fiber parameter defined inside the back cover. If r_d denotes the shift in the peak field, then

$$r_d = \frac{V^2}{2\Delta} \frac{r_0^4}{R_c\rho^2}. \quad (36-56)$$

This shift is the predominant effect of bending on the fields. In the direction orthogonal to the plane of the bend ($\phi = \pi/2$), there is no shift, so that the field pattern is distorted as well as shifted outwards.

REFERENCES

1. Kapany, N. S. and Burke, J. J. (1972) *Optical Waveguides*, Academic Press, New York, p. 74.
2. Johnson, C. C. (1965) *Field and Wave Electrodynamics*, McGraw-Hill, New York.
3. Goodman, J. (1968) *Fourier Optics*, McGraw-Hill, New York.
4. Gloge, D. and Marcattili, E. A. J. (1973) Multimode theory of graded-core fibers. *Bell. Syst. Tech. J.*, **52**, 1563-78.
5. Love, J. D. and Snyder, A. W. (1976) Optical fiber eigenvalue equation: plane wave derivation. *Appl. Opt.*, **15**, 2121-5.
6. Ankiewicz, A. (1978) Comparison of wave and ray techniques for solution of graded index optical waveguide problems. *Opt. Acta.*, **25**, 361-73.
7. Snyder, A. W. and Mitchell, D. J. (1974) Leaky rays on circular optical fibres. *J. Opt. Soc. Am.*, **69**, 599-607.
8. Marcuse, D. (1974) *Theory of Dielectric Optical Waveguides*. Academic Press, New York, p. 33.
9. Love, J. D. and Winkler, C. (1978) Goos-Hanchen shift for leaky rays on step-index waveguides. *Electron. Lett.*, **14**, 379-81.
10. Love, J. D., Winkler, C., Sammut, R. and Barrell, K. (1978) Leaky modes and rays on multimode step-index waveguides—a comparison. *Electron. Lett.*, **14**, 489-90.
11. Feynman, R. P., Leighton, R. B. and Sands, M. (1965) *The Feynman Lectures on Physics*, Addison-Wesley, New York.
12. Snyder, A. W. and Pask, C. (1973) Incoherent illumination of an optical fibre. *J. Opt. Soc. Am.*, **63**, 806-12.
13. Pask, C., Snyder, A. W. and Mitchell, D. J. (1975) Number of modes on optical waveguides. *J. Opt. Soc. Am.*, **65**, 356-7.
14. Gambling, W. A., Matsumura, H. and Ragdale, C. M. (1979) Curvature and microbending losses in single-mode optical fibres. *Opt. Quant. Elect.*, **11**, 43-59.

Mathematical formulae

37-1	Trigonometric, hyperbolic and related functions	709
37-2	Vectors, vector operators and integral theorems	710
37-3	Bessel functions	712
37-4	Integrals of Bessel functions	716
37-5	Miscellaneous functions and integrals	717
References		720

In this final chapter, we bring together for handy reference the mathematical formulae which are used throughout the book. The following list is not meant to be comprehensive, but avoids the need to look for relationships elsewhere, particularly the less familiar ones. All of the results below are given by, or are readily deducible from, standard texts [1-4].

37-1 Trigonometric, hyperbolic and related functions***Trigonometric relationships***

$$\sin \theta = \{e^{i\theta} - e^{-i\theta}\}/2i; \quad \cos \theta = \{e^{i\theta} + e^{-i\theta}\}/2, \quad (37-1)$$

$$\sin^2 \theta + \cos^2 \theta = 1; \quad 1 + \tan^2 \theta = 1/\cos^2 \theta, \quad (37-2)$$

$$1 + \cot^2 \theta = 1/\sin^2 \theta; \quad \tan \theta = 1/\cot \theta = \sin \theta / \cos \theta, \quad (37-3)$$

$$\cos 2\theta = 2 \cos^2 \theta - 1 = 1 - 2 \sin^2 \theta; \quad \sin 2\theta = 2 \sin \theta \cos \theta, \quad (37-4)$$

$$\sin(\theta_1 \pm \theta_2) = \sin \theta_1 \cos \theta_2 \pm \sin \theta_2 \cos \theta_1, \quad (37-5)$$

$$\cos(\theta_1 \pm \theta_2) = \cos \theta_1 \cos \theta_2 \mp \sin \theta_1 \sin \theta_2, \quad (37-6)$$

$$\sin^{-1} \theta = \pi/2 - \cos^{-1} \theta; \quad \tan\{\sin^{-1} \theta\} = \theta/(1 - \theta^2)^{1/2}. \quad (37-7)$$

Sine rule

If a triangle has sides of length a , b and c , and the angles opposite these sides are A , B and C , then

$$a/\sin A = b/\sin B = c/\sin C. \quad (37-8)$$

Expansions for small argument

$$\sin \theta \cong \theta - \theta^3/6 + \dots; \quad \cos \theta \cong 1 - \theta^2/2 + \dots, \quad (37-9)$$

$$\tan \theta \cong \theta + \theta^3/3 + \dots; \quad \cot \theta \cong 1/\theta - \theta/3 + \dots \quad (37-10)$$

Hyperbolic functions

$$\sinh z = (e^z - e^{-z})/2; \quad \cosh z = (e^z + e^{-z})/2, \quad (37-11)$$

$$\cosh^2 z - \sinh^2 z = 1; \quad 1 - \tanh^2 z = 1/\cosh^2 z, \quad (37-12)$$

$$\coth^2 z - 1 = 1/\sinh^2 z; \quad \tanh z = 1/\coth z = \sinh z/\cosh z, \quad (37-13)$$

$$\cosh 2z = 2 \cosh^2 z - 1 = 1 + 2 \sinh^2 z; \quad \sinh 2z = 2 \sinh z \cosh z, \quad (37-14)$$

$$\sinh(z_1 \pm z_2) = \sinh z_1 \cosh z_2 \pm \sinh z_2 \cosh z_1, \quad (37-15)$$

$$\cosh(z_1 \pm z_2) = \cosh z_1 \cosh z_2 \pm \sinh z_1 \sinh z_2, \quad (37-16)$$

$$\sinh^{-1} z = \ln\{z + (z^2 + 1)^{1/2}\}; \quad \cosh^{-1} z = \ln\{z + (z^2 - 1)^{1/2}\}. \quad (37-17)$$

Expansions close to $z = 1$

$$\cosh^{-1} z \cong (z^2 - 1)^{1/2} - (z^2 - 1)^{3/2}/6 + \dots; \quad z \gtrsim 1, \quad (37-18)$$

$$\cosh^{-1}(1/z) \cong (1 - z^2)^{1/2} + (1 - z^2)^{3/2}/3 + \dots; \quad z \lesssim 1. \quad (37-19)$$

Logarithmic function

$$\lim_{z \rightarrow \infty} (\ln z)/z^a = 0, \quad a > 0; \quad \lim_{a \rightarrow \infty} a\{z^{1/a} - 1\} = 0. \quad (37-20)$$

Series expansions

$$\ln(1+z) \cong z - z^2/2 + z^3/3 - \dots; \quad \ln(1-z) = -z - z^2/2 - z^3/3 - \dots \quad (37-21)$$

37-2 Vectors, vector operators and integral theorems**Vector operations**

$$\mathbf{A} \cdot \mathbf{A} = A^2; \quad \mathbf{A} \cdot \mathbf{A}^* = |\mathbf{A}|^2, \quad (37-22)$$

$$\mathbf{A} \cdot (\mathbf{B} \times \mathbf{C}) = \begin{vmatrix} A_x & A_y & A_z \\ B_x & B_y & B_z \\ C_x & C_y & C_z \end{vmatrix}; \quad \mathbf{A} \cdot (\mathbf{B} \times \mathbf{C}) = \mathbf{B} \cdot (\mathbf{C} \times \mathbf{A}) = \mathbf{C} \cdot (\mathbf{A} \times \mathbf{B}), \quad (37-23)$$

$$= -\mathbf{A} \cdot (\mathbf{C} \times \mathbf{B})$$

$$\mathbf{A} \times (\mathbf{B} \times \mathbf{C}) = -\mathbf{A} \times (\mathbf{C} \times \mathbf{B}) = (\mathbf{A} \cdot \mathbf{C})\mathbf{B} - (\mathbf{A} \cdot \mathbf{B})\mathbf{C}. \quad (37-24)$$

Vector operators

Subscript t denotes the transverse operator, as defined in Table 30-1, page 592.

$$\nabla(\Psi_1 \Psi_2) = \Psi_1 \nabla \Psi_2 + \Psi_2 \nabla \Psi_1; \quad \nabla_t(\Psi_1 \Psi_2) = \Psi_1 \nabla_t \Psi_2 + \Psi_2 \nabla_t \Psi_1, \quad (37-25)$$

$$\nabla \cdot (\Psi \mathbf{A}) = \Psi \nabla \cdot \mathbf{A} + \mathbf{A} \cdot \nabla \Psi; \quad \nabla_t \cdot (\Psi \mathbf{A}_t) = \Psi \nabla_t \cdot \mathbf{A}_t + \mathbf{A}_t \cdot \nabla_t \Psi, \quad (37-26)$$

$$\nabla \times (\Psi \mathbf{A}) = \Psi \nabla \times \mathbf{A} + \nabla \Psi \times \mathbf{A}; \quad \nabla_t \times (\Psi \mathbf{A}_t) = \Psi \nabla_t \times \mathbf{A}_t + \nabla_t \Psi \times \mathbf{A}_t, \quad (37-27)$$

$$\nabla \cdot (\mathbf{A} \times \mathbf{B}) = \mathbf{B} \cdot (\nabla \times \mathbf{A}) - \mathbf{A} \cdot (\nabla \times \mathbf{B});$$

$$\nabla_t \cdot (\mathbf{A} \times \mathbf{B}) = \mathbf{B} \cdot (\nabla_t \times \mathbf{A}) - \mathbf{A} \cdot (\nabla_t \times \mathbf{B}), \quad (37-28)$$

$$\nabla^2 \Psi = \nabla \cdot (\nabla \Psi); \quad \nabla_t^2 \Psi = \nabla_t \cdot (\nabla_t \Psi), \quad (37-29)$$

$$\nabla^2 \mathbf{A} = \nabla(\nabla \cdot \mathbf{A}) - \nabla \times (\nabla \times \mathbf{A}); \quad \nabla_t^2 \mathbf{A} = \nabla_t(\nabla_t \cdot \mathbf{A}) - \nabla_t \times (\nabla_t \times \mathbf{A}). \quad (37-30)$$

The following relationships hold *only if A has cartesian components*

$$\nabla^2 \mathbf{A} = \nabla^2 \mathbf{A}, \quad \nabla_t^2 \mathbf{A} = \nabla_t^2 \mathbf{A}; \quad \mathbf{A} = (A_x, A_y, A_z). \quad (37-31)$$

Cartesian coordinates

The scalar function Ψ and the vector function \mathbf{A} depend on cartesian coordinates (x, y, z) . If \hat{x} , \hat{y} and \hat{z} are unit vectors parallel to the x -, y - and z -axes, respectively, and \mathbf{A} has cartesian components A_x , A_y and A_z , then

$$\mathbf{A} = (A_x, A_y, A_z) = A_x \hat{x} + A_y \hat{y} + A_z \hat{z}, \quad (37-32)$$

$$\nabla \Psi = \frac{\partial \Psi}{\partial x} \hat{x} + \frac{\partial \Psi}{\partial y} \hat{y} + \frac{\partial \Psi}{\partial z} \hat{z} = \nabla_t \Psi + \frac{\partial \Psi}{\partial z} \hat{z}, \quad (37-33)$$

$$\nabla \cdot \mathbf{A} = \frac{\partial A_x}{\partial x} + \frac{\partial A_y}{\partial y} + \frac{\partial A_z}{\partial z} = \nabla_t \cdot \mathbf{A}_t + \frac{\partial A_z}{\partial z}, \quad (37-34)$$

$$\nabla \times \mathbf{A} = \begin{vmatrix} \hat{x} & \hat{y} & \hat{z} \\ \frac{\partial}{\partial x} & \frac{\partial}{\partial y} & \frac{\partial}{\partial z} \\ A_x & A_y & A_z \end{vmatrix}; \quad \nabla_t \times \mathbf{A}_t = \left(\frac{\partial A_y}{\partial x} - \frac{\partial A_x}{\partial y} \right) \hat{z}, \quad (37-35)$$

$$\nabla^2 \Psi = \frac{\partial^2 \Psi}{\partial x^2} + \frac{\partial^2 \Psi}{\partial y^2} + \frac{\partial^2 \Psi}{\partial z^2} = \nabla_t^2 \Psi + \frac{\partial^2 \Psi}{\partial z^2}, \quad (37-36)$$

$$\nabla^2 \mathbf{A} = \nabla^2 \mathbf{A} = (\nabla^2 A_x) \hat{x} + (\nabla^2 A_y) \hat{y} + (\nabla^2 A_z) \hat{z}, \quad (37-37)$$

$$\nabla_t^2 \mathbf{A} = \nabla_t^2 \mathbf{A}; \quad \nabla^2 \mathbf{A} = \nabla_t^2 \mathbf{A} + \frac{\partial^2 \mathbf{A}}{\partial z^2}, \quad (37-38)$$

Cylindrical polar coordinates

The scalar function Ψ and the vector function \mathbf{A} depend on cylindrical polar coordinates (r, ϕ, z) . If \hat{r} , $\hat{\phi}$ and \hat{z} are unit vectors parallel to the radial, azimuthal and longitudinal directions, respectively, and \mathbf{A} has cylindrical polar components A_r , A_ϕ and A_z , then

$$\mathbf{A} = (A_r, A_\phi, A_z) = A_r \hat{r} + A_\phi \hat{\phi} + A_z \hat{z}, \quad (37-39)$$

$$\nabla \Psi = \frac{\partial \Psi}{\partial r} \hat{r} + \frac{1}{r} \frac{\partial \Psi}{\partial \phi} \hat{\phi} + \frac{\partial \Psi}{\partial z} \hat{z} = \nabla_t \Psi + \frac{\partial \Psi}{\partial z} \hat{z}, \quad (37-40)$$

$$\nabla \cdot \mathbf{A} = \frac{1}{r} \frac{\partial}{\partial r} (r A_r) + \frac{1}{r} \frac{\partial A_\phi}{\partial \phi} + \frac{\partial A_z}{\partial z} = \nabla_t \cdot \mathbf{A}_t + \frac{\partial A_z}{\partial z}, \quad (37-41)$$

$$\nabla \times \mathbf{A} = \frac{1}{r} \begin{vmatrix} \hat{r} & r \hat{\phi} & \hat{z} \\ \frac{\partial}{\partial r} & \frac{\partial}{\partial \phi} & \frac{\partial}{\partial z} \\ A_r & r A_\phi & A_z \end{vmatrix}; \quad \nabla_t \times \mathbf{A}_t = \frac{1}{r} \left\{ \frac{\partial}{\partial r} (r A_\phi) - \frac{\partial A_r}{\partial \phi} \right\} \hat{z}, \quad (37-42)$$

$$\nabla^2 \Psi = \frac{\partial^2 \Psi}{\partial r^2} + \frac{1}{r} \frac{\partial \Psi}{\partial r} + \frac{1}{r^2} \frac{\partial^2 \Psi}{\partial \phi^2} + \frac{\partial^2 \Psi}{\partial z^2} = \nabla_t^2 \Psi + \frac{\partial^2 \Psi}{\partial z^2}, \quad (37-43)$$

$$\nabla^2 \mathbf{A} = \left\{ \nabla^2 A_r - \frac{2}{r^2} \frac{\partial A_\phi}{\partial \phi} - \frac{A_r}{r^2} \right\} \hat{r} + \left\{ \nabla^2 A_\phi + \frac{2}{r^2} \frac{\partial A_r}{\partial \phi} - \frac{A_\phi}{r^2} \right\} \hat{\phi} + (\nabla^2 A_z) \hat{z}, \quad (37-44)$$

$$\nabla_t^2 \mathbf{A} = \nabla^2 \mathbf{A} - \frac{\partial^2 \mathbf{A}}{\partial z^2}. \quad (37-45)$$

Relationships between cartesian and cylindrical polar coordinates

The orientation of the coordinate systems is shown in Fig. 14-1. In terms of the notation defined above, we have

$$x = r \cos \phi, \quad y = r \sin \phi; \quad r = (x^2 + y^2)^{1/2}, \quad \phi = \tan^{-1} (y/x), \quad (37-46)$$

$$\frac{\partial \Psi}{\partial x} = \cos \phi \frac{\partial \Psi}{\partial r} - \frac{\sin \phi}{r} \frac{\partial \Psi}{\partial \phi}; \quad \frac{\partial \Psi}{\partial y} = \sin \phi \frac{\partial \Psi}{\partial r} + \frac{\cos \phi}{r} \frac{\partial \Psi}{\partial \phi}, \quad (37-47)$$

$$\frac{\partial \Psi}{\partial r} = \cos \phi \frac{\partial \Psi}{\partial x} + \sin \phi \frac{\partial \Psi}{\partial y}; \quad \frac{1}{r} \frac{\partial \Psi}{\partial \phi} = -\sin \phi \frac{\partial \Psi}{\partial x} + \cos \phi \frac{\partial \Psi}{\partial y}, \quad (37-48)$$

$$A_r = A_x \cos \phi + A_y \sin \phi; \quad A_\phi = -A_x \sin \phi + A_y \cos \phi, \quad (37-49)$$

$$A_x = A_r \cos \phi - A_\phi \sin \phi; \quad A_y = A_r \sin \phi + A_\phi \cos \phi, \quad (37-50)$$

Relationships between unit vectors

$$\hat{\mathbf{r}} = \hat{\mathbf{x}} \cos \phi + \hat{\mathbf{y}} \sin \phi; \quad \hat{\phi} = -\hat{\mathbf{x}} \sin \phi + \hat{\mathbf{y}} \cos \phi, \quad (37-51)$$

$$\hat{\mathbf{x}} = \hat{\mathbf{r}} \cos \phi - \hat{\phi} \sin \phi; \quad \hat{\mathbf{y}} = \hat{\mathbf{r}} \sin \phi + \hat{\phi} \cos \phi, \quad (37-52)$$

$$\hat{\mathbf{r}} \times \hat{\phi} = \hat{\mathbf{z}}; \quad \hat{\mathbf{z}} \times \hat{\mathbf{r}} = \hat{\phi}, \quad (37-53)$$

$$\frac{\partial \hat{\mathbf{r}}}{\partial r} = 0, \quad \frac{\partial \hat{\mathbf{r}}}{\partial \phi} = \hat{\phi}; \quad \frac{\partial \hat{\phi}}{\partial r} = 0, \quad \frac{\partial \hat{\phi}}{\partial \phi} = -\hat{\mathbf{r}}. \quad (37-54)$$

Integral theorems

The following theorems apply to a planar surface S with perimeter l , on which, $\hat{\mathbf{n}}$ is the unit outward normal, and $\hat{\mathbf{z}}$ is the unit vector orthogonal to S and parallel to the increasing z -direction. The exception is the second relationship in Eq. (37-55) which applies to volume \mathcal{V} bounded by the surface S , on which $\hat{\mathbf{n}}$ is the unit outward normal.

$$\int_S \nabla_t \cdot \mathbf{A}_t dS = \oint_l \mathbf{A}_t \cdot \hat{\mathbf{n}} dl; \quad \int_{\mathcal{V}} \nabla \cdot \mathbf{A} d\mathcal{V} = \oint_S \mathbf{A} \cdot \hat{\mathbf{n}} dS, \quad (37-55)$$

$$\int_S \nabla \cdot \mathbf{A} dS = \frac{\partial}{\partial z} \int_S \mathbf{A} \cdot \hat{\mathbf{z}} dS + \oint_l \mathbf{A} \cdot \hat{\mathbf{n}} dl, \quad (37-56)$$

$$\int_S \{ \mathbf{A}_t \cdot \nabla_t^2 \mathbf{B}_t - \mathbf{B}_t \cdot \nabla_t^2 \mathbf{A}_t \} dS = \oint_l \{ \mathbf{A}_t (\nabla_t \cdot \mathbf{B}_t) - \mathbf{B}_t (\nabla_t \cdot \mathbf{A}_t) \} \cdot \hat{\mathbf{n}} dl, \quad (37-57)$$

$$\int_S \{ \Psi \nabla_t^2 \chi - \chi \nabla_t^2 \Psi \} dS = \oint_l \{ \Psi \nabla_t \chi - \chi \nabla_t \Psi \} \cdot \hat{\mathbf{n}} dl. \quad (37-58)$$

37-3 Bessel functions**Differential equations**

The Bessel functions of the first and second kinds, $J_\nu(z)$ and $Y_\nu(z)$, and the Hankel functions of the first and second kinds, $H_\nu^{(1)}(z)$ and $H_\nu^{(2)}(z)$, all satisfy the same

differential equation. If $F_v(z)$ denotes one of these functions, then

$$z^2 \frac{d^2 F_v}{dz^2} + z \frac{dF_v}{dz} + (z^2 - v^2) F_v = 0. \quad (37-59)$$

If $G_v(z)$ denotes a modified Bessel function of the first or second kind, $I_v(z)$ or $K_v(z)$, then

$$z^2 \frac{d^2 G_v}{dz^2} + z \frac{dG_v}{dz} - (z^2 + v^2) G_v = 0. \quad (37-60)$$

Integral and series definitions

In the following, v is taken to be real and nonnegative, and m is a nonnegative integer.

$$J_v(z) = \frac{1}{\pi} \int_0^\pi \cos(z \sin \theta - v\theta) d\theta - \frac{\sin(v\pi)}{\pi} \int_0^\infty \exp(-z \sinh t - vt) dt, \quad (37-61)$$

$$J_m(z) = \frac{1}{2\pi i^m} \int_0^{2\pi} \exp(iz \cos \theta) \cos(m\theta) d\theta = \frac{i^m}{2\pi} \int_0^{2\pi} \exp(-iz \cos \theta) \cos(m\theta) d\theta, \quad (37-62)$$

$$J_v(z) = \left(\frac{z}{2}\right)^v \sum_{j=0}^{\infty} \frac{(-z^2/4)^j}{j! \Gamma(j+v+1)}, \quad (37-63)$$

$$I_m(z) = \frac{1}{2\pi} \int_0^{2\pi} \cos(m\theta) \exp(z \cos \theta) d\theta, \quad (37-64)$$

$$I_0(z) = \frac{1}{2\pi} \int_0^{2\pi} \exp\{z \cos(\theta - i\chi)\} d\theta, \quad (37-65)$$

$$K_v(z) = \int_0^\infty \exp(-z \cosh t) \cosh(vt) dt, \quad (37-66)$$

$$K_{iv}(z) = \int_0^z \exp(-z \cosh t) \cos(vt) dt, \quad (37-67)$$

where $K_{\frac{1}{2}}(z)$ is a modified Bessel function of the second kind of pure imaginary order.

Relationships between Bessel, Hankel and modified Bessel functions

$$H_v^{(1)}(z) = J_v(z) + iY_v(z); \quad H_v^{(2)}(z) = J_v(z) - iY_v(z), \quad (37-68)$$

$$J_m(iz) = i^m I_m(z); \quad J_0(iz) = I_0(z); \quad J_1(iz) = iI_1(z), \quad (37-69)$$

$$\{J_m(z)\}^* = J_m(z^*); \quad J_{-m}(z) = (-)^m J_m(z), \quad (37-70)$$

$$K_m(-iz) = (\pi/2)i^{m+1} H_m^{(1)}(z); \quad K_{-m}(z) = K_m(z). \quad (37-71)$$

Recurrence relations

The recurrence relations for the J_m are also satisfied by the Y_m , $H_m^{(1)}$ and $H_m^{(2)}$.

$$J_m(z) = \frac{z}{2m} \{J_{m-1}(z) + J_{m+1}(z)\}; \quad \frac{dJ_m(z)}{dz} = \frac{1}{2} \{J_{m-1}(z) - J_{m+1}(z)\}, \quad (37-72a)$$

$$J_{m+1}(z) = \frac{m}{z} J_m(z) - \frac{dJ_m(z)}{dz}; \quad J_{m-1}(z) = \frac{m}{z} J_m(z) + \frac{dJ_m(z)}{dz}, \quad (37-72b)$$

$$K_m(z) = \frac{z}{2m} \{K_{m+1}(z) - K_{m-1}(z)\}; \quad \frac{dK_m(z)}{dz} = -\frac{1}{2} \{K_{m-1}(z) + K_{m+1}(z)\}, \quad (37-73a)$$

$$K_{m+1}(z) = \frac{m}{z} K_m(z) - \frac{dK_m(z)}{dz}; \quad K_{m-1}(z) = -\frac{m}{z} K_m(z) - \frac{dK_m(z)}{dz}, \quad (37-73b)$$

$$I_m(z) = \frac{z}{2m} \{I_{m-1}(z) - I_{m+1}(z)\}; \quad \frac{dI_m(z)}{dz} = \frac{1}{2} \{I_{m-1}(z) + I_{m+1}(z)\}, \quad (37-74a)$$

$$I_{m+1}(z) = -\frac{m}{z} I_m(z) + \frac{dI_m(z)}{dz}; \quad I_{m-1}(z) = \frac{m}{z} I_m(z) + \frac{dI_m(z)}{dz}, \quad (37-74b)$$

$$\frac{dJ_0(z)}{dz} = -J_1(z); \quad \frac{dK_0(z)}{dz} = -K_1(z); \quad \frac{dI_0(z)}{dz} = I_1(z). \quad (37-75)$$

Wronskians

$$W\{J_m(z), Y_m(z)\} = J_m(z) \frac{dY_m(z)}{dz} - Y_m(z) \frac{dJ_m(z)}{dz} = \frac{2}{\pi z} \quad (37-76a)$$

$$= Y_m(z) J_{m+1}(z) - J_m(z) Y_{m+1}(z) \quad (37-76b)$$

$$= J_m(z) Y_{m-1}(z) - Y_m(z) J_{m-1}(z), \quad (37-76c)$$

$$W\{J_m(z), H_m^{(1)}(z)\} = J_m(z) \frac{dH_m^{(1)}(z)}{dz} - H_m^{(1)}(z) \frac{dJ_m(z)}{dz} = \frac{2i}{\pi z} \quad (37-77a)$$

$$= H_m^{(1)}(z) J_{m+1}(z) - J_m(z) H_{m+1}^{(1)}(z) \quad (37-77b)$$

$$= J_m(z) H_{m-1}^{(1)}(z) - H_m^{(1)}(z) J_{m-1}(z), \quad (37-77c)$$

$$W\{K_m(z), I_m(z)\} = K_m(z) \frac{dI_m(z)}{dz} - I_m(z) \frac{dK_m(z)}{dz} = \frac{1}{z}, \quad (37-78)$$

$$W\{K_0(z), I_0(z)\} = K_0(z) I_1(z) + I_0(z) K_1(z) = 1/z. \quad (37-79)$$

Series of Bessel and modified Bessel functions

$$\exp(iz \cos \theta) = J_0(z) + 2 \sum_{m=1}^{\infty} i^m J_m(z) \cos(m\theta), \quad (37-80a)$$

$$\cos(z \cos \theta) = J_0(z) + 2 \sum_{m=1}^{\infty} (-)^m J_{2m}(z) \cos(2m\theta), \quad (37-80b)$$

$$\sin(z \cos \theta) = 2 \sum_{m=0}^{\infty} (-)^m J_{2m+1}(z) \cos(2m+1)\theta. \quad (37-80c)$$

Relative to the coordinates in Fig. 18-4, the addition formula is

$$K_m(ar_1) \begin{cases} \cos(m\phi_1) \\ \sin(m\phi_1) \end{cases} = \pm \sum_{p=-\infty}^{\infty} (-)^p K_{m+p}(ad) I_p(ar_2) \begin{cases} \cos(p\phi_2) \\ \sin(p\phi_2) \end{cases} \quad (37-81)$$

Limiting forms for small argument ($z \rightarrow 0$)

$$J_m(z) \cong \frac{1}{m!} \left(\frac{z}{2}\right)^m; \quad J_0(z) \cong 1 - \frac{z^2}{4}; \quad J_1(z) \cong \frac{z}{2} - \frac{z^3}{16}, \quad (37-82)$$

$$Y_m(z) \cong -\frac{(m-1)!}{\pi} \left(\frac{2}{z}\right)^m \quad (m \neq 0); \quad H_m^{(1)}(z) \cong -\frac{i(m-1)!}{\pi} \left(\frac{2}{z}\right)^m \quad (m \neq 0), \quad (37-83)$$

$$Y_0(z) \cong (2/\pi) \ln z; \quad H_0^{(1)}(z) \cong (2i/\pi) \ln z, \quad (37-84)$$

$$I_m(z) \cong \frac{1}{m!} \left(\frac{z}{2}\right)^m; \quad I_0(z) \cong 1 + \frac{z^2}{4}; \quad I_1(z) \cong \frac{z}{2} + \frac{z^3}{16}, \quad (37-85)$$

$$K_m(z) \cong \frac{(m-1)!}{2} \left(\frac{2}{z}\right)^m \quad (m = 0); \quad K_0(z) \cong -\ln z + (\ln 2 - \gamma), \quad (37-86)$$

where Euler's constant $\gamma \cong 0.577$.

Asymptotic expansions for large argument ($z \rightarrow \infty$)

$$J_v(z) \cong \left(\frac{2}{\pi z}\right)^{1/2} \cos\left\{z - v\frac{\pi}{2} - \frac{\pi}{4}\right\}; \quad H_v^{(1)}(z) \cong \left(\frac{2}{\pi z}\right)^{1/2} \exp\left(i\left\{z - v\frac{\pi}{2} - \frac{\pi}{4}\right\}\right), \quad (37-87)$$

$$I_v(z) \cong \frac{e^z}{(2\pi z)^{1/2}} \left\{1 - \frac{4v^2 - 1}{8z}\right\}; \quad K_v(z) \cong \left(\frac{\pi}{2z}\right)^{1/2} e^{-z} \left\{1 + \frac{4v^2 - 1}{8z}\right\}. \quad (37-88)$$

Debye asymptotic expansions

When the argument is larger than the order and satisfies $z - v \gg v^{1/3}$, then

$$J_v(z) \cong \left(\frac{2}{\pi}\right)^{1/2} \frac{\cos \chi}{(z^2 - v^2)^{1/4}}; \quad H_v^{(1)}(z) \cong \left(\frac{2}{\pi}\right)^{1/2} \frac{\exp(i\chi)}{(z^2 - v^2)^{1/4}}, \quad (37-89a)$$

$$\frac{dJ_v(z)}{dz} \cong -\left(\frac{2}{\pi}\right)^{1/2} \frac{(z^2 - v^2)^{1/4}}{z} \sin \chi; \quad \frac{dH_v^{(1)}(z)}{dz} \cong i\left(\frac{2}{\pi}\right)^{1/2} \frac{(z^2 - v^2)^{1/4}}{z} \exp(i\chi), \quad (37-89b)$$

$$\chi = (z^2 - v^2)^{1/2} - v \cos^{-1}(v/z) - \pi/4. \quad (37-89c)$$

If the argument is smaller than the order and satisfies $v - z \gg v^{1/3}$, $v \gg 1$, then

$$J_v(z) \cong \frac{1}{(2\pi)^{1/2}} \frac{\exp(-\chi)}{(v^2 - z^2)^{1/4}}; \quad H_v^{(1)}(z) \cong iY_v(z) \cong -i\left(\frac{2}{\pi}\right)^{1/2} \frac{\exp(\chi)}{(v^2 - z^2)^{1/4}}, \quad (37-90a)$$

$$\chi = v \cosh(v/z) - (v^2 - z^2)^{1/2} \cong \frac{1}{3z^2} (v^2 - z^2)^{3/2} \cong \frac{z}{3} \left(\frac{v^2}{z^2} - 1\right)^{3/2}, \quad (37-90b)$$

where the approximations to χ apply when z is close to v .

37-4 Integrals of Bessel functions

Indefinite integrals

$$\int z J_0(az) dz = \frac{z}{a} J_1(az); \quad \int \frac{J_1^2(az)}{z} dz = -\frac{1}{2} \{J_0^2(az) + J_1^2(az)\}, \quad (37-91)$$

$$\int z J_m^2(az) dz = \frac{z^2}{2} \{J_m^2(az) - J_{m-1}(az) J_{m+1}(az)\}, \quad (37-92a)$$

$$\int z J_0^2(az) dz = \frac{z^2}{2} \{J_0^2(az) + J_1^2(az)\}, \quad (37-92b)$$

$$\int z K_m^2(az) dz = \frac{z^2}{2} \{K_m^2(az) - K_{m-1}(az) K_{m+1}(az)\}, \quad (37-93a)$$

$$\int z K_0^2(az) dz = \frac{z^2}{2} \{K_0^2(az) - K_1^2(az)\}, \quad (37-93b)$$

$$\int z J_m(az) J_m(bz) dz = \frac{z}{a^2 - b^2} \{b J_m(az) J_{m-1}(bz) - a J_m(bz) J_{m-1}(az)\}, \quad (37-94)$$

$$\int z K_m(az) K_m(bz) dz = \frac{z}{a^2 - b^2} \{b K_m(az) K_{m+1}(bz) - a K_m(bz) K_{m+1}(az)\}, \quad (37-95)$$

$$\int z^2 J_0(az) J_1(az) dz = \frac{z^2}{2a} J_1^2(az), \quad (37-96)$$

$$\int z^2 K_0(az) K_1(az) dz = -\frac{z^2}{2a} K_1^2(az), \quad (37-97)$$

$$\int z J_m(az) K_m(bz) dz = \frac{z}{a^2 + b^2} \{a K_m(bz) J_{m+1}(az) - b J_m(az) K_{m+1}(bz)\}, \quad (37-98)$$

$$\int z J_0(az) I_0(bz) dz = \frac{z}{a^2 + b^2} \{b J_0(az) I_1(bz) + a I_1(az) I_0(bz)\}, \quad (37-99)$$

Definite integrals

$$\int_0^\infty J_1(bz) \exp(-a^2 z^2) dz = \frac{1 - \exp(-b^2/4a^2)}{b}, \quad (37-100a)$$

$$\int_0^\infty z^{m+1} J_m(bz) \exp(-a^2 z^2) dz = \frac{b^m \exp(-b^2/4a^2)}{(2a^2)^{m+1}}, \quad (37-100b)$$

$$\int_0^\infty z I_0(bz) \exp(-a^2 z^2) dz = \frac{\exp(b^2/4a^2)}{2a^2}, \quad (37-101a)$$

$$\int_0^\infty I_0(bz) \exp(-az) dz = \frac{1}{(a^2 - b^2)^{1/2}}, \quad (37-101b)$$

$$\int_0^\infty z I_0(bz) \exp(-az) dz = \frac{a}{(a^2 - b^2)^{3/2}}, \quad (37-102a)$$

$$\int_0^\infty z I_1(bz) \exp(-az) dz = \frac{b}{(a^2 - b^2)^{3/2}}, \quad (37-102b)$$

where $a > b > 0$ in Eq. (37-101b) and in Eq. (37-102).

37-5 Miscellaneous functions and integrals**Special functions**

The complete elliptic integrals of the first and second kinds are, respectively,

$$K(v) = \int_0^{\pi/2} \frac{d\theta}{(1-v\sin^2\theta)^{1/2}}; \quad E(v) = \int_0^{\pi/2} (1-v\sin^2\theta)^{1/2} d\theta, \quad (37-103)$$

and the gamma and beta functions have the respective definitions

$$\Gamma(z) = \int_0^\infty t^{z-1} e^{-t} dt; \quad B(z, w) = \int_0^1 t^{z-1} (1-t)^{w-1} dt. \quad (37-104)$$

Special relationships and particular values are

$$\Gamma(m+1) = m! = \int_0^\infty t^m e^{-t} dt; \quad B(z, w) = \frac{\Gamma(z)\Gamma(w)}{\Gamma(z+w)}, \quad (37-105)$$

$$\Gamma(z+1) = z\Gamma(z); \quad \Gamma(\tfrac{1}{4}) \cong 3.625; \quad \Gamma(\tfrac{1}{3}) \cong 2.679, \quad (37-106a)$$

$$\Gamma(\tfrac{1}{2}) = \pi^{1/2} \cong 1.772; \quad \Gamma(\tfrac{2}{3}) \cong 1.354; \quad \Gamma(\tfrac{3}{4}) \cong 1.225, \quad (37-106b)$$

where $m = 0, 1, \dots$. Low-order Hermite polynomials are

$$H_0 = 1; \quad H_1 = 2z; \quad H_2 = 4z^2 - 2; \quad H_3 = 8z^3 - 12z. \quad (37-107)$$

Equivalent definitions of the Dirac delta function are

$$\delta(z-z_0) = \frac{1}{2\pi} \int_{-\infty}^{\infty} \exp(\pm i(z-z_0)t) dt \quad (37-108a)$$

$$\delta(z-z_0) = \frac{1}{2\pi} \sum_{m=-\infty}^{\infty} \cos m(z-z_0) = \frac{1}{2\pi} \sum_{m=-\infty}^{\infty} \exp\{im(z-z_0)\}. \quad (37-108b)$$

If \mathbf{r} and \mathbf{r}_0 are position vectors, then relative to cartesian and cylindrical polar coordinates we have, respectively,

$$\delta(\mathbf{r}-\mathbf{r}_0) = \delta(x-x_0)\delta(y-y_0)\delta(z-z_0); \quad \delta(\mathbf{r}-\mathbf{r}_0) = \frac{\delta(r-r_0)}{r_0} \delta(\phi-\phi_0)\delta(z-z_0). \quad (37-109)$$

Indefinite and definite integrals

$$\int_0^\pi \cos(m\theta) \sin(z \cos \theta) d\theta = 0, \quad (m \text{ even}), \quad (37-110a)$$

$$\int_0^\pi \cos(m\theta) \cos(z \cos \theta) d\theta = 0, \quad (m \text{ odd}) \quad (37-110b)$$

$$\sin(m\theta) \exp(\pm iz \cos \theta) d\theta = 0; \quad \int_{-\infty}^{\infty} \frac{\sin^2(az)}{z^2} dz = a\pi, \quad (a > 0). \quad (37-111)$$

$$\int_{-\pi/2}^{\pi/2} \frac{d\theta}{1+a^2 \sin^2 \theta} = \frac{\pi}{(a^2+1)^{1/2}}, \quad (37-112a)$$

$$\int \frac{d\theta}{a+b \cos^2 \theta} = \frac{1}{\{a(a+b)\}^{1/2}} \tan^{-1} \left\{ \left(\frac{a}{a+b} \right)^{1/2} \tan \theta \right\}, \quad (37-112b)$$

$$\int \frac{d\theta}{\cos^3 \theta} = \frac{\sin \theta}{2 \cos^2 \theta} + \frac{1}{2} \ln \left\{ \tan \left(\frac{\pi}{4} + \frac{\theta}{2} \right) \right\}, \quad (37-113a)$$

$$\int z \sin^{-1} \left(\frac{1}{z} \right) dz = \frac{z^2}{2} \sin^{-1} \left(\frac{1}{z} \right) + \frac{1}{2} (z^2 - 1)^{1/2}, \quad (37-113b)$$

$$\int \sin^2(bz) \exp(-az) dz = -\frac{\{a^2 \sin^2(bz) + ab \sin(2bz) + 2b^2\}}{a(a^2 + 4b^2)} \exp(-az), \quad (37-114a)$$

$$\int \cos^2(bz) \exp(-az) dz = -\frac{\{a^2 \cos^2(bz) - ab \sin(2bz) + 2b^2\}}{a(a^2 + 4b^2)} \exp(-az), \quad (37-114b)$$

$$\int \frac{dz}{a + \cosh z} = \frac{1}{(a^2 - 1)^{1/2}} \ln \left\{ \frac{a + e^z - (a^2 - 1)^{1/2}}{a + e^z + (a^2 - 1)^{1/2}} \right\}, \quad (a > 1) \quad (37-115)$$

$$\int_{-\infty}^{\infty} \frac{dz}{1+z^2} = \pi; \quad \int_0^1 \frac{dz}{a^2+z^2} = \frac{1}{a} \tan^{-1} \left(\frac{1}{a} \right), \quad (37-116)$$

$$\int (a^2 - z^2)^{1/2} dz = \frac{a^2}{2} \left\{ \sin^{-1} \left(\frac{z}{a} \right) + \frac{z}{a} \left(1 - \frac{z^2}{a^2} \right)^{1/2} \right\}, \quad (a > z > 0), \quad (37-117)$$

$$\int_b^a \left\{ \frac{a^2}{z^2} - 1 \right\}^{1/2} dz = a \ln \left\{ \frac{a}{b} + \frac{(a^2 - b^2)^{1/2}}{b} \right\} - (a^2 - b^2)^{1/2}, \quad (37-118a)$$

$$= a \cosh^{-1} \left(\frac{a}{b} \right) - (a^2 - b^2)^{1/2} \cong \frac{1}{3a^2} (a^2 - b^2)^{3/2}, \quad (37-118b)$$

where $a > b > 0$ and the approximation holds when $b \lesssim a$.

$$\int \frac{dz}{\{1 - (a/z)^2\}^{1/2}} = (z^2 - a^2)^{1/2}; \quad \int \left\{ 1 - \frac{a^2}{z^2} \right\}^{1/2} dz = (z^2 - a^2)^{1/2} - a \cos^{-1} \left(\frac{a}{z} \right), \quad (37-119)$$

$$\int_{z_0}^z \frac{dz}{\{z^2 - a^2 - (b/z)^2\}^{1/2}} = \frac{1}{2} \cosh^{-1} \left\{ \frac{2z^2 - a^2}{(4b^2 + a^4)^{1/2}} \right\}, \quad (37-120)$$

where z_0 is the smaller root of the denominator in the integrand.

$$\int_b^z \frac{z dz}{(a^2 - z^2)^{1/2} (z^2 - b^2)^{1/2}} = \frac{1}{2} \cos^{-1} \left\{ \frac{(a^2 - z^2) - (z^2 - b^2)}{a^2 - b^2} \right\}, \quad (37-121)$$

where $a > b > 0$ and $a > z > b$.

$$\int_b^a \frac{z^3 dz}{(a^2 - z^2)^{1/2} (z^2 - b^2)^{1/2}} = \frac{\pi}{4} (a^2 + b^2), \quad (a > b > 0), \quad (37-122)$$

$$\int \frac{\{(z^2 - a^2)(z^2 - b^2)\}^{1/2}}{z} dz = \frac{1}{2} \left[(z^2 - a^2)^{1/2} (z^2 - b^2)^{1/2} - (a^2 + b^2)X + abY \right], \quad (37-123a)$$

$$X = \ln \left\{ \frac{(z^2 - a^2)^{1/2} + (z^2 - b^2)^{1/2}}{(a^2 - b^2)^{1/2}} \right\}, \quad (37-123b)$$

$$Y = \ln \left\{ \frac{(a - b)^2 + [(z^2 - a^2)^{1/2} + (z^2 - b^2)^{1/2}]^2}{(a + b)^2 + [(z^2 - a^2)^{1/2} + (z^2 - b^2)^{1/2}]^2} \right\}, \quad z > a, z > b \quad (37-123c)$$

$$\int_0^z z \exp(-a^2 z^2) dz = \frac{1}{2a^2} \{1 - \exp(-a^2 z^2)\}, \quad (37-124a)$$

$$\int_0^z z^3 \exp(-a^2 z^2) dz = \frac{1}{2a^4} \{1 - (1 + a^2 z^2) \exp(-a^2 z^2)\}, \quad (37-124b)$$

$$I_m = \int_0^\infty z^m \exp(-a^2 z^2) dz = \frac{1}{2a^{m+1}} \Gamma\{(m+1)/2\}, \quad (37-125a)$$

$$I_0 = \frac{\sqrt{\pi}}{2a}; \quad I_1 = \frac{1}{2a^2}; \quad I_2 = \frac{\sqrt{\pi}}{4a^3}; \quad I_3 = \frac{1}{2a^4}, \quad (37-125b)$$

$$\int_{-\infty}^\infty z^m \exp(-a^2 z^2) dz = \frac{1}{a^{m+1}} \Gamma\{(m+1)/2\}, \quad m = 0, 2, 4, \dots, \quad (37-126a)$$

$$\int_{-\infty}^\infty z^m \exp(-a^2 z^2) dz = 0, \quad m = 1, 3, \dots, \quad (37-126b)$$

$$\int_{-\infty}^\infty \exp(-az^2 - bz) \exp(-pz^2 - qz) dz = \left\{ \frac{\pi}{a+p} \right\}^{1/2} \exp \left\{ \frac{(b+q)^2}{4(a+p)} \right\}, \quad (37-127)$$

where $a > 0$, $p > 0$. If $L_{m-1}^{(l)}(z)$ is a generalized Laguerre polynomial, then

$$\int_0^\infty z^l e^{-z} \left\{ L_{m-1}^{(l)}(z) \right\}^2 dz = \frac{(l+m-1)!}{(m-1)!}, \quad l \geq 0, m \geq 1. \quad (37-128)$$

Jacobian transformation

The Jacobian for the two-dimensional transformation $(u, v) \rightarrow (p, q)$ is

$$J = \frac{\partial(u, v)}{\partial(p, q)} = \frac{\partial u}{\partial p} \frac{\partial v}{\partial q} - \frac{\partial u}{\partial q} \frac{\partial v}{\partial p}. \quad (37-129)$$

Laplace's method

If x is large and positive, and the function $h(z)$ takes its maximum value at the lower limit of integration $z = a$ in the integral

$$G(x) = \int_a^b g(z) \exp\{xh(z)\} dz, \quad (37-130)$$

then the value of $G(x)$ is well approximated by [3]

$$G(x) = g(a) \exp\{xh(a)\} \left\{ \frac{-\pi}{2xh''(a)} \right\}^{1/2}, \quad (37-131)$$

where $h''(a)$ is the value of $d^2h(z)/dz^2$ at $z = a$.

Euler's theorem

If cartesian axes are oriented at position P on a surface of arbitrary curvature such that the x -axis is normal to the surface, and the x - y and x - z planes contain the principal radii of curvature ρ_y and ρ_z , respectively, then, for any other plane containing the x -axis and making angle Ω with the z -axis, the radius of curvature $\bar{\rho}$ in the plane is given by [4]

$$\frac{1}{\bar{\rho}} = \frac{\cos^2 \Omega}{\rho_z} + \frac{\sin^2 \Omega}{\rho_y} \quad \text{or} \quad \bar{\rho} = \frac{\rho_y \rho_z}{\rho_y \cos^2 \Omega + \rho_z \sin^2 \Omega}. \quad (37-132)$$

For the situation in Fig. 35-7(a), it follows by geometry that the angle Ω , which the plane of incidence makes with the z -axis, is related to α and θ_z by $\cos \Omega = \cos \theta_z / \sin \alpha$ and $\sin \Omega = \cos \theta_y / \sin \alpha$. Consequently

$$\bar{\rho} = \frac{\rho_y \rho_z \sin^2 \alpha}{\rho_y \cos^2 \theta_z + \rho_z \cos^2 \theta_y}. \quad (37-133)$$

The plane of incidence at P in Fig. 35-7(b) makes angle θ_z with the z -axis. Thus, $\Omega = \theta_z$ and

$$\bar{\rho} = \frac{\rho_y \rho_z}{\rho_y \cos^2 \theta_z + \rho_z \sin^2 \theta_z}. \quad (37-134)$$

REFERENCES

1. Abramowitz, M. and Stegun, I. A. (eds) (1965) *Handbook of Mathematical Functions*, Dover, New York.
2. Gradshteyn, I. S. and Ryzhik, I. M. (1965) *Tables of Integrals, Series and Products*, Academic Press, New York.
3. Erdelyi, A. (1956) *Asymptotic Expansions*, Dover, New York, p. 36.
4. Korn, G. A. and Korn, T. M. (1961) *Mathematical Handbook for Scientists and Engineers*, McGraw-Hill, New York, sect. 17-3-5.

Author index

Bold page numbers denote complete references given at the end of a chapter.

- Abramowitz, M., 148, **152**, 266, 269, 271,
279, 360, 364, 365, **365**, 690, **691**,
709, **720**
- Adams, M. J., 58, **61**, 141, 145, **152**, **153**,
178, 490, **513**
- Adler, R. B., 213, **237**, **444**, **459**, 591, 592,
600
- Albertin, F., 69, **88**
- Allan, W. B., 104, 110, **119**
- Anderssen, R. S., 343, 345, 346, 349, 353,
353
- Ankiewicz, A., **25**, **49**, **50**, **61**, **88**, **118**, **133**,
153, **178**, **279**, **708**
- Arnaud, J. A., 103, **119**, 281, **300**
- Barrell, K. F., **50**, **61**, **88**, **133**, **178**, **440**, **708**
- Birch, R. D., 300, **300**
- Born, M., 8, 13, **25**, 65, 66, **88**, 124, 127,
133, 135, 136, **152**, 234, 235, **237**,
358, **365**, 435, **440**, 598, **600**, 667,
668, 670, 673, 680, **690**
- Bracewell, R. N., 190, **202**
- Brouillon, L., 453, **459**
- Brown, J. M., 606, **621**
- Burke, J. J., **152**, **202**, **279**, **440**, **512**, **584**,
708
- Burman, R., 269, **279**
- Cardama, A., 421, **440**
- Carrier, G. F., 535, 538, 540, **541**
- Chynoweth, A. G., 5, **237**
- Collin, R. E., 205, **207**, 490, **512**, 535, 540,
541
- Davies, O. J., **552**
- Debye, P., **207**
- de Hoog, F., **353**
- de la Rue, R., **279**, **335**
- Di-Vita, P., **88**
- Dyott, R. B., 219, 220, **237**, **440**
- Erdelyi, A., 709, 720, **720**
- Felsen, L. B., 205, **207**, 490, **512**, 535, 540,
541, 667, 670, 690, **690**
- Feshbach, H., **541**, **655**, **665**
- Feynman, R. P., 704, **708**
- Fletcher, A., 24, **25**, 54, **61**
- Friedman, B., 603, **621**, 656, 660, 663, 664,
665
- Gambling, W. A., 206, **207**, 219, 220, **237**,
327, **335**, 337, 350, **353**, 483, 485,
486, 706, 707, **708**
- Ghatak, A. K., **188**, **279**, **365**, **406**
- Gloge, D., 24, **25**, 51, 54, **61**, 116, **119**, 123,
133, 281, 285, **300**, 696, 700, **708**
- Goodman, J., 190, **202**, 696, **708**
- Gordon, J., 266, **279**
- Gradshteyn, I. S., 709, **720**
- Hammond, C. R., 58, **61**
- Hartog, A. H., **61**
- Herriott, D. R., **49**
- Hondros, A., 206, **207**
- Horowitz, B. R., 196, **202**
- Hussey, C. D., **335**, **353**, **373**, **406**, **459**, **639**,
655
- Inabe, K., **335**
- Itoh, T., **440**
- Jackson, J. D., 12, **25**, 58, **61**, 65, **88**, 113,
119, 409, **420**
- Johnson, C. C., 190, **202**, 205, **207**, 218,
224, **237**, 667, **690**, 695, **708**
- Jones, A. L., 582, **585**
- Jones, D. S., 116, **119**, 151, **153**, 448, 449,
459, 464, 465, **473**, 667, 688, **690**, **691**
- Kaminow, I. P., 295, **300**, 381, **405**
- Kapany, N. S., 141, **152**, 175, **178**, 196, 199,
202, 272, 278, **279**, 421, **440**, 490,
512, 568, **584**, 693, 703, **708**
- Kawakami, S., 262, **279**
- Keck, D. B., 3, 4, 5, **61**
- Khular, E., **365**
- Kirschfeld, K., 381, 382, **405**
- Kogelnik, H., 196, 197, 198, 199, **202**, 266,
279
- Korn, G. A., 688, 689, **691**, 709, 720, **720**
- Korn, T. M., **691**, **720**

- Kornhauser, E. T., 440
 Koyamada, Y., 279
 Krook, M., 541
 Krueger, D. A., 13, 25
 Kumar, A., 406
 Kurtz, C. N., 306, 334
- Landau, L. D., 103, 118, 215, 234, 235, 237, 266, 279
 Leighton, R. B., 708
 Li, T., 207
 Lifshitz, E. M., 118, 237, 279
 Lipson, H., 50
 Lipson, S. G., 36, 50
 Lotsch, H. K. V., 196, 202
 Love, J. D., 118, 133, 152, 153, 178, 188, 202, 279, 335, 353, 373, 406, 513, 639, 655, 665, 690, 691, 708
- Makimoto, T., 279
 Marcatili, E. A. J., 21, 61, 61, 62, 207, 708
 Marcuse, D., 8, 13, 25, 94, 100, 103, 104, 116, 118, 119, 248, 254, 279, 324, 335, 337, 353, 427, 440, 462, 473, 483, 486, 500, 513, 515, 533, 543, 552, 554, 566, 603, 621, 703, 708
 Marcuvitz, N., 207, 512, 541, 690
 Mathews, J., 338, 353, 367, 373, 610, 621, 643, 645, 655, 656, 660, 663, 664, 665, 677, 678, 679, 690
 Matsumura, H., 207, 237, 335, 353, 486, 708
 McIntyre, P., 566, 585
 McKenna, J., 49
 Menzel, R., 207, 405, 512, 584
 Midwinter, J. E., 4, 5
 Miller, S. E., 4, 5, 206, 207, 219, 237
 Mitchell, D. J., 119, 152, 178, 188, 440, 485, 513, 708
 Mitra, R., 440
 Morse, P. M., 540, 541, 643, 645, 655, 656, 660, 663, 664, 665
 Mostafavi, M., 427, 441
 Murphy, T., 25, 61
- Neumann, E. G., 334
 Nishida, S., 279
- Oliner, A. A., 541
 Olshansky, R., 54, 55, 58, 61, 61, 62
- Papas, C. H., 448, 449, 459, 658, 659, 665
 Pask, C., 25, 49, 50, 61, 62, 88, 118, 119, 133, 152, 178, 202, 237, 334, 440, 513, 655, 708
 Payne, D. N., 61, 152, 300, 300, 335, 486, 513
- Peace, M., 440
 Pearson, C. E., 541
 Personick, S. D., 94, 118
 Potter, R. J., 175, 178
- Ragdale, C. M., 207, 237, 486, 708
 Ramaswamy, V., 272
 Ramo, S., 448, 449, 459, 638, 639, 658, 659, 665
 Ramskov-Hansen, J. J., 149, 153, 173, 178
 Rawson, E. G., 33, 49, 462, 473
 Renard, R. H., 196, 202
 Rudolph, H. D., 317, 334
 Rühl, F., 300
 Rumsey, V. H., 610, 621
 Ryzhik, I. M., 720
- Sakai, J. I., 405, 485, 486
 Sammut, R. A., 335, 353, 406, 513, 533, 541, 621, 639, 655, 665, 708
 Sands, M., 708
 Sharma, A., 364, 365
 Shevchenko, V. V., 500, 513
 Sladen, F. M. E., 61, 152, 513
 Snitzer, E., 224, 237, 490, 512
 Smyth, W. R., 402, 406
 Snyder, A. W., 49, 88, 118, 119, 133, 152, 153, 178, 188, 202, 207, 237, 279, 300, 334, 335, 353, 373, 405, 406, 419, 440, 459, 472, 473, 485, 512, 513, 533, 552, 566, 584, 585, 621, 622, 639, 655, 665, 690, 708
- Sommerfield, A., 189, 202
 Stegun, I. A., 152, 279, 365, 691, 720
 Stern, J. R., 237, 427, 440
 Stewart, W. J., 141, 145, 152, 490, 512, 513, 666, 690
 Stokes, A. R., 234, 237
 Stratton, J. A., 402, 406, 462, 473, 590, 597, 600
 Streiffer, W., 334
- Tamir, T., 202, 490, 512, 540, 541
 Tarbox, E. J., 300, 300
 Teh, G. A., 419
 Thyagarajan, K., 365, 395, 406
 Tien, P. K., 200, 202
 Tjaden, D. L. A., 624, 639
 Tsuchiya, H., 383, 405
- Van Duzer, T., 459, 639, 665
 Vannucci, R., 88
 Varnham, M. P., 300, 300
- Walker, R. L., 353, 373, 621, 655, 665, 690
 Watson, G. N., 621
 Weber, H. P., 202

Whinnery, J. R., 459, 639, 665
 White, I. A., 202, 473, 485, 486
 Whittaker, E. T., 611, 621
 Wilson, M. G. F., 415, 419
 Winkler, C., 152, 188, 690, 691, 708
 Winston, R., 111, 119
 Wolf, E., 25, 88, 133, 152, 237, 365, 440,
 600, 690

Yamada, R., 326, 335
 Yamamoto, S., 272, 279
 Yeh, C., 263, 279
 Yip, G. L., 658, 665
 Young, A., 25, 61
 Young, W. R., 300, 334, 406, 639
 Zucher, F. J., 512

Subject index

Bold page numbers denote the main text discussion of the subject.

- Absorbing waveguides **120, 231, 405, 597, 700**
 - absorbed power 597
 - absorbing media 121, 232, 597
 - absorption coefficient 232
 - arrays 581
 - cladding 124, 130, 131
 - core 122, 130, 131
 - dependence on polarization 291
 - leaky rays 151
 - low- V 702
 - multimode 702
 - nonuniform 122
 - power transmission coefficient 675, 680, 686
 - pulse shape 130
 - ray and modal power attenuation 700
 - slight absorption 233, 380
 - weakly guiding 291
- Adiabatic invariant 102, 409
- Alpha profiles, *see* Clad power-law profiles
- Angle of acceptance, *see* Numerical aperture
- Anisotropic waveguides **234, 272, 295, 598**
 - biaxial 235
 - dielectric media 286, 296
 - planar 273
 - polarization maintaining 299
 - slight anisotropy 381
 - uniaxial 235
 - uniform media 234
 - weakly guiding 295
- Antenna methods **442, 460, 477, 656**
 - 'free space' 450
- Approximations
 - adiabatic 102, 409
 - asymptotic 94, 409, 666, 692
 - equivalent step profile (ESI) 350
 - 'free space' 450
 - fundamental modes 311, 333, 336
 - higher-order modes 317
 - local plane waves **666**
 - paraxial 20
 - perturbation method **374**
 - quasi-static 402
 - scalar **280, 623**
 - step-profile 350
 - variational methods **336, 366**
 - weak guidance **280, 623**
 - WKB 676
- Arrays of fibers 579
- Asymmetric planar waveguides 25, 248
- Asymptotic modal methods **692**
 - absorbing waveguides 700
 - free-space decomposition of the fields 695
 - leaky modes and rays 703
 - modal fields 696
 - propagation constants 697
 - ray decomposition of a mode 693
 - transit time 700
- Attenuation
 - absorption 231
 - coefficient 121, 127, 182, 186
 - material absorption 121
 - tunneling rays 145, 164
- Attenuation coefficient, *see* Power attenuation coefficient
- Backward-propagating modes 210
- Beams
 - collimated 66, 73
 - diffraction 190
 - Fourier transform 190
 - Gaussian 190
 - illumination 424
 - waist, *see* Spot size
- Beat length 391, 392, 394, 399, 410, 415
- Bends **179, 474**
 - antenna 477
 - classification of rays 180
 - differing radii 483
 - field shift 706
 - local modes 418
 - microbends 485
 - multimode fibers 185
 - multimode planar waveguides 180
 - radiation caustic 181
 - ray invariant 181
 - single-mode fibers 474
 - transition losses 483
 - weakly guiding fibers 476
- Bessel functions 712

- Biaxial fibers 235
- Birefringence
 - anisotropic material 295, 381
 - isotropic material 285, 354, 366, 382
 - material 296
 - single polarization 299
 - structural 295
- Bound modes **208**
 - absorbing waveguides 231
 - allowed propagation constants 226
 - coupling of the field components 222
 - derivation of the fields 220
 - excitation **420, 442**
 - hybrid nature of the fields 223
 - in terms of the longitudinal fields 222
 - longitudinal field equations 222
 - normalization 212
 - orthogonality 212
 - orthonormal 214
 - power 215, 232, 291
 - properties 230
 - representation on nonabsorbing waveguides 212
 - symmetry properties 212
 - vector wave equations 221
 - weakly guiding fibers **280**
- Bound rays **6, 26**
 - absorption **120**
 - circular fibers 26, 35, 38
 - noncircular fibers 46
 - planar waveguides 6, 15
 - power density 71
 - power distribution 71
 - total power 70
- Boundary conditions
 - Maxwell's equations 591
 - scalar wave equation 641
- Cartesian field components 283, 624
- Caustics 14, 47, 492, 689
 - arbitrary curvature 149
 - inner 29
 - radiation 37
 - turning-point 14
- Characteristic length scales 96, 409
- Circular fibers **26, 301**
 - bound modes **300**
 - bound rays **26**
 - fundamental modes 284
 - Gaussian approximation **336**
 - weakly guiding **301**
- Clad inverse-square profile 269
- Clad parabolic profile 72
- Clad power-law profiles 24, 44, 59
- Clad profiles 210
- Cladding 3, 7, 27, 209
 - absorption 124
 - finite 533
 - propagation in 193
- Coherence 437
- Collimated beam 66, 73
 - illumination 73
 - lens 74
 - taper 108
- Complement of the critical angle 8, 246, 490, 668
- Complement of the local critical angle 17, 39
- Concentrators 107, 192
- Concentric elliptical profiles 355
- Condition for weak guidance 308
- Confinement, maximum possible 192
- Connection formulae 679
- Construction of ray paths 8, 13, 28, 32
- Core 3, 7, 27, 209
- Core-cladding interface 7, 27, 209
- Corrections
 - 'free-space' 455, 532
 - tubular source 533, 660
 - waveguide polarization 286
- Coupled local-mode equations **553, 567**
 - coupling coefficients 554, 618, 652
 - derivation 554, 616
 - guided power 555
 - induced current solution 556
 - local radiation modes 560
 - physical derivation 620
 - radiated power 561, 563
 - slow-variation condition 556
 - strong power transfer 560
 - tapered couplers 564
 - twisted elliptical fiber 558
 - weak power transfer 556
 - weakly guiding waveguides 555
- Coupled mode equations **542, 567**
 - cross-coupling coefficients 546
 - cross-talk 569
 - derivation 543, 649
 - induced current solution 545
 - physical derivation 615
 - polarization effects 543
 - self-coupling coefficients 546
 - sinusoidally perturbed fibers 546
 - strong power transfer 545
 - weak power transfer 544, 550
 - weakly guiding waveguides 543
- Couplers 387, 567
 - tapered 413, 415, **553**
 - uniform 387, **567**
- Coupling coefficients 544, 554, 555, 618, 619, 651, 653
- Coupling of modes **542, 567**
 - arrays of fibers 579
 - local modes **553**
 - nonuniform fibers 553

- Coupling of modes (*contd.*)
 - parallel fibers 567
 - sinusoidal perturbations 546
 - weak power transfer 545
- Critical angle 8, 17, 29, 39, 668
- Cross-talk 387, 413, 567
 - absorption 581
 - arrays of fibers 579
 - coupled equations 569, 576
 - finite polygonal arrays 583
 - identical pairs of fibers 570, 578
 - infinite arrays 579
 - multimode fibers 575
 - nearly identical fibers 570
 - parallel fibers 387, 391, 397, 568
 - periodic illumination 579
 - slowly varying fibers 415, 575
 - tapered couplers 413, 415
 - unequal fibers 397, 574
- Crystalline fibers, *see* Anisotropic fibers
- Current dipole, *see* Dipole
- Current sources
 - bound modes 608
 - dyadic Green's function 657
 - radiation modes 608
 - scalar modes 653
- Curvature loss 134, 179
- Cutoff 228
 - equal volume profiles 332
 - far from 229
 - propagation below 489
 - second mode 352
 - step-profile approximation 352
- Cylindrical polar coordinates 711
- Cylindrical symmetry 7, 211, 375

- Debye asymptotic forms of Bessel functions 715
- Decomposition of the radiation field 534
- Depth of penetration 316
- Dichroic fibers 382
- Dielectric constant 590
- Diffraction 190
 - beam 190
 - lateral shift 195
 - light containment 192
 - preferred ray directions 200
 - rays 120, 124
 - total internal reflection 194
- Diffuse illumination 69, 436
 - partially 61, 111
 - source 65, 76
- Diffusion equation 115
- Dipole 445, 446, 451, 457, 532
 - bound modes 442
 - dyadic Green's function 657
 - electrostatic 627
 - 'free-space' fields 530
 - leaky modes 508
 - radiation 451, 530
 - radiation modes 532
 - superposition 656
- Direction angles 29, 33, 492
- Discontinuous profiles 400, 611, 615
- Dispersion 219, 294
 - intermodal 51
 - intramodal 219
 - linear 58
 - material 12, 20, 42, 51, 88
 - nonlinear 60
 - profile 58
 - ray 51, 55, 57
- Displacement vector 591, 598
- Distortion parameter 229, 292, 294, 340
- Distribution function
 - bound-ray power 79
 - scattering 112
 - tunneling rays 157
- Double-parabolic profile 364, 394

- Eccentricity 355, 371
- Effective core half-width 199, 702
- Effective profile 706
- EH modes 224
- Eigenfunction expansion 205, 611, 636
- Eigenvalue equation 211, 218, 221
 - absorbing waveguides 233
 - asymptotic derivation for higher-order modes 697
 - integral form 222, 292, 643
 - leaky modes 489, 538
 - local modes 419
 - local plane-wave derivation 247, 262, 698
 - poles 535
 - weakly guiding waveguides 284
- Eikonal equation 13, 667, 669
- Electromagnetic fields 590
 - anisotropic media 598
 - displacement vector 598
 - forward- and backward-propagating 593
 - Maxwell's equations 590, 598
 - nonabsorbing waveguides 593
 - polarization parallel to a principal axis 600
 - refractive-index tensor 598
 - relationships between components 591
 - translational invariance 591
 - uniaxial waveguides 599
 - vector wave equations 594, 598
- Elliptical fibers 262, 355, 366, 382, 405
 - slight eccentricity 371, 382
 - twisted 412
- Elliptical profiles
 - Gaussian 373

- infinite parabolic 49, 355
 - step 262, 372, 385, 663
- Energy of a mode 214, 607
- Equal-volume profiles 71, 330, 347
- Equalization of transit times 18, 24, 42, 54, 56
- Equivalent step-index approximation (ESI) 350
- Euler's theorem 688, 689, 720
- Evanescent fields 124, 675
- Evanescent modes 516
- Exact modal solutions **238**
- Excitation
 - bound modes **420, 442**
 - leaky modes 501
 - radiation field 448
 - radiation modes 519
 - rays **63**
- Expansion of the modal fields 259, 624
- Expansion over the modal fields 210
- Far-field correction 347, 664
- Fiber parameter 27, 227
- Field shift on bent fibers 483, 706
- Finite cladding 533
- Fraction of modal power in the core 216, 292
- Fraction of total power in the core 217
- 'Free-space'
 - decomposition of the radiation fields **534**
 - Green's function 660
 - radiation modes 520
 - uniform media 281
- Fresnel power transmission coefficient 136, 674
- Frustrated total internal reflection 36, 493, 680
- Fundamental modes 206, 228
 - approximations 317, 333, **336**
 - dependence on profile volume 330
 - Gaussian approximation **336, 366**
 - LP modes 285, 287
 - polarization corrections 286
 - propagation constant 284
 - single polarization fibers 299
 - small- V limit 333
 - step-profile approximation (ESI) 350
 - two parallel fibers 389, 397
 - weakly guiding fibers 284, 630
- Gaussian approximation **336, 366**
 - circular fibers **336**
 - concentric elliptical fibers 369
 - far field 347, 664
 - fundamental modes 336, 366
 - higher-order modes 349
 - noncircular fibers **366**
 - slight eccentricity 371
- Gaussian beam 190
- Gaussian profile 342
- Generalized parameters 164
- Geometric optics 4, 666
 - applicability 193
 - validity 439
- Geometrical birefringence 358
- Goos-Haenchen shift 196, 702
- Graded-profile fibers **27, 238, 280, 301, 336**
 - exact solutions 263
 - Gaussian approximation 336, 366
 - multimode 32
 - single-mode **336**
 - weakly guiding 280, 301
- Graded-profile planar waveguides **13, 238**
- Green's functions **442, 656**
 - antenna radiation 442
 - arbitrary current sources 656
 - correction factor 661
 - dipole 657
 - far-field correction 664
 - 'free-space' 660
 - higher-order field corrections 637
 - perturbation problems 663
 - polarization corrections 636
 - reciprocity theorem 657
 - slightly elliptical fibers 663
 - tubular sources 660
 - vector potential 658
- Group delay 219
- Group index 12, 20, 42, 57, 59, 220
- Group velocity 218, 608
 - Gaussian approximation 340
 - higher-order corrections 294
 - ray and modal transit times 700
 - reciprocity theorem 608
 - scalar wave equation 643
 - weakly guiding waveguides 292
- Hankel functions 712
- HE modes 224
 - nature of the fields 223
 - physical explanation 225
 - ray decomposition 693
- Higher-order field corrections 309
- Homogeneous function profiles 46, 49, 361, 364
- Hybrid modes 223
 - nature of the fields 223
 - physical explanation 225
 - ray decomposition 695
- Hyperbolic functions 710
- Hyperbolic-secant profile 19, 23, 54
- Ideal fibers 205, 209

- Illumination 63, 420**
 - beam 73, 424
 - collimated beam 73
 - comparison with geometric optics 434
 - diffuse 65, 69, 110, 157, 167, 436
 - error in geometric optics analysis 439
 - fields of the beam 424
 - fields on the fiber endface 423
 - Gaussian approximation 430
 - Gaussian beam 425, 427
 - incoherent 437
 - junctions between fibers 430
 - Lambertian 65, 69
 - lens 74, 434
 - mismatch 430
 - mode launching 421, 425
 - multimode fibers 63
 - nonuniform 72
 - oblique incidence 76, 429, 431
 - offset beam 428
 - on-axis beam 428
 - single-mode fibers 430
 - sources of 65
 - tilted beam 427
 - uniform beam 424, 428
 - weakly guiding waveguides 423
- Implicit conditions for radiation modes 529**
- Implicit time dependence 590**
- Impulse response 64, 83**
 - material dispersion 88
 - mean 85
 - numerical determination 87
 - rms width 85
- Induced current method 460**
 - absorption 597
 - coupled local-mode equations 553, 556
 - coupled mode equations 542, 545, 615
- Infinite linear profile 363**
- Infinite parabolic profile 21, 43, 306, 698**
- Infinite power-law profiles 309, 699**
- Inner caustic 29, 35, 81, 695**
- Integral theorems 712**
- Intensity 215, 292**
 - distribution 65, 75, 78, 173
- Interface wave 540**
- Intermodal dispersion 51, 219**
- Intramodal dispersion 219**
- Invariants**
 - adiabatic 102, 409
 - ray 10, 16, 31, 33, 38, 45, 83, 231
- ITE and ITM modes 523, 524, 528**
- Jacket 3**
- Junctions 431**
- Kramers-Kronig relations 215**
- Lambertian source 65**
- Laplace equation 228, 333, 402**
- Large- V limit 692**
- Laser 66**
- Lateral shift 195**
 - absorption 199, 700
 - transit time 197, 700
- Lateral wave 540**
- Leaky modes 487, 534, 538**
 - applications 507
 - attenuation 495
 - characteristics 490
 - classification 492
 - comparison with leaky rays 499, 703
 - decomposition of the radiation field 534
 - eigenvalue equation 502
 - excitation 501
 - guided portion of power 496
 - heuristic derivation 489
 - normalization 499
 - orthogonality 499, 647
 - power 495
 - reciprocity theorem 603
 - refracting 492
 - tunneling 492
- Leaky rays 30, 45, 134, 149**
 - classification 143
 - comparison with leaky modes 499, 703
 - excitation 157, 161
 - graded-profile fibers 38
 - noncircular fibers 45
 - tunneling 36, 134
 - refracting 9, 15, 30, 35, b134
- LED 66**
- Length scales 96**
- Lens illumination 74, 435**
- Light concentration 74, 107**
- Light containment 192**
- Linear dispersion 58**
- Linear taper 109**
- Lissajous figures 49**
- Local critical angle 17, 39**
- Local modes 407, 553**
 - beat length 410, 415
 - bent fibers 418
 - composite waveguides 413, 415, 563
 - coupled equations 554, 617
 - coupling 553
 - coupling coefficients 555, 619, 650, 653
 - cross-talk 414, 417
 - modal half-period 410
 - mode and ray transit times 419
 - multimode fibers 410, 419
 - nonuniform fibers 413, 415, 564
 - physical derivation of the coupled equations 620
 - power 409

- radiation 410, 561
- scalar 651
- tapered couplers 413, 415, 564
- validity 409, 556
- Local numerical aperture 28, 70
- Local plane waves **666**
 - absorbing cladding 675
 - curved interface 687
 - evanescent fields 675
 - Fresnel coefficients 674, 687
 - local plane waves 667
 - loss phenomena 671
 - polarization 669
 - power attenuation coefficient 672
 - power flow 667, 669
 - power transmission coefficient 672
 - ray-path equations 670
 - ray power 672
 - slowly varying media 668
 - Snell's laws 668
 - tunneling 678
 - uniform media 667
 - weakly guiding waveguides 672
- Local speed of light 12, 18, 226
- Locally valid power transmission coefficients 149
- Longitudinal fields 291, 591
- Loss coefficient, *see* Power transmission coefficient
- Loss mechanisms
 - absorption **120**, 231, 380, 405
 - bends **179**, **474**
 - interface roughness 466
 - junctions 431
 - microbends 485
 - nonuniformities **89**, 105, b460
 - offsets 430, 485
 - polarization coupling 299
 - radiation 105, 463
 - refraction 134, 154, 487
 - scatterers 116, 464
 - tilts 431, 485
 - transition 483
 - tunneling 134, 154, 487
- LP modes
 - fundamental 285
 - higher-order 287
 - inaccuracies of 321
- Magnetic permeability 221, 590
- Material absorption 380
- Material anisotropy 296
- Material birefringence 234
- Material dispersion 51, 57, 220, 607
 - impulse response 88
 - nonuniform media 20, 42
 - optimum profile 59
- ray and modal transit times 700
- uniform media 12, 32
- Maximum light concentration 344
- Maxwell's equations 211, 220, 408, 554, b590, 607, 695
 - anisotropic media 598
 - fields of z-dependent waveguides 616
 - modal methods **208**, **601**
 - reciprocity theorem 602
- Meridional rays 29, 34, 54, 56, 140, 224, 695
- Metal-clad waveguides 603, 605
- Microbends 485
- Modal amplitudes
 - bound 211
 - leaky 490, 501
 - radiation 517, 520
- Modal expansion
 - bound 205, 210
 - leaky 499
 - radiation 515, 517
 - scalar 636
- Modal half-period 410
- Modal methods for Maxwell's equations **601**
- Modal methods for the scalar wave equation 640
- Modal parameters 227
- Modes
 - arbitrary waveguides **208**
 - circular fibers **301**
 - composite structures 387
 - confinement 192
 - coupling **460**, **542**
 - decomposition into rays 693
 - excitation **420**, **442**, 608
 - number of 704
 - perturbed fibers **374**
 - scalar wave equation **640**
 - slowly varying fibers **407**
 - weakly guiding waveguides 280
- Monomode, *see* Single mode
- Multilayered waveguides 248, 262
- Multimode 4, 7, 227
- Nearly circular fibers 289, 360
- Noncircular fibers 45, **354**, **366**
 - anisotropic 298
 - bound rays 45
 - concentric elliptical 369
 - elliptical 355, 369
 - Gaussian approximation 366
 - leaky rays 149
 - planar waveguides **6**, 239, 263
 - ray dispersion 57
 - spatial transient 172
 - weakly guiding 280
- Noncircular power-law profiles 46
- Nonlinear dispersion 60

- Nonuniform fibers, *see also* Nonuniformities
 - multimode 89
 - pulse propagation 89
 - single-mode 407
- Nonuniform illumination 72, 423
- Nonuniformities 89, 407, 460, 474
 - change in core radius 465
 - continuously varying 90
 - coupling of modes 467, 471
 - discontinuous 112
 - distributed nonuniformities 464
 - interface roughness 465, 471
 - isolated 469
 - junctions 430
 - offsets 430
 - power redistribution 112, 460
 - prolonged 94
 - radiation from 105, 116, 463
 - random 93
 - slight 104
 - slowly varying 94, 407, 470
 - small amplitude 94, 98, 460
 - tilts 430
- Normalization
 - bound modes 212
 - 'free-space' radiation modes 520
 - leaky modes 500
 - orthonormal modes 214
 - radiation modes 517
 - scalar modes 647
- Normalized distribution function 81
- Number of modes
 - bound 211, 229
 - leaky modes 494
 - tunneling leaky modes 494, 704
 - refracting leaky modes 494, 704
- Number of reflections 11, 17, 32, 39
- Numerical aperture 27
- Oblique incidence 76
- Offsets 429
- Optical axes 285, 287, 296, 631
- Optical path length 11, 17, 31, 39
- Optimum bound-ray power 77
- Optimum profile 54, 59, 102
- Orthogonality
 - absorbing waveguides 214, 605
 - bound modes 212, 604
 - leaky modes 500, 605
 - radiation modes 517, 604
 - scalar radiation modes 647
 - scalar wave equation 292, 641
 - weakly guiding waveguides 292
- Orthonormal modes
 - bound modes 214, 409
 - local modes 409
 - radiation modes 518
- Overmoded, *see* Multimode
- Parabolic profile, *see* Clad parabolic profile; Infinite parabolic profile
- Parabolic taper 108
- Parallel fibers
 - nonuniform 413
 - uniform 387, 567
- Parametric dependence of the modal fields 227, 624
- Paraxial approximation 20, 246
- Partially diffuse source 66, 76, 79
- Path length 11, 17, 31, 39
- Perturbations 374
 - core radius 380, 403
 - cross-talk 387, 567
 - elliptical 382
 - isolated nonuniformity 380
 - large profile height 399
 - sinusoidal 465, 470
 - slight absorption 380, 405
 - slight anisotropy 381
 - slight eccentricity 360, 371, 382
 - slight profile height 378
 - uniform 377
- Phase velocity 211, 607, 643
- Planar waveguides 6, 237
 - anisotropic 272
 - bound rays 6
 - graded profiles 13, 263
 - lateral shift 198
 - multimode 7
 - power transmission coefficients 673, 675
 - ray parameters 16
 - ray paths 13
 - weak-guidance approximation 354
- Plane of incidence 150, 688, 689, 720
- Plane polarized modes, *see* LP modes
- Plane-wave decomposition 246, 262, 494, 524, 693
- Plane-wave reflection 224
- Polarization, *see also* Birefringence
 - corrections 286, 291
 - coupling 222, 299, 470
 - dependence on absorption 291
 - maintaining fibers 299
 - perturbed fibers 377
 - properties of waveguides 222, 309, 358
 - structural 222, 309
 - structural birefringence 295
 - vector 669
- Power
 - absorption coefficients 232, 381
 - attenuation coefficients 121, 127, 129, 137, 672
 - bound-ray 70, 77
 - density 215, 292

- distribution among bound rays 79
- flow 215
- fraction in the core 216
- power transmission coefficients 68, 125, 136
- ray tubes 64
- total guided 216
- Power-law profiles, *see* Clad power-law profiles; Infinite power-law profiles
- Power-series solution 327
- Power transmission coefficients 671
 - absorption 125, 675, 680, 686
 - analytic continuation 683, 685
 - continuous and discontinuous profiles 682
 - definition 672
 - evanescent fields 675
 - Fresnel coefficients 674, 686
 - frustrated total internal reflection 680
 - linear approximation 681, 685
 - locally valid 149
 - ray power 672
 - refracting rays 673, 680, 686
 - scalar approximation 673
 - tunneling rays 678, 685, 688
 - universal 148
 - weakly guiding fibers 672
 - WKB solution 676
- Poynting vector 215, 597
- Preferred ray directions 200
- Principal axes 234, 235, 296, 598, 600
- Profile
 - alpha, *see* Clad power-law
 - anisotropic step-profile planar waveguide 272
 - clad 210
 - clad inverse-linear 269
 - clad inverse-square 269
 - clad parabolic 83
 - clad power-law 22
 - dispersion 58
 - double-parabolic 364
 - equal-volume 71, 347
 - exponential 266
 - Gaussian 342, 373
 - graded 3
 - height parameter 227, 302
 - homogeneous-function 46, 361
 - hyperbolic-secant 23
 - hyperbolic-tangent 266
 - infinite elliptical parabolic 49
 - infinite linear 363
 - infinite parabolic 306
 - infinite power-law 309
 - inverse square 266
 - optimum 54, 59, 171
 - separable 47
 - shape 70
 - smoothed-out 345
 - step 239, 248
 - tangent profile 266
 - uniaxial step profile 278
 - volume 70, 81, 300, 331, 347
- Propagation constant 207, 211, 222, 226
 - absorbing waveguides 232
 - anisotropic media 236
 - asymptotic derivation 697
 - evanescent modes 516
 - forward- and backward-propagating modes 211
 - Gaussian approximation 340
 - integral expressions 222, 292, 606, 643
 - leaky modes 488, 489, 491
 - perturbed fibers 399, 610
 - polarization corrections 286, 294, 625, 628
 - radiation modes 516
 - range for bound modes 226, 236
 - reciprocity relations 644
 - relationship with ray invariant 231, 695
 - slightly elliptical fibers 371
 - two parallel fibers 389, 398
 - uniformly perturbed fibers 648
 - weakly guiding waveguides 283
- Pulse shape 64, 83
 - absorption 130
 - radiation 169
- Pulse spreading 51, 99, 100, 102, 169, 219, 286
- Quasi-static approximation 333, 402
- Radiation 154, 448, 514
 - absorption 176
 - antenna method 442, 656
 - correction due to profile 455
 - diffuse source 157
 - dipole 451, 530, 532
 - 'free-space' approximation 450, 520
 - Green's function 442, 656
 - modal methods 514
 - multimode fibers 134
 - slowly varying fibers 105
 - tubular source 453, 455, 531, 533
- Radiation caustic 37, 492, 677
- Radiation field
 - close to the fiber axis 488
 - correction due to the fiber profile 455
 - decomposition 534
 - integral representation 535
 - leaky mode contribution 538
 - space wave contribution 539
 - total power 518
- Radiation modes 514
 - construction 523
 - dipole excitation 530, 532

Radiation modes (*contd.*)

- excitation 519, 610
 - evanescent modes 516
 - finite cladding 533
 - 'free-space' modes 520
 - ITE and ITM modes 523, 524
 - local 560
 - normalization 517, 527
 - orthogonality 517, 527
 - orthonormal modes 518
 - plane-wave decomposition 524
 - power 518
 - propagation constant 516
 - reciprocity theorem 603
 - representation of the modal fields 515
 - scalar 526, 646
 - vector direction of the modal fields 526
 - weakly guiding 526
- Random nonuniformities 93, 463, 464
- Range of single-mode operation 342
- Rationalized MKS units 590
- Ray caustics, *see* Caustics
- Rayleigh scattering 116
- Rays
- angles 29, 33
 - asymptotic modal methods **692**
 - bound **6, 26**
 - caustic 14, 37
 - classification 29, 35, 48, 186
 - decomposition of a mode 693
 - dispersion **51**
 - equalization of transit times 18
 - equation 13
 - half-period 11, 17, 31, 39
 - invariants 10, 16, 31, 32, 45, 68, 83, 231
 - leaky 30, 45, **134**
 - local plane waves **666**
 - meridional 29, 54, 56, 140
 - number of reflections 11, 17, 32, 39
 - parameters 10, 16, 31, 38
 - paraxial 20
 - path 11, 16, 28, 39
 - path equations 14, 33, 45, 91, 667, 669, 670
 - path length 11, 17, 31, 39
 - preferred directions 200
 - relation to local plane waves **666**
 - refracting 9, 15, 30, 35, **134**, 158
 - skew 29, 54, 140
 - tracing 4
 - trajectory, *see* path
 - transit time 12, 18, 32, 42, 84, 91, 95, 198, 700
 - tubes 64, 667, 669
 - tunneling 30, 36, **134**
 - tunneling-refracting 45, 149
 - turning point 14

- whispering gallery 182
- Reciprocity relations **644**
- Reciprocity theorem **601**
- conjugated form 602
 - coupled mode equations 613
 - current dipole 657
 - dyadic Green's function 657
 - excitation by sources 608
 - generalized 607
 - group velocity 607
 - leaky modes 603
 - line integral formulation 604
 - modal amplitudes 612
 - orthogonality, conjugated form 604
 - orthogonality, unconjugated form 605
 - phase velocity 607
 - propagation constant 606, 610
 - radiation modes 603
 - slightly perturbed waveguides 612
 - stored electric and magnetic energies 607
 - unconjugated form 604
 - uniformly perturbed waveguides 610
- Reflection
- caustic 151
 - interface 150
- Refracting leaky modes 492
- Refracting rays 9, 15, 30, **134**, 158
- fiber endface 67
 - graded-profile fibers 35, 38, 140
 - graded-profile planar waveguides 15, 137
 - power transmission coefficient 673, 680, 686
 - step-profile fiber 30, 38, 138
 - step-profile planar waveguide 136
 - transition to tunneling rays 148
- Refractive-index profile 283, 302
- Resonant conditions 210, 448, 545, 560
- Scalar
- approximation **280**
 - leaky modes 647
 - radiation modes 647
- Scalar wave equation 223, 283, 357, **640**, 674
- anisotropic media 599
 - arbitrary step-profile waveguides 223
 - bound modes 641
 - continuity properties 641
 - correction factor 661
 - current sources 653
 - derivative of the modal parameter 644
 - field shift on bent fibers 707
 - group velocity 643
 - integral for the propagation constant 643
 - leaky modes 647
 - modal methods **640**
 - normalization 642

- orthogonality 641
- phase velocity 643
- power transmission coefficient 674, 676, 683
- propagation constant 284, 625, 626, 628
- radiation modes 646
- small- V limit 333
- TE modes 245, 252
- Scatterers 112
- Separable profiles 47, 362
- Sine rule 709
- Single mode 4, 227
 - fibers 336
 - range of operation 342, 347
 - single-polarization 299
- Sinusoidal deformations 509, 546
- Skew rays 29, 35, 225, 695
- Slightly elliptical fibers 360, 371, 373
- Slowly varying fibers **89, 407, 575**
 - bent fibers 419
 - criterion for 409
 - local modes 407
 - media 668
 - multimode 94
 - ray transit time 95
 - tapered couplers 415
 - tapers 107, 413, 415
- Smoothed-out profiles 345
- Snell's laws, 8, 9, 13, 14, 28, 29, 67, 668
- Sources
 - correction factor 455
 - diffuse 65, 76, 157, 436
 - dipole 446, 451
 - efficiency 70
 - endface illumination 423
 - 'free-space' radiation 450
 - incoherent, *see* Diffuse
 - Lambertian 65
 - modal excitation 442, 520
 - partially diffuse 66, 79
 - power 69
 - radiated power 449
 - sinusoidal line current 509
 - tubular source 447, 453, 458, 533
 - weakly guiding fibers 444
 - within fibers **442**
- Space wave 490, 539
- Spatial coherence 437
- Spatial pulse spread 53
- Spatial steady state 155, 205, 488, 514
- Spatial transient **154, 205, 487, 514**
- Spot size
 - circular fiber 338
 - noncircular fiber 367
- Stationary expressions 292, 338, 610, 643, 645
- Steepest descent 537
- Step-profile approximation 350
- Step-profile waveguides
 - exact solutions 238
 - fibers 248, 301
 - noncircular fibers 262
 - planar waveguides 354
 - weakly guiding 280
- Stored electric and magnetic energy 214, 607
- Structural anisotropy 286, 295
- Synchronous condition, *see* Resonant condition
- Tapered couplers 415
- Tapers 107
- TE modes 223, 224, 235, 599, 629, 695
- TEM waves 283
- Three-layer fiber 378
- Tilts 427, 430
- Time dependence of the fields 211, 221
- TM modes 224, 235, 599, 695
- Total guided power
 - bound modes 216
 - bound rays 70
- Total internal reflection 194, 195, 282, 668
 - curved interface 140
 - planar interface 135
- Transit time
 - rays 12, 419, 700
 - modes 219, 247, 262
- Translational invariance 7, 211
- Transmission coefficient, *see* Power transmission coefficient
- Trapped modes, *see* Bound modes
- Trapped rays, *see* Bound rays
- Trigonometric functions 709
- Tubular source 447, 453, 458, 531, 533
- Tunneling leaky modes 492
- Tunneling rays **30, 140**
 - attenuation 145
 - frustrated total internal reflection 680
 - graded-profile fibers 36, 38, 141, 145
 - power transmission coefficient 678
 - step-profile fiber 30, 31, 38, 143, 147
 - transition to bound rays 686
 - transition to refracting rays 148
- Tunneling-refracting rays 45, 48
- Turning-point caustic 14, 35, 81
- Twisted elliptical fiber 412
- Two parallel fibers 413
- Uniaxial fibers 235, 278, 599
- Uniform beam 190
- Uniform dielectric media 232, 234, 281, 381
- Uniform fibers 123, **374**
- Uniformly perturbed fibers **374**
 - absorption 380, 405

- Uniformly perturbed fibers (*contd.*)
 - anisotropic 381
 - core and cladding indices 378
 - core radius 380, 404
 - ellipticity 382, 405, 663
 - isolated nonuniformity 380, 401
 - modal fields 399, 611
 - propagation constants 399, 610
 - scalar modes 648
 - step discontinuity 400
 - three-region fiber 378
- Universal transmission coefficients 148
- Variational methods 336, 366
- Vector operations 710
- Vector potential 658
- Vector wave equations 221, 594, 598, 623
 - anisotropic media 598
 - cartesian component equations 595
 - coupling of the field components 221, 222, 594
 - cylindrical polar component equations 594
 - equations for the longitudinal fields 222, 597
 - expansion of the exact fields 624
 - homogeneous 594, 595
 - limit of small V 228
 - sources 637
 - step-profile waveguides 239
 - uniaxial waveguides 599
 - weakly guiding waveguides 623
- Wave building block 120, 131
- Wave effects, *see* Diffraction
- Waveguide dispersion 219, 220, 229
 - distortion parameter 229, 294
 - zero of 346
- Waveguide parameter or frequency 7, 27, 227
- Weakly guiding waveguides 280, 623
 - accuracy for leaky modes 506
 - alternative representation for modes 635
 - anisotropic waveguides 236, 278, 295
 - circular fibers 284, 287, 301, 632
 - conditions for weak guidance 308, 311, 359
 - coupled local-mode equations 554
 - coupled mode equations 544
 - general properties 288, 292
 - leaky modes 494
 - modal methods 640
 - noncircular waveguides 285, 289, 354
 - paraxial approximation 20
 - physical interpretation 627
 - polarization corrections to the modal fields 623, 636
 - polarization corrections to the propagation constant 628
 - propagation constant 628
 - radiation modes 526, 638
 - sources 637
 - symmetry properties of modes on fibers 633
 - vector direction of the modal fields 630
- WKB solutions 577, 676
 - circular fibers 683
 - connection formulae 679
 - continuous and discontinuous profiles 682
 - local plane-wave derivation 677, 684
 - planar waveguides 678
 - ray caustics 677, 689
 - uniform approximations 690
- z -dependent nonuniformities, *see* Nonuniform fibers
- z -independent nonuniformities, *see* Uniformly perturbed fibers
- Zero of waveguide dispersion 346

ELECTROMAGNETIC QUANTITIES

$\varepsilon = \varepsilon_0 n^2$	Dielectric constant
ε_0	Free-space dielectric constant
μ_0	Free-space permeability
$c = \frac{1}{(\varepsilon_0 \mu_0)^{1/2}} = \frac{\omega}{k}$	Free-space speed of light
$\omega = kc$	Angular frequency
$\exp(-i\omega t)$	Implicit time dependence

MODAL PARAMETERS

	Exact (n_{co} , n_{cl} arbitrary)	Weak guidance ($n_{co} \cong n_{cl}$)
Propagation constant	$\beta = \frac{1}{\rho} \left\{ \frac{V^2}{2\Delta} - U^2 \right\}^{1/2}$	$\tilde{\beta} = \frac{1}{\rho} \left\{ \frac{V^2}{2\Delta} - \tilde{U}^2 \right\}^{1/2}$
Core parameter	$U = \rho(k^2 n_{co}^2 - \beta^2)^{1/2}$	$\tilde{U} = \rho(k^2 n_{co}^2 - \tilde{\beta}^2)^{1/2}$
Cladding parameter (bound modes)	$W = \rho(\beta^2 - k^2 n_{cl}^2)^{1/2}$	$\tilde{W} = \rho(\tilde{\beta}^2 - k^2 n_{cl}^2)^{1/2}$
Cladding parameter (radiation modes)	$Q = \rho(k^2 n_{cl}^2 - \beta^2)^{1/2} = iW$	$Q = \rho(k^2 n_{cl}^2 - \tilde{\beta}^2)^{1/2} = i\tilde{W}$
Relations with fiber or waveguide parameter	$V^2 = U^2 + W^2$ $= U^2 - Q^2$	$V^2 = \tilde{U}^2 + \tilde{W}^2$ $= \tilde{U}^2 - Q^2$
Cutoff condition	$U = V = V_c$; $W = 0$	$\tilde{U} = V = V_c$; $\tilde{W} = 0$
Range of bound modes	$kn_{cl} < \beta \leq kn_{co}$	$kn_{cl} < \tilde{\beta} \leq kn_{co}$
Range of radiation modes	$0 \leq \beta < kn_{cl}$	$0 \leq \beta < kn_{cl}$